ADVANCED INORGANIC CHEMISTRY CHEM-5020: FALL 2026



Yulia Zaikina
Iowa State University

LibreTexts™

Advanced Inorganic Chemistry CHEM-5020: Fall 2026

Yulia Zaikina

Iowa State University

This text is disseminated via the Open Education Resource (OER) LibreTexts Project (https://LibreTexts.org) and like the thousands of other texts available within this powerful platform, it is freely available for reading, printing, and "consuming."

The LibreTexts mission is to bring together students, faculty, and scholars in a collaborative effort to provide an accessible, and comprehensive platform that empowers our community to develop, curate, adapt, and adopt openly licensed resources and technologies; through these efforts we can reduce the financial burden born from traditional educational resource costs, ensuring education is more accessible for students and communities worldwide.

Most, but not all, pages in the library have licenses that may allow individuals to make changes, save, and print this book. Carefully consult the applicable license(s) before pursuing such effects. Instructors can adopt existing LibreTexts texts or Remix them to quickly build course-specific resources to meet the needs of their students. Unlike traditional textbooks, LibreTexts' web based origins allow powerful integration of advanced features and new technologies to support learning.



LibreTexts is the adaptable, user-friendly non-profit open education resource platform that educators trust for creating, customizing, and sharing accessible, interactive textbooks, adaptive homework, and ancillary materials. We collaborate with individuals and organizations to champion open education initiatives, support institutional publishing programs, drive curriculum development projects, and more.

The LibreTexts libraries are Powered by NICE CXone Expert and was supported by the Department of Education Open Textbook Pilot Project, the California Education Learning Lab, the UC Davis Office of the Provost, the UC Davis Library, the California State University Affordable Learning Solutions Program, and Merlot. This material is based upon work supported by the National Science Foundation under Grant No. 1246120, 1525057, and 1413739.

Any opinions, findings, and conclusions or recommendations expressed in this material are those of the author(s) and do not necessarily reflect the views of the National Science Foundation nor the US Department of Education.

Have questions or comments? For information about adoptions or adaptions contact info@LibreTexts.org or visit our main website at https://LibreTexts.org.

The LibreTexts name, logo, and book covers are trademarked by LibreTexts, Inc. (a 501(c)(3) not-for-profit organization) and protected against unauthorized use.

This text was compiled on 08/23/2026

TABLE OF CONTENTS

Licensing

1: Introduction to Inorganic Chemistry

1.1: What is Inorganic Chemistry?

1.2: Inorganic vs Organic Chemistry

1.3: History of Inorganic Chemistry

1.4: Perspectives

1.5: Practice problems

2: Atomic Structure

2.1: Historical Development of Atomic Theory

2.1.1: The Periodic Table

2.1.2: Discovery of Subatomic Particles and the Bohr Atom

2.2: The Schrödinger equation, particle in a box, and atomic wavefunctions

2.2.1: Particle in a Box

2.2.2: Quantum Numbers and Atomic Wave Functions

2.2.3: Aufbau Principle

2.2.4: Shielding

2.3: Periodic Properties of Atoms

2.3.1: Ionization energy

2.3.2: Electron Affinity

2.3.3: Covalent and Ionic Radii

2.4: Problems

3: Simple Bonding Theory

3.1: Lewis Electron-Dot Diagrams

3.1.1: Resonance

3.1.2: Breaking the octet rule with higher electron counts (hypervalent atoms)

3.1.3: Formal Charge

3.1.4: Lewis Fails to Predict Unusual Cases - Boron and Beryllium

3.2: Valence Shell Electron-Pair Repulsion

3.2.1: Lone Pair Repulsion

3.2.2: Multiple Bonds

3.2.3: Electronegativity and Atomic Size Effects

3.2.4: Ligand Close Packing

3.3: Molecular Polarity

3.4: Hydrogen Bonding

4: Symmetry and Group Theory

4.1: Symmetry Elements and Operations

4.2: Point Groups

4.2.1: Groups of Low and High Symmetry

4.2.2: Other Groups

4.3: Properties and Representations of Groups

4.3.1: Matrices

4.3.2: Representations of Point Groups

4.3.3: Character Tables

4.4: Examples and Applications of Symmetry

4.4.1: Chirality

4.4.2: Molecular Vibrations

4.5: Problems (under construction)

5: Molecular Orbitals

5.1: Formation of Molecular Orbitals from Atomic Orbitals

5.1.1: Molecular Orbitals from s Orbitals

5.1.2: Molecular Orbitals from p Orbitals

5.1.3: Molecular orbitals from d orbitals

5.1.4: Nonbonding Orbitals and Other Factors

5.2: Homonuclear Diatomic Molecules

5.2.1: Molecular Orbitals

5.2.2: Orbital Mixing

5.2.3: Diatomic Molecules of the First and Second Periods

5.2.4: Photoelectron Spectroscopy

5.3: Heteronuclear Diatomic Molecules

5.3.1: Orbital ionization energies

5.3.2: Polar bonds

5.3.3: Ionic Compounds and Molecular Orbitals

5.4: Larger (Polyatomic) Molecules

5.4.1: Bifluoride anion

5.4.2: Carbon Dioxide

5.4.3: H_2O

5.4.4: NH_3

5.4.5: CO_2 (Revisted with Projection Operators)

5.4.6: BF_3

5.5: Problems

6: Chemistry of the Main Group Elements (Barron)

6.1: General Concepts and Trends

6.1.1: Fundamental Properties - Oxidation State
6.1.2: Fundamental Properties - Ionization Energy
6.1.3: Fundamental Properties - Electron Affinity
6.1.4: Fundamental Properties - Electronegativity
6.1.5: Structure and Bonding - Valence Shell Electron Pair Repulsion (VSEPR) Theory
6.1.6: Structure and Bonding - Crystal Structure
6.1.7: Structure and Bonding - Stereochemistry
6.1.8: Acids, Bases, and Solvents - Choosing a Solvent
6.1.9: Chemical Reactivity - The Basics of Combustion
6.1.10: Periodic Trends for the Main Group Elements

6.2: Hydrogen
6.2.1: Discovery of Hydrogen
6.2.2: The Physical Properties of Hydrogen
6.2.3: Synthesis of Molecular Hydrogen
6.2.4: Atomic Hydrogen
6.2.5: The Proton
6.2.6: Hydrides
6.2.7: The Hydrogen Bond
6.2.8: Isotopes of Hydrogen
6.2.9: Nuclear Fusion
6.2.10: Storage of Hydrogen for Use as a Fuel

6.3: Group 1 - The Alkali Metals
6.3.1: The Alkali Metal Elements
6.3.2: Compounds of the Alkali Metals
6.3.3: The Anomalous Chemistry of Lithium
6.3.4: Organolithium Compounds

6.4: Group 2 - The Alkaline Earth Metals
6.4.1: The Alkaline Earth Elements
6.4.2: Calcium the Archetypal Alkaline Earth Metal
6.4.3: Differences for Beryllium and Magnesium
6.4.4: Organometallic Compounds of Magnesium

6.5: Group 12
6.5.1: The Group 12 Elements
6.5.2: Cadmium Chalcogenide Nanoparticles
6.5.3: Organometallic Chemistry of Zinc
6.5.4: Organomercury Compounds
6.5.5: The Myth, Reality, and History of Mercury Toxicity

6.6: Group 13
6.6.1: The Group 13 Elements

6.6.2: Trends for the Group 13 Compounds
6.6.3: Borides
6.6.4: Boron Hydrides
6.6.5: Wade's Rules
6.6.6: Trends for the Oxides of the Group 13 Elements
6.6.7: Boron Oxides, Hydroxides, and Oxyanions
6.6.8: Aluminum Oxides, Hydroxides, and Hydrated Oxides
6.6.9: Ceramic Processing of Alumina
6.6.10: Boron Compounds with Nitrogen Donors
6.6.11: Properties of Gallium Arsenide
6.6.12: Electronic Grade Gallium Arsenide
6.6.13: Chalcogenides of Aluminum, Gallium, and Indium
6.6.14: Group 13 Halides

6.7: Group 14

6.7.1: The Group 14 Elements
6.7.2: Carbon Black- From Copying to Communication
6.7.3: Carbon Nanomaterials
6.7.4: Nitrogen Compounds of Carbon
6.7.5: Carbon Monoxide
6.7.6: Carbon Dioxide
6.7.7: Suboxides of Carbon
6.7.8: Carbon Halides
6.7.9: Comparison Between Silicon and Carbon
6.7.10: Semiconductor Grade Silicon
6.7.11: Oxidation of Silicon
6.7.12: Applications for Silica Thin Films

6.8: Group 15 - The Pnictogens

6.8.1: The Group 15 Elements- The Pnictogens
6.8.2: Reaction Chemistry of Nitrogen
6.8.3: Hydrides
6.8.4: Oxides and Oxoacids
6.8.5: Halides of Phosphorous

6.9: Group 16

6.9.1: The Group 16 Elements- The Chalcogens
6.9.2: Ozone
6.9.3: Water - The Fuel for the Medieval Industrial Revolution
6.9.4: Hydrogen Peroxide
6.9.5: Hydrogen Peroxide Providing a Lift for 007
6.9.6: Comparison of Sulfur to Oxygen
6.9.7: Chalconide Hydrides

6.9.8: Oxides and Oxyacids of Sulfur

6.9.9: Sulfur Halides

6.10: The Halogens

6.10.1: The Group 17 Elements- The Halogens

6.10.2: Compounds of Fluorine

6.10.3: Compounds of Chlorine

6.10.4: Oxyacids of Chlorine

6.10.5: Bromine Trifluoride as a Solvent

6.11: Group 18 - The Noble Gases

6.11.1: The Group 18 Elements- The Noble Gases

6.12: Front Matter

6.12.1: Table of Contents

7: Acid-Base and Donor-Acceptor Chemistry

7.1: Acid-Base Models as Organizing Concepts

7.2: Lewis Concept and Frontier Orbitals

7.2.1: The frontier orbital approach considers Lewis acid-base reactions in terms of the donation of electrons from the base's highest occupied orbital into the acid's lowest unoccupied orbital.

7.2.2: All other things being equal, electron withdrawing groups tend to make Lewis acids stronger and bases weaker while electron donating groups tend to make Lewis bases stronger and acids weaker

7.2.3: The electronic spectra of charge transfer complexes illustrate the impact of frontier orbital interactions on the electronic structure of Lewis acid-base adducts

7.2.4: Bulky groups weaken the strength of Lewis acids and bases because they introduce steric strain into the resulting acid-base adduct.

7.2.5: Frustrated Lewis pair chemistry uses Lewis acid and base sites within a molecule that are sterically restricted from forming an adduct with each other.

7.3: Hard and Soft Acids and Bases

7.3.1: Hard-Hard and Soft-Soft preferences may be explained and quantified in terms of electrostatic and covalent and electronic stabilization on the stability of Lewis acid-base adducts

8: Organometallic Chemistry (Evans)

8.1: Introduction to Organometallic Chemistry

8.1.1: Resources for Organometallic Chemistry

8.1.2: What is Organometallic Chemistry?

8.2: Organometallic Ligands

8.2.1: Carbenes

8.2.2: Carbon Monoxide

8.2.3: σ Complexes

8.2.4: Dative Ligands of N, O, and S

8.2.5: Metal Alkyls

8.2.6: Metal Hydrides

8.2.7: N-heterocyclic Carbenes

8.2.8: Odd-numbered π Systems
8.2.9: Phosphines
8.2.10: π Systems

8.3: Structural Fundamentals
8.3.1: Ligand Field Theory and Frontier Molecular Orbital Theory
8.3.2: Open Coordination Site
8.3.3: Periodic Trends of the Transition Metals
8.3.4: Predicting the Geometry of Organometallic Complexes
8.3.5: Simplifying the Organometallic Complex (Part 1)
8.3.6: Simplifying the Organometallic Complex (Part 2)
8.3.7: Simplifying the Organometallic Complex (Part 3)

8.4: Fundamentals of Organometallic Chemistry
8.4.1: β-Elimination Reactions
8.4.2: Associative Ligand Substitution
8.4.3: Dissociative Ligand Substitution Reactions
8.4.4: Ligand substitution
8.4.5: Migratory Insertion- 1,2-Insertions
8.4.6: Migratory Insertion- Introduction and CO Insertions
8.4.7: Oxidative Addition- General Ideas
8.4.8: Oxidative Addition of Non-polar Reagents
8.4.9: Oxidative Addition of Polar Reagents
8.4.10: Quirky Ligand Substitutions
8.4.11: Reductive Elimination- General Ideas
8.4.12: The trans/cis Effects and Influences

8.5: Parallels between Main Group and Organometallic Chemistry
8.5.1: Parallels between Main Group and Binary Carbonyl Complexes
8.5.2: The Isolobal Analogy
8.5.2.1: Extensions of the Analogy
8.5.2.2: Some Applications of the Isolobal Analogy

8.5.3: Metal-Metal Bonds
8.5.3.1: Metal-Metal Multiple Bonds

8.5.4: Cluster Compounds
8.5.4.1: Boranes
8.5.4.2: Heteroboranes
8.5.4.3: Metallaboranes and Metallacarboranes
8.5.4.4: Carbonyl Clusters
8.5.4.5: Carbon-Centered Clusters
8.5.4.6: Additional Comments on Clusters

8.5.5: Problems

9: Introduction to Solid State Chemistry

9.1: The Nature of Crystalline Solids

9.1.1: Crystal Structures of Metals

9.1.2: Ionic and Covalent Solids - Structures

9.1.2.1: Prelude to Ionic and Covalent Solids - Structures

9.1.2.2: Close-packing and Interstitial Sites

9.1.2.3: Structures Related to NaCl and NiAs

9.1.2.4: Tetrahedral Structures

9.1.2.5: Layered Structures and Intercalation Reactions

9.1.2.6: Bonding in TiS_2, MoS_2, and Pyrite Structures

9.1.2.7: Spinel, Perovskite, and Rutile Structures

9.1.2.8: Discussion Questions

9.1.2.9: References

9.2: Bonding in Metals, Semiconductors and Insulators – Band Structure

9.2.1: Prelude to Electronic Properties of Materials - Superconductors and Semiconductors

9.2.2: Periodic Trends- Metals, Semiconductors, and Insulators

9.2.3: Bonding in Metals

9.2.4: Conduction in Metals

9.2.5: Superconductors

9.2.6: Semiconductors- Band Gaps, Colors, Conductivity and Doping

9.2.7: Semiconductor p-n Junctions

9.2.8: Diodes, LEDs and Solar Cells

9.3: X-rays and X-ray Diffraction

9.4: The Imperfect Solid State

9.5: Glasses

9.6: Phase Equilibria and Phase Diagrams

Index

Glossary

Detailed Licensing

This page titled Advanced Inorganic Chemistry CHEM-5020: Fall 2026 is shared under a license and was authored, remixed, and/or curated by Yulia Zaikina.

Licensing

A detailed breakdown of this resource's licensing can be found in ***Back Matter/Detailed Licensing***.

This page titled Licensing is shared under a Public Domain license and was authored, remixed, and/or curated by Yulia Zaikina.

This page titled 6.12.1: Table of Contents is shared under a license and was authored, remixed, and/or curated by LibreTexts.

1: INTRODUCTION TO INORGANIC CHEMISTRY

This chapter introduces some history and context about the field of Inorganic Chemistry.

1.1: What is Inorganic Chemistry?

1.2: Inorganic vs Organic Chemistry

1.3: History of Inorganic Chemistry

1.4: Perspectives

1.5: Practice problems

This page titled 1: Introduction to Inorganic Chemistry is shared under a license and was authored, remixed, and/or curated by Kathryn Haas.

- 1: Introduction to Inorganic Chemistry by Kathryn Haas is licensed CC BY-NC-SA 4.0.

1.1: What is Inorganic Chemistry?

Where did the name "Inorganic Chemistry" come from? Well, the term "Organic Chemistry" literally means the *chemistry of life*. Organic chemistry is the study of carbon-based molecules because the first molecules that were isolated from living organisms contained carbon. On the other hand, minerals and other non-living things seemed to be made of other elements. For some time in our history, scientists believed that the chemical difference between living and non-living things was carbon. So, if "organic" molecules are the molecules of life, then is "inorganic chemistry" the "chemistry of death"? Almost? "Inorganic" chemistry historically meant the chemistry of "non-living" things; and these were non-carbon based molecules and ions.

The names "organic" and "inorganic" come from science history, and still today a generally-accepted definition of *Inorganic Chemistry is the study of non-carbon molecules, or all the elements on the periodic table except carbon (*Figure 1.1.1. But, this definition is not completely correct because the field of Inorganic Chemistry also includes organometallic compounds and the study of some carbon-based molecules that have properties that are familiar to metals (like conduction of electricity). This makes the field of inorganic chemistry very broad, and practically limitless. A great way to understand the breadth of the field is to take a look at the abstracts in the latest article of Inorganic Chemistry. Or, check out the 20 most-read articles from this past year using the links below.

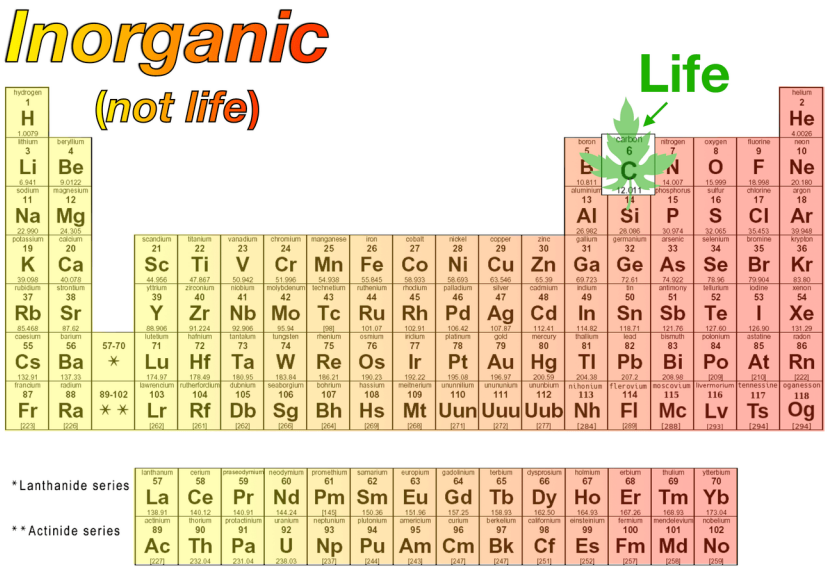


Figure 1.1.1. An illustration of the historic meaning of "organic" and "inorganic". The modern understanding of organic and inorganic chemistry is not consistent with these historical meanings. (Kathryn Haas; CC-NC-BY-SA)

External links:

- The journal, Inorganic Chemistry: https://pubs.acs.org/journal/inocaj
- The latest issue of Inorganic chemistry: https://pubs.acs.org/toc/inocaj/current
- The most popular Inorganic Chemistry articles from the past month and the past year: https://pubs.acs.org/action/showMostReadArticles?journalCode=inocaj

Practice

What are the Sub-Fields of Inorganic Chemistry?

To appreciate the breadth of Inorganic Chemistry, go to the most recent issue of Inorganic Chemistry and look at the titles and visual abstracts. Identify at least 4 sub-fields of Inorganic Chemistry.

Answer available at the end of this section.

Answers

What are the Sub-Fields of Inorganic Chemistry?

There are a lot of correct answers here! The point here is that you notice that Inorganic Chemistry is a very broad field. It has something for almost everyone because many other fields overlap with Inorganic Chemistry. You might notice that some of the sub-fields you identified are also interdisciplinary fields between inorganic chemistry and another discipline. For a list of some of the subfields of Inorganic Chemistry, check this Wikipedia article.

This page titled 1.1: What is Inorganic Chemistry? is shared under a CC BY-NC-SA 4.0 license and was authored, remixed, and/or curated by Kathryn Haas.

- 1.1: What is Inorganic Chemistry? by Kathryn Haas is licensed CC BY-NC-SA 4.0.

1.2: Inorganic vs Organic Chemistry

The division between the fields of Inorganic and Organic chemistry has become blurred. For example, let's look at one of the major classes of catalysts used for organic synthesis reactions: organometalic catalysts (Figure 1.2.1). Organometallic catalysts like these, and all organometallic compounds, contain metals that are bonded to carbon or carbon-containing molecules. So, are they "inorganic" because they contain metals, or "organic" because they contain carbon? These illustrate that clear divisions between organic and inorganic chemistry do not exist. Further, metal ions are common in biology and so the idea that metals are "inorganic" and thus classed as "non-living or non-biological" is incorrect. A canonical example is the organometallic catalyst adenosylcobalbumin, which is an important biological cofactor containing a cobalt (Co) ion (Figure 1.2.1, right) and a cobalt-carbon bond.

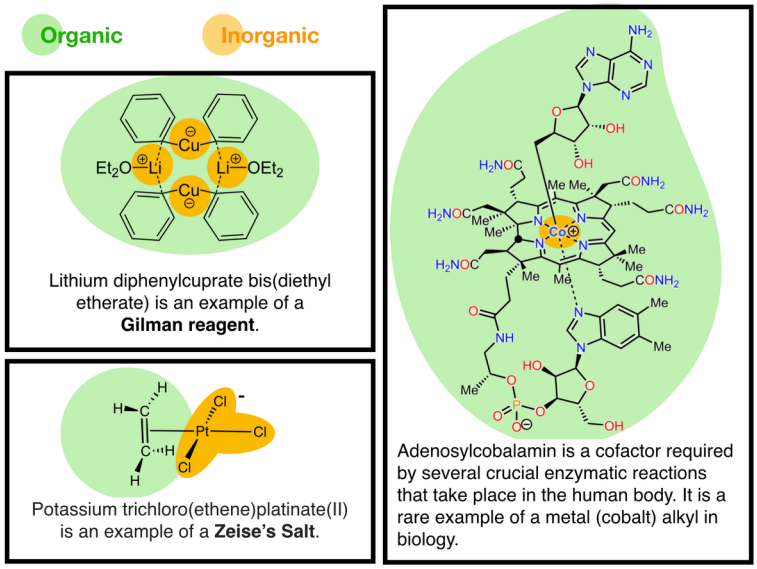
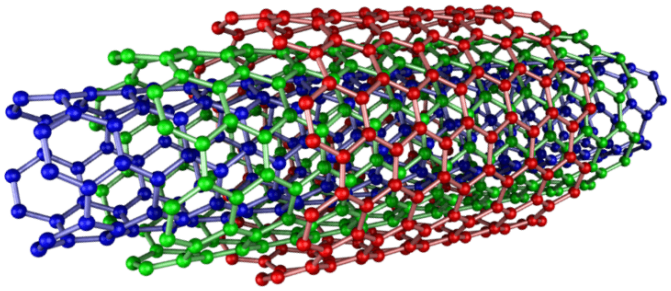


Figure 1.2.1: Some examples of organometallic catalysts. These compounds catalyze organic reactions or biochemical reactions and they are compounds that contain both carbon and metals. These compounds are examples of molecules that cannot be defined only as organic molecules or only as inorganic molecules. Adenosylcobalbumin is an example of an organometallic catalyst that is present in biology, further illustrating that "inorganic" metals are important cofactors in biology. This image is based on information on the Wikipedia article on Organometallic Chemistry and is created from images found there; attribution to images created by Alsosaid1987, AdoCbl-ColorCoded, CC BY-SA 4.0 and Smokefoot, Zeise'sSalt, CC BY-SA 3.0. (Kathryn Haas; CC-BY-SA)

Some of the subfields of Inorganic Chemistry focus on electrical conductivity of inorganic materials (i.e., conduction, superconduction, and semiconduction) and on the study of optical and electronic properties of inorganic nanomaterials. Electrical conductivity is a canonical property of metals, but carbon-based materials also demonstrate electrical conductivity. For example, carbon nanotubes conduct electricity through their extended conjugated π systems. Fullerenes, of which the most famous is Buckminsterfullerene, or Buckeyball (C_{60}), demonstrate interesting properties that are similar to nanoparticles, and when combined with metals and crystallized can demonstrate superconductivity.



Buckminsterfullerene is a type of fullerene with the formula C_{60}



Triple-walled armchair **carbon nanotube**

Figure 1.2.2: This figure is created from information found on the Wikipedia articles for Buckmisterfullerene and carbon nanotubes. Attribution Eric Wieser, Multi-walled Carbon Nanotube, CC BY-SA 3.0. (Kathryn Haas; CC-BY-SA)

Although carbon nanotubes and fullerenes are allotropes of carbon, their material properties are somewhat foreign to many organic chemists, who traditionally have focused on smaller organic molecules having very different properties. However, these properties are familiar to inorganic chemists. Thus, inorganic chemists have embraced these molecules as "inorganic" due to the fact that they behave more like inorganic materials than smaller organic molecules. This class of carbon-based molecules serves as another example of molecules that are not perfectly matched to the traditional definitions of "organic" and "inorganic" chemistry. Certainly, the future will hold more and more examples of molecules that do not fit into the traditional disciplines of chemistry.

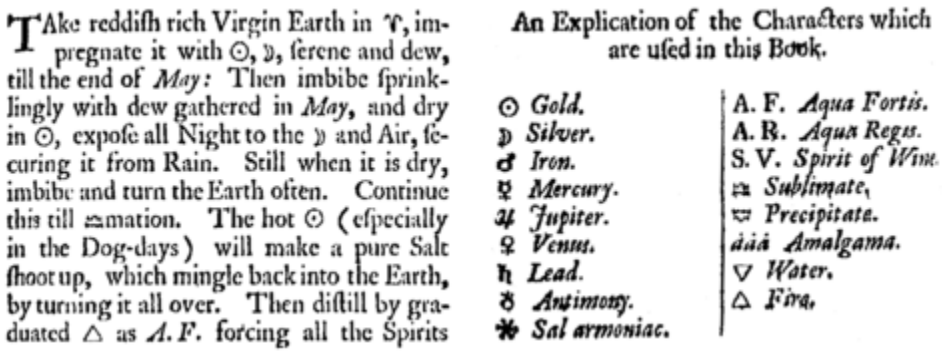
This page titled 1.2: Inorganic vs Organic Chemistry is shared under a CC BY-NC-SA 4.0 license and was authored, remixed, and/or curated by Kathryn Haas.

- 1.2: Inorganic vs Organic Chemistry by Kathryn Haas is licensed CC BY-NC-SA 4.0.

1.3: History of Inorganic Chemistry

Metals serve an essential role in many aspects of human civilization and have defined ages of human history. The period of time from about 3300 BC to 1200 BC is often referred to as the Bronze Age. During this period our ancestors first started using metal and learned to mix various elements with copper to make a strong alloy, called bronze. This age yielded significant advancement in the crafting of sharper knives and stronger weapons out of metal instead of rock, wood and bone. Around 1200 BC the human race found an even harder metal and discovered a much stronger alloy called steel. This period is known as the Iron Age. More recently, periods of time known as Gold Rushes have caused huge changes in population distributions and wealth in some countries. Metal has obvious importance in our modern way of life. Today, iron and steel are used for making buildings, machines, automobiles, jewelry, cooking pots, tools, weapons, vehicles, electronics, surgical instruments and symbolic structures like the Eiffel Tower and the Statue of Liberty. Gold, silver, and copper still serve as currency for trade and exchange of goods and services.

The existence of chemistry as a field of study owes much to the fact that gold was a valuable commodity throughout our history. In both the ancient Egyptian society and during the Roman Empire, gold mines were the property of the state, not an individual or group. So there were few ways for most people to legally get any gold for themselves. The Alchemists were a varied group of scholars and charlatans who aimed to solve this problem by creating the **Philosopher's Stone** (which caused the transmutation of lead into gold). Three major streams of alchemy are known: Chinese, Indian, and European, with all three streams having some factors in common. Techniques developed in the European stream ultimately influenced the development of the science of chemistry.



TAke reddiſh rich Virgin Earth in ♈, impregnate it with ☉, ☽, ſerene and dew, till the end of *May*: Then imbibe ſprinklingly with dew gathered in *May*, and dry in ☉, expoſe all Night to the ☽ and Air, ſecuring it from Rain. Still when it is dry, imbibe and turn the Earth often. Continue this till ♎mation. The hot ☉ (eſpecially in the Dog-days) will make a pure Salt ſhoot up, which mingle back into the Earth, by turning it all over. Then diſtill by graduated △ as *A. F.* forcing all the Spirits

An Explication of the Characters which are uſed in this Book.

☉ *Gold.*
☽ *Silver.*
♂ *Iron.*
☿ *Mercury.*
♃ *Jupiter.*
♀ *Venus.*
♄ *Lead.*
♁ *Antimony.*
✱ *Sal armoniac.*

A. F. *Aqua Fortis.*
A. R. *Aqua Regis.*
S. V. *Spirit of Wine.*
♎ *Sublimate.*
♍ *Precipitate.*
ȧȧȧ *Amalgama.*
▽ *Water.*
△ *Fire.*

Figure 1.3.1. Alchemist recipe. Many of the specific approaches that alchemists used when they tried changing lead into gold are vague and unclear. Each alchemist had his own code for recording his data. The processes were kept secret so others could not profit from them. Different scholars developed their own set of symbols as they recorded the information they came up with. Many alchemists were not very honest, taking money from a nobleman by claiming to be able to make gold from lead, then leaving town in the middle of the night. Sometimes the nobleman would detect the fraud and have the alchemist hung. By the 1300's, several European rules had declared alchemy to be illegal and set out strict punishments for those practicing the alchemical arts.

Although alchemists were never successful in changing lead into gold, they made several contributions to modern-day chemistry. Strong acids and bases were discovered, including nitric acid ($ceHNO3$), sulfuric acid ($\mathrm{H_2SO_4}$), and hydrochloric acid (HCl), as well as sodium hydroxide (NaOH). Glassware for running chemical reactions was developed, as were methods for distillation, crystallization, and sublimation. Alchemy helped improve the study of metallurgy and the extraction of metals from ores. More systematic approaches to research were developed that allowed the discovery of atoms and laid the groundwork for development of the periodic table. For more about the History of Chemistry in general, try the LibreText page A Brief History of Chemistry.

Inorganic compounds have been known and used since antiquity; probably the oldest is the deep blue pigment called Prussian blue ($\mathrm{Fe_4[Fe(CN)_6]_3}$). However, the chemical nature of these substances was unknown until the late nineteenth and early twentieth century when the modern field of coordination chemistry emerged. Much of what we know about inorganic chemistry is based largely on the work of and debates between Alfred Werner (1866–1919; Nobel Prize in Chemistry in 1913) and Sophus Mads Jørgensen (1837 –1914). After Werner succeeded in these debates, the field of inorganic chemistry declined in popularity until the mid-twentieth century, when the second world war stimulated renewed interest. During the post-war era, several important discoveries and theories were developed. For example, important theories of bonding in coordination compounds were developed.

Soon after World War II, Crystal Field Theory (CFT) and Ligand Field Theory (LFT) were developed. These are two critical and complimentary theories that provide explanations of spectroscopic, chemical, and structural properties of inorganic coordination compounds, CFT being more simple, and LFT more accurate. In the 1950's, organometallic catalysts were discovered that catalyzed important organic reactions and the Haber-Bosch Process was discovered. The Haber-Bosch Process is catalyzed by an inorganic oxide catalyst and is one of the world's most important industrial reactions. It provides for the synthesis of ammonia directly from elemental nitrogen, N_2, and hydrogen, H_2.

$$\mathrm{N_2\,(g) + 3\,H_2\,(g)\ \rightleftharpoons 2\,NH_3\,(g)} \tag{1.3.1}$$

Since its development in the early twentieth century, it has led to the production of an enormous quantity of fertilizer, vastly increasing global food production. As a result, it is estimated that a significant fraction of the nitrogen content in the typical human body is ultimately derived from this process. Yet while the reaction must be run at high temperatures and pressures in the industrial setting, the nitrogenase enzyme in the roots of plants can carry out this reaction at the mild conditions within the soil. Intense investigations were then aimed at improving inorganic catalysts through understanding the metal cofactors in enzymes. The link between the Haber-Bosch industrial process and the nitrogenase enzyme was an early bridge between the fields of organometallic chemistry and biochemistry.

Contributions

Part of this page is adapted from K.Haas Ph.D. dissertation

Part of this page is adapted from the following LibreTexts pages

- Alchemy contributed by CK-12 Foundation by Sharon Bewick, Richard Parsons, Therese Forsythe, Shonna Robinson, and Jean Dupon.
- Werner's Theory of Coordination Compounds
- The Haber-Bosch Process Worksheet

This page titled 1.3: History of Inorganic Chemistry is shared under a CC BY-NC-SA 4.0 license and was authored, remixed, and/or curated by Kathryn Haas.

- 1.3: History of Inorganic Chemistry by Kathryn Haas is licensed CC BY-NC-SA 4.0.

1.4: Perspectives

The field of inorganic chemistry stands on the shoulders of giants (or in this case, many talented and dedicated scientists). If you are lucky enough to have journal access, peruse the titles and pages of the first issues of Inorganic Chemistry. You will find some lively debate about the puzzles of determining inorganic structure and reactivity. The scientists that made early discoveries in this field practiced elegant science.

The inorganic chemists who built our field are diverse. They are the ones who discovered new elements, developed new materials, characterized the fundamental principles of reactions, and developed the theories that we use to understand and predict metal structure and reactivity. And, there are people who are still working on these things today.

To gain more perspective on Inorganic Chemistry, compare the topics in the very first issue (Feb 1, 1962) to the most recent issue or the current most popular articles using the links below.

- The very first issue of Inorganic Chemistry from 1962: https://pubs.acs.org/toc/inocaj/1/1
- The latest issue of Inorganic chemistry: https://pubs.acs.org/toc/inocaj/current
- The most popular Inorganic Chemistry articles from the past month and the past year: https://pubs.acs.org/action/showMostReadArticles?journalCode=inocaj

This page titled 1.4: Perspectives is shared under a CC BY-NC-SA 4.0 license and was authored, remixed, and/or curated by Kathryn Haas.

- 1.4: Perspectives by Kathryn Haas is licensed CC BY-NC-SA 4.0.

1.5: Practice problems

These questions are designed to check your understanding of the reading in this chapter.

1. What is the historic definition of *inorganic chemistry*? What are some problems that arise from this definition?
2. Name three sub-fields of inorganic chemistry.
3. What is the class of inorganic compounds that have bonds between metals and carbon?

This page titled 1.5: Practice problems is shared under a CC BY-NC-SA 4.0 license and was authored, remixed, and/or curated by Kathryn Haas.

- 1.5: Practice problems by Kathryn Haas is licensed CC BY-NC-SA 4.0.

2: ATOMIC STRUCTURE

2.1: Historical Development of Atomic Theory

2.1.1: The Periodic Table

2.1.2: Discovery of Subatomic Particles and the Bohr Atom

2.2: The Schrödinger equation, particle in a box, and atomic wavefunctions

2.2.1: Particle in a Box

2.2.2: Quantum Numbers and Atomic Wave Functions

2.2.3: Aufbau Principle

2.2.4: Shielding

2.3: Periodic Properties of Atoms

2.3.1: Ionization energy

2.3.2: Electron Affinity

2.3.3: Covalent and Ionic Radii

2.4: Problems

This page titled 2: Atomic Structure is shared under a license and was authored, remixed, and/or curated by Kathryn Haas.

- 2: Atomic Structure by Kathryn Haas is licensed CC BY-NC-SA 4.0.

2.1: Historical Development of Atomic Theory

Notes about this page

The page below is a brief overview on the history of atomic theory. It contains lots of video media.

Alternatives pages on the history of atomic theory are:

- A more detailed overview that includes practice problems is here (click).
- Another brief overview is here (click).

Skills to Develop

By the end of this section, you will be able to:

- State the postulates of Dalton's atomic theory
- Use postulates of Dalton's atomic theory to explain the laws of definite and multiple proportions
- Outline milestones in the development of modern atomic theory
- Summarize and interpret the results of the experiments of Thomson, Millikan, and Rutherford

A Video Introduction to Atomic Theory through the Nineteenth Century From Crash Course Chemistry

YouTube Video

This interactive element is not available in this format. Visit the link or scan the QR code to access it online.

View this YouTube Video online

***Video* 2.1.1*:* Lavoisier's discovery of The Law of Conservation of Matter led to the Laws of Definite and Multiple Proportions and eventually Dalton's Atomic Theory.**

Atomic Theory through the Nineteenth Century

The earliest recorded discussion of the basic structure of matter comes from ancient Greek philosophers, the scientists of their day. In the fifth century BC, Leucippus and Democritus argued that all matter was composed of small, finite particles that they called *atomos*, a term derived from the Greek word for "indivisible." They thought of atoms as moving particles that differed in shape and size, and which could join together. Later, Aristotle and others came to the conclusion that matter consisted of various combinations of the four "elements"—fire, earth, air, and water—and could be infinitely divided. Interestingly, these philosophers thought about atoms and "elements" as philosophical concepts, but apparently never considered performing experiments to test their ideas.

The Aristotelian view of the composition of matter held sway for over two thousand years, until English schoolteacher John Dalton helped to revolutionize chemistry with his hypothesis that the behavior of matter could be explained using an atomic theory. First published in 1807, many of Dalton's hypotheses about the microscopic features of matter are still valid in modern atomic theory. Here are the postulates of Dalton's atomic theory.

1. Matter is composed of exceedingly small particles called atoms. An atom is the smallest unit of an element that can participate in a chemical change.
2. An element consists of only one type of atom, which has a mass that is characteristic of the element and is the same for all atoms of that element (Figure 2.1.1). A macroscopic sample of an element contains an incredibly large number of atoms, all of which have identical chemical properties.
3. Atoms of one element differ in properties from atoms of all other elements.
4. A compound consists of atoms of two or more elements combined in a small, whole-number ratio. In a given compound, the numbers of atoms of each of its elements are always present in the same ratio (Figure 2.1.2).
5. Atoms are neither created nor destroyed during a chemical change, but are instead rearranged to yield substances that are different from those present before the change (Figure 2.1.3).

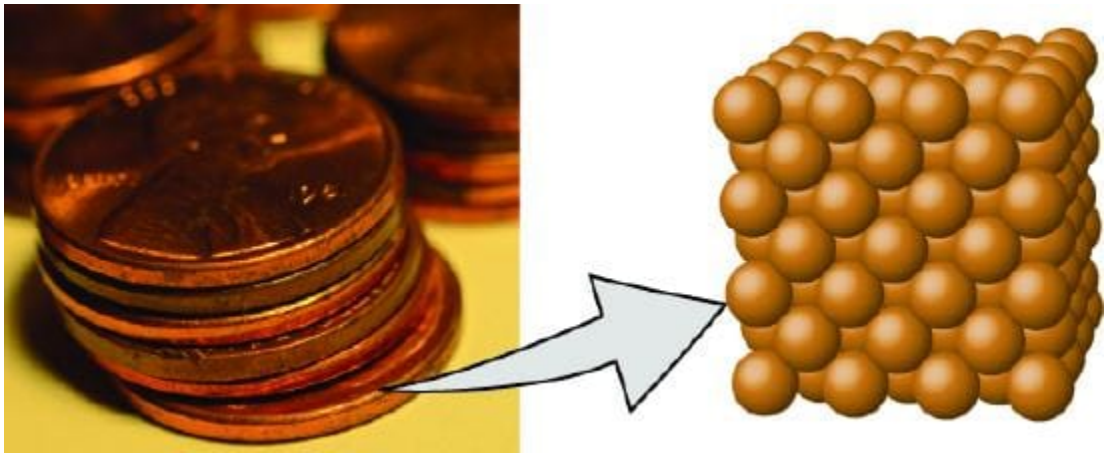


Figure 2.1.1***:*** *A pre-1982 copper penny (left) contains approximately* 3×10^{22} *copper atoms (several dozen are represented as brown spheres at the right), each of which has the same chemical properties. (credit: modification of work by "slgckgc"/Flickr)*

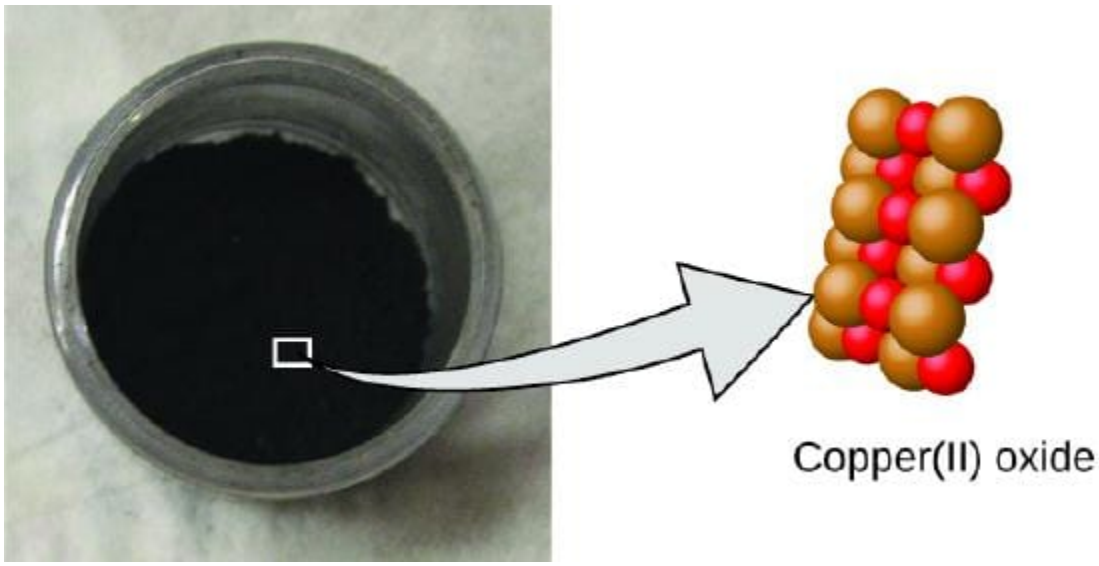


Figure 2.1.2***:*** *Copper(II) oxide, a powdery, black compound, results from the combination of two types of atoms—copper (brown spheres) and oxygen (red spheres)—in a 1:1 ratio. (credit: modification of work by "Chemicalinterest"/Wikimedia Commons)*

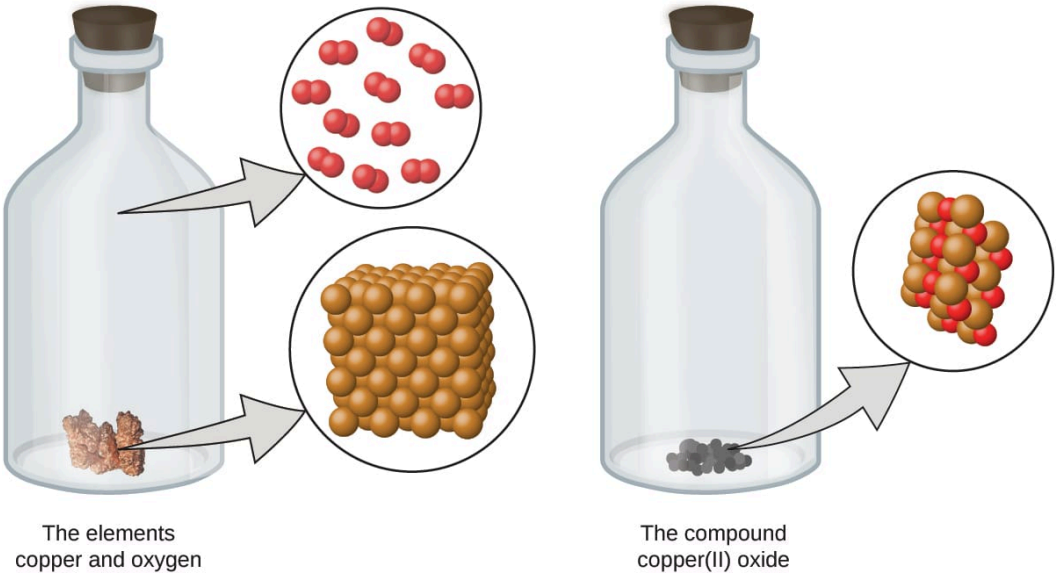


Figure 2.1.3*: When the elements copper (a shiny, red-brown solid, shown here as brown spheres) and oxygen (a clear and colorless gas, shown here as red spheres) react, their atoms rearrange to form a compound containing copper and oxygen (a powdery, black solid). (credit copper: modification of work by http://images-of-elements.com/copper.php).*

Dalton's atomic theory provides a microscopic explanation of the many macroscopic properties of matter that you've learned about. For example, if an element such as copper consists of only one kind of atom, then it cannot be broken down into simpler substances, that is, into substances composed of fewer types of atoms. And if atoms are neither created nor destroyed during a chemical change, then the total mass of matter present when matter changes from one type to another will remain constant (the law of conservation of matter (or mass)).

Want to learn more about the Law of Conservation of Mass?

YouTube Video

This interactive element is not available in this format. Visit the link or scan the QR code to access it online.

View this YouTube Video online

Video 2.1.2***: "We are made of star stuff" - Carl Sagan.***

Example 2.1.1: Testing Dalton's Atomic Theory

In the following drawing, the green spheres represent atoms of a certain element. The purple spheres represent atoms of another element. If the spheres touch, they are part of a single unit of a compound. Does the following chemical change represented by these symbols violate any of the ideas of Dalton's atomic theory? If so, which one?

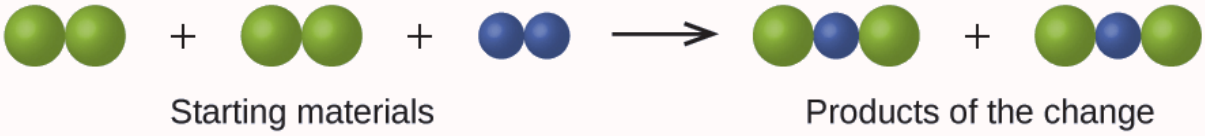


Solution

The starting materials consist of two green spheres and two purple spheres. The products consist of only one green sphere and one purple sphere. This violates Dalton's postulate that atoms are neither created nor destroyed during a chemical change, but are merely redistributed. (In this case, atoms appear to have been destroyed.)

Exercise 2.1.1

In the following drawing, the green spheres represent atoms of a certain element. The purple spheres represent atoms of another element. If the spheres touch, they are part of a single unit of a compound. Does the following chemical change represented by these symbols violate any of the ideas of Dalton's atomic theory? If so, which one



Answer

The starting materials consist of four green spheres and two purple spheres. The products consist of four green spheres and two purple spheres. This does not violate any of Dalton's postulates: Atoms are neither created nor destroyed, but are redistributed in small, whole-number ratios.

Dalton knew of the experiments of French chemist Joseph Proust, who demonstrated that *all samples of a pure compound contain the same elements in the same proportion by mass*. This statement is known as the law of definite proportions or the law of constant composition. The suggestion that the numbers of atoms of the elements in a given compound always exist in the same ratio is consistent with these observations. For example, when different samples of isooctane (a component of gasoline and one of the standards used in the octane rating system) are analyzed, they are found to have a carbon-to-hydrogen mass ratio of 5.33:1, as shown in Table 2.1.1.

Table 2.1.1*: Constant Composition of Isooctane*

Sample	Carbon	Hydrogen	Mass Ratio
A	14.82 g	2.78 g	$\frac{14.82\ \text{g carbon}}{2.78\ \text{g hydrogen}} = \frac{5.33\ \text{g carbon}}{1.00\ \text{g hydrogen}}$
B	22.33 g	4.19 g	$\frac{22.33\ \text{g carbon}}{4.19\ \text{g hydrogen}} = \frac{5.33\ \text{g carbon}}{1.00\ \text{g hydrogen}}$
C	19.40 g	3.64 g	$\frac{19.40\ \text{g carbon}}{3.63\ \text{g hydrogen}} = \frac{5.33\ \text{g carbon}}{1.00\ \text{g hydrogen}}$

It is worth noting that although all samples of a particular compound have the same mass ratio, the converse is not true in general. That is, samples that have the same mass ratio are not necessarily the same substance. For example, there are many compounds other than isooctane that also have a carbon-to-hydrogen mass ratio of 5.33:1.00.

Dalton also used data from Proust, as well as results from his own experiments, to formulate another interesting law. The law of multiple proportions states that *when two elements react to form more than one compound, a fixed mass of one element will react with masses of the other element in a ratio of small, whole numbers*. For example, copper and chlorine can form a green,

crystalline solid with a mass ratio of 0.558 g chlorine to 1 g copper, as well as a brown crystalline solid with a mass ratio of 1.116 g chlorine to 1 g copper. These ratios by themselves may not seem particularly interesting or informative; however, if we take a ratio of these ratios, we obtain a useful and possibly surprising result: a small, whole-number ratio.

$$\frac{\frac{1.116\ \text{g Cl}}{1\ \text{g Cu}}}{\frac{0.558\ \text{g Cl}}{1\ \text{g Cu}}} = \frac{2}{1} \tag{2.1.1}$$

This 2-to-1 ratio means that the brown compound has twice the amount of chlorine per amount of copper as the green compound.

This can be explained by atomic theory if the copper-to-chlorine ratio in the brown compound is 1 copper atom to 2 chlorine atoms, and the ratio in the green compound is 1 copper atom to 1 chlorine atom. The ratio of chlorine atoms (and thus the ratio of their masses) is therefore 2 to 1 (Figure 2.1.4).

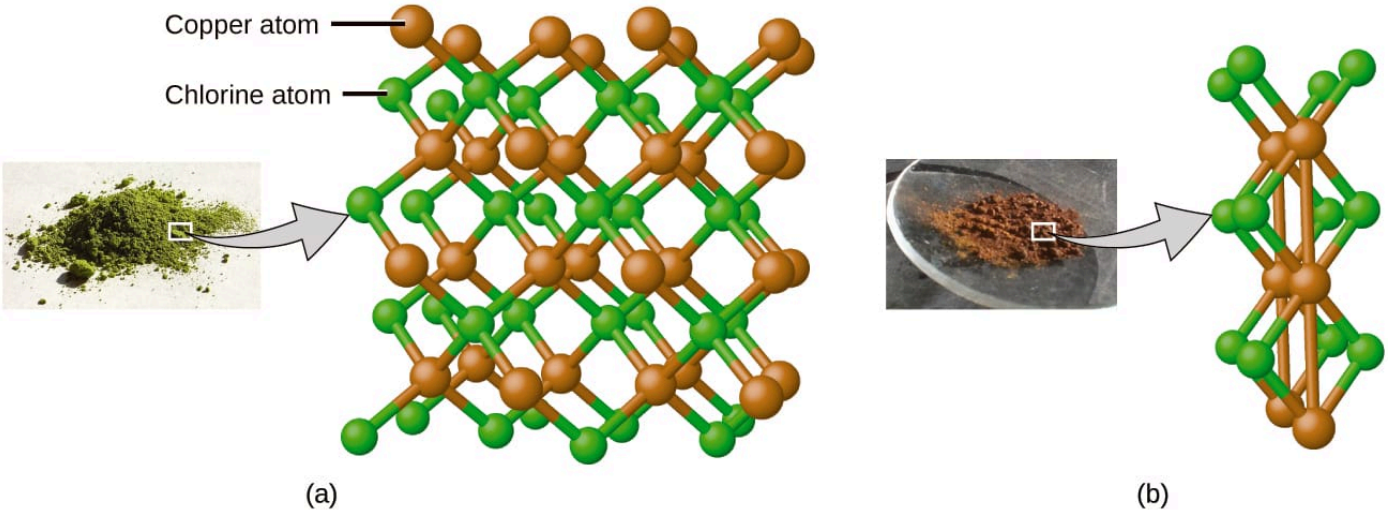


Figure 2.1.4*: Compared to the copper chlorine compound in (a), where copper is represented by brown spheres and chlorine by green spheres, the copper chlorine compound in (b) has twice as many chlorine atoms per copper atom. (credit a: modification of work by "Benjah-bmm27"/Wikimedia Commons; credit b: modification of work by "Walkerma"/Wikimedia Commons)*

Example 2.1.2: Laws of Definite and Multiple Proportions

A sample of compound A (a clear, colorless gas) is analyzed and found to contain 4.27 g carbon and 5.69 g oxygen. A sample of compound B (also a clear, colorless gas) is analyzed and found to contain 5.19 g carbon and 13.84 g oxygen. Are these data an example of the law of definite proportions, the law of multiple proportions, or neither? What do these data tell you about substances A and B?

Solution

In compound A, the mass ratio of carbon to oxygen is:

$$\frac{1.33\ \text{g O}}{1\ \text{g C}}$$

In compound B, the mass ratio of carbon to oxygen is:

$$\frac{2.67\ \text{g O}}{1\ \text{g C}}$$

The ratio of these ratios is:

$$\frac{\frac{1.33\ \text{g O}}{1\ \text{g C}}}{\frac{2.67\ \text{g O}}{1\ \text{g C}}} = \frac{1}{2}$$

This supports the law of multiple proportions. This means that A and B are different compounds, with A having one-half as much carbon per amount of oxygen (or twice as much oxygen per amount of carbon) as B. A possible pair of compounds that would fit this relationship would be A = CO_2 and B = CO.

Exercise 2.1.2

A sample of compound X (a clear, colorless, combustible liquid with a noticeable odor) is analyzed and found to contain 14.13 g carbon and 2.96 g hydrogen. A sample of compound Y (a clear, colorless, combustible liquid with a noticeable odor that is slightly different from X's odor) is analyzed and found to contain 19.91 g carbon and 3.34 g hydrogen. Are these data an example of the law of definite proportions, the law of multiple proportions, or neither? What do these data tell you about substances X and Y?

Answer

In compound X, the mass ratio of carbon to hydrogen is $\frac{14.13\ \text{g C}}{2.96\ \text{g H}}$.

In compound Y, the mass ratio of carbon to oxygen is $\frac{19.91\ \text{g C}}{3.34\ \text{g H}}$.

The ratio of these ratios is

$$\frac{\frac{14.13\ \text{g C}}{2.96\ \text{g H}}}{\frac{19.91\ \text{g C}}{3.34\ \text{g H}}} = \frac{4.77\ \text{g C/g H}}{5.96\ \text{g C/g H}} = 0.800 = \frac{4}{5}.$$

This small, whole-number ratio supports the law of multiple proportions. This means that X and Y are different compounds.

In the two centuries since Dalton developed his ideas, scientists have made significant progress in furthering our understanding of atomic theory. Much of this came from the results of several seminal experiments that revealed the details of the internal structure of atoms. Here, we will discuss some of those key developments, with an emphasis on application of the scientific method, as well as understanding how the experimental evidence was analyzed. While the historical persons and dates behind these experiments can be quite interesting, it is most important to understand the concepts resulting from their work.

Atomic Theory after the Nineteenth Century

If matter were composed of atoms, what were atoms composed of? Were they the smallest particles, or was there something smaller? In the late 1800s, a number of scientists interested in questions like these investigated the electrical discharges that could be produced in low-pressure gases, with the most significant discovery made by English physicist J. J. Thomson using a cathode ray tube. This apparatus consisted of a sealed glass tube from which almost all the air had been removed; the tube contained two metal electrodes. When high voltage was applied across the electrodes, a visible beam called a cathode ray appeared between them. This beam was deflected toward the positive charge and away from the negative charge, and was produced in the same way with identical properties when different metals were used for the electrodes. In similar experiments, the ray was simultaneously deflected by an applied magnetic field, and measurements of the extent of deflection and the magnetic field strength allowed Thomson to calculate the charge-to-mass ratio of the cathode ray particles. The results of these measurements indicated that these particles were much lighter than atoms (Figure 2.1.1).

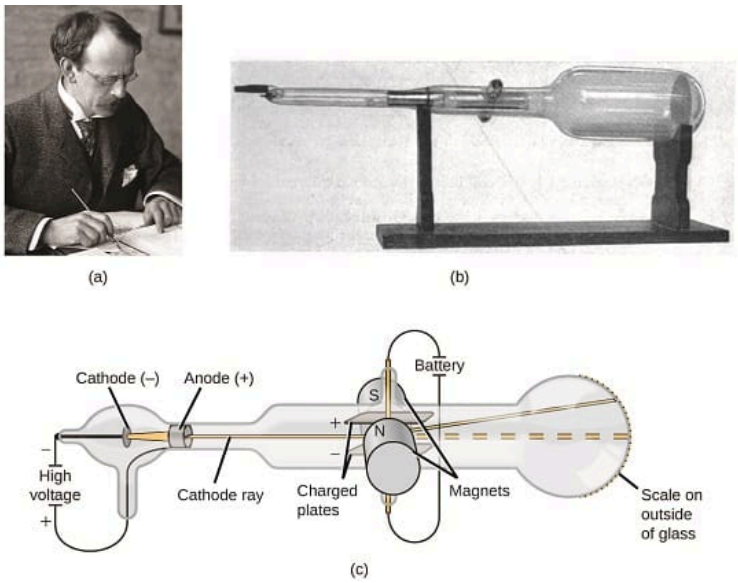
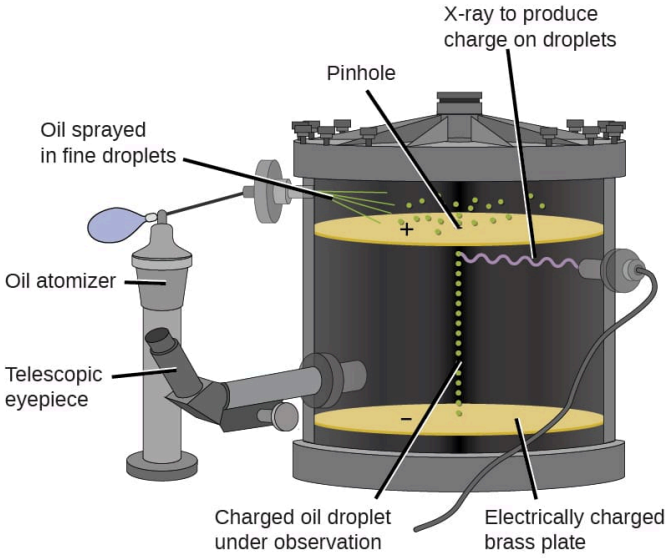


Figure 2.1.5*: (a) J. J. Thomson produced a visible beam in a cathode ray tube. (b) This is an early cathode ray tube, invented in 1897 by Ferdinand Braun. (c) In the cathode ray, the beam (shown in yellow) comes from the cathode and is accelerated past the anode toward a fluorescent scale at the end of the tube. Simultaneous deflections by applied electric and magnetic fields permitted Thomson to calculate the mass-to-charge ratio of the particles composing the cathode ray. (credit a: modification of work by Nobel Foundation; credit b: modification of work by Eugen Nesper; credit c: modification of work by "Kurzon"/Wikimedia Commons).*

Based on his observations, here is what Thomson proposed and why: The particles are attracted by positive (+) charges and repelled by negative (–) charges, so they must be negatively charged (like charges repel and unlike charges attract); they are less massive than atoms and indistinguishable, regardless of the source material, so they must be fundamental, subatomic constituents of all atoms. Although controversial at the time, Thomson's idea was gradually accepted, and his cathode ray particle is what we now call an electron, a negatively charged, subatomic particle with a mass more than one thousand-times less that of an atom. The term "electron" was coined in 1891 by Irish physicist George Stoney, from "*electr*ic i*on*."

In 1909, more information about the electron was uncovered by American physicist Robert A. Millikan via his "oil drop" experiments. Millikan created microscopic oil droplets, which could be electrically charged by friction as they formed or by using X-rays. These droplets initially fell due to gravity, but their downward progress could be slowed or even reversed by an electric field lower in the apparatus. By adjusting the electric field strength and making careful measurements and appropriate calculations, Millikan was able to determine the charge on individual drops (Figure 2.1.2).



Oil drop	Charge in coulombs (C)
A	4.8×10^{-19} C
B	3.2×10^{-19} C
C	6.4×10^{-19} C
D	1.6×10^{-19} C
E	4.8×10^{-19} C

Figure 2.1.6***: Millikan's experiment measured the charge of individual oil drops. The tabulated data are examples of a few possible values.***

Looking at the charge data that Millikan gathered, you may have recognized that the charge of an oil droplet is always a multiple of a specific charge, 1.6×10^{-19} C. Millikan concluded that this value must therefore be a fundamental charge—the charge of a single electron—with his measured charges due to an excess of one electron (1 times 1.6×10^{-19} C), two electrons (2 times 1.6×10^{-19} C), three electrons (3 times 1.6×10^{-19} C), and so on, on a given oil droplet. Since the charge of an electron was now known due to Millikan's research, and the charge-to-mass ratio was already known due to Thomson's research (1.759×10^{11} C/kg), it only required a simple calculation to determine the mass of the electron as well.

$$\text{Mass of electron} = 1.602 \times 10^{-19} \cancel{\text{C}} \times \frac{1 \text{ kg}}{1.759 \times 10^{11} \cancel{\text{C}}} = 9.107 \times 10^{-31} \text{ kg} \tag{2.3.1}$$

Scientists had now established that the atom was not indivisible as Dalton had believed, and due to the work of Thomson, Millikan, and others, the charge and mass of the negative, subatomic particles—the electrons—were known. However, the positively charged part of an atom was not yet well understood. In 1904, Thomson proposed the "plum pudding" model of atoms, which described a positively charged mass with an equal amount of negative charge in the form of electrons embedded in it, since all atoms are electrically neutral. A competing model had been proposed in 1903 by Hantaro Nagaoka, who postulated a Saturn-like atom, consisting of a positively charged sphere surrounded by a halo of electrons (Figure 2.1.3).

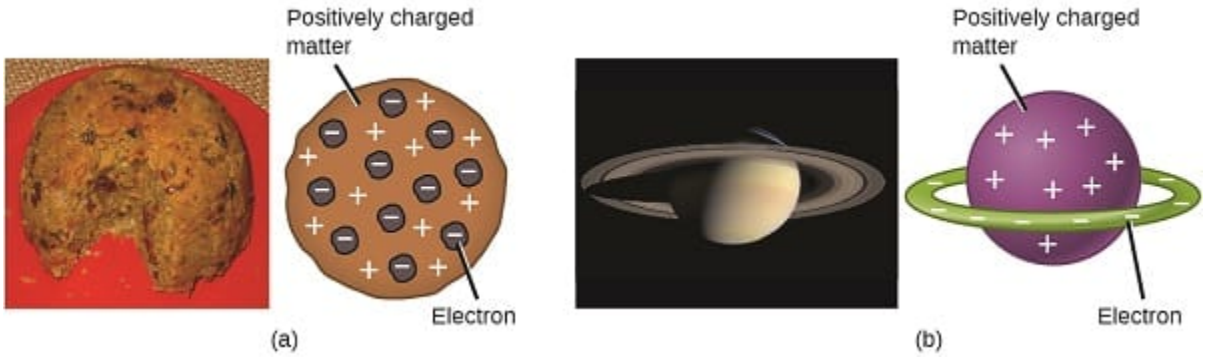


Figure 2.1.7*: (a) Thomson suggested that atoms resembled plum pudding, an English dessert consisting of moist cake with embedded raisins ("plums"). (b) Nagaoka proposed that atoms resembled the planet Saturn, with a ring of electrons surrounding a positive "planet." (credit a: modification of work by "Man vyi"/Wikimedia Commons; credit b: modification of work by "NASA"/Wikimedia Commons).*

The next major development in understanding the atom came from Ernest Rutherford, a physicist from New Zealand who largely spent his scientific career in Canada and England. He performed a series of experiments using a beam of high-speed, positively charged alpha particles (α particles) that were produced by the radioactive decay of radium; α particles consist of two protons and two neutrons (you will learn more about radioactive decay in the chapter on nuclear chemistry). Rutherford and his colleagues Hans Geiger (later famous for the Geiger counter) and Ernest Marsden aimed a beam of α particles, the source of which was embedded in a lead block to absorb most of the radiation, at a very thin piece of gold foil and examined the resultant scattering of the α particles using a luminescent screen that glowed briefly where hit by an α particle.

What did they discover? Most particles passed right through the foil without being deflected at all. However, some were diverted slightly, and a very small number were deflected almost straight back toward the source (Figure 2.1.4). Rutherford described finding these results: "It was quite the most incredible event that has ever happened to me in my life. It was almost as incredible as if you fired a 15-inch shell at a piece of tissue paper and it came back and hit you"[1] (p. 68).

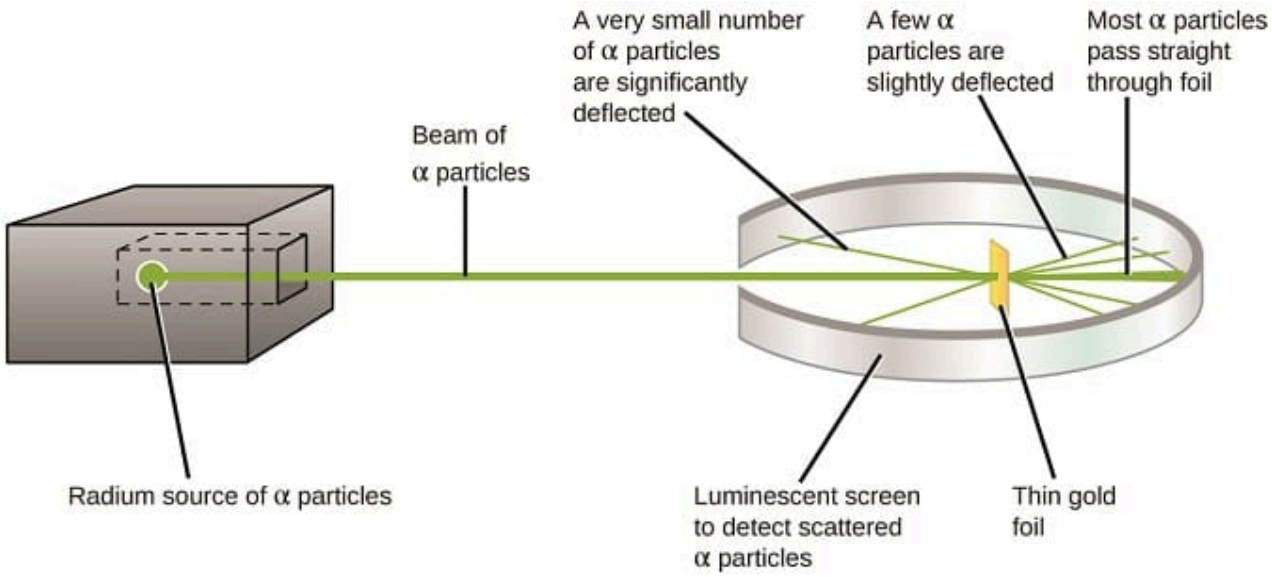


Figure 2.1.8***:*** *Geiger and Rutherford fired α particles at a piece of gold foil and detected where those particles went, as shown in this schematic diagram of their experiment. Most of the particles passed straight through the foil, but a few were deflected slightly and a very small number were significantly deflected.*

Here is what Rutherford deduced: Because most of the fast-moving α particles passed through the gold atoms undeflected, they must have traveled through essentially empty space inside the atom. Alpha particles are positively charged, so deflections arose when they encountered another positive charge (like charges repel each other). Since like charges repel one another, the few positively charged α particles that changed paths abruptly must have hit, or closely approached, another body that also had a highly concentrated, positive charge. Since the deflections occurred a small fraction of the time, this charge only occupied a small amount of the space in the gold foil. Analyzing a series of such experiments in detail, Rutherford drew two conclusions:

1. The volume occupied by an atom must consist of a large amount of empty space.
2. A small, relatively heavy, positively charged body, the nucleus, must be at the center of each atom.

This analysis led Rutherford to propose a model in which an atom consists of a very small, positively charged nucleus, in which most of the mass of the atom is concentrated, surrounded by the negatively charged electrons, so that the atom is electrically neutral (Figure 2.1.5).

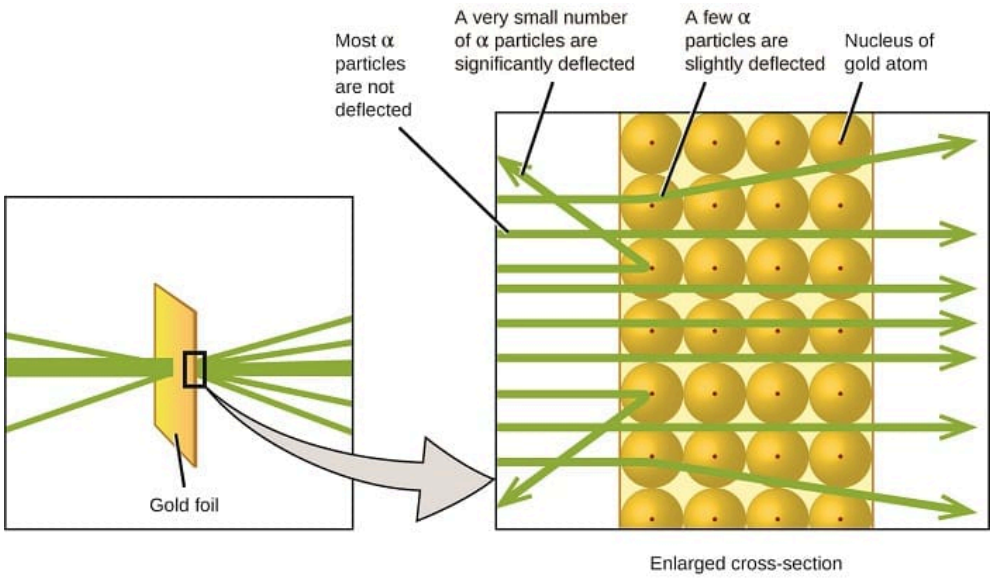


Figure 2.1.9*: The α particles are deflected only when they collide with or pass close to the much heavier, positively charged gold nucleus. Because the nucleus is very small compared to the size of an atom, very few α particles are deflected. Most pass through the relatively large region occupied by electrons, which are too light to deflect the rapidly moving particles.*

After many more experiments, Rutherford also discovered that the nuclei of other elements contain the hydrogen nucleus as a "building block," and he named this more fundamental particle the proton, the positively charged, subatomic particle found in the nucleus. With one addition, which you will learn next, this nuclear model of the atom, proposed over a century ago, is still used today.

Another important finding was the discovery of isotopes. During the early 1900s, scientists identified several substances that appeared to be new elements, isolating them from radioactive ores. For example, a "new element" produced by the radioactive decay of thorium was initially given the name mesothorium. However, a more detailed analysis showed that mesothorium was chemically identical to radium (another decay product), despite having a different atomic mass. This result, along with similar findings for other elements, led the English chemist Frederick Soddy to realize that an element could have types of atoms with different masses that were chemically indistinguishable. These different types are called isotopes—atoms of the same element that differ in mass. Soddy was awarded the Nobel Prize in Chemistry in 1921 for this discovery.

One puzzle remained: The nucleus was known to contain almost all of the mass of an atom, with the number of protons only providing half, or less, of that mass. Different proposals were made to explain what constituted the remaining mass, including the existence of neutral particles in the nucleus. As you might expect, detecting uncharged particles is very challenging, and it was not until 1932 that James Chadwick found evidence of neutrons, uncharged, subatomic particles with a mass approximately the same as that of protons. The existence of the neutron also explained isotopes: They differ in mass because they have different numbers of neutrons, but they are chemically identical because they have the same number of protons. This will be explained in more detail later in this unit.

YouTube Video

This interactive element is not available in this format. Visit the link or scan the QR code to access it online.

View this YouTube Video online

Video 2.1.2***: An Introduction to Subatomic Particles***

Summary

YouTube Video

This interactive element is not available in this format. Visit the link or scan the QR code to access it online.

View this YouTube Video online

Video 2.1.3***:*** *A summary of discoveries in atomic theory.*

YouTube Video

This interactive element is not available in this format. Visit the link or scan the QR code to access it online.

View this YouTube Video online

Video 2.1.4***:*** *A different summary of discoveries in atomic theory.*

The ancient Greeks proposed that matter consists of extremely small particles called atoms. Dalton postulated that each element has a characteristic type of atom that differs in properties from atoms of all other elements, and that atoms of different elements can combine in fixed, small, whole-number ratios to form compounds. Samples of a particular compound all have the same elemental proportions by mass. When two elements form different compounds, a given mass of one element will combine with masses of the other element in a small, whole-number ratio. During any chemical change, atoms are neither created nor destroyed.

Although no one has actually seen the inside of an atom, experiments have demonstrated much about atomic structure. Thomson's cathode ray tube showed that atoms contain small, negatively charged particles called electrons. Millikan discovered that there is a fundamental electric charge—the charge of an electron. Rutherford's gold foil experiment showed that atoms have a small, dense, positively charged nucleus; the positively charged particles within the nucleus are called protons. Chadwick discovered that the nucleus also contains neutral particles called neutrons. Soddy demonstrated that atoms of the same element can differ in mass; these are called isotopes.

Footnotes

1. Ernest Rutherford, "The Development of the Theory of Atomic Structure," ed. J. A. Ratcliffe, in *Background to Modern Science*, eds. Joseph Needham and Walter Pagel, (Cambridge, UK: Cambridge University Press, 1938), 61–74. Accessed September 22, 2014, https://ia600508.us.archive.org/3/it...e032734mbp.pdf.

Glossary

Dalton's atomic theory
: set of postulates that established the fundamental properties of atoms

law of constant composition
: (also, law of definite proportions) all samples of a pure compound contain the same elements in the same proportions by mass

law of multiple proportions
: when two elements react to form more than one compound, a fixed mass of one element will react with masses of the other element in a ratio of small whole numbers

law of definite proportions
: (also, law of constant composition) all samples of a pure compound contain the same elements in the same proportions by mass

alpha particle (α particle)
: positively charged particle consisting of two protons and two neutrons

electron
: negatively charged, subatomic particle of relatively low mass located outside the nucleus

isotopes
: atoms that contain the same number of protons but different numbers of neutrons

neutron
: uncharged, subatomic particle located in the nucleus

proton
: positively charged, subatomic particle located in the nucleus

nucleus
: massive, positively charged center of an atom made up of protons and neutrons

Contributors

- Paul Flowers (University of North Carolina - Pembroke), Klaus Theopold (University of Delaware) and Richard Langley (Stephen F. Austin State University) with contributing authors. Textbook content produced by OpenStax College is licensed under a Creative Commons Attribution License 4.0 license. Download for free at http://cnx.org/contents/85abf193-2bd...a7ac8df6@9.110).

- Adelaide Clark, Oregon Institute of Technology
- Crash Course Chemistry: Crash Course is a division of Complexly and videos are free to stream for educational purposes.
- TED-Ed's commitment to creating lessons worth sharing is an extension of TED's mission of spreading great ideas. Within TED-Ed's growing library of TED-Ed animations, you will find carefully curated educational videos, many of which represent collaborations between talented educators and animators nominated through the TED-Ed website.

Feedback

Have feedback to give about this text? Click here.

Found a typo and want extra credit? Click here.

This page titled 2.1: Historical Development of Atomic Theory is shared under a license and was authored, remixed, and/or curated by LibreTexts.

- 2.1: Historical Development of Atomic Theory is licensed CC BY-NC-SA 4.0.

2.1.1: The Periodic Table

Learning Objectives

- To become familiar with the history of the periodic table.

The modern periodic table has evolved through a long history of attempts by chemists to arrange the elements according to their reactivity and other properties as an aid in predicting chemical behavior. Now that we have arranged the table according to electronic structure, it makes sense to go back and look at earlier efforts in the light of what we know about electronic structure.

One of the first to suggest such an arrangement was the German chemist Johannes Dobereiner (1780–1849), who noticed that many of the known elements could be grouped in triads, sets of three elements that have similar properties—for example, chlorine, bromine, and iodine; or copper, silver, and gold. Dobereiner proposed that all elements could be grouped in such triads, but subsequent attempts to expand his concept were unsuccessful. We now know that portions of the periodic table—the *d* block in particular—contain triads of elements with substantial similarities. The middle three members of most of the other columns, such as sulfur, selenium, and tellurium in group 16 or aluminum, gallium, and indium in group 13, also have remarkably similar chemistry.

By the mid-19th century, the atomic masses of many of the elements had been determined. The English chemist John Newlands (1838–1898), hypothesizing that the chemistry of the elements might be related to their masses, arranged the known elements in order of increasing atomic mass and discovered that every seventh element had similar properties (Figure 3.4.1). Newlands therefore suggested that the elements could be classified into octaves: a group of seven elements (not counting the noble gases, which were unknown at the time) that correspond to the *horizontal* rows in the main group elements. Unfortunately, Newlands's "law of octaves" did not seem to work for elements heavier than calcium, and his idea was publicly ridiculed. At one scientific meeting, Newlands was asked why he didn't arrange the elements in alphabetical order instead of by atomic mass, since that would make just as much sense! Actually, Newlands was on the right track—with only a few exceptions, atomic mass does increase with atomic number, and similar properties occur every time a set of ns^2np^6 subshells is filled. Despite the fact that Newlands's table had no logical place for the *d*-block elements, he was honored for his idea by the Royal Society of London in 1887.

John Newlands (1838–1898)

Newlands noticed that elemental properties repeated every seventh (or multiple of seven) element, as musical notes repeat every eighth note.

No.	No.	No.	No.	No.	No.	No.	No.
H 1	F 8	Cl 15	Co & Ni 22	Br 29	Pd 36	I 42	Pt & Ir 50
Li 2	Na 9	K 16	Cu 23	Rb 30	Ag 37	Cs 44	Tl 51
G 3	Mg 10	Ca 17	Zn 25	Sr 31	Bd [sic-Cd] 38	Ba & V 45	Pb 54
Bo 4	Al 11	Cr 19	Y 24	Ce & La 33	U 40	Ta 46	Th 56
C 5	Si 12	Ti 18	In 26	Zr 32	Sn 39	W 47	Hg 52
N 6	P 13	Mn 20	As 27	Di & Mo 34	Sb 41	Nb 48	Bi 55
O 7	S 14	Fe 21	Se 28	Ro & Ru 35	Te 43	Au 49	Os 51

NOTE. Where two elements happen to have the same equivalent, both are designated by the same number.

Figure 3.4.1 The arrangement of the elements into octaves as proposed by **Newlands:** *The table shown here accompanied a letter from a 27-year-old Newlands to the editor of the journal Chemical News in which he wrote: "If the elements are arranged in the order of their equivalents, with a few slight transpositions, as in the accompanying table, it will be observed that elements belonging to the same group usually appear on the same horizontal line. It will also be seen that the numbers of analogous elements generally differ either by 7 or by some multiple of seven; in other words, members of the same group stand to each other in the same relation as the extremities of one or more octaves in music. Thus, in the nitrogen group, between nitrogen and phosphorus there are 7 elements; between phosphorus and arsenic, 14; between arsenic and antimony, 14; and lastly, between antimony and bismuth, 14 also. This peculiar relationship I propose to provisionally term the Law of Octaves. I am, &c. John A. R. Newlands, F.C.S. Laboratory, 19, Great St. Helen's, E.C., August 8, 1865."*

The periodic table achieved its modern form through the work of the German chemist Julius Lothar Meyer (1830–1895) and the Russian chemist Dimitri Mendeleev (1834–1907), both of whom focused on the relationships between atomic mass and various physical and chemical properties. In 1869, they independently proposed essentially identical arrangements of the elements. Meyer aligned the elements in his table according to periodic variations in simple atomic properties, such as "atomic volume" (Figure 3.4.2), which he obtained by dividing the atomic mass (molar mass) in grams per mole by the density of the element in grams per cubic centimeter. This property is equivalent to what is today defined as molar volume, the molar mass of an element divided by its density (measured in cubic centimeters per mole):

$$\frac{molar\ mass\left(\not{g}/mol\right)}{density\left(\not{g}/cm^3\right)} = molar\ \ volume\left(cm^3/mol\right)$$

As shown in Figure 3.4.2 , the alkali metals have the highest molar volumes of the solid elements. In Meyer's plot of atomic volume versus atomic mass, the nonmetals occur on the rising portion of the graph, and metals occur at the peaks, in the valleys, and on the down slopes.

Dimitri Mendeleev (1834–1907)

When his family's glass factory was destroyed by fire, Mendeleev moved to St. Petersburg, Russia, to study science. He became ill and was not expected to recover, but he finished his PhD with the help of his professors and fellow students. In addition to the periodic table, another of Mendeleev's contributions to science was an outstanding textbook, *The Principles of Chemistry*, which was used for many years.

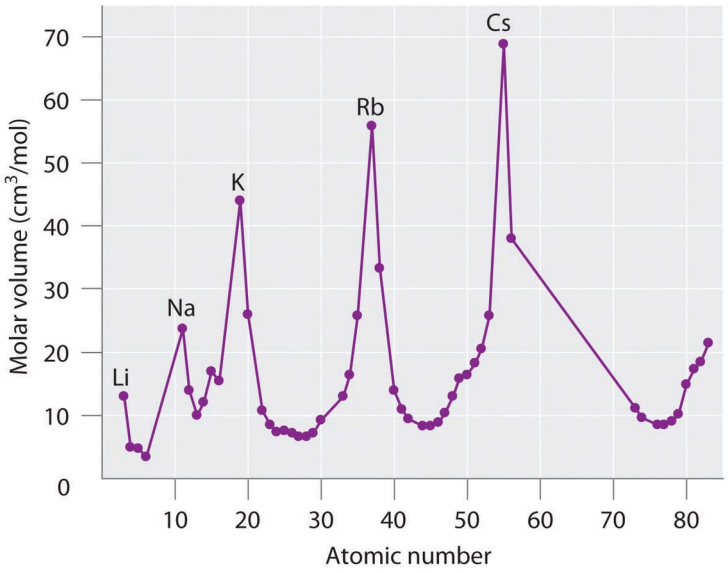


Figure 3.4.2 Variation of atomic volume with atomic number, adapted from Meyer's plot of **1870:** *Note the periodic increase and decrease in atomic volume. Because the noble gases had not yet been discovered at the time this graph was formulated, the peaks correspond to the alkali metals (group 1).*

Mendeleev's Periodic Table

Mendeleev, who first published his periodic table in 1869 (Figure 3.4.3), is usually credited with the origin of the modern periodic table. The key difference between his arrangement of the elements and that of Meyer and others is that Mendeleev did not assume that all the elements had been discovered (actually, only about two-thirds of the naturally occurring elements were known at the time). Instead, he deliberately left blanks in his table at atomic masses 44, 68, 72, and 100, in the expectation that elements with those atomic masses would be discovered. Those blanks correspond to the elements we now know as scandium, gallium, germanium, and technetium.

Reihen	Gruppe I. — R^2O	Gruppe II. — RO	Gruppe III. — R^2O^3	Gruppe IV. RH^4 RO^2	Gruppe V. RH^3 R^2O^5	Gruppe VI. RH^2 RO^3	Gruppe VII. RH R^2O^7	Gruppe VIII. — RO^4
1	H=1							
2	Li=7	Be=9,4	B=11	C=12	N=14	O=16	F=19	
3	Na=23	Mg=24	Al=27,3	Si=28	P=31	S=32	Cl=35,5	
4	K=39	Ca=40	— =44	Ti=48	V=51	Cr=52	Mn=55	Fe=56, Co=59, Ni=59, Cu=63.
5	(Cu=63)	Zn=65	— =68	— =72	As=75	Se=78	Br=80	
6	Rb=85	Sr=87	?Yt=88	Zr=90	Nb=94	Mo=96	— =100	Ru=104, Rh=104, Pd=106, Ag=108.
7	(Ag=108)	Cd=112	In=113	Sn=118	Sb=122	Te=125	J=127	
8	Cs=133	Ba=137	?Di=138	?Ce= 40	—	—	—	— — — —
9	(—)	—	—	—	—	—	—	
10	—	—	?Er=178	?La=180	Ta=182	W=184	—	Os=195, Ir=197, Pt=198, Au=199.
11	(Au=199)	Hg=200	Tl=204	Pb=207	Bi=208	—	—	
12	—	—	—	Th=231	—	U=240	—	— — — —

Figure 3.4.3 Mendeleev's periodic table, as published in the German journal *Annalen der Chemie und Pharmacie* in 1872: *The column headings "Reihen" and "Gruppe" are German for "row" and "group." Formulas indicate the type of compounds formed by each group, with "R" standing for "any element" and superscripts used where we now use subscripts. Atomic masses are shown after equal signs and increase across each row from left to right.*

The groups in Mendeleev's table are determined by how many oxygen or hydrogen atoms are needed to form compounds with each element. For example, in Group I, two atoms of hydrogen (H), lithium (Li), sodium (Na), and potassium (K) form compounds

with one atom of oxygen. In Group VII, one atom of fluorine (F), chlorine (Cl), and bromine (Br), reacts with one atom of hydrogen. Notice how this approach has trouble with the transition metals. Until roughly 1960, a rectangular table developed from Mendeleev's table and based on reactivity was standard at the front of chemistry lecture halls.

The most convincing evidence in support of Mendeleev's arrangement of the elements was the discovery of two previously unknown elements whose properties closely corresponded with his predictions (Table 3.4.1). Two of the blanks Mendeleev had left in his original table were below aluminum and silicon, awaiting the discovery of two as-yet-unknown elements, *eka*-aluminum and *eka*-silicon (from the Sanskrit *eka*, meaning "one," as in "one beyond aluminum"). The observed properties of gallium and germanium matched those of *eka*-aluminum and *eka*-silicon so well that once they were discovered, Mendeleev's periodic table rapidly gained acceptance.

YouTube Video

This interactive element is not available in this format. Visit the link or scan the QR code to access it online.

View this YouTube Video online

Table 3.4.1 Comparison of the properties predicted by Mendeleev in 1869 for *eka*-aluminum and *eka*-silicon with the properties of gallium (discovered in 1875) and germanium (discovered in 1886)

Property	*eka*-Aluminum (predicted)	Gallium (observed)	*eka*-Silicon (predicted)	Germanium (observed)
atomic mass	68	69.723	72	72.64
element	metal	metal	dirty-gray metal	gray-white metal
	low mp*	mp = 29.8°C	high mp	mp = 938°C
	d = 5.9 g/cm^3	d = 5.91 g/cm^3	d = 5.5 g/cm^3	d = 5.323 g/cm^3
oxide	E_2O_3	Ga_2O_3	EO_2	GeO_2
	d = 5.5 g/cm^3	d = 6.0 g/cm^3	d = 4.7 g/cm^3	d = 4.25 g/cm^3
chloride	ECl_3	$GaCl_3$	ECl_4	$GeCl_4$
	volatile	mp = 78°C bp* = 201°C	bp < 100°C	bp = 87°C
***mp = melting point; bp = boiling point.**				

When the chemical properties of an element suggested that it might have been assigned the wrong place in earlier tables, Mendeleev carefully reexamined its atomic mass. He discovered, for example, that the atomic masses previously reported for beryllium, indium, and uranium were incorrect. The atomic mass of indium had originally been reported as 75.6, based on an assumed stoichiometry of InO for its oxide. If this atomic mass were correct, then indium would have to be placed in the middle of the nonmetals, between arsenic (atomic mass 75) and selenium (atomic mass 78). Because elemental indium is a silvery-white *metal*, however, Mendeleev postulated that the stoichiometry of its oxide was really In_2O_3 rather than InO. This would mean that indium's atomic mass was actually 113, placing the element between two other metals, cadmium and tin.

One group of elements absent from Mendeleev's table was the noble gases, all of which were discovered more than 20 years later, between 1894 and 1898, by Sir William Ramsay (1852–1916; Nobel Prize in Chemistry 1904). Initially, Ramsay did not know where to place these elements in the periodic table. Argon, the first to be discovered, had an atomic mass of 40. This was greater than chlorine's and comparable to that of potassium; so Ramsay, using the same kind of reasoning as Mendeleev, decided to place the noble gases between the halogens and the alkali metals.

The Role of the Atomic Number in the Periodic Table

Despite its usefulness, Mendeleev's periodic table was based entirely on empirical observation supported by very little understanding. It was not until 1913, when a young British physicist, H. G. J. Moseley (1887–1915), while analyzing the frequencies of x-rays emitted by the elements, discovered that the underlying foundation of the order of the elements was the *atomic number*, not the atomic mass. Moseley hypothesized that the placement of each element in his series corresponded to its atomic number Z, which is the number of positive charges (protons) in its nucleus. Argon, for example, although having an atomic mass greater than that of potassium (39.9 amu versus 39.1 amu, respectively), was placed *before* potassium in the periodic table. While analyzing the frequencies of the emitted x-rays, Moseley noticed that the atomic number of argon is 18, whereas that of potassium is 19, which indicated that they were indeed placed correctly. Moseley also noticed three gaps in his table of x-ray frequencies, so he predicted the existence of three unknown elements: technetium (Z = 43), discovered in 1937; promethium (Z = 61), discovered in 1945; and rhenium (Z = 75), discovered in 1925.

H. G. J. Moseley (1887–1915)

Moseley left his research work at the University of Oxford to join the British army as a telecommunications officer during World War I. He was killed during the Battle of Gallipoli in Turkey.

Example 3.4.1

Before its discovery in 1999, some theoreticians believed that an element with a Z of 114 existed in nature. Use Mendeleev's reasoning to name element 114 as *eka*-_____; then identify the known element whose chemistry you predict would be most similar to that of element 114.

Given: atomic number

Asked for: name using prefix *eka*-

Strategy:

A Using the periodic table locate the n = 7 row. Identify the location of the unknown element with Z = 114; then identify the known element that is directly above this location.

B Name the unknown element by using the prefix *eka*- before the name of the known element.

Solution:

A The n = 7 row can be filled in by assuming the existence of elements with atomic numbers greater than 112, which is underneath mercury (Hg). Counting three boxes to the right gives element 114, which lies directly below lead (Pb). **B** If Mendeleev were alive today, he would call element 114 *eka*-lead.

Exercise

Use Mendeleev's reasoning to name element 112 as *eka*-_____; then identify the known element whose chemistry you predict would be most similar to that of element 112.

Answer: *eka*-mercury

Summary

The periodic table arranges the elements according to their electron configurations, such that elements in the same column have the same valence electron configurations. Periodic variations in size and chemical properties are important factors in dictating the types of chemical reactions the elements undergo and the kinds of chemical compounds they form. The modern periodic table was based on empirical correlations of properties such as atomic mass; early models using limited data noted the existence of **triads** and **octaves** of elements with similar properties. The periodic table achieved its current form through the work of Dimitri Mendeleev and Julius Lothar Meyer, who both focused on the relationship between atomic mass and chemical properties. Meyer arranged the elements by their atomic volume, which today is equivalent to the **molar volume**, defined as molar mass divided by

molar density. The correlation with the electronic structure of atoms was made when H. G. J. Moseley showed that the periodic arrangement of the elements was determined by atomic number, not atomic mass.

Key Takeaways

- The elements in the periodic table are arranged according to their properties, and the periodic table serves as an aid in predicting chemical behavior.

Conceptual Problems

1. Johannes Dobereiner is credited with developing the concept of chemical triads. Which of the group 15 elements would you expect to compose a triad? Would you expect B, Al, and Ga to act as a triad? Justify your answers.

2. Despite the fact that Dobereiner, Newlands, Meyer, and Mendeleev all contributed to the development of the modern periodic table, Mendeleev is credited with its origin. Why was Mendeleev's periodic table accepted so rapidly?

3. How did Moseley's contribution to the development of the periodic table explain the location of the noble gases?

4. The *eka*- naming scheme devised by Mendeleev was used to describe undiscovered elements.

    1. Use this naming method to predict the atomic number of *eka*-mercury, *eka*-astatine, *eka*-thallium, and *eka*-hafnium.
    2. Using the *eka*-prefix, identify the elements with these atomic numbers: 79, 40, 51, 117, and 121.

Numerical Problem

1. Based on the data given, complete the table.

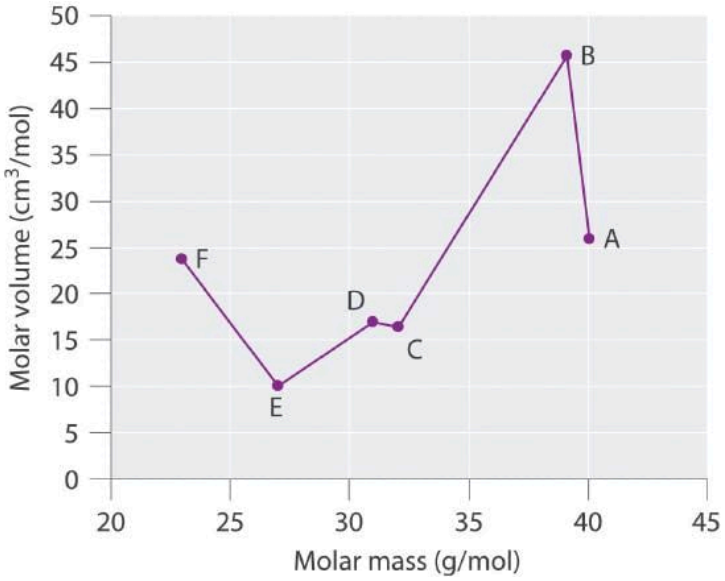
Species	Molar Mass (g/mol)	Density (g/cm^3)	Molar Volume (cm^3/mol)
A	40.078		25.85
B	39.09	0.856	
C	32.065		16.35
D		1.823	16.98
E	26.98		9.992
F	22.98	0.968	

Plot molar volume versus molar mass for these substances. According to Meyer, which would be considered metals and which would be considered nonmetals?

Answer

1.

Species	Molar Mass (g/mol)	Density (g/cm^3)	Molar Volume (cm^3/mol)
A	**40.078**	1.550	**25.85**
B	**39.09**	**0.856**	45.67
C	**32.065**	1.961	**16.35**
D	30.95	**1.823**	**16.98**
E	**26.98**	2.700	**9.992**
F	**22.98**	**0.968**	23.7



Meyer found that the alkali metals had the highest molar volumes, and that molar volumes decreased steadily with increasing atomic mass, then leveled off, and finally rose again. The elements located on the rising portion of a plot of molar volume versus molar mass were typically nonmetals. If we look at the plot of the data in the table, we can immediately identify those elements with the largest molar volumes (A, B, F) as metals located on the left side of the periodic table. The element with the smallest molar volume (E) is aluminum. The plot shows that the subsequent elements (C, D) have molar volumes that are larger than that of E, but smaller than those of A and B. Thus, C and D are most likely to be nonmetals (which is the case: C = sulfur, D = phosphorus).

Contributors and Attributions

- Anonymous

Modified by Joshua Halpern

Video from TED-Ed Lou Serocp

This page titled 2.1.1: The Periodic Table is shared under a license and was authored, remixed, and/or curated by LibreTexts.

- 2.1.1: The Periodic Table is licensed CC BY-NC-SA 4.0.

2.1.2: Discovery of Subatomic Particles and the Bohr Atom

Hydrogen Absorption and Emission Spectra

When a high-voltage electrical discharge is passed through a sample of hydrogen gas (H_2) at low pressure, the result is individual isolated hydrogen atoms that emit a red light. Unlike blackbody radiation, the color of the light emitted by the hydrogen atoms does not depend greatly on the temperature of the gas in the tube. When the emitted light is passed through a prism, only a few narrow lines of particular wavelengths, called a line spectrum, are observed rather than a continuous range of wavelengths (Figure 2.1.2.1). The light emitted by hydrogen atoms is red because, of its four characteristic lines, the most intense line in its spectrum is in the red portion of the visible spectrum, at 656 nm.

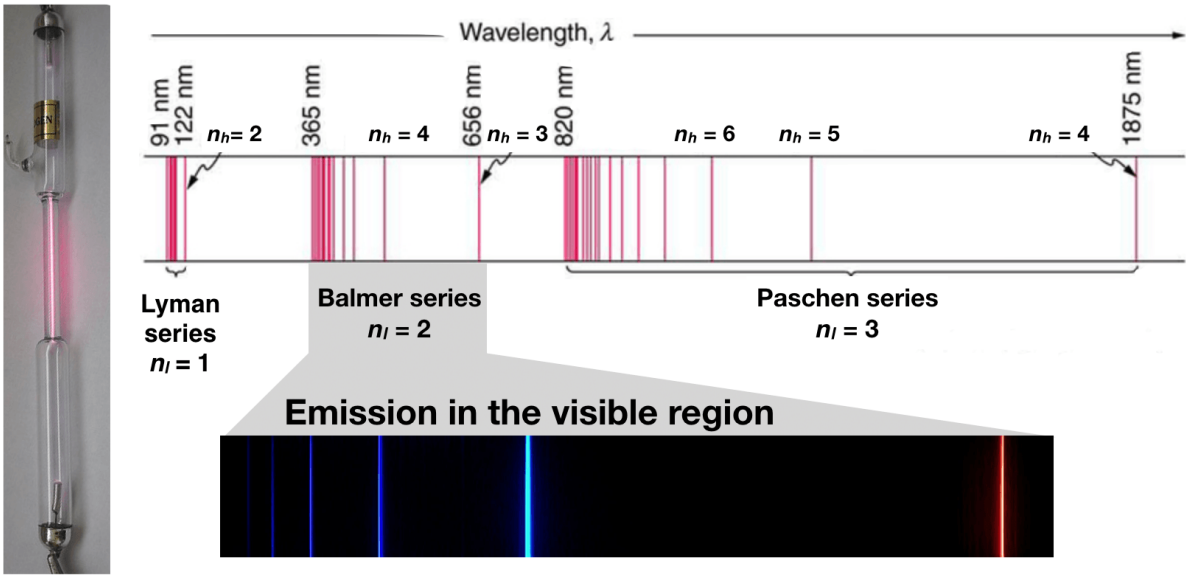


Figure 2.1.2.1: The emission of light by hydrogen atoms. (left) A sample of excited hydrogen atoms emits a characteristic red light. (bottom) When the light emitted by a sample of excited hydrogen atoms is split into its component wavelengths by a prism, four characteristic violet, blue, green, and red emission lines can be observed, with the most intense at 656 nm. (top) A diagram showing extended regions of the electromagnetic spectrum and the hydrogen line spectra that are observed. (Kathryn Haas; CC-BY-SA)

The Balmer Series

In 1885, a Swiss mathematics teacher, Johann Balmer (1825–1898), showed that the frequencies of the lines observed in the visible region of the hydrogen line spectrum fit a simple equation that can be expressed as follows:

$$u = constant\ \left(\frac{1}{2^2} - \frac{1}{n^2}\right) \tag{2.1.2.1}$$

where *n* = 3, 4, 5, 6. As a result, these lines are known as the *Balmer series*. The Swedish physicist Johannes Rydberg (1854–1919) subsequently restated and expanded Balmer's result in the *Rydberg equation*:

$$\frac{1}{\lambda} = R_H\ \left(\frac{1}{n_l^2} - \frac{1}{n_h^2}\right) \tag{2.1.2.2}$$

,

where n_l and n_h are positive integers, $n_h > n_l$, and R_H, the *Rydberg constant*, has a value of 1.09737 × 10^7 m^{-1}. Like Balmer's equation, Rydberg's simple equation described the wavelengths of the visible lines in the emission spectrum of hydrogen (with $n_l = 2, n_h = 3, 4, 5, ...$). More importantly, Rydberg's equation also predicted the wavelengths of other series of lines that would be observed in the emission spectrum of hydrogen: one in the ultraviolet ($n_l = 1, n_h = 2, 3, 4, ...$) and one in the infrared ($n_l = 3, n_h$

$= 4, 5, 6$).

Other Series

The results given by Balmer and Rydberg for the spectrum in the visible region of the electromagnetic spectrum start with $n_h = 3$, and $n_l = 2$.

Is there a different series with the following formula (e.g., $n_l = 1$)?

$$\frac{1}{\lambda} = R_{\mathrm{H}} \left(\frac{1}{1^2} - \frac{1}{n^2} \right) \tag{2.1.2.3}$$

The values for n_h and wavenumber u for this series would be:

Table 2.1.2.1*: The Lyman Series of Hydrogen Emission Lines* ($n_l = 1$)

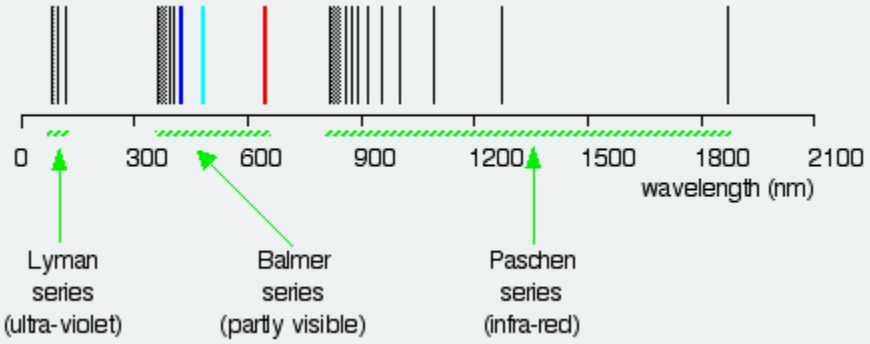
n_h	2	3	4	5
λ **(nm)**	121	102	97	94
$\tilde{u}$ **(cm^{-1})**	82,2291	97,530	102,864	105,332

Do you know what region of the electromagnetic radiation these lines are in? Of course, these lines are in the UV region, and they are not visible, but they are detected by instruments; these lines form a **Lyman series**. The existences of the Lyman series and Balmer's series suggest the existence of more series. For example, the series with $n_2^2 = 3$ and n_1^2 = 4, 5, 6, 7, ... is called the **Pashen series**.

Multiple series

The spectral lines are grouped into series according to n_1 values. Lines are named sequentially starting from the longest wavelength/lowest frequency of the series using Greek letters within each series. For example, the ($n_1 = 1/n_2 = 2$) line is called "Lyman-alpha" (Ly-α), while the ($n_1 = 3/n_2 = 7$) line is called "Paschen-delta" (Pa-δ). The first six series have specific names:

- Lyman series with $n_1 = 1$
- Balmer series with $n_1 = 2$
- Paschen series (or Bohr series) with $n_1 = 3$
- Brackett series with $n_1 = 4$
- Pfund series with $n_1 = 5$
- Humphreys series with $n_1 = 6$



The spectral series of hydrogen based on the Rydberg Equation (on a logarithmic scale).

Example 2.1.2.1: The Lyman Series

The so-called Lyman series of lines in the emission spectrum of hydrogen corresponds to transitions from various excited states to the *n* = 1 orbit. Calculate the wavelength of the lowest-energy line in the Lyman series to three significant figures. In what region of the electromagnetic spectrum does it occur?

Given: lowest-energy orbit in the Lyman series

Asked for: wavelength of the lowest-energy Lyman line and corresponding region of the spectrum

Strategy:

A. Substitute the appropriate values into Equation $Ref2.1.2.2$ (the Rydberg equation) and solve for λ.
B. Locate the region of the electromagnetic spectrum corresponding to the calculated wavelength.

Solution:

We can use the Rydberg equation (Equation $Ref2.1.2.2$ to calculate the wavelength:

$$\frac{1}{\lambda} = R_H \left(\frac{1}{n_l^2} - \frac{1}{n_h^2} \right)$$

A For the Lyman series, $n_1 = 1$.

$$\begin{aligned} \frac{1}{\lambda} &= R_H \left(\frac{1}{n_l^2} - \frac{1}{n_h^2} \right) \\ &= 1.097 \times m^{-1} \left(\frac{1}{1} - \frac{1}{4} \right) \\ &= 8.228 \times 10^6 \; m^{-1} \end{aligned}$$

Spectroscopists often talk about energy and frequency as equivalent. The cm^{-1} unit (wavenumbers) is particularly convenient. We can convert the answer in part A to cm^{-1}.

$$\begin{aligned} \tilde{u} &= \frac{1}{\lambda} \\ &= 8.228 \times 10^6 \; \cancel{m^{-1}} \left(\frac{\cancel{m}}{100 \; cm} \right) \\ &= 82,280 \; cm^{-1} \end{aligned}$$

and

$$\lambda = 1.215 \times 10^{-7} \; m = 122 \; nm$$

This emission line is called Lyman alpha and is the strongest atomic emission line from the sun; it drives the chemistry of the upper atmosphere of all the planets producing ions by stripping electrons from atoms and molecules. It is completely absorbed by oxygen in the upper stratosphere, dissociating O_2 molecules to O atoms, which react with other O_2 molecules to form stratospheric ozone (O_3).

B This wavelength is in the ultraviolet region of the spectrum.

Exercise 2.1.2.1: The Pfund Series

The Pfund series of lines in the emission spectrum of hydrogen corresponds to transitions from higher excited states to $n_1 = 5$. Calculate the wavelength of the *second* line in the Pfund series to three significant figures. In which region of the spectrum does it lie?

Answer available at the end of this section.

The above discussion presents only a phenomenological description of hydrogen emission lines. Balmer and Rydberg could predict where emission lines could occur, but they could not explain why lines followed this pattern using any useful theory. For an explanation of why atoms demonstrate discrete emission spectra, quantum theories were developed.

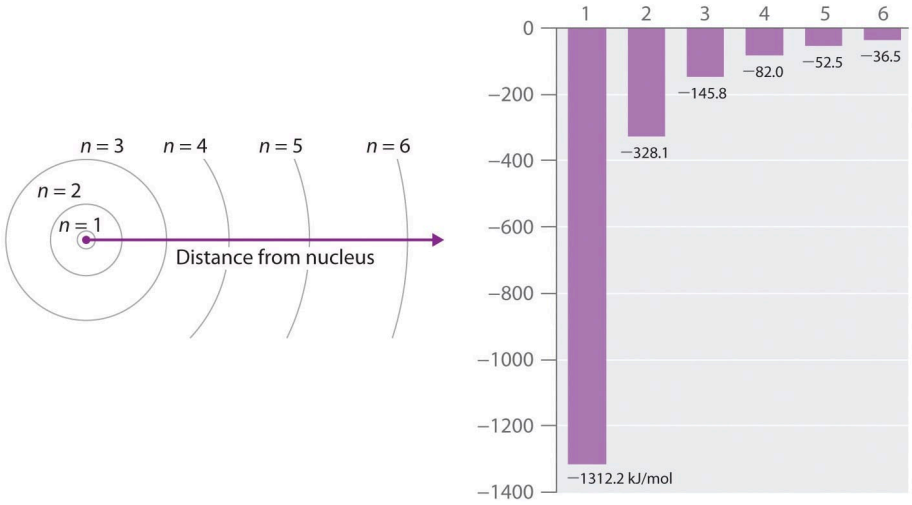
The Bohr Model

In 1913, a Danish physicist, Niels Bohr (1885–1962; Nobel Prize in Physics, 1922), proposed a theoretical model for the hydrogen atom that explained its emission spectrum. Bohr's model required only one assumption: *The electron moves around the nucleus in circular orbits that can have only certain allowed radii.* Rutherford's earlier model of the atom had also assumed that electrons moved in circular orbits around the nucleus and that the atom was held together by the electrostatic attraction between the positively charged nucleus and the negatively charged electron. Although we now know that the assumption of circular orbits was incorrect, Bohr's insight also posited that *the electron could occupy only certain regions of space*.

Using classical physics, Niels Bohr showed that the energy of an electron in a particular orbit is given by

$$E_n = \frac{-R_H hc}{n^2} \tag{2.1.2.4}$$

where R_H is the Rydberg constant, *h* is Planck's constant, *c* is the speed of light, and *n* is a positive integer corresponding to the number assigned to the orbit, with *n* = 1 corresponding to the orbit closest to the nucleus. In this model *n* = ∞ corresponds to the level where the energy holding the electron and the nucleus together is zero. In that level, the electron is unbound from the nucleus and the atom has been separated into a negatively charged (the electron) and a positively charged (the nucleus) ion. In this state the radius of the orbit is also infinite. The atom has been ionized.



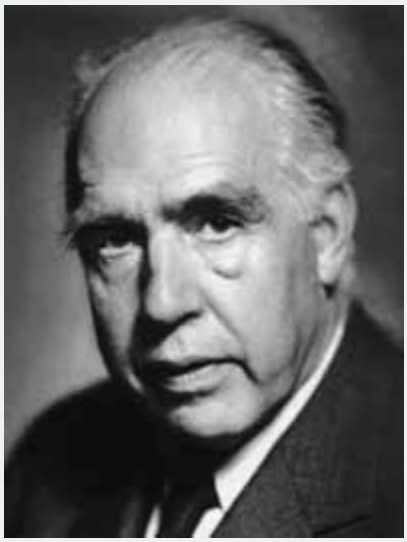
(a) Hydrogen orbits (Bohr model). Orbits are not drawn to scale.

(b) Hydrogen orbit energy (kJ/mol) vs. *n*

Figure 2.1.2.2: *The Bohr Model of the hydrogen atom (a) The distance of the orbit from the nucleus increases with increasing n. (b) The energy of the orbit becomes increasingly less negative with increasing n.*

Niels Bohr (1885–1962)

During the Nazi occupation of Denmark in World War II, Bohr escaped to the United States, where he became associated with the Atomic Energy Project.



In his final years, he devoted himself to the peaceful application of atomic physics and to resolving political problems arising from the development of atomic weapons.

As n decreases, the energy holding the electron and the nucleus together becomes increasingly negative; the radius of the orbit shrinks and more energy is needed to ionize the atom. The orbit with n = 1 is the lowest lying and most tightly bound. The negative sign in Equation ??? indicates that the electron-nucleus pair is more tightly bound (i.e. at a lower potential energy) when they are near each other than when they are far apart. Because a hydrogen atom with its one electron in this orbit has the lowest possible energy, this is the **ground state** (the most stable arrangement of electrons for an element or a compound) for a hydrogen atom. As n increases, the radius of the orbit increases; the electron is farther from the proton, which results in a less stable arrangement with higher potential energy (Figure $2.1.2.2a$). A hydrogen atom with an electron in an orbit with n > 1 is therefore in an **excited state**, defined as any arrangement of electrons that is higher in energy than the ground state. When an atom in an excited state undergoes a transition to the ground state in a process called decay, it loses energy by emitting a photon whose energy corresponds to the *difference* in energy between the two states (Figure $2.1.2.1$).

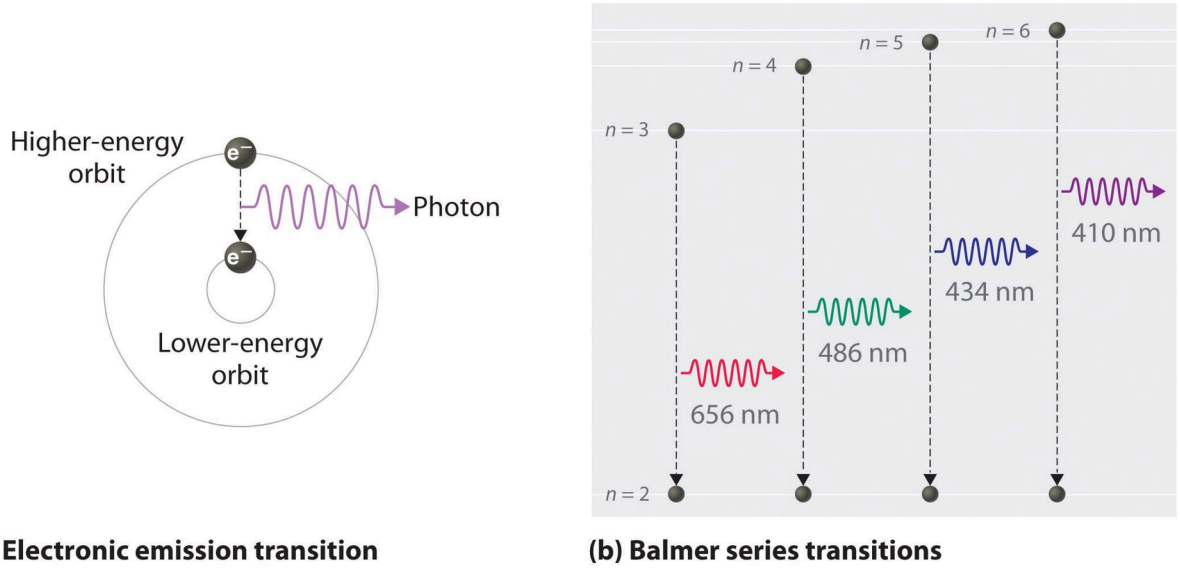


Figure 2.1.2.3: *The emission of light by a hydrogen atom in an excited state. (a) Light is emitted when the electron undergoes a transition from an orbit with a higher value of n (at a higher energy) to an orbit with a lower value of n (at lower energy). (b) The Balmer series of emission lines is due to transitions from orbits with n ≥ 3 to the orbit with n = 2. The differences in energy between these levels correspond to light in the visible portion of the electromagnetic spectrum.*

So the difference in energy (Δ*E*) between any two orbits or energy levels is given by $\Delta E = E_{n_l} - E_{n_h}$, where n_l is the final orbit and n_h the initial orbit. Substituting from Bohr's equation (Equation 2.1.2.4) for each energy value gives

$$\Delta E = E_{final} - E_{initial} = -\frac{R_H hc}{n_h^2} - \left(-\frac{R_H hc}{n_l^2}\right) = -R_H hc\left(\frac{1}{n_h^2} - \frac{1}{n_l^2}\right) \tag{2.1.2.5}$$

If $n_h > n_l$, the transition is from a higher energy state (larger-radius orbit) to a lower energy state (smaller-radius orbit), as shown by the dashed arrow in part (a) in Figure 2.1.2.3. Substituting *hc*/λ for Δ*E* gives

$$\Delta E = \frac{hc}{\lambda} = -R_H hc\left(\frac{1}{n_h^2} - \frac{1}{n_l^2}\right) \tag{2.1.2.6}$$

Canceling *hc* on both sides gives

$$\frac{1}{\lambda} = -R_H\left(\frac{1}{n_h^2} - \frac{1}{n_l^2}\right) \tag{2.1.2.7}$$

Except for the negative sign, this is the same equation that Rydberg obtained experimentally. The negative sign in Equations 2.1.2.6 and 2.1.2.7 indicates that energy is released as the electron moves from orbit n_h to orbit n_l because orbit n_h is at a higher energy than orbit n_l. Bohr calculated the value of R_H from fundamental constants such as the charge and mass of the electron and Planck's constant and obtained a value of 1.0974 × 10^7 m^{-1}, the same number Rydberg had obtained by analyzing the emission spectra.

We can now understand the physical basis for the Balmer series of lines in the emission spectrum of hydrogen (2.1.2.3*b*); the lines in this series correspond to transitions from higher-energy orbits (n > 2) to the second orbit (n = 2). Thus, the hydrogen atoms in the sample have absorbed energy from the electrical discharge and decayed from a higher-energy excited state (n > 2) to a lower-energy state (n = 2) by emitting a photon of electromagnetic radiation whose energy corresponds exactly to the difference in energy between the two states (Figure 2.1.2.3*a*). The n = 3 to n = 2 transition gives rise to the line at 656 nm (red), the n = 4 to n = 2 transition to the line at 486 nm (green), the n = 5 to n = 2 transition to the line at 434 nm (blue), and the n = 6 to n = 2 transition to the line at 410 nm (violet). Because a sample of hydrogen contains a large number of atoms, the intensity of the various lines in a line spectrum depends on the number of atoms in each excited state. At the temperature in the gas discharge tube, more atoms are in the n = 3 than the n ≥ 4 levels. Consequently, the n = 3 to n = 2 transition is the most intense line, producing the characteristic red color of a hydrogen discharge (Figure 2.1.2.1*a*). Other families of lines are produced by transitions from excited states with n > 1 to the orbit with n = 1 or to orbits with n ≥ 3. These transitions are shown schematically in Figure

2.1.2.4 :

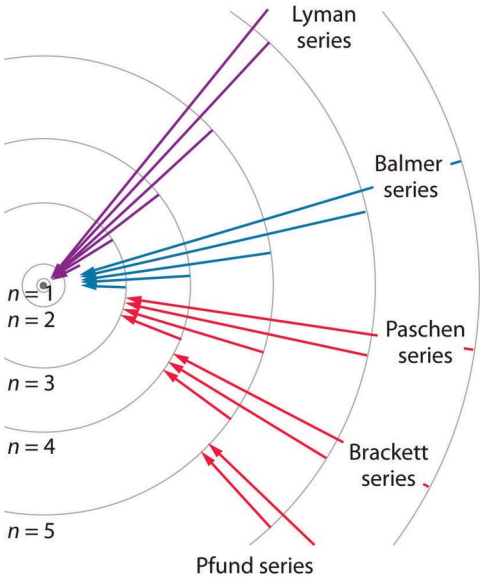


Figure 2.1.2.4: Electron transitions responsible for the various series of lines observed in the emission spectrum of hydrogen. The Lyman series of lines is due to transitions from higher-energy orbits to the lowest-energy orbit (n = 1); these transitions release a great deal of energy, corresponding to radiation in the ultraviolet portion of the electromagnetic spectrum. The Paschen, Brackett, and Pfund series of lines are due to transitions from higher-energy orbits to orbits with n = 3, 4, and 5, respectively; these transitions release substantially less energy, corresponding to infrared radiation. (Orbits are not drawn to scale.)

Using Atoms to Time

In contemporary applications, electron transitions are used in timekeeping that needs to be exact. Telecommunications systems, such as cell phones, depend on timing signals that are accurate within a millionth of a second per day; the same goes for the devices that control the US power grid. Global positioning system (GPS) signals must be accurate within a billionth of a second per day, which is equivalent to gaining or losing no more than one second in 1,400,000 years. Quantifying time requires finding an event with an interval that repeats on a regular basis.

To achieve the accuracy required for modern purposes, physicists have turned to the atom. The current standard used to calibrate clocks is the cesium atom. Supercooled cesium atoms are placed in a vacuum chamber and bombarded with microwaves whose frequencies are carefully controlled. When the frequency is exactly right, the atoms absorb enough energy to undergo an electronic transition to a higher-energy state. Decay to a lower-energy state emits radiation. The microwave frequency is continually adjusted, serving as the clock's pendulum.

In 1967, the second was defined as the duration of 9,192,631,770 oscillations of the resonant frequency of a cesium atom, called the *cesium clock*. Research is currently under way to develop the next generation of atomic clocks that promise to be even more accurate. Such devices would allow scientists to monitor vanishingly faint electromagnetic signals produced by nerve pathways in the brain and allow geologists to measure variations in gravitational fields, which cause fluctuations in time, that would aid in the discovery of oil or minerals.

Example 2.1.2.1: The Lyman Series

The so-called Lyman series of lines in the emission spectrum of hydrogen corresponds to transitions from various excited states to the n = 1 orbit. Calculate the wavelength of the lowest-energy line in the Lyman series to three significant figures. In what region of the electromagnetic spectrum does it occur?

Given: lowest-energy orbit in the Lyman series

Asked for: wavelength of the lowest-energy Lyman line and corresponding region of the spectrum

Strategy:

A. Substitute the appropriate values into Equation 2.1.2.4 (the Rydberg equation) and solve for λ.
B. Use Figure 2.2.1 to locate the region of the electromagnetic spectrum corresponding to the calculated wavelength.

Solution:

We can use the Rydberg equation to calculate the wavelength:

$$\frac{1}{\lambda} = -R_H \left(\frac{1}{n_h^2} - \frac{1}{n_l^2} \right)$$

A For the Lyman series, /(n_l = 1\). The lowest-energy line is due to a transition from the *n* = 2 to *n* = 1 orbit because they are the closest in energy.

$$\frac{1}{\lambda} = -R_H \left(\frac{1}{n_h^2} - \frac{1}{n_l^2} \right) = 1.097 \times m^{-1} \left(\frac{1}{1} - \frac{1}{4} \right) = 8.228 \times 10^6 \; m^{-1}$$

It turns out that spectroscopists (the people who study spectroscopy) use cm^{-1} rather than m^{-1} as a common unit. Wavelength is inversely proportional to energy but frequency is directly proportional as shown by Planck's formula, E=hu.

Spectroscopists often talk about energy and frequency as equivalent. The cm^{-1} unit is particularly convenient. The infrared range is roughly 200 - 5,000 cm^{-1}, the visible from 11,000 to 25,000 cm^{-1} and the UV between 25,000 and 100,000 cm^{-1}. The units of cm^{-1} are called wavenumbers, although people often refer to the unit as inverse centimeters. We can convert the answer in part A to cm^{-1}.

$$\tilde{u} = \frac{1}{\lambda} = 8.228 \times 10^6 \; \cancel{m^{-1}} \left(\frac{\cancel{m}}{100 \; cm} \right) = 82,280 \; cm^{-1}$$

and

$$\lambda = 1.215 \times 10^{-7} \; m = 122 \; nm$$

This emission line is called Lyman alpha. As the strongest atomic emission line from the sun, it drives the chemistry of the upper atmosphere of all the planets, producing ions by stripping electrons from atoms and molecules. It is completely absorbed by oxygen in the upper stratosphere, dissociating O_2 molecules to O atoms which react with other O_2 molecules to form stratospheric ozone.

B This wavelength is in the ultraviolet region of the spectrum.

Exercise 2.1.2.1: The Pfund Series

The Pfund series of lines in the emission spectrum of hydrogen corresponds to transitions from higher excited states to the *n* = 5 orbit. Calculate the wavelength of the *second* line in the Pfund series to three significant figures. In which region of the spectrum does it lie?

Answer available at the end of this section.

Bohr's model of the hydrogen atom gave an exact explanation for its observed emission spectrum. The following are his key contributions to our understanding of atomic structure:

- Electrons can occupy only certain regions of space, called *orbits*.
- Orbits closer to the nucleus are lower in energy.
- Electrons can move from one orbit to another by absorbing or emitting energy, giving rise to characteristic spectra.

Unfortunately, Bohr could not explain *why* the electron should be restricted to particular orbits. Also, despite a great deal of

conjecturing, such as assuming that orbits could be ellipses rather than circles, his model could not quantitatively explain the emission spectra of any element other than hydrogen (Figure 2.1.2.5). In fact, Bohr's model worked only for species that contained just one electron: H, He^+, Li^{2+}, and so forth. Scientists needed a fundamental change in their way of thinking about the electronic structure of atoms to advance beyond the Bohr model.

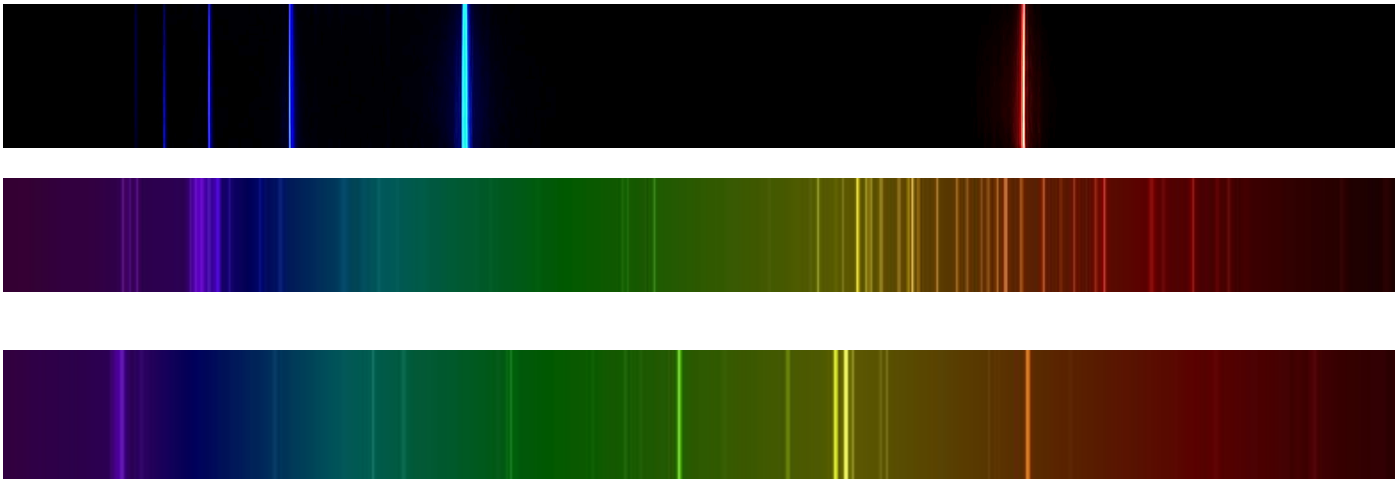


Figure 2.1.2.5: The emission spectra of elements compared to hydrogen. **Top:** hydrogen gas (atomized to hydrogen atoms in the discharge tube). **Middle:** neon. **Bottom:** mercury. The strongest lines in the hydrogen spectrum are in the far UV Lyman series starting at 124 nm and below. The strongest lines in the mercury spectrum are at 181 and 254 nm, also in the UV. These are not shown. Attribution: Hydrogen (Jan Homann / CC BY-SA); Neon (Teravolt at en.Wikipedia / Public domain); Mercury (Teravolt at en.Wikipedia / Public domain)

The Energy States of the Hydrogen Atom

Thus far, we have explicitly considered only the emission of light by atoms in excited states, which produces an emission spectrum (a spectrum produced by the emission of light by atoms in excited states). The converse, absorption of light by ground-state atoms to produce an excited state, can also occur, producing an absorption spectrum (a spectrum produced by the absorption of light by ground-state atoms).

> When an atom emits light, it decays to a lower energy state; when an atom absorbs light, it is excited to a higher energy state.

If white light is passed through a sample of hydrogen, hydrogen atoms absorb energy as an electron is excited to higher energy levels (orbits with $n \geq 2$). If the light that emerges is passed through a prism, it forms a continuous spectrum with *black* lines (corresponding to no light passing through the sample) at 656, 468, 434, and 410 nm. These wavelengths correspond to the $n = 2$ to $n = 3$, $n = 2$ to $n = 4$, $n = 2$ to $n = 5$, and $n = 2$ to $n = 6$ transitions. Any given element therefore has both a characteristic emission spectrum and a characteristic absorption spectrum, which are essentially complementary images.

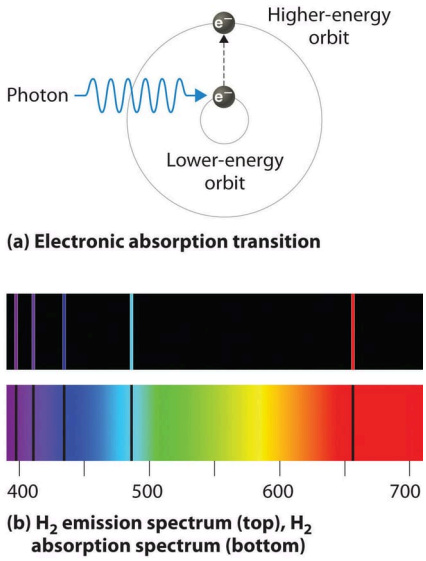


Figure 2.1.2.6: Absorption and emission spectra. Absorption of light by a hydrogen atom. (a) When a hydrogen atom absorbs a photon of light, an electron is excited to an orbit that has a higher energy and larger value of n. (b) Images of the emission and absorption spectra of hydrogen are shown here.

Emission and absorption spectra form the basis of *spectroscopy*, which uses spectra to provide information about the structure and the composition of a substance or an object. In particular, astronomers use emission and absorption spectra to determine the composition of stars and interstellar matter. As an example, consider the spectrum of sunlight shown in Figure 2.1.2.7. Since the sun is very hot, it emits light in the form of a continuous emission spectrum. Superimposed on the spectrum, however, is a series of dark lines primarily resulting from the absorption of specific frequencies of light by cooler atoms in the outer atmosphere of the sun. By comparing these lines with the spectra of elements measured on Earth, we now know that the sun contains large amounts of hydrogen, iron, and carbon, along with smaller amounts of other elements. During the solar eclipse of 1868, the French astronomer Pierre Janssen (1824–1907) observed a set of lines that did not match those of any known element. He suggested that they were due to the presence of a new element, which he named *helium*, from the Greek *helios*, meaning "sun." Helium (He) was finally discovered in uranium ores on Earth in 1895. Alpha particles are helium nuclei. Alpha particles emitted by radioactive uranium nuclei pick up electrons from the rocks to form helium atoms.

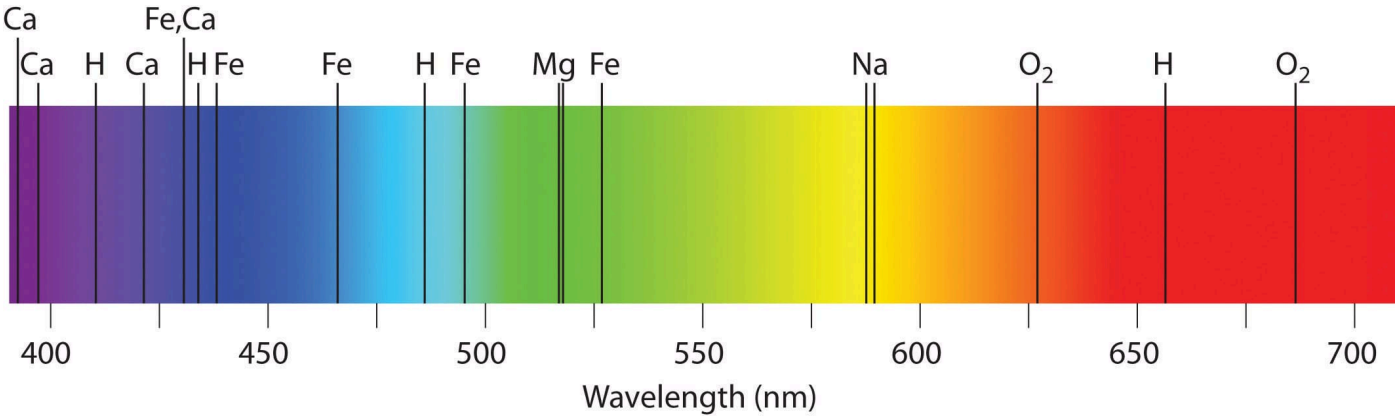


Figure 2.1.2.7: *The visible spectrum of sunlight. The characteristic dark lines are mostly due to the absorption of light by elements that are present in the cooler outer part of the sun's atmosphere; specific elements are indicated by the labels. The lines at 628 and 687 nm, however, are due to the absorption of light by oxygen molecules in Earth's atmosphere.*

The familiar red color of neon signs used in advertising is due to the emission spectrum of neon shown in part (b) in Figure 2.1.2.5 . Similarly, the blue and yellow colors of certain street lights are caused, respectively, by mercury and sodium discharges. In all these cases, an electrical discharge excites neutral atoms to a higher energy state, and light is emitted when the atoms decay to the ground state. In the case of mercury, most of the emission lines are below 450 nm, which produces a blue light (part (c) in Figure 2.1.2.5). In the case of sodium, the most intense emission lines are at 589 nm, which produces an intense yellow light.

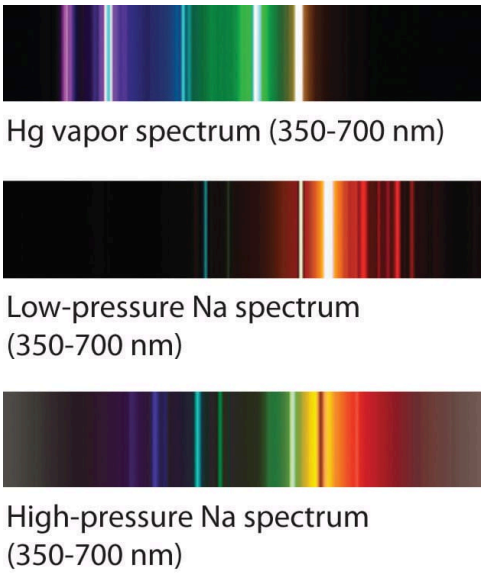


Figure 2.1.2.8: *The emission spectra of sodium and mercury. Many street lights use bulbs that contain sodium or mercury vapor. Due to the very different emission spectra of these elements, they emit light of different colors. The lines in the sodium lamp are broadened by collisions. The dark line in the center of the high pressure sodium lamp where the low pressure lamp is strongest is caused by absorption of light in the cooler outer part of the lamp.*

Summary

There is an intimate connection between the atomic structure of an atom and its spectral characteristics. Atoms of individual elements emit light at only specific wavelengths, producing a **line spectrum** rather than the continuous spectrum of all wavelengths produced by a hot object. Niels Bohr explained the line spectrum of the hydrogen atom by assuming that the electron moved in circular orbits and that orbits with only certain radii were allowed. Lines in the spectrum were due to transitions in which an electron moved from a higher-energy orbit with a larger radius to a lower-energy orbit with smaller radius. The orbit closest to the nucleus represented the **ground state** of the atom and was most stable; orbits farther away were higher-energy **excited states**. Transitions from an excited state to a lower-energy state resulted in the emission of light with only a limited number of wavelengths. Atoms can also absorb light of certain energies, resulting in a transition from the ground state or a lower-energy excited state to a higher-energy excited state. This produces an **absorption spectrum**, which has dark lines in the same position as the bright lines in the **emission spectrum** of an element. Bohr's model revolutionized the understanding of the atom but could not explain the spectra of atoms heavier than hydrogen.

Contributors and Attributions

- Modified by Joshua Halpern (Howard University)

Answers

Exercise 2.1.2.1: The Pfund Series

$4.65 \times 10^3\ nm$; infrared

Exercise 2.1.2.1: The Pfund Series

4.65 × 10^3 nm; infrared

This page titled 2.1.2: Discovery of Subatomic Particles and the Bohr Atom is shared under a CC BY-NC-SA 3.0 license and was authored, remixed, and/or curated by LibreTexts.

- 2.1.2: Discovery of Subatomic Particles and the Bohr Atom is licensed CC BY-NC-SA 3.0.

2.2: The Schrödinger equation, particle in a box, and atomic wavefunctions

Considering the failures of the Bohr model, Erwin Schrödinger and Werner Heisenberg proposed a major change in the paradigm regarding the electron. In several breakthrough papers (1925-1927) they attributed wave properties to electrons and they each received Nobel prizes for developing the theories of Wave Mechanics (or the "New Quantum Mechanics"). This approach treated electrons as having "dual" nature: possessing properties of *both* waves and particles.

Schrödinger's Equation describes the behavior of the electron (in a hydrogen atom) in three dimensions. It is a mathematical equation that defines the electron's position, mass, total energy, and potential energy. The simplest form of the Schrödinger Equation is as follows:

$$\hat{H}\psi = E\psi$$

where $\hat{H}$ is the **Hamiltonian operator**, E is the **energy of the electron**, and ψ is the **wavefunction**.

The Hamiltonian, $\hat{H}$

The Hamiltonian operator is like a set of instructions that tells us what to do with the function that follows it. A Hamiltonian operator is a function over three-dimensional space that corresponds to the sum of kinetic energies and potential energies of the particles in a system, one electron and its nucleus in this case. The Hamiltonian operator for a one-electron system is:

$$\hat{H} = \frac{-h^2}{8\pi^2 m_e}\left(\frac{\partial^2}{\partial x^2} + \frac{\partial^2}{\partial y^2} + \frac{\partial^2}{\partial z^2}\right) - \frac{Ze^2}{4\pi\epsilon_0 r},$$

where h is Planck's constant, m_e is the mass of the electron, e is the charge of the electron, r is the distance from the nucleus ($r = \sqrt{x^2+y^2+z^2}$), Z is the charge of the nucleus, and $4\pi\epsilon_0$ is the permittivity of a vacuum.

Kinetic Energy

The first part of the Hamiltonian written above, $\frac{-h^2}{8\pi^2 m_e}\left(\frac{\partial^2}{\partial x^2} + \frac{\partial^2}{\partial y^2} + \frac{\partial^2}{\partial z^2}\right)$ describes the kinetic energy of the electron. This is the energy due to motion of the electron.

Potential energy

The second part written above, $\frac{-Ze^2}{4\pi\epsilon_0 r}$, describes the potential energy of the electron, and is commonly written as $V(r)$ or $V(x,y,z)$.

$$V(x,y,x) = \frac{-Ze^2}{4\pi\epsilon_0 r} = \frac{-Ze^2}{4\pi\epsilon_0\sqrt{x^2+y^2+z^2}}$$

The potential energy depends on the attractive electrostatic force between the electron and the nucleus. You might notice that this attraction is essentially the same as the electrostatic force defined by Coulomb's law. And, just as in Coulomb's law, when two opposite charges are attracted to one another, the potential energy of the force is negative. Thus, when an electron is close to the nucleus, the potential energy is a large negative number corresponding to a strong attractive force. When an electron is farther from the nucleus, the potential energy is still negative but with a smaller magnitude, corresponding to a weaker attractive force. If the electron is very far from the nucleus ($r = \infty$) then the attractive force, and the potential energy, is zero.

The Wavefunction, ψ

In simple terms, the wavefunction (ψ) of an electron describes the electron's position in space, relative to the nucleus. The square of the ψ describes an atomic orbital. We can't define the position too exactly because we would violate the Heisenberg Uncertainty principle, but we can define its wave. A simple example of a ψ is described in the next section: Particle in a Box. Here, we will describe the ψ in general terms. Generally, in a one-electron atom, the electron ψ is defined by the wave's distance from the nucleus and its angle with respect to the x, y, and z axes of the atom's Cartesian coordinates (the nucleus is at the origin). The general form of the (ψ) for an electron in a hydrogen atom can be written as follows:

$$\psi_{n,l,m_l} = R_{n,l}(r) * Y_{l,m_l}(\theta, \phi)$$

Quantum Numbers define ψ

The (ψ) is defined by three of the quantum numbers: n, l, and m_l. These quantum numbers will be discussed more in a later section (2.2.2) The radial variation, R, depends on the electron's distance from the nucleus. The quantum numbers n (energy level) and l (orbital type) define R. Since n must be an integer, there are only certain allowed values for the solution to the wavefunction.

The angular variation, Y, depends on the angle with respect to the x, y, and z coordinates, and depends on the quantum numbers l (the orbital type) and m_l (the angular momentum, or the specific orbital). For example p_x lies along the x axis, while p_y points in a different direction in space.

For review, a list of the quantum numbers, their values, and meanings are in the table below.

SYMBOL	NAME	VALUES	MEANING
n	principal	$1, 2, 3...$(any integer)	energy level, shell
l	angular momentum	$0 \rightarrow n-1$	subshell, $0 = s, 1 = p, 2 = d, 3 = f...$ this is the angular dependence of the orbital, shape of the orbital *letters have historical meaning, sharp, principle, diffuse, fundamental
m_l	magnetic	$+l \rightarrow -l$	orientation of angular momentum in space, orbital
m_s	spin	$+\frac{1}{2}, -\frac{1}{2}$	the imaginary property we call "spin", up or down

---

Some important considerations and limitations

Although it might seem like there could be any value of x, y, and z for the Hamiltonian, these values are limited by the allowed positions of electrons according to ψ, which is limited by integer values of n. In other words the allowed solutions are *quantized*. However, there are an infinite number of values for n from $n = 1 \rightarrow \infty$, so there are also infinite solutions to the Schrödinger equation.

The ψ describes the wave properties of an electron. The probability of finding the electron somewhere in space is the square of the wavefunction (ψ^2 or $\psi\psi^*$). In other words, ψ^2 describes the shape and size of an electron's orbital (the shapes you already know).

There are some requirements for a physically realistic and meaningful solution for ψ, and thus ψ^2.

1. There is only one possible value for ψ for any set of the three quantum numbers n, l, m_l.
2. The ψ approaches zero as r approaches infinity, and so ψ^2 also approaches zero as $r \rightarrow \infty$.
3. The wavefunction must be normalized. In other words, the total probability of finding the electron in all of space must be 1.

$$\int_{\text{all space}} \psi_A \psi_A^* d\tau = 1$$

4. Any two orbitals must not occupy the same space. In other words, any two orbitals in an atom are orthogonal. If ψ_A and ψ_B

are wavefunctions for different orbitals in the same atom,

$$\int_{\text{all space}} \psi_A \psi_B^* d\tau = 0$$

5. The probability of finding the electron anywhere in infinite space must be defined. This means that the wave functions and their first derivatives must be continuous (i.e. not change abruptly from one point to the next).

Awesome Sources for further reading

- +Plus: https://plus.maths.org/content/schrodinger-1

This page titled 2.2: The Schrödinger equation, particle in a box, and atomic wavefunctions is shared under a CC BY-NC-SA 4.0 license and was authored, remixed, and/or curated by Kathryn Haas.

- 2.2: The Schrödinger equation, particle in a box, and atomic wavefunctions by Kathryn Haas is licensed CC BY-NC-SA 4.0.

2.2.1: Particle in a Box

The particle in the box is a model that can illustrate how a wave equation works. Although it does not represent a real situation, we can limit our model to just one dimension (the x-dimension, for instance) such that the Schrödinger equation becomes significantly simplified. Despite being unrealistic, this simplification is quite useful for gaining an understanding of the Schrödinger equation.

The model of a particle in a box

The particle in the box is a hypothetical situation with a particle trapped in a one-dimensional "box". Let's not get hung-up on the fact that the common object called a "box" is typically an object with three dimensions instead of just one dimension. And let's also not get hung up on the word "particle". This is a particle that has properties of a wave...so it is unlike the macroscopic particle that you're probably imagining. This "box" is more like a line, or an x-axis; it is just a one-dimensional space in which a particle-wave is trapped.

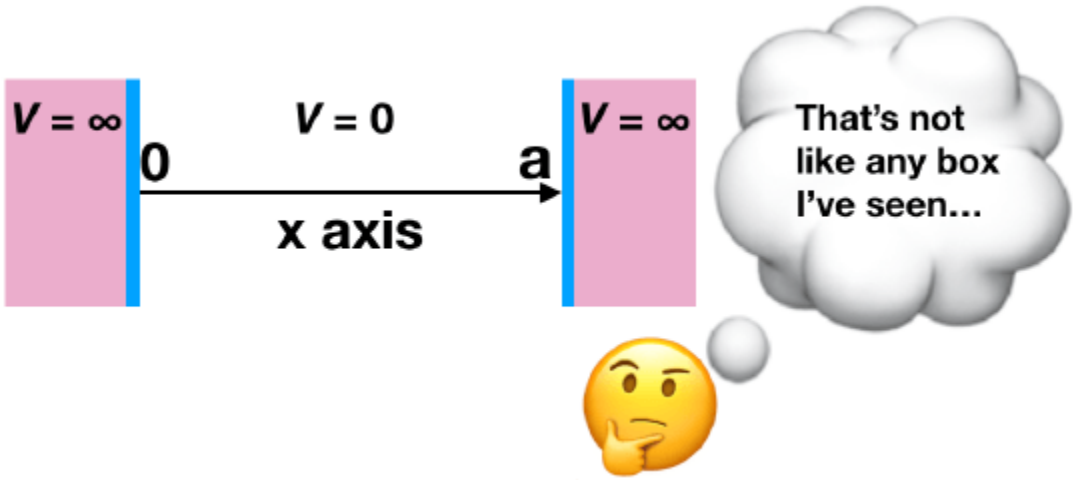


Figure 2.2.1.1. An illustration of the particle in the box model (particle not shown). The box is actually just a one-dimensional space, often assigned to the x-dimension (the x-axis). The particle has wave properties and is trapped in the box. Since no forces act on the particle inside the box, the particle's potential energy inside the box is zero ($V = 0$) and its potential energy outside the box is infinite ($V = \infty$). (CC-BY-NC-SA; Kathryn Haas)

The particle-wave can only exist inside the walls (where \(0a\)). This means that it is infinitely unfavorable for the particle-wave to exist outside the box, and so it never does. The particle-wave is trapped between the walls, along the 1-dimensional x axis, and there are no forces acting on the particle-wave inside this "box".

The Schrödinger wave equation for a particle in a box

The particle in a box model lets us consider a simple version of the Schrödinger equation. Before we simplify, let's take another look at the full Hamiltonian for a particle-wave in three dimensions (see equation 2.2.2) and the simplest form of the Schrödinger equation (see equation 2.2.1). Both of these equations are described in the previous section and are written below for convenience.

The Schrödinger Equation (from equation 2.2.1): $\hat{H}\psi = E\psi$

The Hamiltonian in three dimensions (from equation 2.2.2):

$$\hat{H} = \frac{-h^2}{8\pi^2 m_e}\left(\frac{\partial^2}{\partial x^2} + \frac{\partial^2}{\partial y^2} + \frac{\partial^2}{\partial z^2}\right) - \frac{Ze^2}{4\pi\epsilon_0 r}$$

In the particle in a box model, there is only one dimension, x. Because the y and z values are zero, we can drop y and z out of our Hamiltonian equation. And, since $V = 0$ inside the box, we can drop the whole part of the Hamiltonian equation that describes the potential energy ($\frac{-Ze^2}{4\pi\epsilon_0 r}$). This leaves us with a much simplified Hamiltonian operator, which we can then use to write the Schrödinger wave equation for a particle moving in one dimension. One last thing we'll do is use a more general value m for the mass of the particle, rather than m_e that specifically represents the mass of an electron. The Schrödinger equation for a particle-wave in a one-dimensional box is:

$$\frac{-h^2}{8\pi^2 m}\left(\frac{\partial^2\psi(x)}{\partial x^2}\right) = E\psi \tag{2.2.1.1}$$

Exercise 2.2.1.1

Follow the steps that were described in the last paragraph to find Equation 2.2.1.1 from equation 2.2.1 and 2.2.2. In other words, derive the Schrödinger Equation for the particle in a box given the three-dimensional Hamiltonian and Schrödinger Equations.

Answer available at the end of this section.

The wavefunction of a one-dimensional wave

Although we've simplified the Schrödinger Equation by considering the particle in the box, Equation 2.2.1.1 may still look mysterious to you. But it's simpler than you might realize. Let's unpack it! Here we'll go through the steps of deriving the 1-dimensional wavefunction for the particle in a box. We won't try to derive a three-dimensional wavefunction for a "real" electron, but when you understand how to find the 1-dimensional wavefunction, and what it tells us, then you can conceptually extend this to understand what the wavefunction tells us about electrons in three dimensions.

Let's dissect Equation 2.2.1.1. Here it is again for reference:

$$\frac{-h^2}{8\pi^2 m_e}\left(\frac{\partial^2\psi(x)}{\partial x^2}\right) = E\psi$$

The expression $\frac{-h^2}{8\pi^2 m_e}$ is just a negative constant. This negative constant is multiplied by the second derivative of the wavefunction in the expression above. And E is a constant multiplied by that same function. We can rearrange this equation as follows:

$$\frac{\partial^2\psi(x)}{\partial x^2} = \frac{-8\pi^2 m_e E}{h^2}\psi = -C\psi \tag{2.2.1.2}$$

where C is just the constant; $C = \frac{8\pi^2 m_e E}{h^2}$

To an expert in the mathematical field of Differential Equations, this expression 2.2.1.1 follows a familiar pattern that makes it easy to translate. If you're not an expert in differential equations, that is OK; you'll just have to bear with this while things get a little "hand-wavy" and try Exercise 2.2.1.2 to prove it to yourself that the following "hand waviness" is true. An expert in differential equations could tell you that when the second derivative of a function is equal to a negative constant times that same function, the function can be written in terms of sin and cos, as shown in Equation 2.2.1.3 (that was the hand-wavy part...see, not so bad):

$$\psi = A\sin(rx) + B\cos(sx) \tag{2.2.1.3}$$

A, B, r, and s are constants in Equation 2.2.1.3. This expression is useful because it is in a form that we could plot with a graphing program (or calculator). However, to do so we must know the constants A, B, r, and s.

What are r and s?

If we substitute expression 2.2.1.3 into Equation 2.2.1.1 and solve for r and s, we find the expressions below.

$$r = s = \sqrt{2m_e E}\left(\frac{2\pi}{h}\right) \tag{2.2.1.4}$$

This shows us that r and s are equal and constant; we know the values for $\pi, h,$ and m_e, and we can solve for the constant E.

Exercise 2.2.1.2: Prove that Equation 2.2.1.3 is true

Show that Equation 2.2.1.3 is true in the case that Equation 2.2.1.2 ($\frac{\partial^2\psi(x)}{\partial x^2} = -C\psi$) is true. Also consider Equation 2.2.1.4 (r, s are constants and $r = s$) and explain why the constant r must equal s.

To do this problem, you'll also need to know the basic differentiation rules of $\sin$ and $\cos$ functions, given below for convenience.

Differentiation Rules for sin and cos:

$\frac{d}{dx}\Big(\sin(rx)\Big) = r\cos(rx)$, where r is a constant.

$\frac{d}{dx}\Big(\cos(rx)\Big) = -r\sin(rx)$, where r is a constant.

Answer available at the end of this section.

Exercise 2.2.1.4

*Complete Exercise 2.2.1.2 before attempting this one.

Derive the expression for r below (from Equation 2.2.1.4) using the 1-D wavefunction (2.2.1.3: $\psi = A\sin(rx) + B\cos(sx)$) and the 1-D Schrödinger equation (2.2.1.1: $\left(\frac{-h^2}{8\pi^2 m_e}\left(\frac{\partial^2\psi(x)}{\partial x^2}\right) = E\psi\right)$).

$r = \frac{2\pi}{h}\sqrt{2m_eE}$

Answer available at the end of this section.

What are A and B?

We can find the possible values of A and B by looking at the possible extremes for the value of x. In our model in Figure 2.2.1.1 , we can see that x can have values from $0 \rightarrow a$. The two extremes, where $x = 0$ and $x = a$, lie at the walls of the box. The electron cannot exist beyond these values because it is trapped inside the walls, so its wavefunction must be zero at $x = 0$ and $x = a$.

The case where $x = 0$ can help us find the value of B. We just said that the wavefunction must be zero where $x = 0$. This means:

$$\psi_{x=0} = A\sin(rx) + B\cos(sx) = A\sin(0) + B\cos(0) = 0$$

Because $A\sin(0) = 0$, the expression can be simplified to:

$$\psi_{x=0} = B\cos(0) = B(1) = 0$$

Now we can see that there is only one possible value for the constant, B, that would allow this expression to be true, $B = 0$. And since B is constant then it will always be zero despite the value of x. This simplifies our 1-D wavefunction:

$$\psi = A\sin(rx) \tag{2.2.1.5}$$

The case where $x = a$ can help us find the value for A. Since the wavefunction must be zero where $x = a$:

$$\psi_{x=a} = A\sin(rx) = A\sin(ra) = 0$$

In this case, A cannot be zero because if both A and B are zero, the wavefunction is zero at all values of x, and so our wavefunction would not exist inside the box. So, let's assume A is not zero. Then, it must be the case that

$$\sin(ra) = 0$$

and then because of the way that $\sin$ functions work, the quantity ra must be an integer value of π if $\sin(ra) = 0$.

$$ra = \pm n\pi$$

where $n = 1, 2, 3...$ any non-zero integer. We can ignore negative values here since both positive and negative values of r will give the same value for $\sin(ra)$. We can then solve for r:

$$r = \frac{n\pi}{a} \tag{2.2.1.6}$$

and substitute the value $r = \frac{n\pi}{a}$ into Equation 2.2.1.5 to get:

$$\psi = A \sin\left(\frac{n\pi x}{a}\right) \tag{2.2.1.7}$$

Recall that the square of the wavefunction (ψ^2) gives the probability of finding the electron anywhere in space. In our model, the probability of finding the particle-wave inside the box is unity (it is 1). Mathematically, this is the normalizing requirement (expressed as $\int \psi_A \psi_A^* d\tau = 1$), which can be solved to find the value of A.

$$A = \sqrt{\frac{2}{a}}$$

Now, we can substitute the value of A into expression 2.2.1.7, and we have a wavefunction that can be visualized using any graphing program/calculator!

$$\psi = \sqrt{\frac{2}{a}} \left(\sin\left(\frac{n\pi x}{a}\right)\right) \tag{2.2.1.8}$$

What is the energy (E) of a particle in the box?

So, now you can see how a 1-D wavefunction can be solved. But how do we find the E of the electron from this? Well, in order to not distract you earlier, we skipped over a very simple way to do this. The E falls right out of the equations you just saw. We can set the two expressions we found above for the constant r, (equations 2.2.1.4 and 2.2.1.6) equal to one another and then solve for E:

$$r = \frac{n\pi}{a} = \sqrt{2mE}\left(\frac{2\pi}{h}\right)$$

$$E = \frac{n^2 h^2}{8ma^2} \tag{2.2.1.9}$$

Expression 2.2.1.9 can be used to calculate the energy of a particle in a one-dimensional box of length a, given its integer energy level, n. Here we can see that the energy is quantized because n is an integer ($n = 1, 2, 3...$). In other words, n is a **quantum number**.

Making sense of the particle in a box: plotting the 1-D ψ and ψ^2.

No matter whether you're dealing with a 1-dimensional or 3-dimensional wave equation, the wavefunction itself (ψ) describes the particle's wave properties. This ψ doesn't have actual physical meaning, so it's hard to imagine what it "looks like" other than just plotting its function. However, the probability of finding the particle-wave at any specific position along the x-axis between $x = 0$ and $x = a$ is more physically meaningful. The probability of finding the particle is proportional to the square of the wave function, which is represented by either ψ^2 or, sometimes, $\psi\psi^*$. The plots of the functions for ψ and ψ^2 for the first three possible values of n are shown below in Figure 2.2.1.2. You could create plots similar to these simply by plotting the function shown in Equation 2.2.1.8 . To plot, you just need to assign a value of n, and it is convenient to assign the length of the box as $a = 1$. The plot generated would have the general ratio of $\frac{x}{a}$ on the x axis, and thus would be relevant for any length box.

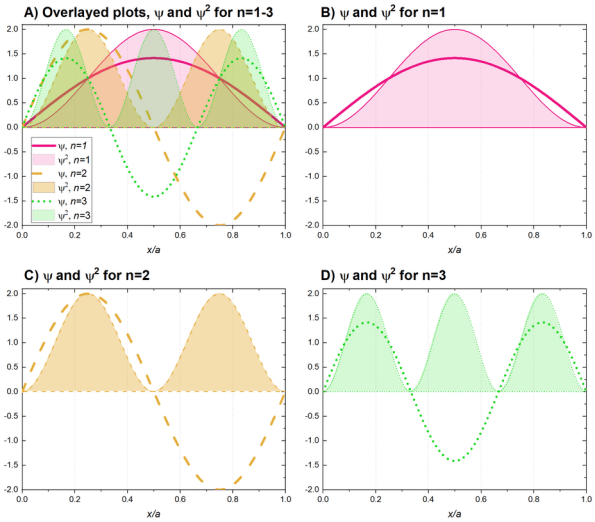


Figure 2.2.1.2. Plots of the 1-D ψ and ψ^2 for $n = 1$, $n = 2$, and $n = 3$ of a box of length a. The wavefunction (ψ) is plotted as a thick solid, dashed, or dotted line. The square of the wavefunction (ψ), which represents the probability of finding the particle at position x, is plotted as the thinner lines and is shaded. Solid lines represent $n = 1$, dashed lines represent $n = 2$, and dotted lines represent $n = 3$. (CC-BY-NC-SA; Kathryn Haas)

The graphs above represent "solutions" to the wave function. For example, the solution $n = 1$ gives the plot shown in Figure 2.2.1.2 B. The solution of $n = 2$ is plotted in Figure 2.2.1.2 C, and so on. These values for n are some of the possible solutions to the 1-dimensional ψ, and they yield descriptions of the wave behavior and probability of finding a particle in 1-dimensional space.

How does this apply to atoms?

The 1-dimensional particle in a box does not represent a real situation; but rather, it is a simple model that we can use to understand a more complex system, like a electron orbiting the nucleus in three dimensions. It's useful to recognize the analogies here that might represent something familiar in a real situation.

$x = 0$ is analogous to the nucleus in an atom. Here in the particle in a box model, $\psi = 0$ and there is zero probability of finding an electron. When this is extended to an atom, this position is analogous to the nucleus (at the origin of a coordinate system where $x = y = z = 0$. A 3-dimensional ψ is also zero at the nucleus and the electron cannot exist there; also, ψ approaches zero as it approaches this position in both the particle in a box model and in a more realistic case of an electron in an atom.

$x = a$ is analogous to a boundary surface far from the nucleus. In the particle in a box model, the 1-dimensional ψ is zero at $x = a$. This is analogous to an electron's ψ approaching zero as it gets further from the nucleus. There will be a more in depth description of boundary surface in the next section (2.2.2). You already know this as the outermost surface of an electron orbital. One minor but notable difference between the 1-dimensional particle in a box and the case of a real atom is that the ψ in three dimensions approaches but never quite reaches zero as distance from the nucleus increases, while $\psi = 0$ for $x = a$ in the more simple case of a 1-dimensional particle in a box.

A change in sign of the ψ (and where both $psi = 0$ and $\psi^2 = 0$) is a node. In both the 1-dimensional particle in a box model and in the more realistic 3-dimensional case, a node is found where the ψ changes sign. At this point, $\psi = \psi^2 = 0$; in other words there is zero probability of finding the particle or electron at these points. It is easy to spot these points in the plots above because the wave function crosses the x-axis and the ψ^2 meets zero.

Exercise 2.2.1.4

Identify the points on plots B, C, and D in Figure 2.2.1.2 that are nodes. How many nodes are there for $n = 1, n = 2$, and $n = 3$?

Answer available at the end of this section.

Exercise 2.2.1.5

Use a graphing program to plot the 1-dimensional ψ and ψ^2 for $n = 1, 2, 3, 4$. How many nodes are there for $n = 4$? Is this expected? Predict how many nodes we should expect for $n = 5$.

You can use any plotting program to do this, and if you aren't familiar with any, try this one: Desmos

Answer available at the end of this section.

In the next section, we will extend these ideas qualitatively to three dimensions. While there is only one quantum number in one dimension, there are three quantum numbers in three dimensions that (when combined) give discrete descriptions of an electron in three-dimensional space (plus a fourth quantum number that explains other properties of the electron).

Answers

Exercise 2.2.1.1

Here is the Hamiltonian Equation for in three dimensions.

$$\hat{H} = \frac{-h^2}{8\pi^2 m}\left(\frac{\partial^2}{\partial x^2} + \frac{\partial^2}{\partial y^2} + \frac{\partial^2}{\partial z^2}\right) - \frac{Ze^2}{4\pi\epsilon_0 r}$$

There are two parts to this equation: the kinetic energy contribution and the potential energy contribution. While the first part of this expression, $\frac{-h^2}{8\pi^2 m}\left(\frac{\partial^2}{\partial x^2} + \frac{\partial^2}{\partial y^2} + \frac{\partial^2}{\partial z^2}\right)$, is the **kinetic energy** contribution, the second part of the expression, $-\frac{Ze^2}{4\pi\epsilon_0 r}$, is the **potential energy (V)** contribution.

(1) Simplify the expression for kinetic energy

Your particle-wave is moving in only one dimension. We can arbitrarily choose the dimension x. This means that x is a variable and will have some value from 0 to a. On the other hand, the particle does not move in the other two dimensions, y and z. You can assign the position of the particle along x and y axes as zero or you can just understand that they do not exist in any significant capacity in our 1-D space. Either way, you can just drop them out of the kinetic energy part of the Hamiltonian, as so:

When $y = z = 0$ and the particle-wave only exists/moves in the x dimension, $\frac{-h^2}{8\pi^2 m}\left(\frac{\partial^2}{\partial x^2} + \frac{\partial^2}{\partial y^2} + \frac{\partial^2}{\partial z^2}\right) = \frac{-h^2}{8\pi^2 m}\left(\frac{\partial^2}{\partial x^2}\right)$

And the overall Hamiltonian is simplified:

$$\hat{H} = \frac{-h^2}{8\pi^2 m}\left(\frac{\partial^2}{\partial x^2}\right) - \frac{Ze^2}{4\pi\epsilon_0 r}$$

(2) Simplify the expression for potential energy (V).

The particle's potential energy inside the box is zero ($V = 0$). Therefore, $V = -\frac{Ze^2}{4\pi\epsilon_0 r} = 0$. We can simply drop the potential energy portion from the Hamiltonian because its value is zero.

The simplified Hamiltonian is now:

$$\hat{H} = \frac{-h^2}{8\pi^2 m}\left(\frac{\partial^2}{\partial x^2}\right)$$

(3) Substitute the simplified Hamiltonian into the Schrödinger Equation.

The Schrödinger is: $\hat{H}\psi = E\psi$

When the simplified Hamiltonian is substituted into this equation, the result is the 1-D Schrödinger Equation 2.2.1.1.

$$\left(\frac{-h^2}{8\pi^2 m}\left(\frac{\partial^2\psi(x)}{\partial x^2}\right)\right) = E\psi$$

Exercise 2.2.1.2**: Prove that Equation** 2.2.1.3 **is true**

You can show that 2.2.1.3 is true by substituting 2.2.1.3 back into Equation 2.2.1.2; in other words take the second derivative of the function, $\psi = A\sin(rx) + B\cos(sx)$ to show that $\frac{\partial^2\psi(x)}{\partial x^2} = -C\psi$. C, r, and s are arbitrary constants, and $r = s$. The actual value of these constants is irrelevant for this problem. Here is one way to approach the problem:

(1) Substitute $\psi = A\sin(rx) + B\cos(sx)$ into $\frac{\partial^2\psi(x)}{\partial x^2} = -C\psi$.

$$\frac{\partial^2}{\partial x^2}\left(A\sin(rx) + B\cos(sx)\right) = -C\psi$$

(2) Take the first and second derivative of $A\sin(rx) + B\cos(sx)$.

The result of taking the first derivative...

$$\frac{\partial}{\partial x}\left(rA\cos(rx) - sB\sin(sx)\right) = -C\psi$$

...and the second derivative...

$$-r^2 A\sin(rx) - s^2 B\cos(sx) = -C\psi$$

This is where we see that the only way $\psi = A\sin(rx) + B\cos(sx)$ is if we can factor the values r^2 and s^2 out of the left side. We have a hint that $r = s$ from the discussion above and Equation 2.2.1.4. Now we see that this is a necessary condition for the expression $-r^2 A\sin(rx) - s^2 B\cos(sx) = -C\psi$ to be true.

(3) Simplify

If $r = s$, then $r^2 = s^2$ and we can replace s with r in the equation above, as so...

$$-r^2 A\sin(rx) - r^2 B\cos(sx) = -C\psi$$

Now, we can factor the constant, $-r^2$ out of the left side of this expression,

$$-r^2\left(A\sin(rx) + B\cos(sx)\right) = -C\psi$$

Now we see that $\psi = A\sin(rx) + B\cos(sx)$ when $-C = -r^2$. In other words, we have shown that $\psi = A\sin(rx) + B\cos(sx)$ is true.

Why is this a useful exercise?

Although it is difficult to explain the derivation of the expression $\psi = A\sin(rx) + B\cos(sx)$ without differential equations and only knowing that $\frac{\partial^2\psi(x)}{\partial x^2} = -C\psi$, to show this is true is as simple as solving this exercise. This exercise is here to help you review your calculus and to show you that the "hand waving" in the text above is not magic, but it is coming from math that you have seen in your calculus courses. Math is crucial for explaining the nature of the universe! Eat your vegetables and practice your math.

Exercise 2.2.1.4

The steps below could be carried out in a different sequence:

(1) Rearrange

Let's move **all constants** to the right side of 2.2.1.1 so that we arrive at the expression that is shown in part of Equation 2.2.1.2 .

$$\frac{\partial^2\psi(x)}{\partial x^2} = \frac{-8\pi^2 m_e E}{h^2}\psi$$

(2) Take the second derivative of ψ, which we found in Exercise 2.2.1.2.

$$\frac{\partial^2\psi(x)}{\partial x^2} = -r^2\left(A\sin(rx) + B\cos(sx)\right) = \frac{-8\pi^2 m_e E}{h^2}\psi$$

And since $\psi = A\sin(rx) + B\cos(sx)$, we can simplify this by dividing both sides by ψ (or by $A\sin(rx) + B\cos(sx)$).

**recall that $s = r$. So, you could have substituted r for s in the expression above, and you'd still be on the right track.*

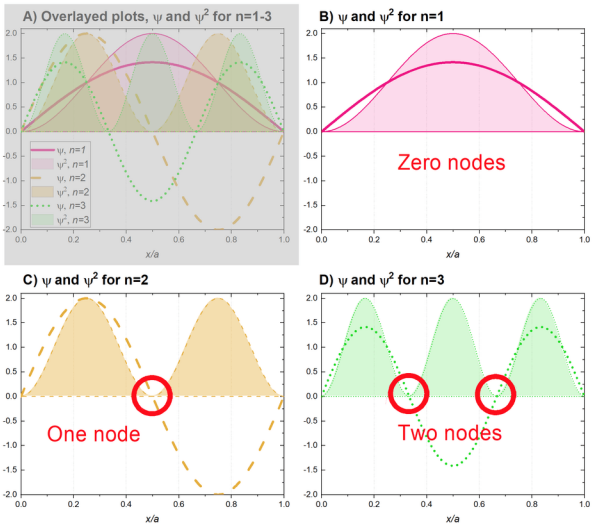
$$-r^2 = \frac{-8\pi^2 m_e E}{h^2}$$

(3) Solve for r (*we already showed $r = s$ in the Exercise 2.2.1.2).

$$r = \sqrt{\frac{8\pi^2 m_e E}{h^2}} = \frac{2\pi}{h}\sqrt{2m_e E}$$

Exercise 2.2.1.4

The nodes are annotated with red circles on the figure below. **Panel B** ($n = 1$) has zero nodes. There are two points where $\psi = 0$ in the case of $n = 1$, but these points are at the walls of the box and they are not nodes. The walls of the box are analogous to the nucleus and the boundary surface of an electron orbital. **Panel C** ($n = 2$) has one node where the ψ crosses zero. **Panel D** ($n = 3$) shows two nodes.



Exercise 2.2.1.5

You can use any plotting program to do this. This is the function you should plot (it is Equation 2.2.1.8):

$\psi = \sqrt{\frac{2}{a}}\left(\sin\left(\frac{n\pi x}{a}\right)\right)$

For n=1: Assign a value of $n = 1$, as stated in the problem. In the text above, it also states that it is convenient to assign a value of $a = 1$. Assigning these values results in the following function:

$\psi = \sqrt{\frac{2}{1}}\left(\sin\left(\frac{1\pi x}{1}\right)\right)$ and simplifying leads to $\psi = \sqrt{2}\left(\sin\left(\pi x\right)\right)$

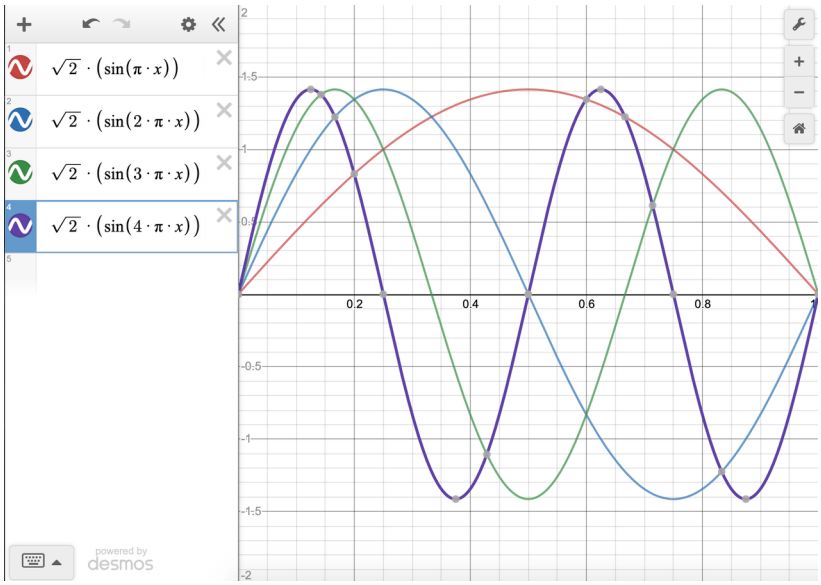
For n=2,3,4 you would repeat the process above. You will get the following functions:

For n=2: $\psi = \sqrt{2}\left(\sin\left(2\pi x\right)\right)$

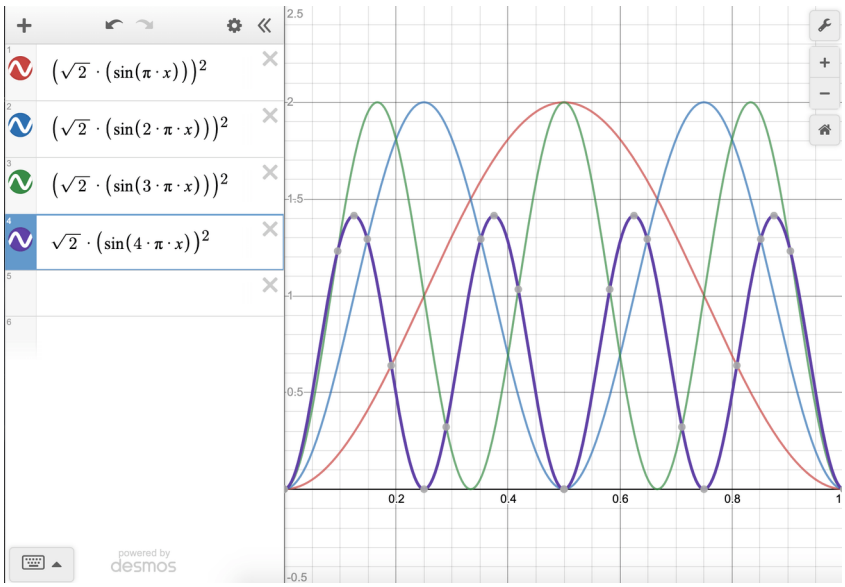
For n=3: $\psi = \sqrt{2}\left(\sin\left(3\pi x\right)\right)$

For n=4: $\psi = \sqrt{2}\left(\sin\left(4\pi x\right)\right)$

In a program like Desmos, you need to input the function correctly. It's useful to know the code for at least one graphing program. For Desmos, and most others, you can find help online. For example, the correct input for Desmos for the n=4 case is sqrt(2)*(sin(4*pi*x)). But, you have to type it in because copy/paste doesn't work. You'll also want to display your graph only from $x = 0$ to $x = 1$ by hitting the settings button (a little wrench in the upper right corner) and changing the x scale. Go ahead and change the y scale too, to $y = -2$ to $y = 2$. If you do this, you should get something that looks like this:



To graph the square of each wavefunction, you'd just square the functions that we just plotted:



In both the case of ψ and ψ^2, the $n = 4$ function shows three nodes (see the bolded purple line, where nodes are tiny grey spots on the axis). This follows a pattern that you might have noticed with the cases of $n = 1, 2,$ and 3 where the number of nodes is $n - 1$ (nodes = $n - 1$). We should expect three nodes for $n = 4$ based on this pattern, and four nodes for $n = 5$.

This page titled 2.2.1: Particle in a Box is shared under a CC BY-NC-SA 4.0 license and was authored, remixed, and/or curated by Kathryn Haas.

- 2.2.1: Particle in a Box by Kathryn Haas is licensed CC BY-NC-SA 4.0.

2.2.2: Quantum Numbers and Atomic Wave Functions

The one-dimensional particle in a box model from the previous section shows us how a wavefunction works in one dimension (the x- dimension). In one dimension, the wavefunction requires only one quantum number, n. A full explanation of the three-dimensional wavefunction for an electron is outside of the scope of this course. Instead, we will focus on gaining a conceptual understanding by extending knowledge of the one-dimensional wavefunction to a three-dimensional space.

Quantum numbers

Extending the wavefunction to three dimensions requires a total of three quantum numbers. In addition to n, which we saw in the one-dimensional case, we also need l and m_l to express the wavefunction in three dimensions. A complete solution to the Schrödinger equation, both the three-dimensional wavefunction and energy, includes a set of three quantum numbers (n, l, m_l). The wavefunction describes what we know as an atomic orbital; it defines the region in space where the electron is located. Additionally, there is a fourth quantum number, m_s. The m_s quantum number accounts for the observed interaction of electrons with an applied magnetic field; it is an additional postulate that is not part of the wavefunction. These four quantum numbers are described below.

The quantum number, n: This is the principle quantum number. This number represents the shell, including both the overall energy of the electron in that shell and the size of that shell. An allowed value for n is any non-zero, positive integer (1, 2, 3, 4, ... etc are allowed, but 4.1 is not allowed).

The quantum number, l: This is the angular momentum quantum number that corresponds to the subshell and its shape. It represents the angular dependence of the subshell, or the "shape" of the orbitals within a subshell. The allowed values of l depend on n. The allowed values of l for an electron in shell n are integer values between 0 to $n-1$, or $l = 0 \rightarrow n-1$. These values correspond to the orbital shape where $l = 0$ is an s-orbital, $l = 1$ is a p-orbital, $l = 2$ is a d-orbital, and $l = 3$ is an f-orbital.

The quantum number m_l: This is the magnetic quantum number. Its possible values give the number of orbitals within a subshell and its specific value gives the orbital's orientation in space. The allowed values of m_l depend on the value of l. The value of m_l is allowed to be any positive or negative integer between $+l$ and $-l$. In other terms, $m_l = +l \rightarrow -l$. For example, if the electron is in a 3-p-orbital, then $n = 3, l = 1$, and the possible values of m_l are $-1, 0,$ and $+1$. Since there are three possible values of m_l there are three orbitals in the p subshell. The specific m_l value defines in which of the three possible p-orbitals (p_x, p_y, or p_z) the electron exists. In the case of the s subshell, there is only one value, $m_l = 0$ because $l = 0$. The one value corresponds to the fact that there is only one s orbital in any shell.

The quantum number m_s: This quantum number accounts for the electron's "spin". In short, electrons interact with magnetic fields in a way that is similar to how a tiny bar magnet would interact with a magnetic field. The allowed values for m_s are $+\frac{1}{2}$ and $-\frac{1}{2}$.

Table 2.2.2.1. Quantum Numbers

SYMBOL	NAME	VALUES	MEANING
n	principal	$1, 2, 3...$(any integer)	energy level, shell
l	angular momentum	$0 \rightarrow n-1$	subshell, $0 = s, 1 = p, 2 = d, 3 = f...$ this is the angular dependence of the orbital, shape of the orbital *letters have historical meaning, sharp, principle, diffuse, fundamental
m_l	magnetic	$+l \rightarrow -l$	orientation of angular momentum in space, orbital
m_s	spin	$+\frac{1}{2}, -\frac{1}{2}$	the imaginary property we call "spin", up or down

1-Electron Wavefunctions (Atomic orbitals)

One simplified representation of the three-dimensional wavefunction is shown below. This representation breaks the wavefunction into two parts: the **radial contribution** ($R_{n,l}(r)$) and the **angular contribution** ($Y_{l,m_l}(\theta,\phi)$).

$$\psi_{(n,l,m_l)} = R_{n,l}(r) \times Y_{l,m_l}(\theta,\phi) \tag{2.2.2.1}$$

Allowed Energies

From the wavefunction, we can find the allowed energies of an electron in an atom. We have not given you the more complex form of the wavefunction where you'd need to derive 2.2.2.2 from 2.2.2.1 because it is outside the scope of this course. Instead, consider the process that we used to derive the energy of a particle in a one-dimensional box in the previous section. A similar process can be used to find the energy of an electron in three dimensions, shown in 2.2.2.2.

$$E_n = -\frac{hcRZ^2}{n^2} = -(13.607\,eV)\left(\frac{Z}{n}\right)^2 \tag{2.2.2.2}$$

,

where n is the principle quantum number, h is Planck's constant, c is the speed of light, R is the Rydberg constant, and Z is the charge of the nucleus. It is useful to know that the value of $hcR = 13.6eV$. This is also the value of the ionization energy of an electron in a hydrogen atom. This equation only works for **hydrogenic atoms** (atoms or ions that are "like" hydrogen in that they have only one electron).

Exercise 2.2.2.1

The energy that it takes to eject a ground-state electron from a hydrogen atom (its ionization energy, IE) is measured to be approximately 13.6 eV, while the IE energy of a He^+ ion is four times greater at 54.4 eV. These values can be predicted using both Equation 2.2.2.2 and the Rydberg equation.

a. Using Equation 2.2.2.2 for allowed energies of electrons in a hydrogen atom, derive the energy of the ground state electron in H. Then repeat this process for a He^+ ion. What do the values indicate about the relative attraction between an electron and the nuclei of these two hydrogenic atoms?
b. Show that the IE of H's 1s electron can also be predicted by the Rydberg formula (equation 2.1.2.2).

Answer (a) available at the end of this section.

Answer (b) available at the end of this section.

Exercise 2.2.2.2

Which of the following are hydrogenic atoms? H, H^+, H^-, He, He^{2+}, He^+, He^-, Li, Li^{3+}, Li^{2+}, Li^+, Li^- .

Answer available at the end of this section.

Radial and Angular contributions to the wavefunction:

Radial contribution, $R_{n,l}(r)$

The radial part of the wavefunction, $R_{n,l}(r)$ gives the radial variation of ψ. In other words, $R_{n,l}(r)$ defines how the wavefunction depends on the distance of the electron from the nucleus (the radius). The $R_{n,l}(r)$ parts of the wavefunction for a hydrogenic atom are listed in Table 2.2.2.2, and they are plotted in Figure 2.2.2.1. Notice that the $R_{n,l}(r)$ of all s-orbitals (solid lines) reaches a maximum at $r = 0$. This is unique to the s-orbitals' $R_{n,l}(r)$. The $R_{n,l}(r)$ of p- and d-orbitals orbitals approaches zero as r approaches zero. This has important consequences for how closely an electron in these orbitals can approach the nucleus.

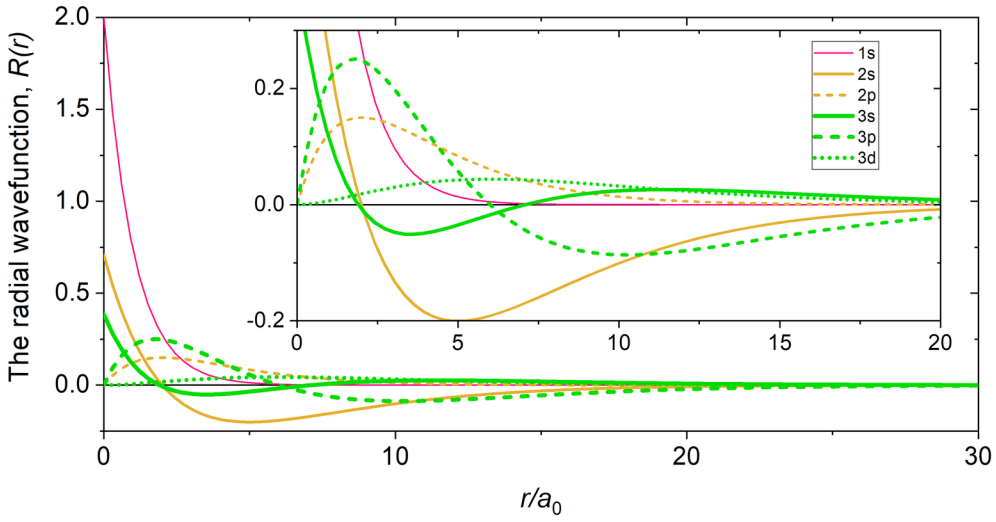


Figure 2.2.2.1. Plots of the radial wavefunction, $R_{n,l}(r)$, for the first three shells. The wavefunctions are plotted relative to $\frac{r}{a_0}$, where $a_0 = 52.9pm = 0.529\mathring{A}$ is the Bohr Radius (the radius of a hydrogen 1s orbital). The expressions for these radial wavefunctions ($R_{n,l}(r)$) are shown in Table 2.2.2.2. (Kathryn Haas; CC-NC-BY-SA)

Table 2.2.2.2. Radial wavefunctions ($R(r)$) for the first three shells of a hydrogen atom. Z is the nuclear charge, and $a_0 = 52.9pm = 0.529\mathring{A}$ is the Bohr radius (the radius of a hydrogen 1s orbital). For the H atom, $Z = 1$ (the nuclear charge of hydrogen). Plotting of the functions can be simplified if we set $a_0 = 1$ and plot the functions with respect to r/a_0, which was done to find the plots shown in Figure 2.2.2.1.

Orbital	n	l	$R_{n,l}(r)$
1s	1	0	$2\left[\frac{Z}{a_0}\right]^{3/2} e^{-Zr/a_0}$
2s	2	0	$2\left[\frac{Z}{2a_0}\right]^{3/2}\left(2-\frac{Zr}{a_0}\right) e^{-Zr/2a_0}$
2p	2	1	$\frac{1}{\sqrt{3}}\left[\frac{Z}{3a_0}\right]^{3/2}\left(\frac{Zr}{a_0}\right) e^{-Zr/2a_0}$
3s	3	0	$\frac{2}{27}\left[\frac{Z}{3a_0}\right]^{3/2}\left(27-18\frac{Zr}{a_0}-2(\frac{Zr}{a_0})^2\right) e^{-Zr/3a_0}$
3p	3	1	$\frac{1}{81\sqrt{3}}\left[\frac{2Z}{a_0}\right]^{3/2}\left(6-\frac{Zr}{a_0}\right)(\frac{Zr}{a_0}) e^{-Zr/3a_0}$
3d	3	2	$\frac{1}{81\sqrt{15}}\left[\frac{2Z}{a_0}\right]^{3/2}\left(\frac{Zr}{a_0}\right)^2 e^{-Zr/3a_0}$

Radial probability function, $4\pi r^2(R_{n,l}(r))^2$

Just like in the particle-in-a-box model, the square of the wavefunction is proportional to the probability of finding a particle (electron) at some point in space. The square of the radial part of the wavefunction is called the radial distribution function $4\pi r^2(R_{n,l}(r))^2$, and it describes the probability of locating the electron at some distance r away from the nucleus. When we normalize the probability functions by dividing the function by its integral over all space, we get the plots shown in Figure 2.2.2.2. The normalized probability functions are compared to the original radial part of the wavefunctions in Figure 2.2.2.3. The most probable distance for finding an electron is shown by the maximum value of the function. For an electron in the 1s orbital of H, the most probable distance from the nucleus occurs at $r = 1a_0$. This is the Bohr Radius, and it has a value of $a_0 = 52.9pm = 0.529\mathring{A}$. It is convenient to plot the functions of the hydrogen atomic orbitals relative to the size of its smallest orbital, the 1s orbital; this is the reason we plot $R_{n,l}(r)$ and $4\pi r^2(R_{n,l}(r))^2$ relative to $\frac{r}{a_0}$.

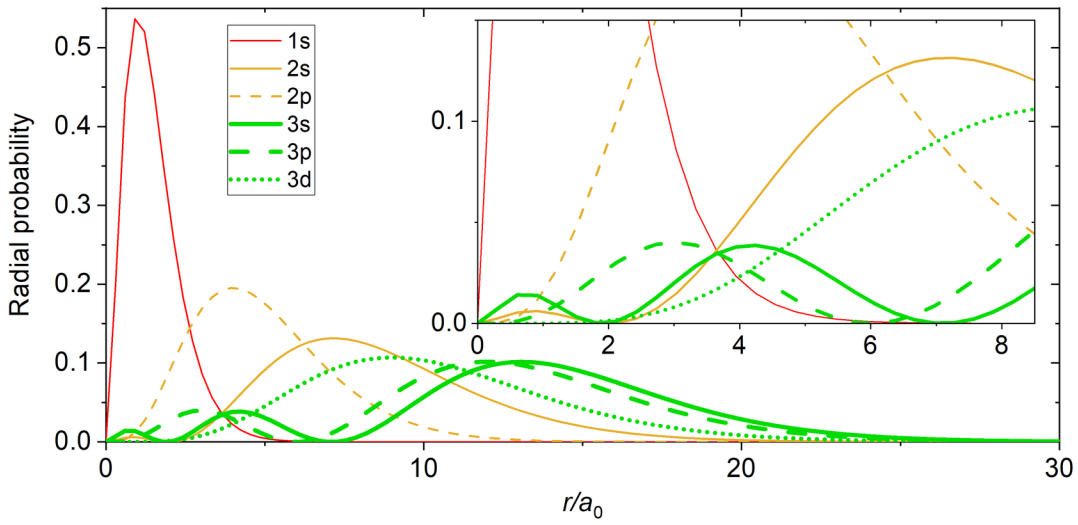


Figure 2.2.2.2: Plots of the normalized radial probability functions for the first three shells. The radial wavefunctions ($R_{n,l}(r)$) are shown in Table 2.2.2.2. (Kathryn Haas; CC-NC-BY-SA)

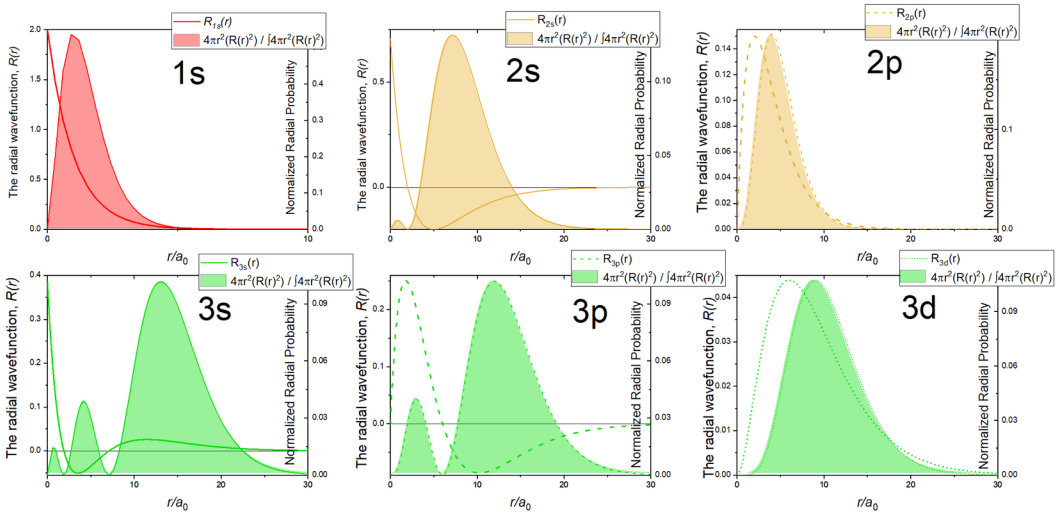


Figure 2.2.2.2. Plots of the normalized radial probability function for each orbital in the first three shells (shaded curves). The radial wavefunctions are also shown (Table 2.2.2.2). The y-axis on the left of each plot corresponds to the radial wavefunction (line); the y-axis on the right of each plot corresponds to the radial probability function (shaded). (Kathryn Haas; CC-NC-BY-SA)

Radial nodes

From the discussion of the 1-dimensional particle in a box, we learned that nodes exist where $\psi = 0$. In the case of the 3-dimensional wavefunction, there are two different types of nodes: radial nodes and angular nodes. **Radial nodes occur where the radial part of the wavefunction is zero ($R(x) = 0$)**. These are easy to find by plotting the radial part of the wavefunction and finding where the radial part of the wavefunction (and the radial probability function) is zero (where $R_{n,l}(r) = 0$) and where $4\pi r^2 (R_{n,l}(r))^2 = 0$. These nodes are spherical in shape and depend on the energy level and subshell (the values of n and l). **The number of radial nodes is** $n - l - 1$. An example of a radial node is the single node that occurs in the $2s$ orbital ($2 - 0 - 1 = 1$ node). In contrast, the 1s orbital has zero radial nodes ($1 - 0 - 1 = 0$ nodes). Where there is a node, there is zero probability of finding an electron.

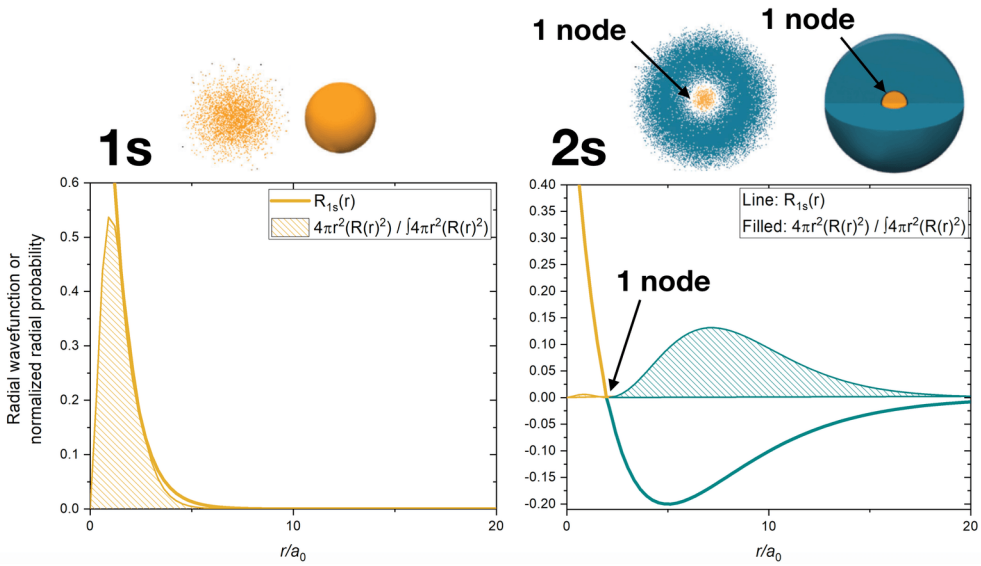


Figure 2.2.2.3: Visualization of the 1s and 2s atomic orbitals. Each orbital is shown as both an electron probability density plot and a contour plot above its wavefunction and probability density function. The 1s orbital has zero radial nodes. The 2s orbital has one radial node where its wavefunction changes sign and its radial probability function is zero. (Kathryn Haas; CC-BY-SA)

Boundary surfaces

A true node occurs where the probability of finding an electron is zero. Nodes occur where $\psi = \psi^2 = 0$. Far from the nucleus, the probability of finding the electron rapidly approaches zero, but is never *exactly* zero. What this means is that it is rather improbable to find the electron at far distances from the nucleus, but it's not impossible. The rapid fall of probability creates a boundary surface rather than a node. The boundary surface represents the area around the nucleus where the electron exists most of the time.

Exercise 2.2.2.1

How many radial nodes are in the s, p, d, and f orbitals in the first four shells? $n = 1, 2, 3, 4$?

Answer available at the end of this section.

Exercise 2.2.2.1

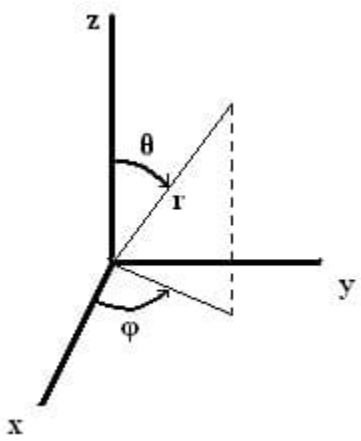
Draw a rough plot of the following:

a. The radial wavefunction, $R_{n,l}(r)$ and the probability density function, $4\pi r^2(R_{n,l}(r))^2$, for the 1s orbital.
b. The radial wavefunction, $R_{n,l}(r)$ and the probability density function, $4\pi r^2(R_{n,l}(r))^2$, for the 4s orbital.

Answer, 1s available at the end of this section.

Answer, 4s available at the end of this section.

Angular contribution, $Y_{l,m_l}(\theta,\phi)$, and angular probability function, $(Y_{l,m_l}(\theta,\phi))^2$



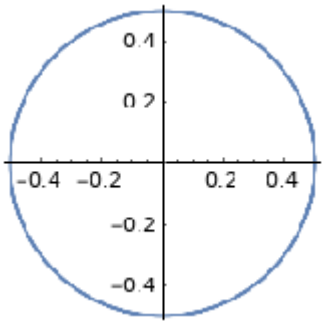
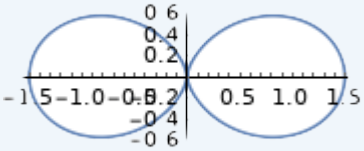
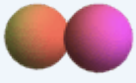
The angular contribution to the wavefunction, $Y_{l,m_l}(\theta,\phi)$, describes the wavefunction's shape, or the angle with respect to a coordinate system. To describe the direction in space, we use spherical coordinates that tell us distance *and* orientation in 3-dimensional space. There are three spherical coordinates: r, ϕ, and θ. r is the radius, or the actual distance from the origin. ϕ and θ are angles. ϕ is measured from the positive x axis in the xy plane and may be between 0 and 2π. θ is measured from the positive z axis towards the xy plane and may be between 0 and π.

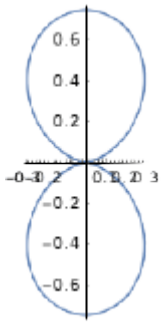
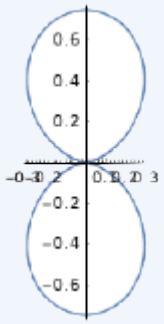
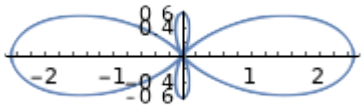
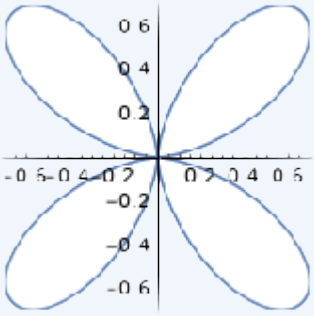
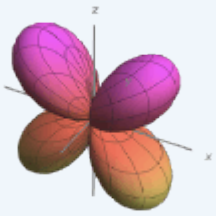
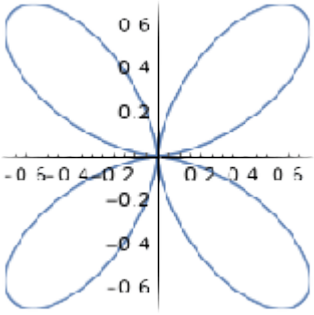
$$Y_{l,m_l}(\theta,\phi) = \left(\frac{1}{4\pi}\right)^{1/2} y(\theta,\phi)$$

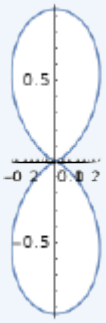
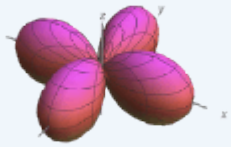
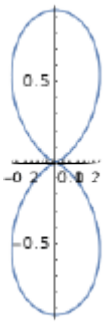
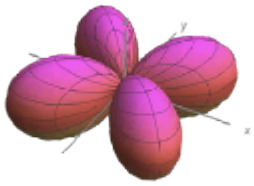
$Y_{l,m_l}(\theta,\phi)$, is slightly more difficult to describe than the radial contribution was. This is partly because $Y_{l,m_l}(\theta,\phi)$ contains imaginary numbers, which have no real, physical meaning. However, the angular part of the wavefunction becomes more "real" when you square it to get angular probability density, a more tangible concept described as the **shapes of orbitals**.

The values of θ, ϕ, and $y(\theta,\phi)$ for orbitals in the hydrogen atom are listed in Table 2.2.2.3. But $Y_{l,m_l}(\theta,\phi)$ is only a mathematical function and has no real physical meaning. The square of the radial wavefunction, $Y_{l,m_l}(\theta,\phi)^2$, gives the probability of finding the electron at a point in space on a ray described by (ϕ,θ). Thus $Y_{l,m_l}(\theta,\phi)^2$ describes the shape of the orbital.

Table 2.2.2.3. Components of the angular wavefunction and the resulting orbital shapes. The plots in the two right hand columns were created using Desmos and Mathematica: specifically "Spherical Harmonics" from the Wolfram Demonstrations Project, http://demonstrations.wolfram.com/SphericalHarmonics/ and "Visualizing Atomic Orbitals" demonstrations.wolfram.com/Vi...tomicOrbitals/.

subshell	m_l (orbital)	θ	ϕ	Plots of θ^2	orbital shapes
$l=0$, s	$m_l=0$	$\frac{1}{\sqrt{2}}$	$\frac{1}{\sqrt{2\pi}}$		
$l=1$, p	$m_l=0$	$\frac{\sqrt{6}}{2}\cos\theta$	$\frac{1}{\sqrt{2\pi}}$		

subshell	m_l (orbital)	θ	ϕ	Plots of θ^2	orbital shapes
$l = 1$, p	$m_l = +1$	$\frac{\sqrt{3}}{2}\sin\theta$	$\frac{1}{\sqrt{2\pi}}e^{i\phi}$		
$l = 1$, p	$m_l = -1$	$\frac{\sqrt{3}}{2}\sin\theta$	$\frac{1}{\sqrt{2\pi}}e^{-i\phi}$		
$l = 2$, d	0	$\frac{\sqrt{10}}{4}\left(3\cos^2\theta - 1\right)$	$\frac{1}{\sqrt{2\pi}}$		
$l = 2$, d	$m_l = +1$	$\frac{\sqrt{15}}{2}\sin\theta\cos\theta$	$\frac{1}{\sqrt{2\pi}}e^{i\phi}$		
$l = 2$, d	$m_l = -1$	$\frac{\sqrt{15}}{2}\sin\theta\cos\theta$	$\frac{1}{\sqrt{2\pi}}e^{-i\phi}$		

subshell	m_l (orbital)	θ	ϕ	Plots of θ^2	orbital shapes
$l = 2$, d	$m_l = +2$	$\frac{\sqrt{15}}{4}\sin^2\theta$	$\frac{1}{\sqrt{2\pi}}e^{i2\phi}$		
$l = 2$, d	$m_l = -2$	$\frac{\sqrt{15}}{4}\sin^2\theta$	$\frac{1}{\sqrt{2\pi}}e^{-i2\phi}$		

Angular nodes

Angular nodes exist where $(Y_{l,m_l}(\theta,\phi))^2 = 0$. These nodes are planar in shape, and they depend on the value of l. The number of angular nodes in any orbital is equal to l. This means that s-orbitals ($l = 0$) have zero angular nodes, p-orbitals ($l = 1$) have one angular node, d-orbitals ($l = 2$) have two angular nodes, and so on. Planar nodes can be flat planes (like the nodes in all p orbitals) or they can have a conical shape, like the two angular nodes in the d_{Z^2} orbital. Angular nodes in some p and d orbitals are shown in Figure 2.2.2.4.

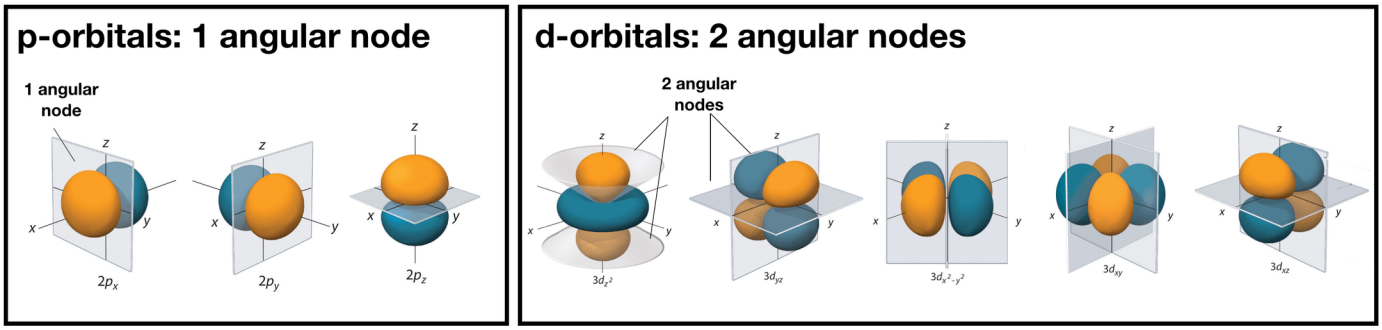
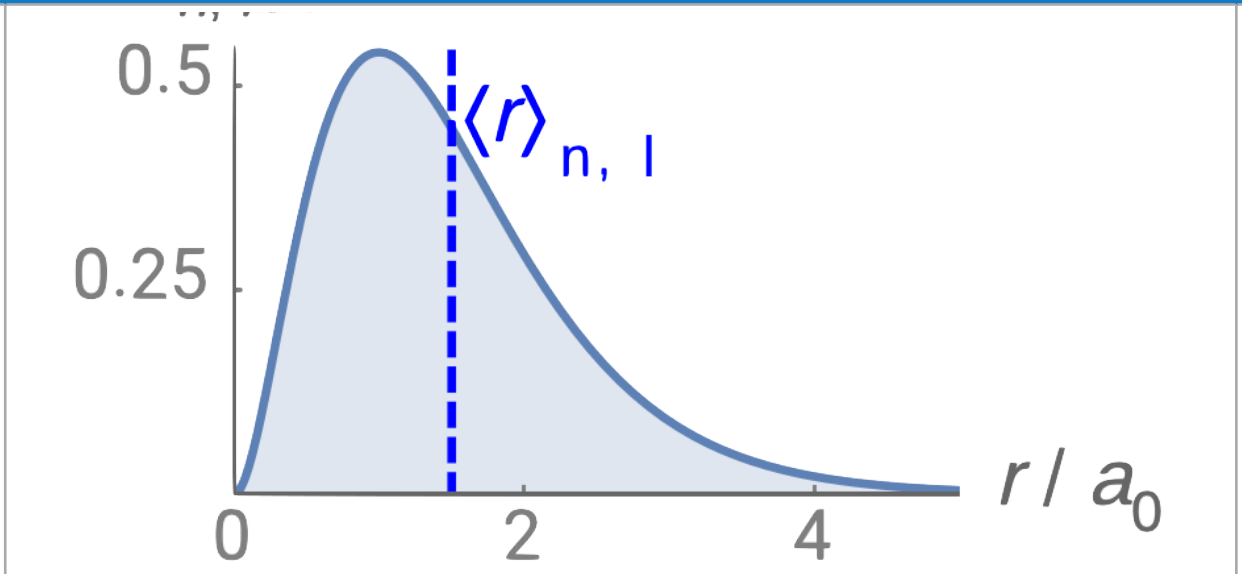
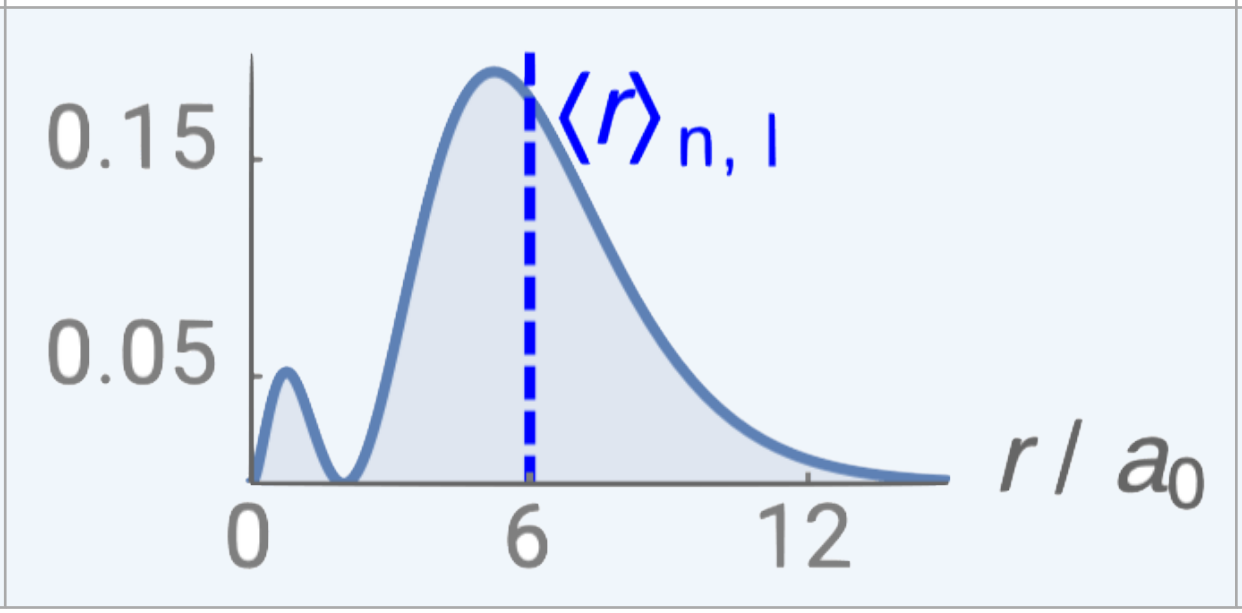


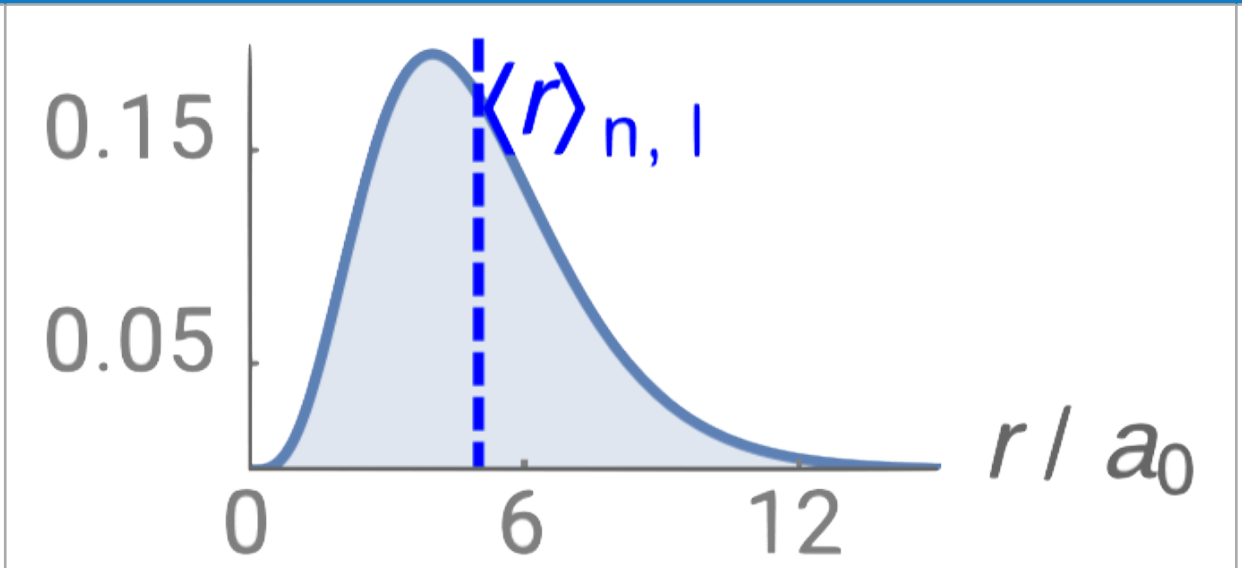
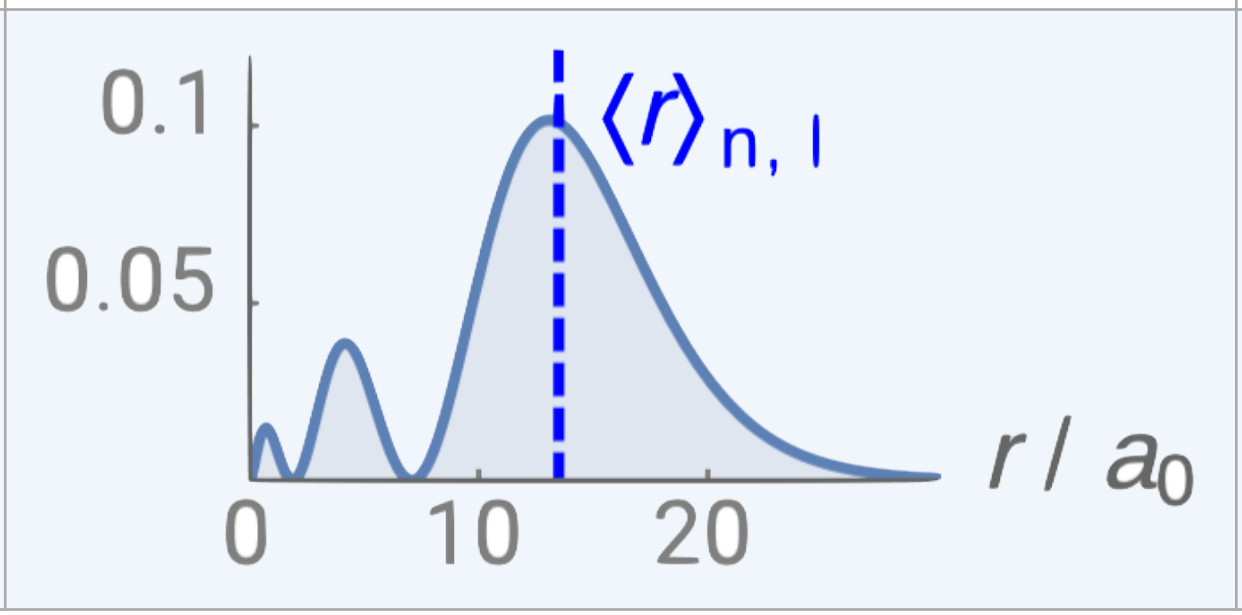
Figure 2.2.2.4: The angular nodes in p-orbitals and d-orbitals are shown. Every p orbital has one angular node, and every d orbital has two angular nodes. The number of angular nodes in any orbital is equal to the value of the quantum number, l. (CC BY-NC-SA; anonymous by request)

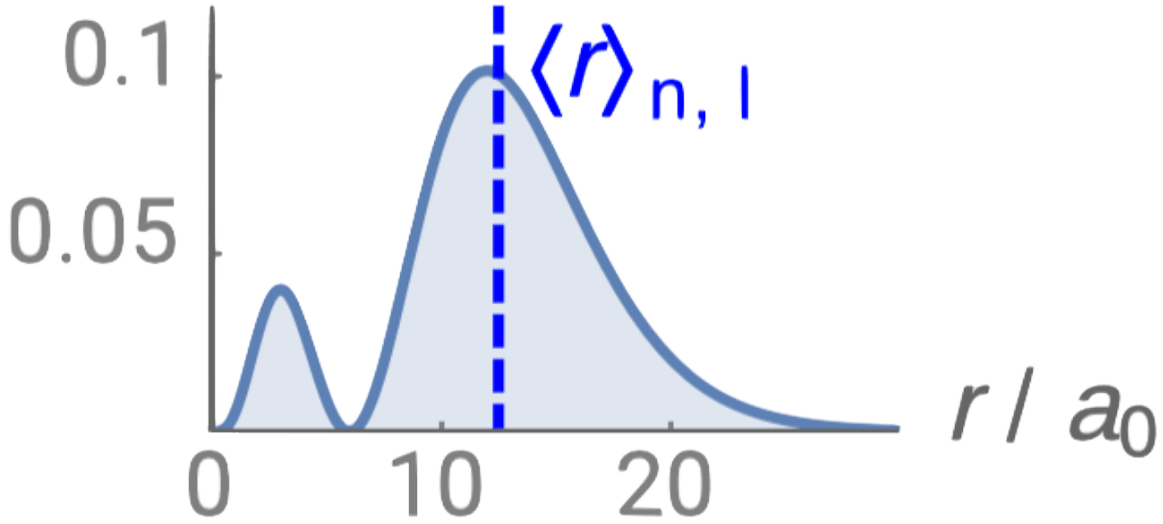
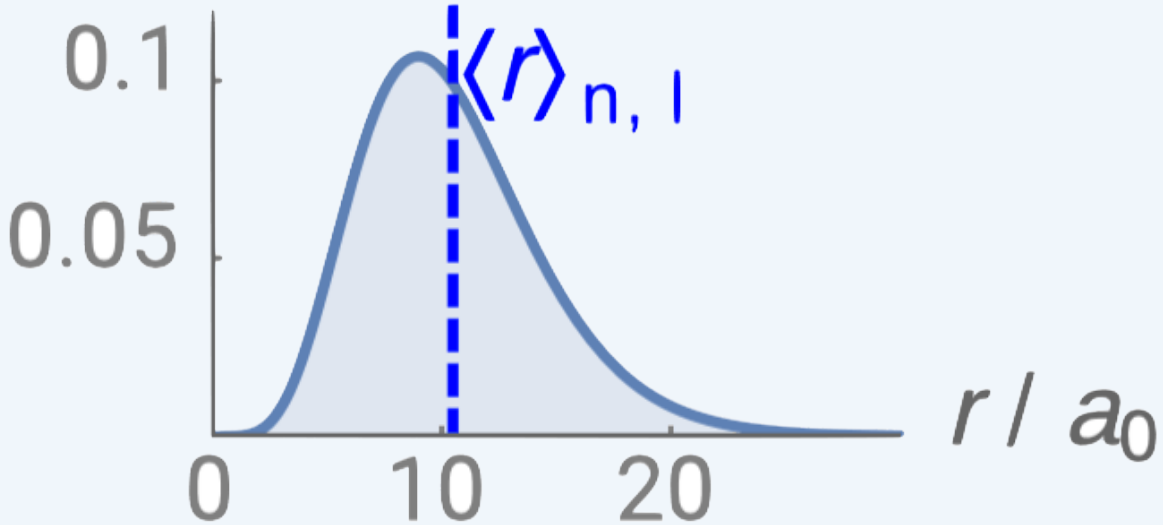
Atomic Orbitals

Atomic orbitals result from a combination of both the radial and angular contributions of the wavefunction. Atomic orbitals can have both angular nodes and radial nodes, depending on the values of n and l.

The chart below compares the radial variation, angular variation, and their combinations (orbitals).

Orbital	Radial Probability	Radi Nod
1s		0
2s		1

Orbital	Radial Probability	Radi Node
2p		0
3s		2

Orbital	Radial Probability	Radi Nod
3p		1
3d		0

Answers

Exercise 2.2.2.1

Use Equation 2.2.2.2 . For a hydrogen atom with one proton, $Z = 1$, and the ground state energy level is the lowest energy level, $n = 1$. Therefore, the energy of an electron in the ground state of a H atom is:

$E_n = -\frac{hcRZ^2}{n^2} = -13.607\ eV(\frac{1}{1})^2 = -13.607\ eV$, or *approximately* $-13.6\ eV$. Thus, the IE (energy necessary to remove that electron) is +13.6 eV.

We can use the same process to find the ground state energy of an electron in He^+. This time, $Z = 2$ because helium has two protons in its nucleus, and as before, the ground state is $n = 1$.

$E_n = -\frac{hcRZ^2}{n^2} = -13.607\ eV(\frac{2}{1})^2 = -54.428eV$, or *approximately* $-54.4\ eV$. Thus, the IE is +54.4 eV.

These ground-state energies are the same as the energy required to remove the ground state electron from H and He^+. In other words, these are the predicted ground state IE values for one electron in H and He^+. The *measured* IEs for these two species are in fact 13.6 eV and 54.4 eV, respectively.

The He^+ ion has a more negative value for its ground state energy with a magnitude four times greater than that of the ground state H electron. This means that

the He^+ electron is more strongly attracted to the (+2) nucleus than the H electron is attracted to the (+1) nucleus, and more energy is required to eject the He^+ electron than the H electron. It takes more energy to remove the electron from He^+ than from H. This makes sense in light of Coulomb's law: The attractive force between the H nucleus (+1) and an electron (-1) would be weaker than that of a He nucleus (+2) and an electron (-1) because the positive charge of the He nucleus has a greater magnitude.

Exercise 2.2.2.1

The Rydberg equation is: $\frac{1}{\lambda} = E(cm^{-1}) = R_H \left(\frac{1}{n_l^2} - \frac{1}{n_h^2}\right)$ where n_l and n_h are positive integers, $n_h > n_l$, and the *Rydberg constant* (R_H), has a value of 1.09737 × $10^7 m^{-1}$. We should set $n_l = 1$ to represent the initial ground state, and $n_h = \infty$ to represent the removal of the electron from the atom.

Step 1.

Calculate Energy (in m^{-1}) using the Rydberg equation:

$E = R_H \left(\frac{1}{n_l^2} - \frac{1}{n_h^2}\right) = 1.09737 \times 10^7 m^{-1} \left(\frac{1}{1^2} - \frac{1}{\infty^2}\right) = 1.09737 \times 10^7 m^{-1} (1 - 0) = 1.09737 \times 10^7 m^{-1}$

Ultimately, we want a value of energy in units of eV so we can compare it to the answers in part (a), but our value here is in units of inverse meters (m^{-1}). A quick internet search can tell you the conversion between inverse centimeters (cm^{-1}) and eV is $1eV = 8065.6cm^{-1}$.

Step 2.

Convert from m^{-1} to cm^{-1} to eV so that we can compare to the answer in part (a):

$1.09737 \times 10^7 \frac{1}{m} \times \frac{1m}{100cm} \times \frac{1eV}{8065.6 \frac{1}{cm}} = 13.6056eV$, or approximately 13.6 eV.

Exercise 2.2.2.2

Hydrogenic atoms are atoms or ions that contain only one electron. H, He^+, and Li^{2+} are hydrogenic atoms/ions that contain only one electron.

Exercise 2.2.2.1

You can approach this answer by using the mathematical relationship between the number of radial nodes and the values of n and l: **number of radial nodes is** $n - 1 - l$. You could also notice the pattern that the first orbital of any type (1s, 2p, 3d...) has zero radial nodes, the second orbital of a type (2s, 3p, 4d...) has one radial node, the third orbital of a type has two radial nodes (3s, 4p, 5d...)...etc.

A full list of all of the orbitals in the first four shells and their number of radial nodes is below. It's a good idea to prove to yourself that the numbers given below are consistent with the plots of the orbitals' wavefunctions for those orbitals in the first three shells:

s-orbitals:

1s: $n - 1 - l = 1 - 1 - 0 = 0$, zero radial nodes

2s: $n - 1 - l = 2 - 1 - 0 = 1$, one radial node

3s: $n - 1 - l = 3 - 1 - 0 = 2$, two radial nodes

4s: $n - 1 - l = 4 - 1 - 0 = 3$, three radial nodes

p-orbitals

2p: $n - 1 - l = 2 - 1 - 1 = 0$, zero radial nodes

3p: $n - 1 - l = 3 - 1 - 1 = 1$, one radial node

4p: $n - 1 - l = 4 - 1 - 1 = 2$, two radial nodes

d-orbitals

3d: $n - 1 - l = 3 - 1 - 2 = 0$, zero radial nodes

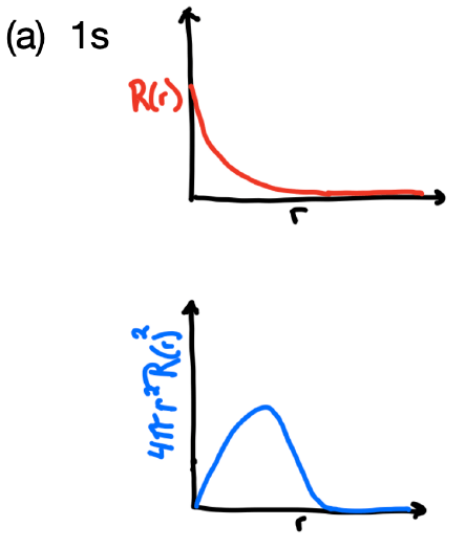
4d: $n - 1 - l = 4 - 1 - 2 = 1$, one radial nodes

f-orbital

4f: $n - 1 - l = 4 - 1 - 3 = 0$, zero radial nodes

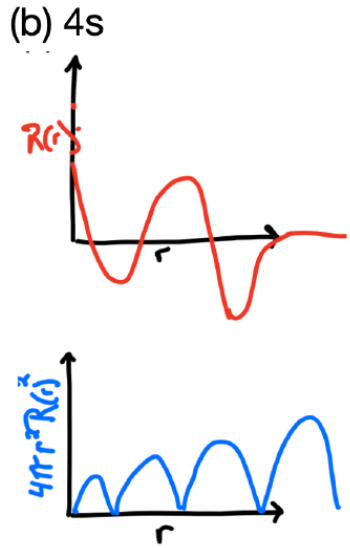
Exercise 2.2.2.1

The 1s orbital's $R_{n,l}(r)$ reaches a maximum near the origin and approaches zero far from the nucleus. The $4\pi r^2 (R_{n,l}(r))^2$ approaches zero at the origin, has a maximum intensity at the Bohr radius, and approaches zero far from the nucleus (its boundary surface).



Exercise 2.2.2.1

Like all s orbitals, the 4s orbital's $R_{n,l}(r)$ reaches a maximum near X=0, but it would be less intense than the function of the 1s, 2s, and 3s orbitals. It should have three radial nodes and so its wavefunction would change sign three times. This would give four regions of electron density in the probability function while the function would approach zero (boundary surface) far from the nucleus.



This page titled 2.2.2: Quantum Numbers and Atomic Wave Functions is shared under a CC BY-NC-SA 4.0 license and was authored, remixed, and/or curated by Kathryn Haas.

- 2.2.2: Quantum Numbers and Atomic Wave Functions by Kathryn Haas is licensed CC BY-NC-SA 4.0.

2.2.3: Aufbau Principle

Introduction

The **Aufbau Principle** (also called the **building-up principle** or the **Aufbau rule**) states that, in the ground state of an atom or ion, electrons fill atomic orbitals of the lowest available energy level before occupying higher-energy levels. In general, an electron will occupy an atomic orbital with the lowest value of n, l, m_l, in that order of priority. The value of m_s for an unpaired electron is conventionally assigned a value of $+\frac{1}{2}$. Each electron in an atom/ion must have a unique set of values for all four quantum numbers.

The Ground State of Hydrogenic Atoms/Ions

In a hydrogenic atom/ion, there is only one electron. In this case, the *only factor determining energy is the value of* n. The ground state will always be the 1s orbital ($n = 1, l = 0, m_l = 0, m_s = +\frac{1}{2}$).

The Ground State of Multi-electron Atoms/Ions

In atoms/ions with two or more electrons, the ground state electron configuration (1) minimizes the total energy of the electrons, (2) obeys the Pauli exclusion principle, (3) obeys Hunds rule of maximum multiplicity, and (4) considers the exchange interaction. These "rules" are described below.

---

(1) Electrons will occupy the lowest energy orbitals in order to minimize the total energy. The two quantum numbers that are related to energy in multi-electron atoms are n, and l. Thus, orbitals with the lowest values of n and l will fill first.

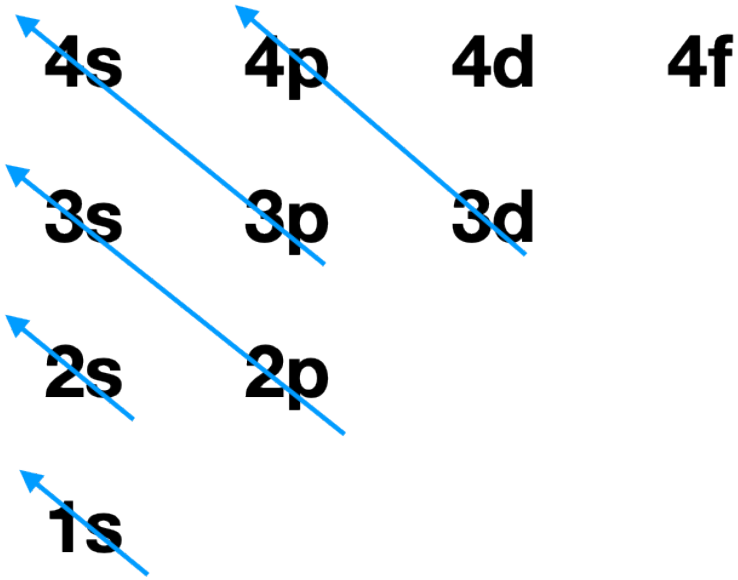
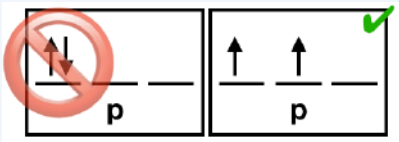


Figure 2.2.3.1. The order of filling of ground state electron orbitals is 1s, 2s, 2p, 3s, 3p, 4s, 3d, 4p, etc... (CC-BY-NC-SA; Kathryn Haas)

(2) Hund's rule of maximum multiplicity states that for a given electron configuration, the lowest energy arrangement of electrons in degenerate orbitals is the one with the greatest "multiplicity," where multiplicity is the number of unpaired electrons (n) plus 1 (multiplicity = n + 1). This rule is used to predict the ground state of an atom or molecule with one or more open electronic shells.

Hund's rule is based on empirical observation of atomic spectra, and it is a consequence of the energy required to pair two electrons in the same orbital. This energy of repulsion between two electrons in the same orbitals is a Coulombic energy of repulsion, Π_c, caused by two electrons with like charge sharing the same area of space (an orbital). When more than one electron occupies a set of degenerate orbitals, the most favorable arrangement is one where the number of paired electrons is minimized.

A simplified definition of Hund's rule is that **the lowest energy arrangement is the one with the greatest number of unpaired electrons**. This implies that if two or more orbitals of equal energy are available, electrons will occupy them singly before filling them in pairs. Examples of ground state arrangements of electrons in three degenerate p-orbitals is given in the figure shown here.



# of electrons in a p-subshell	Arrangement (unpaired electrons, n)	Spin Multiplicity (n + 1)
1	(n = 1)	2
2	(n = 2)	3
3	(n = 3)	4
4	(n = 2)	3
5	(n = 1)	2
6	(n = 0)	1

Figure 2.2.3.2**.** Hund's rule is that spin multiplicity must be maximized in the ground state. (Kathryn Haas; CC-NC-BY-SA)

(3) The Pauli exclusion principle states that it is impossible for two electrons of a multi-electron atom to have the same set of values for all four quantum numbers. Two electrons in different orbitals will have a different set of n, l, and m_l values. When two electrons reside in the same orbital, they posses the same n, l, and m_l values, therefore their m_s must be different. Thus, two electrons in the same orbital must have opposite half-integer spin projections of $+\frac{1}{2}$ and $-\frac{1}{2}$.

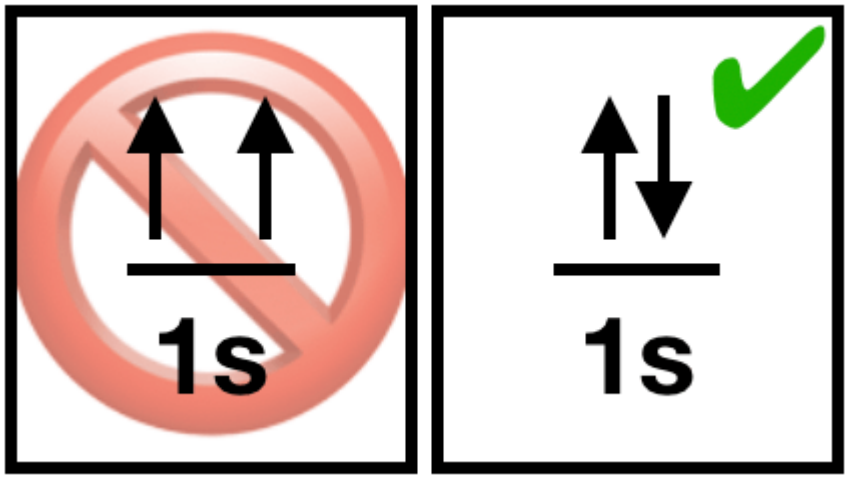


Figure 2.2.3.3**.** Pauli's principle tells us that paired electrons must have opposite spin. (Kathryn Haas; CC-NC-BY-SA)

(4) The exchange interaction is sometimes called the *exchange energy* or *exchange force*. However, it is not a true energy or force. Rather, it is a quantum mechanical effect that takes place between identical particles. The exchange interaction results in a ground state electron configuration with unpaired electrons all being of the same spin. Unpaired electrons are conventionally written in the "spin up" direction.

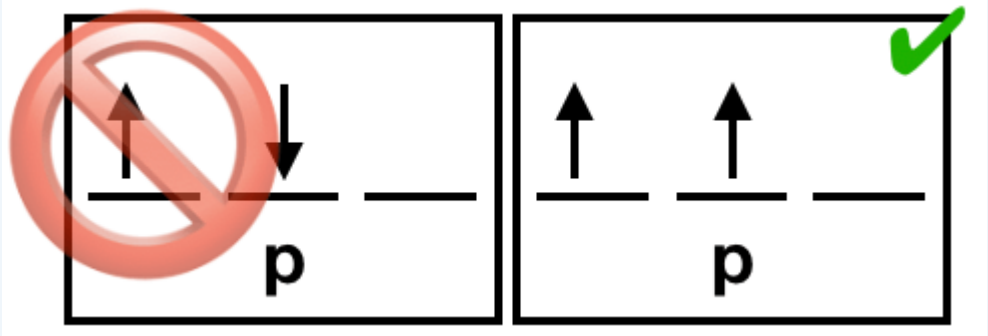


Figure 2.2.3.4**.** Unpaired electrons should have identical spins due to the exchange interaction. (Kathryn Haas; CC-NC-BY-SA)

Trends in Expected Electron Configuration

The four "rules" above can be used as guidelines to predict the ground state electron configuration of atoms, the filling of subshells, and the configuration of electrons in degenerate orbitals. However, the utility of these guidelines for predicting actual electron configurations requires more nuanced knowledge of the relative energy levels of orbitals.

Generally, orbital energy levels directly correspond to their shell number. Additionally, orbitals within a shell generally follow the energetic trend where s

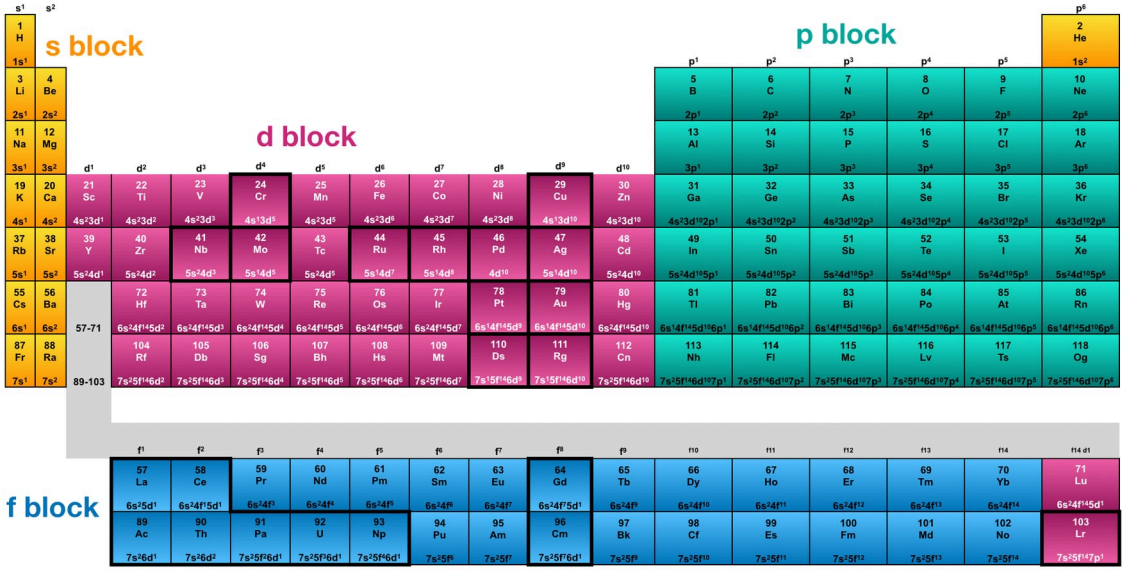


Figure 2.2.3.5. This is a depiction of the periodic table that highlights the s-, p-, d-, and f- blocks in different colors. Violations of the expected trend in electron configurations are outlined in a heavy black line. Several elements of the d block and f block violate the general trends in electron configuration because their orbital energy levels do not follow *general* trends. (CC-BY-NC-SA; Kathryn Haas)

Elements that violate general trends in electron configuration are outlined with a dark line in Figure 2.2.3.5. All of the exceptions are within the d- and f- blocks, and the violations are caused by an unexpected order of the orbital energy levels.

In the next section you will learn why the orbital energy levels correlate with shell number and why subshells within a shell usually follow the trend that s

References

1. Miessler, Gary L., and Donald A. Tarr. *Inorganic Chemistry*. Upper Saddle River, NJ: Pearson Prentice Hall, 2010. Print.
2. Brown, Ian David. *The Chemical Bond in Inorganic Chemistry the Bond Valence Model*. Oxford: Oxford UP, 2006. Print.

This page titled 2.2.3: Aufbau Principle is shared under a CC BY-NC-SA 4.0 license and was authored, remixed, and/or curated by Kathryn Haas.

- 2.2.3: Aufbau Principle by Kathryn Haas is licensed CC BY-NC-SA 4.0.

2.2.4: Shielding

Introduction

Coulomb's Law is from classical physics; it tells us that particles with opposite electrostatic charge are attracted to each other, and the larger the charge on either particle or the closer the distance between them, the stronger the attraction. Coulomb's law explains why atomic size decreases as the charge on the nucleus increases, but it can't explain the nuances and variations in size as we go across the periodic table. Coulomb's Law also explains why electrons in different shells (*n*), at different distances from the nucleus, have different energies. But on its own, Coulomb's law doesn't quite explain why electron subshells within a shell (like 2s vs. 2p) would have different energies. To explain these things, we need to consider how both electron **shielding** and **penetration** result in variations in effective nuclear charge (Z*) that depend on shell and subshell.

Effective Nuclear Charge (Z*)

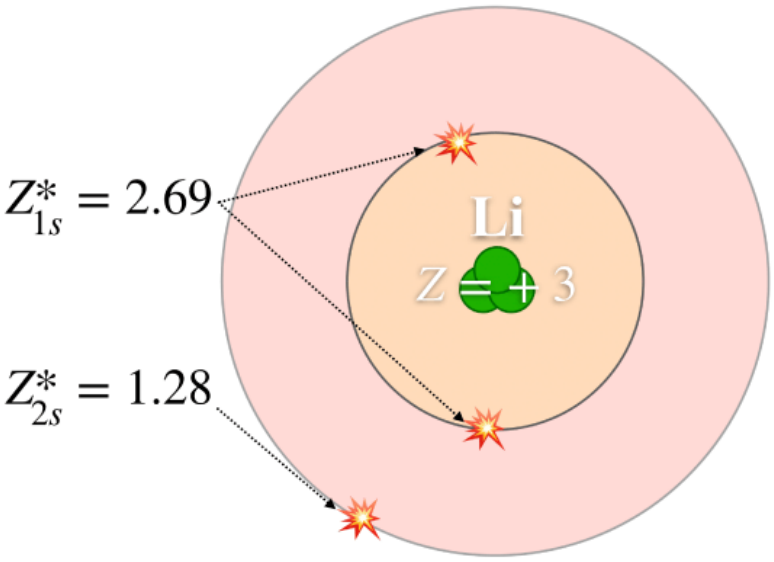


Figure 2.2.4.1. In a lithium atom, the nuclear charge (Z) is +3. 1s electrons experience an effective nuclear charge (Z*) of +2.69, and 2s electrons experience an Z* of +1.28. (CC-BY-NC-SA; Kathryn Haas)

Coulombs' law works well for predicting the energy of an electron in a hydrogen atom (because H has only one electron). It also works for hydrogen-like atoms: any nucleus with exactly one electron (a He^+ ion, for example, has one electron). However, Coulomb's law is insufficient for predicting the energies of electrons in multi-electron atoms and ions.

Electrons within a multi-electron atom interact with the nucleus and with all other electrons. Each electron in a multi-electron atom experiences both attraction to the nucleus and repulsion from interactions with other electrons. The presence of multiple electrons decreases the nuclear attraction to some extent. Each electron in a multi-electron atom experiences a different magnitude of (and attraction to) the nuclear charge depending on what specific shell and subshell the electron occupies. The amount of positive nuclear charge experienced by any individual electron is the **effective nuclear charge (Z*)**.

For example, in lithium (Li), none of the three electrons "feel" the full +3 charge from the nucleus (see Figure 2.2.4.1). Rather, each electron "feels" a Z* that is less than the actual Z and that depends on the electron's orbital. The actual nuclear charge in Li is $Z = +3$; the 1s electrons experience a $Z^* = +2.69$, and the 2s electron experiences a $Z^* = +1.28$. In general, core electrons (or the electrons closest to the nucleus), "feel" a Z* that is close to, but less than, Z. On the other hand, outer valence electrons experience a Z* that is much less than Z.

In summary:

- Core electrons: $Z^* \lessapprox Z$
- Valence electrons: $Z^* \ll Z$

Shielding:

Shielding is the reduction of true nuclear charge (Z) to the effective nuclear charge (Z*) by other electrons in a multi-electron atom or ion. Shielding occurs in all atoms and ions that have more than one electron. H is the only atom in which shielding does not occur.

Explanation of shielding: Electrons in a multi-electron atom interact with the nucleus and all other electrons in the atom. To describe shielding, we can use a simplified model of the atom: we will choose an electron-of-interest in a multi-electron atom and treat all the "other" electrons as a group of spherically-distributed negative charge. Classical electrostatics allows us to treat spherical distribution of charge as a point of charge at the center of the distribution. Thus, we consider all the "other" electrons in our atom as a point of negative charge in the center of the atom. While the positive charge of the nucleus provides an attractive force toward our electron, the negative charge distribution at the center of the atom would provide a repulsive force. The attractive and repulsive forces would partially cancel each other; but since there are less "other" electrons than there are protons in our atom, the nuclear charge is never completely canceled. The "other" electrons partially block, or shield, part of the nuclear charge so that our electron-of-interest experiences a partially-reduced nuclear charge, the Z*.

In reality, there is not a one-for-one "canceling" of the nuclear charge by each electron. Partly due to *penetration*, no single electron can completely shield a full unit of positive charge. Core electrons shield valence electrons, but valence electrons have little effect on the Z* of core electrons. The ability to shield, and be shielded by, other electrons strongly depends the electron orbital's average distance from the nucleus and its *penetration*; thus shielding depends on both shell (n) and subshell (l).

Shielding depends on electron penetration

Coulomb's law shows us that distance of an electron from its nucleus is important in determining the electron's energy (its attraction to the nucleus). The shell number (n) determines approximately how far an electron is from the nucleus *on average*. Thus, all orbitals in the same shell (s,p,d) have similar sizes and similar average distance of their electrons from the nucleus. But there is another distance-related factor that plays a critical role in determining orbital energy levels: *penetration*. **Penetration** describes the ability of an electron in a given subshell to penetrate into other shells and subshells to get close to the nucleus. Penetration is the **extent to which an electron can approach the nucleus**. Penetration depends on both the shell (n) and subshell (l).

The penetration of individual orbitals can be visualized using the radial probability functions. For example, Figure $2.2.4.2$ below shows plots of the radial probability function of the 1s, 2s, and 2p orbitals. From these plots, we can see that the 1s orbital is able to approach the closest to the nucleus; thus it is the most penetrating. While the 2s and 2p have most of their probability at a farther distance from the nucleus (compared to 1s), the 2s orbital and the 2p orbital have different extents of penetration. Notice that the 2s orbital is able to penetrate the 1s orbital because of the central 2s lobe. The 2p orbital penetrates somewhat into the 1s, but it cannot approach the nucleus as closely as the 2s orbital can. While the 2s orbital penetrates more than 2p (the 2s orbital can approach closer to the nucleus), the 2p is slightly *closer on average* than 2s. The order of Z* in 2s and 2p subshells depends on which factor (average distance or penetration) is more important. In the first two rows of the periodic table, penetration is the dominant factor that results in 2s having a lower energy than 2p (see Figure $2.2.4.4$ for values).

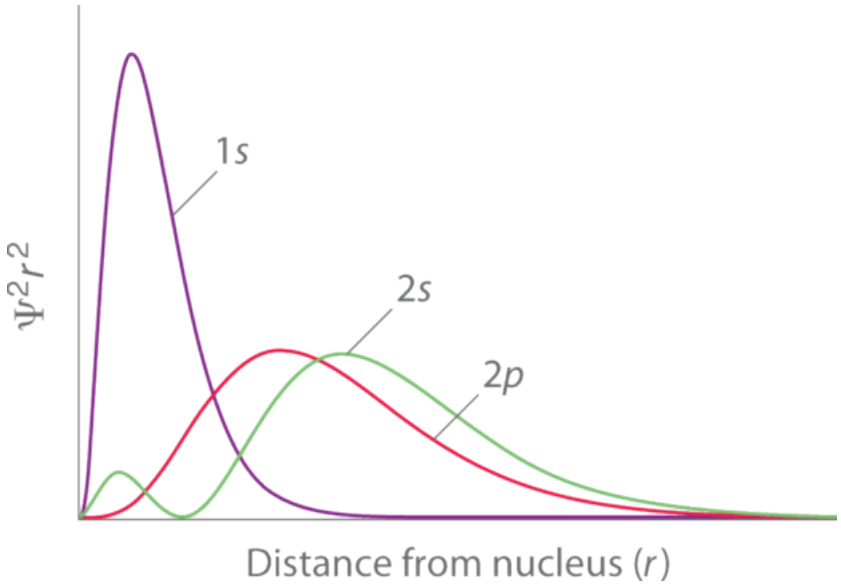


Figure 2.2.4.2. Orbital Penetration. A comparison of the radial probability distribution of the 2s and 2p orbitals for various states of the hydrogen atom shows that the 2s orbital penetrates inside the 1s orbital more than the 2p orbital does. Consequently, when an electron is in the small inner lobe of the 2s orbital, it experiences a relatively large value of Z*, which causes the energy of the 2s orbital to be lower than the energy of the 2p orbital.

An electron orbital's penetration affects its ability to shield other electrons and affects the extent to which it is shielded by other electrons. In general, electron orbitals that have greater penetration experience stronger attraction to the nucleus and less shielding by other electrons; these electrons thus experience a larger Z*. Electrons in orbitals that have greater penetration also shield other electrons to a greater extent.

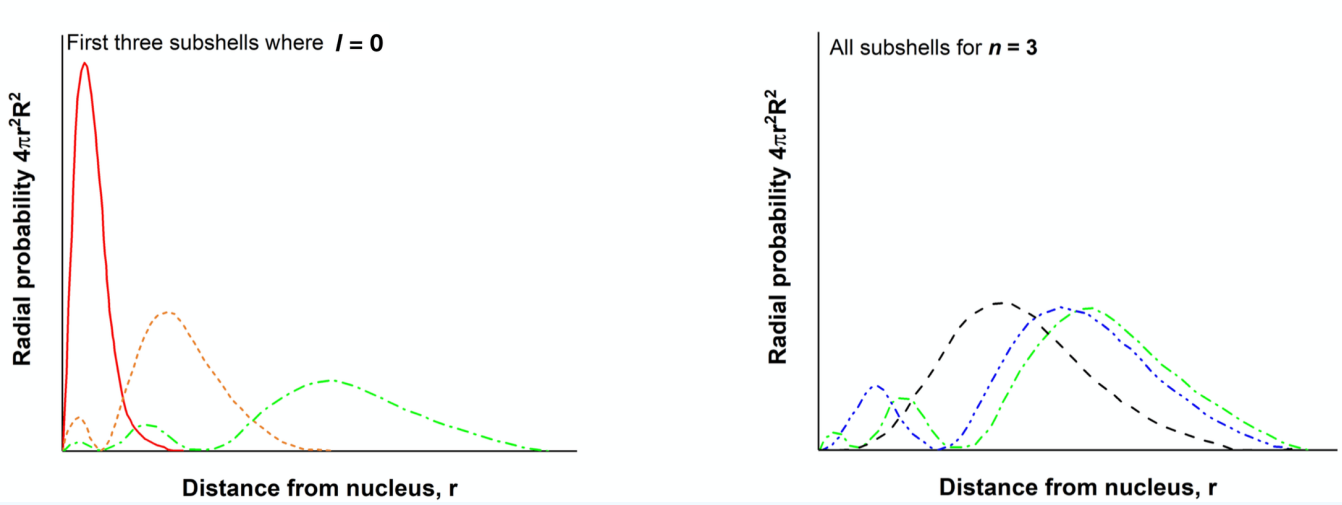
Within the same shell value (n), the penetrating power of an electron follows this trend in subshells (m_l):

s>p>d>f

Exercises

Exercises

1. Compare the 2s and 2p orbitals:
   (a) Which is closer to the nucleus on average?
   (b) Which is more penetrating?
   (c) Which orbital experiences a stronger Z* and is thus lower in energy (consider your experience, but also inspect Figures 1.1.2.3 and 1.1.2.4 from the previous page)? Please explain.
2. Peruse the Hyperphysics page (click) that shows radial probability functions of several orbitals (click around on various orbitals). Compare the 2p and 3s orbitals:
   (a) Which is farther from the nucleus on average?
   (b) Which is more penetrating?
   (c) Which orbital is lower in energy?
3. Which atom, Li, or N, has a stronger valence Z*? Explain why.
4. Explain why 2s and 2p subshells are completely degenerate in a hydrogen atom.
5. Which atom has a smaller radius: Be or F? Explain.
6. Which electrons shield others more effectively: 3p or 3d?
7. Use the clues given in the figures below to label the radial distribution functions shown.



8. Examine the plots on the right in the previous question, above. Note that this is a plot showing the probability density for the 3s, 3p, and 3d subshells.
(a) For which of these three functions is the highest probability density at the smallest r value (which is closest to the nucleus on average)? Is this the same subshell that penetrates most?
(b) Use this example to describe how penetration and shielding result in a splitting of subshell energy level in multi-electron atoms.

9. Explain why the ground state (most energetically favorable) electron configuration of Be is $1s^2 2s^2$ rather than alternative configurations like $1s^2 2s^1 2p^1$ or $1s^2 2p^2$.

Answer 1 available at the end of this section.

Slater's rules for estimating Z*

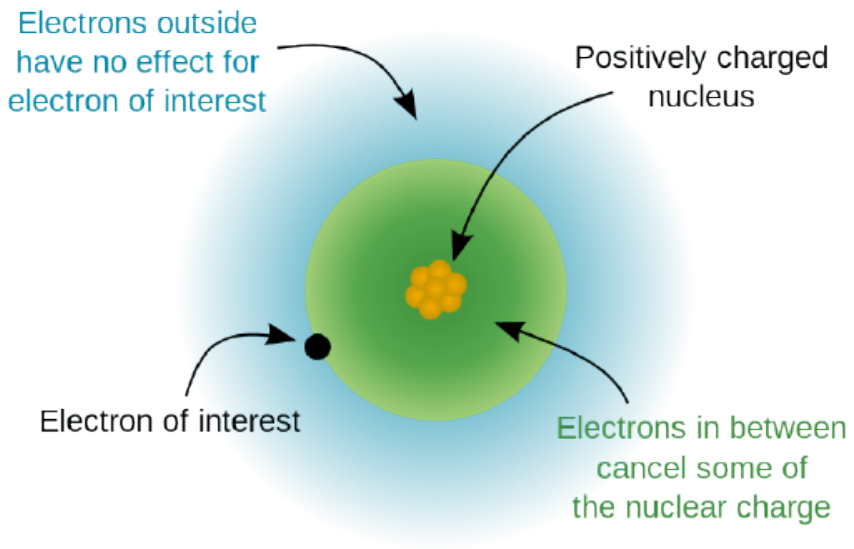


Figure 2.2.4.3. Diagram illustrating effective nuclear charge according to Slater's rules.

The Z* can be estimated using a number of different methods; probably the best known and most commonly used method is known as **Slater's Rules**. Slater developed a set of rules to estimate Z* based on how many other electrons exist in the atom and on the orbital location of the electron-of-interest. These two factors are important determinants in shielding, and they are used to

calculate a **shielding constant (S)** used in Slater's formula:

$$Z* = Z - S$$

where Z is the actual nuclear charge (the atomic number) and Z* is the effective nuclear charge.

In the calculation of S, it is assumed that electrons closer to the nucleus than our electron-of-interest cancel some of the nuclear charge; those farther from the nucleus have no effect. To calculate S, all the relevant orbitals in an atom are written out in order of increasing energy, separating them into in "groups". Each change in shell number is a new group; s and p subshells are in the same group but d and f orbitals are their own group. You write out all the orbitals using parentheses until you get to the group of the electron-of-interest, like this:

(1s)(2s,2p)(3s,3p)(3d)(4s,4p)(4d)(4f)(5s,5p) etc.

**Critical: The orbitals must be written in order of increasing energy!

1. **Electrons in the same Group():** Each other electron (not counting the electron-of-interest) in the same group () as the chosen electron, contributes 0.35 to S.
   Conceptually, this means electrons in the same group shield each other 35%.
2. **Electrons in Groups() to the left:**
   - If the electron-of-interest is in a d or f subshell, every electron in groups () to the left contributes 1.00 to S.
     Conceptually, this means that d and f electrons are shielded 100% by all electrons in the same shell with a smaller value of l, as well as all electrons in lower shells (n).
   - If the electron-of-interest is in an s or p subshell, all electrons in the next lower shell (n - 1) contribute 0.85 to S. And all the electrons in even lower shells contribute 1.00 to S.
     Conceptually, this means that s and p electrons are shielded 85% by the electrons one shell lower, and 100% by all electrons in shells n - 2 or lower.
3. ***1s electrons:*** *S of a 1s electron is just S=0.3, no matter the element.*

A video explaining how to use Slater's Rules

Example 2.2.4.1: Fluorine, Neon, and Sodium

What is the Z* experienced by the valence electrons in the three isoelectronic species: fluorine anion (F^-), neutral neon atom (Ne), and sodium cation (Na^+)?

Solution

Each species has 10 electrons, and the number of core electrons is 2 (10 total electrons - 8 valence), but the effective nuclear charge varies because each has a different atomic number (Z). The approximate Z* can be found with Slater's Rules. For all of these species, we would calculate the same sigma value:

Calculating S: (1s)(2s,2p), $S = 2(0.85) + 7(0.35) = 1.7 + 2.45 = 4.15$

Fluorine anion: $Z* = 9 - S = 9 - 4.15 = 4.85$

Neon atom: $Z* = 10 - S = 10 - 4.15 = 5.85$

Sodium Cation: $Z* = 11 - S = 11 - 4.15 = 6.85$

So, the sodium cation has the greatest effective nuclear charge.

Exercise 2.2.4.1

Calculate Z* for a 3d-electron in a zinc (Zn) atom.

Answer available at the end of this section.

"Best" values for Z*

Slater's rules are a set of simple rules for predicting S and Z* based on empirical evidence from quantum mechanical calculations. In other words, the Z* calculated from Slater's rules are approximate values. The values considered to be the most accurate are derived from quantum mechanical calculations directly. You can find these values in a nice chart on the Wikipedia article of Effective Nuclear Charge. The chart is recreated here in Figure 2.2.4.3 for convenience:

Z or Z_{eff}	H																	He
Z	1.00																	2.00
1s	1.00																	1.69
	Li	Be											B	C	N	O	F	Ne
Z	3.00	4.00											5.00	6.00	7.00	8.00	9.00	10.00
1s	2.69	3.69											4.68	5.67	6.67	7.66	8.65	9.64
2s	1.28	1.91											2.58	3.22	3.85	4.49	5.13	5.76
2p													2.42	3.14	3.83	4.45	5.10	5.76
	Na	Mg											Al	Si	P	S	Cl	Ar
Z	11.00	12.00											13.00	14.00	15.00	16.00	17.00	18.00
1s	10.63	11.61											12.59	13.58	14.56	15.54	16.52	17.51
2s	6.57	7.39											8.21	9.02	9.83	10.63	11.43	12.23
2p	6.80	7.83											8.96	9.95	10.96	11.98	12.99	14.01
3s	2.51	3.31											4.12	4.90	5.64	6.37	7.07	7.76
3p													4.07	4.29	4.89	5.48	6.12	6.76
	K	Ca	Sc	Ti	V	Cr	Mn	Fe	Co	Ni	Cu	Zn	Ga	Ge	As	Se	Br	Kr
Z	19.00	20.00	21.00	22.00	23.00	24.00	25.00	26.00	27.00	28.00	29.00	30.00	31.00	32.00	33.00	34.00	35.00	36.00
1s	18.49	19.47	20.46	21.44	22.43	23.41	24.40	25.38	26.37	27.35	28.34	29.33	30.31	31.29	32.28	33.26	34.25	35.23
2s	13.01	13.78	14.57	15.38	16.18	16.98	17.79	18.60	19.41	20.21	21.02	21.83	22.60	23.37	24.13	24.89	25.64	26.40
2p	15.03	16.04	17.06	18.07	19.07	20.08	21.08	22.09	23.09	24.10	25.10	26.10	27.09	28.08	29.07	30.07	31.06	32.05
3s	8.68	9.60	10.34	11.03	11.71	12.37	13.02	13.68	14.32	14.96	15.59	16.22	17.00	17.79	18.60	19.40	20.22	21.03
3p	7.73	8.66	9.41	10.10	10.79	11.47	12.11	12.78	13.44	14.09	14.73	15.37	16.20	17.01	17.85	18.71	19.57	20.43
4s	3.50	4.40	4.63	4.82	4.98	5.13	5.28	5.43	5.58	5.71	5.84	5.97	7.07	8.04	8.94	9.76	10.55	11.32
3d			7.12	8.14	8.98	9.76	10.53	11.18	11.86	12.53	13.20	13.88	15.09	16.25	17.38	18.48	19.56	20.63
4p													6.22	6.78	7.45	8.29	9.03	9.34
	Rb	Sr	Y	Zr	Nb	Mo	Tc	Ru	Rh	Pd	Ag	Cd	In	Sn	Sb	Te	I	Xe
Z	37.00	38.00	39.00	40.00	41.00	42.00	43.00	44.00	45.00	46.00	47.00	48.00	49.00	50.00	51.00	52.00	53.00	54.00
1s	36.21	37.19	38.18	39.16	40.14	41.13	42.11	43.09	44.08	45.06	46.04	47.03	48.01	48.99	49.97	50.96	51.94	52.92
2s	27.16	27.90	28.62	29.37	30.13	30.88	31.63	32.38	33.16	33.88	34.63	35.39	36.12	36.86	37.60	38.33	39.07	39.80
2p	33.04	34.03	35.00	35.99	36.98	37.97	38.94	39.95	40.94	41.93	42.92	43.91	44.90	45.89	46.87	47.86	48.85	49.84
3s	21.84	22.66	23.55	24.36	25.17	25.98	26.79	27.60	28.44	29.22	30.03	30.84	31.63	32.42	33.21	34.00	34.79	35.58
3p	21.30	22.17	23.09	23.85	24.62	25.47	26.38	27.22	28.15	29.02	29.81	30.69	31.52	32.35	33.18	34.01	34.84	35.67
4s	12.39	13.44	14.26	14.90	15.28	16.10	17.20	17.66	18.58	18.99	19.87	20.87	21.76	22.66	23.54	24.41	25.30	26.17
3d	21.68	22.73	25.40	25.57	26.25	27.23	28.35	29.36	30.41	31.45	32.54	33.61	34.68	35.74	36.80	37.84	38.90	39.95
4p	10.88	11.93	12.75	13.46	14.08	14.98	15.81	16.44	17.14	17.72	18.56	19.41	20.37	21.27	22.18	23.12	24.03	24.96
5s	4.99	6.07	6.26	6.45	5.92	6.11	7.23	6.49	6.64	(empty)	6.76	8.19	9.51	10.63	11.62	12.54	13.40	14.22
4d			15.96	13.07	11.24	11.39	12.88	12.81	13.44	13.62	14.76	15.88	16.94	17.97	18.97	19.96	20.93	21.89
5p													8.47	9.10	10.00	10.81	11.61	12.43

Figure 2.2.4.4. This chart shows Z* values calculated by Clementi et al. in 1963 and 1967 that are consistent with SCF Calculations. This chart was created using data from the Wikipedia article on Effective Nuclear Charge. (Kathryn Haas; CC-NC-BY-SA)

Z* modulates attraction

When valence electrons experience less nuclear charge than core electrons, different electrons experience different magnitudes of attraction to the nucleus. A modified form of Coulomb's Law is written below, where e is the charge of an electron, Z* is the effective nuclear charge experienced by that electron, and r is the radius (distance of the electron from the nucleus).

$$F_{eff} = k\frac{Z * e^2}{r^2}$$

This formula suggests that if we can estimate Z*, then we can predict the attractive force experienced by, and the energy of, an electron in a multi-electron atom (ex. Li).

The attraction of the nucleus to valence electrons determines the atomic or ionic size, ionization energy, electron affinity, and electronegativity. The stronger the attraction, and the stronger Z*, the closer the electrons are pulled toward the nucleus. This in turn results in a smaller size, higher ionization energy, higher electron affinity, and stronger electronegativity.

General Periodic Trends in Z*

Close inspection of Figure 2.2.4.3 and analysis of Slater's rules indicate that there are some predictable trends in Z*. The data from Figure 2.2.4.3 is plotted below in Figure 2.2.4.4 to provide a visual aid to the discussion below.

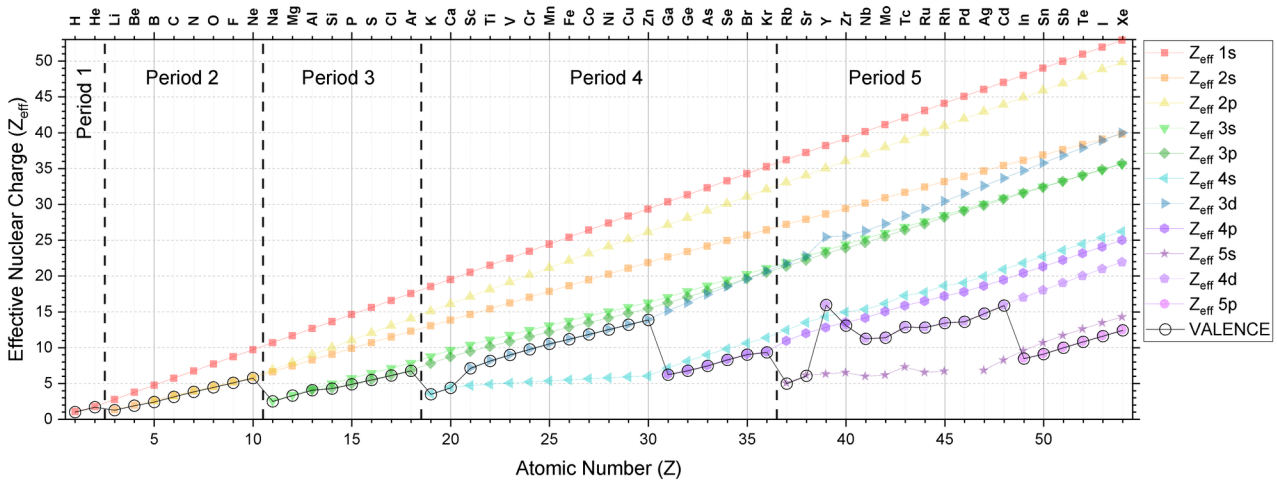


Figure 2.2.4.5: The Z* values for electrons in each subshell of the first 54 elements (H to Xe). Each subshell is plotted as a different series (see legend) and the valence shell is highlighted by a solid black line with open circles. (Kathryn Haas; CC-NC-BY-SA)

Trends in Z* for electrons in a specific shell and subshell

The Z* for electrons in a given shell and subshell generally increases as atomic number increases; this trend holds true going across the periodic table and down the periodic table. Convince yourself that this is true for any subshell by examining Figure 2.2.4.4. (CC-BY-NC-SA; Kathryn Haas)

Do you notice any exceptions to this general trend?

Inspection of Figure 2.2.4.4 should confirm for you that the Z* increases as Z increases for electrons in any subshell (like the 1s subshell for example, which is plotted above as a red line with square points). You can see this trend as the positive slope in each series. There is one obvious exception in Period 5 in elements 39 (Y) to 41 (Nb; the Z* of 4s actually decreases across these three elements as atomic number increases. There is also an exception between Y and Zr in the 3d subshell, and between Tc and Ru in the 5s subshell.

For valence electrons:

It is useful to understand trends in valence Z* because the valence Z* determines atomic/ionic properties and chemical reactivity. The trends in the valence Z* are not simple because as atomic number increases, the valence shell and/or subshell also changes. The valence Z* is indicated in Figure 2.2.4.4 as a black line with open circles.

Down the table: As we go down a column of the periodic table, the valence Z* increases. This is a simple trend because type of subshell is consistent and there is an increase only in shell and in atomic number, Z. This trend is best illustrated by inspection of Figure 2.2.4.3.

Across the table: the trend depends on shell and subshell, but generally Z* increases across a period.

Periods 1-3 (s and p only): As we go across the table in periods 1-3, the shell stays constant as Z increases and the subshell changes from s to p. In these periods, there is a gradual increase in valence Z* as we move across any of the first three periods.

Periods 4 and 5 (s, p, and d): Now we have some more complex trends because valence subshell and shell are changing as we increase in atomic number. Notice that the valence Z* generally increases going across a period as long as the subshell isn't changing; the exception is within the 4d subshell (elements 39-44 or Y-Ru). In general, going from an $(n)s$ subshell to an $(n-1)d$ subshell, there a relatively large increase in valence Z*. And in going from an $(n-1$d\) subshell to an $(n)p$ subshell, there is a relatively large decrease in Z*.

From one period to another: From Figure 2.2.4.4, we can see that as we increase Z by one proton, going from one period to the next, there is a relatively large decrease in Z* (from Ne to Na, for example). This is because as Z increases by a small

interval, the shell number increases, and so the electrons in the valence shell are much farther from the nucleus and are more shielded by all the electrons in the lower shell numbers.

Exercises

Exercise 2.2.4.2

1. Compare trends in Z* and atomic size. Explain how and why atomic size depends on Z*.
2. Compare trends in Z* and ionization energy. Explain how and why ionization energy depends on Z*.

Answer available at the end of this section.

References

1. Petrucci, Ralph H., William S. Harwood, F. Geoffrey Herring, and Jeffry D. Madura. General Chemistry: Principles and Modern Applications, Ninth Edition. Pearson Education Inc. Upper Saddle River, New Jersey: 2007.
2. Raymond Chang. Physical Chemistry for Biological Sciences. Sausalito, California: University Science Books, 2005
3. R. S. Mulliken, Electronic Structures of Molecules and Valence. II General Considerations, Physical Review, vol. 41, pp. 49-71 (1932)
4. Anastopoulos, Charis (2008). *Particle Or Wave: The Evolution of the Concept of Matter in Modern Physics*. Princeton University Press. pp. 236–237. ISBN 0691135126. http://books.google.com/?id=rDEvQZhpltEC&pg=PA236.

Contributors and Attributions

- Sidra Ayub (UCD), Alan Chu (UCD)
- Emily V Eames (City College of San Francisco)
- Curated or created by Kathryn Haas

Answers

Exercises

(a) The 2s orbital is closer to the nucleus on average.

(b) The 2s orbital is more penetrating than 2p.

(c) You might "know" that the 2s orbital is lower in energy than 2p because 2s fills first. But a close inspection of Figures 1.1.2.3 and 1.1.2.4 from the previous page indicates that while the 2s and 2p elements are degenerate in Ne (element 10), for elements with atomic number 11 and greater 2p has a higher Z* than 2s! This example illustrates that both average distance and penetration are factors in determining Z*, and the factor that is more important may change as we increase in atomic number.

(a) The 3s orbital reaches farther away from the nucleus and is on average farther from the nucleus than 2p.

(b) The 3s orbital is more penetrating than 2p, even though 3s is farther on average!

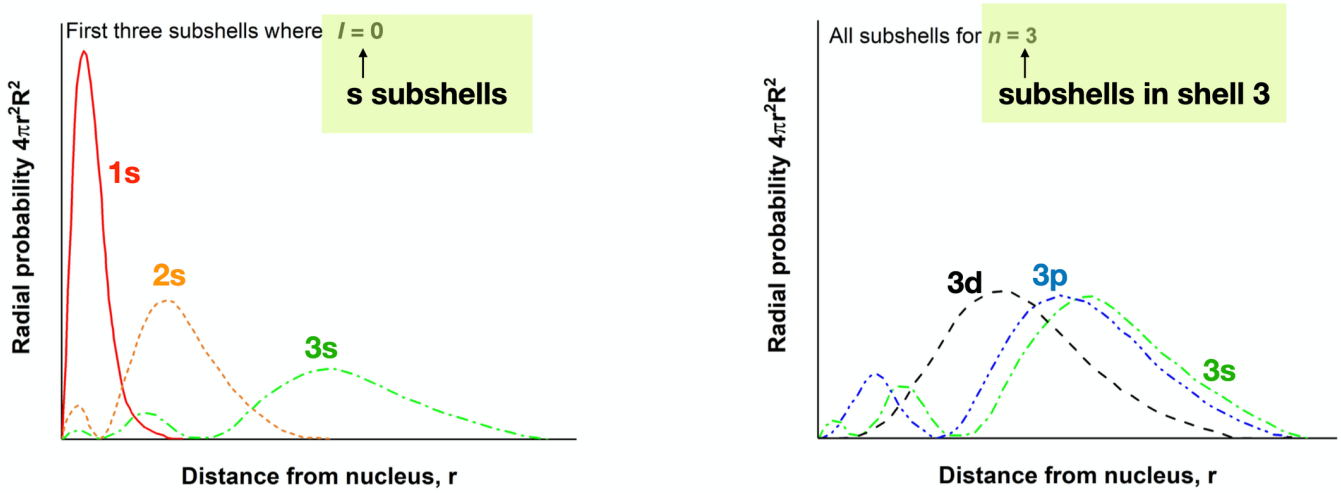
(c) The 2p orbital is lower in energy than 3s; this is because 2p is still significantly closer to the nucleus on average and experiences a stronger Z*. (Penetration is not the only consideration!)

A nitrogen atom has a stronger effective nuclear charge (Z*) than lithium due to its greater number of protons; even though N also has more electrons that would shield the nuclear charge, each electron only partially shields each proton. This means that atoms with greater atomic number always have greater Z* for any given electron.

The hydrogen atom has only one electron; thus there is no shielding to consider. When there are not other electrons to shield the nucleus, penetration and shielding are irrelevant, and subshells within a shell are degenerate.

Fluorine has a smaller radius than beryllium because F has a greater valence Z* and therefore pulls the valence electrons closer to the nucleus and provides a smaller atomic radius.

3p shields better than 3d because p orbitals penetrate more than d orbitals within the same shell.



3d is closest on average, but 3s penetrates most. The three subshells of $n = 3$ differ in their average distance and in their ability to penetrate; these factors result in differences in the Z* experienced by electrons in each orbital. We would expect 3s to be lowest in energy followed by 3p and then 3d.

This question is asking why the 2s orbital fills in Be before 2p is occupied. This is a multi-electron atom, therefore core electrons shield the 2s and 2p orbitals to different extents. In Be we expect the 2s orbital to fill before 2p because 2s penetrates more and experiences a higher Z*.

Exercise 2.2.4.1

Write out the relevant orbitals: (1s)(2s,2p)(3s,3p)(3d) ~~(4s)~~

Notice that although 4s is fully occupied, we don't include it because in Zn, 4s is higher in energy than 3d. Therefore, 4s is to the right of the d electrons we are considering. The electron-of-interest is in 3d, so the other nine electrons in 3d each contribute 0.35 to the value of S. The other 18 electrons each contribute 1 to the value of S.

$S = 18(1) + 9(0.35) = 21.15$

$Z* = 30 - 21.15 = 8.85$

So, although the nuclear charge of Zn is 30, the 3d electrons only experience a $Z* \approx 8.85$!

Exercise 2.2.4.2

1. On the periodic table, atomic radius generally decreases across the periods (left to right) and increases down the groups. As atomic number increases across the periodic table, nuclear charge (Z) increases and Z* increases. In turn, the atomic radius decreases because the higher nuclear charge (and thus higher Z*) pulls electrons closer to the nucleus. Atomic radius increases down the periodic table because the shell number increases. Despite an increase in Z* going down the periodic table, larger atomic radii result from electrons occupying higher shells.

2. Ionization energies (IE) are inversely related to atomic radius; IE increases across the periods and decreases down the groups. Since the nucleus holds valence electrons more strongly (due to higher Z*) across the periods, IE increases because valence electrons are harder to remove. Down the periodic table, larger atomic radii cause electrons in valence orbitals to be shielded by core electrons. Recall that shielding reduces the nuclear charge available to electrons in higher orbital levels, resulting in a lower Z*. With more shielding and lower Z*, the valence electrons are held less tightly by the nucleus such that ionization energy decreases (i.e., valence electrons are easier to remove).

This page titled 2.2.4: Shielding is shared under a CC BY-NC-SA 4.0 license and was authored, remixed, and/or curated by Kathryn Haas.

- 2.2.4: Shielding by Kathryn Haas is licensed CC BY-NC-SA 4.0.

2.3: PERIODIC PROPERTIES OF ATOMS

General periodic trends are specific patterns that are present within the periodic table; these are patterns in properties like electronegativity, ionization energy, electron affinity, atomic radius, melting point, and metallic character. General periodic trends provide chemists with an invaluable tool to quickly predict an element's properties. These trends exist because of the similar atomic structure of the elements within their respective group families or periods, and because of the periodic nature of the elements. Some of the general periodic trends are described in this section.

2.3.1: Ionization energy

2.3.2: Electron Affinity

2.3.3: Covalent and Ionic Radii

References

1. Russo, Steve, and Mike Silver. Introductory Chemistry. San Francisco: Pearson, 2007.
2. Petrucci, Ralph H, et al. General Chemistry: Principles and Modern Applications. 9th Ed. New Jersey: Pearson, 2007.
3. Atkins, Peter et. al, *Physical Chemistry*, 7th Edition, 2002, W.H Freeman and Company, New York, pg. 390.
4. Alberty, Robert A. et. al, *Physical Chemistry*, 3rd Edition, 2001, John Wiley & Sons, Inc, pg. 380.
5. Kots, John C. et. al, *Chemistry & Chemical Reactivity*, 5th Edition, 2003, Thomson Learning Inc, pg. 305-309.

This page titled 2.3: Periodic Properties of Atoms is shared under a license and was authored, remixed, and/or curated by Kathryn Haas.

- 2.3: Periodic Properties of Atoms by Kathryn Haas is licensed CC BY-NC-SA 4.0.

2.3.1: Ionization energy

Ionization energy (IE) is the energy required to **remove an electron from a neutral atom or cation in its gaseous phase**. IE is also known as *ionization potential*.

$$A^{n+}_{(g)} \longrightarrow A^{(n+1)+}_{(g)} + e^- \qquad IE = \Delta U$$

Conceptually, ionization energy is the affinity of an element for its outermost electron (an electron it already has in its valence shell).

1st, 2nd, and 3rd Ionization Energies

The symbol I_1 stands for the ***first ionization energy*** (energy required to take away an electron from a neutral atom, where $n = 0$). The symbol I_2 stands for the ***second ionization energy*** (energy required to take away an electron from an atom with a +1 charge, $n = 2$.)

- **First Ionization Energy,** I_1 (general element, A):

$$A_{(g)} \rightarrow A^{1+}_{(g)} + e^-$$

- **Second Ionization Energy,** I_2 (general element, A):

$$A^{1+}_{(g)} \rightarrow A^{2+}_{(g)} + e^-$$

- **Third Ionization Energy,** I_3 (general element, A):

$$A^{2+}_{(g)} \rightarrow A^{3+}_{(g)} + e^-$$

Each succeeding ionization energy is larger than the preceding energy. This means that $I_1 < I_2 < I_3 < ... < I_n$ will always be true. For example, ionization energy increases as succeeding electrons are taken away from Mg.

$$Mg_{\,(g)} \rightarrow {Mg^+}_{\,(g)} + e^- \quad I_1 = 738\,kJ/mol$$

$${Mg^+}_{\,(g)} \rightarrow {Mg^{2+}}_{\,(g)} + e^- \quad I_2 = 1451\,kJ/mol$$

Ionization energy is correlated with the strength of attraction between the positively-charged nucleus and the negatively-charged valence electrons. The higher the ionization energy, the stronger the attractive force between nucleus and valence electrons, and the more energy is required to remove a valence electron. The lower the ionization energy, the weaker the attractive force between nucleus and valence electrons, and the less energy required to remove a valence electron.

General periodic trends in electron affinity

In general, ionization energies increase from left to right and decrease down a group; however, there are variations in these trends that would be expected from the effects of penetration and shielding. The trends in **first ionization energy** are shown in Figure $2.3.1.1$ and are summarized below.

- **Across a period:** As Z* increases across a period, the ionization energy of the elements generally increases from left to right. However there are breaks or variation in the trends in the following cases:
  - IE is especially low when removal of an electron creates a newly empty p subshell (examples include I_1 of B, Al, Sc)
  - IE energy is especially low where removal of an electron results in a half-filled p or d subshell (examples include I_1 of O, S)
  - IE increases more gradually across the d- and f-subshells compared to s- and p- subshells. This is because d- and f-electrons are weakly penetrating and experience especially low Z*.
- **From one period to the next:** There is an especially large decrease in IE with the start of every new period (from He to Li or from Ne to Na for example). This is consistent with the idea that IE is especially low when removal of an electron creates a newly empty s-subshell.

- **Noble gases:** The noble gases posses very high ionization energies. Note that helium has the highest ionization energy of all the elements.
- **Down a group:** Although Z* increases going down a group, there is no reliable trend in IE going down any group; in some cases IE increases going down a group, while in other cases IE decreases going down a group.

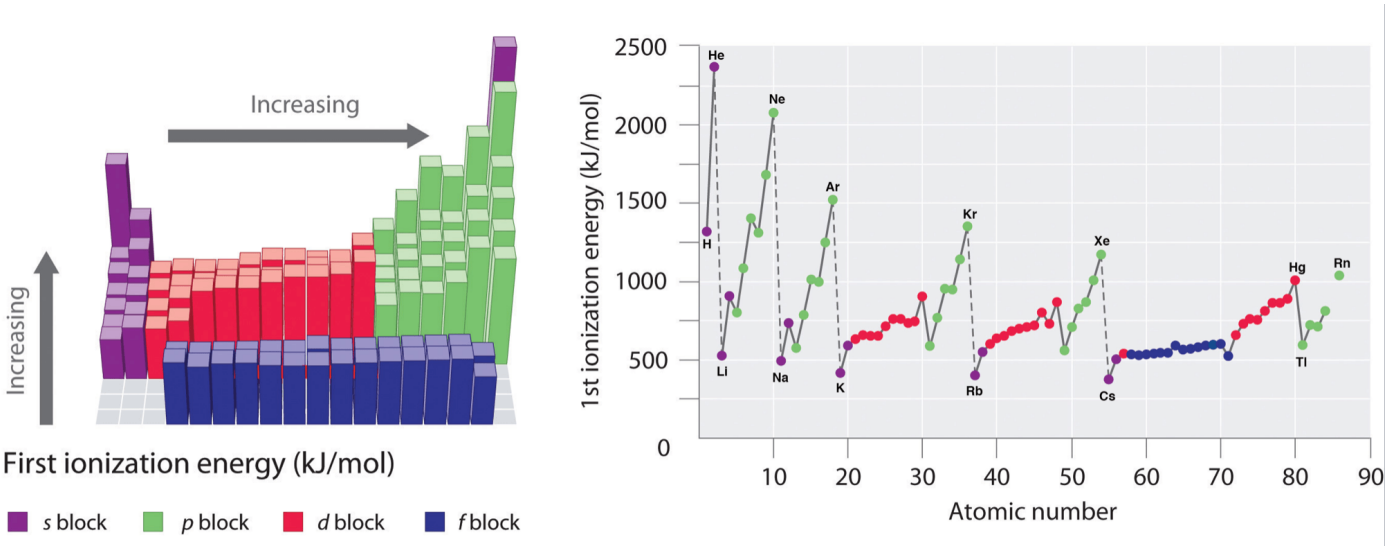


Figure 2.3.1.1: Graph showing the First Ionization Energy of the Elements. Left: ionization energies are mapped onto the periodic table, where the magnitude of ionization energy is depicted as a bar graph. Right: the first ionization energy is plotted against atomic number. In both panels the elements of the s-block are shown in purple, p-block are shown in green, d-block are shown in red, and f-block are shown in blue. (CC BY-NC-SA 3.0; anonymous)

Plots of the I_1, I_2, and I_3 of elements from hydrogen to krypton (first four periods) are shown in Figure 2.3.1.2. Notice that $I_3 > I_2 > I_1$. Also notice that trends mentioned above for I_1 hold true for subsequent ionizations when electron configurations are considered!

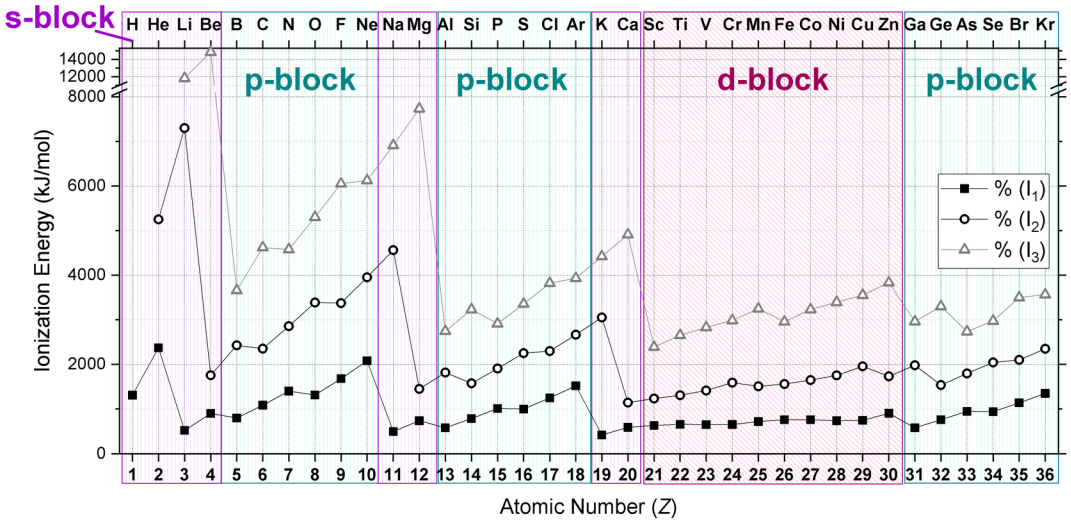


Figure 2.3.1.2. The first (I_1), second (I_2), and third (I_3) ionization energies plotted for elements with Z = 1 to 36 (H to Kr). The position of each element in its atomic form is indicated as s- p- or d-block. (CC-BY-NC-SA; Kathryn Haas)

This page titled 2.3.1: Ionization energy is shared under a CC BY-NC-SA 3.0 license and was authored, remixed, and/or curated by Bingyao Zheng, Emily Nguyen, Kathryn Haas, & Swetha Ramireddy.

- 2.3.1: Ionization energy by Bingyao Zheng, Emily Nguyen, Kathryn Haas, Swetha Ramireddy is licensed CC BY-NC-SA 3.0.

2.3.2: Electron Affinity

Definitions of Electron Affinity

According to IUPAC, there are two different, but equivalent, definitions of **electron affinity (EA)**.[1]

Definition: Electron Affinity defined as removal of an electron

Electron affinity can be defined as the energy *required* when an electron is removed from a gaseous anion. The reaction as shown in equation 2.3.2.1 is *endothermic* (positive ΔU) for elements except noble gases and alkaline earth metals. Under this definition, the more positive the EA value, the higher an atom's affinity for electrons.

$$A^-_{(g)} \longrightarrow A_{(g)} + e^- \qquad EA = \Delta U \tag{2.3.2.1}$$

The reaction shown in Equation 2.3.2.1 is similar those that define ionization energy. For this reason, the EA is also described as the *zeroth ionization energy*.

Definition: Electron Affinity defined as addition of an electron

An alternate and more common definition is the microscopic reverse of Equation 2.3.2.1. This more common definition states that electron affinity is the energy *released* when an electron is added to a gaseous atom, as shown in Equation 2.3.2.2. The reaction as shown in equation 2.3.2.2 is *exothermic* (negative ΔU) for elements except noble gases and alkaline earth metals. The more negative this EA value, the higher an atom's affinity for electrons.

$$A_{(g)} + e^- \longrightarrow A^-_{(g)} \qquad EA = \Delta U \tag{2.3.2.2}$$

Conceptually, this second definition is quite similar to the concept of electronegativity; but unlike electronegativity, EA is a well-defined quantitative measurement.

Trends in Electron Affinity

For this discussion, we will use the definition of EA that is consistent with it being a *zeroth ionization energy:* a more positive (larger) value means that the EA is higher (meaning stronger affinity toward an electron).

- **Across a period**: Similar to ionization energy, EA generally increases across a row of the periodic table; this observation is consistent with the increase in effective nuclear charge (Z*) from left to right across a period. However, there are variations across a period that are similar to variations in ionization energy and that can be explained by shielding, penetration, and electron configuration.
- **Down a group**: Like the case of ionization energy trends, EA does not consistently decrease going down a column of the periodic table despite the fact that Z^* increases down a group.

The trend in EA follows a zig-zag pattern similar to the one seen with ionization energies, except that it is displaced by one unit from the trend in I_1, two units from I_2, and so on. For example, EA peaks at F, while I_1 peaks at Ne, I_2 peaks at Na, and I_3 peaks at Mg. A plot of EA for the first 13 elements is shown overlaid on plots of I_1, I_2 and I_3 in Figure 2.3.2.1., where the shifts in the peaks and valleys within each zig-zag trend are indicated.

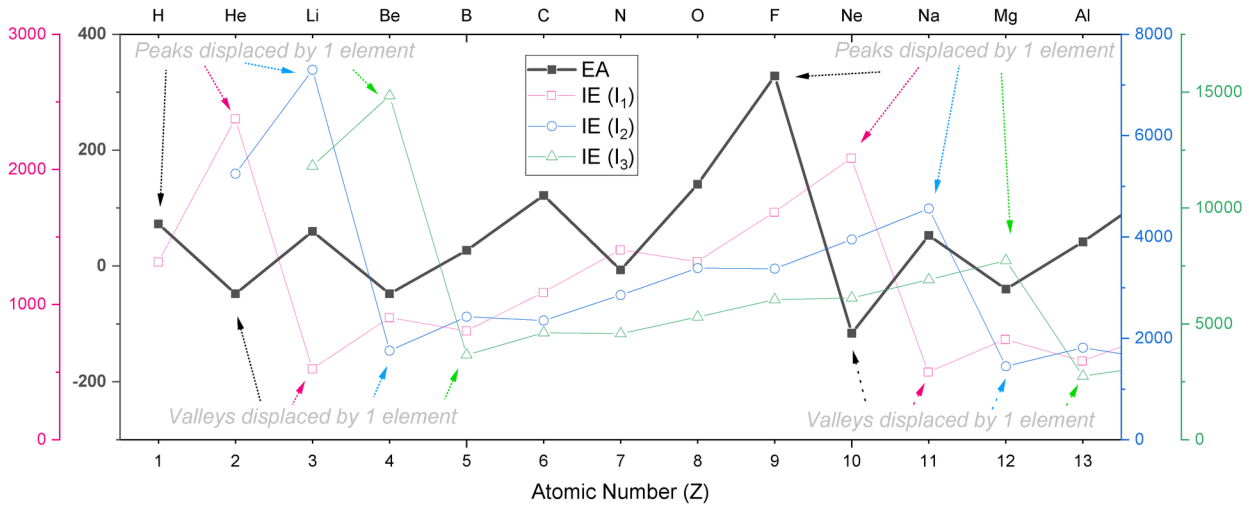


Figure 2.3.2.1. A plot of electron affinity (the zeroth ionization energy) is overlaid on plots of the first (I_1), second (I_2), and third (I_3) ionization energies. Each plot is shown using separate y-axes. Trends in EA are similar to those in ionization energies, except that the peaks and valleys of the trends are shifted by one unit, as indicated. These plots are shown in units of kJ/mole. (CC-BY-NC-SA; Kathryn Haas)

Sources

1. IUPAC. Compendium of Chemical Terminology, 2nd ed. (the "Gold Book"). Compiled by A. D. McNaught and A. Wilkinson. Blackwell Scientific Publications, Oxford (1997). Online version (2019-) created by S. J. Chalk. ISBN 0-9678550-9-8. doi.org/10.1351/goldbook.
2. Electron Affinity (data page), Wikipedia. en.Wikipedia.org/wiki/Electron_affinity_(data_page) Accessed 12/3/19.

This page titled 2.3.2: Electron Affinity is shared under a CC BY-NC 4.0 license and was authored, remixed, and/or curated by Kathryn Haas.

- 2.3.2: Electron Affinity by Kathryn Haas is licensed CC BY-NC-SA 4.0.

2.3.3: Covalent and Ionic Radii

Measurement of Radius

There are several methods that can be used to determine radii of atoms and ions:

- **Nonpolar atomic radii:** The radius of an atom is derived from the bond lengths within nonpolar molecules; one-half the distance between the nuclei of two atoms within a covalent bond.
- **van der Waals radius:** The radius of an atom is determined by collision with other atoms.
- **Crystal radii**: The atomic or ionic radius is determined using electron density maps from X-ray data.

The measurement of atomic or ionic size will depend on a number of factors, including the covalent character of bonding in any particular molecule, coordination number, physical state (liquid, solid, gas), the identity of nearby atoms/ions, variation in crystal structure, and distortions within regular crystal structures. You should keep in mind that the size of an atom or ion is a "fuzzy" measure, and the radius under a different set of conditions will probably change slightly.

Regardless, measured atomic and ionic radii reveal obvious trends across the periodic table and between atoms and ions. The relative atomic sizes shown in Figure 2.3.3.1 were derived from crystallographic data.[1]

Trends in Atomic Radius

Atomic size generally decreases gradually from left to right across a period of elements. As nuclear charge (Z) increases, we expect the effective nuclear charge (Z*) of the valence electrons to also increase. Increasing Z pulls electrons closer to the nucleus. However, with each additional unit of Z, there is also an additional electron. The change in size is a balance of a compression caused by increasing Z and an expansion in the number of electrons. As a result, the atomic radius decreases *gradually* across a period.

Atomic size generally increases going down a group. As valence electrons occupy higher level shells due to the increasing quantum number (n), size increases despite the fact that Z and Z* are increasing going down the group.

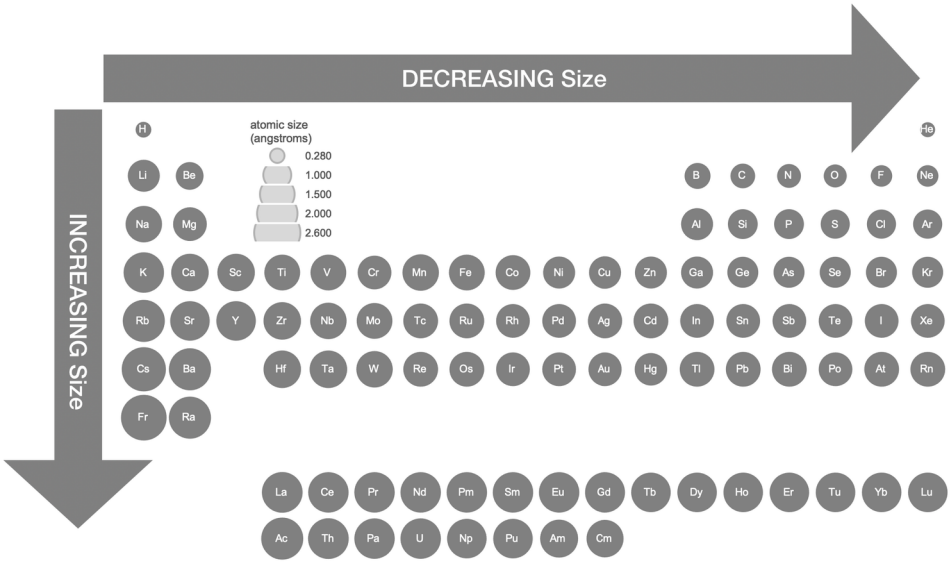


Figure 2.3.3.1. *Atomic Radii Calculated from Crystalographic Data. Data from Cordero, Beatriz, Veronica Gomez, Ana E. Platero-Prats, Marc Reves, Jorge Echeverria, Eduard Cremades, Flavia Barragan, and Santiago Alvarez. "Covalent Radii Revisited." Dalton Transactions, no. 21 (2008): 2832–38. doi:10.1039/b801115j.* (Kathryn Haas; CC-NC-BY-SA)

Trends in Ionic Radius

Trends in ionic radius follow general trends in atomic radius for ions of the same charge. Ionic radius varies with the charge of the ion (and number of electrons) and the electron configuration (e.g. high spin or low spin).

Cations

Compared to their atoms, cations have the same Z but fewer electrons. Removal of electrons from an atom to form a cation results in a significant increase in effective nuclear charge, resulting in all other electrons being more strongly attracted to the nucleus, and having a lower energy level. The result is a contraction in size from the atom to cation. Figure 2.3.3.2 visually illustrates the relative size of atoms and some cations of the first four periods; the data is available in tabular format in Figure 2.3.3.3.

Anions

Compared to their atoms, anions have the same Z but more electrons. Addition of electrons to an atom to form an anion results in a decrease in effective nuclear charge, which corresponds to a decrease in attractive force between the nucleus and electrons. Lower attractive force leads to expansion, where the size of the atom becomes larger in the formation of an anion. Figure 2.3.3.2 visually illustrates the relative size of atoms and some anions of the first four periods, while the data is available in tabular format in Figure 2.3.3.3.

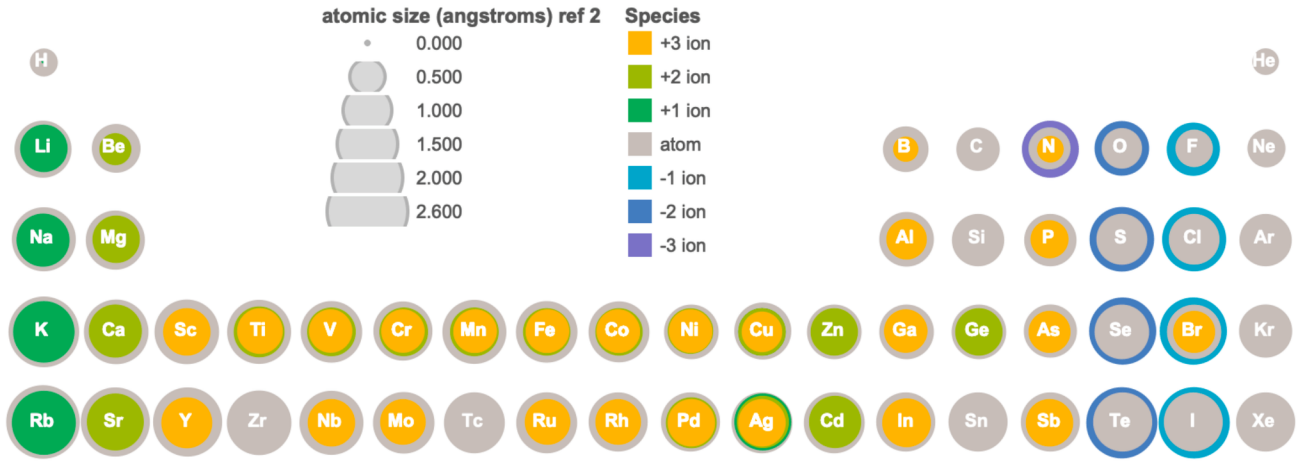


Figure 2.3.3.2. This figure illustrates relative size of atoms and ions of the first four periods of the periodic table. Atomic radius is indicated by grey circles. Radius of cations is shown in green (+1), lime (+2), and yellow (+3) circles. Radius of anions are shown as aqua (-1), blue (-2), and purple (-3) circles. Data from sources 1-3. (Kathryn Haas; CC-NC-BY-SA)

H																	**He**
0.31 (atom) 0 (+1)																	0.28 (atom)
Li	**Be**											**B**	**C**	**N**	**O**	**F**	**Ne**
1.28 (atom) 0.9 (+1) - -	0.96 (atom) 0.41 (+2) - -											0.84 (atom) 0.25 (+1)	0.76 (atom) 0.29 (+4)	1.32 (-3) 0.71 (atom) 0.3 (+3) 0.27 (+5)	1.21 (-2) 0.66 (atom)	1.145 (-1) 0.57 (atom)	0.58 (atom)
Na	**Mg**											**Al**	**Si**	**P**	**S**	**Cl**	**Ar**
1.66 (atom) 1.16 (+1)	1.41 (atom) 0.86 (+2)											1.21 (atom) 0.675 (+3)	1.11 (atom) 0.4 (+4)	1.07 (atom) 0.58 (+3) 0.31 (+5)	1.7 (-2) 1.05 (atom) 0.51 (+4) 0.26 (+6)	1.67 (-1) 1.02 (atom)	1.06 (atom)
K	**Ca**	**Sc**	**Ti**	**V**	**Cr**	**Mn**	**Fe**	**Co**	**Ni**	**Cu**	**Zn**	**Ga**	**Ge**	**As**	**Se**	**Br**	**Kr**
2.03 (atom) 1.52 (+1)	1.76 (atom) 1.14 (+2)	1.7 (atom) 0.885 (+3)	1.6 (atom) 1 (+2) 0.81 (+3) 0.745 (+4)	1.53 (atom) 0.93 (+2) 0.78 (+3) 0.72 (+4)	1.39 (atom) 0.94 (+2 hs) 0.87 (+2 ls) 0.7555 (+3) 0.69 (+4) 0.63 (+5) 0.58 (+6)	1.61 (atom) 0.97 (+2 hs) 0.81 (+2 ls) 0.785 (+3 hs) 0.72 (+3 ls) 0.67 (+4) 0.47 (+5) 0.395 (+6) 0.39 (+7)	1.52 (atom) 0.92 (+2 hs) 0.785 (+3 hs) 0.75 (+2 ls) 0.725 (+4) 0.69 (+3 ls) 0.39 (+6)	1.5 (atom) 0.885 (+2 hs) 0.79 (+2 ls) 0.75 (+3 hs) 0.685 (+3 ls) 0.67 (+4 hs)	1.24 (atom) 0.83 (+2) 0.74 (+3 hs) 0.7 (+3 ls) 0.62 (+4)	1.32 (atom) 0.91 (+1, cn6) 0.87 (+2, cn6) 0.68 (+3, cn6)	1.22 (atom) 0.88 (+2)	1.22 (atom) 0.76 (+3)	1.2 (atom) 0.87 (+2) 0.67 (+4)	1.19 (atom) 0.72 (+3) 0.6 (+5)	1.84 (-2) 1.2 (atom) 0.64 (+4) 0.56 (+6)	1.82 (-1) 1.2 (atom) 0.73 (+3) 0.53 (+7) 0.45 (+5)	1.16 (atom)
Rb	**Sr**	**Y**	**Zr**	**Nb**	**Mo**	**Tc**	**Ru**	**Rh**	**Pd**	**Ag**	**Cd**	**In**	**Sn**	**Sb**	**Te**	**I**	**Xe**
2.2 (atom) 1.66 (+1)	1.95 (atom) 1.32 (+2)	1.9 (atom) 1.04 (+3)	1.75 (atom) 0.86 (+4)	1.64 (atom) 0.86 (+3) 0.82 (+4) 0.78 (+5)	1.54 (atom) 0.83 (+3) 0.79 (+4) 0.75 (+5) 0.73 (+6)	1.47 (atom) 0.785 (+4) 0.74 (+5) 0.7 (+7)	1.46 (atom) 0.82 (+3) 0.76 (+4) 0.705 (+5) 0.52 (+7) 0.5 (+8)	1.42 (atom) 0.805 (+3) 0.74 (+4) 0.69 (+5)	1.39 (atom) 0.73 (+1) 1 (+2) 0.9 (+3) 0.755 (+4)	1.45 (atom) 1.29 (+1) 1.08 (+2) 0.89 (+3)	1.44 (atom) 1.09 (+2)	1.42 (atom) 0.94 (+3)	1.39 (atom) 0.83 (+4)	1.39 (atom) 0.9 (+3) 0.74 (+5)	2.07 (-2) 1.38 (atom) 1.1 (+4) 0.7 (+6)	2.06 (-1) 1.39 (atom) 1.09 (+5) 0.67 (+7)	1.4 (atom) 0.62 (+8)

Figure
2.3.3.3.

This figure shows radii (in Angstroms) of atoms and ions of the first four periods of the periodic table. Radii from each element are listed from largest to smallest, ionic charge indicated in parentheses (); hs = high spin, ls = low spin, cn6 = coordination number is 6. Data from sources 1-3. (Kathryn Haas; CC-NC-BY-SA)

References

1. Cordero, Beatriz, Veronica Gomez, Ana E. Platero-Prats, Marc Reves, Jorge Echeverria, Eduard Cremades, Flavia Barragan, and Santiago Alvarez. *"Covalent Radii Revisited." Dalton Transactions, no. 21 (2008): 2832–38. doi:10.1039/b801115j.*
2. R. D. Shannon (1976). "Revised effective ionic radii and systematic studies of interatomic distances in halides and chalcogenides". *Acta Crystallogr A.* **32** (5): 751–767. Bibcode:1976AcCrA..32..751S. doi:10.1107/S0567739476001551.
3. Wikipedia articles on Atomic Radius and Ionic Radius.

This page titled 2.3.3: Covalent and Ionic Radii is shared under a CC BY-NC 4.0 license and was authored, remixed, and/or curated by Bingyao Zheng.

- 2.3.3: Covalent and Ionic Radii by Bingyao Zheng, Emily Nguyen, Kathryn Haas, Swetha Ramireddy is licensed CC BY-NC-SA 4.0.

2.4: Problems

Example Exercises

The following series of problems reviews general understanding of the aforementioned material.

Exercises

1. Based on the periodic trends for ionization energy, which element has the highest ionization energy?
2. Which has a larger atomic radius: nitrogen or oxygen?
3. Which element is more electronegative, sulfur (S) or selenium (Se)?
4. Why is the electronegativity value of most noble gases zero?
5. Rewrite the following list in order of decreasing electron affinity: fluorine (F), phosphorous (P), sulfur (S), boron (B).
6. Which of these elements has a smaller atomic radius than sulfur (S): O, Cl, Ca, Li

Answer 1 available at the end of this section.

Answers

Exercises

Helium (He).

Atomic radius increases from right to left on the periodic table. Therefore, nitrogen is larger than oxygen.

Sulfur (S). Note that sulfur and selenium share the same column. Electronegativity increases up a column. This indicates that sulfur is more electronegative than selenium.

Because of their full valence electron shell, the noble gases are extremely stable and do not readily lose or gain electrons.

Fluorine (F)>Sulfur (S)>Phosphorous (P)>Boron (B). Explanation: Electron affinity generally increases from left to right and from bottom to top.

Oxygen (O) is the only element in the list with a smaller atomic radius than S. Periodic trends indicate that atomic radius increases down a group (from top to bottom) and from left to right across a period.

This page titled 2.4: Problems is shared under a license and was authored, remixed, and/or curated by Kathryn Haas.

- 2.4: Problems by Kathryn Haas is licensed CC BY-NC-SA 4.0.

3: SIMPLE BONDING THEORY

3.1: Lewis Electron-Dot Diagrams

3.1.1: Resonance

3.1.2: Breaking the octet rule with higher electron counts (hypervalent atoms)

3.1.3: Formal Charge

3.1.4: Lewis Fails to Predict Unusual Cases - Boron and Beryllium

3.2: Valence Shell Electron-Pair Repulsion

3.2.1: Lone Pair Repulsion

3.2.2: Multiple Bonds

3.2.3: Electronegativity and Atomic Size Effects

3.2.4: Ligand Close Packing

3.3: Molecular Polarity

3.4: Hydrogen Bonding

This page titled 3: Simple Bonding Theory is shared under a license and was authored, remixed, and/or curated by Kathryn Haas.

- 3: Simple Bonding Theory by Kathryn Haas is licensed CC BY-NC-SA 4.0.

3.1: Lewis Electron-Dot Diagrams

In 1916, Gilbert Lewis Newton introduced a simple way to show the bonding between atoms in a molecule though Lewis electron dot diagrams. Creating Lewis diagrams is rather simple and requires only a few steps and some accounting of the valence electrons on each atom. Valence electrons are represented as dots. When two electrons are paired (lone pairs), they are represented by two adjacent dots located on an atom, and when two paired electrons are shared between atoms (bonds), they are shown as lines. For example, below are the electron dot structures of atoms and the Lewis electron dot structures of the molecules.

These diagrams are helpful because they allow us to show how atoms are connected, and when coupled with Valence Shell Electron Repulsion Theory (VSEPR), we can use Lewis structures to predict the shape of the molecule.

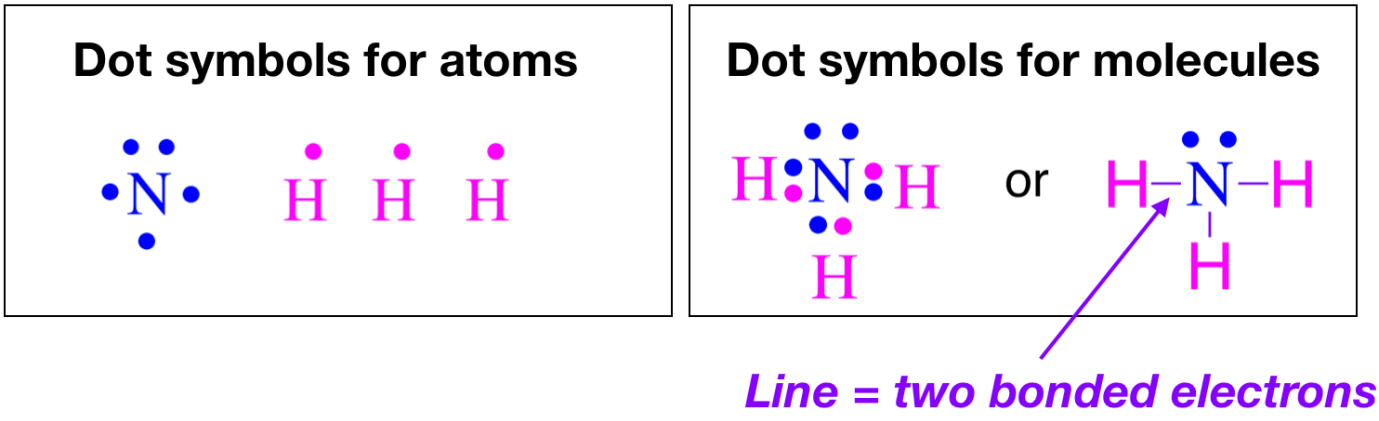


Figure 3.1.1: Lewis dot structure of atoms comprising ammonia and the dot structure of the molecule. (Kathryn Haas; CC-NC-BY-SA)

The drawing of Lewis electron-dot structures is guided largely by the **octet rule**: that atoms form bonds to achieve eight electrons in their valence shell. For many elements, a full valence shell has an electron configuration of s^2p^6, or eight electrons. A common exception to this rule is the first row elements, H and He. These two elements have $n = 1$ as their valence shell, and so they have only two electrons in a full valence shell ($1s^2$ electron configuration). Although H and He are exceptions to the "octet rule", they still form bonds to achieve a full valence shell. It may be better to think of this as the "full valence" rule of bonding. We will see many more violations to the "octet" rule as we progress through this course. In the case of metals and metalloids, breaking of the rules is particularly common. (CC-BY-NC-SA; Kathryn Haas)

Common violations of the octet rule

- **Less than eight electrons (hypovalency)**: H and He are examples of elements that cannot have more than two electrons in their full valence shell. Additionally, there are cases where a valid Lewis structure contains atoms with ***hypovalency:*** *partially-filled valence shells*. An example of this is a *carbocation, a positively charged carbon with only six electrons in its valence shell*. Carbocations are important intermediates in organic chemistry, and they are highly reactive (unstable) Lewis acids (electrophiles). Another example of hypovalency is the Lewis structure for BH_3, which shows boron with three bonds, and only six electrons in its valence shell. Boron hydride is a strong Lewis Acid. (Side note: the actual chemical form of BH_3 is not well-predicted by the Lewis structure and we'll see more about this in Section 3.1.4.)
- **More than eight electrons (hypervalency)**: This is a case where an element has more than eight electrons in its valence shell. It is common for larger atoms ($n \geq 3$), and it is discussed further in Section 3.1.2.

Pitfall alert! There are different rules for counting electrons depending on the purpose of the counting. These are the rules for counting for "octets". The rules for counting for calculation of an atom's formal charge are !!different!! and are described in Section 3.1.1. When an atom is part of a molecule, all electrons that are associated with the atom are counted as contributing to the atom's valence. This includes electrons that are lone pairs on the atoms, and *all* electrons that are shared in bonds. If four electrons are shared between two atoms, it is a double bond. If six electrons are shared between atoms, it is a triple bond.

Electrons in valence (octet) = total unbonded electrons on the atom + total bonded electrons (2 electrons per bond)

Even if you're an old pro at drawing Lewis structures, it's a good idea to polish up. Please complete the practice exercises below. You should get out an actual piece of paper (I know...just do it. It's good for you.) and a writing tool and try to complete each problem before checking the answer.

Exercise 3.1.1

Draw the Lewis structures for H_2O, CO_2, and N_2.

Answer available at the end of this section.

Exercise 3.1.2

Draw the Lewis structures for H_2, BH_3 and BF_3.

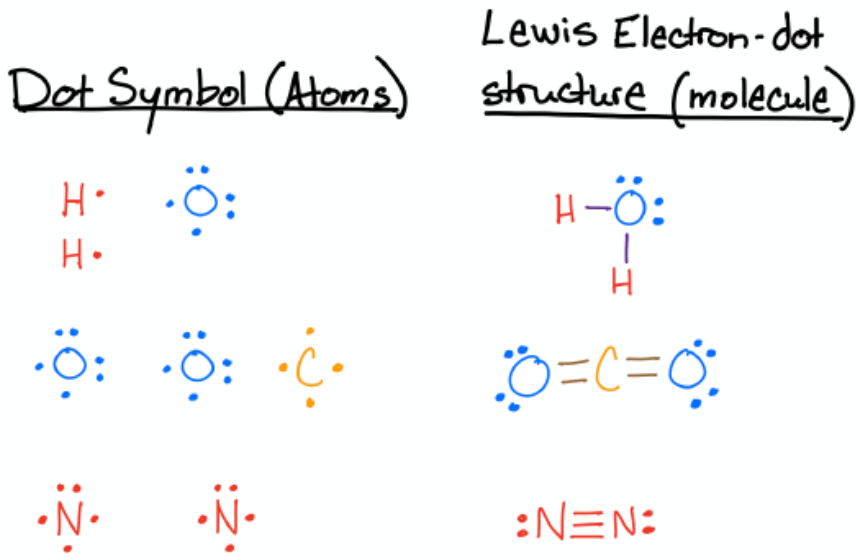
Answer available at the end of this section.

Outside Links

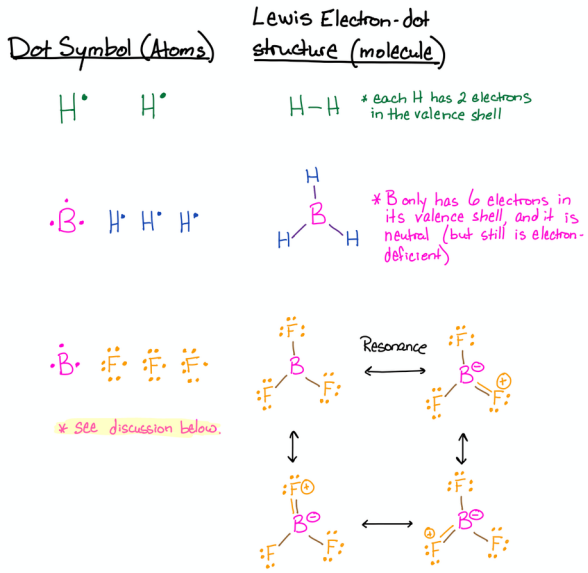
- en.Wikipedia.org/wiki/Lewis_structures
- http://www.ausetute.com.au/lewisstr.html
- cost.georgiasouthern.edu/chem...cule/lewis.htm

Answers

Exercise 3.1.1



Exercise 3.1.2



These three examples include atoms that have less than eight electrons in their valence shell. In the case of H, it is satisfied with only two electrons in its valence, as was discussed earlier in this section. The case of BH_3 was also discussed above. In the Lewis structure of BH_3, the boron can only have six electrons in its octet and it is neutral in charge. The boron is electron deficient even though it has neutral charge.

The case of BF_3 deserves a discussion: If you are unfamiliar with resonance and formal charge, see Sections 3.1.1 (Resonance) and 3.1.3 (Formal Charge) first and come back to this afterward. You might have drawn the BF_3 structure similar to the one that is drawn for BH_3, where boron has three bonds and only six electrons in its valence shell. If you did that, then you are correct; but if you only gave this structure, then your answer is not complete. There are three other correct ways to draw the structure. Since F has lone pairs of electrons, other valid Lewis structures would each have a double bond to one of the fluorines (three total). All of these structures are called resonance structures, and based on the four of them, we could predict that BF_3 would have B-F bonds that have some double-bond character. If fact, this is the case for BF_3; it has bond lengths that are shorter than single bonds, but longer than double bonds. Read more about it on its Wikipedia page here (click).

This page titled 3.1: Lewis Electron-Dot Diagrams is shared under a CC BY-NC 4.0 license and was authored, remixed, and/or curated by Kathryn Haas.

- 3.1: Lewis Electron-Dot Diagrams by Kathryn Haas is licensed CC BY-NC-SA 4.0.
- 2.1B: Lewis Structures by Andrew Iskandar is licensed CC BY 4.0.

3.1.1: Resonance

Learning Objectives

- To understand the concept of resonance.

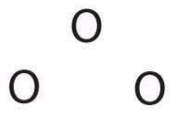
Resonance structures are a set of two or more Lewis Structures that collectively describe the electronic bonding of a single polyatomic species including fractional bonds and fractional charges. Resonance structures are capable of describing delocalized electrons that cannot be expressed by a single Lewis formula with an integral number of covalent bonds.

Sometimes one Lewis Structure is not Enough

Sometimes, even when formal charges are considered, the bonding in some molecules or ions cannot be described by a single Lewis structure. Resonance is a way of describing delocalized electrons within certain molecules or polyatomic ions where the bonding cannot be expressed by a single Lewis formula. A molecule or ion with such delocalized electrons is represented by several contributing structures (also called resonance structures or canonical forms). Such is the case for ozone (O_3), an allotrope of oxygen with a V-shaped structure and an O–O–O angle of 117.5°.

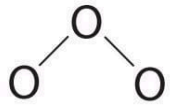
Ozone (O_3)

1. We know that ozone has a V-shaped structure, so one O atom is central:



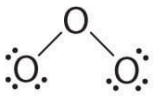
2. Each O atom has 6 valence electrons, for a total of 18 valence electrons.

3. Assigning one bonding pair of electrons to each oxygen–oxygen bond gives



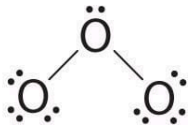
with 14 electrons left over.

4. If we place three lone pairs of electrons on each terminal oxygen, we obtain



and have 2 electrons left over.

5. At this point, both terminal oxygen atoms have octets of electrons. We therefore place the last 2 electrons on the central atom:

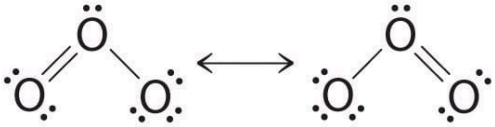


6. The central oxygen has only 6 electrons. We must convert one lone pair on a terminal oxygen atom to a bonding pair of electrons—but which one? Depending on which one we choose, we obtain either



Which is correct? In fact, neither is correct. Both predict one O–O single bond and one O=O double bond. As you will learn, if the bonds were of different types (one single and one double, for example), they would have different lengths. It turns out, however, that both O–O bond distances are identical, 127.2 pm, which is shorter than a typical O–O single bond (148 pm) and longer than the O=O double bond in O_2 (120.7 pm).

Equivalent Lewis dot structures, such as those of ozone, are called **resonance structures**. The position of the *atoms* is the same in the various resonance structures of a compound, but the position of the *electrons* is different. Double-headed arrows link the different resonance structures of a compound:



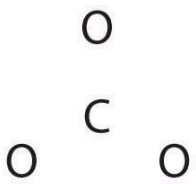
The double-headed arrow indicates that the actual electronic structure is an *average* of those shown, not that the molecule oscillates between the two structures.

> When it is possible to write more than one equivalent resonance structure for a molecule or ion, the actual structure is the average of the resonance structures.

The Carbonate (CO_3^{2-}) Ion

Like ozone, the electronic structure of the carbonate ion cannot be described by a single Lewis electron structure. Unlike O_3, though, the actual structure of CO_3^{2-} is an average of *three* resonance structures.

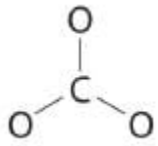
1. Because carbon is the least electronegative element, we place it in the central position:



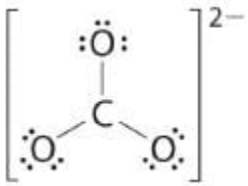
The three oxygens are drawn in the shape of a triangle with the carbon at the center of the triangle.

2. Carbon has 4 valence electrons, each oxygen has 6 valence electrons, and there are 2 more for the –2 charge. This gives 4 + (3 × 6) + 2 = 24 valence electrons.

3. Six electrons are used to form three bonding pairs between the oxygen atoms and the carbon:



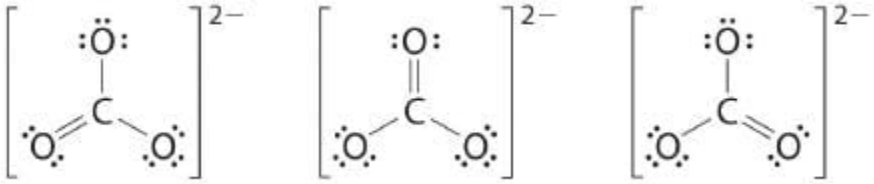
4. We divide the remaining 18 electrons equally among the three oxygen atoms by placing three lone pairs on each and indicating the –2 charge:



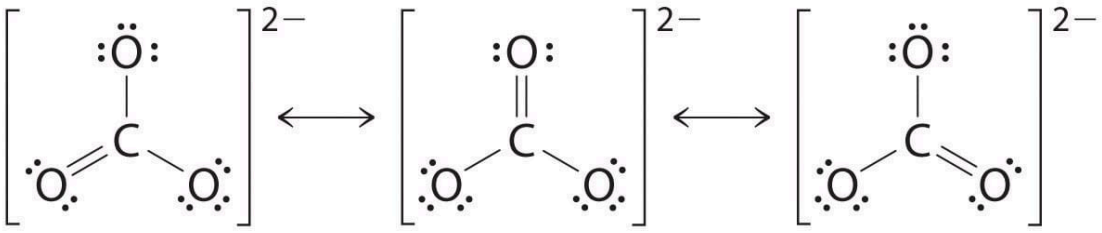
The Lewis dot structure has a central carbon that is bonded to 3 oxygens. Each oxygen has 3 lone pairs. The molecule is inside square brackets and has a charge of minus 2.

5. No electrons are left for the central atom.

6. At this point, the carbon atom has only 6 valence electrons, so we must take one lone pair from an oxygen and use it to form a carbon–oxygen double bond. In this case, however, there are *three* possible choices:



As with ozone, none of these structures describes the bonding exactly. Each predicts one carbon–oxygen double bond and two carbon–oxygen single bonds, but experimentally all C–O bond lengths are identical. We can write resonance structures (in this case, three of them) for the carbonate ion:



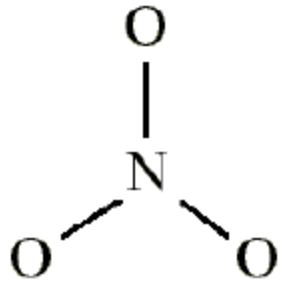
The resonance structure includes all three Lewis dot structures with double headed arrows between them.

The actual structure is an average of these three resonance structures.

The Nitrate (NO_3^-) ion

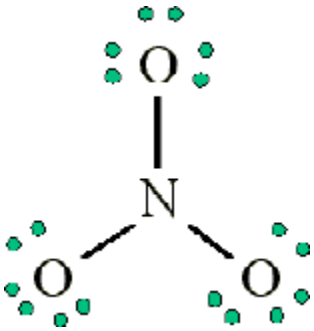
1. Count up the valence electrons: (1*5) + (3*6) + 1(ion) = **24** electrons

2. Draw the bond connectivities:

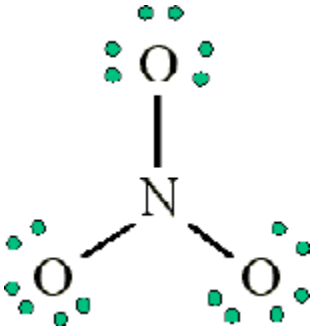


The three oxygens are drawn in the shape of a triangle with the nitrogen at the center of the triangle.

3. Add octet electrons to the atoms bonded to the center atom:

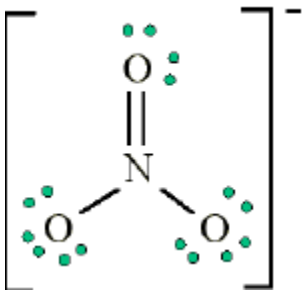


4. Place any leftover electrons (24-24 = **0**) on the center atom:



5. Does the central atom have an octet?

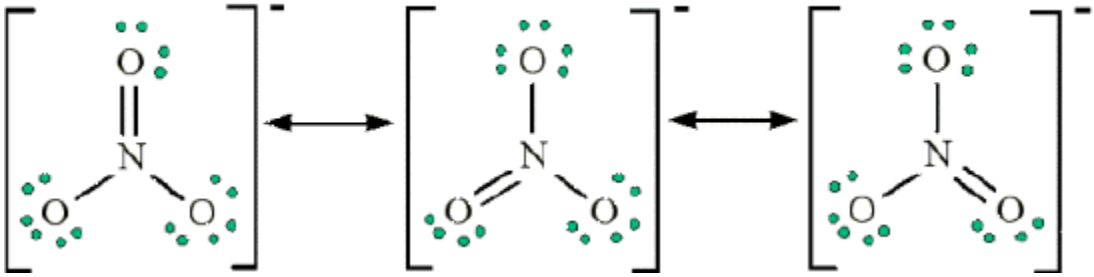
- **NO**, it has 6 electrons
- Add a multiple bond (first try a double bond) to see if the central atom can achieve an octet:



A double bond is added between one oxygen and the central nitrogen. The molecule has a negative charge.

6. Does the central atom have an octet?

- YES
- Are there possible resonance structures? YES



Note: We would expect that the bond lengths in the NO_3^- ion to be somewhat shorter than a single bond.

YouTube Video

This interactive element is not available in this format. Visit the link or scan the QR code to access it online.

View this YouTube Video online

Example 3.1.1.1: Benzene

Benzene is a common organic solvent that was previously used in gasoline; it is no longer used for this purpose, however, because it is now known to be a carcinogen. The benzene molecule (C_6H_6) consists of a regular hexagon of carbon atoms, each of which is also bonded to a hydrogen atom. Use resonance structures to describe the bonding in benzene.

Given: molecular formula and molecular geometry

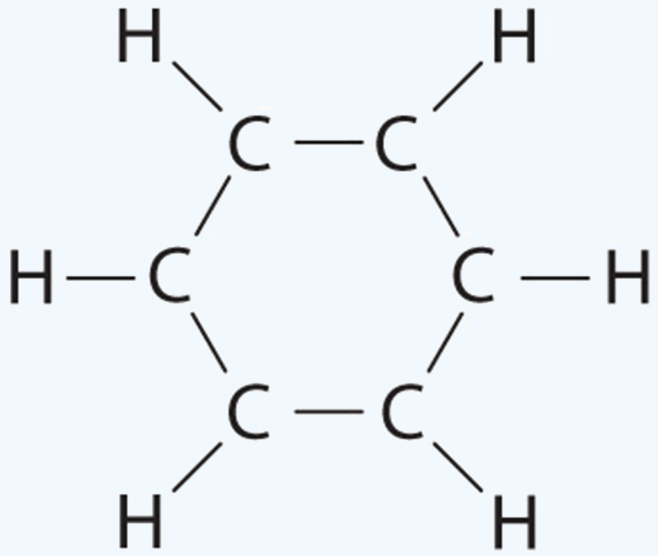
Asked for: resonance structures

Strategy:

A. Draw a structure for benzene illustrating the bonded atoms. Then calculate the number of valence electrons used in this drawing.
B. Subtract this number from the total number of valence electrons in benzene and then locate the remaining electrons such that each atom in the structure reaches an octet.
C. Draw the resonance structures for benzene.

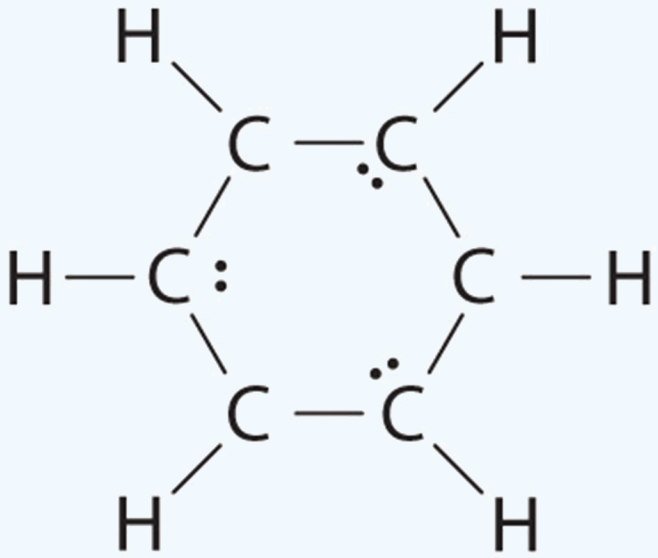
Solution:

A Each hydrogen atom contributes 1 valence electron, and each carbon atom contributes 4 valence electrons, for a total of (6 × 1) + (6 × 4) = 30 valence electrons. If we place a single bonding electron pair between each pair of carbon atoms and between each carbon and a hydrogen atom, we obtain the following:



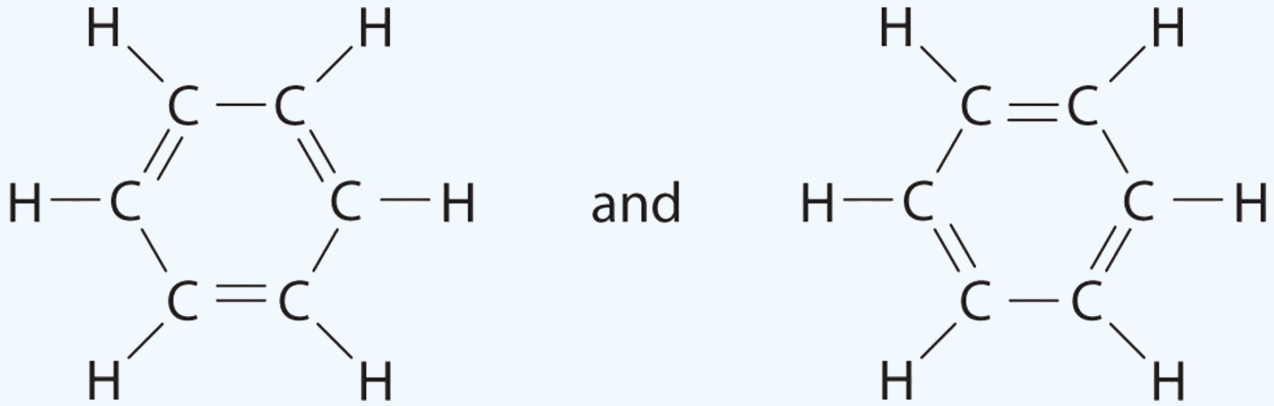
Each carbon atom in this structure has only 6 electrons and has a formal charge of +1, but we have used only 24 of the 30 valence electrons.

B If the 6 remaining electrons are uniformly distributed pairwise on alternate carbon atoms, we obtain the following:

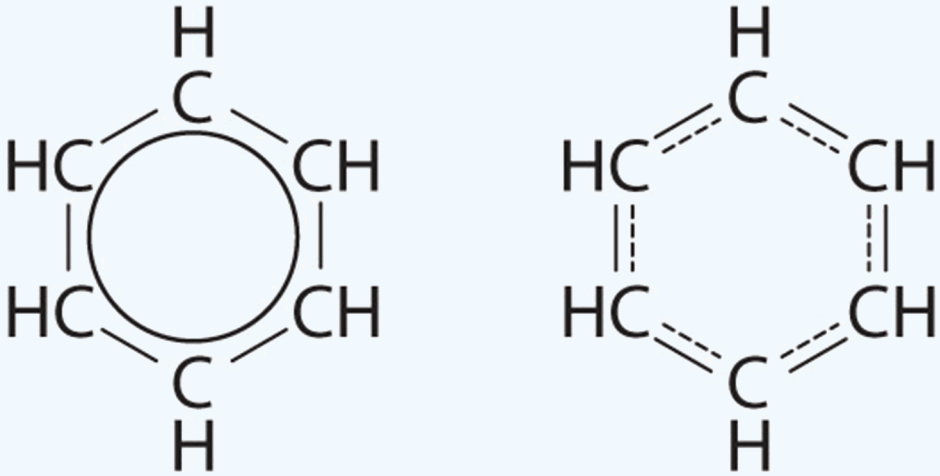


Three carbon atoms now have an octet configuration and a formal charge of –1, while three carbon atoms have only 6 electrons and a formal charge of +1. We can convert each lone pair to a bonding electron pair, which gives each atom an octet of electrons and a formal charge of 0, by making three C=C double bonds.

C There are, however, two ways to do this:



Each structure has alternating double and single bonds, but experimentation shows that each carbon–carbon bond in benzene is identical, with bond lengths (139.9 pm) intermediate between those typically found for a C–C single bond (154 pm) and a C=C double bond (134 pm). We can describe the bonding in benzene using the two resonance structures, but the actual electronic structure is an average of the two. The existence of multiple resonance structures for aromatic hydrocarbons like benzene is often indicated by drawing either a circle or dashed lines inside the hexagon:



Benzene

Exercise 3.1.1.1: Nitrite Ion

The sodium salt of nitrite is used to relieve muscle spasms. Draw two resonance structures for the nitrite ion (NO_2^-).

Answer available at the end of this section.

Warning

If several reasonable resonance forms for a molecule exists, the "actual electronic structure" of the molecule will probably be intermediate between all the forms that you can draw. The classic example is benzene in Example 3.1.1.1. One would expect the double bonds to be shorter than the single bonds, but if one overlays the two structures, you see that one structure has a single bond where the other structure has a double bond. The best measurements that we can make of benzene do not show two bond lengths - instead, they show that the bond length is intermediate between the two resonance structures.

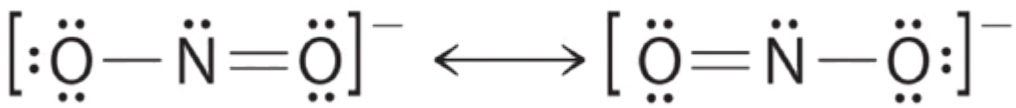
Resonance structures is a mechanism that allows us to use all of the possible resonance structures to try to predict what the actual form of the molecule would be. Single bonds, double bonds, triple bonds, +1 charges, -1 charges, these are our limitations in explaining the structures, and the true forms can be in between - a carbon-carbon bond could be mostly single bond with a little bit of double bond character and a partial negative charge, for example.

Summary

Some molecules have two or more chemically equivalent Lewis electron structures, called resonance structures. Resonance is a mental exercise and method within the Valence Bond Theory of bonding that describes the delocalization of electrons within molecules. These structures are written with a **double-headed arrow** between them, indicating that none of the Lewis structures accurately describes the bonding but that the actual structure is an average of the individual resonance structures. Resonance structures are used when one Lewis structure for a single molecule cannot fully describe the bonding that takes place between neighboring atoms relative to the empirical data for the actual bond lengths between those atoms. The net sum of valid resonance structures is defined as a resonance hybrid, which represents the overall delocalization of electrons within the molecule. A molecule that has several resonance structures is more stable than one with fewer. Some resonance structures are more favorable than others.

Answers

Exercise 3.1.1.1**: Nitrite Ion**



There is a double bond between one oxygen and the nitrogen, It can be found on the left oxygen or the right oxygen.

Resonance structures are particularly common in oxoanions of the *p*-block elements, such as sulfate and phosphate, and in aromatic hydrocarbons, such as benzene and naphthalene.

This page titled 3.1.1: Resonance is shared under a CC BY-NC 3.0 license and was authored, remixed, and/or curated by Kathryn Haas.

- 8.6: Resonance Structures is licensed CC BY-NC-SA 3.0.

3.1.2: Breaking the octet rule with higher electron counts (hypervalent atoms)

The octet rule applies well to atoms in the second row of the periodic table, where a full valence shell includes eight electrons with an electron configuration of s^2p^6. Even elements in the third and fourth row are known to follow this rule *sometimes*, but not always. In larger atoms, where $n \geq 3$ the valence shell contains additional subshells: the $d, f, g...$ subshells. Therefore, atoms with $n \geq 3$ can have higher valence shell counts by "expanding" into these additional subshells. When atoms contain more than eight electrons in their valence shell, they are said to be **hypervalent**. Hypervalency allows atoms with $n \geq 3$ to break the octet rule by having more than eight electrons. This also means they can have five or more bonds; something that is nearly unheard of for atoms with $n \leq 2$. Complete the exercises below to see examples of molecules containing hypervalent atoms.

Exercise 3.1.2.1

Draw the Lewis structures for sulfur hexafluoride ($\mathrm{SF_6}$).

Answer available at the end of this section.

Exercise 3.1.2.1

Draw the Lewis structure for chlorine trifluoride ($\mathrm{ClF_3}$.

Answer available at the end of this section.

Is hypervalency real? Not exactly. Hypervalency is a concept associated with hybrid orbital theory and Lewis theory. It's useful for some simple things, like predicting how atoms are connected and predicting molecular shape. But the idea that the d-orbitals are involved in bonding isn't accurate according to wave mechanics.

For main group molecules, chemists (like Pauling) thought a long time ago that hypervalence is due to expanded s^2p^6 octets. The consensus is now clear that d orbitals are NOT involved in bonding in molecules like SF_6 any more than they are in SF_4 and SF_2. In all three cases, there is a small and roughly identical participation of d-orbitals in the wavefunctions. This has been established in both MO and VB theory. However, using hybrid orbitals with d-orbital contributions equips us with a language which can pragmatically describe the geometries of highly coordinated substances.

While hybrid orbitals are a powerful tool to describe the geometries and shape of molecules and metal complexes, in "real" molecules their significance may be debated. Often a more realistic molecular orbitals approach is needed. However, from an epistemologically simple point of view, bonding theories can only be judged by their predictions. To the extent that hybridization can explain the shapes of PF_5 and SF_6, valence bond theory is a perfectly good theory. To the extent that if you write out the valence bond wavefunction using hybridized orbitals and calculate energies and other properties à la Pauling (i.e., ionization energy and electron affinities) and find them to be off from experimental results (by tens of kcals/mol), then valence bond theory is not accurate.

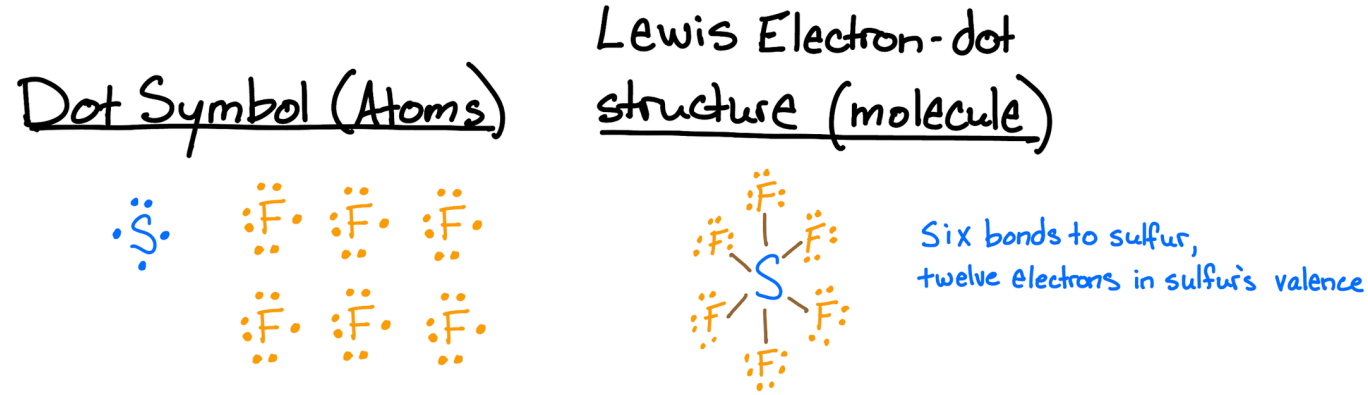
> Bonding theories can only be judged by their predictions.

A simple explanation that can be given is that molecular wavefunctions constructed out of hybridized atomic orbitals are accurate enough to predict some things, but not others. Predictions of any theory must be compared with empirical evidence to assess when they work and when they fail. When a theory gives the wrong answer, at least one assumption must not hold. In this case, the valence bond wavefunction is not accurate enough to capture some important features of a system's electronic structure. It may not be the most intellectually satisfying answer, but to say more would result in a much more complicated answer and certainly far beyond the level reasonably expected from general chemistry discussions.

Answers

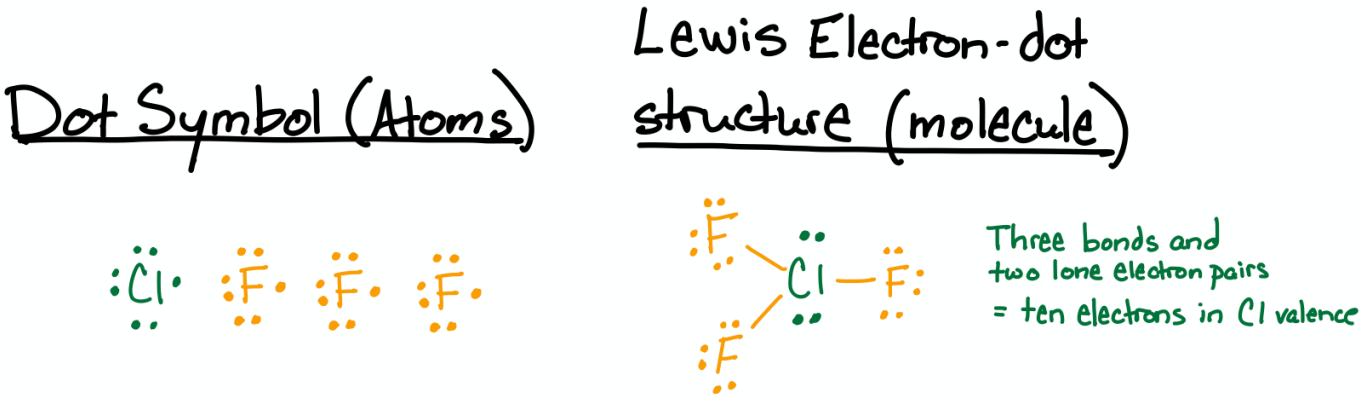
Exercise 3.1.2.1

Each fluorine atom has one valence electron and will make one bond each. The sulfur has six valence electrons, and must make six bonds to form a molecule with the six fluorine atoms. The molecular structure has six bonds to sulfur, with twelve valence electrons. The sulfur is hypervalent.



Exercise 3.1.2.1

All atoms are halogens and each has seven valence electrons. Chlorine is capable of hypervalency because it is in the third row of the periodic table; however fluorine cannot have more than eight valence electrons in its valence because it is in the second row. The structure has the three fluorine atoms bonded to a central chlorine atom. The chlorine has a valence of ten electrons due to its three bonds and two lone pairs.



.

This page titled 3.1.2: Breaking the octet rule with higher electron counts (hypervalent atoms) is shared under a CC BY-NC 4.0 license and was authored, remixed, and/or curated by Kathryn Haas.

- 3.1.2: Breaking the octet rule with higher electron counts (hypervalent atoms) by Kathryn Haas is licensed CC BY-NC-SA 4.0.

3.1.3: Formal Charge

The formal charge of an atom in a molecule is the *hypothetical* charge the atom would have if we could redistribute the electrons in the bonds evenly between the atoms. Another way of saying this is that formal charge results when we take the number of valence electrons of a neutral atom, subtract the nonbonding electrons, and then subtract the number of bonds connected to that atom in the Lewis structure.

Calculating Formal Charges

We calculate the formal charge of an atom in a molecule or polyatomic ions as follows:

Formal Charge = (valence electrons of the "free" element) - (unshared electrons) - (bonds).

We can double-check formal charge calculations by determining the sum of the formal charges for the whole structure. The sum of the formal charges of all atoms in a molecule must be zero; the sum of the formal charges in an ion should equal the charge of the ion.

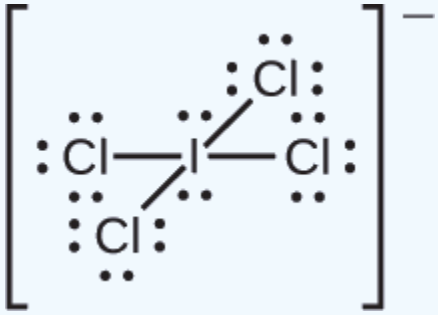
We must remember that the formal charge calculated for an atom is not the *actual* charge of the atom in the molecule. Formal charge is only a useful bookkeeping procedure; it does not indicate the presence of actual charges.

Calculating Formal Charge from Lewis Structures

Assign formal charges to each atom in the interhalogen ion $\mathrm{ICl_4^-}$.

Solution

We divide the bonding electron pairs equally for all $\mathrm{I{-}Cl}$ bonds:



We assign lone pairs of electrons to their atoms. Each Cl atom now has seven electrons assigned to it, and the I atom has eight.

Subtract this number from the number of valence electrons for the neutral atom:

- I: 7 – 8 = –1
- Cl: 7 – 7 = 0

The sum of the formal charges of all the atoms equals –1, which is identical to the charge of the ion (–1).

Exercise 3.1.3.1

Calculate the formal charge for each atom in the carbon monoxide molecule:



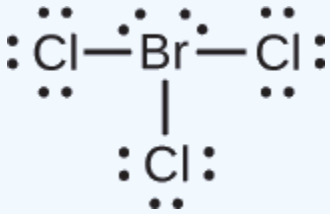
Answer available at the end of this section.

Example: Calculating Formal Charge from Lewis Structures

Assign formal charges to each atom in the interhalogen molecule $\mathrm{BrCl_3}$.

Solution

Assign one of the electrons in each Br–Cl bond to the Br atom and one to the Cl atom in that bond:



Assign the lone pairs to their atom. Now each Cl atom has seven electrons and the Br atom has seven electrons.

Subtract this number from the number of valence electrons for the neutral atom. This gives the formal charge:

- Br: 7 – 7 = 0
- Cl: 7 – 7 = 0

All atoms in $\mathrm{BrCl_3}$ have a formal charge of zero, and the sum of the formal charges totals zero, as it must in a neutral molecule.

Exercise 3.1.3.2

Determine the formal charge for each atom in $\mathrm{NCl_3}$.

Answer available at the end of this section.

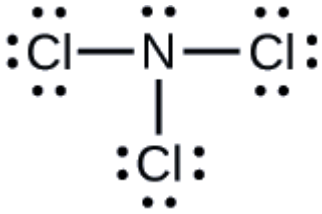
Answers

Exercise 3.1.3.1

C –1, O +1

Exercise 3.1.3.2

N: 0; all three Cl atoms: 0



This page titled 3.1.3: Formal Charge is shared under a CC BY-NC 4.0 license and was authored, remixed, and/or curated by Kathryn Haas.

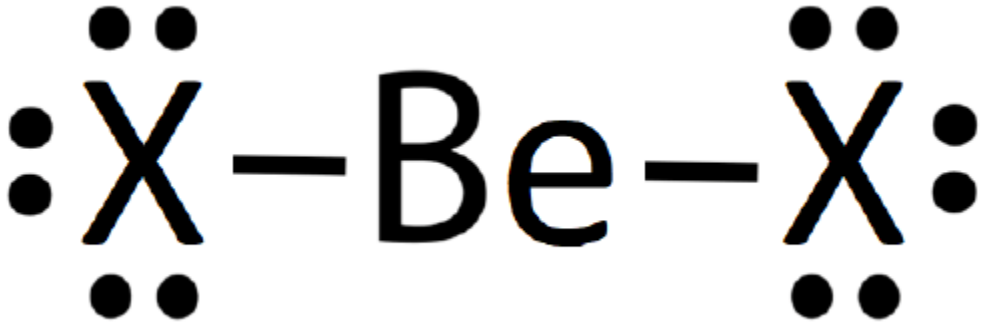
- 7.5: Formal Charges and Resonance by OpenStax is licensed CC BY 4.0. Original source: https://openstax.org/details/books/chemistry-2e.

3.1.4: Lewis Fails to Predict Unusual Cases - Boron and Beryllium

Two notable cases where Lewis theory fails to predict structure are the cases of beryllium (Be) and boron (B). These two atoms are in period 2 ($n = 2$) of the periodic table and their atoms have the valence electron configurations of $2s^2$ and $2s^2 2p^1$, respectively.

Beryllium

The Lewis electron dot structures are shown below for $\mathrm{BeX_2}$, where X is one of the halogens, F or Cl.



Each of the structures above would predict a linear geometry for the $\mathrm{BeX_2}$ molecule. Together the three resonance structures suggest partial double-bond character in the Be-X bond, which results in an intermediate bond length between a single and double bond.

There are issues with each of these resonance structures. The structure on the left would predict only four electrons around Be ; thus, the atom does not fulfill the octet rule. The structure on the left suggests multiple bonds for the halogen (X) and high separation of charge with formal charge on each atom. The structure in the middle is a mix of these problems. None of these situations is ideal according to Lewis theory. Further, experimental data is not consistent with any of these structures or their resonance hybrid (except in the case of $\mathrm{BeCl_2}$ at very high temperatures).

It turns out that the monomer of $\mathrm{BeX_2}$ does exist, but only at very high temperatures and low pressures. Even under extreme conditions, the monomer is not particularly stable due to the electron deficiency around Be.

BeF_2

At ambient temperature and pressure, BeF_2 is a solid that looks similar to quartz (Figure $3.1.4.1$) The Be is four-coordinate with tetrahedral geometry; each F is two-coordinate and the Be-F bond length is 1.54 Å. This structure is possible due to an extended 3-dimensional network in the solid where adjacent BeF_2 units are bonded to one another, as shown in Figure $3.1.4.1$.



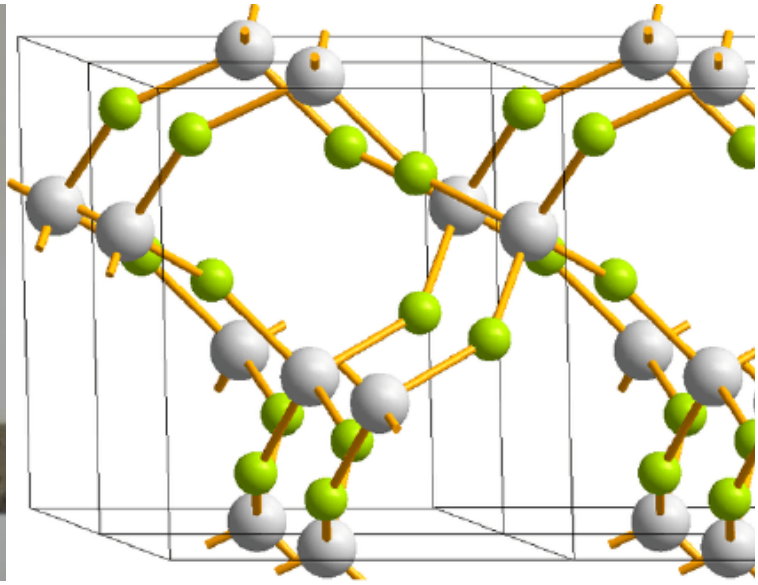


Figure 3.1.4.1: (left) A nugget of beryllium fluoride obtained from Materion. Black spots are carbon (CC BY-SA 3.0; Bckelleher via Wikipedia). (right) BeF2 structure (CC BY-SA 3.0 Unported; Materialscientist via Wikipedia)

In the liquid phase, $\mathrm{BeF_2}$ has a fluctuating tetrahedral structure where Be and F ions exchange. The vapor phase is reached at temperatures higher than 1000 °C (at ~ 1 atm). In the vapor phase, $\mathrm{BeF_2}$ exists as a monomer with linear geometry and a bond length of 1.43 Å, consistent with a double bond between Be and F.

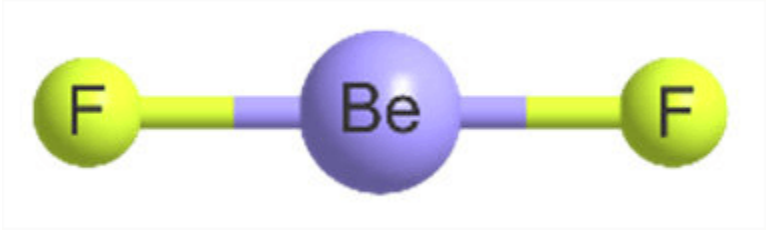


Figure 3.1.4.2: Geometries of $\mathrm{BeF_2}$. (CC BY; Ibon Alkorta and Anthony C. Legoe via Inorganics)

$\mathrm{BeCl_2}$

At ambient temperature and pressure, $\mathrm{BeCl_2}$ is a solid. As in $\mathrm{BeF_2}$ described above, $\mathrm{BeCl_2}$ has four-coordinate, tetrahedral Be and two-coordinate Cl. In contrast to $\mathrm{BeF_2}$, solid $\mathrm{BeCl_2}$ is a 1-dimensional polymer consisting of edge-shared tetrahedral.

In the gas phase, $\mathrm{BeCl_2}$ exists as a dimer with two chlorine atoms bridging two Be atoms. In the dimer, the Be atoms are 3-coordinate. Bridging Cl atoms are two-coordinate, while terminal Cl atoms are one-coordinate. At higher temperatures in the vapor phase, the linear monomer also exists.

Boron ($2s^2 2p^1$)

Prediction based on Lewis structures:

Lewis structures of $\mathrm{BH_3}$ and $\mathrm{BF_3}$ were described in Exercise 3.1.2, and are drawn again below for convenience.

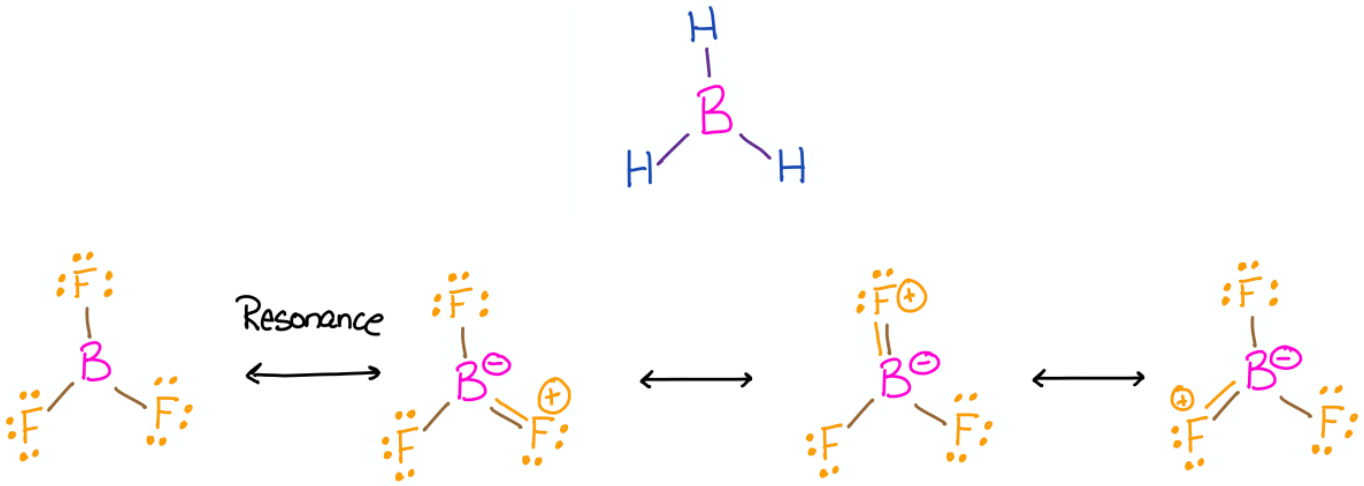


Figure 3.1.4.2: Lewis structures of $\mathrm{BH_3}$ and $\mathrm{BF_3}$. (Kathryn Haas; CC-NC-BY-SA)

Boron trihalides

Boron trihalides, like $\mathrm{BF_3}$, have properties that are largely predicted by Lewis structures and VSEPR theory. The Lewis structure for $\mathrm{BF_3}$ includes several resonance structures. The structure with only single bonds is the most common representation for this molecule because the charge separation shown in the other structures is considered to be unfavorable. The highly polarized B-F bond has a dipole moment that lies opposite to the indicated formal charges shown in the resonance structures with double bonds between boron and fluorine.

The resonance hybrid of $\mathrm{BF_3}$ predicts partial double bond character between boron and fluorine, thus a bond length shorter than a single bond. Using the Lewis structures and VSEPR theory, we would predict a trigonal planar geometry around boron. In fact, the actual structure of $\mathrm{BF_3}$ is a monomer with trigonal planar geometry and with bond length that is shorter than a single bond. The case is similar to structures of other boron trihalides as well.

Boron trihalides are electron deficient at the boron center and react readily with Lewis bases. In other words they are strong Lewis acids (electrophiles).

Boron trihydride (BH_3 is really B_2H_6)

The properties of boron trihydride $(\mathrm{BH_3})$ are not predicted by the simple predictions made through Lewis structures and VSEPR. The monomer, BH_3, is not stable, but when dissolved in the presence of a Lewis base, BH_3 can form a stable acid-base adduct. In its pure form, the compound actually exists as a dimeric gas with a molecular unit of B_2H_6 (try drawing a valid Lewis structure for that!). Its unexpected structure includes two H's that bridge the two boron atoms in 3-center-2-electron bonds. You can read more about B_2H_6 on the Wikipedia page for Diborane(6). The unique bonding observed for boron is described more in Chapter 8 and Chapter 15.

This page titled 3.1.4: Lewis Fails to Predict Unusual Cases - Boron and Beryllium is shared under a CC BY-NC 4.0 license and was authored, remixed, and/or curated by Kathryn Haas.

- 3.1.4: Lewis Fails to Predict Unusual Cases - Boron and Beryllium by Kathryn Haas is licensed CC BY-NC-SA 4.0.

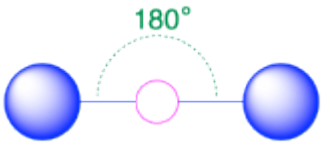
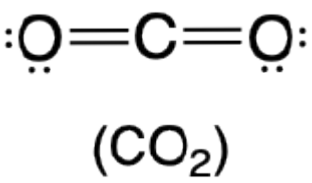
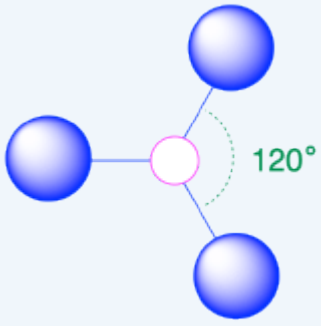
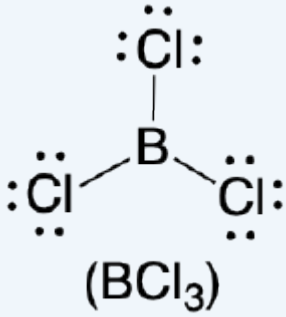
3.2: Valence Shell Electron-Pair Repulsion

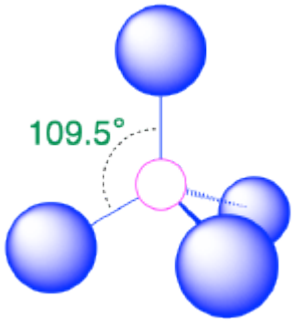
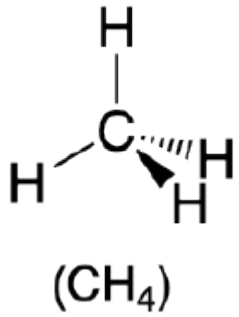
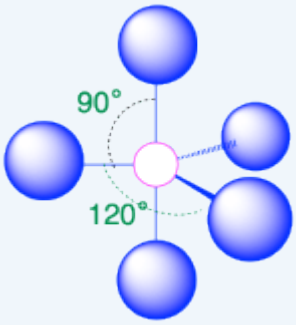
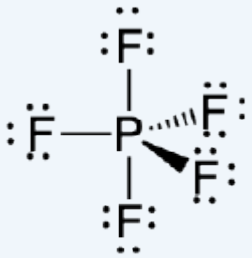
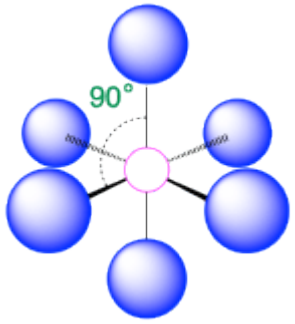
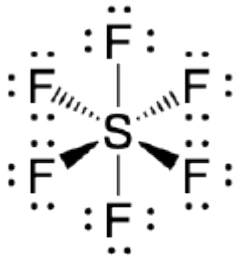
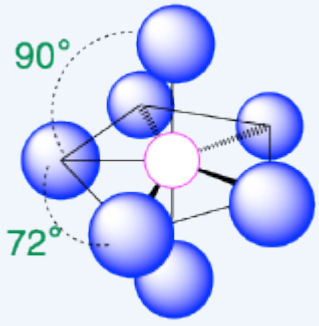
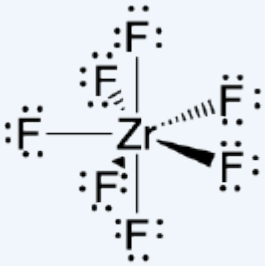
Introduction to VSEPR

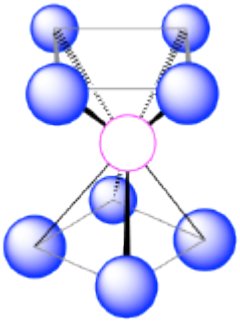
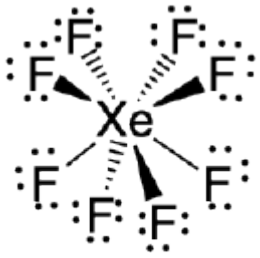
The **Valence Shell Electron Repulsion (VSEPR)** model can predict the structure of most molecules and polyatomic ions in which the central atom is a nonmetal; it also works for some structures in which the central atom is a metal. VSEPR builds on Lewis electron dot structures (discussed in Section 3.1(opens in new window)); Lewis structures alone predict only connectivity while the Lewis structure and VSEPR together can predict the geometry of each atom in a molecule. The main idea of VSEPR theory is that pairs of electrons (in bonds and in lone pairs) repel each other. The pairs of electrons (in bonds and in lone pairs) are called "groups". Because electrons repel each other electrostatically, the most stable arrangement of electron groups (i.e., the one with the lowest energy) is the one that minimizes repulsion. Groups are positioned around the central atom in a way that produces the molecular structure with the lowest energy. In other words, the repulsion between groups around an atom favors a geometry in which the groups are as far apart from each other as possible. Although VSEPR is simplistic because it does not account for the subtleties of orbital interactions that influence molecular shapes, it accurately predicts the three-dimensional structures of a large number of compounds.

We can use the VSEPR model to predict the geometry around the atoms in a polyatomic molecule or ion by focusing on the number of electron pairs (groups) around a *central atom* of interest. Groups include bonded and unbonded electrons; a single bond, a double bond, a triple bond, a lone pair of electrons, or even a single unpaired electron each count as one group. The molecule or polyatomic ion is given an $\mathbf{AX}_{\boldsymbol{m}}\mathbf{E}_{\boldsymbol{n}}$ designation, where **A is the central atom**, **X is a bonded atom**, **E is a nonbonding** valence electron group (usually a lone pair of electrons), and $\boldsymbol{m}$ and $\boldsymbol{n}$ are integers. The number of groups is equal to the sum of $\boldsymbol{m}$ and $\boldsymbol{n}$. Using this information, we can describe the molecular geometry around a central atom, that is, the arrangement of the *bonded atoms* in a molecule or polyatomic ion. The geometries that are predicted from VSEPR when a central atom has only bonded groups ($n = 0$) are listed below in Table 3.2.1. The cases where lone pairs contribute to the total groups ($n \geq 1$) are discussed in the next section about lone pair repulsion(opens in new window).

Table 3.2.1. Geometries predicted using VSEPR theory (bonded groups only).

Groups around central atom ($m + n$)	Geometry Name	Geometry Sketch	Predicted bond Angle	Example
2	linear		180°	 (CO_2)
3	trigonal plane(opens in new window)		120°	 (BCl_3)

Groups around central atom ($m + n$)	Geometry Name	Geometry Sketch	Predicted bond Angle	Example
4	tetrahedron		109.5°	 (CH_4)
5	trigonal bipyramid		90° and 120°	 (PF_5)
6	octahedron		90°	 (SF_6)
7	pentagonal bipyramid		90° and 72°	 ($[ZrF_7]^{3-}$)

Groups around central atom ($m + n$)	Geometry Name	Geometry Sketch	Predicted bond Angle	Example
8	square antiprism		70.5°, 99.6° and 109.5°	 $([XeF_8]^{2-})$

Practice

VSEPR to predict Molecular Geometry

You can follow these four steps to predict the geometry around an atom using VSEPR:

1. Draw the Lewis electron structure of the molecule or polyatomic ion.
2. For the central atom of interest, assign the AX_mE_n designation and the total number of groups ($m+n$).
3. Determine the electron group arrangement around the central atom that minimizes repulsions.
4. Describe the molecular geometry.

Use the procedure above to complete the exercises below

Exercise 3.2.1

Predict the geometry around the central atom in BeH_2 and CO_2.

Answer BeH2 available at the end of this section.

Answer CO2 available at the end of this section.

2. The carbon atom forms two double bonds. Each double bond is counted as one group, so there are two groups around the central atom. Once again, both groups around the central atom are bonds, so CO_2 is designated as AX_2.

3. Like BeH_2, the arrangement that minimizes repulsions places the groups 180° apart.

4. VSEPR only recognizes groups around the *central* atom (the carbon). Thus the lone pairs on the oxygen atoms do not influence the molecular geometry. With two bonded groups on the central atom and no lone pairs, the molecular geometry of CO_2 is linear (Table 3.2.1). The structure of CO_2 is shown in Table 3.2.1.

Exercise 3.2.2

Predict the geometry around the central atom in BCl_3 and CO_3^{2-}.

Answer BCl3 available at the end of this section.

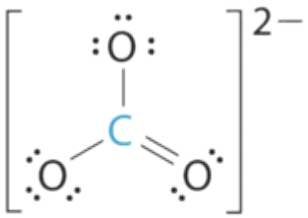
2. There are three groups around the central atom and all are single bonds. The structure is designated as AX_3.

3. To minimize repulsions, the groups are placed 120° apart (Table 3.2.1).

4. From Table 3.2.1 we see that with three bonding pairs around the central atom, the molecular geometry of BCl_3 is *trigonal planar*.

Answer CO_3^{2-}

1. The central atom, carbon, has four valence electrons, and each oxygen atom has six valence electrons. The Lewis electron structure of one of three resonance forms is represented as

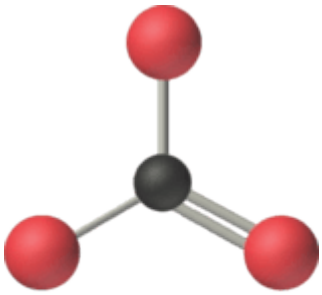


Lewis structure

2. The structure of CO_3^{2-} is a resonance hybrid. It has three identical bonds, each with a bond order of $1\frac{1}{3}$. All electron groups are bonds. With three bonding groups around the central atom, the structure is designated as AX_3.

3. We minimize repulsions by placing the three groups 120° apart (Table 3.2.1).

4. We see from Table 3.2.1 that the molecular geometry of CO_3^{2-} is trigonal planar with bond angles of 120°.



Molecular geometry
(trigonal planar)

In our next example we encounter the effects of lone pairs and multiple bonds on molecular geometry for the first time.

Exercise 3.2.3

Predict the geometry around the central atom in CH_4, PCl_5 and SF_6.

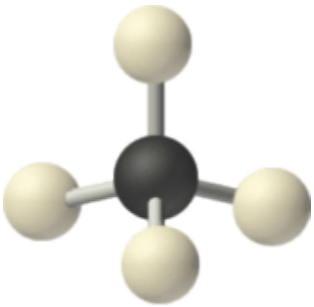
Answer CH4 available at the end of this section.

2. There are four electron groups around the central atom. All electron groups are bonding pairs, so the structure is designated

as AX_4.

3. As shown in Table 3.2.1, repulsions are minimized by placing the groups in the corners of a tetrahedron with bond angles of 109.5°.

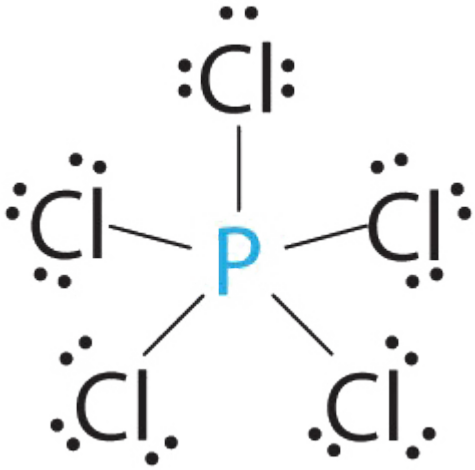
4. With four bonding pairs, the molecular geometry of methane is *tetrahedral* (Table 3.2.1).



Molecular geometry
(tetrahedral)

Answer PCl_5

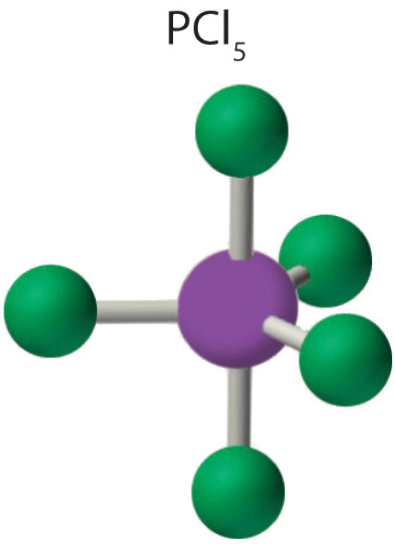
1. Phosphorus has five valence electrons and each chlorine has seven valence electrons, so the Lewis electron structure of PCl_5 is



2. There are five bonding groups around phosphorus, the central atom. All electron groups are bonds, so the structure is designated as AX_5.

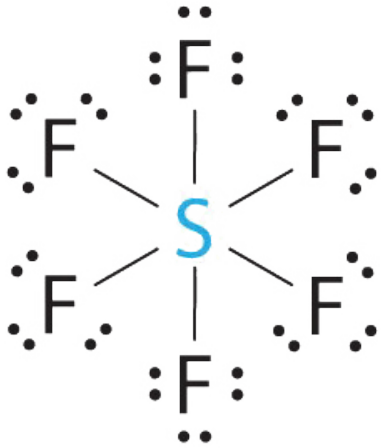
3. The structure that minimizes repulsions is a *trigonal bipyramid*, which consists of two trigonal pyramids that share a base (Table 3.2.1).

4. The molecular geometry of PCl_5 is *trigonal bipyramidal*, as shown below. The molecule has three atoms in a plane in *equatorial* positions and two atoms above and below the plane in *axial* positions. The three equatorial positions are separated by 120° from one another, and the two axial positions are at 90° to the equatorial plane. The axial and equatorial positions are not chemically equivalent.



Answer SF_6

1. The central atom, sulfur, contributes six valence electrons, and each fluorine atom has seven valence electrons, so the Lewis electron structure is



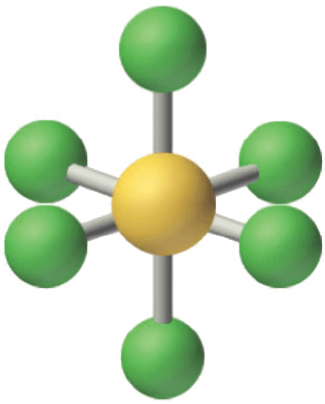
Lewis structure

With an expanded valence, this species is an exception to the octet rule.

2. There are six electron groups around the central atom, each a bonding pair. We see from Figure 3.2.2 that the geometry that minimizes repulsions is *octahedral*.

3. With only bonding pairs, SF_6 is designated as AX_6. All positions are chemically equivalent, so all electronic interactions are equivalent.

4. There are six nuclei, so the molecular geometry of SF_6 is octahedral.

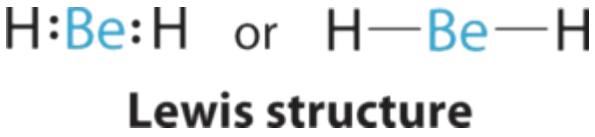


Molecular geometry
(octahedral)

Answers

Exercise 3.2.1

1. The central atom, beryllium, contributes two valence electrons, and each hydrogen atom contributes one. The Lewis electron structure is

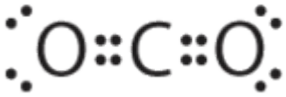


Lewis structure

2. There are two groups around the central atom, and both groups are single bonds. Thus BeH_2 is designated as AX_2.
3. We see from Table 3.2.1 that the arrangement that minimizes repulsions places the groups 180° apart.
4. From Table 3.2.1 we see that with two bonding pairs, the molecular geometry that minimizes repulsions in BeH_2 is *linear*.

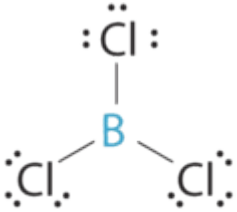
Exercise 3.2.1

1. The central atom, carbon, contributes four valence electrons, and each oxygen atom contributes six. The Lewis electron structure is



Exercise 3.2.2

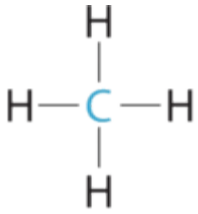
1. The central atom, boron, contributes three valence electrons, and each chlorine atom contributes seven valence electrons. The Lewis electron structure is



Lewis structure

Exercise 3.2.3

1. The central atom, carbon, contributes four valence electrons, and each hydrogen atom has one valence electron, so the full Lewis electron structure is



Lewis structure

This page titled 3.2: Valence Shell Electron-Pair Repulsion is shared under a CC BY-NC-SA 4.0 license and was authored, remixed, and/or curated by Kathryn Haas.

- 3.2: Valence Shell Electron-Pair Repulsion by Kathryn Haas is licensed CC BY-NC-SA 4.0.

3.2.1: Lone Pair Repulsion

In the previous section, we saw how to use VSEPR to predict the geometry around a central atom based on the number of groups attached to a central atom. However, our previous discussion was limited to the simple cases where all of the groups were bonded groups (i.e., in the designation $\mathbf{AX_mE_n}$, n=0). When all of the groups are bonds, the geometries can be predicted using information in Table 3.2.1 in the previous section. Now we will consider cases where one or more of these groups are lone pairs.

Lone pairs have stronger repulsive forces than bonded groups.

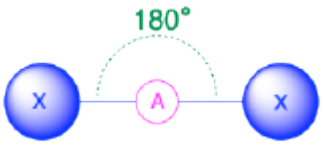
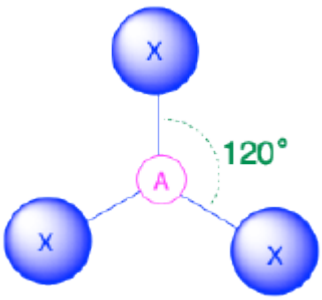
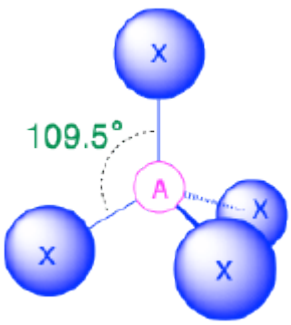
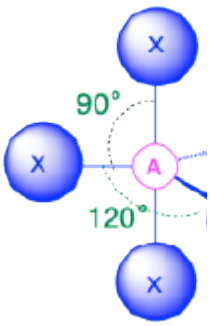
When one or more of the groups is a lone pair of electrons (non-bonded electrons), the experimentally-observed geometry around an atom is slightly different than in the case where all groups are bonds. The actual bond angles are similar, but not exactly the same, as those predicted based on the *total number of groups* (the "parent" geometry). When there is a mixture of group types (**lone pairs (E)** ***and*** **bonded groups (X)**) there are three different types of angles to consider: bond angles between two bonded atoms (**X-X** angles), angles between a bonded atom and a lone pair (**X-E** angles), and angles between two lone pairs (**E-E** angles). Empirical evidence shows the following trend in the degree of bond angles around atoms with a mixture of group types:

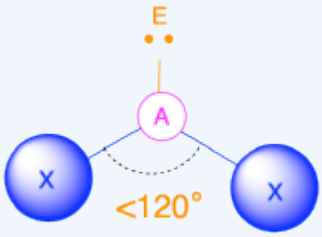
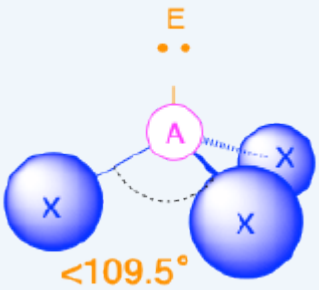
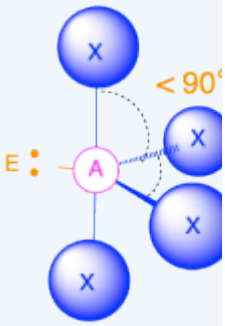
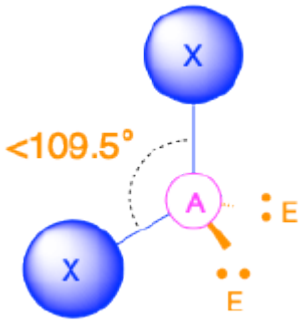
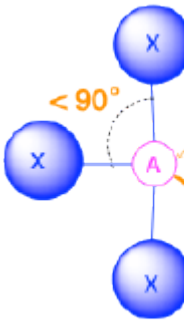
Trend in bond angles:

E-E >**X-E** >**X-X**

Using empirical evidence as a guide, we can predict that lone pairs repel other electron groups more strongly than bonded pairs. The molecular geometry of molecules with lone pairs of electrons is better predicted when we consider that electronic repulsion created by lone pairs is stronger than the repulsion from bonded groups. It is difficult to predict the exact bond angle based on this principle, but we can predict approximate angles, as described and summarized below in Table 3.2.1.1.

Table 3.2.1.1: Predictions of molecular geometry and bond angles around atoms with a mixture of bonded (X) and unbonded (E) elec

	Electron Groups (*m* + *n*)			
	2 (steric number = 2)	**3** (steric number = 3)	**4** (steric number = 4)	**5** (steric number
Parent Geometry (**0 lone pairs**) **AX_m**	 **AX_2**, linear 180°	 **AX_3**, trig. plane 120°	 **AX_4**, tetrahedron 109.5°	 **AX_5**, trig. bipyra 90°, 120°

	Electron Groups (m + n)			
	2 (steric number = 2)	3 (steric number = 3)	4 (steric number = 4)	5 (steric number
1 lone pair **AX_mE_1**		 **AX_2E_1**, bent <120°	 **AX_3E_1**, trig. pyramid <109.5°	 **AX_4E_1**, see-s <90°, <120°
2 lone pairs **AX_mE_2**			 **AX_2E_2**, bent <109.5°	 **AX_3E_2**, T-sha <90°

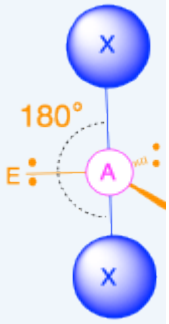
	Electron Groups (m + n)			
	2 (steric number = 2)	3 (steric number = 3)	4 (steric number = 4)	5 (steric number
3 lone pairs **AX_mE_3**				 **AX_2E_3**, linea 180°

Table 3.2.1.1 summarizes the geometries and bond angles predicted for nearest-neighbor bonded groups on central atoms with a mixture of lone pairs and bonded groups. The table does not cover all possible situations; it only includes cases where there are two bonded groups in which an X-X angle is measurable between nearest-neighbors. A more detailed description of some selected cases is given below.

Two Electron Groups (m + n = 2)

(Steric number = 2) In the case that there are only two electron groups around a central atom, those groups will lie 180° from one another. This results in a linear molecular geometry with 180° bond angles.

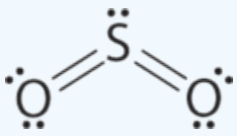
Three Electron Groups (m + n = 3)

(Steric number = 3) In the case that there are three electron groups around a central atom, those groups will lie approximately 120° from one another in space. This results in an electronic geometry that is approximately **trigonal planar**. There are two different molecular geometries that are possible in this category:

- When all of the electron groups are bonds (m = 3 or AX_3), the molecular geometry is a ***trigonal plane*** with **120°** bond angles.
- When there is one lone pair (m=2, n=1 or AX_2E_1), the molecular geometry is ***bent*** with a bond angle that is slightly **less than 120°**.

AX_2E Molecules: Example SO_2

1. The central atom, sulfur, has 6 valence electrons, as does each oxygen atom. With 18 valence electrons, the Lewis electron structure is shown below.



2. There are three electron groups around the central atom: two double bonds and one lone pair. We initially place the groups in

a trigonal planar arrangement to minimize repulsions (Table 3.2.1.1).

3. With two bonding pairs and one lone pair, the structure is designated as AX_2E. This designation has a total of three electron pairs, two X and one E. The lone pair occupies more space around the central atom than a bonding pair (even double bonds!). Bonding pairs and lone pairs repel each other electrostatically in the order BP–BP < LP–BP < LP–LP. In SO_2, we have one BP–BP interaction and two LP–BP interactions.

4. The molecular geometry is described only by the positions of the nuclei, *not* by the positions of the lone pairs. Thus, with two nuclei and one lone pair the shape is *bent*, or *V shaped*, which can be viewed as a trigonal planar arrangement with a missing vertex. The O-S-O bond angle is expected to be *less than* 120° because of the extra space taken up by the lone pair.

Four Electron Groups (m + n = 4)

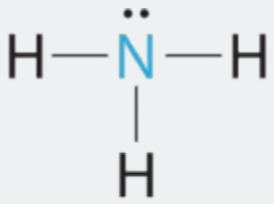
(Steric number = 4) In the case that there are four electron groups around a central atom, those groups will lie approximately 109.5° from one another in space. This results in an electronic geometry that is approximately **tetrahedral**. There are three different molecular geometries that are possible in this category:

- When all electron groups are bonds (m=4 or AX_4), the molecular geometry is a ***tetrahedron*** with bond angles of **109.5°**.
- When there is one lone pair (m=3, n=1 or AX_3E_1), the molecular geometry is a ***trigonal pyramid*** with bond angles of **slightly less than 109.5°**.
- When there are two lone pairs (m=2, n=2 or AX_2E_2), the molecular geometry is ***bent*** with bond angles of **slightly less than 109.5°**.

AX_3E Molecules: Example NH_3

One of the limitations of Lewis structures is that they depict molecules and ions in only two dimensions. With four electron groups, we must learn to show molecules and ions in three dimensions.

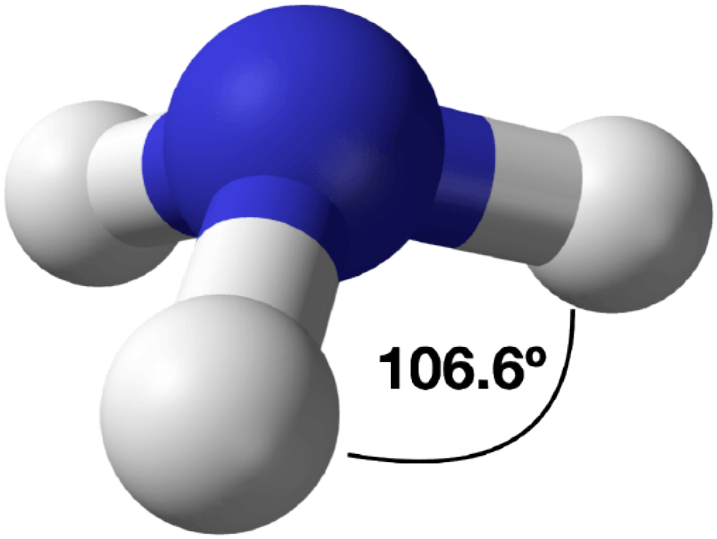
1. In ammonia, the central atom, nitrogen, has five valence electrons and each hydrogen donates one valence electron, producing the Lewis electron structure



Lewis structure

2. There are four electron groups around nitrogen, three bonding pairs and one lone pair. Repulsions are minimized by directing each hydrogen atom and the lone pair to the corners of a tetrahedron.

3. With three bonding pairs and one lone pair, the structure is designated as AX_3E. This designation has a total of four electron pairs, three X and one E. We expect the LP–BP interactions to cause the bonding pair angles to deviate significantly from the angles of a perfect tetrahedron.



The Difference in the Space Occupied by a Lone Pair of Electrons and by a Bonding Pair

As with SO_2, this composite model of electron distribution and negative electrostatic potential in ammonia shows that a lone pair of electrons occupies a larger region of space around the nitrogen atom than does a bonding pair of electrons that is shared with a hydrogen atom.

4. There are three nuclei and one lone pair, so the molecular geometry is *trigonal pyramidal*. In essence, this is a tetrahedron with a vertex missing. However, the H–N–H bond angles are less than the ideal angle of 109.5° because of LP–BP repulsion. The bond angles in ammonia are 106.6°.

AX_2E_2 Molecules: Example H_2O

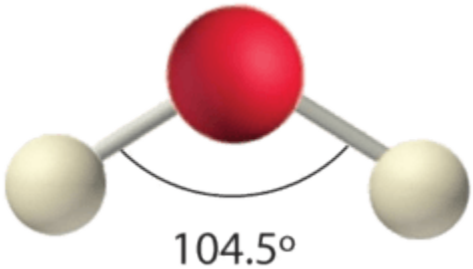
1. Oxygen has six valence electrons and each hydrogen has one valence electron, producing the Lewis electron structure



2. There are four groups around the central oxygen atom, two bonding pairs and two lone pairs. Repulsions are minimized by directing the bonding pairs and the lone pairs to the corners of a tetrahedron.

3. With two bonding pairs and two lone pairs, the structure is designated as AX_2E_2 with a total of four electron pairs. Due to LP–LP, LP–BP, and BP–BP interactions, we expect a significant deviation from idealized tetrahedral angles.

4. With two hydrogen atoms and two lone pairs of electrons, the structure has significant lone pair interactions. There are two nuclei about the central atom, so the molecular shape is *bent*, or *V shaped*, with an H–O–H angle that is even less than the H–N–H angles in NH_3, as we would expect because of the presence of two lone pairs of electrons on the central atom rather than one. This molecular shape is essentially a tetrahedron with two missing vertices.



Five Electron Groups (m + n = 5)

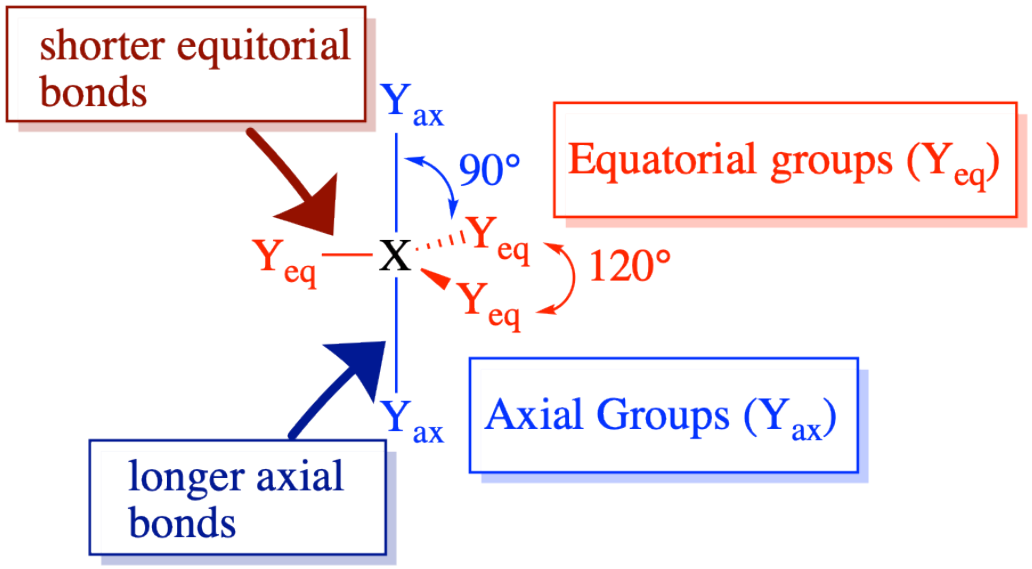


Figure: Trigonal pyramidal molecules (steric number 5) possess different bond angles and lengths for axial (ax) and equatorial (eq) pendant atoms. (CC-BY-NC-SA; Kathryn Haas).

(Steric number = 5) In the case that there are five electron groups around a central atom, there are two different types of positions around the central atom: equatorial positions and axial positions. The three equatorial ligands are 120° from one another and are 90° from each of the two axial ligands. The axial positions have three adjacent groups oriented 90° away in space. Axial groups are thus more crowded than the equatorial positions with only two adjacent groups at 90°. The crowding of axial positions results in slight differences in bond distances; crowded axial groups have longer bonds than the less crowded equatorial groups. Lone pairs of electrons generally prefer to occupy equatorial positions rather than axial positions. The justification for this preference, according to VSEPR theory, is that the lone electron pairs are more repulsive than bonding electron pairs, and thus the lone pairs prefer the less crowded equatorial positions.

The arrangement of five groups around a central atom results in a **trigonal bipyramidal** electronic geometry. There are four different molecular geometries that are possible in this category, depending upon the number of bonded groups and lone pairs of electrons:

- When all electron groups are bonds (m=5 or AX_5), the molecular geometry is a ***trigonal bipyramid*** with bond angles of **120°** and **90°** between adjacent ligands.
- When there is one lone pair (m=4, n=1 or AX_4E_1), the lone pair occupies one of the equatorial positions. The molecular geometry is called a ***see saw*** with bond angles of **slightly less than 120°** and **slightly less than 90°**.
- When there are two lone pairs (m=3, n=2 or AX_3E_2), each lone pair occupies one of the three equatorial positions. The molecular geometry is ***T-shaped*** with bond angles of **slightly less than 120°** and **slightly less than 90°**.
- When there are three lone pairs (m=1, n=3 or AX_3E_2), the lone pairs occupy the three equatorial positions. The molecular geometry is ***linear*** with bond angles of **180°**.

AX_4E Molecules: SF_4

1. The sulfur atom has six valence electrons and each fluorine has seven valence electrons, so the Lewis electron structure is



Lewis structure

With an expanded valence, this species is an exception to the octet rule.

2. There are five groups around sulfur, four bonding pairs and one lone pair. With five electron groups, the lowest energy arrangement is a trigonal bipyramid.

3. We designate SF_4 as AX_4E; it has a total of five electron pairs. However, because the axial and equatorial positions are not chemically equivalent, where do we place the lone pair? If we place the lone pair in the axial position, we have three LP–BP repulsions at 90°. If we place it in the equatorial position, we have two 90° LP–BP repulsions at 90°. With fewer 90° LP–BP repulsions, we can predict that the structure with the lone pair of electrons in the *equatorial position is more stable than the one with the lone pair in the axial position*. We also expect a deviation from ideal geometry because a lone pair of electrons occupies more space than a bonding pair.

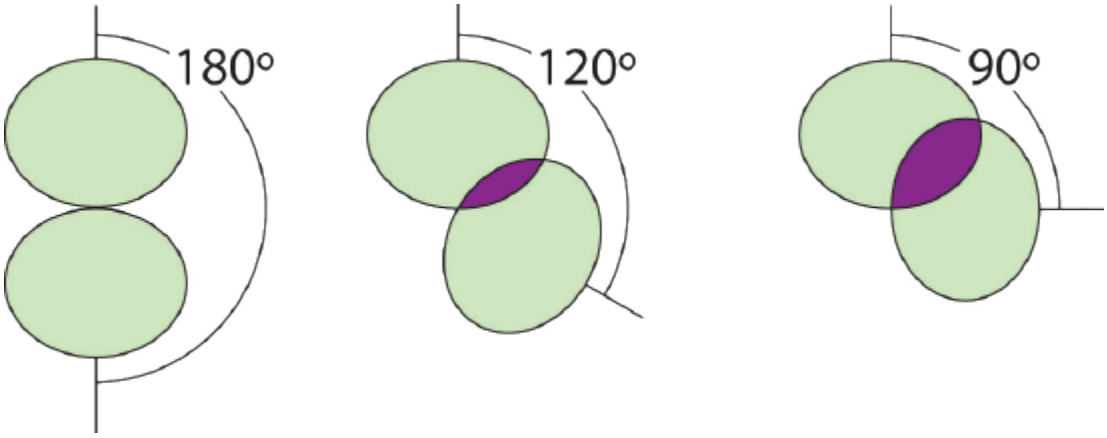
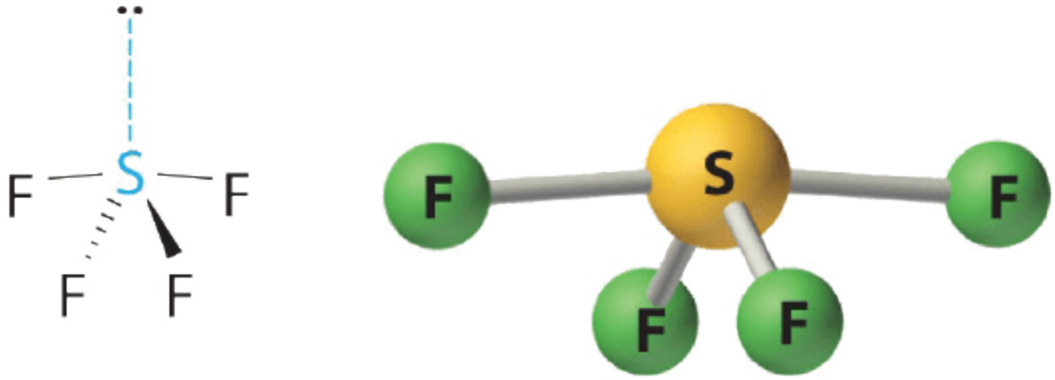


Illustration of the Area Shared by Two Electron Pairs versus the Angle between Them

At 90°, the two electron pairs share a relatively large region of space, which leads to strong repulsive electron–electron interactions.

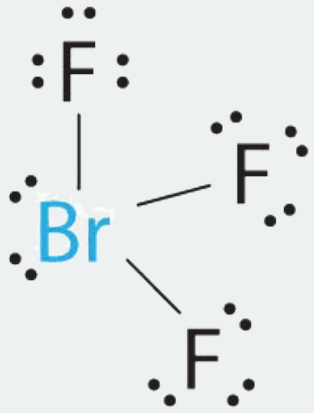
4. With four nuclei and one lone pair of electrons, the molecular structure is based on a trigonal bipyramid with a missing equatorial vertex; it is described as a *seesaw*. The F_{axial}–S–F_{axial} angle is 173° rather than 180° because of the lone pair of electrons in the equatorial plane.



Molecular geometry (seesaw)

AX_3E_2 Molecules: BrF_3

1. The bromine atom has seven valence electrons, and each fluorine has seven valence electrons, so the Lewis electron structure is

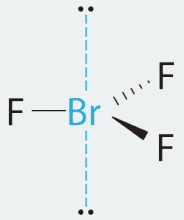


Lewis structure

Once again, we have a compound that is an exception to the octet rule.

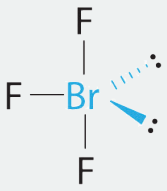
2. There are five groups around the central atom, three bonding pairs and two lone pairs. We again direct the groups toward the vertices of a trigonal bipyramid.

3. With three bonding pairs and two lone pairs, the structural designation is AX_3E_2 with a total of five electron pairs. Because the axial and equatorial positions are not equivalent, we must decide how to arrange the groups to minimize repulsions. If we place both lone pairs in the axial positions, we have six LP–BP repulsions at 90°. If both are in the equatorial positions, we have four LP–BP repulsions at 90°. If one lone pair is axial and the other equatorial, we have one LP–LP repulsion at 90° and three LP–BP repulsions at 90°:



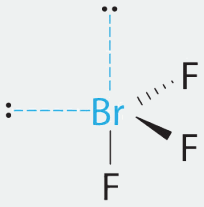
Lone pairs axial

(a)



Lone pairs equatorial

(b)



Lone pairs axial and equatorial

(c)

Interactions

90° LP–LP	0	0	1
90° LP–BP	6	4	3

Structure (c) can be eliminated because it has a LP–LP interaction at 90°. Structure (b), with fewer LP–BP repulsions at 90° than (a), is lower in energy. However, we predict a deviation in bond angles because of the presence of the two lone pairs of electrons.

4. The three nuclei in BrF_3 determine its molecular structure, which is described as *T shaped*. This is essentially a trigonal bipyramid that is missing two equatorial vertices. The F_{axial}–Br–F_{axial} angle is 172°, less than 180° because of LP–BP repulsions.

Because lone pairs occupy more space around the central atom than bonding pairs, electrostatic repulsions are more important for lone pairs than for bonding pairs.

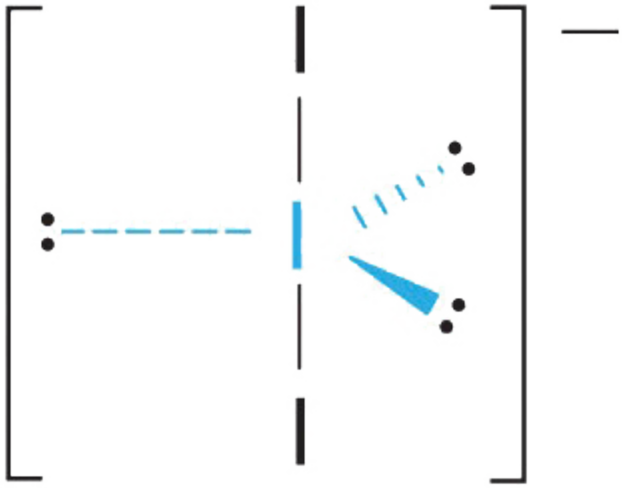
AX_2E_3 Molecules: I_3^-

1. Each iodine atom contributes seven electrons and the negative charge one, so the Lewis electron structure is



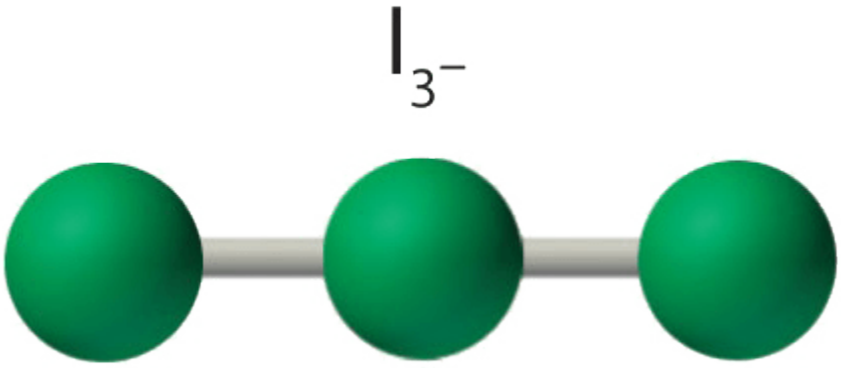
2. There are five electron groups about the central atom in I_3^-, two bonding pairs and three lone pairs. To minimize repulsions, the groups are directed to the corners of a trigonal bipyramid.

3. With two bonding pairs and three lone pairs, I_3^- has a total of five electron pairs and is designated as AX_2E_3. We must now decide how to arrange the lone pairs of electrons in a trigonal bipyramid in a way that minimizes repulsions. Placing them in the equatorial positions eliminates 90° LP–LP repulsions and minimizes the number of 90° LP–BP repulsions.



The three lone pairs of electrons have equivalent interactions with the three iodine atoms, so we do not expect any deviations in bonding angles.

4. With three nuclei and three lone pairs of electrons, the molecular geometry of I_3^- is linear. This can be described as a trigonal bipyramid with three equatorial vertices missing. The ion has an I–I–I angle of 180°, as expected.



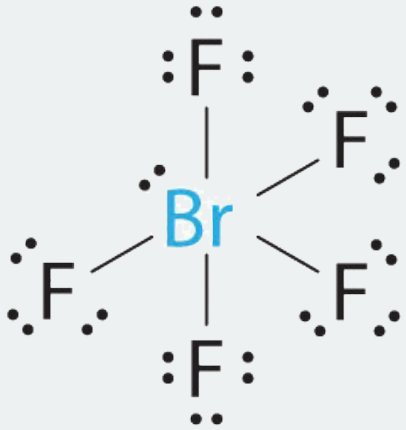
Six Electron Groups (m + n = 6)

(Steric number = 6) In the case that there are six electron groups around a central atom, the nearest groups will lie approximately 90° from one another in space. This results in an electronic geometry that is approximately **octahedral**. There are three relevant molecular geometries in this category:

- When all electron groups are bonds (m=6 or AX_6), the molecular geometry is an ***octahedron*** with bond angles of **90°** between adjacent bonds.
- When there is one lone pair (m=5, n=1 or AX_5E_1) we now distinguish between the axial and equitorial positions; the lone pair is considered to be in one of the axial positions, while the bond directly opposite of the lone pair is the axial bond. The molecular geometry is a ***square pyramid*** with bond angles of **90°** between adjacent equatorial bonds and **slightly less than 90°** between the axial bond and equatorial groups.
- When there are two lone pairs (m=4, n=2 or AX_4E_2), the lone pairs are opposite of one another and each occupy an axial position. The molecular geometry is ***square planar*** with bond angles of **90°**.

AX_5E Molecules: BrF_5

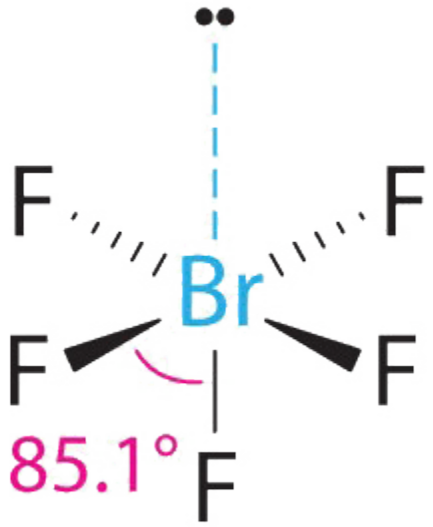
1. The central atom, bromine, has seven valence electrons, as does each fluorine, so the Lewis electron structure is



Lewis structure

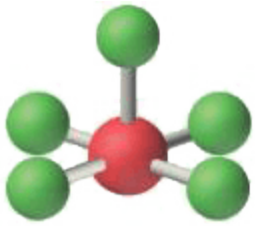
With its expanded valence, this species is an exception to the octet rule.

2. There are six electron groups around the Br, five bonding pairs and one lone pair. Placing five F atoms around Br while minimizing BP–BP and LP–BP repulsions gives the following structure:



3. With five bonding pairs and one lone pair, BrF_5 is designated as AX_5E; it has a total of six electron pairs. The BrF_5 structure has four fluorine atoms in a plane in an equatorial position and one fluorine atom and the lone pair of electrons in the axial positions. We expect all F_{axial}–Br–$F_{equatorial}$ angles to be less than 90° because of the lone pair of electrons, which occupies more space than the bonding electron pairs.

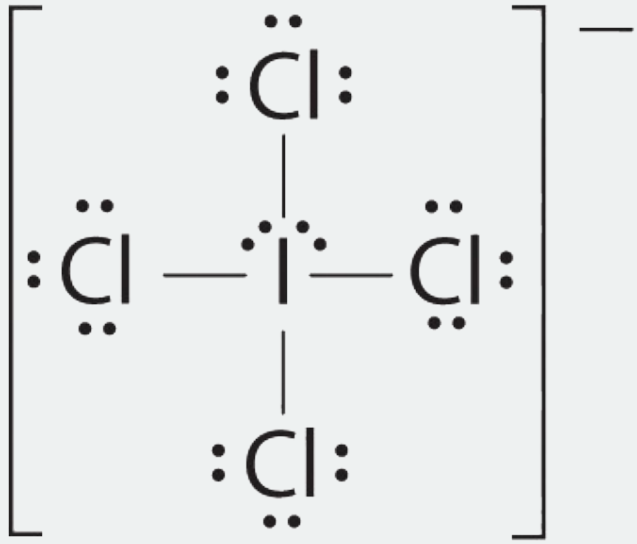
4. With five nuclei surrounding the central atom, the molecular structure is based on an octahedron with a vertex missing. This molecular structure is *square pyramidal*. The F_{axial}–B–$F_{equatorial}$ angles are 85.1°, less than 90° because of LP–BP repulsions.



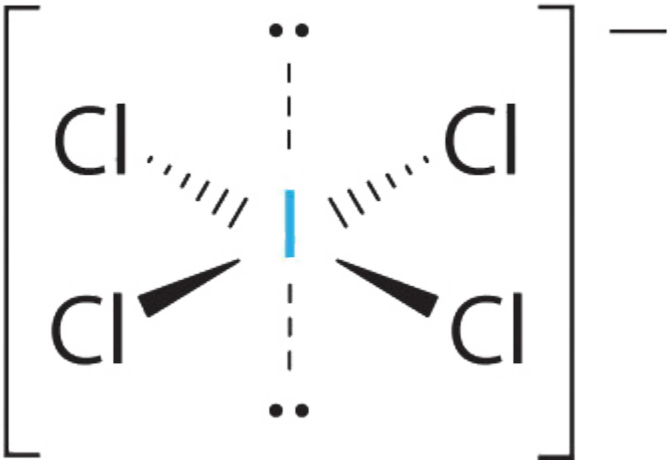
Molecular geometry
(square pyramidal)

AX_4E_2 Molecules: ICl_4^-

1. The central atom, iodine, contributes seven electrons. Each chlorine contributes seven, and there is a single negative charge. The Lewis electron structure is



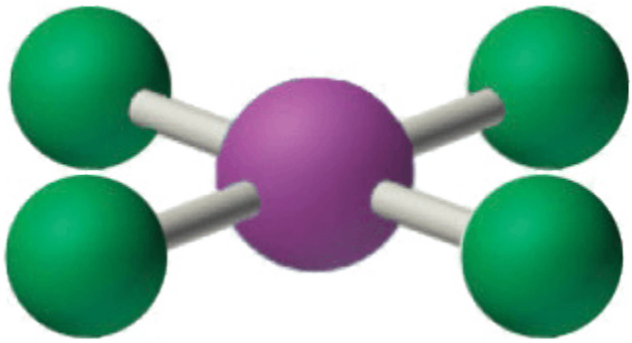
2. There are six electron groups around the central atom, four bonding pairs and two lone pairs. The structure that minimizes LP–LP, LP–BP, and BP–BP repulsions is



3. ICl_4^- is designated as AX_4E_2 and has a total of six electron pairs. Although there are lone pairs of electrons, with four bonding

electron pairs in the equatorial plane and the lone pairs of electrons in the axial positions, all LP–BP repulsions are the same. Therefore, we do not expect any deviation in the Cl–I–Cl bond angles.

4. With five nuclei, the ICl4− ion forms a molecular structure that is *square planar*, an octahedron with two opposite vertices missing.



Summary

The arrangement of bonded atoms in a molecule or polyatomic ion is crucial to understanding the chemistry of a molecule, but Lewis electron structures give no information about **molecular geometry**. The **valence-shell electron-pair repulsion (VSEPR) model** allows us to predict which of the possible structures is actually observed in most cases. VSEPR is based on the assumption that pairs of electrons occupy space, and the lowest-energy structure is the one that minimizes repulsions between electron pairs. In the VSEPR model, the molecule or polyatomic ion is given an AX_mE_n designation, where A is the central atom, X is a bonded atom, E is a nonbonding valence electron group (usually a lone pair of electrons), and *m* and *n* are integers. Each group around the central atom is designated as a bonding pair (BP) or lone (nonbonding) pair (LP). From the BP and LP interactions we can predict both the relative positions of the atoms and the angles between the bonds, called the **bond angles**. From this we can describe the **molecular geometry**. The VSEPR model can be used to predict the shapes of many molecules and polyatomic ions, but it gives no information about bond lengths and the presence of multiple bonds. A combination of VSEPR and a bonding model, such as Lewis electron structures, is necessary to understand the presence of multiple bonds.

The relationship between the number of electron groups around a central atom, the number of lone pairs of electrons, and the molecular geometry is summarized in Table 3.2.1.1.

Example Excercises

Example 3.2.1.1

Using the VSEPR model, predict the molecular geometry of each molecule or ion.

1. PF_5 (phosphorus pentafluoride, a catalyst used in certain organic reactions)
2. H_3O^+ (hydronium ion)

Given: two chemical species

Asked for: molecular geometry

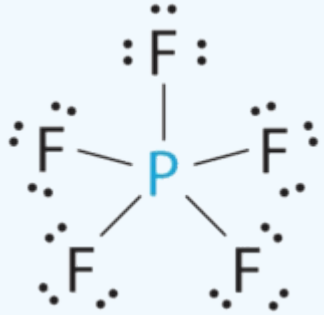
Strategy:

A. Draw the Lewis electron structure of the molecule or polyatomic ion.
B. Determine the electron group arrangement around the central atom that minimizes repulsions.
C. Assign an AX_mE_n designation; then identify the LP–LP, LP–BP, or BP–BP interactions and predict deviations in bond angles.

D. Describe the molecular geometry.

Solution:

1. **A** The central atom, P, has five valence electrons and each fluorine has seven valence electrons, so the Lewis structure of PF_5 is



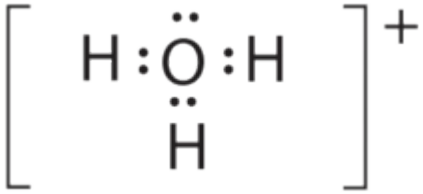
B There are five bonding groups about phosphorus. The structure that minimizes repulsions is a trigonal bipyramid.

C All electron groups are bonding pairs, so PF_5 is designated as AX_5. Notice that this gives a total of five electron pairs. With no lone pair repulsions, we do not expect any bond angles to deviate from the ideal.

D The PF_5 molecule has five nuclei and no lone pairs of electrons, so its molecular geometry is trigonal bipyramidal.



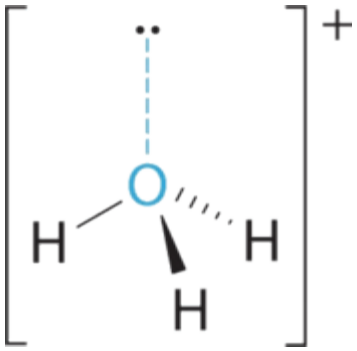
- **A** The central atom, O, has six valence electrons, and each H atom contributes one valence electron. Subtracting one electron for the positive charge gives a total of eight valence electrons, so the Lewis electron structure is



B There are four electron groups around oxygen, three bonding pairs and one lone pair. Like NH_3, repulsions are minimized by directing each hydrogen atom and the lone pair to the corners of a tetrahedron.

C With three bonding pairs and one lone pair, the structure is designated as AX_3E and has a total of four electron pairs (three X and one E). We expect the LP–BP interactions to cause the bonding pair angles to deviate significantly from the angles of a perfect tetrahedron.

D There are three nuclei and one lone pair, so the molecular geometry is *trigonal pyramidal*, in essence a tetrahedron missing a vertex. However, the H–O–H bond angles are less than the ideal angle of 109.5° because of LP–BP repulsions:



Exercise 3.2.1.1

Using the VSEPR model, predict the molecular geometry of each molecule or ion.

a. XeO_3
b. PF_6^-
c. NO_2^+

Answer a available at the end of this section.

Example 3.2.1.2

Predict the molecular geometry of each molecule.

1. XeF_2
2. $SnCl_2$

Given: two chemical compounds

Asked for: molecular geometry

Strategy:

Use the strategy given in Example3.2.1.1.

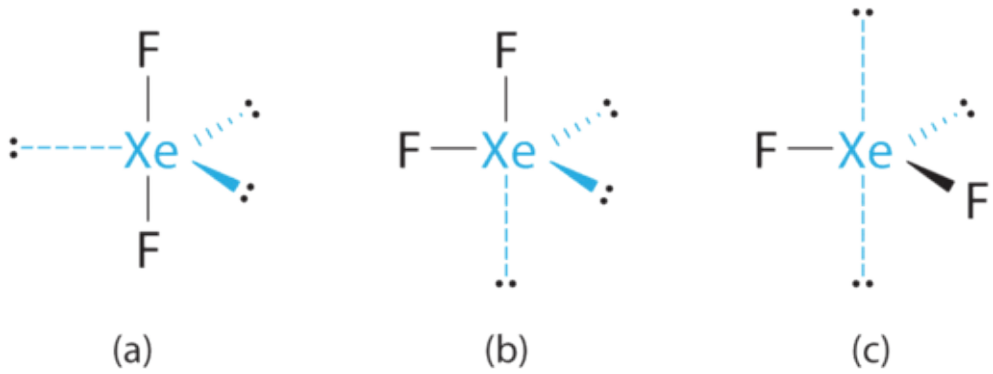
Solution:

1. **A** Xenon contributes eight electrons and each fluorine seven valence electrons, so the Lewis electron structure is



B There are five electron groups around the central atom, two bonding pairs and three lone pairs. Repulsions are minimized by placing the groups in the corners of a trigonal bipyramid.

C From B, XeF_2 is designated as AX_2E_3 and has a total of five electron pairs (two X and three E). With three lone pairs about the central atom, we can arrange the two F atoms in three possible ways: both F atoms can be axial, one can be axial and one equatorial, or both can be equatorial:



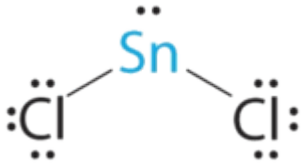
Interactions

90 LP–LP	0	2	2

The structure with the lowest energy is the one that minimizes LP–LP repulsions. Both (b) and (c) have two 90° LP–LP interactions, whereas structure (a) has none. Thus both F atoms are in the axial positions, like the two iodine atoms around the central iodine in I_3^-. All LP–BP interactions are equivalent, so we do not expect a deviation from an ideal 180° in the F–Xe–F bond angle.

D With two nuclei about the central atom, the molecular geometry of XeF_2 is linear. It is a trigonal bipyramid with three missing equatorial vertices.

- **A** The tin atom donates 4 valence electrons and each chlorine atom donates 7 valence electrons. With 18 valence electrons, the Lewis electron structure is



B There are three electron groups around the central atom, two bonding groups and one lone pair of electrons. To minimize repulsions the three groups are initially placed at 120° angles from each other.

C From B we designate $SnCl_2$ as AX_2E. It has a total of three electron pairs, two X and one E. Because the lone pair of electrons occupies more space than the bonding pairs, we expect a decrease in the Cl–Sn–Cl bond angle due to increased LP–BP repulsions.

D With two nuclei around the central atom and one lone pair of electrons, the molecular geometry of $SnCl_2$ is bent, like SO_2, but with a Cl–Sn–Cl bond angle of 95°. The molecular geometry can be described as a trigonal planar arrangement with one vertex missing.

Exercise 3.2.1.2

Predict the molecular geometry of each molecule.

a. SO_3
b. XeF_4

Answer a available at the end of this section.

Answers

Exercise 3.2.1.1

trigonal pyramidal

octahedral

linear

Exercise 3.2.1.2

trigonal planar

square planar

This page titled 3.2.1: Lone Pair Repulsion is shared under a CC BY-NC-SA 4.0 license and was authored, remixed, and/or curated by Kathryn Haas.

- 3.2.1: Lone Pair Repulsion by Kathryn Haas is licensed CC BY-NC-SA 4.0.
- 3.2.2: Multiple Bonds by Kathryn Haas is licensed CC BY-NC-SA 4.0.

3.2.2: Multiple Bonds

In the previous sections, we saw how to predict the approximate geometry around an atom using VSEPR theory, and we learned that lone pairs of electrons slightly distort bond angles from the "parent" geometry. This page discusses the effect of multiple (double and triple) bonds between bonded atoms.

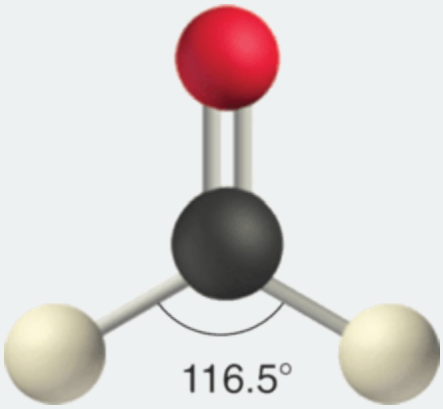
Double and triple bonds are more repulsive than single bonds

VSEPR theory predicts that double and triple bonds have stronger repulsive forces than single bonds. Like lone pairs of electrons, multiple bonds occupy more space around the central atom than a single bond. The result is that bond angles are slightly distorted compared to the parent geometry. Since a multiple bond has a higher electron density than a single bond, its electrons occupy more space than those of a single bond. Double and triple bonds distort bond angles in a way similar to what lone pairs do. Due to the stronger repulsion, double and triple bonds occupy positions similar to those of lone pairs in groups with 5 and 6 electron groups.

Examples 3.2.2.1

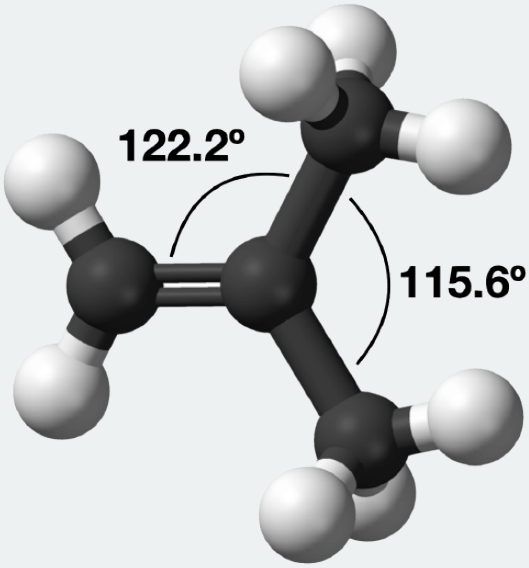
CH_2O

In a molecule such as CH_2O (AX_3), whose structure is shown below, the double bond repels the single bonds more strongly than the single bonds repel each other. This causes a deviation from ideal geometry (an H–C–H bond angle of 116.5° rather than 120°).



2-methybutene

In the molecule, $CH_2C(CH_3)_2$, the methyl—C—methyl bond angle is 115.6°, which is less than the 120° bond angle that would be expected of the parent geometry. On the other hand, the acetyl—C—methyl bond angle is greater than 120°, with an actual bond angle of 122.2°.



Atoms with both lone pairs and multiple bonds

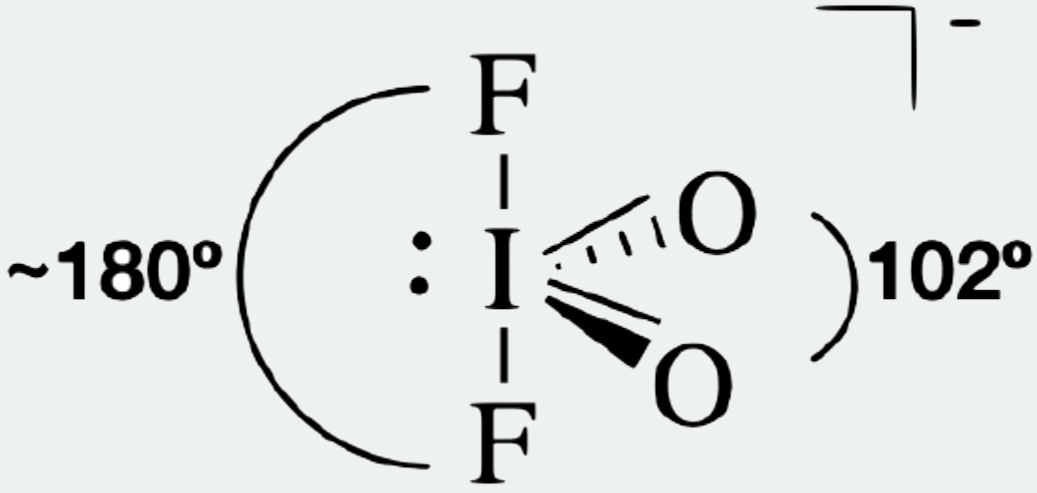
In general, we expect that a lone pair has slightly greater repulsive force than a multiple bond, and that a multiple bond has slightly greater repulsive force than a single bond. The **order of expected repulsive force** is:

$$\text{lone pair} > \text{double or triple bond} > \text{single bond}$$

Examples3.2.2.1

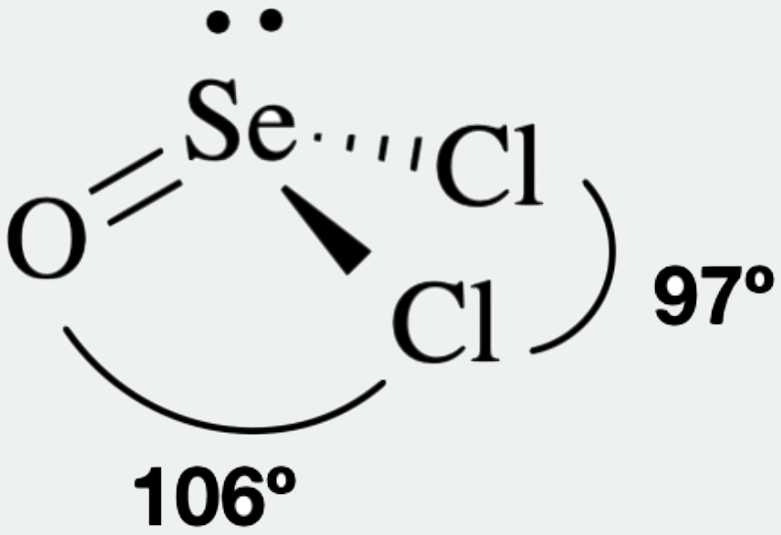
$IO_2F_2^-$

With five electron groups, the IO_2F_2 molecule has an approximately trigonal bipyramidal electronic (parent) geometry. The central iodine atom has a single bond to each of the fluorine atoms, a double bond to each oxygen, and a lone pair. The lone pair and the double bonds will occupy more space around iodine than each of the single bonds. Thus, we expect the lone pair and double bonds to occupy equatorial positions around the central iodine. The O=I=O bond angle is 102° (*much* smaller than the 120° angle expected from the parent geometry). This dramatically smaller angle is a result of the increased repulsion between the lone pair and the double bond.



$SeOCl_2$

With four electron groups, the $SeOCl_2$ molecule has four electron groups and approximately tetrahedral electronic (parent) geometry. It has both a lone pair and a double bond on the central selenium atom. The two chlorine atoms are singly bonded to selenium, while the oxygen is double bonded. The lone pair is most repulsive, followed by the double bonded oxygen, and then the chlorine bonds. This gives a Cl—Se—Cl bond angle of 97° and a Cl—Se—O bond angle of 106°; both angles are less than the 109.5° angles expected for the ideal tetrahedral geometry.



Practice

Exercise 3.2.2.1

Use VSEPR theory to predict the geometries and draw the structures of the following.

a. $XeOF_4$
b. NO_2^-
c. $SOCl_2$
d. IOF_3^-

Answer a available at the end of this section.

Answer b available at the end of this section.

Answer c available at the end of this section.

Answer d available at the end of this section.

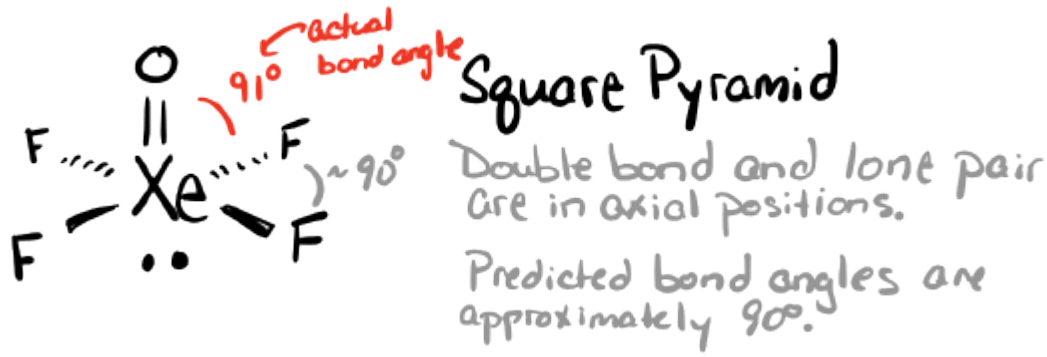
References

- Miessler, G.; Fischer, P.J.; Tarr, D. (2014). Inorganic Chemistry. New Jersey: Prentice-Hall. pp. 55

Answers

Exercise 3.2.2.1

This molecule has six electron groups around the central Xe atom (steric number 6), and thus has an approximately octahdral electronic (parent) geometry. There is a double bond to O and a lone pair, both of which are more strongly repulsive than the single bonds to F. The double bond and lone pair will be directly opposite to each other, designated as axial positions. The result is a square pyramidal molecular geometry. VSEPR theory predicts F—Xe—F bond angles of 90°. As a general rule, lone pairs are slightly more repulsive than multiple bonds, and so we might expect the O—Xe—F bond angles to be <90°; *however in this case the actual O—Xe—F bond angle is observed to be 91°* (you could not have predicted the latter).



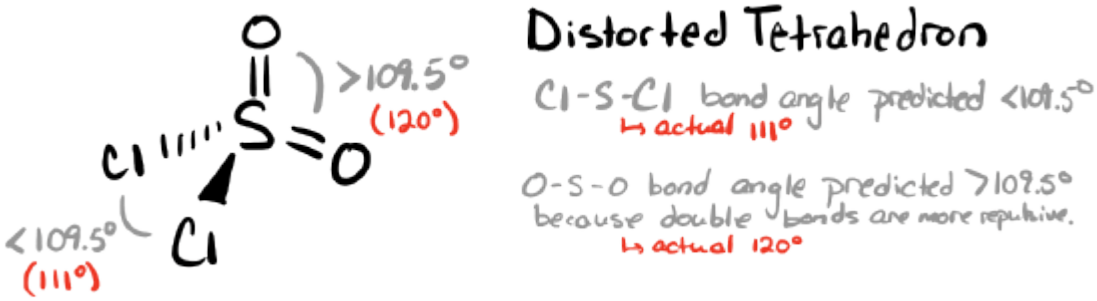
Exercise 3.2.2.1

This molecule has three electron groups around the central atom: one lone pair and two double bonds to oxygen atoms. This results in an approximately trigonal planar electronic (parent geometry). We expect the lone pair to be slightly more repulsive than double bonds, and so we expect the O—N—O bond angle to be slightly less than 120°. *The actual O—N—O angle is 115°.*



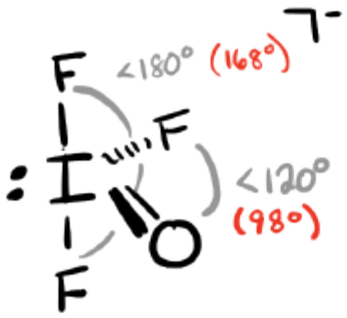
Exercise 3.2.2.1

This molecule has four electron groups (steric number 4) with an approximately tetrahedral electronic (parent) geometry. Each double bonded oxygen will take up more space around the central S than the single bonded Cl atoms. We should expect the double bonds to repel each other more strongly than they repel each single bond, with the least repulsive interaction being between the two single bonds. The bond angle for Cl—S—Cl is expected to be <109.5° according to VSEPR theory (however, it is actually 111°). We would expect the bond angle for O—S—O to be larger than the angle for Cl—S—Cl and for Cl—S—O. The O—S—O bond angle is predicted to be >109.5° (and the actual bond angle is 120°). The molecular geometry is a distorted tetrahedron.



Exercise 3.2.2.1

This molecule has five electron groups (steric number 5) with an approximately trigonal bipyramidal electronic (parent) geometry. There is one lone pair, a double bond to O, and three single bonds to F atoms around the central I atom. The lone pair and double bond are most repulsive, and should occupy the less crowded equatorial positions rather than the more crowded axial positions. This results in a seesaw molecular geometry. With the more repulsive lone pair and the strongest equatorial repulsive force being between the double bond and lone pair, we should expect the $F_{equatorial}$—I—O bond angle to be less than the 120° angle expected for the parent geometry (*it is actually much less, at 98°*). Due to repulsion between the axial F atoms and both the lone pair and double bond, we should expect the F—S—F bond angles to be compressed. The F_{axial}—I—F_{axial} is actually 168°.



Distorted see saw

Lone pair and double bond in equitorial positions.

Predicted bond angles:

F-I-O <120° / actual 98°

F_{axial}-I-F_{axial} <180° / actual 168°

This page titled 3.2.2: Multiple Bonds is shared under a CC BY-NC-SA 4.0 license and was authored, remixed, and/or curated by Kathryn Haas.

- 3.2.2: Multiple Bonds by Kathryn Haas is licensed CC BY-NC-SA 4.0.

3.2.3: Electronegativity and Atomic Size Effects

Introduction

We saw in previous sections how lone pairs of electrons and multiple bonds distort bond angles between non-central atoms (ligands) around a central atom. This section describes how ligand **electronegativity and size also influence bond angles and molecular geometry**. Electronegativity is generally correlated with atomic size going down any group of the periodic table. There are some cases where bond angles can be predicted by these correlations. However, size and electronegativity can also work as competing factors in determining bond angles.

Definitions of Electronegativity

Linus Pauling introduced the first electronegativity scale in 1932 in order to explain the extra stability of molecules with polar bonds.[1] The electronegativity of an atom, represented by the Greek letter χ (chi), can be defined as the tendency of an atom to draw electrons to itself in a chemical bond. On the Pauling scale, the electronegativity difference between two atoms A and B was defined in terms of the dissociation energies E_d of the A-A, B-B, and A-B bonds:

$$\chi_A - \chi_B = \sqrt{E_d(AB) - [E_d(AA) + E_d(BB)]/2}$$

where the energies are expressed in electron volts. Pauling's scale of electronegativity ranges from Fluorine (most electronegative = 4.0) to Francium (least electronegative = 0.7). [2,3] The polarity of bonds and assignment of formal charges is predicted by electronegativity differences.

Periodic table of electronegativity using the Pauling scale

→ Atomic radius decreases → Ionization energy increases → Electronegativity increases →

Group →	1	2	3	4	5	6	7	8	9	10	11	12	13	14	15	16	17	18
↓ Period																		
1	H 2.20																	He
2	Li 0.98	Be 1.57											B 2.04	C 2.55	N 3.04	O 3.44	F 3.98	Ne
3	Na 0.93	Mg 1.31											Al 1.61	Si 1.90	P 2.19	S 2.58	Cl 3.16	Ar
4	K 0.82	Ca 1.00	Sc 1.36	Ti 1.54	V 1.63	Cr 1.66	Mn 1.55	Fe 1.83	Co 1.88	Ni 1.91	Cu 1.90	Zn 1.65	Ga 1.81	Ge 2.01	As 2.18	Se 2.55	Br 2.96	Kr 3.00
5	Rb 0.82	Sr 0.95	Y 1.22	Zr 1.33	Nb 1.6	Mo 2.16	Tc 1.9	Ru 2.2	Rh 2.28	Pd 2.20	Ag 1.93	Cd 1.69	In 1.78	Sn 1.96	Sb 2.05	Te 2.1	I 2.66	Xe 2.60
6	Cs 0.79	Ba 0.89	*	Hf 1.3	Ta 1.5	W 2.36	Re 1.9	Os 2.2	Ir 2.20	Pt 2.28	Au 2.54	Hg 2.00	Tl 1.62	Pb 1.87	Bi 2.02	Po 2.0	At 2.2	Rn 2.2
7	Fr 0.7	Ra 0.9	**	Rf	Db	Sg	Bh	Hs	Mt	Ds	Rg	Cn	Uut	Fl	Uup	Lv	Uus	Uuo

* Lanthanoids	La 1.1	Ce 1.12	Pr 1.13	Nd 1.14	Pm 1.13	Sm 1.17	Eu 1.2	Gd 1.2	Tb 1.1	Dy 1.22	Ho 1.23	Er 1.24	Tm 1.25	Yb 1.1	Lu 1.27
** Actinoids	Ac 1.1	Th 1.3	Pa 1.5	U 1.38	Np 1.36	Pu 1.28	Am 1.13	Cm 1.28	Bk 1.3	Cf 1.3	Es 1.3	Fm 1.3	Md 1.3	No 1.3	Lr 1.3

Figure 3.2.3.1: Table of Pauling electronegativities from Wikipedia's Electronegativity page (click).

While directly relevant to the strength of chemical bonds, the Pauling definition of electronegativity has a significant limitation: calculating each value requires data from several compounds in which specific atoms are bonded. This means that the scale cannot be successfully applied to all situations. To overcome this limitation, alternative electronegativity scales were developed based on different thermochemical measurements or calculations. These other scales are listed in the table below. More thorough descriptions of how values in each scale are calculated are described on Wikipedia's Electronegativity page (click) and a concise history of electronegativity scales is summarized in ref 4.

Scale Developer	Year first described	Characteristics
Linus Pauling[1]	1932	Based on bond energies
Robert S. Mulliken[5,6]	1934	Based on valence electron properties of atoms (electron affinity and ionization energy)
Louis Allred & Eugene G. Rochow[7]	1958	Based on electrostatic force (effective nuclear charge)
Robert T. Sanderson[8]	1983	Based on atomic electron density
Ralph G. Pearson[9]	1985	Related to Hard-Soft Acid-Based theory
Leland C. Allen, Joseph Mann, Terry L. Meek[10,11,12]	1989, 2000	Average ionization energies of valence shell electrons, configuration energies (CE) $$\mathrm{CE} = \frac{n\varepsilon_s + m\varepsilon_p}{n+m}$$ $n =$ number of s electrons $m =$ number of p electrons $\varepsilon_s, \varepsilon_p =$ experimental 1-electron s and p energies

The primary advantage to this scale developed by Mann, Meek, and Allen[12] is that it is based on configuration energy (CE), the average ionization energies of valence electrons in ground state free atoms. A scale based on ionization energies can be calculated more directly for any element. However, a critique of all electronegativity scales, including this one, is that they are all based on assumptions that fail in some cases.

There is a relationship between electronegativity and atomic size because both are related to ionization energy. Like ionization energy, there is a general trend across the periodic table for both electronegativity and atomic size; in general, smaller atoms toward the top right-hand side of the periodic table have greater electronegativity values and smaller atomic size. We will see below that both electronegativity and atomic size influence bond angles and absolute molecular geometry around a central atom. In some cases, the size and electronegativity affects are aligned; in some cases these effects compete.

Electronegativity and Size Influence Bond Angles

Let's begin by examining the bond angles of several trigonal pyramidal molecules. The molecules shown in Figure 3.2.3.2 each have three identical "pendant groups" on the central atom (Figure 3.2.3.2). *Pendant atoms* or *pendant groups* are the atoms, or groups of atoms, that are bonded directly to the central atom. The molecules shown here are arranged according to the size of the central and pendant atoms. Central atoms increase in size going down this figure, and pendant atoms increase in size going across from left to right. The bond angles and bond lengths are labeled in each case.

What trends can you identify?

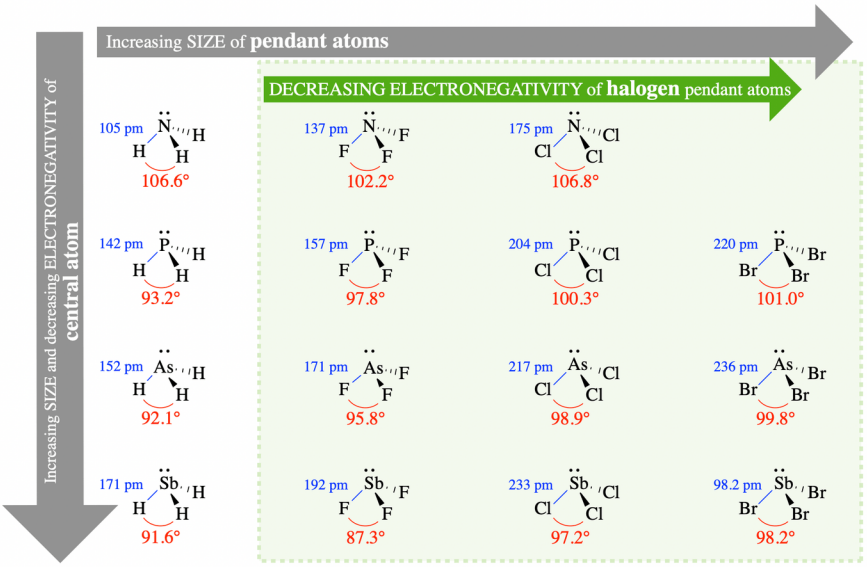


Figure 3.2.3.2: Several molecules with trigonal pyramidal electronic geometry are shown arranged according to size of the central atom (increasing size of central atom from top to bottom) and pendant atom (increasing size of pendant atoms from left to right). Bond angles and bond lengths are indicated. (Kathryn Haas; CC-NC-BY-SA)

Trends in Size

First, let's examine how the size of the central and pendant groups might influence bond angle. In VSEPR theory, **the size of atoms (or groups of atoms) will affect bond angles due to changes in steric interactions between pendant groups.**

Size of the central atom

Examine the relationship between the size of the central atom and the bond angles in Figure 3.2.3.2 (go down any column in the figure). For example, compare NH_3, PH_3, AsH_3, and SbH_3, with bond angles 106.6°, 93.2°, 92.1°, and 91.6°, respectively. In this series, the size of the central atom increases from N to Sb while the size of the pendant atom (hydrogen) remains constant. *As the size of the central atom increases, the bond angles decrease; thus, we observe a negative relationship between size of the central atom and the bond angle in these molecules*. This relationship is explained by sterics. As the central atom increases in size, the bond lengths also increase and the pendant atoms are farther from each other in space. In VSEPR theory, this will reduce steric interactions between the pendant groups. Since the lone pair on these molecules is more repulsive than bonded groups, the decrease in steric interactions between bonded groups results in a decrease in bond angles.

Size of the pendant atoms (or groups)

Examine the relationships between size of the halogen pendant atoms and bond angle in Figure 3.2.3.2 (go across any row within the shaded region). For example, compare PF_3, PCl_3, and PBr_3, with bond angles 97.8°, 100.3°, and 101.0°, respectively. In this series, the size of the pendant atom increases from F to Br while the central atom remains constant (phosphorous). *As the size of pendant atoms increases, the bond angle increases; thus, we observe a direct relationship between size of the pendant group and the bond angle in these molecules*. Again, we can explain this using sterics. As the size of the pendant atoms increases, sterics between the pendant groups will increase (despite small changes in bond length). Increased steric interactions between pendant groups will prefer larger bond angles between the groups.

This trend fails, however, if we consider the molecules with hydrogen as the pendant atoms. Notice, for example, that H is the smallest pendant atom. If we consider the trend described above, we should assume that XH_3 (where X is a variable atom) would have the smallest bond angle in the series of XH_3, XF_3, XCl_3, and XBr_3. However this is not the case of NH_3, NF_3, and NCl_3, with bond angles 106.6°, 102.2°, and 106.8°, respectively. To explain the variation in these bond angles, we need to consider electronegativity.

Trends in Electronegativity

Now let's examine how electronegativity influences bond angles around a central atom. In VSEPR theory, **electronegativity of atoms/groups will affect bond angles due to changes in the distribution of electron pairs around the central atom (and thus changes in the severity of electron pair repulsion).** This really comes down to bond polarity caused by the difference in electronegativity between the central atom and pendant groups (bond polarity in the context of valence bond theory). In a polar bond, the more electronegative atom will pull electron density towards itself. When a pendant atom is more electronegative, it will pull the bonded electron pair towards itself and away from the central atom; this will reduce the electron pair repulsion between bonded electron pairs on the central atom. A decrease in electron pair repulsion on the central atom should decrease bond angles between the groups (Figure 3.2.3.3).

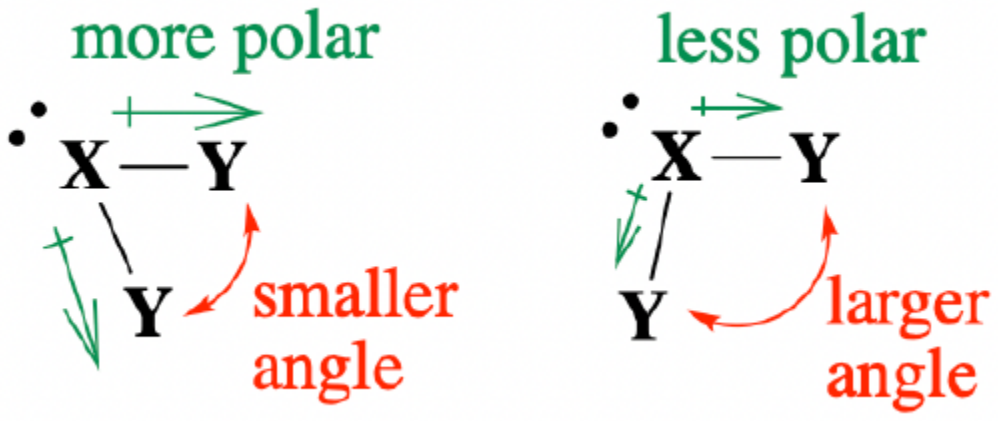


Figure 3.2.3.3. When electron pairs are distributed away from the central atom, repulsions are decreased, allowing smaller bond angles. (Kathryn Haas; CC-NC-BY-SA)

Electronegativity is an alternative explanation to the trends we already examined above in Figure 3.2.3.2 . For example, when we compare the halogen pendant atoms (shaded region in Figure 3.2.3.2) , the electronegativity of pendant groups decreases, bond polarity of the bonds decreases, and bond angles increase going from left to right and from F to Br. As more electron density remains on the central atom, electron repulsion between the bonded pairs increases and bond angles increase.

The electronegativity argument can also be used to explain the fact that NH_3 (106.6°) has a larger bond angle than NF_3 (102.2°). This particular case illustrates how electronegativity and size can be competing factors. While electronegativity differences seem to dominate in the case of NH_3 (106.6°) compared to NF_3 (102.2°), size differences still dominate in the cases of other XH_3 and XF_3 examples in Figure 3.2.3.2).

Exercise 3.2.3.1

Predict the geometry and approximate bond angles. Then put the molecules in each series in order of smallest to largest bond angle. Defend your answer.

a. The X-S-X bond angle in OSF_2, $OSCl_2$, $OSBr_2$
b. H_2O, H_2S, H_2Se, H_2Te
c. H_2O, OF_2, OCl_2

Answer (a) available at the end of this section.

Group Electronegativities

You probably heard the terms "electron donating group" and "electron withdrawing group" from your coursework in Organic Chemistry. For example, the acid trifluoroacetic acid (TFA) is more acidic than acetic acid due to the electron withdrawing effects of the CF_3 group compared to CH_3. CF_3 is an electron withdrawing group, while CH_3 is an electron donating group. In other words,

CF_3 is more electronegative than CH_3.

The electron withdrawing ability (electronegativity) of groups can be estimated and compared, just as they are with atoms. Although there is no one scale that is used for group electronegativities, and published values even for the same groups vary widely, there are reliable trends within similar groups. The same size and electronegativity factors discussed above that affect bond angles for *pendant atoms*, also can be used to rationalize distorted bond angles for *pendant groups* around a central atom.

Exercise 3.2.3.2

Consider the relative electronegativities and sizes of the pendant atoms/groups in the following examples. Is the trend in bond angles what you would expect from the relative group electronegativities and relative sizes? What, if any, is the more dominant factor in determining the trend?

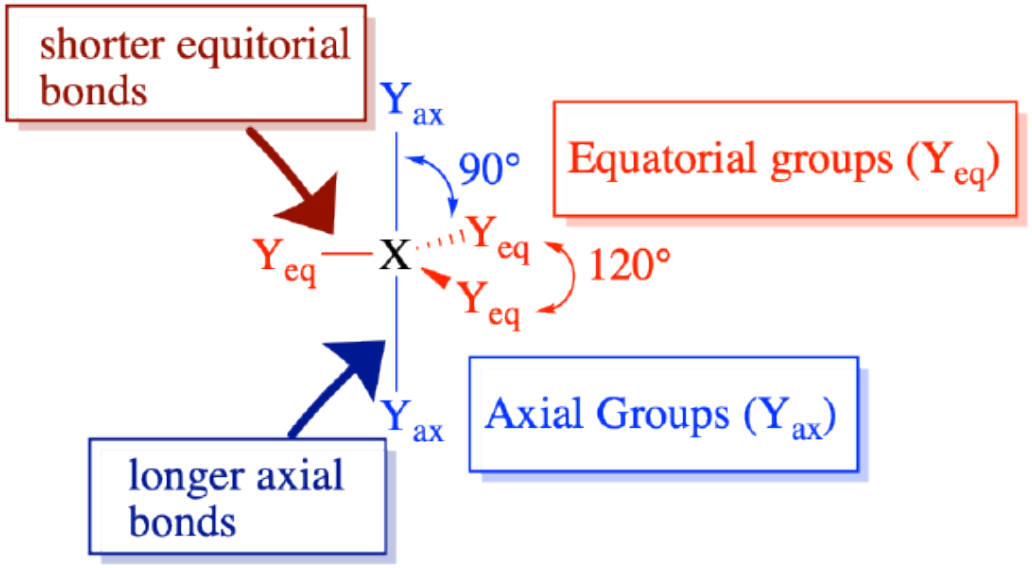
a. $N(CH_3)_3$ has an C-N-C bond angle of 110.9°, while $N(CF_3)_3$ has a bond angle of 117.9°.
b. The X-S-X bond angles in molecules of the form $SO_2(X)_2$ are: $SO_2(OH)_2$ 101.3°; $SO_2(CF_3)_2$ 102.0°; $SO_2(CH_3)_2$ 102.6°.

Answer (a) available at the end of this section.

Answer (b) available at the end of this section.

Special case of electronegativity and size in steric number 5 (trigonal bypyramid)

Molecules with steric number 5 are interesting because they posses two different types of positions (equatorial and axial). These positions have unique bond angles and bond lengths. Pendant atoms/groups have different preferences for the axial and equatorial positions that depend somewhat on their electronegativity.



Molecules with steric number 5 possess different bond angles and lengths for axial (ax) and equatorial (eq) pendant atoms. (CC-BY-NC-SA; Kathryn Haas)

In a previous section, we discussed the preference of lone pairs and multiple bonds for the equatorial positions in trigonal bipyramidal molecules. VSEPR theory rationalizes this by assuming that lone pairs and multiple bonds are more repulsive than the electron pairs in single bonds. Equatorial positions are less crowded (with only two closest neighbors at 90°, and two farther neighbors at 120°) compared to axial positions (with three closest neighbors at 90°), thus the more repulsive groups prefer the less crowded equatorial positions.

Pendant groups that are more electronegative result in weaker electron pair repulsion around the central atom, while groups that

are less electronegative result in stronger electron-pair repulsion around the central atom (as described above). The result for steric number 5: **bonding pairs to *less electronegative elements* are *more repulsive*, and *generally prefer equatorial* positions.** Still, lone pairs and multiple bonds are more repulsive than single bonds and would show a stronger preference for equatorial positions.

Examples and Nuances

Exercise 3.2.3.3

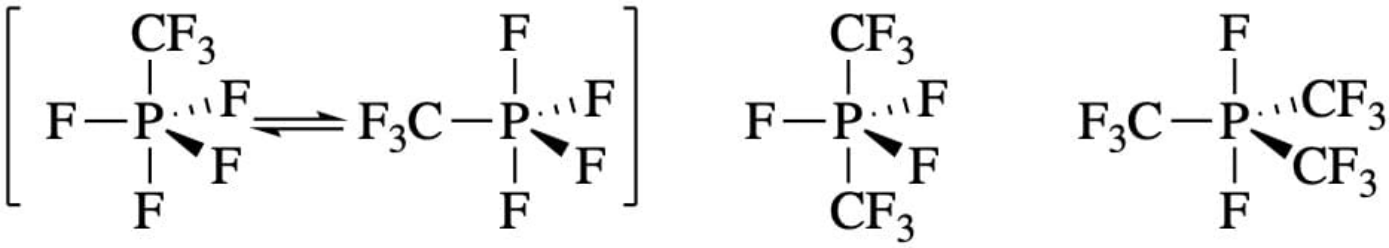
Some examples of molecule that demonstrate the equatorial preference of less electronegative groups are below. Predict (draw) their structures.

a. PF_4Cl, PF_3Cl_2, and PF_2Cl_3
b. $PF_4(CH_3)$ $PF_3(CH_3)_2$, and $PF_2(CH_3)_3$

Answer (a) available at the end of this section.

Answer (b) available at the end of this section.

In the exercise above, the structures can be explained by the electronegativity of the pendant groups; less electronegative groups prefer the equatorial positions. There are other similar molecules for which explanations (or predictions) are difficult. For example, the series of molecules below seems to have completely random placement of F and CF_3 groups. **These structures could not be predicted based on VSEPR theory.** It seems that in this case, the more symmetrical arrangements of pendant groups is preferred.



References and resources

1. Pauling, L. (1932). "The Nature of the Chemical Bond. IV. The Energy of Single Bonds and the Relative Electronegativity of Atoms". *J. Am. Chem. Soc.* **54**(9): 3570–3582. doi:10.1021/ja01348a011.
2. Housecroft, Catherine E. et. al. "Inorganic Chemistry" 3rd Edition. Pearson Education Limited 2008. Chapter 2.5 "Electronegativity Values" pgs. 42-44
3. International Union of Pure and Applied Chemistry. "Electronegativity". goldbook.iupac.org/E01990.html.
4. Pearson, R.G. *Acc. Chem. Res.* 1990, 23, 1, 1–2. https://doi.org/10.1021/ar00169a001
5. Mulliken, R. S. (1934). "A New Electroaffinity Scale; Together with Data on Valence States and on Valence Ionization Potentials and Electron Affinities". *J. Chem. Phys.***2** (11): 782–793. doi:10.1063/1.1749394.
6. Mulliken, R. S. (1935). "Electronic Structures of Molecules XI. Electroaffinity, Molecular Orbitals and Dipole Moments". J. Chem. Phys. **3** (9): 573–585. doi:10.1063/1.1749731.
7. Allred, A. L.; Rochow, E. G. (1958). "A scale of electronegativity based on electrostatic force". *Journal of Inorganic and Nuclear Chemistry*. **5** (4): 264–268. doi:10.1016/0022-1902(58)80003-2
8. Sanderson, R. T. (1983). "Electronegativity and bond energy". *Journal of the American Chemical Society*. **105** (8): 2259–2261. doi:10.1021/ja00346a026
9. Pearson, R. G. (1985). "Absolute electronegativity and absolute hardness of Lewis acids and bases". J. Am. Chem. Soc. 107 (24): 6801. doi:10.1021/ja00310a009.
10. Allen, Leland C. (1989). "Electronegativity is the average one-electron energy of the valence-shell electrons in ground-state free atoms". Journal of the American Chemical Society. 111 (25): 9003–9014. doi:10.1021/ja00207a003.
11. Mann, Joseph B.; Meek, Terry L.; Allen, Leland C. (2000). "Configuration Energies of the Main Group Elements". Journal of the

American Chemical Society. 122 (12): 2780–2783. doi:10.1021/ja992866e.
12. Mann, Joseph B.; Meek, Terry L.; Knight, Eugene T.; Capitani, Joseph F.; Allen, Leland C. (2000). "Configuration energies of the d-block elements". Journal of the American Chemical Society. 122 (21): 5132–5137. doi:10.1021/ja9928677

Acknowledgment

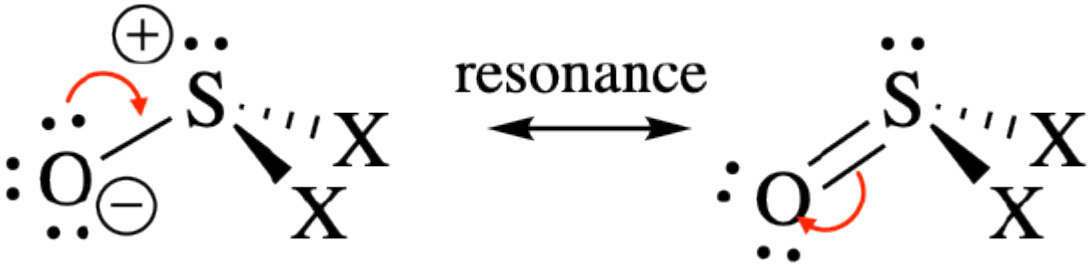
- Matthew Salem (UC Davis) (Pauling Electronegativity)
- Introduction to Inorganic Chemistry Wikibook (https://chem.libretexts.org/Bookshel..._Bond_Strength)

- Curated or created by Kathryn Haas

Answers

Exercise 3.2.3.1

Geometry and predicted bond angles: These are molecules with steric number 4. They can be written as two different resonance structures, and the resonance hybrid would have double bond character between S and O.



We would expect a trigonal pyramidal geometry with all bond angles <109.5° because the lone pair is more repulsive than bonds. Because the double bond is more repulsive than single bonds, we should also expect the O-S-X bond angles to be greater than the X-S-X bond angles.

Trend: This is a series of molecules that varies in the identity of the pendant atoms; the variation is within the halogens. The size of the halogens increases, and the electronegativity decreases in the order F, Cl, Br. Both size and electronegativity would lead us to conclude that the X-S-X bond angles would increase in the order $OSF_2 < OSCl_2 < OSBr_2$

Explanation: (1) Increasing electonegativity of the pendant atom (F > Cl > Br) increases the polarity of the bond and reduces the electron density of the bonded pair on the central atom. This reduces the e-e repulsions of adjacent bonded electron pairs on S, allowing the halogens to become closer. The more electronegative pendant atoms can have smaller bond angles. (2) Increasing size of pendant atoms (F < Cl < Br) increases steric repulsions and increases bond angle. Both explanations lead to the same predicted trend.

The actual measured X-S-X bond angles are OSF_2 (92.3°) / $OSCl_2$ (96.2°) / $OSBr_2$ (98.2°). The trend in these bond angles is consistent with the prediction.

Geometry and predicted bond angles: These are molecules with steric number 4, bent molecular geometry, with predicted bond angles <109.5° because the two lone pairs are each more repulsive than the bonds. There are two lone pairs and two single bonds to H around each central atom.

Trend: This is a series of molecules that varies in the identity of the central atom. The central atom increases in the order O < S < Se < Te, where Te is the largest element and O is the smallest. Arguments based on size would lead us to predict that the pendant groups of H_2Te would be less sterically crowded and thus have a smaller bond angle than the pendant groups of H_2O. The electronegativity decreases in the order O > S > Se > Te, where O is the most electronegative element and Te is the least. Thus, we expect the bonding electro pairs to be closer to the central atom on O than they would be on Te; we should expect H_2Te to have the least electron pair repulsions and thus smallest bond angle in this series, while H_2O would have the strongest electron pair repulsions and largest bond angles.

Both arguments lead to the same conclusion, that the order of increasing bond angle is $H_2Te < H_2Se < H_2S < H_2O$.

The actual measured bond angles are H_2Te (90.2°) / H_2Se (90.6°) / H_2S (92.1°) / H_2O (104.5). The trend in these bond angles is consistent with prediction.

Geometry and predicted bond angles: These are molecules with steric number 4, bent molecular geometry, with predicted bond angles <109.5° because the two lone pairs are each more repulsive than the bonds. There are two lone pairs and two single bonds to H around each central atom. (This is similar to the case in (b)).

Trend: This is a series of molecules that varies in the identity of the pendant atoms; two of the molecules have halogens, and the other has hydrogen pendant atoms. This is a case where size and electronegativity will be conflicting factors because trends in electronegativity do not mirror the trend in size.

- *Size:* The size of pendant atoms increases in the order H < F < Cl where H is smallest and Cl is largest. Prediction of bond angles based on size alone would lead to the predicted order of increasing bond angle $H_2O < OF_2 < OCl_2$.
- *Electronegativity*: The electronegativity decreases in the order F > Cl > H where F has the greatest electronegativity and H has the least. Since we expect the most electronegative pendant atoms to have the smallest bond angles, prediction based on electronegativity alone would lead to the predicted order of increasing bond angle $OF_2 < OCl_2 < H_2O$.

The points above illustrate how the two different arguments would lead to different predictions about the trend in bond angle. This makes it difficult to predict the actual order of increasing bond angle. However, we saw above in the example of NH_3 vs NF_3 that electronegativity is more important than size; yet in the case of NH_3 vs NCl_3, the much larger size of the pendant atom is more important. If we apply this lesson to the current problem, we might predict the order $OF_2 < H_2O < OCl_2$, and in fact this more nuanced prediction, based on a similar case, matches the actual order for measured bond angles: OF_2 (103.3°) < H_2O (104.5°) < OCl_2 (110.9°).

Exercise 3.2.3.2

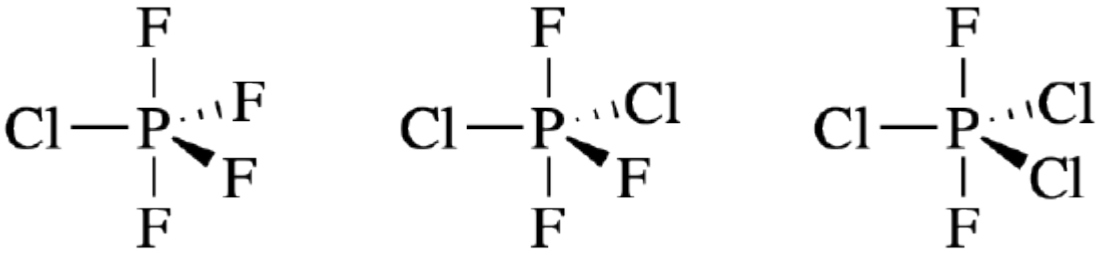
Add texts here. Do not delete this text first.

Exercise 3.2.3.2

Add texts here. Do not delete this text first.

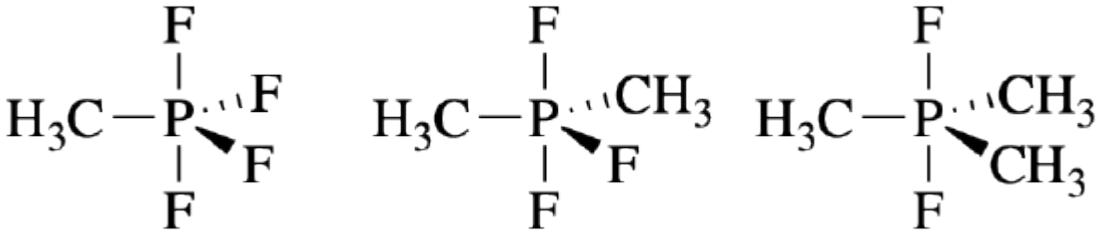
Exercise 3.2.3.3

Cl is less electronegative than F; thus we expect Cl to have stronger preference for the equatorial positions.



Exercise 3.2.3.3

CH_3, an electron donating group, is less electronegative than F. We expect CH_3 to have a stronger preference for the equatorial positions.



This page titled 3.2.3: Electronegativity and Atomic Size Effects is shared under a CC BY-NC-SA 4.0 license and was authored, remixed, and/or curated by Kathryn Haas.

- 3.2.3: Electronegativity and Atomic Size Effects by Kathryn Haas is licensed CC BY-NC-SA 4.0.

3.2.4: Ligand Close Packing

Introduction

Ligand Close Packing (LCP) theory is complimentary to VSEPR, except that LCP focuses on repulsions between pendant *atoms* ("outer" atoms that are not directly bonded to one another), rather than focusing on the chemical environment around the central atom in a molecule. Both LCP and the VSEPR models were developed by Robert Gillespie.

The LCP model assumes that ligands (or pendant atoms) "pack" as closely as possible around a central atom. A given ligand will have a specific atomic radius when bound to a central atom. The distance between two ligands around the same central atom is simply the sum of the atomic radii of the pendant atoms. Therefore for a specific set of ligands around a specific central atom, the ligand-ligand distances are constant despite the coordination number or bond angles. In other words, for a series of similar molecules with the same central atom, while bond angles and bond distances of pendant atoms may change, the distances between two pendant atoms remain the same.

Ligand Close Packing Theory

According to LCP, distances between two pendant atoms are similar...

- even when steric number changes
- even when bond angles change
- Reason: pendant atoms "pack" around the central atom.

Ligand Close Packing and Bond Distances

If the distance between non-bonded atoms remains constant even while bond angles change, then the bond length between the pendant and central atom must change to accommodate. For example, $\mathrm{PF_4}^+$ and $\mathrm{PF_3O}$ have almost identical $\mathrm{F-F}$ distances of 238 and 237 pm, respectively. As expected from VSEPR, the $\mathrm{F-P-F}$ bond angle in $\mathrm{PF_4}^+$ is 109.5°. The $\mathrm{F-P-F}$ bond angle in $\mathrm{PF_3O}$ (101.1°) is smaller due to the increased repulsion of the oxygen double bond. Therefore the P-F bond lengths must be different. In fact, the P-F bond distances are 145.7 pm in $\mathrm{PF_4}^+$ and 154 pm in $\mathrm{PF_3O}$.

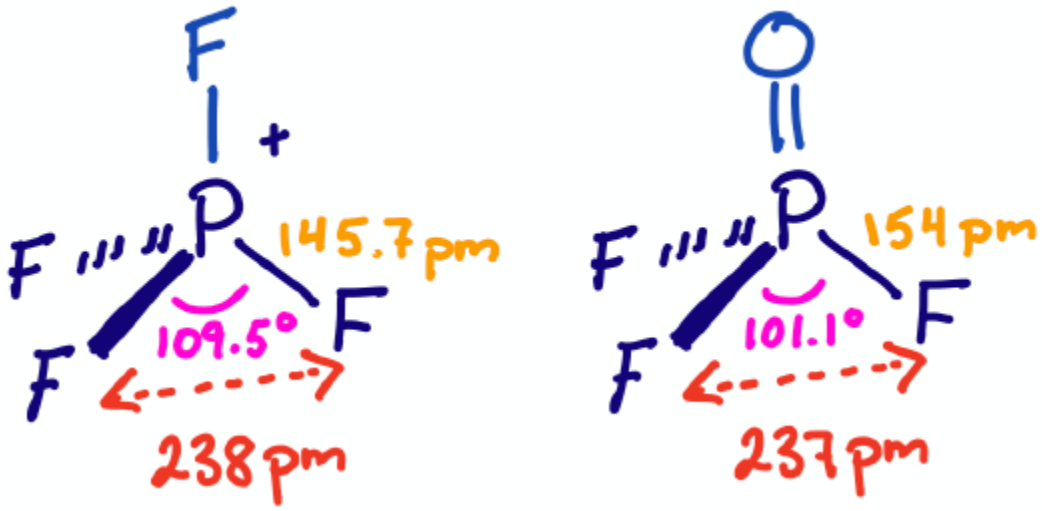


Figure 3.2.4.1: The molecular structures of $\mathrm{PF_4}^+$ and $\mathrm{PF_3O}$. The distances between neighboring F atoms are similar in the two molecules, while bond lengths and angles differ. The $\mathrm{PF_4}^+$ ion has a $\mathrm{P-F}$ bond length of 145.7 pm, an $\mathrm{F-P-F}$ bond angle of 109.5°, and a distance of 238 pm between neighboring F atoms. The $\mathrm{PF_3O}$ molecule has a $\mathrm{P-F}$ bond length of 154 pm, an $\mathrm{F-P-F}$ bond angle of 101.1°, and a distance of 237 pm between neighboring F atoms. (CC-BY-NC-SA; Kathryn Haas)

The relationship between bond angles, bond lengths, and close-packing distance is described by right angle trigonometry (recall SOA-CAH-TOA). In a right triangle, the hypotenuse is the longest side, opposite to the right angle. For either of the other two angles in the triangle, the angle (θ) and lengths of the sides (*opposite* and *adjacent* to θ) are related by the trigometric functions shown in Figure 3.2.4.2 .

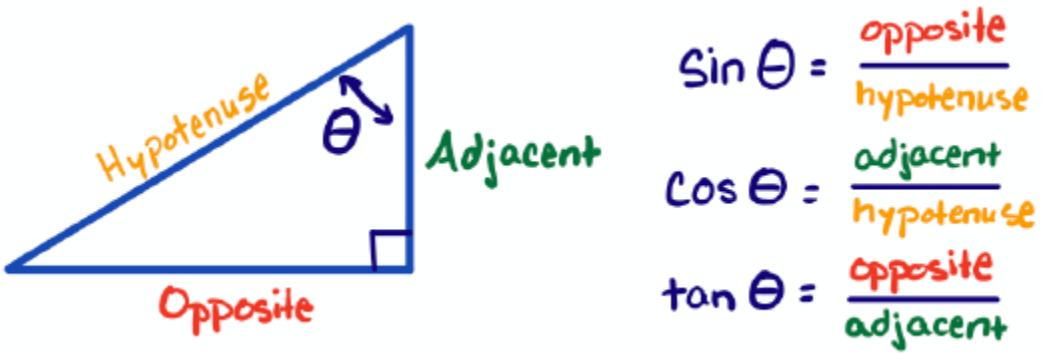


Figure 3.2.4.2: Visual depiction of SOA-CAH-TOA. (CC-BY-NC-SA; Kathryn Haas)

In the case of a molecule, we can apply right angle trigonometry by imagining that the bond angle is divided into two right angles, as illustrated in Figure 3.2.4.2. The hypotenuse of the triangles is the bond length, the opposite side is one half of the close-packing distance, and θ is one half the bond angle.

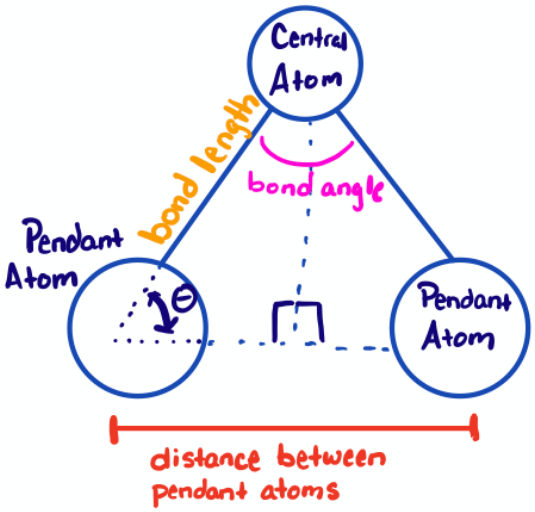


Figure 3.2.4.1: Illustration of how right angle trigonometry can be applied to determine bond angle, bond length, or distance between neighboring atoms: any bond angle can be divided into two right angles where the bond length is the hypotenuse, the distance between neighbors is twice the opposite side, and the bond angle is twice θ. (CC-BY-NC-SA; Kathryn Haas)

Exercise 3.2.4.1

The distance between F atoms is 212 pm in both NF_4^+ and NF_3. The bond angles are 109.5° and 102.3°, respectively. What are the expected $N-F$ bond lengths?

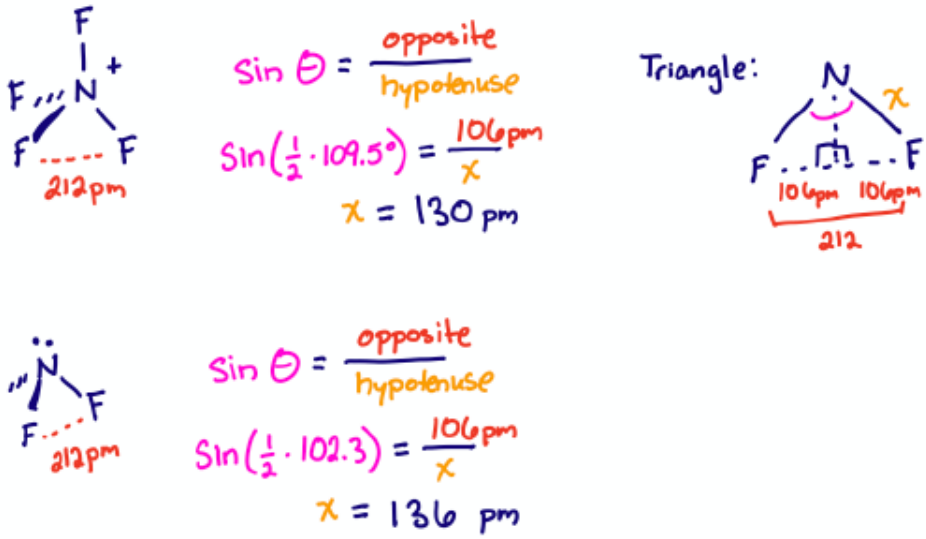
Answer available at the end of this section.

Sources and Resources

- https://en.Wikipedia.org/wiki/LCP_th...ieNyholm1957-3

Answers

Exercise 3.2.4.1



The actual measured bond lengths are 130 pm for NF_4^+ and 136.5 pm for NF_3.

This page titled 3.2.4: Ligand Close Packing is shared under a CC BY-NC-SA 4.0 license and was authored, remixed, and/or curated by Kathryn Haas.

- 3.2.4: Ligand Close Packing by Kathryn Haas is licensed CC BY-NC-SA 4.0.

3.3: Molecular Polarity

Dipole moments occur when there is a separation of charge. They can occur between two ions in an ionic bond or between atoms in a covalent bond; dipole moments arise from differences in electronegativity. The larger the difference in electronegativity, the larger the dipole moment. The distance between the charge separation is also a deciding factor in the size of the dipole moment. The dipole moment is a measure of the polarity of the molecule.

Introduction

When atoms in a molecule share electrons unequally, they create what is called a dipole moment. This occurs when one atom is more electronegative than another, resulting in that atom pulling more tightly on the shared pair of electrons, or when one atom has a lone pair of electrons and the difference of electronegativity vector points in the same way. One of the most common examples is the water molecule, made up of one oxygen atom and two hydrogen atoms. The differences in electronegativity and lone electrons give oxygen a partial negative charge and each hydrogen a partial positive charge.

Dipole Moment

When two electrical charges, of opposite sign and equal magnitude, are separated by a distance, an electric dipole is established. The size of a dipole is measured by its dipole moment (μ). Dipole moment is measured in Debye units, which is equal to the distance between the charges multiplied by the charge (1 Debye equals $3.34 \times 10^{-30}\ C\ m$). The dipole moment of a molecule can be calculated by Equation 3.3.1:

$$\vec{\mu} = \sum_i q_i \vec{r}_i \tag{3.3.1}$$

where

- $\vec{\mu}$ is the dipole moment vector
- q_i is the magnitude of the ith charge, and
- $\vec{r}_i$ is the vector representing the position of ith charge.

The dipole moment acts in the direction of the vector quantity. An example of a polar molecule is $\mathrm{H_2O}$. Because of the lone pair on oxygen, the structure of $\mathrm{H_2O}$ is bent (via VSEPR theory), which means that the vectors representing the dipole moment of each bond do not cancel each other out. Hence, water is polar.

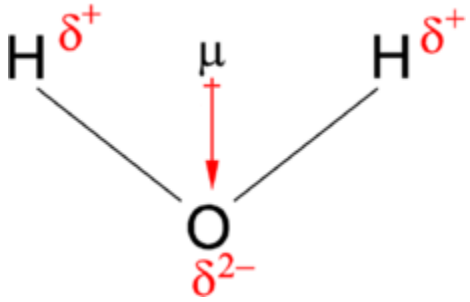


Figure 3.3.1: Dipole moment of water. The convention in chemistry is that the arrow representing the dipole moment goes from positive to negative. Physicist tend to use the opposite orientation.

The vector points from positive to negative, on both the molecular (net) dipole moment and the individual bond dipoles. Table A2 shows the electronegativity of some of the common elements. The larger the difference in electronegativity between the two atoms, the more electronegative that bond is. To be considered a polar bond, the difference in electronegativity must be large. The dipole moment points in the direction of the vector quantity of each of the bond electronegativities added together.

It is relatively easy to measure dipole moments: just place a substance between charged plates (Figure 3.3.2); polar molecules increase the charge stored on the plates, and the dipole moment can be obtained (i.e., via the capacitance of the system).

Nonpolar CCl_4 is not deflected; moderately polar acetone deflects slightly; highly polar water deflects strongly. In general, polar molecules will align themselves: (1) in an electric field, (2) with respect to one another, or (3) with respect to ions (Figure 3.3.2).

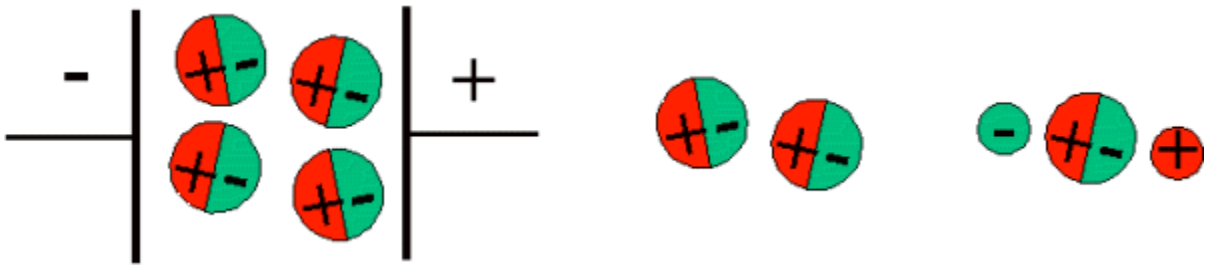


Figure 3.3.2: Polar molecules align themselves in an electric field (left), with respect to one another (middle), and with respect to ions (right)

Equation 3.3.1 can be simplified for a simple separated two-charge system like diatomic molecules or when considering a bond dipole within a molecule

$$\mu_{diatomic} = Q \times r \tag{3.3.2}$$

This bond dipole is interpreted as the dipole from a charge separation over a distance r between the partial charges Q^+ and Q^- (or the more commonly used terms δ^+ - δ^-); the orientation of the dipole is along the axis of the bond. Consider a simple system of a single electron and proton separated by a fixed distance. When the proton and electron are close together, the dipole moment (degree of polarity) decreases. However, as the proton and electron get farther apart, the dipole moment increases. In this case, the dipole moment is calculated as (via Equation 3.3.2):

$$\begin{aligned} \mu &= Qr \\ &= (1.60 \times 10^{-19}\, C)(1.00 \times 10^{-10}\, m) \\ &= 1.60 \times 10^{-29}\, C \cdot m \end{aligned}$$

The Debye characterizes the size of the dipole moment. When a proton and electron are 100 pm apart, the dipole moment is 4.80 D:

$$\begin{aligned} \mu &= (1.60 \times 10^{-29}\, C \cdot m)\left(\frac{1\ D}{3.336 \times 10^{-30}\, C \cdot m}\right) \\ &= 4.80\ D \end{aligned}$$

$4.80\ \ D$ is a key reference value and represents a pure charge of +1 and -1 separated by 100 pm. If the charge separation is increased then the dipole moment increases (linearly):

- If the proton and electron are separated by 120 pm:

$$\mu = \frac{120}{100}(4.80\ D) = 5.76\, D \tag{3.3.3}$$

- If the proton and electron are separated by 150 pm:

$$\mu = \frac{150}{100}(4.80\ D) = 7.20\, D \tag{3.3.4}$$

- If the proton and electron are separated by 200 pm:

$$\mu = \frac{200}{100}(4.80\ D) = 9.60\, D \tag{3.3.5}$$

Example 3.3.1: Water

The water molecule in Figure 3.3.1 can be used to determine the direction and magnitude of the dipole moment. From the electronegativities of oxygen and hydrogen, the difference in electronegativity is 1.2e for each of the hydrogen-oxygen bonds. Next, because the oxygen is the more electronegative atom, it exerts a greater pull on the shared electrons; it also has two lone pairs of electrons. From this, it can be concluded that the dipole moment points from between the two hydrogen atoms

toward the oxygen atom. Using the equation above, the dipole moment is calculated to be 1.85 D by multiplying the distance between the oxygen and hydrogen atoms by the charge difference between them and then finding the components of each that point in the direction of the net dipole moment (the angle of the molecule is 104.5°).

The bond moment of the O-H bond =1.5 D, so the net dipole moment is

$$\mu = 2(1.5)\cos\left(\frac{104.5^\circ}{2}\right) = 1.84\ D$$

Polarity and Structure of Molecules

The shape of a molecule and the polarity of its bonds determine the OVERALL POLARITY of that molecule. A molecule that contains polar bonds might not have any overall polarity, depending upon its shape. The simple definition of whether a complex molecule is polar or not depends upon whether its overall centers of positive and negative charges overlap. If these centers lie at the same point in space, then the molecule has no overall polarity (and is non polar). If a molecule is completely symmetric, then the dipole moment vectors on each molecule will cancel each other out, making the molecule nonpolar. A molecule can only be polar if the structure of that molecule is not symmetric.

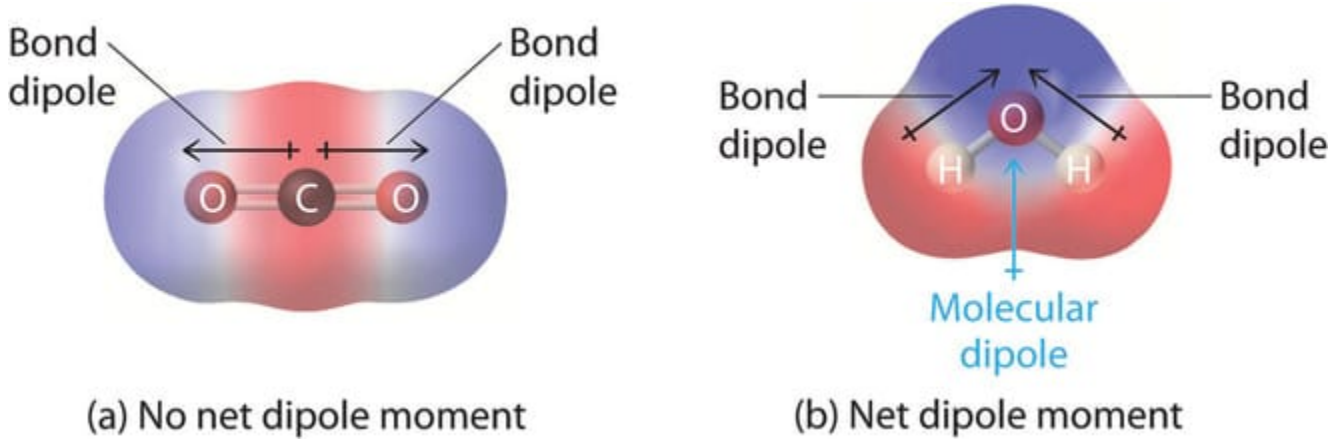


Figure 3.3.3: Charge distributions of CO_2 and H_2O\). Blue and red colored regions are negatively and positively signed regions, respectively. (CC BY-SA-NC 3.0; anonymous)

A good example of a nonpolar molecule that contains polar bonds is carbon dioxide (Figure $3.3.3a$). This is a linear molecule and each C=O bond is, in fact, polar. The central carbon will have a net positive charge, and the two outer oxygen atoms a net negative charge. However, since the molecule is linear, these two bond dipoles cancel each other out (i.e. the vector addition of the dipoles equals zero) and the overall molecule has a zero dipole moment ($\mu = 0$).

> Although a polar bond is a prerequisite for a molecule to have a dipole, not all molecules with polar bonds exhibit dipoles

For AB_n molecules, where A is the central atom and B are all the same types of atoms, there are certain molecular geometries which are symmetric. Therefore, they will have no dipole even if the bonds are polar. These geometries include linear, trigonal planar, tetrahedral, octahedral and trigonal bipyramid.

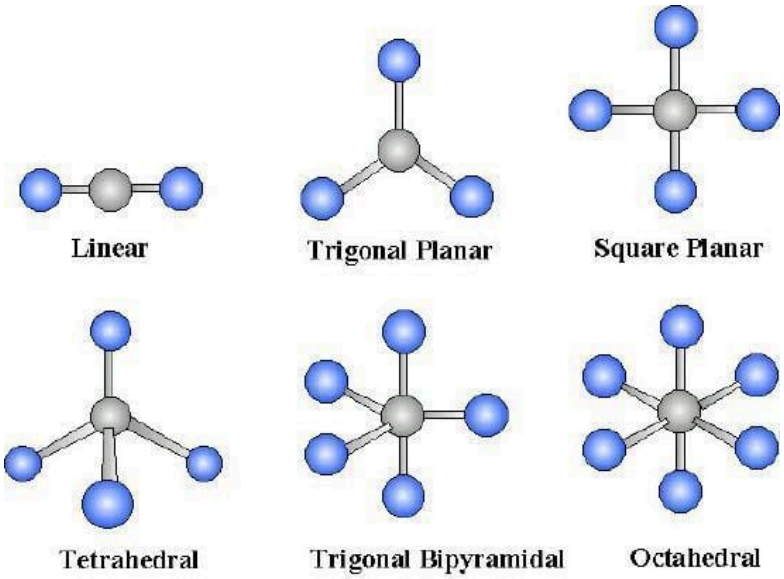
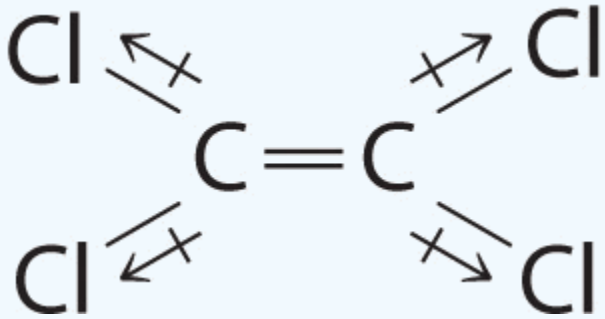


Figure 3.3.4: Molecular geometries with exact cancellation of polar bonding to generate a non-polar molecule ($\mu = 0$)

Example 3.3.3: C_2Cl_4

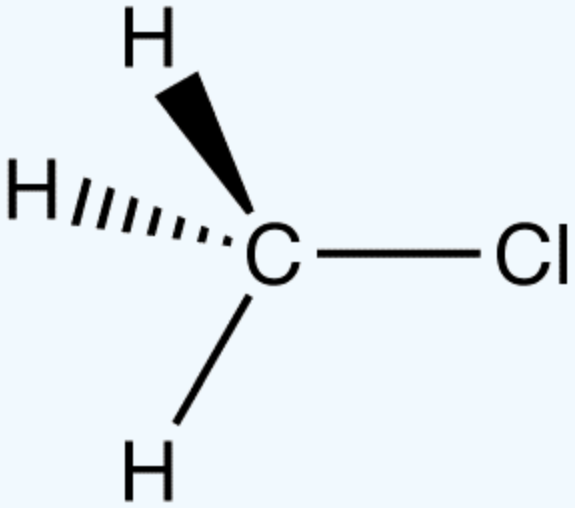
Although the C–Cl bonds are rather polar, the individual bond dipoles cancel one another in this symmetrical structure, and $Cl_2C{=}CCl_2$ does not have a net dipole moment.



Example 3.3.3: CH_3Cl

C-Cl, the key polar bond, is 178 pm. Measurement reveals 1.87 D. From this data, % ionic character can be computed. If this bond were 100% ionic (based on proton & electron),

$$\mu = \frac{178}{100}(4.80\ D)$$
$$= 8.54\ D$$



Although the bond length is ***increasing***, the dipole is ***decreasing*** as you move down the halogen group. The electronegativity decreases as we move down the group. Thus, the greater influence is the electronegativity of the two atoms (which influences the ***charge*** at the ends of the dipole).

Table 3.3.1: Relationship between Bond length, Electronegativity and Dipole moments in simple Diatomics

Compound	Bond Length (Å)	Electronegativity Difference	Dipole Moment (D)
HF	0.92	1.9	1.82
HCl	1.27	0.9	1.08
HBr	1.41	0.7	0.82
HI	1.61	0.4	0.44

References

1. *Housecroft, Catherine E. and Alan G. Sharpe. Inorganic Chemistry. 3rd ed. Harlow: Pearson Education, 2008. Print. (Pages 44-46)*
2. *Tro, Nivaldo J. Chemistry: A Molecular Approach. Upper Saddle River: Pearson Education, 2008. Print. (Pages 379-386)*

This page titled 3.3: Molecular Polarity is shared under a CC BY 4.0 license and was authored, remixed, and/or curated by Kathryn Haas.

- Dipole Moments by Delmar Larsen, Mike Blaber is licensed CC BY 4.0.

3.4: Hydrogen Bonding

A hydrogen bond is an intermolecular force (IMF) that forms a special type of dipole-dipole attraction when a hydrogen atom bonded to a strongly electronegative atom exists in the vicinity of another electronegative atom with a lone pair of electrons. Intermolecular forces (IMFs) occur between molecules. Other examples include ordinary dipole-dipole interactions and dispersion forces. Hydrogen bonds are are generally stronger than ordinary dipole-dipole and dispersion forces, but weaker than true covalent and ionic bonds.

The evidence for hydrogen bonding

Many elements form compounds with hydrogen. If you plot the boiling points of the compounds of the group 14 elements with hydrogen, you find that the boiling points increase as you go down the group.

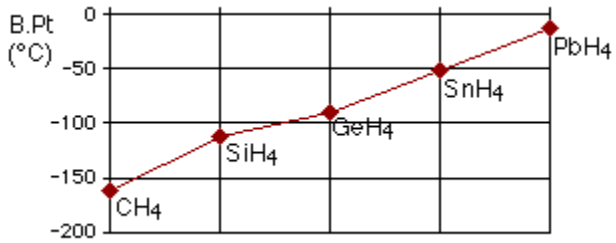


Figure 1: Boiling points of group 14 elemental halides.

The increase in boiling point happens because the molecules are getting larger with more electrons, and so van der Waals dispersion forces become greater. If you repeat this exercise with the compounds of the elements in groups 15, 16, and 17 with hydrogen, something odd happens.

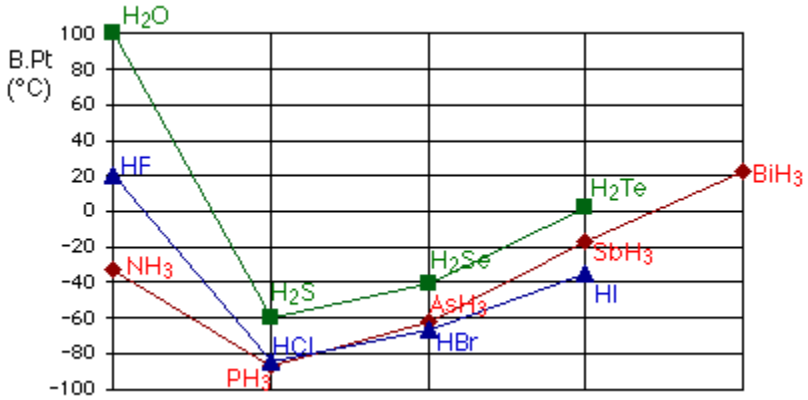


Figure 2: Boiling points of group 15-17 elemental halides.

Although the same reasoning applies for group 4 of the periodic table, the boiling point of the compound of hydrogen with the first element in each group is abnormally high. In the cases of NH_3, H_2O and HF there must be some additional intermolecular forces of attraction, requiring significantly more heat energy to break the IMFs. These relatively powerful intermolecular forces are described as hydrogen bonds.

Origin of Hydrogen Bonding

The molecules capable of hydrogen bonding include the following:

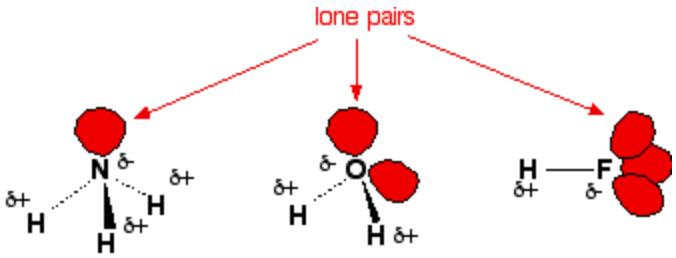


Figure 3: The lone pairs responsible for hydrogen bonding in NH_3, H_2O, and HF. The solid line represents a bond in the plane of the screen or paper. Dotted bonds are going back into the screen or paper away from you, and wedge-shaped ones are coming out towards you.

Notice that in each of these molecules:

- The hydrogen is attached directly to a highly electronegative atoms, causing the hydrogen to acquire a highly positive charge.
- Each of the highly electronegative atoms attains a high negative charge and has at least one "active" lone pair. Lone pairs at the 2-level have electrons contained in a relatively small volume of space, resulting in a high negative charge density. Lone pairs at higher levels are more diffuse and, resulting in a lower charge density and lower affinity for positive charge.

If you are not familiar with electronegativity, you should follow this link before you go on.

Consider two water molecules coming close together.

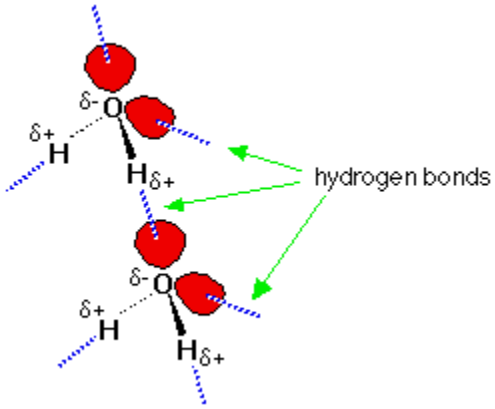


Figure 4: Hydrogen bonding in water

The δ^+ hydrogen is so strongly attracted to the lone pair that it is almost as if you were beginning to form a co-ordinate (dative covalent) bond. It doesn't go that far, but the attraction is significantly stronger than an ordinary dipole-dipole interaction. Hydrogen bonds have about a tenth of the strength of an average covalent bond, and are constantly broken and reformed in liquid water. If you liken the covalent bond between the oxygen and hydrogen to a stable marriage, the hydrogen bond has "just good friends" status.

Water is an ideal example of hydrogen bonding. Notice that each water molecule can potentially form four hydrogen bonds with surrounding water molecules: two with the hydrogen atoms and two with the with the oxygen atoms. There are exactly the right numbers of δ^+ hydrogens and lone pairs for every one of them to be involved in hydrogen bonding.

This is why the boiling point of water is higher than that of ammonia or hydrogen fluoride. In the case of ammonia, the amount of hydrogen bonding is limited by the fact that each nitrogen only has one lone pair. In a group of ammonia molecules, there are not enough lone pairs to go around to satisfy all the hydrogens. In hydrogen fluoride, the problem is a shortage of hydrogens. In water, two hydrogen bonds and two lone pairs allow formation of hydrogen bond interactions in a lattice of water molecules. Water is thus considered an ideal hydrogen bonded system.

More complex examples of hydrogen bonding

The hydration of negative ions

When an ionic substance dissolves in water, water molecules cluster around the separated ions. This process is called hydration. Water frequently attaches to positive ions by co-ordinate (dative covalent) bonds. It bonds to negative ions using hydrogen bonds.

> If you are interested in the bonding in hydrated positive ions, you could follow this link to co-ordinate (dative covalent) bonding.

The diagram shows the potential hydrogen bonds formed with a chloride ion, Cl-. Although the lone pairs in the chloride ion are at the 3-level and would not normally be active enough to form hydrogen bonds, they are made more attractive by the full negative charge on the chlorine in this case.

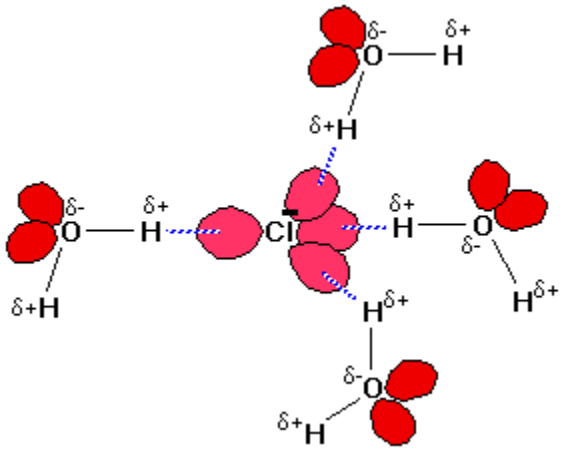


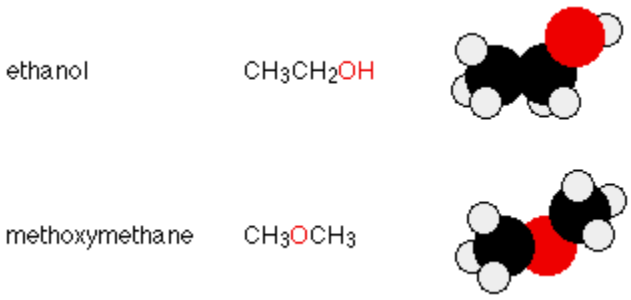
Figure 5: Hydrogen bonding between chloride ions and water.

However complicated the negative ion, there will always be lone pairs that the hydrogen atoms from the water molecules can hydrogen bond to.

Hydrogen bonding in alcohols

An alcohol is an organic molecule containing an -OH group. Any molecule which has a hydrogen atom attached directly to an oxygen or a nitrogen is capable of hydrogen bonding. Hydrogen bonds also occur when hydrogen is bonded to fluorine, but the HF group does not appear in other molecules. Molecules with hydrogen bonds will always have higher boiling points than similarly sized molecules which don't have an -O-H or an -N-H group. The hydrogen bonding makes the molecules "stickier," such that more heat (energy) is required to separate them. This phenomenon can be used to analyze boiling point of different molecules, defined as the temperature at which a phase change from liquid to gas occurs.

Ethanol, CH_3CH_2-O-H, and methoxymethane, CH_3-O-CH_3, both have the same molecular formula, C_2H_6O.



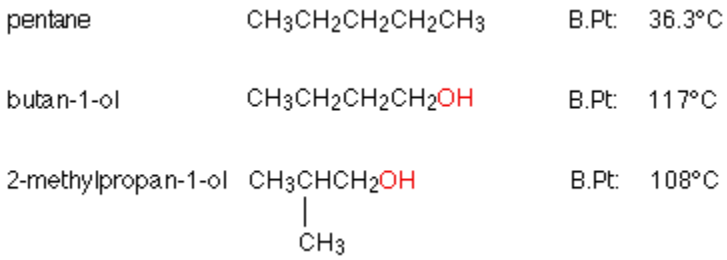
They have the same number of electrons, and a similar length. The van der Waals attractions (both dispersion forces and dipole-

dipole attractions) in each will be similar. However, ethanol has a hydrogen atom attached directly to an oxygen; here the oxygen still has two lone pairs like a water molecule. Hydrogen bonding can occur between ethanol molecules, although not as effectively as in water. The hydrogen bonding is limited by the fact that there is only one hydrogen in each ethanol molecule with sufficient $\delta+$ charge.

In methoxymethane, the lone pairs on the oxygen are still there, but the hydrogens are not sufficiently $\delta+$ for hydrogen bonds to form. Except in some rather unusual cases, the hydrogen atom has to be attached directly to the very electronegative element for hydrogen bonding to occur. The boiling points of ethanol and methoxymethane show the dramatic effect that the hydrogen bonding has on the stickiness of the ethanol molecules:

ethanol (with hydrogen bonding)	78.5°C
methoxymethane (without hydrogen bonding)	-24.8°C

The hydrogen bonding in the ethanol has lifted its boiling point about 100°C. It is important to realize that hydrogen bonding exists in addition to van der Waals attractions. For example, all the following molecules contain the same number of electrons, and the first two have similar chain lengths. The higher boiling point of the butan-1-ol is due to the additional hydrogen bonding.



Comparing the two alcohols (containing -OH groups), both boiling points are high because of the additional hydrogen bonding; however, the values are not the same. The boiling point of the 2-methylpropan-1-ol isn't as high as the butan-1-ol because the branching in the molecule makes the van der Waals attractions less effective than in the longer butan-1-ol.

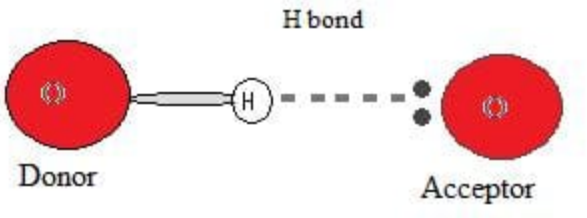
Hydrogen bonding in organic molecules containing nitrogen

Hydrogen bonding also occurs in organic molecules containing N-H groups; recall the hydrogen bonds that occur with ammonia. Examples range from simple molecules like CH_3NH_2 (methylamine) to large molecules like proteins and DNA. The two strands of the famous double helix in DNA are held together by hydrogen bonds between hydrogen atoms attached to nitrogen on one strand, and lone pairs on another nitrogen or an oxygen on the other one.

Donors and Acceptors

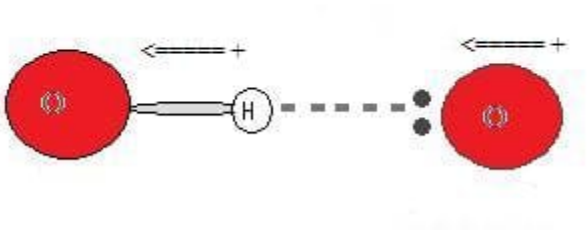
In order for a hydrogen bond to occur there must be both a hydrogen donor and an acceptor present. The donor in a hydrogen bond is usually a strongly electronegative atom such as N, O, or F that is covalently bonded to a hydrogen bond.

The hydrogen acceptor is an electronegative atom of a neighboring molecule or ion that contains a lone pair that participates in the hydrogen bond.



Why does a hydrogen bond occur?

Since the hydrogen donor (N, O, or F) is strongly electronegative, it pulls the covalently bonded electron pair closer to its nucleus, and away from the hydrogen atom. The hydrogen atom is then left with a partial positive charge, creating a dipole-dipole attraction between the hydrogen atom bonded to the donor and the lone electron pair of the acceptor. This results in a hydrogen bond.(see Interactions Between Molecules With Permanent Dipoles)

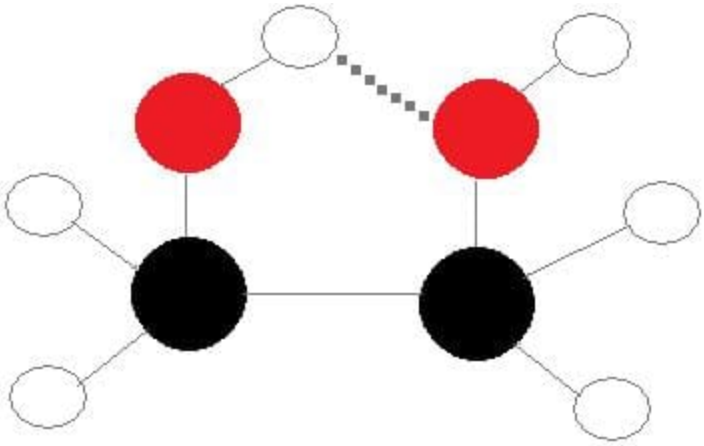


Types of hydrogen bonds

Although hydrogen bonds are well-known as a type of IMF, these bonds can also occur within a single molecule, between two identical molecules, or between two dissimilar molecules.

Intramolecular hydrogen bonds

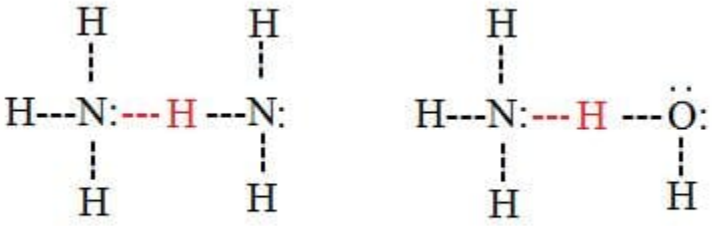
Intramolecular hydrogen bonds are those which occur *within* one single molecule. This occurs when two functional groups of a molecule can form hydrogen bonds with each other. In order for this to happen, both a hydrogen donor a hydrogen acceptor must be present within one molecule, and they must be within close proximity of each other in the molecule. For example, intramolecular hydrogen bonding occurs in ethylene glycol ($C_2H_4(OH)_2$) between its two hydroxyl groups due to the molecular geometry.



Intramolecular h-bonding in Ethylene Glycol molecule

Intermolecular hydrogen bonds

Intermolecular hydrogen bonds occur *between* separate molecules in a substance. They can occur between any number of like or unlike molecules as long as hydrogen donors and acceptors are present in positions where they can interact with one another. For example, intermolecular hydrogen bonds can occur between NH_3 molecules alone, between H_2O molecules alone, or between NH_3 and H_2O molecules.



Properties and effects of hydrogen bonds

On Boiling Point

When we consider the boiling points of molecules, we usually expect molecules with larger molar masses to have higher normal boiling points than molecules with smaller molar masses. This, without taking hydrogen bonds into account, is due to greater dispersion forces (see Interactions Between Nonpolar Molecules). Larger molecules have more space for electron distribution and thus more possibilities for an instantaneous dipole moment. However, when we consider the table below, we see that this is not always the case.

Compound	Molar Mass	Normal Boiling Point
H_2O	18 g/mol	373 K
HF	20 g/mol	292.5 K
NH_3	17 g/mol	239.8 K
H_2S	34 g/mol	212.9 K

Compound	Molar Mass	Normal Boiling Point
HCl	36.4 g/mol	197.9 K
PH_3	34 g/mol	185.2 K

We see that H_2O, HF, and NH_3 each have higher boiling points than the same compound formed between hydrogen and the next element moving down its respective group, indicating that the former have greater intermolecular forces. This is because H_2O, HF, and NH_3 all exhibit hydrogen bonding, whereas the others do not. Furthermore, H_2O has a smaller molar mass than HF but partakes in more hydrogen bonds per molecule, so its boiling point is higher.

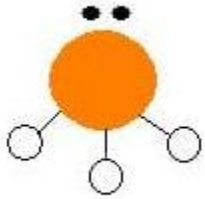
On Viscosity

The same effect that is seen on boiling point as a result of hydrogen bonding can also be observed in the viscosity of certain substances. Substances capable of forming hydrogen bonds tend to have a higher viscosity than those that do not form hydrogen bonds. Generally, substances that have the possibility for multiple hydrogen bonds exhibit even higher viscosities.

Factors preventing Hydrogen bonding

Electronegativity

Hydrogen bonding cannot occur without significant electronegativity differences between hydrogen and the atom it is bonded to. Thus, we see molecules such as PH_3, which do not participate in hydrogen bonding. PH_3 exhibits a trigonal pyramidal molecular geometry like that of ammonia, but unlike NH_3 it cannot hydrogen bond. This is due to the similarity in the electronegativities of phosphorous and hydrogen. Both atoms have an electronegativity of 2.1, and thus, there is no dipole moment. This prevents the hydrogen atom from acquiring the partial positive charge needed to hydrogen bond with the lone electron pair in another molecule. (see Polarizability)



Atom Size

The size of donors and acceptors can also affect the ability to hydrogen bond. This can account for the relatively low ability of Cl to form hydrogen bonds. When the radii of two atoms differ greatly or are large, their nuclei cannot achieve close proximity when they interact, resulting in a weak interaction.

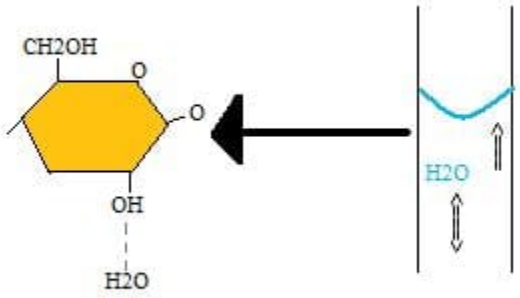


Hydrogen Bonding in Nature

Hydrogen bonding plays a crucial role in many biological processes and can account for many natural phenomena such as the Unusual properties of Water. In addition to being present in water, hydrogen bonding is also important in the water transport system of plants, secondary and tertiary protein structure, and DNA base pairing.

Plants

The cohesion-adhesion theory of transport in vascular plants uses hydrogen bonding to explain many key components of water movement through the plant's xylem and other vessels. Within a vessel, water molecules hydrogen bond not only to each other, but also to the cellulose chain that comprises the wall of plant cells. Since the vessel is relatively small, the attraction of the water to the cellulose wall creates a sort of capillary tube that allows for capillary action. This mechanism allows plants to pull water up into their roots. Furthermore, hydrogen bonding can create a long chain of water molecules, which can overcome the force of gravity and travel up to the high altitudes of leaves.



Proteins

Hydrogen bonding is present abundantly in the secondary structure of proteins, and also sparingly in tertiary conformation. The secondary structure of a protein involves interactions (mainly hydrogen bonds) between neighboring polypeptide backbones which contain nitrogen-hydrogen bonded pairs and oxygen atoms. Since both N and O are strongly electronegative, the hydrogen atoms bonded to nitrogen in one polypeptide backbone can hydrogen bond to the oxygen atoms in another chain and vice-versa. Though they are relatively weak, these bonds offer substantial stability to secondary protein structure because they repeat many times and work collectively.

In tertiary protein structure, interactions are primarily between functional R groups of a polypeptide chain; one such interaction is called a hydrophobic interaction. These interactions occur because of hydrogen bonding between water molecules around the hydrophobe that further reinforces protein conformation.

References

1. Brown, et al. Chemistry:The Central Science. 11th ed. Upper Saddle River, New Jersey: Pearson/Prentice Hall, 2008.
2. Chang, Raymond. General Chemistry:The Essential Concepts. 3rd ed. New York: Mcgraw Hill, 2003
3. Petrucci, et al. General Chemistry: Principles & Modern Applications. 9th ed. Upper Saddle River, New Jersey: Pearson/Prentice Hall, 2007.

This page titled 3.4: Hydrogen Bonding is shared under a CC BY-NC-SA 4.0 license and was authored, remixed, and/or curated by Jim Clark.

- Hydrogen Bonding by Jim Clark, Jose Pietri is licensed CC BY-NC-SA 4.0.

4: SYMMETRY AND GROUP THEORY

4.1: Symmetry Elements and Operations

4.2: Point Groups

4.2.1: Groups of Low and High Symmetry

4.2.2: Other Groups

4.3: Properties and Representations of Groups

4.3.1: Matrices

4.3.2: Representations of Point Groups

4.3.3: Character Tables

4.4: Examples and Applications of Symmetry

4.4.1: Chirality

4.4.2: Molecular Vibrations

4.5: Problems (under construction)

This page titled 4: Symmetry and Group Theory is shared under a CC BY 4.0 license and was authored, remixed, and/or curated by Kathryn Haas.

- 4: Symmetry and Group Theory by Kathryn Haas has no license indicated.

4.1: Symmetry Elements and Operations

Click here to see a lecture on this topic.

Introduction

The symmetry of a molecule consists of **symmetry operations** and **symmetry elements**. A symmetry operation is an operation that is performed to a molecule which leaves it indistinguishable and superimposable on the original position. Symmetry operations are performed with respect to symmetry elements (points, lines, or planes).

An example of a symmetry operation is a 180° rotation of a water molecule in which the resulting position of the molecule is indistinguishable from the original position (see Figure 4.1.1). In this example, the symmetry operation is the rotation and the symmetry element is the axis of rotation.

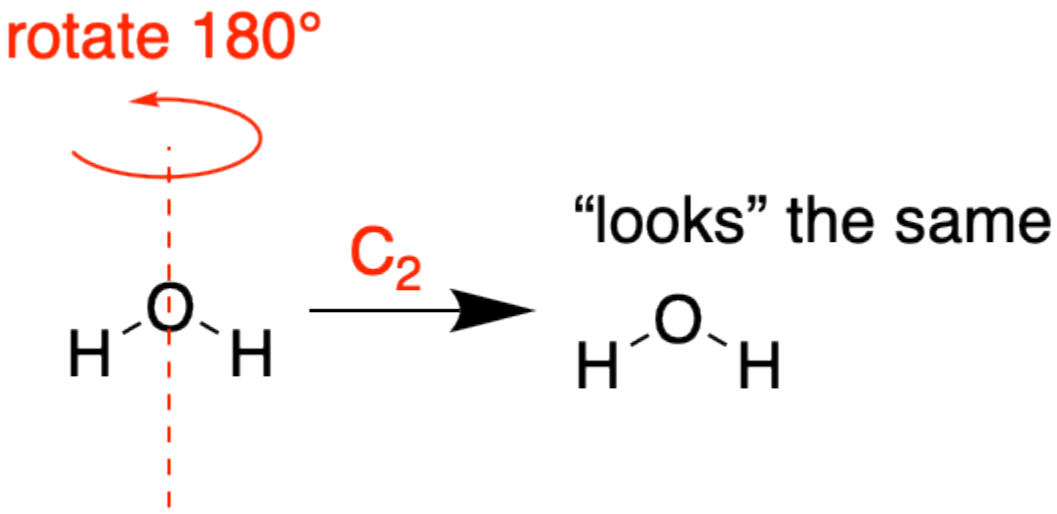


Figure 4.1.1: An example of a symmetry operation is a 180° rotation where the resulting position is indistinguishable from the original. A 180° rotation is called a C_2 operation; the axis of rotation is the symmetry element. (Kathryn Haas; CC-NC-BY-SA)

There are five types of symmetry operations including **identity**, **reflection**, **inversion**, **proper rotation**, and **improper rotation**. The improper rotation is the sum of a rotation followed by a reflection. The symmetry elements that correspond to the five types of symmetry operations are listed in Table 4.1.1.

Table 4.1.1: Table of elements and operations

Element	Operation	Symbol
Identity	identity	E
Proper axis	rotation by $(360/n)^o$	C_n
Symmetry plane	reflection in the plane	σ
Inversion center	inversion of a point at (x,y,z) to (-x,-y,-z)	*i*
Improper axis	rotation by $(360/n)^o$, followed by reflection in the plane perpendicular to the rotation axis	S_n

Symmetry Operations and Elements

Identity (E)

All molecules have the identity element. The identity operation is doing nothing to the molecule (it doesn't rotate, reflect, or invert...it just is).

Proper Rotation and Proper Axis (C_n)

A "proper" rotation is just a simple rotation operation about an axis. The symbol for any proper rotation or proper axis is $C_{(360/n)}$, where n is the degree of rotation. Thus, a 180° rotation is a C_2 rotation around a C_2 axis, and a 120° rotation is a C_3 rotation about a C_3 axis.

> **PRINCIPAL AXIS**: The principal axis of a molecule is the highest order proper rotation axis. For example, if a molecule had C_2 and C_4 axes, the C_4 is the principal axis.

Reflection and Symmetry Planes (σ)

Symmetry planes are mirror planes within the molecule. A reflection operation occurs with respect to a plane of symmetry. There are three classes of symmetry elements:

1. σ_h (horizontal): horizontal planes are perpendicular to principal axis
2. σ_v (vertical): vertical planes are parallel to the principal axis
3. σ_d (dihedral): dihedral planes are parallel to the principal axis and bisecting two C_2' axes

Inversion and Inversion Center (i)

The inversion operation requires a point of symmetry (a center of symmetry within a molecule). In other words, a point at the center of the molecule that can transform (x,y,z) into (-x,-y,-z) coordinate. Structures of tetrahedrons, triangles, and pentagons lack an inversion center.

Improper rotation (S_n)

Improper rotation is a combination of a rotation with respect to an axis of rotation (C_n), followed by a reflection through a plane perpendicular to that C_n axis. In short, an S_n operation is equivalent to C_n followed by σ_h.

References

1. Introduction to Molecular Symmetry by J. S Ogden
2. Inorganic Chemistry by Catherine Housecroft And Alan G. Sharpe.

This page titled 4.1: Symmetry Elements and Operations is shared under a CC BY-NC-SA 4.0 license and was authored, remixed, and/or curated by Kathryn Haas.

- 4.1: Symmetry Elements and Operations by Kathryn Haas is licensed CC BY-NC-SA 4.0.

4.2: Point Groups

Click here to see a lecture on this topic.

Introduction

A **Point Group** describes all the symmetry operations that can be performed on a molecule that result in a conformation indistinguishable from the original. Point groups are used in Group Theory, the mathematical analysis of groups, to determine properties such as a molecule's molecular orbitals.

Assigning Point Groups

While a point group contains all of the symmetry operations that can be performed on a given molecule, it is not necessary to identify all of these operations to determine the molecule's overall point group. Instead, a molecule's point group can be determined by following a set of steps which analyze the presence (or absence) of particular symmetry elements.

Steps for assigning a molecule's point group:

1. Determine if the molecule is of high or low symmetry.
2. If not, find the highest order rotation axis, C_n.
3. Determine whether the molecule has any C_2 axes perpendicular to the principal C_n axis. If so, then there are n such C_2 axes, and the molecule is in the D set of point groups. If not, it is in either the C or S set of point groups.
4. Determine whether the molecule has a horizontal mirror plane (σ_h) perpendicular to the principal C_n axis. If so, the molecule is either in the C_{nh} or D_{nh} set of point groups.
5. Determine whether the molecule has a vertical mirror plane (σ_v) containing the principal C_n axis. If so, the molecule is either in the C_{nv} or D_{nd} set of point groups. If not, and if the molecule has n perpendicular C_2 axes, then it is part of the D_n set of point groups.
6. Determine whether there is an improper rotation axis, S_{2n}, collinear with the principal C_n axis. If so, the molecule is in the S_{2n} point group. If not, the molecule is in the C_n point group.

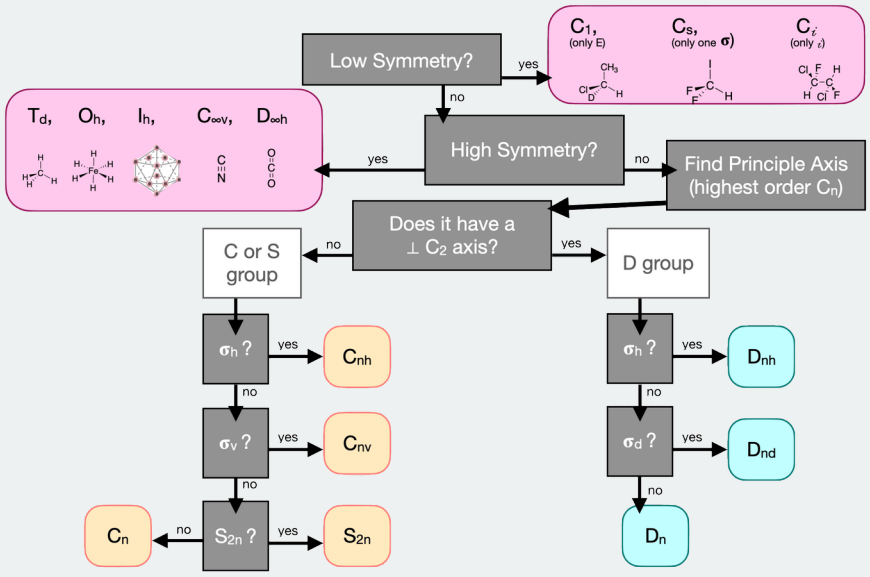


Figure 4.2.1: Decision tree for determining a molecule's point group (CC-BY-NC-SA; Kathryn Haas)

Example 4.2.1

Find the point group of benzene (C_6H_6).

Answer available at the end of this section.

See Also

Symmetry Gallery

Answers

Example 4.2.1

Solution

1. Benzene is neither high nor low symmetry
2. Highest order rotation axis: C_6
3. There are 6 C_2 axes perpendicular to the principal axis
4. There is a horizontal mirror plane (σ_h)

Benzene is in the D_{6h} point group.

This page titled 4.2: Point Groups is shared under a CC BY-NC-SA 4.0 license and was authored, remixed, and/or curated by Kathryn Haas.

- 4.2: Point Groups by Kathryn Haas has no license indicated.

4.2.1: Groups of Low and High Symmetry

Click here to see a lecture on this topic.

Low Symmetry Point Groups

Low symmetry point groups include the C_1, C_s, and C_i groups

Group	Description	Example
C_1	only the identity operation (E)	CHFClBr
C_s	only the identity operation (E) and one mirror plane	C_2H_2ClBr
C_i	only the identity operation (E) and a center of inversion (i)	$C_2H_2Cl_2Br$

High Symmetry Point Groups

High symmetry point groups include the T_d, O_h, I_h, $C_{\infty v}$, and $D_{\infty h}$ groups. The table below describes their characteristic symmetry operations. The full set of symmetry operations included in the point group is described in the corresponding character table.

Group	Description	Example
$C_{\infty v}$	linear molecule with an infinite number of rotation axes and vertical mirror planes (σ_v)	HBr
$D_{\infty h}$	linear molecule with an infinite number of rotation axes, vertical mirror planes (σ_v), perpendicular C_2 axes, a horizontal mirror plane (σ_h), and an inversion center (i)	CO_2
T_d	typically have tetrahedral geometry, with 4 C_4 axes, 3 C_2 axes, 3 S_4 axes, and 6 dihedral mirror planes (σ_d)	CH_4
O_h	typically have octahedral geometry, with 3 C_4 axes, 4 C_3 axes, and an inversion center (i) as characteristic symmetry operations	SF_6
I_h	typically have an icosahedral structure, with 6 C_5 axes as characteristic symmetry operations	$B_{12}H_{12}^{2-}$

See Also

Symmetry Gallery

This page titled 4.2.1: Groups of Low and High Symmetry is shared under a CC BY-NC-SA 4.0 license and was authored, remixed, and/or curated by Kathryn Haas.

- 4.2.1: Groups of Low and High Symmetry by Kathryn Haas has no license indicated.
- 1.2: Molecular Point Groups by Wikipedia is licensed CC BY-SA 4.0. Original source: https://en.wikibooks.org/wiki/Advanced_Inorganic_Chemistry.

4.2.2: Other Groups

Click here to see a lecture on this topic.

D Groups

The D set of point groups is classified as D_{nh}, D_{nd}, or D_n, where n refers to the principal axis of rotation. Overall, the D groups are characterized by the presence of n C_2 axes perpendicular to the principal C_n axis. Further classification of a molecule in the D groups depends on the presence of horizontal or vertical/dihedral mirror planes.

Group	Description	Example
D_{nh}	n perpendicular C_2 axes, and a horizontal mirror plane (σ_h)	benzene, C_6H_6 is D_{6h}
D_{nd}	n perpendicular C_2 axes, and a vertical mirror plane (σ_v)	propadiene, C_3H_4 is D_{2d}
D_n	n perpendicular C_2 axes, no mirror planes	$[Co(en)_3]^{3+}$ is D_3

C Groups

The C set of point groups is classified as C_{nh}, C_{nv}, or C_n, where n refers to the principal axis of rotation. The C set of groups is characterized by the absence of n C_2 axes perpendicular to the principal C_n axis. Further classification of a molecule in the C groups depends on the presence of horizontal or vertical/dihedral mirror planes.

Group	Description	Example
C_{nh}	horizontal mirror plane (σ_h) perpendicular to the principal C_n axis	boric acid, H_3BO_3, is C_{3h}
C_{nv}	vertical mirror plane (σ_v) containing the principal C_n axis	ammonia, NH_3, is C_{3v}
C_n	no mirror planes	$P(C_6H_5)_3$ is C_3

S Groups

The S set of point groups is classified as S_{2n}, where n refers to the principal axis of rotation. The S set of groups is characterized by the absence of n C_2 axes perpendicular to the principal C_n axis, as well as the absence of horizontal and vertical/dihedral mirror planes. However, there is an improper rotation (or a rotation-reflection) axis collinear with the principal C_n axis.

Group	Description	Example
S_{2n}	improper rotation (or a rotation-reflection) axis collinear with the principal C_n axis	12-crown-4 is S_4

See Also

Symmetry Gallery

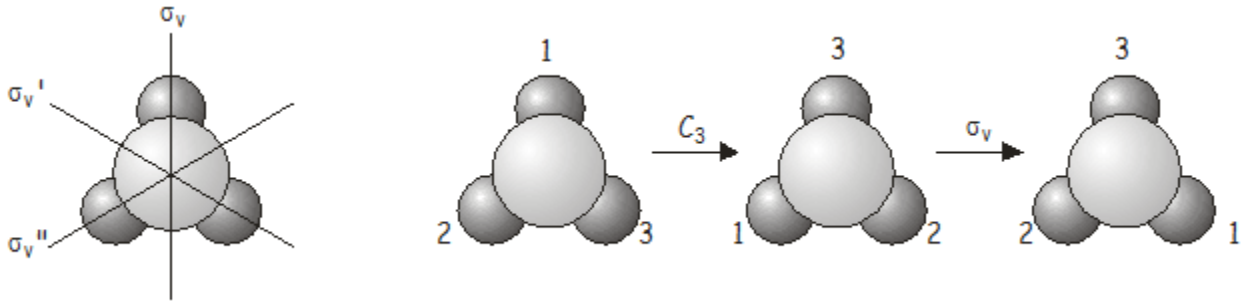
This page titled 4.2.2: Other Groups is shared under a CC BY-NC-SA 4.0 license and was authored, remixed, and/or curated by Kathryn Haas.

- 4.2.2: Other Groups by Kathryn Haas has no license indicated.
- 1.2: Molecular Point Groups by Wikipedia is licensed CC BY-SA 4.0. Original source: https://en.wikibooks.org/wiki/Advanced_Inorganic_Chemistry.

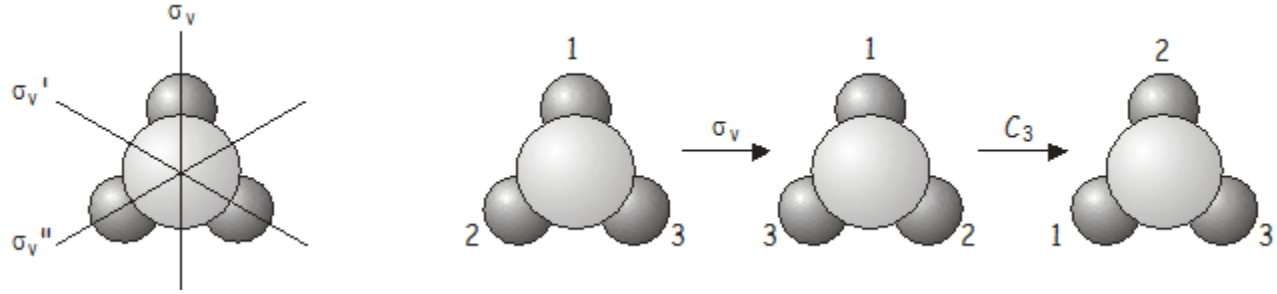
4.3: Properties and Representations of Groups

Group Multiplication

Now we will investigate what happens when we apply two symmetry operations in sequence. As an example, consider the NH_3 molecule, which belongs to the C_{3v} point group. Consider what happens if we apply a C_3rotation (120˚ counter-clockwise) followed by a σ_v reflection (reflection over the σ_v axis). We write this combined operation $\sigma_v C_3$ (when written, symmetry operations operate on the thing directly to their right, just as operators do in quantum mechanics – we therefore have to work backwards from right to left from the notation to get the correct order in which the operators are applied). As we shall soon see, the order in which the operations are applied is important.



The combined operation $\sigma_v C_3$ is equivalent to σ_v'' (note the double prime on σ_v''!), which is also a symmetry operation of the C_{3v} point group. Now let's see what happens if we apply the operators in the reverse order, i.e., $C_3\sigma_v$ is (σ_v followed by C_3).



Again, the combined operation $C_3\sigma_v$ is equivalent to another operation of the point group, this time σ_v' (note the single prime on σ_v'!).

There are two important points that are illustrated by this example:

1. The order in which two operations are applied is important. For two symmetry operations A and B, AB is not necessarily the same as BA, i.e. symmetry operations do not in general ***commute***. In some groups the symmetry elements do commute; such groups are said to be ***Abelian***.
2. If two operations from the same point group are applied in sequence, the result will be equivalent to another operation from the point group. Symmetry operations that are related to each other by other symmetry operations of the group are said to belong to the same ***class***. In NH_3, the three mirror planes σ_v, σ_v' and σ_v'' belong to the same class (related to each other through a C_3 rotation), as do the rotations C_3^+ and C_3^- (anticlockwise and clockwise rotations about the principal axis, related to each other by a vertical mirror plane).

Four Properties of Mathematical Groups

Now that we have explored some of the properties of symmetry operations and elements and their behavior within point groups,

we are ready to introduce the formal mathematical definition of a group. The definitions below will be put into the context of *molecular* symmetry.

A mathematical group is defined as a set of elements (A_1, A_2, A_3...) together with a rule for forming combinations A_i,A_j... For our purposes, A_1, A_2, A_3, etc. are symmetry elements and A_i, A_j, etc. are symmetry operations described in a previous section. The elements of the group and the rule for combining them must satisfy the following four criteria.

1. The group must include the **identity** E, which commutes with other members of the group. In other terms, $EA_i = A_i$ for all the elements of the group. Application of the identity operation before or after another operation, A_i, results in the same outcome as A_i alone.
2. The elements must satisfy the group property that the combination of any pair of elements is also an element of the group. For example, in the C_{3v} point group, a C_3 rotation followed by a σ_v gives another operation that is already part of the group: a σ_v ″.
3. Each symmetry operation A_i must have an inverse A_i^{-1}, which is also an element of the group, such that
$$A_i A_i^{-1} = A_i^{-1} A_i = E$$
The inverse g_i^{-1} effectively 'undoes' the effect of the symmetry operation g_i. For example, in the C_{3v} point group, the inverse of C_3^+ is C_3^-.
4. The rule of combination must be associative
$$(A_i A_j)(A_k) = A_i(A_j A_k)$$
Or $A(BC) = (AB)C$. In other words, the order of operations should not matter.

Group theory is an important area in mathematics, and luckily for chemists the mathematicians have already done most of the work for us. Along with the formal definition of a group comes a comprehensive mathematical framework that allows us to carry out a rigorous treatment of symmetry in molecular systems and learn about its consequences.

Many problems involving operators or operations (such as those found in quantum mechanics or group theory) may be reformulated in terms of matrices. Any of you who have come across transformation matrices before will know that symmetry operations such as rotations and reflections may be represented by matrices. It turns out that the set of matrices representing the symmetry operations in a group obey all the conditions laid out above in the mathematical definition of a group, and using matrix representations of symmetry operations simplifies carrying out calculations in group theory. Before we learn how to use matrices in group theory, it will probably be helpful to review some basic definitions and properties of matrices.

*This page was adapted from here (click).

Contributors and Attributions

- Claire Vallance (University of Oxford)
- Curated or created by Kathryn Haas

This page titled 4.3: Properties and Representations of Groups is shared under a CC BY-NC-SA 4.0 license and was authored, remixed, and/or curated by Kathryn Haas.

- 4.3: Properties and Representations of Groups by Kathryn Haas is licensed CC BY-NC-SA 4.0.

4.3.1: Matrices

The symmetry of molecules is essential for understanding the structures and properties of organic and inorganic compounds. The properties of chemical compounds are often easily explained by consideration of symmetry. For example, the symmetry of a molecule determines whether the molecule has a permanent dipole moment or not. The theories that describe optical activity, infrared and ultraviolet spectroscopy, and crystal structure involve the application of symmetry considerations. Matrix algebra is the most important mathematical tool in the description of symmetry.

The properties of symmetry groups are organized in character tables (discussed later in this chapter). Character tables are constructed based on matrices. This page is a brief description of matrices and matrix multiplication.

What is a matrix?

An $m \times n$ matrix $\mathbf{A}$ is a rectangular array of numbers with m rows and n columns. The numbers m and n are the dimensions of $\mathbf{A}$. The numbers in the matrix are called its entries. The entry in row i and column j is called a_{ij}.

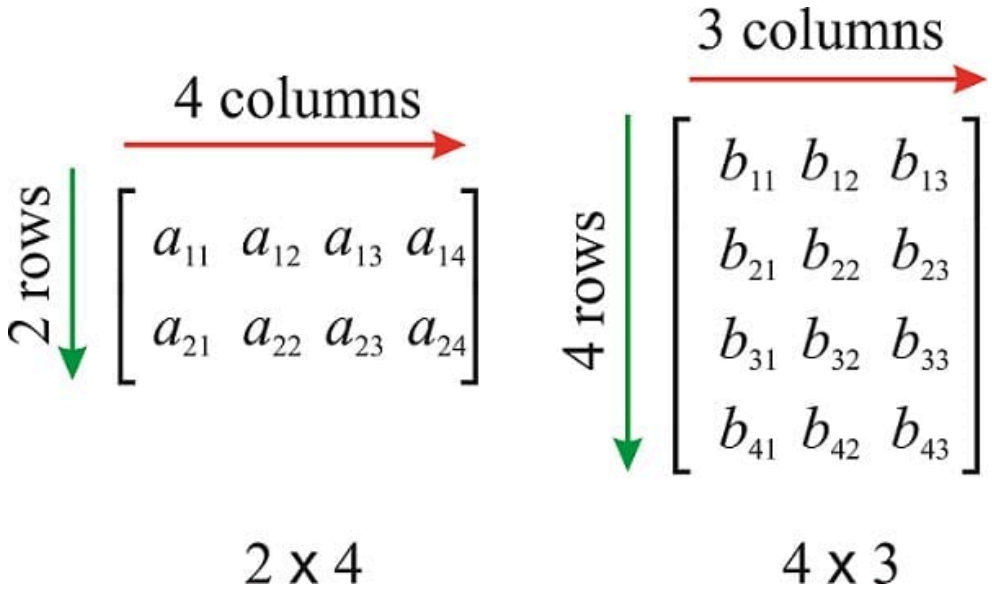


Figure 4.3.1.1: Matrices of different dimensions

Some types of matrices have special names:

- A square matrix:

$$\begin{pmatrix} 3 & -2 & 4 \\ 5 & 3i & 3 \\ -i & 1/2 & 9 \end{pmatrix}$$

  with $m = n$
- A rectangular matrix:

$$\begin{pmatrix} 3 & -2 & 4 \\ 5 & 3i & 3 \end{pmatrix}$$

  with $m \neq n$
- A column vector:

$$\begin{pmatrix} 3 \\ 5 \\ -i \end{pmatrix}$$

with $n = 1$

- A row vector:

$$\begin{pmatrix} 3 & -2 & 4 \end{pmatrix}$$

with $m = 1$

- The identity matrix:

$$\begin{pmatrix} 1 & 0 & 0 \\ 0 & 1 & 0 \\ 0 & 0 & 1 \end{pmatrix}$$

with $a_{ij} = \delta_{i,j}$, where $\delta_{i,j}$ is a function defined as $\delta_{i,j} = 1$ if $i = j$ and $\delta_{i,j} = 0$ if $i \neq j$.

- A diagonal matrix:

$$\begin{pmatrix} a & 0 & 0 \\ 0 & b & 0 \\ 0 & 0 & c \end{pmatrix}$$

with $a_{ij} = c_i \delta_{i,j}$.

- An upper triangular matrix:

$$\begin{pmatrix} a & b & c \\ 0 & d & e \\ 0 & 0 & f \end{pmatrix}$$

All the entries below the main diagonal are zero.

- A lower triangular matrix:

$$\begin{pmatrix} a & 0 & 0 \\ b & c & 0 \\ d & e & f \end{pmatrix}$$

All the entries above the main diagonal are zero.

- A triangular matrix is one that is either lower triangular or upper triangular.

The Trace of a Matrix

The trace of an $n \times n$ square matrix $\mathbf{A}$ is the sum of the diagonal elements, and formally defined as $Tr(\mathbf{A}) = \sum_{i=1}^{n} a_{ii}$.

For example,

$$\mathbf{A} = \begin{pmatrix} 3 & -2 & 4 \\ 5 & 3i & 3 \\ -i & 1/2 & 9 \end{pmatrix} ; Tr(\mathbf{A}) = 12 + 3i$$

Singular and Nonsingular Matrices

A square matrix with nonzero determinant is called *nonsingular*. A matrix whose determinant is zero is called *singular*. (Note that you cannot calculate the determinant of a non-square matrix).

For a 2x2 matrix,

$$\mathbf{B} = \begin{pmatrix} a & b \\ c & d \end{pmatrix} ; det(\mathbf{B}) = ad - cb$$

For a 3x3 matrix,

$$\mathbf{C} = \begin{pmatrix} a & b & c \\ d & e & f \\ g & h & i \end{pmatrix}$$

$$det(\mathbf{C}) = a \begin{pmatrix} e & f \\ h & i \end{pmatrix} - b \begin{pmatrix} d & f \\ g & i \end{pmatrix} + c \begin{pmatrix} d & e \\ g & h \end{pmatrix}$$

$$det(\mathbf{C}) = aei - ahf - bdi + bgf + cdh - cge$$

The Matrix Transpose

The matrix transpose, most commonly written $\mathbf{A}^T$, is the matrix obtained by exchanging $\mathbf{A}$'s rows and columns. It is obtained by replacing all elements a_{ij} with a_{ji}. For example:

$$\mathbf{A} = \begin{pmatrix} 3 & -2 & 4 \\ 5 & 3i & 3 \end{pmatrix} \rightarrow \mathbf{A}^T = \begin{pmatrix} 3 & 5 \\ -2 & 3i \\ 4 & 3 \end{pmatrix}$$

Matrix Multiplication

To multiply two matrices, the number of vertical columns in the first matrix must be the same as the number of rows in the second matrix. If $\mathbf{A}$ has dimensions $m \times n$ and $\mathbf{B}$ has dimensions $n \times p$, then the product $\mathbf{AB}$ is defined, and has dimensions $m \times p$.

$$c_{ij} = \sum a_{ij} \times b_{ij}$$

The entry $a_{ij} \times b_{ij}$ is obtained by multiplying row i of $\mathbf{A}$ by column j of $\mathbf{B}$, which is done by multiplying corresponding entries together and then adding the results:

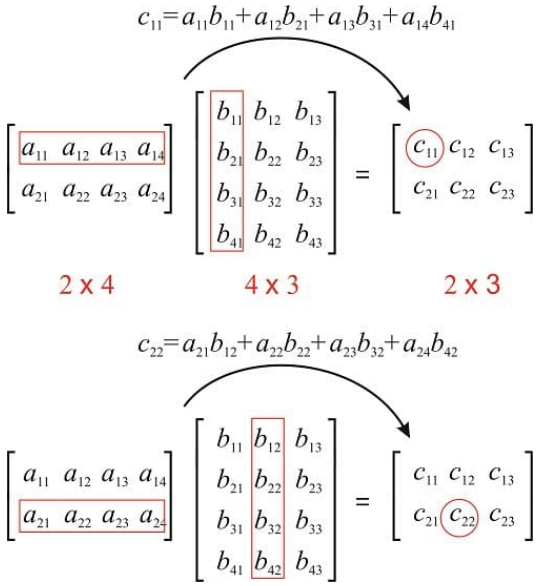


Figure 4.3.1.1: Matrix multiplication

Example 4.3.1.1

Calculate the product

$$\begin{pmatrix} 1 & -2 & 4 \\ 5 & 0 & 3 \\ 0 & 1/2 & 9 \end{pmatrix} \begin{pmatrix} 1 & 0 \\ 5 & 3 \\ -1 & 0 \end{pmatrix}$$

Solution

We need to multiply a 3×3 matrix by a 3×2 matrix, so we expect a 3×2 matrix as a result.

$$\begin{pmatrix}1 & -2 & 4\\ 5 & 0 & 3\\ 0 & 1/2 & 9\end{pmatrix}\begin{pmatrix}1 & 0\\ 5 & 3\\ -1 & 0\end{pmatrix}=\begin{pmatrix}a & b\\ c & d\\ e & f\end{pmatrix}$$

To calculate a, which is entry (1,1), we use row 1 of the matrix on the left and column 1 of the matrix on the right:

$$\begin{pmatrix}1 & -2 & 4\\ 5 & 0 & 3\\ 0 & 1/2 & 9\end{pmatrix}\begin{pmatrix}1 & 0\\ 5 & 3\\ -1 & 0\end{pmatrix}=\begin{pmatrix}a & b\\ c & d\\ e & f\end{pmatrix}\rightarrow a=1\times 1+(-2)\times 5+4\times(-1)=-13$$

To calculate b, which is entry (1,2), we use row 1 of the matrix on the left and column 2 of the matrix on the right:

$$\begin{pmatrix}1 & -2 & 4\\ 5 & 0 & 3\\ 0 & 1/2 & 9\end{pmatrix}\begin{pmatrix}1 & 0\\ 5 & 3\\ -1 & 0\end{pmatrix}=\begin{pmatrix}a & b\\ c & d\\ e & f\end{pmatrix}\rightarrow b=1\times 0+(-2)\times 3+4\times 0=-6$$

To calculate c, which is entry (2,1), we use row 2 of the matrix on the left and column 1 of the matrix on the right:

$$\begin{pmatrix}1 & -2 & 4\\ 5 & 0 & 3\\ 0 & 1/2 & 9\end{pmatrix}\begin{pmatrix}1 & 0\\ 5 & 3\\ -1 & 0\end{pmatrix}=\begin{pmatrix}a & b\\ c & d\\ e & f\end{pmatrix}\rightarrow c=5\times 1+0\times 5+3\times(-1)=2$$

To calculate d, which is entry (2,2), we use row 2 of the matrix on the left and column 2 of the matrix on the right:

$$\begin{pmatrix}1 & -2 & 4\\ 5 & 0 & 3\\ 0 & 1/2 & 9\end{pmatrix}\begin{pmatrix}1 & 0\\ 5 & 3\\ -1 & 0\end{pmatrix}=\begin{pmatrix}a & b\\ c & d\\ e & f\end{pmatrix}\rightarrow d=5\times 0+0\times 3+3\times 0=0$$

To calculate e, which is entry (3,1), we use row 3 of the matrix on the left and column 1 of the matrix on the right:

$$\begin{pmatrix}1 & -2 & 4\\ 5 & 0 & 3\\ 0 & 1/2 & 9\end{pmatrix}\begin{pmatrix}1 & 0\\ 5 & 3\\ -1 & 0\end{pmatrix}=\begin{pmatrix}a & b\\ c & d\\ e & f\end{pmatrix}\rightarrow e=0\times 1+1/2\times 5+9\times(-1)=-13/2$$

To calculate f, which is entry (3,2), we use row 3 of the matrix on the left and column 2 of the matrix on the right:

$$\begin{pmatrix}1 & -2 & 4\\ 5 & 0 & 3\\ 0 & 1/2 & 9\end{pmatrix}\begin{pmatrix}1 & 0\\ 5 & 3\\ -1 & 0\end{pmatrix}=\begin{pmatrix}a & b\\ c & d\\ e & f\end{pmatrix}\rightarrow f=0\times 0+1/2\times 3+9\times 0=3/2$$

The result is:

$$\begin{pmatrix}1 & -2 & 4\\ 5 & 0 & 3\\ 0 & 1/2 & 9\end{pmatrix}\begin{pmatrix}1 & 0\\ 5 & 3\\ -1 & 0\end{pmatrix}=\begin{pmatrix}-13 & -6\\ 2 & 0\\ -13/2 & 3/2\end{pmatrix}$$

Example 4.3.1.2

Calculate

$$\begin{pmatrix}1 & -2 & 4\\ 5 & 0 & 3\end{pmatrix}\begin{pmatrix}1\\ 5\\ -1\end{pmatrix}$$

Solution

We are asked to multiply a 2×3 matrix by a 3×1 matrix (a column vector). The result will be a 2×1 matrix (a vector).

$$\begin{pmatrix} 1 & -2 & 4 \\ 5 & 0 & 3 \end{pmatrix} \begin{pmatrix} 1 \\ 5 \\ -1 \end{pmatrix} = \begin{pmatrix} a \\ b \end{pmatrix}$$

$$a = 1 \times 1 + (-2) \times 5 + 4 \times (-1) = -13$$

$$b = 5 \times 1 + 0 \times 5 + 3 \times (-1) = 2$$

The solution is:

$$\begin{pmatrix} 1 & -2 & 4 \\ 5 & 0 & 3 \end{pmatrix} \begin{pmatrix} 1 \\ 5 \\ -1 \end{pmatrix} = \begin{pmatrix} -13 \\ 2 \end{pmatrix}$$

Need help? The link below contains solved examples: Multiplying matrices of different shapes (three examples): http://tinyurl.com/kn8ysqq

External links:

- Multiplying matrices, example 1: http://patrickjmt.com/matrices-multiplying-a-matrix-by-another-matrix/
- Multiplying matrices, example 2: http://patrickjmt.com/multiplying-matrices-example-2/
- Multiplying matrices, example 3: http://patrickjmt.com/multiplying-matrices-example-3/

The Commutator

Matrix multiplication is not, in general, commutative. For example, we can perform

$$\begin{pmatrix} 1 & -2 & 4 \\ 5 & 0 & 3 \end{pmatrix} \begin{pmatrix} 1 \\ 5 \\ -1 \end{pmatrix} = \begin{pmatrix} -13 \\ 2 \end{pmatrix}$$

but cannot perform

$$\begin{pmatrix} 1 \\ 5 \\ -1 \end{pmatrix} \begin{pmatrix} 1 & -2 & 4 \\ 5 & 0 & 3 \end{pmatrix}$$

Even with square matrices, that can be multiplied both ways, multiplication is not commutative. In this case, it is useful to define the **commutator**, defined as:

$$[\mathbf{A}, \mathbf{B}] = \mathbf{AB} - \mathbf{BA}$$

Example 4.3.1.3

Given $\mathbf{A} = \begin{pmatrix} 3 & 1 \\ 2 & 0 \end{pmatrix}$ and $\mathbf{B} = \begin{pmatrix} 1 & 0 \\ -1 & 2 \end{pmatrix}$

Calculate the commutator $[\mathbf{A}, \mathbf{B}]$

Solution

$$[\mathbf{A}, \mathbf{B}] = \mathbf{AB} - \mathbf{BA}$$

$$\mathbf{AB} = \begin{pmatrix} 3 & 1 \\ 2 & 0 \end{pmatrix} \begin{pmatrix} 1 & 0 \\ -1 & 2 \end{pmatrix} = \begin{pmatrix} 3 \times 1 + 1 \times (-1) & 3 \times 0 + 1 \times 2 \\ 2 \times 1 + 0 \times (-1) & 2 \times 0 + 0 \times 2 \end{pmatrix} = \begin{pmatrix} 2 & 2 \\ 2 & 0 \end{pmatrix}$$

$$\mathbf{BA} = \begin{pmatrix} 1 & 0 \\ -1 & 2 \end{pmatrix} \begin{pmatrix} 3 & 1 \\ 2 & 0 \end{pmatrix} = \begin{pmatrix} 1\times 3 + 0 \times 2 & 1 \times 1 + 0 \times 0 \\ -1 \times 3 + 2 \times 2 & -1 \times 1 + 2 \times 0 \end{pmatrix} = \begin{pmatrix} 3 & 1 \\ 1 & -1 \end{pmatrix}$$

$$[\mathbf{A}, \mathbf{B}] = \mathbf{AB} - \mathbf{BA} = \begin{pmatrix} 2 & 2 \\ 2 & 0 \end{pmatrix} - \begin{pmatrix} 3 & 1 \\ 1 & -1 \end{pmatrix} = \begin{pmatrix} -1 & 1 \\ 1 & 1 \end{pmatrix}$$

$$[\mathbf{A}, \mathbf{B}] = \begin{pmatrix} -1 & 1 \\ 1 & 1 \end{pmatrix}$$

Multiplication of a vector by a scalar

The multiplication of a vector $\vec{v}_1$ by a scalar n produces another vector of the same dimensions that lies in the same direction as $\vec{v}_1$;

$$n \begin{pmatrix} x \\ y \end{pmatrix} = \begin{pmatrix} nx \\ ny \end{pmatrix}$$

The scalar can stretch or compress the length of the vector, but cannot rotate it (figure [fig:vector_by_scalar]).

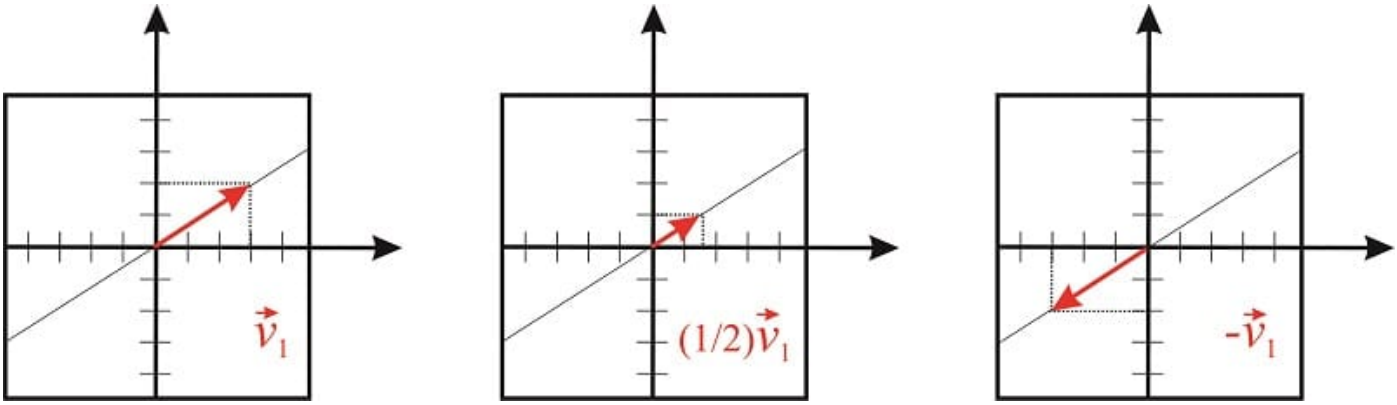


Figure 4.3.1.2: Multiplication of a vector by a scalar

Multiplication of a square matrix by a vector

The multiplication of a vector $\vec{v}_1$ by a square matrix produces another vector of the same dimensions of $\vec{v}_1$. For example, we can multiply a 2×2 matrix and a 2-dimensional vector:

$$\begin{pmatrix} a & b \\ c & d \end{pmatrix} \begin{pmatrix} x \\ y \end{pmatrix} = \begin{pmatrix} ax + by \\ cx + dy \end{pmatrix}$$

For example, consider the matrix

$$\mathbf{A} = \begin{pmatrix} -2 & 0 \\ 0 & 1 \end{pmatrix}$$

The product

$$\begin{pmatrix} -2 & 0 \\ 0 & 1 \end{pmatrix} \begin{pmatrix} x \\ y \end{pmatrix}$$

is

$$\begin{pmatrix} -2x \\ y \end{pmatrix}$$

We see that 2×2 matrices act as operators that transform one 2-dimensional vector into another 2-dimensional vector. This

particular matrix keeps the value of y constant and multiplies the value of x by -2 (Figure $4.3.1.3$).

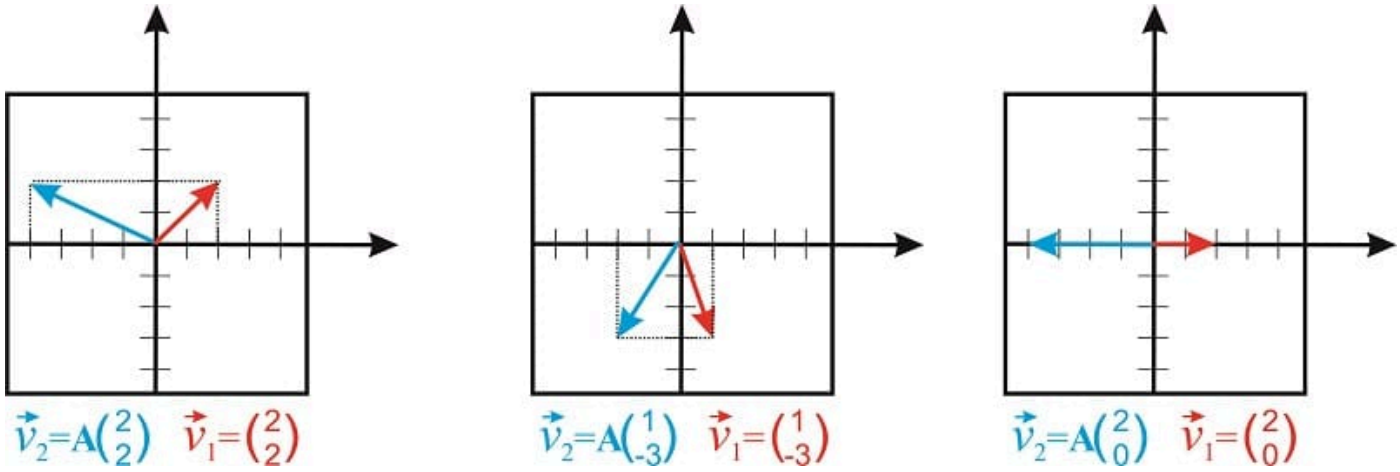


Figure $4.3.1.3$: Multiplication of a vector by a square matrix

Notice that matrices are useful ways of representing operators that change the orientation and size of a vector. An important class of operators that are of particular interest to chemists are the so-called symmetry operators.

Attribution

This page was adapted from Matrices (click here), contributed by Marcia Levitus, Associate Professor (Biodesign Institute) at Arizona State University.

Curated or created by Kathryn Haas

This page titled 4.3.1: Matrices is shared under a CC BY-NC-SA 4.0 license and was authored, remixed, and/or curated by Kathryn Haas.

- 4.3.1: Matrices by Kathryn Haas is licensed CC BY-NC-SA 4.0.

4.3.2: Representations of Point Groups

Symmetry Operations: Matrix Representations

A **symmetry operation**, such as a rotation around a symmetry axis or a reflection through a plane, is an operation that, when performed on an object, results in a new orientation of the object that is indistinguishable from the original. For example, if we rotate a square in the plane by $\pi/2$ or π, the new orientation of the square is superimposable on the original one (Figure $4.3.2.1$).

If rotation by an angle θ of a molecule (or object) about some axis results in an orientation of the molecule (or object) that is superimposable on the original, the axis is called a rotation axis. The molecule (or object) is said to have an n-fold rotational axis, where n is $2\pi/\theta$. The axis is denoted as C_n. The square of Figure $4.3.2.1$ has a C_4 axis perpendicular to the plane because a 90° rotation leaves the figure indistinguishable from the initial orientation. This axis is also a C_2 axis because a 180° degree rotation leaves the square indistinguishable from the original square. In addition, the figure has several other C_2 axis that lie on the same plane as the square:

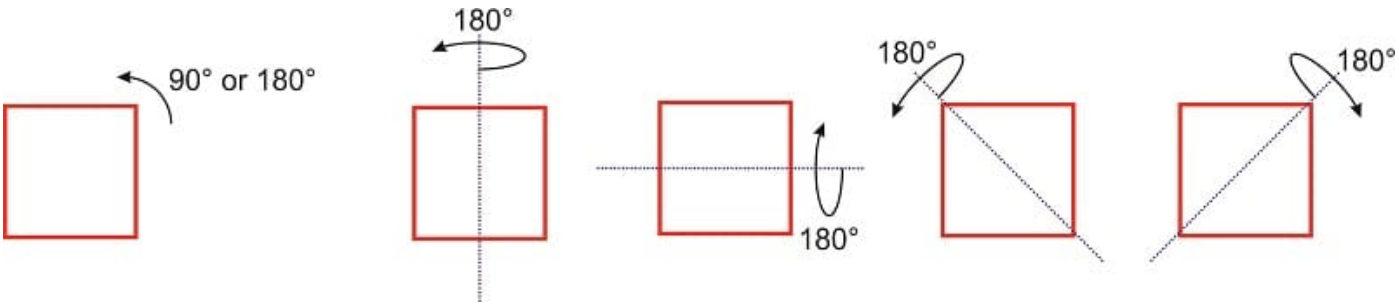


Figure $4.3.2.1$: Symmetry operations performed on a square

A symmetry operation moves all the points of the object from one initial position to a final position, and that means that symmetry operators are 3×3 square matrices (or 2×2 in two dimensions). Each symmetry operation can be expressed as a **transformation matrix** where the vector (x', y', z') represents the new coordinates of the point (x, y, z) after the symmetry operation.

$$[\text{New Coordinates}(x', y', z')] = [\text{Transformation Matrix}] \times [\text{Old Coordinates}(x, y, z)]$$

We will use the example of water, which is in the C_{2v} point group, to illustrate how transformation matrices can be used to represent the symmetry of a group.

Figure $4.3.2.2$ shows the three symmetry elements of the molecule of water (H_2O). This molecule has only one rotation axis, which is 2-fold, and therefore we call it a "C_2 axis." It also has two mirror planes, one that contains the two hydrogen atoms (σ_{yz}), and another one perpendicular to it (σ_{xz}). Both planes contain the C_2 axis.

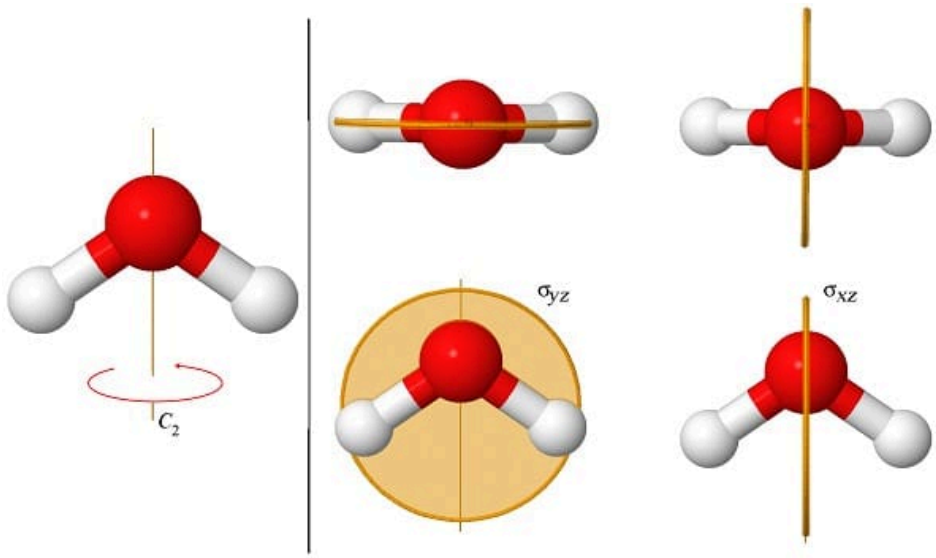


Figure 4.3.2.2: The symmetry elements of the molecule of water

Transformation Matrix of C_2 rotation

A 2-fold rotation around the z −axis changes the location of a point (x, y, z) to $(-x, -y, z)$ (see Figure 4.3.2.3). By convention, rotations are always taken in the counterclockwise direction.

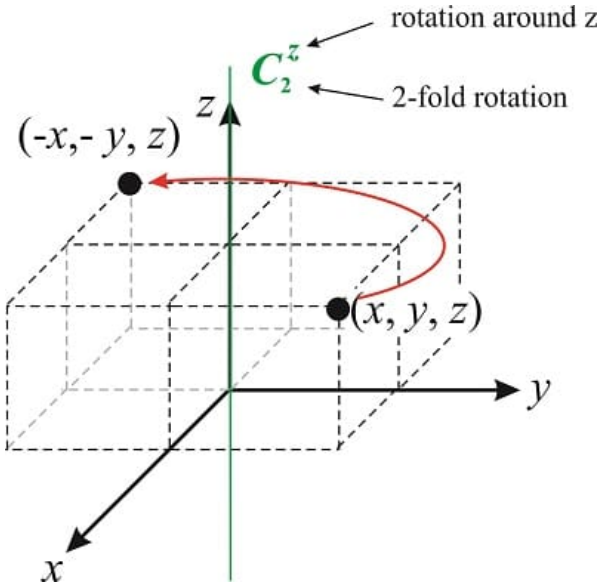


Figure 4.3.2.3: A 2-fold rotation around the z-axis

What is the matrix that represents the C_2 rotation? The matrix transforms the vector (x, y, z) into $(-x, -y, z)$, so

$$C_2(x, y, z) = (-x, -y, z)$$

$$\begin{pmatrix} a_{11} & a_{12} & a_{13} \\ a_{21} & a_{22} & a_{23} \\ a_{31} & a_{32} & a_{33} \end{pmatrix} \begin{pmatrix} x \\ y \\ z \end{pmatrix} = \begin{pmatrix} -x \\ -y \\ z \end{pmatrix}$$

We know the matrix is a 3×3 square matrix because it needs to multiply a 3-dimensional vector. In addition, we write the vector as a vertical column to satisfy the requirements of matrix multiplication.

$$\begin{pmatrix} a_{11} & a_{12} & a_{13} \\ a_{21} & a_{22} & a_{23} \\ a_{31} & a_{32} & a_{33} \end{pmatrix} \begin{pmatrix} x \\ y \\ z \end{pmatrix}$$

$$a_{11}x + a_{12}y + a_{13}z = -x$$

$$a_{21}x + a_{22}y + a_{23}z = -y$$

$$a_{31}x + a_{32}y + a_{33}z = z$$

and we conclude that $a_{11} = -1$, $a_{12} = a_{13} = 0$, $a_{22} = -1$, $a_{21} = a_{23} = 0$ and $a_{33} = 1$, $a_{31} = a_{32} = 0$. The transformation matrix of the C_2 operation of the C_{2v} point group is:

$$C_2 = \begin{pmatrix} -1 & 0 & 0 \\ 0 & -1 & 0 \\ 0 & 0 & 1 \end{pmatrix}$$

Transformation Matrix of σ_{xz} reflection

Rotations are not the only symmetry operations we can perform on a molecule. Figure 4.3.2.4 illustrates the reflection of a point through the xz plane. This operation transforms the vector (x, y, z) into the vector $(x, -y, z)$. Symmetry operators involving reflections through a plane are usually denoted with the letter σ, so the operator that reflects a point through the xz plane is $\hat{\sigma}_{xz}$:

$$\sigma_{xz}(x, y, z) = (x, -y, z)$$

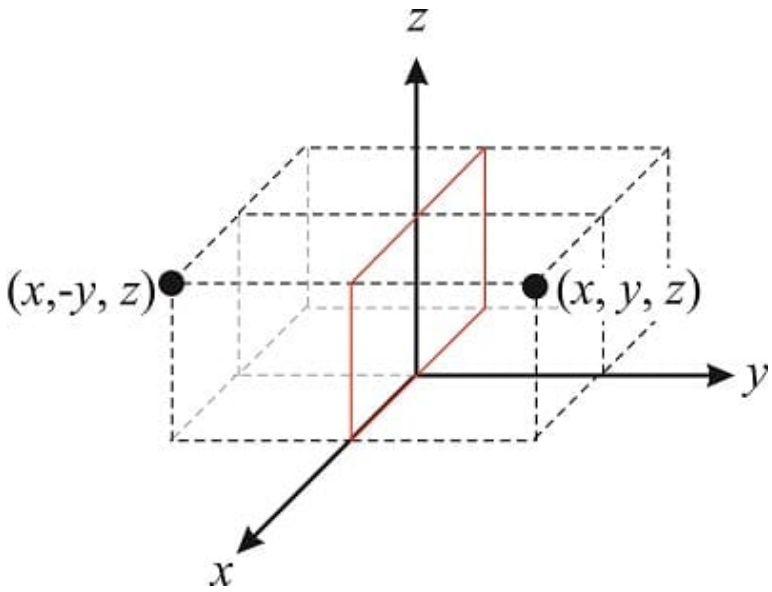


Figure 4.3.2.3: A reflection through the xz plane

Following the same logic we used for the rotation matrix, we can write the σ_{xz} transformation matrix as:

$$\sigma_{x,z} = \begin{pmatrix} 1 & 0 & 0 \\ 0 & -1 & 0 \\ 0 & 0 & 1 \end{pmatrix}$$

This is true because

$$\begin{pmatrix} 1 & 0 & 0 \\ 0 & -1 & 0 \\ 0 & 0 & 1 \end{pmatrix} \begin{pmatrix} x \\ y \\ z \end{pmatrix} = \begin{pmatrix} x \\ -y \\ z \end{pmatrix}$$

Exercise 4.3.2.1

Find the transformation matrix of the identity (E) and the $\sigma_{y,z}$ operations under the C_{2v} point group.

Answer available at the end of this section.

Characters

For a square matrix, the ***character*** is the trace of the matrix. For the C_2 operation, with the transformation matrix

$$\begin{pmatrix} -1 & 0 & 0 \\ 0 & -1 & 0 \\ 0 & 0 & 1 \end{pmatrix},$$

the trace is $(-1) + (-1) + 1 = -1$.

The set of characters for a point group is called a **reducible representation (Γ)**. The reducible representation for the C_{2v} point group is:

C_{2v}	E	C_2	σ_v	σ_v'
Γ	3	-1	1	1

Exercise 4.3.2.1

Prove that the characters in the reducible representation for C_{2v} are correct:

C_{2v}	E	C_2	σ_v	σ_v'
Γ	3	-1	1	1

Answer available at the end of this section.

Reducible and Irreducible Representations

Let us now go back and look in more detail at the transformation matrices of the C_{2v} point group that we derived above. If we look at the matrices carefully we see that they all take the same block diagonal form (a square matrix is said to be **block diagonal** if all the elements are zero except for a set of submatrices lying along the diagonal).

$$E = \begin{pmatrix} [1] & 0 & 0 \\ 0 & [1] & 0 \\ 0 & 0 & [1] \end{pmatrix}, C_2 = \begin{pmatrix} [-1] & 0 & 0 \\ 0 & [-1] & 0 \\ 0 & 0 & [1] \end{pmatrix}, \sigma'_{v(xz)} = \begin{pmatrix} [1] & 0 & 0 \\ 0 & [-1] & 0 \\ 0 & 0 & [1] \end{pmatrix}, \sigma_{v(yz)''} = \begin{pmatrix} [-1] & 0 & 0 \\ 0 & [1] & 0 \\ 0 & 0 & [1] \end{pmatrix}$$

All the non-zero elements become 1x1 matrices that each represent individual x, y, z coordinates. In other words, the element a_{11} represents x, a_{22} represents y, and a_{33} represents z. The matrix elements for x from each transformation matrix combine to form an irreducible representation of the C_{2v} point group. Likewise, the matrix elements for y combine to form a second irreducible representation, and the same is true for z elements. These irreducible representations are shown below:

C_{2v}	E	C_2	σ_v	σ_v'	Coordinate Used
	1	-1	1	-1	x
	1	-1	-1	1	y
	1	1	1	1	z
Γ	3	-1	1	1	

The irreducible representations add to form the reducible representation, Γ. This Γ, which is the set of 3x3 matrices, can be reduced to the set of 1x1 matrices of the irreducible representations. The irreducible representations cannot be reduced further,

hence their name.

Sources & Attribution

- Parts of this page was adapted from Matrices (click here) (Symmetry Operators), contributed by Marcia Levitus, Associate Professor (Biodesign Institute) at Arizona State University.
- Parts of this page were adapted from Reductions of Representations, contributed by

  Claire Vallance (University of Oxford)

- Curated or created by Kathryn Haas

Answers

Exercise 4.3.2.1

The transformation matrix for E is $\begin{pmatrix} 1 & 0 & 0 \\ 0 & 1 & 0 \\ 0 & 0 & 1 \end{pmatrix}$.

The transformation matrix for $\sigma_{v(yz)''}$ is $\begin{pmatrix} -1 & 0 & 0 \\ 0 & 1 & 0 \\ 0 & 0 & 1 \end{pmatrix}$.

Exercise 4.3.2.1

For the E operation, with the transformation matrix $\begin{pmatrix} 1 & 0 & 0 \\ 0 & 1 & 0 \\ 0 & 0 & 1 \end{pmatrix}$, the trace is $1+1+1=3$.

For the C_2^z operation, with the transformation matrix $\begin{pmatrix} -1 & 0 & 0 \\ 0 & -1 & 0 \\ 0 & 0 & 1 \end{pmatrix}$, the trace is $(-1)+(-1)+1=-1$.

For the $\sigma_{v(xz)'}$ operation, with the transformation matrix $\begin{pmatrix} 1 & 0 & 0 \\ 0 & -1 & 0 \\ 0 & 0 & 1 \end{pmatrix}$, the trace is $1+(-1)+1=1$.

For the $\sigma_{v(yz)''}$ operation, with the transformation matrix $\begin{pmatrix} -1 & 0 & 0 \\ 0 & 1 & 0 \\ 0 & 0 & 1 \end{pmatrix}$, the trace is $-1+1+1=1$.

This gives the reducible representation

C_{2v}	E	C_2	σ_v	σ_v'
Γ	3	−1	1	1

This page titled 4.3.2: Representations of Point Groups is shared under a CC BY-NC-SA 4.0 license and was authored, remixed, and/or curated by Kathryn Haas.

- 4.3.2: Representations of Point Groups by Kathryn Haas is licensed CC BY-NC-SA 4.0.

4.3.3: Character Tables

Introduction to Character Tables, using C_{2v} as example

A character table is the complete set of irreducible representations of a symmetry group. In the previous section, we derived three of the four irreducible representations for the C_{2v} point group. These three irreducible representations are labeled A_1, B_1, and B_2. The fourth irreducible representation, A_2, can be derived using the properties (or "rules") for irreducible representations listed below.

Properties of Characters of Irreducible Representations in Point Groups

1. There is always a totally symmetric representation in which all the characters are 1.
   e.g. In C_{2v}, A_1 is totally symmetric.
2. The order of the group (h) is the total number of symmetry operations in the group.
   e.g. In C_{2v}, $h = 4$
3. Similar operations are listed as classes (R) and appear as columns in the table.
   e.g. In C_{2v}, there are four classes of operations, E, C_2, $\sigma_{v(xz)}$, and $\sigma'_{v(yz)}$
4. The number of irreducible representations (rows) must equal the number of classes (columns). This results in all character tables being square.
   e.g. In C_{2v}, there are four classes and four irreducible representations.
5. The sum of squares of all characters under E is equal to the order of the group: $h = \sum [\chi_i]^2$
   e.g. In C_{2v}, $h = 1^2 + 1^2 + 1^2 + 1^2 = 4$
6. For any irreducible representation (i), the sum of squares of its characters multiplied by the number of operations in the class is the order of the group: $h = \sum [\chi_i(R)]^2$
   e.g. For A_2 in C_{2v}, $h = (1 \times 1)^2 + (1 \times 1)^2 + (-1 \times 1)^2 + (-1 \times 1)^2 = 4$
7. Irreducible representations are orthogonal. For any two representations (i and j): $\sum [\chi_i * (R) \chi_j(R)] = 0$
   e.g. For B_1 and B_2 of C_{2v}, $[1 \times 1] + [-1 \times -1] + [1 \times -1] + [-1 \times 1] = 0$

The complete character table for C_{2v} is given below.

C_{2v}	E	C_2	σ_v	σ'_v	$h = 4$	
A_1	1	1	1	1	z	x^2, y^2, z^2
A_2	1	1	-1	-1	R_z	xy
B_1	1	-1	1	-1	x, R_y	xz
B_2	1	-1	-1	1	y, R_x	yz

The various sections of the table are as follows:

i. The first element in the table gives the name of the point group, usually in Schoenflies (C_{2v}) notation.
ii. Along the first row are the symmetry operations of the group, E, C_2, σ_v and σ_v ″, followed by the order of the group, h.
iii. In the first column are the irreducible representations of the group, represented by Mulliken Labels. In C_{2v} the irreducible representations are A_1, A_2, B_1 and B_2. The Mulliken labels indicate the symmetry of each representation (explained further below).
iv. The characters (χ) of the irreducible representations under each symmetry operation are given in the bulk of the table.
v. The final column(s) of the table lists a number of functions that transform as the various irreducible representations of the group. These are the Cartesian axes (x, y, z), the Cartesian products $(z^2, x^2 + y^2, xy, xz, yz)$, and the rotations (R_x, R_y, R_z) (explained further below).

Another example: C_{3v}

Th C_{3v} point group has three classes of operations: E, C_3, and $\sigma_{v(xz)}$. The derivation of transformation matrices for E and $\sigma_{v(xz)}$ is similar to the case for C_{2v}. However, the C_{3v} operation does not give simple 1 or -1 characters. If we carry out a rotation about z by

an angle θ, our x and y axes are transformed onto new axes x' and y'. The new axes can each be written as a linear combination of our original x and y axes. The derivation of the rotation matrices will not be covered in this text, but is described elsewhere:

$$\begin{aligned} x' &= x\cos\theta + y\sin\theta \\ y' &= -x\sin\theta + y\cos\theta \end{aligned}$$

For a C_3 rotation counterclockwise through 120° (or $\frac{2\pi}{3}$):

$$\begin{aligned} x' &= x\cos(2\pi/3) + y\sin(2\pi/3) &&= -\tfrac{1}{2}x - \tfrac{\sqrt{3}}{2}y \\ y' &= -x\sin(2\pi/3) + y\cos(2\pi/3) &&= \tfrac{\sqrt{3}}{2}x - \tfrac{1}{2}y \end{aligned}$$

The transformation matrices for symmetry operations of C_{3v} are as follows:

$$E = \begin{pmatrix} 1 & 0 & 0 \\ 0 & 1 & 0 \\ 0 & 0 & 1 \end{pmatrix} \; C_3 = \begin{pmatrix} -\frac{1}{2} & -\frac{\sqrt{3}}{2} & 0 \\ \frac{\sqrt{3}}{2} & -\frac{1}{2} & 0 \\ 0 & 0 & 1 \end{pmatrix} \; \sigma'_{v(xz)} = \begin{pmatrix} 1 & 0 & 0 \\ 0 & -1 & 0 \\ 0 & 0 & 1 \end{pmatrix}$$

The C_3 transformation matrix contains off-diagonal entries, and therefore it cannot be block diagonalized as 1x1 matrices. However, the first two lines can be diagonalized as a 2x2 and the last line as a 1x1 matrix (Figure 4.3.3.1):

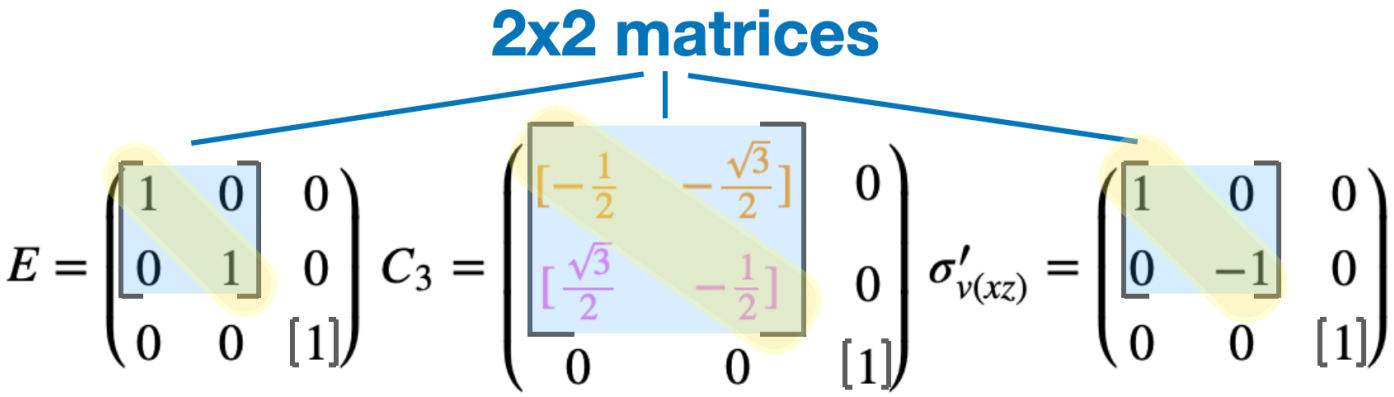


Figure 4.3.3.1: The C_3 transformation matrix contains off-diagonal entries, and therefore it cannot be block diagonalized as 1x1 matrices. However, the first two lines can be diagonalized as a 2x2 and the last line as a 1x1 matrix. (CC-BY-NC-SA; Kathryn Haas)

The character from a 2x2 matrix is the sum of the trace of that matrix. So, for the C_3 operation, the 2x2 matrix gives the character -1 (from $-\frac{1}{2} + -\frac{1}{2}$).

The character table for C_{3v} is shown below.

C_{3v}	E	$2C_3$	$3\sigma_v$	$h = 6$
A_1	1	1	1	$z, z^2, x^2 + y^2$
A_2	1	1	-1	R_z
E	2	-1	0	$(x, y), (xy, x^2 + y^2), (xz, yz), (R_x, R_y)$

Additional features of character tables

Additional Features of Character Tables

1. Symmetry operations of the same class are grouped into the same column (class) in the character table and not listed separately.
   e.g. In the C_{3v} point group, there are four operations: E, C_3, C_3^2, and σ_v. The C_3 and C_3^2 operations are listed together in the character table as $2C_3$.

2. IF there are multiple C_2 axes (in a D group), the C_2 axes that are perpendicular to the principle axis are labeled with primes (e.g. C_2' and C_2''); when there are multiple types of perpendicular C_2 axes, one prime (C_2') means that it passes through more atoms, while a double prime (C_2'') means it goes between atoms.
3. Mirror planes that are perpendicular to the principle axis are "horizontal" mirror planes and are designated with an h subscript (σ_h). Mirror planes that are in-plane with the principle axis are "vertical" mirror planes, σ_v. When there are two types of vertical mirror planes, those that run through more atoms are σ_v while those that run between atoms are "dihedral", σ_d.
4. Matching the symmetry operations listed in the character table to the symmetry operations of a molecule can confirm its point group.
5. Irreducible representations are each assigned a Mulliken label, listed in the left-hand column, that indicates the symmetry of that representation as follows:

Mulliken Labels	**meaning**
A	singly degenerate (1x1), symmetric to principle axis
B	singly degenerate (1x1), antisymmetric to principle axis
E	doubly degenerate (2x2)
T	triply degenerate (3x3)
Subscripts and superscripts	**meaning**
1	symmetric to $\sigma_v$or perpendicular to C_2
2	anti-symmetric to $\sigma_v$or perpendicular to C_2
g	symmetric to inversion center
u	anti-symmetric to inversion center
$'$	symmetric to σ_h
$''$	anti-symmetric to σ_h

6. The right-hand columns of the character table list a number of functions that transform as the various irreducible representations of the group. These are the Cartesian axes (x, y, z), the Cartesian products $(z^2, x^2 + y^2, xy, xz, yz)$, and the rotations (R_x, R_y, R_z). These expressions indicate the properties of orbitals within the symmetry group. The s-orbital, which is totally symmetric, corresponds to the irreducible representation that possesses symmetry of x^2, y^2 and z^2 combined. The p-orbitals each possess the symmetry of the corresponding axis (e.g. p_x corresponds to the x axis). Each of the d-orbitals possess the symmetry of the corresponding binary product (e.g. d_{xy} corresponds to the binary product, xy, in the character table).

The functions listed in the final column of the table are important in many chemical applications of group theory, particularly in spectroscopy. For example, by looking at the transformation properties of x, y and z (sometimes given in character tables as T_x, T_y, T_z) we can discover the symmetry of translations along the x, y, and z axes. Similarly, R_x, R_y and R_z represent rotations about the three Cartesian axes. The transformation properties of x, y, and z can be used to determine whether or not a molecule is IR-active or whether or not it can absorb a photon of x-, y-, or z-polarized light and undergo a spectroscopic transition. The Cartesian products play a similar role in determining selection rules for Raman transitions, which involve two photons.

A visual summary of the sections and their significance is given in Figure 4.3.3.2. Character tables for common point groups are given in the References section of LibreTexts Bookshelves.

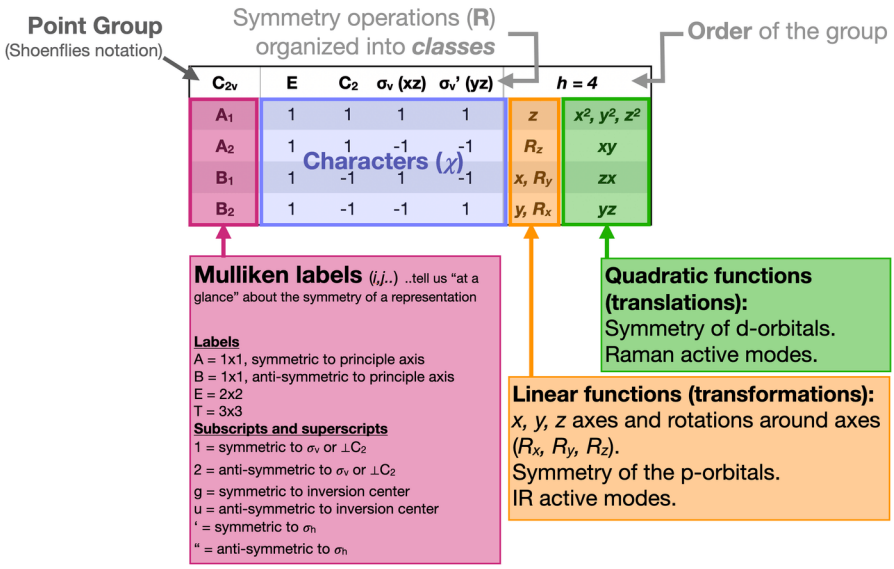


Figure 4.3.3.2: Visual summary of the sections of a character table and their meaning. (CC-BY-NC-SA; Kathryn Haas)

Contributors and Attributions

- Curated or created by Kathryn Haas
- Claire Vallance (University of Oxford)

  adapted from Character Tables (click here)

This page titled 4.3.3: Character Tables is shared under a CC BY-NC-SA 4.0 license and was authored, remixed, and/or curated by Kathryn Haas.

- 4.3.3: Character Tables by Kathryn Haas is licensed CC BY-NC-SA 4.0.

4.4: EXAMPLES AND APPLICATIONS OF SYMMETRY

The purpose of learning group theory is that molecular symmetry can be applied to understand the properties of molecules. This chapter introduces two applications of symmetry: chirality and molecular vibrations (in the context of analyzing IR and Raman spectra). An additional application of symmetry, to understand molecular bonding, deserves its own chapter and will be explored in Chapter 5.

4.4.1: Chirality

4.4.2: Molecular Vibrations

This page titled 4.4: Examples and Applications of Symmetry is shared under a license and was authored, remixed, and/or curated by Kathryn Haas.

- 4.4: Examples and Applications of Symmetry by Kathryn Haas has no license indicated.

4.4.1: Chirality

Introduction

Around the year 1847, the French scientist Louis Pasteur provided an explanation for the optical activity of tartaric acid salts. When he carried out a particular reaction, Pasteur observed that two types of crystals precipitated. Patiently and carefully using tweezers, Pasteur was able to separate the two types of crystals. Pasteur noticed that the types rotated plane-polarized light by the same amount but in different directions. These two compounds are called enantiomers.

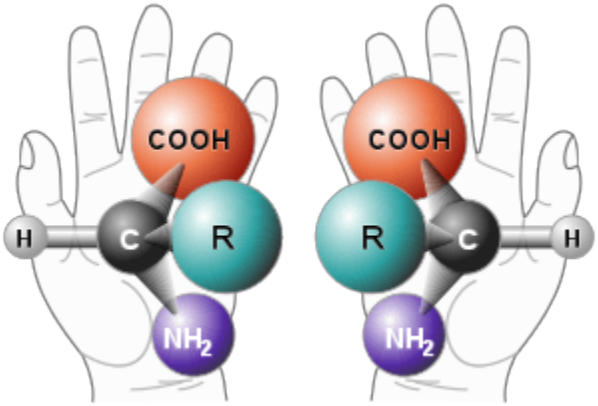


Figure 4.4.1.1: Two enantiomers of an amino acid (with side chain R).

What is chirality?

A molecule is **chiral** (or **dissymetric**) if it is non-superimposable on its mirror image. The two mirror images of a chiral molecule are called enantiomers. Enantiomers have the same physical properties (e.g., melting point, etc.). They differ in their ability to rotate plane polarized light and in their reactivity with other chiral molecules. Due to their ability to rotate plane polarized light, they are referred to as being *optically active*.

Using Symmetry to Determine Chirality

There are some general rules of thumb that help determine whether a molecule is chiral or achiral. The point group of the molecule, and the symmetry operations within that point group, can give clues as to whether the molecule is chiral.

Symmetry operations of chiral molecules

A chiral molecule cannot possess a plane of symmetry (σ), a center of inversion (i), or an improper rotation (S_n). Due to the fact that all groups that lack both σ and i also lack S_n, **a molecule that belongs to any group that lacks S_n is chiral.**

An example of an inorganic coordination complex is tris(ethylenediamine)cobalt(III) (Figure 4.4.1.1). Figure 4.4.1.1 shows the two enantiomers of tris(ethylenediamine)cobalt(III): the Δ and Λ isomers.

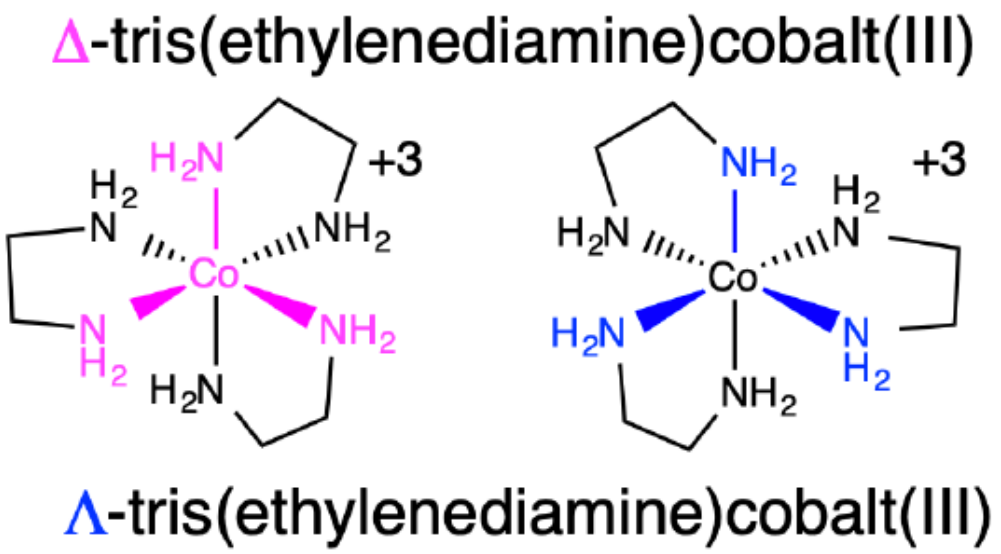


Figure 4.4.1.2: Two chiral enantiomers of tris(ethylenediamine)coalt(III).

You can visualize the Λ and Δ isomers by imagining that the ligands around the metal centers are blades of a fan. To push the air toward you, you would need to rotate the Δ isomer clockwise, and the Λ isomer counter-clockwise.

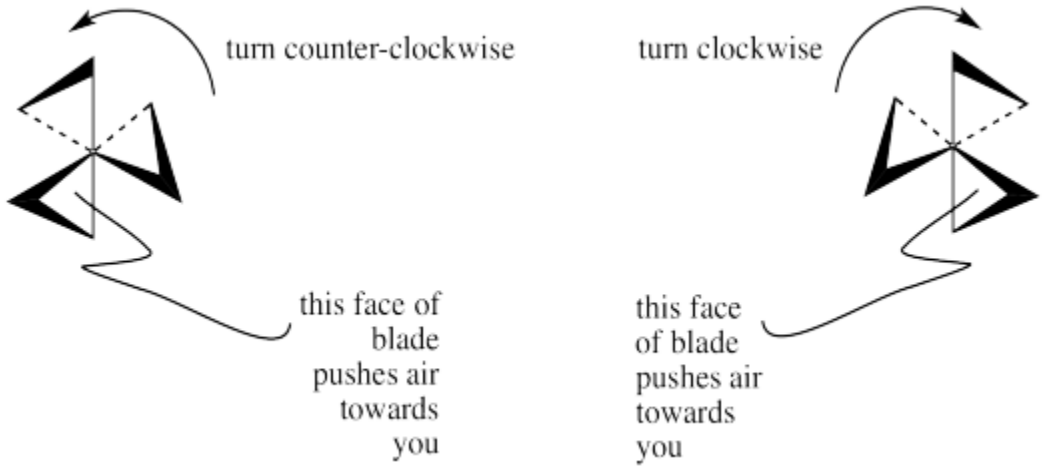


Figure 4.4.1.3: Another way of thinking about the chirality of the two chiral enantiomers of tris(ethylenediamine)coalt(III) shown in Figure 4.4.1.2. This figure was taken from Structure and Reactivity in Organic, Biological, and Inorganic Chemistry.

Exercise 4.4.1.1

Which point groups are possible for chiral molecules?

Answer available at the end of this section.

Answers

Exercise 4.4.1.1

As a result of the previous discussion, there are a few classes of point groups that lack an improper axis. Those classes are C_1, C_n, and D_n.

This page titled 4.4.1: Chirality is shared under a CC BY-NC 4.0 license and was authored, remixed, and/or curated by Kathryn Haas.

- 4.4.1: Chirality by Kathryn Haas is licensed CC BY-NC 4.0.

4.4.2: Molecular Vibrations

Symmetry and group theory can be applied to understand molecular vibrations. This is particularly useful in the context of predicting the number of peaks expected in the infrared (IR) and Raman spectra of a given compound.

We will use water as a case study to illustrate how group theory is used to predict the number of peaks in IR and Raman spectra.

How many IR and Raman peaks would we expect for $\mathrm{H_2O}$?

To answer this question with group theory, a pre-requisite is that you **assign the molecule's point group and assign an axis system** to the entire molecule. By convention, the z axis is collinear with the principle axis, the x axis is in-plane with the molecule or the most number of atoms. It is a good idea to stick with this convention (see Figure 4.4.2.1).

What is the point group for $\mathrm{H_2O}$? (click to see answer)

$\mathrm{H_2O}$ has the following operations: E, C_2, σ_v, σ_v'. The point group is C_{2v}.

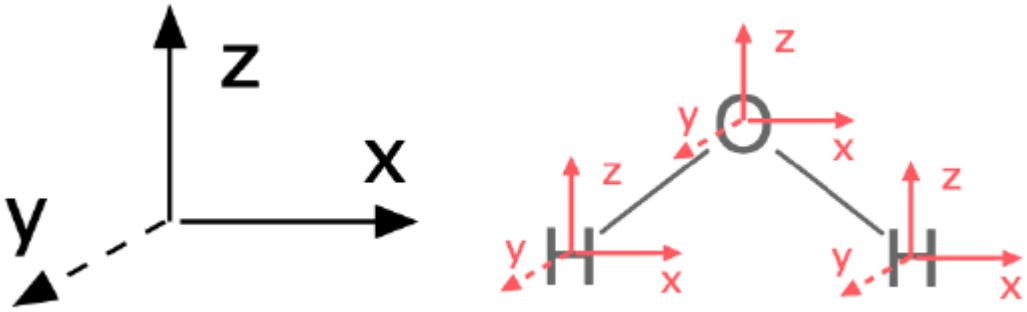


Figure 4.4.2.1: The first step to finding normal modes is to assign a consistent axis system to the entire molecule and to each atom. (CC-BY-SA; Kathryn Haas)

Now that we know the molecule's point group, we can use group theory to determine the symmetry of all motions in the molecule, or the symmetry of each of its degrees of freedom. Then we will subtract rotational and translational degrees of freedom to find the vibrational degrees of freedom. The number of degrees of freedom depends on the number of atoms (N) in a molecule. Each atom in the molecule can move in three dimensions (x, y, z), and so the number of degrees of freedom is three dimensions times N number of atoms, or $3N$. The total degrees of freedom include a number of vibrations, three translations (in x, y, and z), and either two or three rotations. Linear molecules have two rotational degrees of freedom, while non-linear molecules have three. The vibrational modes are represented by the following expressions:

$$\begin{aligned} \text{Linear Molecule Degrees of Freedom} &= 3N-5 \\ \text{Non-Linear Molecule Degrees of Freedom} &= 3N-6 \end{aligned}$$

Our goal is to find the symmetry of all degrees of freedom, and then determine which are vibrations that are IR- and Raman-active.

STEP 1: Find the reducible representation for all normal modes Γ_{modes}.

The first major step is to **find a reducible representation (Γ)** for the movement of all atoms in the molecule (including rotational, translational, and vibrational degrees of freedom). We'll refer to this as Γ_{modes}. To find normal modes using group theory, **assign an axis system** to each individual atom to represent the three dimensions in which each atom can move. Each axis on each atom should be consistent with the conventional axis system you previously assigned to the entire molecule (see Figure 4.4.2.1).

Γ_{modes} is the sum of the characters (trace) of the transformation matrix for the entire molecule (in the case of water, there are 9 degrees of freedom and this is now a 9x9 matrix). Let's walk through this step-by-step. The transformation matrix of E and C_2 are

shown below:

$$E = \begin{pmatrix} 1 & 0 & 0 & 0 & 0 & 0 & 0 & 0 & 0 \\ 0 & 1 & 0 & 0 & 0 & 0 & 0 & 0 & 0 \\ 0 & 0 & 1 & 0 & 0 & 0 & 0 & 0 & 0 \\ 0 & 0 & 0 & 1 & 0 & 0 & 0 & 0 & 0 \\ 0 & 0 & 0 & 0 & 1 & 0 & 0 & 0 & 0 \\ 0 & 0 & 0 & 0 & 0 & 1 & 0 & 0 & 0 \\ 0 & 0 & 0 & 0 & 0 & 0 & 1 & 0 & 0 \\ 0 & 0 & 0 & 0 & 0 & 0 & 0 & 1 & 0 \\ 0 & 0 & 0 & 0 & 0 & 0 & 0 & 0 & 1 \end{pmatrix} \begin{pmatrix} x_{oxygen} \\ y_{oxygen} \\ z_{oxygen} \\ x_{hydrogen-a} \\ y_{hydrogen-a} \\ z_{hydrogen-a} \\ x_{hydrogen-b} \\ y_{hydrogen-b} \\ z_{hydrogen-b} \end{pmatrix} = \begin{pmatrix} x'_{oxygen} \\ y'_{oxygen} \\ z'_{oxygen} \\ x'_{hydrogen-a} \\ y'_{hydrogen-a} \\ z'_{hydrogen-a} \\ x'_{hydrogen-b} \\ y'_{hydrogen-b} \\ z'_{hydrogen-b} \end{pmatrix}, \chi = 9$$

$$C_2 = \begin{pmatrix} -1 & 0 & 0 & 0 & 0 & 0 & 0 & 0 & 0 \\ 0 & -1 & 0 & 0 & 0 & 0 & 0 & 0 & 0 \\ 0 & 0 & 1 & 0 & 0 & 0 & 0 & 0 & 0 \\ 0 & 0 & 0 & 0 & 0 & 0 & -1 & 0 & 0 \\ 0 & 0 & 0 & 0 & 0 & 0 & 0 & -1 & 0 \\ 0 & 0 & 0 & 0 & 0 & 0 & 0 & 0 & 1 \\ 0 & 0 & 0 & -1 & 0 & 0 & 0 & 0 & 0 \\ 0 & 0 & 0 & 0 & -1 & 0 & 0 & 0 & 0 \\ 0 & 0 & 0 & 0 & 0 & 1 & 0 & 0 & 0 \end{pmatrix} \begin{pmatrix} x_{oxygen} \\ y_{oxygen} \\ z_{oxygen} \\ x_{hydrogen-a} \\ y_{hydrogen-a} \\ z_{hydrogen-a} \\ x_{hydrogen-b} \\ y_{hydrogen-b} \\ z_{hydrogen-b} \end{pmatrix} = \begin{pmatrix} x'_{oxygen} \\ y'_{oxygen} \\ z'_{oxygen} \\ x'_{hydrogen-a} \\ y'_{hydrogen-a} \\ z'_{hydrogen-a} \\ x'_{hydrogen-b} \\ y'_{hydrogen-b} \\ z'_{hydrogen-b} \end{pmatrix}, \chi = 1$$

It is unnecessary to find the transformation matrix for each operation since it is only the TRACE that gives us the character, and any off-diagonal entries do not contribute to Γ_{modes}. The values that contribute to the trace can be found simply by performing each operation in the point group and assigning a value to each individual atom to represent how it is changed by that operation. If the atom moves away from itself, that atom gets a character of zero (this is because any non-zero characters of the transformation matrix are off of the diagonal). If the atom remains in place, each of its three dimensions is assigned a value of $\cos\theta$**.** For the example of H_2O under the C_{2v} point group, the axes that remain unchanged ($\theta = 0^\circ$) are assigned a value of $\cos(0^\circ) = 1$, while those that are moved into the negative of themselves (rotated or reflected to $\theta = 180^\circ$) are assigned $\cos(180^\circ) = -1$. The character for Γ is the sum of the values for each transformation.

Let's walk through the steps to assign characters of Γ_{modes} for H_2O to illustrate how this works:

For the operation E, performed on H_2O, all three atoms remain in place. The three axes x, y, z on each atom remain unchanged. Thus, each of the three axes on each of three atom (nine axes) is assigned the value $\cos(0^\circ) = 1$, resulting in a sum of $\chi = 9$ for the Γ_{modes}.

For the operation C_2, the two hydrogen atoms are moved away from their original position, and so the hydrogens are assigned a value of zero. The oxygen remains in place; the z-axis on oxygen is unchanged ($\cos(0^\circ) = 1$), while the x and y axes are inverted ($\cos(180^\circ)$). The sum of these characters gives $\chi = -1$ in the Γ_{modes}.

Now you try! Find the characters of $\sigma_{v(xz)}$ and $\sigma_{v(yz)}$ under the C_{2v} point group. Compare what you find to the Γ_{modes} for all normal modes given below.

C_{2v}	E	C_2	σ_v	σ'_v
Γ_{modes}	9	-1	3	1

(4.4.2.1)

STEP 2: Break Γ_{modes} into its component irreducible representations

Now that we've found the Γ_{modes} (4.4.2.1), we need to break it down into the individual irreducible representations ($i, j, k...$) for the point group. We can do this systematically using the following formula:

$$\#\text{ of } i = \frac{1}{h}\sum(\#\text{ of operations in class}) \times (\chi_\Gamma) \times (\chi_i) \tag{4.4.2.2}$$

In other words, the number of irreducible representations of type i is equal to the sum of the number of operations in the class $\times$ the character of the Γ_{modes} $\times$ the character of i, and that sum is divided by the order of the group (h).

Using equation 4.4.2.2, we find that for all normal modes of H_2O:

$$\Gamma_{modes} = 3A_1 + 1A_2 + 3B_1 + 2B_2. \tag{4.4.2.3}$$

Notice there are 9 irreducible representations in Equation 4.4.2.3. These irreducible representations represent the symmetries of all 9 motions of the molecule: vibrations, rotations, and translations.

Exercise 4.4.2.1: Derive the irreducible representation in equation 4.4.2.3.

Derive the nine irreducible representations of Γ_{modes} for H_2O, expression 4.4.2.3.

Hint available at the end of this section.

Answer available at the end of this section.

STEP 3: Subtract rotations and translations to find vibrational modes.

Because we are interested in molecular vibrations, we need to subtract the rotations and translations from the total degrees of freedom.

$$\text{Vibrations} = \Gamma_{modes} - \text{Rotations} - \text{Translations}$$

In the example of H_2O, the total degrees of freedom are given above in equation 4.4.2.3, and therefore the vibrational degrees of freedom can be found by:

$$H_2O \text{ vibrations} = (3A_1 + 1A_2 + 3B_1 + 2B_2) - \text{Rotations} - \text{Translations} \tag{4.4.2.4}$$

But which of the irreducible representations are ones that represent rotations and translations? The symmetry of rotational and translational degree modes can be found by inspecting the right-hand columns of any character table. Rotational modes correspond to irreducible representations that include R_x, R_y, and R_z in the table, while each of the three translational modes has the same symmetry as the x, y and z axes. For a non-linear molecule, subtract three rotational irreducible representations and three translational irreducible representations from the total Γ_{modes}.

In the specific case of water, we refer to the C_{2v} character table:

C_{2v}	E	C_2	σ_v	σ_v'	$h = 4$	
A_1	1	1	1	1	z	x^2, y^2, z^2
A_2	1	1	−1	−1	R_z	xy
B_1	1	−1	1	−1	x, R_y	xz
B_2	1	−1	−1	1	y, R_x	yz

In C_{2v}, translations correspond to B_1, B_2, and A_1 (respectively for x, yz), and rotations correspond to B_2, B_1, and A_1 (respectively for R_x, R_y, R_z). Subtracting these six irreducible representations from Γ_{modes} will leave us with the irreducible representations for vibrations.

$$\begin{aligned} H_2O \text{ vibrations} &= \Gamma_{modes} - \text{Rotations} - \text{Translations} \\ &= (3A_1 + 1A_2 + 3B_1 + 2B_2) - (A_1 + B_1 + B_2) - (A_2 + B_1 + B_2) \\ &= 2A_1 + 1B_1 \end{aligned}$$

The three vibrational modes for H_2O are $2A_1 + 1B_1$. Note that we have the correct number of vibrational modes based on the expectation of $3N - 6$ vibrations for a non-linear molecule.

STEP 4: Determine which of the vibrational modes are IR-active and Raman-active.

The next step is to determine which of the vibrational modes is IR-active and Raman-active. To do this, we apply the IR and Raman Selection Rules below:

IR and Raman Selection Rules

Infrared selection rules:

If a vibration results in the change in the molecular dipole moment, it is IR-active. In the character table, we can recognize the vibrational modes that are IR-active by those with symmetry of the x, y, and z axes.

In C_{2v}, any vibrations with A_1, B_1 or B_2 symmetry would be IR-active.

Raman selection rules:

If a vibration results in a change in the molecular polarizability, it will be Raman-active. In the character table, we can recognize the vibrational modes that are Raman-active by those with symmetry of any of the binary products (xy, xz, yz, x^2, y^2, and z^2) or a linear combination of binary products (e.g. $x^2 - y^2$).

In C_{2v}, any vibrations with A_1, A_2, B_1 or B_2 symmetry would be Raman-active.

In our H_2O example, we found that of the three vibrational modes, two have A_1 and one has B_1 symmetry. Both A_1 and B_1 are IR-active, and both are also Raman-active. ***There are three possible IR peaks and three possible Raman peaks expected for water***.*

*It is important to note that this prediction tells only what is possible, but not what we might actually see in the IR and Raman spectra. For example, if two IR peaks overlap, we might actually notice only one peak in the spectrum. Or, if one or more peaks is off-scale, we wouldn't see it in actual data. Group theory tells us what is *possible and allows us to make predictions or interpretations of spectra*.

Summary of Analysis for Water

Each molecular motion for water, or any molecule, can be assigned a symmetry under the molecule's point group. For water, we found that there are a total of 9 molecular motions; $3A_1 + A_2 + 3B_1 + 2B_2$. Six of these motions are not the translations and rotations. The remaining motions are vibrations; two with A_1 symmetry and one with B_1 symmetry.

We can tell what these vibrations would look like based on their symmetries. The two A_1 vibrations must be completely symmetric, while the B_1 vibration is antisymmetric with respect to the principal C_2 axis.

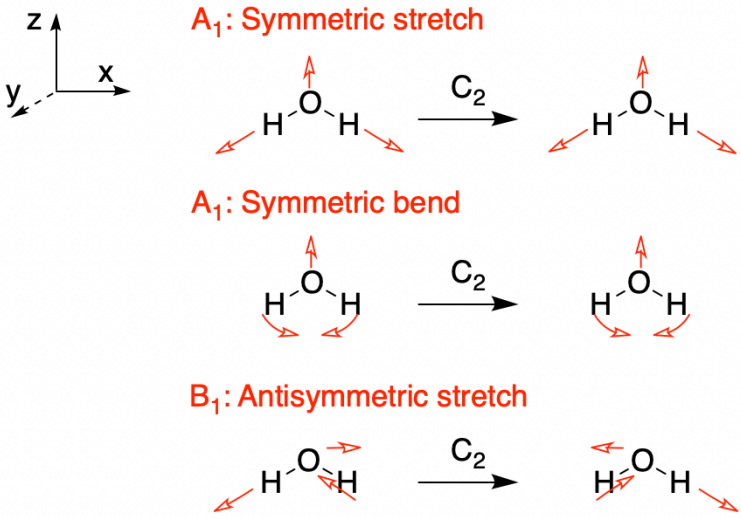


Figure 4.4.2.2: Illustration of the vibrational motions of water. The antisymmetric stretch has B_1 symmetry, while the symmetric stretch and symmetric bend both have A_1 symmetry. (Click here to see animation) (CC-BY-NC-SA; Kathryn Haas)

Table 4.4.2.1: Summary of the Symmetry of Molecular Motions for Water

All Motions (step 2 above)	Translations (x,y,z)	Rotations (R_x, R_y, R_z)	Remaining Vibrations	Description of Vibration
$3A_1$	$1A_1$		$2A_1$	One is a symmetric stretch. The other is a symmetric bend. Both are *IR-active* and *Raman-active*
A_2		$1A_2$		
$3B_1$	$1B_1$	$1B_1$	$1B_1$	Antisymmetric stretch that is *IR-active* and *Raman-active*.
$2B_2$	$1B_2$	$1B_2$		

Exercise 4.4.2.2

Find the symmetries of all motions of the square planar complex, tetrachloroplatinate (II). Determine which are rotations, translations, and vibrations. Determine which vibrations are IR and Raman active.

Answer available at the end of this section.

Selected Vibrational Modes

The interpretation of CO stretching vibrations in an IR spectrum is particularly useful. Symmetry and group theory can be applied to predict the number of CO stretching bands that appear in a vibrational spectrum for a given metal coordination complex. A classic example of this application is in distinguishing isomers of metal-carbonyl complexes. For example, the *cis*- and *trans*-isomers of square planar metal dicarbonyl complexes ($ML_2(CO)_2$) have a different number of IR stretches that can be predicted and interpreted using symmetry and group theory. Another example is the case of *mer*- and *fac*- isomers of octahedral metal tricarbonyl complexes ($ML_3(CO)_3$). Structures of the two types of metal carbonyl configurations and their isomers are shown in Figure 4.4.2.1. The isomers in each case can be distinguished using vibrational spectroscopy.

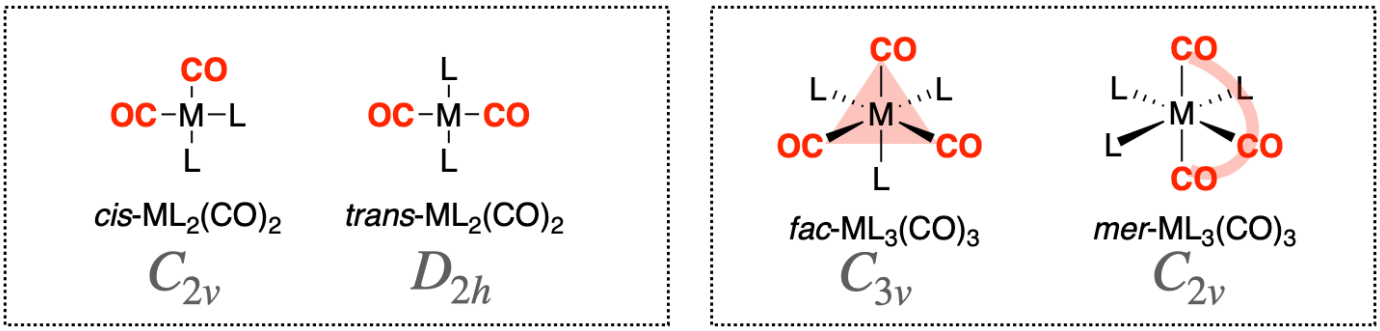


Figure 4.4.2.3: Cis- and *trans*- isomers of square planar metal dicarbonyl complexes ($ML_2(CO)_2$) are shown in the left box. *Mer*- and *fac*- isomers of octahedral metal tricarbonyl complexes ($ML_3(CO)_3$) are shown in the right box. The point group for each of the general structures is also shown. (CC-BY-NC-SA; Kathryn Haas)

EXAMPLE 1: Distinguishing *cis*- and *trans*- isomers of square planar metal dicarbonyl complexes

General structures of the *cis*- and *trans*- isomers of square planar metal dicarbonyl complexes ($ML_2(CO)_2$) are shown in the left box in Figure 4.4.2.1. We can use symmetry and group theory to predict how many carbonyl stretches we should expect for each isomer following the steps below.

Step 1: Assign the point group and Cartesian coordinates for each isomer.

The *cis*-isomer has C_{2v} symmetry and the *trans*-isomer has D_{2h} symmetry. We assign the Cartesian coordinates so that z is colinear with the principle axis in each case. For the D_2h isomer, there are several orientations of the z axis possible. The axes shown in Figure 4.4.2.2 will be used here.



Figure 4.4.2.4: Cis- and *trans*- isomers of square planar metal dicarbonyl complexes ($ML_2(CO)_2$) are shown and oriented with respect to the Cartesian coordinates shown at the left so that the highest-order rotation axis is colinear with z and the molecule is co-planar with the xz plane. The vector along each C—O bond is shown using a red arrow (→). These vectors represent the direction of C—O stretching motions. (CC-BY-NC-SA; Kathryn Haas)

Step 2: Produce a reducible representation (Γ) for CO stretches in each isomer

First, assign a vector along each C—O bond in the molecule to represent the direction of C—O stretching motions, as shown in Figure 4.4.2.2 (red arrows →). These vectors are used to produce a reducible representation (Γ) for the C—O stretching motions in each molecule. Using the symmetry operations under the appropriate character table, assign a value of 1 to each vector that remains in place during the operation, and a value of 0 if the vector moves out of place. There will be no occasion where a vector remains in place but is inverted, so a value of -1 will not occur.

cis- $ML_2(CO)_2$:

For *cis*- $ML_2(CO)_2$, the point group is C_{2v} and so we use the operations under the C_{2v} character table to create the Γ_{cis-CO}.



trans- $ML_2(CO)_2$:

For trans- $ML_2(CO)_2$, the point group is D_{2h} and so we use the operations under the D_{2h} character table to create the $\Gamma_{trans-CO}$.



Step 3: Break each Γ into its component irreducible representations

Each Γ can be reduced using inspection or by the systematic method described previously.

In the case of the *cis*- $ML_2(CO)_2$, the CO stretching vibrations are represented by A_1 and B_1 irreducible representations:



(4.4.2.5)

In the case of *trans*- $ML_2(CO)_2$, the CO stretching vibrations are represented by A_1 and B_{3u} irreducible representations:



These irreducible representations correspond to the symmetries of only the selected C—O vibrations. Since these motions are isolated to the C—O group, they do not include any rotations or translations of the entire molecule, and so we do not need to find and subtract rotationals or translations (unlike the previous cases where all motions were considered).

Step 4: Determine which vibrational modes are IR-active and/or Raman-active

Apply the infrared selection rules described previously to determine which of the CO vibrational motions are IR-active and Raman-active. The two isomers of $ML_2(CO)_2$ are described below.

In the case of the *cis*- $ML_2(CO)_2$, the CO stretching vibrations are represented by A_1 and B_1 irreducible representations. The characters of both representations and their functions are shown above, in 4.4.2.5 (and can be found in the C_{2v} character table). Under C_{2v}, both the A_1 and B_1 CO vibrational modes are IR-active and Raman-active. Therefore, two bands in the IR spectrum and two bands in the Raman spectrum are possible.

In the case of the trans- $ML_2(CO)_2$, the CO stretching vibrations are represented by A_g and B_{3u} irreducible representations. The characters of both representations and their functions are shown above, in 4.4.2.5 (and can be found in the D_{2h} character table). Under D_{2h}, the A_g vibrational mode is is Raman-active only, while the B_{3u} vibrational mode is IR-active only. Therefore, only one IR band and one Raman band are possible for this isomer.

Summary

It is possible to distinguish between the two isomers of square planar $ML_2(CO)_2$ using either IR or Raman vibrational spectroscopy. The *cis*- $ML_2(CO)_2$ can produce two CO stretches in an IR or Raman spectrum, while the *trans*- $ML_2(CO)_2$ isomer

can produce only one band in either type of vibrational spectrum. If a sample of $ML_2(CO)_2$ produced two CO stretching bands, we could rule out the possibility of a pure sample of *trans*-$ML_2(CO)_2$.

Exercise 4.4.2.3

Repeat the steps outlined above to determine how many CO vibrations are possible for *mer*-$ML_3(CO)_3$ and *fac*-$ML_3(CO)_3$ isomers (see Figure 4.4.2.1) in both IR and Raman spectra. Could either of these vibrational spectroscopies be used to distinguish the two isomers?

Answer available at the end of this section.

Answers

Exercise 4.4.2.1: Derive the irreducible representation in equation 4.4.2.3.

To find the number of each kind of irreducible representation that combine to form the Γ_{modes}, we need the characters of Γ_{modes} that we found above (4.4.2.1), the C_{2v} character table (below), and equation 4.4.2.2.

C_{2v}	$1E$	$1C_2$	$1\sigma_v$	$1\sigma_v'$	$h=4$	
A_1	1	1	1	1	z	x^2, y^2, z^2
A_2	1	1	−1	−1	R_z	xy
B_1	1	−1	1	−1	x, R_y	xz
B_2	1	−1	−1	1	y, R_x	yz

In the C_{2v} point group, each class has only one operation, so the number of operations in each class (from equation 4.4.2.2) is 1 for each class. This has been explicitly added to the character table above for emphasis.

Exercise 4.4.2.1: Derive the irreducible representation in equation 4.4.2.3.

The number of $A_1 = \frac{1}{4}[(1\times 9\times 1)+(1\times(-1)\times 1)+(1\times 3\times 1)+(1\times 1\times 1)] = 3A_1$

The number of $A_2 = \frac{1}{4}[(1\times 9\times 1)+(1\times(-1)\times 1)+((-1)\times 3\times 1)+((-1)\times 1\times 1)] = 1A_2$

The number of $B_1 = \frac{1}{4}[(1\times 9\times 1)+((-1)\times(-1)\times 1)+(1\times 3\times 1)+((-1)\times 1\times 1)] = 3B_1$

The number of $B_2 = \frac{1}{4}[(1\times 9\times 1)+((-1)\times(-1)\times 1)+((-1)\times 3\times 1)+(1\times 1\times 1)] = 2B_2$

Exercise 4.4.2.2

The point group of $[PtCl_4]^{2-}$ is D_{4h} (refer to its character table). There are five atoms and 15 vectors (x, y, z for each atom × 5 atoms).

STEP 1: The first major step is to **find a reducible representation (Γ)** for the movement of all atoms in the molecule.

C_{2v}	E	$2C_4$	C_2	$2C_2'$	$2C_2''$	i	$2S_4$	σ_h	$2\sigma_v$	$2\sigma_d$
Γ_{modes}	15	1	−1	−3	−1	−3	−1	5	3	1

(4.4.2.6)

.

STEP 2: Break Γ_{modes} into its component irreducible representations.

Following the process described earlier, we come to $A_{1g}+A_{2g}+B_{1g}+B_{2g}+E_g+2A_{2u}+B_{2u}+3E_u$. This accounts for all modes of movement, including rotations and translations.

STEP 3: Subtract rotations and translations to find vibrational modes.

The translations are $A_{2u}+E_u$ and the rotations are $A_{2g}+E_g$.
The remaining normal modes are: $A_{1g}+B_{1g}+B_{2g}+A_{2u}+B_{2u}+2E_u$

STEP 4: Determine which of the vibrational modes are IR-active and Raman-active:

$A_{2u}+E_u$ are IR-active. Since A_{2u} is singly degenerate and E_u is doubly degenerate, we expect three possible IR bands.
$A_{1g}+B_{1g}+B_{2g}$ are Raman-Active. Each of these is singly degenerate, so we expect three possible Raman bands.

Exercise 4.4.2.3

Step 1: Assign the point group and Cartesian coordinates for each isomer.
The *fac*-isomer is C_{3v}. The *mer*-isomer is C_{2v}.

Step 2: Produce a reducible representation for CO stretches in each isomer.

Step 3: Break each into its component irreducible representations.

Step 4: Determine which vibrational modes are IR-active and/or Raman-active.

***For fac*-$ML_3(CO)_3$**, the point group is C_{3v} and so we use the operations under the C_{3v} character table to create the Γ_{fac-CO}. Then break it into its irreducible representations and determine which are IR and Raman active:



This reduces to A_1+E. Both of these are IR active, and since one is singly degenerate while the other is doubly degenerate, we expect three possible IR bands from this isomer. Both vibrational modes are also Raman active, and again we would expect three possible bands in the Raman spectrum.

For mer-$ML_3(CO)_3$, the point group is C_{2v} and so we use the operations under the C_{2v} character table to create the Γ_{mer-CO}. Then break it into its irreducible representations and determine which are IR and Raman active:



This reduces to $2A_1 + B_1$; both A_1 and B_1 are IR and Raman active. So this isomer would have three possible IR bands and three possible Raman Bands.

These two isomers have the same number of possible bands in both IR and Raman spectroscopy. It would not be straightforward to distinguish them from each other based on the number of possible bands in the vibrational spectrum.

This page titled 4.4.2: Molecular Vibrations is shared under a CC BY-NC 4.0 license and was authored, remixed, and/or curated by Kathryn Haas.

- 4.4.2: Molecular Vibrations by Kathryn Haas is licensed CC BY-NC 4.0.

4.5: Problems (under construction)

Problems

1. Chlorophyll *a* is a green pigment that is found in plants. Its molecular formula is $C_{55}H_{77}O_5N_4Mg$. How many degrees of freedom does this molecule possess? How many vibrational degrees of freedom does it have?
2. CCl_4 was commonly used as an organic solvent until its severe carcinogenic properties were discovered. How many vibrational modes does CCl_4 have? Are they IR and/or Raman active?
3. The same vibrational modes in H_2O are IR and Raman active. WF_6^- has IR active modes that are not Raman active and vice versa. Explain why this is the case.
4. How many IR peaks do you expect from SO_3? Estimate where these peaks are positioned in an IR spectrum.
5. Calculate the symmetries of the normal coordinates of planar BF_3.

Answers to Problems

1. Chlorophyll *a* has 426 degrees of freedom and 420 vibrational modes.
2. The point group is T_d, $T_{vib} = a_1 + e + 2t_2$; a_1 and e are Raman active, t_2 is both IR and Raman active.
3. For molecules that possess a center of inversion i, modes cannot be simultaneously IR and Raman active.
4. Point group is D_{3h}; one would expect three IR active peaks. Asymmetric stretch highest (1391 cm^{-1}), two bending modes (both around 500 cm^{-1}). The symmetric stretch is IR inactive.
5. $T_{3N} = A_1' + A_2' + 3E' + 2\ A_2'' + E''$ and $T_{vib} = A_1' + 2E' + A_2''$

Contributors and Attributions

- Kristin Kowolik, University of California, Davis

Problems

1. The water molecule H_2O was used as an example; it was mentioned that when water was rotated 180 degrees around an axis bisecting the oxygen, the molecule was superimposable on the original water molecule. How about CO_2? Will it be like the water molecule since CO_2 also has 2 atoms of oxygen?

Of course not, because every molecule has a different molecular shape. To recognize the symmetry of any molecule, the structure and the molecular shape of that molecule should be defined. The water molecule is bent but CO_2 is not, and if CO_2 is rotated 360 degrees around the axis bisecting the C atom, then it can be superimposed on the original molecule. We then see the symmetry for the CO_2.

2. Why should all of the five symmetry elements be done on a molecule in order to find the point group the molecule belongs to? Why is performing only one or two of the symmetry elements not enough for recognizing the point group?

One or two of the symmetry elements will not be able to tell us everything about the molecule's symmetry, since those one or two properties do not tell us everything about the molecule. Also, while different molecules may have one or two symmetrical properties in common, the five properties will not be the same for all molecules.

3. What does the symbol C_n stand for and what does n represent? Why is it important to identify n?

C is the axis of rotation and n is the order of the axis.

4. How are the character tables helpful?

The character table tells us about all the operational elements performed on the molecule and indicates whether we have forgotten to perform any of the symmetry elements. The tables serve as a checklist because all the operational elements should be done on the molecule in order to find the point group of the molecule.

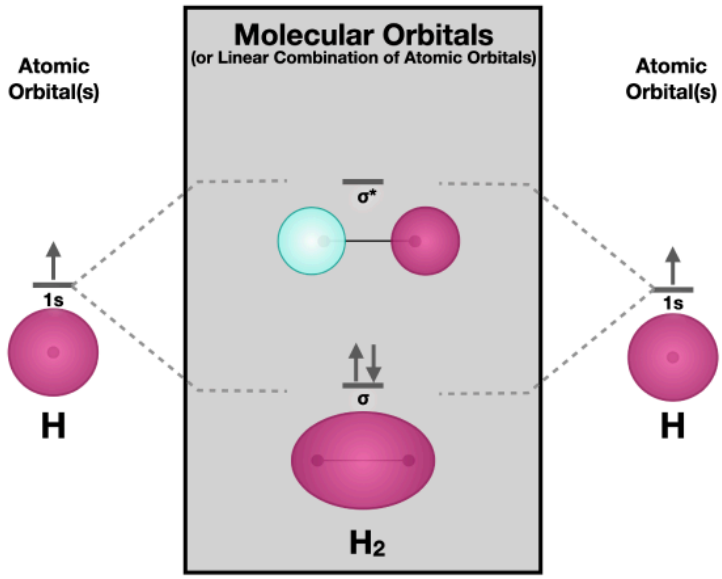
5. Why is important to find symmetry in molecules?

Symmetry tells us about bonding for that molecule.

This page titled 4.5: Problems (under construction) is shared under a CC BY-NC-SA 4.0 license and was authored, remixed, and/or curated by Kathryn Haas.

- 4.P: Problems (under construction) by Kathryn Haas has no license indicated.

5: MOLECULAR ORBITALS



Molecular Orbital Theory

Molecular Orbital (MO) Theory is a sophisticated bonding model. It is generally considered to be more powerful than *Lewis* and *Valence Bond Theories* for predicting molecular properties; however, this power comes at the price of complexity. In its full development, MO Theory requires complex mathematics, though the ideas behind it are simple. Atomic orbitals (AOs) that are localized on individual atoms combine to make molecular orbitals (MOs) that are distributed over the molecule. The simplest example is the molecule dihydrogen (H_2), in which two independent hydrogen 1s orbitals combine to form the σ bonding MO and the σ antibonding MO of the dihydrogen molecule (see figure). The MO's are also called Linear Combinations of Atomic Orbitals (LCAO).

5.1: Formation of Molecular Orbitals from Atomic Orbitals

5.1.1: Molecular Orbitals from s Orbitals

5.1.2: Molecular Orbitals from p Orbitals

5.1.3: Molecular orbitals from d orbitals

5.1.4: Nonbonding Orbitals and Other Factors

5.2: Homonuclear Diatomic Molecules

5.2.1: Molecular Orbitals

5.2.2: Orbital Mixing

5.2.3: Diatomic Molecules of the First and Second Periods

5.2.4: Photoelectron Spectroscopy

5.3: Heteronuclear Diatomic Molecules

5.3.1: Orbital ionization energies

5.3.2: Polar bonds

5.3.3: Ionic Compounds and Molecular Orbitals

5.4: Larger (Polyatomic) Molecules

5.4.1: Bifluoride anion

5.4.2: Carbon Dioxide
5.4.3: H_2O
5.4.4: NH_3
5.4.5: CO_2 (Revisted with Projection Operators)
5.4.6: BF_3
5.5: Problems

This page titled 5: Molecular Orbitals is shared under a CC BY-SA 4.0 license and was authored, remixed, and/or curated by Kathryn Haas.

- 5: Molecular Orbitals by Kathryn Haas is licensed CC BY-SA 4.0.

5.1: Formation of Molecular Orbitals from Atomic Orbitals

Molecular orbital theory extends from quantum theory and the atomic orbital wavefunctions (ψ) described by the Schrödinger equation. While the Schrödinger equation defines a Ψ for electrons in individual atoms, we can approximate the molecular wavefunction (what Ψ would look like if we combined the ψ of individual atoms). The addition or subtraction of wavefunctions is termed **linear combination of atomic orbitals** (LCAO). Molecular orbital theory is applied to LCAO to describe bonding.

The LCAO for the wavefunction of two atoms (ψ_a and ψ_b) is represented by the general expression below. The coefficients c_a and c_b quantify the contribution of each atomic ψ to the molecular Ψ.

$$\Psi = c_a\psi_a + c_b\psi_b$$

For two atomic ψs to form a bond, three conditions must be satisfied:

- First, the **distance between the atoms** must be small enough to provide good overlap. This is because the two orbitals must be able to overlap using regions of ψ^2 where the probability of finding electrons is significant. If atoms are not close enough, ψ_a and ψ_b cannot interact productively. At the same time, the atoms must be far enough apart that their nuclei do not repel each other.
- The **symmetry of the orbitals** must be compatible such that regions of ψ_a and ψ_b with the same sign constructively interfere more than regions with opposite sign destructively interfere. In other words, for a productive interaction, there must be a relatively high probability of finding an electron between the two nuclei, and this depends on the symmetry (and sign of the ψ) of the atomic orbitals.
- Third, the **energies of the atomic orbitals** must be similar. Orbitals with similar energy combine to make the most stable bonding molecular orbitals. Atomic orbitals with very different energies form less stable bonding interactions, and the larger the difference in the atomic orbitals, the weaker the bonding interaction will be.

Atomic orbitals combine to form molecular orbitals when these three conditions are met. The result is a set of bonding molecular orbitals that are lower in energy than the original atomic orbital energies.

This page titled 5.1: Formation of Molecular Orbitals from Atomic Orbitals is shared under a CC BY-SA 4.0 license and was authored, remixed, and/or curated by Kathryn Haas.

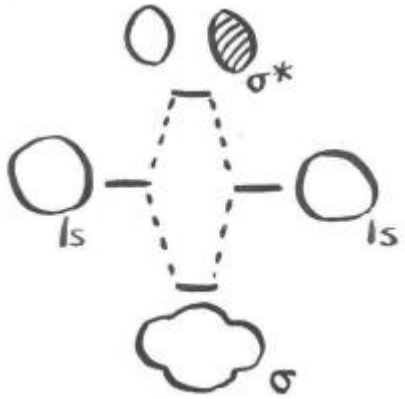
- 5.1: Formation of Molecular Orbitals from Atomic Orbitals by Kathryn Haas is licensed CC BY-SA 4.0.

5.1.1: Molecular Orbitals from s Orbitals

In the case of the hydrogen molecule, we took two atomic orbitals and combined them to form two molecular orbitals. These new molecular orbitals had different wavelengths than the two atomic orbitals: one had a longer wavelength and was a little lower in energy, while the other had a shorter wavelength and was a little higher in energy. If we take into account the energy of the two original atomic wavefunctions, and compare them to the total energy of the two new molecular wavefunctions, there is no change overall.

We started with two atomic orbitals, and by combining them we produced two molecular orbitals. Both of these ideas are useful in considering the formation of more complex molecules from individual atoms.

- ◦ The average energy of the orbitals has remained almost constant.
  ◦ Also, the number of wavefunctions has remained constant.



◦

Of course, from the point of view of the two real electrons, some remarkable changes have occurred. Both of these electrons have adopted a longer wavelength and a lower energy and that has made all the difference. There is an occupied molecular orbital and an unoccupied molecular orbital; only the occupied orbital makes a real energetic contribution to the overall stability of the molecule. The unoccupied orbital is completely imaginary.

A bonding picture of He_2 would look exactly the same, because it would also involve the overlap of 1s electrons on one atom with 1s electrons on the other atom. There would be a different electronic energy, however. That difference would affect the prospects of helium-helium bond formation.

- The electrons have lower kinetic energy in the bond than they had before bonding.
- Electronic energy has decreased. A stable bond has formed.

Exercise 5.1.1.1

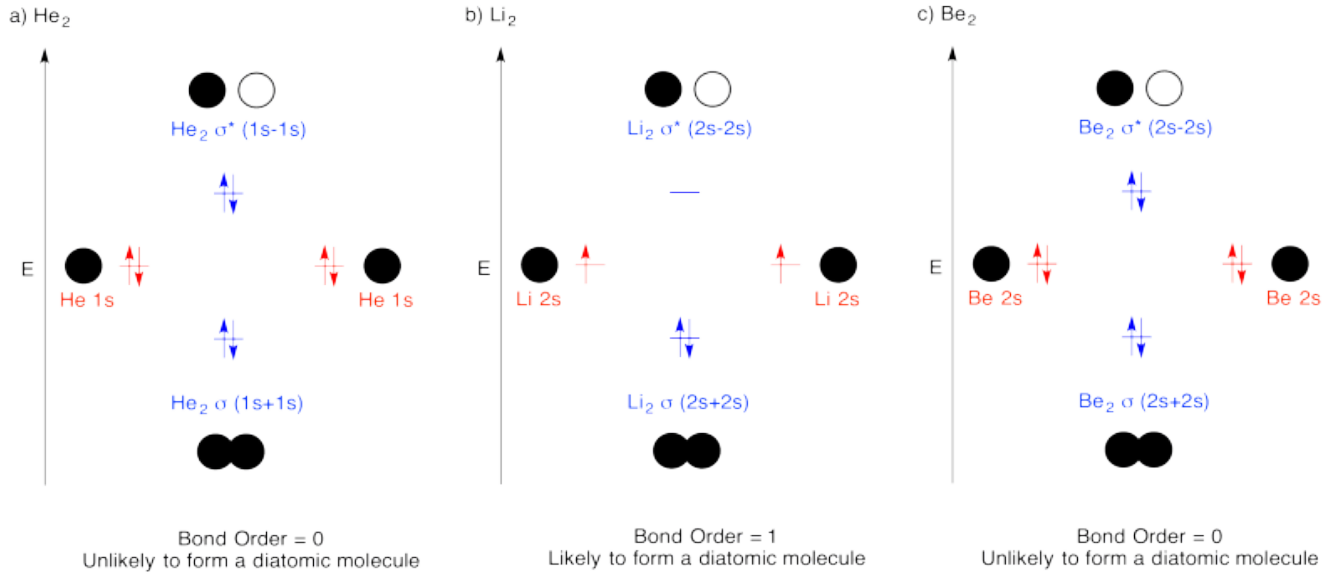
Construct molecular orbital diagrams for the following diatomic species and discuss the likelihood of bond formation in each case.

a. He_2.
b. Li_2.
c. Be_2.

Answer available at the end of this section.

Answers

Exercise 5.1.1.1



Bond Order = 0
Unlikely to form a diatomic molecule

Bond Order = 1
Likely to form a diatomic molecule

Bond Order = 0
Unlikely to form a diatomic molecule

This page titled 5.1.1: Molecular Orbitals from s Orbitals is shared under a CC BY-NC 3.0 license and was authored, remixed, and/or curated by Chris Schaller.

5.1.2: Molecular Orbitals from p Orbitals

Bonding with P-orbitals

Sigma bonding with p-orbitals

Other diatomic molecules in the upper right corner of the periodic table can be constructed in a similar way. Look at dinitrogen, N_2.

We can think about how dinitrogen would form if two nitrogen atoms were placed close enough together to share electrons. Nitrogen has more electrons than hydrogen, so this interaction is more complicated.

In our qualitative examination of bonding in main group diatomics, we will take the approach used in Lewis structures and just look at the valence electrons. A quantitative molecular orbital calculation with a computer would not take this shortcut, but would include all of the electrons in the atoms that are bonding together.

Nitrogen has five valence electrons, and these electrons are found in the 2s and 2p levels. There are three possible atomic orbitals in the 2p level where some of these electrons could be found: p_x, p_y and p_z. We need to look at the interaction between the s and p_x, p_y and p_z orbitals on one nitrogen atom with the s and p_x, p_y and p_z orbitals on the other nitrogen. That process could be extremely complicated, but:

- Orbital interactions are governed by symmetry.

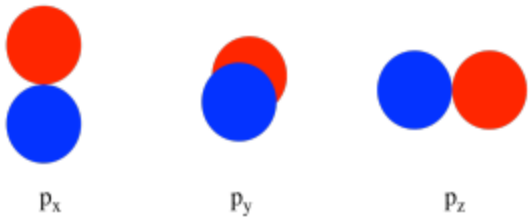
Orbitals interact most easily with other orbitals that have the same element of symmetry. For now, we can simplify and say that orbitals on one atom only interact with the same type of orbitals on the other atom.

- s orbitals interact with s orbitals. We can already see how that will work out in dinitrogen, because that is what happened in dihydrogen.
- p_x orbitals interact with p_x orbitals.
- p_y orbitals interact with p_y orbitals.
- p_z orbitals interact with p_z orbitals.

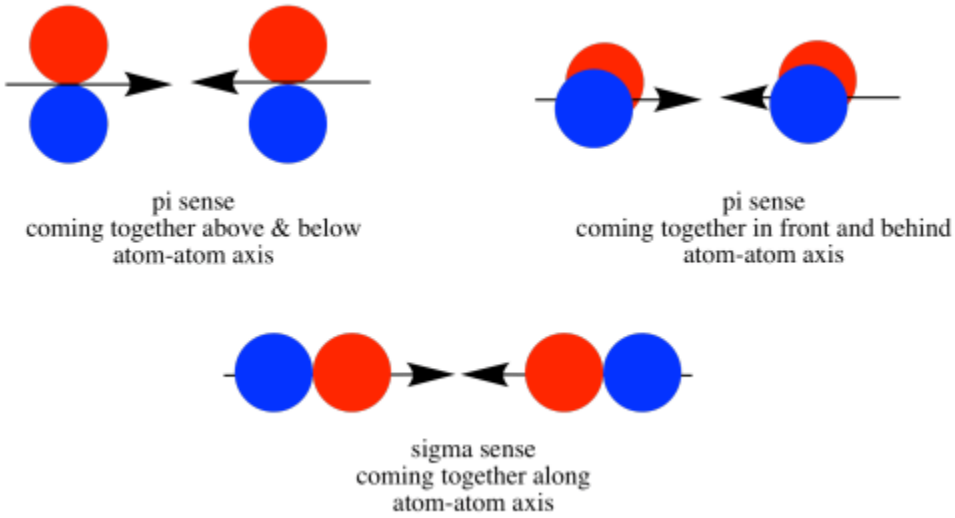
Another complication here is that the s and p orbitals do not start out at the same energy level. When the orbitals mix, one combination goes up in energy and one goes down. Does the s antibonding combination go higher in energy than the combinations from p orbitals? Do the p bonding combinations go lower in energy than the combinations from s orbitals? We will **simplify** and **assume** that the s and p levels remain completely separate from each other. This is not always true, but the situation varies depending on what atoms we are dealing with.

- The combination of one s orbital with another is just like in hydrogen. Two original orbitals will combine and rearrange to produce two new orbitals.
- There is a bonding combination in which the orbitals are in phase. The new orbital produced has a longer wavelength than the original orbital. It is lower in energy.
- There is an antibonding combination in which the orbitals are out of phase. The new orbital produced has a shorter wavelength than the original orbital. It is higher in energy.

In considering the interaction of two p orbitals, we have to keep in mind that p orbitals are directional. A p orbital lies along a particular axis: x, y or z. The three p orbitals on nitrogen are all mutually perpendicular (or orthogonal) to each other. That situation is in contrast to s orbitals, which are spherical and thus look the same from any direction.

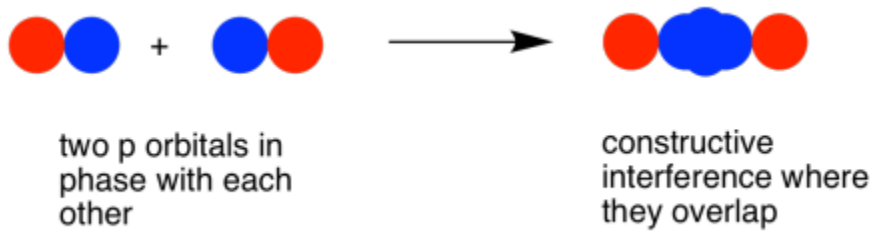


We first need to define one axis as lying along the N-N bond. It does not really matter which one. We arbitrarily say the N-N bond lies along the z axis. The p_z orbitals have a different spatial relationship to each other compared to the p_y and p_x. The p_z orbitals lie along the bond axis, whereas the p_y and p_x are orthogonal to it.

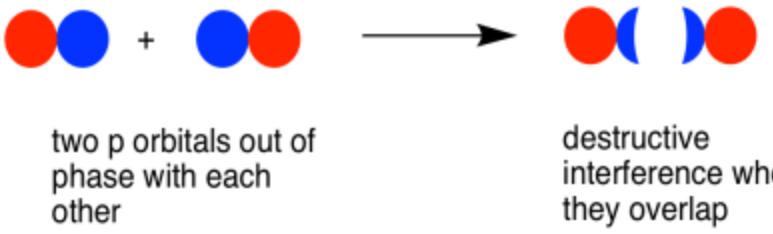


As the nitrogen atoms are brought together, one lobe on one p_z orbital overlaps strongly with one lobe on the other p_z orbital. The other lobes point away from each other and do not interact in any obvious way.

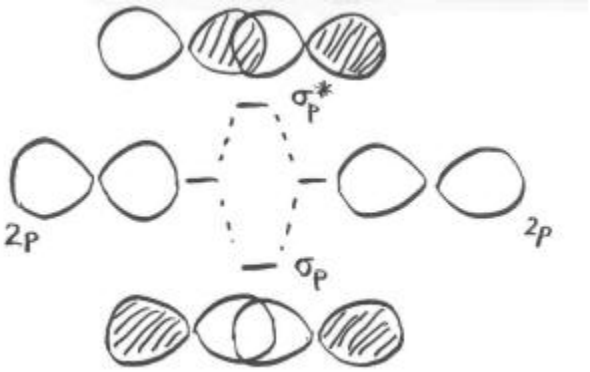
As with the s orbital, the p_z orbitals can be in-phase or out-of-phase. The in-phase combination results in constructive interference. (Here, "in-phase" means the lobes that overlap are in-phase; for that to happen the two p orbitals are actually completely out-of-phase with each other mathematically, so that one orbital is the mirror image of the other.) This combination is at a longer wavelength than the original orbital. It is a lower energy combination.



The out-of-phase combination (meaning in this case that the overlapping lobes are out-of-phase) results in destructive interference. This combination is at shorter wavelength than the original orbital. It is a higher energy combination.



As a result, we have two different combinations stemming from two different p orbitals coming together in two different ways. We get a low-energy, in-phase, bonding combination and a high-energy, out-of-phase, antibonding combination.



What about those other p orbitals, the ones that do not lie along the bond axis? We'll take a look at that problem on the next page.

Exercise 5.1.2.2

Draw an MO cartoon of a sigma bonding orbital formed by the overlap of two p orbitals between two oxygen atoms. Label the positions of the oxygen nuclei with the symbol "O". Label the O-O bond axis.

Answer available at the end of this section.

Exercise 5.1.2.3

Chemical reactions can be described by MO diagrams too! Consider the following reaction in which a new sigma bond is formed.



Draw an MO diagram for the reaction above. In other words, start from the one frontier MO on each reactant to build the MO's of the new sigma bond in the product.

- Draw the orbital from the base (hydroxide) that is likely to donate its electrons.
- Draw the orbital from the acid (aluminum chloride) that is likely to accept electrons.
- Complete the MO mixing diagram of these two orbitals:

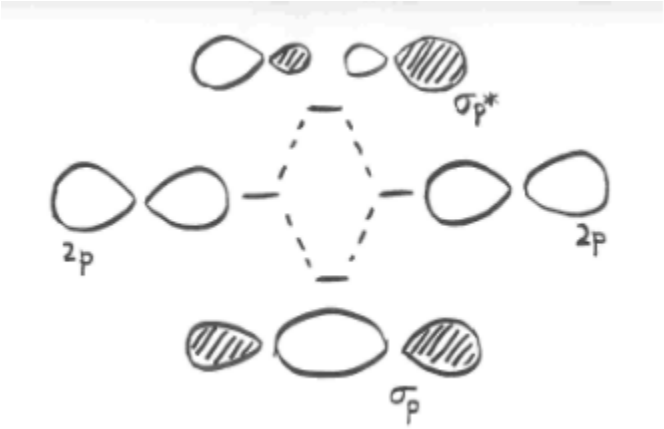
- Label the electron donating orbital
- Label the electron accepting orbital
- Populate the MO mixing diagram with electrons

o Draw a cartoon showing each reactant and product MO that contributes to the bonding interaction.

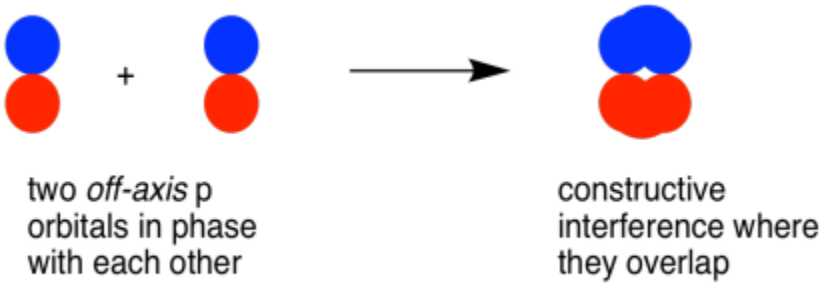
Answer available at the end of this section.

Pi-bonding with p-orbitals

Earlier, we saw that p orbitals that lie along the same axis can interact to form bonds.



Parallel, but not collinear, p orbitals can also interact with each other. They would approach each other side by side, above and below the bond axis between the two atoms. They can be close enough to each other to overlap, although they do not overlap as strongly as orbitals lying along the bond axis. They can make an in-phase combination, as shown below.

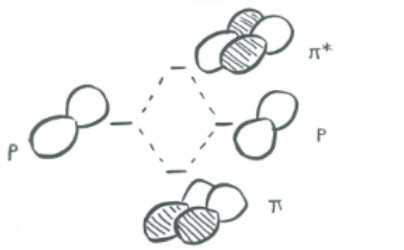


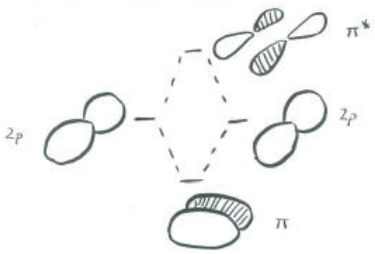
They could also make an out-of-phase combination, as shown below.



- parallel p orbitals can overlap to produce bonding and antibonding combinations.
- the resulting orbitals contain nodes along the bond axis.
- the electron density is found above and below the bond axis.
- this is called a p (pi) bond.

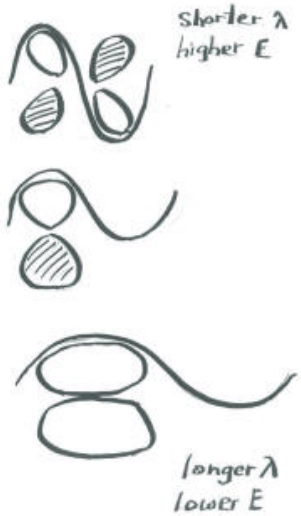
The illustration above is for one set of p orbitals that are orthogonal to the bond axis. The second picture shows the result of the constructive (or destructive) interference. A similar picture could be shown for the other set of p orbitals.



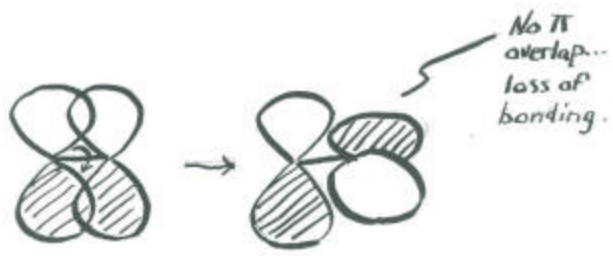


In a main group diatomic species like dinitrogen, one p orbital lying along the bond axis can engage in s bonding. The two p orbitals orthogonal to the bond axis can engage in p bonding. There will be both bonding and antibonding combinations.

Just as the sigma-bonding orbitals display progressively shorter wavelengths along the bonding axis as they go to higher energy, so do the pi bonding orbitals. In other words, there are more nodes in the higher-energy orbitals than in the lower-energy ones.



An important consequence of the spatial distribution or "shape" of a p orbital is that it is not symmetric with respect to the bond axis. An s orbital is not affected when the atom at one end of the bond is rotated with respect to the other. A p orbital is affected by such a rotation. If one atom turns with respect to the other, the p orbital would have to stretch to maintain the connection. The orbitals would not be able to overlap, so the connection between the atoms would be lost.



Exercise 5.1.2.4

The combinations of _____ atomic orbitals leads to σ orbitals.

Draw pictures.

Answer available at the end of this section.

Exercise 5.1.2.5

The combinations of _____ atomic orbitals leads to π orbitals.

Draw pictures.

Answer available at the end of this section.

Exercise 5.1.2.6

Which molecular orbital is typically the highest in energy?
a. p
b. σ
c. π*
d. π
e. σ*

Answer available at the end of this section.

Exercise 5.1.2.7

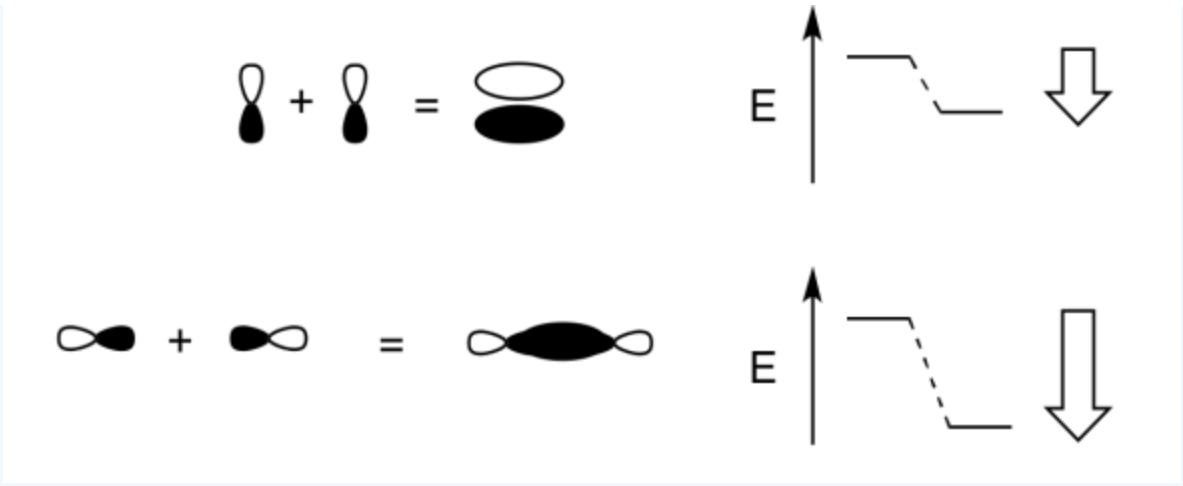
Why would a *core* 1s orbital not interact with a *valence* 2s orbital?

Hint: Why is a Li_2O bond stronger than a K_2O bond?

Answer available at the end of this section.

Exercise 5.1.2.8

Add a few words to explain the ideas conveyed in these drawings.



Answer available at the end of this section.

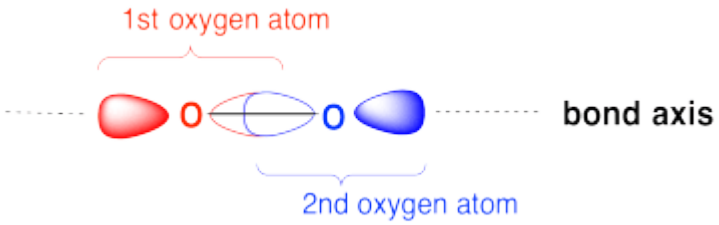
Attribution

Chris P Schaller, Ph.D., (College of Saint Benedict / Saint John's University)

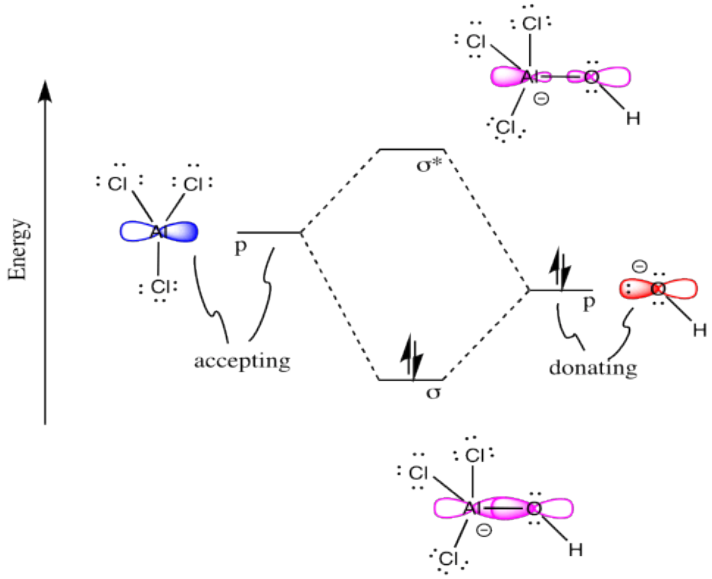
Curated or created by Kathryn Haas

Answers

Exercise 5.1.2.2

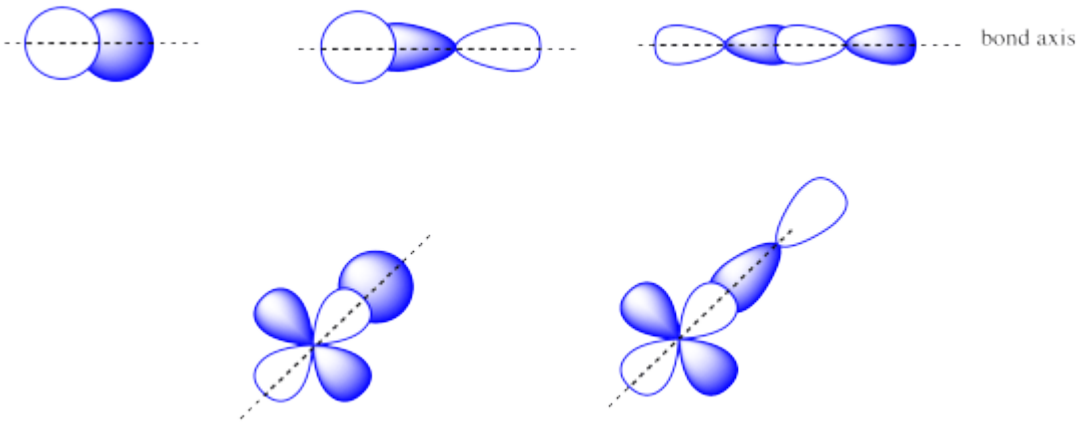


Exercise 5.1.2.3



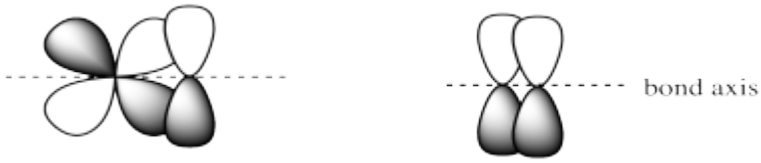
Exercise 5.1.2.4

The combinations of ***s* + *s*** OR ***s* + *p*** OR ***p* + *p*** OR ***s* + *d*** OR ***p* + *d*** atomic orbitals can lead to σ orbitals.



Exercise 5.1.2.5

The combinations of side by side p + p or p + d atomic orbitals leads to π orbitals.



Exercise 5.1.2.6

e) σ*

Exercise 5.1.2.7

Li^+ and O^{2-} are more similar in size than K^+ and O^{2-}, so the bond between Li^+ and O^{2-} is stronger.

The energy difference between any core orbitals and valence orbitals is too large, so they cannot interact. In order for orbitals to interact, the orbitals need to have the same symmetry, be in the same plane, and be similar in energy.

Exercise 5.1.2.8

When two parallel p orbitals combine out-of-phase, destructive interference occurs.

There is a node between the atoms.

The energy of the electrons increases.

When two parallel p orbitals combine in-phase, constructive interference occurs.

There is no node between the atoms; the electrons are found above and below the axis connecting the atoms.

The energy of the electrons decreases.

This page titled 5.1.2: Molecular Orbitals from p Orbitals is shared under a CC BY-NC 3.0 license and was authored, remixed, and/or curated by Chris Schaller.

- 5.1.2: Molecular Orbitals from p Orbitals by Chris Schaller is licensed CC BY-SA 3.0.

5.1.3: Molecular orbitals from d orbitals

In transition metals and other heavier elements, the d orbitals may combine with other orbitals of compatible symmetry (and energy) to form molecular orbitals. Generally, there are three types of bonding and antibonding interactions that may occur with d orbitals: sigma (σ), pi (π), and delta (δ) bonds.

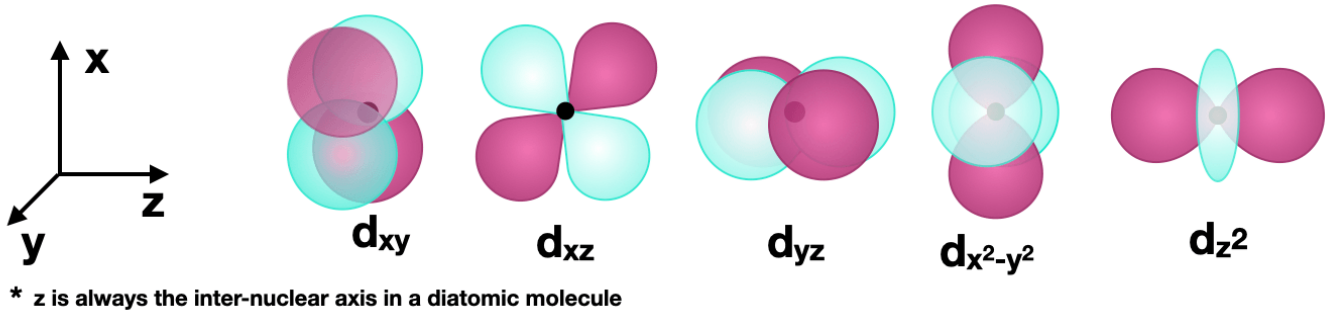


Figure 5.1.3.1: The five $3d$ orbitals are shown. The orientation of the axes is consistent and the z axis is horizontal for convenience in drawing bonding along the z axis (see examples below). (CC-BY-SA; Kathryn Haas)

Sigma (σ) bonding with d orbitals

σ bonds are symmetric with respect to the inter-nuclear axis (in a diatomic molecule, this is the z axis). An example of a σ bond formed by d orbitals is that of two d_{z^2} orbitals (see Figure 5.1.3.2). If a bonded atom is in a position other than on the z axis (in an octahedral geometry, for example), σ bonds can also form. For example, two $d_{x^2-y^2}$ orbitals on atoms bonded along the x or y axes could also form a σ bond.

d orbitals can also form σ bonds with other types of orbitals with the appropriate symmetry. Examples of orbitals with appropriate symmetry are the s orbital and certain p orbitals on another atom, as shown below in Figure 5.1.3.2.

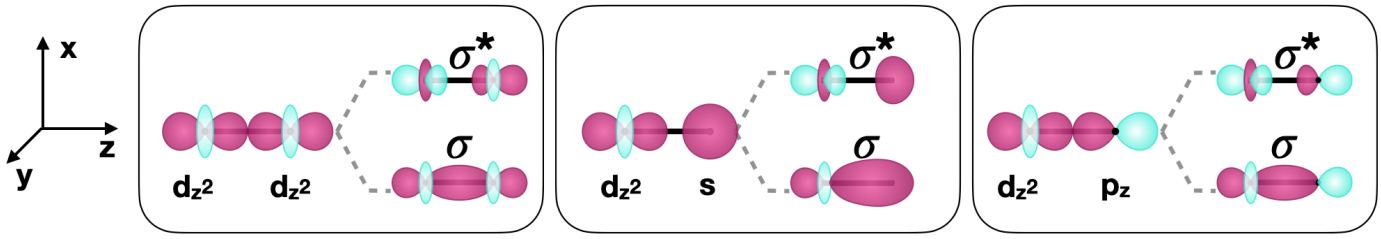


Figure 5.1.3.2: Selected examples of σ bonds involving d orbitals along the z internuclear axis (shown as a bold horizontal line) between two atoms. (CC-BY-SA; Kathryn Haas)

Pi (π) bonding with d orbitals

π bonds are those with one node that is in-plane with the internuclear axis. A π bond can form between two d orbitals or between d orbitals and other types of orbitals with comparable symmetry. An example of a π bond between two d orbitals is that formed by two d_{xz} orbitals along the z axis (shown in Figure 5.1.3.3). d orbitals can also form π bonds using p orbitals with compatible symmetry, as shown in Figure 5.1.3.3.

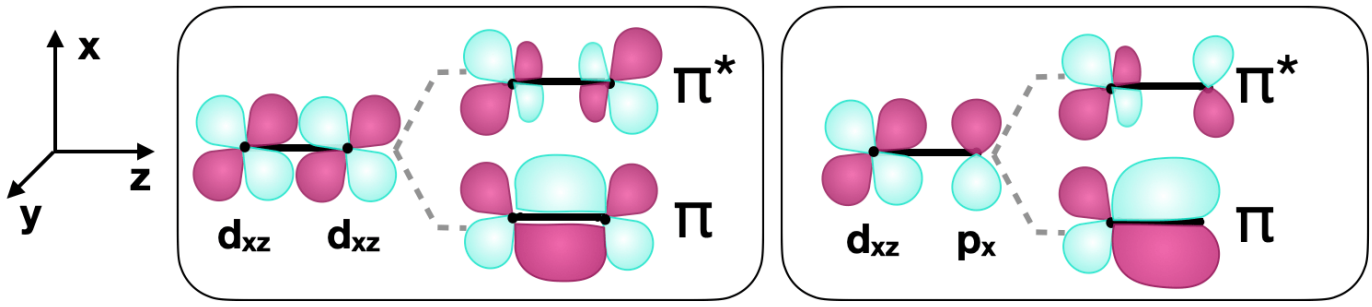


Figure 5.1.3.3: Selected examples of π bonds involving d orbitals along the z internuclear axis (shown as a bold horizontal line) between two atoms. (CC-BY-SA; Kathryn Haas)

Delta (δ) bonding with d orbitals

δ bonds are those with two nodes that are in-plane with the internuclear axis. δ bonds can form between two d orbitals with appropriate symmetry. For example, when two atoms bond along the z axis, the d_{xy} orbitals and the two $d_{x^2-y^2}$ orbitals can form δ bonds (Figure 5.1.3.4).

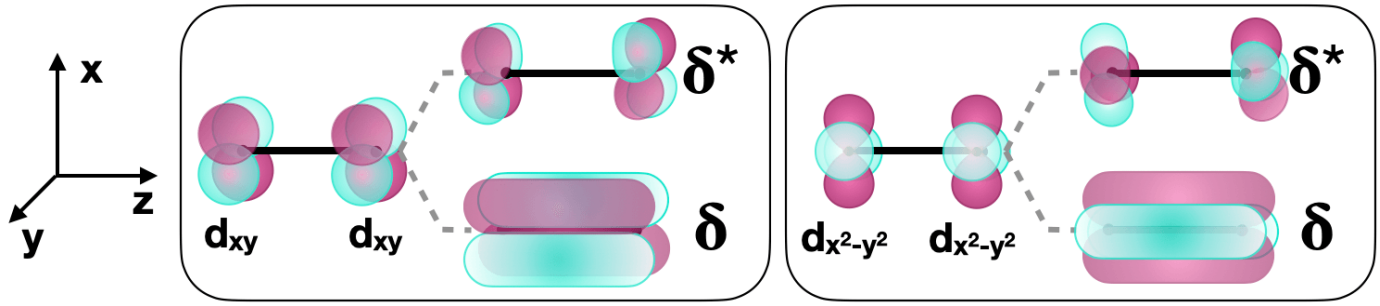


Figure 5.1.3.4: Selected examples of δ bonds involving d orbitals along the z internuclear axis (shown in bold horizontal line) between two atoms. (CC-BY-SA; Kathryn Haas)

Incompatible orbitals

In the descriptions above, we focused on how bonds (and antibonds) can be formed with d orbitals. All bonding and non-bonding interactions require that orbitals have compatible symmetry to form productive interactions. It is worth mentioning that orbitals with symmetry that is incompatible with the d orbitals will not have bonding or antibonding interactions with d orbitals. The figure below shows several sets of orbitals that are incompatible for bonding.

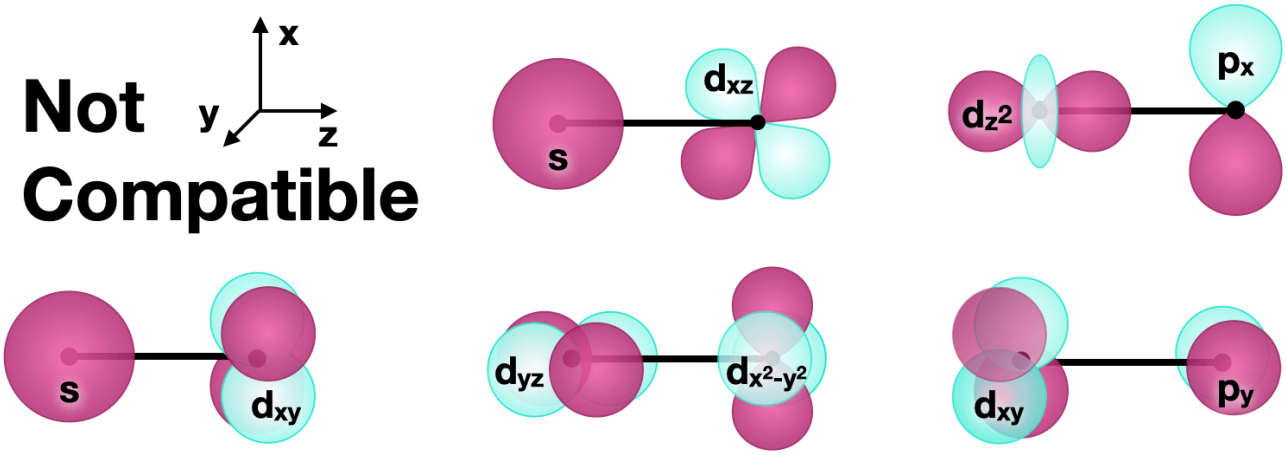


Figure 5.1.3.5: Several incompatible pairs of orbitals. (CC-BY-SA; Kathryn Haas)

Curated or created by Kathryn Haas

This page titled 5.1.3: Molecular orbitals from d orbitals is shared under a CC BY-SA 4.0 license and was authored, remixed, and/or curated by Kathryn Haas.

- 5.1.3: Molecular orbitals from d orbitals by Kathryn Haas is licensed CC BY-SA 4.0.

5.1.4: Nonbonding Orbitals and Other Factors

The simplest case is when there is an even number of atomic orbitals that all combine to form strong bonding and antibonding orbitals. But what if there is an uneven number of atomic orbitals? Or what if there are some orbitals that don't meet the criteria for bonding? Or what if the bonding interactions are weak? In these cases, there will be molecular orbitals on the molecule that have non-bonding character.

It is important to note that the bonding, non-bonding, and antibonding nature of orbitals exist on a spectrum. Some bonding and anti-bonding orbitals may have some non-bonding character depending on where their energies lie with respect to the original atomic orbital energies. When molecular orbitals have energies similar to their original atomic orbitals, they will have some non-bonding character. The closer the energies of atomic and molecular orbitals, the more non-bonding the molecular orbitals.

Two major factors to consider

Uneven number of atomic orbitals: In the case that there is an uneven number of atomic orbitals with compatible symmetry, orbitals with non-bonding character will form. For example, in the case where three atomic orbitals combine, the most common result is formation of a low-energy bonding orbital, a high energy antibonding orbital, and a non-bonding orbital of intermediate energy (Figure 5.1.4.1).

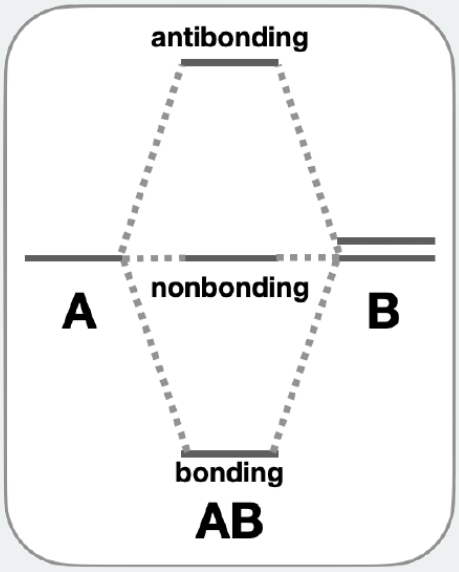


Figure 5.1.4.1. This figure illustrates the most common case for three atomic orbitals that combine to form three molecular orbitals; formation of one low-energy bonding, one high-energy antibonding, and one intermediate energy non-bonding molecular orbital. (CC-BY-NC-SA, Kathryn Haas)

Differences in energy: Combination of orbitals with different energies may lead to orbitals with non-bonding character. Atomic orbitals that have similar energies will have the strongest interactions, and result in bonding molecular orbitals with much lower energies than the component atomic orbitals. On the other hand, atomic orbitals with very unequal energies have a weaker interaction because the molecular orbitals are closer in energy to the atomic orbital energies, thus there is less energy benefit to putting electrons in the bonding molecular orbitals (Figure 5.1.4.2). When bonding or antibonding orbitals are close to the energies of the contributing atomic orbitals, those molecular orbitals may have some non-bonding character.

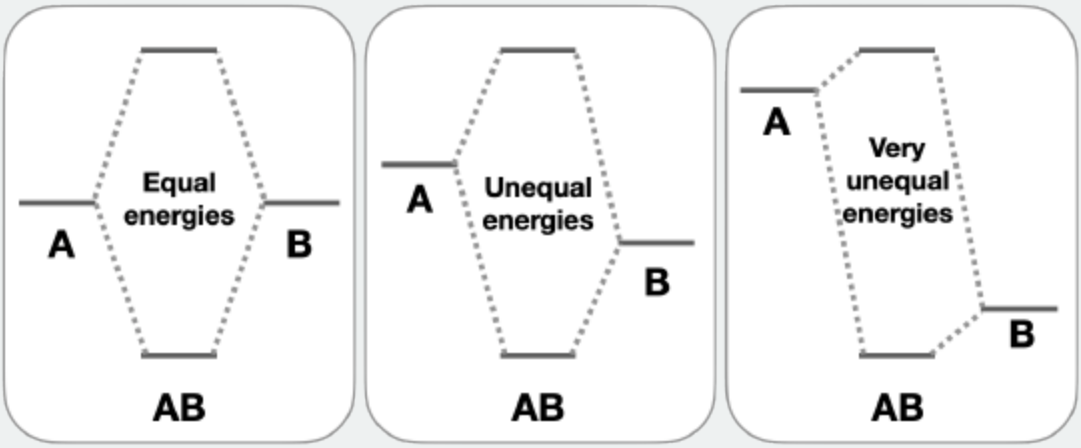


Figure 5.1.4.2. This figure illustrates how relative energies of atomic orbitals result in molecular orbitals that are more or less favorable. The greater the energy difference between atomic orbitals and the bonding molecular orbital, the more eneretically favorable it is for bonding to occur. (CC-BY-NC-SA, Kathryn Haas)

This page titled 5.1.4: Nonbonding Orbitals and Other Factors is shared under a CC BY-SA 4.0 license and was authored, remixed, and/or curated by Kathryn Haas.

- 5.1.4: Nonbonding Orbitals and Other Factors by Kathryn Haas is licensed CC BY-SA 4.0.

5.2: HOMONUCLEAR DIATOMIC MOLECULES

In this section you will be introduced to the molecular orbital diagrams of several homonuclear diatomic molecules. Homonuclear diatomic molecules are molecules made of exactly two identical atoms, and they are relatively simple.

5.2.1: Molecular Orbitals

5.2.2: Orbital Mixing

5.2.3: Diatomic Molecules of the First and Second Periods

5.2.4: Photoelectron Spectroscopy

This page titled 5.2: Homonuclear Diatomic Molecules is shared under a CC BY-SA 4.0 license and was authored, remixed, and/or curated by Kathryn Haas.

- 5.2: Homonuclear Diatomic Molecules by Kathryn Haas is licensed CC BY-SA 4.0.

5.2.1: Molecular Orbitals

There are several cases where our more elementary models of bonding (like Lewis Theory and Valence Bond Theory) fail to predict the actual molecular properties and reactivity. A classic example is the case of O_2 and its magnetic properties. At very cold temperatures, O_2 is attracted to a magnetic field, and thus it must be paramagnetic (unpaired electrons give rise to magnetism). Watch the video below!

YouTube Video

This interactive element is not available in this format. Visit the link or scan the QR code to access it online.

View this YouTube Video online

The magnetic properties of O_2 are easily rationalized by its **molecular orbital diagram**. A molecular orbital diagram is a diagram that shows the relative energies and identities of each molecular orbital in a molecule. Figure $5.2.1.1$ shows a simplified and generic molecular orbital diagram for a second-row homonuclear diatomic molecule. The diagram is simplified in that it assumes that interactions are limited to degenerate orbitals from two atoms (see next section).

There are some things you should note as you inspect Figure $5.2.1.1$ (and keep these in mind as you draw your own diagrams!). First, notice that there are the **same number of molecular orbitals as there are atomic orbitals**. Second, notice that **each orbital in the diagram is rigorously labeled** using labels (σ and π) that include the subscripts u and g. These labels and subscripts indicate the symmetry of the orbitals. The σ symbol indicates that the orbital is symmetric with respect to the internuclear axis, while the π label indicates that there is one node along that axis. The g and u stand for *gerade* and *ungerade*, the German words for *even* and *uneven*, respectively. The subscript g is given to orbitals that are *even*, or *symmetric*, with respect to an inversion center. The subscript u is given to orbitals that are *uneven*, or *antisymetric*, with respect to an inversion center. The pictures of calculated molecular orbitals are shown in Figure $5.2.1.1$ to illustrate the symmetry of each orbital.

Another important thing to notice is that the diagram in Figure $5.2.1.1$ lacks electrons (because it is generic for any second-row diatomic molecule). If this were a *complete* molecular orbital diagram it would **include the electrons for each atom and for the molecule**. Electrons in molecular orbitals are filled in the same way an atomic orbital diagram would be filled, where electrons occupy lower energy orbitals before higher energy orbitals, and electrons occupy empty degenerate orbitals before pairing. A complete molecular orbital diagram would show whether the molecule is diamagnetic or paramagnetic. It can also be used to calculate the bond order of the molecule (the number of bonds between atoms) using the formula below:

$$\text{Bond order } = \frac{1}{2}\left[\begin{pmatrix}\text{number of electrons}\\ \text{in bonding orbitals}\end{pmatrix} - \begin{pmatrix}\text{number of electrons}\\ \text{in antibonding orbitals}\end{pmatrix}\right]$$

In general, non-valence (core) electrons can be ignored because they contribute nothing to the bond order. In fact, many molecular orbital diagrams will ignore the core orbitals, as they are insignificant for bonding interactions and reactivity.

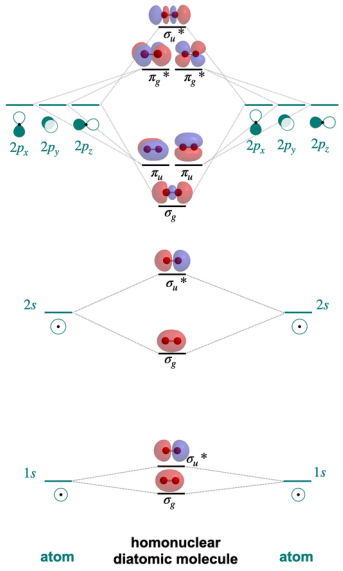


Figure 5.2.1.1: A generic molecular orbital diagram for a homonuclear diatomic molecule of second-row elements assuming no orbital mixing (interactions are formed by orbitals of the same energy from each atom). (CC-BY-NC-SA, Kathryn Haas)

Now, to see how this molecular orbital diagram can explain the magnetic behaviour of O_2, complete the example below.

Example 5.2.1.1

Let's change Figure 5.2.1.1 to make it specific for O_2. Re-draw the MO diagram (no need to draw the shapes of orbitals). Fill in the correct number of electrons for each oxygen atom on either side of the diagram. Then, fill in the total molecular electrons in the center. Calculate the bond order and determine whether it is diamagnetic or paramagnetic.

Solution

The diagram in Figure 5.2.1.1 includes core orbitals (the 1s) and valence electrons (2s, 2p). Therefore, we will consider all the electrons in an oxygen atom and a dioxygen molecule. An oxygen atom has eight total electrons. So we fill eight electrons into the atomic orbitals for the oxygen atom on the right, and eight electrons into the atomic orbitals for oxygen on the left. The total number of electrons for the molecule is sixteen, so fill in 16 electrons into the molecular orbitals, being sure to apply Hund's rule and the Aufbau principle. The result is a diagram that looks like the one drawn below in Figure 5.2.1.2.

The bond order is calculated using the molecular orbitals (we can ignore atomic orbitals). There are 10 electrons in binding orbitals and 6 electrons in antibonding orbitals). This gives a bond order of $\frac{1}{2}(10-6)=2$. This bond order is consistent with valence bond theory!

This diagram indicates that dioxygen is paramagnetic; it has two unpaired electrons in the π^* orbitals. This paramagnetic electron configuration explains why dioxygen is attacted to magnetic fields!

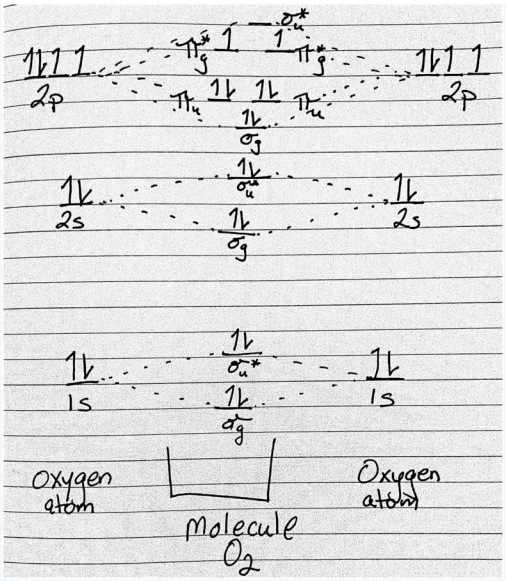


Figure 5.2.1.2: Hand-drawn molecular orbital diagram for dioxygen. (CC-BY-SA; Kathryn Haas)

Exercise 5.2.1.1

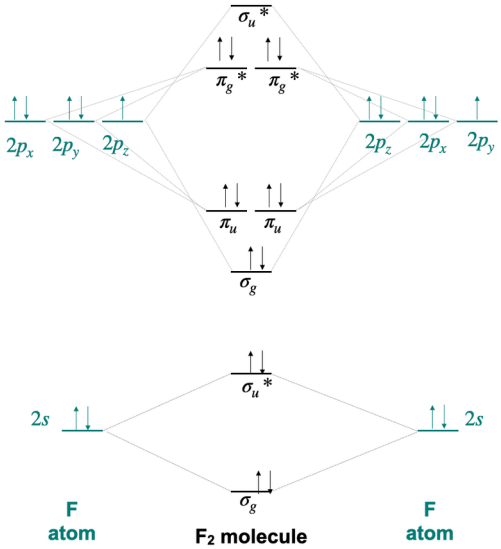
Draw the molecular orbital diagram for F_2; be sure to label your orbitals with the appropriate symmetry and count your orbitals to make sure that the total number of atomic orbitals and molecular orbitals is the same. As a shortcut, include only the valence orbitals and electrons. What is the bond order? Is the molecule diamagnetic or paramagnetic?

Answer available at the end of this section.

Answers

Exercise 5.2.1.1

The valence orbitals on an F atom are 2s and 2p. And, there are seven valence electrons in F. This gives fourteen total valence electrons. The MO diagram of the valence molecular orbitals can be constructed by combining the valence 2s and valence 2p orbitals from each F atom. The bond order is 1 and the molecule is diamagnetic.



This page titled 5.2.1: Molecular Orbitals is shared under a CC BY-SA 4.0 license and was authored, remixed, and/or curated by Kathryn Haas.

- 5.2.1: Molecular Orbitals by Kathryn Haas is licensed CC BY-SA 4.0.

5.2.2: Orbital Mixing

In the previous section, we introduced a simplified molecular orbital (MO) diagram, assuming that interactions were limited to degenerate orbitals of compatible symmetry. A version of that *simplified* diagram for second-row homonuclear diatomics is shown on the left side of Figure $5.2.2.1$ (only valence orbitals shown).

In reality, orbitals of compatible symmetry can combine, or mix, even when they have different energies. When sets of orbitals mix, it has the effect of decreasing the energy of the lower-energy set and increasing the energy of the higher-energy set. There are two ways to explain mixing, described in the points below. The diagram on the right of side of Figure $5.2.2.1$ shows how energy levels are affected by orbital mixing.

- **Starting from the simplified MO diagram and mixing molecular orbitals of like symmetry**: If we start with the "no mixing" simplified diagram shown on the left, we can pick out the orbitals with like symmetry and consider what will happen if these molecular orbitals mix. For example, starting from the MO diagram on the left side of Figure $5.2.2.1$, we see that there are two σ_g orbitals that have identical symmetry (hence they have identical symmetry labels). Upon mixing, the lower-energy $\sigma_g(2s)$ will decrease in energy while the higher-energy $\sigma_g(2p)$ will increase in energy. Likewise, there are two σ_u^* orbitals that will mix, decreasing the energy of $\sigma_u^*(2s)$ while increasing the energy of $\sigma_u^*(2p)$.
- **Starting from and mixing atomic orbitals of compatible symmetry**: Starting from the atomic orbitals, we can select the orbitals that have compatible symmetry to make productive interactions, and combine them as a set to make molecular orbitals. From the two sets of atomic orbitals on the right panel in Figure $5.2.2.1$, there are two sets of four orbitals with compatable symmetry; one is the set of two $2s$ and two $2p_z$ orbitals. These four orbitals can combine to form molecular orbitals with σ symmetry. They combine to form one lowest-energy bonding σ_g, a highest-energy σ_u^*, and two orbitals with intermediate energy (σ_g, and σ_u^*). This treatment can be expressed as the linear combination of four atomic orbitals:

  $$\Psi = c_1\psi\,(2s_a) \pm c_2\psi\,(2s_b) \pm c_3\psi\,(2p_a) \pm c_4\psi\,(2p_b)$$

  where the coefficients $c_1 = c_2$ and $c_3 = c_4$ for homonuclear diatomic molecules.

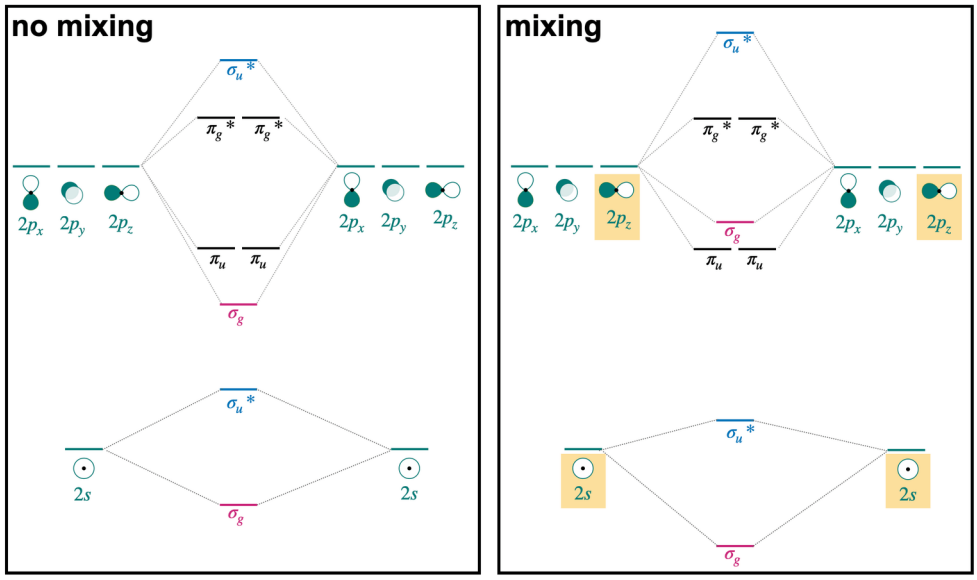


Figure $5.2.2.1$: Mixing of orbitals with like symmetry affects the energies of molecular orbitals. The simplified case where no mixing occurs is shown on the left. The effects of mixing are shown on the right. The σ_g orbitals of like symmetry are highlighted in fuschia and the σ_u^* orbitals of like symmetry are highlighted in blue. A group of atomic orbitals of similar symmetry are highlighted in yellow boxes; these atomic orbitals combine to give all σ molecular orbitals. (CC-BY-SA, Kathryn Haas)

In the case of homonuclear diatomic molecules of the second row, orbital mixing has important consequences for the energetic order of the $\sigma_g(2p)$ and $\pi_u(2p)$ orbitals. This will be discussed in the next section.

This page titled 5.2.2: Orbital Mixing is shared under a CC BY-SA 4.0 license and was authored, remixed, and/or curated by Kathryn Haas.

- 5.2.2: Orbital Mixing by Kathryn Haas is licensed CC BY-SA 4.0.

5.2.3: Diatomic Molecules of the First and Second Periods

First Period Homonuclear Diatomic Molecules

In the first row of the periodic table, the valence atomic orbitals are $1s$. There are two possible homonuclear diatomic molecules of the first period:

Dihydrogen, H_2 $[\sigma_g^2(1s)]$: This is the simplest diatomic molecule. It has only two molecular orbitals (σ_g and σ_u^*), two electrons, a bond order of 1, and is diamagnetic. Its bond length is 74 pm. MO theory would lead us to expect bond order to decrease and bond length to increase if we either add or subtract one electron. The calculated bond length for the H_2^+ ion is approximately 105 pm.[1]

Dihelium, He_2 $[\sigma_g^2\sigma_u^{*2}(1s)]$: This molecule has a bond order of zero due to equal number of electrons in bonding and antibonding orbitals. Like other nobel gases, He exists in the atomic form and does not form bonds at ordinary temperatures and pressures.

Exercise 5.2.3.1

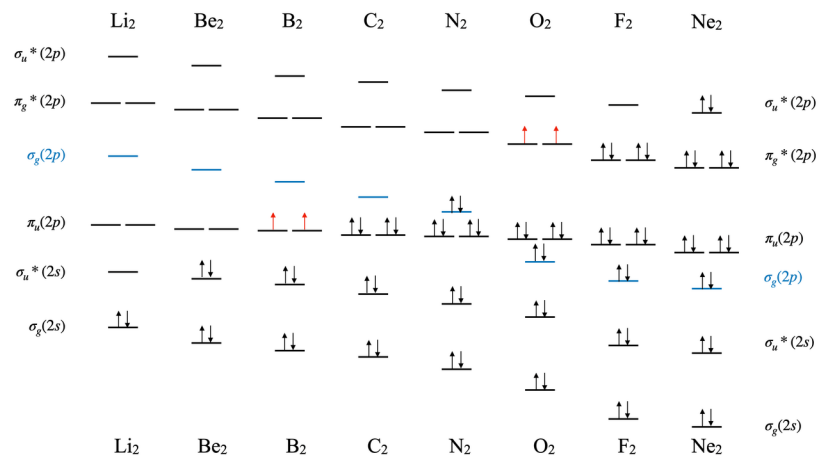
Draw the complete molecular orbital diagrams for H_2 and for He_2. Include sketches of the atomic and molecular orbitals.

Answer available at the end of this section.

Second Period Homonuclear Diatomic Molecules

The second period elements span from Li to Ne. The valence orbitals are 2s and 2p. In their molecular orbital diagrams, non-valence orbitals (1s in this case) are often disregarded in molecular orbital diagrams.

Orbital mixing has significant consequences for the magnetic and spectroscopic properties of second period homonuclear diatomic molecules because it affects the order of filling of the $\sigma_g(2p)$ and $\pi_u(2p)$ orbitals. Early in period 2 (up to and including nitrogen), the $\pi_u(2p)$ orbitals are lower in energy than the $\sigma_g(2p)$ (see Figure 5.2.3.1). However, later in period 2, the $\sigma_g(2p)$ orbitals are pulled to a lower energy. This lowering in energy of $\sigma_g(2p)$ is not unique; all of the σ orbitals in the molecule are pulled to lower energy due to the increasing positive charge of the nucleus. The π orbitals in the molecule are also affected, but to a much lesser extent than σ orbitals. The reason has to do with the high penetration of s atomic orbitals compared to p atomic orbitals (recall our previous discussion on penetration and shielding, and its effect on periodic trends). The σ molecular orbitals have more s character and thus their energy is more influenced by increasing nuclear charge. As nuclear charge increases, the energy of the $\sigma_g(2p)$ orbital is lowered significantly more than the energy of the $\pi_u(2p)$ orbitals (Figure 5.2.3.1).



	Li_2	Be_2	B_2	C_2	N_2	O_2	F_2	Ne_2
Unpaired e^-	0	0	2	0	0	2	0	0
Bond Order	1	0	1	2	3	2	1	0
Experimental* Bond Length (pm)	267.3	246.0	159.0	124.3	109.8	120.8	141.2	310.0

*Experimental bond lengths from "List of Experimental Diatomic Bond Lengths", NIST, https://cccbdb.nist.gov/diatomicexpbondx.asp

Figure 5.2.3.1: Molecular orbital energy-level diagrams for the diatomic molecules of the period 2 elements. Unlike earlier diagrams, *only the valence molecular orbital energy levels for the **molecules** are shown here (atomic orbitals not shown for simplicity).* For Li_2 through N_2, the $\sigma_g(2p)$ orbital is higher in energy than the $\pi_u(2p)$ orbitals. In contrast, from O_2 onward, the $\sigma_g(2p)$ orbital is *lower* in energy than the $\pi_u(2p)$ orbitals because the nuclear charge increases across the row. The experimental bond lengths correlate with the calculated bond order. (CC-BY-NC-SA, Kathryn Haas)

Dilithium, Li_2 $[\sigma_g^2(2s)]$**:** This molecule has a bond order of one and is observed experimentally in the gas phase to have one Li-Li bond.

Diberylium, Be_2 $[\sigma_g^2\sigma_u^{*2}(2s)]$**:** This molecule has a bond order of zero due to the equal number of electrons in bonding and antibonding orbitals. Although Be_2 does not exist under ordinary conditions, it can be produced in a laboratory and its bond length measured (Figure 5.2.3.2). Although the bond is very weak, its bond length is surprisingly ordinary for a covalent bond of the second period elements.[2]

Diboron, B_2 $[\sigma_g^2\sigma_u^{*2}(2s)\pi_u^1\pi_u^1(2p)]$**:** The case of diboron is one that is much better described by molecular orbital theory than by Lewis structures or valence bond theory. This molecule has a bond order of one. The molecular orbital description of diboron also predicts, accurately, that diboron is paramagnetic. The paramagnetism is a consequence of orbital mixing, resulting in the σ_g orbital's being at a higher energy than the two degenerate π_u^* orbitals.

Dicarbon, C_2 $[\sigma_g^2\sigma_u^{*2}(2s)\pi_u^2\pi_u^2(2p)]$**:** This molecule has a bond order of two. Molecular orbital theory predicts two bonds with π symmetry, and no σ bonding. C_2 is rare in nature because its allotrope, diamond, is much more stable.

Dinitrogen, N_2 $[\sigma_g^2\sigma_u^{*2}(2s)\pi_u^2\pi_u^2\sigma_g^2(2p)]$**:** This molecule is predicted to have a triple bond. This prediction is consistent with its short bond length and bond dissociation energy. The energies of the $\sigma_g(2p)$ and $\pi_u(2p)$ orbitals are very close, and their relative energy levels have been a subject of some debate (see next section for discussion).

Dioxygen, O_2 $[\sigma_g^2\sigma_u^{*2}(2s)\sigma_g^2\pi_u^2\pi_u^2\pi_g^{*1}\pi_g^{*1}(2p)]$**:** This is another case where valence bond theory fails to predict actual properties. Molecular orbital theory correctly predicts that dioxygen is paramagnetic, with a bond order of two. Here, the molecular orbital diagram returns to its "normal" order of orbitals where orbital mixing could be somewhat ignored, and where $\sigma_g(2p)$ is lower in energy than $\pi_u(2p)$.

Difluorine, F_2 $[\sigma_g^2\sigma_u^{*2}(2s)\sigma_g^2\pi_u^2\pi_u^2\pi_g^{*2}\pi_g^{*2}(2p)]$**:** This molecule has a bond order of one and like oxygen, the $\sigma_g(2p)$ is lower in energy than $\pi_u(2p)$.

Dineon, Ne_2 $[\sigma_g^2\sigma_u^{*2}(2s)\sigma_g^2\pi_u^2\pi_u^2\pi_g^{*2}\pi_g^{*2}\sigma_u^{*2}(2p)]$**:** Like other noble gases, Ne exists in the atomic form and does not form bonds at ordinary temperatures and pressures. Like Be_2, Ne_2 is an unstable species that has been created in extreme laboratory conditions and its bond length has been measured (Figure 5.2.3.2)

Exercise 5.2.3.2

Draw the complete molecular orbital diagram for O_2. Show calculation of its bond order and tell whether it is diamagnetic or paramagnetic.

Answer available at the end of this section.

Exercise 5.2.3.3: The Peroxide Ion

Use a qualitative molecular orbital energy-level diagram to predict the electron configuration, the bond order, and the number of unpaired electrons in the peroxide ion (O_2^{2-}).

Answer available at the end of this section.

Bond Lengths in Homonuclear Diatomic Molecules

The trends in experimental bond lengths are predicted by molecular orbital theory, specifically by the calculated bond order. The values of bond order and experimental bond lengths for the second period diatomic molecules are given in Figure 5.2.3.1, and shown in graphical format on the plot in Figure 5.2.3.2. From the plot, we can see that bond length correlates well with bond order, with a minimum bond length occurring where the bond order is greatest (N_2). The shortest bond distance is at N_2 due to its high bond order of 3. From N_2 to F_2 the bond distance increases despite the fact that atomic radius decreases.

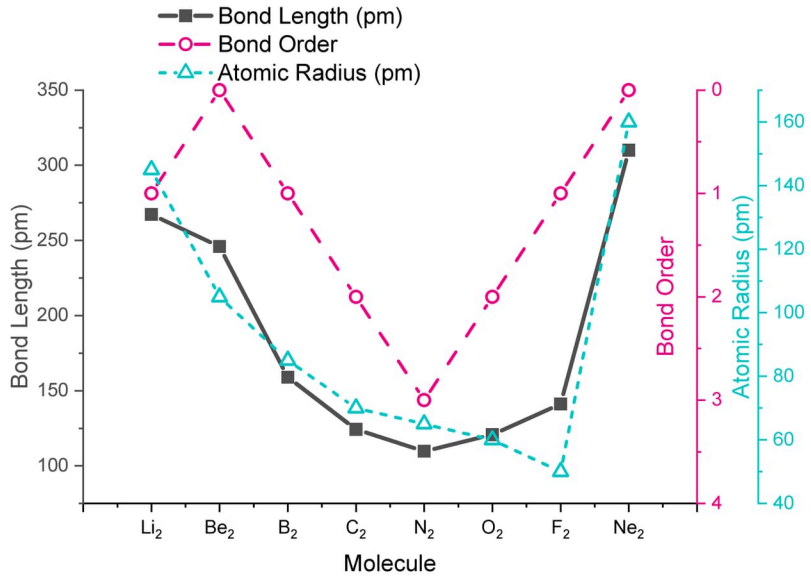


Figure 5.2.3.2: Overlayed plots of bond length (black squares), bond order (pink circles), and atomic radius (teal triangles) versus atomic number for second period homonuclear diatomic molecules. (CC-BY-NC-SA; Kathryn Haas)

References

1. NIST, Calculated Geometries available for H_2^+ (Hydrogen cation) 2Σg+ D∞h, available at https://cccbdb.nist.gov/diatomicexpbondx.asp
2. Merritt, J. M.; Bondybey, V. E.; Heaven, M. C., Beryllium Dimer-Caught in the Act of Bonding. *Science* **2009,** *324* (5934), 1548-1551.

Answers

Exercise 5.2.3.1

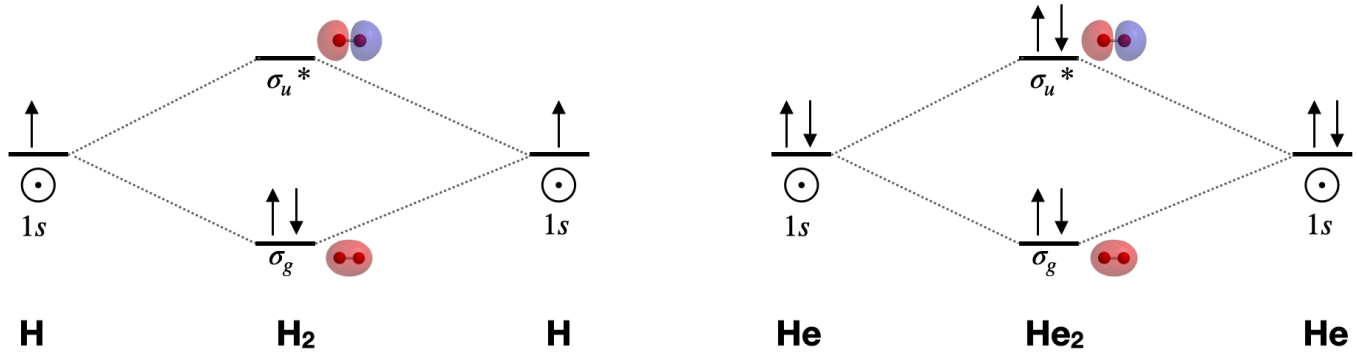


Figure for Exercise 5.2.3.1: Molecular orbital diagrams for dihydrogen and dihelium. Molecular orbital surfaces calculated using Spartan software. (CC-BY-NC-SA; Kathryn Haas)

A complete molecular orbital diagram includes all atomic orbitals and molecular orbitals, their symmetry labels, and electron filling.

Exercise 5.2.3.2

O_2 is paramagnetic with a bond order of 2. Its $\sigma_g(2p)$ molecular orbital is lower in energy that the set of $\pi_u(2p)$ orbitals.

Bond order $= \frac{1}{2}\left[\left(\begin{array}{c}\text{8 electrons in}\\ \text{valence bonding orbitals}\end{array}\right) - \left(\begin{array}{c}\text{4 electrons in}\\ \text{valence antibonding orbitals}\end{array}\right)\right]$

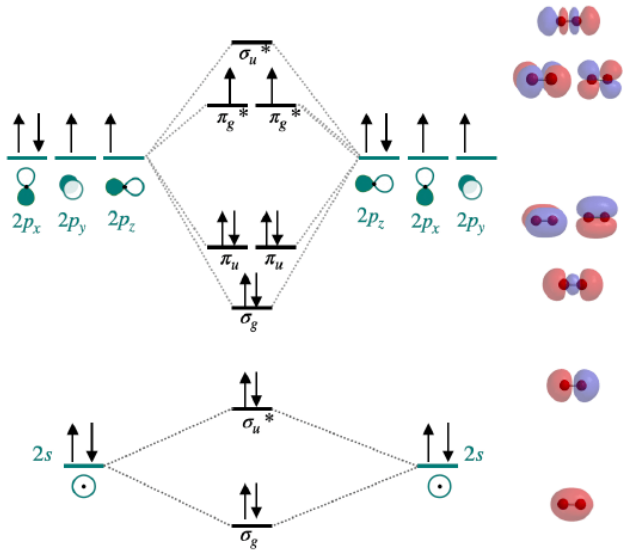


Figure for Exercise 5.2.3.2. Molecular orbital diagram of O_2. (CC-BY-NC-SA, Kathryn Haas)

Exercise 5.2.3.3**: The Peroxide Ion**

This diagram looks similar to that of O_2, except that there are two additional electrons.
$(\sigma_g(2s))^2 (\sigma_u^*(2s))^2 (\sigma_g(2p))^2 (\pi_u(2p))^4 (\pi_g(2p))^4$; bond order of 1; no unpaired electrons.

This page titled 5.2.3: Diatomic Molecules of the First and Second Periods is shared under a CC BY-SA 4.0 license and was authored, remixed, and/or curated by Kathryn Haas.

- 5.2.3: Diatomic Molecules of the First and Second Periods by Kathryn Haas is licensed CC BY-SA 4.0.
- 5.P: Problems is licensed CC BY-SA 4.0.

5.2.4: Photoelectron Spectroscopy

A photoelectron spectrum can show the relative energies of occupied molecular orbitals by ionization. The *ionization energy* is a direct measure of the energy required to just remove the electron concerned from its initial level to the vacuum level (free electron). Photoelectron spectroscopy measures the relative energies of the ground and excited positive ion states that are obtained by removal of single electrons from the neutral molecule.

$$A + \text{photon} \rightarrow A^+ + e^-$$

The information obtained from photoelectron spectroscopy is typically discussed in terms of the electronic structure and bonding in the ground states of neutral molecules, with ionization of electrons occurring from bonding molecular orbitals, lone pairs, antibonding molecular orbitals, or atomic cores. These descriptions reflect the relationship of ionization energies to the molecular orbital model of electronic structure.

Ionization energies are directly related to the energies of molecular orbitals (by Koopmans' theorem).

Example: Photoelectron spectrum of dihydrogen

The molecular orbital description of dihydrogen involves two $1s$ atomic orbitals generating two molecular orbitals: a bonding σ_g and an antibonding σ_u^*. The two electrons occupy the σ_g bonding orbital, leaving the molecule with a bond order of one (Figure $5.2.4.1$). The PES spectrum of dihydrogen (Figure $5.2.4.1$) has a single band that corresponds to the ionization of one electron from the σ_g. The multiple peaks are due to electrons ejecting from a range of stimulated vibrational energy levels. When extensive vibrational structure is resolved in a PES molecular orbital, then the removal of an electron from that molecular orbital induces a significant change in the bonding (in this case an increase in the bond length due to decrease in bond order).

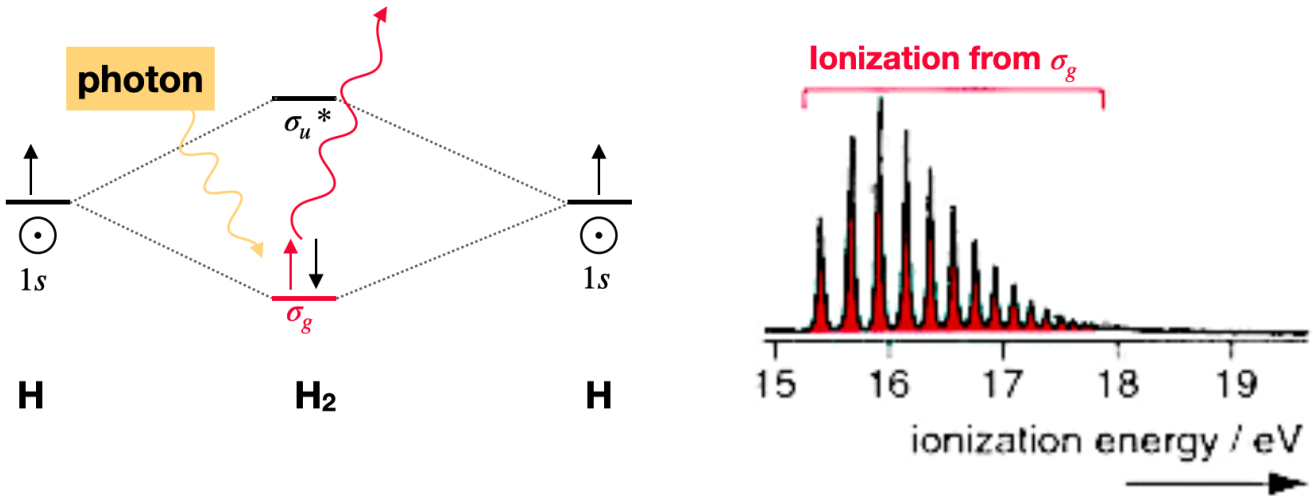


Figure $5.2.4.1$: The molecular orbital diagram and photoelectron spectrum of dihydrogen. (CC-BY-NC-SA; Libretexts)

Example: Photoelectron spectrum of dinitrogen

Diatomic nitrogen is more complex than hydrogen since multiple molecular orbitals are occupied. Five molecular orbitals are occupied; two of them are degenerate. Three bands in the photoelectron spectrum correspond to ionization of an electron in $\sigma_g(2p)$, $\pi_u(2p)$ and $\sigma_u^*(2s)$ molecular orbitals. Ionization of the fourth type of orbital, $\sigma_g(2s)$, does not appear in Figure $5.2.4.2$ because it is either off scale or because the incident light $h\nu$ used did not have sufficient energy to ionize electrons in that deeply stabilized molecular orbital. Note that extensive vibrational structure for the $\pi_u(2p)$ band indicates that the removal of an electron from this molecular orbital causes a significant change in the bonding.

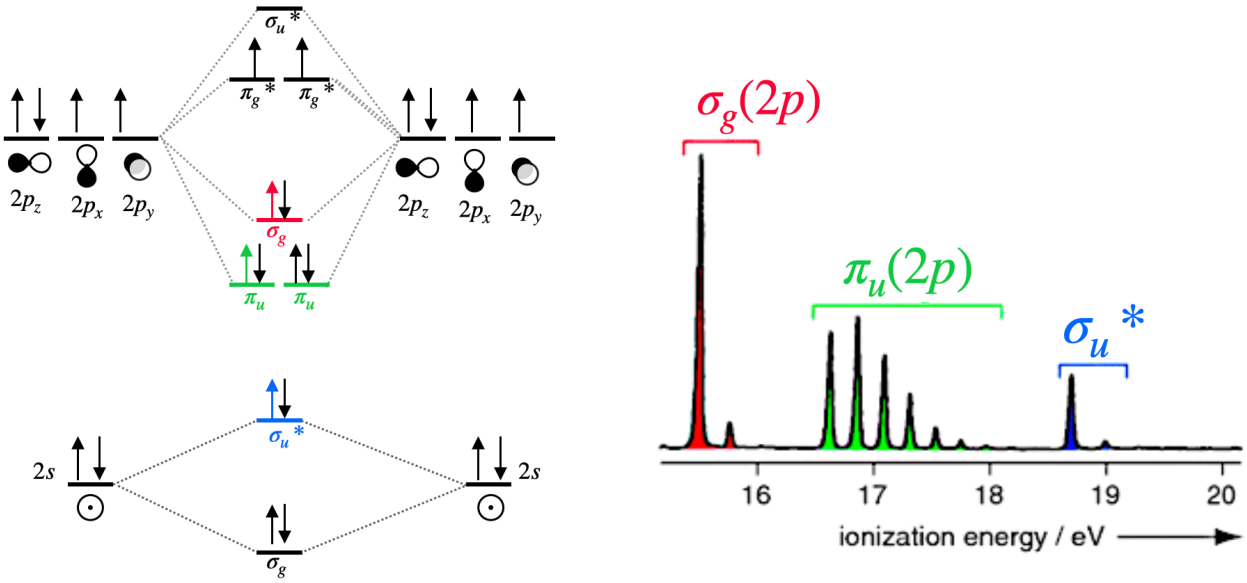


Figure 5.2.4.2: The molecular orbital diagram and photoelectron spectrum of dinitrogen. (CC-BY-NC-SA; Libretexts)

From the photoelectron spectrum of dinitrogen, we can see that the electrons in the $\sigma_g(2p)$ orbital can be ionized using less energy than required to ionize electrons in the $\pi_u(2p)$ orbital. This is evidence for $\sigma_g(2p)$ existing at a higher energy than the $\pi_u(2p)$ orbitals.

This page titled 5.2.4: Photoelectron Spectroscopy is shared under a CC BY-SA 4.0 license and was authored, remixed, and/or curated by Kathryn Haas.

- 10.4: Photoelectron Spectroscopy by Roger Nix is licensed CC BY 4.0.

5.3: HETERONUCLEAR DIATOMIC MOLECULES

Diatomic molecules with two non-identical atoms are called **heteronuclear** diatomic molecules. When atoms are not identical, the molecule forms by combining atomic orbitals of unequal energies. *The result is a polar bond in which atomic orbitals contribute unevenly to each molecular orbital.*

The application of molecular orbital theory to heteronuclear diatomic molecules is similar to the case of homonuclear diatomics, except that the atomic orbitals from each atom have different energies and contribute unequally to molecular orbitals. Recall that atomic orbitals must have compatible symmetry and similar energy to combine into molecular orbitals. In the case where atomic orbitals of like symmetry have different energies, they combine less favorably than orbitals that are closer to one another in energy. As a general rule, orbitals that have energy differences of greater than 10-14 eV do not combine favorably. In the molecular orbital diagram, the closer a molecular orbital is to an atomic orbital, the more that atomic orbital contributes to the molecular orbital. This last point is helpful for back-of-the napkin estimations of what the molecular orbitals "look" like.

In this section, you should learn how to generate molecular orbital diagrams of heteronuclear diatomic molecules. To approach such a problem, we must start with a knowledge of the relative energies of electrons in different atomic orbitals. In other words, we need knowledge of the orbital potential energies (or orbital ionization energies).

5.3.1: Orbital ionization energies

5.3.2: Polar bonds

5.3.3: Ionic Compounds and Molecular Orbitals

Sources:

- Gray, Harry. *Electrons and Chemical Bonding*, Benjamin, 1964.
- Miessler, Gary L, and Donald A. Tarr. *Inorganic Chemistry*. Upper Saddle River, N.J: Pearson Education, 2014. Print.

This page titled 5.3: Heteronuclear Diatomic Molecules is shared under a CC BY-SA 4.0 license and was authored, remixed, and/or curated by Kathryn Haas.

- 5.3: Heteronuclear Diatomic Molecules by Kathryn Haas is licensed CC BY-SA 4.0.

5.3.1: Orbital ionization energies

To generate molecular orbital diagrams of heteronuclear diatomic molecules, we must start with a knowledge of the relative energies of electrons in different atomic orbitals. In other words, we need knowledge of the orbital potential energies (or orbital ionization energies).

Orbital Ionization Energies

There are two approaches you can use to "know" or estimate the atomic orbital energy levels.

1. Use a table of atomic orbital ionization energies, like those found in Table 5.3.1.1.
2. When you do not have access to a table of values like the one below, use periodic trends in electronegativity and/or ionization energies as your guide to approximate relative values for different atoms.

Table 5.3.1.1: These are one-electron ionization energies of the valence orbitals calculated by average energies of both the ground-state and ionized-state configurations. (From Harry Gray, “Electrons and Chemical Bonding,” Benjamin, 1964, Appendix) Values are expressed in eV.



This page titled 5.3.1: Orbital ionization energies is shared under a CC BY-SA 4.0 license and was authored, remixed, and/or curated by Kathryn Haas.

- 5.3: Heteronuclear Diatomic Molecules by Kathryn Haas is licensed CC BY-SA 4.0.

5.3.2: Polar bonds

Molecular orbital diagrams for heteronuclear diatomic molecules

The molecular orbital diagram of a heteronuclear diatomic molecule is approached in a way similar to that of a homonuclear diatomic molecule. The orbital diagrams may also look similar. A major difference is that the more electronegative atom will have orbitals at a lower energy level. Two examples of heteronuclear diatomic molecules will be explored below as illustrative examples.

Carbon monoxide MO diagram

Carbon monoxide is an example of a heteronuclear diatomic molecule where both atoms are second-row elements. The valence molecular orbitals in both atoms are the $2s$ and $2p$ orbitals. The molecular orbital diagram for carbon monoxide (Figure $5.3.2.1$) is constructed in a way similar to how you would construct dicarbon or dioxygen, except that the oxygen orbitals have a lower potential energy than analogous carbon orbitals. The labeling of molecular orbitals in this diagram follows a convention by which orbitals are given serial labels according to type of orbital (σ, π, etc.). The lowest energy orbitals of any type are assigned a value of 1 and higher energy orbitals of the same type are assigned by increasing intervals (..2, 3, 4...). The orbital labeling system described previously is inappropriate for heteronuclear diatomic molecules that cannot be assigned g and u subscripts.

A consequence of unequal atomic orbital energy levels is that orbital mixing is significant. Notice the order of the molecular orbitals labeled 1π and 3σ in Figure $5.3.2.1$. This is a similar order of π and σ orbitals to the one we saw in the case of the σ_g and π_u orbitals of N_2 and lighter diatomics of the second period. Because the oxygen $2p_z$ orbital is close in energy to both the carbon $2p_z$ and carbon $2s$, these three orbitals will have significant interaction (mixing). The result is an increase in the energy of the 3σ orbital and a decrease in energy of the $2\sigma^*$ orbital, resulting in the diagram shown in Figure $5.3.2.1$.

In the case of carbon monoxide (Figure $5.3.2.1$), atomic orbitals contribute unequally to each molecular orbital. For example, because the $2s$ orbital of oxygen is very close in energy to the 2σ moelcular orbital, it contributes to that molecular orbital more than the $2s$ orbital from carbon. Notice the shape of this 2σ orbital and how it is unevenly distributed over the two atoms; it is more heavily distributed on the oxygen because it is most like the oxygen $2s$. This is in line with the assumption that electron density is distributed more on oxygen because it is more electronegative than carbon. Likewise, the 1π orbitals are unevenly distributed, with more distribution close to the oxygen.

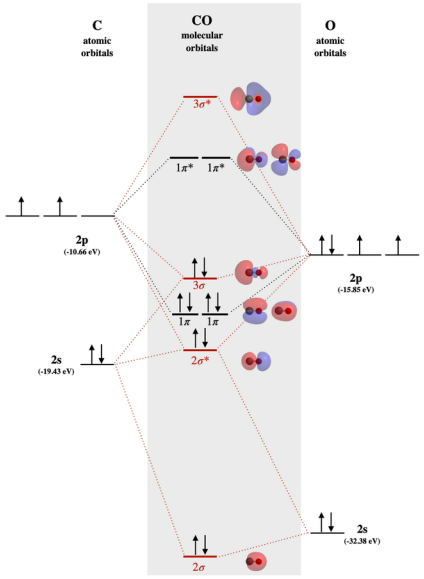
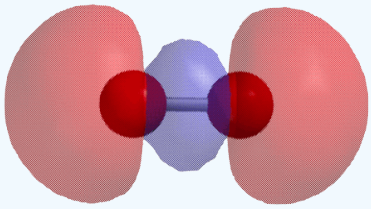


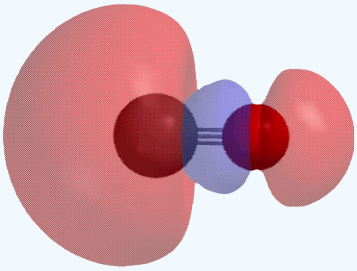
Figure $5.3.2.1$: Molecular orbital diagram of carbon monoxide. The labeling of molecular orbitals in this diagram follows a convention by which orbitals are given serial names according to the type of orbital (σ, π, etc.). The lowest energy orbitals of any type are assigned a value of 1 and higher energy orbitals of the same type are assigned by increasing intervals (..2, 3, 4...). The orbital labeling system described previously is inappropriate for heteronuclear diatomic molecules that cannot be assigned g and u subscripts. Molecular orbital surfaces were calculated using Spartan software. (Kathryn Haas, CC-BY-NC-SA)

Exercise 5.3.2.1

Examine the shape of the 3σ orbital of carbon monoxide in Figure 5.3.2.1. Describe what ways this shape is different from the shape of the σ_g orbitals from second period homonuclear diatomic molecules (see Fig. 5.2.1.1). Rationalize these differences. Both orbitals are re-created below for convenience.



σ_g of homonuclear diatomic



3σ of CO

Answer available at the end of this section.

Hydrogen fluoride MO diagram

Hydrogen fluoride is an example of a heteronuclear diatomic molecule in which the two atoms are from different periods. In this case, the valence orbital of H is $1s$ while those of F are $2s$ and $2p$. The molecular orbital diagram for HF is shown in Figure 5.3.2.2.

Three of these orbitals have compatible symmetry for mixing; these are the hydrogen $1s$, fluorine $2s$, and fluorine $2p$. However, the extent to which they will interact depends on their relative energies. Fluorine is more electronegative than H, and the fluorine atom has a higher first ionization energy than does hydrogen. From these trends, we can expect that the fluorine valence orbitals are lower in energy than that of hydrogen. From Table 5.3.1, we find that the 1s orbital of H (-13.6 eV) is higher in energy than both fluorine orbitals (-18.7 and -40.2 eV, respectively for $2p$ and $2s$). The energies of hydrogen $1s$ and fluorine $2p$ are a good match for combination; however, the fluorine $2s$ orbital is much too different to create a productive interaction. Therefore, we expect that the fluorine $2s$ will create a non-bonding molecular orbital, while the $1s$ and $2p_z$ orbitals combine to make σ bonding and σ^* antibonding molecular orbitals. The remaining $2p_x$ and $2p_y$ orbitals do not have compatible symmetry for bonding with hydrogen, and they will form non-bonding π molecular orbitals. The non-bonding orbitals will have similar energy and character as their component atomic orbitals.

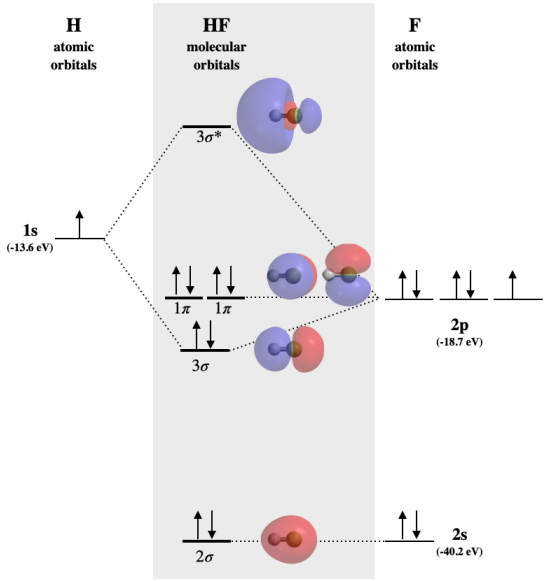


Figure 5.3.2.2: Molecular Orbital diagram of hydrogen fluoride. Molecular orbitals calculated using Spartan software. (Kathryn Haas, CC-BY-NC-SA)

Chemical reactions take place at the HOMO and LUMO orbitals

Knowledge of molecular orbital diagrams, and the shapes of molecular orbitals, can be used to accurately explain and predict chemical reactivity. Chemical reactions take place using the highest occupied molecular orbitals (HOMO) of a nucleophile or Lewis base, and the lowest unoccupied molecular orbital (LUMO) of an electrophile or Lewis acid.

> Lewis bases react using electrons in the HOMO, while Lewis acids react using the empty LUMO.

Example: Reactivity of CO with metal ions

CO is an excellent ligand for many metal ions. In fact, the strong affinity between CO and the heme iron (Fe) ions in hemoglobin can explain the mechanism of carbon monoxide poisoning. When CO binds in place of O_2 to hemoglobin, that hemoglobin can no longer carry O_2 to tissue cells. CO binding to hemoglobin is strong and practically irreversible. When CO binds to metal ions, it does so through the carbon atom. This is contrary to expectations based on the Lewis structure and the known bond polarity, where electron density is polarized toward oxygen. The distribution of the electron density of the HOMO of CO can explain this observation!

Exercise 5.3.2.2

Refer to the MO diagram for CO. Identify the HOMO and explain why CO bonds to metal ions through the carbon atom rather than through the oxygen atom.

Answer available at the end of this section.

Answers

Exercise 5.3.2.1

The 3σ orbital is like the σ_g in that it has three lobes and two nodes distributed along the internuclear bond. They are different in their distribution. The two external lobes of σ_g are evenly distributed because they are an equal combination of two p_z orbitals (one from each atom). The 3σ orbital is more heavily distributed toward the carbon atom, the less electronegative atom, than toward the oxygen. The unequal distribution of 3σ is apparent in the unequal sizes of its exterior lobes and the uneven shape of the interior lobe. The heavier distribution within the exterior lobe on carbon is caused by the mixing of the carbon $2s$ orbital with carbon and oxygen $2p_z$ orbitals. The uneven shape of the interior lobe, where it leans toward oxygen, is best explained by the fact that the 3σ orbital is closer in energy to the oxygen $2p_z$ than the carbon $2p_z$.

Exercise 5.3.2.2

In the interaction between CO and a metal ion, CO would act as a Lewis base; thus it will react using electrons in its HOMO. The MO diagram for CO is shown in

Figure 5.3.2.1: the HOMO is the 3σ orbital (also discussed in Exercise 5.3.2.1). The electron density of that MO is centered around the carbon atom, thus the carbon atom will be a better Lewis base than the O atom.

This page titled 5.3.2: Polar bonds is shared under a CC BY-SA 4.0 license and was authored, remixed, and/or curated by Kathryn Haas.

- 5.3.2: Polar bonds by Kathryn Haas is licensed CC BY-SA 4.0.

5.3.3: Ionic Compounds and Molecular Orbitals

Ionic interactions lie at one extreme on a spectrum of bonding. On the opposite end of the spectrum are the non-polar covalent bonds (e.g., homonuclear diatomics). In these molecules, molecular orbitals are formed by equal-energy atomic orbitals, resulting in electron density evenly distributed over the molecule. In the middle of the spectrum are the cases of polar covalent bonds (e.g., heteronuclear diatomics), in which atomic orbitals of unequal energies contribute unequally to molecular orbitals, resulting in uneven distribution of electron density across the molecule. In the case of polar bonds, the electron density is shifted toward the more electronegative atom since that atom contributes more to the lowest energy bonding molecular orbitals. Molecular orbital diagrams can be drawn for ionic compounds as if they are extremely polar bonds in which electrons are not only shifted toward, but are transferred completely to the more electronegative atom.

Example: NaCl

In NaCl, the sodium $3s$ orbital (-5.2 eV) is significantly higher in energy than the chlorine valence orbitals. The chlorine $3s$ and $3p_z$ orbitals have compatible symmetry, yet only the $3p_z$ orbital (-13.8 eV) is close enough in energy to interact with the Na $3s$; still, the energy difference is large enough to make bonding weak. The Na $3s$ orbital combines with Cl $3p_z$ to form the molecular orbitals labeled 4σ and $4\sigma^*$ in Figure $5.3.3.1$. The 4σ orbital is weakly bonding, but is very close in energy to the Cl $3p_z$ orbital, and is mostly Cl-like in character. Notice that all σ orbitals look very much like either s or p orbitals centered on the Cl atom, while the $4\sigma^*$ orbital is centered almost entirely on Na. The lack of molecular orbitals that are distributed over both atoms at once is consistent with a lack of significant covalent bond character in NaCl. The bonding here is characterized by transfer of one electron from Na to Cl and is almost entirely electrostatic. Bonding that is mostly electrostatic in character is non-directional, unlike true covalent bonding.

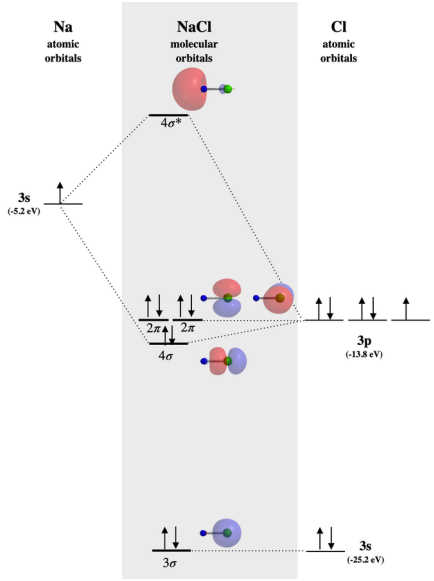


Figure $5.3.3.1$: The molecular orbital diagram for sodium chloride. Molecular orbital surfaces calculated using Spartan software indicate almost no covalent nature of bonding. (CC-BY-NC-SA, Kathryn Haas)

Exercise $5.3.3.1$

Draw the molecular orbital diagram for LiF. Make sure to label all molecular orbitals appropriately, and specify whether they are mostly bonding, non-bonding, or antibonding. Identify the HOMO and LUMO. Sketch the approximate shapes of all orbitals.

Answer available at the end of this section.

Answers

Exercise 5.3.3.1

We expect LiF to be an ionic compound because the energy difference in valence orbitals is at least 10-14 eV. (See Table 5.3.1) There are a variety of ways used to label molecular orbitals. In the figure below, we are using the convention of labeling each type of orbital with numbers starting from the lowest-energy orbitals. The 1σ orbital would be mostly F $1s$ in character and is not shown. The 2σ orbital is mostly non-bonding in nature, although it has a very small contribution from $2s$ of Li due to compatible symmetry. The 3σ orbital is slightly bonding but it is mostly F$2p$ in character. The two 1π orbitals are completely non-bonding. The $3\sigma^*$ orbital is antibonding.

- HOMO is 1π
- LUMO is $3\sigma^*$

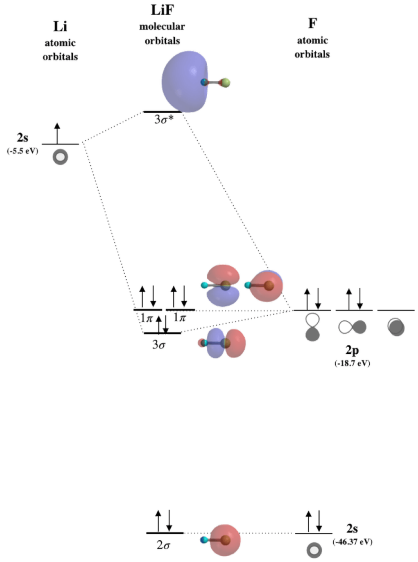


Figure for Exercise 5.3.3.1: Molecular orbital diagram for the ionic compund, LiF. (CC-BY-NC-SA, Kathryn Haas)

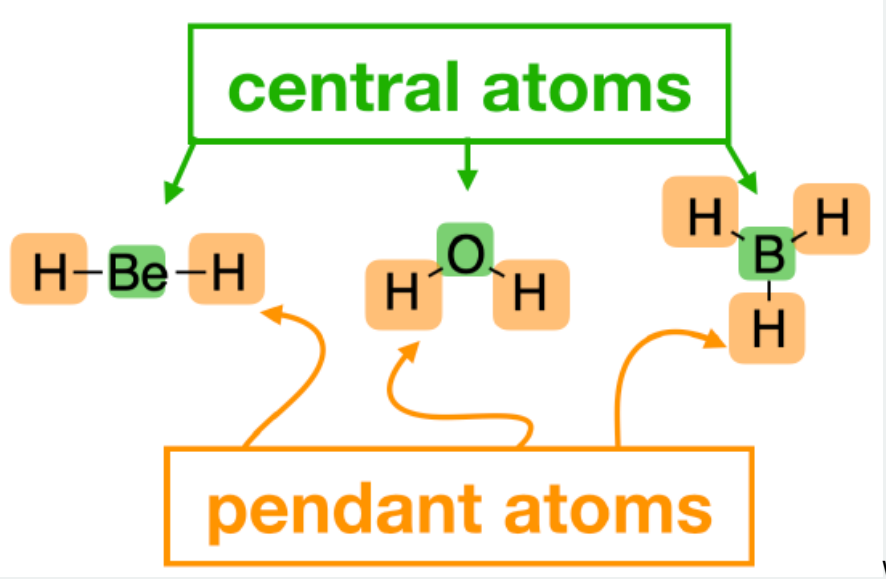
This page titled 5.3.3: Ionic Compounds and Molecular Orbitals is shared under a CC BY-SA 4.0 license and was authored, remixed, and/or curated by Kathryn Haas.

- 5.3.3: Ionic Compounds and Molecular Orbitals by Kathryn Haas is licensed CC BY-SA 4.0.

5.4: LARGER (POLYATOMIC) MOLECULES

We can extend the method we used for diatomic molecules to draw the molecular orbitals of more complicated, polyatomic molecules (molecules with more than two atoms). To combine several different atoms in a molecular orbital diagram, we will group orbitals from different atoms into sets that match the symmetry of a central atom. These **group orbitals** are also referred to as **symmetry adapted linear combinations (SALCs)**. We'll use a stepwise approach to do this as summarized below.

Symmetry adapted linear combinations (SALCs)



We need SALCs (aka group orbitals) to draw molecular orbital (MO) diagrams of *polyatomic* molecules. SALCs are groups of orbitals on **pendant atoms**. These groups of orbitals much match the symmetry of valence orbitals on the **central atom** in order to create a productive interaction. When we combine SALCs with the atomic orbitals on the central atom, we can generate an MO diagram that gives us information about the molecule's bonding and electronic states.

Below is a set of steps you can follow to find SALCs and draw an MO Diagram. Each step will be illustrated in detail through the examples in the subsections that follow this page.

1. Find the **point group** of the molecule and assign Cartesian coordinates so that z is the principal axis.
   Sometimes we can simplify things by looking only at the point group of the relevant orbitals. Only simplify when instructed to do so.*
2. Identify and count the pendant atoms' valence orbitals.
   Is there more than 1 type for each atom (ex. just s, or s and p?) We expect 1 SALC for each ligand orbital.
3. Generate a **reducible representation (Γ)** for the group of pendant atom orbitals using the appropriate character table.
   You have to do this for each set of orbital types. If you only have s orbitals for each ligand, you only need to generate 1 reducible representation. If you have p orbitals, you would generate additional Γ's for p_x, p_y, and p_z.
4. Break the Γ into its component **irreducible representations** from the character table. Note the symmetry of each irreducible representation, its associated orbitals, and their degeneracy.
5. If you are asked to sketch the shapes of SALCs, determine what they "look like" using one of the following strategies.
   (a) Shortcut: if the reducible representations are listed with s, p, or d orbitals in the character table, just draw them (... and skip steps b-c)
   (b) Systematic (Projection Operator) method: Draw an expanded character table and draw your molecule with each ligand identified by letters or numbers (*a,b,c...* or *i,j,k...* or *1,2,3...*) Determine where each pendant atom/orbital ends up under each of the operations of your expanded table. Project the values for each irreducible representation onto the chart you created and then add up the values. Positive and negative values are opposite signed orbitals.

6. Draw the MO diagram by combining SALCs with AO's of like symmetry. When drawing SALC energy levels, remember that the more nodal planes in your SALC orbital drawing, the higher the energy for that SALC orbital.

** When we are focused on orbitals, as in the case for finding group orbitals and drawing molecular orbital diagrams, the symmetry of the orbitals is what we are interested in. In the case of high-symmetry point groups, like $D_{\infty h}$ and $C_{\infty v}$, even though the molecule may have a C_∞ axis, the orbitals do not necessarily retain this symmetry element. For example, the p_x orbital would not have a C_∞ axis, but rather a C_2 axis. It is sufficient and useful to substitute D_{2h} for $D_{\infty h}$ and C_{2v} for $C_{\infty v}$ to simplify the problem.*

5.4.1: Bifluoride anion

5.4.2: Carbon Dioxide

5.4.3: H_2O

5.4.4: NH_3

5.4.5: CO_2 (Revisted with Projection Operators)

5.4.6: BF_3

This page titled 5.4: Larger (Polyatomic) Molecules is shared under a CC BY-SA 4.0 license and was authored, remixed, and/or curated by LibreTexts.

- 5.4: Larger (Polyatomic) Molecules is licensed CC BY-SA 4.0.

5.4.1: Bifluoride anion

Finding SALCs and drawing the MO diagram for [F-H-F]$^-$

The linear anion [F-H-F]$^-$ is a good place to start as an example to illustrate the process of generating pendant atom SALCs and then constructing a molecular orbital diagram for a polyatomic molecule. We will proceed using the steps outlined on the previous page for generating SALCs and a molecular orbital diagram.

Step 1. Find the point group of the molecule and assign Cartesian coordinates so that z is the principal axis.

We begin by assigning the appropriate point group for this molecule: $D_{\infty h}$ (Figure $5.4.1.1$). As mentioned in the previous page, it is useful to substitute D_{2h} for $D_{\infty h}$ when generating SALCs and molecular orbital diagrams. The z axis is assigned to be colinear with the principal axis, and in this case is the same as the C_∞ axis (Figure $5.4.1.1$).

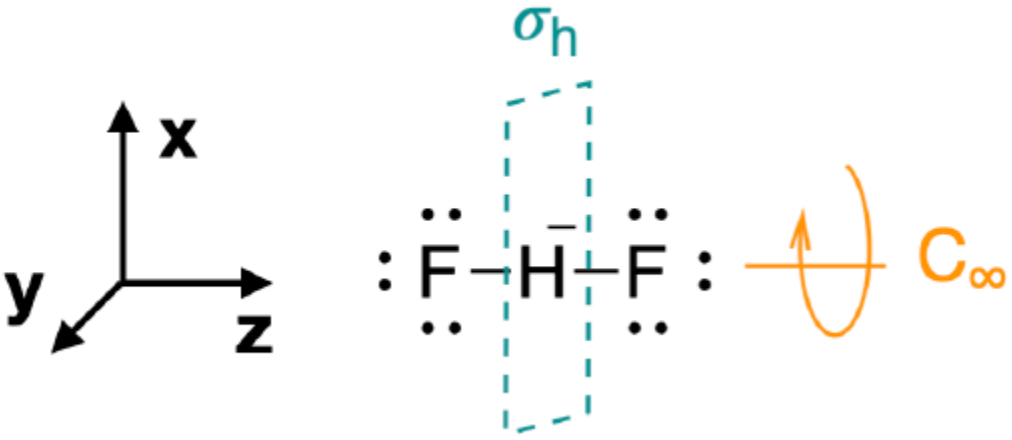


Figure $5.4.1.1$: The [FHF]$^-$ anion belongs to the $D\infty_h$ point group. (CC-BY-NC-SA; Kathryn Haas)

Step 2. Identify and count the pendant atoms' valence orbitals.

The next step is to identify the valence orbitals on the pendant F atoms that will form SALCs. In most cases, you should consider all of the valence orbitals. In this case, each of the fluorine atoms has four valence orbitals ($2s$, $2p_x$, $2p_y$, and $2p_z$). From these eight fluorine valence orbitals, we should expect eight group orbitals (SALCs).

3. - 5. Generate SALCS (shortcut)

To draw these SALCs for this molecule is rather simple, and we don't need to follow all the steps of finding the Γ's and reducing them. Rather, you can proceed as if you are creating bonding and antibonding molecular orbitals between the two F atoms, except that the F orbitals are separated by the H atom. Approximate sketches of the eight SALCs from F valence orbitals are shown in Figure $5.4.1.2$.

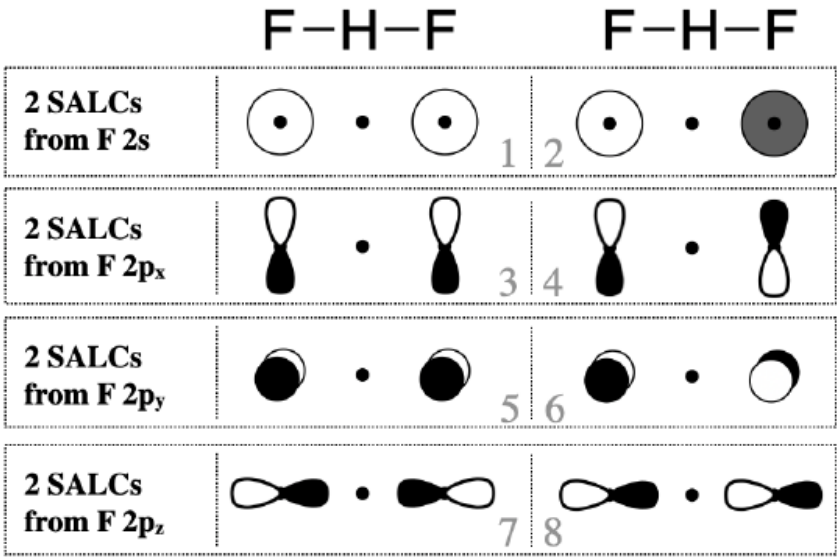


Figure 5.4.1.2: Eight SALCs from the valence orbitals of two fluorine atoms. (CC-BY-NC-SA; Kathryn Haas)

6. Draw the MO diagram by combining SALCs with AO's of like symmetry.

SALCs can productively interact with the central atom only when symmetry is compatible. Just some of the groups of orbitals in Figure 5.4.1.2 possess appropriate symmetry to combine with the hydrogen atom valence orbital (the H $1s$). In this simple case, you can decide whether orbitals have compatible symmetry by visually inspecting the shapes of the group orbitals. The F $2p_y$ and $2p_x$ orbitals do not have appropriate symmetry to bond to the H $1s$ orbital because the nodes of these orbitals run through the center of the H $1s$ orbital, thus we can eliminate all SALCs composed from F $2p_x$ and $2p_y$ (*these are SALCs numbered 3-6 in Figure* 5.4.1.2). On the other hand, the F $2s$ and $2p_z$ orbitals individually do have appropriate shape and direction in space for productive interaction with an H $1s$ orbital. However only SALCs where the *entire group* has appropriate symmetry will combine with H $1s$ to produce bonding or antibonding molecular orbitals. Only the SALCs labeled with numbers 1 and 7 can combine with an s orbital in the center of the group. The ways in which these SALCs are able to combine with H $1s$ are illustrated in Figure 5.4.1.3.

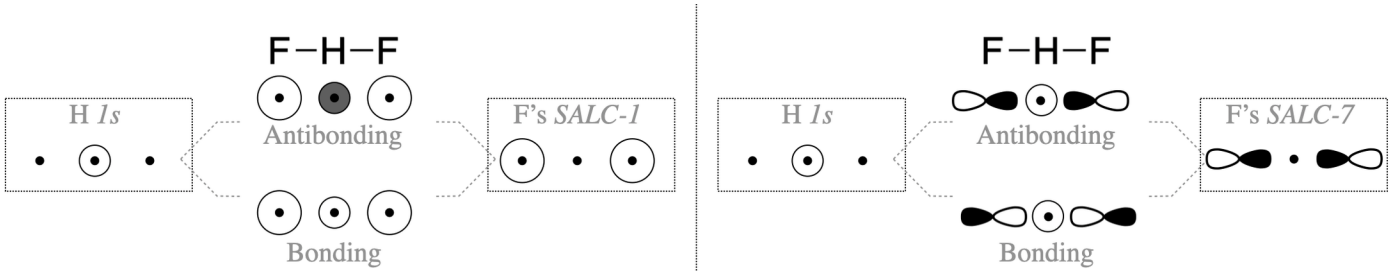


Figure 5.4.1.3: Combinations of a central H $1s$ orbital with the group orbitals, SALC-1 and SALC-7 from Figure 5.4.1.2, to create bonding and antibonding interactions. (CC-BY-NC-SA; Kathryn Haas)

Before we assume that both SALC-1 and SALC-7 will combine with the H $1s$ orbital, we must consider the energies of all atomic orbitals. The F $2p_z$ orbital has a potential energy of -18.7 eV (see Table 5.3.1). This is a good match for the H $1s$ orbital (-13.6 eV). However, the F $2s$ orbital has a much lower energy of -46.37 eV and would have weak interaction with the H $1s$.

The molecular orbital diagram for [F-H-F]$^-$ is shown in Figure 5.4.1.4. Notice that all atomic orbitals, group orbitals (SALCs), and molecular orbitals in Figure 5.4.1.4 are assigned a symmetry label that corresponds to each element's symmetry under the D_{2h} point group. The molecular orbital labels correspond to **lower-case Mulliken Labels** of individual reducible representations from the D_{2h} character table. Upper-case symbols are used to indicate symmetry and irreducible representations, while lower-case symbols are used to indicate the identity of an orbital with that symmetry. The labeling methods described for simple diatomic linear molecules (σ, π) are not sufficient to indicate the more complex symmetries of the molecular orbitals in polyatomic molecules. The use of lower-case Mulliken symbols is the most rigorous way to label the orbitals. Refer to your instructor for how you should label orbitals for any graded work.

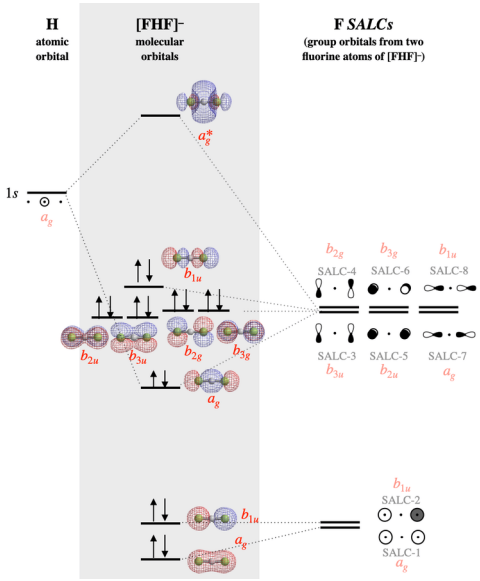
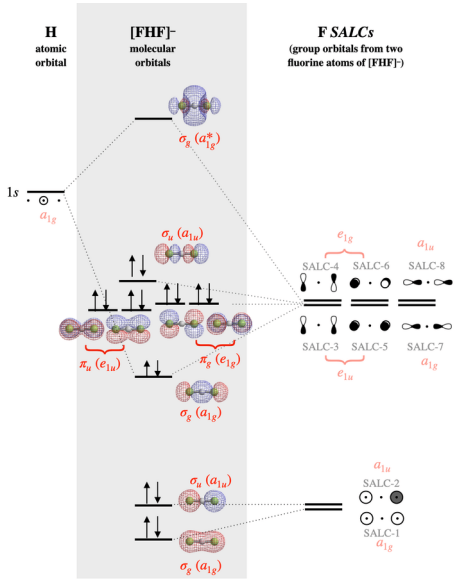


Figure 5.4.1.4:The molecular orbital diagram for $[F\text{-}H\text{-}F]^-$. The molecular orbital surfaces and relative energy levels were calculated using Spartan software. SALCs are labeled according to numbers assigned in Figure 5.4.1.2. The symmetry of each SALC and orbital under the D_{2h} **point group** is shown in red font. (CC-BY-NC-SA; Kathryn Haas)

Click here for a version of Figure 5.4.1.4 using $D_{\infty h}$ labeling:

For high-symmetry groups, a shortcut is to use a lower-symmetry group that maintains the critical symmetry elements. In the case of the $D_{\infty h}$ point group, it is often sufficient to use the approximation of the D_{2h} point group and character table. This is the same MO diagram as shown above, but using the symmetry labels appropriate for the D_{2h} approximation.



Alternate Figure 5.4.1.4: The molecular orbital diagram for $[F\text{-}H\text{-}F]^-$. The molecular orbital surfaces and relative energy levels were calculated using Spartan software. SALCs are labeled according to numbers assigned in Figure 5.4.1.2. The symmetry of each SALC and orbital under the D_{2h} **point group** is shown in red font. (CC-BY-NC-SA; Kathryn Haas)

Constructing the MO diagram

After identifying the atomic orbitals and constructing SALCs, place the atomic orbitals of H on one side of the diagram and all SALCs from F on the other side. Molecular orbitals are in the center.

The lowest-energy fluorine SALCs will be those composed of the lowest-energy atomic orbitals of fluorine; these would be SALC-1 (a_{1g}) and SALC-2 (a_{1u}) that are constructed from fluorine s atomic orbitals. Of these two orbitals, the one with zero nodes would be slightly lower in energy than the one with one node. When these two orbitals form molecular orbitals, the completely symmetric SALC-1 will be mostly non-bonding with slight bonding character from minor combination with the hydrogen $1s$ orbital. SALC-2, however is symmetrically incompatible with hydrogen $1s$ and will be a truly non-bonding orbital distributed over both F atoms.

The six SALCs constructed of fluorine p orbitals will have higher energy since the fluorine p atomic orbitals are higher in energy than the s orbitals (SALC-3 through SALC-8). Again, we expect SALCs with more nodes (SALC-4, -6, -8) to have slightly higher energy than those with fewer nodes (SALC-3, -5, -7). SALC-7 will form a bonding and antibonding interaction with the hydrogen $1s$ orbital. All other SALCS are truly non-bonding, but are non-degenerate non-bonding orbitals.

In bifluoride, there is an important distinction between the Lewis structure and molecular orbital description of lone pairs. In Lewis theory, the lone pairs are localized to individual fluorine atoms, while in the molecular orbital description each lone pair is distributed over both fluorine atoms at once (see surface depiction of each molecular orbital in Figure $5.4.1.4$).

This page titled 5.4.1: Bifluoride anion is shared under a CC BY-SA 4.0 license and was authored, remixed, and/or curated by LibreTexts.

- 5.4.1: Bifluoride anion is licensed CC BY-SA 4.0.

5.4.2: Carbon Dioxide

Construct SALCs and the molecular orbital diagram for CO_2

Carbon dioxide is another linear molecule. This example is slightly more complex than the previous example of the bifluoride anion. While bifluoride had only one valence orbital to consider in its central H atom (the $1s$ orbital), carbon dioxide has a larger central atom, and thus more valence orbitals that will interact with SALCs.

Preliminary Steps

Step 1. Find the point group of the molecule and assign Cartesian coordinates so that z is the principal axis.

The CO_2 molecule is linear and its point group is $D_{\infty h}$. The z axis is collinear with the C_∞ axis. We will use the D_{2h} point group as a substitute since the orbital symmetries are retained in the D_{2h} point group.

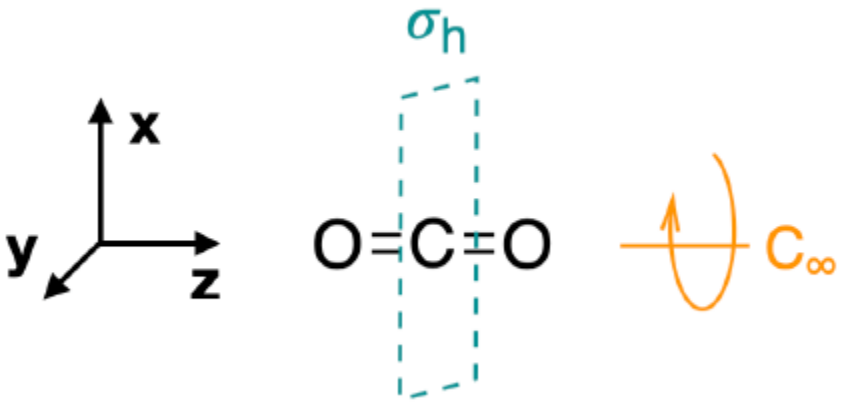


Figure $5.4.2.1$: CO_2 belongs to the $D_{\infty h}$ point group. (CC_BY-NC-SA; Kathryn Haas)

Step 2. Identify and count the pendant atoms' valence orbitals.

Each of the two pendant oxygen atoms has four valence orbitals; $2s$, $2p_x$, $2p_y$, and $2p_z$. Thus, we can expect a total of eight SALCs.

Generate SALCs

The SALCs for CO_2 are identical in shape and symmetry to those described in the previous example for the bifluoride anion. But instead of cutting to the shortcut, we will systematically derive the SALCs here to demonstrate the process.

Step 3. Generate the Γ's

Use the D_{2h} character table to generate four reducible representations ($\Gamma's$); one for each of the four types of pendant atom orbitals ($s,\ p_x,\ p_y,\ p_z$). For each s orbital, assign a value of 1 if it remains in place during the operation or zero if it moves out of its original place. For each p orbital, assign 1 if there is no change, -1 if it remains in place but is inverted, and 0 if it moves out of its original position. The four Γ's are given below:



Step 4. Break Γ's into irreducible representations for individual SALCs

Reduce each Γ into its component irreducible representations. There are two strategies that can be used to do this. The quick and easy way is to do it "by inspection", but this only works well for simple cases. The other is by using the systematic approach for breaking a Γ into reducible representations described previously in section 4.4.2 using the following formula:

$$\text{number of } i = \frac{1}{h}\sum(\text{number of operations in class}) \times (\chi_\Gamma) \times (\chi_i) \tag{5.4.2.1}$$

In other words, the number of irreducible representations of type i is equal to the sum of the number of operations in the class $\times$ the character of the Γ_{modes} $\times$ the character of i, and that sum is divided by the order of the group (h).

Using either approach results in the following eight irreducible representations ($2A_g + 2B_{1u} + B_{2g} + B_{3u} + B_{3g} + B_{2u}$):



Step 5. Sketch the SALCs

From the systematic process above, you have found the symmetries (the irreducible representations) of all eight SALCs under the D_{2h} point group. To sketch the SALC that corresponds to each irreducible representation, again we use the D_{2h} character table, and specifically the functions listed on the right side columns of the table.

Two A_g SALCs (one from s and one from p_z): The A_g SALCs are each singly degenerate and symmetric with respect to both the principal axis (z) and the inversion center (i) (based on its Mulliken Label). We can look at the functions in the D_{2h} character table that correspond to A_g and see that it is completely symmetric under the group (because the combination of x^2, y^2, z^2 shows that it is totally symmetric). This would be the same symmetry as an s orbital on the central atom. From this information, we know that these SALCs must have symmetry compatible with an s orbital on the central atom, and we can draw the two A_g SALCs shown in Figure 5.4.2.2.

Two B_{1u} SALCs (one from s and one from p_z): The Mulliken Label tells us that the B_{1u} SALCs are each antisymmetric with respect to both the principal axis and the inversion center. The function, z, appearing with B_{1u} in the character table tells us that these SALCs have the same symmetry as the z axis, or a p_z orbital on the central atom. From this information, we know that these two SALCs should be compatible with a p_z orbital on the central atom, and we can draw the two B_{1u} SALCs shown in Figure 5.4.2.2 .

All other SALCs shown below are derived using a strategy similar to the one in the two cases described above.

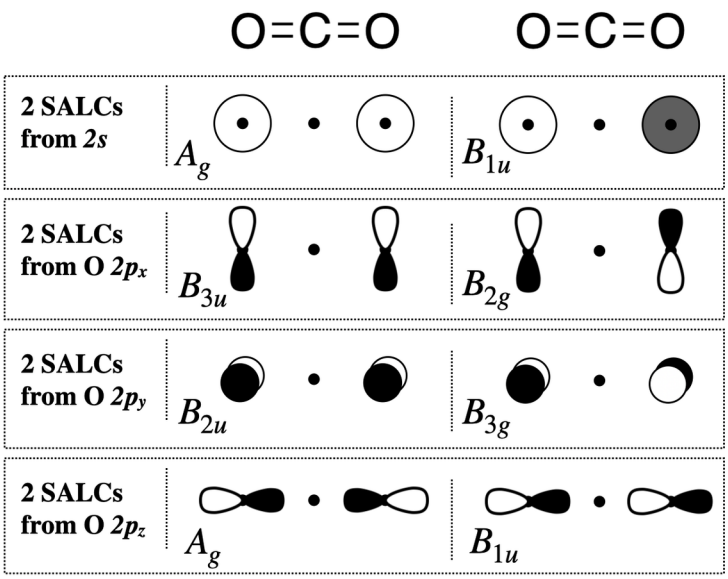


Figure 5.4.2.2: SALCs from the valence orbitals of oxygen atoms in CO_2. (CC-BY-NC-SA; Kathryn Haas)

Draw the MO diagram for CO_2

Step 6. Combine SALCs with AO's of like symmetry.

First we identify the valence orbitals on carbon: there are four including $2s$, $2p_x$, $2p_y$, and $2p_z$. Now we identify the symmetry of each using the D_{2h} character table. The symmetry of a central s orbital corresponds to the combination of functions x^2, y^2, and z^2 in the character table; this is A_g. The p_z orbital corresponds to the symmetry of the linear function z in the character table; this is B_{1u}. And so on... The symmetries of the C valence orbitals are listed below.

$$2s = A_g$$
$$2p_x = B_{3u}$$
$$2p_y = B_{2u}$$
$$2p_z = B_{1u}$$

Now that we have identified the symmetries of the eight oxygen SALCs and the four valence orbitals on carbon, we know which atomic orbitals and SALCs may combine based on compatible symmetries. We also need to know the relative orbital energy levels so that we can predict the relative strength of orbital interactions. The orbital ionization energies are listed in Section 5.3.

With knowledge of both orbital symmetries and energies, we can construct the molecular orbital diagram. The carbon atom goes on one side of the diagram while the oxygen SALCs are drawn on the opposite side. Molecular orbitals are drawn in the center column of the diagram:

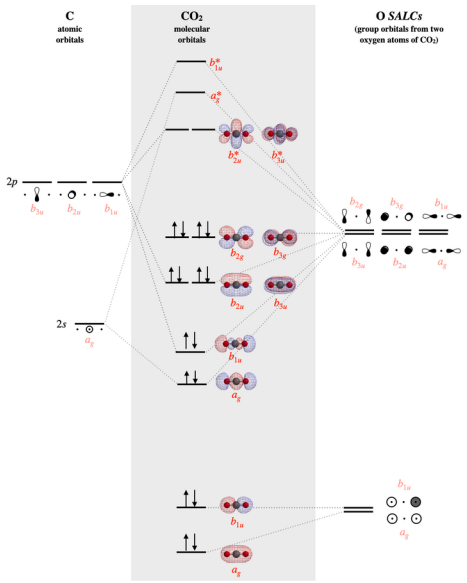


Figure 5.4.2.3: Molecular orbital diagram for carbon dioxide. (CC-BY-NC-SA; Kathryn Haas)

The SALCs on the right side of the diagram above are constructed from groups of either the $2s$ atomic orbitals of oxygen, or the $2p$ atomic orbitals of oxygen. Each SALC will combine with the atomic orbitals of carbon that have compatible symmetry; but the strength of the interaction depends on their relative energies. The individual valence atomic orbitals of oxygen have energies of $-32.36eV$ ($2s$) and $-15.87eV$ ($2p$), while the valence orbitals of carbon have energies of $-19.47eV$ ($2s$) and $-10.66eV$ ($2p$). The $2s$ orbitals of the oxygen are far lower in energy ($-32.36eV$) than all other valence orbitals, and so we should expect that molecular orbitals that are constructed from these oxygen $2s$ will be mostly non-bonding. These mostly non-bonding orbitals are the a_{1g} and b_{1g} orbitals shown at the bottom of Figure 5.4.2.3. The a_g orbital is lower in energy than the b_{1u} due to slight mixing with other orbitals of a_g symmetry.

The bonding orbitals of CO_2 include two $sigma$ molecular orbitals of a_g and b_{1u} symmetry and two π molecular orbitals of b_{2u} and b_{3u} symmetry. Each of these bonding molecular orbitals possesses a higher-energy antibonding partner. The b_{2g} and b_{3g} SALCs that are formed from oxygen $2p_x$ and $2p_y$ orbitals have no compatible match with carbon valence orbitals; thus they form two b_{2g} and b_{3g} molecular orbitals, which are truly non-bonding and mostly oxygen in character. Still, notice that each orbital is spread across both oxygen atoms at once, and again we see that each non-bonding electron pair in the HOMO is very different in molecular orbital theory compared to Lewis theory. Each non-bonding pair is distributed over both oxygen atoms at once in molecular orbital theory, while in Lewis theory each lone pair is isolated to one atom or to localized bonds attached to that atom.

This page titled 5.4.2: Carbon Dioxide is shared under a CC BY-SA 4.0 license and was authored, remixed, and/or curated by Kathryn Haas.

- 5.4.2: Carbon Dioxide by Kathryn Haas is licensed CC BY-SA 4.0.

5.4.3: H_2O

Construct SALCs and the molecular orbital diagram for H_2O.

This is the first example so far that is not a linear molecule. Water is a bent molecule, and so it is important to remember that interactions of pendant ligands are dependent on their positions in space. You should consider the positions of the three atoms in water to be essentially fixed in relation to each other. The process for constructing the molecular orbital diagram *for a non-linear molecule*, like water, is similar to the process for linear molecules. We will walk through the steps below to construct the molecular orbital diagram of water.

Preliminary Steps

Step 1. Find the point group of the molecule and assign Cartesian coordinates so that z is the principal axis.

The H_2O molecule is bent and its point group is C_{2v}. The z axis is collinear with the principal axis, the C_2 axis. There is no need to simplify this problem, as we had done for previous examples. The C_{2v} point group is simple enough.

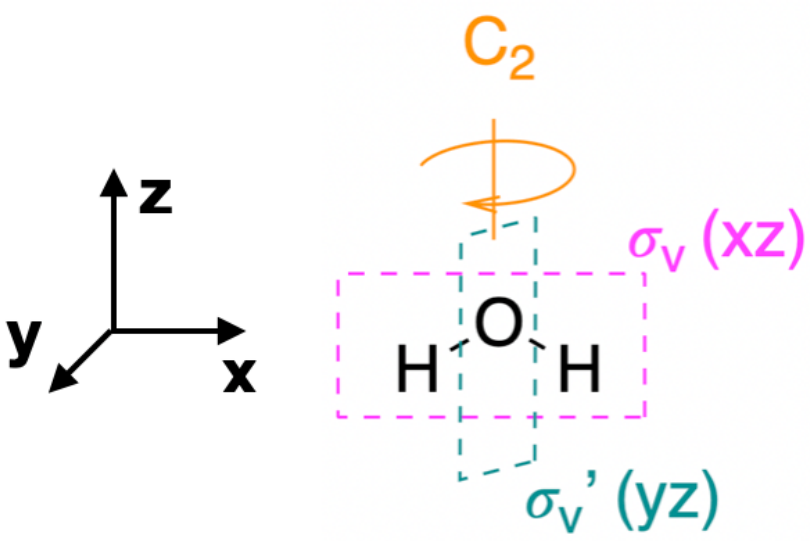


Figure 5.4.3.1: The water molecular is in the C_{2v} point group. (CC-BY-NC-SA; Kathryn Haas)

Step 2. Identify and count the pendant atoms' valence orbitals.

Each of the two pendant hydrogen atoms has one valence orbital, the $1s$. Thus, we can expect a total of two SALCs from these two atoms.

Generate SALCs

The SALCs for H_2O are quite simple, yet we will systematically derive the SALCs here to demonstrate the process.

Step 3. Generate the Γ's

Use the C_{2v} character table to generate one reducible representation (Γ); in this case we need only one Γ because there is only one type of valence orbital (the $1s$). For each s orbital, assign a value of 1 if it remains in place during the operation or zero if it

moves out of its original place. The Γ is given below:

[redacted]

Step 4. Break Γ's into irreducible representations for individual SALCs

Reduce each Γ into its component irreducible representations. Using either of the processes described previously, we find that the Γ reduces to the two irreducible representations A_1 and B_1 under the C_{2v} point group.

[redacted]

Step 5. Sketch the SALCs

From the systematic process above, you have found the symmetries (the irreducible representations) of both SALCs under the C_{2v} point group. To sketch the SALC that corresponds to each irreducible representation, again we use the C_{2v} character table, and specifically the functions listed on the right side columns of the table.

One A_1 SALC: The A_1 SALC is singly degenerate and symmetric with respect to both the principle axis (z) and the inversion center (i) (based on its Mulliken Label). We can look at the functions in the C_{2v} character table that correspond to A_1 and see that it is completely symmetric under the group (because the combination of x^2, y^2, z^2 shows that it is totally symmetric). This would be the same symmetry as an s orbital on the central oxygen atom. From this information, we know that this SALC must have symmetry compatible with an s orbital on the central atom. We can also see from the character table that the z axis, and thus a p_z orbital on oxygen, also possesses A_1 symmetry. This tells us that in addition to being compatible with the oxygen s orbital, it should also be compatible with the oxygen p_z orbital. From this information we can draw the A_1 SALC shown in Figure 5.4.3.2 . *If it is not obvious how the A_1 sketch in Fig. 5.4.3.2 is compatible with the s and p_z orbitals of oxygen, inspect the drawings corresponding to molecular orbitals $2a_1$ and $3a_1$ in Fig. 5.4.3.3.*

One B_1 SALC: The Mulliken Label tells us that the B_1 SALC is singly degenerate and antisymmetric with respect to both the principal axis and the inversion center. The function, x, appearing with B_1 in the character table tells us that this SALC has the same symmetry as the x axis, or a p_x orbital on the central oxygen atom. From this information, we know that this SALC should be compatible with a p_x orbital on the central atom, and we can draw the B_1 SALCs shown in Figure 5.4.3.2. *If it is not obvious how the B_1 sketch in Fig. 5.4.3.2 is compatible with the p_x orbital of oxygen, inspect the drawing corresponding to molecular orbital $1b_1$ in Fig. 5.4.3.3.*

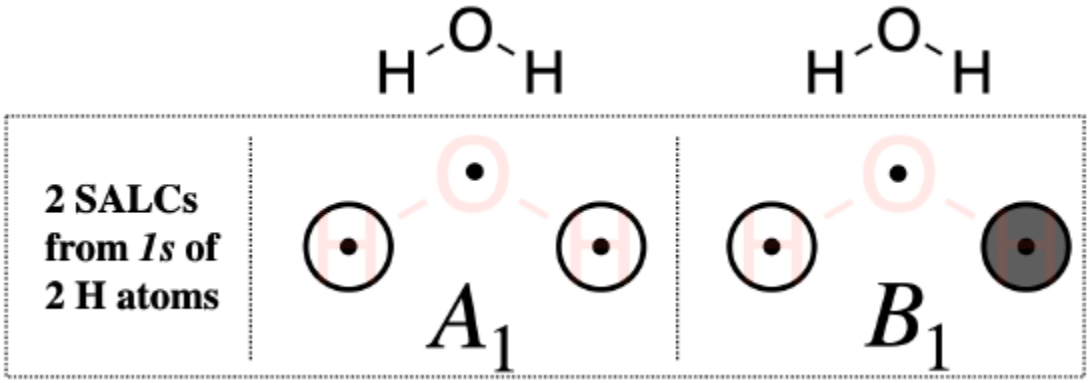


Figure 5.4.3.2: Sketch of the A_1 and B_1 hydrogen SALCs of water. (CC-BY-NC-SA; Kathryn Haas)

Not convinced about the sketches of these SALCs? You can convince yourself by putting them to the test. Try the exercise below.

Exercise 5.4.3.1

Perform all operations of the C_{2v} point group on the two sketches of H SALCs shown in Figure 5.4.3.2, and convince yourself that each sketch does possess the A_1 and B_1 symmetries assigned to them, respectively, under the C_{2v} point group.

Answer available at the end of this section.

Draw the MO diagram for H_2O

Step 6. Combine SALCs with AO's of like symmetry.

First we must identify the valence orbitals on the central oxygen: there are four including $2s$, $2p_x$, $2p_y$, and $2p_z$. Now we identify the symmetry of each using the C_{2v} character table. The symmetry of a central $2s$ orbital corresponds to the combination of functions x^2, y^2, and z^2 in the character table; this is A_1. The p_z orbital also corresponds to A_1. And so on... The symmetries of oxygen valence orbitals are listed below.

$$2s = A_1$$
$$2p_x = B_1$$
$$2p_y = B_2$$
$$2p_z = A_1$$

Now that we have identified the symmetries of the two hydrogen SALCs and the four valence orbitals on oxygen, we know which atomic orbitals and SALCs may combine based on compatible symmetries. We also need to know the relative orbital energy levels so that we can predict the relative strength of orbital interactions. The orbital ionization energies are listed in Section 5.3.1.

With knowledge of both orbital symmetries and energies, we can construct the molecular orbital diagram. The valence orbitals of oxygen go on one side of the diagram while the hydrogen group orbitals are drawn on the opposite side. Molecular orbitals are drawn in the center column of the diagram, as shown in Figure 5.4.3.3:

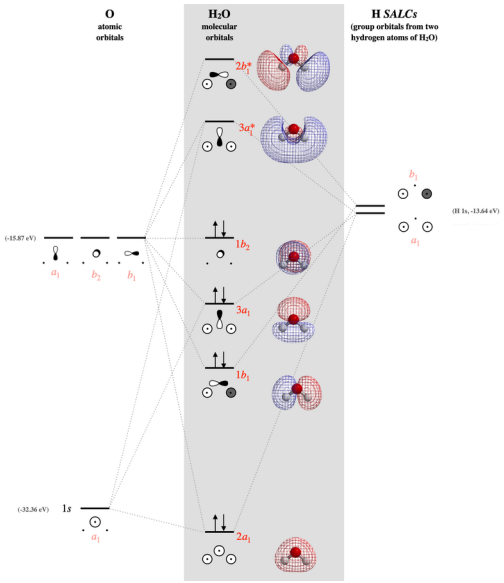


Figure 5.4.3.3: The molecular orbital diagram of water. Molecular orbital surfaces calculated using Spartan software. The surface of the $3a_1^*$ orbital has been trimmed. (CC-BY-NC-SA; Kathryn Haas)

Example 5.4.3.1

In the previous examples shown for the molecular orbital diagrams of the bifluoride anion and carbon dioxide, we discussed differences in the understanding of those molecules from molecular orbital theory compared to Lewis structures. Water contains two lone pairs in its Lewis structure. Compare the predictions about water's lone pairs of electrons and its reactivity based on (1) the combination of elementary models (Lewis, Valence Bond, and Hybridized Orbital theories) and (2) Molecular Orbital theory. Specifically address and explain how the elementary models differ from molecular orbital theory in the following respects:

a. Where are the lone pairs in water?
b. Are the two lone pairs equivalent or are they different?
c. Where are sites on the molecule that will undergo reaction with electrophiles and nucleophiles?

Solution

1) Elementary models: The Lewis structure predicts that two lone pairs are (a) localized on the oxygen atom of water and that (b) both lone pairs are equivalent. The Lewis structure, combined with Valence Bond Theory, would predict that lone pairs occupy two equivalent hybridized sp^3 atomic orbitals on oxygen. (c) Lewis theory would predict that the oxygen lone pairs are nucleophiles; thus an electrophile would react with the oxygen atom lone pairs. The polarized O-H bond leaves the H atoms as the most electrophilic locations on the water molecule; thus nucleophiles would react at the H atoms of water.

2) Molecular orbital theory: The molecular orbitals predict that (a) the two lone pairs of water are not equivalent, and that (b) each is distributed over the entire molecule. One lone pair is in the truly non-bonding $1b_2$ orbital (Figure $5.4.3.3$), which is also the HOMO. There is not another truly non-bonding orbital in the molecule, but the lowest-energy $2a_1$ orbital could be considered mostly non-bonding due to the large energy difference between it and other valence orbitals. (c) Although the $2a_1$ orbital can be considered mostly non-bonding, we cannot expect the electrons in $2a_1$ to react readily, as they are in the lowest-energy molecular orbital. Molecular orbital theory predicts that reactions occur at the HOMO and LUMO orbitals. The HOMO reacts with electrophiles, and in this case, the HOMO is distributed over the top and bottom faces of the molecule, and is centered on the oxygen atom. The LUMO would react with nucleophiles. The LUMO is the orbital labeled $3a_1^*$ in Figure $5.4.3.3$, and has a major lobe that is distributed more heavily over the H atoms, and from this we should predict H atoms to be the preferred site of reaction for nucleophiles.

Expressing molecular orbitals in terms of Ψ

The general expression for a molecular orbital, or the linear combination of atomic orbitals (LCAO), was given previously as $\Psi = c_a\psi_a + c_b\psi_b$. In this expression, the wavefunction of two atoms (ψ_a and ψ_b) is combined to form the wavefunction of the molecular orbital. The coefficients c_a and c_b quantify the contribution of each atomic ψ to the molecular Ψ.

$$\Psi = c_a\psi_a + c_b\psi_b$$

In the case of polyatomic orbitals, each LCAO is constructed of atomic orbitals from a central atom and group orbitals (SALCs) from the pendent atoms. In the case of water, the expression above could be modified to give the expression below.

$$\Psi = c_{oxygen}\left(\psi_{oxygen}\right) + c_{SALCs}\left(N(\psi_{H_a} \pm \psi_{H_b})\right)$$

N represents the normalizing requirement that was mentioned previously in reference to the requirements for electron wavefunctions and probability functions. The normalizing requirement simply stated is the requirement that the probability of finding the electron in any orbital, including group orbitals, is 1. In general, the value of N for a group orbital is...

$$N = \frac{1}{\sum c_i^2}$$

...where c_i is the coefficient of each unique atomic orbital that contributes to the group. For the hydrogen SALCs of water, there are two atomic orbitals that contribute to equally to each SALC, and so the coefficient on each of the two orbitals is 1. This gives $N = \left(\frac{1}{\sqrt{1^2+1^2}}\right) = \frac{1}{\sqrt{2}}$ for the H SALCs of water.

There are only two hydrogen SALCs: the one in which the hydrogen wavefunctions are added ($N(\psi_{H_a} + \psi_{H_b})$) has A_1 symmetry, and the one in which the hydrogen wavefunctions are subtracted ($N(\psi_{H_a} - \psi_{H_b})$) has B_1 symmetry.

The molecular orbitals from Figure $5.4.3.3$ are expressed below in terms of their LCAO of individual wavefunctions. Yet, note that these expressions are simplifications that ignore orbital mixing. For example, as expressed below, they ignore contributions of oxygen $2s$ to the higher energy moelcular orbitals with A_1 symmetry (the $3a_1$ and $3a_1^*$ in Figure $5.4.3.3$).



Answers

Exercise $5.4.3.1$

Add texts here. Do not delete this text first.

This page titled 5.4.3: H_2O is shared under a CC BY-SA 4.0 license and was authored, remixed, and/or curated by LibreTexts.

- 5.4.3: H_2O is licensed CC BY-SA 4.0.

5.4.4: NH_3

Construct SALCs and the molecular orbital diagram for $\mathrm{NH_3}$

This is the first example so far that has more than two pendant atoms and the first example in which the molecule has atoms that lie in three dimensions (i.e., it is not flat). Ammonia is a trigonal pyramidal molecule, with three pendant hydrogen atoms. The three-dimensional shape and the odd number of pendant atoms makes this example more complicated than the previous cases of water, carbon dioxide, and bifluoride. In this case, sketching the shapes (step 5) of pendant atom SALCs is less straightforward; rather, an alternative method, the **projection operator method**, is preferred for generating pictorial representations of the SALCs.

As in previous examples, it is important to remember that interactions of pendant ligands are dependent on their positions in three-dimensional space. You should consider the positions of the four atoms in ammonia to be essentially fixed in relation to each other. We will walk through the steps used to construct the molecular orbital diagram of ammonia. The first few steps are the same as you've seen before:

Step 1. Find the point group of the molecule and assign Cartesian coordinates so that z is the principal axis.

The NH_3 molecule is trigonal pyramidal and its point group is C_{3v}. The z axis is collinear with the principal axis, the C_3 axis.

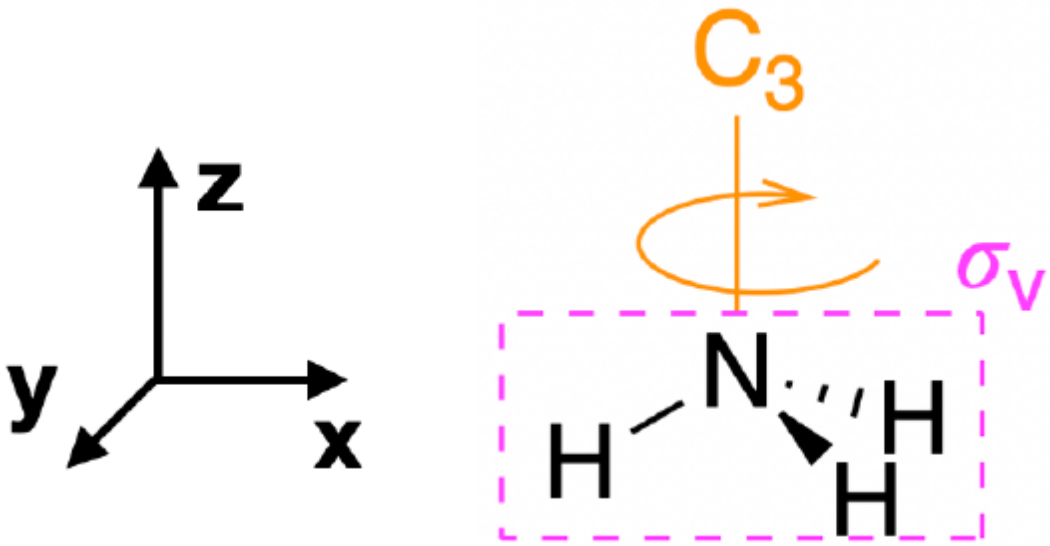


Figure 5.4.4.1: The ammonia molecule is in the C_{3v} point group. (CC-BY-NC-SA; Kathryn Haas)

Step 2. Identify and count the pendant atoms' valence orbitals.

Each of the three pendant hydrogen atoms has one valence orbital; the $1s$. Thus, we can expect a total of three SALCs from these three atoms.

Step 3. Generate the Γ's

Use the C_{3v} character table to generate one reducible representation (Γ); in this case we need only one Γ because there is only one type of valence orbital (the $1s$). For each s orbital, assign a value of 1 if it remains in place during the operation or zero if it moves out of its original place. The Γ is given below:

[redacted]

Step 4. Break Γ's into irreducible representations for individual SALCs

Reduce each Γ into its component irreducible representations. Using either of the processes described previously, we find that the Γ reduces to the two irreducible representations A_1 and E under the C_{3v} point group.

[redacted]

Notice that we only found TWO irreducible representations. But, in fact we have THREE different SALCs. The E irreducible representation is doubly degenerate, which in this context means that it corresponds to two degenerate SALCs. Thus, we have already found the symmetries of the three SALCs for ammonia: Two of the SALCs are degenerate with E symmetry under the C_{3v} point group, while the third SALC has A_1 symmetry.

Step 5. Sketch the SALCs using the PROJECTION OPERATOR METHOD

From the first four steps (described above), you have found the symmetries (the irreducible representations) of all three SALCs under the C_{3v} point group. To sketch the SALC that corresponds to each irreducible representation, again we use the C_{3v} character table. But now we will introduce the **projection operator method** to derive the surface representation of each SALC.

Step 5.1: Label the pendent atoms

In the projection operator method, first **label each of the pendant atoms so that we can distinguish identical atoms from one another**; for example, identify the three hydrogen atoms on ammonia as H_a, H_b, and H_c (Figure 5.4.4.2).

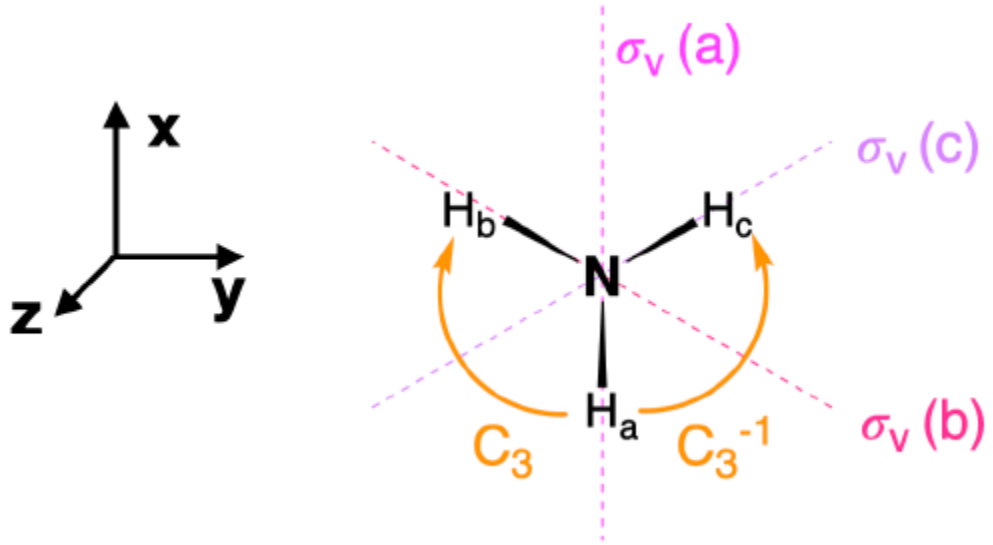


Figure 5.4.4.2: The three H's in NH_3 are chemically identical, but we can distinguish them using labels for the purpose of applying the projection operator method. In this figure, we have placed the z axis along the principal C_3 axis and placed the x axis colinear with one H. Each of the three H atoms has been labeled as H_a, H_b, or H_c. The σ_v that is coplanar with each H is labeled similarly (a, b, c) to keep account of each individual plane of symmetry. (CC-BY-NC-SA; Kathryn Haas)

Step 5.2: Create an expanded character table with one pendant atom's projected position after each operation

We will **perform each operation of the C_{3v} point group on this labeled molecule** and follow where one of the atoms is projected after the operation is complete. We will arbitrarily choose H_a. For example, upon performing the identity operation, E, the H_a atom is projected onto itself. On the other hand, H_a is projected onto H_b upon a clockwise C_3 rotation (as drawn in Figure 5.4.4.2). We take into account the result of each operation using an expanded character table (refer to the table below, 5.4.4.1). In the expanded character table, each operation within each class is written separately (i.e., $2C_3$ is accounted for separately as C_3 and C_3^{-1}).

Table 5.4.4.1: The expanded character table, and the projection of H_a by each operation is shown below.

[redacted] (5.4.4.1)

Step 5.3: Find the contribution of each pendant atom to each SALC

Next, **create a linear combination of the projections for each of the SALCs** (the irreducible representations found in step 4). For each of the irreducible representations, multiply the projection by the respective character of the operation.

$$\text{Contribution of each atom to the SALC } = \sum(\text{Projection of } H_a \times \chi)$$

The linear combination for all irreducible representations of C_3v is shown below.

Table 5.4.4.2: The symmetry adapted linear combination (SALC) for each irreducible representation of C_3v is shown.

[redacted] (5.4.4.2)

Notice that there are only two irreducible representations that produce SALCs, and these are the same that were found in Step 4, above. This illustrates the fact that only the irreducible representations found through the reduction of the Γ will produce SALCs. We can ignore any irreducible representations that were not found in Step 4. Or, you can check your work in Step 4 by applying the projection operator to any irreducible representations not found in Step 4, and finding that they produce a sum of zero.

Step 5.4: Sketch the SALCs

The meaning of the linear combinations found in Table 5.4.4.2 is as follows:

- **Sketch the SALC with A_1 symmetry:** The linear combination $2H_a + 2H_b + 2H_c$ indicates all contributions to this SALC are of the same sign (of the wavefunction). Qualitatively, this means there is no node in this SALC. We can take this SALC almost literally to assume that all three H 1s wavefunctions contribute equally to the SALC. We can also use the fact that the A_1 representation possesses the full symmetry of the C_3v point group, is compatible with an s orbital on N, and thus is a totally symmetric SALC.

  Quantitatively, we can apply the normalizing factor, N, for this SALC. The linear combination for the A_1 SALC in Table 5.4.4.2 shows us that the coefficient for each orbital is 1. Thus, the normalizing factor for the A_1 SALC is $N = \left(\frac{1}{\sqrt{1^2+1^2+1^2}}\right) = \frac{1}{\sqrt{3}}$. This tells us that H_a, H_b, and H_c each contribute $\frac{1}{\sqrt{3}}$ to the normalized A_1 group orbital:

  $$A_1 \text{ group orbital } = \frac{1}{\sqrt{3}}\left[\psi_{H_a} + \psi_{H_b} + \psi_{H_c}\right]$$

  This is shown visually in Figure 5.4.4.3.
- **Sketch two SALCs with E symmetry:** The linear combination $2H_a - H_b - H_c$ indicates that there are contributions with both positive and negative sign to the wavefunction for each of the E group orbitals. Qualitatively, this tells us that there is a node within each of these two SALCs, and that the total contribution of the positive portion of the wavefunction is equal to

the contribution of the negative portion.

- **Finding the first E SALC:**
  For one of the SALCs, we can take the linear combination from Table 5.4.4.2 almost literally: The contribution from H_a is equal and opposite to the sum of the contributions from $H_b + H_c$. This would result in a SALC as shown in Figure 5.4.4.3 (E, left), that would have symmetry of the x axis and that would be compatible with the p_x orbital on N. The node exists in the yz plane and there is an equal contribution of positive and negative parts of the total wavefunction.

  We can also apply the normalizing factor, N, to find this SALC. The linear combination for the E SALC in Table 5.4.4.2 shows us that the coefficients for orbital contributions are 2, -1, and -1. Thus, the normalizing factor for the first E SALC is $N = \left(\frac{1}{\sqrt{2^2+(-1)^2+(-1)^2}}\right) = \frac{1}{\sqrt{6}}$. This normalized E group orbital is:

$$\text{First } E \text{ group orbital } = \frac{1}{\sqrt{6}}\left[2\psi_{H_a} - \psi_{H_b} - \psi_{H_c}\right]$$

  This is shown visually in Figure 5.4.4.3 (E, left).
- **Finding the second E SALC:**
  The second SALC is less obvious at first glance. We must use clues from the character table to help us determine what it should "look like". Since the E representation transforms as the group, (x, y), we know that one of the SALCs will have the symmetry of the x axis and p_x orbital on the central nitrogen atom, while the other should possess the symmetry of the y axis and be compatible with the p_y orbital on nitrogen. This alone could lead you to the sketch of the second SALC with E symmetry shown in Figure 5.4.4.3 (E, right). This second E SALC must have a node in the xz plane, and because H_a lies in this node, H_a cannot contribute to this group orbital. Retaining the fact that the positive and negative contributions of the linear combination must be equal, we can arrive at a SALC that has equal but opposite contributions of H_b and H_c, and no contribution by H_c (Figure 5.4.4.3, right).

  We can also apply the normalizing factor, N, to find this SALC. But we must apply the fact that H_a cannot contribute to the SALC with "y" symmetry. We remove the contribution of H_a, leaving us with coefficients of 0 for H_a and 1 for H_b and H_c. Thus, the normalizing factor for the second E SALC is $N = \left(\frac{1}{\sqrt{0^2+1^2+1^2}}\right) = \frac{1}{\sqrt{2}}$. To this, we must add positive and negative coefficients so that the entire wavefunction of this SALC is normalized. The result for this normalized E group orbital is:

$$\text{Second } E \text{ group orbital } = \frac{1}{\sqrt{2}}\left[\psi_{H_b} - \psi_{H_c}\right]$$

  This is shown visually in Figure 5.4.4.3.

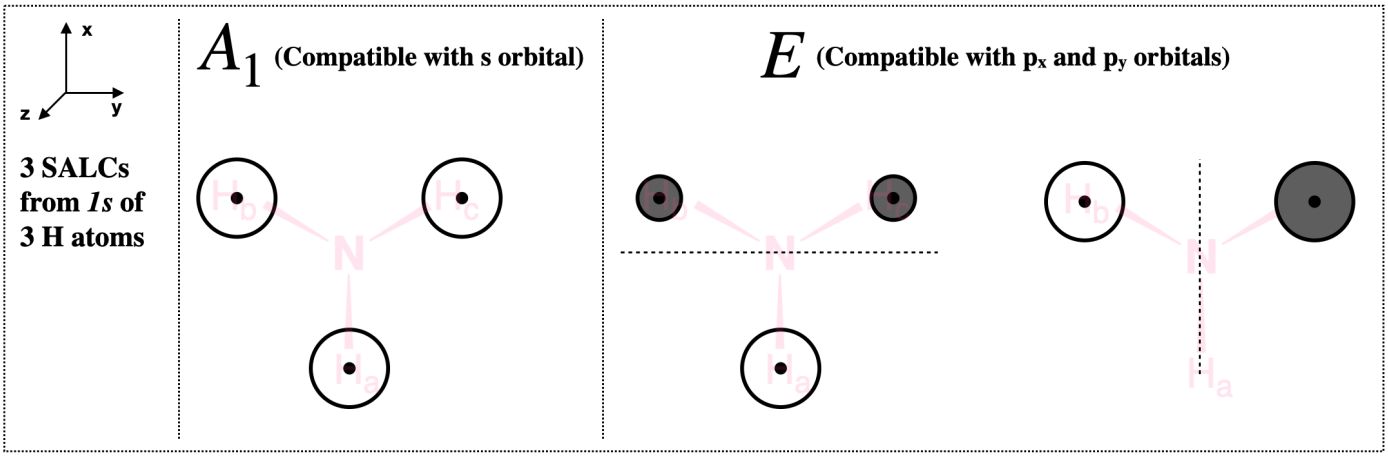


Figure 5.4.4.3: Sketches of H SALCs of ammonia from the perspective of the C_3 axiz (z axis). The A_1 SALC is shown at the left, while two degenerate SALCs with E symmetry are shown on the right. Nodes for E group orbitals are shown as dashed lines. (CC-BY-NC-SA; Kathryn Haas)

Step 6. Combine SALCs with AO's of like symmetry to draw the MO diagram for NH_3

First we must identify the valence orbitals on the central nitrogen: there are four including $2s$, $2p_x$, $2p_y$, and $2p_z$. Now we identify the

symmetry of each using the C_{3v} character table. The symmetry of a central $2s$ orbital corresponds to the combination of functions x^2, y^2, and z^2 in the character table; this is A_1. The p_z orbital also corresponds to A_1. And so on... The symmetries of nitrogen valence orbitals are listed below.

$$2s = A_1$$
$$(2p_x,\ 2p_y) = E$$
$$2p_z = A_1$$

The next step is to get a sense of the relative energies of valence atomic orbitals for nitrogen and hydrogen, and then construct the molecular orbital diagram. The nitrogen $2s$ orbital is about 12 eV lower in energy than a H $1s$. This difference is an acceptable energy-match for the H orbitals to interact, but would not usually result in a strong interaction. On the other hand, the nitrogen 2p orbitals have an energy very close to the hydrogen 1s, different by only 0.5 eV. Knowledge of the relative energies of the atomic orbitals tells us that, when constructing a diagram, we can place the H SALCs at an energy similar to that of the N $2p$ orbitals, while the N $2s$ is much lower (Figure 5.4.4.4).

The $2s$ and $2p_z$ orbitals have A_1 symmetry and can combine with the A_1 SALC. These orbitals will give three molecular orbitals. The $2s$ orbital will not have strong interactions with the other orbitals of A_1 symmetry due to the large energy difference. The $2p_z$ orbital will not have good overlap with the wavefunctions for the three hydrogen orbitals due to their positions in space: The $2p_z$ orbital has half of its angular distribution pointed away from the hydrogen orbitals, and half pointed toward the center of a triangle formed by the three hydrogen atoms. The nitrogen $2s$ and $2p_z$ will combine with the hydrogen SALC of A_1 symmetry to give three molecular orbitals; one low-energy bonding orbital, one mid-energy non-bonding orbital, and one high-energy antibonding orbital. The mid-level non-bonding a_1 molecular orbital is close in energy to, and resembles, the nitrogen $2p_z$ orbital. The lowest energy a_1 molecular orbital will be lower in energy, but be similar to the nitrogen $2s$.

The remaining two $2p$ orbitals are degenerate and possess E symmetry under the C_{3v} point group. Although these orbitals are a good energy match, again, their orientation and positions in space do not allow for good orbital overlap, and their bonding and antibonding interactions are relatively weak compared to what we might otherwise expect from such a good energy match. The e atomic orbitals of nitrogen will combine with the e SALCs to give a set of two degenerate bonding molecular orbitals and a set of two degenerate antibonding orbitals (four total molecular orbitals of e symmetry). The MO diagram for NH_3 is shown in Figure 5.4.4.4, with calculated electron density surfaces of each MO shown.

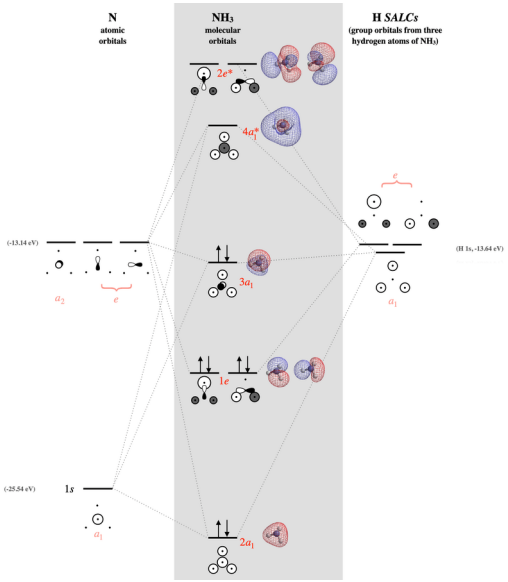


Figure 5.4.4.4: The molecular orbital diagram of ammonia. Molecular orbitals surfaces calculated using Spartan software. (CC-BY-NC-SA; Kathryn Haas)

This page titled 5.4.4: NH_3 is shared under a CC BY-SA 4.0 license and was authored, remixed, and/or curated by Kathryn Haas.

- 5.4.4: NH_3 by Kathryn Haas is licensed CC BY-SA 4.0.

5.4.5: CO_2 (Revisted with Projection Operators)

The process for finding SALCs and constructing the molecular orbital diagram for carbon dioxide was described in a previous section (Section 5.4.2). However, we also just presented an alternative strategy, the projection operator method, to finding the shapes of SALCs in Section 5.4.4. Let's revisit carbon dioxide and demonstrate how you can use the projection operator method to find SALCs for carbon dioxide.

Just as before, we can simplify the problem by approximating the $D_{\infty h}$point group using D_{2h}. The first four steps for constructing the MO diagram would be the same as described in Section 5.4.2. and we will pick up from that point (with Step 5) to find what the SALCs look like using the projection operator method.

The projection operator method applied to $\mathrm{CO_2}$

Step 5.1: Label the pendent atoms.

We can label the pendant atoms as O_a and O_b, as in Figure 5.4.5.1.

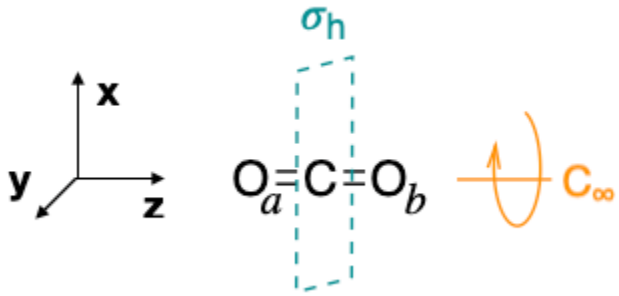


Figure 5.4.5.1: The structure of carbon dioxide with pendant oxygen atoms distinguished with labels a and b. Note that we will approximate the C_∞ axis as a C_2 axis to simplify the process of finding the SALCs. (CC-BY-SA; Kathryn Haas)

Step 5.2: Create an expanded character table with one pendant atom's projected position for each operation

The D_{2h} character table needs no expansion because each operation is in its own class. We will arbitrarily choose to determine the new position of O_a after each operation.

[redacted]

Step 5.3: Find the contribution of each pendant atom to each SALC

Create a linear combination of the projections for each or the SALCs. The irreducible representations were found in step 4 in Section 5.4.2. Eight irreducible representations were found to be: $2A_g + 2B_{1u} + B_{2g} + B_{3u} + B_{3g} + B_{2u}$. For each of the irreducible representations, multiply the projection by the respective character of the operation.

$$\text{Contribution of each atom to the SALC } = \sum(\text{Projection of } H_a \times \chi)$$

The linear combination for all irreducible representations of D_{2h} are shown below.

Table 5.4.5.1: The symmetry adapted linear combination (SALC) for each irreducible representations of C_3v are shown.



(5.4.5.1)

Notice that there are only two irreducible representations that produce SALCs, the A_g and the B_{1u}. Since we found two of each ($2A_g + 2B_{1u}$) when we found the irreducible representations, we know that there will be two SALCs of A_g symmetry and two of B_{1u} symmetry; that is four total SALCs from the pendant oxygens. This is the same as what we found in Section 5.4.2 using a different method.

Step 5.4: Sketch the SALCs

The SALCs with A_g symmetry: Quantitatively, we can apply the normalizing factor, N, for these SALCs. Each atom contributes equally to the SALCs, thus the normalizing factor for the A_g SALC is $N = \left(\frac{1}{\sqrt{1^2+1^2}}\right) = \frac{1}{\sqrt{2}}$. This tells us that each oxygen contributes $\frac{1}{\sqrt{2}}$ to each of the normalized A_g group orbitals:

$$A_g \text{ group orbital } = \frac{1}{\sqrt{2}}\left[\psi_{O_a} + \psi_{O_b}\right]$$

The linear combination $4\mathrm{O}_a + 4\mathrm{O}_b$ indicates that wavefunctions from each oxygen atom contribute equally to each of the two SALCs, with the same sign of the wavefunction for each. Because we know that A_g is totally symmetric (all 1's in the characters), we can assume that the SALC's will look like a symmetric arrangement of oxygen orbitals. But which orbitals contribute? We could peek at the character table to get a hint. But we'll treat this problem systematically.

The SALCs with B_{1u} symmetry: The linear combination $4\mathrm{O}_a - 4\mathrm{O}_b$ indicates that each oxygen atom contributes equally, but that they have opposite wavefunctions. Application of the normalizing factor would give us:

$$B_{1u} \text{ group orbital } = \frac{1}{\sqrt{2}}\left[\psi_{O_a} + \psi_{O_b}\right]$$

But how do we know what the SALCs look like? Again, the character table can give us some hints, but we'll use a systematic process, below.

What do the SALCs look like? One way to systematically derive the SALC shapes is to perform the projection (Step 5.3) on specific groups of orbitals on the oxygen atom. For example, if we replicate Table 5.4.5.1 using just the group of oxygen 2s orbitals and the A_g and B_{1u} representations, we get the following:



(5.4.5

This tells us that one of the A_g SALCs looks like two oxygen 1s orbitals with equal signs and contributions. It also tells us that one of the B_{1u} SALCs looks like two s orbitals with opposite signs and equal magnitudes. These two SALCs are shown in Figure 5.4.5.2 .

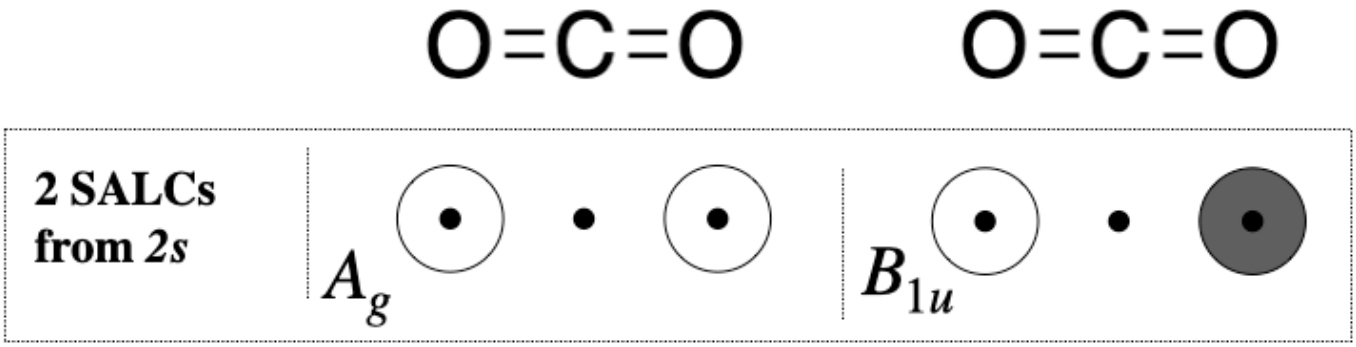


Figure $5.4.5.2$: SALCs derived from two oxygen $2s$ orbitals from carbon dioxide. Compare to Section 5.4.2. (CC-BY-SA; Kathryn Haas)

If we do the same for the $2p_z$ orbitals, we need to pay attention to the orientation of the p orbital lobes. If the orbital is moved into the opposite orientation, it would get a negative sign in the projection (see below).



This tells us that one of the A_g SALCs is derived from two $2p_z$ orbitals of opposite sign but equal magnitude. In other words, the two p orbitals are pointing in opposite directions, but the lobes that are facing one another are of the same sign (see Figure $5.4.5.3$, left). This also tells us that one of the B_{1u} orbitals is derived from two p_z orbitals of equal magnitude and equal sign (pointing in the same directions, with lobes facing one another of opposite sign!) (see Figure $5.4.5.3$, right).

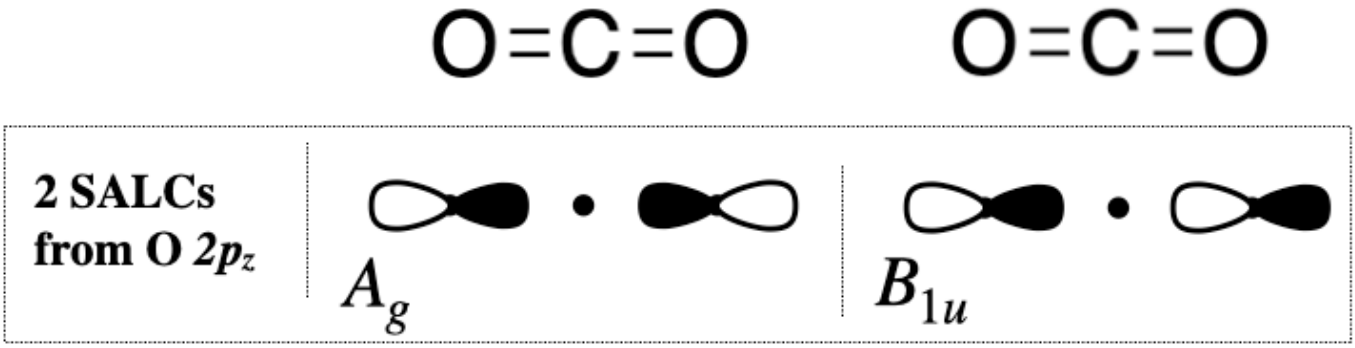


Figure $5.4.5.3$: SALCs derived from two oxygen $2p_z$ orbitals from carbon dioxide. Compare to Section 5.4.2. (CC-BY-SA; Kathryn Haas)

Now we have reached the same SALCs that we found previously in Section 5.4.2, but by an alternate method.

This page titled 5.4.5: CO_2 (Revisted with Projection Operators) is shared under a CC BY-SA 4.0 license and was authored, remixed, and/or curated by LibreTexts.

- 5.4.4: NH_3 by Kathryn Haas is licensed CC BY-SA 4.0.

5.4.6: BF_3

The case of boron trifluoride (BF_3) is an example of a molecule with one more layer of complexity than the other examples we have seen in previous sections in this chapter. (BF_3) is more complex than previous examples because it is the first case in which there are multiple types of valence orbitals on the pendant atoms. (BF_3) possesses s and p orbitals on *both* the central atom and all of the pendant atoms. We can follow the same steps that we have previously to derive other molecular orbital diagrams; however, there is one important difference: we will treat each type of pendant orbital as an individual set of SALCs.

Step 1. Find the point group of the molecule and assign Cartesian coordinates so that z is the principal axis.

The BH_3 molecule is trigonal planar, and its point group is D_{3h}. The z axis is colinear with the principle axis, the C_3 axis.

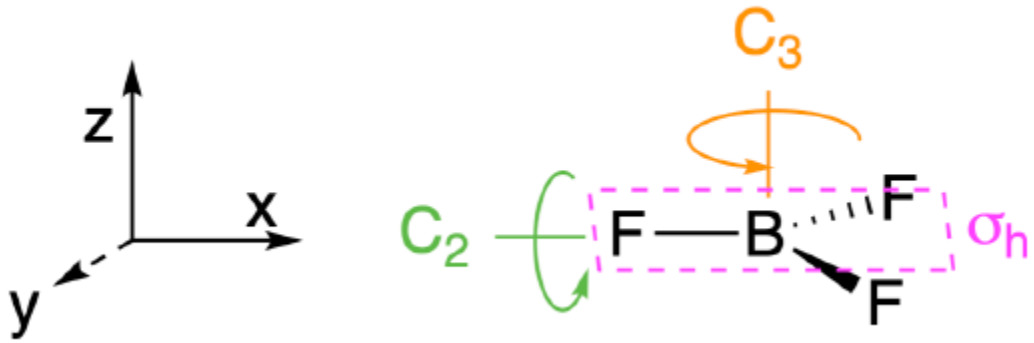


Figure 5.4.6.1: The molecule is in the D_{3h} point group. (CC-BY-NC-SA; Kathryn Haas)

Step 2. Identify and count the pendant atoms' valence orbitals.

Each of the three pendant fluorine atoms has four valence orbitals: one $2s$ and three $2p$ orbitals. Thus, we can expect a total of twelve SALCs from the three atoms. However, we will treat each type of orbital from the F atoms as its own set; each will have its own set of coordinates, with the y axis along the M-L bond. Thus we expect the following:

- One set of $2s$ SALCs: there is one 2s orbital on each of three atoms. This set will have three SALCs.
- One set of $2p_x$ SALCs: there is one $2p_x$ orbital on each of three atoms. Each of these individual orbitals is perpendicular to the M-L bond and coplanar with the molecule. This set will have three SALCs.
- One set of $2p_y$ SALCs: there is one $2p_y$ orbital on each of three atoms. Each of these individual orbitals is colinear with the M-L bond. This set will have three SALCs.
- One set of $2p_z$ SALCs: there is one $2p_z$ orbital on each of three atoms. Each of these individual orbitals is perpendicular to the M-L bond and parallel with the principal axis of the molecule. This set will have three SALCs.

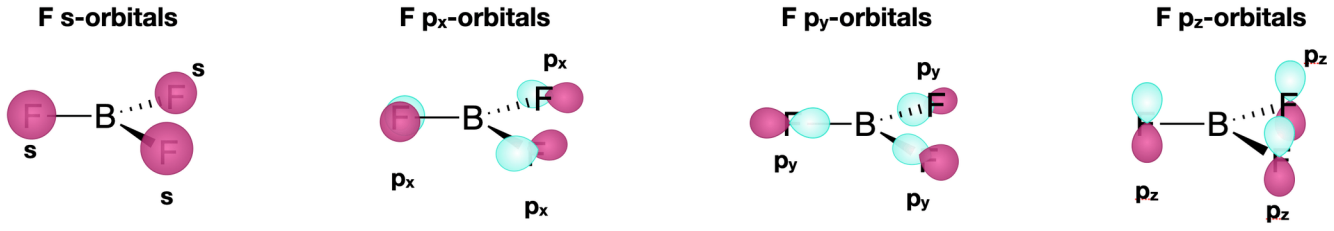


Figure 5.4.6.2: Individual sets of pendant fluorine atomic orbitals will create separate sets of SALCs. (CC-BY-SA; Kathryn Haas)

Step 3. Generate the Γ's for each set of SALCs

Use the D_{3h} character table to generate one reducible representation (Γ) for each of the four sets of pendant atomic orbitals shown in Figure $5.4.6.2$; in this case we need four Γ because there are four types of valence orbital (the s, p_x, p_y, p_z).

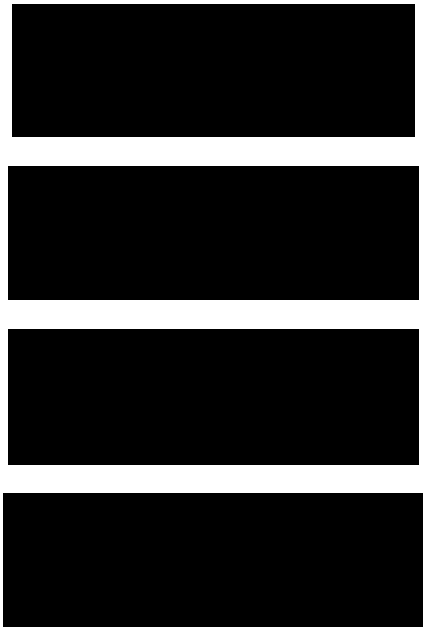
- For the set of s orbitals: perform the operation for each class in the character table. Each s orbital is assigned a value depending on whether it moves or not: assign a value of 1 if it remains in place during the operation, or 0 (zero) if it moves out of its original place.
- for each set of p orbitals: Now there are phases (signs of the wavefunction), so a negative value is possible. Assign a value of 1 to each p orbital if it remains in place and in phase during the operation; assign a -1 if the atom's position remains, while the phase of the orbital is inverted (the positive lobe moves to the position of the negative lobe and vice versa); assign a 0 if it moves out of its original position.

The Γ for each type is given below:



Step 4. Break Γ's into irreducible representations for individual SALCs

Reduce each Γ into its component irreducible representations. Using either of the processes described previously, we find that each of the Γ reduces to two irreducible representations under the D_{3h} point group; in each case one is singly degenerate (A) and the other doubly degenerate (E). This equates to three SALCs for each Γ (orbital type) and a total of twelve SALCs. This should give us confidence! We were in fact expecting 12 SALCs because we found that there were twelve pendant atomic orbitals to start with.



Step 5: Sketch the SALCs

We'll skip this step for now to make this problem simpler.

Step 6: Draw the MO diagram by combining SALCs with AO's of like symmetry.

We now know the symmetries of different pendant orbital SALCs - and it is helpful if we also know their relative energies, and the energies of the valence orbitals on the central boron atom. We can make predictions based on periodic trends, or we can use a table of ionization energies as a guide. The symmetries of the boron $2s$ and $2p$ orbitals can be found from the D_{3h} character table.

This page titled 5.4.6: BF_3 is shared under a CC BY-SA 4.0 license and was authored, remixed, and/or curated by LibreTexts.

- 5.4.4: NH_3 by Kathryn Haas is licensed CC BY-SA 4.0.

5.5: Problems

Concept Review Questions

1. What are the assumptions (axioms) of molecular orbital (MO) theory?

2. Explain qualitatively why the vectorial addition of atomic orbitals creates molecular orbitals (which underlying physical phenomenon is described by the vectorial addition?).

3. Explain qualitatively why molecular orbital theory is suitable to describe covalent bonding.

4. What are the three criteria that determine the degree of covalent interaction in MO theory?

5. Which three rules determine the degree of orbital overlap in MO theory?

6. Explain why the combination of a large, diffuse orbital and a small orbital produces only weak covalent interaction.

7. Explain why sigma interactions between atomic orbitals typically produce larger orbital overlaps than pi interactions.

8. Explain why the combination of orbitals of the same energy leads to the largest degree of covalent interaction.

9. What can be said about energy and location of a bonding and an anti-bonding molecular orbital that are made from atomic orbitals of large energy difference?

10. MO theory – even though designed for covalent bonding – can also make statements about ionic bonding. Explain why.

11. Explain the principles of SALC.

Dr. Kai Landskron (Lehigh University). If you like this textbook, please consider to make a donation to support the author's research at Lehigh University: Click Here to Donate.

Homework Problems

Section 1

Exercise 1

What will most likely lead to the smallest covalent interaction?

a) Overlap of a small and a large orbital.

b) Overlap of two small orbitals.

c) Overlap of two large orbitals.

Answer available at the end of this section.

Exercise 2

What will most likely lead to the largest covalent interaction?

a) orbital overlap in sigma-fashion

b) orbital overlap in pi-fashion

c) orbital overlap in delta-fashion

Answer available at the end of this section.

Exercise 3

Qualitatively construct the MO diagrams composed of

a) two 2s atom orbitals A and B of equal energy.

b) two 2s atom orbitals where the orbital energy of atom A is significantly higher than that of B. If both the bonding and the antibonding MO are filled with electrons, where will bonding and antibonding electrons primarily be located? Briefly explain your decision.

Answer available at the end of this section.

Exercise 4

Decide by “inspection” which of the following combinations of orbitals have the “right” symmetries to form molecular orbitals.

a) The $2p_x$ orbital of the first N atom and the $2p_y$ orbital of the second N atom in the molecule N_2. The z axis is defined as the bond axis in N_2.

b) The F $2p_x$ and the H 1s orbital in the HF molecule. The z axis is defined as the bond axis.

c) The $2p_z$ orbital of F and the 1s orbital in the HF molecule. The z axis is defined as the bond axis.

Answer available at the end of this section.

Exercise 5

The CH_4 molecule belongs to the point group T_d. You can find the character table of the point group in the internet.

a) Calculate the reducible representation for the ligand group orbitals (LGOs).

b) Calculate the irreducible representations of the ligand group orbitals (LGOs).

c) Draw a qualitative molecular orbital diagram for CH_4.

Answer available at the end of this section.

Exercise 6

Which are the symmetry types of the central atom orbitals in the PCl_5 molecule?

Answer available at the end of this section.

Exercise 7

For the hypothetical $BrKr^+$ molecule: Toward which atom is the HOMO polarized? Explain briefly why.

Answer available at the end of this section.

Exercise 8

Reconstruct the MO diagram for water and NH_3 (repeat what we did in class without looking at your notes (only use the respective character tables).

Answer available at the end of this section.

Dr. Kai Landskron (Lehigh University). If you like this textbook, please consider to make a donation to support the author's research at Lehigh University: Click Here to Donate.

Exercise 5.5.1

A Molecular Orbital Diagram for a diatomic molecule (two atoms) always has the same basic pattern.

- Draw a picture of the levels.
- Label each level with σ, σ*, π, π*

Answer available at the end of this section.

Exercise 5.5.2

A Molecular Orbital Diagram for a diatomic molecule (two atoms) varies in the number of electrons. How do you populate the electrons?

Answer available at the end of this section.

Exercise 5.5.3

Construct a qualitative molecular orbital diagram for chlorine, Cl_2. Compare the bond order to that seen in the Lewis structure (remember that an electron in an antibonding orbital cancels the stabilization due to bonding of an electron in a bonding orbital).

Answer available at the end of this section.

Exercise 5.5.4

a. Construct a qualitative molecular orbital diagram for oxygen, O_2.
b. Compare the bond order to that seen in the Lewis structure.
c. How else does this MO picture of oxygen compare to the Lewis structure? What do the two structures tell you about electron pairing?
d. Compounds that have all of their electrons paired are referred to as diamagnetic. Those with unpaired electrons are referred to as paramagnetic. Paramagnetic materials are attracted by a magnetic field, but diamagnetic things are not. How would you expect molecular oxygen to behave?

Answer available at the end of this section.

Exercise 5.5.5

a. Construct a qualitative molecular orbital diagram for peroxide anion, O_2^{2-}.
b. Compare the bond order to that seen in the Lewis structure.
c. How else does this MO picture of oxygen compare to the Lewis structure? What do the two structures tell you about electron pairing?
d. Based on molecular orbital pictures, how easily do you think dioxygen could be reduced to peroxide (through the addition of two electrons)?

Answer available at the end of this section.

Exercise 5.5.6

Construct a qualitative molecular orbital diagram for diboron, B_2. Do you think boron-boron bonds could form easily, based on this picture?

Answer available at the end of this section.

Exercise 5.5.7

a. Construct a qualitative molecular orbital diagram for dicarbon, C_2.
b. Compare the bond order to that seen in the Lewis structure.
c. How else does this MO picture of oxygen compare to the Lewis structure? What do the two structures tell you about electron pairing?

Answer available at the end of this section.

Exercise 5.5.8

a. Construct a qualitative molecular orbital diagram for acetylide anion, C_2^{2-}.
b. Compare the bond order to that seen in the Lewis structure.
c. How else does this MO picture of oxygen compare to the Lewis structure? What do the two structures tell you about electron pairing?
d. Based on molecular orbital pictures, how easily do you think dicarbon could be reduced to acetylide (through the addition of two electrons)?

Answer available at the end of this section.

Exercise 5.5.9

Make drawings and notes to summarize the effect of populating antibonding orbitals.

Answer available at the end of this section.

Exercise 5.5.10

Researchers at Johns Hopkins recently reported the formation of Na_4Al_2 in a pulsed arc discharge (they put a lot of electric current through a sample of sodium and aluminum; Xinxing Zhang, Ivan A. Popov, Katie A. Lundell, Haopeng Wang, Chaonan Mu, Wei Wang, Hansgeorg Schnöckel, Alexander I. Boldyrev, Kit H. Bowen, *Angewandte Chemie International Edition*, **2018**, *57*(43), 14060-14064. Copyright 2018, John Wiley & Sons. Used with permission.).

a. The compound is ionic. Explain which atoms form the cations, based on periodic trends.
b. Therefore, what atoms form the anion?
c. The anion is one molecule. What is the charge on this molecule?
d. Show how to calculate the total valence electrons in this molecular anion.
e. Draw a Lewis structure for this molecular anion.
f. Construct a diatomic molecular orbital energy level diagram for this molecule. Label the energy levels (sigma, pi, etc.) and add in the correct number of electrons.
g. Show how to calculate the bond order in the molecule.

Answer available at the end of this section.

Exercise 5.5.1

Draw the molecular orbital diagram for (NO^-).

Answer available at the end of this section.

Exercise 5.5.1

Draw and compare the molecular orbital diagrams to the Lewis structure diagrams for O_2, O_2^-, and O_2^{2-}.

Answer available at the end of this section.

Exercise 5.5.1

Draw the molecular orbital diagram for hydroxide ion (OH^-).

Answer available at the end of this section.

Exercise 5.5.1

Draw the molecular orbital diagram for hydroxide fluoride (HF).

Answer available at the end of this section.

Exercise 5.5.1

Draw the molecular orbital diagram for borane (BN).

Answer available at the end of this section.

BH3

Exercise 5.5.1

Draw the molecular orbital diagram for (FeH_6).

Answer available at the end of this section.

Exercise 5.5.1

Draw the molecular orbital diagram for boron trifluoride (BF_3).

- What is the non-bonding orbital?
- What are the HOMO and LUMO orbitals?
- Why does e' have 2 lines of energy levels compared to a1', which has only a 1-line energy level?
- What is the bond order of BH_3 in this MO diagram?

Answer available at the end of this section.

Answers

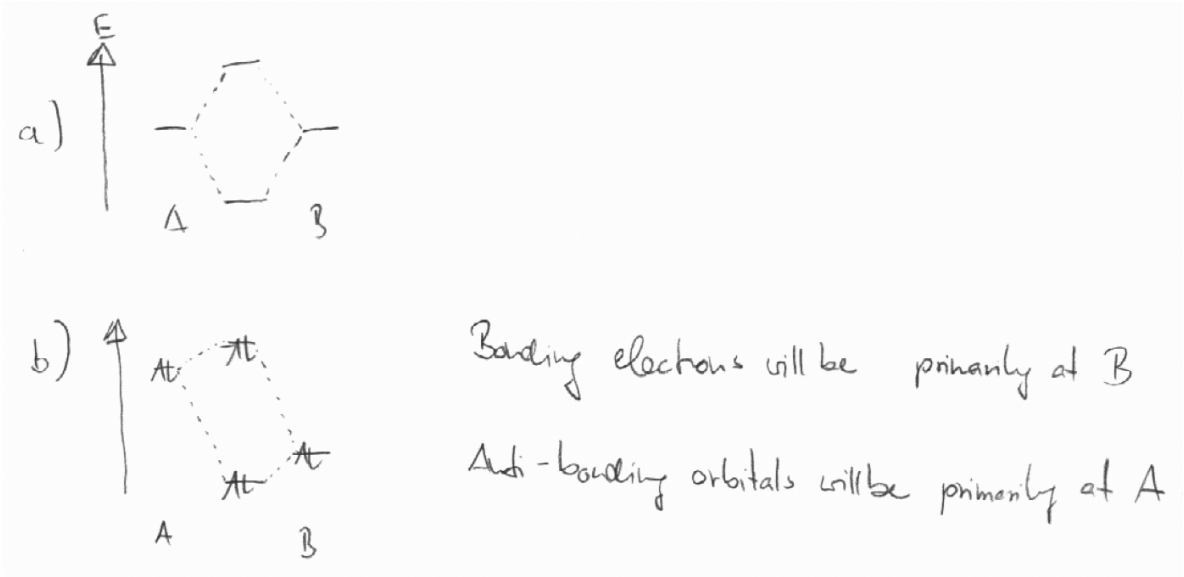
Exercise 1

a) Overlap of a small and a large orbital.

Exercise 2

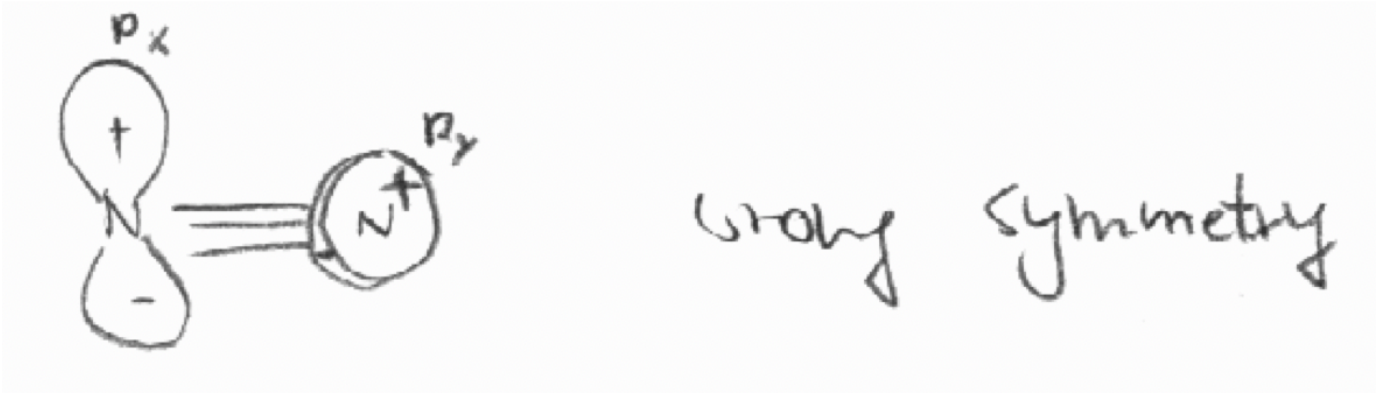
a) orbital overlap in sigma-fashion

Exercise 3

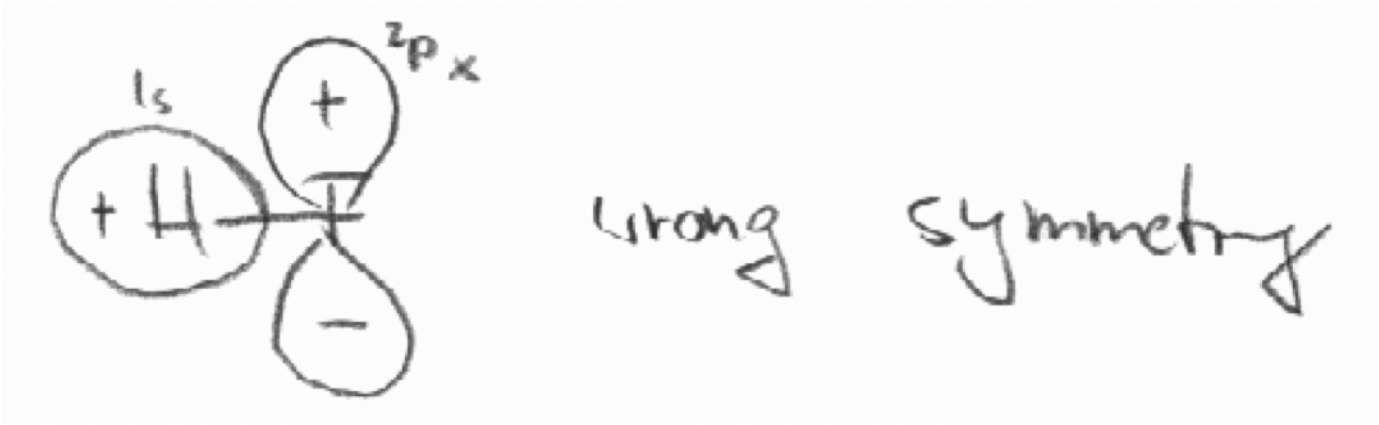


Exercise 4

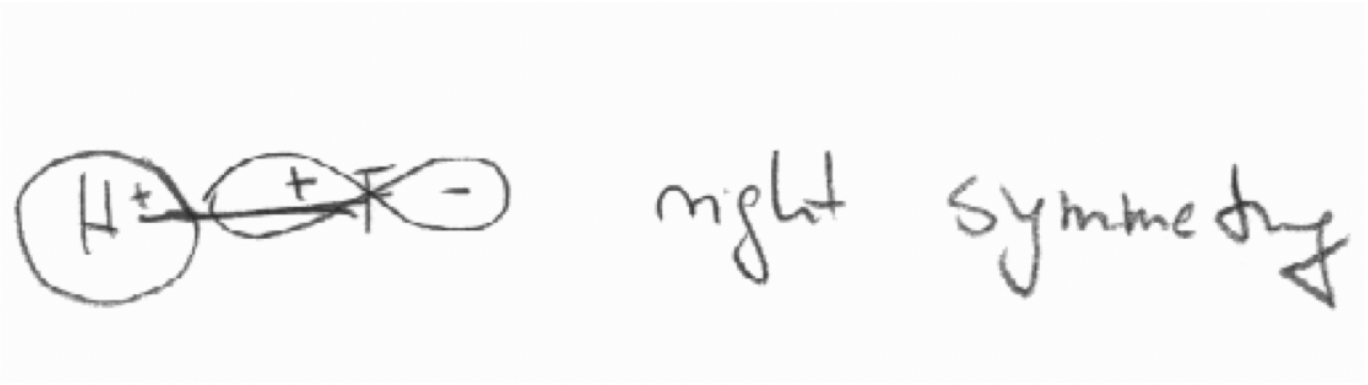
a)



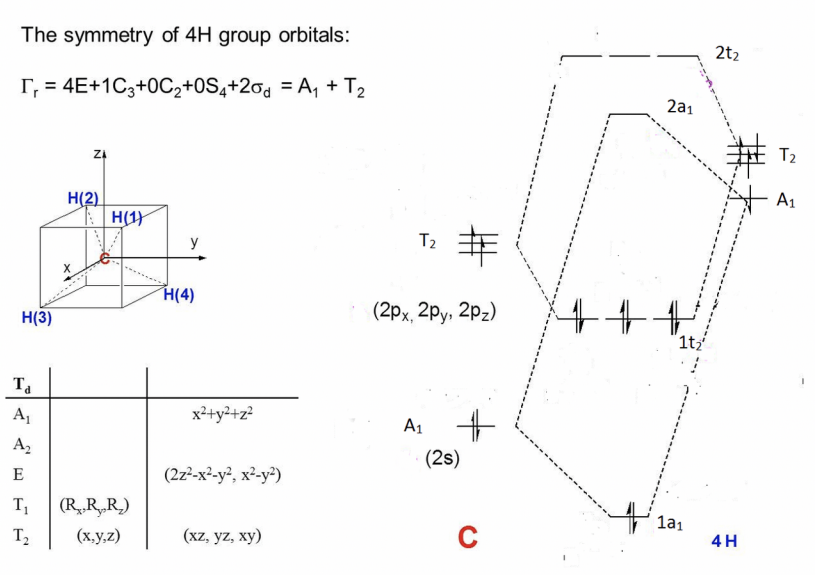
b)



c)



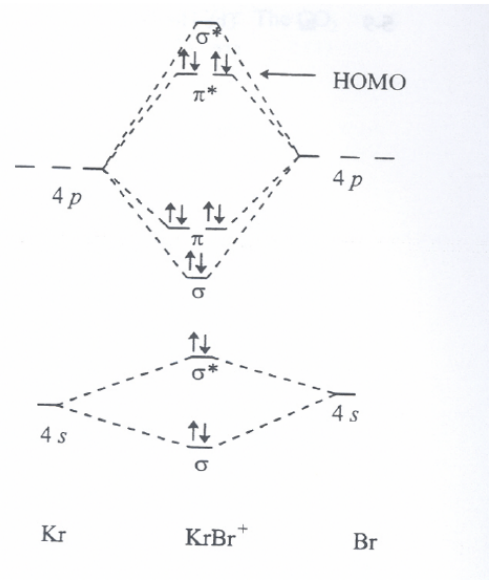
Exercise 5



Exercise 6

1. Determine point group of PCl_5. --> D_{3h}.
2. Decide what are the valence orbitals of the central atom: 3s, 3p
3. Look up the character table of D_{3h}, e.g., in the internet. You will find their symmetries to be: A_1' (3s), A_2'' ($3p_z$), E'($3p_x$, $3p_y$)

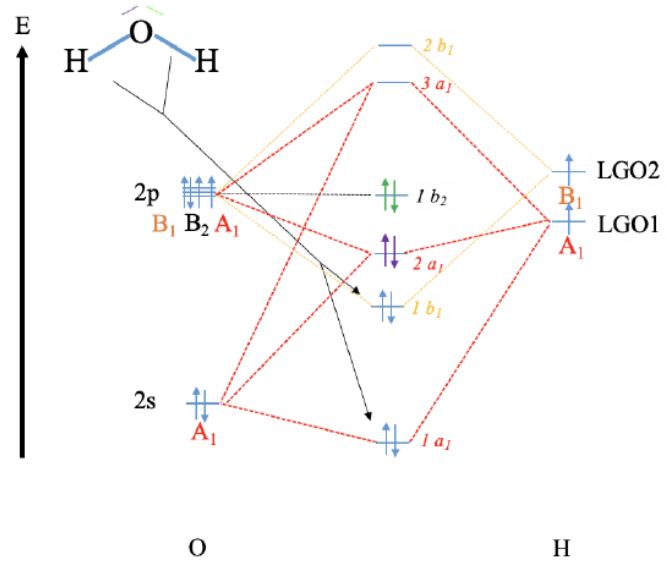
Exercise 7



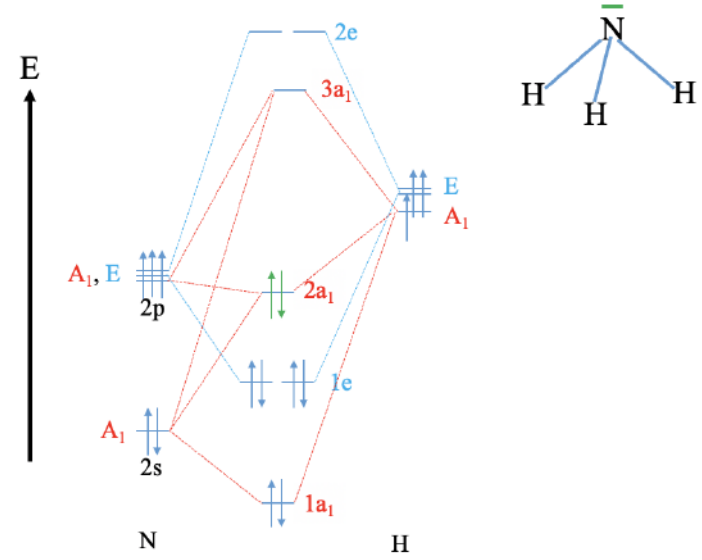
Orbital energies of Kr must be somewhat lower than the ones of Br because the electrons experience higher effective nuclear charge (Z_{eff} increases within a period). This means that the antibonding HOMO is polarized towards Br (HOMO energetically closer to 4p(Br) than 4p(Kr)).

Exercise 8

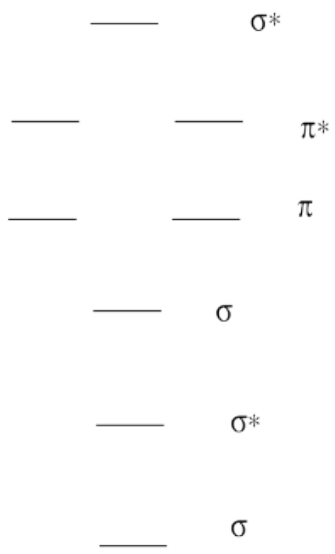
Water



NH_3



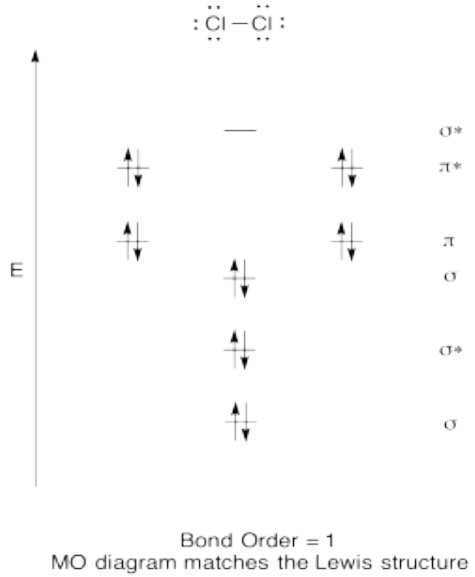
Exercise 5.5.1



Exercise 5.5.2

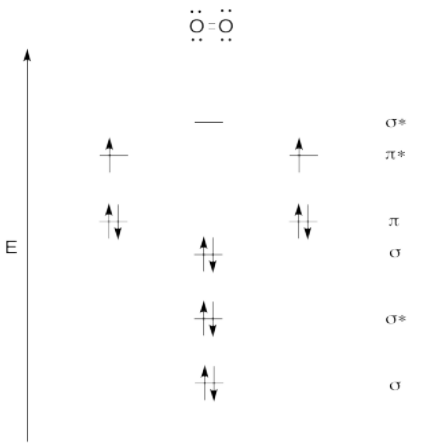
- Count the valence electrons on the molecule. That's the number of valence electrons on each atom, adjusted for any charge on the molecule. (eg C_2^{2-} has 10 valence electrons: 4 from each carbon -- that's 8 -- and two more for the 2- charge).
- Fill electrons into the lowest energy orbitals first.
- Pair electrons after all orbitals at the same energy level have one electron.

Exercise 5.5.3



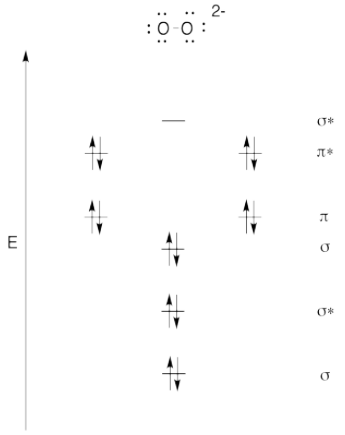
Bond Order = 1
MO diagram matches the Lewis structure

Exercise 5.5.4



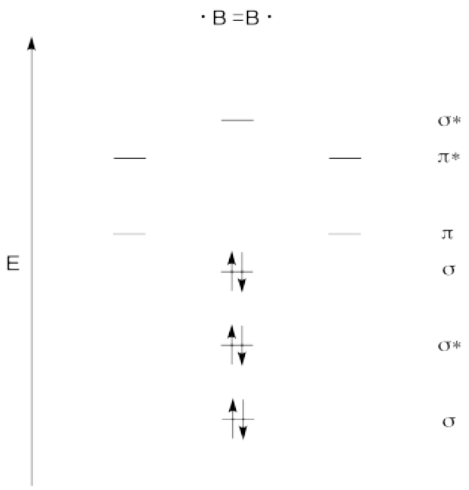
Bond Order = 2
MO diagram indicates two unpaired electrons and therefore does not match the Lewis structure. Based on the MO diagram oxygen would be paramagnetic and would be attracted to a magnetic field

Exercise 5.5.5



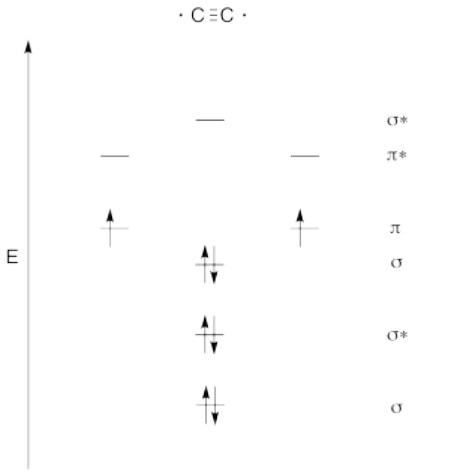
Bond Order = 1
MO diagram matches the Lewis structure. Both predict a Bond Order of 1 and 6 lone pairs of electrons. The addition of two electrons to O_2 to O_2^{2-} would be possible.

Exercise 5.5.6



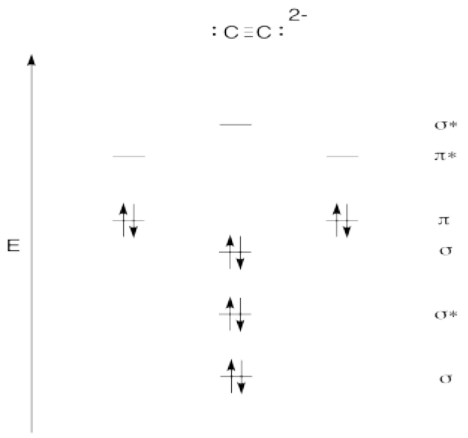
Bond Order = 1
Boron-Boron bonding should be possible

Exercise 5.5.7



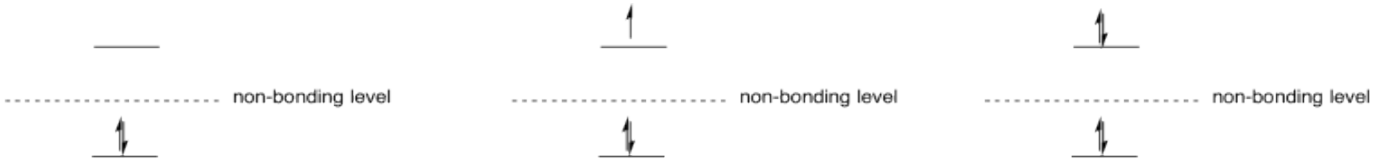
Bond Order = 2
MO diagram does not match the Lewis structure.
However, the MO diagram does concur about the
2 unpaired electrons.

Exercise 5.5.8



Bond Order = 3
MO diagram matches the Lewis structure. Both predict a Bond Order of 3 and 2 lone pairs of electrons. The addition of two electrons to C_2 to C_2^{2-} would be possible.

Exercise 5.5.9



I'm stable!!!
And I have ONE FULL BOND!!!!

I'm kinda stable I guess...
Still got a half a bond...
Don't worry about me...

Not stable together.
No bonds here.

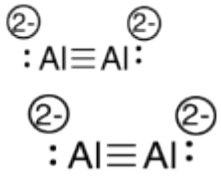
Exercise 5.5.10

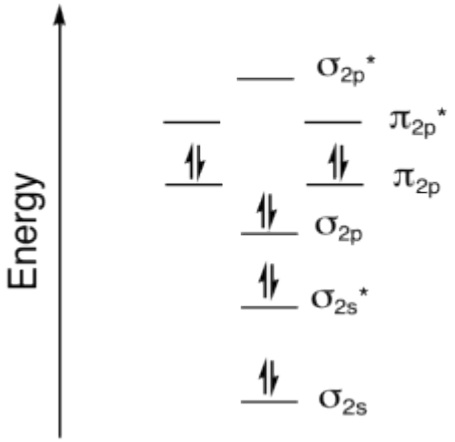
a) Na, because Na has a lower ionization potential (and a lower electronegativity) than Al.

b) Al

c) 4-, because there are four Na^+

d) total e^- = 2 x 3 e^- (per Al) + 4 e^- (for the negative charge) = 10 e-





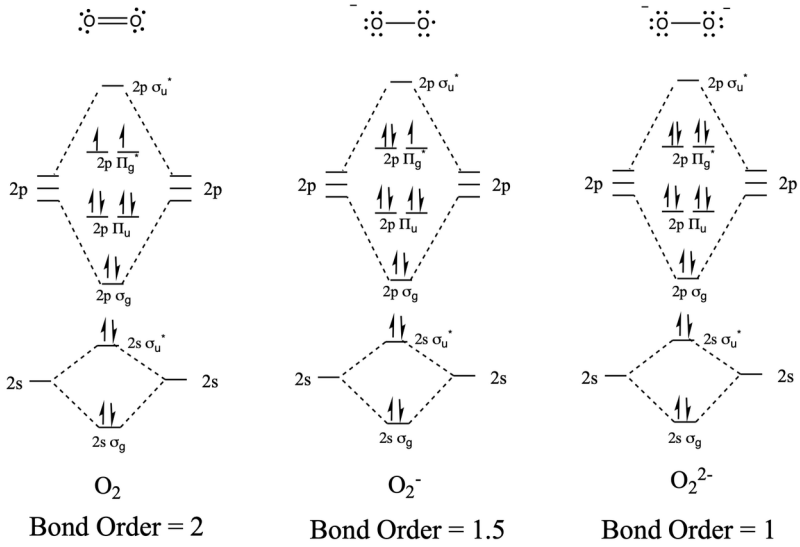
g) bond order $= \frac{(\#bonding\ e^- - \#antibonding\ 3^-)}{2} = \frac{8-2}{2} = 3$

Exercise 5.5.1

Add texts here. Do not delete this text first.

Exercise 5.5.1

The Lewis structures and MO diagrams are shown below. In general, the bond order derived from the MO diagram agrees with the Lewis structure for each species. In the case of the two ions, the number of unpaired electrons from MO theory and the Lewis structure also agrees. In the case of dioxygen, however, there is an inconsistency between the Lewis representation and the MO diagram. While the Lewis structure would lead us to believe that all electrons are paired, the MO diagram indicates paramagnetism, with two unpaired electrons. The MO diagram explains the magnetic behaviour of dioxygen.



Exercise 5.5.1

Add texts here. Do not delete this text first.

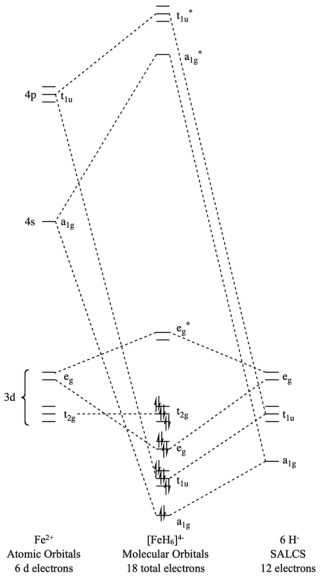
Exercise 5.5.1

Add texts here. Do not delete this text first.

Exercise 5.5.1

Add texts here. Do not delete this text first.

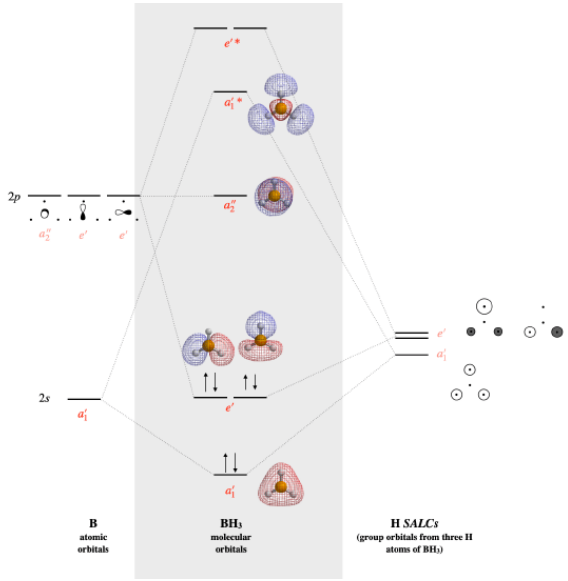
Exercise 5.5.1



Exercise 5.5.1

The calculated MO diagram is shown below.

- a_2'' is the lone non-bonding orbital.
- The HOMO is the a_2'' nonbonding orbital, the LUMO is a bonding e' set of two degenerate orbitals/
- e' is doubly degenerate
- The bond order is 3



This page titled 5.5: Problems is shared under a CC BY-SA 4.0 license and was authored, remixed, and/or curated by LibreTexts.

- Concept Review Questions Chapter 3 by Kai Landskron is licensed CC BY 4.0.
- Homework Problems Chapter 3 by Kai Landskron is licensed CC BY 4.0.
- 13.6: Assembling the Complete Diagram and Electron Population by Chris Schaller is licensed CC BY-NC 3.0. Original source: https://employees.csbsju.edu/cschaller/structure.htm.

6: CHEMISTRY OF THE MAIN GROUP ELEMENTS (BARRON)

The main group (*s*- and *p*-block) elements are among the most diverse in the Periodic Table. Ranging from non-metallic gases (e.g., hydrogen and fluorine), through semi-metals (e.g., metalloids such as silicon) to highly reactive metals (e.g., sodium and potassium). The study of the main group elements is important for a number of reasons. On an academic level they exemplify the trends and predictions in structure and reactivity that are the key to the Periodic Table. They represent the diversity of inorganic chemistry, and the fundamental aspects of structure and bonding that are also present for the transition metal, lanthanide and actinide elements.

6.1: General Concepts and Trends

6.1.1: Fundamental Properties - Oxidation State

6.1.2: Fundamental Properties - Ionization Energy

6.1.3: Fundamental Properties - Electron Affinity

6.1.4: Fundamental Properties - Electronegativity

6.1.5: Structure and Bonding - Valence Shell Electron Pair Repulsion (VSEPR) Theory

6.1.6: Structure and Bonding - Crystal Structure

6.1.7: Structure and Bonding - Stereochemistry

6.1.8: Acids, Bases, and Solvents - Choosing a Solvent

6.1.9: Chemical Reactivity - The Basics of Combustion

6.1.10: Periodic Trends for the Main Group Elements

6.2: Hydrogen

6.2.1: Discovery of Hydrogen

6.2.2: The Physical Properties of Hydrogen

6.2.3: Synthesis of Molecular Hydrogen

6.2.4: Atomic Hydrogen

6.2.5: The Proton

6.2.6: Hydrides

6.2.7: The Hydrogen Bond

6.2.8: Isotopes of Hydrogen

6.2.9: Nuclear Fusion

6.2.10: Storage of Hydrogen for Use as a Fuel

6.3: Group 1 - The Alkali Metals

6.3.1: The Alkali Metal Elements

6.3.2: Compounds of the Alkali Metals

6.3.3: The Anomalous Chemistry of Lithium

6.3.4: Organolithium Compounds

6.4: Group 2 - The Alkaline Earth Metals

6.4.1: The Alkaline Earth Elements

6.4.2: Calcium the Archetypal Alkaline Earth Metal

6.4.3: Differences for Beryllium and Magnesium

6.4.4: Organometallic Compounds of Magnesium

6.5: Group 12

6.5.1: The Group 12 Elements

6.5.2: Cadmium Chalcogenide Nanoparticles

6.5.3: Organometallic Chemistry of Zinc

6.5.4: Organomercury Compounds

6.5.5: The Myth, Reality, and History of Mercury Toxicity

6.6: Group 13

6.6.1: The Group 13 Elements

6.6.2: Trends for the Group 13 Compounds

6.6.3: Borides

6.6.4: Boron Hydrides

6.6.5: Wade's Rules

6.6.6: Trends for the Oxides of the Group 13 Elements

6.6.7: Boron Oxides, Hydroxides, and Oxyanions

6.6.8: Aluminum Oxides, Hydroxides, and Hydrated Oxides

6.6.9: Ceramic Processing of Alumina

6.6.10: Boron Compounds with Nitrogen Donors

6.6.11: Properties of Gallium Arsenide

6.6.12: Electronic Grade Gallium Arsenide

6.6.13: Chalcogenides of Aluminum, Gallium, and Indium

6.6.14: Group 13 Halides

6.7: Group 14

6.7.1: The Group 14 Elements

6.7.2: Carbon Black- From Copying to Communication

6.7.3: Carbon Nanomaterials

6.7.4: Nitrogen Compounds of Carbon

6.7.5: Carbon Monoxide

6.7.6: Carbon Dioxide

6.7.7: Suboxides of Carbon

6.7.8: Carbon Halides

6.7.9: Comparison Between Silicon and Carbon

6.7.10: Semiconductor Grade Silicon

6.7.11: Oxidation of Silicon

6.7.12: Applications for Silica Thin Films

6.8: Group 15 - The Pnictogens

6.8.1: The Group 15 Elements- The Pnictogens

6.8.2: Reaction Chemistry of Nitrogen

6.8.3: Hydrides

6.8.4: Oxides and Oxoacids
6.8.5: Halides of Phosphorous

6.9: Group 16

6.9.1: The Group 16 Elements- The Chalcogens
6.9.2: Ozone
6.9.3: Water - The Fuel for the Medieval Industrial Revolution
6.9.4: Hydrogen Peroxide
6.9.5: Hydrogen Peroxide Providing a Lift for 007
6.9.6: Comparison of Sulfur to Oxygen
6.9.7: Chalconide Hydrides
6.9.8: Oxides and Oxyacids of Sulfur
6.9.9: Sulfur Halides

6.10: The Halogens

6.10.1: The Group 17 Elements- The Halogens
6.10.2: Compounds of Fluorine
6.10.3: Compounds of Chlorine
6.10.4: Oxyacids of Chlorine
6.10.5: Bromine Trifluoride as a Solvent

6.11: Group 18 - The Noble Gases

6.11.1: The Group 18 Elements- The Noble Gases

6.12: Front Matter

6.12.1: Table of Contents

This page titled 6: Chemistry of the Main Group Elements (Barron) is shared under a CC BY 3.0 license and was authored, remixed, and/or curated by Andrew R. Barron via source content that was edited to the style and standards of the LibreTexts platform.

6.1: General Concepts and Trends

This page titled 6.1: General Concepts and Trends is shared under a CC BY 3.0 license and was authored, remixed, and/or curated by Andrew R. Barron (CNX) via source content that was edited to the style and standards of the LibreTexts platform.

6.1.1: Fundamental Properties - Oxidation State

The oxidation state of an element is defined as *the formal charge on the atom if all bonds were assumed to be fully ionic*.

In an ionic compound the oxidation state is equal to the charge on the ion, e.g., in NaCl the charge on the sodium is +1 and the oxidation state is also +1. In contrast, the charge on an atom in a covalent compound never approaches the charge implied from the oxidation number, e.g., in CCl4, the oxidation state of carbon is +4 but the charge on the carbon atom is signicantly less.

Thus, while oxidation state is a simple formulism it is very useful in a number of ways:

1. Classication of compounds of elements, especially those of the transition metals.
2. Enables the balance of reduction-oxidation (redox) reactions.

To determine the oxidation state of an element within a particular compound the following steps act as a guideline:

1. The oxidation state of any atom of any element in its elemental form is zero.
2. The oxidation state of a monatomic ion is equal to its charge.
3. Any homoleptic X-X bonds (e.g., the C-C bond in H3C-CH3) are assumed to be non-ionic and do not contribute to the oxidation state of X.
4. Fluorine always has oxidation state of 1
5. Elements of Group 1 (IA) (except hydrogen) have an oxidation state of +1 in compounds.
6. Elements of Group 2 (IIA) have an oxidation state of +2 in compounds.
7. Elements of Group 17 (VIIA) have an oxidation state of -1 when they combine with elements below or to the left of their position in the periodic table
8. Oxygen is usually assigned the oxidation state of 2, except in compounds with uorine, oxygen has a positive oxidation number.
9. Hydrogen is assigned the oxidation state of +1 with non-metals and 1 with metals.
10. In any compound the sum of the oxidation states (oxidation numbers) is equal to the overall charge.

Exercises

Exercise 6.1.1.1

What is the oxidation state of sulfur in Na_2SO_4?

Solution available at the end of this section.

Exercise 6.1.1.2

What is the oxidation state of sulfur in Na_2SO_3?

Solution available at the end of this section.

Exercise 6.1.1.3

What is the oxidation state of sulfur in H_2S?

Solution available at the end of this section.

In writing the oxidation state of an element within a compound it is common to use a Roman numeral, rather than the charge, i.e., Al(III) rather than Al^{3+}.

Answers

The two sodium atoms each have an oxidation state of +1, while the oxygen atoms have an oxidation state of 2, and the overall charge is 0.

1. overall charge = sum of oxidation states
2. 0 = (2 x oxidation state of Na) + (oxidation state of S) + (4 x oxidation state of O)
3. 0 = (2 x +1) + (oxidation state of S) + (4 x -2)
4. oxidation state of S = 0 (2 x +1) - (4 x 2)
5. oxidation state of S = +6

The two sodium atoms each have an oxidation state of +1, while the oxygen atoms have an oxidation state of 2, and the overall charge is 0.

1. overall charge = sum of oxidation states
2. 0 = (2 x oxidation state of Na) + (oxidation state of S) + (3 x oxidation state of O)
3. 0 = (2 x +1) + (oxidation state of S) + (3 x -2)
4. oxidation state of S = 0 (2 x +1) - (3 x 2)
5. oxidation state of S = +4

The two hydrogen atoms each have an oxidation state of +1 and the overall charge is 0.

- overall charge = sum of oxidation states
- 0 = (2 x oxidation state of H) + (oxidation state of S)
- 0 = (2 x +1) + (oxidation state of S)
- oxidation state of S = 0 (2 x +1)
- oxidation state of S = -2

This page titled 6.1.1: Fundamental Properties - Oxidation State is shared under a CC BY 3.0 license and was authored, remixed, and/or curated by Andrew R. Barron (CNX) via source content that was edited to the style and standards of the LibreTexts platform.

6.1.2: Fundamental Properties - Ionization Energy

The ionization energy (IE), or more properly the ionization enthalpy, is defined as the energy required to loose an electron from a gaseous atom or ion.

$$M_{(g)}^{n+} \rightarrow M_{(g)}^{(n+1)+} + e^- \tag{6.1.2.1}$$

Each subsequent ionization energy is greater than the previous one because of the increase in charge on the ion. For example, for any given atom or ion the 1st ionization energy is less than the 2nd ionization energy, and so on. This is shown in Table 6.1.2.1.1.

Table 6.1.2.1.1: The first three ionization energies for aluminum.

Ionization	
$Al^0 \rightarrow Al^+ + e^-$	(6.1.2.2)
$Al^+ \rightarrow Al^{2+} + e^-$	(6.1.2.3)
$Al^{2+} \rightarrow Al^{3+} + e^-$	(6.1.2.4)

How does the ionization energy vary with elements in the periodic table? If we consider the 1st ionization potential of the elements in a particular group of the periodic table we note that there is a decrease in ionization potential as you go down the Group. The reason for this trend is due to the increased shielding of the outer shell electrons (ns^1) by the completed (filled) inner shells. The ns^1 electron thus exhibits a lower effective nuclear charge and makes it easier to remove. For example, Table 6.1.2.1.2 shows the 1st ionization potential for the Group 1 alkali metals.

Table 6.1.2.1.2: Variation of the first ionization potential (M0 → M+) for the Group 1 (IA) elements.

Element	**Ionization energy (kJ/mol)**
Li	526
Na	502
K	425
Rb	409
Cs	382

In contrast, to individual Groups, moving across a particular Period results in a general increase in the ionization potential as is shown in Figure 6.1.2.1.1. The lack of additional screening of filled shells across the Period means that the ionization energy for the outer shell electrons is dominated by the increase in nuclear charge (number of protons) with increased atomic number.

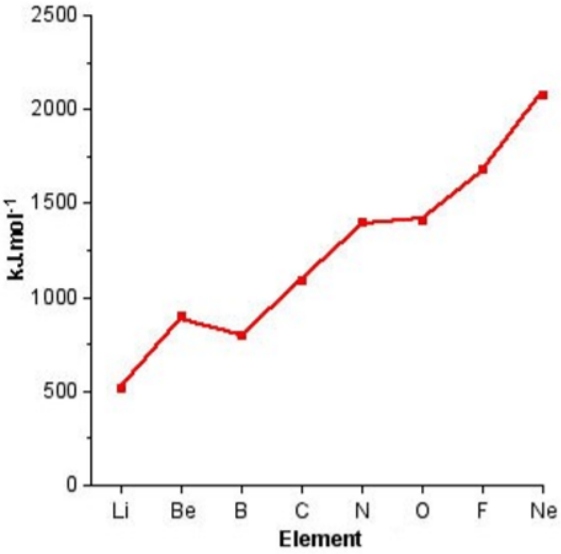


Figure 6.1.2.1: Plot of the first ionization potential for the elements Li to Ne.

From Figure 6.1.2.1.1 it can be seen that the Periodic trend is not linear, there are significant steps in the plot. Boron, for example, has a lower first ionization potential than beryllium, why? A consideration of the electron configuration for the elements provides in answer (Figure 6.1.2.1.2). Beryllium has a $2s^2$ outer shell configuration, while boron has a $2s^2$ $2p^1$ configuration. The $2p^1$ electron is easy to remove because it exhibits increased shielding from the nucleus due to the filled 2s orbital.

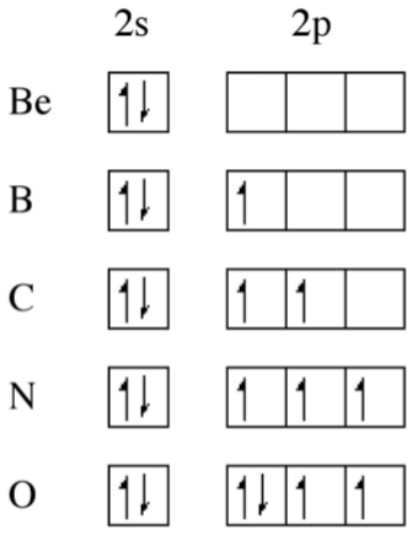


Figure 6.1.2.2: Outer shell electron configuration of beryllium through oxygen.

As we move from, boron to nitrogen, the 2p shell is filled (Figure 6.1.2.1.2) without additional shielding and the effect of the increased nuclear charge dominates. Finally, the $2p^4$ configuration for oxygen (Figure 6.1.2.1.2) results in an electron pair, which repel each other, thus making it easier to remove an electron (lower ionization potential) that expected from the increased nuclear charge. From Figure 6.1.2.1 we can see that the effect of electron pairing is less than that of a filled shell.

The trend for the 2nd ionization potential is similar, but different, to that of the 1st ionization potential. As may be seen in Figure 6.1.2.1.3 the steps observed for the 1st ionization energy plot (i.e., between Be/B and N/O have moved one element to the right. A view of the electron conguration for the E^+ ions (Figure 6.1.2.1.4) shows that the rational for the trend in the 1st ionization potential trends still applies but to the ion of the element to the right in the Periodic table. Now B+ has a $2s^2$ outer shell conguration, while C^+ has a $2s^2$ $2p^1$ configuration. A similar plot for the 3rd ionization energy would move the steps another element to the right.

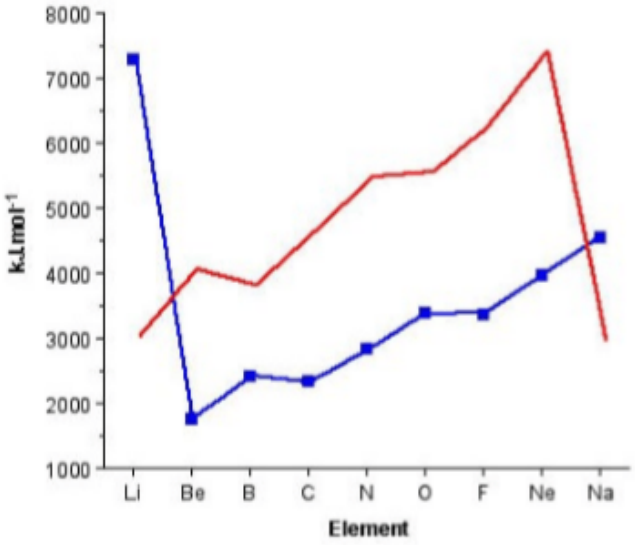


Figure 6.1.2.3: A plot of 2nd ionization energy (enthalpy) for elements Li to Na (blue with square data points) showing the relative trend to the 1st ionization potential (red line not to scale).

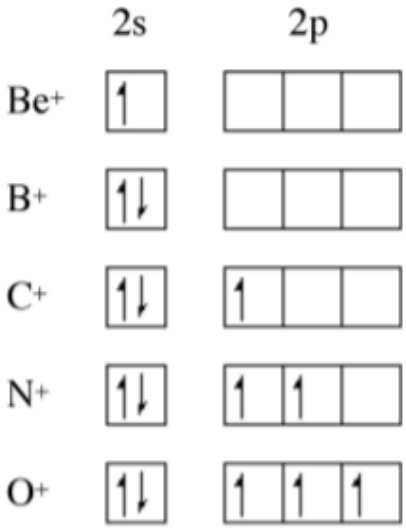


Figure 6.1.2.4: Outer shell electron conguration of E+ for beryllium through oxygen.

The other observation to be made from Figure 6.1.2.1.3 is the very large 2nd ionization potential for lithium associated with the ionization of Li^+ to Li^{2+}. The large increase is due to the removal of an electron from the filled $1s^2$ shell.

This page titled 6.1.2: Fundamental Properties - Ionization Energy is shared under a CC BY 3.0 license and was authored, remixed, and/or curated by Andrew R. Barron (CNX) via source content that was edited to the style and standards of the LibreTexts platform.

6.1.3: Fundamental Properties - Electron Affinity

The electron affinity (EA) of an element is defined as the energy given of when a neutral atom in the gas phase gains an extra electron to form a negatively charged ion.

$$X_{(g)}^{n-} + e^- \rightarrow X_{(g)}^{(n+1)-} \tag{6.1.3.1}$$

Electron anities are more difficult to measure than ionization energies and are usually less accurately known. Electron affinities are large and negative for elements such as fluorine and oxygen, and small and positive for metals.

Electron affinities generally become smaller as you go down a Group of the periodic table (Table 6.1.3.1.3). This is because the electron being added to the atom is placed in a larger orbital, where it spends less time near the nucleus of the atom, and also the number of electrons on an atom increases as we go down a column, so the force of repulsion between the electron being added and the electrons already present on a neutral atom becomes larger. Electron anities are further complicated since the repulsion between the electron being added to the atom and the electrons already present on the atom depends on the volume of the atom. Thus, for the nonmetals in Groups 6 (VIA) and 7 (VIIA), this force of repulsion is largest for the very smallest atoms in these columns: oxygen and uorine. As a result, these elements have a smaller electron anity than the elements below them in these columns as shown in Table 6.1.3.1.3.

Table 6.1.3.1.3: The electron anity for the non-metallic halogens.

Element	Electron affinity (kJ/mol)
F	-322
Cl	-349
Br	-325
I	-295

Although there is a general trend that for Group 1 (IA) to Group 17 (VIIA) elements the electron affinity increases across the Periodic table from left to right, the details of the trend are more complex. As may be seen from Figure 6.1.3.1.5, there is a cyclic trend. The explanation of this is a consequence of the unusually stable electron configurations exhibited by atoms with filled or half filled shells, i.e., helium, beryllium, nitrogen and neon (see Table 6.1.3.1.4). These configurations are so stable that it actually takes energy to force one of these elements to pick up an extra electron to form a negative ion.

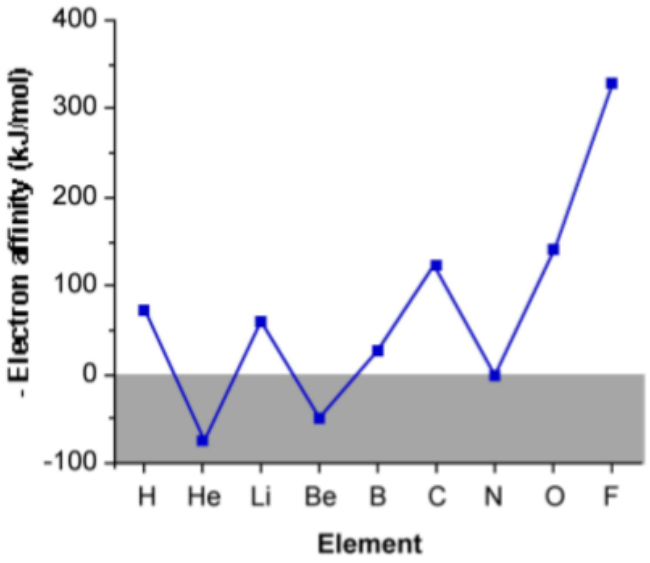


Figure 6.1.3.5: Plot of the electron affinity for the elements hydrogen to fluorine. N.B. Values for helium, beryllium, nitrogen, and neon are not known with any accuracy but are all positive.

Table 6.1.3.1.4: Electron affinities of the elements hydrogen to neon. N.B. Values for helium, beryllium, nitrogen, and neon are not known with any accuracy but are all positive.

Element	Electron affinity (kJ/mol)	Electron configuration
H	-72.8	$1s^1$
He	+ve	$1s^2$
Li	-59.8	[He] $2s^1$
Be	+ve	[He] $2s^2$
B	-27	[He] $2s^2 2p^1$
C	-122.3	[He] $2s^2 2p^2$
N	+ve	[He] $2s^2 2p^3$
O	-141.1	[He] $2s^2 2p^4$
F	-328.0	[He] $2s^2 2p^5$
Ne	+ve	[He] $2s^2 2p^6$

This page titled 6.1.3: Fundamental Properties - Electron Affinity is shared under a CC BY 3.0 license and was authored, remixed, and/or curated by Andrew R. Barron (CNX) via source content that was edited to the style and standards of the LibreTexts platform.

6.1.4: Fundamental Properties - Electronegativity

An issue with ionization potential and electron affinity is that they are defined and measured as reactions in the gas phase. Although values have been determined for molecular fragments it is still difficult to correlate with reaction trends in solution. To overcome this issue the concept of electronegativity was developed.

Electronegativity is defined as *the tendency of an atom in a molecule to attract electrons to itself*. Although several electronegativity scales have been developed, that by Linus Pauling (Figure 6.1.4.1.6) is the most often used. Table 6.1.4.1.5 provides selected Pauling electronegativity values (unit less).

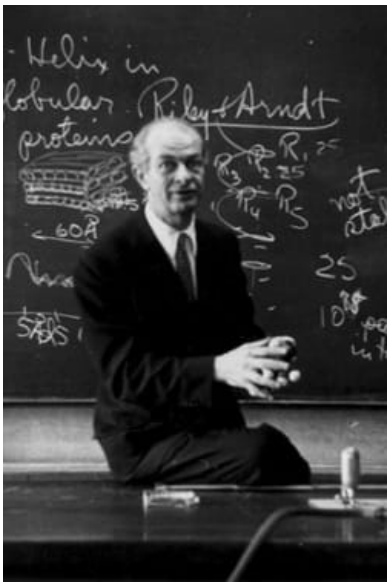


Figure 6.1.4.6: American chemist Linus Carl Pauling (1901 1994).

Table 6.1.4.1.5: Selected Pauling electronegativity values.

Element	Pauling Scale
F	4.0
O	3.5
Cl	3.0
N	3.0
S	2.5
C	2.5
H	2.1
B	2.0
Na	0.9

The advantage of the Pauling electronegativity scale is that it allows the prediction of general behavior. For example, the larger the dierence in electronegativity between two elements the more ionic character or more polar the bonding interaction. Thus, a H-O bond (3.5 - 2.1 = 1.4) is more polar than a H-S bond (2.5 2.1 = 0.4).

This page titled 6.1.4: Fundamental Properties - Electronegativity is shared under a CC BY 3.0 license and was authored, remixed, and/or curated by Andrew R. Barron (CNX) via source content that was edited to the style and standards of the LibreTexts platform.

6.1.5: Structure and Bonding - Valence Shell Electron Pair Repulsion (VSEPR) Theory

The idea of a correlation between molecular geometry and the number of valence electrons was first presented in 1940 by Sidgwick and Powell; however, in 1957, Ronald Gillespie (Figure 6.1.5.1.7) and Sir Ronald Nyholm (Figure 6.1.5.1.8) refined this concept to build a more detailed theory. It is their work that provides the basis of the valence shell electron pair repulsion (VSEPR) theory, and as such it is also known as the Gillespie-Nyholm theory.

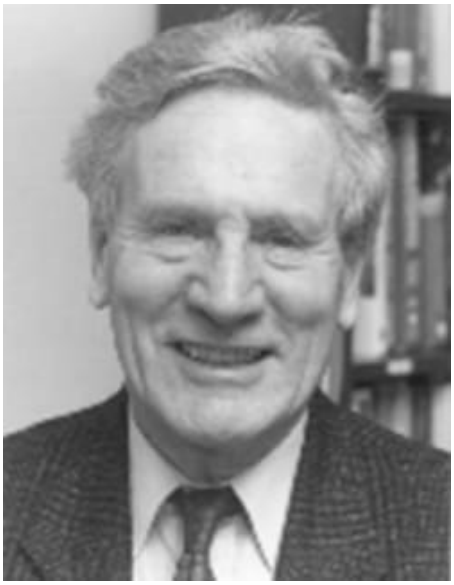


Figure 6.1.5.7: Chemist Ronald J. Gillespie (1924 -).



Figure 6.1.5.8: Australian chemist Sir Ronald Sydney Nyholm (1917 -).

One attribute of VSEPR is that with the ability to predict the shape of a molecule for a compound comes the ability to predict some of the physical and chemical properties of that compound.

The formal definition that is the basis for VSEPR is as follows: *Pairs of electrons in the valence shell of a central atom of a molecule repel each other and take up positions as far apart as possible*.

Within this definition it is implicitly assumed that the core shells are not polarized and therefore take no part in bonding, and therefore can be ignored. Since the maximum repulsion of the electron pairs (be they associated with a bonding interaction or a lone pair) control the shape of a molecule, for each number of electron pairs we can dene the geometric optimum position that maximizes the distance between the electron pairs (Table 6.1.5.1.6). The number of electron pairs surrounding an atom, both bonding and nonbonding, is called its steric number.

Table 6.1.5.1.6: Shapes of molecules and ions

Number of central atom electron pairs	Bonding pairs	Non-bonding pairs	Shape	Example
2	2	0	Linear	$BeCl_2$
3	3	0	Triangular	BF_3
3	2	1	Bent	$SnCl_2$
4	4	0	Tetrahedral	CCl_4
4	3	1	Pyramidal	NH_3
4	2	2	Bent	H_2O
5	5	0	Trigonal bipyramidal (tbp)	PF_5
5	4	1	Pseudo-tdp	BrF_4^-
5	3	2	T-Shaped	BrF_3
5	2	3	Linear	XeF_2
6	6	0	Octahedral	SF_6,PF_6^-
6	5	1	Square pyramidal	IF_5
6	4	2	Square planar	XeF_4,IF_4^-

The steps for dening the molecular shape are as follows:

1. Draw a simple Lewis structure including single, double, and triple bonds where appropriate.
2. Count the number of electrons on the central atom assuming it is neutral.
3. Add one electron for each σ-bond.
4. Subtract one electron for each π-bond.
5. Subtract one electron for each positive (+) charge.
6. Add one electron for each negative (-) charge.
7. Divide the number of electrons by two to give the number of electron pairs.
8. Use the list in Table 6.1.5.1.6 to predict the structure of the molecule.

6.1.5.1Exa

What is the shape of NH_4^+

Solution

1. Nitrogen has 5 valence electrons
2. Add 4 electrons for the four σ-bonds: 5 + 4 = 9
3. Subtract one electron for the positive (+) charge: 9 1 = 8
4. Divide the number of electrons by two to give the number of electron pairs: 8/2 = 4
5. Four bonding pairs and no lone pairs = tetrahedral geometry

Exercises

Exercise 6.1.5.1

What is the shape of $HgCl_2$?

Answer available at the end of this section.

Exercise 6.1.5.2

What is the shape of H_2CO?

Answer available at the end of this section.

Lone pairs versus bonding pairs

The prediction of the detailed molecular structure (including bond angles) is not as simple as shown in Table 6.1.5.1.6. In molecules with either lone pair electrons or multiple (double or triple) bonds the angles about the central atom are distorted due to the increased electron repulsion (Figure 6.1.5.1.9). The differences in repulsion caused by a lone pair or a bonding pair may be rationalized in a simple manner by a lone pair taking up more space than a bonding pair (Figure 6.1.5.1.10).

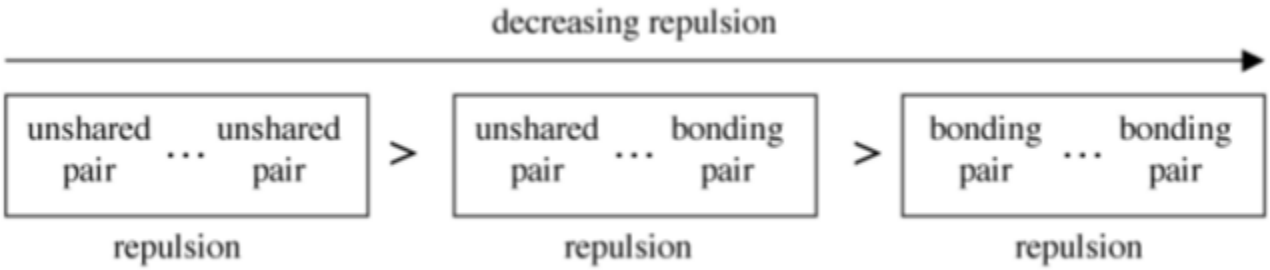


Figure 6.1.5.9: The order of decreasing repulsion between non-bonding (unshared) and bonding electron pairs.

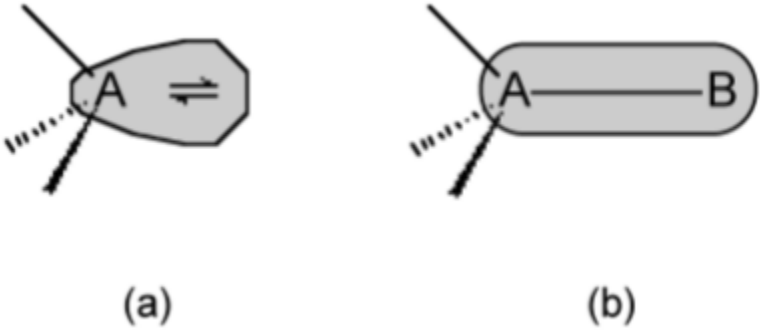


Figure 6.1.5.10: Representation of the relative space taken up by (a) a lone pair of electrons and (b) a bonding pair of electrons.

Water is one of the classic cases in considering the issue of non-bonding (unshared) electron pairs.

1. Oxygen has 6 valence electrons
2. Add 2 electrons for the two σ-bonds: 6 + 2 = 8
3. Divide the number of electrons by two to give the number of electron pairs: 8/2 = 4
4. Two bonding pairs and two lone pairs = tetrahedral geometry

From this an idealized tetrahedral geometry would give the H-O-H angle as 109.5°, however, from Figure 6.1.5.1.9 we know that the lone pair...lone pair repulsion is greater than the lone pair...bonding pair repulsion which is greater than the bonding pair...bonding pair repulsion, and thus, the H-O-H angle should be decreased from the ideal tetrahedral. The experimentally determined H-O-H angle in water is in fact 104.5°.

Ethylene is a good case in considering the issue of multiple bonds. Ethylene contains both σ-bond and π-bond between the carbon atoms. This combination can be thought of as a super bond, and as such its effect is similar to a lone pair.

Carbon has 4 valence electrons

Add 3 electrons for the two σ-bonds: 4 + 3 = 7

Subtract one electron for each π-bond: 7 1 = 6

Divide the number of electrons by two to give the number of electron pairs: 6/2 = 3

Three bonding pairs and no lone pairs = triangular geometry

From this an idealized tetrahedral geometry would give the H-C-H angle as 120°, however, the π-bond repulsion is greater than the σ-bond repulsion, and thus, the H-C-H angle should be decreased from the ideal tetrahedral. The experimentally determined H-O-H angle in water is in fact 118.3°.

Resonance structures

If a molecule or ion has two or more resonance forms it is necessary to consider each form before angles are predicted. For example, the carbonate anion, CO_3^-, can be drawn as a single structure from which it would be predicted that two groups of O-C-O angles would result (Figure 6.1.5.1.11).

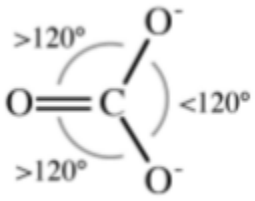


Figure 6.1.5.11: VSEPR predicted structure of a single resonance form of CO_3^{2-}.

However, CO_3^- should actually be drawn in each of its resonance forms as in Figure 6.1.5.1.12.

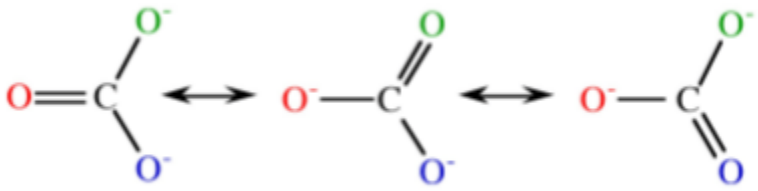


Figure 6.1.5.12: Resonance forms of CO_3^{2-}.

From Figure 6.1.5.1.12 it is clear that the real structure will be an average of the three resonance forms, and hence there will be a single O-C-O angle = 120° (Figure 6.1.5.1.13).

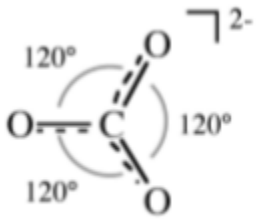


Figure 6.1.5.13: Structure of CO_3^{2-}.

Atom electronegativities

In an A-X bond where the atom electronegativities are very different the bonding pair is assumed to occupy less space than in bond between two atoms of similar electronegativities. As the bonding pair occupies less space it will repel neighboring electron pairs less.

For example, based on the above, a comparison of the tetrahedral compounds H_2O and F_2O would suggest that the F-O-F angle be smaller than the H-O-H angle since fluorine has a higher electronegativity than hydrogen (4.0 and 2.1, respectively). This is indeed observed (Figure 6.1.5.1.14).

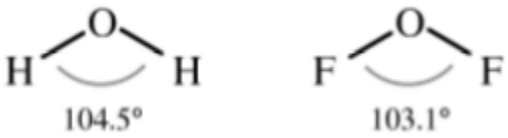


Figure 6.1.5.14: Structures of H_2O and F_2O.

In many cases, inter-ligand steric interactions can also be used to explain the dffierence in angle. For example, while fluorine is more electronegative than chlorine (4.0 versus 3.0, respectively) it is also significantly smaller (Table 6.1.5.1.7). Thus, a larger Cl-X-Cl angle than a F-X-F angle in the homologous compound, can be attributed to a greater steric interactions, rather than difference in electronegativities.

Table 6.1.5.1.7: Comparison of size between fluoride and chloride ligands.

Ligand	Covalent Radius (Å)	Van der Waal radius (Å)
F	0.57	1.35
Cl	1.02	1.80

Bent's rule

There is the potential for more than one isomer for molecules that adopt structures in which there is a symmetry difference between at least two of the ligand positions. For example a trigional bipyramidal compound of the formula PXY_4 has two possible structures. One where the X occupies an axial position (Figure 6.1.5.1.15a) and the other where it occupies an equatorial position (Figure 6.1.5.1.15b).

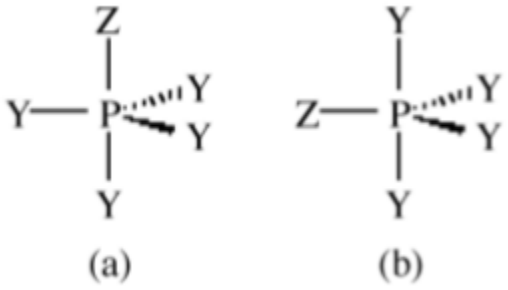


Figure 6.1.5.15: The two possible structures of PXY_4.

Through the consideration of structures Henry Bent suggested a rule: *More electronegative substituents prefer hybrid orbitals with less s character, and conversely, more electropositive substituents prefer hybrid orbitals with greater s character.*

For example, in $PFCl_5$ the fluorine is the most electronegative substituent and will therefore occupy the axial (p-character only) position.

Bibliography

- H. A. Bent, *J. Chem. Educ.*, 1960, **37**, 616.
- H. A. Bent, *Chem. Rev.*, 1961, **61**, 275.
- R. J. Gillespie, *J. Chem. Educ.*, 1970, **47**, 18.
- R. J. Gillespie, *Chem. Soc. Rev.*, 1992, **21**, 59.
- R. J. Gillespie and R. S. Nyholm, *Quart. Rev.*, 1957, **11**, 339.

Answers

1. Mercury has 2 valence electrons
2. Add 2 electrons for the two σ-bonds: 2 + 2 = 4
3. Divide the number of electrons by two to give the number of electron pairs: 4/2 = 2
4. Two bonding pairs and no lone pairs = linear geometry

1. Carbon has 4 valence electrons
2. Add 3 electrons for the three σ-bonds: 4 + 3 = 7
3. Subtract one electron for each π-bond: 7 1 = 6
4. Divide the number of electrons by two to give the number of electron pairs: 6/2 = 3
5. Two bonding pairs and no lone pairs = triangular geometry

This page titled 6.1.5: Structure and Bonding - Valence Shell Electron Pair Repulsion (VSEPR) Theory is shared under a CC BY 3.0 license and was authored, remixed, and/or curated by Andrew R. Barron (CNX) via source content that was edited to the style and standards of the LibreTexts platform.

6.1.6: Structure and Bonding - Crystal Structure

Introduction

In any sort of discussion of crystalline materials, it is useful to begin with a discussion of crystallography: the study of the formation, structure, and properties of crystals. A crystal structure is defined as the particular repeating arrangement of atoms (molecules or ions) throughout a crystal. Structure refers to the internal arrangement of particles and not the external appearance of the crystal. However, these are not entirely independent since the external appearance of a crystal is often related to the internal arrangement. For example, crystals of cubic rock salt (NaCl) are physically cubic in appearance. Only a few of the possible crystal structures are of concern with respect to simple inorganic salts and these will be discussed in detail, however, it is important to understand the nomenclature of crystallography.

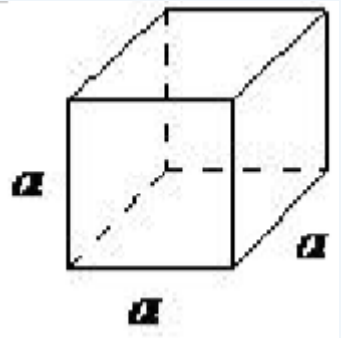
Crystallography

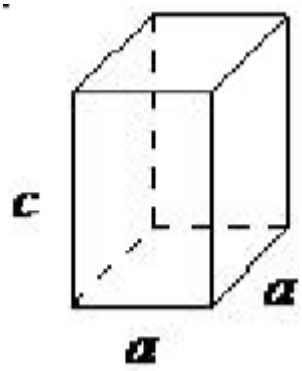
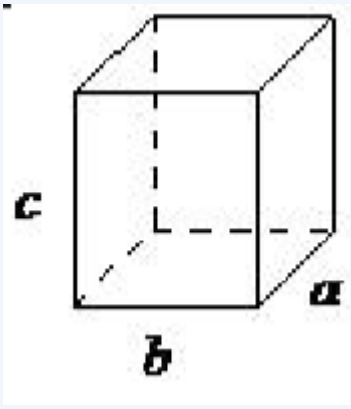
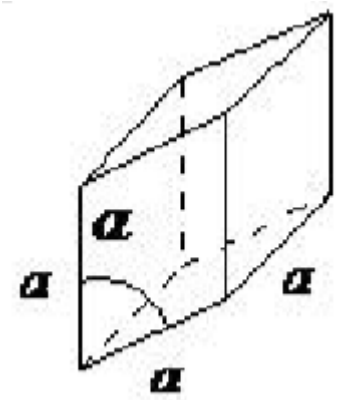
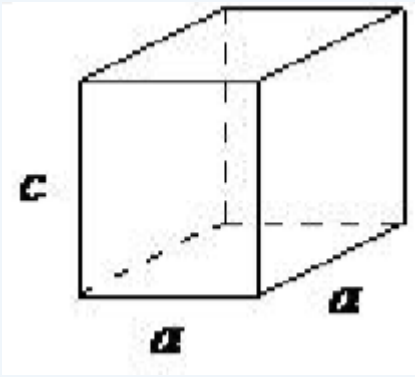
Bravais lattice

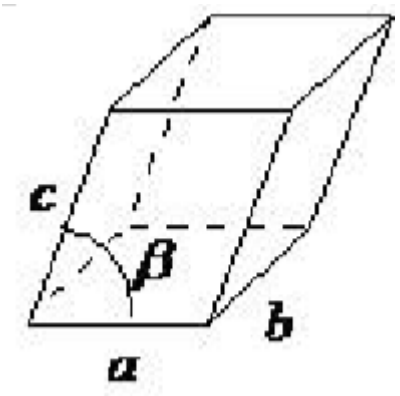
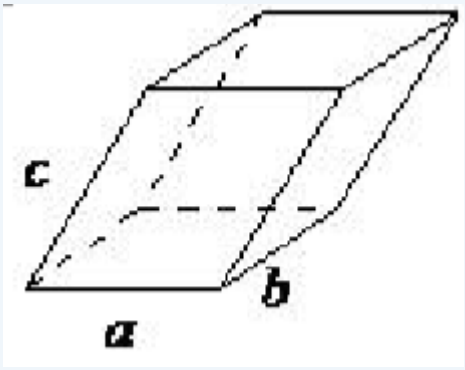
The Bravais lattice is the basic building block from which all crystals can be constructed. The concept originated as a topological problem of finding the number of different ways to arrange points in space where each point would have an identical atmosphere. That is each point would be surrounded by an identical set of points as any other point, so that all points would be indistinguishable from each other. Mathematician Auguste Bravais discovered that there were 14 different collections of the groups of points, which are known as Bravais lattices. These lattices fall into seven different "crystal systems, as differentiated by the relationship between the angles between sides of the unit cell and the distance between points in the unit cell. The unit cell is the smallest group of atoms, ions or molecules that, when repeated at regular intervals in three dimensions, will produce the lattice of a crystal system. The lattice parameter is the length between two points on the corners of a unit cell. Each of the various lattice parameters are designated by the letters *a*, *b*, and *c*. If two sides are equal, such as in a tetragonal lattice, then the lengths of the two lattice parameters are designated *a* and *c*, with *b* omitted. The angles are designated by the Greek letters *α*, *β*, and *γ*, such that an angle with a specific Greek letter is not subtended by the axis with its Roman equivalent. For example, *α* is the included angle between the *b* and *c* axis.

Table 6.1.6.1.8 shows the various crystal systems, while Figure 6.1.6.1.16 shows the 14 Bravais lattices. It is important to distinguish the characteristics of each of the individual systems. An example of a material that takes on each of the Bravais lattices is shown in Table 6.1.6.1.9.

Table 6.1.6.1.8: Geometrical characteristics of the seven crystal systems.

System	Axial lengths and angles	Unit cell geometry
cubic	a = b = c, α = β = γ= 90°	

tetragonal	$a = b \neq c$, $\alpha = \beta = \gamma = 90^\circ$	
orthorhombic	$a \neq b \neq c$, $\alpha = \beta = \gamma = 90^\circ$	
rhombohedral	$a = b = c$, $\alpha = \beta = \gamma \neq 90^\circ$	
hexagonal	$a = b \neq c$, $\alpha = \beta = 90^\circ$, $\gamma = 120^\circ$	

monoclinic	$a \neq b \neq c$, $\alpha = \gamma = 90^\circ$, $\beta \neq 90^\circ$	
triclinic	$a \neq b \neq c$, $\alpha \neq \beta \neq \gamma$	

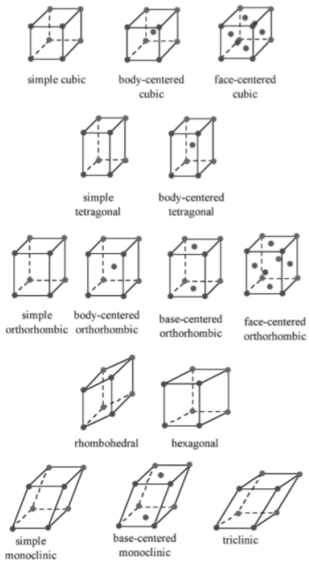


Figure 6.1.6.16: Bravais lattices.

Table 6.1.6.1.9: Examples of elements and compounds that adopt each of the crystal systems.

Crystal system	**Example**
triclinic	$K_2S_2O_8$
monoclinic	As_4S_4, KNO_2
rhombohedral	Hg, Sb
hexagonal	Zn, Co, NiAs

orthorhombic	Ga, Fe_3C
tetragonal	In, TiO_2
cubic	Au, Si, NaCl

The cubic lattice is the most symmetrical of the systems. All the angles are equal to 90°, and all the sides are of the same length ($a = b = c$). Only the length of one of the sides (a) is required to describe this system completely. In addition to simple cubic, the cubic lattice also includes body-centered cubic and face-centered cubic (Figure 6.1.6.1.16). Body-centered cubic results from the presence of an atom (or ion) in the center of a cube, in addition to the atoms (ions) positioned at the vertices of the cube. In a similar manner, a face-centered cubic requires, in addition to the atoms (ions) positioned at the vertices of the cube, the presence of atoms (ions) in the center of each of the cubes face.

The tetragonal lattice has all of its angles equal to 90°, and has two out of the three sides of equal length ($a = b$). The system also includes body-centered tetragonal (Figure 6.1.6.1.16).

In an orthorhombic lattice all of the angles are equal to 90°, while all of its sides are of unequal length. The system needs only to be described by three lattice parameters. This system also includes body-centered orthorhombic, base-centered orthorhombic, and face-centered orthorhombic (Figure 6.1.6.1.16). A base-centered lattice has, in addition to the atoms (ions) positioned at the vertices of the orthorhombic lattice, atoms (ions) positioned on just two opposing faces.

The rhombohedral lattice is also known as trigonal, and has no angles equal to 90°, but all sides are of equal length ($a = b = c$), thus requiring only by one lattice parameter, and all three angles are equal ($\alpha = \beta = y$).

A hexagonal crystal structure has two angles equal to 90°, with the other angle (y) equal to 120°. For this to happen, the two sides surrounding the 120° angle must be equal ($a = b$), while the third side (c) is at 90° to the other sides and can be of any length.

The monoclinic lattice has no sides of equal length, but two of the angles are equal to 90°, with the other angle (usually defined as β) being something other than 90°. It is a tilted parallelogram prism with rectangular bases. This system also includes base-centered monoclinic (Figure 6.1.6.1.16).

In the triclinic lattice none of the sides of the unit cell are equal, and none of the angles within the unit cell are equal to 90°. The triclinic lattice is chosen such that all the internal angles are either acute or obtuse. This crystal system has the lowest symmetry and must be described by 3 lattice parameters *(a*, *b*, and *c*) and the 3 angles (α, β, and y).

Atom positions, crystal directions and Miller indicies

Atom positions and crystal axes

The structure of a crystal is defined with respect to a unit cell. As the entire crystal consists of repeating unit cells, this definition is sufficient to represent the entire crystal. Within the unit cell, the atomic arrangement is expressed using coordinates. There are two systems of coordinates commonly in use, which can cause some confusion. Both use a corner of the unit cell as their origin. The first, less-commonly seen system is that of Cartesian or orthogonal coordinates (X, Y, Z). These usually have the units of Angstroms and relate to the distance in each direction between the origin of the cell and the atom. These coordinates may be manipulated in the same fashion are used with two- or three-dimensional graphs. It is very simple, therefore, to calculate inter-atomic distances and angles given the Cartesian coordinates of the atoms. Unfortunately, the repeating nature of a crystal cannot be expressed easily using such coordinates. For example, consider a cubic cell of dimension 3.52 Å. Pretend that this cell contains an atom that has the coordinates (1.5, 2.1, 2.4). That is, the atom is 1.5 Å away from the origin in the x direction (which coincides with the a cell axis), 2.1 Å in the y (which coincides with the b cell axis) and 2.4 Å in the z (which coincides with the c cell axis). There will be an equivalent atom in the next unit cell along the x-direction, which will have the coordinates (1.5 + 3.52, 2.1, 2.4) or (5.02, 2.1, 2.4). This was a rather simple calculation, as the cell has very high symmetry and so the cell axes, a, b and c, coincide with the Cartesian axes, X, Y and Z. However, consider lower symmetry cells such as triclinic or monoclinic in which the cell axes are not mutually orthogonal. In such cases, expressing the repeating nature of the crystal is much more difficult to accomplish.

Accordingly, atomic coordinates are usually expressed in terms of fractional coordinates, (x, y, z). This coordinate system is

coincident with the cell axes (a, b, c) and relates to the position of the atom in terms of the fraction along each axis. Consider the atom in the cubic cell discussion above. The atom was 1.5 Å in the a direction away from the origin. As the a axis is 3.52 Å long, the atom is ($^{1.5}/_{3.52}$) or 0.43 of the axis away from the origin. Similarly, it is ($^{2.1}/_{3.52}$) or 0.60 of the b axis and ($^{2.4}/_{3.5}$) or 0.68 of the c axis. The fractional coordinates of this atom are, therefore, (0.43, 0.60, 0.68). The coordinates of the equivalent atom in the next cell over in the a direction, however, are easily calculated as this atom is simply 1 unit cell away in a. Thus, all one has to do is add 1 to the x coordinate: (1.43, 0.60, 0.68). Such transformations can be performed regardless of the shape of the unit cell. Fractional coordinates, therefore, are used to retain and manipulate crystal information.

Crystal directions

The designation of the individual vectors within any given crystal lattice is accomplished by the use of whole number multipliers of the lattice parameter of the point at which the vector exits the unit cell. The vector is indicated by the notation [*hkl*], where *h*, *k*, and *l* are reciprocals of the point at which the vector exits the unit cell. The origination of all vectors is assumed defined as [000]. For example, the direction along the *a*-axis according to this scheme would be [100] because this has a component only in the *a*-direction and no component along either the *b* or *c* axial direction. A vector diagonally along the face defined by the *a* and *b* axis would be [110], while going from one corner of the unit cell to the opposite corner would be in the [111] direction. Figure 6.1.6.1.17 shows some examples of the various directions in the unit cell. The crystal direction notation is made up of the lowest combination of integers and represents unit distances rather than actual distances. A [222] direction is identical to a [111], so [111] is used. Fractions are not used. For example, a vector that intercepts the center of the top face of the unit cell has the coordinates x = 1/2, y = 1/2, z = 1. All have to be inversed to convert to the lowest combination of integers (whole numbers); i.e., [221] in Figure 6.1.6.1.17. Finally, all parallel vectors have the same crystal direction, e.g., the four vertical edges of the cell shown in Figure 6.1.6.1.17 all have the crystal direction [*hkl*] = [001].

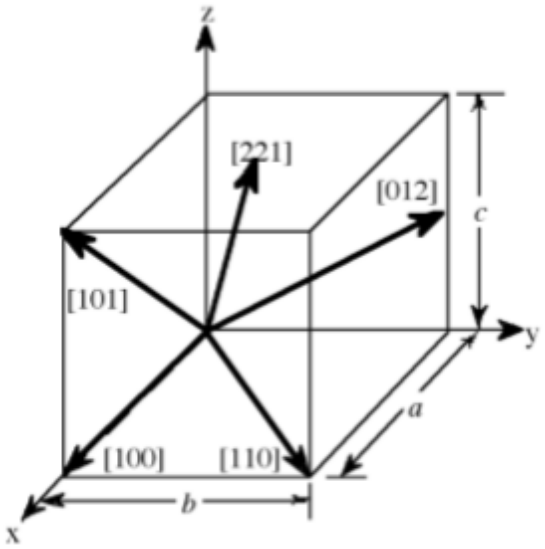


Figure 6.1.6.17: Some common directions in a cubic unit cell.

Crystal directions may be grouped in families. To avoid confusion there exists a convention in the choice of brackets surrounding the three numbers to differentiate a crystal direction from a family of direction. For a direction, square brackets [*hkl*] are used to indicate an individual direction. Angle brackets <*hkl*> indicate a family of directions. A family of directions includes any directions that are equivalent in length and types of atoms encountered. For example, in a cubic lattice, the [100], [010], and [001] directions all belong to the <100> family of planes because they are equivalent. If the cubic lattice were rotated 90°, the *a*, *b*, and *c* directions would remain indistinguishable, and there would be no way of telling on which crystallographic positions the atoms are situated, so the family of directions is the same. In a hexagonal crystal, however, this is not the case, so the [100] and [010] would both be <100> directions, but the [001] direction would be distinct. Finally, negative directions are identified with a bar over the negative number instead of a minus sign.

Crystal planes

Planes in a crystal can be specified using a notation called Miller indices. The Miller index is indicated by the notation [*hkl*] where

h, *k*, and *l* are reciprocals of the plane with the *x*, *y*, and *z* axes. To obtain the Miller indices of a given plane requires the following steps:

1. The plane in question is placed on a unit cell.
2. Its intercepts with each of the crystal axes are then found.
3. The reciprocal of the intercepts are taken.
4. These are multiplied by a scalar to insure that is in the simple ratio of whole numbers.

For example, the face of a lattice that does not intersect the y or z axis would be (100), while a plane along the body diagonal would be the (111) plane. An illustration of this along with the (111) and (110) planes is given in Figure 6.1.6.1.18.

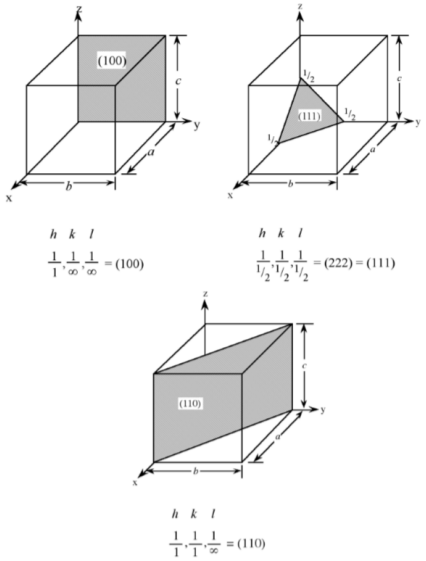


Figure 6.1.6.18: Examples of Miller indices notation for crystal planes.

As with crystal directions, Miller indices directions may be grouped in families. Individual Miller indices are given in parentheses (*hkl*), while braces {*hkl*} are placed around the indices of a family of planes. For example, (001), (100), and (010) are all in the {100} family of planes, for a cubic lattice.

Description of crystal structures

Crystal structures may be described in a number of ways. The most common manner is to refer to the size and shape of the unit cell and the positions of the atoms (or ions) within the cell. However, this information is sometimes insufficient to allow for an understanding of the true structure in three dimensions. Consideration of several unit cells, the arrangement of the atoms with respect to each other, the number of other atoms they in contact with, and the distances to neighboring atoms, often will provide a better understanding. A number of methods are available to describe extended solid-state structures. The most applicable with regard to elemental and compound semiconductor, metals and the majority of insulators is the close packing approach.

Close packed structures: hexagonal close packing and cubic close packing

Many crystal structures can be described using the concept of close packing. This concept requires that the atoms (ions) are arranged so as to have the maximum density. In order to understand close packing in three dimensions, the most efficient way for equal sized spheres to be packed in two dimensions must be considered.

The most efficient way for equal sized spheres to be packed in two dimensions is shown in Figure 6.1.6.1.19, in which it can be seen that each sphere (the dark gray shaded sphere) is surrounded by, and is in contact with, six other spheres (the light gray spheres in Figure 6.1.6.1.19). It should be noted that contact with six other spheres the maximum possible is the spheres are the same size, although lower density packing is possible. Close packed layers are formed by repetition to an infinite sheet. Within these close packed layers, three close packed rows are present, shown by the dashed lines in Figure 6.1.6.1.19.

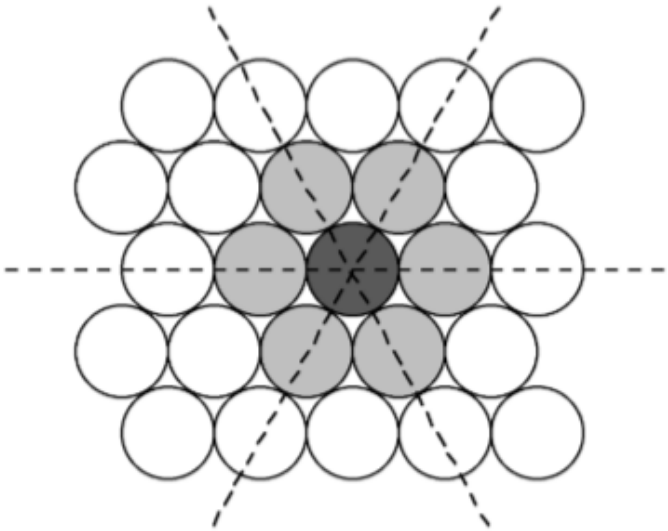


Figure 6.1.6.19: Schematic representation of a close packed layer of equal sized spheres. The close packed rows (directions) are shown by the dashed lines.

The most efficient way for equal sized spheres to be packed in three dimensions is to stack close packed layers on top of each other to give a close packed structure. There are two simple ways in which this can be done, resulting in either a hexagonal or cubic close packed structures.

Hexagonal close packed

If two close packed layers A and B are placed in contact with each other so as to maximize the density, then the spheres of layer B will rest in the hollow (vacancy) between three of the spheres in layer A. This is demonstrated in Figure 6.1.6.1.20. Atoms in the second layer, B (shaded light gray), may occupy one of two possible positions (Figure 6.1.6.1.20a or b) but not both together or a mixture of each. If a third layer is placed on top of layer B such that it exactly covers layer A, subsequent placement of layers will result in the following sequence ...ABABAB.... This is known as hexagonal close packing or *hcp*.

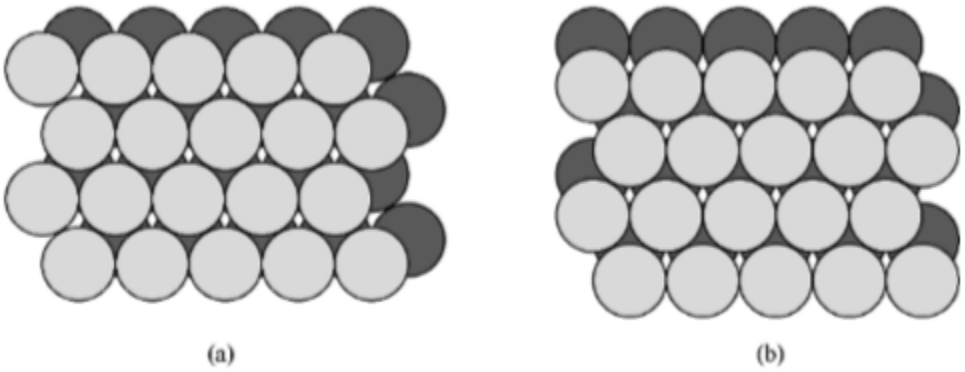


Figure 6.1.6.20: Schematic representation of two close packed layers arranged in A (dark grey) and B (light grey) positions. The alternative stacking of the B layer is shown in (a) and (b).

The hexagonal close packed cell is a derivative of the hexagonal Bravais lattice system (Figure 6.1.6.1.16) with the addition of an atom inside the unit cell at the coordinates ($^1/_3$,$^2/_3$,$^1/_2$). The basal plane of the unit cell coincides with the close packed layers (Figure 6.1.6.1.21). In other words the close packed layer makes-up the {001} family of crystal planes.

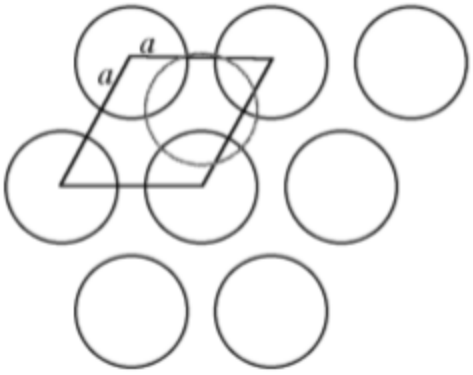


Figure 6.1.6.21: A schematic projection of the basal plane of the hcp unit cell on the close packed layers.

The packing fraction in a hexagonal close packed cell is 74.05%; that is 74.05% of the total volume is occupied. The packing fraction or density is derived by assuming that each atom is a hard sphere in contact with its nearest neighbors. Determination of the packing fraction is accomplished by calculating the number of whole spheres per unit cell (2 in hcp), the volume occupied by these spheres, and a comparison with the total volume of a unit cell. The number gives an idea of how open or filled a structure is. By comparison, the packing fraction for body-centered cubic (Figure 6.1.6.1.16) is 68% and for diamond cubic (an important semiconductor structure to be described later) is it 34%.

Cupic close packed: face-centered cubic

In a similar manner to the generation of the hexagonal close packed structure, two close packed layers are stacked (Figure 6.1.6.1 .19) however, the third layer (C) is placed such that it does not exactly cover layer A, while sitting in a set of troughs in layer B (Figure 6.1.6.1.22), then upon repetition the packing sequence will be ...ABCABCABC.... This is known as cubic close packing or *ccp*.

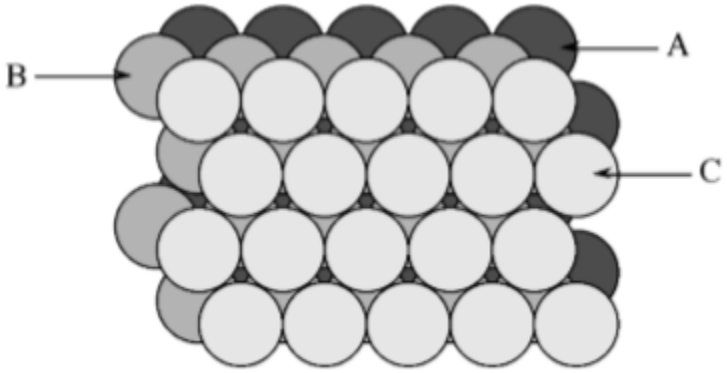


Figure 6.1.6.22: Schematic representation of the three close packed layers in a cubic close packed arrangement: A (dark grey), B (medium grey), and C (light grey).

The unit cell of cubic close packed structure is actually that of a face-centered cubic (*fcc)* Bravais lattice. In the *fcc* lattice the close packed layers constitute the {111} planes. As with the *hcp* lattice packing fraction in a cubic close packed (*fcc*) cell is 74.05%. Since face centered cubic or *fcc* is more commonly used in preference to cubic close packed (*ccp*) in describing the structures, the former will be used throughout this text.

Coordination number

The coordination number of an atom or ion within an extended structure is defined as the number of nearest neighbor atoms (ions of opposite charge) that are in contact with it. A slightly different definition is often used for atoms within individual molecules: the number of donor atoms associated with the central atom or ion. However, this distinction is rather artificial, and both can be employed.

The coordination numbers for metal atoms in a molecule or complex are commonly 4, 5, and 6, but all values from 2 to 9 are

known and a few examples of higher coordination numbers have been reported. In contrast, common coordination numbers in the solid state are 3, 4, 6, 8, and 12. For example, the atom in the center of body-centered cubic lattice has a coordination number of 8, because it touches the eight atoms at the corners of the unit cell, while an atom in a simple cubic structure would have a coordination number of 6. In both fcc and hcp lattices each of the atoms have a coordination number of 12.

Octahedral and tetrahedral vacancies

As was mentioned above, the packing fraction in both fcc and hcp cells is 74.05%, leaving 25.95% of the volume unfilled. The unfilled lattice sites (interstices) between the atoms in a cell are called interstitial sites or vacancies. The shape and relative size of these sites is important in controlling the position of additional atoms. In both fcc and hcp cells most of the space within these atoms lies within two different sites known as octahedral sites and tetrahedral sites. The difference between the two lies in their coordination number, or the number of atoms surrounding each site. Tetrahedral sites (vacancies) are surrounded by four atoms arranged at the corners of a tetrahedron. Similarly, octahedral sites are surrounded by six atoms which make-up the apices of an octahedron. For a given close packed lattice an octahedral vacancy will be larger than a tetrahedral vacancy.

Within a face centered cubic lattice, the eight tetrahedral sites are positioned within the cell, at the general fractional coordinate of ($^{n}/_{4}$,$^{n}/_{4}$,$^{n}/_{4}$) where n = 1 or 3, e.g., ($^{1}/_{4}$,$^{1}/_{4}$,$^{1}/_{4}$), ($^{1}/_{4}$,$^{1}/_{4}$,$^{3}/_{4}$), etc. The octahedral sites are located at the center of the unit cell ($^{1}/_{2}$,$^{1}/_{2}$,$^{1}/_{2}$), as well as at each of the edges of the cell, e.g., ($^{1}/_{2}$,0,0). In the hexagonal close packed system, the tetrahedral sites are at (0,0,$^{3}/_{8}$) and ($^{1}/_{3}$,$^{2}/_{3}$,$^{7}/_{8}$), and the octahedral sites are at ($^{1}/_{3}$,$^{1}/_{3}$,$^{1}/_{4}$) and all symmetry equivalent positions.

Important structure types

The majority of crystalline materials do not have a structure that ts into the one atom per site simple Bravais lattice. A number of other important crystal structures are found, however, only a few of these crystal structures are those of which occur for the elemental and compound semiconductors and the majority of these are derived from fcc or hcp lattices. Each structural type is generally defined by an archetype, a material (often a naturally occurring mineral) which has the structure in question and to which all the similar materials are related. With regard to commonly used elemental and compound semiconductors the important structures are diamond, zinc blende, Wurtzite, and to a lesser extent chalcopyrite. However, rock salt, *β*-tin, cinnabar and cesium chloride are observed as high pressure or high temperature phases and are therefore also discussed. The following provides a summary of these structures. Details of the full range of solid-state structures are given elsewhere.

Diamond Cubic

The diamond cubic structure consists of two interpenetrating face-centered cubic lattices, with one offset $^{1}/_{4}$ of a cube along the cube diagonal. It may also be described as face centered cubic lattice in which half of the tetrahedral sites are filled while all the octahedral sites remain vacant. The diamond cubic unit cell is shown in Figure 6.1.6.1.23. Each of the atoms (e.g., C) is four coordinate, and the shortest interatomic distance (C-C) may be determined from the unit cell parameter (*a*).

$$ C\text{-}C = a\dfrac{\sqrt{3}}{4} \approx 0.442a $$

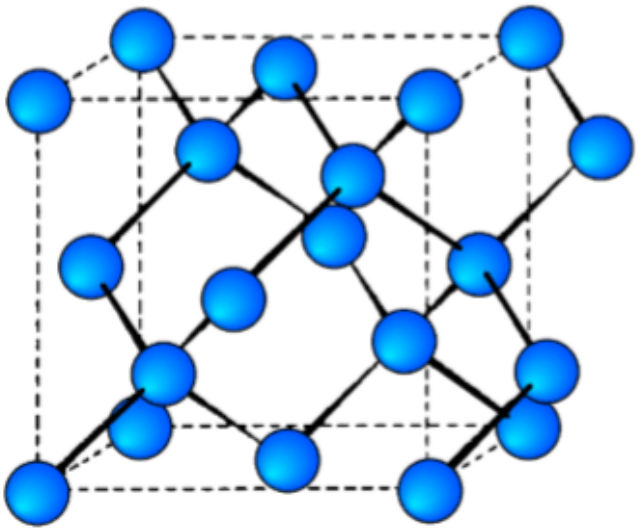


Figure 6.1.6.23: Unit cell structure of a diamond cubic lattice showing the two interpenetrating face-centered cubic lattices.

Zinc blende

This is a binary phase (ME) and is named after its archetype, a common mineral form of zinc sulfide (ZnS). As with the diamond lattice, zinc blende consists of the two interpenetrating fcc lattices. However, in zinc blende one lattice consists of one of the types of atoms (Zn in ZnS), and the other lattice is of the second type of atom (S in ZnS). It may also be described as face centered cubic lattice of S atoms in which half of the tetrahedral sites are filled with Zn atoms. All the atoms in a zinc blende structure are 4-coordinate. The zinc blende unit cell is shown in Figure 6.1.6.1.24. A number of inter-atomic distances may be calculated for any material with a zinc blende unit cell using the lattice parameter (*a*).

\[Zn-S = a\dfrac{\sqrt{3}}{4} \approx 0.442a \]

$$Zn - Zn = \frac{a}{\sqrt{2}} \approx 0.707a \tag{6.1.6.1}$$

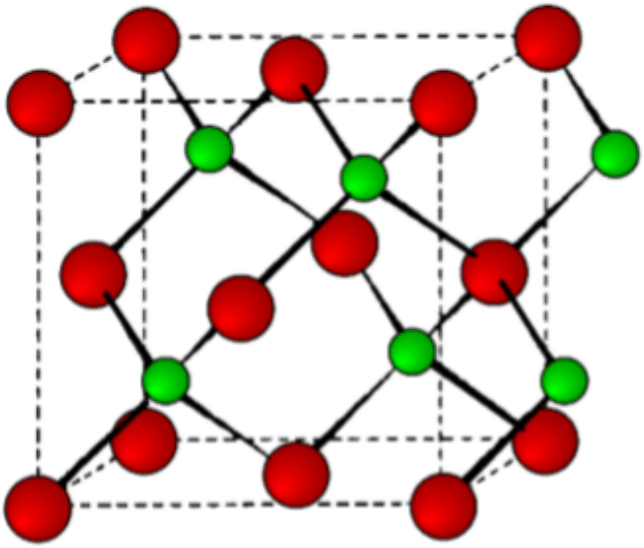


Figure 6.1.6.24: Unit cell structure of a zinc blende (ZnS) lattice. Zinc atoms are shown in green (small), sulfur atoms shown in red (large), and the dashed lines show the unit cell.

Chalcopyrite

The mineral chalcopyrite $CuFeS_2$ is the archetype of this structure. The structure is tetragonal ($a = b \neq c$, $\alpha = \beta = y = 90^{\circ}$, and is essentially a superlattice on that of zinc blende. Thus, is easiest to imagine that the chalcopyrite lattice is made-up of a lattice of sulfur atoms in which the tetrahedral sites are filled in layers, ...FeCuCuFe..., etc. (Figure 6.1.6.1.25). In such an idealized structure c = 2*a*, however, this is not true of all materials with chalcopyrite structures.

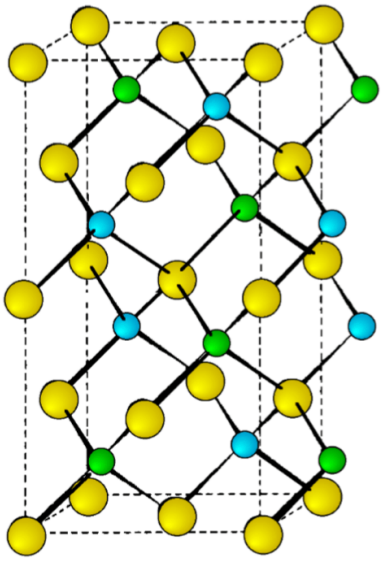


Figure 6.1.6.25: Unit cell structure of a chalcopyrite lattice. Copper atoms are shown in blue, iron atoms are shown in green and sulfur atoms are shown in yellow. The dashed lines show the unit cell.

Rock salt

As its name implies the archetypal rock salt structure is NaCl (table salt). In common with the zinc blende structure, rock salt consists of two interpenetrating face-centered cubic lattices. However, the second lattice is offset 1/2*a* along the unit cell axis. It may also be described as face centered cubic lattice in which all of the octahedral sites are filled, while all the tetrahedral sites remain vacant, and thus each of the atoms in the rock salt structure are 6-coordinate. The rock salt unit cell is shown in Figure 6.1.6.1.26. A number of inter-atomic distances may be calculated for any material with a rock salt structure using the lattice parameter (*a*).

$$Na - Cl = \frac{a}{2} \approx 0.5a \tag{6.1.6.2}$$

$$Na - Na = Cl - Cl = \frac{a}{\sqrt{2}} \approx 0.707a \tag{6.1.6.3}$$

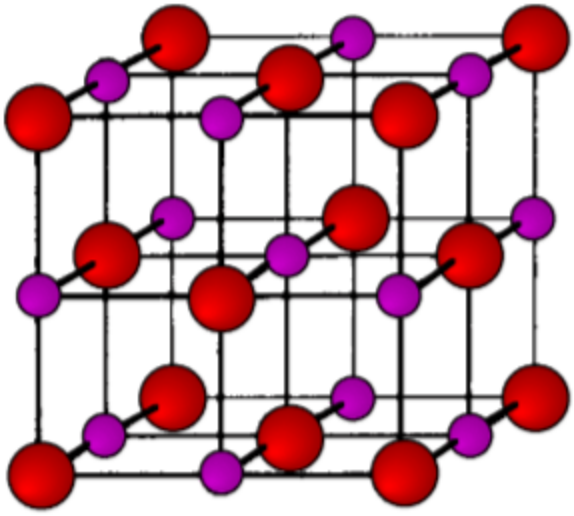


Figure 6.1.6.26: Unit cell structure of a rock salt lattice. Sodium ions are shown in purple (small spheres) and chloride ions are shown in red (large spheres).

Cinnabar

Cinnabar, named after the archetype mercury sufilde, HgS, is a distorted rock salt structure in which the resulting cell is rhombohedral (trigonal) with each atom having a coordination number of six.

Wurtzite

This is a hexagonal form of the zinc sulfide. It is identical in the number of and types of atoms, but it is built from two interpenetrating hcp lattices as opposed to the fcc lattices in zinc blende. As with zinc blende all the atoms in a wurtzite structure are 4-coordinate. The wurtzite unit cell is shown in Figure 6.1.6.1.27. A number of inter atomic distances may be calculated for any material with a wurtzite cell using the lattice parameter (*a*).

$$Zn - S = a\sqrt{\frac{3}{8}} \approx 0.612a = \frac{3c}{8} = 0.375c \tag{6.1.6.4}$$

$$Zn - Zn = S - S = a = 1.632c \tag{6.1.6.5}$$

However, it should be noted that these formulae do not necessarily apply when the ratio a/c is different from the ideal value of 1.632.

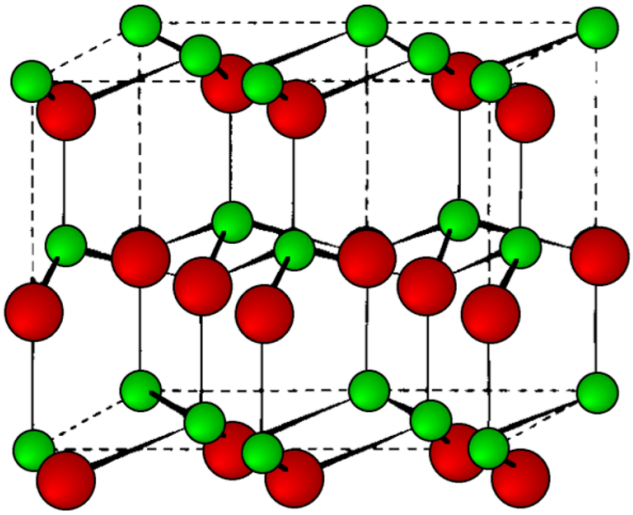


Figure 6.1.6.27: Unit cell structure of a wurtzite lattice. Zinc atoms are shown in green (small spheres), sulfur atoms shown in red (large spheres), and the dashed lines show the unit cell.

Cesium Chloride

The cesium chloride structure is found in materials with large cations and relatively small anions. It has a simple (primitive) cubic cell (Figure 6.1.6.1.16) with a chloride ion at the corners of the cube and the cesium ion at the body center. The coordination numbers of both Cs+ and Cl-, with the inner atomic distances determined from the cell lattice constant (*a*).

$$Cs - Cl = \frac{a\sqrt{3}}{2} = 0.866a \tag{6.1.6.6}$$

$$Cs - Cs = Cl - Cl = a \tag{6.1.6.7}$$

β-Tin

The room temperature allotrope of tin is *β*-tin or white tin. It has a tetragonal structure, in which each tin atom has four nearest neighbors (Sn-Sn = 3.016 Å) arranged in a very flattened tetrahedron, and two next nearest neighbors (Sn-Sn = 3.175 Å). The overall structure of *β*-tin consists of fused hexagons, each being linked to its neighbor via a four-membered Sn_4 ring.

Defects in crystalline solids

Up to this point we have only been concerned with ideal structures for crystalline solids in which each atom occupies a designated point in the crystal lattice. Unfortunately, defects ordinarily exist in equilibrium between the crystal lattice and its environment. These defects are of two general types: point defects and extended defects. As their names imply, point defects are associated with a single crystal lattice site, while extended defects occur over a greater range.

Point defects: too many or too few or just plain wrong

Point defects have a significant effect on the properties of a semiconductor, so it is important to understand the classes of point defects and the characteristics of each type. Figure 6.1.6.1.28 summarizes various classes of native point defects, however, they may be divided into two general classes; defects with the wrong number of atoms (deficiency or surplus) and defects where the identity of the atoms is incorrect.

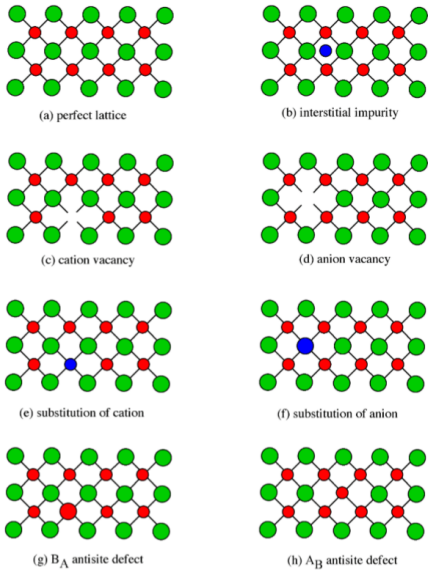


Figure 6.1.6.28: Point defects in a crystal lattice.

Interstitial Impurity

An interstitial impurity occurs when an extra atom is positioned in a lattice site that should be vacant in an ideal structure (Figure 6.1.6.1.28b). Since all the adjacent lattice sites are filled the additional atom will have to squeeze itself into the interstitial site, resulting in distortion of the lattice and alteration in the local electronic behavior of the structure. Small atoms, such as carbon, will prefer to occupy these interstitial sites. Interstitial impurities readily diffuse through the lattice via interstitial diffusion, which can result in a change of the properties of a material as a function of time. Oxygen impurities in silicon generally are located as interstitials.

Vacancies

The converse of an interstitial impurity is when there are not enough atoms in a particular area of the lattice. These are called vacancies. Vacancies exist in any material above absolute zero and increase in concentration with temperature. In the case of compound semiconductors, vacancies can be either cation vacancies (Figure 6.1.6.1.28c) or anion vacancies (Figure 6.1.6.1.28d), depending on what type of atom are missing.

Substitution

Substitution of various atoms into the normal lattice structure is common, and used to change the electronic properties of both compound and elemental semiconductors. Any impurity element that is incorporated during crystal growth can occupy a lattice site. Depending on the impurity, substitution defects can greatly distort the lattice and/or alter the electronic structure. In general, cations will try to occupy cation lattice sites (Figure 6.1.6.1.28e), and anion will occupy the anion site (Figure 6.1.6.1.28f). For example, a zinc impurity in GaAs will occupy a gallium site, if possible, while a sulfur, selenium and tellurium atoms would all try to substitute for an arsenic. Some impurities will occupy either site indiscriminately, e.g., Si and Sn occupy both Ga and As sites in GaAs.

Antisite Defects

Antisite defects are a particular form of substitution defect, and are unique to compound semiconductors. An antisite defect occurs when a cation is misplaced on an anion lattice site or vice versa (Figure 6.1.6.1.28g and h). Dependent on the arrangement these are designated as either AB antisite defects or BA antisite defects. For example, if an arsenic atom is on a gallium lattice site the defect would be an AsGa defect. Antisite defects involve tting into a lattice site atoms of a different size than the rest of the lattice, and therefore this often results in a localized distortion of the lattice. In addition, cations and anions will have a different number of electrons in their valence shells, so this substitution will alter the local electron concentration and the electronic properties of this area of the semiconductor.

Extended Defects: Dislocations in a Crystal Lattice

Extended defects may be created either during crystal growth or as a consequence of stress in the crystal lattice. The plastic deformation of crystalline solids does not occur such that all bonds along a plane are broken and reformed simultaneously. Instead, the deformation occurs through a dislocation in the crystal lattice. Figure 6.1.6.1.29 shows a schematic representation of a dislocation in a crystal lattice. Two features of this type of dislocation are the presence of an extra crystal plane, and a large void at the dislocation core. Impurities tend to segregate to the dislocation core in order to relieve strain from their presence.

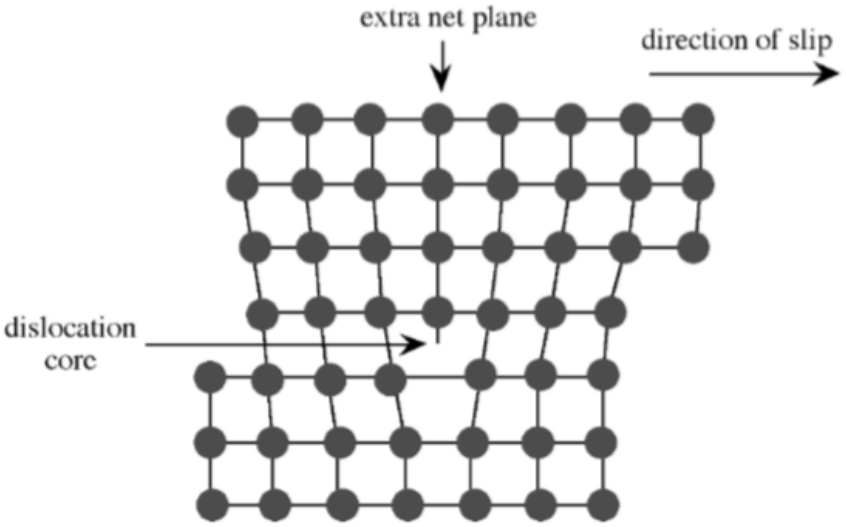


Figure 6.1.6.29: Dislocation in a crystal lattice.

Epitaxy

Epitaxy, is a transliteration of two Greek words *epi*, meaning "upon", and *taxis*, meaning "ordered". With respect to crystal growth it applies to the process of growing thin crystalline layers on a crystal substrate. In epitaxial growth, there is a precise crystal orientation of the lm in relation to the substrate. The growth of epitaxial films can be done by a number of methods including molecular beam epitaxy, atomic layer epitaxy, and chemical vapor deposition, all of which will be described later.

Epitaxy of the same material, such as a gallium arsenide lm on a gallium arsenide substrate, is called homoepitaxy, while epitaxy where the lm and substrate material are different is called heteroepitaxy. Clearly, in homoepitaxy, the substrate and lm will have the identical structure, however, in heteroepitaxy, it is important to employ where possible a substrate with the same structure and similar lattice parameters. For example, zinc selenide (zinc blende, a = 5.668 Å) is readily grown on gallium arsenide (zinc blende, a = 5.653 Å). Alternatively, epitaxial crystal growth can occur where there exists a simple relationship between the structures of the substrate and crystal layer, such as is observed between Al2O3 (1̄00) on Si (100). Whichever route is chosen a close match in the lattice parameters is required, otherwise, the strains induced by the lattice mismatch results in distortion of the lm and formation of dislocations. If the mismatch is signicant epitaxial growth is not energetically favorable, causing a textured lm or polycrystalline untextured lm to be grown. As a general rule of thumb, epitaxy can be achieved if the lattice parameters of the two materials are within about 5% of each other. For good quality epitaxy, this should be less than 1%. The larger the mismatch, the larger the strain in the lm. As the lm gets thicker and thicker, it will try to relieve the strain in the lm, which could include the loss of epitaxy of the growth of dislocations. It is important to note that the <1̄00> directions of a lm must be parallel to the <1̄00> direction of the substrate. In some cases, such as Fe on MgO, the [111] direction is parallel to the substrate [1̄00]. The epitaxial relationship is specified by giving first the plane in the film that is parallel to the substrate [1̄00].

Bibliography

- *International Tables for X-ray Crystallography*. Vol. IV; Kynoch Press: Birmingham, UK (1974).
- B. F. G. Johnson, in *Comprehensive Inorganic Chemistry*, Pergamon Press, Vol. 4, Chapter 52 (1973).
- A. R. West, *Solid State Chemistry and its Applications*, Wiley, New York (1984).

This page titled 6.1.6: Structure and Bonding - Crystal Structure is shared under a CC BY 3.0 license and was authored, remixed, and/or curated by Andrew R. Barron (CNX) via source content that was edited to the style and standards of the LibreTexts platform.

6.1.7: Structure and Bonding - Stereochemistry

Stereo isomers

Stereo isomers have the same empirical formula or molecular formula but different structural formulas. A typical example is butane, C_4H_{10}, which can have two different possible structures: *n*-butane (Figure 6.1.7.1.30a) and iso-butane also known as 1-methylpropane (Figure 6.1.7.1.30b).

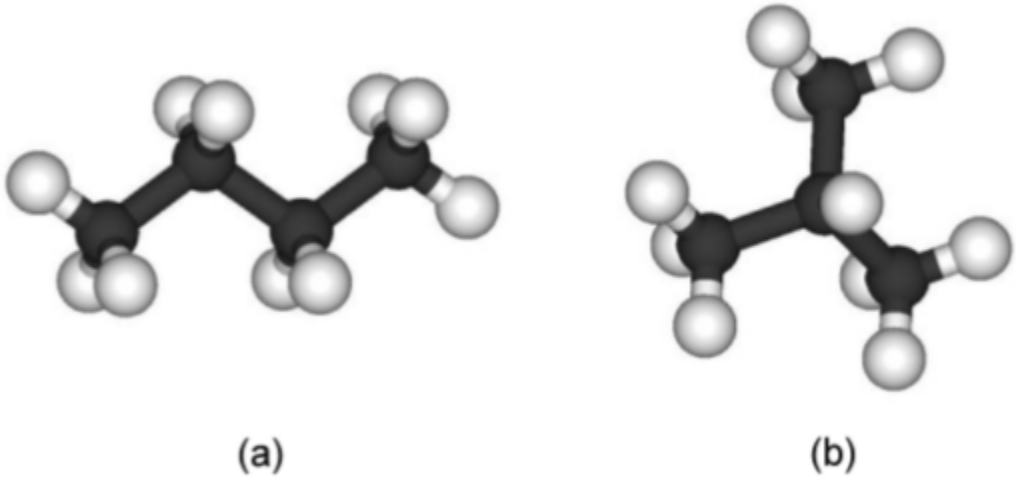


Figure 6.1.7.30: The two stereo isomers of butane: (a) *n*-butane and (b) iso-butane.

Geometric isomers

Geometric isomers have the same empirical formula or molecular formula and also the same structural formula, but have a different relative arrangement of the substituent groups. For example, the two geometric isomers of 1,2-dichloroethene (Figure 6.1.7.1.31) have the molecular formula of $C_2H_2Cl_2$, and the same structural formula of Cl(H)C=C(H)Cl, but the relative position of the two chlorine atoms can either be the same side of the C=C double bond (i.e., *cis*, see Figure 6.1.7.1.31a) or on opposite sides of the C=C double bond (i.e., *trans*, see Figure 6.1.7.1.31b). The use of *cis* and *trans* is not limited to organic compounds such as olefins, but can also be used in metal complexes, e.g., Figure 6.1.7.1.32.

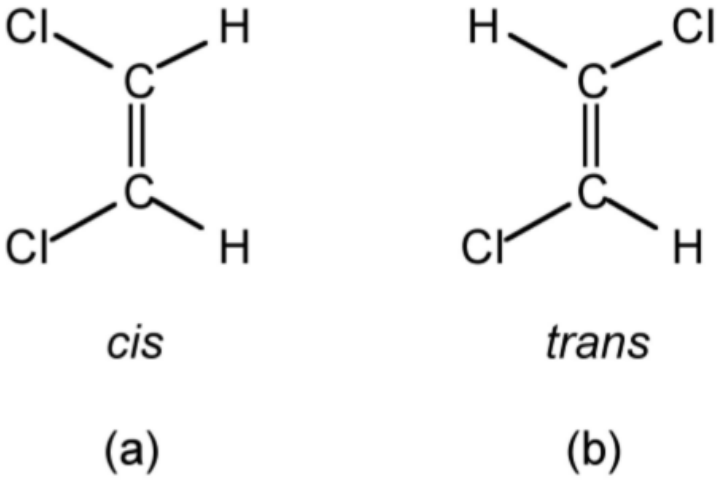


Figure 6.1.7.31: The two geometric isomers of 1,2-dichloroethene.

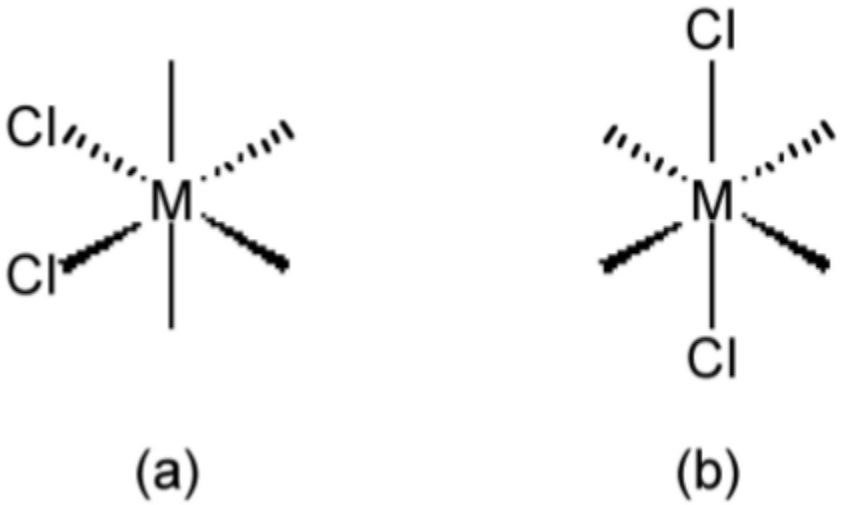


Figure 6.1.7.32: Examples of (a) *cis* and (b) *trans* geometric isomers for metal complexes.

When it is not possible to describe geometric isomers by the terms *cis* or *trans*, the terms facial (*fac*, Figure 6.1.7.1.33a) or meridinal (*mer*, Figure 6.1.7.1.33b) are commonly employed.

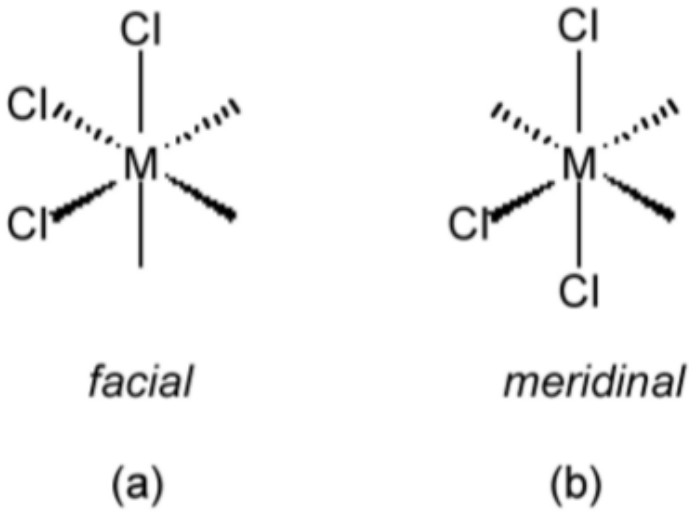


Figure 6.1.7.33: Examples of (a) fac and (b) mer geometric isomers for metal complexes.

Optical isomers

If the mirror object and mirror image of a molecule are not the same (i.e., they are not superimposable) they are known as *enantiomers*. If they also have optical activity they are called *chiral* and are described as having *chirality*. Enantiomers of a particular compound have the same general properties with two exceptions:

1. Their behavior to polarized light.
2. Their reaction with other chiral molecules

It is possible to determine if a molecule is chiral or not from its symmetry. Chiral molecules will have no symmetry or axis of rotation. The optical activity of a chiral molecule will turn the plane of polarized light either to the right (+) or the left (-). The former is known as *dextrorotatory* (D), while the latter is known as *levorotatory* (L).

Configuration

The configuration of a chiral molecule may be represented in a number of ways. Lactic acid ($C_3H_6O_3$) provides a suitable and simple example. The two optical isomers of lactic acid can be represented in 3-dimensional (3D) form as shown in Figure 6.1.7.1.34; however, it is also possible to draw the same molecules in 2D using the Fischer projection (Figure 6.1.7.1.35). While the Fisher projection does not appear to dene the geometry about the central carbon atom, the convention is that the side chains are out of the plane of the page (towards the observer), while the top and bottom groups are into the plane of the page (away from the observer). Thus, Figure 6.1.7.1.35a is a representation of Figure 6.1.7.1.34a, and Figure 6.1.7.1.35b is a representation of Figure 6.1.7.1.34b.

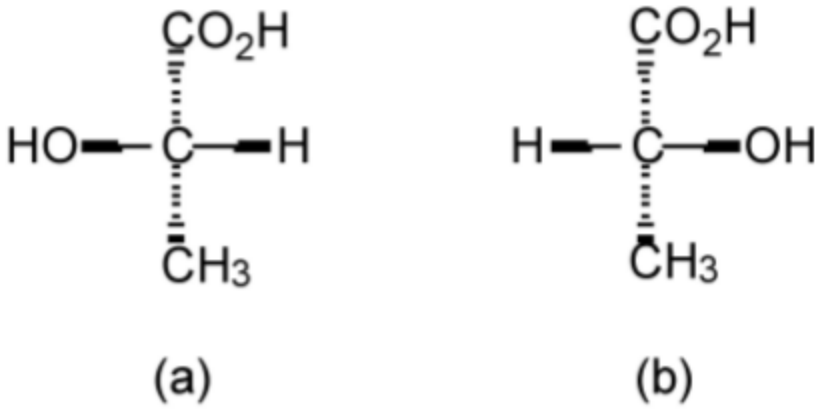


Figure 6.1.7.34: 3D representations of lactic acid.

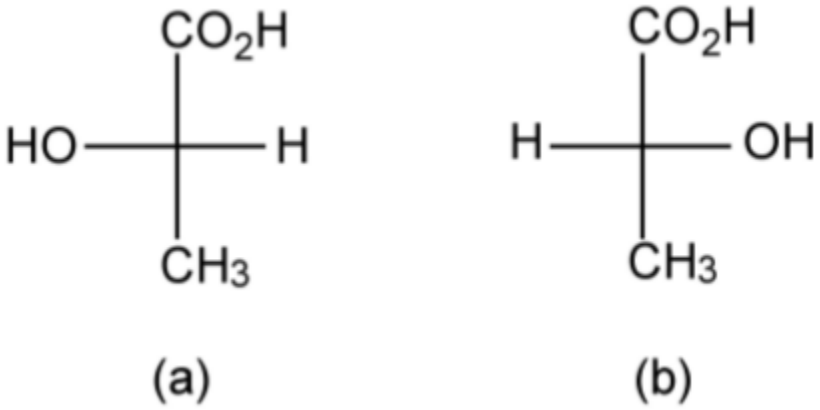


Figure 6.1.7.35: 2D Fischer representations of lactic acid.

Fischer-Rosenoff convention

The Fischer-Roseno convention defines chirality of a molecule using the Fischer projection. The convention is based upon D-(+)-glyceraldehydes (Figure 6.1.7.1.36).

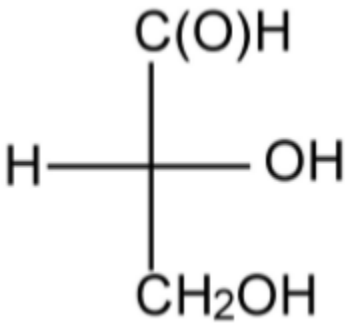


Figure 6.1.7.36: The Fischer projection of D-(+)-glyceraldehyde.

To determine the chiral label for a molecule, the Fischer projection is drawn with the longest carbon chain pointing away from the observer, i.e., into the plain of the page. The number 1 carbon (that of the highest substitution) is positioned at the top of the diagram. If the functional group is on the right of the diagram the isomer is given the label D (from the dextrorotatory enantiomer of glyceraldehydes rather than the molecule being dextrorotatory per se), i.e., Figure 6.1.7.1.36. On the other hand if the functional group is on the left of the diagram the isomer is given the label L (from the levorotatory enantiomer of glyceraldehyde rather than

the molecule being levorotatory per se).

Rules

Where molecules are large and complex a number of additional rules are useful:

1. Make any alcohol substituent to be nearest to the top, e.g., a butan-2-ol (Figure 6.1.7.1.37a) rather than a butan-3-ol (Figure 6.1.7.1.37b).
2. Aldehydes and ketones are the number 1 carbon atom.
3. If there are both sets of substituents, rule 1 has precedence over rule 2.

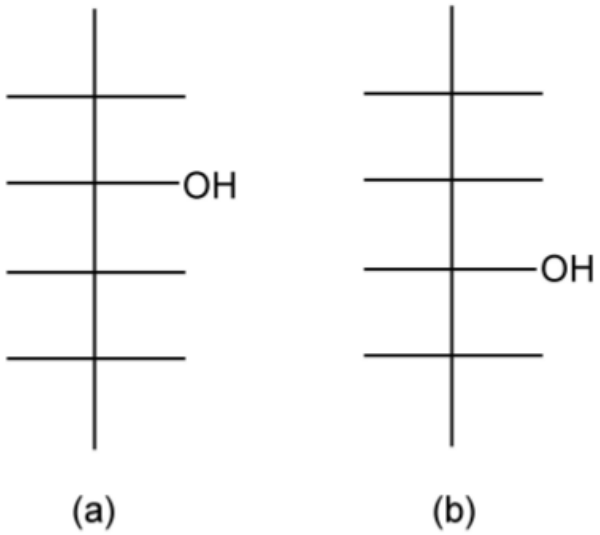


Figure 6.1.7.37: Preferred positioning of an alcohol substituent to be nearest the top (a) rather than at the bottom (b), according to the rules of the Fischer-Roseno convention.

Nomenclature in terms of *R* and S

The *R/S* nomenclature is a more widely used alternative to the *D/L* nomenclature, and is based upon the hierarchical order of the substituents. From the Fischer projection, the groups are ordered with the largest atom first, as shown in Figure 6.1.7.1.38. The lowest numbered substituent is then oriented away from the observer (i.e., H in Figure 6.1.7.1.38). The order of the remaining substituents 1, 2, 3 is then traced: if it goes clockwise the molecule is labeled *R*, if it goes anti-clockwise (counter-clockwise) the molecule is labeled S.

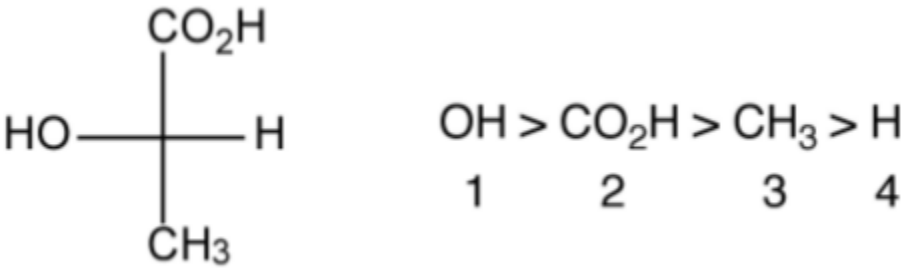


Figure 6.1.7.38: The structure of Slactic acid, and the ordering of the substituents.

The advantage of the *R/S* methodology is that it can also be used for geometric isomers. Thus, while *cis* and *trans* are useful when the groups either side of a C=C double bond are the same (e.g., cis-1,2dichloroethene, Figure 6.1.7.1.39a); however, when four different groups are present (e.g., A, B, X, and Y as seen in Figure 6.1.7.1.39b) then an alternative must be used. By taking either group A/B or X/Y and placing in order of precedence, the relative order defines the isomer. Thus, if in Figure 6.1.7.10b A>B and

X>Y the label Z (*zusammen* from the German for *together*) is used. Conversely, if in Figure 6.1.7.10b A**Y the label E (*entgegen* from the German for *opposite*) is used.**

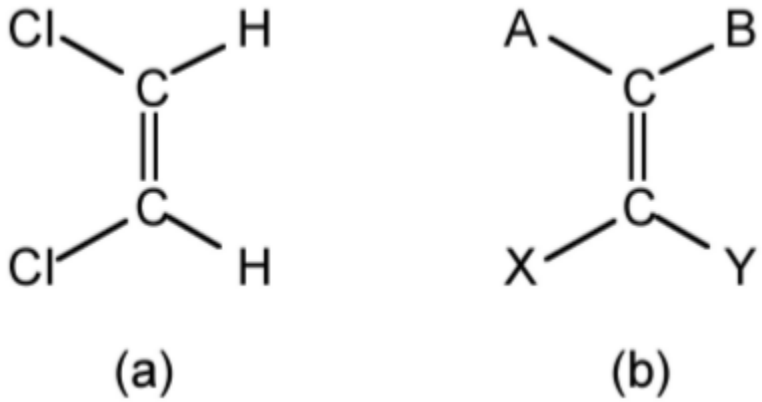


Figure 6.1.7.39: The structures of (a) cis-1,2-dichloroethene and (b) a generic olen with four different substituent groups.

More complex molecules

As molecules become more complex with multiple functional groups and multiple chiral centers the *D/L* nomenclature has the potential to become confusing. Erythrose has two chiral centers, and based upon the Fischer projections it may be seen that since the alcohol substituents in the 2 and 3 positions are on the same side of the backbone in the Fischer projection irrespective if it is D-(-)-erythrose or *L*-(+)-erythrose (Figure 6.1.7.1.40a and b). Thus, the naming is simplified despite the presence of multiple side groups. However, in threose (Figure 6.1.7.1.40c) the substituents are on different sides of the Fischer projection raising the issue as to whether this should be L or D. However, in such cases the substituent at the bottom of the side chain takes priority, thus Figure 6.1.7.1.40c is *D*-(-)-threose.

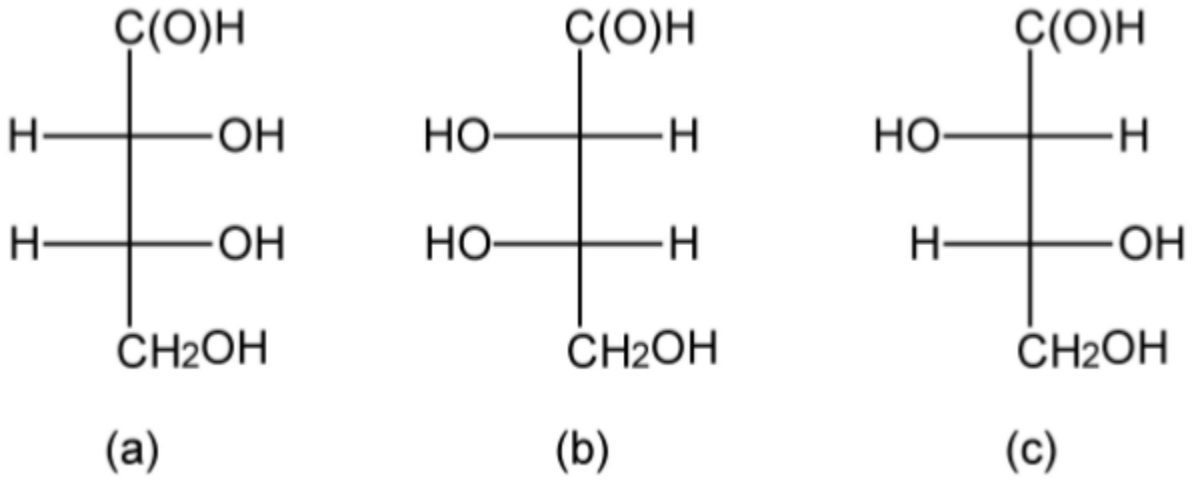


Figure 6.1.7.40: The Fischer projections of (a) D-(-)-erythrose, (b) L-(+)-erythrose, and (c) D-(-)-threose.

Note

***D*-(-)-erythrose and *L*-(+)-erythrose are enantiomers, and *D*-(+)-threose and *L*-(+)-threose are also enantiomers, but threose and erythrose are *diasteriomers*. Enantiomers have the same physical properties (just different behavior to polarized light), while diasteriomers may have different physical properties such as melting points and solubility.**

Amino Acids

Amino acids (or more properly α-amino acids) are compounds containing both an amine (NH_2) group and a carboxylic acid (CO_2H) attached to the same carbon atom. The presence of both acid and base groups can result in the formation of the Zwitterionic form with ammonium (NH_3^+) and carboxylate (CO_2^-) groups.

In defining the labels for amino acids, the basis is D-(-)-allothreonine (Figure 6.1.7.1.41), whereas for an amino acid such as threonine the top substituent is used for a label, e.g., Figure 6.1.7.1.42.

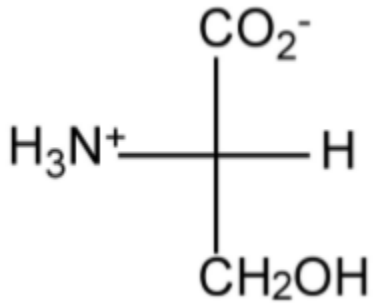


Figure 6.1.7.41: The Fischer projection of D-(-)-allothreonine.

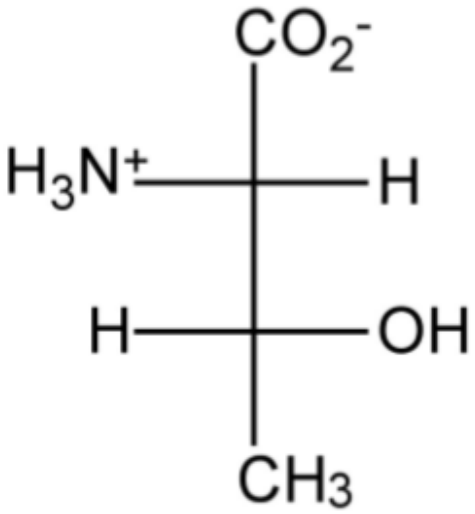


Figure 6.1.7.42: The Fischer projection of D-(-)-threonine.

Similar chiral centers

Just because a compound has more than one chiral center does not mean that it is optically active. A consideration of erythritol shows the presence of a mirror plane of symmetry (Figure1.43). As such, erythritol is not optically active, i.e., there is no effect on polarized light. In contrast, while threitol has the same molecular and geometric formula, the lack of a mirror plane of symmetry (Figure 6.1.7.1.44) means that the *L*- and *D*+ forms are optically active.

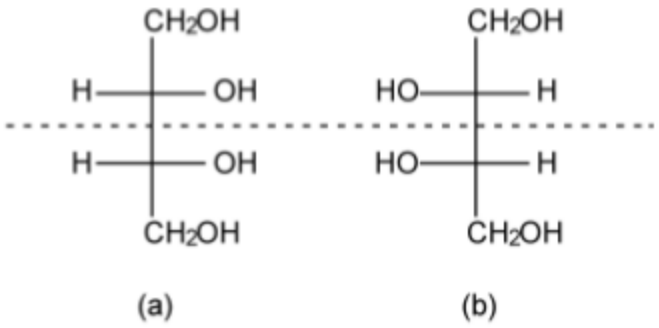


Figure 6.1.7.43**: The Fischer projections of *D* and *L* erythritol showing the presence of a mirror plane of symmetry. N.B. The presence of a mirror plane means that erythritol is not optically active and hence there is no need to label with + or -.**

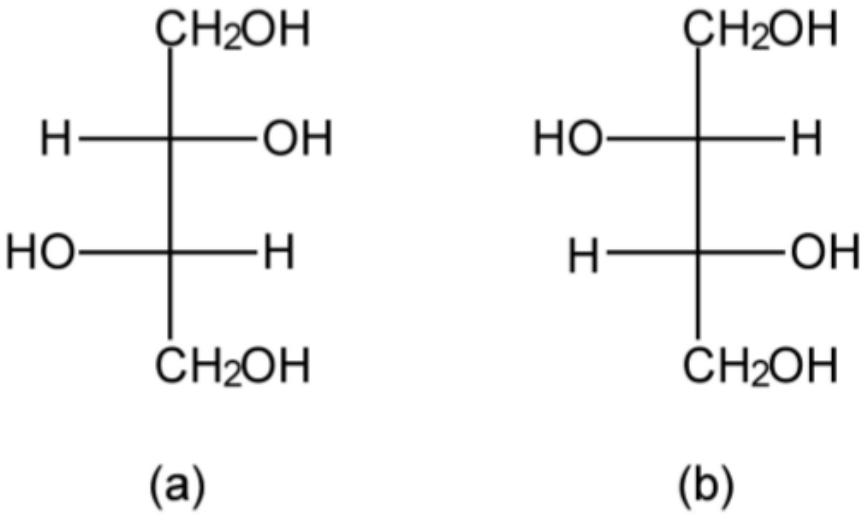


Figure 6.1.7.44**: The Fischer projections of (a) *L*-(-)-threitol and (b) *D*-(+)-threitol.**

Compounds with a *D*:*L* ratio of 1:1 are called racemic compounds and are totally optically inactive. However, it is also possible for a racemic solution of a compound to crystallize to form crystals of pure D or L, which may be manually separated.

Optical isomers that are not tetrahedral

Pyrimidal molecules

Pyramidal molecules can also exhibit chirality when the three substituents are distinct, e.g., $PR_1R_2R_3$ (Figure 6.1.7.1**.45). Unfortunately, most pyramidal compounds undergo an inversion of their isomers (in a similar manner to turning an umbrella inside out), such that the chiral forms interconvert rapidly. In such a case, it is not possible to resolve (separate) the different forms. Phosphines may generally be resolved because the barrier to their inversion is suficiently large (ca. 132 kJ/mol)**

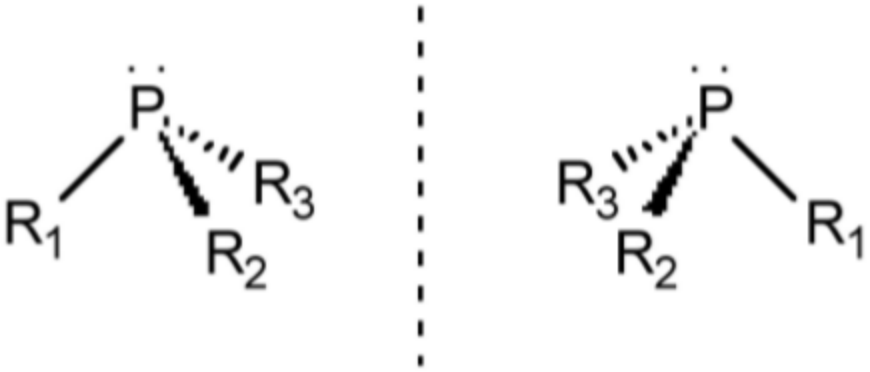


Figure 6.1.7.45**: An example of a chiral phosphine where R1 ≠ R2 ≠ R3.**

The notation used for pyramidal molecules is the same as that for tetrahedral molecules, in that the individual substituents are ordered with the largest atom first. The lone pair is defined as having the lowest numbering and thus is oriented away from the observer. The order of the remaining substituents 1, 2, and 3 is then traced: if it goes clockwise the molecule is labeled R, if it goes anti-clockwise (counter-clockwise) the molecule is labeled S.

Chirality in octohedral complexes

The presence of a chelate ligand on an octahedral complex can induce chirality in the complex.

Note

A chelate ligand is a molecule or ion that is bonded to at least two points of a central atom or ion. The term chelate is from the Greek chelè, meaning claw.

Unlike tetrahedral based compounds, chiral octahedral compounds have their nomenclature based on the structure of a helix. For example, in the case of a bis-chelate complex (Figure 6.1.7.1**.46), with one of the chelate ligands pointing straight up the helix, the direction of the other defines the chirality of the helix, i.e., if it is a left or right hand helix. If the ligand points up to the left the complex is assigned the symbol shown in Figure** 6.1.7.1**.46a, while if the ligand points up to the right the complex is assigned the symbol shown in Figure** 6.1.7.1**.46b.**

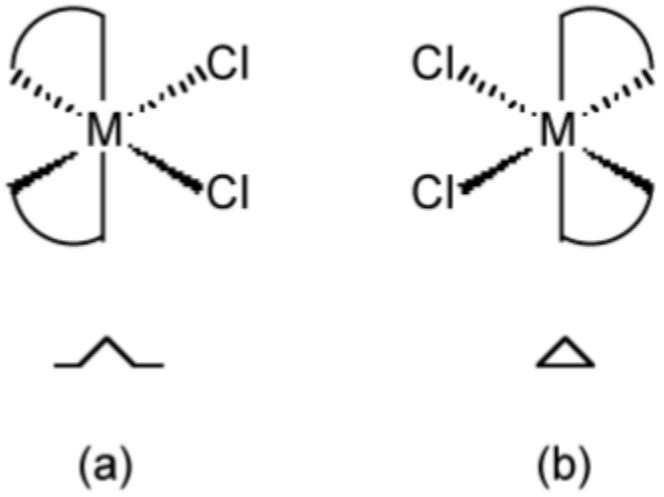


Figure 6.1.7.46**: The two optical isomers of a bis-chelate metal complex.**

In complexes with three chelate ligands (i.e., a tris-chelate complex, Figure 6.1.7.1.47), the same methodology applies, in that any two ligands can be chosen and the same rules applied.

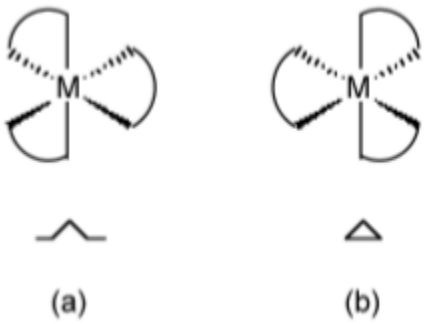


Figure 6.1.7.47: The two optical isomers of a tris-chelate metal complex.

Methods of resolution of racemic mixtures

A racemic mixture, or racemate, is one that has equal amounts of left- and right-handed enantiomers of a chiral molecule. The first known racemic mixture was "racemic acid," which Louis Pasteur (Figure 6.1.7.1.48) found to be a mixture of the two enantiomeric isomers of tartaric acid (Figure 6.1.7.1.49).



Figure 6.1.7.48: French microbiologist and chemist Louis Pasteur who is remembered for his remarkable breakthroughs in the causes and preventions of disease (1822 1895).

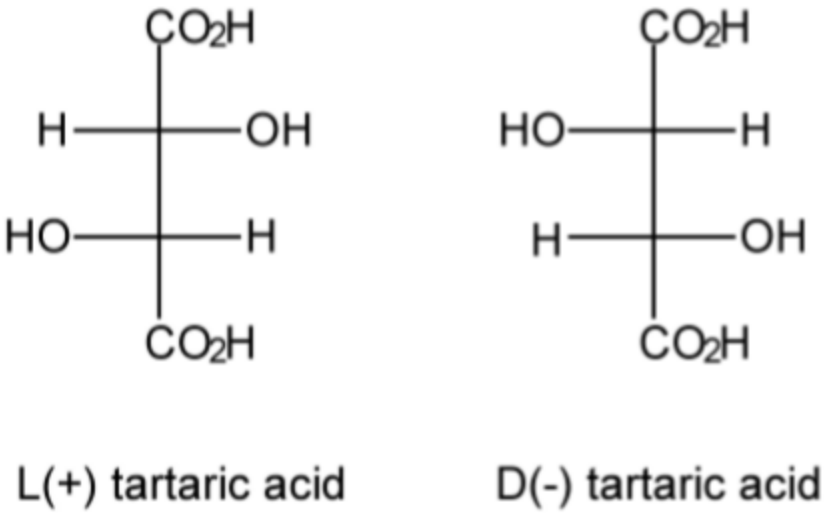


Figure 6.1.7.49**: The Fischer projections of the two enantiomeric isomers of tartaric acid.**

In nature, it is common that only one of an optical isomers is naturally produced, but in laboratory synthesis it is more common that both isomers are made in equal amounts. The separation of a racemate into its components (the pure enantiomers) is called a chiral resolution.

Mechanical seperation

The crystals of enantiomerically pure compounds often have different appearances. Thus, just as Pasteur did in 1848, it is often possible to look under a microscope and physically separate the two different enantiomers.

Resolution by formation of diasteriomers

One of the differentiating properties of a chiral molecule is that each enantiomer reacts with another chiral molecule to form a diastereomeric pair of compounds. For example, a racemic acid, (+)HA and (-)HA, will react with a chiral base, (-)B, to form a mixture of diasteriomers, [(-)BH+.(+)A-] and [(-)BH+.(-)A-]. Because diasteriomers have different physical properties they can be separated by recrystallization. Once separated by recrystallization, the addition of excess acid will liberate the enantiomerically pure compound, i.e., (+)HA or (-)HA. A typical chiral base would be a natural alkaloid base to ensure that it is pure + or -. If it is a base that is needed to be separated, then (-)malic acid is a suitable acid.

Resolution by chromatography

In a related method to resolution by the formation of diasteriomers, a chiral column material will allow for the chromatographic separation of an enantiomeric mixture. Thus, the retention rate for (+)X will be different from (-)X on a column in which the stationary phase is chiral, i.e., (-)A. Many common chiral stationary phases are based on oligosaccharides such as cellulose or cyclodextrin (in particular with β-cyclodextrin).

Labile stereo isomers and racemization

It is only possible to separate (resolve) racemic mixtures if the molecule stays as one form for a long time. In other words, if there is a mechanism by which the two forms are interconverted, then resolution cannot be achieved.

Intramolecular rearrangement

Intramolecular rearrangements involve no bonds being broken. The classic example is the inversion of an amine, (1.12), which has a low energy barrier (24.7 kJ/mol).



Another example of an intramolecular rearrangement is the conversion of a square-based pyramidal geometry via a trigonal bipyramidal geometry to the isomeric square-based pyramidal geometry, or the alternative isomerization of one trigonal bipyramidal geometry to another via a square-based pyramidal transition state. Such a process is known as a ***Berry rotation***. The Berry mechanism is a pseudorotation process for simultaneously interchanging two equatorial groups with the two axial groups, while the third equatorial group (called the pivot group) remains an equatorial group (**Figure** 6.1.7.1**.50**).

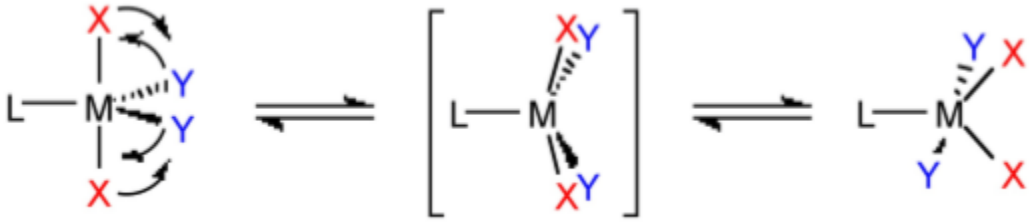


Figure 6.1.7.50**: The Berry pseudorotation.**

Intermolecular processes

Intermolecular processes involve bond breaking (and bond formation). For example a tetrahedral compound could loose one ligand, which creates a labile pyramidal compound. Rapid inversion of the pyramidal compound is followed by re-attachment of the ligand. Such a process is often so fast that resolution cannot be achieved.

Intramolecular processes

Intramolecular processes with bond breaking (and making) also lead to racemization. For example, in an octahedral complex with chelate ligands, if one of the ends of a chelate ligand detaches, it can reattach in the same configuration, or attach differently to change the chirality. In this manner the chirality can be changed from one form to another.

Conformation

The conformation of a molecule arises from the rotation of a single bond (**Figure** 6.1.7.1**.51**). However, even though there is rotation about the bond, there are energy barriers due to steric interactions of the substituents. In order to understand (and predict) these interactions, it is necessary to visualize the molecule in such a manner as to highlight the across-bond interactions; this is done by using a Newman projection.

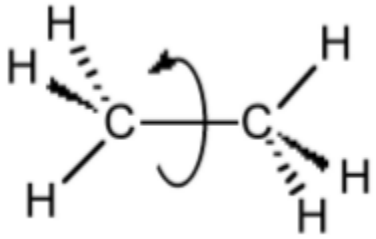


Figure 6.1.7.51**: The rotation about the C-C single bond in ethane.**

A Newman projection, useful in alkane stereochemistry, visualizes chemical conformations of a carbon-carbon chemical bond from front to back, with the front carbon represented by a dot and the back carbon as a circle (**Figure** 6.1.7.1**.52**).

The front carbon atom is called proximal, while the back atom is called distal. This type of representation is useful for assessing the torsional angle between bonds. Using ethane as an example, the Newman projection along the C-C single bond results in two basic conformations: eclipsed (Figure 6.1.7.1.52a) and staggered (Figure 6.1.7.1.52b). The staggered conformation will be energetically favored since the substituents are the most distant from each other. Conversely, the staggered will be the highest in energy. The difference in energy between the two conformations will define the barrier to rotation. In the case of ethane this is very small (12.5 kJ/mol).

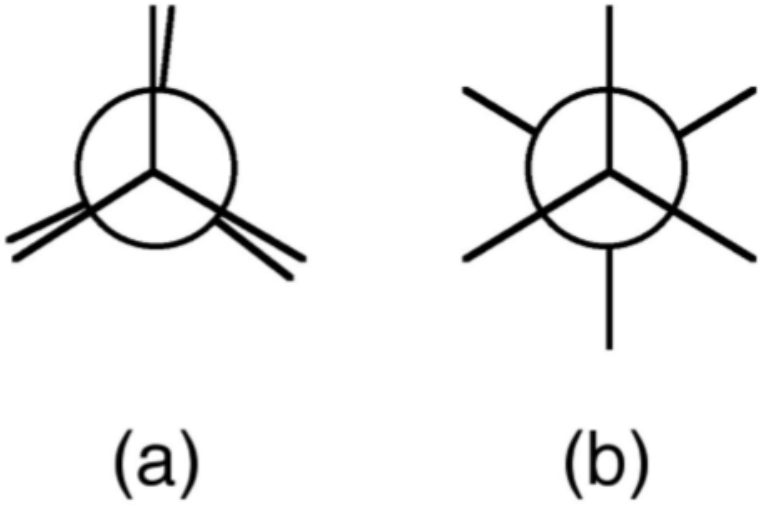


Figure 6.1.7.52: The Newman projection of ethane showing (a) eclipsed (E) and (b) staggered (S) conformations.

Although we often only consider the two extreme conformations, in reality there is a continuum around 360◦ rotation of the C-C bond. Figure 6.1.7.1.53 shows the relative energy as a function of the dihedral angle for ethane. Since each carbon in ethane has equivalent substitution (i.e., three H atoms) the energy for each staggered conformation is the same. This is not true for more complex molecules such as butane (Figure 6.1.7.1.54).

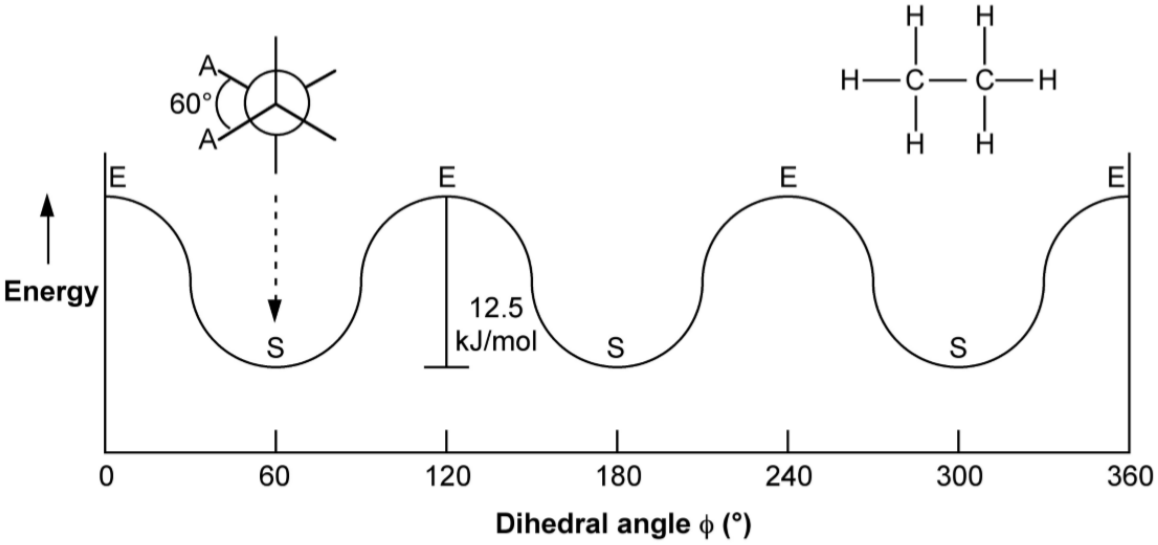


Figure 6.1.7.53: The relative energy as a function of the dihedral angle for ethane.

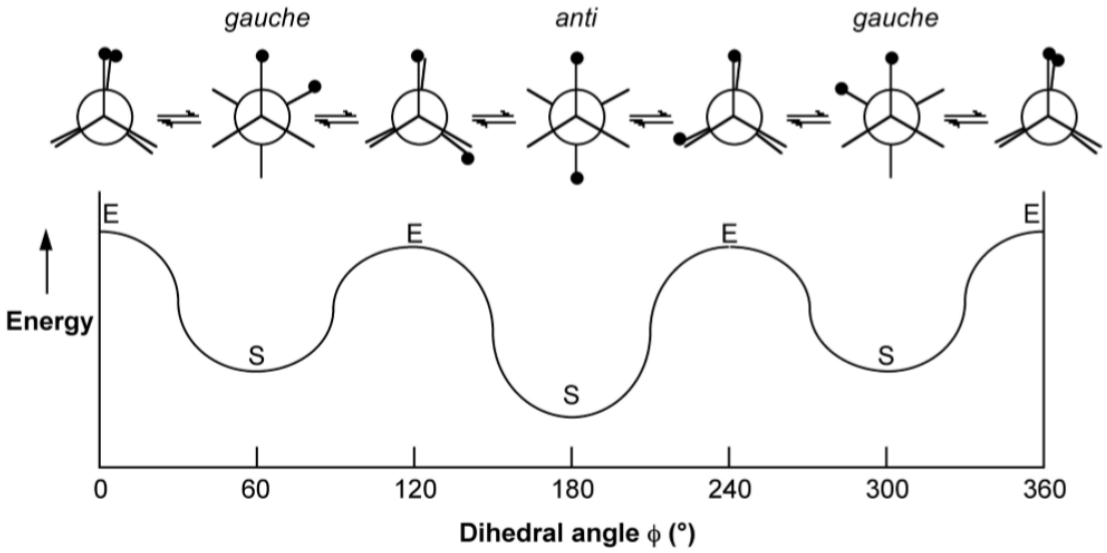


Figure 6.1.7.54**: The relative energy as a function of the dihedral angle for butane.**

As may be seen from Figure 6.1.7.1**.54, the staggered conformation in which the two methyl groups (represented by the black circles) are as far away from each other (*anti*) is the most energetically favored. The other two staggered conformations (*gauche*) are mirror images of each other and are hence conformation enantiomers. It should also be noted from Figure** 6.1.7.1**.54 that the eclipsed conformations vary in energy since the presence of methyl‴methyl near neighbors is clearly less energetically favorable than methyl‴H near neighbors.**

Generally the rotation about C-C bonds has a low barrier to rotation, however, if substituents are suciently bulky the molecule will not twist around the bond, e.g., substituted bi-phenyl with sterically bulky substituents (Figure 6.1.7.1**.55).**

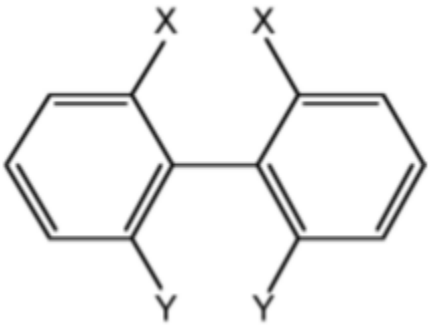


Figure 6.1.7.55**: The ease of rotation about the C-C bond of a substituted bi-phenyl will depend on the steric bulk of X and Y.**

Free rotation about a C-C bond is not fully possible when you have a ring system, e.g., in a cyclic compound such as cyclohexane, C_6H_{12}. The limited rotation about the C-C bonds results in the ipping of the ring conformation from the chair form (Figure 6.1.7.1**.56a) to the boat form (Figure** 6.1.7.1**.56b). Since the boat form has steric hindrance between the hydrogen atoms, the chair form is the more stable.**

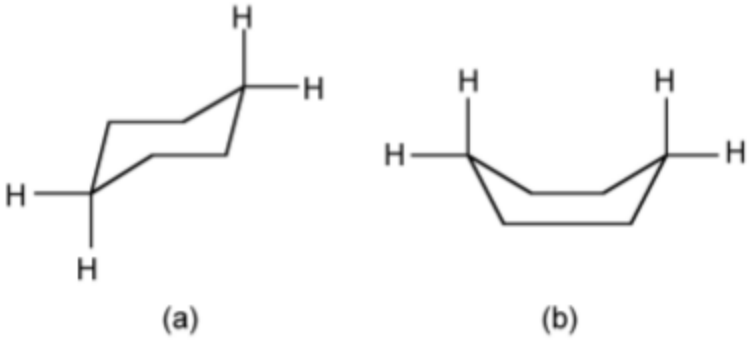


Figure 6.1.7.56**: The chair (a) and boat (b) conformations of cyclohexane, C_6H_{12}.**

Conformation of compounds with lone pairs

Lone pairs often behave in a different manner to substituents in regard to conformations. Thus, methylamine (CH_3NH_2) would be predicted to have the staggered conformation shown in Figure 6.1.7.1**.57a. However, the lower steric bulk of the lone pair results in the nitrogen being 0.09 Å away from the true center of the CH_3 projection (Figure** 6.1.7.1**.57b).**

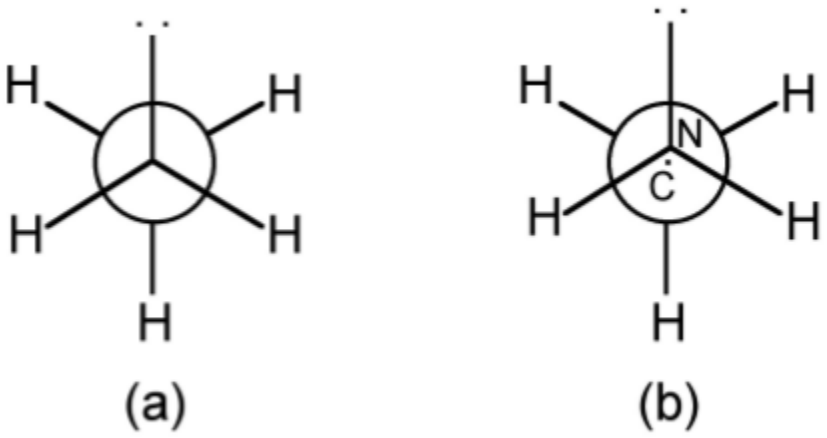


Figure 6.1.7.57**: The ideal (a) and observed (b) conformations of methylamine, CH_3NH_2.**

In compounds with more than one lone pair, the lowest energy form is not always the *anti* conformation. For example, at 20 °C hydrazine (H_2NNH_2) is 100% *gauche* (Figure 6.1.7.1**.58a); but for substituted hydrazines (i.e., a diamine, R_2NNR_2) if the substituent groups are suficiently large then the anti conformation will dominate (Figure** 6.1.7.1**.58b).**

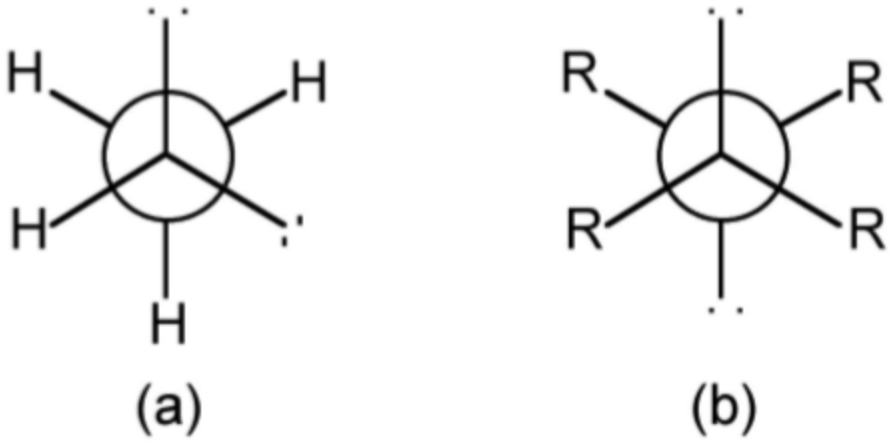


Figure 6.1.7.1.58: The stable conformation of hydrazine (H2NNH2) at 20 ◦C (a) as compared to the anti conformation (b) observed for diamines (R2NNR2).

The conformation of hydrogen peroxide (H2O2) is dominated by the lone pairs rather than the hydrogen atoms. Instead of the expected anti conformation (c.f., Figure 6.1.7.1.54 where the black circles would represent the hydrogen atoms) in the free state the dihedral angle is 94° (Figure 6.1.7.1.59). The conformation of hydrogen peroxide is therefore neither eclipsed nor staggered but an intermediate structure. When in the solid state hydrogen bonding will cause the shape and angles to change.

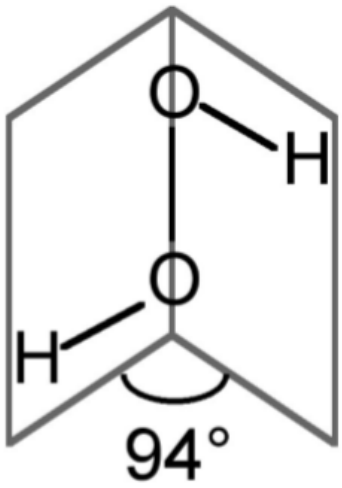


Figure 6.1.7.59: The structure of hydrogen peroxide in the free state.

Bibliography

- **R. S. Berry, *J. Chem. Phys.*, 1960, 32, 933.**
- **A. Keys, S. G. Bott, and A. R. Barron, *J. Chem. Cryst.*, 1998, 28, 629.**

This page titled 6.1.7: Structure and Bonding - Stereochemistry is shared under a CC BY 3.0 license and was authored, remixed, and/or curated by Andrew R. Barron (CNX) via source content that was edited to the style and standards of the LibreTexts platform.

6.1.8: Acids, Bases, and Solvents - Choosing a Solvent

The choice of solvent is an important parameter for any chemical reaction. The following provides a guide to some of the consideration to be made in choosing a solvent to ensure the desired reaction occurs.

Solvation

Solvation may be defined as the interaction between the solvent and the solute, however, two general classes of solvation have different consequences to the stability of either reagents or products in a chemical reaction, and hence the potential of a reaction to occur

- **Specific solvation** is where the solvent interacts with one of the ions (or molecules) in solution via a covalent interaction. Furthermore, there will be a specific number of solvent molecules bound to each ion (or molecule), e.g., $[Cu(NH_3)_4]^{2+}$ and $[Mg(H_2O)6]^{2+}$ (Figure 6.1.8.1.60a).
- **Non-specific solvation** is as a result of van der Waals or dipole-dipole forces between the solvent and an ion (or molecule). There will be no defined number of interactions and the solvent…ion interaction will be highly fluxional, e.g., while water solvates the chloride ion (Figure 6.1.8.1.60b) the number of water molecules around each anion is not fixed

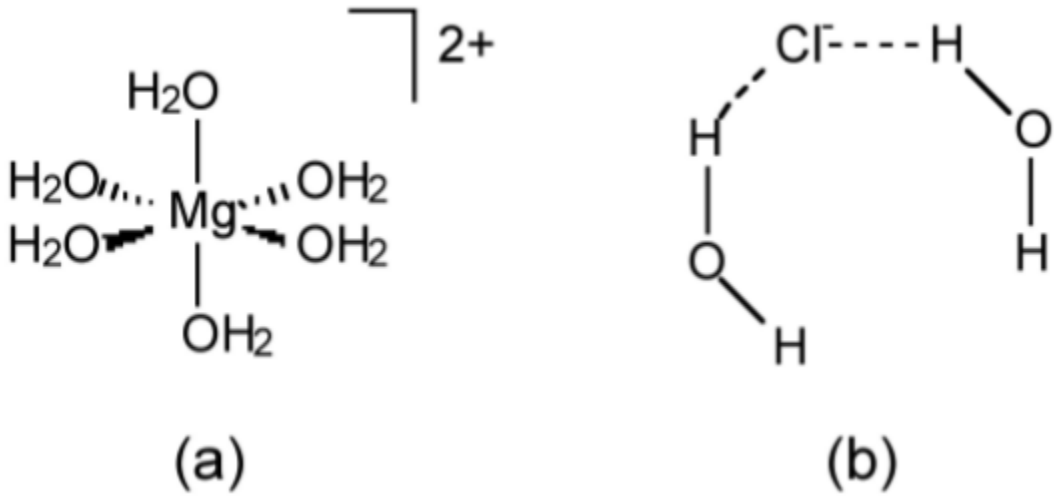


Figure 6.1.8.60: Examples of (a) specific and (b) non-specific solvation.

Table 6.1.8.1.10 shows the ability of three solvents to act with specific and non-specific solvation. The relative solvation ability of each solvent results in three different products from the dissolution of iron(III) chloride ($FeCl_3$).

Solvation	DMSO (Me_2SO)	Pyridine (C_5H_5N)	Acetonitrile (MeCN)
Specific	Good	Very good	Poor
Non-specific	Good	Poor	Moderately good

Dissolution of $FeCl_3$ in DMSO results in the dissociation of a chloride ligand, (1.8.1), due to both the specific solvation of the $FeCl^{2+}$ cation and the non-specific solvation of the Cl- anion. In fact, the good solvation properties of DMSO means that depending on the concentration (and temperature) a series of dissociations may occur, (1.8.2).

$$FeCl_3 \overset{DMSO}{\rightleftharpoons} [FeCl_2(DMSO)_4]^+ Cl^-_{(solv)} \tag{6.1.8.1}$$

$$[FeCl_2(DMSO)_4]^+ \xleftrightarrow{-Cl^-_{(solv)}} +DMSO[FeCl(DMSO)_5]^{2+} \xleftrightarrow{-Cl^-_{(solv)}} +DMSO[Fe(DMSO)_6]^{3+}$$

In contrast, if $FeCl_3$ is dissolved in pyridine (py) the neutral Lewis acid-base complex is formed, (1.8.3), because while pyridine is a very good at specific solvation (Table 6.1.8.1.10), it is poor at solvating the chloride anion.

$$FeCl_3 + py \rightarrow FeCl_3(py) \tag{6.1.8.3}$$

In a similar manner, $FeCl_3(MeCN)_3$ will be formed by the dissolution in acetonitrile, because although it is not good at specific solvation, it is not sufficiently good at non-specific solvation to stabilize the chloride anion. However, since the $FeCl_4^-$ anion has a lower charge density that Cl-, it can be supported by the non-specific solvation of acetonitrile and thus a disproportionation reaction occurs, (1.8.4).

$$2FeCl_3(MeCN)_3 \rightleftharpoons [FeCl_2(MeCN)_4]^+ + FeCl_4^- \tag{6.1.8.4}$$

Interference by the solvent

Rather than solvating a molecule or ion, the solvent can take an active and detrimental role in the synthesis of a desired compound.

Solvolysis

The archetypal solvolysis reaction is the reaction with water, i.e., hydrolysis, (6.1.8.5). However, solvolysis is a general reaction, involving bond breaking by the solvent. Thus, the reaction with ammonia is **ammonolysis**, (6.1.8.6), the reaction with acetic acid is **acetolysis**, (6.1.8.7), and the reaction with an alcohol is **alcoholysis**, (6.1.8.8) where Et = C_2H_5. In each case the same general reaction takes place yielding the cation associated with the solvent.

$$SO_2Cl_2 + 4\,H_2O \rightarrow SO_2(OH)_2 + 2\,H_3O^+ + 2\,Cl^- \tag{6.1.8.5}$$

$$SO_2Cl_2 + 4\,NH_3 \rightarrow SO_2(NH_2)_2 + 2\,NH_4{}^+ + 2\,Cl^- \tag{6.1.8.6}$$

$$SO_2Cl_2 + 4\,MeCO_2H \rightarrow SO_2(O_2CMe)_2 + 2\,MeCO_2H_2{}^+ + 2\,Cl^- \tag{6.1.8.7}$$

$$SO_2Cl_2 + 4\,EtOH \rightarrow SO_2(OEt)_2 + 2\,EtOH_2{}^+ + 2\,Cl^- \tag{6.1.8.8}$$

Competition reactions

Where more than one reaction could occur the reaction involving the solvent can often compete with the desired reaction.

If it is desired to synthesis the Lewis acid-base complex between diethylether (Et_2O) and boron triuoride (BF_3) it is important to choose a solvent that will not compete with the complex formation. For example, pyridine is a poor choice because the nitrogen donor is a stronger Lewis base than the diethylether, (1.8.9), and thus no reaction would occur between diethylether and boron trifluoride. In contrast, since acetonitrile (MeCN) is a poor Lewis base, then the reaction will occur.

$$BF_3(Et_2O) + py \rightarrow BF_3(py) + Et_2O \tag{6.1.8.9}$$

If the synthesis of $GeCl_6^{2-}$ from germanium tetrachloride ($GeCl_4$) and a source of chloride anion, then water would be a poor choice of solvent since hydrolysis of $GeCl_4$ would result. Liquid hydrogen chloride would be equally poor solvent since strong Cl-...H-Cl hydrogen bonding would stabilize the chloride anion and preclude reaction. In contrast, nitromethane (CH_3NO_2) would be a polar enough solvent to solvate the $GeCl_4$, but it will be displaced by the chloride anion, which would be only weakly solvated.

Salt formation

The formation of a salt via a double displacement reaction, (1.8.10), can be promoted by the choice of solvent by shifting the equilibrium by stabilization of one or more reagent/product.

$$MX + M'X' \rightleftharpoons MX' + M'X \tag{6.1.8.10}$$

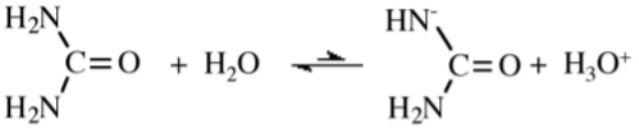
Salt stabilization through relative acidity

The attempted formation of nitronium perchlorate from nitric acid and perchloric acid, (1.8.11), in water will result in the decomposition of the NO_2^+ cation, (1.24). However, if the reaction is carried out in a stronger acid, i.e., sulfuric acid, the NO_2^+ cation is stable, and the resulting salt can be recystallized, (1.8.12).

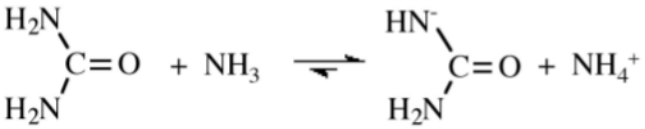
$$HNO_3 + HClO_4 \rightarrow NO_2^+ + ClO_4^- + H_2O \tag{6.1.8.11}$$

$$NO_2^+ + 2H_2O \rightarrow HNO_3 + H_3O^+ \tag{6.1.8.12}$$

In a similar manner, the weak basic character of water means the equilibrium reaction, (1.25), has a very small equilibrium constant, K. However, if the reaction is carried out in a strongly basic solvent such as ammonia the uride anion is stabilized, (1.26), and can be precipitated by cation exchange.



(1.25)



(1.26)

Salt stabilization through solvation

The following observations may be explained by a consideration of the solvation ability of the solvent.

1. The reaction of silver nitrate with barium chloride in water yields silver chloride and barium nitrate, (1.8.13).
2. The reaction of barium nitrate with silver chloride in ammonia yields barium chloride and silver nitrate, (1.8.14).

$$2AgNO_3 + BaCl_2 \xrightarrow{H_2O} 2AgCl\downarrow + Ba^{2+} + 2NO_3^- \tag{6.1.8.13}$$

$$2AgCl + Ba(NO_3)_2 \xrightarrow{NH_2} BaCl_2\downarrow + 2Ag^+ + 2NO_3^- \tag{6.1.8.14}$$

Since silver nitrate and barium nitrate are soluble in both solvents, the differences must be due to differences in the solubility of the chlorides in each solvent. A consideration of the relative stability of solid silver chloride versus the solvated species (Figure 6.1.8.1.61) shows that the enthalpy of solvation in water is less than the lattice energy. Thus, if silver chloride were present as Ag+ and Cl- in water it would spontaneously precipitate. In contrast, the enthalpy of solvation in ammonia is greater than the lattice energy, thus solid AgCl will dissolve readily in liquid ammonia. The reason for the extra stabilization from the specific solvation of the silver cation by the ammonia, i.e., the formation of the covalent complex $[Ag(NH_3)_2]^+$.

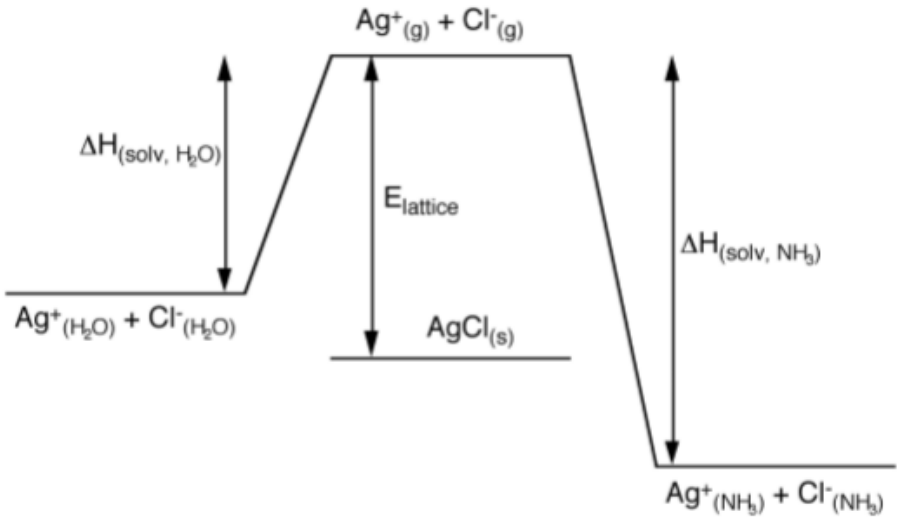


Figure 6.1.8.61: Enthalpy of solvation of silver chloride in water and ammonia in comparison to the lattice energy.

As may be seen from Figure 6.1.8.1.62, the opposite effect occurs for barium chloride. Here the enthalpy of solvation in ammonia is less than the lattice energy. Thus, if barium chloride were present as Ba^{2+} and Cl^- in ammonia it would spontaneously precipitate. In contrast, the enthalpy of solvation in water is greater than the lattice energy, thus solid $BaCl_2$ will dissolve readily in water. The stabilization of Ba^{2+}(aq) occurs because water will have a larger sphere of non-specific solvation as a consequence of having two lone pairs, allowing interaction with the Ba^{2+} as well as other water molecules (Figure 6.1.8.1.63).

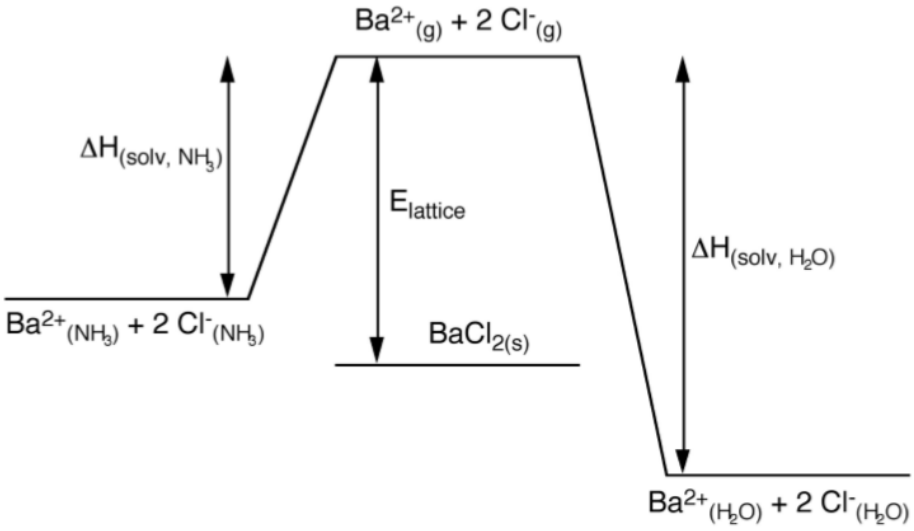


Figure 6.1.8.62: Enthalpy of solvation of barium chloride in water and ammonia in comparison to the lattice energy.

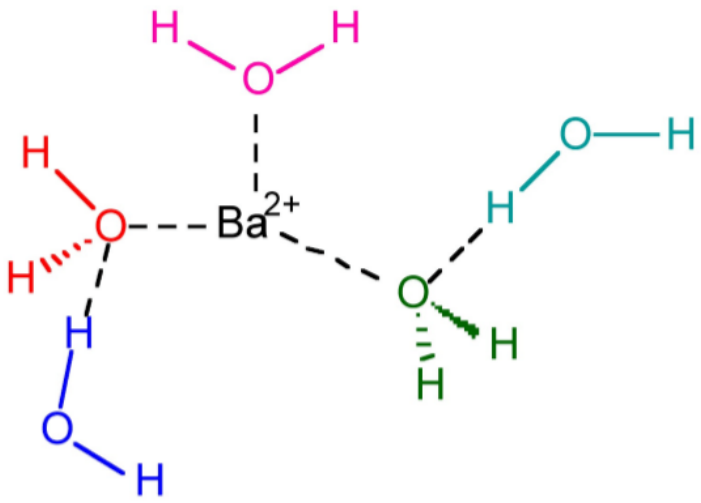


Figure 6.1.8.63: Schematic representation of the extended water solvation (aquation) sphere about Ba2+ cation.

Electron transfer reaction

A consideration of the oxidation, (1.8.15), and reduction, (1.8.16), reactions that occur for pure water at neutral pH (where $[H^+]$ = 10^{-7}) would suggest that water will not tolerate oxidants whose E0 is greater than 0.82 V nor tolerate reductants whose E0 is less than -0.41 V.

$$2H^+ + \frac{1}{2}O_2 + 2e^- \rightarrow H_2O \qquad E_0 = +0.82V \tag{6.1.8.15}$$

$$H^+ + e^- \rightarrow \frac{1}{2}H_2 \qquad E_0 = -0.41V \tag{6.1.8.16}$$

Thus, while water has a fair range to support redox reactions it is not very good at the extremes with strong reducing agents or strong oxidizing agents. Liquid ammonia is an excellent solvent for very strong reducing agents because of the stabilization of solvated electrons, i.e., $[e^-(NH_3)_6]$. In contrast, hydrochloric acid is a good solvent for reactions involving very strong oxidizing agents.

This page titled 6.1.8: Acids, Bases, and Solvents - Choosing a Solvent is shared under a CC BY 3.0 license and was authored, remixed, and/or curated by Andrew R. Barron (CNX) via source content that was edited to the style and standards of the LibreTexts platform.

6.1.9: Chemical Reactivity - The Basics of Combustion

When discussing the combustion of a compound it is ordinarily referring to the reaction of an organic compound (hydrocarbon) with oxygen, in which the carbon is converted to carbon dioxide (CO_2) and the hydrogen forms water (H_2O) as a vapor, e.g., (1.9.1).

$$CH_4 + 2O_2 \rightarrow CO_2 + 2H_2O \tag{6.1.9.1}$$

However, this only a narrow view of combustion, and a more general denition should be that combustion or burning is the sequence of exothermic chemical reactions between a fuel and an oxidant accompanied by the production of heat and conversion of chemical species. Based upon this definition methane can combust in the presence of fluorine (F_2) as strong oxidant, (1.9.2).

$$CH_4 + 4F_2 \rightarrow CF_4 + 4HF \tag{6.1.9.2}$$

In considering the combustion of any flammable compound, for example gasoline, it should be noted that the compounds that make up gasoline are quiet stable in the absence of a source of oxygen (usually from the air). Furthermore, some form of energy input (heat, flame, or spark) must be provided. Thus, the combustion of gasoline provides the archetypal example of the three component explosive system typical of a traditional chemical explosive: fuel (something that will burn), an oxidizer (usually a source of oxygen), and energy (ignition). In this regard, combustion also includes the exothermic reactions of many metals with oxygen, (1.9.3).

$$6Al + 3O_2 \rightarrow 2Al_2O_3 \tag{6.1.9.3}$$

It is not just reactive metals that can be used as the fuel component of combustion, but many of their compounds as well. The formation of water from the hydrogen in organic compounds, in combination with an oxygen source, releases significant energy. It stands to reason therefore that any compound comprising of hydrogen and an element can be a potential fuel: a compound of hydrogen and another element is known as a hydride. This is especially true for the hydrides of reactive metals such as aluminum and sodium (and metalloids such as boron, (1.9.4)), but is also true for the hydrides of silicon and phosphorus. These hydride compounds react with an oxidizer in a manner analogous to that of a hydrocarbon, as may be seen by a comparison of (1.9.5) and (1.9.1).

$$2BH_3 + 3O_2 \rightarrow B_2O_3 + 3H_2O \tag{6.1.9.4}$$

$$SiH_4 + 2O_2 \rightarrow SiO_2 + 2H_2O \tag{6.1.9.5}$$

Figure 6.1.9.1.64 shows a comparison of the heat of combustion of various inorganic fuels with commonly used jet fuels (JP-10 and JP-8). Hydrocarbons heat of combustion is limited by the C:H ratio, while graphite is the limiting case. Boron and boron compounds have greater volumetric and gravimetric energy density than hydrocarbons, and therefore were studied as potential high-energy fuels.

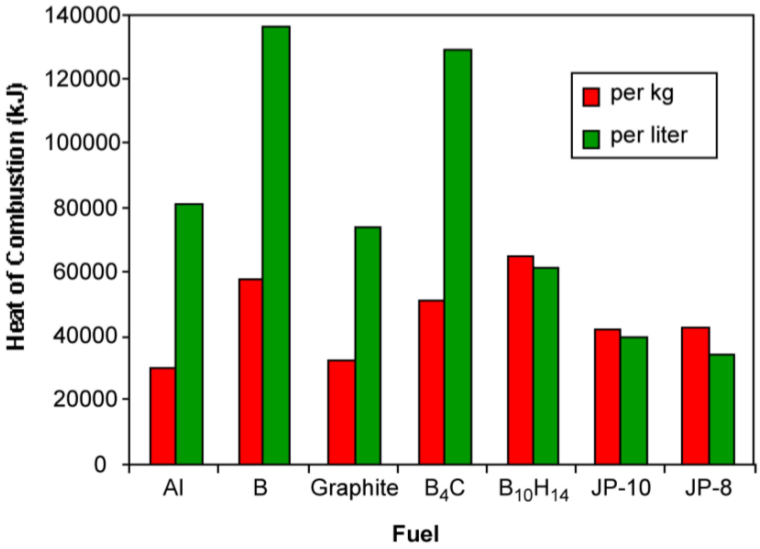


Figure 6.1.9.64: Heat of combustion of various fuels.

Note

Ammonia has been proposed as a practical alternative to fossil fuel for internal combustion engines. The energy value of ammonia is 22.5 MJ/kg, which is about half that of diesel. In a normal engine, in which the water vapor is not condensed, the caloric value of ammonia will be about 21% less than this value; however, it can be used in existing engines with only minor modifications to carburetors/fuel injectors.

Oxygen (O_2) from the air does not have to be the source of oxidizer. Alternatives such as hydrogen peroxide (H_2O_2), nitrous oxide (N_2O), and nitrates (e.g., ammonium nitrate, $NH_4(NO_3)$) are all sources of oxygen for combustion or explosions. However, this does not mean that every compound containing oxygen can be an oxidizer. For example, alcohols such as methanol will burn (in the presence of additional oxygen), but they will not act as an oxidizer. The oxygen within any compound must be reactive. By this we mean that it must be able to be released, preferentially as the more reactive oxygen atom (O) rather than O_2, or be attached (chemically bonded to an element that wants to get rid of the oxygen (i.e., an element that is readily reduced). The most likely element in this case is nitrogen, with sulfur and phosphorus also potential candidates. Almost all compounds containing nitrogen bonded to oxygen can act as an oxidizer. Generally, the more oxygen atoms attached to nitrogen the more reactive the compound.

The efficiency of a chemical reaction such as combustion is dependent on how well the fuel and oxidizer are mixed at the molecular scale. Obviously the best situation is if both components are in the same molecule. Self-oxidizers are compounds containing oxygen in a reactive form as well as a suitable fuel (carbon or hydrogen). The most common self-oxidizers are organic nitrates. It should be pointed out that in spite of the presence of reactive oxygen, self-oxidizers may still require an external source of oxygen to ensure complete reaction, and some form of energy input (ignition) is still required.

Oxygen balance

While many compounds contain oxygen that does not mean they will combust efficiently in the absence of an external oxidizer, or whether they have sufficient oxygen to completely self-combust, or whether they can act as an oxidizer for other compounds. The simplest test for a compound's potential to fulfill these roles is its oxygen balance. The oxygen balance for a chemical is the amount of oxygen needed or produced to ensure the complete oxidation of all the carbon, hydrogen, or other elements.

Compounds such as trinitrotoluene (TNT, Figure 6.1.9.1.65a) have a negative oxygen balance since extra oxygen is needed for complete formation of all the CO_2 and H_2O possible, (1.9.6). Thus, despite its reputation as an explosive, TNT is only efficient in the presence of an external oxidant, which may be air or another compound that provides a positive oxygen balance.

$$2C_7H_5N_3O_6 + 21''O'' \rightarrow 14CO_2 + 5H_2O + 3N_2 \tag{6.1.9.6}$$

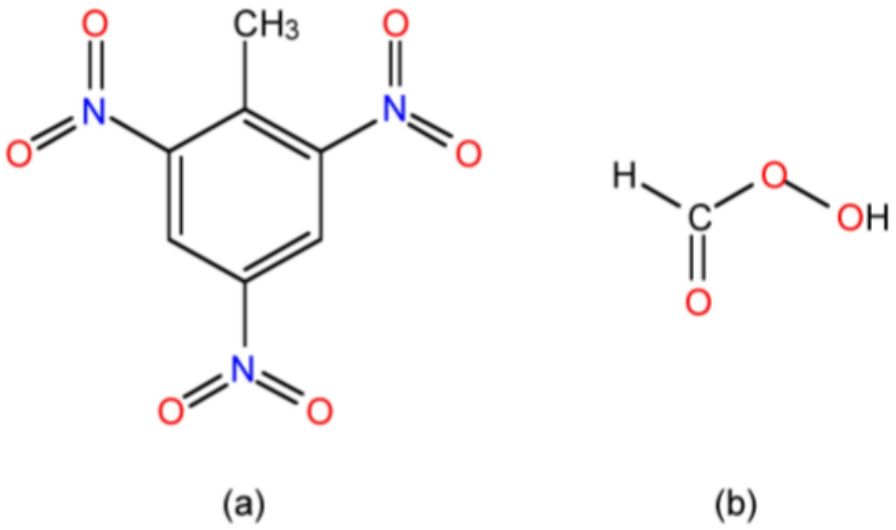


Figure 6.1.9.65: The structures of (a) trinitrotoluene (TNT) and (b) The structure of performic acid.

In contrast to TNT, performic acid (Figure 6.1.9.1.65b) is an example of a compound with a zero oxygen balance: it has all the oxygen it needs for complete combustion, (1.9.7), and hence only requires energy to detonate making at a much more dangerous compound per se than TNT.

$$2CH_2O_3 \rightarrow CO_2 + H_2O \tag{6.1.9.7}$$

A positive oxygen balance means that the compound liberates oxygen surplus to its own needs, for example the decomposition of ammonium nitrate provides one atom of oxygen per molecule, (1.9.8). Clearly, any compound with a positive oxygen balance makes a good oxidizer and is highly incompatible with combustible chemicals.

$$NH_4(NO_3) \rightarrow 2H_2O + N_2 + "O" \tag{6.1.9.8}$$

Quantification of oxygen balance

A quantification of oxygen balance allows for the determination of approximate ratio of reagents to optimize combustion/explosion. In this regard *oxygen balance* is defined as the number of moles of oxygen (excess or deficient) for 100 g of a compound of a known molecular weight (M_w), (1.8.9) where x = number of atoms of carbon, y = number of atoms of hydrogen, z = number of atoms of oxygen, and m = number of atoms of metal oxide produced.

$$OB\% = \frac{-1600}{M_w} \times (2x + \frac{y}{2} + m - z) \tag{6.1.9.9}$$

6.1.9.1 Exa

In the case of TNT, the M_w = 227.1 g/mol, the number of carbon atoms (x) = 7, the number of hydrogen atoms (y) = 5, the number of oxygen atoms (z) = 6, and the number of atoms of metal oxide produced (m) = 0. Therefore:

$$OB\% = \frac{-1600}{227.1} \times (14 + 2.5 + 0 - 6) = -74\% \tag{6.1.9.10}$$

A summary of selected oxygen balance values is given in Table 6.1.9.1.11.

Table 6.1.9.1.11: Oxygen balance of selected compounds.

Element or Compound	Oxygen balance (%)
Carbon	-266.7

Element or Compound	Oxygen balance (%)
Sulfur	-100
Aluminum powder	-89
Trinitrotoluene	-74
Nitroglycerine	+3.5
Ammonium nitrate	+20
Ammonium perchlorate	+27
Potassium chlorate	+26
Sodium chlorate	+45
Sodium nitrate	+37
Tetranitromethane	+57
Lithium perchlorate	+45

This page titled 6.1.9: Chemical Reactivity - The Basics of Combustion is shared under a CC BY 3.0 license and was authored, remixed, and/or curated by Andrew R. Barron (CNX) via source content that was edited to the style and standards of the LibreTexts platform.

6.1.10: Periodic Trends for the Main Group Elements

Within the main group (s- and p-block) elements of the Periodic Table (Figure 6.1.10.1.66) there are some general trends that we can observe for the elemental form, as well as the hydrides, oxides, and halides.

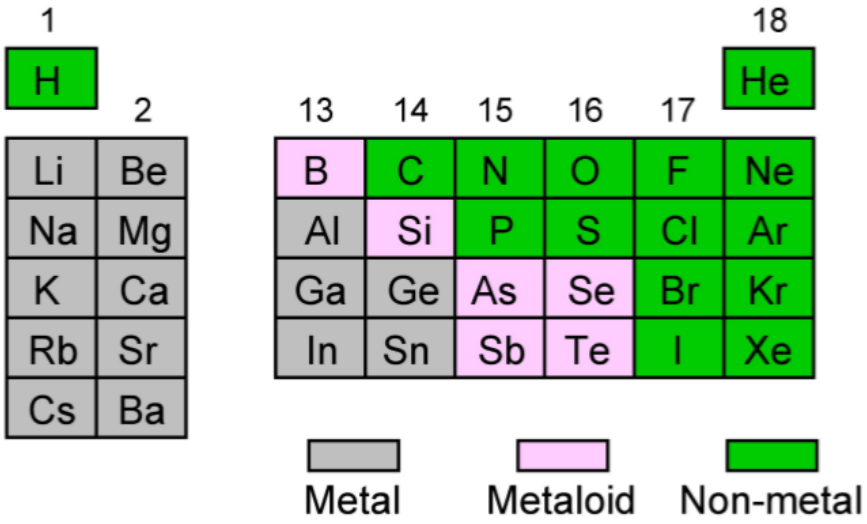


Figure 6.1.10.66: The main group elements (Adapted from www.meta-synthesis.com).

Periodic trends for the main group elements

Within the main group (s- and p-block) elements there are some general trends that we can observe.

- The further down a given Group the elements have increased metallic character, i.e., good conductors of both heat and electricity, and exhibit delocalized bonding.
- Moving from left to right across a Period the elements have greater non-metallic character, they are insulators with localized bonding.
- Within the p-block at the boundary between the metallic elements (Figure 6.1.10.1.66, grey elements) and nonmetal elements (Figure 6.1.10.1.66, green elements) there is positioned boron and silicon that are metalloid in character (Figure 6.1.10.1.66, pink elements), i.e., they have low electrical conductivity but it increases with temperature.

As an example of these changes Table 6.1.10.1.12 shows the trends across one Period.

Table 6.1.10.1.12: Summary of trends for elements across the Periodic Table.

Element	Na	Mg	Al	Si	P	S	Cl	Ar
Properties	Electropositive metal	Electropositive metal	Metal but forms covalent bonds	Metalloid semiconductor metal/non-metal characteristics	E-E bonding in elements	E-E bonding in elements	Simple molecule	Monoatomic gas

Periodic trends for the main group hydrides

The properties of main group hydrides are dependant on the difference in electronegativity between the element and hydrogen (Table 6.1.10.1.13). Elements on the left of the Periodic Table are highly electropositive and form ionic hydrides, while those of the center and right are covalent in character. However, of those with covalent E-H bonds, there is a change from polymeric hydrides to molecular compounds. For example, the Group 13 element hydrides (i.e., BH_3) form hydrogen-bridged oligomers (i.e., B_2H_6). In

contrast, HCl is a diatomic molecule.

Table 6.1.10.1.13: Summary of properties of selected main group hydrides as a function of the relative electronegativities.

Hydride	Element electronegativity	Hydrogen electronegativity	E-H polarity	Structure	Comments
NaH	0.9	2.1	M^+H^-	Ionic	Reacts with H_2O to liberate H_2
BH_3	2.0	2.1	$B^{\delta+}$-$H^{\delta-}$	Oligomeric and polymeric	Reacts slowly with H_2O
CH_4	2.4	2.1	$C^{\delta-}$-$H^{\delta+}$	Molecular	Insoluble in H_2O
HCl	3.0	2.1	$Cl^{\delta-}$-$H^{\delta+}$	Molecular	Dissolves in H_2O to form H^+ and Cl^-

Periodic trends for the main group oxides

As with hydrides the properties of main group oxides are dependant on the difference in electronegativity between the element and oxygen. Highly electropositive metals for ionic oxides, while other elements for covalent bonds (albeit polar in character) with oxygen. In addition, the aggregation of covalent oxides decreased across the Period from left to right (Table 6.1.10.1.14). As may also be seen from Table 6.1.10.1.14, oxides of elements on the left of the Periodic Table dissolve in water to form basic solutions, while those on the right form acidic solutions. There is a class of oxides (especially those of Group 13 and 14) that can react as either an acid or a base. These are known as amphoteric substances.

Note

The word is from the Greek prefix *ampho* meaning "both"

Table 6.1.10.1.14: Comparison of oxides across the Periodic Table.

Oxide	Bonding	Reactivity with H_2O	Description
Na_2O	Ionic	Dissolves to give a strong base	Basic
Al_2O_3	Covalent polymeric	Dissolves in both acidic and basic solution	Amphoteric
SiO_2	Covalent polymeric	Dissolves in both acidic and basic solution	Amphoteric
CO_2	Covalent molecular	Dissolves to give a weak acid	Acidic
SO_3	Covalent molecular	Dissolves to give a strong acid	Aci

In summary, oxides of the main group elements show two trends.

1. From left to right across a Period, the oxides change from ionic → oligomeric/polymeric covalent → molecular covalent
2. From left to right across a Period, the oxides change from ionic → oligomeric/polymeric covalent → molecular covalent.

Periodic trends for the main group chlorides

The trend between ionic and non-ionic/covalent in moving across a Period is also true for the chlorides of the main group elements. Those on the left (i.e., Group 1 and 2) are ionic and soluble in water, while those to the right tend to give acidic solutions due to reactions with the water and the formation of hydrochloric acid, e.g., (1.10.1).

$$SiCl_4 + 2H_2O \rightarrow SiO_2 + 4HCl_{(aq)} \tag{6.1.10.1}$$

This page titled 6.1.10: Periodic Trends for the Main Group Elements is shared under a CC BY 3.0 license and was authored, remixed, and/or curated by Andrew R. Barron (CNX) via source content that was edited to the style and standards of the LibreTexts platform.

6.2: Hydrogen

Thumbnail: Zeppelin the Hindenburg on fire at the mooring mast of Lakehurst (United States of America) 6 May 1937. (Public Domain; Sam Shere via Wikipedia)

This page titled 6.2: Hydrogen is shared under a CC BY 3.0 license and was authored, remixed, and/or curated by Andrew R. Barron (CNX) via source content that was edited to the style and standards of the LibreTexts platform.

6.2.1: Discovery of Hydrogen

Hydrogen gas, H2, was first artificially synthesized by Phillip von Hohenheim (known as Paracelsus, Figure 6.2.1.2.1) by mixing metals with strong acids. He was unaware that the flammable gas produced by this chemical reaction was a new chemical element. In 1671, Robert Boyle (Figure 6.2.1.2.2) rediscovered the reaction between iron lings and dilute acids, which results in the production of hydrogen gas. He noted that these fumes were highly flammable and that the flame gave o a lot of heat but not much light.



Figure 6.2.1.1: Renaissance physician, botanist, alchemist, and astrologer Paracelsus (1493 1541).



Figure 6.2.1.2: Irish philosopher, chemist, physicist, and inventor Robert Boyle (1627 1691).

In 1766, Henry Cavendish (Figure 6.2.1.2.3) was the first to recognize hydrogen gas as a discrete substance, by identifying the gas from a metal-acid reaction as *flammable* air. One of the richest men in Britain at the time, he lived in London and spent his time in his private laboratory at his home. In 1781 he was the first person to nd that the gas produces water when burned. This was a key experiment in disproving the Aristotelian theory of the four elements. As a consequence of his work he is usually given credit for its discovery as an element. However, it was Antoine Lavoisier (Figure 6.2.1.2.4) who in 1783 named the element *hydrogen* (from the Greek *hydro* meaning water and *genes* meaning creator) after he reproduced Cavendish's findings.

The four Aristotalian elements were *Earth, Fire, Air* and *Water*. A fifth element, *Aether*, was ascribed as a divine substance that made up the heavenly spheres and heavenly bodies (stars and planets).



Figure 6.2.1.3: British scientist Henry Cavendish (1731 - 1810).



Figure 6.2.1.4: French chemist and biologist Antoine-Laurent de Lavoisier (1743 1794).

Using his invention, the vacuum flask, James Dewar (Figure 6.2.1.2.5) was the first to liquefy hydrogen in 1898. He produced solid hydrogen the next year.



Figure 6.2.1.5: Scottish chemist and physicist Sir James Dewar FRS (1842 1923).

This page titled 6.2.1: Discovery of Hydrogen is shared under a CC BY 3.0 license and was authored, remixed, and/or curated by Andrew R. Barron (CNX) via source content that was edited to the style and standards of the LibreTexts platform.

6.2.2: The Physical Properties of Hydrogen

Table 6.2.2.2.1: Physical properties of hydrogen.

Chemical Symbol	H
Atomic number	1
Electron configuration	$1s^1$
Atomic weight	1.00794
Melting point	-259 °C
Boiling point	-253 °C
Density (gas)	0.090 g/L
Density (liquid)	0.70g/L
Ionization potential	13.598 eV
Pauling electronegativity	2.1
Ionic radius (H^-)	1.54 Å
van der Waal radius	1.2 Å
Explosive limit	4 - 75%
Ignition temperature	585 °C

This page titled 6.2.2: The Physical Properties of Hydrogen is shared under a CC BY 3.0 license and was authored, remixed, and/or curated by Andrew R. Barron (CNX) via source content that was edited to the style and standards of the LibreTexts platform.

6.2.3: Synthesis of Molecular Hydrogen

Although hydrogen is the most abundant element in the universe, its reactivity means that it exists as compounds with other elements. Thus, molecular hydrogen, H_2, must be prepared from other compounds. The following outlines a selection of synthetic methods.

Steam reforming of carbon and hydrocarbons

Many reactions are available for the production of hydrogen from the reaction of steam with a carbon source. The choice of reaction is guided by the availability of raw materials and the desired purity of the hydrogen. The simplest reaction involves passing steam over coke at high temperatures (1000 °C).

$$\mathrm{C(s) + H_2O(g) \rightarrow H_2(g) + CO(g)}$$

Coke is a grey, hard, and porous carbonaceous material derived from destructive distillation of low-ash, low-sulfur bituminous coal. As an alternative to coke, methane may be used at a slightly higher temperature (1100 °C).

$$\mathrm{CH_4(g) + H_2O(g) \rightarrow 3\,H_2(g) + CO(g)}$$

In each case the carbon monoxide formed in the reaction can react further with steam in the presence of a suitable catalyst (usually iron or cobalt oxide) to generate further hydrogen.

$$\mathrm{CO(g) + H_2O(g) \rightleftharpoons H_2(g) + CO_2(g)}$$

This reaction is known as the water gas-shift reaction, and was discovered by Italian physicist Felice Fontana (Figure 6.2.3.2.6) in 1780.



Figure 6.2.3.6: Italian physicist Felice Fontana (1730 - 1805).

The dominant industrial process for hydrogen production uses natural gas or oil refinery feedstock in the presence of a nickel catalyst at 900 °C.

$$C_2H_{8(g)} + 3H_2O_{(g)} \rightarrow 7H_{2(g)} + 3CO_{(g)}$$

Electrolysis of water

Electrolysis of acidified water in with platinum electrodes is a simple (although energy intensive) route to hydrogen.

$$2H_2O_{(l)} \rightarrow 2H_{2(g)} + O_{2(g)}$$

On a larger scale hydrolysis of warm aqueous solutions of barium hydroxide can yield hydrogen of purity greater than 99.95%. Hydrogen is also formed as a side product in the production of chlorine from electrolysis of brine (NaCl) solutions in the presence of a mercury electrode.

$$2NaCl_{(aq)} + 2Hg_{(l)} \rightarrow Cl_{2(g)} + 2NaHg_{(l)}$$

The sodium mercury amalgam reacts with water to yield hydrogen.

$$NaHg_{(l)} + 2H_2O_{(l)} \rightarrow H_{2(g)} + 2NaOH_{(aq)} + 2Hg_{(l)}$$

Thus, the overall reaction can be written as:

$$NaCl_{(aq)} + H_2O_{(l)} \rightarrow H_{2(g)} + 2NaOH_{(aq)} + Cl_2$$

However, this method is being phased out for environmental reasons.

Reaction of metal with acid

Hydrogen is produced by the reaction of highly electropositive metals with water, and less reactive metals with acids, e.g.,

$$Fe_{(s)} + 2H_3O^+_{(aq)} \rightarrow H_{2(g)} + 2H_2O_{(aq)} + Fe^{2+}_{(aq)}$$

This method was originally used by Henry Cavendish (Figure 6.2.3.2.7) during his studies that led to the understanding of hydrogen as an element (Figure 6.2.3.2.8).



Figure 6.2.3.7: Henry Cavendish (1731 - 1810).

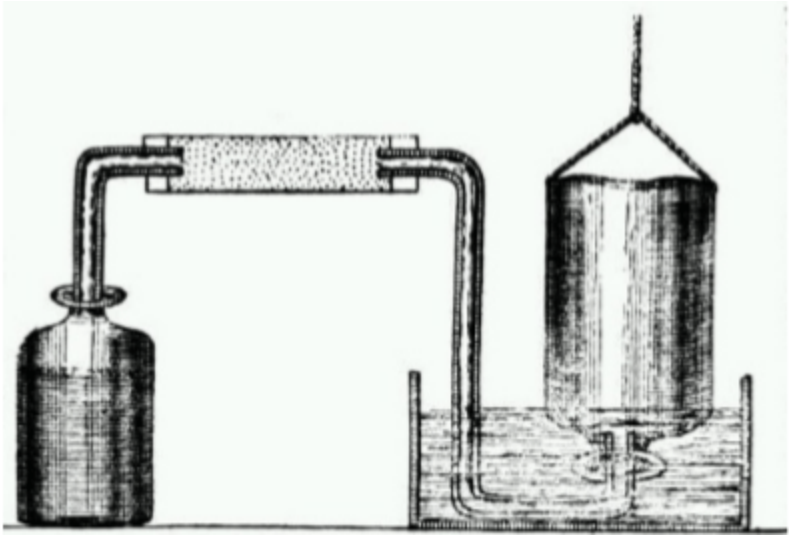


Figure 6.2.3.8: Cavendish's apparatus for making hydrogen in the left hand jar by the reaction of a strong acid with a metal and collecting the hydrogen gas above water in the right hand inverted jar.

The same method was employed by French inventor Jacques Charles (Figure 6.2.3.2.9) for the first ight of a hydrogen balloon on 27th August 1783. Unfortunately, terrified peasants destroyed his balloon when it landed outside of Paris.



Figure 6.2.3.9: Jacques Alexandre César Charles (1746 1823).

Hydrolysis of metal hydrides

Reactive metal hydrides such as calcium hydride (CaH_2) undergo rapid hydrolysis to liberate hydrogen.

$$CaH_{2(s)} + 2H_2O_{(l)} \rightarrow 2H_{2(g)} + 2OH^-_{(aq)} + Ca^{2+}_{(aq)}$$

This reaction is sometimes used to inflate life rafts and weather balloons where a simple, compact means of generating H_2 is desired.

This page titled 6.2.3: Synthesis of Molecular Hydrogen is shared under a CC BY 3.0 license and was authored, remixed, and/or curated by Andrew R. Barron (CNX) via source content that was edited to the style and standards of the LibreTexts platform.

6.2.4: Atomic Hydrogen

Atomic hydrogen has the electron conguration of $1s^1$ and as such represents the simplest atomic conguration. However, as a consequence there is dispute as to its proper position within the Periodic Table. Its electron conguration is similar to the valence electron conguration of the alkali metals (ns^1) suggesting it be listed at the top of Group 1 (1A). However, its reaction chemistry is dissimilar to the alkali metals. Hydrogen is also one electron short of a Nobel gas conguration, and therefore it is possible to think of its relationship to the halogens.

Vapor phase

Atomic hydrogen ($H^{\cdot}$) is highly reactive and consequently has a short lifetime due to its reaction chemistry. Consequently, in order to generate and observe the reactivity they must be generate at low pressures.

Thermolysis of hydrogen compound (commonly halide) or photolysis at an energy above the bond dissociation energy results in the homoleptic cleavage of the H-X bond to generate the appropriate radical species.

$$H-X\xleftrightarrow{\Delta \ or \ h\nu}H+X \tag{6.2.4.1}$$

Alternatively, atomic hydrogen can be generated from elemental hydrogen.

$$H-H\xleftrightarrow{\Delta \ or \ h\nu}H^{\cdot}+H^{\cdot} \tag{6.2.4.2}$$

The reverse reaction (recombination of two hydrogen atoms) is highly exothermic (-434 $kJ.mol^{-1}$) and forms the basis of the heat generated in arc welding.

Solution

Atomic hydrogen may be generated in aqueous solution through the solvation of electrons.

$$e^{-}_{(aq)}+H_3O^{+}\leftrightharpoons H^{\cdot}+H_2O \tag{6.2.4.3}$$

The formation equilibrium constant (K_{eq}) is very small resulting in very low concentrations being generated (10^{-5} M). As expected solvated atomic hydrogen is a strong reducing agent.

$$Ag^{+}+H^{\cdot}\rightarrow Ag+H^{+} \tag{6.2.4.4}$$

$$2I^{-}+2H^{\cdot}\rightarrow 2H^{+}+I_2 \tag{6.2.4.5}$$

Solid state

Hydrogen atoms may be trapped in the solid state lattice upon generation by photolysis of HX. Observation by electron spin resonance (esr) of a signal split by s = $^1/_2$ nucleus (i.e., ^1H) results in a doublet with a coupling of 1428 MHz.

This page titled 6.2.4: Atomic Hydrogen is shared under a CC BY 3.0 license and was authored, remixed, and/or curated by Andrew R. Barron (CNX) via source content that was edited to the style and standards of the LibreTexts platform.

6.2.5: The Proton

The proton, H^+, is the name given to hydrogen in the +1 oxidation state.

Gas phase

The proton can be formed from the photolysis of atomic hydrogen in the vapor phase at low pressure.

$$H_{(g)} + h\nu \rightarrow H^+_{(g)} + e^-_{(g)} \tag{6.2.5.1}$$

The proton is more reactive than the hydrogen atom because of its high charge density. In addition, the proton's small ionic radius, 1.5 x 10^{-15} cm, means that it can get close to other atoms and hence form strong bonds.

$$H^+_{(g)} + NR_3 \rightarrow HNR^+_{3(g)} \tag{6.2.5.2}$$

The strength of the bonding interaction is such that it is very hard to measure directly. Instead the relative bond strength between the proton and an appropriate base, B_1, is measured in the presence of a competing base, B_2.

$$B_1H^+_{(g)} + B_{2(g)} \leftrightharpoons B_2H^+_{(g)} + B_{2(g)} \tag{6.2.5.3}$$

In measuring the exchange reaction, the *relative proton affinity* of B_1 and B_2 is measured. This is also known as the gas phase acidity, and as such it is a measure of the inherent acidity of a species X-H because it obviates any solvent effects.

Liquid and solution

The high reactivity of the proton means that it does not exist free in solution. There are however many H^+ containing species. These are generally classified as *acids*.

$$\underset{\text{acid}}{B_1H^+_{(sol)}} + \underset{\text{base}}{B_{2(sol)}} \leftrightharpoons \underset{\text{acid}}{B_2H^+_{(sol)}} + \underset{\text{base}}{B_{1(sol)}} \tag{6.2.5.4}$$

The reaction between the acid and the base is a proton transfer reaction. While the proton travels from B_1 to B_2, it is never free in solution. Instead a bridged transition state or intermediate is formed, B_1‴H^+‴B_2.

Acidity and pH

The most common solvent for H+ is water. The acid form is usually defined as the hydronium ion or H_3O^+, (2.5.5). The terms oxonium, hydroxonium and oxidanium are also used for the H_3O^+. Although we commonly use H_3O^+ it is known from spectroscopy that larger complexes are formed such as $H_9O_4^+$ (Figure 6.2.5.2.10).

$$H_2O + H^+ \rightarrow H_3O^+ \tag{6.2.5.5}$$

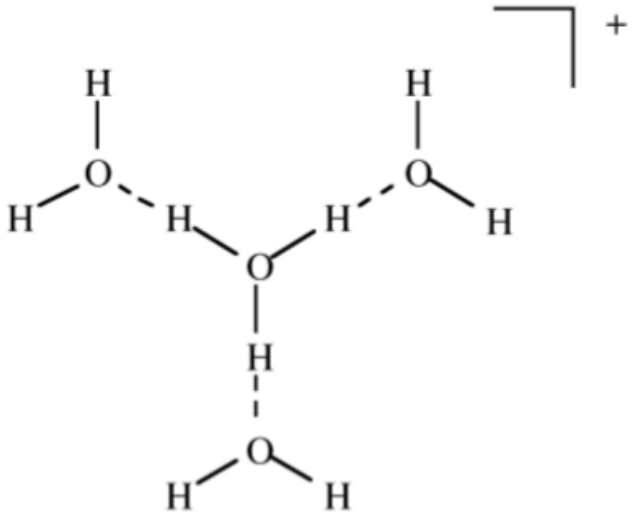


Figure 6.2.5.10: Structure of $H_9O_4^+$.

Acids and bases have been characterized in a number of different ways. In 1680 Robert Boyle (Figure 6.2.5.2.11) defined an acid as a compound that dissolved many other compounds, had a sour taste, and reacted with alkali (base).



Figure 6.2.5.11: Portrait of Robert Boyle (1627 1691).

Boyle's simple observational description was rationalized by Danish physical chemist Johannes Brønsted (Figure 6.2.5.2.12). Brønsted proposed that acids are *proton donors*, and bases are *proton acceptors*. An acid-base reaction is one in which a proton is transferred from a proton donor (acid) to a proton acceptor (base). Based upon Brønsted's proposal simple acids contain an ionizable proton. Examples of simple acids include neutral molecules (HCl, H2SO4), anions (HSO_4^-, $H_2PO_4^-$), and cations (NH_4^+). The most common Brønsted bases include metal hydroxides (MOH).



Figure 6.2.5.12: Johannes Nicolaus Brønsted (1879 1947).

Brønsted noted that when an acid donates a proton it forms a conjugate base. The following are examples of an acid and its conjugate base.

$$\underset{\text{acid}}{H_2O} \rightarrow \underset{\text{conjugate base}}{H^+ + OH^-} \tag{6.2.5.6}$$

$$\underset{\text{acid}}{H_2SO_4} \rightarrow \underset{\text{conjugate base}}{H^+ + HSO_4^-} \tag{6.2.5.7}$$

$$\underset{\text{acid}}{NH_4^+} \rightarrow \underset{\text{conjugate base}}{H^+ + NH_3} \tag{6.2.5.8}$$

Exercises

Exercise 6.2.5.1\

What is the conjugate base of HCl?

Answer available at the end of this section.

Exercise 6.2.5.2\

What is the conjugate base of HSO_4^-

Answer available at the end of this section.

Exercise 6.2.5.3\

What is the conjugate base of $[Al(H_2O)_6]^{3+}$

Answer available at the end of this section.

The same occurs when a base accepts a proton it forms a conjugate acid. The following are examples of a base and its conjugate acid.

$$\underset{\text{base}}{H_2O} + H^+ \rightarrow \underset{\text{conjugate acid}}{H_3O^+} \tag{6.2.5.9}$$

$$\underset{\text{base}}{HCO_3^-} + \underset{\text{conjugate acid}}{H^+} \rightarrow H_2CO_3 \tag{6.2.5.10}$$

$$\underset{\text{base}}{F^-} + \underset{\text{conjugate acid}}{H^+} \rightarrow HF \tag{6.2.5.11}$$

Exercises

Exercise 6.2.5.4\

What is the conjugate acid of NH_3?

Answer available at the end of this section.

Exercise 6.2.5.5\

What is the conjugate acid of S^{2-}?

Answer available at the end of this section.

Exercise 6.2.5.6\

What is the conjugate acid of CO_3^{2-}?

Answer available at the end of this section.

Thus, the reaction between an acid and a base results in the formation of the appropriate conjugate base and conjugate acid.

$$acid_1 + base_1 \leftrightharpoons acid_2 + base_2 \tag{6.2.5.12}$$

A specific example is as follows:

$$\underset{acid_1}{HNO_3} + \underset{base_1}{NH_3} \leftrightharpoons \underset{acid_2}{NH_4^+} + \underset{base_2}{NO_3^-} \tag{6.2.5.13}$$

6.2.5.7Exe

What is the conjugate acid and base formed from the reaction of NH_4^+ with S_2^+?

Answer available at the end of this section.

In the equilibrium reactions shown in (2.12) and (2.13) there is a competition between the two bases for the proton. As would be expected the strongest base wins.

When a strong acid is added to (dissolved in) water it will react with the water as a base:

$$\underset{acid}{HCl} + \underset{base}{H_2O} \leftrightharpoons \underset{acid}{H_3O^+} + \underset{base}{Cl^-} \tag{6.2.5.14}$$

In contrast, when a strong base is added to (dissolved in) water it will react with the water as an acid:

$$\underset{acid}{H_2O} + \underset{base}{NH_3} \leftrightharpoons \underset{acid}{NH_4^+} + \underset{base}{OH^-} \tag{6.2.5.15}$$

pH a measure of acidity

The acidity of a water (aqueous) solution depends on the concentration of the hydronium ion, i.e., [H_3O^+]. The acidity of a solution is therefore the ability of the solution to donate a proton to a base. The acidity or pH of a solution is defined as:

$$pH = -log[H_3O_a^+] \tag{6.2.5.16}$$

It is important to note that the value is the *activity* of H_3O^+ and not the *concentration*.

Note

Activity is a measure of the eective concentration of a species in a mixture. The dierence between activity and other measures of composition such as concentration arises because molecules in non-ideal gases or solutions interact with each other, either to attract or to repel each other.

The activity of the H_3O^+ ion can be measured by

(a) A gas electrode

(b) Acid-base indicators

Proton Transfer Reactions

The proton transfer reaction is one of the simplest reactions in chemistry. It involves no electrons and low mass transfer/change, giving it a low energy of activation. For proton transfer between O-H or N-H groups and their associated bases the reaction is very fast. The proton transfer occurs across a hydrogen-bonded pathway during which the proton is never free.

Answers

Cl^-

SO_4^{2-}

$[Al(H_2O)_5(OH)]^{2+}$

NH_4^+

HS^-

HCO_3^-

$$\underset{acid_1}{NH_4^+} + \underset{base_1}{S^{2-}} \leftrightharpoons \underset{acid_2}{HS^-} + \underset{base_2}{NH_3} \tag{6.2.5.17}$$

This page titled 6.2.5: The Proton is shared under a CC BY 3.0 license and was authored, remixed, and/or curated by Andrew R. Barron (CNX) via source content that was edited to the style and standards of the LibreTexts platform.

6.2.6: Hydrides

The combination of hydrogen with another element produces a hydride, E_xH_y. The formal charge or oxidation state of the hydrogen in these compounds is dependant on the relative electronegativity of the element in question.

Ionic hydrides

Hydrogen compounds with highly electropositive metals, i.e., those in which the metal has an electronegativity of less than 1.2, are ionic with the hydrogen having a s^2 configuration (H^-). Typical ionic metal hydrides are those of the Group 1 (IA) metals and the heavier Group 2 (IIA) metals.

The ionic radius of the hydride ion is in between that of fluoride and chloride and the same as oxide (Table 6.2.6.2.2). As a consequence, in the solid state the hydride ion replicates that of a halide ion (e.g., Cl^-), and as such similar solid state structures are observed (Table 6.2.6.2.3).

Table 6.2.6.2.2: Selected ionic radii.

Ion	Ionic Radius (Å)
H^-	1.40
F^-	1.36
Cl^-	1.81
O^{2-}	1.40

Table 6.2.6.2.3: Lattice parameters (Å) for hydrides, and halides of the Group 1 metal salts with cubic rock salt structures.

Metal	Hydride	Fluoride	Chloride
Li	4.085	4.0173	5.129
Na	4.880	4.620	5.640
K	5.700	5.347	6.292
Rb	6.037	5.640	6.581
Cs	6.376	6.008	7.020

Unlike the halide ions that are soluble in water, the hydride ion reacts with water, (2.32), and consequently NaH and CaH_2 are commonly used as drying agents. The liberation of hydrogen was used as a commercial source of hydrogen for small-scale applications.

$$H^- + H_2O \rightarrow OH^- + H_{2(g)} \tag{6.2.6.1}$$

WARNING

Group 1 and 2 metal hydrides can ignite in air, especially upon contact with water to release hydrogen, which is also flammable. Hydrolysis converts the hydride into the analogous hydroxide, which are caustic bases. In practice, most ionic hydrides are dispensed as a dispersion in oil, which can be safely handled in air.

Covalent Hydrides

The most common binary compounds of hydrogen are those in which hydrogen bonds have covalent bond character. The E-H bond is usually polar ranging from those in which the hydrogen is polarized positively (e.g., those with non-metals such as F, O, S, and C) to where it is negative (e.g., those with metals and metalloids such as B, Al, etc). Magnesium hydride is intermediate between covalent and ionic since it has a polymeric solid similar to AlH_3, but reacts rapidly with water like ionic hydrides. Table 6.2.6.2.4 lists the important covalent hydrides of p-block elements. It should be noted that all organic hydrocarbons can be thought of as simply the hydrides of carbon!

Group 13	Group 14	Group 15	Group 16	Group 17
B_2H_6	C_nH_{2n+2}, C_nH_{2n}, C_nH_{2n-2}	NH_3, N_2H_4	H_2O, H_2O_2	HF
$(AlH_3)_n$	Si_nH_{2n+2}	PH_3, P_2H_4	H_2S, H_2S_n	HCl
Ga_2H_6	Ge_nH_{2n+2}	AsH_3	H_2Se	HBr
	SnH_4	SbH_3	H_2Te	HI

The elements of Group 14 to 17 all form hydrides with normal covalent bonds in which the hydrogen is bonded by a single bond to the element in question. In contrast, the elements of Group 13 (as typified by boron) all exhibit a second type of covalent bond: the electron deficient **hydrogen bridged bond**. In this type of bond the hydrogen nucleus is embedded in a molecular orbital that covers more than two atoms to create a multi-center two-electron bond. Diborane (Figure 6.2.6.2.13) represents the archetypal compound containing the hydrogen bridge bond. Hydrides are not limited to terminal (E-H) or those bridging two atoms (E-H-E), but are also known where the hydrogen bridges (or caps) more than two atoms, i.e., Figure 6.2.6.2.14.

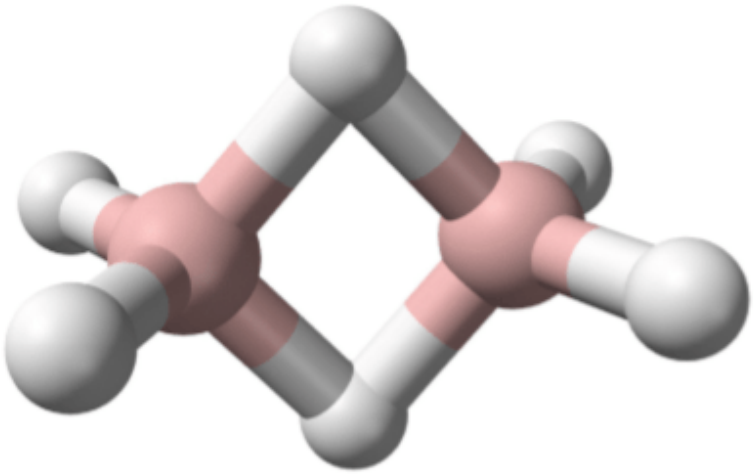


Figure 6.2.6.13: Structure of diborane (B2H6); where pink = boron; white = hydrogen.

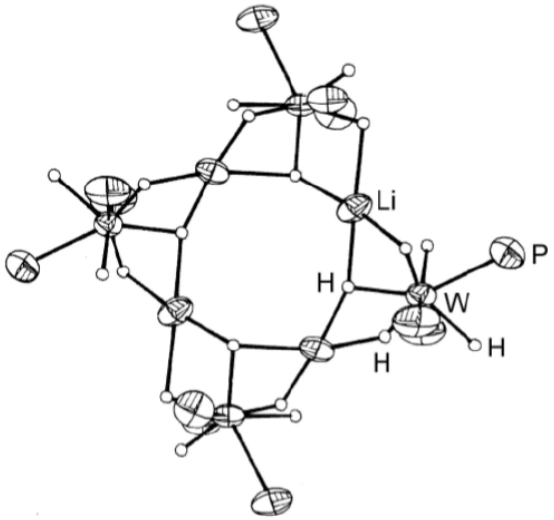


Figure 6.2.6.14: The structure of {[$(Me_3P)_3WH_5$]$^-$$Li^+$}4 showing the presence of terminal, bridging, and trifurcated hydrides. The methyl groups have been omitted for clarity. Adapted from A. R. Barron, M. B. Hursthouse, M. Motevalli, and G. Wilkinson, *J. Chem. Soc., Chem. Commun.*, 1986, 81.

Synthesis of covalent hydrides

Covalent hydrides can be made by a range of synthetic routes. The simplest is direct combination of the elements (in a similar manner to that used with ionic hydrides).

$$2H_2 + O_2 \rightarrow 2H_2O \tag{6.2.6.2}$$

The use of a hydride as a reagent to reduce a halide or oxide of the desired element

$$SiCl_4 + LiAlH_4 \rightarrow SiH_4 + LiAlCl_4 \tag{6.2.6.3}$$

Metal phosphides, carbides, silicides, and borides result in the formation of the hydride.

$$Ca_3P_2 + 6H_2O \rightarrow 2PH_3 + 3Ca(OH)_2 \tag{6.2.6.4}$$

Hydride compounds can be interconverted in the presence of a catalyst, heat, or an electrical discharge. This is the basis of catalytic cracking of petroleum mixtures.

Interstitial hydrides

Many transition metal, lanthanides and actinides absorb hydrogen to give a metallic hydride which retain the properties of a metal, although the presence of hydrogen does result in embrittlement of the metal. As such these hydrides are best considered as alloys since they do not have defined stoichiometries. For example, vanadium absorbs hydrogen to form an alloy with a maximum hydrogen content of $VH_{1.6}$. In a similar manner palladium forms $PdH_{0.6}$. The hydrogen atoms are present in interstitial sites in the metal's lattice; hence *interstitial hydride*. Interstitial hydrides show certain promise as a way for safe hydrogen storage.

Bibliography

- A. R. Barron, M. B. Hursthouse, M. Motevalli, and G. Wilkinson, *J. Chem. Soc., Chem. Commun.*, 1986, 81.

This page titled 6.2.6: Hydrides is shared under a CC BY 3.0 license and was authored, remixed, and/or curated by Andrew R. Barron (CNX) via source content that was edited to the style and standards of the LibreTexts platform.

6.2.7: The Hydrogen Bond

Hydrogen bonds are formed between a species with a polar $X^{\delta-}$-$H^{\delta+}$ bond and a species with a lone pair ($Y^{\delta-}$), i.e., $X^{\delta-}$-$H^{\delta+}$...$Y^{\delta-}$. The most common species for X are oxygen and nitrogen, and to a lesser extent carbon, fluorine, and sulfur. However, as long as the X-H bond is polar then hydrogen bonding is possible. Similarly, the most common Lewis bases that hydrogen bond involve oxygen, nitrogen, and fluorine as the donor atom. Again there are many examples of other atoms, but as long as the atom has a lone pair that is chemically active, hydrogen bonding can occur.

The majority of hydrogen bonds are asymmetrical, that is the hydrogen is closer to one atom than the other (Figure 6.2.7.2.15), even when X and Y are the same element, i.e., O-H...O. While the typical hydrogen bond involves one Lewis base (lone pair donor), there are many examples where the hydrogen interacts with two Lewis base lone pairs (Figure 6.2.7.2.16).

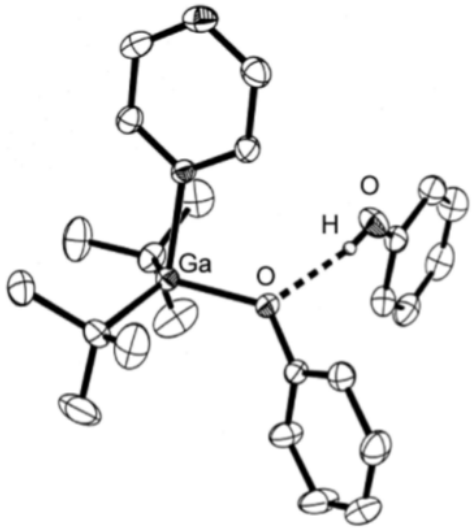


Figure 6.2.7.15: Structure of $(^{t}Bu)_2Ga(OPh)(pyz)\cdot(PhOH)$ from X-ray crystallographic data showing the presence of an asymmetrical hydrogen bond. Hydrogen atoms attached to carbon are omitted for clarity. Adapted from L. H. van Poppel, S. G. Bott and A. R. Barron, *Polyhedron*, 2002, **21**, 1877.

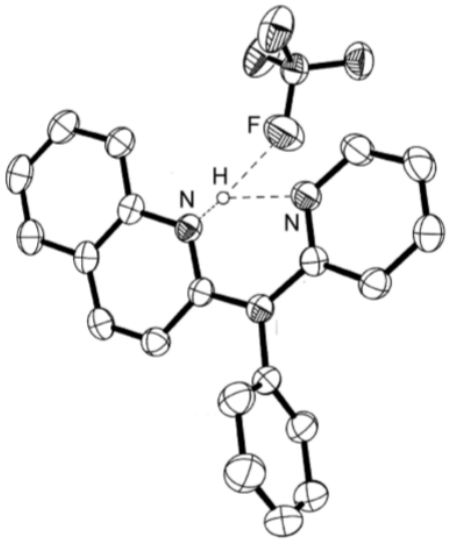


Figure 6.2.7.16: Structure of [H{PhN(py)(quin)}]BF_4 from X-ray crystallographic data showing the presence of a trifurcated asymmetrical hydrogen bond. Hydrogen atoms attached to carbon are omitted for clarity. Adapted from J. J. Allen, C. E. Hamilton, and A. R. Barron, *J. Chem. Cryst.*, 2009.

Hydrogen bonds are mostly electrostatic attractions, and as such they are weaker than covalent bonds, but stronger than van der Waal interactions. With bond strengths generally covering the range of 5 50 kJ/mol, the energy required to break a hydrogen bond is comparable to that of thermal motion within the temperature range of 0 200°C. As a consequence the number of groups involved in hydrogen bonding decreases with increasing temperature, until few hydrogen bonds are observed in the vapor phase. One noted exception is the hydrogen bridged anion $[F\text{-}H\text{-}F]^-$, in which the strong interaction (243 kJ/mol) is covalent in character involving a three-center molecular orbital bond.

Classes of hydrogen bond

Although hydrogen bonds may be characterized with respect to the X and Y atom, it is more useful to classify them as either intramolecular or intermolecular hydrogen bonds. This is due to the difference in physical and chemical properties between these two classes.

Intramolecular

Intramolecular hydrogen bonds (X-H...Y) arise where the X and Y atoms are in the same molecule (Figure 6.2.7.2.17).

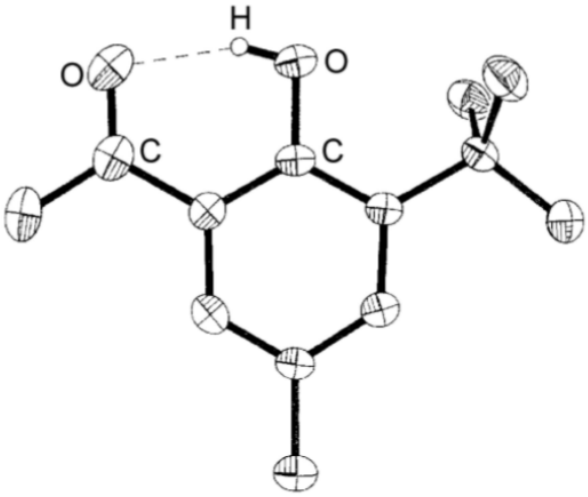


Figure 6.2.7.17: Structure of 3-*tert*-butyl-2-hydroxy-5-methylacetophenone showing the presence of an intramolecular hydrogen bond. Hydrogen atoms attached to carbon are omitted for clarity. Adapted from M. B. Power, A. R. Barron, S. G. Bott, E. J. Bishop, K. D. Tierce and J. L. Atwood, *J. Chem. Soc.*, Dalton Trans., 1991, 241.

Intermolecular

If the hydrogen bond (X-H···Y) involves X and Y being from different molecules this is an intermolecular hydrogen bond. Within the range of intermolecular hydrogen bonded compounds there are two sub-categories: those involving discrete molecular species (oligomers) and those resulting in polymeric species.

Carboxylic acids are a typical example of a discrete oligomeric species that are held together by intermolecular hydrogen bonds (Figure 6.2.7.2.18a). A wide range of structurally analogous compounds also form head-to-tail hydrogen bonded dimers (e.g., Figure 6.2.7.2.19). In a polymeric hydrogen bonded species every molecule hydrogen bonds but in a random form. As an example, liquid primary alcohols form extended hydrogen networks (Figure 6.2.7.2.18b). Such an arrangement is labile and as such it is difficult to determine definitive speciation. Liquids that form this type of hydrogen-bonded network are known as associated liquids. In the solid state the networks generally adopt a more ordered structure. For example as is seen in the structure of ice.

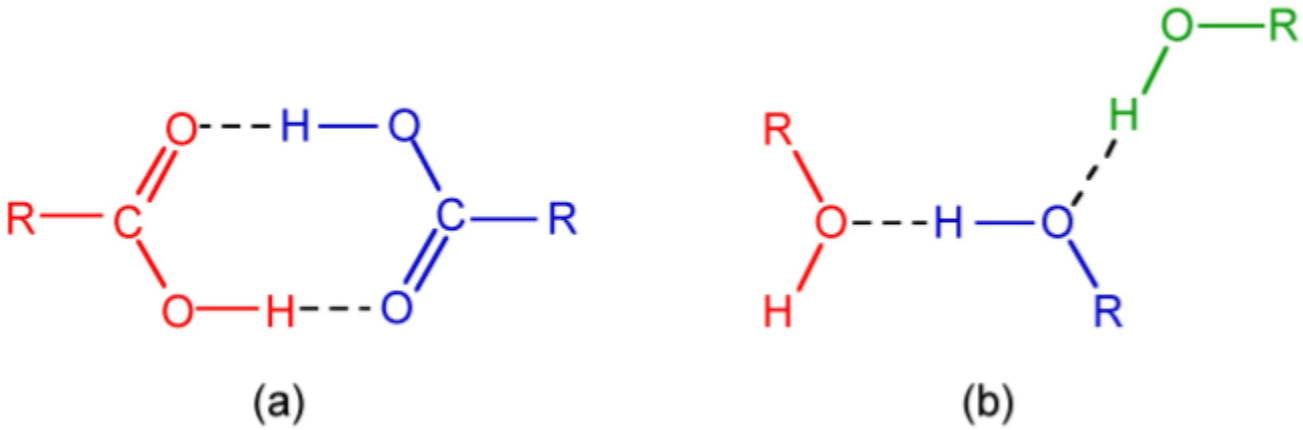


Figure 6.2.7.18: Structure of (a) the head-to-tail dimmer formed between two carboxylic acid molecules, and (b) a typical network of a primary alcohol in the liquid phase.

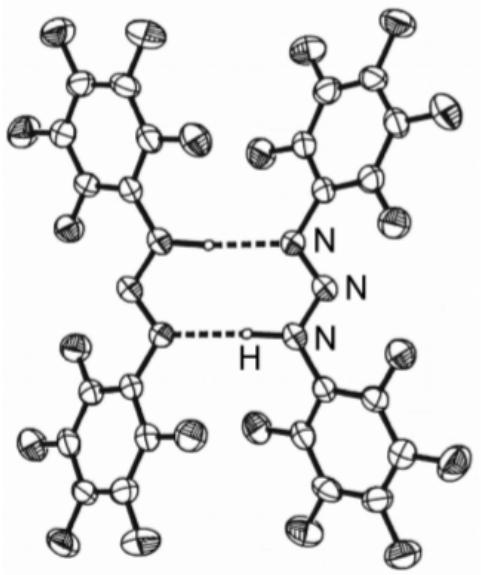


Figure 6.2.7.19: Structure of the hydrogen bonded diner of (C6H5)NNN(H)(C6F5). Adapted from J. T. Leman, J. Braddock-Wilking, A. J. Coolong, and A. R. Barron, *Inorg. Chem.*, 1993, **32**, 4324.

Methods of study

The study of the structure arising from hydrogen bonding and the properties exhibited due to the presence of hydrogen bonds is very important.

Diffraction methods

X-raydiffraction of single crystals is the most common structural method employed to determine the presence, effect, and strength of a hydrogen bond. Unfortunately, in order for the location of the hydrogen to be determined with some degree of accuracy, diffraction data of a high quality is needed and/or low temperature (e.g., -196 °C) data collection is required. Neutron scattering can be used where very accurate data is required because hydrogen atoms scatter neutrons better than they do X-rays. Figure 6.2.7.2.20 summarizes the key parameters that are obtained from X-ray (and neutron) diffraction experiments.

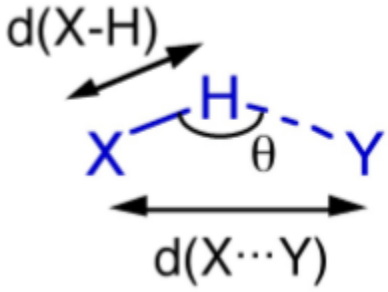


Figure 6.2.7.20: Structural parameters obtained from diraction methods.

Given the electrostatic nature of a hydrogen bond between a polar X-H bond and a Lewis base it is reasonable that the X-H...Y angle (θ) is roughly linear (i.e., 180°). However, it is not always so and nonlinear interactions are known where steric or conformational restrictions limit the orientation of the X-H bond with respect to Y.

The distance between X and Y, d(X...Y), is less than the sum of the van der Waal radii of X and Y (Table 6.2.7.2.5). This is in line with the relative strength of these interactions. As would be expected the shorter the X...Y distance the stronger the hydrogen bond.

Table 6.2.7.2.5: Comparison of the X...Y distance in hydrogen bonded species with the sum of the van der Waal radii.

X	Y	Sum of van der Waal radii (Å)	Typical X···Y distance (Å)
O	O	2.8	2.50-2.69
O	N	2.9	2.75-2.85
N	N	3.0	2.69-2.98

The bond distance to hydrogen, d(X-H), is often longer in hydrogen bonded species. For example the O-H distance for an alcohol in the absence of hydrogen bonding is typically 0.97 Å. In contrast, the value typically seen for a hydrogen-bonded analog is 1.05 Å.

Spectroscopy

Spectroscopy is a simple method of comparing hydrogen-bonded systems in particular in the solution or liquid phase.

Infra red and Raman

The X-H stretching frequency in the IR (and Raman) spectrum is dependant on the identity of X, i.e., O-H = 3610 - 3640 cm^{-1} and N-H = 3400 - 3500 cm^{-1}. However, the ν(X-H) is shifted to lower energy (lower frequency) as a consequence of hydrogen bonding. In addition, while non-hydrogen bonded X-H stretches are sharp, the presence of hydrogen bonding results in the peak being broadened. Figure X demonstrates both these effects. The O-H stretch for dilute ^{n}BuOH in CCl_4 is a sharp peak at 3650 cm^{-1} due to the lack of hydrogen bonding between the two components (Figure 6.2.7.2.21a), and the presence of hydrogen bonding between ^{n}BuOH and ^{n}BuOH is limited by the dilution. By contrast, a dilute solution of ^{n}BuOH in Et_2O results in a shift to lower frequency and a significant increase of peak width (Figure 6.2.7.2.21b) as a result of fairly strong O-H···O bonds. Finally, a dilute solution of ^{n}BuOH in NMe_3 results in a further shift to 3250 cm^{-1} and a very broad peak (Figure 6.2.7.2.21c). The broadening of the peaks is due to the distribution of X-H distances within a X-H···Y hydrogen bond.

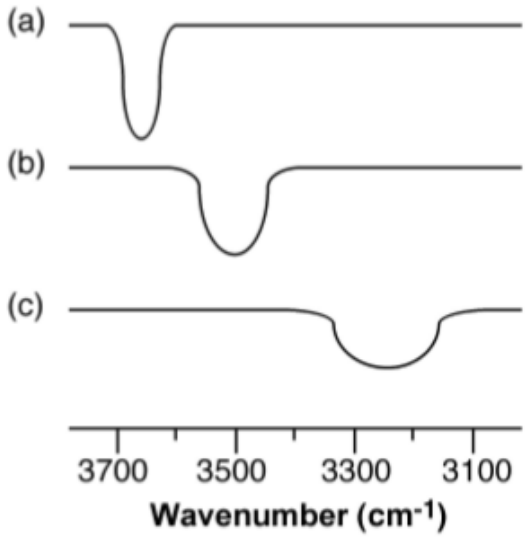


Figure 6.2.7.21: Schematic representation of the O-H stretch region in the IR spectra of a dilute solution of ^{n}BuOH in (a) CCl4, (b) Et_2O, and (c) NEt_3.

NMR

The presence of hydrogen bonding results the shift to higher ppm (lower frequency) of the ^{1}H NMR resonance for the proton.

This shift is due to the decrease in shielding of the proton. A dilute solution of ^{n}BuOH in CCl_4 shows a resonance typical of a non-hydrogen bonded compound (Figure 6.2.7.2.22a), while that for ^{n}BuOH in NMe_3 (Figure 6.2.7.2.22b) shows a significant low field shift. Very strong intra or intermolecular hydrogen bonded species show a very large ^{1}H NMR shift (e.g., Figure 6.2.7.2.22c).

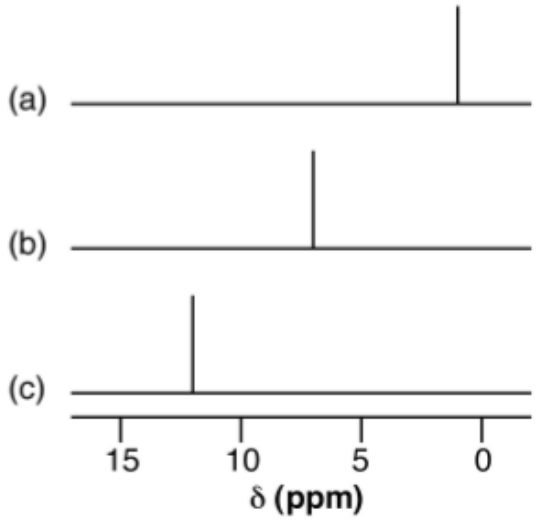


Figure 6.2.7.22: Schematic representation of the relative shift of the OH resonance for (a) ^{n}BuOH in CCl_4, (b) ^{n}BuOH in NEt_3, and (c) concentrated acetic acid.

Effects of hydrogen bonding

Physical effects

The presence of intermolecular hydrogen bonding provides additional attractive forces between molecules. Thus, properties that depend on intramolecular forces are affected.

Liquids with significant hydrogen bonding exhibit higher boiling points, higher viscosity, and higher heat of vaporization (ΔH_v) as compared to analogous compounds without extensive hydrogen bonding. For solids the presence of hydrogen bonding results in an increase in the melting point of the solid and an increase in the associated heat of fusion (ΔH_f).

The archetypal case for the effect of hydrogen bonding is the melting and boiling points of the hydrides of the Group 16 elements, i.e., H_2E. For a series of analogous compounds with the same molecular structure it would be expected that the boiling points would be related to the molecular mass. However, as can be seen from Table 6.2.7.2, the melting and boiling points of water are anomalously higher than those of its heavier analogs. In fact from Figure 6.2.7.2.23 it is clear that just considering H_2S, H_2Se, and H_2Te, the expected trend is observed, and it is similar to that for the Group 14 hydrides (CH_4, SiH_4, etc). Therefore, water must have additional intermolecular forces as compared to its heavier homologs. This observation is consistent with the strong hydrogen bonding in water, and the very weak if nonexistent hydrogen bonding in the sulfur, selenium, and tellurium analogs.

Table 6.2.7.2: Summary of physical properties for the hydrides of the Group 16 elements.

Compound	Molecular weight (g/mol)	Melting point (°C)	Boiling Point (°C)
H_2O	18.01	0	100
H_2S	24.08	-85.5	-60.7
H_2Se	80.98	-60.4	-41.5
H_2Te	129.62	-49	-2

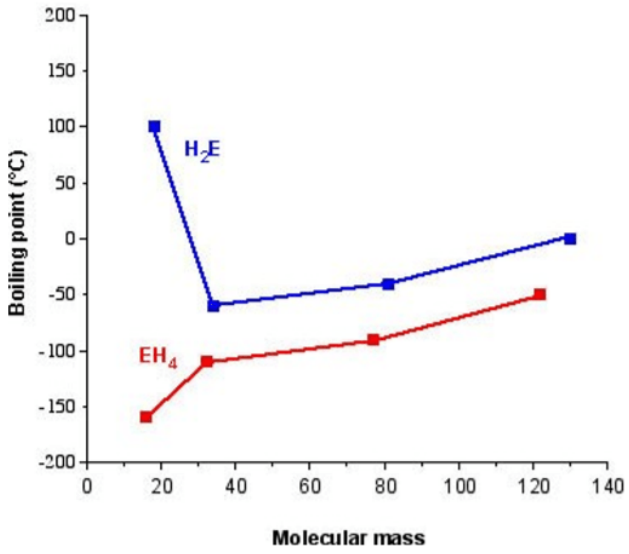


Figure 6.2.7.23: Plot of boiling point as a function of molecular weight for the hydrides of the Group 14 (EH_4) and 16 (H_2E) elements.

A similar but not as pronounced trend is observed for the Group 15 hydrides, where ammonia's higher values are associated with the presence of significant hydrogen bonding (Table 6.2.7.2.7).

Table 6.2.7.2: Summary of physical properties for the hydrides of the Group 15 elements.

Compound	Molecular weight (g/mol)	Melting point (°C)	Boiling Point (°C)
NH_3	17.03	-77.7	-33.35
PH_3	34.00	-133.5	-87.4
AsH_3	77.95	-113.5	-55
ShH_3	124.77	-88.5	-17

6.2.7.1Exe

Would you expect H_2S_2 to have a higher or lower boiling point that H_2O_2? Why?

Answer available at the end of this section.

The types of hydrogen bond can also have a signicant effect on the physical properties of a compound. For example, the cis isomer of hydroxybenzaldehyde melts at 1 °C, while the trans isomer has melting and boiling points of 112 °C. Both compounds exhibit strong hydrogen bonding in the solid state, however, as may be seen from Figure 6.2.7.2.24a, *cis*-hydroxybenzaldehyde (salicylaldehyde) has a configuration that allows strong intramolecular hydrogen bonding, which precludes any intermolecular hydrogen bonding. The melting point of *cis*-hydroxybenzaldehyde is going to be controlled by the van der Waal forces between adjacent molecules. In contrast, since intramolecular hydrogen bonding is precluded in the *trans* isomer (Figure 6.2.7.2.24b) it can form strong intermolecular hydrogen bonds in the solid state, and thus, it is these that define the melting point. The boiling points are controlled in a similar manner.

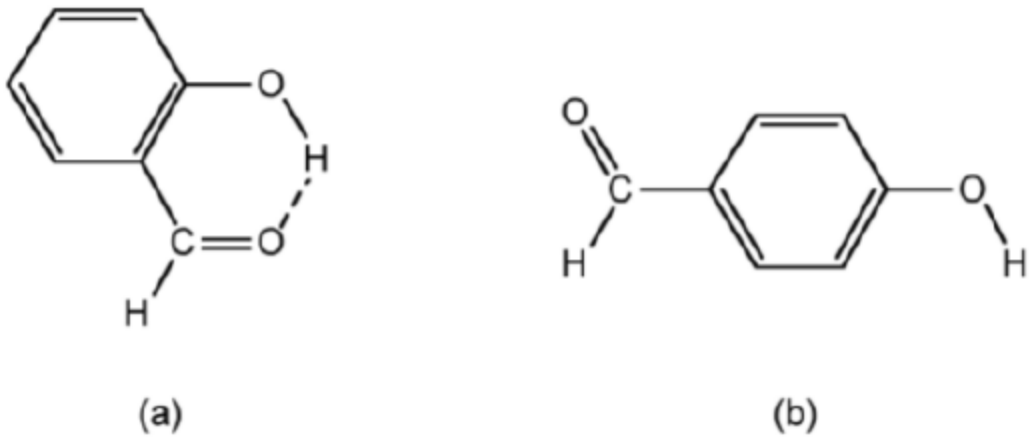


Figure 6.2.7.24: Structures of (a) salicylaldehyde and (b) trans-hydroxybenzaldehyde.

6.2.7.2Exe

4-Hydroxybenzoic acid melts at 213 °C, while 2-hydroxybenzoic acid melts at 158 °C. Explain this observation.

Answer available at the end of this section.

Melting and boiling are not the only physical properties that are aected by hydrogen bonding. Solubility can also be aected. Consider two isomers of $C_4H_{10}O$: ^{n}BuOH and Et_2O. The n-butanol is much more soluble in water than diethyl ether. The reason for this is that while both compounds can hydrogen bond to water, those between nBuOH and water are much stronger than those between Et_2O and water, and thus, dissolution of ^{n}BuOH in water does not disrupt the very strong hydrogen bonding in water as much as Et_2O does.

Acid strength

The acidity of a protic species can be affected by the presence of hydrogen bonding. For example, consider the di-carboxylic acid derivatives of ethylene (fumaric acid). Each of the carboxylic acid groups has sequential equilibria that may be defined by the pK values, (2.36). Table 6.2.7.2 lists the pK values for the *cis* and *trans* isomers. The acidity of the first and second carboxylic group for the *trans* isomer is similar, the difference being due to the increased charge on the molecule. In contrast, the second proton in the cis isomer is much less acidic than the first proton: why? A consideration of the structure of the mono anion of the cis isomer (Figure 6.2.7.2.25) shows that a very strong intramolecular hydrogen bond is formed once the first proton is removed. This hydrogen bond makes the second acidic proton much more difficult to remove and thus lowers the acidity of the proton.

$$HO_2C{-}HC{=}CH{-}CO_2H \overset{pK_1}{\rightleftharpoons} O_2{}^{-}C{-}HC{=}CH{-}CO_2H \overset{pK_2}{\rightleftharpoons} O_2{}^{-}C{-}HC{=}CH{-}CO_2{}^{-}$$

Table 6.2.7.2: Acidity equilibrium constants for cis and trans isomers of fumaric acid.

Isomer	pK_1	pK_2	Ratio
Trans	3	4.5	25:1
Cis	1.9	6.2	10,000:1

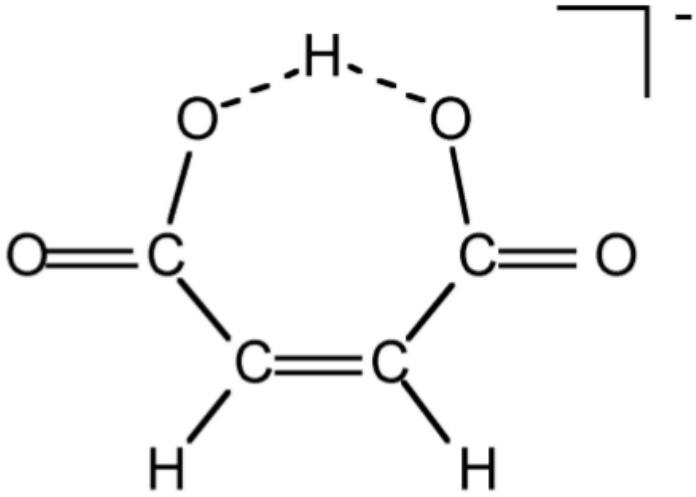


Figure 6.2.7.25: Structure of *cis*-[O_2C-HC=CH-CO_2H]$^-$.

Solid state structure

In the solid state, molecules that can form hydrogen bonds will tend to arrange themselves so as to maximize the formation of linear hydrogen bonds. The structure of ice is a typical example, where each water molecule's hydrogen bonds to four other molecules creating a diamond-like lattice (Figure 6.2.7.2.26). However, ice isn't the only compound whose solid state structure is defined by its hydrogen bonding. Cyanuric acid forms six strong intermolecular hydrogen bonds to three other molecules in the plane of the heterocyclic ring and thus creates a graphite-like structure (Figure 6.2.7.2.27).

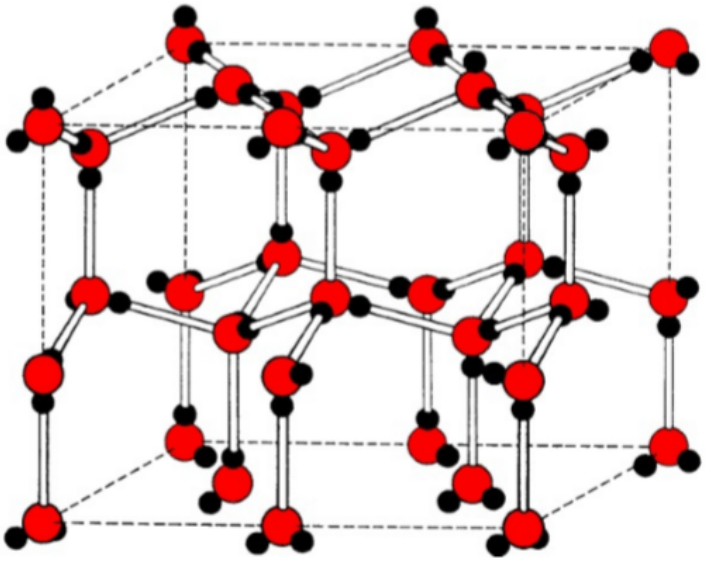


Figure 6.2.7.26: The diamond-like structure formed in ice by hydrogen bonding.

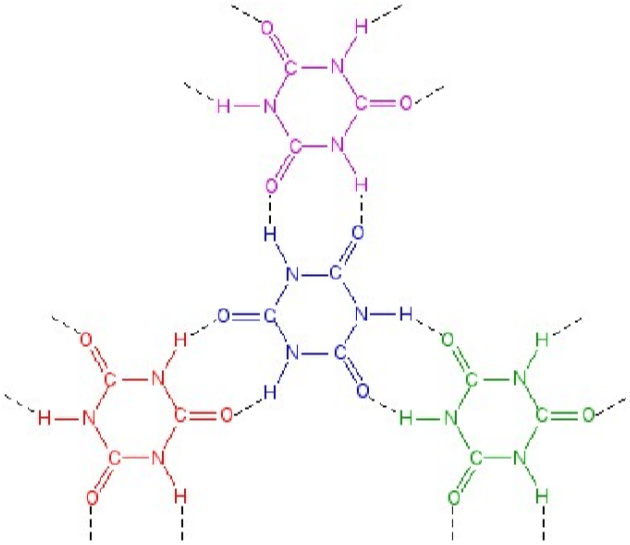


Figure 6.2.7.27: The hydrogen bonding of cyanuric acid.

Conformational stabilization

The presence of hydrogen bonding can stabilize certain conformations over others that in the absence of hydrogen bonding would be more favored. For example, based on steric considerations $H_2NCH_2CH_2C(O)H$ would be expected to adopt a staggered conformation as is typical for compounds with free rotation about a C-C bond. However, due to the presence of a strong intramolecular hydrogen bond it adopts a sterically disfavored eclipsed conformation (Figure 6.2.7.2.28).

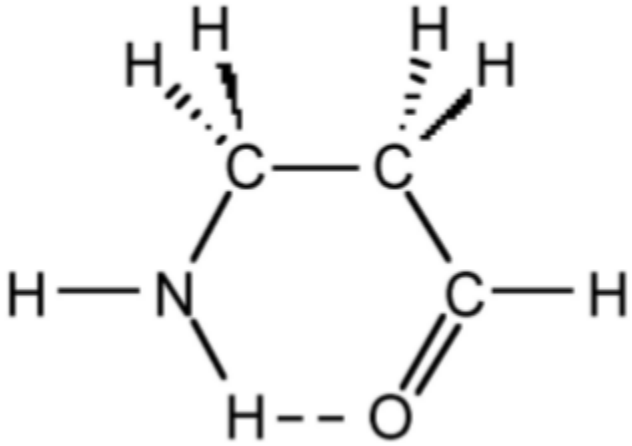


Figure 6.2.7.28: Stable conformation of $H_2NCH_2CH_2C(O)H$.

This conformational stabilization is even more important in biopolymers such as peptides. If we assume that a peptide chain (Figure 6.2.7.2.29) made from a sequence of amino acids would not adopt any eclipsed conformations on steric grounds, and that the amide group (H-N-C=O) is near planar due to delocalization, then there will be 3^2 possible conformations per nitrogen in the peptide chain, i.e., three each for the C-C and C-N bonds (Figure 6.2.7.2.29). Assuming a modest peptide has 50 amino acids, there will be 3^{2x50} potential conformations of the polymer chain, i.e., over 5×10^{47} conformations. However, in reality there are limits to the number of conformations observed since particular ones are stabilized by intramolecular hydrogen bonds. The most important of these are the α-helix (Figure 6.2.7.2.30) and β-sheet structures.

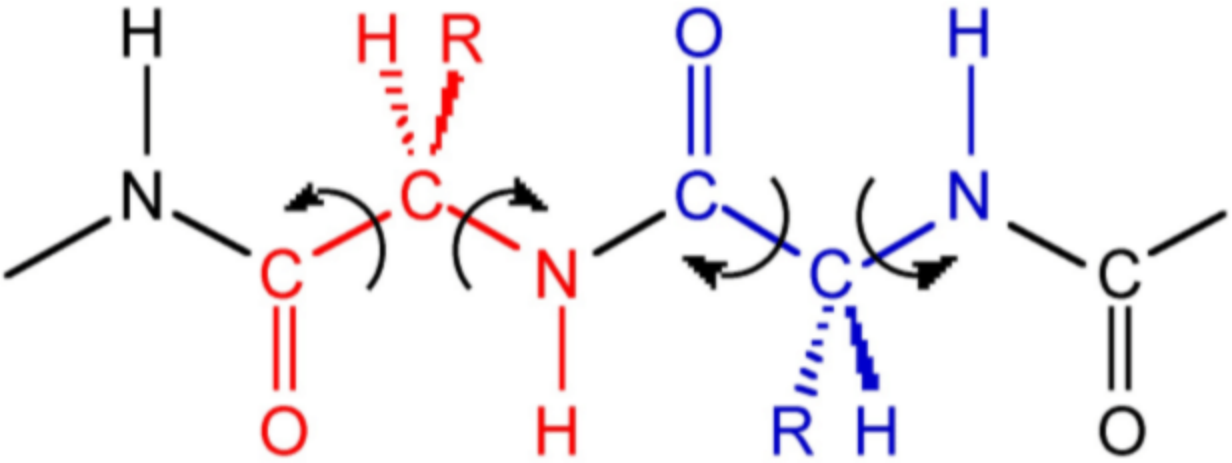


Figure 6.2.7.29: A section of a peptide polymer chain showing the possible rotational freedom of the C-C and C-N bonds.

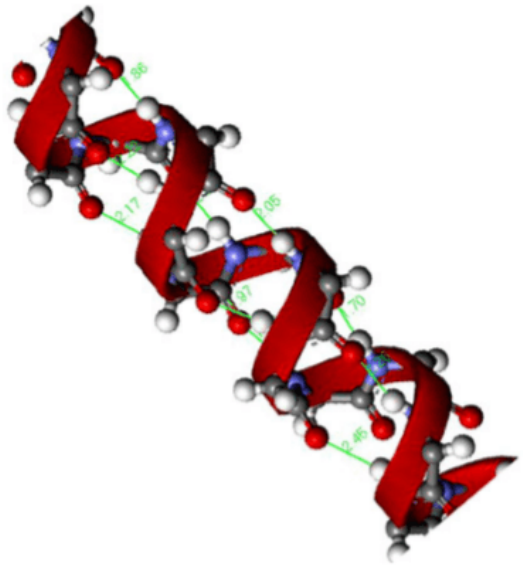


Figure 6.2.7.30: A representation of a peptide α-helix structure showing the stabilizing hydrogen bonds.

Bibliography

J. T. Leman, J. Braddock-Wilking, A. J. Coolong, and A. R. Barron*, Inorg. Chem.*, 1993, **32**, 4324.

K. Nakamoto, M. Margoshes, and R. E. Rundle, *J. Am. Chem. Soc.*, 1955, **77**, 6480.

M. B. Power, A. R. Barron, S. G. Bott, E. J. Bishop, K. D. Tierce and J. L. Atwood, *J. Chem. Soc., Dalton Trans.,* 1991, 241.

R. Taylor and O. Kennard, *Acc. Chem. Res.*, 1984, **17**, 320.

Answers

The boiling point for H_2O_2 is 150.2 °C, while that of 70.7 °C. The difference in boiling point is due to the stronger intermolecular hydrogen bonding in H_2O_2 than in H_2S_2.

2-Hydroxybenzoic acid exhibits strong intramolecular hydrogen bonding while 4-hydroxybenzoic acid has strong intermolecular hydrogen bonding.

This page titled 6.2.7: The Hydrogen Bond is shared under a CC BY 3.0 license and was authored, remixed, and/or curated by Andrew R. Barron (CNX) via source content that was edited to the style and standards of the LibreTexts platform.

6.2.8: Isotopes of Hydrogen

Physical effects

The presence of intermolecular hydrogen bonding provides additional attractive forces between molecules. Thus, properties that depend on intramolecular forces are affected.

Table 6.2.8.2.9: Summary of isotopes of hydrogen.

Isotope	Hydrogen-1	Hydrogen-2	Hydrogen-3
Special name	Hydrogen	Deuterium	Tritium
Symbol	H	D	T
Atomic number	1	1	1
Number of neutrons	0	1	2
Mass number	1	2	3
Natural abundance	99.9844%	0.0156%	very small

Synthesis of deuterium compounds

Electrolysis of water

The electrolysis of hydrogen-1 water (H_2O) in the presence of an alkali results in the formation of hydrogen and oxygen.

$$2H_2O_{(l)} \rightarrow 2H_{2(g)} + O_{2(g)} \tag{6.2.8.1}$$

In a similar manner the hydrolysis of deuterated water (D_2O) yields deuterium and oxygen.

$$2D_2O_{(l)} \rightarrow 2D_{2(g)} + O_{2(g)} \tag{6.2.8.2}$$

However, the rate of electrolysis of D_2O is slightly slower than that of H_2O. Thus, the partial hydrolysis of water with a mixture of natural isotopes results in the slight enrichment of the water with D_2O. The level of enrichment in one step is less than 1%. In order to obtain high levels of D_2O (e.g., ca. 30%) it is necessary to reduce the original volume of water by 1/100,000th.

Chemical equilibrium

Proton exchange reactions can be used to enrich compounds in deuterium. For example, the reaction of HSD with water shown in (2.8.3) has a slight preference for the formation of H_2S, i.e., K_{eq} = 1.012. Thus, bubbling HSD through water results in the enrichment of the water in HOD. However, about 30% enrichment is about the best that can be achieved by this method.

$$H_2O_{(l)} + HSD_{(g)} \leftrightharpoons HOD_{(l)} + H_2S_{(g)} \tag{6.2.8.3}$$

Fractional distillation

The boiling point of H_2O is (by definition) 100 $^{\circ}$C, in contrast the boiling point of D_2O is 101.4 $^{\circ}$C. Thus, it is possible to separate H_2O from D_2O by fractional distillation. This method provides the most suitable route to high isotopic enrichment and D_2O of 99.8% can be produced this way.

Note

The term *heavy water* is used for D_2O of greater than 99.8% enrichment.

Uses of deuterium compounds

Possible nuclear fusion

The largest use of D_2O is as a moderator and heat exchanger for fission nuclear reactors, however, the biggest potential application will be if nuclear fusion is realized as a commercial process.

The fusion of two deuterium atoms to form a helium atom and energy would be one source of energy, (2.8.4), however, deuterium-tritium fusion is the most promising, (2.8.5).

$$ {}^{2}_{1}H + {}^{2}_{1}H \rightarrow {}^{3}_{2}He + {}^{1}_{0}n + energy \tag{6.2.8.4} $$

$$ {}^{2}_{1}H + {}^{3}_{1}H \rightarrow {}^{4}_{2}He + {}^{1}_{0}n + energy \tag{6.2.8.5} $$

The deuterium part of the fuel does not pose a great problem because about 1 part in 5000 of the hydrogen in seawater is deuterium. This amounts to an estimate that there is over 10^{15} tons of deuterium in the oceans. The tritium part of the fuel is more problematic since there is no significant natural source (Table $6.2.8.2.9$), and the tritium would have to be obtained by breeding the tritium from lithium.

$$ {}^{6}_{3}Li + {}^{1}_{0}n \rightarrow {}^{4}_{2}He + {}^{3}_{1}H \tag{6.2.8.6} $$

Since a gallon of seawater could produce as much energy as 300 gallons of gasoline, there is clearly a large amount of energy that can potentially be realized through nuclear fusion. Unfortunately, this advantage is also a disadvantage since the temperatures attained are similar to the surface of the sun, which would vaporize any conventional container. Fusion experiments therefore use a magnetic field to contain the reaction. The shape of the eld is like a bottle, hence the term "magnetic bottle".

One demonstrated fusion process is the so-called hydrogen bomb or thermonuclear bomb in which a fission atom bomb is used to initiate a fusion reaction. The atomic bomb is surrounded by a layer of lithium deuteride. Neutrons from the atomic explosion (fission) cause the lithium to be converted into helium, tritium, and energy, (2.8.6). The atomic explosion also supplies the 50,000,000 $^{\circ}$C temperature needed for the subsequent fusion of deuterium with tritium, (2.8.5). So in-fact the hydrogen bomb is misnamed and it should be called a deuterium bomb.

Note

The original calculations to model the hydrogen bomb were performed using ENIAC (short for Electronic Numerical Integrator And Computer) that was originally designed to generate tables of trajectories of shells red from large artillery. The artillery ring tables were made by women mathematicians who were called calculators hence the name used today. Built in 1946 ENIAC is often assumed to be the first programmable electronic computer, however, it was predated by the six Colossus machines that were used to successfully crack the German Enigma code as early as 1944. However, the existence of the Colossus machines was kept secret until 1975.

Spectroscopy

In the chemical laboratory deuterium compounds are commonly used in spectroscopy for:

a) The assignment of resonances in IR, Raman, and NMR spectroscopy.

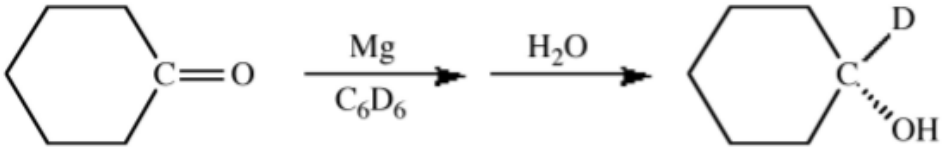
b) As a non-proton containing solvent in 1H NMR spectroscopy.

A description of these applications is given below.

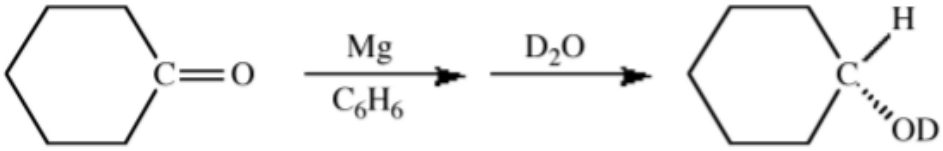
Reaction mechanism and rate determination

Given the larger mass of deuterium over hydrogen there is an associated dierence in the rate of reactions (see below) and therefore investigations using hydrogen and deuterium analogs can provide information as to reaction mechanisms.

The spectroscopic dierences between hydrogen and deuterium can also be used as a tracer to uniquely determine the source of particular substituents. For example, the magnesium (or Grignard) reduction of a ketone yields upon hydrolysis the secondary alcohol. If the reaction is carried out in a deuterated solvent and H_2O used for hydrolysis then the secondary carbon is deuterated, (2.43). In contrast, if the reaction is carried out in a non-deuterated solvent and hydrolysis is accomplished with D_2O then the deuterated alcohol is formed, (2.44). These experiments define that the initial reduction occurs at the ketone's α-carbon.



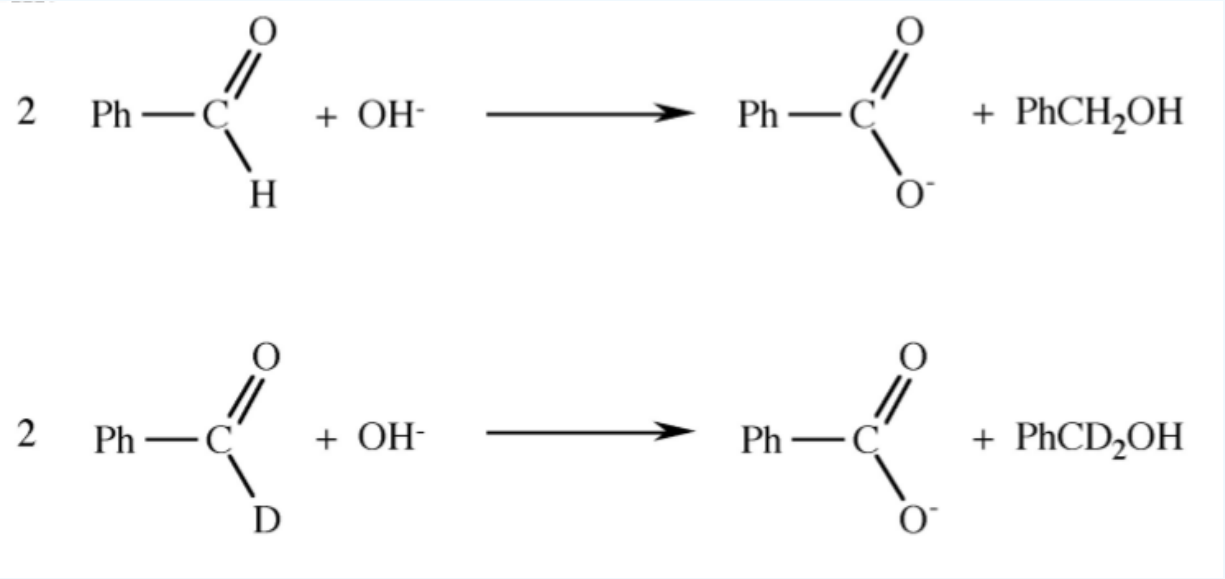
(2.43)



(2.44)

6.2.8.1Exe

Given the following reactions and the isotope distribution of the products suggest the reaction mechanism.



Answer available at the end of this section.

Differences between hydrogen and deuterium

Properties that depend on nuclei properties

The nuclear magnetic moment of an atomic nucleus arises from the spins of the protons and neutrons within the nucleus. As a consequence the magnetic moment for hydrogen and deuterium are very different and hence the conditions for detection by NMR are very different. Thus, in observing the ^{1}H NMR spectrum of a compound not only are the deuterium atoms not observed, but the coupling is now H-D rather than H-H (Figure 6.2.8.2.31).

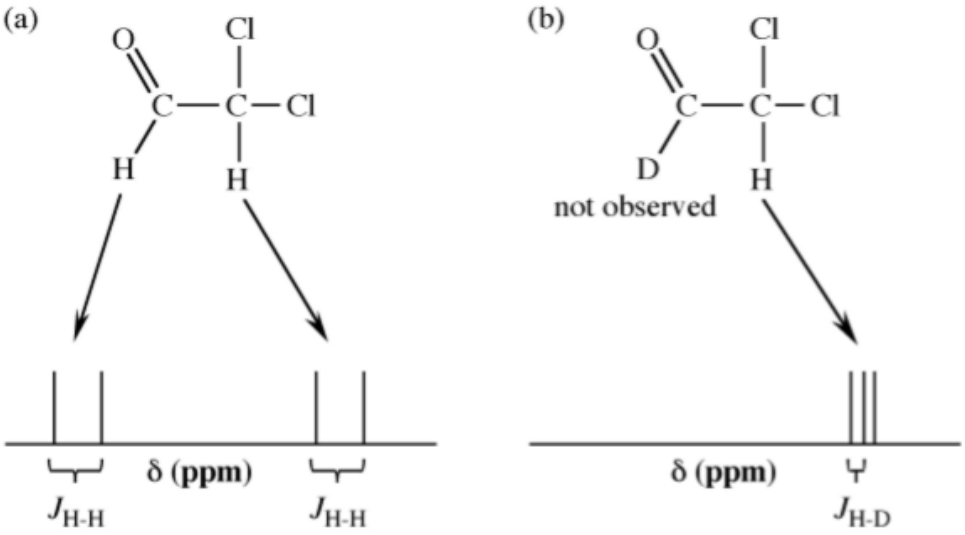


Figure 6.2.8.31: An example of the differences in the ^{1}H NMR spectrum upon deuterium substitution.

Deuterium is better at scattering neutrons than hydrogen. The H and D cross sections are very distinct and different in sign, which allows contrast variation in such experiments. Hydrogen's low electron density makes it difficult to determine its position by X-ray diffraction methods, neutron diffraction methods allow for highly accurate structure determination. Hydrogen can be seen by neutron diffraction and scattering, however, it has a large incoherent neutron cross-section. This is nil for deuterium and thus delivers much clearer signals may be obtained for deuterated samples. Neutron scattering of deuterated samples is indispensable for many studies of macromolecules in biology.

Properties that depend on mass

The difference in mass between hydrogen and deuterium obviously results in a difference in molecular mass of their analogous compounds. This difference can be used for analysis by mass spectrometry, but it also results in different densities of compounds. For example, the density of H_2O at 25 °C is 0.997 g/cm^3, while the density of D_2O at 25 °C is 1.104 g/cm^3.

The vibrational frequency for a diatomic molecule, H-X, can be defined by the equation:

$$v_{H-X} = \frac{1}{2\pi}\sqrt{\frac{f_{H-X}}{\mu_{H-X}}} \tag{6.2.8.7}$$

where $f_{H\text{-}X}$ is the H-X bond force constant, and $\mu_{H\text{-}X}$ is the reduced mass.

$$\mu_{H-X} = \frac{m_h \cdot m_X}{m_H + m_X} \tag{6.2.8.8}$$

If substitute H for D the D-X force constant is the same as the H-X force constant, but the reduced mass is twice the value for the H-X bond. As a result the ratio of the vibrational frequency of an H-X bond to that of the analogous D-X bond is given by the following equation.

$$\frac{\mu_{D-X}}{\mu_{H-X}} = (\frac{\mu_{H-X}}{\mu_{D-X}})^{\frac{1}{2}} = \frac{1}{\sqrt{2}} \tag{6.2.8.9}$$

With the change in vibrational energy there is concomitant change in the bond strength.

$$E_{D-X} > E_{H-X} \tag{6.2.8.10}$$

Thus, the rate of reactions will be faster for hydrogen derivative than the deuterium analog. The ratio of the rate constants will be dependant on the involvement of H-X bond breaking or forming in the rate limiting step (the slowest reaction step within the overall reaction mechanism). When an H-X bond is made or broken in the rate limiting step, then the ratio of the rate constants upon deuterium substitution will be:

$$\frac{k_{H-X}}{k_{D-X}} \approx 7 \tag{6.2.8.11}$$

This is known as the *primary isotope effect*. In this case where H-X bond breaking or forming is not part of the rate limiting step, then the isotope effect will be much smaller and is known as a *secondary isotope effect*.

The position of equilibrium reactions that involve hydrogen exchange, (2.8.12), will be effected by the presence of deuterium to favor the deuterium being concentrated in the more stable bond. This is the basis of the concentration of HOD from HSD and water, (2.8.3).

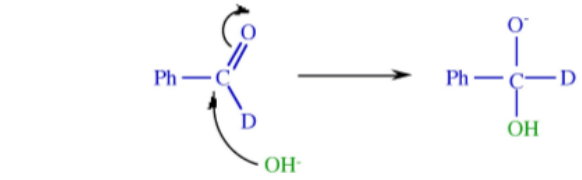
$$\text{X-H} + \text{Y-D} \leftrightharpoons \text{X-D} + \text{Y-H} \tag{6.2.8.12}$$

Bibliography

- M. B. Power, S. G. Bott, J. L. Atwood, and A. R. Barron. *J. Am. Chem. Soc.*, 1990, **112**, 3446.
- A. S. Borovik and A. R. Barron, *Main Group Chem.* 2005, **4**, 135.

Answers

Step 1.



Step 2.



Step 3.



This page titled 6.2.8: Isotopes of Hydrogen is shared under a CC BY 3.0 license and was authored, remixed, and/or curated by Andrew R. Barron (CNX) via source content that was edited to the style and standards of the LibreTexts platform.

6.2.9: Nuclear Fusion

The process of nuclear fission and radioactive decay are both associated with the conversion of an atom with a large nucleus to an atom (or atoms) with a smaller nucleus. In the process, mass is lost and energy is produced. However, what happens if two atoms with small nuclei are combined to give a single atom with a larger nucleus? In such a process the nuclei would be fused together, and this process is called nuclear fusion.

One of the simplest fusion processes involves the fusing of two hydrogen-2 (deuterium) atoms:

$$ {}^{2}_{1}H + {}^{2}_{1}H \rightarrow {}^{4}_{2}He \tag{6.2.9.1} $$

The mass of each deuterium atom is 2.0140 amu, while the mass of the resulting helium is 4.0026 amu. The mass defect of the reaction is 0.0254 amu or 0.63% of the original mass. While this percentage of the original mass may not seem much, it should be noted that the mass defect for the conversion of uranium-238 to lead-206 is only 0.026%, and that for splitting uranium-235 is 0.056%. Based upon these comparisons it is clear that fusion of hydrogen produces 24x the energy kg/kg than natural radioactivity and 11x that of nuclear fission.

In addition to being a plentiful source of energy, fusion is actually the most important process in the universe. Since the statement in 1847 of the Law of conservation of energy (the total amount of energy in an isolated system remains constant) scientists had wondered how the sun works. No source of energy was known in the 19th century that could explain the sun. Based upon the age of the earth it is known that the sun is 4,550,000,000 years old, and it was marveled at the continued source of energy over that span of time. By the 1920s nuclear energy was defined as being the most powerful source of energy, and British astrophysicist Arthur Eddington (Figure 6.2.9.2.32) suggested that the sun's energy arises from the fusion of hydrogen into helium.



Figure 6.2.9.32: (left) Arthur Stanley Eddington (1882 1944). (middle) Henry Norris Russell (1877 - 1957). (right) Hans Albrecht Bethe (1906 - 2005).

In 1929 American Henry Norris Russell (Figure 6.2.9.33) studied the spectrum of the sun. Based upon his studies he calculated the composition of the sun to be 90% hydrogen, 9% helium, and 1% of all other elements up to iron (but nothing of higher atomic number). Given the composition it became clear that the only reaction possible to account for the sun's energy was the fusion of hydrogen. In 1938 Hans Bethe (Figure 6.2.9.2.34) demonstrated a model for how the sun worked. The energy source is the fusion of hydrogen to give helium (Figure 6.2.9.2.35), while in massive starts the presence of heavier elements such as carbon, oxygen, nitrogen, neon, silicon, and iron are the result of the fusion of helium.

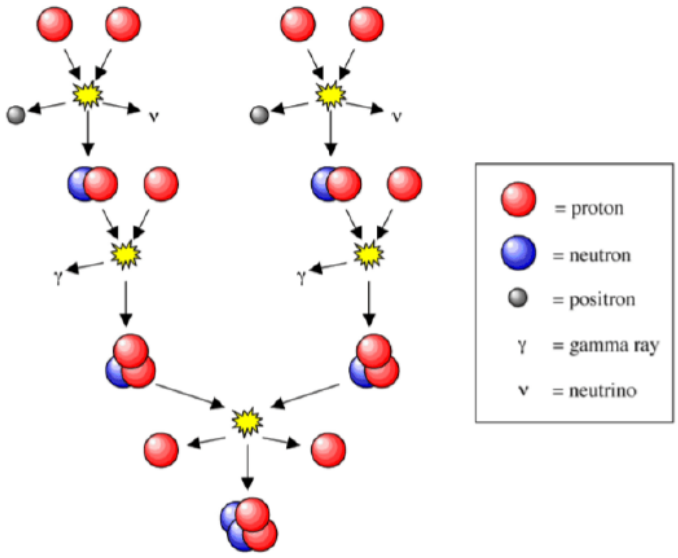


Figure 6.2.9.35: The proton-proton chain dominates in stars the size of the Sun or smaller.

Why is it that uranium, thorium and other radioactive elements undergo radioactive decay, but hydrogen does not undergo spontaneous fusion? The reason for this difference is that any change that uranium undergoes occurs inside a nucleus that is already formed, while fusion requires that two nuclei must come together. This process results in extremely large repulsive forces. So why does it happen in a star? The temperatures inside a star approach 15,000,000 $^{\circ}$C, while the high pressure results in a density of approximately 160 g/cm^3 which for comparison is 8x that of gold. Under these conditions the nuclei are free to move in a sea of electrons. Nuclear fusion takes place in the core of the sun where the density is at the highest but an explosion does not result due to the extreme gravity of the sun: 333,000x that of Earth.

Research into controlled fusion, with the aim of producing fusion power for the production of electricity, has been conducted for over 50 years. It has been accompanied by extreme scientific and technological difficulties, but has resulted in progress. At present, break-even (self-sustaining) controlled fusion reactions have not been demonstrated, however, work continues since the fuel for such a fusion reaction is hydrogen (in its compounds including water) is the 3rd most abundant element on the Earth.

This page titled 6.2.9: Nuclear Fusion is shared under a CC BY 3.0 license and was authored, remixed, and/or curated by Andrew R. Barron (CNX) via source content that was edited to the style and standards of the LibreTexts platform.

6.2.10: Storage of Hydrogen for Use as a Fuel

Note

This module is based upon the Connexions course *Methods of Hydrogen Storage for Use as a Fuel Case Study* by Christian Cioce.

Introduction

Dihydrogen is a colorless and odorless gas at room temperature which is highly ammable, releasing a large amount of energy when combusted. As compared with combustion of the current fuels which operate automobiles, for example petrol or diesel, the energy released when hydrogen is combusted is more than three times greater. The heat of combustion for hydrogen is 141.9 kJ/mol as compared to 47.0 kJ/mol and 45.0 kJ/mol for gasoline and diesel, respectively.

Furthermore, the combustion of hydrocarbons releases the greenhouse gas carbon dioxide (CO_2) into the atmosphere, and is therefore not a "clean" fuel. When hydrogen is combusted in the presence of oxygen (from air) the only product is water, (2.52). Both its clean reactivity and the large chemical energy make H_2 extremely appealing for use as a fuel in automobiles.

$$2H_{2(g)} + O_{2(g)} \rightarrow 2H_2O_{(g)} \tag{6.2.10.1}$$

If hydrogen has such a potential as a fuel why has it not been widely implemented? Dihydrogen is a gas at room temperature. Gases, compared to the other states of matter (liquid and solid), occupy the most volume of space, for a given number of molecules. Octane and the other hydrocarbons found in gasoline are liquids at room temperature, demanding relatively small fuel tanks. Liquids are therefore easier to store than compressed gases.

Hydrogen has a high energy content per weight (more than three times as much as gasoline), but the energy density per volume is rather low at standard temperature and pressure. Volumetric energy density can be increased by storing the gaseous hydrogen under increased pressure or storing it at extremely low temperatures as a liquid. Hydrogen can also be adsorbed into metal hydrides and highly porous materials (Table 6.2.10.2.10). The current available methods of storing hydrogen include compressed hydrogen and liqueed hydrogen, however many promising methods exist, namely metal organic materials (MOMs), metal hydrides and carbon nanostructures.

Table 6.2.10.2.10: Comparison of hydrogen storage ability of metal hydrides.

Material	**H-atoms per cm^3 (x 10^{22})**	**% of weight that is H_2**
H2 gas, 200 bar (2850 psi)	0.99	100
H2 liquid, 20 K (-253 °C)	4.2	100
H2 solid, 4.2 K (-269 °C)	5.3	100
MgH_2	6.5	7.6
Mg_2NiH_4	5.9	3.6
$FeTiH_2$	6.0	1.89
$LaNi_5H_6$	5.5	1.37

Liquid hydrogen

Liquid hydrogen is made possible by cryogenically cooling it to below its boiling point, -253 °C. As a liquid, the same amount of gaseous hydrogen will require much less volume, and therefore is feasible to individual automobile use. A refrigeration system

is required to keep the liquid cooled, for if the system temperature rises above hydrogen's critical point (-241 $^{\circ}$C), the liquid will become a gas. There must exist a vacuum insulation between the inner and outer walls of liquid hydrogen tank system, for heat cannot travel through a vacuum. There is a tradeo, however, because the tank must be an open system to prevent overpressure. This will lead directly to heat loss, though minimal.

The relative tank size has a broad range, with small tanks having a volume of 100 L, and large spherical tanks sizing all the way up to 2000m^3. Refrigerationsystemsarenotalikelyfeatureforeveryautomobile, and open systems may pose a hazard should an accident occur. Cooling hydrogen down to a liquid is a convenient method of storage, however, and its implementation most likely will be limited to large stationary tanks as well as mobile multi-axle trucks.

Compressed hydrogen

Compressing gas is the process of applying an external force which minimizes the distance between gas particles, therefore forcing the system to occupy less volume. This is attractive since many particles can exist in a reasonably sized tank. At room temperature and atmospheric pressure, 4 kg of hydrogen occupies a volume of 45 m^3, which corresponds to a balloon with a diameter of 5 m. Clearly compression is required to store and transport the gas. When it comes to individual mobility however, these tanks are still far too large for the average sized automobile.

Compressed tanks are regularly lled to 200 atmospheres in most countries. Storing 4 kg of hydrogen still requires an internal volume of 225 L (about 60 gallons). This amount can be divided into 5 tanks with 45 L internal volume.

Metal hydrides for storage

Metal hydrides are coordinated complexes and/or crystal systems which reversibly bind hydrogen. The hydrogen is favorably incorporated into the complex and may be released by applying heat to the system. A major method to determine a particular complex's eectiveness is to measure the amount of hydrogen that can be released from the complex, rather than the amount it can store (Table 6.2.10.2.10).

Some issues with metal hydrides are low hydrogen capacity, slow uptake and release kinetics, as well as cost. The rate at which the complex accepts the hydrogen is a factor, since the time to fuel a car should ideally be minimal. Even more importantly, at the current stage of research, the rate at which hydrogen is released from the complex is too slow for automobile requirements. This technology is still a very promising method, and further research allows for the possibility of highly binding and rapid reversal rates of hydrogen gas.

This page titled 6.2.10: Storage of Hydrogen for Use as a Fuel is shared under a CC BY 3.0 license and was authored, remixed, and/or curated by Andrew R. Barron (CNX) via source content that was edited to the style and standards of the LibreTexts platform.

6.3: Group 1 - The Alkali Metals

This page titled 6.3: Group 1 - The Alkali Metals is shared under a CC BY 3.0 license and was authored, remixed, and/or curated by Andrew R. Barron (CNX) via source content that was edited to the style and standards of the LibreTexts platform.

6.3.1: The Alkali Metal Elements

The Group 1 metals have a particular name: the alkali metals. This is due to the formation of alkali (basic) solutions upon their reaction with water. Table 6.3.1.3.1 lists the derivation of the names of the alkali metals.

Table 6.3.1.3.1: Derivation of the names of each of the alkali metal elements.

Element	Symbol	Name
Lithium	Li	Greek *lithos* meaning *stone*
Sodium	Na	Latin *natrium* or Arabic *natrun* meaning *soda*
Potassium	K	From the Latin *kalium*, and from Arabic *al-qali* meaning *plant ashes*
Rubidium	Rb	Latin *rubidus* meaning *deepest red*
Caesium	Cs	Latin *caesius* meaning *blueish grey*
Francium	Fr	Named after France

Note

Caesium is the international spelling standardized by the IUPAC, but in the United States it is more commonly spelled as cesium.

Discovery

Lithium

Petalite ($Li_2O.Al_2O_3.8SiO_2$) was first discovered in 1800 by José Bonifácio de Andrade e Silva (Figure 6.3.1.3.1), who discovered the mineral in a Swedish mine on the island of Utö. However, it was not until 1817 that Johan August Arfwedson (Figure 6.3.1.3.2) working in the laboratory of Jöns Jakob Berzelius (Figure 6.3.1.3.3), discovered the presence of a new element while analyzing petalite ore. Named from the Greek *lithos* meaning *stone* reflected its discovery in a mineral, as opposed to sodium and potassium, which had been discovered in plant tissue; its name was later standardized as lithium. The element was not isolated until 1821, when William Brande (Figure 6.3.1.3.4) isolated the element by performing electrolysis on lithium oxide, a process previously employed by Sir Humphry Davy to isolate potassium and sodium.



Figure 6.3.1.1: Portuguese statesman and naturalist José Bonifácio de Andrada e Silva (1763 - 1838).



Figure 6.3.1.2: Swedish chemist Johan August Arfwedson (1792 - 1841).



Figure 6.3.1.3: Swedish chemist Friherre J¨ ons Jacob Berzelius (1779 - 1848).

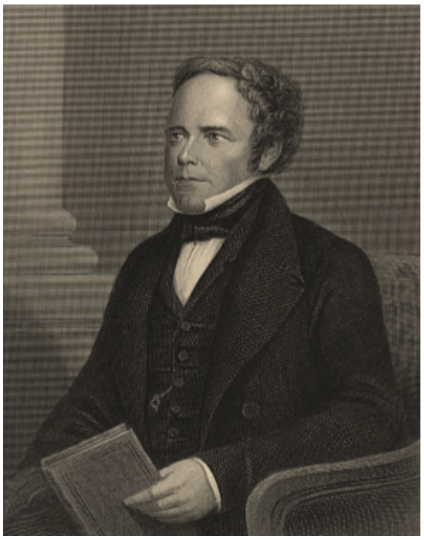


Figure 6.3.1.4: English chemist William Thomas Brande FRS (1788 - 1866).

Sodium

3.1.1.2 Sodium Elemental sodium was first isolated by Sir Humphry Davy (Figure 6.3.1.3.5) in 1806 by passing an electric current through molten sodium hydroxide.



Figure 6.3.1.5: British chemist and inventor Sir Humphry Davy FRS (1778 - 1829).

Potassium

The name *kalium* was taken from the word alkali, which came from Arabic *al qali* meaning the *calcined ashes*. The name potassium was made from the English word *potash*, meaning an alkali extracted in a pot from the ash of burnt wood or tree leaves. Potassium metal was discovered in 1807 by Sir Humphry Davy (Figure 6.3.1.3.5), who derived it from caustic potash (KOH), by the use of electrolysis of the molten salt.

Rubidium

Rubidium was discovered using spectroscopy in 1861 by Robert Bunsen (Figure 6.3.1.3.6) and Gustav Kirchho (Figure 6.3.1.3.7) in the mineral lepidolite. The first rubidium metal was produced by Bunsen from the reaction of rubidium chloride (RbCl) with potassium.



Figure 6.3.1.6: German chemist Robert Wilhelm Eberhard Bunsen (1811 - 1899).

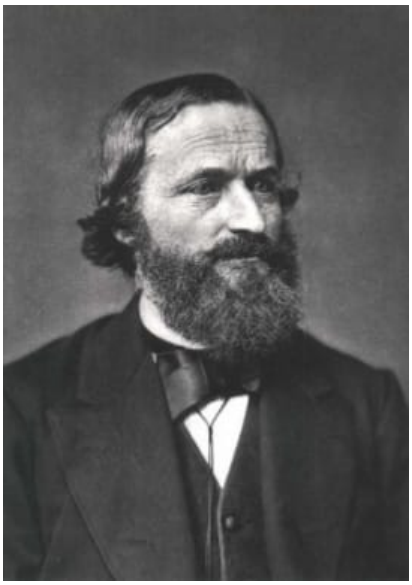


Figure 6.3.1.7: German physicist Gustav Robert Kirchho (1824 - 1887).

Caesium

Like Rubidium, caesium was discovered spectroscopically by Bünsen (Figure 6.3.1.3.6) and Kirchho (Figure 6.3.1.3.7) in 1860 in mineral water from Drkheim, Germany. The residues of 44,000 liters of mineral water yielded several grams of a caesium salt. Its identification was based upon the bright blue lines in its spectrum and it was the first element discovered by spectral analysis. The first caesium metal was subsequently produced in 1882 by electrolysis of caesium chloride.

Francium

Originally known as eka-caesium, francium was discovered in 1939 by Marguerite Perey (Figure 6.3.1.3.8) of the Curie Institute in Paris, France when she purified a sample of actinium-227, which had been reported to have a decay energy of 220 keV. However, Perey noticed decay particles with an energy level below 80 keV. Perey thought this decay activity was caused by a previously unidentified element, which exhibited chemical properties of an alkali metal. This led Perey to believe that it was element 87, caused by the alpha decay of actinium-227. Perey named the new isotope actinium-K (now referred to as francium-223) and in 1946, she proposed the name catium for her newly discovered element, however, she subsequently suggested francium, after France.



Figure 6.3.1.8: French physicist Marguerite Catherine Perey (1909 - 1975), a student of Marie Curie, and the first woman to be elected to the French Académie des Sciences.

Abundance

The abundance of the alkali metals is given in Table 6.3.1.3.2. Sodium's high abundance is due mainly to large underground deposits of rock salt (NaCl). However, sodium is also more abundant in seawater (10,800 ppm) as compared to potassium (380 ppm).

Table 6.3.1.3.2: Abundance of alkali metal elements.

Element	Terrestrial abundance (ppm)
Li	20 (Earth's crust), 40 (soil), 0.17 (sea water)
Na	23,000 (Earth's crust), 10,500 (sea water)
K	21,000 (Earth's crust), 14 (soil), 380 (sea water)
Rb	90 (Earth's crust), 30 - 250 (soil), 0.1 (sea water)
Cs	3 (Earth's crust), 0.0001 (soil), 0.0003 (sea water)
Fr	Essentially nil

Isotopes

The naturally abundant isotopes of the alkali metals are listed in Table 6.3.1.3.3. All of the isotopes of francium are radioactive. Lithium-7 and sodium-23 are both useful NMR nucleus having I = $^{1}/_{2}$.

Table 6.3.1.3.3: Abundance of the major isotopes of the alkali metals.

Isotope	Natural abundance (%)
Lithium-6	7.5
Lithium-7	92.5
Sodium-23	100
Potassium-39	93
Potassium-40	0.0118

Isotope	Natural abundance (%)
Potassium-41	6.9
Caesium-133	100

Potassium has three isotopes (Table 6.3.1.3.3), of which potassium-40 is radioactive and provides the basis for the determination of the age of rocks between 10^5 and 10^9 years old, i.e., those formed in proterozoic and cenozoic periods of geological time. The decay of potassium-40 occurs with a half life of 1.31 x 10^9 years, by two routes. That associated with a beta particle decay accounts for 89% of the decay:

$$\$40_{19}K \rightarrow^{97}_{20} Ca +^{0}_{-1} e \tag{6.3.1.1}$$

While that associated with an electron capture and by positron emission decay accounts for 11% of the decay to give argon-40. Since many rocks contain potassium containing minerals the decay of potassium-40 after solidification of the rock will result in the formation of argon trapped in the rock. The argon-40 content is determined by mass spectrometry, while the potassium content is determined by flame spectrophotometry. The ratio of the two, (3.2), will allow for the determination of the elapsed time since the rock solidified.

$$\frac{[^{40}_{18}Ar]}{[^{40}_{19}K]} \tag{6.3.1.2}$$

Caesium has at least 39 known isotopes (more than any other element except francium) ranging from caesium-112 caesium-151; however, caesium-133 is the only naturally occurring stable isotope. The other isotopes have half-lives from a few days to fractions of a second. The radiogenic isotope caesium-137 is produced from the detonation of nuclear weapons and is produced in nuclear power plants, and was released to the atmosphere most notably from the 1986 Chernobyl accident.

Physical properties

Many of the physical properties of the alkali metals (Table 6.3.1.3.4) are typical of metals, e.g., thermal and electrical conductivity. However, due to the relatively weak inter-atomic forces (weak M-M bonding) they are soft and readily cut with a knife.

Table 6.3.1.3.4: Selected physical properties of the alkali metal elements.

Element	Melting point (°C)	Boiling point (°C)	Density (g/cm^3)	Electrical resistivity (Ω·cm)
Li	453	1615	0.534	12.17 @ 86 °C
Na	370	1156	0.968	5.23 @ 29 °C
K	336	1032	0.89	7.01 @ 22.8 °C
Rb	312	961	1.532	12.52 @ 53 °C
Cs	201	944	1.93	37.38 @ 28.1 °C

Reactivity

All the alkali metals are highly reactive and are as a consequence of the stability of the M^+ ion are strong reducing agents (Table 6.3.1.3.5). The metals react readily with hydrogen and oxygen.

$$\mathrm{M} + \tfrac{1}{2}\,\mathrm{H_2} \rightarrow \mathrm{M^+H^-} \tag{6.3.1.3}$$

$$\mathrm{M} + \mathrm{O_2} \longrightarrow \mathrm{M^+(O_2)^-} \tag{6.3.1.4}$$

Table 6.3.1.3.5: Electrochemical reduction potential for alkali metals.

Reduction	Reduction potential (V)
$Li^+ + e^- \rightarrow Li$	-3.045
$Na^+ + e^- \rightarrow Na$	-2.7109
$K^+ + e^- \rightarrow K$	-2.924
$Rb^+ + e^- \rightarrow Rb$	-2.925
$Cs^+ + e^- \rightarrow Cs$	-2.923

All of the alkali metals react with water to liberate hydrogen.

$$\mathrm{M} + \mathrm{H_2O} \longrightarrow \mathrm{M(OH)} + \tfrac{1}{2}\,\mathrm{H_2} \tag{6.3.1.5}$$

WARNING

The reactions of alkali metals with water are exothermic and the heat generated is sucient to ignite the hydrogen. In addition the solutions formed are highly alkaline. Caution should be taken when handling alkali metals and storage should always be under mineral oil.

A similar, but less violent, reaction is also observed with ammonia when catalyzed by transition metal ions.

$$\mathrm{M} + \mathrm{NH_3} \longrightarrow \mathrm{M(NH_2)} + \tfrac{1}{2}\,\mathrm{H_2} \tag{6.3.1.6}$$

In the absence of a catalyst, the Group 1 metals dissolve in liquid ammonia to form solutions with characteristic properties.

- Highly reducing.
- Blue color.
- ESR signal due to solvated electrons.

As an example, the dissolution of sodium in liquid ammonia results in the formation of solvated Na+ cations and electrons.

$$Na_{(s)} \rightarrow Na_{(solv)} \leftrightharpoons Na^+_{(solv)} + e^-_{(solv)} \tag{6.3.1.7}$$

The solvated electrons are stable in liquid ammonia and form a complex: $[e^-(NH_3)_6]$. It is this solvated electron that gives the strong reducing properties of the solution as well as the characteristic signal in the ESR spectrum associated with a single unpaired electron. The blue color of the solution is often ascribed to these solvated electrons; however, their absorption is in the far infra-red region of the spectrum. A second species, Na-(solv), is actually responsible for the blue color of the solution.

$$2Na_{(solv)} \leftrightharpoons Na^+_{(solv)} + Na^-_{(solv)} \tag{6.3.1.8}$$

The formation of the sodium anion is confirmed by complexation of the cation with a cryptan ligand (C) such as a crown ether.

$$Na^+_{(solv)} + Na^-_{(solv)} + ''C'' \rightarrow [Na(C)]^+ + Na^- \tag{6.3.1.9}$$

The resulting complex is found to be isostructural to the iodide analog in the solid state.

$$Na^+_{(solv)} + I^-_{(solv)} + ''C'' \rightarrow [Na(C)]^+ + I^- \tag{6.3.1.10}$$

Vapor phase

All the alkali metals form M_2 dimers in the vapor phase in an analogous manner to hydrogen. As with dihydrogen the bonding is associated with the molecular orbital combination of the two valence s-orbitals (Figure 6.3.1.3.9).

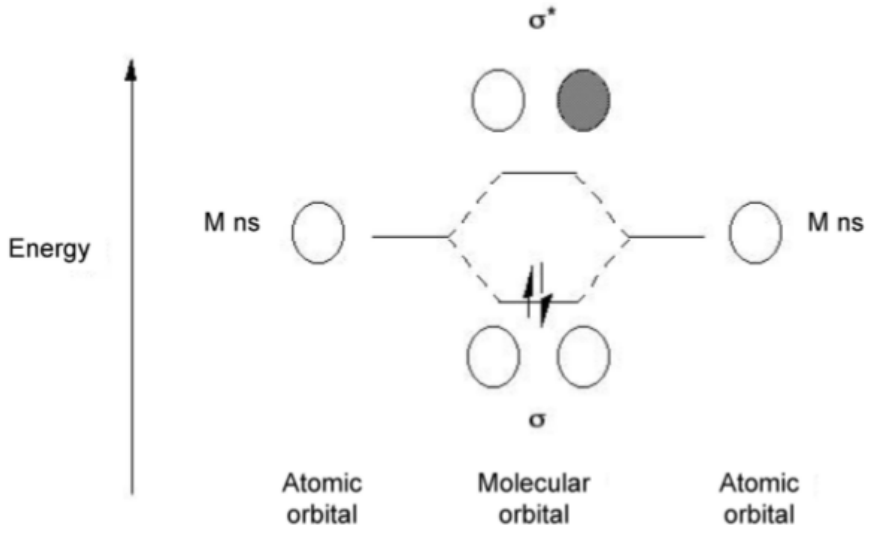


Figure 6.3.1.9: Molecular orbital diagram for the formation of M_2.

Sodium vapor is commonly used for lighting in a gas discharge lamp, which uses sodium in an excited state to produce light (Figure 6.3.1.3.10). There are two varieties of such lamps: low pressure and high pressure.



Figure 6.3.1.10: A low pressure sodium streetlamp.

This page titled 6.3.1: The Alkali Metal Elements is shared under a CC BY 3.0 license and was authored, remixed, and/or curated by Andrew R. Barron (CNX) via source content that was edited to the style and standards of the LibreTexts platform.

6.3.2: Compounds of the Alkali Metals

The chemistry of the alkali metals is dominated by the stability of the +1 oxidation state and the noble gas configuration of the M^+ cation. The alkali metals all have low first ionization energies (Table 6.3.2.3.6) but very high second ionization energies.

Table 6.3.2.3.6: First ionization potentials for the alkali metals.

Element	1st ionization energy (kJ/mol)
Li	526
Na	502
K	425
Rb	409
Cs	382

As a consequence of the stability of M^+, the Group 1 metals have the least variation in chemistry of the any Group in the periodic table. The only exceptions are the subtle trends that exist for lithium due to its small size (Table 6.3.2.3.7). All of the metals are more electropositive than hydrogen (Table 6.3.2.3.8).

Table 6.3.2.3.7: Radii of alkali metals. N.B. Some values are unknown.

Element	Atomic radius (Å)	Ionic radius (Å)	Covalent radius (Å)	Van der Waals radius (Å)
Li	1.52	0.68	1.52	1.82
Na	1.86	0.97	1.53	2.27
K	2.31	1.33	1.90	2.75
Rb	2.44	1.47	2.47	-
Cs	2.62	1.67	2.65	-
Fr	-	1.80	2.70	-

Table 6.3.2.3.8: Pauling electronegativities of Group 1 elements.

Element	Electronegativity
H	2.20
Li	0.98
Na	0.93
K	0.82
Rb	0.82
Cs	0.79
Fr	0.70

Solid State

In the solid state, the compounds of the alkali metals generally form ionic lattices, e.g., Na^+Cl^-. These structures are essentially electrostatic in nature and the lattice energy is usually defined as the enthalpy of formation of the ionic compound from gaseous ions and as such is invariably exothermic.

$$M^{+}_{(vap)} + X^{-}_{(vap)} \rightarrow MX_{(s)} \tag{6.3.2.1}$$

In all cases the lattice energies is high and is found to be proportional to the ratio of the charges on the ions and the sum of the ionic radii (r).

$$U \propto \frac{z^{+}z^{-}}{\sum(r)} \tag{6.3.2.2}$$

The ionic radii for alkali metal cations are given in Table 6.3.2.3.7; those for common anions are given in Table 6.3.2.3.9.

Table 6.3.2.3.9: Ionic radii of common anions.

Anion	Ionic radius (Å)
F^-	1.33
Cl^-	1.81
Br^-	1.96
I^-	2.20
H^-	1.54
O^{2-}	1.32

The ratio of the ionic radii (r^+/r^-) neatly defines the structural type observed for alkali metal salts (Table 6.3.2.3.10). The unit cells for ZnS (zinc blende), NaCl (rock salt), and CsCl are shown in Figure 6.3.2.3.11, Figure 6.3.2.3.12, and Figure 6.3.2.3.13, respectively.

Table 6.3.2.3.10: Defining MX structural types for alkali metal salts.

r^+/r^-	Structural type	Metal coordination number
0.225 - 0.414	ZnS (zinc blende)	4
0.414 - 0.732	NaCl (rock salt)	6
0.732 -	CsCl	8

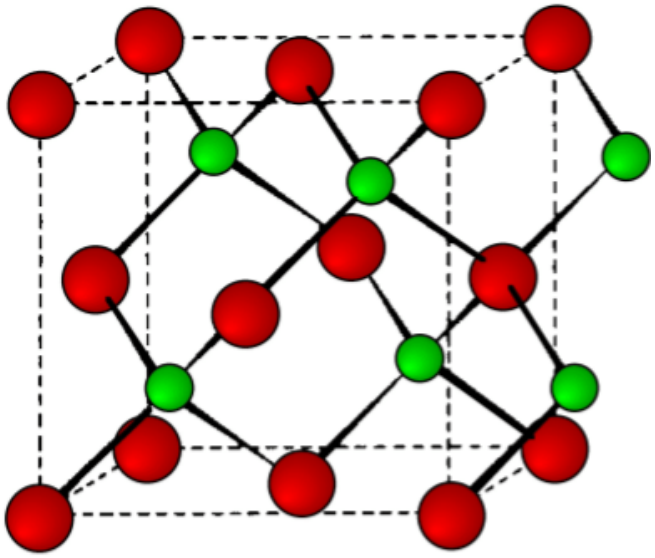


Figure 6.3.2.11: Unit cell structure of a zinc blende (ZnS) lattice.

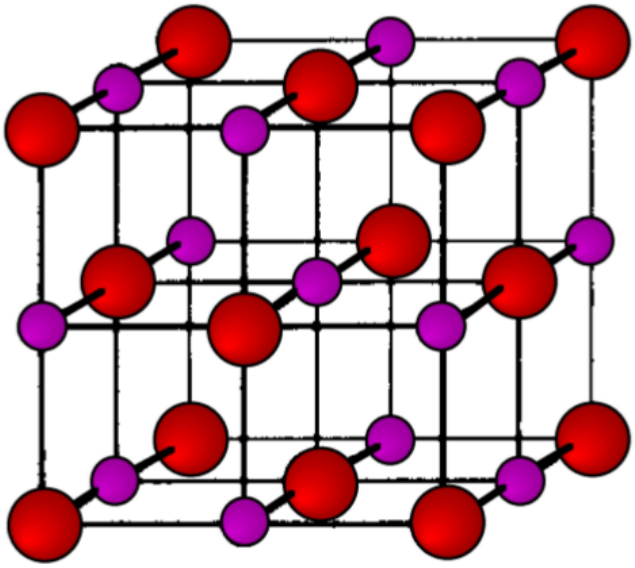


Figure 6.3.2.12: Unit cell structure of a rock salt lattice.

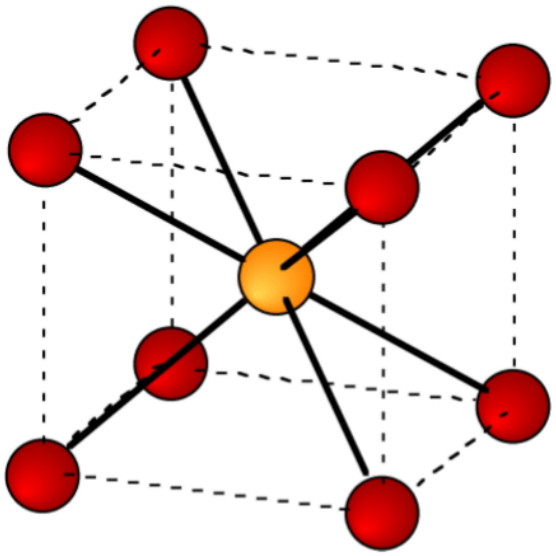


Figure 6.3.2.13: Unit cell of CsCl.

As an example, the structure of KBr can be predicted from the data in Table 6.3.2.3.7 and Table 6.3.2.3.9. The ionic radius of K^+ is 1.33 Å, while that for Br^- is 1.96 Å. The ratio of the ionic radii (r^+/r^-) is 0.67. Hence, KBr has a NaCl (rock salt) structure.

6.3.2.1 Exercise : Sodium Hydride

What is the structure of NaH?

Answer available at the end of this section.

6.3.2.2 Exercise : Rubidium Fluoride

What is the structure of RbF?

Answer available at the end of this section.

Complexes

The coordination complexes of the alkali metal cations (M^+) involve electrostatic, or ion-dipole, interactions (Figure 6.3.2.3.14) that have no preferred direction of interaction. Thus, the ionic radius of the cation (Table 6.3.2.3.7) controls the coordination numbers of the metal in its complexes (Table 6.3.2.3.11).

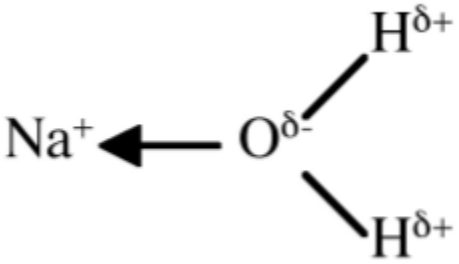


Figure 6.3.2.14: A schematic representation of the ion-dipole or electrostatic interaction of Na+ with water.

Table 6.3.2.3.11: Coordination number for alkali metal ions in aqueous complexes.

Aqua ion	n
$[Li(H_2O)_n]^+$	4
$[Na(H_2O)_n]^+$	6
$[K(H_2O)_n]^+$	6
$[Rb(H_2O)_n]^+$	6-8
$[Cs(H_2O)_n.]^+$	8

In general the alkali metal ions form complexes with hard donor such as oxygen (H_2O, ROH, RCO_2^-, etc.) or nitrogen (e.g., NH_3, NR_3, etc.). The aquo complexes readily exchange the water for other ligands, (3.13); however, the equilibrium constants are small when the ligand is similar in size to water.

$$[M(H_2O)_n]^+ + L \leftrightharpoons [M(H_2O)_{n-1}L]^+ + H_2O \tag{6.3.2.3}$$

As a consequence of the low equilibrium constants for monodentate ligands, the alkali metal cations, M^+, favor coordination to polydentate ligands such as ethylenediaminetetraacetic acid (EDTA, Figure 6.3.2.3.15), polyethers, and even natural polyesters or polypeptides. In each case the polydentate ligand wraps itself around the cation.

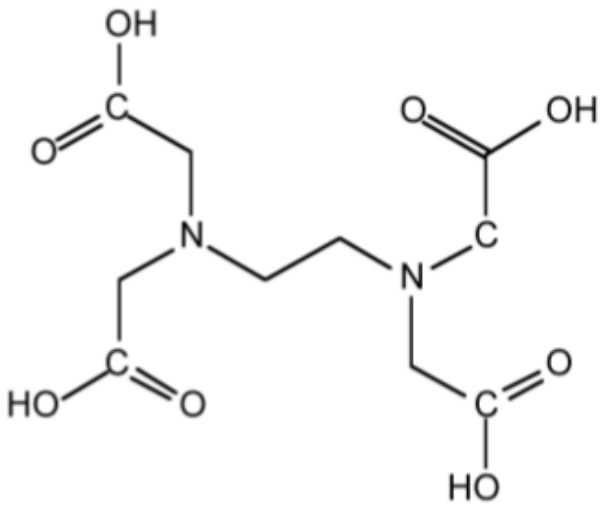


Figure 6.3.2.15: Structure of ethylenediaminetetraacetic acid (EDTA).

Macrocyclic ligands

Macrocyclic ligands represent a special class of polydentate ligand. They are defined as being a cyclic compound with nine or more members including all the heteroatoms and with three or more donor atoms. and are given the special name of **cryptands** when they are synthetic bi- and poly-cyclic multidentate ligands. Crown ethers is the name applied to macrocyclic ligands that consist of a ring containing several ether groups. Figure 6.3.2.3.16 shows several common macrocyclic ligands.

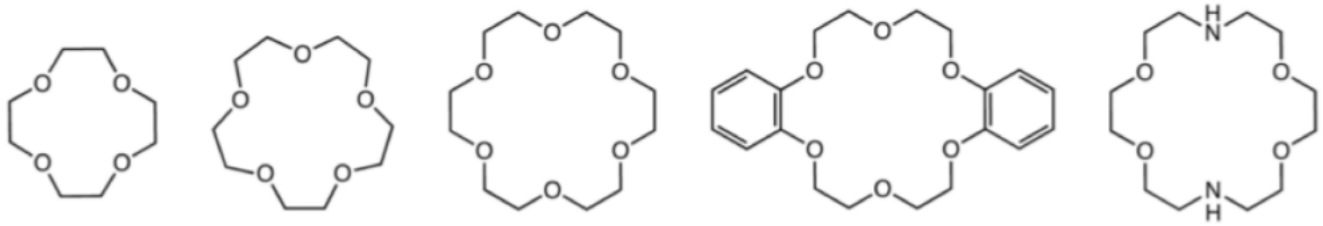


Figure 6.3.2.16: The structures of some common macrocyclic ligands.

Macrocyclic ligands are generally oxygen or nitrogen donor ligands, and they form highly stable 1:1 complexes with alkali metal ions in which all or most of the coordination sites on the metal are occupied, i.e., $[M(L)]^+$ rather than $[M(L)(H_2O)_n]^+$. Since the external surface of the macrocyclic ligands comprises of organic residue (e.g., CH_2 groups) the complexes are soluble in organic solvents. Thus, crown ethers are commonly used to solubilize salts (e.g., NaCl) in organic solvents. They have also been used to create solutions of nanoparticles, such as carbon nanotubes (Figure 6.3.2.3.17), that are ordinarily highly insoluble in common organic solvents (Table 6.3.2.3.12).

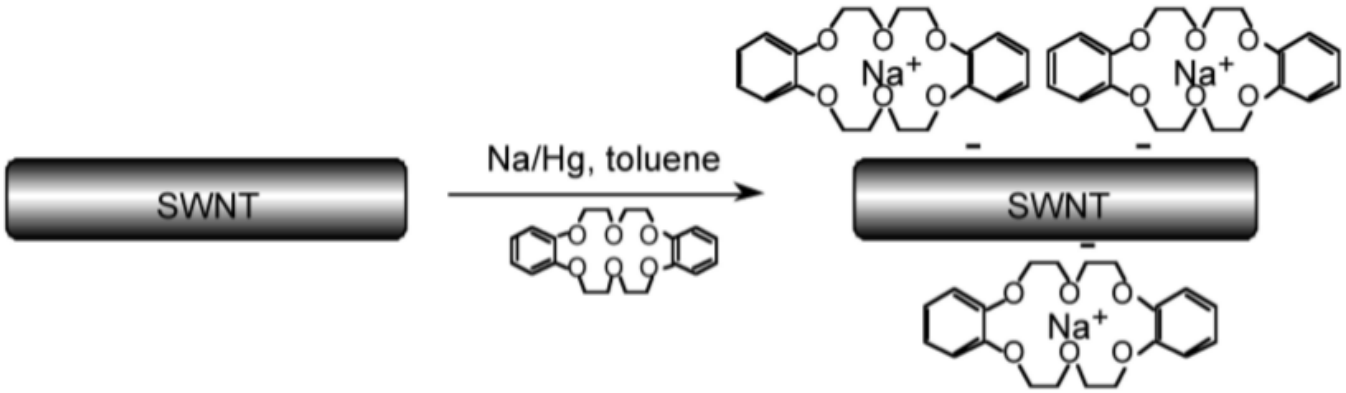


Figure 6.3.2.17: Representation of the reaction between Na/Hg amalgam, dibenzo-18-crown-6, and puried single walled carbon nanotubes (SWNTs) in toluene and the formation of the $[Na(dibenzo\text{-}18\text{-}crown6)]_n[SWNT]$ complex. Adapted from R. E. Anderson and A. R. Barron, *J. Nanosci. Nanotechnol.*, 2007, **7**, 3436

Table 6.3.2.3.12: The concentration of Na/dibenzo-18-crown-6 solubilized reduced single walled carbon nanotubes (SWNTs) in various solvents.

Solvent	SWNT concentration (mg/L)
CH_2Cl_2	14.05
DMF	11.42
hexane	4.65
toluene	3.79
EtOH	2.37
MeOH	2.37
$CHCl_3$	0.30
H_2O	0.10

The most important factor in the coordination of various macrocyclic ligands to alkali metal ions is the relative size of the ion and the ligand cavity. For example, 4,7,13,16,21,24-hexaoxa-1,10diazabicyclo[8,8,8]hexacosane is a potentially octa-dentate ligand; however, the binding eciency is very dependant on the identity of the M+ ion (Figure 6.3.2.3.18). The low binding constant for lithium is probably as a consequence that the ligand would have to distort to coordinate to the small cation. Conversely, the lower equilibrium for caesium is due to its being to large to t completely into the ligand cavity.

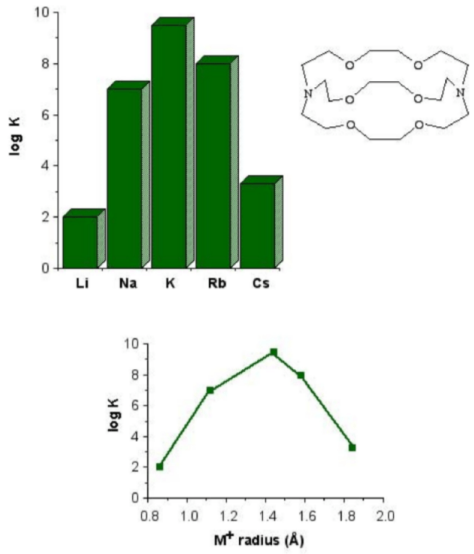


Figure 6.3.2.18: : Relative stability constants (log K) of alkali metal ions to 4,7,13,16,21,24-hexaoxa-1,10diazabicyclo[8,8,8]hexacosane and relationship to the M^+ ionic radius.

One application of the size effect for macrocyclic ligands is the ability to selectively bind different metals. For example, the 4,7,13,16,21-pentaoxa-1,10-diazabicyclo[8,8,5]tricosane and 4,7,13,16,21,24-hexaoxa-1,10diazabicyclo[8,8,8]hexacosane ligands shown in Figure 6.3.2.3.19 have very different binding constants to Na^+ and K^+, as a consequence of the relative size of the cation and the ligand cavity (Table 6.3.2.3.13).

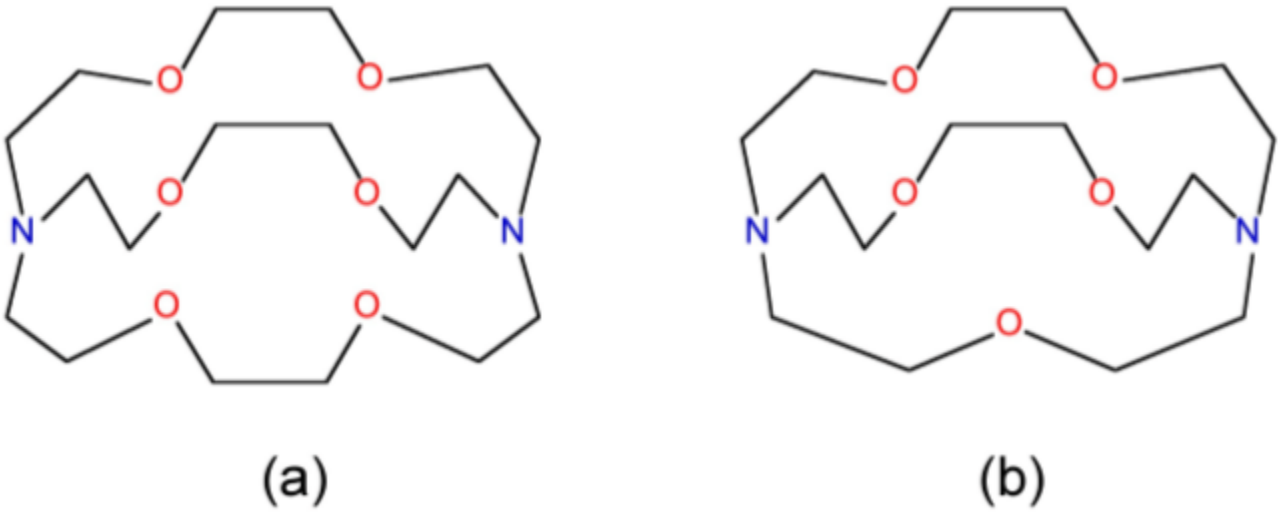


Figure 6.3.2.19: Structure of (a) 4,7,13,16,21-pentaoxa-1,10-diazabicyclo[8,8,5]tricosane [2,2,1] and (b) 4,7,13,16,21,24-hexaoxa-1,10-diazabicyclo[8,8,8]hexacosane [2,2,2].

Table 6.3.2.3.13: Equilbrium constants for the M+ complexes for macrocyclic ligands with different cavity sizes. The structures of the ligands are shown in Figure 6.3.2.3.19.

Cation	[2,2,2]	[2,2,1]
Na^+	800	250,000
K^+	250,000	700

Bibliography

1. R. E. Anderson and A. R. Barron, *J. Nanosci. Nanotechnol.*, 2007, **7**, 3436.
2. J. M. Lehn, *Supramolecular Chemistry: Concepts and Perspectives*. VCH (1995).

Answers

The ionic radius of Na^+ is 0.97 Å, while that for H^- is 1.54 Å. The ratio of the ionic radii (r^+/r^-) is 0.67. Hence, NaH has a NaCl (rock salt) structure

The ionic radius of Rb^+ is 1.47 Å, while that for F^- is 1.33 Å. The ratio of the ionic radii (r^+/r^-) is 1.10. Hence, RbF has a CsCl structure.

This page titled 6.3.2: Compounds of the Alkali Metals is shared under a CC BY 3.0 license and was authored, remixed, and/or curated by Andrew R. Barron (CNX) via source content that was edited to the style and standards of the LibreTexts platform.

6.3.3: The Anomalous Chemistry of Lithium

While lithium shows many properties that are clearly consistent with its position in Group 1, it also has key differences to the other alkali metals. In fact, in many ways it is more similar to its diagonal neighbor magnesium (Mg) than the other Group 1 metals - a phenomenon known as **the diagonal effect**.

Charge/radius

The ionic radius for the +1 cation of lithium is very small in comparison with its next highest homolog, sodium (Table 6.3.3.3.14). This results in a correspondingly high value for the charge density (z/r). As may be seen from Table 6.3.3.1 the charge density for lithium is significantly higher than that of its Group 1 relations.

Table 6.3.3.1: Comparison of charge densities for lithium, sodium, potassium, and magnesium.

Element	z	r (Å)	z/r ($Å^{-1}$)
Li	+1	0.68	1.47
Na	+1	0.97	1.03
K	+1	1.33	0.75
Mg	+2	0.66	3.03

As a result of the high charge density, the Li^+ ion is a highly polarizing ion. One of the main consequences of this is that lithium tends to form polar covalent bonds rather than ionic interactions. For example, alkyl lithium compounds (RLi) contain covalent Li-C bonds in a similar manner to the Mg-C bonds in Grignards (RMgX, where X = Cl, Br)

Lattice energy

Lithium compounds have high lattice energies as compared to the other Group 1 metals (Table 6.3.3.2). As a consequence lithium compounds would be less soluble than the highly soluble sodium compounds. In some cases (Li_2O, Li_3N) they react with water.

Table 6.3.3.2: Comparison of lattice energies for compounds of lithium, sodium, potassium, and magnesium.

Compound	Lattice energy (kJ/mol)
LiF	-1046
NaF	-923
KF	-821
MgF_2	-2957

Coordination number

The small size of lithium results in a lower coordination number (4) for compounds and complexes than observed for the other Group 1 metals. However, lithium and magnesium complexes and organometallic compounds both have most commonly four-coordinate metal centers (in the absence of large steric constraints).

Chemical reactivity

A review of some of the reactions of lithium, magnesium and the other Group 1 metals shows the anomalous behavior of lithium and its similarity to magnesium. Both lithium and magnesium reacts with carbon or nitrogen to form the corresponding carbide and nitride. Whereas sodium and the other Group 1 metals show no reaction under ambient conditions. The combustion of either

lithium or magnesium in air results in the formation of the oxides, Li_2O and MgO, respectively. In contrast, sodium forms the peroxide, Na_2O_2.

It is not only in the reactivity of the elements that this relationship between lithium and its diagonal neighbor exists. Many of the compounds of lithium have a similar reactivity to those of magnesium rather than sodium. For example, the carbonates of lithium and magnesium decompose under thermolysis to yield the oxides, (3.14) and (3.15), in contrast, sodium carbonate (Na_2CO_3) is stable to thermolysis.

$$Li_2CO_3 \rightarrow Li_2O + CO_2 \tag{6.3.3.1}$$

$$MgCO_3 \rightarrow MgO + CO_2 \tag{6.3.3.2}$$

This page titled 6.3.3: The Anomalous Chemistry of Lithium is shared under a CC BY 3.0 license and was authored, remixed, and/or curated by Andrew R. Barron (CNX) via source content that was edited to the style and standards of the LibreTexts platform.

6.3.4: Organolithium Compounds

One of the major uses of lithium is in the synthesis of organolithium compounds, RLi. They have great importance and utility in industry and chemical research. Their reactivity resembles that of Grignard reagents, but they are generally more reactive.

Synthesis

The best general method for RLi synthesis involves the reaction of an alkyl or aryl chloride with lithium metal in benzene or an aliphatic hydrocarbon (e.g., hexane), (3.4.1).

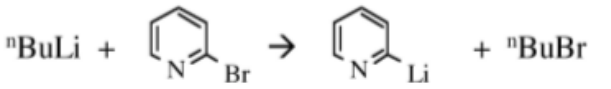
$$RCl + 2Li \rightarrow RLi + LiCl \tag{6.3.4.1}$$

While it is possible to use diethyl ether (Et_2O), the solvent slowly attack the resultant alkyl lithium compound, (3.4.2).

$$Et_2O + {}^{n}\,BuLi \rightarrow EtOLi + H_2C{=}CH_2 + {}^{n}\,BuH \tag{6.3.4.2}$$

Metal-hydrogen exchange, (3.4.3), metal-halogen exchange, (3.19), and metal-metal exchange can also be used, (3.4.4).

$$RH + R'Li \rightarrow R'H + RLi \tag{6.3.4.3}$$



(3.19)

$$2Li + R_2Hg \rightarrow 2RLi + Hg \tag{6.3.4.4}$$

All organolithium compounds are produced as solutions and are hence used in synthetic protocols by volume of solution. It is therefore important to know the exact concentration of RLi in solution. The simplest approach to quantify the amount of organolithium is to react a known volume with water, (3.4.5), and then titrate (with acid) the resultant base that is formed.

$$RLi + H_2O \rightarrow LiOH + RH \tag{6.3.4.5}$$

However, while the concentration of freshly prepared samples of organolithium reagents can the theoretically measured in this way, real samples always contain some amount of LiOH or other bases. A simple titration inevitably results in an over estimation of the organolithium reagent. To overcome this a *double titration* method is used.

Gillman double titration method

The careful addition of a known volume of an organolithium reagent solution (between 0.5 and 1.5 mL) to an excess of water yields a solution of LiOH that can be titrated with a standardized solution of hydrochloric acid, using phenolphthalein as the indicator. The presence of any LiOH in the original organolithium solution will be incorporated into this titration, and thus the result will be a measure of the *total base content* in the solution, i.e., (3.4.6).

$$\text{Total base content} = \text{LiOH formed from the reaction of RLi with } H_2O + \text{LiOH present as impurity in the RLi solution} \tag{6.3}$$

In order to determine the amount of LiOH present as impurity in the organolithium solution it is necessary to react the RLi without the formation of base, then titrate the resulting solution. To do this, an aliquot (the same amount as used before) of the organolithium is reacted slowly with 1,2-dibromoethane ($BrCH_2CH_2Br$) dissolved in dry diethyl ether (Et_2O). After 5 min of stirring, the solution is diluted with an excess of water and then titrated with a standardized solution of hydrochloric acid, again using phenolphthalein as the indicator. The dierence of the two titrations gives the exact concentration of the organolithium.

6.3.4.1Exa

An aliquot of nBuLi in hexanes (0.50 mL) was added to degassed water (20 mL). After any visible reaction had ceased, a few drops of a phenolphthalein solution in water/methanol are added resulting in a pink color indicative of a basic pH. The resulting mixture is titrated with standardized hydrochloric acid ([HCl] = 0.1034 N) until complete disappearance of the pink color (7.90 mL).

A second aliquot of nBuLi in hexanes (0.50 mL) is added to 1,2-dibromoethane (0.20 mL, Et2O). After 5 min of stirring, the mixture was diluted with water (20 mL) and after addition of the phenolphthalein indicator titrated (with vigorous stirring due to the biphasic nature of the system) with standardized hydrochloric acid ([HCl] = 0.1034 N) until complete disappearance of the pink color (0.25 mL).

The concentration of nBuLi is calculated as follows:

Step 1.

$$[\text{total base}] = \frac{\text{volume HCl} \times [\text{HCl}]}{\text{volume } {}^{n}\text{BuLi}} = \frac{7.90 \times 0.1034}{0.50} = 1.633 \tag{6.3.4.7}$$

Step 2.

$$[\text{residual base}] = \frac{\text{volume HC l} \times [\text{HCl}]}{\text{volume } {}^{n}\text{BuLi}} = \frac{0.25 \times 0.1034}{0.50} = 0.013 \tag{6.3.4.8}$$

Step 3.

$$[{}^{n}\text{BuLi}] = [\text{total base}] - [\text{residual base}] = 1.633 - 0.013 = 1.620M \tag{6.3.4.9}$$

Properties

Alkyl lithium compounds are either low melting solids or liquids, and often with high volatility (depending on the substituent) due to the covalent nature of the bonding. They are soluble in aliphatics, aromatics, and ethers. However, while the reaction with ethers is generally slow, (3.17), alkyl lithium compounds can polymerize tetrahydrofuran (THF).

Organolithium compounds react rapidly with air and water (both vapor and liquid). The reaction with water is the basis of the Gillman double titration method for determining the concentration of organolithium reagents in solution.

Structure

The structure of organolithium compounds is dominated by their highly oligomeric nature as a result of 3-center 2-electron bridging bonds. In all cases the extent of oligomerization is dependant on the identity of the alkyl (or aryl) group. The alkyl-bridged bond is similar to those found for beryllium and aluminum compounds.

In the vapor phase any particular organolithium derivative show a range of oligomeric structures. For example, the mass spectrum of EtLi shows ions associated with both tetramers (e.g., $[Et_3Li_4]^+$) and hexamers (e.g., $[Et_5Li_6]^+$). The structures of the different oligomers have been predicted by molecular orbital calculations (Figure 6.3.4.3.20).

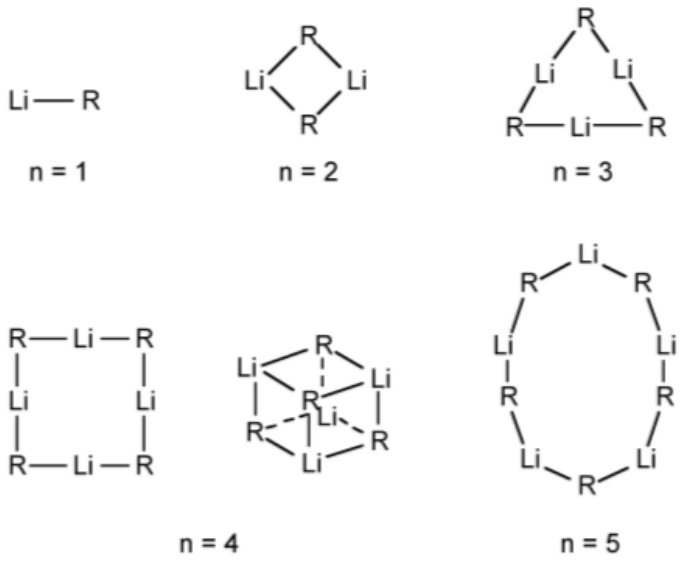


Figure 6.3.4.20: Proposed vapor phase structures for various oligomers of RLi.

Solution molecular weight measurements indicate the oligomerization is present (in the absence of a coordinating ligand such as Et_2O or an amine). The extent of oligomerization depends on the steric bulk of the alkyl group (Table 6.3.4.3.16). Oligomerization and solution structures have also been investigated by ^{7}Li and ^{13}C NMR spectroscopy.

Table 6.3.4.3.16: Extent of oligomerization (n) for organolithium compounds $[RLi]_n$ in benzene solution.

R	$[RLi]_n$	R	$[RLi]_n$
Me	4	Et	6
^{n}Bu	6	^{t}Bu	4

There are a large number of X-ray crystallographically determined structures for organolithium derivatives. The archetypal example is MeLi, which exists as a tetramer in the solid state (Figure 6.3.4.3.21). The lithium atoms are arranged as a tetrahedron and the carbon atoms are positioned on the center of the facial planes, i.e., the carbon is equidistant from each of the lithium atoms. In contrast, EtLi has a similar tetrahedral structure, but the α-carbon of the ethyl groups are asymmetrically arranged such that it is closer to one lithium atom than the other two.

This page titled 6.3.4: Organolithium Compounds is shared under a CC BY 3.0 license and was authored, remixed, and/or curated by Andrew R. Barron (CNX) via source content that was edited to the style and standards of the LibreTexts platform.

6.4: Group 2 - The Alkaline Earth Metals

Thumbnail: A crystal of strontianite. Both strontianite, one of the most important strontium ores, and strontium are named after the town of Strontian, Scotland, the location of one of the first mines for strontium ores.

This page titled 6.4: Group 2 - The Alkaline Earth Metals is shared under a CC BY 3.0 license and was authored, remixed, and/or curated by Andrew R. Barron (CNX) via source content that was edited to the style and standards of the LibreTexts platform.

6.4.1: The Alkaline Earth Elements

The Group 2 metals have a particular name: the alkaline earth metals. The name is derived from the observation that they have such high melting points (Table 6.4.1.4.1) that they remain solids (earths) in a fire. Table 6.4.1.4.2 lists the derivation of the names of the alkali metals.

Table 6.4.1.4.1: Melting points of the alkaline earth metals in comparison with the alkali metals.

Alkali metal	Melting point (°C)	Alkaline earth metal	Melting point (°C)
Li	180.54	Be	1287
Na	97.72	Mg	650
K	63038	Ca	842
Rb	39.31	Sr	777
Cs	28.44	Ba	727
Fr	27 (estimated)	Ra	700

Table 6.4.1.4.2: Derivation of the names of the alkaline earth metals.

Element	Symbol	Name
Beryllium	Be	From the Greek *berullos* meaning *to become pale*, in reference to the pale semiprecious gemstone beryl
Magnesium	Mg	From the *Magensia* district in Greece
Calcium	Ca	From the Latin *calcis* meaning *lime*
Strontium	Sr	From the mineral *strontianite* named after the Scottish village of *Strontian*
Barium	Ba	From the Greek *bary*, meaning *heavy*
Radium	Ra	From the Latin *radius* meaning *ray*

Discovery

Beryllium

Beryllium was discovered by Louis-Nicolas Vauquelin (Figure 6.4.1.4.1) in 1798 as a component in beryls and emeralds; however, Fredrich Wöhler (Figure 6.4.1.4.2) and Antoine Bussy (Figure 6.4.1.4.3) independently isolated the metal in 1828 by reacting potassium with beryllium chloride, (4.1.1).

$$BeCl_2 + 2K \rightarrow Be + 2KCl \tag{6.4.1.1}$$



Figure 6.4.1.1: French pharmacist and chemist Louis Nicolas Vauquelin (1763 - 1829).

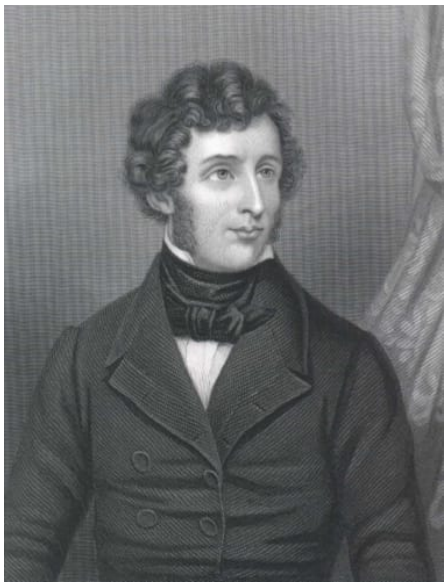


Figure 6.4.1.2: German chemist Friedrich Wöhler (1800 - 1882) also known for his synthesis of urea and, thus, the founding of the field of natural products synthesis.

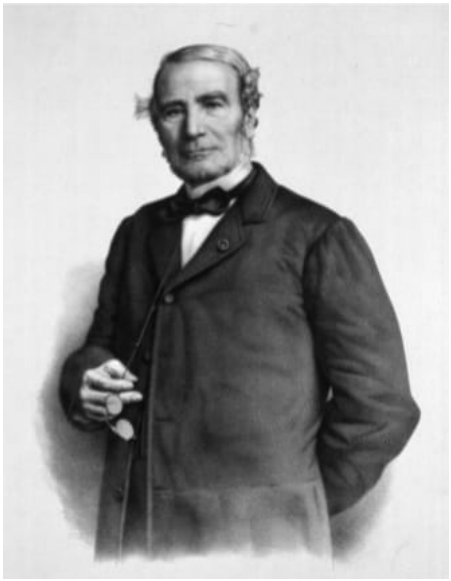


Figure 6.4.1.3: French chemist Antoine Alexandre Brutus Bussy (1794 - 1882).

Magnesium

Magnesium is found in large deposits of magnesite and dolomite, and in mineral waters where the Mg^{2+} ion is soluble. In 1618 a farmer at Epsom in England attempted to give his cows water from a well. The farmer noticed that the water seemed to heal scratches and rashes. These *Epsom salts* were recognized to be hydrated magnesium sulfate, $MgSO_4$. The metal was first isolated in 1808 by Sir Humphry Davy (Figure 6.4.1.4.4) via the electrolysis of a mixture of magnesia and mercury oxide.

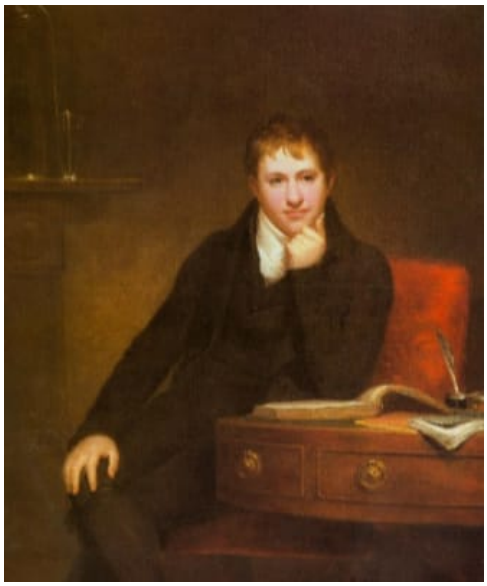


Figure 6.4.1.4: British chemist and inventor Sir Humphry Davy FRS (1778 - 1829).

Antoine Bussy (Figure 6.4.1.4.3) subsequently prepared magnesium by heating magnesium chloride and potassium in a glass tube, (4.1.2). When the potassium chloride was washed out, small globules of magnesium remained.

$$MgCl_2 + 2K \rightarrow Mg + 2KCl \tag{6.4.1.2}$$

Calcium

Calcium oxide or lime was known in ancient Rome, while even in 975 AD, Plaster of Paris (calcium sulphate) was reported to

be useful for setting broken bones. The element itself was not isolated until 1808 when Sir Humphry Davy (Figure 6.4.1.4.4) electrolyzed a mixture of lime and mercuric oxide (HgO). His work was based upon prior work by Jöns Berzelius (Figure 6.4.1.4.5) who had prepared calcium amalgam (an alloy of calcium and mercury) by electrolyzing lime in mercury.



Figure 6.4.1.5: Swedish chemist Jöns Jacob Berzelius (1779 1848).

Strontium

Discovered in lead mines in 1787 the mineral strontianite was named after the Scottish village of Strontian. Although it was realized that this mineral was different from others that contained barium, it wasn't until 1798 that Thomas Hope (Figure 6.4.1.4.6) suggested the presence of a new element. As with calcium, metallic strontium was first isolated by Sir Humphry Davy (Figure 6.4.1.4.4) in 1808 using electrolysis of a mixture containing strontium chloride and mercuric oxide.

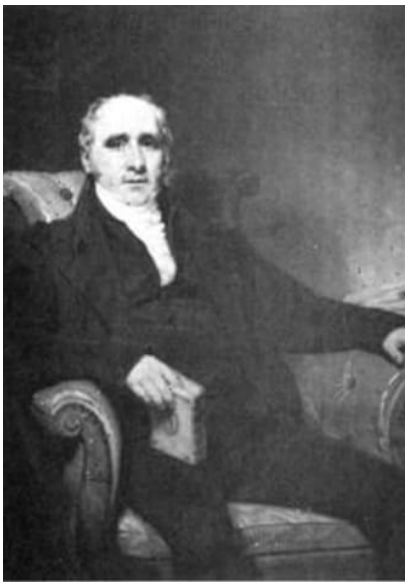


Figure 6.4.1.6: Scottish chemist Thomas Charles Hope (1766 - 1844).

Barium

Barium minerals were known by alchemists in the early Middle Ages. Stones of the mineral barite found in Bologna, Italy (also known as *Bologna stones*), were known to glow after exposure to light. Carl Scheele (Figure 6.4.1.4.7) identified barite in 1774, but

did not isolate barium. Barium was first isolated as Ba^{2+} in solution by Sir Humphry Davy (Figure 6.4.1.4.4) in 1808. The oxidized barium was at first called *barote*, by Guyton de Morveau, (Figure 6.4.1.4.8) which was changed by Antoine Lavoisier (Figure 6.4.1.4.9) to *baryta*, from which barium was derived to describe the metal.



Figure 6.4.1.7: : German-Swedish pharmaceutical chemist Carl Wilhelm Scheele (1742 - 1786). Author Isaac Asimov has called him "hard-luck Scheele" because he made a number of chemical discoveries before others who are generally given the credit.



Figure 6.4.1.8: : French chemist and politician Louis-Bernard Guyton de Morveau (1737 - 1816) changed his name to Guyton-Morveau after the French Revolution.



Figure 6.4.1.9: French chemist and biologist Antoine-Laurent de Lavoisier (1743 1794).

Radium

Radium was discovered by Marie Curie (Figure 6.4.1.4.10) and her husband Pierre (Figure 6.4.1.4.11) in 1898 while studying pitchblende. After removing uranium they found that the remaining material was still radioactive. They then separated out a radioactive mixture consisting mostly of barium and an element that gave crimson spectral lines that had never been documented before. In 1910, radium was isolated as a pure metal by Curie and André-Louis Debierne (Figure 6.4.1.4.12) through the electrolysis of a radium chloride solution by using a mercury cathode and distilling in an atmosphere of hydrogen gas.



Figure 6.4.1.10: Marie Curie (1867-1934). Copyright Academy of Achievement.



Figure 6.4.1.11: French physicist Pierre Curie (1859 1906).



Figure 6.4.1.12: French chemist André-Louis Debierne (1874 - 1949).

Abundance

The abundance of the alkaline earth elements is given in Table 6.4.1.4.3. Beryllium is rare, but found in the mineral beryl ($Be_3Al_2Si_6O_{18}$). While magnesium is widespread within the Earth's crust, commercial sources tend to be from sea water as well as the carbonate minerals magnesite ($MgCO_3$) and dolomite [$(Ca,Mg)CO_3$]. Calcium is also commonly found as the carbonate, however, strontium and barium are present as the sulfates celestine ($SrSO_4$) and barites ($BaSO_4$), respectively.

Table 6.4.1.4.3: Abundance of alkaline earth elements.

Element	Terrestrial abundance (ppm)
Be	2.6 (Earth's crust), 6 (soil), 2 x 10^{-7} (sea water)
Mg	23,000 (Earth's crust), 10,000 (soil), 1,200 (sea water)
Ca	41,000 (Earth's crust), 20,000 (soil), 400 (sea water)
Sr	370 (Earth's crust), 200 (soil), 8 (sea water)

Element	Terrestrial abundance (ppm)
Ba	500 (Earth's crust), 500 (soil), 0.001 (sea water)
Ra	6×10^{-7} (Earth's crust), 8×10^{-7} (soil), 1×10^{-10} (sea water)

Calcium is a key element for living. Not only is it present as the skeletal material for shell sh and crabs ($CaCO_3$) its phosphate derivative, hydroxyapetite [$Ca_5(OH)(PO_4)_3$] is the structural material of bones and teeth. Calcium is also present in soft tissue at a level of ca. 22g/kg. Calcium is a vital metal for the following:

- Links large molecules together.
- Used in the activation of muscles
- Used in enzyme activation by stabilization of particular conformations of proteins to be acted upon by enzymes.

Isotopes

The naturally abundant isotopes of the alkaline earth elements are listed in Table 6.4.1.4.4. All of the 25 isotopes of radium are radioactive, and while radium-223, radium-224, and radium-228 are found in nature as decay products of either uranium or thorium, they are only present in trace amounts.

Table 6.4.1.4.4: Abundance of the major isotopes of the alkaline earth elements.

Isotope	Natural abundance (%)
Beryllium-9	100
Magnesium-24	78.99
Magnesium-25	10
Magnesium-26	11.01
Calcium-40	96.941
Calcium-42	0.647
Calcium-43	0.135
Calcium-44	2.086
Calcium-46	0.004
Calcium-48	0.187
Strontium-84	0.56
Strontium-86	9.86
Strontium-87	7.0
Strontium-88	82.58
Barium-130	0.106
Barium-132	0.101
Barium-134	2.417
Barium-135	6.592
Barium-136	7.854
Barium-137	11.23
Barium-138	71.7
Radium-226	100

Although beryllium-7 and beryllium-10 are found as trace isotopes, they are so rare beryllium is considered mononuclidic element (a chemical element which is found essentially as a single nuclide, of only one atomic mass). Calcium has four stable isotopes plus two more isotopes (calcium-46 and calcium-48) that have such long half-lives (2.8 x 10^{15} and 4 x 10^{19} years, respectively) that for all practical purposes they can be considered stable.

Measurement of the $^{87}Sr/^{86}Sr$ ratio allows for geological dating of minerals and rocks. Strontium-90 (half-life = 28.9 years) is a by-product of nuclear fission and found in nuclear fallout. For example, the 1986 Chernobyl nuclear accident contaminated released a large amount of strontium-90. Since strontium substitutes for calcium in bones it prevents excretion from the body and thus presents a significant health risk, however, strontium-89 is a short-lived artificial radioisotope that is used in the treatment of bone cancer.

Naturally occurring barium is a mix of seven stable isotopes (Table 6.4.1.4.4), but there are a total twenty-two isotopes known, most of which are highly radioactive and have half-lives in the several millisecond to several day range. The only notable exception is barium-133 which has a half-life of 10.51 years.

Industrial production

The industrial production of beryllium is usually from the reaction of beryl ($Be_3Al_2Si_6O_{18}$) with $Na_2(SiF_6)$ which yields the beryllium fluoride, $Na_2(BeF_4)$. Subsequent reactions with base give the hydroxide.

$$Na_2(BeF_4) + 2NaOH \rightarrow Be(OH)_2 + 4NaF \tag{6.4.1.3}$$

Reaction of the hydroxide with the ammonium salt of HF_2^-, followed by thermolysis gives beryllium fluoride (BeF2). Finally, reduction of the fluoride with magnesium yields beryllium.

$$BeF_2 + Mg \rightarrow MgF_2 + Be \tag{6.4.1.4}$$

Although magnesium is an abundant metal in dozens of mineral the majority of commercial production comes from sea water, where it is present at about a level of 12% that of sodium. Calcium hydroxide is added to seawater to form magnesium hydroxide precipitate.

$$MgCl_2 + Ca(OH)_2 \rightarrow Mg(OH)_2 + CaCl_2 \tag{6.4.1.5}$$

Subsequent reaction with hydrochloric acid yields concentrated magnesium chloride solution.

$$Mg(OH)_2 + 2HCl \rightarrow MgCl_2 + 2H_2O \tag{6.4.1.6}$$

Electrolysis of the magnesium chloride produces magnesium. At the cathode, the Mg^{2+} ion is reduced to magnesium metal, (4.1.7), while at the anode chlorine gas is formed, (4.1.8).

$$Mg^{2+} + 2e^- \rightarrow Mg \tag{6.4.1.7}$$

$$2Cl^- \rightarrow Cl_{2(g)} + 2e^- \tag{6.4.1.8}$$

Strontium metal is produced in an analogous manner; however, it may also be prepared from strontium oxide by reduction with aluminum in vacuum at a temperature at which strontium distills off.

$$3SrO + 2Al \rightarrow 3Sr + Al_2O_3 \tag{6.4.1.9}$$

Reactivity and toxicity

The chemistry of the Group 2 elements is dominated by the +2 oxidation state and the noble gas configuration of the M^{2+} cation.

Calcium, strontium, and barium react with water on contact to produce the hydroxide and hydrogen gas. Although the lighter alkaline earth metals do not react violently with water, they do burn in air.

Magnesium burns with a very bright white flame such that caution should be taken not to look at the ame directly. Magnesium is capable of reducing water, (4.1.10), and as a result, water cannot be used to extinguish magnesium res; the hydrogen gas

produced will only intensify the re. In addition, magnesium also reacts with carbon dioxide, (4.1.11), precluding the use of carbon dioxide re extinguishers. Class D dry chemical re extinguisher or sand are used for magnesium res.

$$Mg_{(s)} + 2H_2O \rightarrow Mg(OH)_{2(s)} + H_{2(g)} \tag{6.4.1.10}$$

$$2Mg_{(s)} + CO_2 \rightarrow 2MgO_{(s)} + C_{(s)} \tag{6.4.1.11}$$

Strontium and barium burn in air to produce both the oxide and the nitride, but since the metals do not react with nitrogen except at high temperatures they only form the oxide spontaneously at room temperature.

Beryllium is a class 1 carcinogen, i.e., it is carcinogenic to both animals and humans. Beryllium is harmful if inhaled; if the concentration in air is high enough (greater than 100 µg/m3) an acute condition can result, called acute beryllium disease, which resembles pneumonia. Acute beryllium disease was reported as being associated with the manufacture of fluorescent lighting tubes (a practice that ceased in 1949).

The human body absorbs strontium as if it were calcium, and while stable isotopes have pose no signicant health threat, the uptake of radioactive strontium-90 can lead to various bone disorders and diseases, including bone cancer. All water or acid soluble barium compounds are extremely poisonous. At low doses, barium acts as a muscle stimulant, while higher doses affect the nervous system. Radium is highly radioactive and its decay product, radon gas, is also radioactive.

This page titled 6.4.1: The Alkaline Earth Elements is shared under a CC BY 3.0 license and was authored, remixed, and/or curated by Andrew R. Barron (CNX) via source content that was edited to the style and standards of the LibreTexts platform.

6.4.2: Calcium the Archetypal Alkaline Earth Metal

Calcium represents the typical Group 2 metal. The chemical properties of its compounds can be applied to all the heavier homologs.

Solid state

In the solid state the compounds of the alkaline metals generally form ionic lattices. In fact (except for beryllium and to a lesser extend magnesium) the lattice parameters calculated from the ionic radii of Group 2 metals are within 1% of the experimentally determined values, indicating the highly ionic character.

Due to the increased ionic charge the cations of the alkaline earths are less than that of their alkali metal neighbors. Thus, the ionic radius of Ca^{2+} (0.99 Å) is less than that of K^{+} (1.33 Å), but more similar to Na+ (0.97 Å). This diagonal relationship is seen for the other metals in Group 2.

Oxides

Combustion of the Group 2 metals gives the monoxide, MO. In the case of SrO and BaO further reaction occurs by the absorption of oxygen under pressure to give the peroxides, MO_2. The peroxide and superoxides are not stable for the lighter homologs because the smaller M^{2+} ions are more polarizing and cause the peroxide and superoxides to decompose to the monoxide. Calcium peroxide can be prepared by the reaction of the hydroxide with hydrogen peroxide.

$$Ca(OH)_2 + H_2O_2 + 6H_2O \rightarrow CaO_2 \cdot 8H_2O \tag{6.4.2.1}$$

As typical for the Group 2 oxides, calcium monoxide is basic and reacts with water to give the hydroxide, (4.2.2). In fact, thin films of the Group 2 oxides of calcium, barium and strontium will readily absorb water and form the hydroxides.

$$CaO + H_2O \rightarrow Ca(OH)_2 \tag{6.4.2.2}$$

Carbonate

Calcium carbonate ($CaCO_3$) is a common substance found in rock in all parts of the world, and is the main component of shells of marine organisms, snails, pearls, and eggshells. Calcium carbonate is usually the principal cause of hard water. Most calcium carbonate used is extracted by quarrying or mining. However, pure calcium carbonate (e.g., for pharmaceutical use) can be produced from a pure quarried source (usually marble) or manufactured by the sequential reaction involving the thermal decomposition of the carbonate to the monoxide, (4.2.3), followed by the reaction with water to give the hydroxide, (4.2.2), and finally, the reaction with carbon dioxide to reform the carbonate, (4.2.4).

$$CaCO_3 \rightarrow CaO + CO_2 \tag{6.4.2.3}$$

$$Ca(OH)_2 + CO_2 \rightarrow CaCO_3 + H_2O \tag{6.4.2.4}$$

Calcium carbonate crystallizes as a variety of mineral forms.

- Aragonite
- Calcite (Figure 6.4.2.4.13)
- Vaterite
- Chalk
- Travertine
- Limestone
- Marble

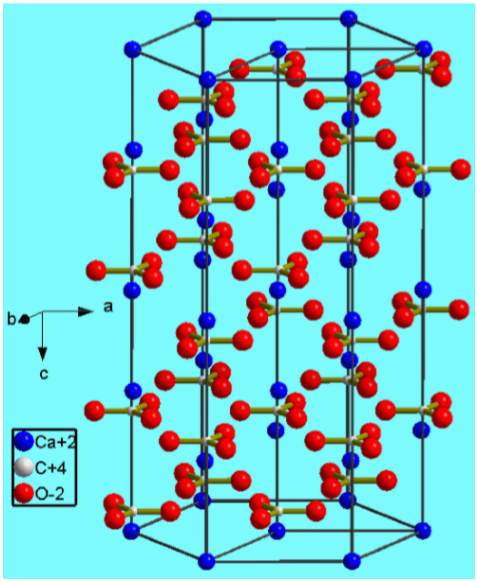


Figure 6.4.2.4.13: Unit cell of calcite a common form of calcium carbonate (CaCO3).

Calcium carbonate is one of the most widely used mineral materials, the following represents a list of some of the main applications.

- Construction industry as a building material (marble) or as an ingredient of cement.
- Purification of iron from iron ore in a blast furnace.
- A drilling fluids in the oil industry.
- Filler material for latex gloves.
- Filler (extender) in paints.
- Filler in plastics.
- Babies' diapers.
- DIY adhesives, sealants, and decorating fillers.
- Whiting in ceramics/glazing application.
- The filler in glossy paper.
- The production of blackboard chalk ($CaSO_4$).
- An abrasive in household cleaning products.
- Dietary calcium supplement.
- Inert filler for tablets and pharmaceuticals.
- Toothpaste.

Halides

Calcium chloride, bromide, and iodide are all ionic, water-soluble salts. In contrast, due to its high lattice energy for the small fluoride ion, CaF_2 is only slightly soluble (Table 6.4.2.4.5). The *fluorite* structure typified for CaF_2 (Figure 6.4.2.4.14) is found for most of the MX_2 ionic solids.

Table 6.4.2.4.5: Solubility of calcium halides in water.

Compound	Solubility @ 20 °C (g/100 mL)	Solubility @ 100 °C (g/100 ml)
CaF_2	0.0016	0.0017
$CaCl_2$	74.5	159
$CaBr_2$	142	312
CaI_2	209	426

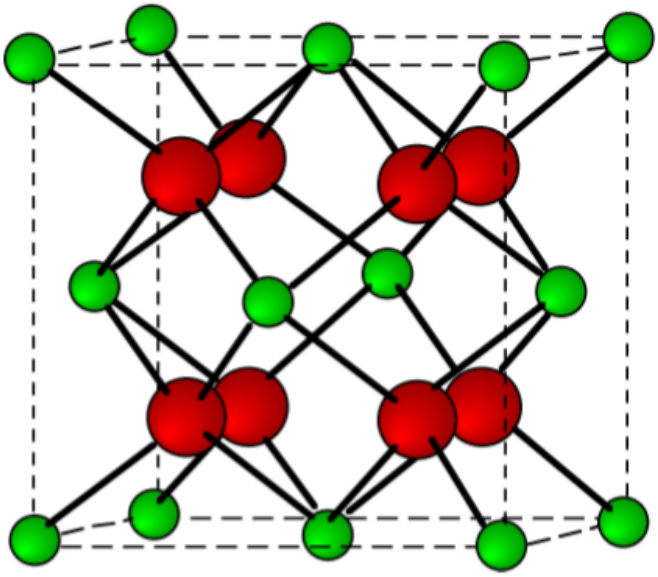


Figure 6.4.2.4.14 Unit cell for the uorite (CaF2) structure. Calcium atoms are shown in green (small), uorine atoms are shown in red (large), and the dashed lines show the unit cell.

Complexes

The coordination complexes of the alkaline earth metal cations (M^{2+}) involve electrostatic, or ion-dipole, interactions that have no preferred direction of interaction. Calcium will tolerate a wide range of coordination numbers, however, 6 and 8 are the most common. Complexes generally form with oxygen donors in a wide range of ligands, including: ROH, R_2O, $R_2C{=}O$, RCO_2^-, and PO_4^{2-}. While complexes with nitrogen donor ligands are known they are usually present with oxygen donors as well. As with the Group 1 metals, the aquo complex readily exchanges the water for other ligands, however, since the bond energy is larger for Ca^{2+} than for Na^+, the equilibrium constants are larger for analogous complexes.

Bibliography

- J. M. Buriak, L. K. Cheatham, R. G. Gordon, J. J. Graham, and A. R. Barron, *Euro J. Solid State Inorg. Chem.*, 1992, **29**, 43.
- R. E. Anderson and A. R. Barron, *Main Group Chem.*, 2005, **4**, 279.
- C, Lupu, R. S. Arvidson, A. Lüttge and A. R. Barron, *Chem. Commun.*, 2005, 2354.

Calcium Carbide: From Gaslight to Fertilizer

Calcium carbide has an interesting role in the societal and commercial changes that took place in the late 19th and early 20th centuries. However, in order to understand the effects of calcium carbide it is important to realize the state of the art of lighting in the late 18th century.

It was in 1792 that William Murdoch (Figure 6.4.2.4.15) first began experimenting with the use of gas, derived from the heating of coal and other materials, for lighting. Murdoch produced this coal gas, or manufactured gas and conveyed it through metal pipes, lighting his cottage and offices in Redruth, Cornwall (Figure 6.4.2.4.16).



Figure 6.4.2.4.15: Scottish engineer, inventor, and pioneer of gas lighting William Murdoch (1754 - 1839).



Figure 6.4.2.4.16: Murdoch's house at Redruth was the first domestic residence to be lit by gas.

In 1802 as part of the public celebrations of the Peace of Amiens (between England and France) Murdoch made a public exhibition of his lighting by illuminating the exterior of the Soho Foundry in Birmingham, England. Then in 1807 an entrepreneur, Fredrick Winsor (originally Friedrich Albrecht Winzer) displayed gaslights along the top of the wall between Carlton House and the Mall in London. This demonstration for city use was a revelation. By 1823 Britain had 300 miles of gas pipe and by 1850 it was 2000 miles. Gaslight had a profound impact on society. Walking the streets at night was safer, and it allowed for longer working hours. It also made evening activities easier. As a consequence reading and evening schools became popular pastimes. Unfortunately, gaslight was rather dull orange in color (Figure 6.4.2.4.17), but it was due to another area of chemical research that a brighter alternative was discovered.



Figure 6.4.2.4.17: A gas light still in use on the streets of London.

In 1895 the Frenchman Henry Moissan (Figure 6.4.2.4.18) was trying to make diamonds by the reaction of carbon (graphite) with almost anything he could lay his hands on. Although highly unsuccessful, one of his experiments did prove useful. By reacting carbon with lime, the common name for calcium oxide (CaO) at 2000 °C (in an electric arc furnace that he had helped develop) he produced calcium carbide (CaC_2).



Figure 6.4.2.4.18:French chemist Ferdinand Frederick Henri Moissan (1852 - 1907).

Pure calcium carbide is colorless, but most samples have a color ranging from black to grayish-white, depending on the grade. As an ionic salt it has a high melting point (2160 °C). While the structure of calcium carbide (Figure 6.4.2.4.19) has a tetragonal lattice, it is related to that of a cubic rock salt structure, but where the anion is the linear C_2^{2-} moiety.

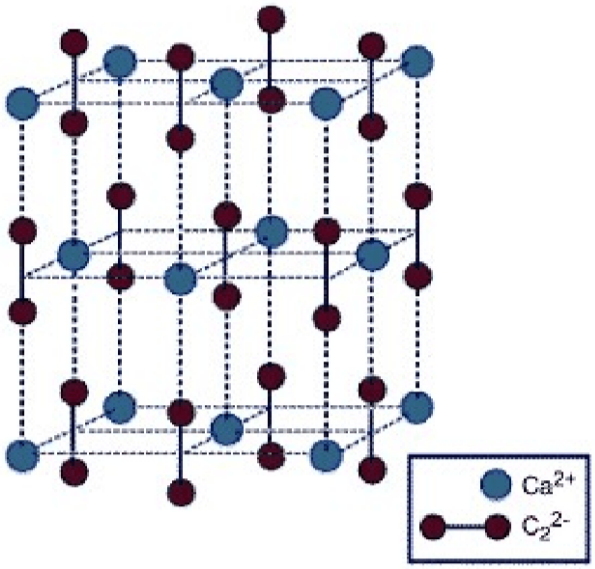


Figure 6.4.2.4.19:The unit cell of calcium carbide (CaC_2). Adapted from N. N. Greenwood and A. Earnshaw, *Chemistry of the Elements*, Butterworth-Heinemann (1984).

Although now used extensively, at the time of its discovery calcium carbide itself did not prove very interesting, its reaction with water had a profound effect on illumination. The reaction of calcium carbide with water yields acetylene, (4.2.5).

$$\mathrm{Ca_2C + H_2O \rightarrow Ca(OH)_2 + HC{=}CH} \tag{6.4.2.5}$$

Unlike coal gas, acetylene burns with a very bright white ame. Although electricity was starting to become more commonly used it was very expensive and acetylene offered a cheaper alternative for domestic lighting. Thus, by 1899 there were over 250,000 acetylene gas jets in Germany alone. The reaction of calcium carbide to form acetylene was used in a variety of portable lamps. These so-called carbide lamps were used in slate, copper and tin mines, and were also used extensively as headlights in early automobiles and bikes (Figure 6.4.2.4.20).



Figure 6.4.2.4.20:The carbide lamp on a 1911 Renault.

Unfortunately for acetylene there was one discovery and one economic change that brought the use of acetylene as a light source to an end. In 1893 Auer von Welsbach (Figure 6.4.2.4.21) invented the gas mantel (Figure 6.4.2.4.22). By the impregnation of silk or cotton with a mixture of thorium dioxide and cerium(IV) oxide (99:1), and using this in combination with gas he was able to produce a very white ame.



Figure 6.4.2.4.21:Austrian scientist and inventor Carl Auer Freiherr von Welsbach (1858 - 1929).



Figure 6.4.2.4.22 Gas mantles. Copyright Science Museum, London.

The other impact on acetylene, was that by 1905 the cost of electricity was significantly lower, and as a consequence the price of CaC_2 dropped to 30%. There were stockpiles of calcium carbide all over Europe and America. This may have been the end of calcium carbide's usefulness, however, in 1895 Heinrich Caro (Figure 6.4.2.4.23) and Adolf Frank (Figure 6.4.2.4.24), at the German chemical giant Badische Anilin- und Soda-Fabrik (BASF), were trying to make hydrogen cyanide (HCN) to use in its color dye business. In 1898, one of their colleagues demonstrated that what was actually produced during the reaction at temperatures exceeding 1000 °C was not cyanide, as they had hoped. It turned out that what Caro and Frank had found was that that when calcium carbide is reacted with nitrogen at 1000 ◦C it forms calcium cyanamide ($CaCN_2$), (4.2.6). The cyanamide anion has the structure $[N=C=N]^{2-}$.

$$CaC_2 + N_2 \rightarrow CaCN_2 + C \tag{6.4.2.6}$$

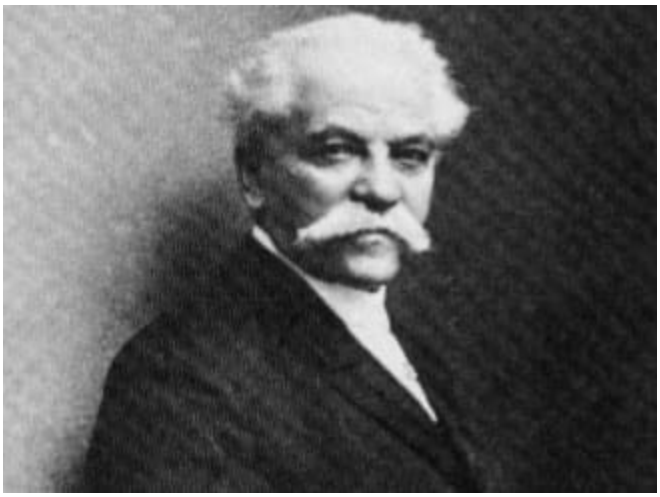


Figure 6.4.2.4.23:German chemist Heinrich Caro (1834 - 1910).



Figure 6.4.2.4.24: German chemist, engineer, and businessman Adolph Frank (1834 1916).

In contact with water calcium cyanamide decomposes and liberates ammonia:

$$CaCN_2 + 3H_2O \rightarrow 2NH_3 + CaCO_3 \tag{6.4.2.7}$$

As such, $CaCN_2$ is an excellent solid fertilizer that is readily plowed into the soil. By 1908 calcium cyanamide was also found to be a plant protection agent, which, at a time when all weed control was performed mechanically, represented a great step forward. Consequently, the output of calcium cyanamide grew enormously. In 1910, 30,000 tons were produced, but in 1928, global production had reached 1.2 million tons. After a temporary decline, demand has again risen in recent years owing to the ban on several pesticides due to the environmental damage they cause. Even after 100 years of use, no harmful long-term effects to the earth or environment have been observed, nor have weeds or pests developed a resistance to calcium cyanamide.

Bibliography

- N.-G. Vannerberg, *Acta Chem. Scand.*, 1962, **16**, 1212.
- M. A. Bredig, *J. Am. Chem. Soc.*, 1942, **64**, 1730.
- Y. Yamamoto, K. Kinoshita, K. Tamaru, and T. Yamanaka, *Bull. Chem. Soc. Japan*, 1958, **31**, 501.

Portland Cement

Chemical Composition of Portland Cement

There are four chief minerals present in a Portland cement grain: tricalcium silicate (Ca_3SiO_5), dicalcium silicate (Ca_2SiO_4), tricalcium aluminate ($Ca_3Al_2O_5$) and calcium aluminoferrite ($Ca_4Al_nFe_{2-n}O_7$). The formula of each of these minerals can be broken down into the basic calcium, silicon, aluminum and iron oxides (Table 6.4.2.4.6). Cement chemists use abbreviated nomenclature based on oxides of various elements to indicate chemical formulae of relevant species, i.e., C = CaO, S = SiO_2, A = Al_2O_3, F = Fe_2O_3. Hence, traditional cement nomenclature abbreviates each oxide as shown in Table 6.4.2.4.6.

Table 6.4.2.4.6: Chemical formulae and cement nomenclature for major constituents of Portland cement. Abbreviation notation: C = CaO, S = SiO_2, A = Al_2O_3, F = Fe_2O_3.

Mineral	Chemical formula	Oxide composition	Abbreviation
Tricalcium silicate (alite)	Ca_3SiO_5	$3CaO.SiO_2$	C3S
Dicalcium silicate (belite)	Ca_2SiO_4	$2CaO.SiO_2$	C2S
Tricalcium aluminate	$Ca_3Al_2O_4$	$3CaO.Al_2O_3$	C3A
Tetracalcium aluminoferrite	$Ca_4Al_nFe_{2-n}O_7$	$4CaO.Al_nFe_{2-n}O_3$	C4AF

The composition of cement is varied depending on the application. A typical example of cement contains 5070% C3S, 1530% C2S, 510% C3A, 515% C4AF, and 38% other additives or minerals (such as oxides of calcium and magnesium). It is the hydration of the calcium silicate, aluminate, and aluminoferrite minerals that causes the hardening, or setting, of cement. The ratio of C3S to C2S helps to determine how fast the cement will set, with faster setting occurring with higher C3S contents. Lower C3A content promotes resistance to sulfates. Higher amounts of ferrite lead to slower hydration. The ferrite phase causes the brownish gray color in cements, so that white cements (i.e., those that are low in C4AF) are often used for aesthetic purposes.

The calcium aluminoferrite (C4AF) forms a continuous phase around the other mineral crystallites, as the iron containing species act as a fluxing agent in the rotary kiln during cement production and are the last to solidify around the others. Figure 6.4.2.4.25 shows a typical cement grain.

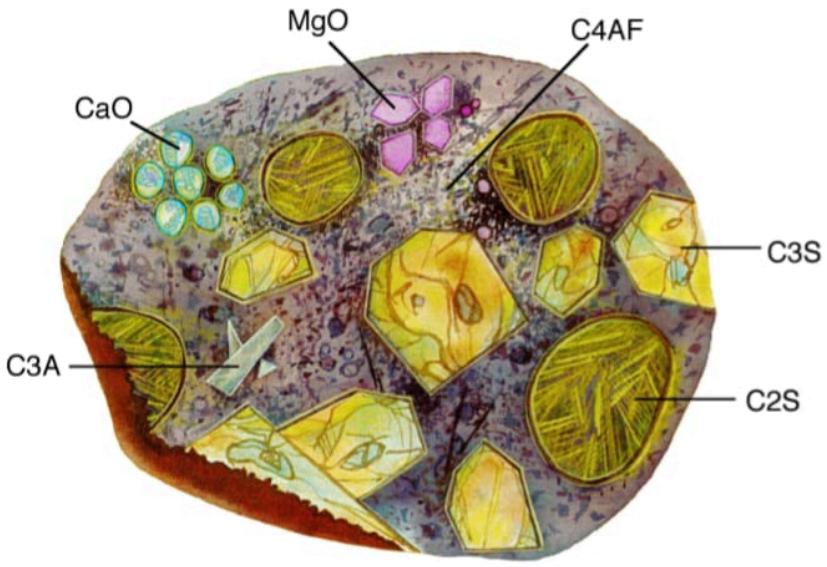


Figure 6.4.2.4.25: A pictorial representation of a cross-section of a cement grain. Adapted from Cement Microscopy, Halliburton Services, Duncan, OK.

It is worth noting that a given cement grain will not have the same size or even necessarily contain all the same minerals as the next grain. The heterogeneity exists not only within a given particle, but extends from grain to grain, batch-to-batch, plant to plant.

Bibliography

- H. F. W. Taylor, *Cement Chemistry*, 2nd Ed., Academic Press, London (1997).

Manufacture of Portland Cement

Portland Cement is manufactured by heating calcium carbonate and clay or shale in a kiln. During this process the calcium carbonate is converted to calcium oxide (also known as lime) and the clay minerals decompose to yield dicalcium silicate (Ca_2SiO_4, C_2S) and other inorganic oxides such as aluminate and ferrite. Further heating melts the aluminate and ferrite phases. The lime reacts with dicalcium silicate to from tricalcium silicate (Ca_3SiO_5, C_3S). As the mixture is cooled, tricalcium aluminate (Ca_3Al2O_6, C_3A) and tetracalcium aluminoferrite ($Ca_4AlnFe_{2-n}O_7$, C_4AF) crystallize from the melt and tricalcium silicate and the remaining dicalcium silicate undergo phase transitions. These four minerals (C_3S, C_2S, C_3A, and C_4AF) comprise the bulk of most cement mixtures. Initially Portland cement production was carried out in a furnace, however, technological developments such as the rotary kiln have enhanced production capabilities and allowed cement to become one of the most widely used construction materials.

Cement plants generally produce various grades of cement by two processes, referred to as either the wet or dry process. The dry process uses a pneumatic kiln system which uses superheated air to convert raw materials to cement, whereas the wet process slurries the raw materials in water in preparation for conversion to cement. Cement manufacturers due to its higher energy efficiency generally favor the dry process, but the wet process tends to produce cement with properties more palatable to the energy services industry. The American Petroleum Institute (API) Class H cement used in energy service applications is produced by the wet process, and thus will be the focus of the following discussion.

The cement manufacturing process begins at the quarry (Figure 6.4.2.4.26), where limestone formations are ripped and crushed in two crushers to a mean particle size of 4". The quarry formation is not entirely limestone, and no attempt is made to isolate the limestone from the other minerals. On the contrary, the rippers act to blend in the impurity minerals as evenly as is feasible while still maintaining an acceptable limestone content so as not to waste the formation. This is accomplished by ripping the formation face at a 45° (Figure 6.4.2.4.27). The rock is quality controlled via mobile X-ray fluorescence (XRF) spectroscopy (Figure 6.4.2.4.28) at the starting point of a mobile covered conveyor belt system (Figure 6.4.2.4.29), which transports the material to a dome storage unit (Figure 6.4.2.4.30).



Figure 6.4.2.4.26: Limestone quarry face in Midlothian, TX (Copyright Halliburton Energy Services).



Figure 6.4.2.4.27: Limestone quarry formation, showing the 45◦ ripping technique (Copyright Halliburton Energy Services).



Figure 6.4.2.4.28: Mobile crusher and XRF unit (Copyright Halliburton Energy Services).



Figure 6.4.2.4.29: Covered conveyor belt for limestone transport (Copyright Halliburton Energy Services).



Figure 6.4.2.4.30: Exterior view of dome storage unit with conveyor loading port (Copyright Halliburton Energy Services).

The dome storage unit has a capacity of 60 kilotons, and is filled by dispensing the rock from the conveyor at the top of the dome into a pile built in a circular pattern (Figure 6.4.2.4.31). The rock is reclaimed from storage via a raking device (Figure 6.4.2.4.32) that grates over the pile at the natural angle of material slide. The raked material slides to the base of the raking unit, where a second conveyor system transfers material to either of two limestone buffer bins (Figure 6.4.2.4.33), each of which is dedicated to a particular kiln process. There is an additional buffer bin for mill scale from a nearby steel plant, as well as a buffer bin for sand. It is worth noting at this point that the mill scale from the steel plant contains significant levels of boron, which acts as an innate retarder and seems to affect adversely, though not overly severely, the early compressive strength development when compared to cement from other plants.

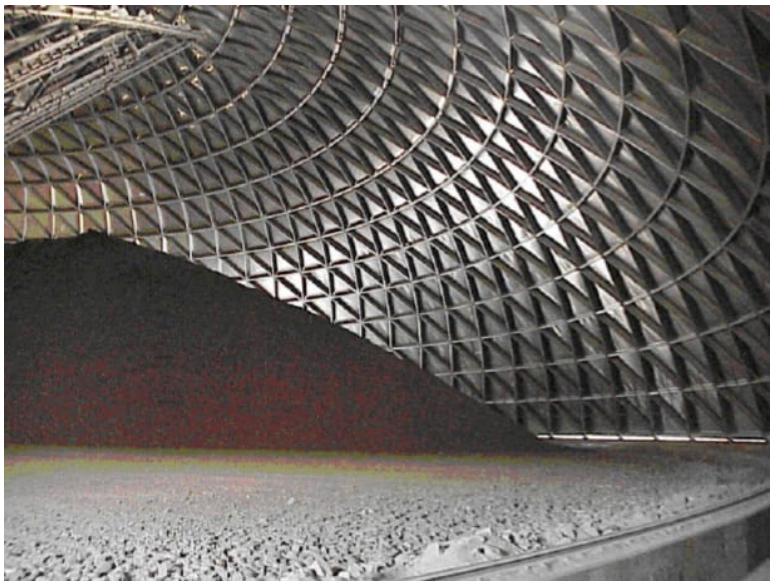


Figure 6.4.2.4.31: Interior view of dome storage unit, illustrating its radial piling (Copyright Halliburton Energy Services).



Figure 6.4.2.4.32: Raking device for reclaiming stored limestone (Copyright Halliburton Energy Services).



Figure 6.4.2.4.33: Buffer bin (Copyright Halliburton Energy Services).

Material leaving the buffer bins is monitored for elemental composition via XRF and feed rates are adjusted for maintaining proper ow of calcium, silicon, aluminum, and iron. The raw materials are carried to ball mills (Figure 6.4.2.4.34) for grinding to ne powder, which is then mixed with water. The resulting slurry is then sent to the rotary kiln for burning (Figure 6.4.2.4.35), or transformation into cement clinker.

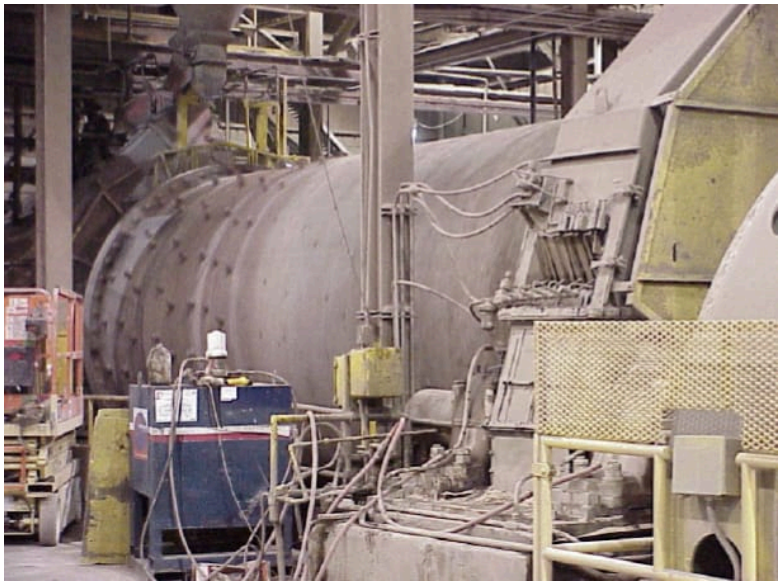


Figure 6.4.2.4.34: Coarse grinder (Copyright Halliburton Energy Services).



Figure 6.4.2.4.35: A wet rotary kiln (Copyright Halliburton Energy Services).

The kilns are red to an internal material temperature of 2700 °F (Figure 6.4.2.4.36) with a fuel of nely ground coal, natural gas, and/or various waste materials. Around fifty percent of the energy expenditure in the wet kiln process is dedicated to evaporating the water from the slurry, in contrast to the dry process, which spends most of its energy on the calcining process. Since the dry process only requires approximately half the energy of the wet process, it is generally more attractive to cement manufacturers. Unfortunately, the dry process in current use produces poor API Class H cement. A fuller understanding of the differences in cement synthesis via the two processes could lead to the development of a more effective dry synthesis of Class H cements, but that is beyond the scope of this work.



Figure 6.4.2.4.36: Interior view of an operational wet kiln (Copyright Halliburton Energy Services).

After the clinker leaves the kiln, it enters a cooler that uses pressurized air to cool the clinker. The energy absorbed by the air in the cooler serves to pre-heat the air for feed into the kiln. The cooled clinker is then taken to storage to await nal grinding with approximately ve percent gypsum by weight. After grinding to the specied fineness, the nal cement powder is pneumatically transferred to storage silos until it is shipped to the customer.

Quality control of the clinker and nal powder is handled via an automated X-ray diffraction/X-ray fluorescence (XRD/XRF) system, simple wet chemical analyses, simple optical microscopy, and periodic performance tests, including compressive strength and thickening time. This entire process results in the heterogeneous nanocomposite of calcium silicate and aluminate particles,

among other materials, which make up a typical cement grain.

Hydration of Portland Cement

The addition of water to dry cement powder results in a thin cement slurry that can be easily manipulated and cast into different shapes. In time, the slurry sets and develops strength through a series of hydration reactions. Hydration of cement is not linear through time, it proceeds very slowly at first, allowing the thin mixture to be properly placed before hardening. The chemical reactions that cause the delay in hardening are not completely understood; however, they are critical to developing a rational methodology for the control of cement setting.

Tri- and di-calcium silicates

The tri- and di-calcium silicates (C_3S and C_2S, respectively) comprise over 80% by weight of most cement. It is known that C_3S is the most important phase in cement for strength development during the first month, while C_2S reacts much more slowly, and contributes to the long-term strength of the cement. Both the silicate phases react with water as shown below to form calcium hydroxide and a rigid calcium-silicate hydrate gel, CSH, (4.2.7) and (4.2.8).

$$2(CaO)_3(SiO_2) + 7H_2O \rightarrow (CaO)_3(SiO_2)_24(H_2O) + 3CA(OH)_2 \tag{6.4.2.8}$$

$$2(CaO)_2(SiO_2) + 5H_2O \rightarrow (CaO)_3(SiO_2)_24(H_2O) + Ca(OH)_2 \tag{6.4.2.9}$$

The detailed structure of CSH is not completely known, however it is generally agreed upon that it consists of condensed silicate tetrahedrally sharing oxygen atoms with a central, calcium hydroxide-like CaO_2 layer. Calcium hydroxide consists of hexagonal layers of octahedrally coordinated calcium atoms and tetrahedrally coordinated oxygen atoms. Taylor has proposed that the structure is most similar to either Tobermorite or Jennite, both of which share a skeletal silicate chain Figure 6.4.2.4.37.

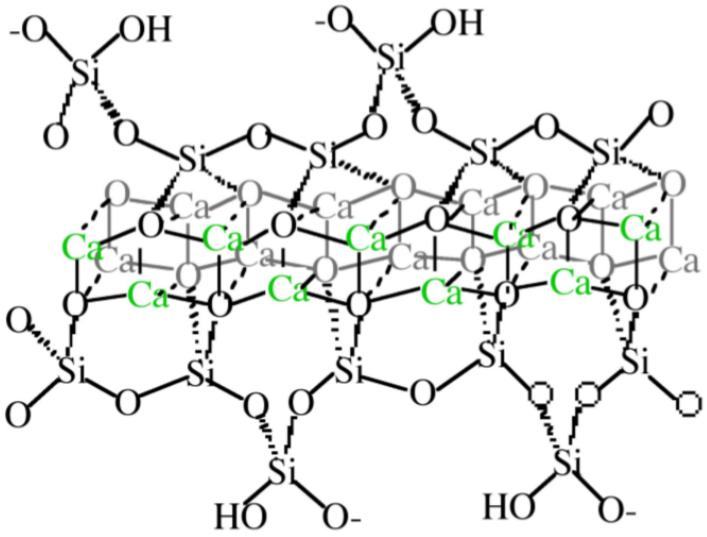


Figure 6.4.2.4.37: Schematic representation of Tobermorite, viewed along a polysilicate chain. Silicate ions either share oxygen atoms with a central CaO_2 core or bridge silicate tetrahedra. Interlayer calcium ions and water molecules are omitted for clarity.

Although the precise mechanism of C3S hydration is unclear, the kinetics of hydration is well known. The hydration of the calcium silicates proceeds via four distinct phases as shown in Figure 6.4.2.4.38. The first 15-20 minutes, termed the pre-induction period (Figure 6.4.2.4.38a), is marked by rapid heat evolution. During this period calcium and hydroxyl ions are released into the solution. The next, and perhaps most important, phase is the induction period (Figure 6.4.2.4.38b), which is characterized by very slow reactivity. During this phase, calcium oxide continues to dissolve producing a pH near 12.5. The chemical reactions that cause the induction period are not precisely known; however, it is clear that some form of an activation barrier must be overcome before hydration can continue. It has been suggested that in pure C3S, the induction period may be the length of time it takes for CSH to begin nucleation, which may be linked to the amount of time required for calcium ions to become supersaturated in solution. Alternatively, the induction period may be caused by the development of a small amount of an impermeable calcium-silicon-hydrate (CSH) gel at the surface of the particles, which slows down the migration of water to the inorganic oxides. The initial Ca/

Si ratio at the surface of the particles is near 3. As calcium ions dissolve out of this CSH gel, the Ca/Si ratio in the gel becomes 0.8-1.5. This change in Ca/Si ratio corresponds to a change in gel permeability, and may indicate an entirely new mechanism for CSH formation. As the initial CSH gel is transformed into the more permeable layer, hydration continues and the induction period gives way to the third phase of hydration, the acceleratory period (Figure 6.4.2.4.38c).

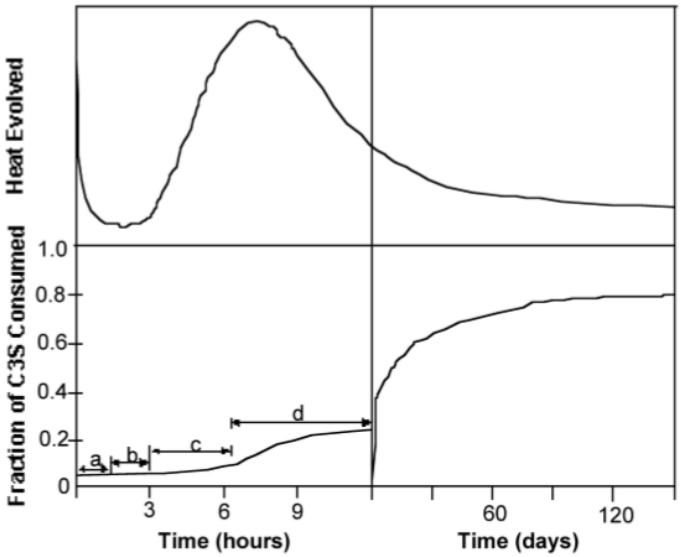


Figure 6.4.2.4.38: Hydration of C3S over time: (a) the preinduction period, (b) the induction, (c) period the acceleratory period, and (d) the deceleratory period.

After ca. 3 hours of hydration, the rate of CSH formation increases with the amount of CSH formed. Solidification of the paste, called setting, occurs near the end of the third period. The fourth stage (Figure 6.4.2.4.38d) is the deceleratory period in which hydration slowly continues hardening the solid cement until the reaction is complete. The rate of hydration in this phase is determined either by the slow migration of water through CSH to the inner, unhydrated regions of the particles, or by the migration of H^+ through the CSH to the anhydrous CaO and SiO_2, and the migration of Ca^{2+} and Si4+ to the OH- ions left in solution.

Calcium aluminate and ferrite

In spite of the fact that the aluminate and ferrite phases comprise less than 20% of the bulk of cement, their reactions are very important in cement and dramatically affect the hydration of the calcium silicate phases, see below. Relative to C3S, the hydration of C3A is very fast. In the absence of any additives, C3A reacts with water to form two intermediate hexagonal phases, C2AH8 and C4AH13, (4.2.9). The structure of C2AH8 is not precisely known, but C4AH13 has a layered structure based on the calcium hydroxide structure, in which one out of every three Ca^{2+} is replaced by either an Al^{3+} or Fe^{3+} with an OH^- anion in the interlayer space to balance the charge. All of the aluminum in C4AH13 is octahedral. C2AH8 and C4AH13 are meta-stable phases that spontaneously transform into the fully hydrated, thermodynamically stable cubic phase, C3AH6, (4.2.10). In C3A, aluminum coordination is tetrahedral. The structure consists of rings of aluminum tetrahedrally linked through bridging oxygen atoms, which slightly distorts the aluminum environment. In C3AH6, aluminum exists as highly symmetrical, octahedral $Al(OH)_6$ units.

$$2(CaO)_3(Al_2O_3) + 21H_2O \rightarrow (CaO)_4(Al_2O_3) \cdot 13(H_2O) + (CaO)_2(Al_2O_3) \cdot 8(H_2O) \tag{6.4.2.10}$$

$$(CaO)_4(Al_2O_3) \cdot 13(H_2O) + (CaO)_2(Al - 2O_3) \cdot 8(H_2O) \rightarrow 2(CaO)_3(Al_2O_3) \cdot 6(H_2O) + 9H_2O \tag{6.4.2.11}$$

If the very rapid and exothermic hydration of C3A is allowed to proceed unhindered in cement, then the setting occurs too quickly and the cement does not develop strength. Therefore, gypsum [calcium sulfate dihydrate, $CaSO_4 \cdot 2(H_2O)$] is added to slow down the C3A hydration. In the presence of gypsum, tricalcium aluminate forms ettringite, $[Ca_3Al(OH)_6.12(H_2O)]_2.(SO_4)_3.2(H_2O)$, (4.2.11), which can also be written as $C3A.3(CaSO_4).32(H_2O)$. Ettringite grows as columns of calcium, aluminum and oxygen surrounded by water and sulfate ions, as shown in Figure 6.4.2.4.39.

$$(CaO)_4(Al_2O_3) + 3CaSO_4 \cdot 2(H_2O) + 26H_2O \rightarrow (CaO)_3(Al_2O_3)(CaSO_4)_3 \cdot 32(H_2O) \tag{6.4.2.12}$$

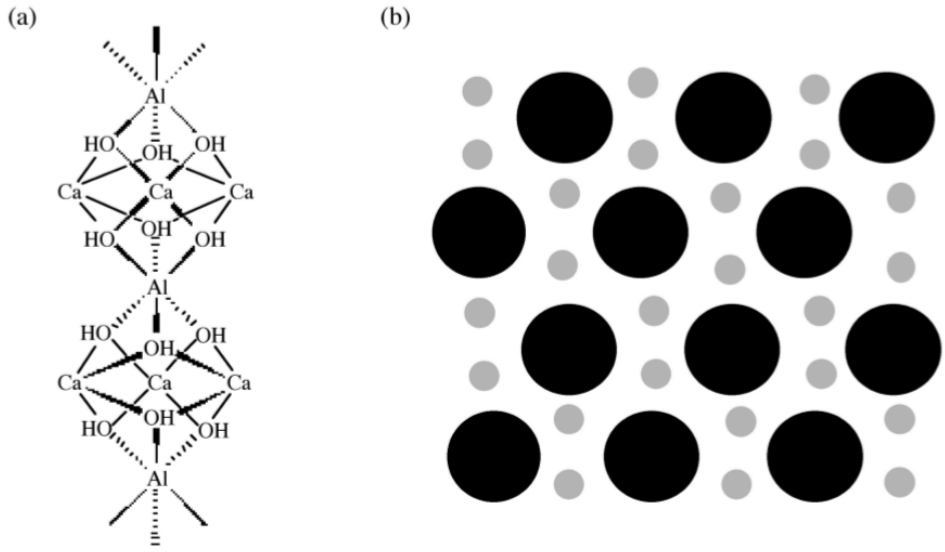


Figure 6.4.2.4.39: Ettringite columns (a) consisting of octahedral aluminum, tetrahedral oxygen, and 8-coordinate calcium. The coordination sphere of each calcium is filled by water and sulfate ions. The packing of the columns (b) represented by large circles, the smaller circles represent channels containing with water and sulfate ions.

Tetracalcium aluminoferrite (C4AF) reacts much like C3A, i.e., forming ettringite in the presence of gypsum. However, hydration the ferrite phase is much slower than hydration of C3A, and water is observed to bead up on the surface of C4AF particles. This may be due to the fact that iron is not as free to migrate in the pastes as aluminum, which may cause the formation of a less permeable iron rich layer at the surface of the C4AF particles and isolated regions of iron hydroxide. In cement, if there is insufficient gypsum to convert all of the C4AF to ettringite, then an iron-rich gel forms at the surface of the silicate particles which is proposed to slow down their hydration.

Portland Cement

The hydration of cement is obviously far more complex than the sum of the hydration reactions of the individual minerals. The typical depiction of a cement grain involves larger silicate particles surrounded by the much smaller C3A and C4AF particles. The setting (hydration) of cement can be broken down into several distinct periods. The more reactive aluminate and ferrite phases react first, and these reactions dramatically affect the hydration of the silicate phase. Scrivener and Pratt used TEM to develop the widely accepted model depicted in Figure 6.4.2.4.40.

In the first few minutes of hydration (Figure 6.4.2.4.40b), the aluminum and iron phases react with gypsum to form an amorphous gel at the surface of the cement grains and short rods of ettringite grow. After this initial period of reactivity, cement hydration slows down and the induction period begins. After about 3 hours of hydration, the induction period ends and the acceleratory period begins. During the period from 3 to 24 hours, about 30% of cement reacts to form calcium hydroxide and CSH. The development of CSH in this period occurs in 2 phases. After ca. 10 hours hydration (Figure 6.4.2.4.40c), C3S has produced outer CSH, which grows out from the ettringite rods rather than directly out from the surface of the C3S particles. Therefore, in the initial phase of the reaction, the silicate ions must migrate through the aluminum and iron rich phase to form the CSH. In the latter part of the acceleratory period, after 18 hours of hydration, C3A continues to react with gypsum, forming longer ettringite rods (Figure 6.4.2.4.40d). This network of ettringite and CSH appears to form a hydrating shell about 1 µm from the surface of anhydrous C3S. A small amount of inner CSH forms inside this shell. After 13 days of hydration, reactions slow down and the deceleratory period begins (Figure 6.4.2.4.40e). C3A reacts with ettringite to form some monosulfate. Inner CSH continues to grow near the C3S surface, narrowing the 1 µm gap between the hydrating shell and anhydrous C3S. The rate of hydration is likely to depend on the diusion rate of water or ions to the anhydrous surface. After 2 weeks hydration (Figure 6.4.2.4.40f), the gap between the hydrating shell and the grain is completely filled with CSH. The original, outer CSH becomes more fibrous.

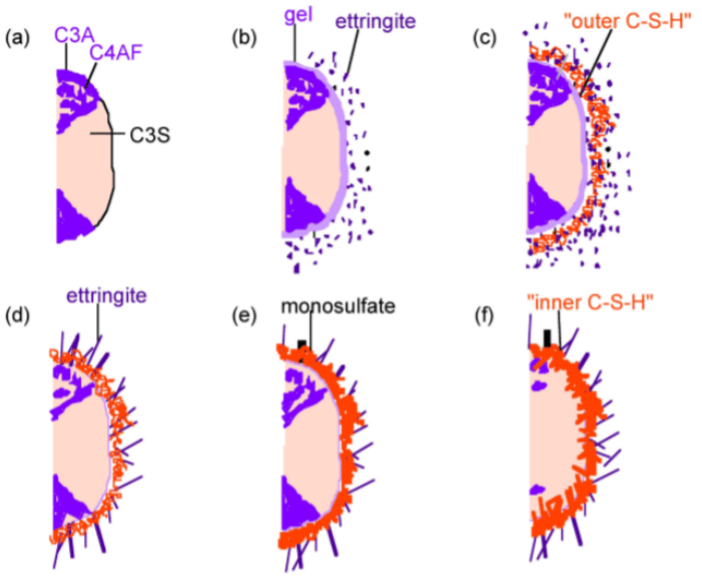


Figure 6.4.2.4.40: Schematic representation of anhydrous cement (a) and the effect of hydration after (b) 10 minutes, (c) 10 hours, (d) 18 hours, (e) 13 days, and (f) 2 weeks. Adapted from M. Bishop, PhD Thesis, Rice University, 2001

Bibliography

- H. F. W. Taylor, *Cement Chemistry*, 2nd Ed., Academic Press, London (1997).
- H. F. W. Taylor, *J. Am. Ceram. Soc.*, 1986, **69**, 464.
- V. S. Ramanchandran, R.F. Feldman, and J. J. Beaudoin, *Concrete Science*, Heyden and Son Ltd., Philadelphia, PA, 1981.
- H. N. Stein and J. Stevels, *J. App. Chem.*, 1964, **14**, 338.
- M. Grutzeck, S. Kwan, J. Thompson, and A. Benesi, *J. Mater. Sci. Lett.*, 1999, **18**, 217.
- V. S. Ramachandran, *Concrete Admixtures Handbook, 2nd Edition, Noyes Publications*, New Jersey (1995).
- K. L. Scrivener and P. L. Pratt, *Mater. Res. Soc. Symp. Proc.*, 1984, **31**, 351.

Hydration Inhibition of Portland Cement

In the oil industry, Portland cement supports boreholes of ever increasing depth. This application requires a high degree of control over the setting kinetics to allow the cement to be pumped down in a liquid form. A number of chemical inhibitors are employed to delay the setting time. The ideal inhibitor for oil well cementing would predictably delay the setting of cement, and then suddenly allow hydration to continue at a rapid rate.

A wide range of compounds show set inhibition of the hydration of Portland cement. Some common examples include, sucrose, tartaric acid, gluconic acid δ-lactone, lignosulfonate, and organic phosphonic acids, in particular nitrilo-tris(methylene)phosphonic acid (H6ntmp). The structures of these retarders are shown in.

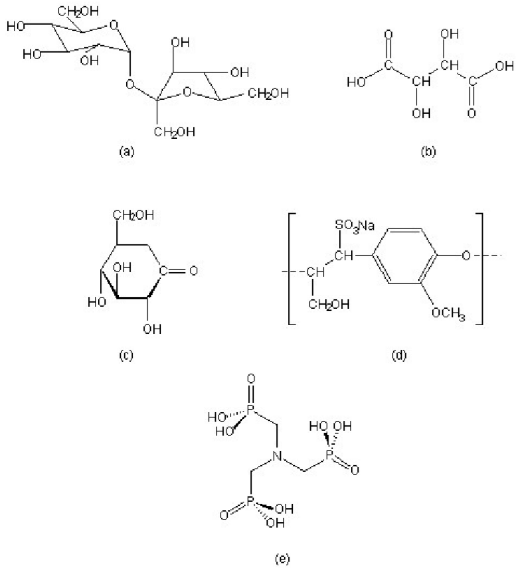


Figure 6.4.2.4.41: Structural formulae of common cement retarders. (a) sucrose, (b) tartaric acid, (c) gluconic acid d-lactone, (d) sodium lignosulfonate, and (e) nitrilo-tris(methylene)phosphonic acid (H6ntmp).

In spite of the fact that the science of cement hydration inhibition has been investigated for over 40 years, the mechanistic details are still the subject of much speculation. There are ve primary models for cement hydration inhibition: calcium complexation, nucleation poisoning, surface adsorption, protective coating/osmotic bursting, and dissolution-precipitation. A summary of the characteristic behavior of selected retarders is shown in Table 6.4.2.4.7.

Table 6.4.2.4.7: Summary of the behavior of various hydration retarders.

Retarder	Characteristic behavior
sucrose	Ca binding, acts directly on silicates, accelerates ettringite formation
tartaric acid	acts via calcium complexation and calcium tartrate coating, inhibits ettringite formation
lignosulfonate	accelerates ettringite formation, calcium becomes incorporated into the polymer matrix during hydration, forms a diffusion barrier
nitrilo-tris(methylene)phosphonic acid (H_6ntmp)	promotes Ca dissolution, forms [Ca(H_6ntmp)], heterogeneous nucleation on aluminates creates a protective coating around the grain

Calcium complexation

Inhibition by calcium complexation relies largely on the requirement that small calcium oxide/hydroxide templates must form in the pore water of cement pastes before silicate tetrahedra can condense into dimeric and oligomeric silicates to form CSH. Calcium complexation involves either removing calcium from solution by forming insoluble salts, or chelating calcium in solution. Calcium complexation lowers the amount of calcium effectively in solution, delaying the time to $Ca(OH)_2$ super-saturation and preventing precipitation of the necessary templates. Simple calcium complexation should dramatically increase the amount of $Si(OH)_4$ tetrahedra in solution, and indeed this is observed with most retarders. However, if the retarder were acting solely by calcium complexation, then one molecule of retarder would be required per calcium ion in solution, and good inhibitors are used in much smaller quantities, on the order of 0.1-2% by weight of cement. In addition, there is no simple correlation between either calcium binding strength or calcium salt solubility and retarding ability. Yet it has been shown that in pure systems, i.e., of C3S and C2S, that the lime concentration in solutions is the most important factor in determining the precipitation of CSH. Therefore, although calcium complexation must play some role in inhibition, other mechanisms of inhibition must be at work as well. An example of a retarder that operates primarily through calcium complexation is tartaric acid, however, the formation of insoluble calcium tartrate on cement grains suggest that dissolution/precipitation occurs in addition (Figure 6.4.2.4.42).

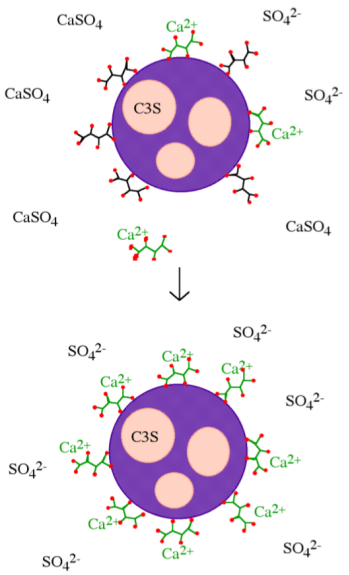


Figure 6.4.2.4.42: Schematic representation of cement hydration in the presence of tartaric acid. The aluminate (and aluminate ferrate) phases (shown in purple) surround the silicate phases (C3S and C2S). Tartaric acid adsorbs onto the aluminum surfaces and reacts with calcium ions from gypsum to deposit a thick calcium tartrate coating on the cement grain. Adapted from M. Bishop, PhD Thesis, Rice University, 2001.

Nucleation poisoning

As with calcium complexation, nucleation poisoning must rely on the formation of small calcium oxide/hydroxide templates in the pore water of cement pastes before silicate tetrahedra can condense into dimeric and oligomeric silicates to form CSH. Inhibition by nucleation poisoning is where the retarder blocks the growth of CSH or $Ca(OH)_2$ crystals through inhibiting agglomerates of calcium ions from forming the necessary hexagonal pattern. Nucleation inhibitors act on the surface of small clusters, therefore, less than one molecule of retarder per calcium ion is required to produce dramatic results. This type of inhibition also results in an increase in the amount of silicate ions in solution, as condensation of silicate chains onto calcium oxide templates to form the CSH is inhibited. As a retarder sucrose acts via nucleation poisoning/surface adsorption.

Surface adsorption

Surface adsorption of inhibitors directly onto the surface of either the anhydrous or (more likely) the partially hydrated mineral surfaces blocks future reactions with water. In addition, if such inhibitors are large and anionic, then they produce a negative charge at the surface of the cement grains, causing the grains to repel each other thereby reducing inter-particle interactions. Lignosulfonates are typical of retarders that act via surface adsorption.

Protective coating/osmotic bursting

The formation of a protective coating with its subsequent bursting due to the build up of osmotic pressure was originally posited to explain the existence of the induction period in C3S and cement hydration, however it may be applied to inhibition in general. In this mechanism, a semi-permeable layer at the surface of the cement grain forms and slows down the migration of water and lengthens the induction period. Osmosis will drive water through the semi-permeable membrane towards the unhydrated mineral, and eventually the ow of water creates higher pressure inside the protective coating and the layer bursts. Hydration is then allowed to continue at a normal rate.

Dissolution-precipitation

A detailed study of several retarders (in particular the organic phophonates) has shown that the actually accelerate certain stages of the hydration process. This is unexpected since the phosphonates have been termed super retarders, due to their increased effect on cement hydration relative to the effect of conventional retarders. So how is it that a retarder can be so efficient at hydration inhibition at the same time as accelerating the process? The ability of phosphonates to retard cement setting is due to the lengthening the induction period, without slowing down the time it takes for setting to occur (once the acceleratory period has begun).

Phosphonates are known to complex calcium and other M^{2+} cations, poison the nucleation and growth of barium sulfate crystals, and inhibit the hydration of Fe_2O_3 and Al_2O_3 surfaces via direct surface adsorption, thus it was assumed that with regard to cement hydration inhibition occurred by one of these mechanism. However, the mechanism by which phosphonates inhibit cement hydration consists of two steps. First dissolution, whereby calcium is extracted from the surface of the cement grains (Figure 6.4.2.4.43a) exposing the aluminum rich surface to enhanced (catalyzes) hydration and ettringite formation (Figure 6.4.2.4 .43b). Second precipitation, whereby the soluble calcium-phosphonate oligomerizes either in solution or on the hydrate surface to form an insoluble polymeric Ca-phosphonate (Figure 6.4.2.4.43c). The Ca-phosphonate material binds to the surface of the cement grains inhibiting further hydration by acting as a diffusion barrier to water as well as a nucleation inhibitor.

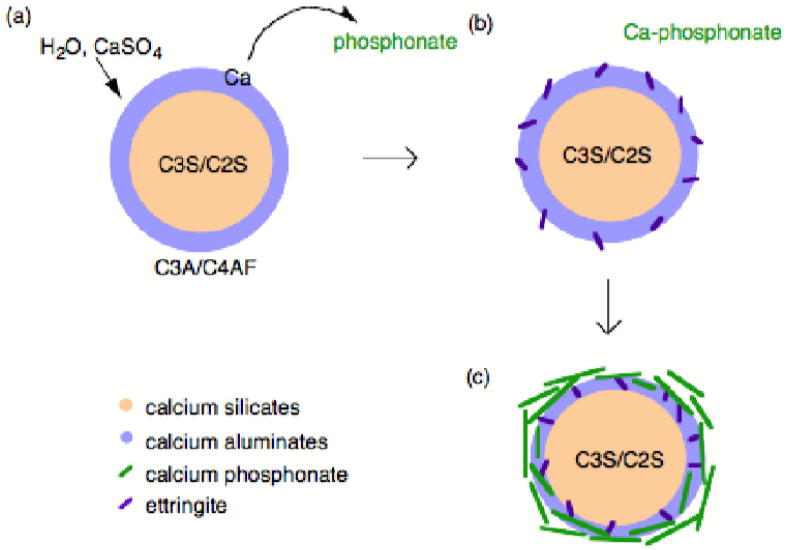


Figure 6.4.2.4.43: Schematic representation of the H6ntmp inhibition of cement showing (a) the phosphonic acid promoting calcium dissolution, allowing water and gypsum to react with the aluminum phases at the surface of the cement grain, (b) the formation of a meta-stable calcium phosphonate, which precipitates onto the hydrating aluminate surfaces (c), forming a barrier to water and sulfate diffusion. Adapted from M. Bishop, PhD Thesis, Rice University, 2001.

Bibliography

- N. Thomas and J. Birchall, *Cement and Concrete Research*, 1983, **13**, 830.
- D. Double, *Phil. Trans. R. Soc. London*, 1983, **A30**, 53.
- M. Bishop, S. G. Bott, and A. R. Barron, *Chem. Mater.*, 2003, **15**, 3074.
- M. Bishop and A. R. Barron, *Ind. Eng. Chem. Res.*, 2006, **45**, 7042.

This page titled 6.4.2: Calcium the Archetypal Alkaline Earth Metal is shared under a CC BY 3.0 license and was authored, remixed, and/or curated by Andrew R. Barron (CNX) via source content that was edited to the style and standards of the LibreTexts platform.

6.4.3: Differences for Beryllium and Magnesium

While the chemistry of strontium, barium (and radium) is similar to that of calcium, magnesium and beryllium show marked differences. In both cases these differences are due to the small size of the ions.

Beryllium

Beryllium can be thought of as being even more covalent than magnesium. The small size (ca. 0.3 Å) results in a very high charge density of Be^{2+}. In addition, the ionization energy for beryllium is a large positive value (1st ionization energy = 899.5 kJ/mol, 2nd ionization energy = 14,848.7 kJ/mol). Both of these factors means that the free ion does not exist. Instead, beryllium forms covalent compounds in a similar manner to its diagonal analog aluminum. Both beryllium and aluminum form covalent compounds or strongly solvated cations, and both form polymeric hydrides, chlorides, and alkyls.

Beryllium chloride is not a lattice structure with a concomitantly high melting and boiling point as observed for the other Group 2 metals (Table4.8). Instead $BeCl_2$ is a polymer in the solid state (Figure 6.4.3.4.44a), and an equilibrium between a monomer (Figure 6.4.3.4.44b) and dimer (Figure 6.4.3.4.44c) in the vapor phase.

Table 6.4.3.4.8: Summary of structures for alkaline earth chlorides (MCl_2).

M	Structure
Be	Polymer (4-coordinate Be)
Mg	Cadmium chloride structure (6-coordinate Mg)
Ca	Deformed rutile structure (6-coordinate Ca)
Ca	Deformed rutile structure (6-coordinate Sr)
Ba	$PbCl_2$ structure (9-coordinate Ba) or fluorite structure (8-coordinate Ba)

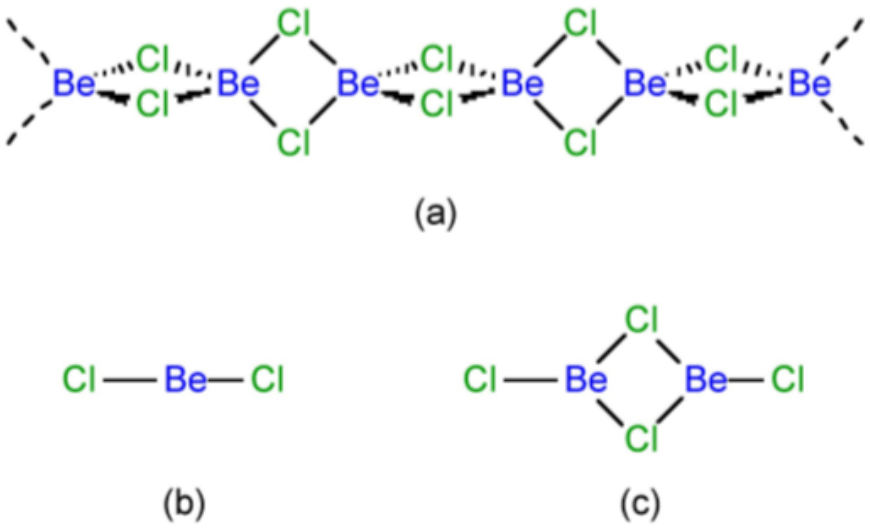


Figure 6.4.3.4.44: Structures of $BeCl_2$.

Magnesium

The ionic radius for the +2 cation of magnesium is fairly small (0.65 Å). As a consequence the charge density (z/r) is high, which results in a high polarizing power of the Mg^{2+} ion. Thus, magnesium tends to form polar covalent bonds rather than ionic

complexes. As with lithium there is a wide range of organometallic derivatives of magnesium, especially the Grignards (RMgX, where X = Cl, Br).

A further consequence of the covalent character of the bonding is that magnesium tends to form either 4-coordinate (tetrahedral) or 6-coordinate (octahedral) complexes with well-defined geometries.

This page titled 6.4.3: Differences for Beryllium and Magnesium is shared under a CC BY 3.0 license and was authored, remixed, and/or curated by Andrew R. Barron (CNX) via source content that was edited to the style and standards of the LibreTexts platform.

6.4.4: Organometallic Compounds of Magnesium

While beryllium makes a range of organometallic compounds, their hazardous nature has limited their study. In contrast, the ionic nature of calcium, strontium, and barium compounds limits the number of stable organometallic derivatives. However, the organometallic chemistry of magnesium is rich and extensive. The importance of Grignards (RMgX, where X = halide) and dialkyl magnesium compounds (R_2Mg) is due to their use in organic synthesis and as synthons for a range of organometallic compounds.

Grignard reagents

Grignard reagents (and the Grignard reaction using these compounds) are named after Victor Grignard (Figure 6.4.4.4.45). After studying mathematics at Lyon he transferred to chemistry, becoming a professor at the University of Nancy in 1910. During World War I, he was involved in the eld of chemical warfare; however, it is for his major contribution to organic chemistry he is remembered.



Figure 6.4.4.4.45: French chemist and Nobel Prize winner François Auguste Victor Grignard (1871 1935).

Preparation

The general the synthesis of a Grignard reagent involves the reaction of an alkyl halide (RX, where X = Cl, Br, I) with magnesium metal in a suitable ether solvent, (4.4.1).

$$RX + Mg \rightarrow RMgX \tag{6.4.4.1}$$

While diethyl ether (Et_2O) and tetrahydrofuran (THF) are commonly used as solvents, other polar nonprotic solvents are suitable, including: triethylamine (NEt_3), dimethylsulphide (Me_2S), dimethylselenide (Me_2Se), and dimethyltelluride (Me_2Te).

In general the alkyl halide is added to an excess of magnesium suspended in the solvent. In most cases it is necessary to activate the magnesium, by the addition of iodine (I_2), 1,2-dibromoethane, or sonication. If the halide is very inert reaction can be promoted by the co-condensation of magnesium and THF under vacuum.

There is often an induction period after the initial addition of alkyl halide. However, since the reaction, (4.4.1), is highly exothermic care should be taken to ensure that the reaction does not run-away. For this reason it is normal to initially add a small quantity of the alkyl halide to ensure the reaction initiates. Once reaction is initiated, the addition of alkyl halide is maintained at a suitable rate to ensure the reaction is maintained until all the alkyl halide is consumed. The excess reaction magnesium is removed from the reaction mixture by filtration.

It is not always necessary to use a liquid or solid halide dissolved in the solvent. Bubbling methyl chloride (MeCl) through an Et_2O suspension of magnesium yields MeMgCl. The advantage of a gaseous alkyl halide is that the reaction is very clean as all the magnesium is consumed and the excess alkyl halide is bubbled away.

The purity of the magnesium is very important. For his original experiments Grignard used magnesium of a purity of 99.2%. However, it is now more typical to use 99.8% pure magnesium. It is important that the magnesium not be too pure since it is thought that the transition metal impurities catalyze the reaction.

The relative order of reactivity of the alkyl halide follows the trend:

$$I > Br > Cl > F \tag{6.4.4.2}$$

In fact alkyl uorides are suciently inert that highly coordinating polar solvents such as THF or dimethylformamide (DMF) must be used.

If the reaction is allowed to get too hot then several possible side reactions can occur. In THF reaction with the solvent occurs:

$$RMgX + THF \rightarrow RH + H_2C = CH_2 + H_2C = C(H)MgX \tag{6.4.4.3}$$

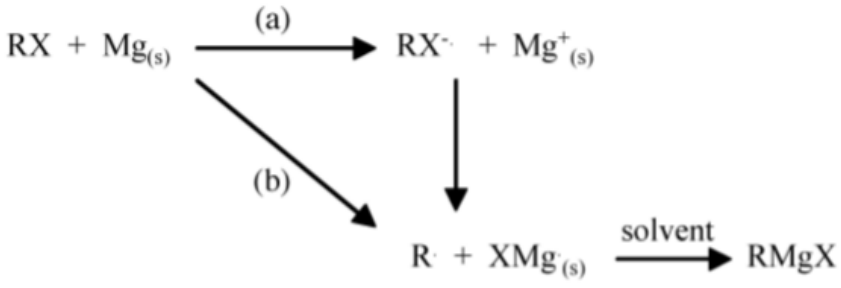
Alternatively, a transition metal catalyzed radical coupling between the Grignard and unreacted alkyl halide is observed irrespective of the identity of the solvent, (4.4.4).

$$RMgX + RX \rightarrow R - R + MgX_2 \tag{6.4.4.4}$$

The mechanism for Grignard formation is thought to be radical in nature; however, a study of the surface of the magnesium during the reaction has shown the presence of corrosion pits. It is generally agreed that initiation occurs at surface dislocations, but the major reaction occurs at a polished surface.

The kinetics of the reaction is 1st order with respect to the alkyl halide concentration, but it has also been claimed to be 1st order with respect to the solvent concentration. It has therefore been concluded that the rate-determining step involves the metal solvent interface.

The reaction of magnesium with aryl bromides has been studied and is proposed to occur by two reactions. The first involves electron transfer between the aryl halide and the metal, while the second involves aryl radical formation.



(4.28)

A number of alternative synthetic routes are used with polyhalogenated hydrocarbons, (4.4.5) and (4.4.6), and where the alkyl radical is unstable, (4.4.7).

$$X_3CH + {}^{i}PrMgX \rightarrow (X_3C)MgX + {}^{i}PrH \tag{6.4.4.5}$$

$$C_6Br_6 + EtMgX \rightarrow (C_6Br_5)MgX + EtBr \tag{6.4.4.6}$$

$$RX + R'MgX' \rightarrow RMgX' + R'X \tag{6.4.4.7}$$

Structure

The solid state structure of Grignard reagents is controlled by the presence and identity of the solvent used in the synthesis. In this regard the size and the basicity of the solvent is important. For example, the structure of EtMgBr crystallized from diethyl

ether exists as a 4-ccordinate monomer (Figure 6.4.4.4.46a), while the use of the sterically less demanding THF results in a 5-coordinate monomeric structure (Figure 6.4.4.4.46b). In contrast, the use of triethylamine yields a dimeric bromide bridged structure (Figure 6.4.4.4.46c), and the use of a chelate bidentate amine gives a structure (Figure 6.4.4.4.46d) similar to that observed with diethyl ether (Figure 6.4.4.4.46a).

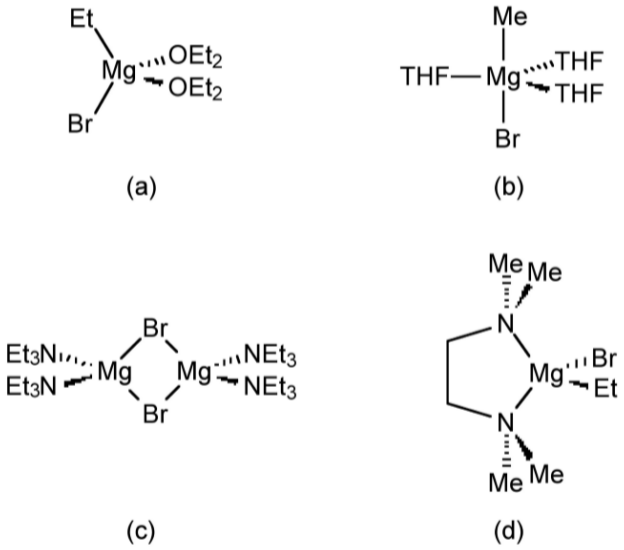


Figure 6.4.4.4.46: Molecular structure of EtMgBr in (a) diethyl ether, (b) THF, (c) triethyl amine, and (d) tetramethyletheylenediamine (TMED).

In solution, Grignards are fluxional such that no single defined structure is present. The series of exchange reactions are known as an extended Schlenk equilibrium (Figure 6.4.4.4.47).

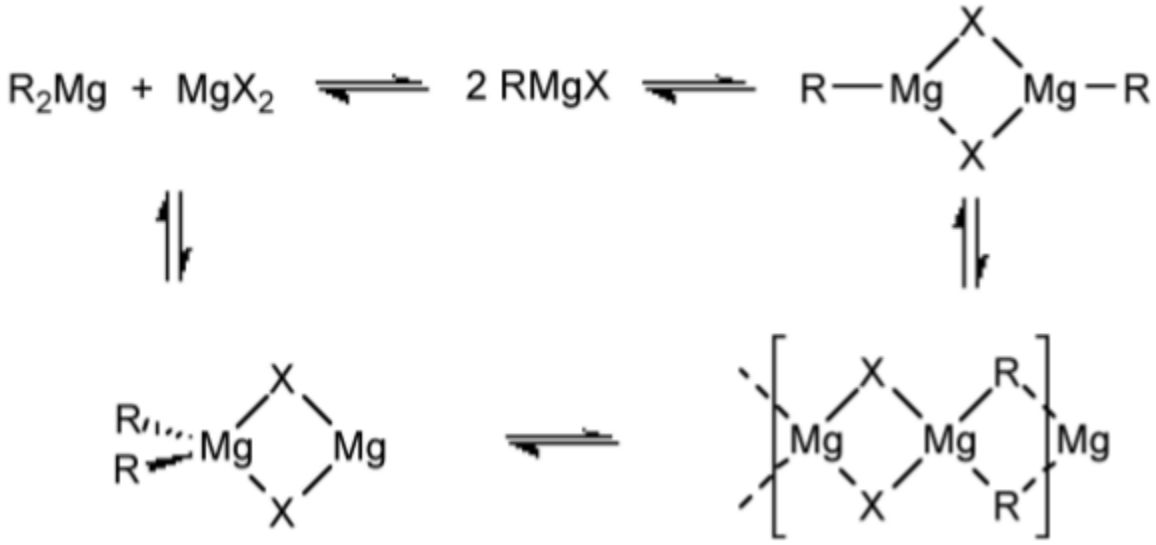


Figure 6.4.4.4.47: Schematic representation of the extended Schlenk equilibrium observed for Grignard compounds in solution.

It is observed that Grignard solutions are also slightly conducting, and magnesium is deposited at both the anode and cathode suggesting the formation of RMg^{+} and $[RMgX_2]^{-}$. The alkyl/halide exchange is thought to occur through a bridging intermediate (Figure 6.4.4.4.48).

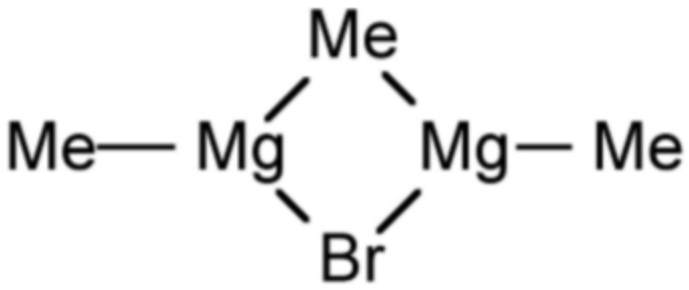


Figure 6.4.4.4.48: Proposed structure for the alkyl/halide exchange bridging intermediate.

Dialkyl magnesium (R_2Mg)

Dialkyl magnesium compounds are involatile white solids. They generally have similar reactivity to their Grignard analogs.

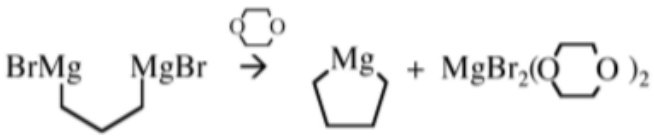
Synthesis

The most common synthesis of R2Mg is by the reaction of a Grignard with dioxane ($C_4H_8O_2$), (4.32), where the precipitation of the dihalide is the reaction driving force.



(4.32)

This method is useful for the synthesis of cyclic compounds, (4.33).



(4.33)

An alternative synthesis that does not require dioxane involves the metal exchange reaction between magnesium metal and a dialkyl mercury compound.

$$R_2Hg + Mg \rightarrow R_2Mg + Hg \tag{6.4.4.8}$$

Finally, in selected cases, magnesium will react with acidic hydrocarbons such as cyclopentadienyl at high temperatures (600 °C).

Structure

In the vapor phase dialkyl magnesium compounds are generally monomeric linear compounds. In solution, in the absence of coordinating solvents R_2Mg form a variety of oligomers (Figure 6.4.4.4.49a-c) in solution as determined by molecular weight measurements. In the presence of coordinating solvents 4-coordinate monomers predominate (Figure 6.4.4.4.49d).

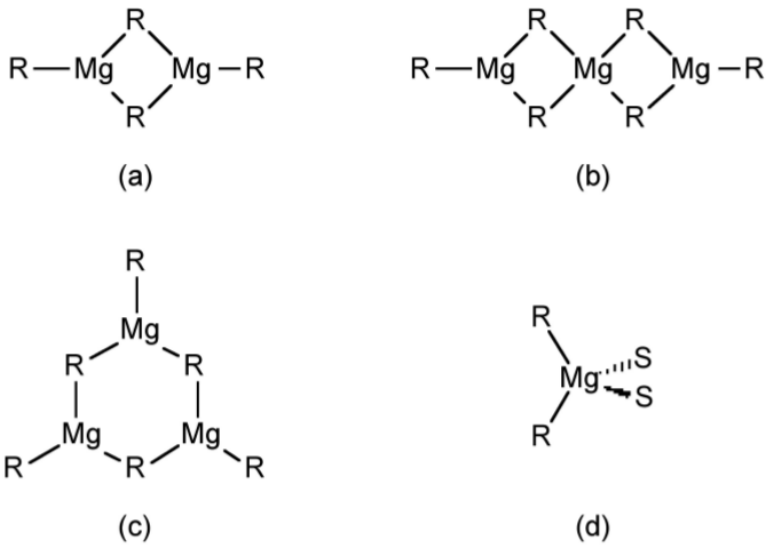


Figure 6.4.4.4.49: Solution structure of R_2Mg (R = Me, Et) in (a c) non-coordinating solvents, and (d) diethyl ether.

As similar trend is observed in the solid state, where polymers have been characterized in the absence of coordinating solvents (Figure 6.4.4.4.50a), while monomers or dimmers are generally observed when crystallized from a coordinating solvent (Figure 6.4.4.4.50b and c).

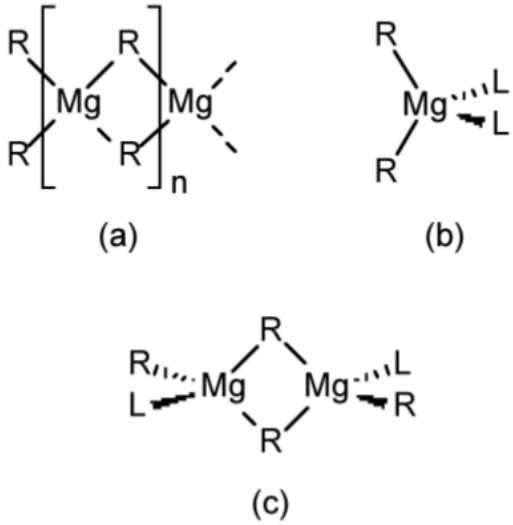


Figure 6.4.4.4.50: Solid state structure of R2Mg (R = Me, Et) crystallized in (a) the absence and (b and c) the presence of a coordinating solvents.

The use of organomagnesium compounds in organic synthesis

Hydrolysis and related reactions

Grignard compounds react with water to give the hydrocarbon, (4.4.9), they also react with other hydroxylic compounds such as alcohols and carboxylic acids. One important use of the hydrolysis reaction is specifically deuteration, (4.4.10).

$$CH_3MgBr + H_2O \rightarrow CH_4 + BrMgOH \tag{6.4.4.9}$$

$$CH_3CH_2(CH_3)_2CMgBr + D_2O \rightarrow CH_3CH_2(CH_3)_2CD + BrMgOD \tag{6.4.4.10}$$

The hydrogen atom on a terminal alkyne is suciently acidic that the reaction with Grignards occurs in an analogous manner to that of hydrolysis.

$$C_6H_5C=CH+C_2H_5MgBr \rightarrow C_6H_5C=CMgBr+C_2H_6 \tag{6.4.4.11}$$

Once formed the alkynyl Grignard undergoes the same hydrolysis reaction.

$$C_6H_5C=CMgBr+D_2O \rightarrow C_6H_5C=CD+BrMgOD \tag{6.4.4.12}$$

Reaction with CO_2

Grignards react readily with carbon dioxide to form the carboxylate, which yields the associated carboxylic acid upon hydrolysis, (4.4.13).

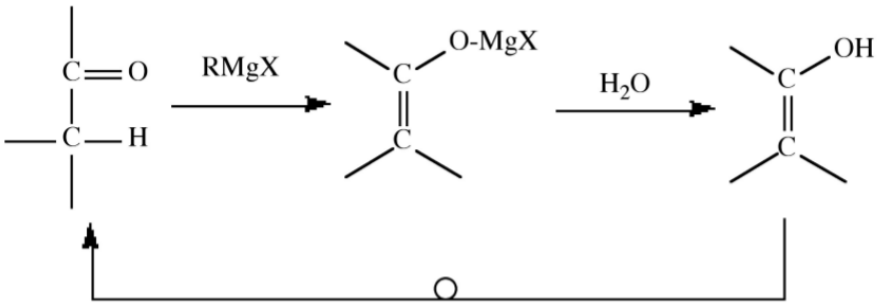
$$RMgX+CO_2 \rightarrow RCO_2MgX \xrightarrow{H_2O} RCO_2H+HOMgX \tag{6.4.4.13}$$

Reaction with carbonyls

Organomagnesium compounds react with organic carbonyls (aldehydes, ketones, and esters) to yield the alcohol on hydrolysis, (4.4.14). This synthetic route is useful for the formation of primary, secondary and terminal alcohols.

$$RMgX+R'_2C=O \rightarrow R'_2(R)COMgX \xrightarrow{H_2O} R'_2(R)COH+HOMgX \tag{6.4.4.14}$$

Unfortunately, for some carbonyls there is a competing side reaction of enolization, where the starting ketone is reformed upon hydrolysis.



(4.41)

When the Grignard reagent has a β-hydrogen another side reaction occurs in which the carbonyl group is reduced and an alkene is formed.

$$R_2C=O+(CH_3CH_2)MgX \rightarrow R_2(H)COH+H_2C=CH_2 \tag{6.4.4.15}$$

Both the enolization and reduction occur via similar 6-membered cyclic transition states (Figure 6.4.4.4.51).

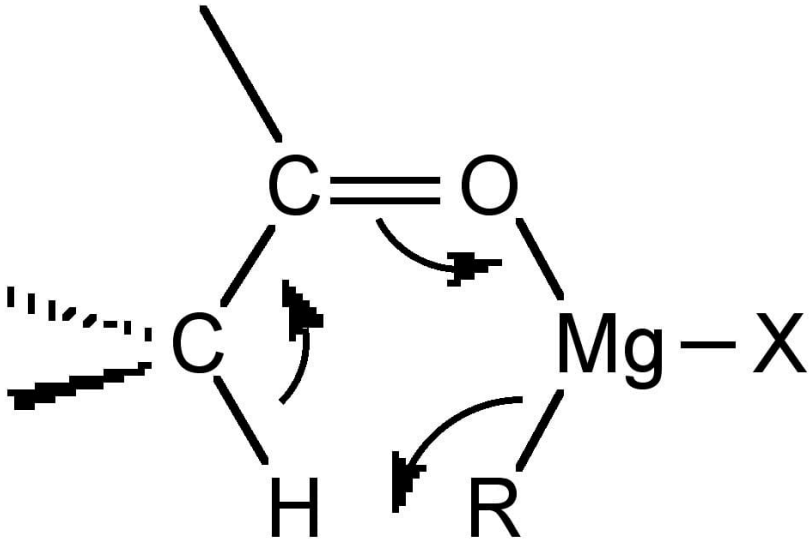


Figure 6.4.4.4.51: Representation of the 6-membered transition state reaction for enolization of a ketone.

Grignards react with α,β-unsaturated ketones to give either the 1,2-addition product or the 1,4-addition product, or both.

$$\mathrm{Ph(H)C{=}C(H)\text{-}C(O)Me + EtMgBr \xrightarrow{H_2O} Ph(H)C{=}C(H)\text{-}C(OH)EtMe + Ph(H)EtC\text{-}CH_2\text{-}C(O)Me} \tag{6.4.4.16}$$

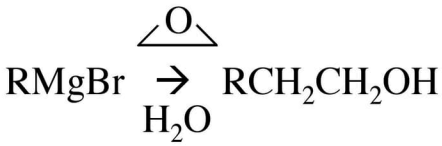
Reaction with acyl halides

Acyl halides react with Grignards to give ketones (4.4.16). Best results are obtained if the reaction is carried out at low temperature and in the presence of a Lewis acid catalysts (e.g., ($FeCl_3$).

$$\mathrm{CH_3C(O)Cl + RMgX \rightarrow CH_3C(O)R + XMgCl} \tag{6.4.4.17}$$

Reaction with epoxides

Oxirane (epoxide) rings are opened by Grignards in a useful reaction that extends the carbon chain of the Grignard by two carbon atoms. This reaction is best performed with ethylene oxide since the magnesium halide formed is a Lewis acid catalyst for further reactions in the case of substituted oxiranes.



Reaction with salts

One of the most useful methods of preparing organometallic compounds is the exchange reaction of one organometallic compound with a salt of a different metal, Equation. This is an equilibrium process, whose equilibrium constant is defined by the reduction potential of both metals. In general the reaction will proceed so that the more electropositive metal will form the more ionic salt (usually chloride).

$$\mathrm{RM + M'X \leftrightharpoons RM' + MX} \tag{6.4.4.18}$$

Grignard reagents are particularly useful in this regard, and may be used to prepare a wide range of organometallic compounds. For example:

$$\mathrm{2\ CH_3CH_2MgCl + CdCl_2 \rightarrow Cd(CH_2CH_3)_2 + 2\ MgCl_2} \tag{6.4.4.19}$$

$$4\ CH_3MgCl + SiCl_4 \rightarrow Si(CH_3)_4 + 4\ MgCl_2 \tag{6.4.4.20}$$

The reaction with a Grignard is milder than the analogous reaction with lithium reagents, and leads to a lower incident of side-products.

Bibliography

- H. Bader and N. M. Smyth, *J. Org. Chem.*, 1964, **29**, 953.
- C. L. Hill, J. B. Vander Sande, G. M. Whitesides, *J. Org. Chem.*, 1980, **45**, 1020.
- E. Weiss, *J. Organomet. Chem.*, 1964, **2**, 314.
- A. R. Barron, *J. Chem. Soc., Dalton Trans.*, 1989, 1625.

This page titled 6.4.4: Organometallic Compounds of Magnesium is shared under a CC BY 3.0 license and was authored, remixed, and/or curated by Andrew R. Barron (CNX) via source content that was edited to the style and standards of the LibreTexts platform.

6.5: Group 12

This page titled 6.5: Group 12 is shared under a CC BY 3.0 license and was authored, remixed, and/or curated by Andrew R. Barron (CNX) via source content that was edited to the style and standards of the LibreTexts platform.

6.5.1: The Group 12 Elements

Although the Group 12 metals (Table 6.5.1.1) are formally part of the d-block elements from their position in the Periodic Table, their electronic configuration in both their elemental form ($d^{10}s^2$) and the vast majority of their compounds (d^{10}) is that of the main group elements. The common oxidation state for all the Group 12 elements is +2, and the chemistry of zinc and cadmium compounds in particular is very similar to the analogous magnesium derivatives.

Note

The IUPAC (International Union of Pure and Applied Chemistry) definition of a transition metal (or transition element) states that a transition metal is "an element whose atom has an incomplete *d* sub-shell, or which can give rise to cations with an incomplete *d* sub-shell." Thus, Group 12 elements are not transition metals.

Element	Symbol	Name
Zinc	Zn	From German *zinke*, meaning *tooth-like, pointed or jagged* (metallic zinc crystals have a needle-like appearance), or meaning *tin-like* because of its relation to German word *zinn* meaning *tin*, or from Persian *seng* meaning *stone*.
Cadmium	Cd	From the Latin *cadmia*, meaning *calamine*
Mercury	Hg	From the Latin *hydrargyrum*, meaning *watery* or *liquid silver*

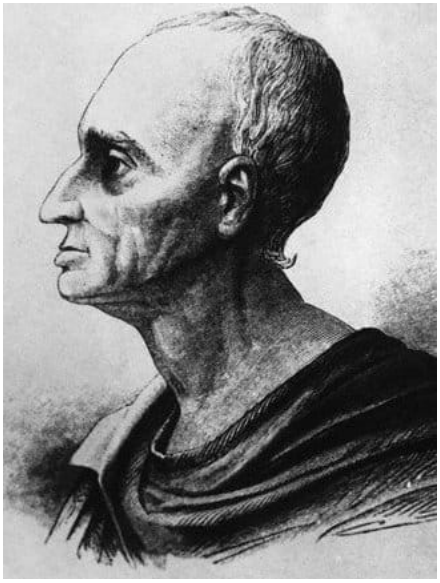
Table 6.5.1.1**:** Derivation of the names of the Group 12 metals.

Discovery

Zinc

Artifacts with a high zinc content (as much as 90%) have been fond to be over 2500 years old, and possibly older. As such it is clear that several cultures had the knowledge of working with zinc alloys, in particular brass (a zinc/copper alloy). Zinc mines at Zawar, near Udaipur in India, have been active since the late 1st millennium BC. However, the smelting of metallic zinc appears to have begun around the 12th century AD.

The isolation of purified metallic zinc was reported concurrently by several people. The extraction of zinc from its oxide (ZnO) was reported as early as 1668, while John Lane is supposed to have smelted zinc in 1726. The first Patent for zinc smelting was granted to English metallurgist William Champion in 1738; however, the credit for discovering pure metallic zinc is often given to Andreas Marggraf in 1746.



Engraving of German chemist Andreas Sigismund Marggraf (1709 –1782).

Cadmium

Cadmium was discovered in 1817 by Friedrich Stromeyer as an impurity in calamine (zinc carbonate, $ZnCO_3$). Stromeyer observed that impure samples of calamine changed color when heated but pure calamine did not. Eventually he was able to isolate cadmium metal by roasting and reduction of the sulfide.



German chemist Friedrich Stromeyer (1776 - 1835).

Mercury

Mercury was known to the ancient Chinese and was found in Egyptian tombs that date from 1500 BC. In China and Tibet, mercury use was thought to prolong life, heal fractures, and maintain generally good health. The ancient Greeks used mercury in ointments; the ancient Egyptians and the Romans used it in cosmetics that sometimes deformed the face.

Abundance

The Group 12 elements mainly occur in sulfide ores, however, as with their Group 2 analogs, carbonate are known, but not as economically viable. The major zinc containing ore is zinc blende (also known as sphalerite), which is zinc sulfide (ZnS). Other important ores include, wurtzite (ZnS), smithsonite (zinc carbonate, $ZnCO_3$), and hemimorphite (calamine, Zn_2SiO_4). The basic

form of zinc carbonate (hydrozincite, $Zn_5(CO_3)_2(OH)_6$) is also mined where economically viable. The main source of cadmium is as an impurity in zinc blende; however, there are several other ores known, e.g., cadmoselite (cadmium selenide, CdSe) and otavite ($CdCO_3$). Mercury sulfide (cinnabar, HgS) is the major source of mercury, and in fact metallic liquid mercury droplets are often found in the ore. The terrestrial abundance of the Group 12 elements is given in Table 6.5.1.2.

Element	Terrestrial abundance (ppm)
Zn	75 (Earth's crust), 64 (soil), 30 x 10^{-6} (sea water)
Cd	0.1 (Earth's crust), 1 (soil), 1 x 10^{-6} (sea water)
Hg	50 x 10^{-6} (Earth's crust), 2 x 10^{-8} (soil), 40 x 10^{-12} (sea water)

Table 6.5.1.2**:** Abundance of Group 12 elements.

Isotopes

The naturally abundant isotopes of the Group 12 metals are listed in Table 6.5.1.3.

Isotope	Natural abundance (%)
Zinc-64	48.6
Zinc-66	27.9
Zinc-67	4.1
Zinc-68	18.8
Zinc-70	0.6
Cadmium-106 *	1.25
Cadmium-108 *	0.89
Cadmium-110	12.49
Cadmium-111	12.8
Cadmium-112	24.13
Cadmium-113 *	12.22
Cadmium-114 *	28.73
Cadmium-116 *	7.49
Mercury-196	0.15
Mercury-198	9.97
Mercury-199	16.87
Mercury-200	23.1
Mercury-201	13.18
Mercury-202	29.86
Mercury-204	6.87

Table 6.5.1.3**:** Abundance of the major (non-synthetic) isotopes of the Group 12 metals. Isotopes labeled with * are radioactive.

Many radioisotopes of zinc have been characterized. Zinc-65 that has a half-life of 244 days, is the most long-lived isotope,

followed by ^{72}Zn with a half-life of 46.5 hours. The most common decay mode of an isotope of zinc with a mass number lower than 64 is electron capture, producing an isotope of copper, (Equation 5.1.1).

$$^{30}_{n}\mathrm{Zn} + \mathrm{e}^{-} \rightarrow ^{29}_{n}\mathrm{Cu} \tag{6.5.1.1}$$

T he most common decay mode of an isotope of zinc with mass number higher than 64 is beta decay (β–), which produces an isotope of gallium, (Equation 5.1.2).

$$^{30}_{n}\mathrm{Zn} \rightarrow ^{31}_{n}\mathrm{Ga} + \mathrm{e}^{-} + \nu_{e} \tag{6.5.1.2}$$

Naturally occurring cadmium is composed of 8 isotopes. For two of them, natural radioactivity was observed, and three others are predicted to be radioactive but their decay is not observed, due to extremely long half-life times. The two natural radioactive isotopes are ^{113}Cd (half-life = 7.7 x 10^{15} years) and ^{116}Cd (half-life = 2.9 x 10^{19} years).

There are seven stable isotopes of mercury with the longest-lived radioisotopes being ^{194}Hg (half-life = 444 years) and ^{203}Hg (half-life = 47 days). ^{199}Hg and ^{201}Hg are the most often studied NMR-active nuclei, having spins of $^{1}/_{2}$ and $^{3}/_{2}$ respectively.

Properties

A summary of the physical properties of the Group 12 metals is given in Table 6.5.1.4. Because of the ns electron in the Group 12 metals are tightly bound, and hence relatively unavailable for metallic bonding, the metals are volatile with low boiling points, as compared to the Group 2 metals.

Element	Mp (°C)	Bp (°C)	Density (g/cm^3)
Zn	419.53	907	7.14
Cd	321.07	767	8.65
Hg	-38.83	356.73	13.534 (liquid)

Table 6.5.1.4**:** Selected physical properties of the Group 12 metals.

The most notable anomaly in the Group 12 metals is the low melting point of mercury compared to zinc and cadmium. In order to completely understand the reasons for mercury's low melting point quantum physics is required; however, the key point is that mercury has a unique electronic configuration, i.e., [Xe] 5*d* 6s. The stability of the 6s shell is due to the presence of a filled 4*f* shell, because an *f* shell poorly screens the nuclear charge that increases the attractive coulomb interaction of the 6s shell and the nucleus. Such a configuration strongly resists removal of an electron and as such mercury behaves similarly to noble gas elements, which form weakly bonded and thus easily melting solids.



Liquid mercury.

Industrial production

The vast majority (95%) of zinc is mined from of the zinc sulfide ores. The zinc is most often mixed with copper, lead, and iron. Zinc metal is produced by extraction, in which the ore is ground and then the minerals are separated from the gangue (commercially worthless mineral matter) by froth flotation (a process for selectively separating hydrophobic materials from hydrophilic). Roasting converts the zinc sulfide concentrate produced to zinc oxide (Equation 5.1.3). Reduction of the zinc oxide with carbon (5.1.4) or carbon monoxide (5.1.5) at 950 °C into the metal is followed by distillation of the metal. Since cadmium is a common impurity in zinc ores, it is most often isolated during the production of zinc. Cadmium is isolated from the zinc metal by vacuum distillation if the zinc is smelted, or cadmium sulfate is precipitated out of the electrolysis solution.

$$2\ \mathrm{ZnS} + 3\ \mathrm{O_2} \rightarrow 2\ \mathrm{ZnO} + 2\ \mathrm{SO_2} \tag{6.5.1.3}$$

$$2\ \mathrm{ZnO} + \mathrm{C} \rightarrow 2\ \mathrm{Zn} + \mathrm{CO_2} \tag{6.5.1.4}$$

$$2\ \mathrm{ZnO} + 2\ \mathrm{CO} \rightarrow 2\ \mathrm{Zn} + 2\ \mathrm{CO} \tag{6.5.1.5}$$

Mercury is extracted by heating cinnabar (HgS) in a current of air, Equation, and condensing the vapor.

$$\mathrm{HgS} + \mathrm{O_2} \rightarrow \mathrm{Hg} + \mathrm{SO_2} \tag{6.5.1.6}$$

This page titled 6.5.1: The Group 12 Elements is shared under a CC BY 3.0 license and was authored, remixed, and/or curated by Andrew R. Barron (CNX) via source content that was edited to the style and standards of the LibreTexts platform.

6.5.2: Cadmium Chalcogenide Nanoparticles

The most studied non-oxide semiconductors are cadmium chalcogenides (CdE, with E = sulfide, selenide and telluride). CdE nanocrystals were probably the first material used to demonstrate quantum size effects corresponding to a change in the electronic structure with size, i.e., the increase of the band gap energy with the decrease in size of particles. These semiconductors nanocrystals are commonly synthesized by thermal decomposition of an organometallic precursor dissolved in an anhydrous solvent containing the source of chalcogenide and a stabilizing material (polymer or capping ligand). Stabilizing molecules bound to the surface of particles control their growth and prevent particle aggregation.

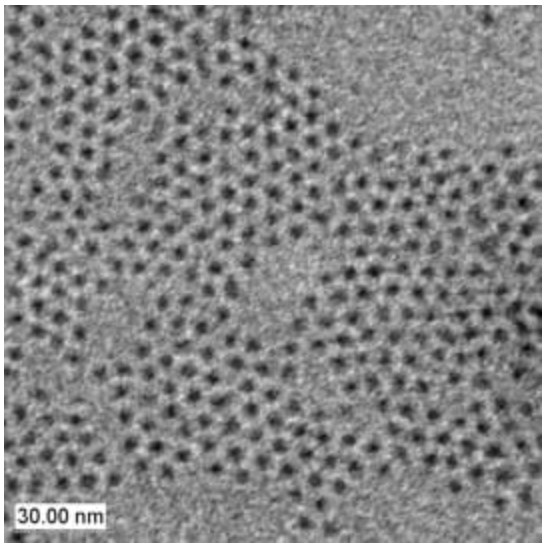


Picture of cadmium selenide (CdSe) quantum dots, dissolved in toluene, fluorescing brightly, as they are exposed to an ultraviolet lamp, in three noticeable different colors (blue ~481 nm, green ~520 nm, and orange ~612 nm) due to the quantum dots' bandgap (and thus the wavelength of emitted light) depends strongly on the particle size; the smaller the dot, the shorter the emitted wavelength of light. The "blue" quantum dots have the smallest particle size, the "green" dots are slightly larger, and the "orange" dots are the largest.

Although cadmium chalcogenides are the most studies semiconducting nanoparticles, the methodology for the formation of semiconducting nanoparticles was first demonstrated independently for InP and GaAs, e.g. Equation 5.1.1. This method has been adapted for a range of semiconductor nanoparticles.

$$\mathrm{InCl_3} + \mathrm{P(SiMe_3)_3} \rightarrow \mathrm{InP} + 3\ \mathrm{Me_3SiCl} \tag{6.5.2.1}$$

In the case of CdE, dimethylcadmium $Cd(CH_3)_2$ is used as a cadmium source and bis(trimethylsilyl)sulfide, $(Me_3Si)_2S$, trioctylphosphine selenide or telluride (TOPSe, TOPTe) serve as sources of selenide in trioctylphosphine oxide (TOPO) used as solvent and capping molecule. The mixture is heated at 230-260 °C over a few hours while modulating the temperature in response to changes in the size distribution as estimated from the absorption spectra of aliquots removed at regular intervals. These particles, capped with TOP/TOPO molecules, are non-aggregated and easily dispersible in organic solvents forming optically clear dispersions. When similar syntheses are performed in the presence of surfactant, strongly anisotropic nanoparticles are obtained, e.g., rod-shaped CdSe nanoparticles can be obtained.



TEM image of CdSe nanoparticles.

Because $Cd(CH_3)_2$ is extremely toxic, pyrophoric and explosive at elevated temperature, other Cd sources have been used. CdO appears to be an interesting precursor. CdO powder dissolves in TOPO and HPA or TDPA (tetradecylphosphonic acid) at about 300 °C giving a colorless homogeneous solution. By introducing selenium or tellurium dissolved in TOP, nanocrystals grow to the desired size.

Nanorods of CdSe or CdTe can also be produced by using a greater initial concentration of cadmium as compared to reactions for nanoparticles. This approach has been successfully applied for synthesis of numerous other metal chalcogenides including ZnS, ZnSe, and $Zn_{1-x}Cd_xS$. Similar procedures enable the formation of MnS, PdS, NiS, Cu_2S nanoparticles, nano rods, and nano disks.

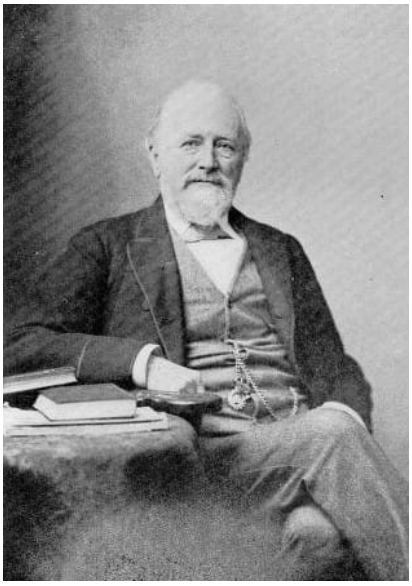
Bibliography

- C. R. Berry, *Phys. Rev.*, 1967, **161**, 848.
- M. D. Healy, P. E. Laibinis, P. D. Stupik, and A. R. Barron, *J. Chem. Soc., Chem. Commun.*, 1989, 359.
- L. Manna, E. C. Scher, and A. P. Alivisatos, *J. Am. Chem. Soc.*, 2000, **122**, 12700.
- C. B. Murray, D. J. Norris, and M. G. Bawendi, *J. Am. Chem. Soc.*, 1993, **115**, 8706.
- Z. A. Peng and X. Peng, *J. Am. Chem. Soc.*, 2002, **12**, 3343.
- R. L. Wells, C. G. Pitt, A. T. McPhail, A. P. Purdy, S. R. B. Shafieezad, and Hallock *Chem. Mater.*, 1989, **1**, 4.
- X. Zong, Y. Feng, W. Knoll, and H. Man, *J. Am. Chem. Soc.*, 2003, **125**, 13559.

This page titled 6.5.2: Cadmium Chalcogenide Nanoparticles is shared under a CC BY 3.0 license and was authored, remixed, and/or curated by Andrew R. Barron (CNX) via source content that was edited to the style and standards of the LibreTexts platform.

6.5.3: Organometallic Chemistry of Zinc

The first dialkyl zinc derivatives, Me_2Zn and Et_2Zn, were prepared in 1848 by Edward Franklin. He also prepared the monoalkyl derivatives, RZnX.



British chemist Sir Edward Franklin FRS (1825 –1899).

Initially alkyl zinc compounds were used in organic synthesis, however, their use diminished significantly once Grignard reagents had been discovered. Little further was investigated of their chemistry until their use in the growth of electronic materials developed in the 1980's.

RZnX

The monoalkyl derivatives are not widely used, but were historically the first to be prepared (Equation 5.3.1).

$$\mathrm{RX + Zn \rightarrow RZnX} \tag{6.5.3.1}$$

While the iodide derivatives can be isolated as unsolvated derivatives, the chloride and bromides need to be prepared in the presence of dimethylformamide (DMF) or dimethyl sulfoxide (DMSO). Alternative methods of synthesis involve the reaction with a Grignard reagent, (Equation 5.3.2), or electrochemical synthesis with a zinc electrode.

$$\mathrm{ZnX_3 + RMgX \rightarrow RZnX + MgX_2} \tag{6.5.3.2}$$

In the solid state RZnI exists as cage oligomers or polymeric chain structures. These structures are broken by the addition of strong Lewis bases to form Lewis acid-base complexes. In solution there exists a Schlenk equilibrium (equation 5.3.3) whose presence has been determined by IR and Raman spectroscopy (Table 6.5.3.1).

$$\mathrm{RZnI \leftrightharpoons R_2Zn + ZnI_2} \tag{6.5.3.3}$$

Stretch	IR (cm^{-1})	Raman (cm^{-1})
symmetric C-Zn-C	Not observed	477
asymmetric C-Zn-C	551	Not observed
C-Zn-I	510	510

Table 6.5.3.1**:** IR and Raman spectroscopic characterization of the components of the Schlenk equilibrium,

R_2Zn

Dialkyl zinc compounds are prepared via the monoalkyl derivatives (Equation 5.3.4). The Schlenk equilibrium is shifted at high temperatures by the distillation of the volatile R_2Zn derivative. The zinc is usually alloyed with copper (10%) to improve the reaction rate.

$$2\ \mathrm{Zn} + 2\ \mathrm{RX} \rightarrow 2\ \mathrm{RZnX} \backslash \mathrm{xleftrightarrow} \Delta \mathrm{R_2Zn} + 2\ \mathrm{MgX_2} \tag{6.5.3.4}$$

Alternative preparation methods include the reaction of ZnX2 with a Grignard (Equation 5.3.5) or by metal-metal exchange (Equation 5.3.6).

$$2\ \mathrm{RMgX} + \mathrm{ZnX_2} \rightarrow \mathrm{R_2Zn} + 2\ \mathrm{MgX_2} \tag{6.5.3.5}$$

$$\mathrm{R_2Hg} + \mathrm{Zn} \rightarrow \mathrm{Hg} + \mathrm{R_2Zn} \tag{6.5.3.6}$$

Bibliography

- E. von Frankland. *Justus Liebigs Ann. Chem.*, 1849, **71**, 171.
- J. J. Habeeb, A. Osman, and D. G. Tuck. *J. Organomet. Chem.*, 1980, **185**, 117

This page titled 6.5.3: Organometallic Chemistry of Zinc is shared under a CC BY 3.0 license and was authored, remixed, and/or curated by Andrew R. Barron (CNX) via source content that was edited to the style and standards of the LibreTexts platform.

6.5.4: Organomercury Compounds

Synthesis

The most common routes to organomercury compounds involve the direct reaction of mercury with an alkyl iodide (Equation 5.4.1) to form the mercury analog of a Grignard reagent.

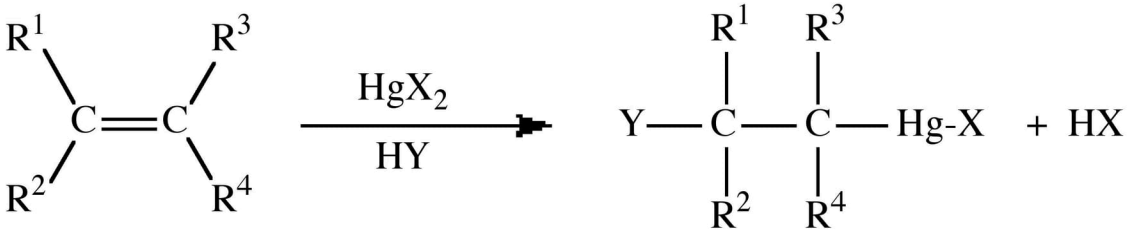
$$\mathrm{Hg} + \mathrm{RX} \rightarrow \mathrm{RHgX} \tag{6.5.4.1}$$

The subsequent reaction of RHgI with potassium cyanide yields the appropriate dialkyl mercury derivative (Equation 5.4.2).

$$2\ \mathrm{RHgI} + 2\ \mathrm{KCN} \rightarrow \mathrm{R_2Hg} + \mathrm{Hg} + 2\ \mathrm{KI} + (\mathrm{NC})_2 \tag{6.5.4.2}$$

Solvomercuration

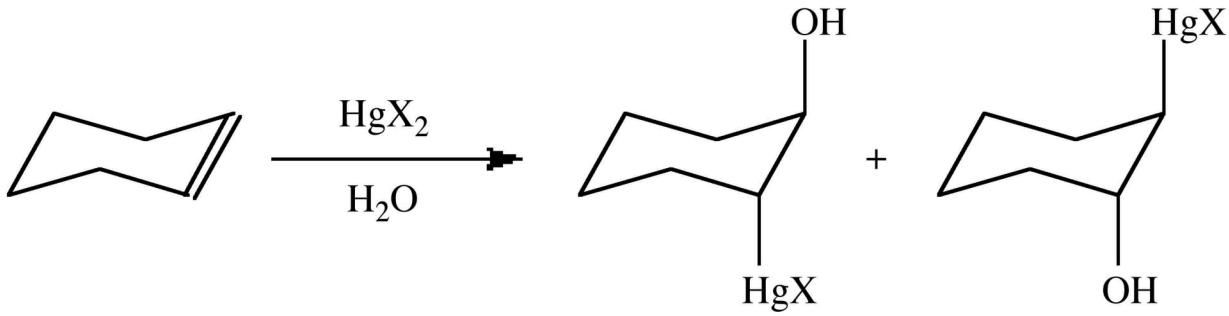
The general process of solvomercuration involves the addition of HgX_2 across an alkene double (or alkyne triple) bond in the presence of a solvent. Solvomercuration applies where HY, from Equation 5.4.3, are part of the solvent system, e.g., in water the process can be described as hydroxymercuration.



The addition to the alkene occurs with Markovnikoff addition, i.e., through the formation of the most stable carbonium ion resulting with the mercury adding to the less substituted carbon. The Hg-C bond can be cleaved by the addition of $NaBH_4$ to yield the C-H bond. It is common to employ mercury acetate, $Hg(OAc)_2$ ($OAc = O_2CCH_3$), with subsequent reaction with NaCl or NaI to form the halide, rather than the mercury halide directly. However, the acetate can also act as a neucleophile resulting in a mixture of products. The order of reactivity for alkenes follows the trend:

$$\mathrm{R_2C{=}CH_2} > \mathrm{R(H)C{=}CH_2} > \textit{cis}\ \mathrm{R(H)C{=}C(H)R} > \textit{trans}\ \mathrm{R(H)C{=}C(H)R} > \mathrm{R_2C{=}C(H)R} > \mathrm{R_2C{=}CR_2} \tag{6.5.4.3}$$

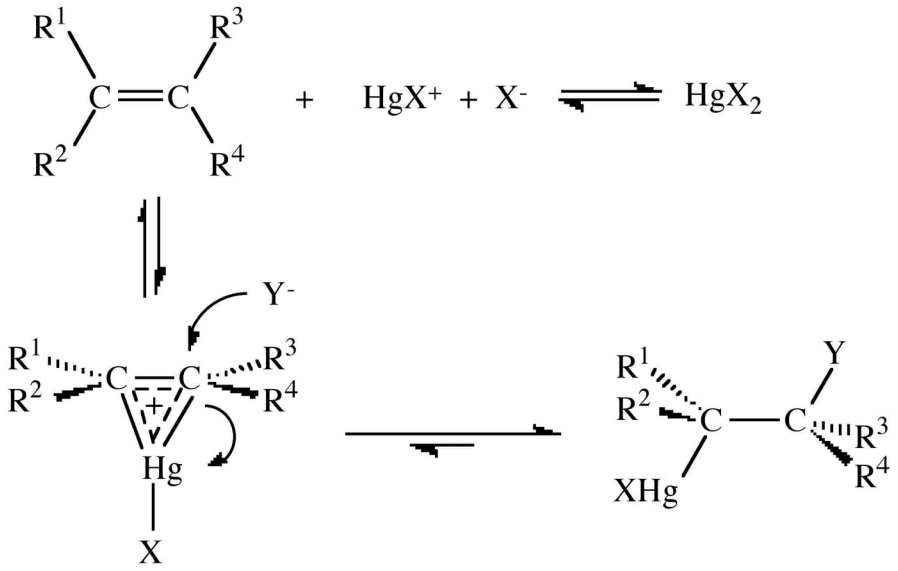
This is due to a combination of steric and electronic effects. The addition occurs in a *trans*/*anti* fashion.



Mercury(II) halides dissociate in polar solvents (Equation 5.4.4) and this species is commonly associated with the initial reaction step.

$$\mathrm{HgX_2} \leftrightharpoons \mathrm{HgX^+} + \mathrm{X^-} \tag{6.5.4.4}$$

The mechanism of solvomercuration is best described by the reaction shown in.

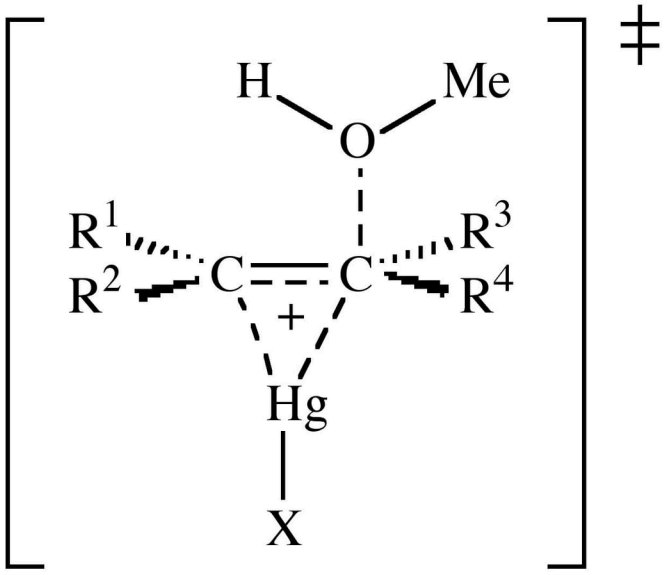


Mechanism of solvomercuration.

Evidence for the mechanism is twofold:

1. The addition is exclusively *trans*.
2. No rearrangement is observed even for $^{t}Bu(H)C=C(H)^{t}Bu$ whose carbonium ion is known to undergo rearrangement.

Isotope studies indicate that the C-O bond formation is present in the transition state. The mercury bridge in the transition state may not be symmetrical, but the structure is similar to the addition of Br^{+} and AuX^{+} to alkenes.



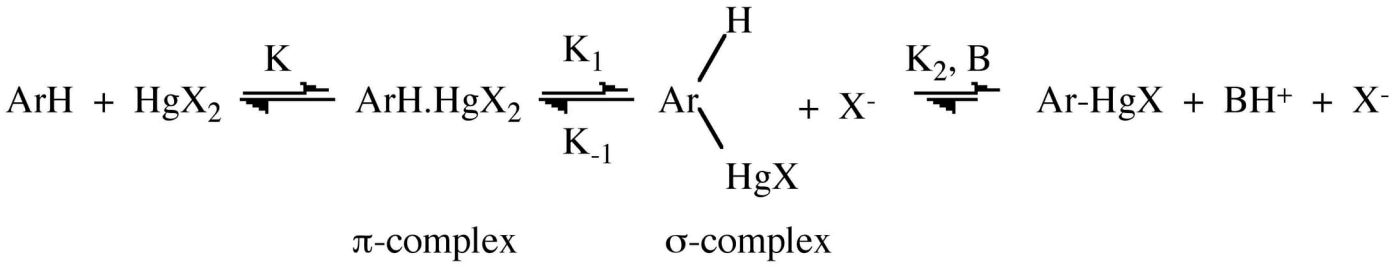
Proposed transition state for the solvomercuration reaction where the solvent is methanol.

The actual reaction was originally carried out with $Hg(OAc)_2$ in benzene at 110 °C for several hours in acetic acid solution. It was found that the reaction was catalyzed by the presence of $HClO_4$, H_2SO_4, and HNO_3, which were found to replace the acetate ion. The reaction rate is also increased by 690,000 times by the use of $Hg(O_2CCF_3)_2$ in HO_2CCF_3.

The solvomercuration of alkynes gives alkenylmercury compounds, but the reaction is more sluggish than for the reaction with alkenes, and the product is always the *trans* isomer.

Mercuration of aromatic compounds

Mercuration is an electrophilic aromatic substitution reaction that is possible for most 2n+2 π-electron species. Evidence for the π-complex intermediate is indicated by UV spectroscopy, which shows an increase in the region 280 – 320 nm for the reaction of aromatic compounds with $Hg(O_2CCF_3)_2$ in HO_2CCF_3. The σ-complex has detected in liquid SO_2.



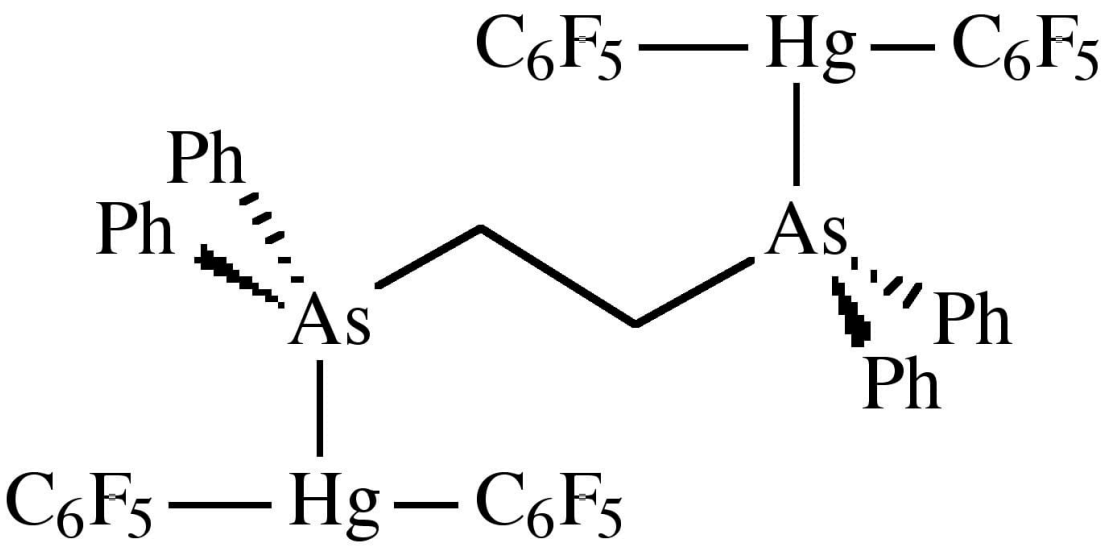
As a preparative method mercuration suffers from alack of selectivity, including an isomerization from *para* substitution at low temperature to *meta* substitution at high temperatures.

Structure

Dialkyl mercury compounds, R_2Hg, are generally air stable and show little Lewis acid behavior. They are monomeric colorless liquids or low melting solids, e.g., Bp = 92.5 °C for Me_2Hg. No solubility is observed in water, except for $(F_3C)_2Hg$ (Equation 5.4.5).

$$(F_3C)_2Hg + H_2O \leftrightharpoons (F_3C)_2Hg(OH)^- + H^+ \tag{6.5.4.5}$$

The hybridization at mercury involves the 6s and 6p orbitals; however, the 5d may be involved. X-ray crystal structures for both R_2Hg and RHgX show linear structures. In general R_2Hg compounds are very weak Lewis acids, but adduct are formed if the alkyl group is sufficiently electron withdrawing, e.g., $(C_6F_5)_2Hg$. The geometry of the Lewis acid-base complex is not triangular as predicted from VSEPR theory, but a *T-shape*. The distortion from a linear C-Hg-C unit is minor. For example, in $(C_6F_5)_2Hg$ the C-Hg-C angle is 176.2°, while in $[(C_6F_5)_2Hg]_2$(diars), where diars = $Ph_2AsCH_2CH_2AsPh_2$, the same angle is 173°. Furthermore, the donor atom-Hg bond distance (e.g., As-Hg = 3.4 Å) is only slightly shorter than the sum of the van der Waal radii (e.g., 3.5 Å).



The structure of $[(C_6F_5)_2Hg]_2$(diars).

Bibliography

- L. C. Damude and P. A. W. Dean. *J. Organomet. Chem.*, 1979, **181**, 1.
- L. C. Damude and P. A. W. Dean. *J. Chem. Soc., Chem. Commun.*, 1978, 1083.
- J. L. Courtneidge, A. G. Davies, P. S. Gregory, D. C. McGuchan, and S. N. Yazdi. *J. Chem. Soc., Chem. Commun.*, 1987, 1192.
- P. B. Hitchcock, J. M. Keates, and G. A. Lawless, *J. Am. Chem. Soc.*, 1998, **120**, 599.

This page titled 6.5.4: Organomercury Compounds is shared under a CC BY 3.0 license and was authored, remixed, and/or curated by Andrew R. Barron (CNX) via source content that was edited to the style and standards of the LibreTexts platform.

6.5.5: The Myth, Reality, and History of Mercury Toxicity

Mercury has a reputation for being a dangerous element, but is its reputation deserved? Given the large-scale use of mercury today it is important to understand the risks and issues related to mercury exposure. Nowhere is this now important than with the use of mercury for small low energy fluorescent lights that are being advocated by everyone from the electricity companies to Greenpeace.



An example of a modern low energy mercury vapor fluorescent light.

When considering the issue of mercury toxicity it is important to separate the effects of mercury metal (as a liquid or vapor) from the compounds of mercury.

Mercury metal

It was found very early on that people who worked with mercury, in mining for example, had very bad health. Other jobs that exposed people to mercury were mirror makers and hatters (people who manufactured hats). The problems in this latter occupation will forever live on with one of the central characters in Lewis Carroll's *Alice's Adventures in Wonderland*; the Mad Hatter.

Hats were made from felt, which is a non-woven textile of animal hair. Wool interlocks naturally due to the surface texture of the individual hairs, but rabbit and beaver have to be artificially roughened. This process was usually accomplished with nitric acid (HNO_3). It was found that if mercury was added to the nitric acid, a better quality of felt was produced. Unfortunately, when the felt was dried a fine dust was formed containing mercury. The hatters who shaped the felt inhaled large quantities of this dust were found to suffer from excessive salivation, erethism (presenting with excessive shyness, timidity and social phobia), and shaking of the limbs, which became known as *hatter's shakes*. The madness that was observed is the derivation of the phrase "mad as a hatter".

Note

It is interesting that while Carroll's Mad Hatter is mad, he does not show the classic symptoms of mercury poisoning. In particular he can be in no way described as shy!

Hatters were not the only people that mercury caused a problem for. Chemists doing research using large quantities of mercury were also affected. They were given to violent headaches, tremors of the hands, "socially troublesome inflammation of the

bladder", loss of memory, and slow mental processes. In 1926 Alfred Stock (Figure) and his research group all suffered from symptoms. However, when the lab was cleaned of mercury the symptoms went away.



German chemist Alfred Stock (1876 –1946).

Many other notable scientists have also suffered from mercury poisoning. Faraday (Figure), Pascal (Figure), and most probably Sir Isaac Newton (Figure) were affected. As part of his research studies, Newton boiled several pounds of mercury a day just before his period of insanity between 1692 and 1693. It is likely that the mercury vapor was the cause of his malady. However, in each case, the symptoms (and insanity) abated once the source of mercury was removed.



An engraving by John Cochran of English chemist and physicist Michael Faraday, FRS (1791 –1867).



French mathematician, physicist, and religious philosopher Blaise Pascal (1623 – 1662).



English physicist, mathematician, astronomer, natural philosopher, alchemist, and theologian Sir Isaac Newton FRS (1643 –1727). Portrait by Godfrey Kneller.

Note

It is important to remember that in all the cases described above it is the inhalation of the mercury vapor that was the cause of the trouble. Solid alloys of mercury such as those found in dental fillings have never been shown to cause any medical issues directly. Despite this the US banned the use of Cu/Hg dental amalgams until 1850! More recently, it has been suggested that dentists are exposed at higher levels during the placing and removal of fillings. Dentists as a group have higher mercury levels than those associated with people with amalgam restorations, but experience no increase in disease or death rates, and in fact tend to be healthier than the general population.

Although elemental mercury was clearly toxic, this did not stop its use in pharmacy for hundreds of years. In the 1500's mercury was used in the treatment (albeit ineffective) of syphilis. Syphilis was a new disease in Europe; it had been brought back from America by Columbus' sailors, and was promptly spread through Europe by the French army, amongst others! Syphilis was much more fatal and had more dramatic symptoms than today.

Initially mercury was used as an ointment, but the patients often got worse. Then there was *the tub*, which was a mercury vapor

bath, and even calomel (Hg_2Cl_2) was used, but with little effect. These treatments were used for over four centuries, but none provided a cure, despite claims at the time. For example, John Hunter, a doctor who gave himself syphilis by mistake (!) claimed he had been cured, but he actually died of a heart attack during an argument, so it is unlikely the mercury worked. Despite this it became known that "a night with Venus results in a lifetime with Mercury".

The reasons that mercury was thought erroneously to cure syphilis are twofold:

1. Until 1906 it was difficult to diagnose syphilis. It was often confused with gonorrhea, and therefore it is likely that some people did not have the far more deadly syphilis.
2. Syphilis occurs in three phases, each with remission between the phases. The period of remission between secondary and tertiary phases can be two to three years, and therefore it may appear that a cure is found. Especially as may patients (like John Hunter) died other deaths during this remission phase.

The prevalent use of mercury and its presence in many cadavers, led some doctors to assume that mercury was a natural part of the body. It was not just humans that were treated with mercury, cattle were also treated, and one druggist sold 25 tons of mercury to a single farmer in one year!

The density of mercury and its liquid state at room temperature led to another unusual application that was somewhat more successful, although equally dangerous: constipation. In medical texts of the time it was noted that "mercury is given in the disease called *Miserere*, unto two or three pounds, and is voided again by siege to the same weight; it is better to take a great deal of it that a little, because a small quantity might be apt to stop in the circumvolutions of the guts, and if some acid humors should happen to join with it, a *sublimate corrosive* would be made; but when a large quantity of it is taken, there's no need to fearing this accident, because it passes through by its own weight."

It is interesting that the mention of the *corrosive sublimate*; this is in fact mercury(II) dichloride ($HgCl_2$) which unlike mercury(I) chloride (Hg_2Cl_2), is a very violent poison. Death is caused by renal failure. So while there is no evidence for elemental mercury itself causing fatalities, its compounds are another matter to be considered.

Organomercury compounds

In 1953 it was noted that the fishing village of Minamata in Japan had an epidemic in which a large number of people died. Initial thoughts of either an infectious disease or malnutrition were discounted; then it was found that the fish eaten by the villagers was highly contaminated by mercury.

It was found that the mercury came from the Chisso Corporation chemical plant that made acetaldehyde from acetylene using a mercury catalyst. The plant was loosing 1 Kg of mercury metal for every ton of acetaldehyde being produced. As a consequence it was originally assumed that the poisoning of the village was due to inorganic mercury. Based upon prior incidents, an obvious response was to ban consumption of all fish and shellfish. As a consequence no new cases were reported, however, people already effected continued to die. This was unlike any previous mercury poisoning.

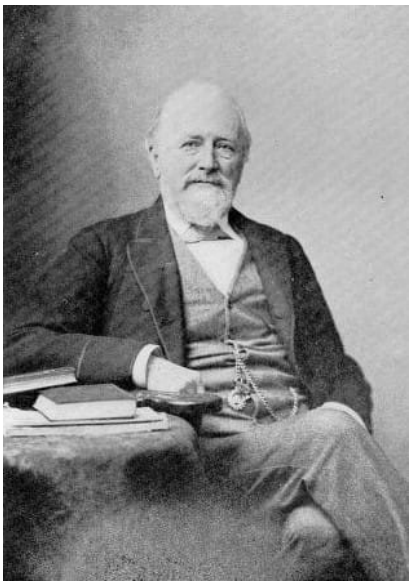
Further analysis showed small quantities of water soluble methyl mercury ($MeHg^+$) was present and sequestered by the shellfish to give MeHgSMe. While the lethal effects of organomercury compounds were known, the source of the methyl mercury was a mystery. A group of Swedish researchers showed that the bacterial action in river sediment or rotting fish converted inorganic mercury to either volatile Me_2Hg or water soluble $MeHg^+$. With this discovery, it was understood how the anaerobic mud of the estuary near Minamata could perform this methylation.

Of course Minamata was not the first report or an organomercury compound, but it was the first time that it was shown that mercury metal could be converted to a highly toxic organometallic derivative in the environment. The hazardous nature of organomercurials was found almost as soon as the first compounds were reported!

While working in Bunsen's research group in Marburg, Edward Franklin discovered the synthesis of the zinc analog of a Grignard reagent. Subsequently, in 1851 Franklin moved to Owens College in Manchester where he extended his work to mercury. In his publication he noted that these organomercury compounds had a "nauseous taste", but didn't realize they were toxic.

$$\mathrm{Zn + MeI \rightarrow MeZnI} \tag{6.5.5.1}$$

$$\mathrm{Hg + RX \rightarrow RHgX} \tag{6.5.5.2}$$



British chemist Sir Edward Franklin FRS (1825 – 1899).

In 1858 George Buckton working at the then Royal College of Chemistry (now Imperial College) reported the synthesis of dimethyl mercury as a volatile liquid.

\[2 \mathrm{MeHgI}+2 \mathrm{KCN} \rightarrow \mathrm{Me}_{2} \mathrm{Hg}+\mathrm{Hg}+2 \mathrm{KI}+(\mathrm{NC})_{2}]



British chemist George Buckton (1818 - 1905).

When Frankland moved his research to St Bartholomew's Hospital ("Barts") London he started looking into the chemistry of R_2Hg with an assistant called Bill Odling in collaboration with Dr Carl Ulrich.

Ulrich died in 1865 as a consequence of exposure to Me_2Hg. In his own statement, he had inhaled a large quantity of the volatile compound without having taken the proper precautions. The following day "his countenance had attained a dull, anxious, and confused expression" and he was admitted to the hospital in a weak condition on 3rd February. On the 9th he became noisy and had to be put under mechanical restraint. The next day his breath and body began to smell offensively and he was in a coma. He would rise from the coma periodically to utter incoherent howls. He died on the 14th of February.

A technician from the same research group (who is only identified as 'T. C.') was also admitted to the hospital on 28th March of the

same year. His symptoms were initially milder than Ulrich's, but soon developed. By that summer he was completely demented, with no control over his body functions. He stayed in this state for many months, only dying on 7th April 1866. Records indicate that a third assistant was also taken ill, but there was no further mention of him, so it is unknown if he died.

Summary and the "green" future

Metallic mercury causes severe symptoms, but all records show that if the patient is removed from the source they recover. Thus, short term exposure to metallic mercury, while dangerous, is not fatal if proper precautions are taken. In contrast, mercury compounds offer different risks. As a general rule, inorganic mercury(I) compounds are far less toxic than their mercury(II) analogs, however, all should be treated with care.

Where mercury compounds offer the greatest risk of fatality is their organometallic derivatives. There is no known cure for exposure to even modest doses of organomercury compounds. Furthermore, the ability of elemental mercury to be transformed into water-soluble organomercury compounds such as $MeHg^+$, offers a future threat to public health.

The new generation of low energy consumption light bulbs contain mercury vapor. While they last longer than a traditional tungsten filament light bulb (Figure), they do have a lifetime. The presence of mercury means that they should be disposed-off separately from household waste to ensure that when the glass is broken the mercury is not released; however, this is unlikely. Most will be disposed off along with household waste which may be subsequently land filled. The lesson from Minamata should be that the bacterial action under anaerobic condition allows for the formation of water soluble $MeHg^+$, that can diffuse into the water table. Although the amount of mercury in each bulb is very small, the highly lethal nature (low LD_{50}) of orgnaomercury compounds should be considered in efforts to conserve energy by the use of the low energy light bulbs. At the very minimum protocols for their efficient disposal and recycling should be in place.

Bibliography

- S. Jensen and A. Jernelöv, *Nature*, 1969, **223**, 753.
- J. C. Clifton II, *Pediatr. Clin. North Am.*, 2007, **54**, 237.
- H. A. Waldron, *Br. Med. J.*, 1983, **287**, 24:
- C. Naleway, R. Sakaguchi, E. Mitchell, T. Muller, W. A. Ayer, and J. J. Hefferren, *J. Amer. Dent. Assoc.*, 1985, **111**, 37.
- D. McComb, *J. Can. Dent. Assoc.*, 1997, **63**, 372.
- T. G. Duplinsky1 and D. V. Cicchetti, *Int. J. Stats. Med. Res.*, 2012, **1**, 1.
- M. Aucott, M. McLinden, and M. Winka, *J. Air. Waste Manag. Assoc.*, 2003, **53**, 143.

This page titled 6.5.5: The Myth, Reality, and History of Mercury Toxicity is shared under a CC BY 3.0 license and was authored, remixed, and/or curated by Andrew R. Barron (CNX) via source content that was edited to the style and standards of the LibreTexts platform.

6.6: Group 13

Thumbnail: Crystals of 99.999% gallium. (CC-SA-BY 3.0; Foobar)

This page titled 6.6: Group 13 is shared under a CC BY 3.0 license and was authored, remixed, and/or curated by Andrew R. Barron (CNX) via source content that was edited to the style and standards of the LibreTexts platform.

6.6.1: The Group 13 Elements

Table 6.6.1.1 lists the derivation of the names of the Group 13 (IIIA) elements.

Element	Symbol	Name
Boron	B	From the Arabic word *buraq* or the Persian word *burah* for the mineral *borax*
Aluminium (Aluminum)	Al	From *alum*
Gallium	Ga	From Named after the Latin word for France (Gaul) *Gallia*
Indium	In	Latin *rubidus* meaning *deepest red*
Thalium	Tl	From the Latin *thallus* meaning *sprouting green twig*

Table 6.6.1.1**:** Derivation of the names of each of the alkali metal elements.

Note

Aluminium is the international spelling standardized by the IUPAC, but in the United States it is more commonly spelled as aluminum.

Discovery

Boron

Borax (a mixture of $Na_2B_4O_7.4H_2O$ and $Na_2B_4O_7.10H_2O$) was known for thousands of years. In Tibet it was known by the Sanskrit name of *tincal*. Borax glazes were used in China in 300 AD, and the writings of the Arabic alchemist Geber appear to mention it in 700 AD. However, it is known that Marco Polo brought some borax glazes back to Italy in the 13th century. In 1600 Agricola in his treatise *De Re Metallica* reported the use of borax as a flux in metallurgy.



A drawing of the *father of chemistry* Abu Musa Jābir ibn Hayyān al azdi known by Geber; the Latinized form of Jabir (721 - 815). Geber was a chemist and alchemist, astronomer and astrologer, engineer, geologist, philosopher, physicist, and pharmacist and physician.



A painting of German author Georg Bauer (1494 - 1555), whose pen-name was the Latinized Georgius Agricola, was most probably the first person to be environmentally conscious.

Boron was not recognized as an element until its isolation by Sir Humphry Davy, Joseph Louis Gay-Lussac and Louis Jacques Thénard in 1808 through the reaction of boric acid and potassium. Davy called the element *boracium*. Jöns Jakob Berzelius identified boron as an element in 1824.



British chemist and inventor Sir Humphry Davy FRS (1778 - 1829).



French chemist and physicist Joseph Louis Gay-Lussac (1778 –1850).



French chemist Louis Jacques Thénard (1777 - 1857).



Swedish chemist Friherre Jöns Jacob Berzelius (1779 - 1848).

Aluminum

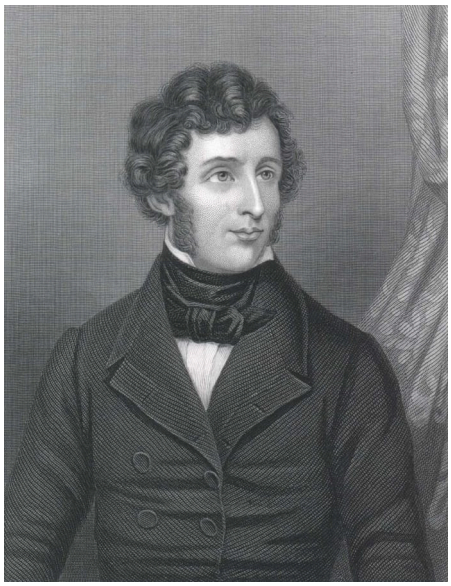
Ancient Greeks and Romans used aluminum salts as dyeing mordants and as astringents for dressing wounds; alum ($KAl(SO_4)_2.12H_2O$) is still used as a styptic (an antihaemorrhagic agent). In 1808, Sir Humphry Davy identified the existence of a metal base of alum, which he at first termed *alumium* and later aluminum.

The metal was first produced in 1825 (in an impure form) by Hans Christian Ørsted by the reaction of anhydrous aluminum chloride with potassium amalgam. Friedrich Wöhler repeated the experiments of Ørsted but suggested that Ørsted had only isolated potassium. By the use of potassium (Equation 6.1.1), he is credited with isolating aluminum in 1827. While Wöhler is generally credited with isolating aluminum, Ørsted should also be given credit.

$$\mathrm{AlCl_3 + 3\ K \rightarrow Al + 3\ KCl} \tag{6.6.1.1}$$



Danish physicist and chemist Hans Christian Ørsted (1777 - 1851).



German chemist Friedrich Wöhler (1800 - 1882) also known for his synthesis of urea and, thus, the founding of the field of natural products synthesis.

In 1846 Henri Deville improved Wöhler's method, and described his improvements in particular the use of sodium in place of the expensive potassium

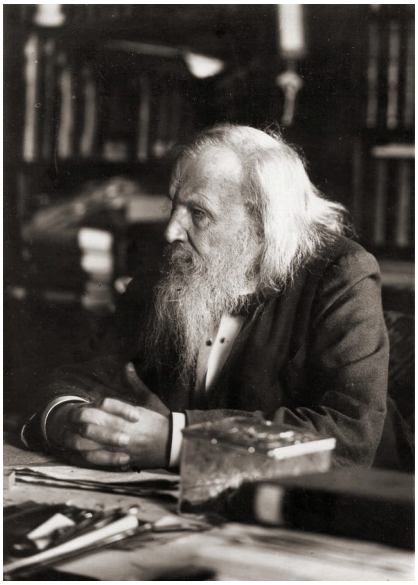
$$\mathrm{AlCl_3 + 3\ Na \rightarrow Al + 3\ NaCl} \tag{6.6.1.2}$$



French chemist Henri Etienne Sainte-Claire Deville (1818 - 1881).

Gallium

The element gallium was predicted, as eka-aluminum, by Mendeleev in 1870, and subsequently discovered by Lecoq de Boisbaudran in 1875; in fact de Boisbaudran had been searching for the missing element for some years, based on his own independent theory. The first experimental indication of gallium came with the observation of two new violet lines in the spark spectrum of a sample deposited on zinc. Within a month of these initial results de Boisbaudran had isolated 1 g of the metal starting from several hundred kilograms of crude zinc blende ore. The new element was named in honor of France (Latin *Gallia*), and the striking similarity of its physical and chemical properties to those predicted by Mendeleev did much to establish the general acceptance of the periodic Law; indeed, when de Boisbaudran first stated that the density of Ga was 4.7 g cm^{-3} rather than the predicted 5.9 g/cm^3, Mendeleev wrote to him suggesting that he redetermine the value (the correct value is 5.904 g/cm^3).



Russian chemist and inventor Dmitri Ivanovich Mendeleev (1834 – 1907).



French chemist Paul Émile (François) Lecoq de Boisbaudran (1838 – 1912).

Indium

While testing ores from the mines around Freiberg, Saxony, Ferdinand Reich and Hieronymous Theodor Richter when they dissolved the minerals pyrite, arsenopyrite, galena and sphalerite in hydrochloric acid, and since it was known that ores from that region contained thallium they searched for the green emission lines by spectroscopy. Although the green lines were absent, a blue line was present in the spectrum. As no element was known with a bright blue emission they concluded that a new element was present in the minerals. They named the element with the blue spectral line indium. Richter went on to isolate the metal in 1864.



German chemist Ferdinand Reich (1799 - 1882).



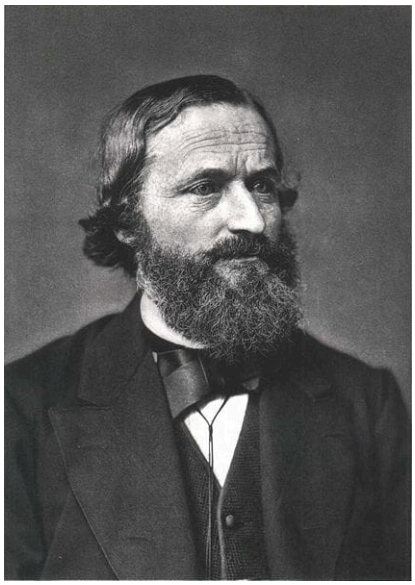
German chemist Hieronymus Theodor Richter (1824 - 1898).

Thallium

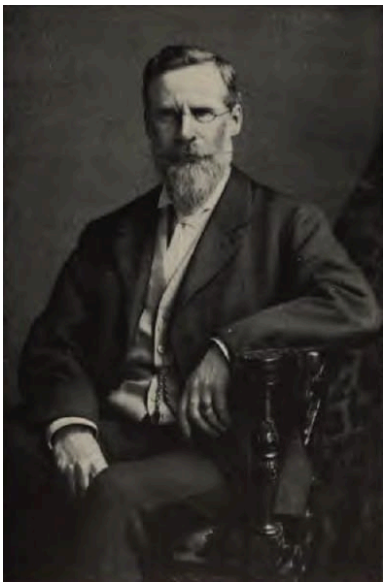
After the publication of their improved method of flame spectroscopy by Robert Bunsen and Gustav Kirchhoff this method became an accepted method to determine the composition of minerals and chemical products. Two chemists, William Crookes and Claude-Auguste Lamy, both started to use the new method and independently employed it in their discovery of thallium.



German chemist Robert Wilhelm Eberhard Bunsen (1811 - 1899).



German physicist Gustav Robert Kirchhoff (1824 - 1887).



English chemist and physicist Sir William Crookes, FRS (1832 –1919) attended the Royal College of Chemistry (now Imperial College) in London.

Crookes was making spectroscopic determinations on selenium compounds deposited in the lead chamber of a sulfuric acid production plant near Tilkerode in the Harz mountains. Using a similar spectrometer to Crookes', Lamy was determining the composition of a selenium-containing substance that was deposited during the production of sulfuric acid from pyrite. Using spectroscopy both researchers both observed a new green line the atomic absorption spectrum and assigned it to a new element. Both set out to isolate the new element. Fortunately for Lamy, he had received his material in larger quantities and thus he was able to isolate sufficient quantities of thallium to determine the properties of several compounds and prepare a small ingot of metallic thallium. At the same time Crookes was able to isolate small quantities of elemental thallium and determine the properties of a few compounds. The claim by both scientists resulted in significant controversy during 1862 and 1863; interestingly this ended when Crookes was elected Fellow of the Royal Society in June 1863.

Abundance

The abundance of the Group 13 elements is given in Table 6.6.1.2. Aluminum is the most abundant metal in the Earth's crust and is found in a wide range of minerals. While boron is not as common it is also found in a range of borate minerals. In contrast, gallium, indium, and thallium are found as impurities in other minerals. In particular indium and thallium are found in sulfide

or selenide mineral rather than oxides, while gallium is found in both sulfides (ZnS) and oxides (bauxite). Although indium and thallium minerals are known, they are rare: indite ($FeIn_2S_4$), lorandite ($TlAsS_2$), crookesite (Cu_7TlSe_4).

Table 6.6.1.2: Abundance of Group 13 elements.

Element	Terrestrial abundance (ppm)
B	10 (Earth's crust), 20 (soil), 4 (sea water)
Al	82,000 (Earth's crust), 100,000 (soil), 5 x 10^{-4} (sea water)
Ga	18 (Earth's crust), 28 (soil), 30 x 10^{-6} (sea water)
In	0.1 (Earth's crust), 0.01 (soil), 0.1 x 10^{-6} (sea water)
Tl	0.6 (Earth's crust), 0.2 (soil), 10 x 10^{-6} (sea water)

Isotopes

The naturally abundant isotopes of the Group 13 elements are listed in Table 6.6.1.3. Thallium has 25 isotopes that have atomic masses that range from 184 to 210. Thallium-204 is the most stable radioisotope, with a half-life of 3.78 years.

Table 6.6.1.3: Abundance of the major isotopes of the Group 13 elements.

Isotope	Natural abundance (%)
Boron-10	19.9
Boron-11	80.1
Aluminum-27	100
Gallium-69	60.11
Gallium-71	39.89
Indium-113	4.3
Indium-115	95.7
Thallium-203	29.52
Thallium-205	70.48

The Group 13 elements offer potential as NMR nuclei (Table 6.6.1.4). In particular ^{11}B and ^{27}Al show promise for characterization in both solution and solid state.

Table 6.6.1.4: Isotopes of Group 13 elements for NMR spectroscopy.

Isotope	Spin	Natural abundance (%)	Quadrupole moment (10^{-30} m^2)	NMR frequency (MHz) at a field of 2.3488 T	Reference
Boron-10	3	19.58	8.459	-10.746	$BF_3.Et_2O$
Boron-11	$^3/_2$	80.42	4.059	-32.084	$BF_3.Et_2O$
Aluminum-27	$^5/_2$	100	14.66	-26.057	$Al(NO_3)_3$
Gallium-69	$^3/_2$	60.4	17.1	-24.003	$Ga(NO_3)_3$
Gallium-71	$^3/_2$	39.6	10.7	-30.495	$Ga(NO_3)_3$
Indium-113	$^9/_2$	4.28	79.9	-21.866	$In(NO_3)_3$
Indium-115	$^9/_2$	95.72	81.0	-21.914	$In(NO_3)_3$

Industrial production

Borax is mined as a mixture of $Na_2B_4O_7.4H_2O$ and $Na_2B_4O_7.10H_2O$. Acidification gives boric acid, $B(OH)_3$, which can be reduced with sodium amalgam (Na/Hg) to give amorphous boron. Pure boron can be prepared by reducing boron halides (e.g., BF_3 and BCl_3) with hydrogen at high temperatures. Ultrapure boron, for the use in semiconductor industry, is produced by the decomposition of diborane (B_2H_6) and then further purified with the zone melting or Czochralski processes.

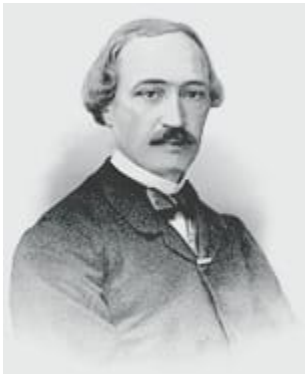
The only two economic sources for gallium are as byproduct of aluminum and zinc production. Extraction during the Bayer process followed by mercury cell electrolysis and hydrolysis of the amalgam with sodium hydroxide leads to sodium gallate. Electrolysis then gives gallium metal.

The lack of indium mineral deposits and the fact that indium is enriched in sulfides of lead, tin, copper, iron and zinc, makes the zinc production the main source for indium. The indium is leached from slag and dust of zinc production. Up until 1924, there was only about a gram of isolated indium on the planet, however, today worldwide production is currently greater 476 tons per year from mining and a 650 tons per year from recycling. This massive increase in demand is due to applications in LCD displays and solar cell applications.

Aluminum

Due to aluminum's position as the most abundant metallic element in the Earth's crust (7.5 - 8.1%) and its enormous industrial importance warrants detailed discussion of its industrial production. Aluminum only appears in its elemental form in nature in oxygen-deficient environments such as volcanic mud. Ordinarily, it is found in a variety of oxide minerals.

In comparison to other metals aluminum is difficult to extract from its ores. Unlike iron, aluminum oxides cannot be reduced by carbon, and so purification is only possible on an economic scale using electrolysis. Prior to electrolysis purified aluminum oxide is obtained by refining bauxite in the process of developed by Karl Bayer.



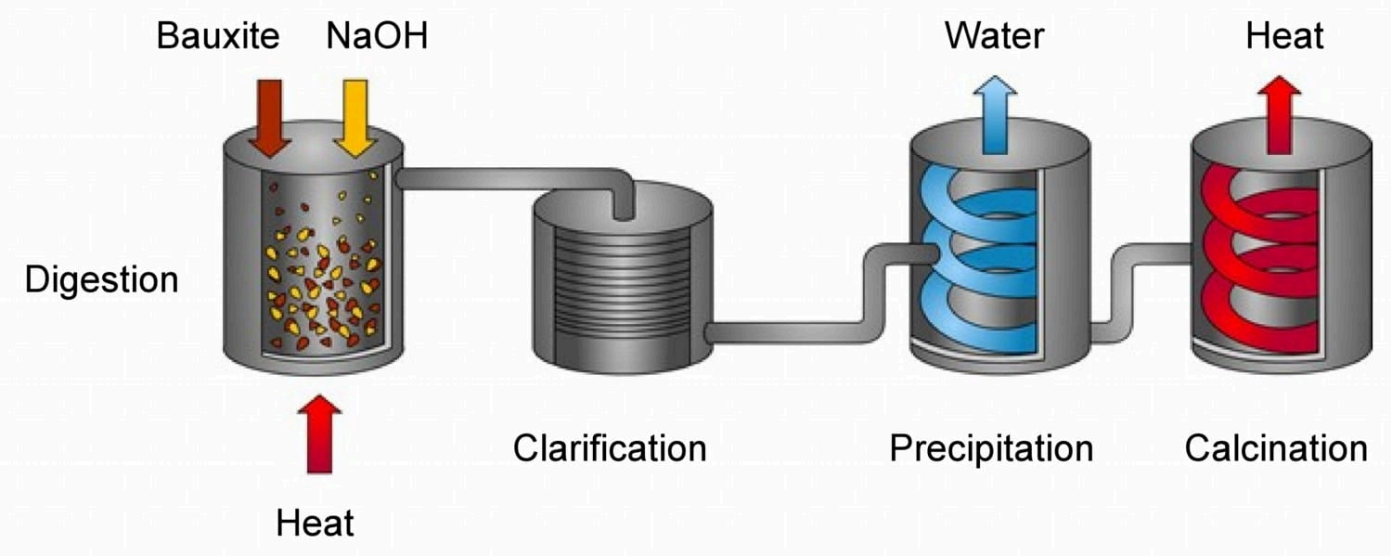
Austrian chemist Karl Josef Bayer (1847 –1904) whose father, Friedrich, founded the Bayer chemical and pharmaceutical company.

Bauxite, the most important ore of aluminum, contains only 30-50% alumina, Al_2O_3, the rest being a mixture of silica, iron oxide, and titanium dioxide. Thus, the alumina must be purified before it can be used as the oxide or refined into aluminum metal. In the Bayer process, bauxite is digested in hot (175 °C) sodium hydroxide (NaOH) solution (Figure). This converts the alumina to aluminum hydroxide, $Al(OH)_3$, which dissolves in the hydroxide solution.

$$\mathrm{Al_2O_3 + 2\ OH^- + 3\ H_2O \rightarrow 2\ [Al(OH)_4]^-} \tag{6.6.1.3}$$

The other components do not dissolve and are filtered off. The hydroxide solution is cooled, and the dissolved aluminum hydroxide precipitates, which when heated to 1050 °C is calcined into alumina.

$$\mathrm{2\ Al(OH)_3 \rightarrow Al_2O_3 + 3\ H_2O} \tag{6.6.1.4}$$



Schematic representation of the Bayer process. Copyright: Andrew Perchard, Alcan Aluminium UK and courtesy of Glasgow University Archives (2007).

Once a pure alumina is formed, it is dissolved in molten cryolite (Na_3AlF_6) and reduced to the pure metal at elevated temperatures (950 - 980 °C) using the Hall-Héroult process, developed independently Charles Hall and Paul Héroult.



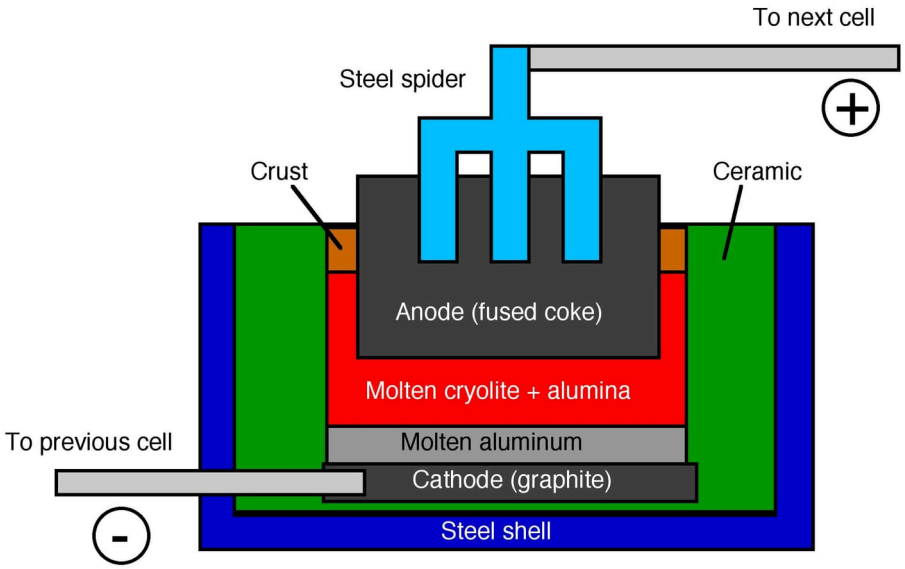
American inventor and engineer Charles Martin Hall (1863 – 1914).



French scientist Paul (Louis-Toussaint) Héroult (1863 – 1914).

Both of the electrodes used in the electrolysis of aluminum oxide are carbon. The reaction at the cathode involves the reduction of the Al^{3+}. The aluminum metal then sinks to the bottom and is tapped off, where it is usually cast into large blocks called aluminum billets.

$$\mathrm{Al^{3+} + 3\ e^- \rightarrow Al} \tag{6.6.1.5}$$



Schematic of the Hall-Héroult cell.

At the anode oxygen is formed, (6.1.6) , where it reacts with the carbon anode is then oxidized to carbon dioxide, (6.1.7). The anodes must be replaced regularly, since they are consumed. While the cathodes are not oxidized they do erode due to electrochemical processes and metal movement.

$$\mathrm{2\ O_2^- \rightarrow O_2 + 4\ e^-} \tag{6.6.1.6}$$

$$\mathrm{C + O_2 \rightarrow CO_2} \tag{6.6.1.7}$$

Although the Hall-Héroult process consumes a lot of energy, alternative processes have always found to be less economically and ecologically viable.

Physical properties

Table summarizes the physical properties of the Group 13 elements. While, aluminum, indium, and thallium have typical metal properties, gallium has the largest liquid range of any element. Boron exists as a molecular compound in the solid state, hence its high melting point.

Element	Mp (°C)	Bp (°C)	Density (g/cm^3)
B	2300	3658	2.3
Al	661	2467	2.7
Ga	30	2403	5.9 (solid), 6.1 (liquid)
In	156	2080	7.3
Tl	304	1457	11.9

Table 6.6.1.5**:** Selected physical properties of the Group 13 elements.

Bibliography

- C. M. Hall. *Process of reducing aluminum from its fluoride salts by electrolysis*. US Patent 400,664 (1886).
- L. B. Alemany, S. Steuernagel, J.-P. Amoureux, R. L. Callender, and A. R. Barron. *Solid State Nuclear Magnetic Resonance*, 1999, **14**, 1.
- L. B. Alemany, R. L. Callender, A. R. Barron, S. Steuernagel, D. Iuga, and A. P. M. Kentgens, *J. Phys. Chem., B.*, 2000, **104**, 11612.
- M. Bishop, N. Shahid, J. Yang, and A. R. Barron, *Dalton Trans.*, 2004, 2621.

This page titled 6.6.1: The Group 13 Elements is shared under a CC BY 3.0 license and was authored, remixed, and/or curated by Andrew R. Barron (CNX) via source content that was edited to the style and standards of the LibreTexts platform.

6.6.2: Trends for the Group 13 Compounds

Boron is a non-metal with metalloidal tenancies. The higher ionization energies for boron than for its other Group homologs are far more than would be compensated by lattice energies, and thus, the B^{3+} ion plays no part in the chemistry of boron, and its chemistry is dominated by the formation of covalent compounds. In contrast, the elements aluminum through thallium each has a low electronegativity and the chemistry of their compounds reflects this characteristic. Each of the Group 13 metals forms both covalent compounds and ionic coordination complexes.

All of the Group 13 (IIIA) elements have a valence shell electron configuration of ns^2np^1. As a consequence all of the Group 13 elements for compounds in which they adopt a +3 oxidation state. While the lighter elements do form compounds with lower oxidation state, they are not the norm; however, the +1 oxidation state is more prevalent for the heavier elements in particular thallium. The rational for this is described as the *inert pair effect*. The inert pair effect is usually explained by the energy of the *n*s orbital is lower making it harder to ionize and stabilizing a ns^2np^0 valence shell. However, as may be seen from Table 6.6.2.1 the sum of the second and third ionization enthalpies is lower for indium (4501 kJ/mol), than for gallium (4916 kJ/mol), but with thallium intermediate (4820 kJ/mol). The true source of the inert pair effect is that the lower bond strengths observed for the heavier elements (due to more diffuse orbitals and therefore less efficient overlap) cannot compensate for the energy needed to promote the ns^2 electrons. For example, the bond energies for gallium, indium, and thallium in MCl_3 are 242, 206, and 153 kJ/mol, respectively. It has also been suggested that relativistic effects make a contribution to the inert pair effect.

Table 6.6.2.1: Summary of first three ionization enthalpies for the Group 13 metals.

Ionization enthalpy (kJ/mol)	Al	Ga	In	Tl
1	576.4	578.3	558.1	589.0
2	1814.1	1969.3	1811.2	1958.7
3	2741.4	2950.0	2689.3	2868.8

In summary, it may be stated that while the chemistry of gallium, indium and thallium is very similar, that of aluminum is slightly different, while boron's chemistry is very different from the rest of the Group.

A second effect is noticed in the transition from aluminum, to gallium, to indium. Based upon their position in the Group it would be expected that the ionic radius and associated lattice parameters should follow the trend:

$$Al < Ga < In < Tl$$

However, as may be seen from Table 6.6.2.2 the values for gallium are either the same as, or smaller, than that of aluminum. In a similar manner, the covalent radius and covalent bond lengths as determined by X-ray crystallography for a range of compounds (Table 6.6.2.3).

Table 6.6.2.2: Lattice parameter (a) for zinc blende forms of the Group 13 phosphides and arsenides. Data from Semiconductors: Group IV Elements and III-V Compounds, Ed. O. Madelung, Springer-Verlag, Berlin (1991).

Element	Phosphide lattice parameter (Å)	Arsenide lattice parameter (Å)
Al	5.4635	5.6600
Ga	5.4505	5.6532
In	5.8687	6.0583

Table 6.6.2.3: Comparative crystallographically determined bond lengths.

Element	M-C (Å)	M-N (Å)	M-O (Å)	M-Cl (Å)
Al	1.96 – 2.02	2.03 – 2.19	1.74 – 1.93	2.09 – 2.11

Ga	1.97 – 2.01	1.95 – 2.12	1.89 - 1.94	2.12 – 2.23
In	2.14 – 2.17	2.23 – 2.31	2.19 – 2.20	2.39 – 2.47

Gallium is significantly smaller than expected from its position within the Group 13 elements (Table 6.6.2.4). The rational for this may be attributed to an analogous effect as seen in the *lanthanide contraction* observed for the lanthanides and the 3rd row of transition elements. In multi-electron atoms, the decrease in radius brought about by an increase in nuclear charge is partially offset by increasing electrostatic repulsion among electrons. In particular, a "shielding effect" results when electrons are added in outer shells, electrons already present shield the outer electrons from nuclear charge, making them experience a lower effective charge on the nucleus. The shielding effect exerted by the inner electrons decreases in the order *s* > *p* > *d* > *f*. As a sub-shell is filled in a period the atomic radius decreases. This effect is particularly pronounced in the case of lanthanides, as the 4*f* sub-shell is not very effective at shielding the outer shell (n = 5 and n = 6) electrons. However, a similar, but smaller effect should be observed with the post-transition metal elements, i.e., gallium. This is indeed observed (Table 6.6.2.4).

Table 6.6.2.4: Comparison of the covalent and ionic radii of Group 13 elements.

Element	**Covalent radius (Å)**	**Ionic radius (Å)**
Aluminum	1.21	0.53
Gallium	1.22	0.62
Indium	1.42	0.80
Iron (low spin)	1.32	0.55
Iron (high spin)	1.52	0.64

The anomalous size of gallium has two positive effects.

1. The similarity in size of aluminum and gallium means that their Group 15 derivatives have near identical lattice parameters (Table 6.6.2.3). This allows for both epitaxial growth of one material on the other, and also the formation of ternary mixtures (i.e., $Al_xGa_{1-x}As$) with matched lattice parameters. The ability to grow hetrojunction structures of Group 13-15 compounds (III-V) is the basis for the fabrication of a wide range of important optoelectronic devices, including: LEDs and laser diodes.
2. The similarity in size of gallium(III) to iron(III) (Table 6.6.2.4) means that gallium can substitute iron in a range of coordination compounds without alteration of the structure. Because of a similar size and charge as Fe^{3+}, Ga^{3+} is widely used as a non-redox-active Fe^{3+} substitute for studying metal complexation in proteins and bacterial populations.

Bibliography

- K. S. Pitzer, *Acc. Chem. Res.*, 1979, **12**, 271.
- K. D. Weaver, J. J. Heymann, A. Mehta, P. L. Roulhac, D. S. Anderson, A. J. Nowalk, P. Adhikari, T. A. Mietzner, M. C. Fitzgerald, and A. L. Crumbliss, *J. Biol. Inorg. Chem.*, 2008, **13**, 887.
- *Semiconductors: Group IV Elements and III-V Compounds*, Ed. O. Madelung, Springer-Verlag, Berlin (1991).

This page titled 6.6.2: Trends for the Group 13 Compounds is shared under a CC BY 3.0 license and was authored, remixed, and/or curated by Andrew R. Barron (CNX) via source content that was edited to the style and standards of the LibreTexts platform.

6.6.3: Borides

The non-metallic nature of boron means that it makes a number of binary compounds with elements more electropositive than itself (i.e., metals). These compounds are called, *borides*, and some are also formed with metalloid elements as well (e.g., arsenic). In this regard, borides may be considered similar to carbides, silicides, and some phosphides.

Borides are prepared in a number of ways, however, direct combination of the elements, (6.3.1), is the simplest. Other routes include, electrolysis of the fused salts, and the reduction of the metal oxide with a mixture of carbon and boron carbide.

$$\mathrm{M} + \mathrm{x\ B} \rightarrow \mathrm{MB_x} \tag{6.6.3.1}$$

Metal borides are generally refractory in character and chemically inert, while they often have properties better that of the constituent elements. For example, the thermal conductivity of TiB_2 is about ten times greater than that of titanium, and the melting point is significantly higher (Table 6.6.3.1).

Table 6.6.3.1: The melting points of Group 4 metals and their borides.

Element	Melting point (°C)	Boride	Melting point (°C)
Ti	1725	TiB_2	3225
Zr	1855	ZrB_2	2990
Hf	2233	HfB_2	3100

The structures of metal borides depends on the M:B ratio. Borides with an isolated boron atom have a low B:M ratio: M_4B, M_3B, M_2B, M_5B_2, and M_7B_3. In such compounds the boron atom is normally in a triangular-prismatic or square-antiprismatic hole in a metal lattice. Borides with equal or near equal metal and boron ratio have structures with either pairs of boron atoms (as in V_3B_2), single boron chains (seen in all MB compounds), or double boron chains (observed for many M_3B_4 compounds). Increasing the boron content results in two-dimensional structures. For example, MB_2 usually consists of alternate hexagonal layers of metal and boron (Figure 6.6.3.1). Finally, boron rich borides (e.g., MB_4, MB_6, and MB_{12}) all have three-dimensional structures.

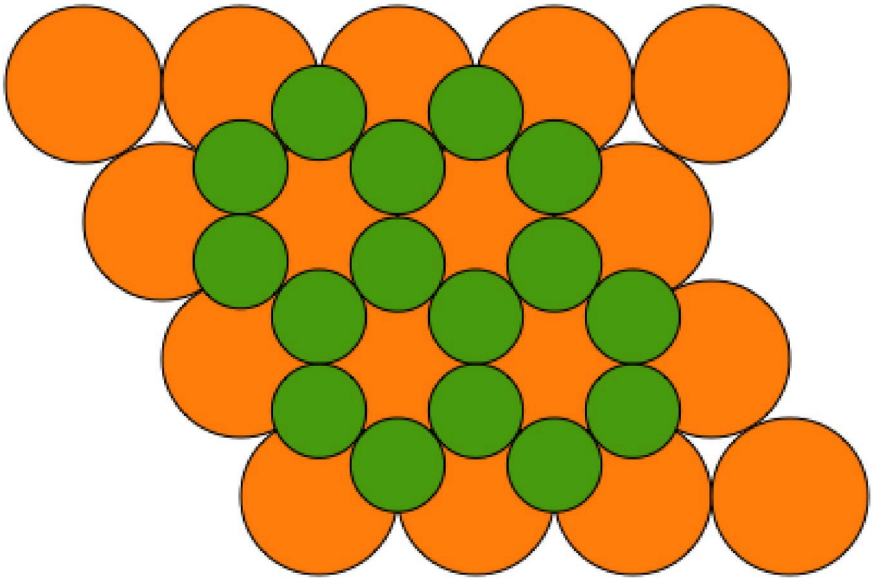


Figure 6.6.3.1: Alternate layers of metal atoms (large circles) and boron (small circles) in MB_2.

This page titled 6.6.3: Borides is shared under a CC BY 3.0 license and was authored, remixed, and/or curated by Andrew R. Barron (CNX) via source content that was edited to the style and standards of the LibreTexts platform.

6.6.4: Boron Hydrides

Borane and diborane

Borane (BH_3) formed in the gaseous state from decomposition of other compounds, (6.4.2) but cannot be isolated except as a Lewis acid-base complex (6.4.1). As such many borane adducts are known.

$$\mathrm{BH_3 + PPh_3 \rightarrow H_3B\text{-}PPh_3} \tag{6.6.4.1}$$

In the absence of a Lewis base the dimeric diborane (B_2H_6) is formed. Diborane is generally synthesized by the reaction if BF_3 with a hydride source, such as $NaBH_4$, (6.4.4), or $LiAlH_4$, (6.4.3).

$$\mathrm{H_3B\text{-}PF_3 \xrightarrow{\Delta} BH_3 + PF_3} \tag{6.6.4.2}$$

$$\mathrm{3\ LiAlH_4 + 4\ BF_3 \rightarrow 2\ B_2H_6\uparrow\ + 3\ LiAlF_4} \tag{6.6.4.3}$$

The structure of diborane (Figure 6.6.4.1 a) is considered to be electron deficient, and has been confirmed by IR spectroscopy and electron diffraction. The four terminal B-H bonds are normal covalent bonds, however, the bridging B-H-B unit consists of two three-centered two-electron bonds, each ordinarily considered to be formed by the combination of two boron sp^3 orbitals and one hydrogen s orbital (Figure 6.6.4.1 b). However, a consideration of the H-B-H bond angle associated with the terminal hydrides (120°) it is perhaps better to consider the BH_2 fragment to be sp^2 hybridized, and the B-H-B bridging unit to be a linear combination of one sp^2 orbital and one p orbital from each boron atom with the two hydrogen s orbitals. Diborane represents the archetypal electron deficient dimeric compound, of which Al_2Me_3 is also a member of this class of electron deficient molecules.

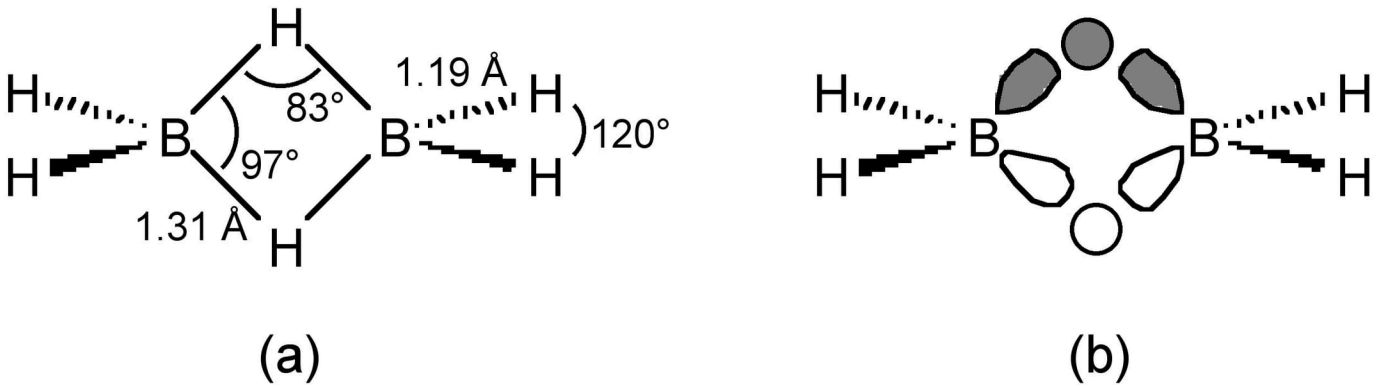


Figure 6.6.4.1: The structure (a) and the typical view of the three-centered two-electron bonds (b) in diborane, B_2H_6.

B_2H_6 is spontaneously and highly exothermically inflammable above 25 °C (ΔH = -2137.7 kJ/mol), (6.4.5). It is often used as one of a range of solvate forms for safety for both its flammability and toxicity.

$$\mathrm{3\ NaBH_4 + 4\ BF_4 \rightarrow 2\ B_2H_6\uparrow\ + 3\ NaBF_4} \tag{6.6.4.4}$$

$$\mathrm{B_2H_6 + 3\ O_2 \rightarrow B_2O_3 + 3\ H_2O} \tag{6.6.4.5}$$

Most reactions of diborane involve the cleavage of the dimeric structure. Hydrolysis of diborane yields boric acid, (6.4.6), while alcoholysis yields the appropriate borate ester, (6.4.7). Diborane reacts with Lewis bases to form the appropriate Lewis acid-base complex, (6.4.8).

$$\mathrm{B_2H_6 + 6\ H_2O \rightarrow 2\ B(OH)_3 + 6\ H_2\uparrow} \tag{6.6.4.6}$$

$$\mathrm{B_2H_6 + 6\ ROH \rightarrow 2\ B(OR)_3 + 6\ H_2\uparrow} \tag{6.6.4.7}$$

$$\mathrm{B_2H_6 + NR_3 \rightarrow 2\ H_3B\text{-}NR_3} \tag{6.6.4.8}$$

Borohydride

The borohydride anion (or more properly the tetrahydridoborate anion), BH_4^-, can be considered as the Lewis acid-base complex between borane and H^-. A typical synthesis involves the reaction of a borate ester with a hydride source, (6.4.9).

$$4\ \mathrm{NaH} + \mathrm{B(OMe)_3} \rightarrow \mathrm{NaBH_4} + 3\ \mathrm{NaOMe} \tag{6.6.4.9}$$

Sodium borohydride is a stable white crystalline solid that is stable in dry air and is non-volatile. The boron in borohydride (BH_4^-) is tetrahedral. Although it is insoluble in Et_2O, it is soluble in water (in which it reacts slowly), THF, ethylene glycol, and pyridine. Interestingly, $NaBH_4$ reacts rapidly with MeOH, but dissolves in EtOH. Sodium borohydride has extensive uses in organic chemistry as a useful reducing agent in which it donates a hydride (H^-).

Higher Boranes

Higher boron hydrides contain, in addition to the bridging B-H-B unit, one or more B-B bonds. The higher boranes are usually formed by the thermal decomposition of diborane, (6.4.10) and (6.4.11).

$$2\ \mathrm{B_2H_6} \rightarrow \mathrm{B_4H_{10}} + \mathrm{H_2} \tag{6.6.4.10}$$

$$5\ \mathrm{B_2H_6} \rightarrow 2\ \mathrm{B_5H_9} + 6\ \mathrm{H_2} \tag{6.6.4.11}$$

These higher boranes have 'open' cluster structures, e.g., Figure 6.6.4.2 - Figure 6.6.4.4. Tetraborane, or to be more precise tetraborane(10) or *arachno*-B_4H_{10}, is a foul-smelling toxic gas. Pentaborane (9) is a toxic liquid (with a distinctive garlic odor) that can detonate in air, and like decaborane(14) was at one time considered as a potential rocket fuel. Because simple boron compounds burn with a characteristic green flame, the nickname for these fuels in the US military was *Green Dragon*. Problems with using boranes as a fuel included their toxicity and the characteristic of bursting into flame on contact with the air; furthermore, the exhaust would also be toxic. The US program resulted in a stockpile of borane fuels, in particular pentaborane(9), which was not destroyed until 2000. The system for the destroying the boranes was appropriately known as *Dragon Slayer*.

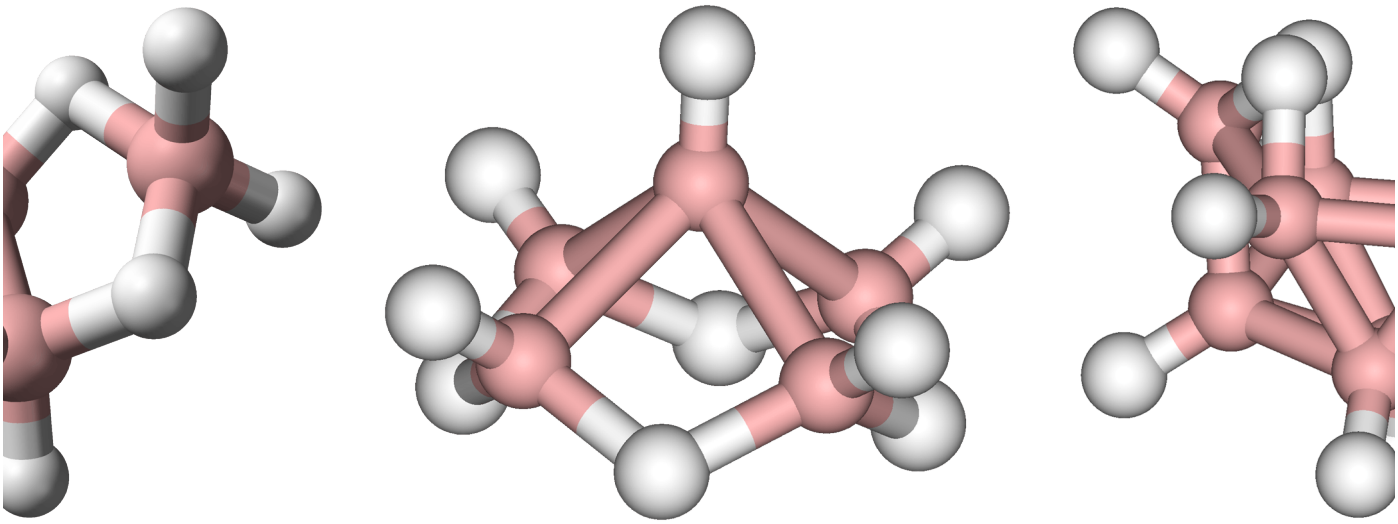


Figure 6.6.4.2: The molecular structure of tetraborane(10), B_4H_{10}, pentaborane(9), B_5H_9, and decaborane(14), $B_{10}H_{14}$ Boron atoms are represented by pink spheres, and hydrogen by white spheres.

Bibliography

- D. F. Gaines, *Acc. Chem. Res.*, 1973, **6**, 416.
- C. E. Housecroft, *Boranes and metalloboranes: structure, bonding and reactivity*, Ellis Horwood, Chichester (1990).
- C. F. Lane, *Chem. Rev.*, 1976, **76**, 773.

This page titled 6.6.4: Boron Hydrides is shared under a CC BY 3.0 license and was authored, remixed, and/or curated by Andrew R. Barron (CNX) via source content that was edited to the style and standards of the LibreTexts platform.

6.6.5: Wade's Rules

Ken Wade (Figure 6.6.5.1) developed a method for the prediction of shapes of borane clusters; however, it may be used for a wide range of substituted boranes (such as carboranes) as well as other classes of cluster compounds.



Figure 6.6.5.1: Chemist Ken Wade FRS.

Wade's rules are used to rationalize the shape of borane clusters by calculating the total number of **skeletal electron pairs (SEP)** available for cluster bonding. In using Wade's rules it is key to understand structural relationship of various boranes (Figure 6.6.5.2).

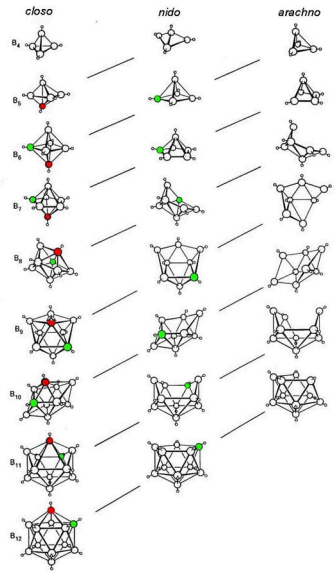


Figure 6.6.5.2: Structural relationship between *closo*, *nido*, and *arachno* boranes (and hetero-substituted boranes). The diagonal lines connect species that have the same number of skeletal electron pairs (SEP). Hydrogen atoms except those of the B-H framework are omitted. The red atom is omitted first, the green atom removed second. Adapted from R. W. Rudolph, *Acc. Chem. Res.*, 1976, **9**, 446.

The general methodology to be followed when applying Wade's rules is as follows:

1. Determine the total number of valence electrons from the chemical formula, i.e., 3 electrons per B, and 1 electron per H.

2. Subtract 2 electrons for each B-H unit (or C-H in a carborane).
3. Divide the number of remaining electrons by 2 to get the number of skeletal electron pairs (SEP).
4. A cluster with *n* vertices (i.e., *n* boron atoms) and *n*+1 SEP for bonding has a *closo* structure.
5. A cluster with *n*-1 vertices (i.e., *n*-1 boron atoms) and *n*+1 SEP for bonding has a *nido* structure.
6. A cluster with *n*-2 vertices (i.e., *n*-2 boron atoms) and *n*+1 SEP for bonding has an *arachno* structure.
7. A cluster with *n*-3 vertices (i.e., *n*-3 boron atoms) and *n*+1 SEP for bonding has an *hypho* structure.
8. If the number of boron atoms (i.e., *n*) is larger than *n*+1 SEP then the extra boron occupies a capping position on a triangular phase.

What is the structure of B_5H_{11}?

1. Total number of valence electrons = (5 x B) + (11 x H) = (5 x 3) + (11 x 1) = 26
2. Number of electrons for each B-H unit = (5 x 2) = 10
3. Number of skeletal electrons = 26 – 10 = 16
4. Number SEP = 16/2 = 8
5. If *n*+1 = 8 and *n*-2 = 5 boron atoms, then *n* = 7
6. Structure of *n* = 7 is pentagonal bipyramid (Figure 6.6.5.2), therefore B_5H_{11} is an *arachno* based upon a pentagonal bipyramid with two apexes missing (Figure 6.6.5.3).

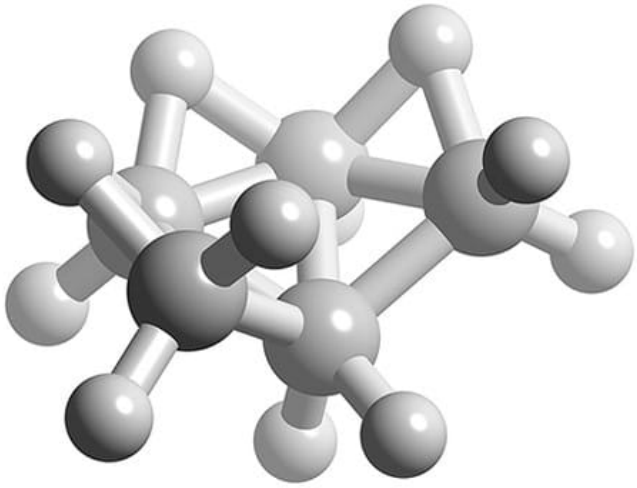


Figure 6.6.5.3: Ball and stick representation of the structure of B_5H_{11}.

What is the structure of B_5H_9?

1. Total number of valence electrons = (5 x B) + (9 x H) = (5 x 3) + (9 x 1) = 24
2. Number of electrons for each B-H unit = (5 x 2) = 10
3. Number of skeletal electrons = 24 – 10 = 14
4. Number SEP = 14/2 = 7
5. If *n*+1 = 7 and *n*-1 = 5 boron atoms, then *n* = 6
6. Structure of *n* = 6 is octahedral (Figure 6.6.5.2), therefore B_5H_9 is a *nido* structure based upon an octahedral structure with one apex missing (Figure 6.6.5.4).

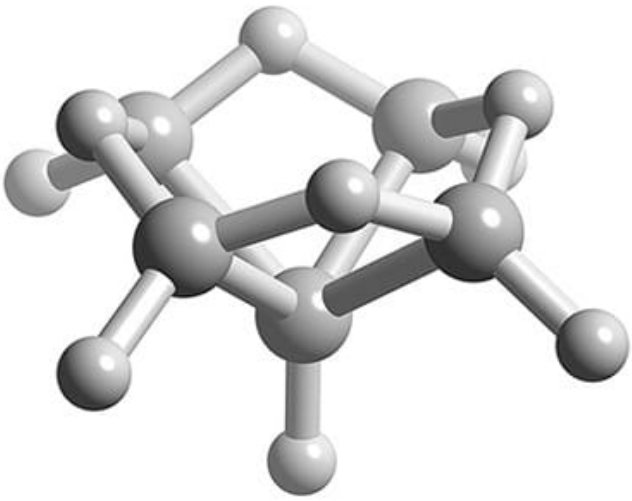


Figure 6.6.5.4: Ball and stick representation of the structure of B_5H_9.

6.6.5.1 Exa

What is the structure of $B_6H_6^{2-}$?

Solution

1. Total number of valence electrons = (6 x B) + (3 x H) = (6 x 3) + (6 x 1) + 2 = 26
2. Number of electrons for each B-H unit = (6 x 2) = 12
3. Number of skeletal electrons = 26 – 12 = 14
4. Number SEP = 14/2 = 7
5. If *n*+1 = 7 and *n* boron atoms, then *n* = 6
6. Structure of *n* = 6 is octahedral (Figure 6.6.5.2), therefore $B_6H_6^{2-}$ is a *closo* structure based upon an octahedral structure (Figure 6.6.5.5).

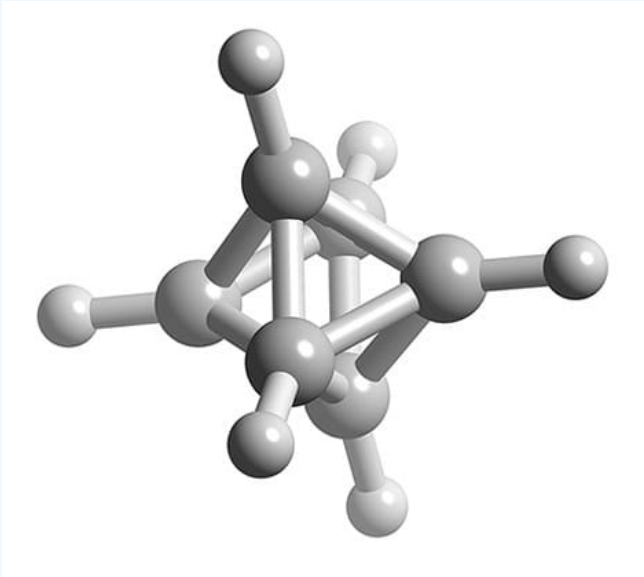


Figure 6.6.5.5: Ball and stick representation of the structure of $B_6H_6^{2-}$.

Table 6.6.5.1 provides a summary of borane cluster with the general formula $B_nH_n^{x-}$ and their structures as defined by Wade's rules.

Table 6.6.5.1: Wade's rules for boranes.

Type	Basic formula	Example	# of verticies	# of vacancies	# of e- in B + charge	# of bonding MOs
Closo	$B_nH_n^{2-}$	$B_6H_6^{2-}$	n	0	3n + 2	n + 1
Nido	$B_nH_n^{4-}$	B_5H_9	n + 1	1	3n + 4	n + 2
Arachno	$B_nH_n^{6-}$	B_4H_{10}	n + 2	2	3n + 6	n + 3
Hypho	$B_nH_n^{8-}$	$B_5H_{11}^{2-}$	n + 3	3	3n + 8	n + 4

Bibliography

- R. W. Rudolph, *Acc. Chem. Res.*, 1976, **9**, 446.
- K. Wade, *Adv. Inorg. Chem. Radiochem.*, 1976, **18**, 1.

This page titled 6.6.5: Wade's Rules is shared under a CC BY 3.0 license and was authored, remixed, and/or curated by Andrew R. Barron (CNX) via source content that was edited to the style and standards of the LibreTexts platform.

6.6.6: Trends for the Oxides of the Group 13 Elements

All of the Group 13 elements form a trivalent oxide (M_2O_3). The chemical properties of the oxides follow the trend acidic to basic going down the Group (Table 6.6.6.1). The physical properties are consistent with the electronegativities and covalent character in the M-O bonds. Thallium oxide is unique in that it decomposes above 100 °C to yield the thalium(I) oxide, Tl_2O. The other oxides are all stable to high temperatures.

Table 6.6.6.1: Properties of the Group 13 oxides.

Oxide	Color	Chemical property	Melting point (°C)
B_2O_3	White/colorless	Weak acid	450 (trigonal), 510 (tetrahedral)
Al_2O_3	White/colorless	Amphoteric	2072 (α)
Ga_2O_3	White/colorless	Amphoteric	1900 (α), 1725 (β)
In_2O_3	Yellow	Weakly basic	1910
Tl_2O_3	Brown-black	Basic, oxidizing	100 (decomposes)

Bibliography

- G. E. Jellison, Jr., L. W. Panek, P. J. Bray, and G. B. Rouse, Jr., *J. Chem. Phys.*, 1977, **66**, 802.

This page titled 6.6.6: Trends for the Oxides of the Group 13 Elements is shared under a CC BY 3.0 license and was authored, remixed, and/or curated by Andrew R. Barron (CNX) via source content that was edited to the style and standards of the LibreTexts platform.

6.6.7: Boron Oxides, Hydroxides, and Oxyanions

Oxides

Boron oxide, B_2O_3, is made by the dehydration of boric acid, (6.7.1). It is a glassy solid with no regular structure, but can be crystallized with extreme difficulty. The structure consists of infinite chains of triangular BO_3 unit (Figure $6.6.7.1$). Boron oxide is acidic and reacts with water to reform boric acid, (6.7.1).

$$2\ \mathrm{B(OH)_3} \overset{\Delta}{\rightleftharpoons} \mathrm{B_2O_3} + \mathrm{H_2O} \tag{6.6.7.1}$$

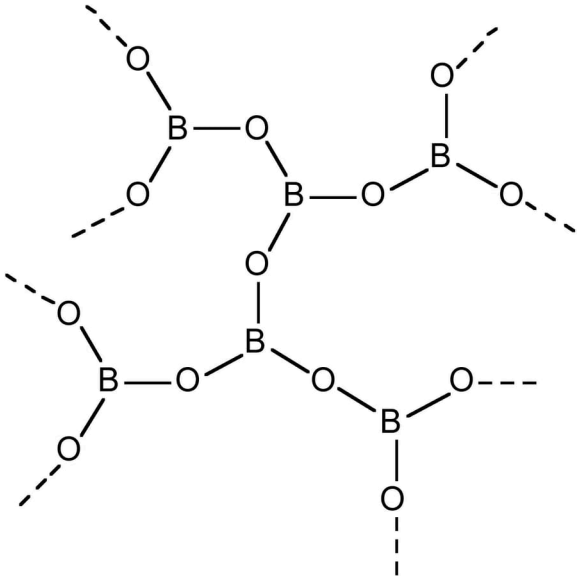


Figure $6.6.7.1$: Glassy structure of B_2O_3.

The reaction of B_2O_3 with hydroxide yields the metaborate ion, (6.7.2), whose planar structure (Figure $6.6.7.2$) is related to metaboric acid. Boron oxide fuses with a wide range of metal and non-metal oxides to give borate glasses.

$$\mathrm{B_2O_3} + 6\ \mathrm{KOH} \rightarrow 2\ \mathrm{K_3[B_3O_6]} + 3\ \mathrm{H_2O} \tag{6.6.7.2}$$

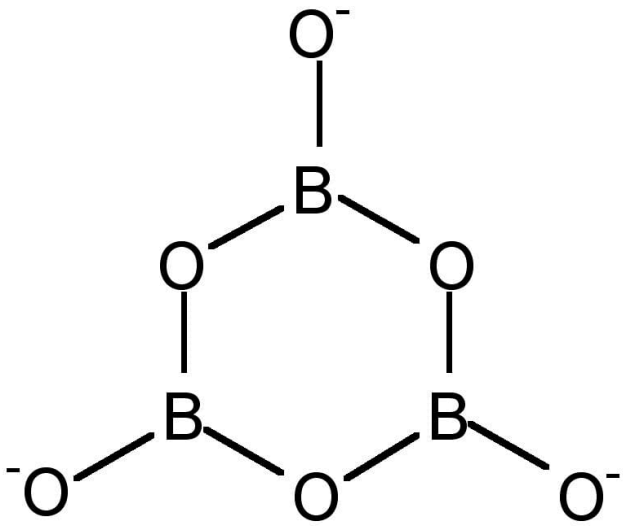


Figure 6.6.7.2: Structure of the metaborate anion, $[B_3O_6]^{3-}$.

Boric acid

Boric acid, $B(OH)_3$, usually obtained from the dissolution of borax, $Na_2[B_4O_5(OH)_4]$, is a planar solid with intermolecular hydrogen bonding forming a near hexagonal layered structure, broadly similar to graphite (Figure 6.6.7.3). The inter layer distance is 3.18 Å.

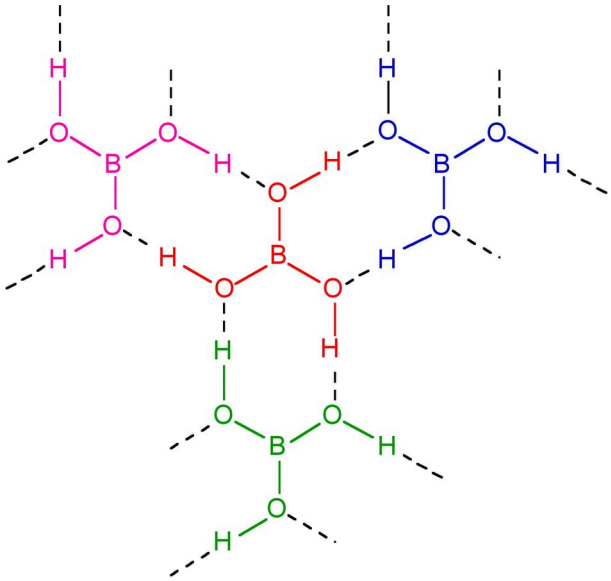


Figure 6.6.7.3: The hydrogen bonded structure of boric acid.

A summary of reactions of the reactivity of boric acid is shown in Figure 6.6.7.4.

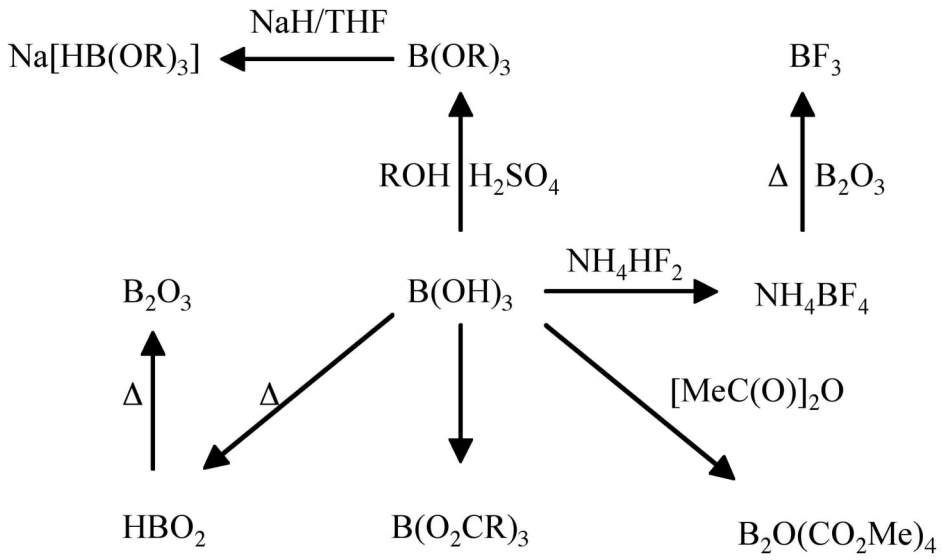


Figure 6.6.7.4: Selected reactions of boric acid. Adapted from F. A. Cotton and G. Wilkinson, *Advanced Inorganic Chemistry*, 4th Ed. Wiley Interscience (1980).

Upon dissolution of boric acid in water, boric acid does not act as a proton acid, but instead reacts as a Lewis acid, (6.7.3).

$$\mathrm{B(OH)_3 + 2\ H_2O \rightleftharpoons B(OH)_4^- + H_3O^+} \tag{6.6.7.3}$$

The reaction may be followed by ^{11}B NMR spectroscopy from the change in the chemical shift (Figure 6.6.7.5).

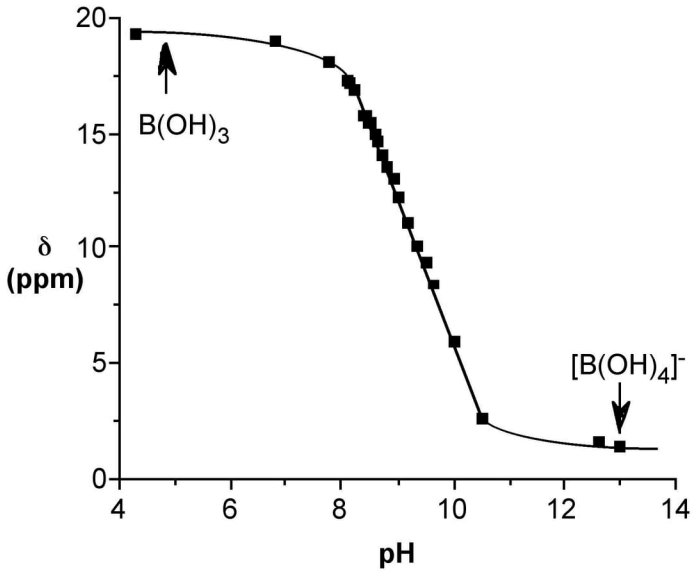


Figure 6.6.7.5: The ^{11}B NMR chemical shift (ppm) of boric acid as a function of pH. Adapted from M. Bishop, N. Shahid, J. Yang, and A. R. Barron, *Dalton Trans*., 2004, 2621.

Since the ^{11}B NMR shift is directly proportional to the mole fraction of the total species present as the borate anion (e.g., $[B(OH)_4]^-$) the ^{11}B NMR chemical shift at a given temperature, $\delta_{(obs)}$, may be used to calculate both the mole fraction of boric acid and the borate anion, i.e., (6.7.4) and (6.7.5), respectively. Using these equations the relative speciation as a function of pH may be calculated for both boric acid (Figure 6.6.7.6). The pH at which a 50:50 mixture of acid and anion for boric acid is *ca*. 9.4.

$$\chi_{(\mathrm{acid})} = \frac{\delta_{(\mathrm{obs})} - \delta_{(\mathrm{anion})}}{\delta_{(\mathrm{acid})} - \delta_{(\mathrm{anion})}} \tag{6.6.7.4}$$

$$\chi_{(\text{acid})} = \frac{\delta_{(\text{acid})} - \delta_{(\text{obs})}}{\delta_{(\text{acid})} - \delta_{(\text{anion})}} \tag{6.6.7.5}$$

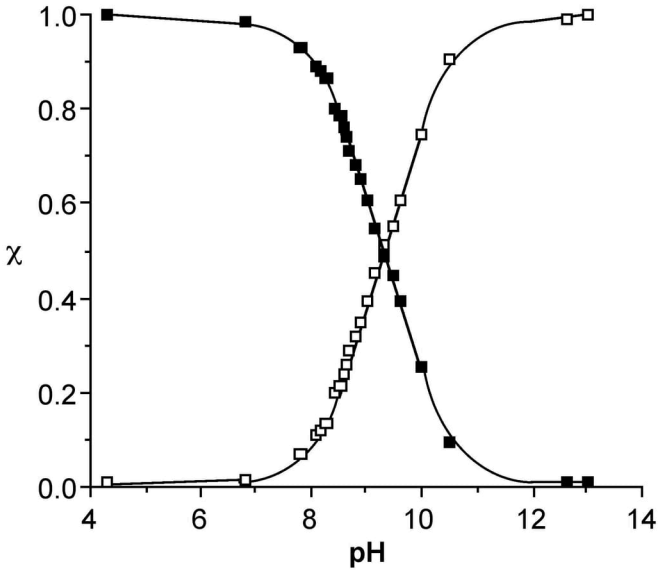


Figure 6.6.7.6: The mole fraction of acid (black squares) and anion (white squares) forms of boric acid as a function of pH. Adapted from M. Bishop, N. Shahid, J. Yang, and A. R. Barron, *Dalton Trans*., 2004, 2621.

In concentrated solutions, the borate ion reacts further to form polyborate ions. The identity of the polyborate is dependent on the pH. With increasing pH, $B_5O_6(OH)_4^-$, (6.7.5), $B_3O_3(OH)_4^-$, (6.7.6), and $B_4O_5(OH)_4^{2-}$, (6.7.7), are formed. The structure of each borate is shown in Figure 6.6.7.7. Once the ratio of $B(OH)_3$ to $B(OH)_4^-$ is greater than 50%, only the mono-borate is observed.

$$4\ \mathrm{B(OH)_3} + \mathrm{B(OH)_4^-} \rightleftharpoons \mathrm{B_5O_6(OH)_4^-} + 6\ \mathrm{H_2O} \tag{6.6.7.6}$$

$$4\ \mathrm{B(OH)_3} + \mathrm{B(OH)_4^-} \rightleftharpoons \mathrm{B_3O_3(OH)_4^-} + 3\ \mathrm{H_2O} \tag{6.6.7.7}$$

$$2\ \mathrm{B(OH)_3} + 2\ \mathrm{B(OH)_4^-} \rightleftharpoons \mathrm{B_4O_5(OH)_4^{2-}} + 5\ \mathrm{H_2O} \tag{6.6.7.8}$$

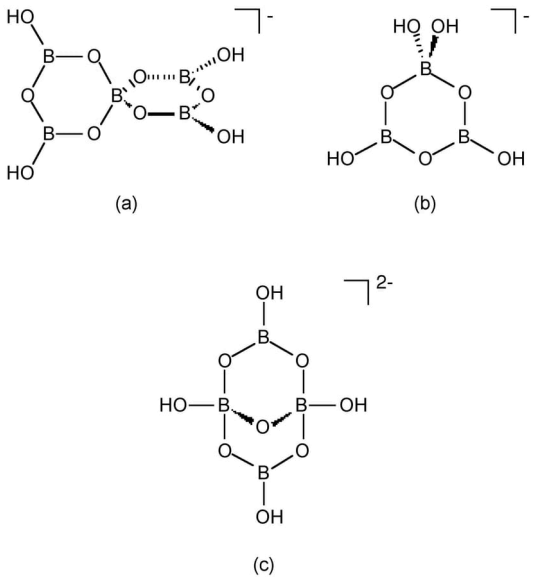


Figure 6.6.7.7: The structures of the borate anions (a) $B_5O_6(OH)_4^-$, (b) $B_3O_3(OH)_4^-$, and (c) $B_4O_5(OH)_4^{2-}$.

Borax, the usual mineral form of boric acid, is the sodium salt, $Na_2[B_4O_5(OH)_4]$, which upon dissolution in water re-equilibrates to $B(OH)_3$.

Enough to make your hair curl

In 1906, a German hairdresser, Charles Nessler who was living in London, decided to help his sister who was fed-up with having to put her straight hair in curlers. While looking for a solution, Nessler noticed that a clothesline contracted in a wavy shape when it was wet. Nessler wound his sister's hair on cardboard tubes; then he covered the hair with borax paste. After wrapping the tubes with paper (to exclude air) he heated the entire mass for several hours. Removing the paper and tubes resulted in curly hair. After much trial and error (presumably at his sisters discomfort) Nessler perfected the method by 1911, and called the process a *permanent wave* (or perm). The process involved the alkaline borax softening the hair sufficiently to be remodeled, while the heating stiffened the borax to hold the hair into shape. The low cost of borax meant that Nessler's methods was an immediate success.

Metaboric acid

Heating boric acid results in the partial dehydration to yield metaboric acid, HBO_2, (6.7.8). Metaboric acid is also formed from the partial hydrolysis of B_2O_3.

$$B(OH)_3 \underset{H_2O}{\overset{\Delta}{\rightleftharpoons}} HBO_2 \underset{H_2O}{\overset{\Delta}{\rightleftharpoons}} B_2O_3 \tag{6.6.7.9}$$

If the heating is carried out below 130 °C, HBO_2-III is formed in which B_3O_3 rings are joined by hydrogen bonding to the hydroxide on each boron atom (Figure 6.6.7.8). Continued heating to 150 °C results in HBO_2-II, whose structure consists of BO_4 tetrahedra and B_2O_5 groups chain linked by hydrogen bonding. Finally, heating above 150 °C yields cubic HBO_2-I with all the boron atoms tetrahedral.

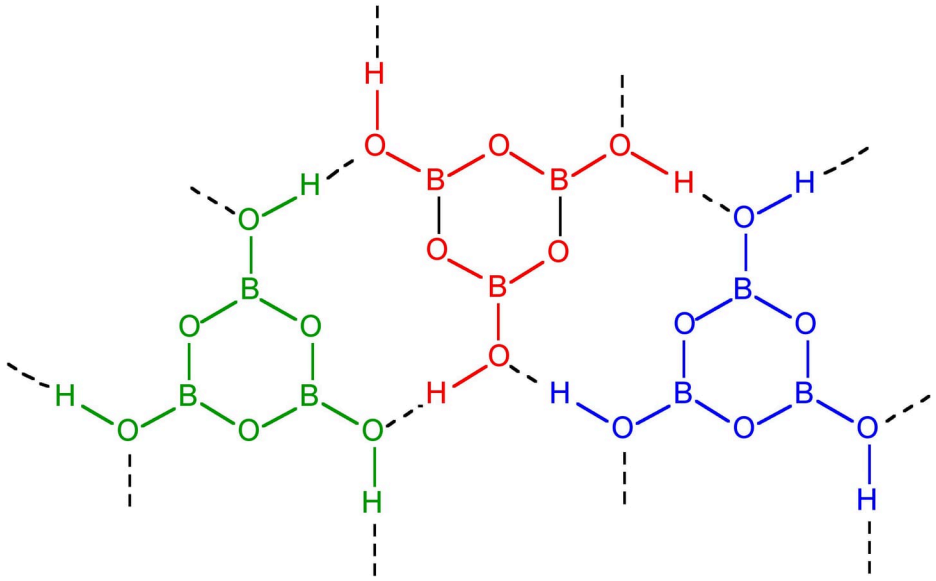


Figure 6.6.7.8: Structure of the layered structure of HBO_2-III.

Borate esters

Boric acid reacts with alcohols in the presence of sulfuric acid to form $B(OR)_3$ (Figure 6.6.7.4). This is the basis for a simple flame test for boron. Treatment of a compounds with methanol/sulfuric acid, followed by placing the reaction product in a flame results in a green flame due to $B(OMe)_3$.

In the presence of diols, polyols, or polysaccharides, boric acid reacts to form alkoxide complexes. In the case of diols, the mono-diol $[B(OH)_2L]^-$ (Figure 6.6.7.9a) and the *bis*-diol $[BL_2]^-$ (Figure 6.6.7.9b) complexes.

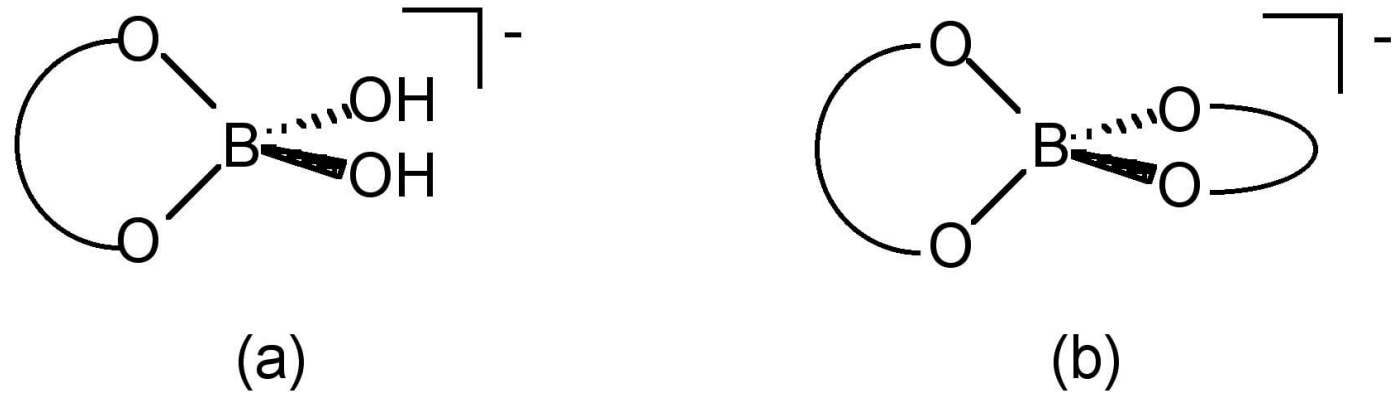


Figure 6.6.7.9: Structure of (a) the $[B(OH)_2L]^-$ and (b) the $[BL_2]^-$ anions formed by the reaction of boric acid (or borate) with a diol.

Originally it was proposed that diols react with the anion rather than boric acid, (6.7.9). In contrast, it was suggested that the optimum pH for the formation of carboxylic acid complexes is under the condition where pK_a (carboxylic acid) < pH < pK_a (boric acid). Under these conditions it is the boric acid, $B(OH)_3$, not the borate anion, $[B(OH)_4]^-$, that reacts to form the complex.

$$[B(OH)_4]^- \overset{+\,LH_2}{\rightleftharpoons} [B(OH)_2L]^- \overset{+\,LH_2}{\rightleftharpoons} [BL_2]^- \tag{6.6.7.10}$$

The conversion of boric acid to borate (6.7.3) must occur through attack of hydroxide or the deprotonation of a coordinated water ligand, either of which is related to the pKa of water. The formation of $[B(OH)_2L]^-$ from $B(OH)_3$ would be expected therefore to occur via a similar initial reaction (attack by RO^- or deprotonation of coordinated ROH) followed by a subsequent elimination of H_2O and the formation of a chelate coordination, and would therefore be related to the pKa of the alcohol. Thus the pH at which $[B(OH)_2L]^-$ is formed relative to $[B(OH)_4]^-$ will depend on the relative acidity of the alcohol. The pK_a of a simple alcohol (e.g., MeOH = 15.5, EtOH = 15.9) are close to the value for water (15.7) and the lowest pH at which $[B(OH)_2L]^-$ is formed should be comparable to that at which $[B(OH)_4]^-$ forms. Thus, the formation of $[B(OH)_2L]^-$ as compared to $[B(OH)_4]^-$ is a competition between the reaction of $B(OH)_3$ with RO^- and OH^- (Figure 6.6.7.10), and as with carboxylic acids it is boric acid not borate that reacts with the alcohol, (6.7.10).

$$B(OH)_3 \overset{+\,LH_2}{\rightleftharpoons} [B(OH)_2L]^- \overset{+\,LH_2}{\rightleftharpoons} [BL_2]^- \tag{6.6.7.11}$$

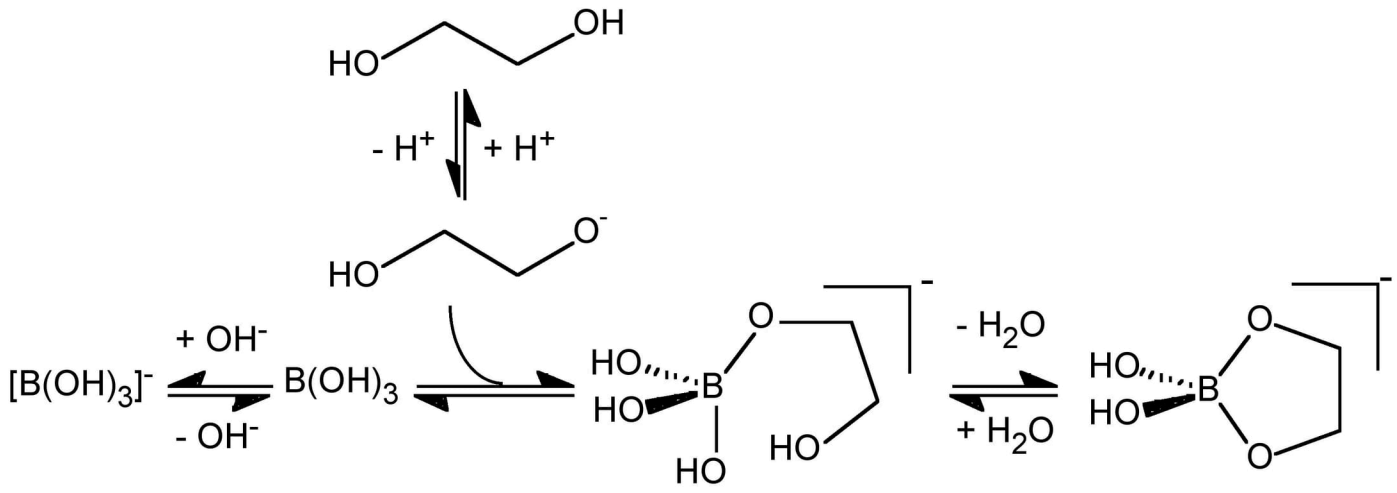


Figure 6.6.7.10: Competition between hydroxide and 1,2-diol for complexation to boron in the aqueous boric acid/diol system.

A key issue in the structural characterization and understanding of the diol/boric acid system is the assignment of the ^{11}B NMR spectral shifts associated with various complexes. A graphical representation of the observed shift ranges for boric acid chelate systems is shown in Figure 6.6.7.11.

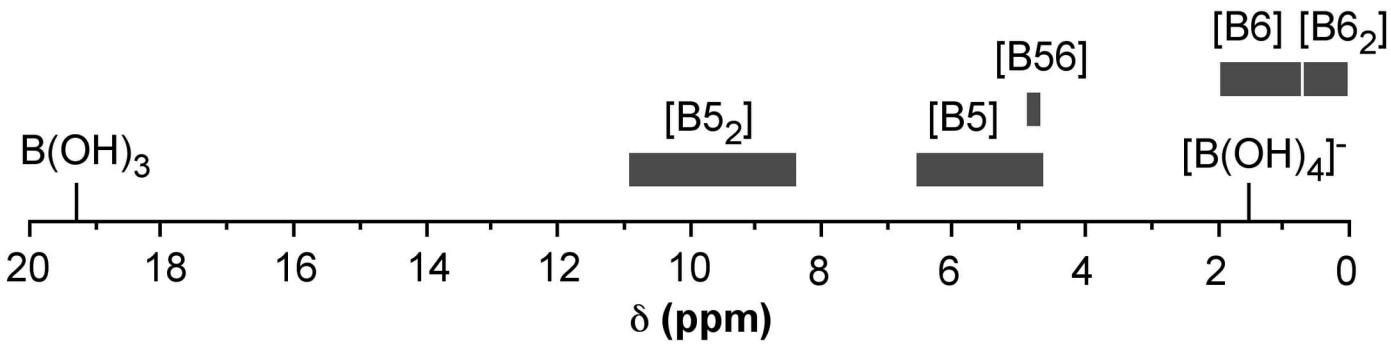


Figure 6.6.7.11: ^{11}B NMR spectroscopic shifts of chelate alkoxide compounds in comparison with boric acid and borate anion. The acronyms [B5] and [B6] are used to denote a borate complex of a 1,2-diol and 1,3-diol forming a chelate 5-membered and 6-membered ring cycle, respectively. Similarly, [B5$_2$] and [B6$_2$] denotes a borate complex of two 1,2-diols or 1,3-diols both forming [BL$_2$]$^-$. Adapted from M. Bishop, N. Shahid, J. Yang, and A. R. Barron, *Dalton Trans*., 2004, 2621.

Boric acid cross-linking of guar gum for hydraulic fracturing fluids

Thick gels of guar gum cross-linked with borax or a transition metal complex are used in the oil well drilling industry as hydraulic fracturing fluids. The polysaccharide guaran ($M_w \approx 10^6$ Da) is the major (>85 wt%) component of guar gum, and consists of a (1→4)-*β*-D-mannopyranosyl backbone with *α*-D-galactopyranosyl side chain units attached via (1→6) linkages. Although the exact ratio varies between different crops of guar gum the general structure is consistent with about one galactose to every other mannose (Figure 6.6.7.12).

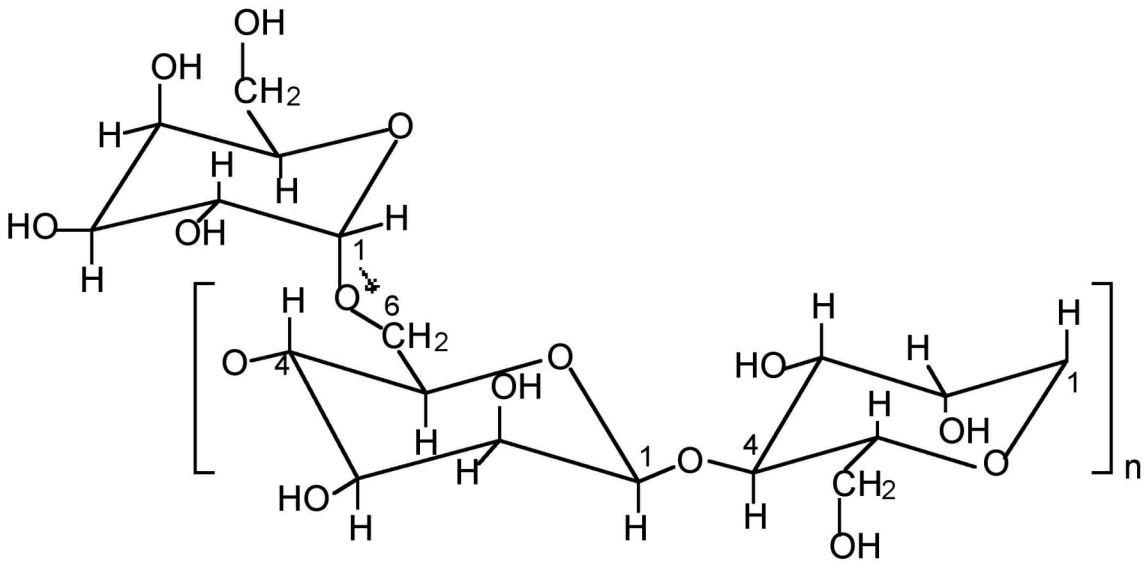


Figure 6.6.7.12: The repeat unit of guaran, a naturally occurring polysaccharide, consisting of (1→4)-*β*-D-mannopyranosyl units with α-D-galactopyranosyl side chains attached to about every other mannose via (1→6) linkages.

The synthesis of a typical boric acid cross-linked guar gel, with viscosity properties suitable for use as a fracturing fluid, involves mixing guar gum, water and boric acid, B(OH)$_3$, in a 10:2000:1 wt/wt ratio. Adjusting the pH to between 8.5 and 9 results in a viscous gel. The boron:guaran ratio corresponds to almost 2 boron centers per 3 monosaccharide repeat units. Such a large excess of boric acid clearly indicates that the system is not optimized for cross-linking, i.e., a significant fraction of the boric acid is ineffective as a cross-linking agent.

The reasons for the inefficiency of boric acid to cross-link guaran (almost 2 borate ions per 3 monosaccharide repeat unit are required for a viscous gel suitable as a fracturing fluid): the most reactive sites on the component saccharides (mannose and galactose) are precluded from reaction by the nature of the guar structure; the comparable acidity (pK_a) of the remaining guaran alcohol substituents and the water solvent, results in a competition between cross-linking and borate formation; a significant

fraction of the boric acid is ineffective in cross-linking guar due to the modest equilibrium (K_{eq}).

Bibliography

- F. A. Cotton and G. Wilkinson, *Advanced Inorganic Chemistry*, 4th Ed. Wiley Interscience (1980).
- M. Bishop, N. Shahid, J. Yang, and A. R. Barron, *Dalton Trans*., 2004, 2621.
- M. Van Duin, J. A. Peters, A. P. G. Kieboom, and H. Van Bekkum, *Tetrahedron*, 1984, **40**, 2901.
- *Zonal Isolation*, "Borate Crosslinked Fluids," by R. J. Powell and J. M Terracina, Halliburton, Duncan, OK (1998).
- R. Schechter, *Oil Well Stimulation*, Prentice-Hall Inc., Englewood Cliffs, NJ (1992).
- S. Kesavan and R. K. Prud'homme, *Macromolecules*, 1992, **25**, 2026.

This page titled 6.6.7: Boron Oxides, Hydroxides, and Oxyanions is shared under a CC BY 1.0 license and was authored, remixed, and/or curated by LibreTexts.

6.6.8: Aluminum Oxides, Hydroxides, and Hydrated Oxides

The many forms of aluminum oxides and hydroxides are linked by complex structural relationships. Bauxite has the formula $Al_x(OH)_{3-2x}$ ($0 < x < 1$) and is thus a mixture of Al_2O_3 (α-alumina), $Al(OH)_3$ (gibbsite), and AlO(OH) (boehmite). The latter is an industrially important compound that is used in the form of a gel as a pre-ceramic in the production of fibers and coatings, and as a fire-retarding agent in plastics.

Knowledge of microstructural evolution in ceramic systems is important in determining their end-use application. In this regard alumina has been the subject of many studies in which the phase, morphology, porosity and crystallinity are controlled by physical and chemical processing. The transformation from boehmite [γ-Al(O)(OH)] o corundum (α-Al_2O_3) has been well characterized and is known to go through the following sequence:

$$\gamma\text{-Al(O)(OH)} \xrightarrow{\approx 500\ ^\circ\text{C}} \gamma\text{-Al}_2\text{O}_3 \xrightarrow{\approx 1000\ ^\circ\text{C}} \theta\text{-Al}_2\text{O}_3 \xrightarrow{> 1100\ ^\circ\text{C}} \alpha\text{-Al}_2\text{O}_3 \tag{6.6.8.1}$$

The phase changes from boehmite through θ-Al_2O_3 are known to be topotactic (i.e., changes in crystal structure are accomplished without changes in crystalline morphology), however, each phase change is accompanied by a change in porosity. The θ- to α-Al_2O_3 phase transition occurs through nucleation and growth of the θ-Al_2O_3 crystallites. The α-Al_2O_3 phase transition temperature can be altered by the addition of certain additives. For example, because the α-Al_2O_3 phase occurs by nucleation, the addition of small seed crystals can lower the transition temperature between 100 and 200 °C. The addition of certain transition metals (chromium, manganese, iron, cobalt, nickel, and copper) has also been shown to decrease the transition temperature, while lanthanum or rare earth metals tend to increase the temperature. Finally, the addition of metal oxides has also shown to affect the growth rate in α-Al_2O_3.

A third form of Al_2O_3 forms on the surface of the clean aluminum metal, (6.8.2). This oxide skin is rapidly self-repairing because its heat of formation is so large (ΔH = 3351 kJ/mol). The thin, tough, transparent oxide layer is the reason for much of the usefulness of aluminum.

$$4\ \text{Al} + 3\ \text{O}_2 \rightarrow 2\ \text{Al}_2\text{O}_3 \tag{6.6.8.2}$$

Bibliography

- K. Wefers and C. Misra, *Oxides and Hydroxides of Aluminum*, Alcoa Laboratories (1987).
- H. L. Wen and F. S. Yen, *J. Cryst. Growth*, 2000, **208**, 696.
- G. K Priya, P. Padmaja, K. G. K. Warrier, A. D. Damodaran, and G. Aruldhas, *J. Mater. Sci. Lett.*, 1997, **16**, 1584.
- E. Prouzet, D. Fargeot, and J. F. Baumard, *J. Mater. Sci. Lett.*, 1990, **9**, 779.

This page titled 6.6.8: Aluminum Oxides, Hydroxides, and Hydrated Oxides is shared under a CC BY 1.0 license and was authored, remixed, and/or curated by LibreTexts.

6.6.9: Ceramic Processing of Alumina

Introduction

While aluminum is the most abundant metal in the earth's crust (*ca.* 8%) and aluminum compounds such as alum, $K[Al(SO_4)_2].12(H_2O)$, were known throughout the world in ancient times, it was not until the isolation of aluminum in the late eighteenth century by the Danish scientist H. C. Öersted that research into the chemistry of the Group 13 elements began in earnest. Initially, metallic aluminum was isolated by the reduction of aluminum trichloride with potassium or sodium; however, with the advent of inexpensive electric power in the late 1800's, it became economically feasible to extract the metal *via* the electrolyis of alumina (Al_2O_3) dissolved in cryolite, Na_3AlF_6, (the Hall-Heroult process). Today, alumina is prepared by the Bayer process, in which the mineral bauxite (named for Les Baux, France, where it was first discovered) is dissolved with aqueous hydroxides, and the solution is filtered and treated with CO_2 to precipitate alumina. With availability of both the mineral and cheap electric power being the major considerations in the economical production of aluminum, it is not surprising that the leading producers of aluminum are the United States, Japan, Australia, Canada, and the former Soviet Union.

Aluminum oxides and hydroxides

The many forms of aluminum oxides and hydroxides are linked by complex structural relationships. Bauxite has the formula $Al_x(OH)_{3-2x}$ ($0 < x < 1$) and is thus a mixture of Al_2O_3 (α-alumina), $Al(OH)_3$ (gibbsite), and AlO(OH) (boehmite). The latter is an industrially important compound which is used in the form of a gel as a pre-ceramic in the production of fibers and coatings, and as a fire retarding agent in plastics.

Heating boehmite and diaspore to 450 °C causes dehydration to yield forms of alumina which have structures related to their oxide-hydroxide precursors. Thus, boehmite produces the low-temperature form γ-alumina, while heating diaspore will give α-alumina (corundum). γ-alumina converts to the hcp structure at 1100 °C. A third form of Al_2O_3 forms on the surface of the clean aluminum metal. The thin, tough, transparent oxide layer is the reason for much of the usefulness of aluminum. This oxide skin is rapidly self-repairing because its heat of formation is so large (ΔH = -3351 kJ/mol).

$$4\ Al + 3\ O_2 \rightarrow 2\ Al_2O_3 \tag{6.6.9.1}$$

Ternary and mixed-metal oxides

A further consequence of the stability of alumina is that most if not all of the naturally occurring aluminum compounds are oxides. Indeed, many precious gemstones are actually corundum doped with impurities. Replacement of aluminum ions with trace amounts of transition-metal ions transforms the formerly colorless mineral into ruby (red, Cr^{3+}), sapphire (blue, $Fe^{2+/3+}$, Ti^{4+}), or topaz (yellow, Fe^{3+}). The addition of stoichiometric amounts of metal ions causes a shift from the α-Al_2O_3 hcp structure to the other common oxide structures found in nature. Examples include the perovskite structure for ABO_3 type minerals (e.g., $CeTiO_7$ or $LaAlO_3$) and the spinel structure for AB_2O_4 minerals (e.g., beryl, $BeAl_2O_4$).

Aluminum oxide also forms ternary and mixed-metal oxide phases. Ternary systems such as mullite ($Al_6Si_2O_{13}$), yttrium aluminum garnet (YAG, $Y_3Al_5O_{12}$), the β-aluminas (e.g., $NaAl_{11}O_{17}$) and aluminates such as hibonite ($CaAl_{12}O_{19}$) possessing β-alumina or magnetoplumbite-type structures can offer advantages over those of the binary aluminum oxides.

Applications of these materials are found in areas such as engineering composite materials, coatings, technical and electronic ceramics, and catalysts. For example, mullite has exceptional high temperature shock resistance and is widely used as an infrared-transparent window for high temperature applications, as a substrate in multilayer electronic device packaging, and in high temperature structural applications. Hibonite and other hexaluminates with similar structures are being evaluated as interfacial coatings for ceramic matrix composites due to their high thermal stability and unique crystallographic structures. Furthermore, aluminum oxides doped with an alkali, alkaline earth, rare earth, or transition metal are of interest for their enhanced chemical and physical properties in applications utilizing their unique optoelectronic properties.

Synthesis of aluminum oxide ceramics

In common with the majority of oxide ceramics, two primary synthetic processes are employed for the production of aluminum oxide and mixed metal oxide materials:

1. The traditional ceramic powder process.
2. The solution-gelation, or "sol-gel" process.

The environmental impact of alumina and alumina-based ceramics is in general negligible; however, the same cannot be said for these methods of preparation. As practiced commercially, both of the above processes can have a significant detrimental environmental impact.

Traditional ceramic processing

Traditional ceramic processing involves three basic steps generally referred to as powder-processing, shape-forming, and densification, often with a final mechanical finishing step. Although several steps may be energy intensive, the most direct environmental impact arises from the shape-forming process where various binders, solvents, and other potentially toxic agents are added to form and stabilize a solid ("green") body (Table 6.6.9.1).

Table 6.6.9.1: Typical composition of alumina green body

Function	Composition	Volume (%)
Powder	alumina (Al_2O_3)	27
Solvent	1,1,1-trichloroethane/ethanol	58
Deflocculant	menhaden oil	1.8
Binder	poly(vinyl butyrol)	4.4
Plasticizer	poly(ethylene glycol)/octyl phthalate	8.8

The component chemicals are mixed to a slurry, cast, then dried and fired. In addition to any innate health risk associated with the chemical processing these agents are subsequently removed in gaseous form by direct evaporation or pyrolysis. The replacement of chlorinated solvents such as 1,1,1-trichloroethylene (TCE) must be regarded as a high priority for limiting environmental pollution. The United States Environmental Protection Agency (EPA) included TCE on its 1991 list of 17 high-priority toxic chemicals targeted for source reduction. The plasticizers, binders, and alcohols used in the process present a number of potential environmental impacts associated with the release of combustion products during firing of the ceramics, and the need to recycle or discharge alcohols which, in the case of discharge to waterways, may exert high biological oxygen demands in the receiving communities. It would be desirable, therefore, to be able to use aqueous processing; however, this has previously been unsuccessful due to problems associated with batching, milling, and forming. Nevertheless, with a suitable choice of binders, etc., aqueous processing is possible. Unfortunately, in many cast-parts formed by green body processing the liquid solvent alone consists of over 50 % of the initial volume, and while this is not directly of an environmental concern, the resultant shrinkage makes near net shape processing difficult.

Sol-gel

Whereas the traditional sintering process is used primarily for the manufacture of dense parts, the solution-gelation (sol-gel) process has been applied industrially primarily for the production of porous materials and coatings.

Sol-gel involves a four stage process: dispersion, gelation, drying, and firing. A stable liquid dispersion or *sol* of the colloidal ceramic precursor is initially formed in a solvent with appropriate additives. By changing the concentration (aging) or pH, the dispersion is "polymerized" to form a solid dispersion or *gel*. The excess liquid is removed from this gel by drying and the final ceramic is formed by firing the gel at higher temperatures.

The common sol-gel route to aluminum oxides employs aluminum hydroxide or hydroxide-based material as the solid colloid, the second phase being water and/or an organic solvent, however, the strong interactions of the freshly precipitated alumina gels with ions from the precursor solutions makes it difficult to prepare these gels in pure form. To avoid this complication, alumina

gels are also prepared from the hydrolysis of aluminum alkoxides, $Al(OR)_3$.

$$Al(OR)_3 + H_2O/H^+ \rightarrow \text{Al-gel} \tag{6.6.9.2}$$

$$\text{Al-gel} \xrightarrow{\Delta} Al_2O_3 \tag{6.6.9.3}$$

The exact composition of the gel in commercial systems is ordinarily proprietary, however, a typical composition will include an aluminum compound, a mineral acid, and a complexing agent to inhibit premature precipitation of the gel, e.g., Table 6.6.9.2.

Table 6.6.9.2: Typical composition of an alumina sol-gel for slipcast ceramics.

Function	Composition
Boehmite precursor	ASB [aluminum *sec*-butoxide, $Al(OC_4H_9)_3$]
Electrolyte	HNO_3 0.07 mole/mole ASB
Complexing agent	glycerol *ca.* 10 wt.%

The principal environmental consequences arising from the sol-gel process are those associated with the use of strong acids, plasticizers, binders, solvents, and *sec*-butanol formed during the reaction. Depending on the firing conditions, variable amounts of organic materials such as binders and plasticizers may be released as combustion products. NO_x's may also be produced in the off-gas from residual nitric acid or nitrate salts. Moreover, acids and solvents must be recycled or disposed of. Energy consumption in the process entails "upstream" environmental emissions associated with the production of that energy.

Bibliography

- *Advances in Ceramics*, Eds. J. A. Mangels and G. L. Messing, American Ceramic Society, Westville, OH, 1984, Vol. 9.
- Adkins, *J. Am. Chem. Soc.*, 1922, **44**, 2175.
- A. R. Barron, *Comm. Inorg. Chem.*, 1993, **14**, 123.
- M. K. Cinibulk, *Ceram. Eng. Sci., Proc.*, 1994, **15**, 721.
- F. A. Cotton and G. Wilkinson, *Advanced Inorganic Chemistry*, 5th Ed., John Wiley and Sons, New York (1988).
- N. N. Greenwood and A. Earnshaw, *Chemistry of the Elements*, Pergamon Press, Oxford (1984).
- P. H. Hsu and T. F. Bates, *Mineral Mag.*, 1964, **33**, 749.
- W. D. Kingery, H. K. Bowen, and D. R. Uhlmann, *Introduction to Ceramics*, 2nd Ed. Wiley, New York (1976).
- H. Schneider, K. Okada, and J. Pask, *Mullite and Mullite Ceramics*, Wiley (1994).
- R. V. Thomas, *Systems Analysis and Water Quality Management*, McGraw-Hill, New York (1972).
- J. C. Williams, in *Treatise on Materials Science and Technology*, Ed. F. F. Y. Wang, Academic Press, New York (1976).

This page titled 6.6.9: Ceramic Processing of Alumina is shared under a CC BY 1.0 license and was authored, remixed, and/or curated by LibreTexts.

6.6.10: Boron Compounds with Nitrogen Donors

The “B-N” unit is isoelectronic (3 + 5 valence electrons) to the “C-C” unit (4 + 4 valence electrons). The two moieties are also isolobal, and as such there are many of the compound types formed by carbon have analogous derivatives in the chemistry of boron-nitrogen.

Lewis acid-base addition compounds

Boron compounds, BX_3, are strong Lewis acids and as such form stable addition compounds with Lewis bases, in particular those with nitrogen donor ligands.

$$\mathrm{BF_3 + NMe_3 \rightarrow F_3B\text{-}NMe_3} \tag{6.6.10.1}$$

In principle these Lewis acid-base complexes should be similar to their isolobal hydrocarbon analogs, however, whereas the dipole in ethane is zero (by symmetry) the dipole in H_3NBH_3 is 5.2 D as a consequence of the difference in the Pauling electronegativities (i.e., B = 2.04 and N = 3.04). It is this dipole that generally differentiates the B-N compounds from their C-C analogs.

Homolytic cleavage of the C-C bond in ethane will yield two neutral methyl radicals, (6.7.2). In contrast, heterolytic cleavage will result in the formation of two charged species, (6.7.3). Thus, the products either have a net spin, (6.7.2), or a net charge, (6.7.3). By contrast, cleavage of the B-N bond in $H_3N\text{-}BH_3$ either yields products with both spin and charge, (6.7.5), or neither, (6.7.4). Heterolytic cleavage of the B-N bond yields neutral compounds, (6.7.4), while hemolytic cleavage results in the formation of radical ions, (6.7.5).

$$\mathrm{H_3C\text{-}CH_3 \rightarrow \cdot CH_3 + \cdot CH_3} \tag{6.6.10.2}$$

$$\mathrm{H_3C\text{-}CH_3 \rightarrow CH_3^+ + \cdot CH_3^-} \tag{6.6.10.3}$$

$$\mathrm{H_3N\text{-}BH_3 \rightarrow NH_3 + BH_3} \tag{6.6.10.4}$$

$$\mathrm{H_3N\text{-}BH_3 \rightarrow NH_3^+ \cdot + BH_3^- \cdot} \tag{6.6.10.5}$$

The difference in bond strength between $H_3N\text{-}BH_3$ and ethane is reflected in the difference in bond lengths (Table 6.6.10.1).

Table 6.6.10.1: A comparison of bonding in $H_3E\text{-}E'H_3$.

Compound	Bond length (Å)	Bond strength (kcal/mol)
$H_3C\text{-}CH_3$	1.533	89
$H_3N\text{-}BH_3$	1.658	31

Aminoboranes

The group $R'_2N\text{-}BR_2$ is isoelectronic and isolobal to the olefin sub-unit $R'_2C{=}CR_2$, and there is even appreciable π-bonding character (Figure 6.6.10.1). A measure of the multiple bond character can be seen from a comparison of the calculated B-N bond in H_2NBN_2 (1.391 Å) as compared to a typical olefin (1.33 Å). It is interesting that a consideration of the possible resonance form (Figure 6.6.10.1) suggest the dipole in the σ-bond is in the opposite direction of that of the π-bond.

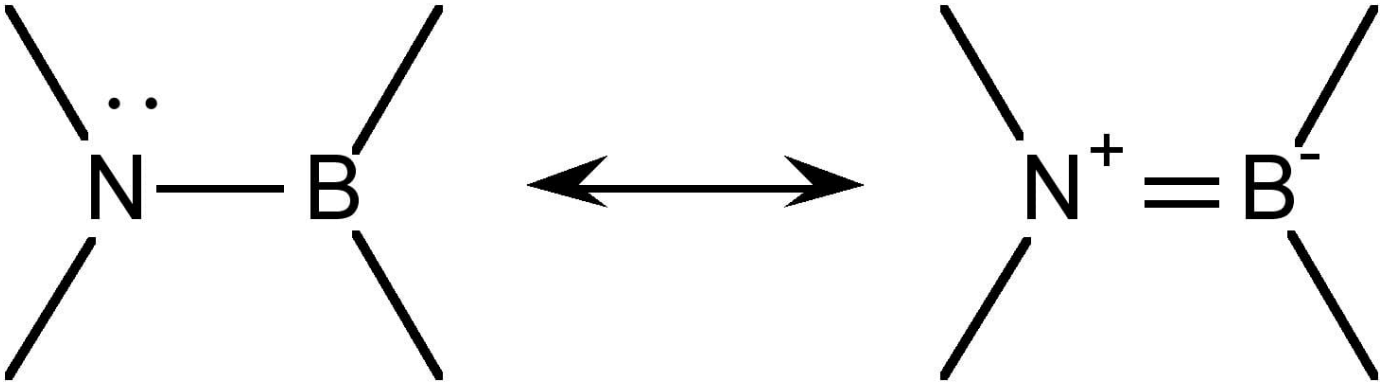


Figure 6.6.10.1: Resonance forms for X_2N-BX'_2.

Unlike olefins, borazines oligomerize to form dimmers and trimers (Figure 6.6.10.2) in the absence of significant steric hindrance. Analogous structures are also observed for the other Group 13-15 homologs ($R_2AlNR'_2$, $R_2GaPR'_2$, etc.).

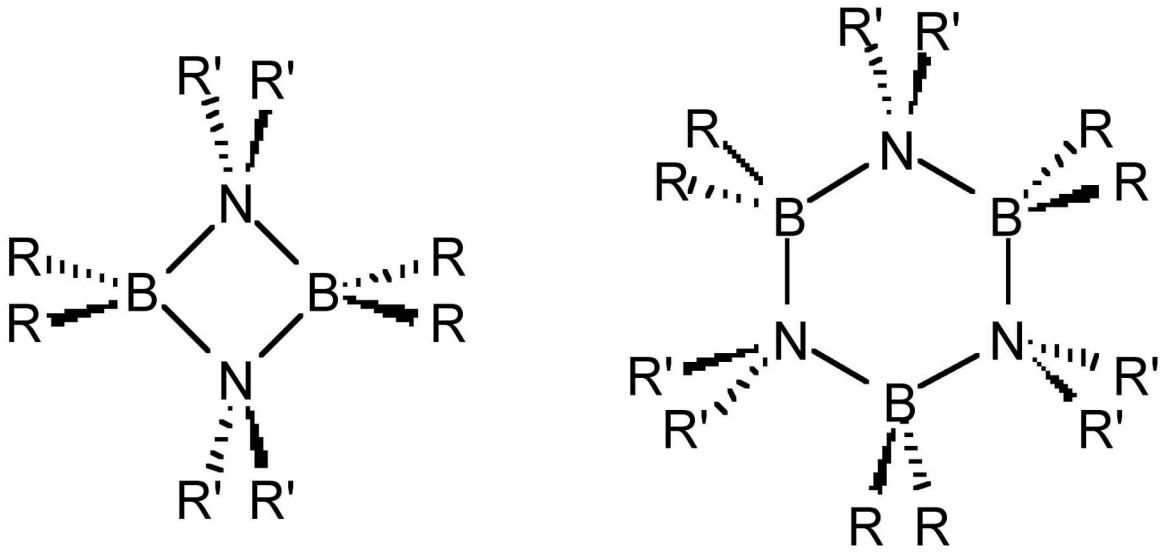


Figure 6.6.10.2: Typical structures of aminoboranes.

Borazines

The condensation of boron hydride with ammonia results in the formation of a benzene analog: borazine, (6.7.6). Substituted derivatives are formed by the reaction with primary amines.

$$BH_3 + NH_3 \rightleftharpoons H_3B\text{-}NH_3 \xrightarrow[-\ H_2]{\Delta} [H_2B\text{-}NH_2]_n \xrightarrow[-\ H_2]{\Delta} [HBNH]_6 \tag{6.6.10.6}$$

Despite the cyclic structure (Figure 6.6.10.3), borazine is not a true analog of benzene. Despite all the B-N bond distances being equal (1.44 Å) consistent with a delocalized structure, the difference in electronegativity of boron and nitrogen (2.04 and 3.04, respectively) results in a polarization of the bonds (i.e., $B^{\delta+}$-$N^{\delta-}$) and hence a limit to the delocalization. The molecular orbitals of the π-system in borazine are lumpy in appearance (Figure 6.6.10.4 a) compared to benzene (Figure 6.6.10.4 b). This uneven distribution makes borazine prone to addition reactions, making it as a molecule less stable than benzene.

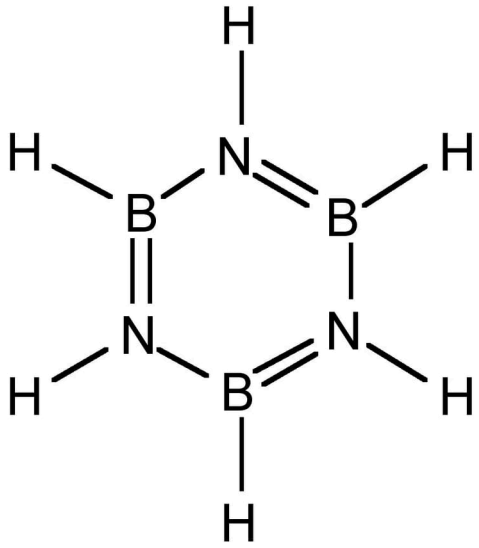


Figure 6.6.10.3: Structure of borazine, the inorganic analog to benzene.

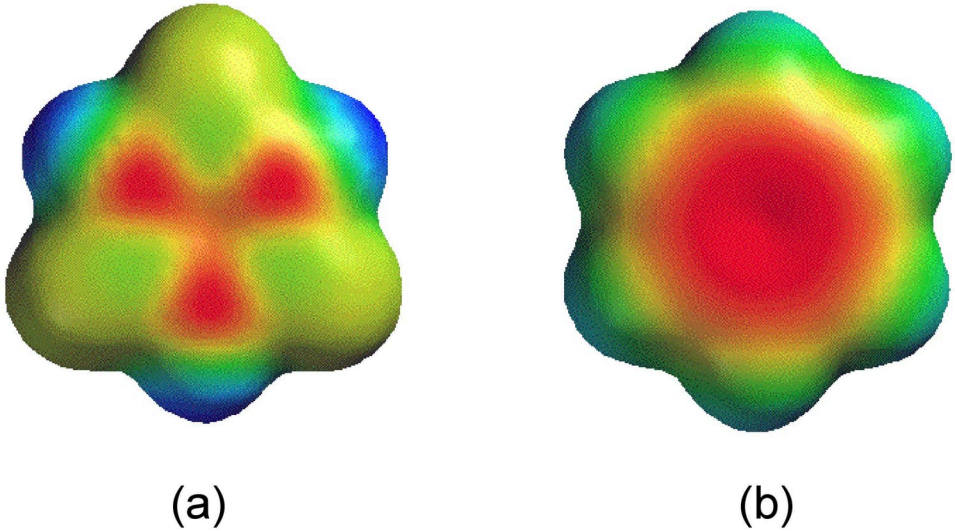


Figure 6.6.10.4: Probability distributions for the π-bond orbitals in (a) borazine and (b) benzene.

Iminoboranes: analogs of acetylene

Iminoboranes, RB=NR', are analogs of alkynes, but like aminoboranes are only isolated as monomers with sterically hindered subsistent. In the absence of sufficient steric bulk oligomerization occurs, forming substituted benzene analogs.

Boron nitrides: analogs of elemental carbon

The fusion of borax, $Na_2[B_4O_5(OH)_4]$ with ammonium chloride (NH_4Cl) results in the formation of hexagonal boron nitride (h-BN). Although h-BN has a planar, layered structure consisting of six-member rings similar to graphite (Figure 6.6.10.5), it is a white solid. The difference in color is symptomatic of the more localized bonding in BN than in graphite.

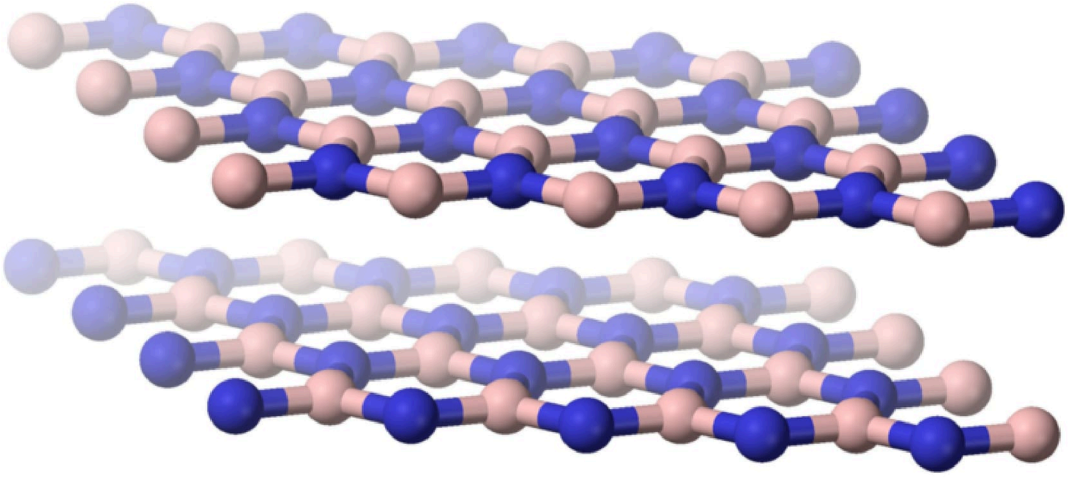


Figure 6.6.10.5: Structure of h-BN.

As is found for its carbon analog, hexagonal boron nitride (h-BN or α-BN) is converted at high temperatures (600 – 2000 °C) and pressures (50 – 200 kbar) to a cubic phase (c-BN or β-BN). In a similar manner to diamond, cubic-BN is very hard being actually able to cut diamond, and as a consequence its main use is as an industrial grinding agent. The cubic form has the sphalerite crystal structure (Figure 6.6.10.6). Finally, a wurtzite form of boron nitride (w-BN) is known that has similar structure as lonsdaleite, rare hexagonal polymorph of carbon. Table 6.6.10.2 shows a comparison of the properties of the hexagonal and cubic phases of BN with their carbon analogs.

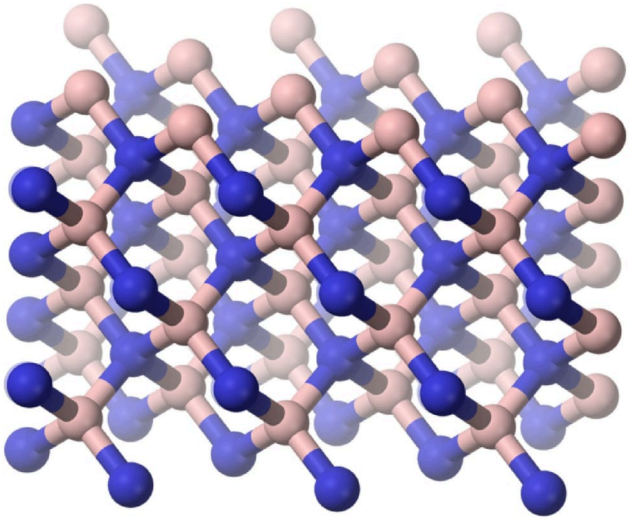


Figure 6.6.10.6: Structure of c-BN.

Table 6.6.10.2: Comparison of structural and physical properties of carbon and boron nitride analogs.

Phase	Carbon	Boron nitride
Cubic	Colorless, hard, mp = 3550 °C. C-C = 1.514 Å	Colorless, hard, B-N = 1.56 Å
Hexagonal	Black solid, planar layers, conductor, mp = 3652 – 3697 °C (sublimes), C-C = 1.415 Å	White solid, planar layers, semiconductor (Eg = 5.2 eV), mp = 2973 °C (sublimes), B-N = 1.45 Å

The partly ionic structure of BN layers in h-BN reduces covalency and electrical conductivity, whereas the interlayer interaction increases resulting in higher hardness of h-BN relative to graphite.

Bibliography

- K. M. Bissett and T. M. Gilbert, *Organometallics*, 2004, **23**, 850.
- P. Paetzold, *Adv. Inorg. Chem.*, 1987, **31**, 123.
- L. R. Thorne, R. D. Suenram, and F. J. Lovas, *J. Chem. Phys.*, 1983, **78**, 167.

This page titled 6.6.10: Boron Compounds with Nitrogen Donors is shared under a CC BY 1.0 license and was authored, remixed, and/or curated by LibreTexts.

6.6.11: Properties of Gallium Arsenide

Gallium: the element

The element gallium was predicted, as eka-aluminum, by Mendeleev in 1870, and subsequently discovered by Lecoq de Boisbaudran in 1875; in fact de Boisbaudran had been searching for the missing element for some years, based on his own independent theory. The first experimental indication of gallium came with the observation of two new violet lines in the spark spectrum of a sample deposited on zinc. Within a month of these initial results de Boisbaudran had isolated 1 g of the metal starting from several hundred kilograms of crude zinc blende ore. The new element was named in honor of France (Latin *Gallia*), and the striking similarity of its physical and chemical properties to those predicted by Mendeleev (Table 6.6.11.1) did much to establish the general acceptance of the periodic Law; indeed, when de Boisbaudran first stated that the density of Ga was 4.7 g/cm^3 rather than the predicted 5.9 g/cm^3, Mendeleev wrote to him suggesting that he redetermine the value (the correct value is 5.904 g/cm^3).

Table 6.6.11.1: Comparison of predicted and observed properties of gallium.

Property	Mendeleev's prediction (1871) for eka-aluminum, M	Observed properties of gallium (discovered 1875)
Atomic weight	ca. 68	69.72
Density, g.cm^{-3}	5.9	5.904
Melting point	Low	29.78
Vapor pressure	Non-volatile	10^{-3} mmHg, 1000 °C
Valence	3	3
Oxide	M_2O_3	Ga_2O_3
Density of oxide (g/cm^3)	5.5	5.88
Properties of metal	M should dissolve slowly in acids and alkalis and be stable in air	Ga metal dissolves slowly in acids and alkalis and is stable in air
Properties of hydroxide	$M(OH)_3$ should dissolve in both acids and alkalis	$Ga(OH)_3$ dissolves in both acids and alkalis
Properties of salts	M salts will tend to form basic salts; the sulfate should form alums; M_2S_3 should be precipitated by H_2S or $(NH_4)_2S$; anhydrous MCl_3 should be more volatile than $ZnCl_2$	Ga salts readily hydrolyze and form basic salts; alums are known; Ga_2S_3 can be precipitated under special conditions by H_2S or $(NH_4)_2S$, anhydrous $GaCl_3$ is more volatile than $ZnCl_2$.

Gallium has a beautiful silvery blue appearance; it wets glass, porcelain, and most other surfaces (except quartz, graphite, and Teflon®) and forms a brilliant mirror when painted on to glass. The atomic radius and first ionization potential of gallium are almost identical with those of aluminum and the two elements frequently resemble each other in chemical properties. Both are amphoteric, but gallium is less electropositive as indicated by its lower electrode potential. Differences in the chemistry of the two elements can be related to the presence of a filled set of 3d orbitals in gallium.

Gallium is very much less abundant than aluminum and tends to occur at low concentrations in sulfide minerals rather than as oxides, although gallium is also found associated with aluminum in bauxite. The main source of gallium is as a by-product

of aluminum refining. At 19 ppm of the earth's crust, gallium is about as abundant as nitrogen, lithium and lead; it is twice as abundant as boron (9 ppm), but is more difficult to extract due to the lack of any major gallium-containing ore. Gallium always occurs in association either with zinc or germanium, its neighbors in the periodic table, or with aluminum in the same group. Thus, the highest concentrations (0.1 - 1%) are in the rare mineral germanite (a complex sulfide of Zn, Cu, Ge, and As); concentrations in sphalerite (ZnS), bauxite, or coal, are a hundred-fold less.

Gallium pnictides

Gallium's main use is in semiconductor technology. For example, GaAs and related compounds can convert electricity directly into coherent light (laser diodes) and is employed in electroluminescent light-emitting diodes (LED's); it is also used for doping other semiconductors and in solid-state devices such as heterojunction bipolar transistors (HBTs) and high power high speed metal semiconductor field effect transistors (MESFETs). The compound $MgGa_2O_4$ is used in ultraviolet-activated powders as a brilliant green phosphor used in Xerox copying machines. Minor uses are as high-temperature liquid seals, manometric fluids and heat-transfer media, and for low-temperature solders.

Undoubtedly the binary compounds of gallium with the most industrial interest are those of the Group 15 (V) elements, GaE (E = N, P, As, Sb). The compounds which gallium forms with nitrogen, phosphorus, arsenic, and antimony are isoelectronic with the Group 14 elements. There has been considerable interest, particularly in the physical properties of these compounds, since 1952 when Welker first showed that they had semiconducting properties analogous to those of silicon and germanium.

Gallium phosphide, arsenide, and antimonide can all be prepared by direct reaction of the elements; this is normally done in sealed silica tubes or in a graphite crucible under hydrogen. Phase diagram data is hard to obtain in the gallium-phosphorus system because of loss of phosphorus from the bulk material at elevated temperatures. Thus, GaP has a vapor pressure of more than 13.5 atm at its melting point; as compared to 0.89 atm for GaAs. The physical properties of these three compounds are compared with those of the nitride in Table 6.6.11.2. All three adopt the zinc blende crystal structure and are more highly conducting than gallium nitride.

Table 6.6.11.2: Physical properties of 13-15 compound semiconductors. [a] Values given for 300 K. [b] Dependent on photon energy; values given for 1.5 eV incident photons. [c] Dependent on temperature; values given for 300 K.

Property	GaN	GaP	GaAs	GaSb
Melting point (°C)	> 1250 (dec)	1350	1240	712
Density (g/cm^3)	ca. 6.1	4.138	5.3176	5.6137
Crystal structure	Würtzite	zinc blende	zinc blende	zinc blende
Cell dimen. (Å)[a]	a = 3.187, c = 5.186	a = 5.4505	a = 5.6532	a = 6.0959
Refractive index[b]	2.35	3.178	3.666	4.388
k ($ohm^{-1}cm^{-1}$)	10^{-9} - 10^{-7}	10^{-2} - 10^{2}	10^{-6} - 10^{3}	6 - 13
Band gap (eV)[c]	3.44	2.24	1.424	0.71

Gallium arsenide versus silicon

Gallium arsenide is a compound semiconductor with a combination of physical properties that has made it an attractive candidate for many electronic applications. From a comparison of various physical and electronic properties of GaAs with those of Si (Table 6.6.11.3) the advantages of GaAs over Si can be readily ascertained. Unfortunately, the many desirable properties of gallium arsenide are offset to a great extent by a number of undesirable properties, which have limited the applications of GaAs based devices to date.

Table 6.6.11.3: Comparison of physical and semiconductor properties of GaAs and Si.

Properties	GaAs	Si
Formula weight	144.63	28.09

Properties	GaAs	Si
Crystal structure	zinc blende	diamond
Lattice constant	5.6532	5.43095
Melting point (°C)	1238	1415
Density (g/cm^3)	5.32	2.328
Thermal conductivity (W/cm.K)	0.46	1.5
Band gap (eV) at 300 K	1.424	1.12
Intrinsic carrier conc. (cm^{-3})	1.79×10^6	1.45×10^{10}
Intrinsic resistivity (ohm.cm)	10^8	2.3×10^5
Breakdown field (V/cm)	4×10^5	3×10^5
Minority carrier lifetime (s)	10^{-8}	2.5×10^{-3}
Mobility ($cm^2/V.s$)	8500	1500

Band gap

The band gap of GaAs is 1.42 eV; resulting in photon emission in the infra-red range. Alloying GaAs with Al to give $Al_xGa_{1-x}As$ can extend the band gap into the visible red range. Unlike Si, the band gap of GaAs is direct, i.e., the transition between the valence band maximum and conduction band minimum involves no momentum change and hence does not require a collaborative particle interaction to occur. Photon generation by inter-band radiative recombination is therefore possible in GaAs. Whereas in Si, with an indirect band-gap, this process is too inefficient to be of use. The ability to convert electrical energy into light forms the basis of the use of GaAs, and its alloys, in optoelectronics; for example in light emitting diodes (LEDs), solid state lasers (light amplification by the stimulated emission of radiation).

A significant drawback of small band gap semiconductors, such as Si, is that electrons may be thermally promoted from the valence band to the conduction band. Thus, with increasing temperature the thermal generation of carriers eventually becomes dominant over the intentionally doped level of carriers. The wider band gap of GaAs gives it the ability to remain 'intentionally' semiconducting at higher temperatures; GaAs devices are generally more stable to high temperatures than a similar Si devices.

Carrier density

The low intrinsic carrier density of GaAs in a pure (undoped) form indicates that GaAs is intrinsically a very poor conductor and is commonly referred to as being semi-insulating. This property is usually altered by adding dopants of either the p- (positive) or n- (negative) type. This semi-insulating property allows many active devices to be grown on a single substrate, where the semi-insulating GaAs provides the electrical isolation of each device; an important feature in the miniaturization of electronic circuitry, i.e., VLSI (very-large-scale-integration) involving over 100,000 components per chip (one chip is typically between 1 and 10 mm square).

Electron mobility

The higher electron mobility in GaAs than in Si potentially means that in devices where electron transit time is the critical performance parameter, GaAs devices will operate with higher response times than equivalent Si devices. However, the fact that hole mobility is similar for both GaAs and Si means that devices relying on cooperative electron and hole movement, or hole movement alone, show no improvement in response time when GaAs based.

Crystal growth

The bulk crystal growth of GaAs presents a problem of stoichiometric control due the loss, by evaporation, of arsenic both in the melt and the growing crystal (> *ca.* 600 °C). Melt growth techniques are, therefore, designed to enable an overpressure of

arsenic above the melt to be maintained, thus preventing evaporative losses. The loss of arsenic also negates diffusion techniques commonly used for wafer doping in Si technology; since the diffusion temperatures required exceed that of arsenic loss.

Crystal Stress

The thermal gradient and, hence, stress generated in melt grown crystals have limited the maximum diameter of GaAs wafers (currently 6" diameter compared to over 12" for Si), because with increased wafer diameters the thermal stress generated dislocation (crystal imperfections) densities eventually becomes unacceptable for device applications.

Physical strength

Gallium arsenide single crystals are very brittle, requiring that considerably thicker substrates than those employed for Si devices.

Native oxide

Gallium arsenide's native oxide is found to be a mixture of non-stoichiometric gallium and arsenic oxides and elemental arsenic. Thus, the electronic band structure is found to be severely disrupted causing a breakdown in 'normal' semiconductor behavior on the GaAs surface. As a consequence, the GaAs MISFET (metal-insulator-semiconductor-field-effect-transistor) equivalent to the technologically important Si based MOSFET (metal-oxide-semiconductor-field-effect-transistor) is, therefore, presently unavailable.

The passivation of the surface of GaAs is therefore a key issue when endeavoring to utilize the FET technology using GaAs. Passivation in this discussion means the reduction in mid-gap band states which destroy the semiconducting properties of the material. Additionally, this also means the production of a chemically inert coating which prevents the formation of additional reactive states, which can effect the properties of the device.

Bibliography

- S. K. Ghandhi, *VLSI Fabrication Principles: Silicon and Gallium Arsenide*. Wiley-Interscience, New York, (1994).
- *Properties of Gallium Arsenide*. Ed. M. R. Brozel and G. E. Stillman. 3rd Ed. Institution of Electrical Engineers, London (1996).

This page titled 6.6.11: Properties of Gallium Arsenide is shared under a CC BY 1.0 license and was authored, remixed, and/or curated by LibreTexts.

6.6.12: Electronic Grade Gallium Arsenide

Introduction

The synthesis and purification of bulk polycrystalline semiconductor material represents the first step towards the commercial fabrication of an electronic device. This polycrystalline material is then used as the raw material for the formation of single crystal material that is processed to semiconductor wafers.

In contrast to electronic grade silicon (EGS), whose use is a minor fraction of the global production of elemental silicon, gallium arsenide (GaAs) is produced exclusively for use in the semiconductor industry. However, arsenic and its compounds have significant commercial applications. The main use of elemental arsenic is in alloys of Pb, and to a lesser extent Cu, while arsenic compounds are widely used in pesticides and wood preservatives and the production of bottle glass. Thus, the electronics industry represents a minor user of arsenic. In contrast, although gallium has minor uses as a high-temperature liquid seal, manometric fluids and heat transfer media, and for low temperature solders, its main use is in semiconductor technology.

Isolation and purification of gallium metal

At 19 ppm gallium (L. Gallia, France) is about as abundant as nitrogen, lithium and lead; it is twice as abundant as boron (9 ppm), but is more difficult to extract due to the lack of any major gallium-containing ore. Gallium always occurs in association either with zinc or germanium, its neighbors in the periodic table, or with aluminum in the same group. Thus, the highest concentrations (0.1-1%) are in the rare mineral germanite (a complex sulfide of Zn, Cu, Ge, and As), while concentrations in sphalerite (ZnS), diaspore [AlO(OH)], bauxite, or coal, are a hundred-fold less. Industrially, gallium was originally recovered from the flue dust emitted during sulfide roasting or coal burning (up to 1.5% Ga), however, it is now obtained as side product of vast aluminum industry and in particular from the Bayer process for obtaining alumina from bauxite.

The Bayer process involves dissolution of bauxite, AlO_xOH_{3-2x}, in aqueous NaOH, separation of insoluble impurities, partial precipitation of the trihydrate, $Al(OH)_3$, and calcination at 1,200 °C. During processing the alkaline solution is gradually enriched in gallium from an initial weight ratio Ga/Al of about 1/5000 to about 1/300. Electrolysis of these extracts with a Hg cathode results in further concentration, and the solution of sodium gallate thus formed is then electrolyzed with a stainless steel cathode to give Ga metal. Since bauxite contains 0.003-0.01% gallium, complete recovery would yield some 500-1000 tons per annum, however present consumption is only 0.1% of this about 10 tons per annum.

A typical analysis of the 98-99% pure gallium obtained as a side product from the Bayer process is shown in Table 6.6.12.1. This material is further purified to 99.99% by chemical treatment with acids and O_2 at high temperatures followed by crystallization. This chemical process results in the reduction of the majority of metal impurities at the ppm level, see Table 6.6.12.1. Purification to seven nines 99.9999% is possible through zone refining, however, since the equilibrium distribution coefficient of the residual impurities $k_0 \approx 1$, multiple passes are required, typically > 500. The low melting point of gallium ensures that contamination from the container wall (which is significant in silicon zone refining) is minimized. In order to facilitate the multiple zone refining in a suitable time, a simple modification of zone refining is employed shown in Figure 6.6.12.1. The gallium is contained in a plastic tube wrapped around a rotating cylinder that is half immersed in a cooling bath. A heater is positioned above the gallium plastic coil. Thus, establishing a series of molten zones that pass upon rotation of the drum by one helical segment per revolution. In this manner, 500 passes may be made in relatively short time periods. The typical impurity levels of gallium zone refined in this manner are given in Table 6.6.12.1.

Table 6.6.12.1: Typical analysis of gallium obtained as a side product from the Bayer process.

Element	Bayer process (ppm)	After acid/base leaching (ppm)	500 zone passes (ppm)
aluminum	100-1,000	7	< 1
calcium	10-100	not detected	not detected
copper	100-1,000	2	< 1
iron	100-1,000	7	< 1

Element	Bayer process (ppm)	After acid/base leaching (ppm)	500 zone passes (ppm)
lead	< 2000	30	not detected
magnesium	10-100	1	not detected
mercury	10-100	not detected	not detected
nickel	10-100	not detected	not detected
silicon	10-100	≈ 1	not detected
tin	10-100	≈ 1	not detected
titanium	10-100	1	< 1
zinc	30,000	≈ 1	not detected

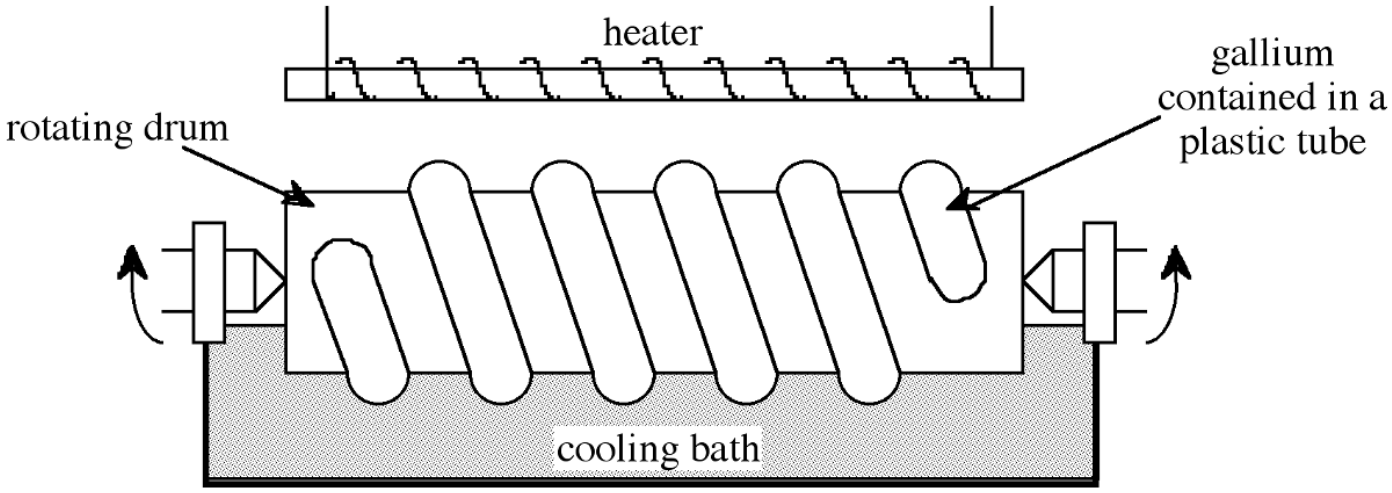


Figure 6.6.12.1: Schematic representation of a zone refining apparatus.

Isolation and purification of elemental arsenic

Elemental arsenic (L. arsenicum, yellow orpiment) exists in two forms: yellow (cubic, As_4) and gray or metallic (rhombohedral). At a natural abundance of 1.8 ppm arsenic is relatively rare, however, this is offset by its presence in a number of common minerals and the relative ease of isolation. Arsenic containing minerals are grouped into three main classes: the sulfides realgar (As_4S_4) and orpiment (As_2S_3), the oxide arsenolite (As_2O_3), and the arsenides and sulfaresenides of the iron, cobalt, and nickel. Minerals in this latter class include: loellinginite ($FeAs_2$), safforlite (CoAs), niccolite (NiAs), rammelsbergite ($NiAs_2$), ansenopyrite or mispickel (FeAsS), cobaltite (CoAsS), enargite (Cu_3AsS_4), gerdsorfite (NiAsS), and the quarturnary sulfide glaucodot [(Co,Fe)AsS]. Table 6.6.12.2 shows the typical impurities in arsenopyrite.

Table 6.6.12.2: Typical impurities in arsenopyrite.

Element	Concentration (ppm)	Element	Concentration (ppm)
silver	90	nickel	< 3,000
gold	8	lead	50
cobalt	30,000	platinum	0.4
copper	200	rhenium	50
germanium	30	selenium	50
manganese	3,000	vanadium	300
molybdenum	60	zinc	400

Arsenic is obtained commercially by smelting either $FeAs_2$ or FeAsS at 650-700 °C in the absence of air and condensing the sublimed element (T_{sub} = 613 °C), (6.12.1).

$$\mathrm{FeAsS} \xrightarrow{650\text{-}700\ ^\circ\mathrm{C}} \mathrm{FeS} + \mathrm{As(vapor)} \xrightarrow{<613\ ^\circ\mathrm{C}} \mathrm{As(solid)} \tag{6.6.12.1}$$

The arsenic thus obtained is combined with lead and then sublimed (T_{sub} = 614 °C) which binds any sulfur impurities more strongly than arsenic. Any residual arsenic that remains trapped in the iron sulfide is separated by forming the oxide (As_2O_3) by roasting the sulfide in air. The oxide is sublimed into the flue system during roasting from where it is collected and reduced with charcoal at 700-800 °C to give elemental arsenic. Semiconductor grade arsenic (> 99.9999%) is formed by zone refining.

Synthesis and purification of gallium arsenide.

Gallium arsenide can be prepared by the direct reaction of the elements, (6.12.2). However, while conceptually simple the synthesis of GaAs is complicated by the different vapor pressures of the reagents and the highly exothermic nature of the reaction. Furthermore, since the synthesis of GaAs at atmospheric pressure is accompanied by its simultaneous decomposes due to the loss by sublimation, of arsenic, the synthesis must be carried out under an overpressure of arsenic in order to maintain a stoichiometric composition of the synthesized GaAs.

$$\mathrm{Ga(liquid)} + \mathrm{As(vapor)} \xrightarrow{>1240\ ^\circ\mathrm{C}} \mathrm{GaAs(solid)} \tag{6.6.12.2}$$

In order to overcome the problems associated with arsenic loss, the reaction is usually carried out in a sealed reaction tube. However, if a stoichiometric quantity of arsenic is used in the reaction a constant temperature of 1238 °C must be employed in order to maintain the desired arsenic overpressure of 1 atm. Practically, it is easier to use a large excess of arsenic heated to a lower temperature. In this situation the pressure in the tube is approximately equal to the equilibrium vapor pressure of the volatile component (arsenic) at the lower temperature. Thus, an over pressure of 1 atm arsenic may be maintained if within a sealed tube elemental arsenic is heated to 600-620 °C while the GaAs is maintained at 1240-1250 °C.

Figure 6.6.12.2 shows the sealed tube configuration that is typically used for the synthesis of GaAs. The tube is heated within a two-zone furnace. The boats holding the reactants are usually made of quartz, however, graphite is also used since the latter has a closer thermal expansion match to the GaAs product. If higher purity is required then pyrolytic boron nitride (PBN) is used. One of the boats is loaded with pure gallium the other with arsenic. A plug of quartz wool may be placed between the boats to act as a diffuser. The tube is then evacuated and sealed. Once brought to the correct reaction temperatures (Figure 6.6.12.2), the arsenic vapor is transported to the gallium, and they react to form GaAs in a controlled manner. Table 6.6.12.3 gives the typical impurity concentrations found in polycrystalline GaAs.

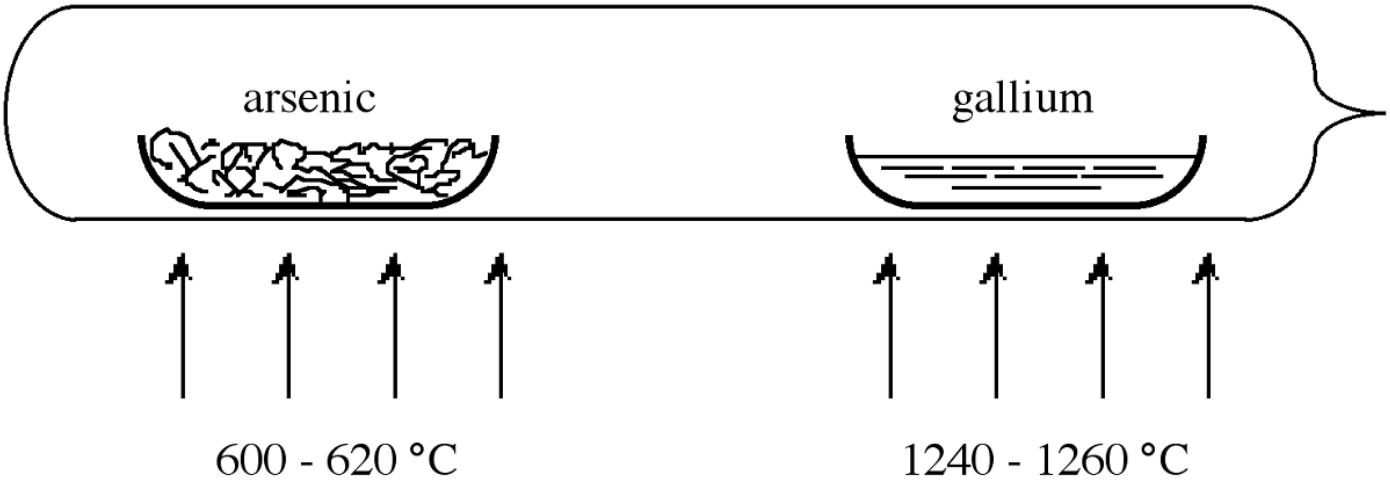


Figure 6.6.12.2: Schematic representation of a sealed tube synthesis of GaAs.

Table 6.6.12.3: Impurity concentrations found in polycrystalline GaAs.

Element	Concentration (ppm)	Element	Concentration (ppm)
boron	0.1	silicon	0.02

Element	Concentration (ppm)	Element	Concentration (ppm)
carbon	0.7	phosphorus	0.1
nitrogen	0.1	sulfur	0.01
oxygen	0.5	chlorine	0.08
fluorine	0.2	nickel	0.04
magnesium	0.02	copper	0.01
aluminum	0.02	zinc	0.05

Polycrystalline GaAs, formed in from the direct reaction of the elements is often used as the starting material for single crystal growth via Bridgeman or Czochralski crystal growth. It is also possible to prepare single crystals of GaAs directly from the elements using in-situ, or direct, compounding within a high-pressure liquid encapsulated Czochralski (HPLEC) technique.

Growth of gallium arsenide crystals

When considering the synthesis of Group 13-15 compounds for electronic applications, the very nature of semiconductor behavior demands the use of high purity single crystal materials. The polycrystalline materials synthesized above are, therefore, of little use for 13-15 semiconductors but may, however, serve as the starting material for melt grown single crystals. For GaAs, undoubtedly the most important 13-15 (III - V) semiconductor, melt grown single crystals are achieved by one of two techniques: the Bridgman technique, and the Czochralski technique.

Bridgman growth

The Bridgman technique requires a two-zone furnace, of the type shown in Figure 6.6.12.3. The left hand zone is maintained at a temperature of *ca*. 610 °C, allowing sufficient overpressure of arsenic within the sealed system to prevent arsenic loss from the gallium arsenide. The right hand side of the furnace contains the polycrystalline GaAs raw material held at a temperature just above its melting point (*ca*. 1240 °C). As the furnace moves from left to right, the melt cools and solidifies.

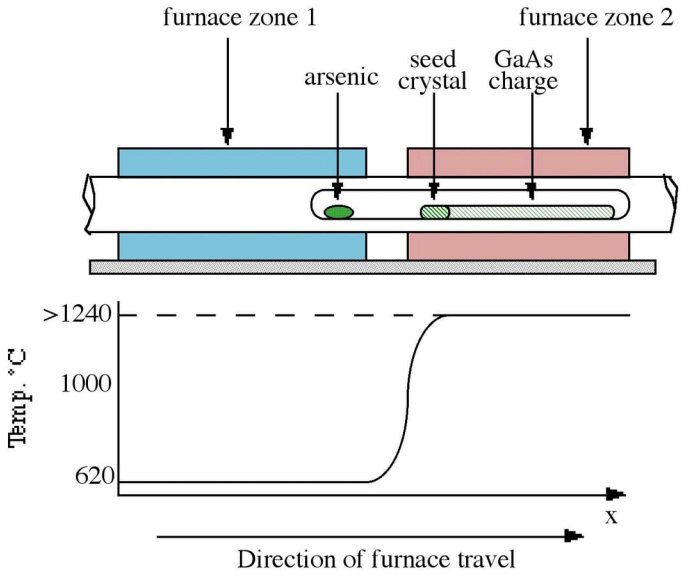


Figure 6.6.12.3: A schematic diagram of a Bridgman two-zone furnace used for melt growths of single crystal GaAs.

If a seed crystal is placed at the left hand side of the melt (at a point where the temperature gradient is such that only the end melts), a specific orientation of single crystal may be propagated at the liquid-solid interface eventually to produce a single crystal.

Czochralski growth

The Czochralski technique, which is the most commonly used technique in industry, is shown in Figure 6.6.12.4. The process relies on the controlled withdrawal of a seed crystal from a liquid melt. As the seed is lowered into the melt, partial melting of the tip occurs creating the liquid solid interface required for crystal growth. As the seed is withdrawn, solidification occurs and the seed orientation is propagated into the grown material. The variable parameters of rate of withdrawal and rotation rate can control crystal diameter and purity. As shown in Figure 6.6.12.4 the GaAs melt is capped by boron trioxide (B_2O_3). The capping layer, which is inert to GaAs, prevents arsenic loss when the pressure on the surface is above atmospheric pressure. The growth of GaAs by this technique is thus termed liquid encapsulated Czochralski (LEC) growth.

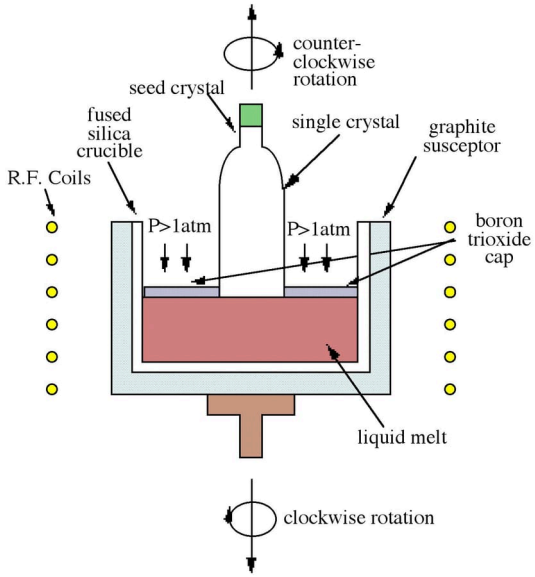


Figure 6.6.12.4: A schematic diagram of the Czochralski technique as used for growth of GaAs single crystal bond.

While the Bridgman technique is largely favored for GaAs growth, larger diameter wafers can be obtained by the Czochralski method. Both of these melt techniques produce materials heavily contaminated by the crucible, making them suitable almost exclusively as substrate material. Another disadvantage of these techniques is the production of defects in the material caused by the melt process.

Bibliography

- S. K. Ghandhi, *VLSI Fabrication Principles: Silicon and Gallium Arsenide*. Wiley-Interscience, New York, (1994).
- J. Krauskopf, J. D. Meyer, B. Wiedemann, M. Waldschmidt, K. Bethge, G. Wolf, and W. Schültze, *5th Conference on Semi-insulating III-V Materials*, Malmo, Sweden, 1988, Eds. G. Grossman and L. Ledebo, Adam-Hilger, New York (1988).
- W. G. Pfann, *Zone Melting*, John Wiley & Sons, New York (1966).
- R. E. Williams, *Gallium Arsenide Processing Techniques*. Artech House (1984).
- *Properties of Gallium Arsenide*. Ed. M. R. Brozel and G. E. Stillman. 3rd Ed. Institution of Electrical Engineers, London (1996).

This page titled 6.6.12: Electronic Grade Gallium Arsenide is shared under a CC BY 1.0 license and was authored, remixed, and/or curated by LibreTexts.

6.6.13: Chalcogenides of Aluminum, Gallium, and Indium

The only stable chalcogenides of aluminum are Al_2S_3 (white), Al_2Se_3 (grey), and Al_2Te_3 (dark grey). They are each prepared by the direct reaction of the elements (100 °C) and hydrolyze rapidly in aqueous solution, (6.13.1). All the chalcogenides have a hexagonal ZnS structure in which $^2/_3$ of the metal sites are occupied.

$$Al_3E_3 + 6\ H_2O \rightarrow 2\ Al(OH)_3 + 3\ H_2E \tag{6.6.13.1}$$

The chalcogenides of gallium and indium are more numerous than those of aluminum, and are listed in Table 6.6.13.1 and Table 6.6.13.2 along with selected physical properties.

Table 6.6.13.1: Stoichiometries, structures and selected physical properties of the crystalline chalcogenides of gallium. [a] *dir = direct, ind = indirect, opt = optical.*

Compound	Structural type	Crystallographic system	Cell parameters (Å, °)	Band Gap (eV)[a]
GaS		Hexagonal	*a* = 3.587, *c* = 15.492	3.05 (dir.), 2.593 (ind.)
GaS	ZnS or NaCl	Cubic	*a* = 5.5	4.0 (opt.)
β-GaSe	GaS	Hexagonal	*a* = 3.742, *c* = 15.919	2.103 (dir.), 2.127 (ind.)
γ-GaSe	GaS	Rhombohedral	*a* = 3.755, *c* = 23.92	
δ-GaSe	GaS	Hexagonal	*a* = 3.755, *c* = 31.99	
β-GaTe	GaS	Hexagonal	*a* = 4.06, *c* = 16.96	
GaTe	GaS	Monoclinic	*a* = 17.44, *b* = 4.077, *c* = 10.456, *β* = 104.4	1.799 (dir.)
α-Ga_2S_3	Wurtzite	Cubic	*a* = 5.181	
α-Ga_2S_3	Wurtzite	Monoclinic	*a* = 12.637, *b* = 6.41, *c* = 7.03, *β* = 131.08	3.438 (opt.)
β-Ga_2S_3	Defect wurtzite	Hexagonal	*a* = 3.685, *c* = 6.028	2.5 - 2.7 (opt.)
α-Ga_2Se_3	Sphalerite	Cubic	*a* = 5.429	2.1 (dir.), 2.04 (ind.)
α-Ga_2Te_3	Sphalerite	Cubic	*a* = 5.886	1.22 (opt.)

Table 6.6.13.2: Stoichiometries, structures and selected physical properties of the crystalline chalcogenides of indium. [a] *dir = direct, ind = indirect, opt = optical.* [b] *High pressure phase.*

Compound	Structural type	Crystallographic system	Cell parameters (Å, °)	Band gap (eV)[a]
β-InS	GaS	Orthorhombic	*a* = 3.944, *b* = 4.447, *c* = 10.648	2.58 (dir.), 2.067 (ind.)
InS[b]	Hg_2Cl_2	Tetragonal		
InSe	GaS	Rhombohedral	*a* = 4.00, *c* = 25.32	1.3525 (dir.), 1.32 (ind.)
β-InSe	GaS	Hexagonal	*a* = 4.05, *c* = 16.93	
InTe	TlSe	Tetragonal	*a* = 8.437, *c* = 7.139	Metallic
InTe[b]	NaCl	Cubic	*a* = 6.18	
α-In_2S_3	γ-Al_2O_3	Cubic	*a* = 5.36	
β-In_2S_3	Spinel	Tetragonal	*a* = 7.618, *c* = 32.33	2.03 (dir.), 1.1 (ind.)
α-In_2Se_3	Defect wurtzite	Hexagonal	*a* = 16.00, *c* = 19.24	
β-In_2Se_3	Defect wurtzite	Rhombohedral	*a* = 4.025, *c* = 19.222	1.2 - 1.5 (ind.)

α-In_2Te_3	Sphalerite	Cubic	a = 6.158	0.92 - 1.15 (opt.)
In_6S_7		Monoclinic	a = 9.090, b = 3.887, c = 17.705, β = 108.20	0.89 (dir.), 0.7 (ind.)
In_6Se_7	In_6S_7	Monoclinic	a = 9.430, b = 4.063, c = 18.378, β = 109.34	0.86 (dir.), 0.34 (ind.)
In_4Se_3		Orthorhombic	a = 15.297, b = 12.308, c = 4.081	0.64 (dir.)
In_4Te_3	In_4Se_3	Orthorhombic	a = 15.630, b = 12.756, c = 4.441	0.48 (dir.)

The hexagonal β-form of Ga_2S_3 is isostructural with the aluminum analogue; however, while the α-phase was proposed to be hexagonal it was later shown to be monoclinic. A cubic α-phase has been reported. Cubic Sphalerite structures are found for Ga_2Se_3, Ga_2Te_3, and In_2Te_3, in which the structure is based on a cubic close packing of the chalcogenides and the metal atoms occupying $^1/_3$ of the tetrahedral sites. These structures are all formed with rapid crystallization; slow crystallization and/or thermal annealing leads to ordering and the formation of more complex structures. The indium sulfides, and selenides derivatives are spinel (γ-Al_2O_3), and defect Würtzite, respectively.

Unlike the chalcogenides of aluminum, those of gallium and indium also form subvalent compounds, i.e., those in which the metal is formally of an oxidation state less than +3. Of these subvalent chalcogenides the (formally) divalent materials are of the most interest. The thermodynamically stable phase of GaS has a hexagonal layer structure (Figure 6.6.13.1) with Ga-Ga bonds (2.48 Å). The compound can, therefore, be considered as an example of Ga(II). Each Ga is coordinated by three sulfur atoms and one gallium, and the sequence of layers along the *z*-axis is ···S-Ga-Ga-S···S-Ga-Ga-S···.

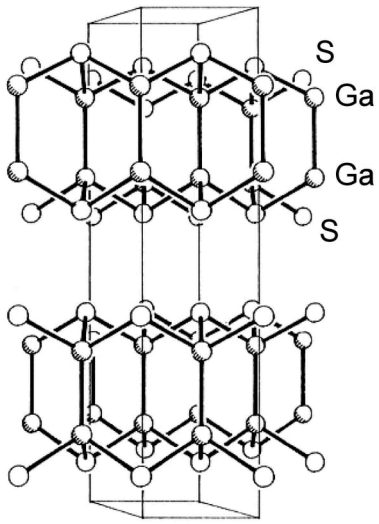


Figure 6.6.13.1: The ···S-Ga-Ga-S···S-Ga-Ga-S··· structure of hexagonal GaS. Gallium atoms are shown shaded.

The structures of β-GaSe, and β-InSe are similar to hexagonal GaS. The layered structure of GaTe is similar in that it consists of ···TeGaGaTe··· layers, but is monoclinic, while InS is found in both a (high pressure) tetragonal phase (Figure 6.6.13.2a) as well as an orthorhombic phase (Figure 6.6.13.2b). By contrast to these M-M bonded layered compounds InTe (Figure 6.6.13.3) has a structure formalized as In(I)[In(III)Te_2]; each In(III) is tetrahedrally coordinated to four Te and these tetrahedra are linked *via* shared edges; the In(I) centers lying between these chains.

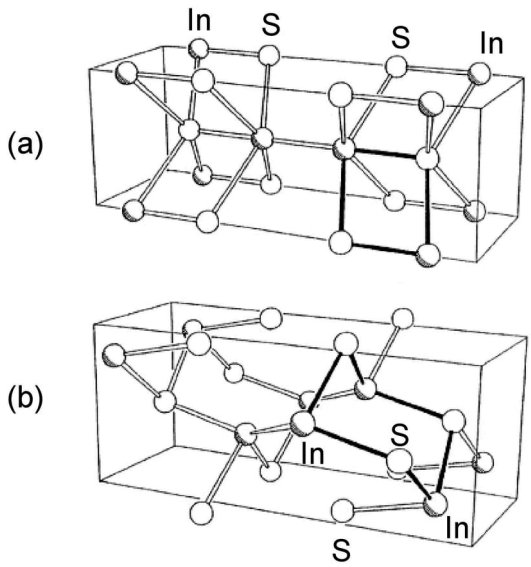


Figure 6.6.13.2: Unit cell of (a) tetragonal InS and (b) orthorhombic InS. Indium atoms are shown shaded, and the solid bonds represent the smallest cyclic structural fragment.

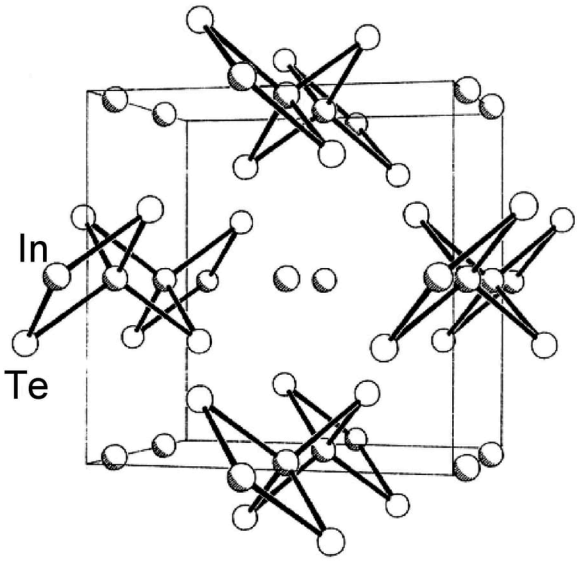


Figure 6.6.13.3: Unit cell of tetragonal InTe. Indium atoms are shown shaded, and the solid bonds represent the $[InTe_2]_\infty$ chains.

Further sub-chalcogenides are known for indium, e.g.; In_4Se_3, which contains $[In(III)_3Se_2]^{5+}$ groups (Figure 6.6.13.4). While the formally In(I) molecule In_2S has been detected in the gas phase, it is actually a mixture of In and InS in the solid state.

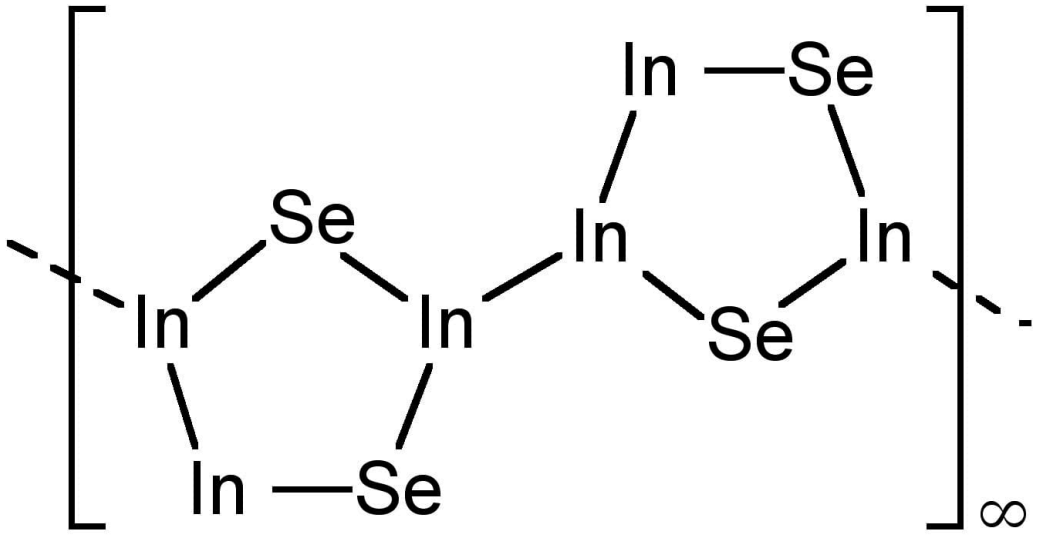


Figure 6.6.13.4: Structure of $[In(III)_3Se_2]^{5+}$ groups in In_4Se_3.

Bibliography

- W. J. Duffin and J. H. C. Hogg, *Acta Crystallogr.*, 1966, **20**, 566.
- J. Goodyear and G. Steigman, *Acta Crystallogr.* 1963, **16**, 946.
- H. Hahn and G. Frank, *Z. Anorg. Allgem. Chem.*, 1955, **278**, 340.
- S. Kabalkina, V. G. Losev, and N. M. Gasanly, *Solid State Commun.*, 1982, **44**, 1383.
- A. Keys, S. G. Bott, and A. R. Barron, *Chem. Mater.*, 1999, **11**, 3578.
- A. N. MacInnes, M. B. Power, and A. R. Barron, *Chem. Mater.*, 1992, **4**, 11.
- A. N. MacInnes, W. M. Cleaver, A. R. Barron, M. B. Power, and A. F. Hepp, *Adv. Mater. Optics. Electron.*, 1992,**1**, 229.
- K. Schubert, E. Dörre, and E. Günzel, *Naturwissenschaften*, 1954, **41**, 488.

This page titled 6.6.13: Chalcogenides of Aluminum, Gallium, and Indium is shared under a CC BY 1.0 license and was authored, remixed, and/or curated by LibreTexts.

6.6.14: Group 13 Halides

Trihalides, MX_3

As shown in Table 6.6.14.1 all the combinations of Group 13 element (M) and halogen (X) exist for the trihalides (MX_3), except thallium(III) iodide. It should be noted that while there is a compound with the general formula TlI_3, it is actually a thallium(I) compound of I_3^-.

Table 6.6.14.1: Selected physical properties of the Group 13 trihalides, MX_3.

Element	Mp (°C)	Bp (°C)
BF_3	-126.8	-100.3
BCl_3	-107.3	12.6
BBr_3	-46.3	91.3
BI_3	49.9	210
AlF_3	1291	-
$AlCl_3$	192.4 (anhydrous), 0.0 (hexahydrate)	120 (hexahydrate)
$AlBr_3$	97.8	265
AlI_3	189.4 (anhydrous) 185 dec. (hexahydrate)	300 subl.
GaF_3	800	1000
$GaCl_3$	77.9	201
$GaBr_3$	121.5	278.8
GaI_3	212	345
InF_3	1172	-
$InCl_3$	586	800
$InBr_3$	220	-
InI_3	210 subl.	-
TlF_3	300 dec.	-
$TlCl_3$	40 dec.	-
$TlBr_3$	40 dec.	-

The trihalides of boron are all monomers with a coordination number of 3 (Table 6.6.14.2), as evidence from their low melting points (Table 6.6.14.1). In contrast, the fluorides and chlorides of the heavier Group 13 elements (except $GaCl_3$) are generally ionic or have a high ionic character, with a coordination number of 6 (Table 6.6.14.2, Figure 6.6.14.1 and Figure 6.6.14.2). The bromides and iodides (except $InBr_3$) are generally dimeric with a coordination number of 4 (Table 6.6.14.2) and have molecular structures involving halide bridging ligands (Figure 6.6.14.3 and Table 6.6.14.3). $AlCl_3$ is unusual in that in the solid state it has an ionic structure, but it is readily sublimed, and in the vapor phase (and liquid phase) it has a dimeric structure (Figure 6.6.14.3).

Table 6.6.14.2: The Group 13 element coordination numbers for the trihalides, MX_3.

Element	Fluoride	Chloride	Bromide	Iodide
B	3	3	3	3

Al	6	6 (4)	4	4
Ga	6	4	4	4
In	6	6	6	4
Tl	6	6	4	-

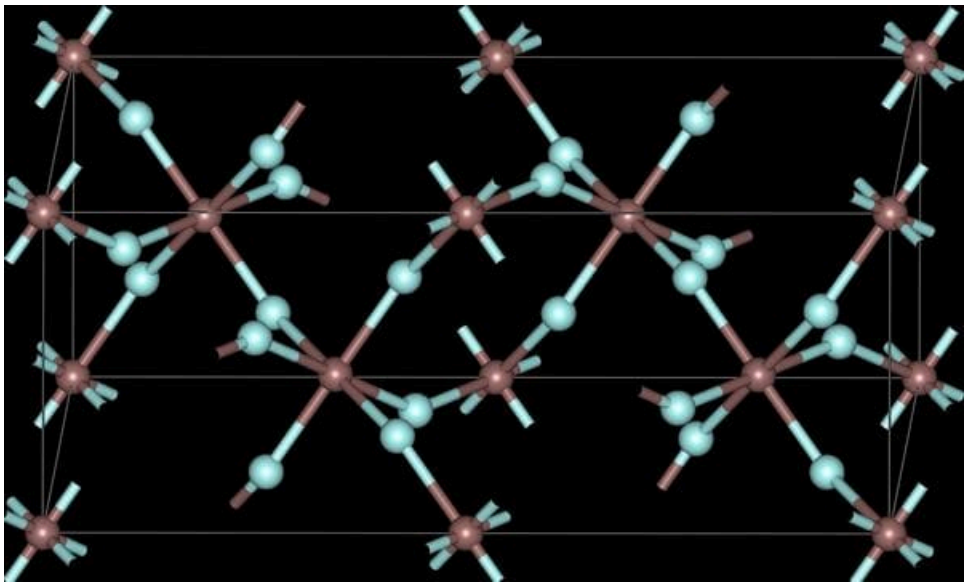


Figure 6.6.14.1: Solid state structure of MF_3 (M = Al, Ga, In). Grey spheres represent the metal, while pale blue spheres represent fluorine.

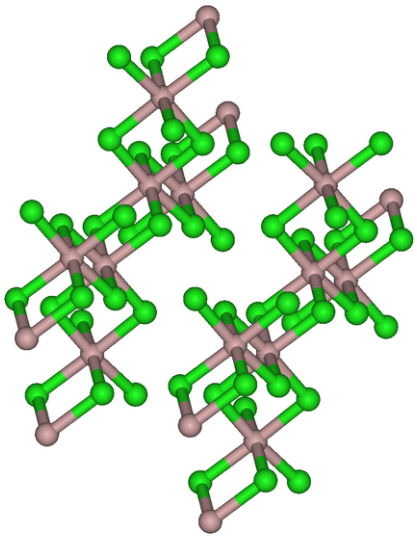


Figure 6.6.14.2: Solid state structure of MCl_3 (M = Al, In, Tl) and MBr_3 (M = In). Grey spheres represent the metal, while green spheres represent the halogen.

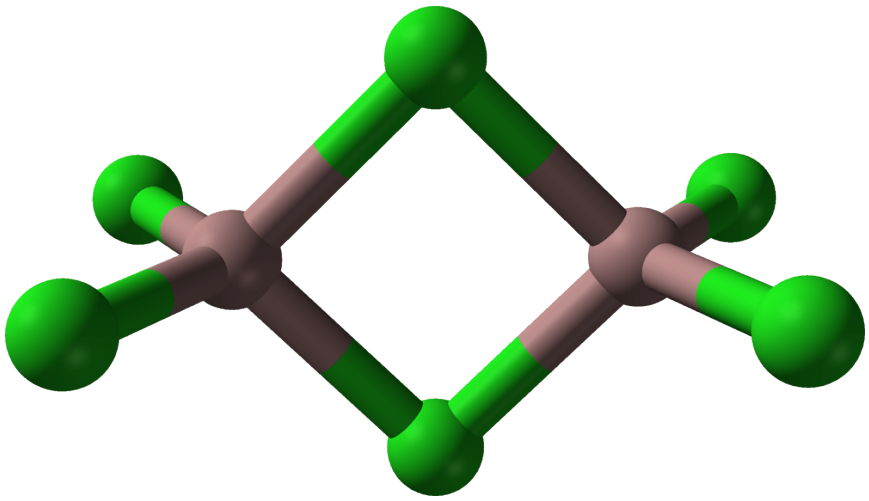


Figure 6.6.14.3: Structure of $GaCl_3$, MBr_3 (M = Al, Ga, Tl), and MI_3 (M = Al, Ga, In). Grey spheres represent the metal, while green spheres represent the halogen.

Table 6.6.14.3: Selected bond lengths and angles for dimeric M_2X_6 compounds. [a] X_t and X_b indicate terminal and bridging halides, respectfully.

Compound	M-X_t (Å)[a]	M-X_b (Å)[a]	X_t-M-X_t (°)[a]	X_b-M-X_b (°)[a]	M-X-M (°)
Al_2Br_6	2.21	2.33	115	93	87
In_2I_6	2.64	2.84	125.1	93.7	86.3

Synthesis

Boron trifluoride (BF_3) is manufactured commercially by the reaction of boron oxides with hydrogen fluoride, (6.14.1). The HF is produced *in-situ* from sulfuric acid and fluorite (CaF_2). On smaller scales, BF_3 is prepared by the thermal decomposition of diazonium salts, (6.14.2).

$$B_2O_3 + 6\ HF \rightarrow 2\ BF_3 + 3\ H_2O \tag{6.6.14.1}$$

$$PhN_2[BF_4] \rightarrow PhF + BF_3 + N_2 \tag{6.6.14.2}$$

Boron trichloride is also made from boron oxide, but in the presence of carbon, (6.14.3).

$$B_2O_3 + 3\ C + 3\ Cl_2 \rightarrow 2\ BCl_3 + 3\ CO \tag{6.6.14.3}$$

Many of the trihalides are readily prepared by either the direct reaction of the metal with the appropriate halogen, (6.14.4) - (6.14.6), or the acid, (6.14.7) and (6.14.8). Thallium tribromide can be prepared in CH_3CN by treating a solution of the monobromide with bromine gas, (6.14.9).

$$2\ Al + 3\ Cl_2 \rightarrow 2\ AlCl_3 \tag{6.6.14.4}$$

$$2\ Al + 3\ Br_2 \rightarrow 2\ AlBr_3 \tag{6.6.14.5}$$

$$2\ Al + 3\ I_2 \rightarrow 2\ AlCl_3 \tag{6.6.14.6}$$

$$2\ Al + 6\ HCl \rightarrow 2\ AlCl_3 + 3\ H_2 \tag{6.6.14.7}$$

$$2\ Al + 6\ HBr \rightarrow 2\ AlBr_3 + 3\ H_2 \tag{6.6.14.8}$$

$$TlBr + Br_2 \rightarrow TlBr_2 \tag{6.6.14.9}$$

Reactivity

The reaction chemistry of the Group 13 trihalides tends to fall into two categories:

- Lewis acid-base complex formation.
- Hydrolysis.

There are, however, a number of reactions involving halide exchange reactions. Aluminum tribromide reacts with carbon tetrachloride at 100 °C to form carbon tetrabromide, (6.14.10), and with phosgene yields carbonyl bromide and aluminum chlorobromide, (6.14.11).

$$4\ \mathrm{AlBr_3} + 3\ \mathrm{CCl_4} \rightarrow 4\ \mathrm{AlCl_3} + 3\ \mathrm{CBr_4} \tag{6.6.14.10}$$

$$\mathrm{AlBr_3} + \mathrm{COCl_2} \rightarrow \mathrm{COBr_2} + \mathrm{AlCl_2Br} \tag{6.6.14.11}$$

Group 13 halides are used as synthons for their organometallic derivatives, (6.14.12) and (6.14.13).

$$\mathrm{MX_3} + 3\ \mathrm{RMgX} \rightarrow \mathrm{MR_3} + \mathrm{MgX_2} \tag{6.6.14.12}$$

$$2\ \mathrm{MR_3} + \mathrm{MX_3} \rightarrow 3\ \mathrm{MXR_2} \tag{6.6.14.13}$$

Lewis acid-base complexes

All of the trihalides are strong Lewis acids, and as such react with Lewis base compounds to form Lewis acid-base complexes, (6.14.12). The extent of the equilibrium is dependant on the Lewis acidity of the trihalide and the basicity of the Lewis base. For example, with BCl_3, oxygen donor ligands result in approximately 50:50 ratio of BCl_3 and BCl_3L, while for nitrogen donor ligands the equilibrium is shifted to the formation of the complex.

$$\mathrm{MX_3} + \mathrm{L} \rightleftharpoons \mathrm{X_3M\text{-}L} \tag{6.6.14.14}$$

The general structure of the Lewis acid-base complexes is such that the Group 13 element is close to tetrahedral (Figure 6.6.14.4). However, for aluminum and the heavier Group 13 elements, more than one ligand can coordinate (Figure 6.6.14.5) up to a maximum of six.

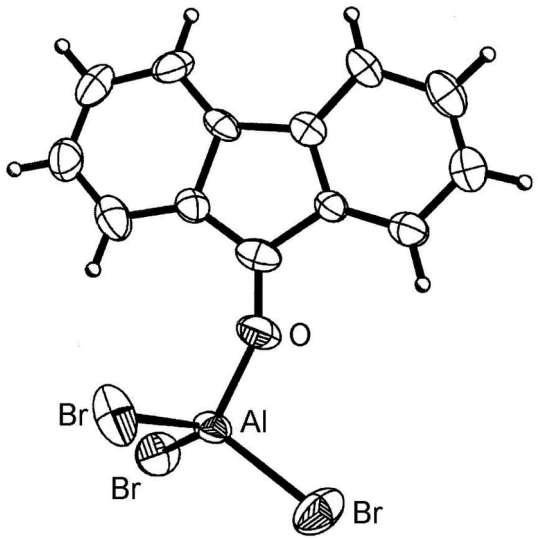


Figure 6.6.14.4: Molecular structure of a typical Group 13 metal trihalide Lewis acid-base complex: $AlBr_3$(9-fluorenone). Adapted from C. S. Branch, S. G. Bott, and A. R. Barron, *J. Organomet. Chem.*, 2003, **666**, 23.

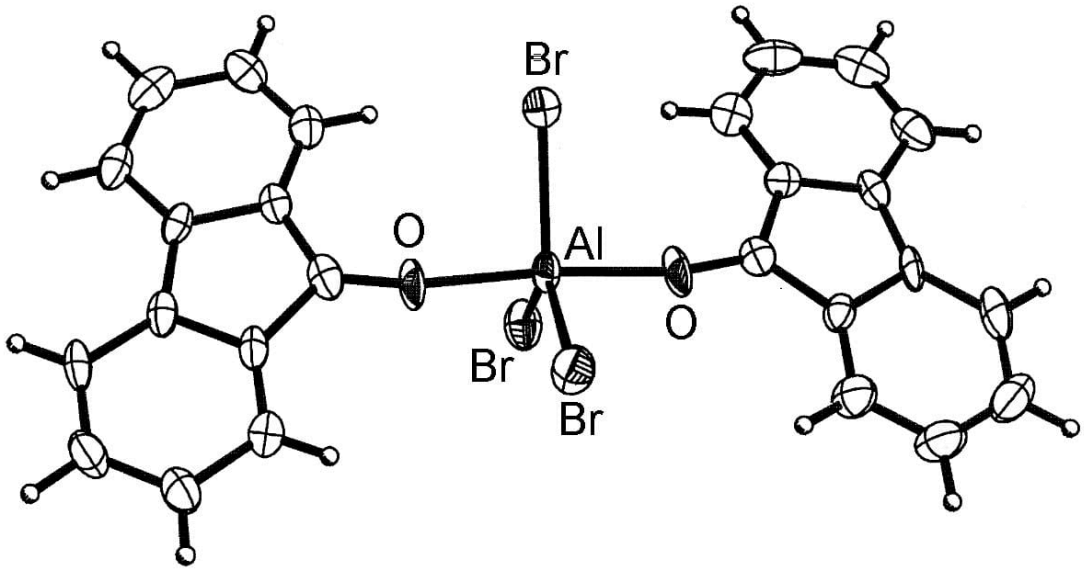


Figure 6.6.14.5: Molecular structure of $AlBr_3$(9-fluorenone)$_2$. Adapted from C. S. Branch, S. G. Bott, and A. R. Barron, *J. Organomet. Chem.*, 2003, **666**, 23.

It should be noted that the dimeric form of MX_3 (Figure 6.6.14.3) can be thought of as mutual Lewis acid-base complexes, in which a Lewis basic lone pair of a halide on one MX_3 unit donates to the Lewis acidic metal on another MX_3 unit.

Hydrolysis

Generally the fluorides are insoluble in water while the heavier halides are more soluble. However, BF_3, BCl_3, and BBr_3 all decompose in the presence of water, (6.14.13). In the case of the fluoride, the HF formed reacts with BF_3 to form fluoroboric acid, (6.14.14). However, there is also a minor equilibrium (2-3%) resulting in the formation of the BF_3 complex of OH^- and H_3O^+, (6.14.15).

$$\mathrm{BX_3 + H_2O \rightarrow B(OH)_3 + 3\ HX} \tag{6.6.14.15}$$

$$\mathrm{HF + BF_3 \rightarrow HBF_4} \tag{6.6.14.16}$$

$$\mathrm{BF_4 + H_3O \rightleftharpoons F_3B\text{-}OH_2 \rightleftharpoons [BF_3OH][BF_3(OH_3)]} \tag{6.6.14.17}$$

While the boron compounds (and $AlBr_3$) decompose even in moist air, $AlCl_3$ reacts more slowly to make aluminum chlorohydrate (ACH) which has the general formula $Al_nCl_{3n-m}(OH)_m$. While ACH has been proposed to exist as a number of cluster species, it is actually a range of nanoparticles.

ACH is also known as polyaluminum chloride (PAC). The latter name is often used in water purification, where ACH is preferred over alum derivatives ($Al_2(SO_4)_3$). The combination of ACH and a high molecular weight quaternized ammonium polymer (e.g., dially dimethyl ammonium chloride (DADMAC)), has been known as an effective combination as a flocculant in water treatment process to remove dissolved organic matter and colloidal particles present in suspension.

Aluminum chlorohydrate (ACH) and aluminum-zirconium compounds, are frequently used as the active ingredient in antiperspirants. The mode of action of most aluminum-based compounds involves the dramatic change in the particle size from nano to micro as a function of pH and electrolyte changes on the skin (as compared to the antiperspirant stick or suspension) and hence forming a gel plug in the duct of the sweat gland. The plugs prevent the gland from excreting liquid and are removed over time by the natural sloughing of the skin. A further mechanism of action involves the absorption of 3-methyl-2-hexenoic acid (Figure 6.6.14.6). Human perspiration is odorless until bacteria ferment it. Bacteria thrive in hot, humid environments such as the underarm. When adult armpits are washed with alkaline pH soaps, the skin loses its acid mantel (pH = 4.5 - 6), raising the skin pH and disrupting the skin barrier. The bacteria thrive in the basic environment, and feed on the sweat from the apocrine glands and on dead skin and hair cells, releasing 3-methyl-2-hexenoic acid, which is the primary cause of body odor. As with all carboxylic acids, 3-methyl-2-hexenoic acid, reacts in a facile manner with the surface of the alumina nanoparticles. Aluminum chloride salts also have a slight astringent effect on the pores; causing them to contract, further preventing sweat from reaching the surface of

the skin.

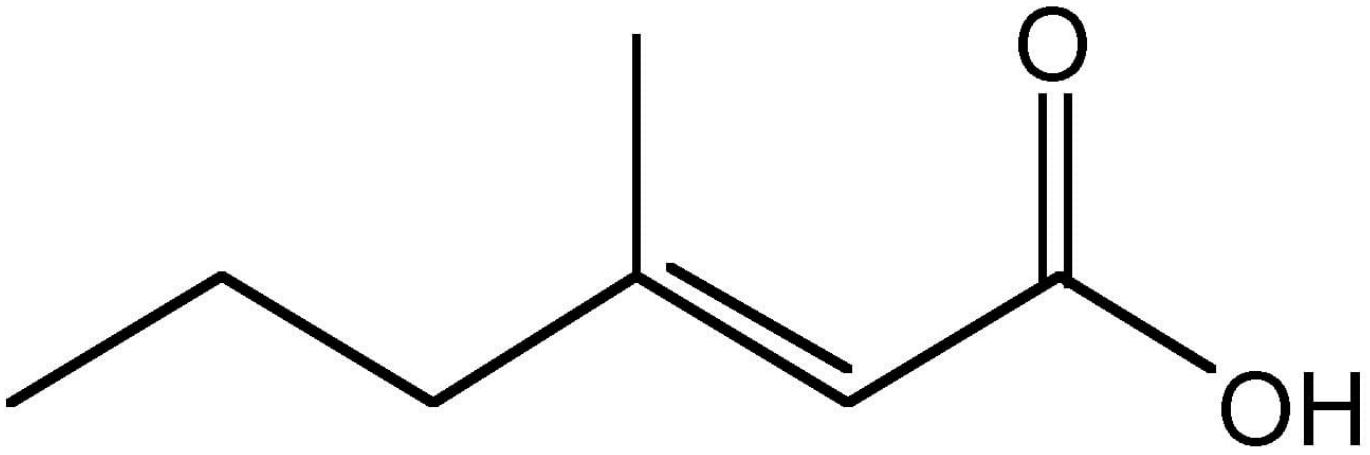


Figure 6.6.14.6: The structure of 3-methyl-2-hexenoic acid.

Boron trihalides: a special case

The three lighter boron trihalides, BX_3 (X = F, Cl, Br) form stable adducts with common Lewis bases. Their relative Lewis acidities can be evaluated in terms of the relative exothermicity of the adduct-forming reaction:

$$BF_3 < BCl_3 < BBr_3(\text{strongest Lewis acid}) \tag{6.6.14.18}$$

This trend is opposite to that expected based upon the electronegativity of the halogens. The best explanation of this trend takes into account the extent of π-donation that occurs between the filled lone pair orbital on the halogens and the empty p-orbital on the planar boron (Figure 6.6.14.7). As such, the greater the π-bonding the more stable the planar BX_3 configuration as opposed to the pyramidalization of the BX_3 moiety upon formation of a Lewis acid-base complex, (6.4.12).

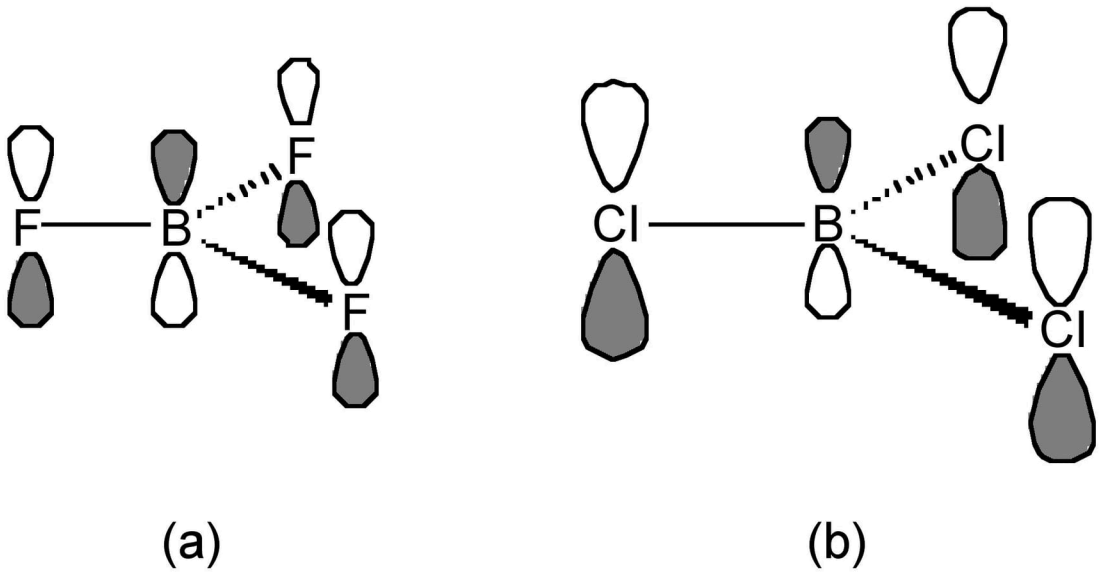


Figure 6.6.14.7: Schematic representation of π-donation from filled halogen p-orbitals into empty p-orbital in the halides BX_3.

The criteria for evaluating the relative strength of π-bonding are not clear, however, one suggestion is that the F atom is small compared to the Cl atom, and the lone pair electron in p_z of F is readily and easily donated and overlapped to empty p_z orbital of boron (Figure 6.6.14.7a). In contrast, the overlap for the large (diffuse) p-orbitals on the chlorine is poorer (Figure 6.6.14.7b). As a result, the π-donation of F is greater than that of Cl. Interestingly, as may be seen from Table 6.6.14.4, any difference in B-X bond

length does not follow the expected trend associated with shortening of the B-X bond with stronger π-bonding. In fact the B-Br distance is the most shortened as compared to that expected from the covalent radii (Table 6.6.14.4).

Table 6.6.14.4: The B-X bond distances in the boron trihalides, BX_3, as compared to the sum of the covalent radii. [a]Covalent radius of B = 0.84(3) Å.

Compound	B-X (Å)	X covalent radius (Å)	Sum of covalent radii (Å)[a]	Δ (Å)
BF_3	1.313	0.57(3)	1.41	0.097
BCl_3	1.75	1.02(4)	1.86	0.11
BBr_3	1.898	1.20(3)	2.04	0.142
BI_3	2.125	1.39(3)	2.23	0.105

At the simplest level the requirements for bonding to occur based upon the molecular or atomic orbital are:

- Directional relationship of the orbitals.
- Relative symmetry of the orbitals.
- Relative energy of the orbitals.
- Extent of orbital overlap

In the case of the boron trihalides, the direction (parallel) and symmetry (p-orbitals) are the same, and the only significant difference will be the relative energy of the donor orbitals (i.e., the lone pair on the halogen) and the extent of the overlap. The latter will be dependant on the B-X bond length (the shorter the bond the greater the potential overlap) and the diffusion of the orbitals (the less diffuse the orbitals the better the overlap). Both of these factors will benefit B-F over B-Cl and B-Br. Thus, the extent of potential overlap would follow the order: (6.14.16). Despite these considerations, it is still unclear of the exact details of the rationalization of the low Lewis basicity of BF_3 as compared to BCl_3 and BBr_3.

Anionic halides

The trihalides all form Lewis acid-base complexes with halide anions, (6.14.17), and as such salts of BF_4^-, $AlCl_4^-$, $GaCl_4^-$, and $InCl_4^-$ are common.

$$\mathrm{MX_3 + X^- \rightarrow MX_4^-} \tag{6.6.14.19}$$

In the case of gallium the $Ga_2Cl_7^-$ anion (Figure 6.6.14.8) is formed from the equilibrium:

$$\mathrm{2\ GaCl_4^- \rightleftharpoons Ga_2Cl_7^- + Cl^-} \tag{6.6.14.20}$$

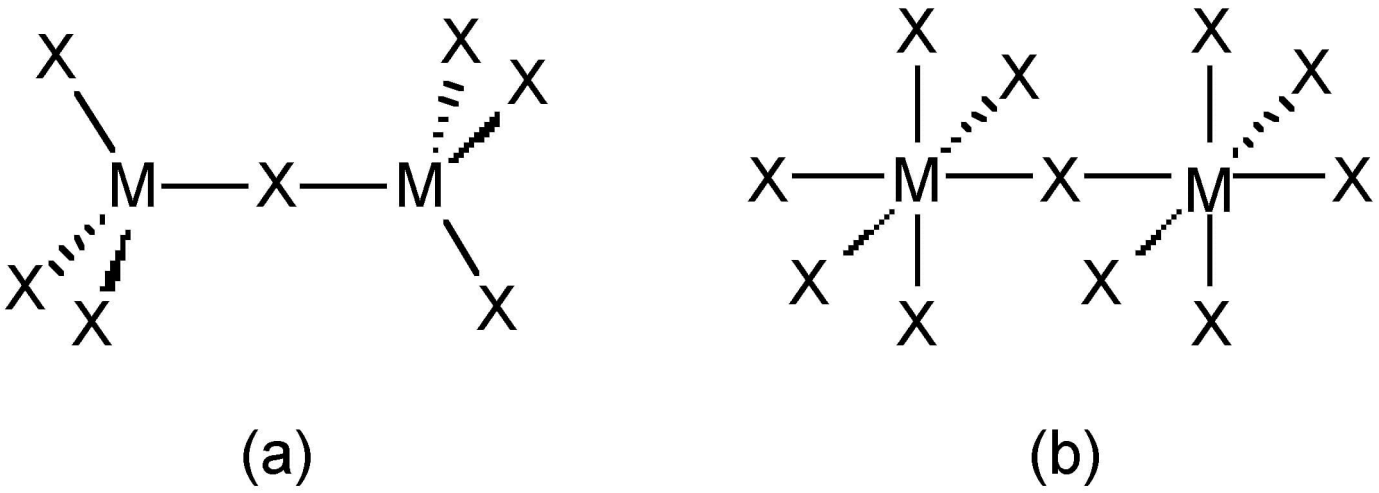


Figure 6.6.14.8: Structures of the (a) $M_2X_7^-$ and (b) $M_2X_9^{3-}$ anions.

As a consequence of its larger size indium forms a wide range of anionic halides addition compounds with trigonal bipyramidal, square pyramidal, and octahedral coordination geometries. For example, salts of $InCl_5^{2-}$, $InBr_5^{2-}$, InF_6^{3-}, $InCl_6^{3-}$ and $InBr_6^{3-}$ have all been made. The $InCl_5^{2-}$ ion has been found to be square pyramidal in the salt $[NEt_4]_2InCl_5$, but is trigonal bipyramidal in the acetonitrile solvate of $[Ph_4P]_2InCl_5$. The oligomeric anionic halides $In_2X_7^-$ and $In_2X_9^{3-}$ (X = Cl and Br) contain binuclear anions with tetrahedral and octahedrally coordinated indium atoms, respectively (Figure 6.6.14.8).

Low valent halides

Oxidation state +2

Boron forms a series of low oxidation halides containing B-B bonds a formal oxidation state of +2. Passing an electric discharge through BCl_3 using mercury electrodes results in the synthesis of B_2Cl_4, (6.14.19). An alternative route is by the co-condensation of copper as a reducing agent with BCl_3, (6.14.20).

$$2\ BCl_3 + 2\ Hg \rightarrow B_2Cl_4 + Hg_2Cl_2 \tag{6.6.14.21}$$

$$2\ BCl_3 + 2\ Cu \rightarrow B_2Cl_4 + 2\ CuCl \tag{6.6.14.22}$$

B_2F_4 has a planar structure (Figure 6.6.14.9) with D2h symmetry, while B_2Cl_4 has the same basic structure it has a staggered geometry (Figure 6.6.14.10). The energy for bond rotation about the B-B bond is very low (5 kJ/mol) that can be compared to ethane (12.5 kJ/mol). The bromide, B_2Br_4, is also observed to be staggered in the solid state. The staggered conformation is favorable on steric grounds, however, for B_2F_4 the planar geometry is stabilized by the smaller size of the halide, and more importantly the presence of strong delocalized π-bonding.

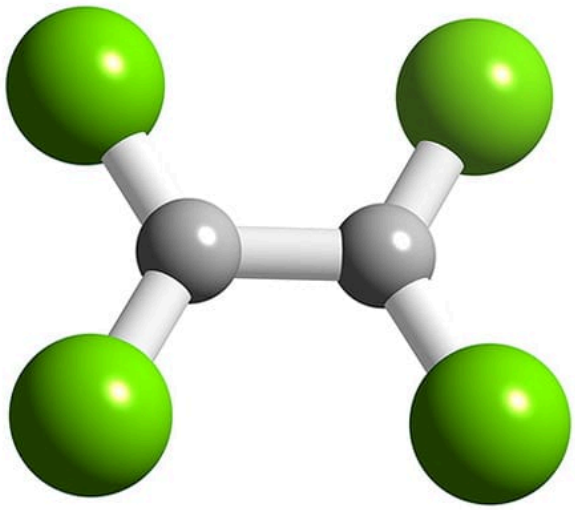


Figure 6.6.14.9: The planar structure of B_2F_4.

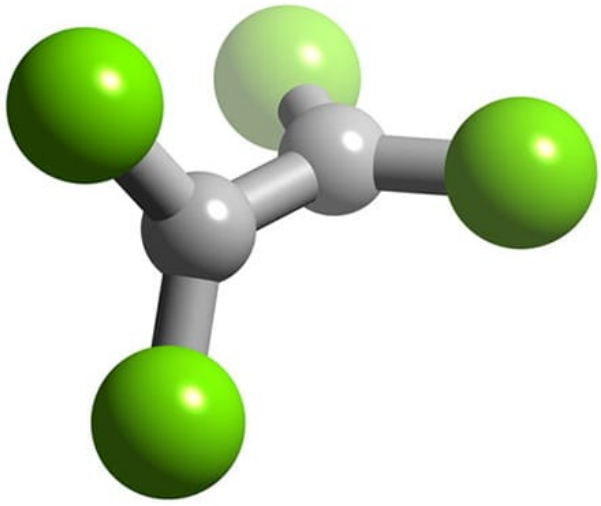


Figure 6.6.14.10: The staggered structure of B_2Cl_4.

Oxidation state +1

Boron forms a number of halides with cluster structures, B_nCl_n where n = 4 (Figure 6.6.14.11), 8, 9, 10, 11, and 12. Each compound is made by the decomposition of B_2Cl_4. For gallium, none of the monohalides are stable at room temperature, but GaCl and GaBr have been produced in the gas form from the reaction of HX and molten gallium. The stability of thallium(I) as compared to thallium(III) results in the monohalides, TlCl, TlBr, and TlI being stable. Each compound is insoluble in water, and photosensitive.

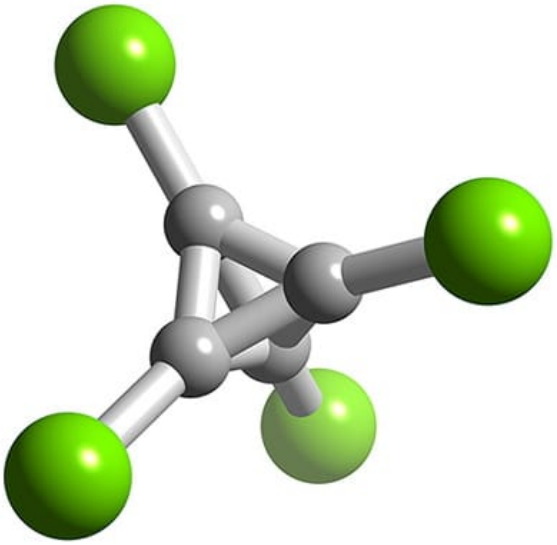


Figure 6.6.14.11: Structure of B_4Cl_4.

Intermediate halides

The dihalides (MX_2) of gallium, indium, and thallium do not actually contain the metal in the +2 oxidation state. Instead they are actually mixed valence compound, i.e., $M^+[MX_4]^-$. The dihalides of gallium are unstable in the presence of water disproportionating to gallium metal and gallium(III) entities. They are soluble in aromatic solvents, where arene complexes have been isolated and the arene is η^6-coordinated to the Ga^+ ion. $InBr_2$ and InI_2 are greenish and yellow crystalline solids, respectively, which are formulated In(I)[In(III)X_4]. $TlCl_2$ and $TlBr_2$ both are of similar formulations.

Ga_2X_3 (X = Br, I) and In_2Br_3 are formulated $M(I)_2[M(II)_2X_6]$. Both anions contain a M-M bond where the metal has a formal oxidation state of +2. The $Ga_2Br_6^{2-}$ anion is eclipsed like the $In2Br6^{2-}$ anion, whereas the $Ga_2I_6^{2-}$ anion is isostructural with Si_2Cl_6 with a staggered conformation. In_2Cl_3 is colorless and is formulated $In(I)_3[In(III)Cl_6]$.

Ga_3Cl_7 contains the $Ga_2Cl_7^-$ ion, which has a structure similar to the dichromate, $Cr_2O_7^{2-}$, ion with two tetrahedrally coordinated gallium atoms sharing a corner (Figure). The compound can be formulated as gallium(I) heptachlorodigallate(III), $Ga(I)[Ga(III)_2Cl_7]$.

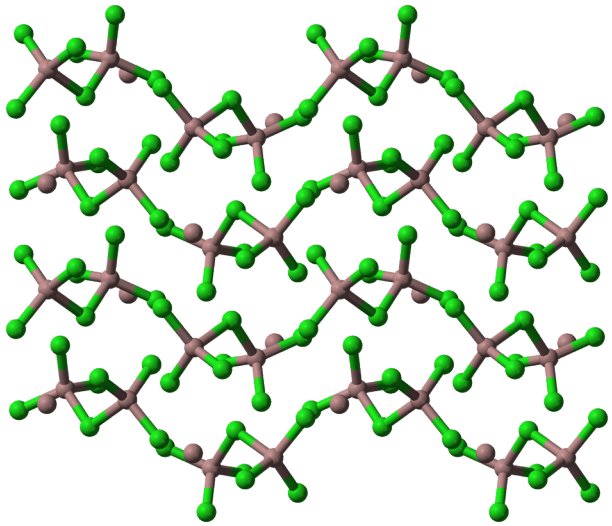


Figure 6.6.14.12: The crystal structure of Ga_3Cl_7, better described as gallium(I) heptachlorodigallate(III), $Ga(I)[Ga(III)_2Cl_7]$. Grey spheres represent the gallium, while green spheres represent the chlorine.

In_4Br_7 is light sensitive (like TlCl and TlBr) decaying to $InBr_2$ and In metal. It is a mixed salt containing the $InBr_4^-$ and $InBr_6^{3-}$ anions balanced by In^+ cations. It is formulated $In(I)_5[In(III)Br_4]_2[In(III)Br_6]$. In_5Br_7 is a pale yellow solid formulated as $In(I)_3[In(II)_2Br_6]Br$. The $In(II)_2Br_6^{2-}$ anion has an eclipsed ethane like structure with an In-In bond length of 2.70 Å. In_5Cl_9 is formulated $In(I)_3[In(III)_2Cl_9]$, with the $In_2Cl_9^{2-}$ anion having two 6 coordinate indium atoms with 3 bridging chlorine atoms, face sharing bioctahedra. Finally, In_7Cl_9 and In_7Br_9 have a structure formulated as $InX_6[In(III)X_6]X_3$.

Bibliography

- P. M. Boorman and D. Potts, *Can. J. Chem.*, 1974, **52**, 2016.
- A. Borovik and A. R. Barron, *J. Am. Chem. Soc.*, 2002, **124**, 3743.
- A. Borovik, S. G. Bott, and A. R. Barron, *J. Am. Chem. Soc.*, 2001, **123**, 11219.
- C. S. Branch, S. G. Bott, and A. R. Barron, *J. Organomet. Chem.*, 2003, **666**, 23.
- W. M. Brown and M. Trevino, *US Patent* 5,395,536 (1995).
- S. K. Dentel, *CRC Critical Reviews in Environmental Control*, 1991, **21**, 41.
- D. E. Hassick and J. P. Miknevich, *US Patent* 4,800,039 (1989).
- M. D. Healy, P. E. Laibinis, P. D. Stupik and A. R. Barron, *J. Chem. Soc., Chem. Commun.*, 1989, 359.
- K. Hedberg and R. Ryan, *J. Chem. Phys.*, 1964, **41**, 2214.
- Y. Koide and A. R. Barron, Organometallics, 1995, **14**, 4026.
- G. Santiso-Quiñones and I. Krossing, *Z. Anorg. Allg. Chem.*, 2008, **634**, 704.

This page titled 6.6.14: Group 13 Halides is shared under a CC BY 1.0 license and was authored, remixed, and/or curated by LibreTexts.

6.7: Group 14

This page titled 6.7: Group 14 is shared under a CC BY 3.0 license and was authored, remixed, and/or curated by Andrew R. Barron (CNX) via source content that was edited to the style and standards of the LibreTexts platform.

6.7.1: The Group 14 Elements

The group was once also known as the *tetrels* (from Greek *tetra* meaning *four*), stemming from the earlier naming convention of this group as Group IVA. Table lists the derivation of the names of the Group 14 elements.

Table 6.7.1.1*: Derivation of the names of each of the Group 14 elements.*

Element	Symbol	Name
Carbon	C	From the Latin *carbo* meaning *coal*
Silicon	Si	From the Latin *silicis* meaning *flints*
Germanium	Ge	From the Latin *Germania* for *Germany*
Tin	Sn	From the Anglo-Saxon and from the Latin *stannum* meaning *melts easily*
Lead	Pb	From the Anglo-Saxon, and from the Latin *plumbum* meaning *soft metal*

Discovery

Carbon

Carbon was known in prehistory in the form of soot; while charcoal was made in Roman times (by heating wood while exclude air) and diamonds were known as early as 2500 BC in China. In 1772, Antoine Lavoisier (Figure 6.7.1.1) showed that diamonds were a form of carbon, when he burned samples of carbon and diamond and showed that both formed the same amount of carbon dioxide per gram of material. Carl Scheele (Figure 6.7.1.2) showed that graphite was a form of carbon rather a form of lead.



Figure 6.7.1.1: French chemist and biologist Antoine-Laurent de Lavoisier (1743 – 1794).



Figure 6.7.1.2: German-Swedish pharmaceutical chemist Carl Wilhelm Scheele (1742 - 1786). Author Isaac Asimov has called him "hard-luck Scheele" because he made a number of chemical discoveries before others who are generally given the credit.

A new allotrope of carbon, fullerene, was discovered in 1985 by Robert Curl, Harry Kroto, and Richard Smalley (Figure 6.7.1.3) who subsequently shared the Nobel Prize in Chemistry in 1996. Fullerenes have been reveled to include nanostructured forms such as buckyballs and nanotubes. The renewed interest in new forms lead to the discovery of further exotic allotropes, including glassy carbon, and the realization that *amorphous carbon* is not amorphous.

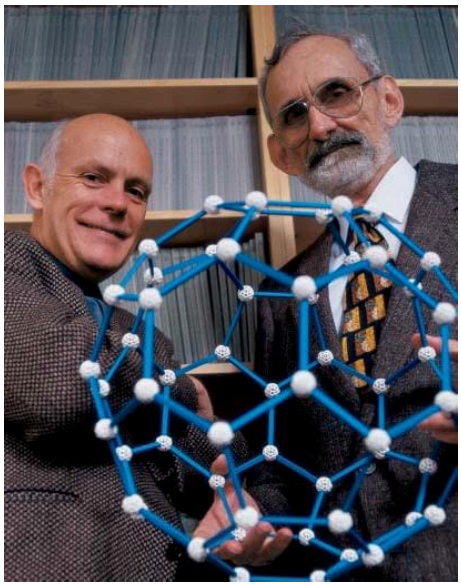


Figure 6.7.1.3: Rice University chemists Richard E. Smalley (1943 - 2005) and Robert F. Curl (1933 -).

Silicon

Silicon was first identified by Antoine Lavoisier (Figure 6.7.1.1) in 1787 as a component of flints, and was later mistaken by Humphry Davy (Figure 6.7.1.4) for a compound rather than an element. In 1824, Berzelius (Figure 6.7.1.5) prepared amorphous silicon by the reaction of potassium with silicon tetrafluoride, (7.1.1).

$$\mathrm{SiCl_4} + 4\ \mathrm{K} \rightarrow \mathrm{Si} + 4\ \mathrm{KCl} \tag{6.7.1.1}$$



Figure 6.7.1.4: British chemist and inventor Sir Humphry Davy FRS (1778 - 1829).



Figure 6.7.1.5: Swedish chemist Jöns Jacob Berzelius (1779 – 1848).

Germanium

In 1869 Dmitri Mendeleev (Figure 6.7.1.6) predicted the existence of several unknown elements, including ekasilicon (Es) between silicon and tin.

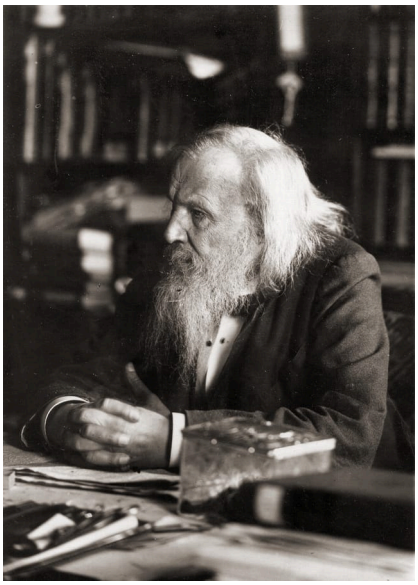


Figure 6.7.1.6: Russian chemist and inventor Dmitri Ivanovich Mendeleev (1834 – 1907).

In 1885 a new mineral (named *argyrodite* because of its high silver content) was found in a mine near Freiberg, Saxony. Clemens Winkler (Figure 6.7.1.7) isolated Mendeleev's missing element. He originally was going to name neptunium because like this element, because like ekasilicon, the planet Neptune had been preceded by mathematical prediction of its existence. However, the name neptunium had already been given to an element and so Winkler named the new metal germanium in honor of his fatherland.



Figure 6.7.1.7: German chemist Clemens Alexander Winkler (1838 –1904).

Winkler was able to isolate sufficient germanium from 500 kg of ore to determine a number properties, including an atomic weight of 72.32 g/mol by analyzing pure germanium tetrachloride ($GeCl_4$). Winkler prepared several new compounds of germanium, including the fluorides, chlorides, sulfides, germanium dioxide, and tetraethylgermane ($Ge(C_2H_5)_4$). The physical data from these compounds, corresponded with Mendeleev's predictions (Table 6.7.1.2).

Table 6.7.1.2: Properties predicted for ekasilicon compared those determined for germanium.

Property	**Ekasilicon**	**Germanium**
Atomic mass	72	72.59
Density (g/cm^3)	5.5	5.35
Melting point (°C)	High	947

Color	Gray	Gray
Oxide type	Refractory dioxide	Refractory dioxide
Oxide density (g/cm^3)	4.7	4.7
Oxide activity	Feebly basic	Feebly basic
Chloride boiling point (°C)	Under 100	86 ($GeCl_4$)
Chloride density (g/cm^3)	1.9	1.9

Tin

Tin is one of the earliest metals known. When the addition of about 5% tim to molten copper produced an alloy (bronze) that was easier to work and much harder than copper, it revolutionized civilization. The widespread use of bronze to make tools and weapons became part of what archaeologists call the Bronze Age. The Bronze Age arrived in Egypt, Mesopotamia and the Indus Valley culture by around 3000 BC.

Lead

Lead has been commonly used for thousands of years because of its ease of extraction, and its ease of smelting. Lead beads dating back to 6400 BC have been found in Çatalhöyük in modern-day Turkey, while lead was used during the Bronze Age.

Abundance

Carbon and silicon are amongst the most abundant elements (Table 6.7.1.3). Silicon is the second most abundant element (after oxygen) in the Earth's crust, making up 28% of the crust. Carbon is the fourth most abundant chemical element in the universe after hydrogen, helium, and oxygen. In combination with oxygen in carbon dioxide, carbon is found in the Earth's atmosphere (in quantities of approximately 810 gigatonnes) and dissolved in all water bodies (approximately 36,000 gigatons). Around 1,900 gigatons are present in the biosphere. Hydrocarbons (such as coal, petroleum, and natural gas) contain carbon amounts to around 900 gigatons. Natural diamonds occur in the rock kimberlite, found in ancient volcanic "necks," or "pipes". Most diamond deposits are in Africa but there are also deposits in Canada, the Russian Arctic, Brazil, and Australia.

Table 6.7.1.3: Abundance of Group 14 elements.

Element	**Terrestrial abundance (ppm)**
C	480 (Earth's crust), 28 (sea water), 350 (atmosphere CO_2), 1.6 (atmosphere, CH_4), 0.25 (atmosphere, CO)
Si	28,000 (Earth's crust), 2 (sea water)
Ge	2 (Earth's crust), 1 (soil), 5 x 10^{-7} (sea water)
Sn	2 (Earth's crust), 1 (soil), 4 x 10^{-6} (sea water)
Pb	14 (Earth's crust), 23 (soil), 2 x 10^{-6} (sea water)

Isotopes

Table 6.7.1.4 summarizes the naturally occurring isotopes of the Group 14 elements.

Table 6.7.1.4: Abundance of the major isotopes of the Group 14 elements.

Isotope	**Natural abundance (%)**
Carbon-12	98.9
Carbon-13	1.1

Carbon-14	trace
Silicon-28	92.23
Silicon-29	4.67
Silicon -30	3.1
Germanium-70	21.23
Germanium-72	27.66
Germanium-73	7.73
Germanium-74	35.94
Germanium-76	7.44
Tin-112	0.97
Tin-114	0.66
Tin-115	0.34
Tin-116	14.54
Tin-117	7.68
Tin-118	24.22
Tin-119	8.59
Tin-120	32.58
Tin-122	4.63
Tin-124	5.79
Lead-204	1.4
Lead-24.1	24.1
Lead-207	22.1
Lead-208	52.4

Although radioactive, carbon-14 is formed in upper layers of the troposphere and the stratosphere, at altitudes of 9–15 km. Thermal neutrons produced by cosmic rays collide with the nuclei of nitrogen-14, forming carbon-14 and a proton. Because of its relatively short half-life of 5730 years, carbon-14 is absent in ancient rocks, but is incorporated in living organisms.

Carbon dating

Carbon dating is a process whereby the age of a material that contains carbon can be determined by comparing the decay rate of that material with that of living material.

Carbon-14 has a half life ($t_{1/2}$) of 5.73 x 10^3 years for its decay to nitrogen-14 by the loss of a β particle, (7.1.2).

$$ {}^{14}_{6}C \rightarrow {}^{14}_{7}N + {}^{0}_{-1}e \tag{6.7.1.2} $$

The rate of radioactive decay can be expressed as a rate constant (k):

$$ \mathrm{k} = \frac{\ln[2]}{\mathrm{t}_{1/2}} = \frac{0.693}{\mathrm{t}_{1/2}} \tag{6.7.1.3} $$

For carbon-14, using (7.1.3),

$$ \mathrm{k} = \frac{0.693}{5.73 \text{ x } 10^3} = 1.21 \text{ x } 10^{-4} \text{ year}^{-1} \tag{6.7.1.4} $$

In 1947 samples of the Dead Sea Scrolls were analyzed by carbon dating. It was found that the carbon-14 present had an activity of d/min.g (where d = disintegration); by contrast in living material the activity is 14 d/min.g. Thus,

$$\ln\frac{14}{11} = (1.21 \text{ x } 10^{-4})\text{ t} \tag{6.7.1.5}$$

$$\text{t} = \frac{\ln 1.272}{1.21 \text{ x } 10^{-4}} = 2.0 \text{ x } 10^{3} \text{ years} \tag{6.7.1.6}$$

From the measurement performed in 1947 the Dead Sea Scrolls were determined to be 2000 years old giving them a date of 53 BC, and confirming their authenticity. This discovery is in contrast to the carbon dating results for the Turin Shroud that was supposed to have wrapped Jesus' body. Carbon dating has shown that the cloth was made between 1260 and 1390 AD. Thus, the Turin Shroud is clearly a fake having been made over a thousand years after its supposed manufacture.

Industrial production

Due to the industrial importance of carbon and silicon, as well as the wide range of fullerene materials, the production of these elements is discussed elsewhere. However, the diamond supply chain is controlled by a limited number of commercial concerns, the largest of which is DeBeers in London (Figure). Diamonds make up only a very small fraction of ore bearing rock. The ore is crushed and subsequently the particles are sorted by density. Diamonds are located in the diamond-rich fraction by X-ray fluorescence, after which the final sorting steps are done by hand.

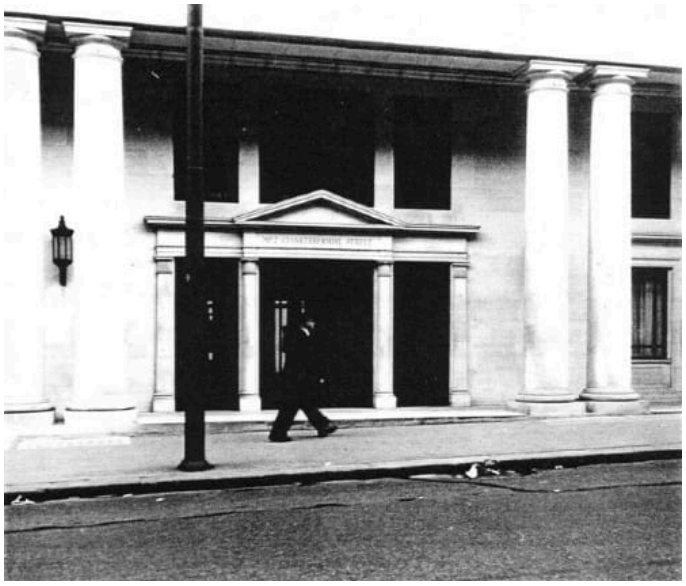


Figure 6.7.1.8: The Charterhouse Street Entrance of the offices of De Beers in London, are the venue for the 10 sights that are held during the year. Sightholders, both manufacturers (of polished diamonds) and dealers (in rough diamonds), meet in London, once every 5 weeks, 10 times a year, to inspect their diamond allocations.

Germanium ore concentrates are mostly sulfidic, e.g., as an impurity in zinc blende. They are converted to the oxides by heating under air (roasting), (7.1.7).

$$\text{GeS}_2 + 3\text{ O}_2 \rightarrow \text{GeO}_2 + 2\text{ SO}_2 \tag{6.7.1.7}$$

Part of the germanium ends up in the dust produced during this process, while the rest is converted to germanates which are leached together with the zinc by sulfuric acid. After neutralisation the germanium and other metals are precipitated (leaving the Zn^{2+} in solution). Germanium dioxide is obtained as a precipitate and converted with chlorine gas or hydrochloric acid to germanium tetrachloride,(7.1.8) (7.1.9), which has a low boiling point and can be purified by distillation.

$$\text{GeO}_2 + 4\text{ HCl} \rightarrow \text{GeCl}_4 + 2\text{ H}_2\text{O} \tag{6.7.1.8}$$

$$\text{GeO}_2 + 2\text{ Cl}_2 \rightarrow \text{GeCl}_4\text{O}_2 \tag{6.7.1.9}$$

The germanium tetrachloride is hydrolyzed to the give pure oxide (GeO_2), which is then converted to germanium glass for the semiconductor industry, (7.1.10). Germanium used in steel production and other applications that do not require the high purity is produced by reduction with carbon, (7.1.11).

$$\mathrm{GeO_2 + 4\ H_2 \rightarrow Ge + H_2O} \tag{6.7.1.10}$$

$$\mathrm{GeO_2 + C \rightarrow Ge + CO_2} \tag{6.7.1.11}$$

Tin is mined and subsequently smelted, and its production has changed little. In contrast, lead-rich ores contain less than 10% lead, but ores containing as little as 3% lead can be economically exploited. Ores are crushed and concentrated to 70%. Sulfide ores are roasted, producing lead oxide and a mixture of sulfates and silicates of lead. Lead oxide from the roasting process is reduced in a coke-fired blast furnace. This converts most of the lead to its metallic form. Metallic lead that results from the roasting and blast furnace processes still contains significant contaminants of arsenic, antimony, bismuth, zinc, copper, silver, and gold. The melt is treated in a reverberatory furnace (Figure 6.7.1.9) with air, steam, and sulfur, which oxidizes the contaminants except silver, gold, and bismuth.

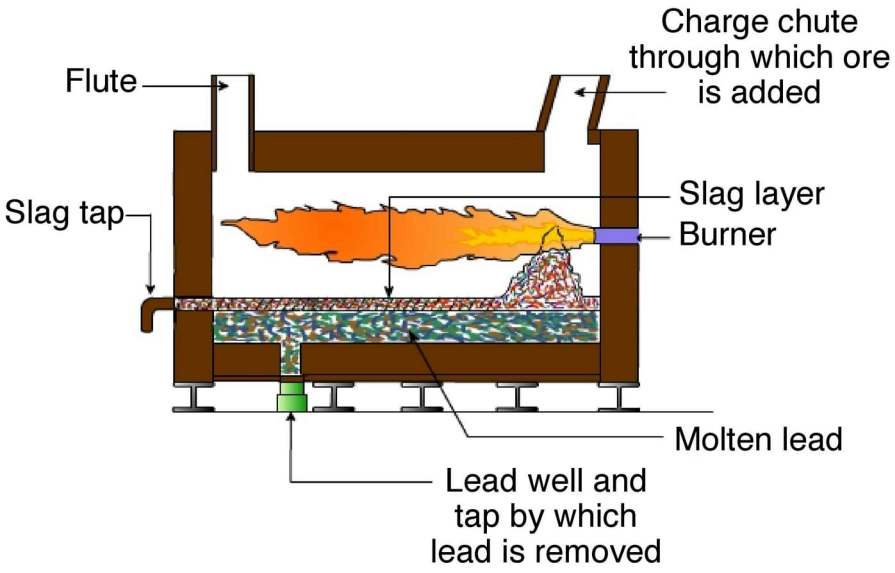


Figure 6.7.1.9: Schematic of a reverberatory furnace.

Physical properties

Table 6.7.1.5 provides a summary of the physical properties of the Group 14 elements.

Table 6.7.1.5: Selected physical properties of the Group 14 elements.

Element	Mp (°C)	Bp (°C)	Density (g/cm^3)
C	642 (sublimes)		2.267 (graphite), 3.515 (diamond), 1.8 - 2.1 (amorphous)
Si	1414	3265	2.3290
Ge	938	2833	5.323
Sn	232	2602	7.365 (white), 5.769 (gray)
Pb	327	1749	11.34

Cubic structure

The elements carbon through tin (in its α form) all exist in diamond cubic structure (Figure 6.7.1.10a), while lead crystallizes in a cubic close packed structure (Figure 6.7.1.10b). As expected the lattice parameter (*a*) increases with increased atomic radius (Table 6.7.1.6). The switch from diamond cubic to close packed cubic may be rationalized by the relative atomic sizes.

The diamond cubic structure comprises of two interpenetrating cubic close packed lattices. As the atomic size increases large interstitial vacancies would result, resulting in an unfavorable low-density structure.

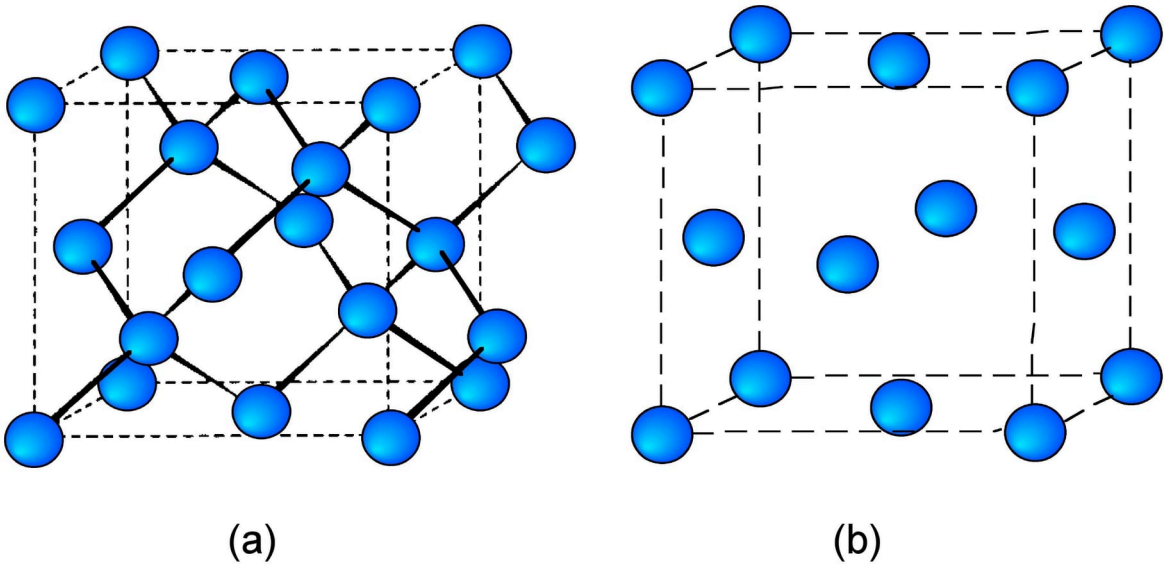


Figure 6.7.1.10: Unit cell structure of (a) the diamond cubic lattice showing the two interpenetrating face-centered cubic lattices, and (b) the cell of cubic close packed structure for comparison.

Table 6.7.1.6: Lattice parameter and crystal density for Group 14 elements.

Element	**Structure**	***a* (Å)**	**Atomic radius (Å)**
C	diamond cubic	3.566	0.70
Si	diamond cubic	5.431	1.10
Ge	diamond cubic	5.657	1.25
α-Sn (gray)	diamond cubic	6.489	1.45
Pb	cubic close packed	4.951	1.80

This page titled 6.7.1: The Group 14 Elements is shared under a CC BY 3.0 license and was authored, remixed, and/or curated by Andrew R. Barron (CNX) via source content that was edited to the style and standards of the LibreTexts platform.

6.7.2: Carbon Black- From Copying to Communication

It is a commonly held fallacy that James Watt (Figure 6.7.2.1) was the inventor of the steam engine. This actually honor belongs to Thomas Newcomen (Figure 6.7.2.2). Watt's actual achievement was to improve Newcomen's design of a steam pump. While Watt was working in the repair shop at the University of Glasgow he was fixing a Newcomen pump when he developed several key improvements on the original design.

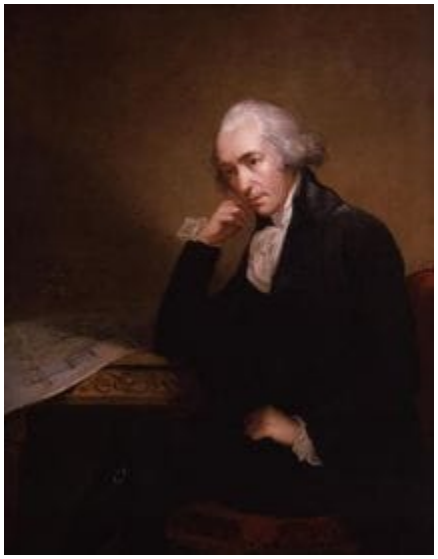


Figure 6.7.2.1: Scottish inventor and mechanical engineer James Watt FRS (1736 –1819).



Figure 6.7.2.2: English ironmonger and inventor of the steam engine Thomas Newcomen (1664 - 1729).

The reason for Watt's success was that Britain was going through a major industrial boom and was in need of significant quantities of raw material including coal. Many of the coalmines, especially those in Devon were prone to flooding. Unfortunately, Newcomen's engine (which was actually a steam pump) could not pump the water out fast enough, whereas Watt's engine was powerful enough to drain the mines. As a result Watt's career as a manufacturer was assured. However, Watt did not see the full potential of his invention, this was left to an employee of his, William Murdock (Figure 6.7.2.3), whose invention of the gearing to allow the steam engine to be used for powering machinery.



Figure 6.7.2.3: Scottish engineer and inventor William Murdock (1754 - 1839).

One outcome that Watt found from his increased business was an increase in paperwork! While he was living in Redruth, Cornwall, close to where many of the mines were situated he told a friend that he was having “excessive difficulty in finding intelligent managing clerks”. In 1780 Watt solved his paperwork problems by inventing the first method of making copies. This was the subject of a Patent entitled “A new method of copying letters and writing expeditiously”. Watt’s invention involved making ink out of gum Arabic and carbon black.

Note

Gum arabic, also known as *gum acacia*, is a natural gum made of the hardened sap taken from two species of the acacia tree; *acacia senegal* and *acacia seyal*. Carbon black is a form of amorphous carbon that has a high surface area to volume ratio it is commonly produced by the incomplete combustion of heavy petroleum products such as coal tar.

Watt’s ink would stay wet for 24 hours. Writing with the ink and then pressing the result against another piece of paper created a copy. Initially there was great resistance to the copy paper. In particular banks believed that this form of copying could result in forgeries. However, by the end of its first year on sale, Watt sold over 200 examples. The real commercial push came after Watt demonstrated his process to the House of Parliament. The resultant consternation amongst the Members of Parliament resulted in their having to be reminded that Parliament was still in session! By 1785 copies were in general use, however, Cyrus P. Dalkin made the biggest advance in 1823. By using a mixture of carbon black and hot paraffin wax the back of a piece of paper was coated. The carbon black was transferred to another piece of paper underneath by the pressure of the pen. Dalkin had created *carbon copies*. Both Ralph Wedgwood in England and Pellegrino Turri in Italy had developed forms of carbon paper between 1806 and 1808, but it was Dalkin’s version of carbon copy paper that found usage.



Figure 6.7.2.4: Modern carbon paper.

Initially there was almost no market for this new carbon copy paper, until in 1868 when American Lebbeus Rogers was talking part in a balloon ascent. Rogers was an owner of biscuit and greengrocer companies, and was intrigued when a reporter for the Associated Press who was interviewing him used Dalkin's carbon paper. Rogers gave up his biscuit business and founded a firm to sell carbon paper. In 1873 he talked with E. Remington and Sons the typewriter manufacturer, and it was this application that created a success out of the carbon paper business.

Note

The term "CC" commonly used in e-mail programs today grew from the use of carbon paper and means *carbon copy*.

Interestingly, carbon black is still used today in modern photocopiers and laser printers. One of the attributes that allow its use is the ability for carbon black particles to become charged. This is related to another application of carbon black in early communications: its ability to conduct electric, and the changes that occur as a function of external pressure.

While Alexander Graham Bell was the first to be awarded a US patent for the electric telephone in March 1876, it was an invention by Thomas Edison (Figure 6.7.2.5) that provided significant improvements. Early telephones relied on a metal diaphragm that was attached to an electromagnet. Speaking into the metal diaphragm caused its vibration, which in tern vibrated the electromagnetic and hence created a current. Unfortunately, the current was very low and subsequent clarity was poor. Between 1877 and 1878 Edison investigated methods to improve the clarity of the signal. The key development was the carbon microphone (Figure 6.7.2.6).

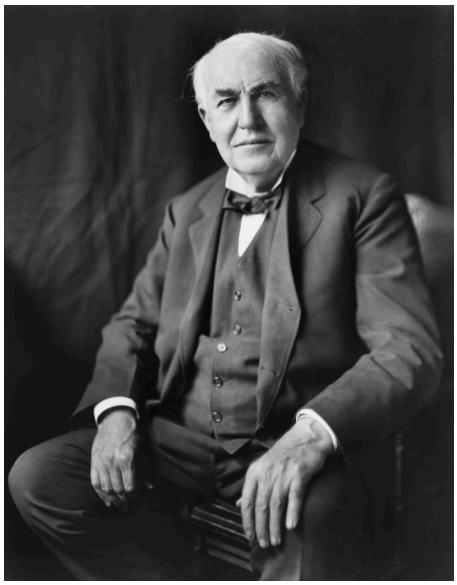


Figure 6.7.2.5: American inventor, scientist and businessman Thomas Alva Edison (1847 –1931).

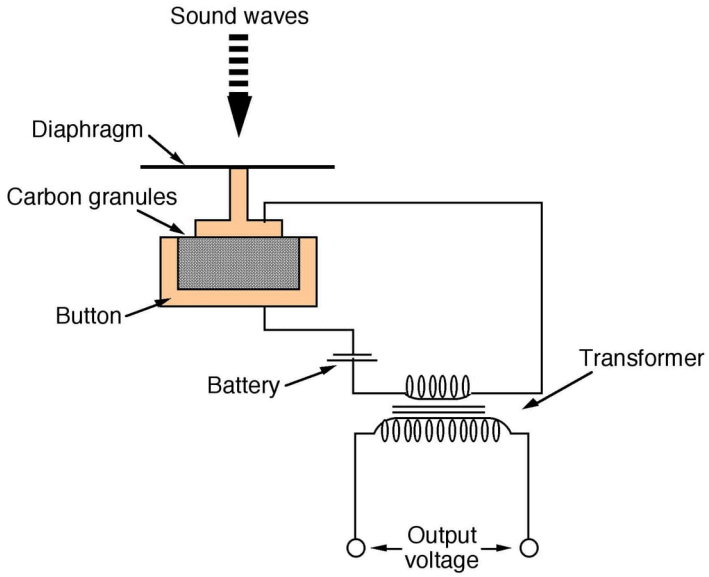


Figure 6.7.2.6: A schematic of a simple carbon “button” microphone.

The carbon microphone, also known as a carbon button microphone consisting of two metal plates separated by granules of carbon. One plate faces outward and acts as a diaphragm. When sound waves strike this plate, the pressure on the granules changes, which in turn changes the electrical resistance between the plates. A direct current is passed from one plate to the other, and the changing resistance results in a changing current, which can be passed through a telephone system. The carbon microphone was used in all telephones until the 1980s.

It was one of Edison’s researchers, Edward Acheson (Figure 6.7.2.7) whose discovery allowed for the extension of communication on a global scale. While trying to make artificial diamonds, Acheson began mixing clay and coke (carbon) at very high temperatures. In an electric furnace at high temperatures he found hexagonal crystals of silicon carbide (SiC) attached to the carbon electrode. He called this material carborundum. When, by mistake, he overheated the mixture to 4150 °C he found that the silicon evaporated (boiling point 3265 °C) leaving pure and highly crystalline carbon: graphite.

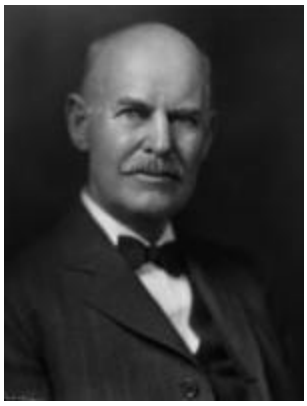


Figure 6.7.2.7: American chemist Edward Goodrich Acheson (1856 – 1931).

Graphite is a natural mineral normally associated with other minerals, although an enormous deposit of graphite was discovered in Cumbria, England, which the locals found very useful for marking sheep! Graphite was named by Abraham Werner (Figure 6.7.2.8) in 1789 from the Greek *graphein* meaning *to draw/write* due to its use in pencils. However, its use was limited due to the cost. The ability to manufacture high purity graphite resulted in its use in electrodes, dynamo brushes, and batteries. The most terrifying application of graphite was as a result of a material problem associated with the V-2 rocket built by Germany during the Second World War.



Figure 6.7.2.8: German geologist Abraham Gottlob Werner (1749 –1817).

The V-2 rockets or Vergeltungswaffen-2 (vengeance weapon-2) was 47 feet long, and reached 3,600 mph with an altitude of 300,000 feet (Figure 6.7.2.9). In order to control the direction of flight the V-2 was guided by four external rudders on the tail fins, and four internal vanes at the exit of the jet (Figure 6.7.2.10). These vanes were made of graphite, it being the only material that would survive the extreme temperatures.



Figure 6.7.2.9: A V-2 rocket at the Peenemünde Museum.

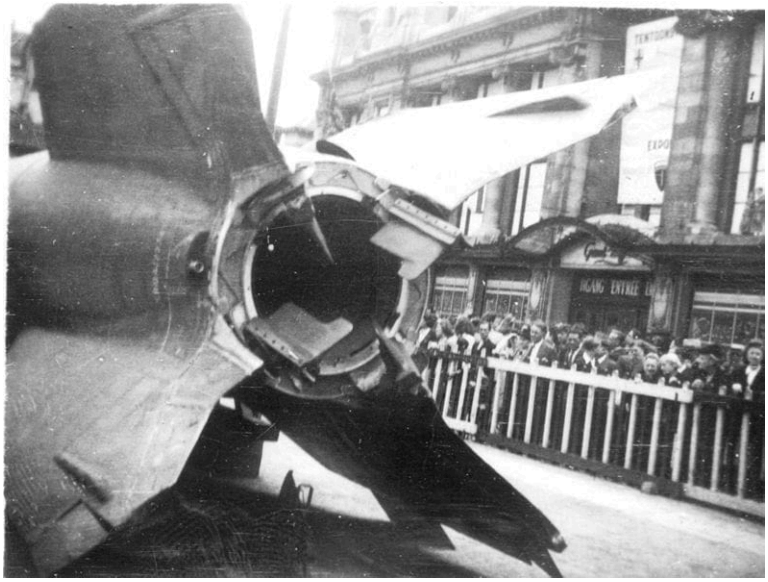


Figure 6.7.2.10: View of the V-2 rocket showing the graphite vanes for directional control.

Of course it was as a result of the same German scientists who worked on the V-2, working for NASA, that allowed rockets of sufficient power to escape the Earth's gravitational pull and send man to the moon, and position many of the satellites that are now vital for global communication.

This page titled 6.7.2: Carbon Black- From Copying to Communication is shared under a CC BY 3.0 license and was authored, remixed, and/or curated by Andrew R. Barron (CNX) via source content that was edited to the style and standards of the LibreTexts platform.

6.7.3: Carbon Nanomaterials

Fullerenes and Nanotubes

Introduction

Although nanomaterials had been known for many years prior to the report of C_{60} the field of nanoscale science was undoubtedly founded upon this seminal discovery. Part of the reason for this explosion in nanochemistry is that while carbon materials range from well-defined nano sized molecules (i.e., C_{60}) to tubes with lengths of hundreds of microns, they do not exhibit the instabilities of other nanomaterials as a result of the very high activation barriers to their structural rearrangement. As a consequence they are highly stable even in their unfunctionalized forms. Despite this range of carbon nanomaterials possible they exhibit common reaction chemistry: that of organic chemistry.

The previously unknown allotrope of carbon: C_{60}, was discovered in 1985, and in 1996, Curl, Kroto, and Smalley were awarded the Nobel Prize in Chemistry for the discovery. The other allotropes of carbon are graphite (sp^2) and diamond (sp^3). C_{60}, commonly known as the "buckyball" or "Buckminsterfullerene", has a spherical shape comprising of highly pyramidalized sp^2 carbon atoms. The C_{60} variant is often compared to the typical soccer football, hence buckyball. However, confusingly, this term is commonly used for higher derivatives. Fullerenes are similar in sheet structure to graphite but they contain pentagonal (or sometimes heptagonal) rings that prevent the sheet from being planar. The unusual structure of C_{60} led to the introduction of a new class of molecules known as fullerenes, which now constitute the third allotrope of carbon. Fullerenes are commonly defined as "any of a class of closed hollow aromatic carbon compounds that are made up of twelve pentagonal and differing numbers of hexagonal faces."

The number of carbon atoms in a fullerene range from C_{60} to C_{70}, C_{76}, and higher. Higher order fullerenes include carbon nanotubes that can be described as fullerenes that have been stretched along a rotational axis to form a tube. As a consequence of differences in the chemistry of fullerenes such as C_{60} and C_{70} as compared to nanotubes, these will be dealt with separately herein. In addition there have also been reports of nanohorns and nanofibers, however, these may be considered as variations on the general theme. It should be noted that fullerenes and nanotubes have been shown to be in flames produced by hydrocarbon combustion. Unfortunately, these naturally occurring varieties can be highly irregular in size and quality, as well as being formed in mixtures, making them unsuitable for both research and industrial applications.

Fullerenes

Carbon-60 (C_{60}) is probably the most studied individual type of nanomaterial. The spherical shape of C_{60} is constructed from twelve pentagons and twenty hexagons and resembles a soccer ball (Figure 6.7.3.1a). The next stable higher fullerene is C_{70} (Figure 6.7.3.1b) that is shaped like a rugby or American football. The progression of higher fullerenes continues in the sequence C_{74}, C_{76}, C_{78}, etc. The structural relationship between each involves the addition of six membered rings. Mathematically (and chemically) two principles define the existence of a stable fullerene, i.e., Euler's theorem and isolated pentagon rule (IPR). Euler's theorem states that for the closure of each spherical network, n (n ≥ 2) hexagons and 12 pentagons are required while the IPR says no two pentagons may be connected directly with each other as destabilization is caused by two adjacent pentagons.

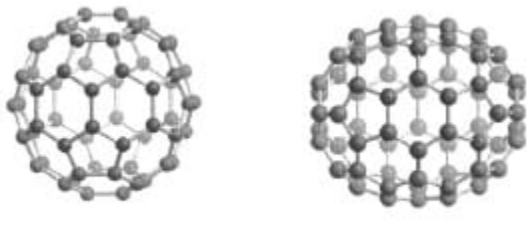


Figure 6.7.3.1: Molecular structures of (a) C_{60} and (b) C_{70}.

Although fullerenes are composed of sp^2 carbons in a similar manner to graphite, fullerenes are soluble in various common organic solvents. Due to their hydrophobic nature, fullerenes are most soluble in CS_2 (C_{60} = 7.9 mg/mL) and toluene (C_{60} = 2.8 mg/mL). Although fullerenes have a conjugated system, their aromaticity is distinctive from benzene that has all C-C bonds of equal lengths, in fullerenes two distinct classes of bonds exist. The shorter bonds are at the junctions of two hexagons ([6, 6] bonds) and the longer bonds at the junctions of a hexagon and a pentagon ([5,6] bonds). This difference in bonding is responsible for some of the observed reactivity of fullerenes.

Synthesis of fullerenes

The first observation of fullerenes was in molecular beam experiments at Rice University. Subsequent studies demonstrated that C_{60} it was relatively easy to produce grams of fullerenes. Although the synthesis is relatively straightforward fullerene purification remains a challenge and determines fullerene's commercial price. The first method of production of measurable quantities of fullerenes used laser vaporization of carbon in an inert atmosphere, but this produced microscopic amounts of fullerenes. Laboratory scales of fullerene are prepared by the vaporization of carbon rods in a helium atmosphere. Commercial production ordinarily employs a simple ac or dc arc. The fullerenes in the black soot collected are extracted in toluene and purified by liquid chromatography. The magenta C_{60} comes off the column first, followed by the red C_{70}, and other higher fullerenes. Even though the mechanism of a carbon arc differs from that of a resistively heated carbon rod (because it involves a plasma) the He pressure for optimum C_{60} formation is very similar.

A ratio between the mass of fullerenes and the total mass of carbon soot defines fullerene yield. The yields determined by UV-Vis absorption are approximately 40%, 10-15%, and 15% in laser, electric arc, and solar processes. Interestingly, the laser ablation technique has both the highest yield and the lowest productivity and, therefore, a scale-up to a higher power is costly. Thus, fullerene commercial production is a challenging task. The world's first computer controlled fullerene production plant is now operational at the MER Corporation, who pioneered the first commercial production of fullerene and fullerene products.

Endohedral fullerenes

Endohedral fullerenes are fullerenes that have incorporated in their inner sphere atoms, ions or clusters. Endohedral fullerenes are generally divided into two groups: endohedral metallofullerenes and non-metal doped fullerenes. The first endohedral metallofullerenes was called La@C_{60}. The @ sign in the name reflects the notion of a small molecule trapped inside a shell.

Doping fullerenes with metals takes place *in-situ* during the fullerene synthesis in an arc reactor or via laser evaporation. A wide range of metals have been encased inside a fullerene, i.e., Sc, Y, La, Ce, Ba, Sr, K, U, Zr, and Hf. Unfortunately, the synthesis of endohedral metallofullerenes is unspecific because in addition a high yield of unfilled fullerenes, compounds with different cage sizes are prepared (e.g., La@C_{60} or La@C_{82}). A characteristic of endohedral metallofullerenes is that electrons will transfer from the metal atom to the fullerene cage and that the metal atom takes a position off-center in the cage. The size of the charge transfer is not always simple to determine, but it is usually between 2 and 3 units (e.g., La_2@C_{80}) but can be as high as 6 electrons (e.g., Sc_3N@C_{80}). These anionic fullerene cages are very stable molecules and do not have the reactivity associated with ordinary empty fullerenes (see below). This lack of reactivity is utilized in a method to purify endohedral metallofullerenes from empty fullerenes.

The endohedral He@C_{60} and Ne@C_{60} form when C_{60} is exposed to a pressure of around 3 bar of the appropriate noble gases. Under these conditions it was possible to dope 1 in every 650,000 C_{60} cages with a helium atom. Endohedral complexes with He, Ne, Ar, Kr and Xe as well as numerous adducts of the He@C_{60} compound have also been proven with operating pressures of 3000 bars and incorporation of up to 0.1 % of the noble gases. The isolation of N@C_{60}, N@C_{70} and P@C_{60} is very unusual and unlike the metal derivatives no charge transfer of the pnictide atom in the center to the carbon atoms of the cage takes place.

Chemically functionalized fullerenes

Although fullerenes have a conjugated aromatic system all the carbons are quaternary (i.e., containing no hydrogen), which results in making many of the characteristic substitution reactions of planar aromatics impossible. Thus, only two types of chemical transformations exist: redox reactions and addition reactions. Of these, addition reactions have the largest synthetic value. Another remarkable feature of fullerene addition chemistry is the thermodymics of the process. Since the sp^2 carbon atoms in a fullerene are paramidalized there is significant strain energy. For example, the strain energy in C_{60} is *ca* 8 kcal/mol, which is 80% of its heat of formation. So the relief of this strain energy leading to sp^3 hybridized C atoms is the major driving force for

addition reactions (Figure 6.7.3.2). As a consequence, most additions to fullerenes are exothermic reactions.

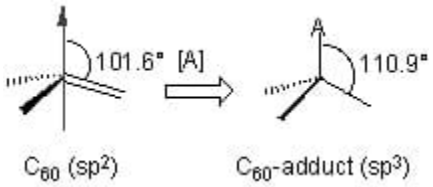


Figure 6.7.3.2: Strain release after addition of reagent A to a pyramidalize carbon of C_{60}.

Cyclic voltammetry (CV) studies show that C_{60} can be reduced and oxidized reversibly up to 6 electrons with one-electron transfer processes. Fulleride anions can be generated by electrochemical method and then be used to synthesize covalent organofullerene derivatives. Alkali metals can chemically reduce fullerene in solution and solid state to form M_xC_{60} (x = 3 - 6). C_{60} can also be reduced by less electropositive metals like mercury to form C_{60}^- and C_{60}^{2-}. In addition, salts can also be synthesized with organic molecules, for example $[TDAE^+][C_{60}^-]$ possesses interesting electronic and magnetic behavior.

Geometric and electronic analysis predicted that fullerene behaves live an electro-poor conjugated polyolefin. Indeed C_{60} and C_{70} undergo a range of nucleophilic reactions with carbon, nitrogen, phosphorous and oxygen nucleophiles. C60 reacts readily with organolithium and Grignard compounds to form alkyl, phenyl or alkanyl fullerenes. Possibly the most widely used additions to fullerene is the Bingel reaction (Figure 6.7.3.3), where a carbon nucleophile, generated by deprotonation of α-halo malonate esters or ketones, is added to form a cyclopropanation product. The α-halo esters and ketones can also be generated in situ with I_2 or CBr_4 and a weak base as 1,8-diazabicyclo[5.4.0]unde-7ene (DBU). The Bingel reaction is considered one of the most versatile and efficient methods to functionalize C_{60}.

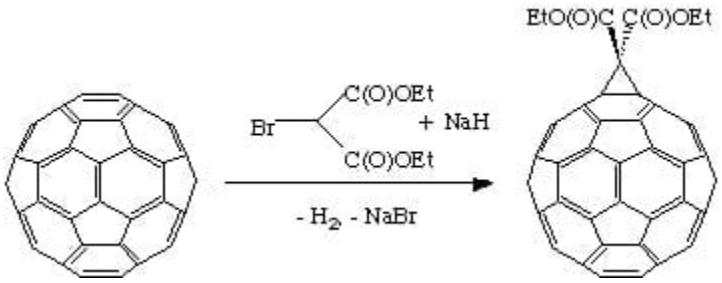


Figure 6.7.3.3: Bingel reaction of C_{60} with 2-bromoethylmalonate.

Cycloaddition is another powerful tool to functionalize fullerenes, in particular because of its selectivity with the 6,6 bonds, limiting the possible isomers (Figure 6.7.3.4). The dienophilic feature of the [6,6] double bonds of C_{60} enables the molecule to undergo various cycloaddition reactions in which the monoadducts can be generated in high yields. The best studies cycloadditon reactions of fullerene are [3+2] additions with diazoderivatives and azomethine ylides (Prato reactions). In this reaction, azomethine ylides can be generated *in situ* from condensation of α-amino acids with aldehydes or ketones, which produce 1,3 dipoles to further react with C_{60} in good yields (Figure 6.7.3.5). Hundreds of useful building blocks have been generated by those two methods. The Prato reactions have also been successfully applied to carbon nanotubes.

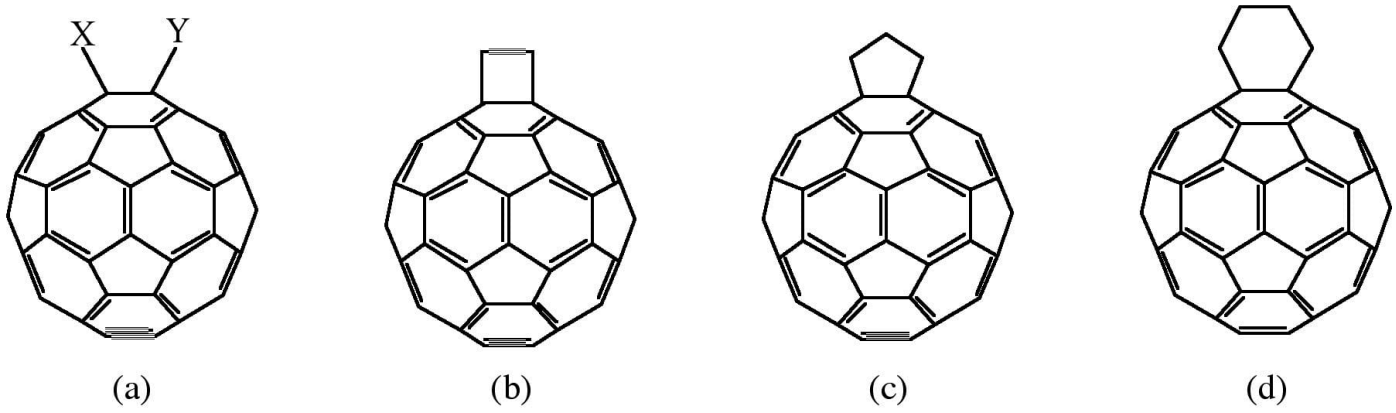


Figure 6.7.3.4: Geometrical shapes built onto a [6,6] ring junction: a) open, b) four-membered ring, c) five-membered ring, and d) six-membered ring.

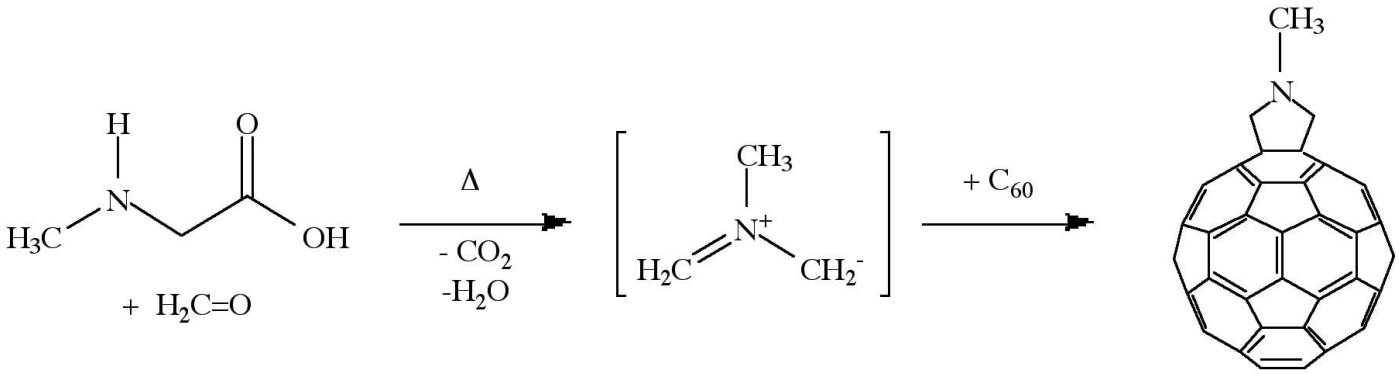


Figure 6.7.3.5: Prato reaction of C_{60} with N-methyglycine and paraformaldehyde.

The oxidation of fullerenes, such as C_{60}, has been of increasing interest with regard to applications in photoelectric devices, biological systems, and possible remediation of fullerenes. The oxidation of C_{60} to $C_{60}O_n$ (n = 1, 2) may be accomplished by photooxidation, ozonolysis, and epoxidation. With each of these methods, there is a limit to the isolable oxygenated product, $C_{60}O_n$ with $n < 3$. Highly oxygenated fullerenes, $C_{60}O_n$ with $3 \leq n \leq 9$, have been prepared by the catalytic oxidation of C_{60} with $ReMeO_3/H_2O_2$.

Carbon nanotubes

A key breakthrough in carbon nanochemistry came in 1993 with the report of needle-like tubes made exclusively of carbon. This material became known as carbon nanotubes (CNTs). There are several types of nanotubes. The first discovery was of multi walled tubes (MWNTs) resembling many pipes nested within each other. Shortly after MWNTs were discovered single walled nanotubes (SWNTs) were observed. Single walled tubes resemble a single pipe that is potentially capped at each end. The properties of single walled and multi walled tubes are generally the same, although single walled tubes are believed to have superior mechanical strength and thermal and electrical conductivity; it is also more difficult to manufacture them.

Single walled carbon nanotubes (SWNTs) are by definition fullerene materials. Their structure consists of a graphene sheet rolled into a tube and capped by half a fullerene (Figure 6.7.3.6). The carbon atoms in a SWNT, like those in a fullerene, are sp2 hybridized. The structure of a nanotube is analogous to taking this graphene sheet and rolling it into a seamless cylinder. The different types of SWNTs are defined by their diameter and chirality. Most of the presently used single-wall carbon nanotubes have been synthesized by the pulsed laser vaporization method, however, increasingly SWNTs are prepared by vapor liquid solid catalyzed growth.

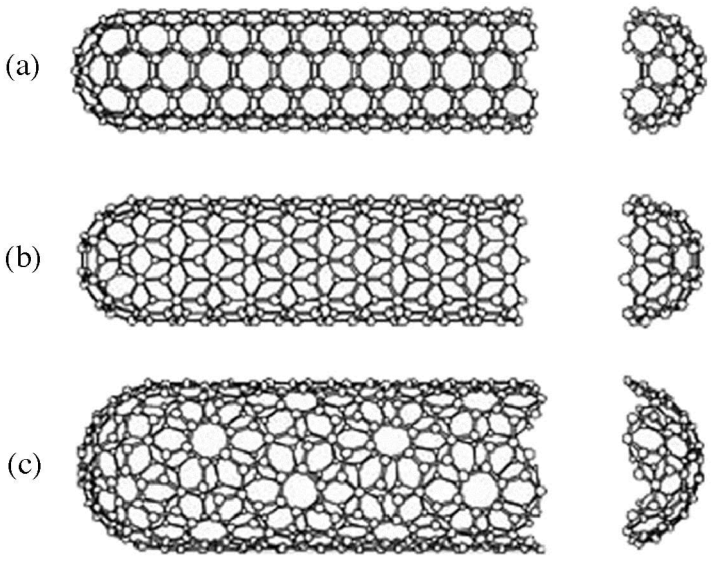


Figure 6.7.3.6: Structure of single walled carbon nanotubes (SWNTs) with (a) armchair, (b) zig-zag, and (c) chiral chirality.

The physical properties of SWNTs have made them an extremely attractive material for the manufacturing of nano devices. SWNTs have been shown to be stronger than steel as estimates for the Young's modulus approaches 1 Tpa. Their electrical conductance is comparable to copper with anticipate current densities of up to 10^{13} A/cm^2 and a resistivity as low as 0.34 x 10^{-4} Ω.cm at room temperatures. Finally, they have a high thermal conductivity (3000 - 6000 W.m/K).

The electronic properties of a particular SWNT structure are based on its chirality or twist in the structure of the tube which is defined by its *n,m* value. The values of *n* and *m* determine the chirality, or "twist" of the nanotube. The chirality in turn affects the conductance of the nanotube, its density, its lattice structure, and other properties. A SWNT is considered metallic if the value *n-m* is divisible by three. Otherwise, the nanotube is semi-conducting. The external environment also has an effect on the conductance of a tube, thus molecules such as O_2 and NH_3 can change the overall conductance of a tube, while the presence of metals have been shown to significantly effect the opto-electronic properties of SWNTs.

Multi walled carbon nanotubes (MWNTs) range from double walled NTs, through many-walled NTs (Figure 6.7.3.7) to carbon nanofibers. Carbon nanofibers are the extreme of multi walled tubes (Figure 6.7.3.8) and they are thicker and longer than either SWNTs or MWNTs, having a cross-sectional of ca. 500 Å^2 and are between 10 to 100 μm in length. They have been used extensively in the construction of high strength composites.

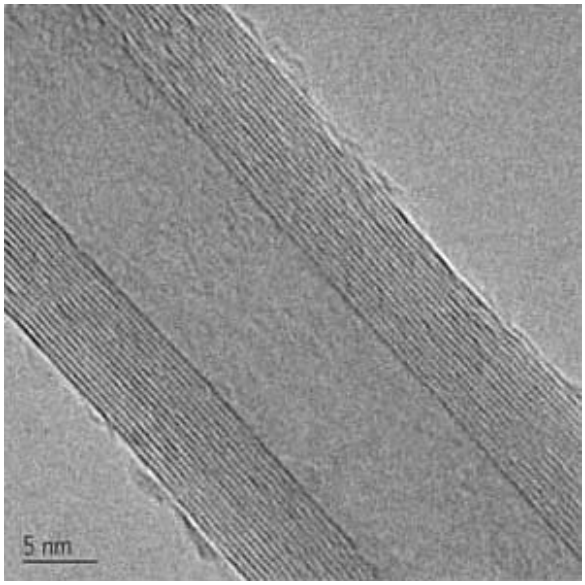


Figure 6.7.3.7: TEM image of an individual multi walled carbon nanotube (MWNTs). Copyright of Nanotech Innovations.

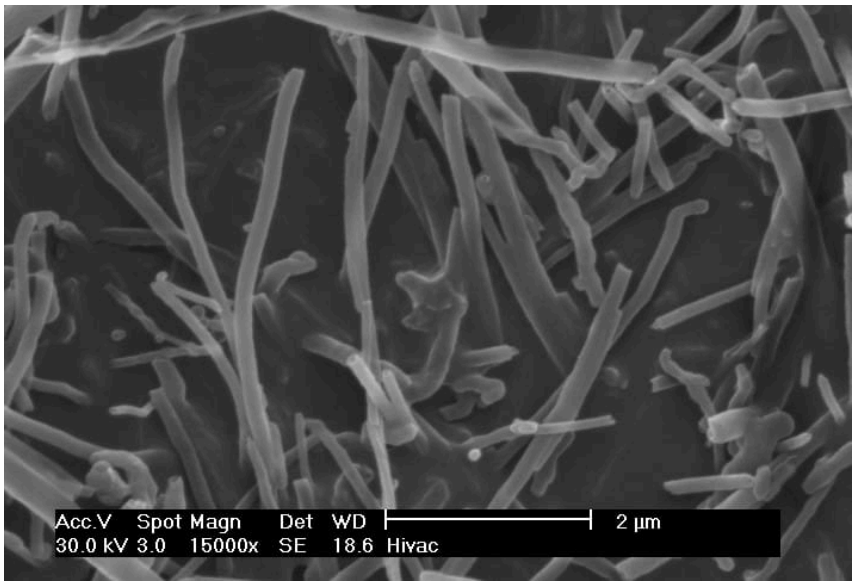


Figure 6.7.3.8: SEM image of vapor grown carbon nanofibers.

Synthesis of carbon nanotubes

A range of methodologies have been developed to produce nanotubes in sizeable quantities, including arc discharge, laser ablation, high pressure carbon monoxide (HiPco), and vapor liquid solid (VLS) growth. All these processes take place in vacuum or at low pressure with a process gases, although VLS growth can take place at atmospheric pressure. Large quantities of nanotubes can be synthesized by these methods; advances in catalysis and continuous growth processes are making SWNTs more commercially viable.

The first observation of nanotubes was in the carbon soot formed during the arc discharge production of fullerenes. The high temperatures caused by the discharge caused the carbon contained in the negative electrode to sublime and the CNTs are deposited on the opposing electrode. Tubes produced by this method were initially multi walled tubes (MWNTs). However, with the addition of cobalt to the vaporized carbon, it is possible to grow single walled nanotubes. This method it produces a mixture of components, and requires further purification to separate the CNTs from the soot and the residual catalytic metals. Producing CNTs in high yield depends on the uniformity of the plasma arc, and the temperature of the deposit forming on the carbon electrode.

Higher yield and purity of SWNTs may be prepared by the use of a dual-pulsed laser. SWNTs can be grown in a 50% yield through direct vaporization of a Co/Ni doped graphite rod with a high-powered laser in a tube furnace operating at 1200 °C. The material produced by this method appears as a mat of “ropes”, 10 - 20 nm in diameter and up to 100 µm or more in length. Each rope consists of a bundle of SWNTs, aligned along a common axis. By varying the process parameters such as catalyst composition and the growth temperature, the average nanotube diameter and size distribution can be varied. Although arc-discharge and laser vaporization are currently the principal methods for obtaining small quantities of high quality SWNTs, both methods suffer from drawbacks. The first is that they involve evaporating the carbon source, making scale-up on an industrial level difficult and energetically expensive. The second issue relates to the fact that vaporization methods grow SWNTs in highly tangled forms, mixed with unwanted forms of carbon and/or metal species. The SWNTs thus produced are difficult to purify, manipulate, and assemble for building nanotube-device architectures for practical applications.

In order to overcome some of the difficulties of these high-energy processes, the chemical catalysis method was developed in which a hydrocarbon feedstock is used in combination with a metal catalyst. The catalyst is typically, but not limited to iron, colbalt, or iron/molybdenum, it is heated under reducing conditions in the presence of a suitable carbon feedstock, e.g., ethylene. This method can be used for both SWNTs and MWNTs; the formation of each is controlled by the identity of the catalyst and the reaction conditions. A convenient laboratory scale apparatus is available from Nanotech Innovations, Inc., for the synthesis of highly uniform, consistent, research sample that uses pre-weighed catalyst/carbon source ampoules. This system, allows for 200 mg samples of MWNTs to be prepared for research and testing. The use of CO as a feedstock, in place of a hydrocarbon, led to the development of the high-pressure carbon monoxide (HiPco) procedure for SWNT synthesis. By this method, it is possible to produce gram quantities of SWNTs, unfortunately, efforts to scale beyond that have not met with complete success.

Initially developed for small-scale investigations of catalyst activity, vapor liquid solid (VLS) growth of nanotubes has been highly studied, and now shows promise for large-scale production of nanotubes. Recent approaches have involved the use of well-defined nanoparticle or molecular precursors and many different transition metals have been employed, but iron, nickel, and cobalt remain to be the focus of most research. The nanotubes grow at the sites of the metal catalyst; the carbon-containing gas is broken apart at the surface of the catalyst particle, and the carbon is transported to the edges of the particle, where it forms the nanotube. The length of the tube grown in surface supported catalyst VLS systems appears to be dependent on the orientation of the growing tube with the surface. By properly adjusting the surface concentration and aggregation of the catalyst particles it is possible to synthesize vertically aligned carbon nanotubes, i.e., as a carpet perpendicular to the substrate.

Of the various means for nanotube synthesis, the chemical processes show the greatest promise for industrial scale deposition in terms of its price/unit ratio. There are additional advantages to the VLS growth, which unlike the other methods is capable of growing nanotubes directly on a desired substrate. The growth sites are controllable by careful deposition of the catalyst. Additionally, no other growth methods have been developed to produce vertically aligned SWNTs.

Chemical functionalization of carbon nanotubes

The limitation of using carbon nanotubes in any practical applications has been its solubility; for example SWNTs have little to no solubility in most solvent due to the aggregation of the tubes. Aggregation/roping of nanotubes occurs as a result of the high van der Waals binding energy of *ca*. 500 eV per mm of tube contact. The van der Waals force between the tubes is so great, that it take tremendous energy to pry them apart, making it very to make combination of nanotubes with other materials such as in composite applications. The functionalization of nanotubes, i.e., the attachment of “chemical functional groups” provides the path to overcome these barriers. Functionalization can improve solubility as well as processibility, and has been used to align the properties of nanotubes to those of other materials. The clearest example of this is the ability to solubilize nanotubes in a variety of solvents, including water. It is important when discussing functionalization that a distinction is made between covalent and non-covalent functionalization.

Current methods for solubilizing nanotubes without covalent functionalization include highly aromatic solvents, super acids, polymers, or surfactants. Non-covalent “functionalization” is generally on the concept of supramolecular interactions between the SWNT and some macromolecule as a result of various adsorption forces, such as van der Waals’ and π-stacking interactions. The chemical speciation of the nanotube itself is not altered as a result of the interaction. In contrast, covalent functionalization relies on the chemical reaction at either the sidewall or end of the SWNT. As may be expected the high aspect ratio of nanotubes means that sidewall functionalization is much more important than the functionalization of the cap. Direct covalent sidewall functionalization is associated with a change of hybridization from sp^2 to sp^2 and a simultaneous loss of conjugation. An alternative approach to covalent functionalization involves the reaction of defects present (or generated) in the structure of the nanotube. Defect sites can be the open ends and holes in the sidewalls, and pentagon and heptagon irregularities in the hexagon graphene framework (often associated with bends in the tubes). All these functionalizations are exohedral derivatizations. Taking the hollow structure of nanotubes into consideration, endohedral functionalization of SWNTs is possible, i.e., the filling of the tubes with atoms or small molecules. It is important to note that covalent functionalization methods have one problem in common: extensive covalent functionalization modifies SWNT properties by disrupting the continuous π–system of SWNTs.

Various applications of nanotubes require different, specific modification to achieve desirable physical and chemical properties of nanotubes. In this regard, covalent functionalization provides a higher degree of fine-tuning the chemistry and physics of SWNTs than non-covalent functionalization. Until now, a variety of methods have been used to achieve the functionalization of nanotubes (Figure 6.7.3.9).

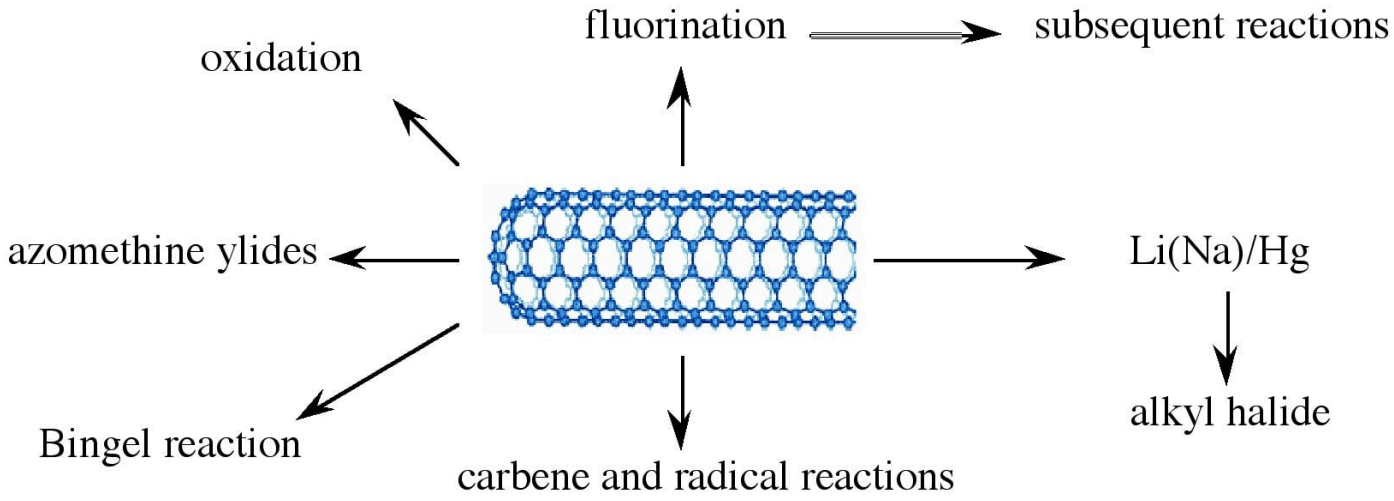


Figure 6.7.3.9: Schematic description of various covalent functionalization strategies for SWNTs.

Taking chemistry developed for C_{60}, SWNTs may be functionalized using 1,3 dipolar addition of azomethine ylides. The functionalized SWNTs are soluble in most common organic solvents. The azomethine ylide functionalization method was also used for the purification of SWNTs. Under electrochemical conditions, aryl diazonium salts react with SWNTs to achieve functionalized SWNTs, alternatively the diazonium ions may be generated *in-situ* from the corresponding aniline, while a solvent free reaction provides the best chance for large-scale functionalization this way. In each of these methods it is possible to control the amount of functionalization on the tube by varying reaction times and the reagents used; functionalization as high as 1 group per every 10 - 25 carbon atoms is possible.

Organic functionalization through the use of alkyl halides, a radical pathway, on tubes treated with lithium in liquid ammonia offers a simple and flexible route to a range of functional groups. In this reaction, functionalization occurs on every 17 carbons. Most success has been found when the tubes are dodecylated. These tubes are soluble in chloroform, DMF, and THF.

The addition of oxygen moieties to SWNT sidewalls can be achieved by treatment with acid or wet air oxidation, and ozonolysis. The direct epoxidation of SWNTs may be accomplished by the direct reaction with a peroxide reagent, or catalytically. Catalytic de-epoxidation (Figure 6.7.3.10) allows for the quantitative analysis of sidewall epoxide and led to the surprising result that previously assumed "pure" SWNTs actually contain *ca*. 1 oxygen per 250 carbon atoms.

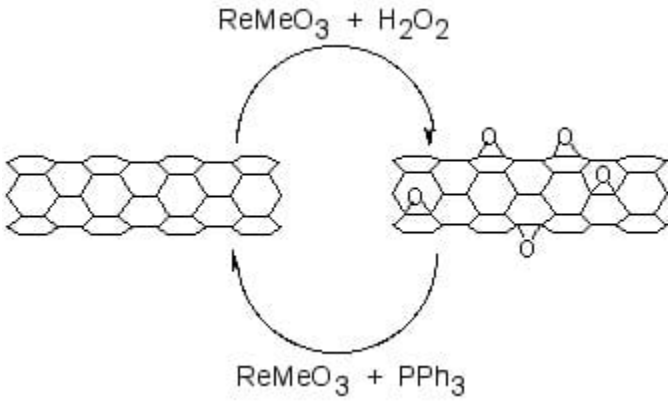


Figure 6.7.3.10: Catalytic oxidation and de-epoxidation of SWNTs.

One of the easiest functionalization routes, and a useful synthon for subsequent conversions, is the fluorination of SWNTs, using elemental fluorine. Importantly, a C:F ratios of up to 2:1 can be achieved without disruption of the tubular structure. The fluorinated SWNTs (F-SWNTs) proved to be much more soluble than pristine SWNTs in alcohols (1 mg/mL in *iso*-propanol), DMF and other selected organic solvents. Scanning tunneling microscopy (STM) revealed that the fluorine formed bands of approximately 20 nm, while calculations using DFT revealed 1,2 addition is more energetically preferable than 1,4 addition, which has been confirmed by solid state ^{13}C NMR. F-SWNTs make highly flexible synthons and subsequent elaboration has been performed with organo lithium, Grignard reagents, and amines.

Functionalized nanotubes can be characterized by a variety of techniques, such as atomic force microscopy (AFM), transmission electron microscopy (TEM), UV-vis spectroscopy, and Raman spectroscopy. Changes in the Raman spectrum of a nanotube sample can indicate if functionalization has occurred. Pristine tubes exhibit two distinct bands. They are the radial breathing mode (230 cm^{-1}) and the tangential mode (1590 cm^{-1}). When functionalized, a new band, called the disorder band, appears at *ca.*1350 cm^{-1}. This band is attributed to sp^3-hybridized carbons in the tube. Unfortunately, while the presence of a significant D mode is consistent with sidewall functionalization and the relative intensity of D (disorder) mode versus the tangential G mode (1550 – 1600 cm^{-1}) is often used as a measure of the level of substitution. However, it has been shown that Raman is an unreliable method for determination of the extent of functionalization since the relative intensity of the D band is also a function of the substituents distribution as well as concentration. Recent studies suggest that solid state ^{13}C NMR are possibly the only definitive method of demonstrating covalent attachment of particular functional groups.

Coating carbon nanotubes: creating inorganic nanostructures

Fullerenes, nanotubes and nanofibers represent suitable substrates for the seeding other materials such as oxides and other minerals, as well as semiconductors. In this regard, the carbon nanomaterial acts as a seed point for the growth as well as a method of defining unusual aspect ratios. For example, silica fibers can be prepared by a number of methods, but it is only through coating SWNTs that silica nano-fibers with of micron lengths with tens of nanometers in diameter may be prepared.

While C_{60} itself does not readily seed the growth of inorganic materials, liquid phase deposition of oxides, such as silica, in the presence of fullerenol, $C_{60}(OH)_n$, results in the formation of uniform oxide spheres. It appears the fullerenol acts as both a reagent and a physical point for subsequent oxide growth, and it is C_{60}, or an aggregate of C_{60}, that is present within the spherical particle. The addition of fullerenol alters the morphology and crystal phase of $CaCO_3$ precipitates from aqueous solution, resulting in the formation of spherical features, 5-pointed flower shaped clusters, and triangular crystals as opposed to the usual rhombic crystals. In addition, the meta-stable vaterite phase is observed with the addition of $C_{60}(OH)_n$.

As noted above individual SWNTs may be obtained in solution when encased in a cylindrical micelle of a suitable surfactant. These individualized nanotubes can be coated with a range of inorganic materials. Liquid phase deposition (LPD) appears to have significant advantages over other methods such as incorporating surfacted SWNTs into a preceramic matrix, *in situ* growth of the SWNT in an oxide matrix, and sol-gel methods. The primary advantage of LPD growth is that individual SWNTs may be coated rather than bundles or ropes. For example, SWNTs have been coated with silica by liquid phase deposition (LPD) using a silica/H_2SiF_6 solution and a surfactant-stabilized solution of SWNTs. The thickness of the coating is dependent on the reaction mixture concentration and the reaction time. The SWNT core can be removed by thermolysis under oxidizing conditions to leave a silica nano fiber. It is interesting to note that the use of a surfactant is counter productive when using MWNTs and VGFs, in this case surface activation of the nanotube offers the suitable growth initiation. Pre-oxidation of the MWNT or VGF allows for uniform coatings to be deposited. The coated SWNTs, MWNTs, and VGFs can be subsequently reacted with suitable surface reagents to impart miscibility in aqueous solutions, guar gels, and organic matrixes. In addition to simple oxides, coated nanotubes have been prepared with minerals such as carbonates and semiconductors.

Bibliography

- S. M. Bachilo, M. S. Strano, C. Kittrell, R. H. Hauge, R. E. Smalley, and R. B. Weisman, *Science*, 2002, **298**, 2361.
- D. S. Bethune, C. H. Klang, M. S. deVries, G. Gorman, R. Savoy, J. Vazquez, and R. Beyers, *Nature*, 1993, **363**, 605.
- J, J. Brege, C. Gallaway, and A. R. Barron, *J. Phys. Chem., C*, 2007, **111**, 17812.
- C. A. Dyke and J. M. Tour, *J. Am. Chem. Soc.*, 2003, **125**, 1156.
- Z. Ge, J. C. Duchamp, T. Cai, H. W. Gibson, and H. C. Dorn, *J. Am. Chem. Soc.*, 2005, **127**, 16292.
- L. A. Girifalco, M. Hodak, and R. S. Lee, *Phys. Rev. B*, 2000, **62**, 13104.
- T. Guo, P. Nikolaev, A. G. Rinzler, D. Tománek, D. T. Colbert, and R. E. Smalley, *J. Phys. Chem.*, 1995, **99**, 10694.
- J. H. Hafner, M. J. Bronikowski, B. R. Azamian, P. Nikolaev, A. G. Rinzler, D. T. Colbert, K. A. Smith, and R. E. Smalley, *Chem. Phys. Lett.*, 1998, **296**, 195.
- A. Hirsch, *Angew. Chem. Int. Ed.*, 2002, **40**, 4002.
- S. Iijima and T. Ichihashi, *Nature*, 1993, **363**, 603.
- H. R. Jafry, E. A. Whitsitt, and A. R. Barron, *J. Mater. Sci.*, 2007, **42**, 7381.
- H. W. Kroto, J. R. Heath, S. C. O'Brien, R. F. Curl, and R. E. Smalley, *Nature*, 1985, **318**, 162.
- F. Liang, A. K. Sadana, A. Peera, J. Chattopadhyay, Z. Gu, R. H. Hauge, and W. E. Billups, *Nano Lett.*, 2004, **4**, 1257.
- D. Ogrin and A. R. Barron, *J. Mol. Cat. A: Chem.*, 2006, **244**, 267.
- D. Ogrin, J. Chattopadhyay, A. K. Sadana, E. Billups, and A. R. Barron, *J. Am. Chem. Soc.*, 2006, **128**, 11322.

- R. E. Smalley, *Acc. Chem. Res.*, 1992, **25**, 98.
- M. M. J. Treacy, T. W. Ebbesen, and J. M. Gibson, *Nature*, 1996, **381**, 678.
- E. A. Whitsitt and A. R. Barron, *Nano Lett.*, 2003, **3**, 775.
- J. Yang and A. R. Barron, *Chem. Commun.*, 2004, 2884.
- L. Zeng, L. B. Alemany, C. L. Edwards, and A. R. Barron, *Nano Res.*, 2008, **1**, 72.

Graphene

Introduction

Graphene is a one-atom-thick planar sheet of sp^2-bonded carbon atoms that are densely packed in a honeycomb crystal lattice (Figure 6.7.3.11). The name comes from “graphite” and “alkene”; graphite itself consists of many graphene sheets stacked together.

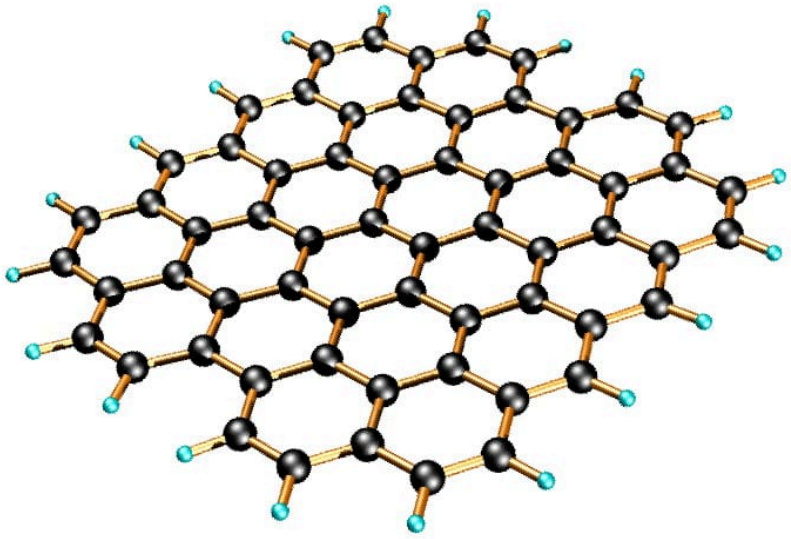


Figure 6.7.3.11: Idealized structure of a single graphene sheet.

Single-layer graphene nanosheets were first characterized in 2004, prepared by mechanical exfoliation (the “scotch-tape” method) of bulk graphite. Later graphene was produced by epitaxial chemical vapor deposition on silicon carbide and nickel substrates. Most recently, graphene nanoribbons (GNRs) have been prepared by the oxidative treatment of carbon nanotubes and by plasma etching of nanotubes embedded in polymer films.

Physical properties of graphene

Graphene has been reported to have a Young’s modulus of 1 TPa and intrinsic strength of 130 GP; similar to single walled carbon nanotubes (SWNTs). The electronic properties of graphene also have some similarity with carbon nanotubes. Graphene is a zero-bandgap semiconductor. Electron mobility in graphene is extraordinarily high (15,000 cm^2/V.s at room temperature) and ballistic electron transport is reported to be on length scales comparable to that of SWNTs. One of the most promising aspects of graphene involves the use of GNRs. Cutting an individual graphene layer into a long strip can yield semiconducting materials where the bandgap is tuned by the width of the ribbon.

While graphene’s novel electronic and physical properties guarantee this material will be studied for years to come, there are some fundamental obstacles yet to overcome before graphene based materials can be fully utilized. The aforementioned methods of graphene preparation are effective; however, they are impractical for large-scale manufacturing. The most plentiful and inexpensive source of graphene is bulk graphite. Chemical methods for exfoliation of graphene from graphite provide the most realistic and scalable approach to graphene materials.

Graphene layers are held together in graphite by enormous van der Waals forces. Overcoming these forces is the major obstacle

to graphite exfoliation. To date, chemical efforts at graphite exfoliation have been focused primarily on intercalation, chemical derivatization, thermal expansion, oxidation-reduction, the use of surfactants, or some combination of these.

Graphite oxide

Probably the most common route to graphene involves the production of graphite oxide (GO) by extremely harsh oxidation chemistry. The methods of Staudenmeier or Hummers are most commonly used to produce GO, a highly exfoliated material that is dispersible in water. The structure of GO has been the subject of numerous studies; it is known to contain epoxide functional groups along the basal plane of sheets as well as hydroxyl and carboxyl moieties along the edges (Figure 6.7.3.12). In contrast to other methods for the synthesis of GO, the the *m*-peroxybenzoic acid (*m*-CPBA) oxidation of microcrystalline synthetic graphite at room temperature yields graphite epoxide in high yield, without significant additional defects.

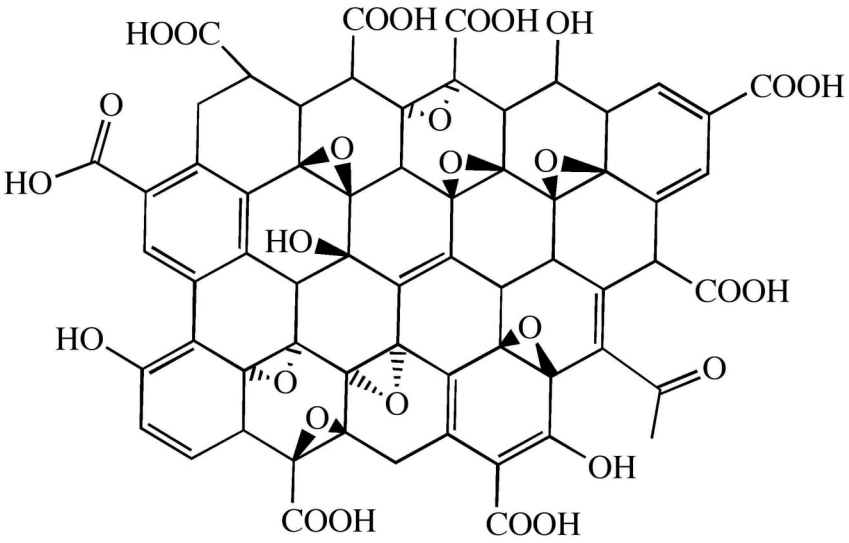


Figure 6.7.3.12: Idealized structure proposed for graphene oxide (GO). Adapted from C. E. Hamilton, PhD Thesis, Rice University (2009).

As graphite oxide is electrically insulating, it must be converted by chemical reduction to restore the electronic properties of graphene. Chemically converted graphene (CCG) is typically reduced by hydrazine or borohydride. The properties of CCG can never fully match those of graphene for two reasons:

1. Oxidation to GO introduces defects.
2. Chemical reduction does not fully restore the graphitic structure.

As would be expected, CCG is prone to aggregation unless stabilized. Graphene materials produced from pristine graphite avoid harsh oxidation to GO and subsequent (incomplete) reduction; thus, materials produced are potentially much better suited to electronics applications.

A catalytic approach to the removal of epoxides from fullerenes and SWNTs has been applied to graphene epoxide and GO. Treatment of oxidized graphenes with methyltrioxorhenium ($MeReO_3$, MTO) in the presence of PPh_3 results in the oxygen transfer, to form $O{=}PPh_3$ and allow for quantification of the C:O ratio.

Homogeneous graphene dispersions

An alternate approach to producing graphene materials involves the use of pristine graphite as starting material. The fundamental value of such an approach lies in its avoidance of oxidation to GO and subsequent (incomplete) reduction, thereby preserving the desirable electronic properties of graphene. There is precedent for exfoliation of pristine graphite in neat organic solvents without oxidation or surfactants. It has been reported that *N*,*N*-dimethylformamide (DMF) dispersions of graphene are possible, but no detailed characterization of the dispersions were reported. In contrast, Coleman and coworkers reported similar dispersions using *N*-methylpyrrolidone (NMP), resulting in individual sheets of graphene at a concentration of ≤0.01 mg/mL. NMP and DMF are highly polar solvents, and not ideal in cases where reaction chemistry requires a nonpolar medium. Further, they are hygroscopic,

making their use problematic when water must be excluded from reaction mixtures. Finally, DMF is prone to thermal and chemical decomposition.

Recently, dispersions of graphene has been reported in *ortho*-dichlorobenzene (ODCB) using a wide range of graphite sources. The choice of ODCB for graphite exfoliation was based on several criteria:

1. ODCB is a common reaction solvent for fullerenes and is known to form stable SWNT dispersions.
2. ODCB is a convenient high-boiling aromatic, and is compatible with a variety of reaction chemistries.
3. ODCB, being aromatic, is able to interact with graphene *via* π-π stacking.
4. It has been suggested that good solvents for graphite exfoliation should have surface tension values of 40 – 50 mJ/m^2. ODCB has a surface tension of 36.6 mJ/m^2, close to the proposed range.

Graphite is readily exfoliated in ODCB with homogenization and sonication. Three starting materials were successfully dispersed: microcrystalline synthetic, thermally expanded, and highly ordered pyrolytic graphite (HOPG). Dispersions of microcrystalline synthetic graphite have a concentration of 0.03 mg/mL, determined gravimetrically. Dispersions from expanded graphite and HOPG are less concentrated (0.02 mg/mL).

High resolution transmission electron microscopy (HRTEM) shows mostly few-layer graphene (n < 5) with single layers and small flakes stacked on top (Figure 6.7.3.13). Large graphitic domains are visible; this is further supported by selected area electron diffraction (SAED) and fast Fourier transform (FFT) in selected areas. Atomic force microscope (AFM) images of dispersions sprayed onto silicon substrates shows extremely thin flakes with nearly all below 10 nm. Average height is 7 - 10 nm. The thinnest are less than 1 nm, graphene monolayers. Lateral dimensions of nanosheets range from 100 – 500 nm.

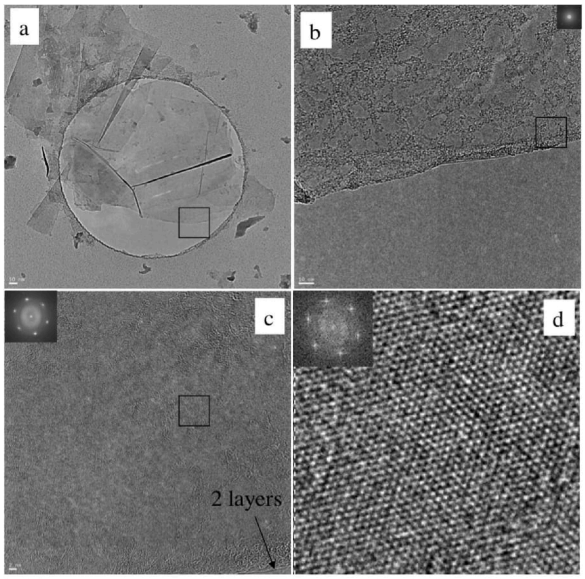


Figure 6.7.3.13: TEM images of single layer graphene from HOPG dispersion. (a) monolayer and few layer of graphene stacked with smaller flakes; (b) selected edge region from (a), (c) selected area from (b) with FFT inset, (d) HRTEM of boxed region in (c) showing lattice fringes with FFT inset. Adapted from C. E. Hamilton, PhD Thesis, Rice University (2009).

As-deposited films cast from ODCB graphene show poor electrical conductivity, however, after vacuum annealing at 400 °C for 12 hours the films improve vastly, having sheet resistances on the order of 60 Ω/sq. By comparison, graphene epitaxially grown on Ni has a reported sheet resistance of 280 Ω/sq.

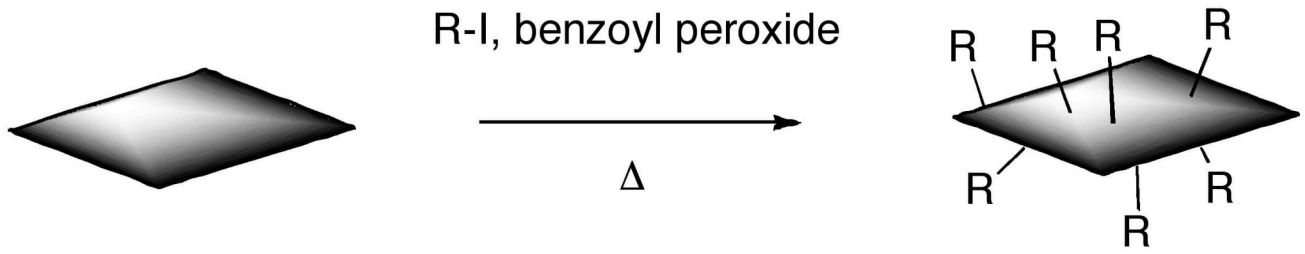
Covalent functionalization of graphene and graphite oxide

The covalent functionalization of SWNTs is well established. Some routes to covalently functionalized SWNTs include esterification/ amidation, reductive alkylation (Billups reaction), and treatment with azomethine ylides (Prato reaction), diazonium salts, or nitrenes. Conversely, the chemical derivatization of graphene and GO is still relatively unexplored.

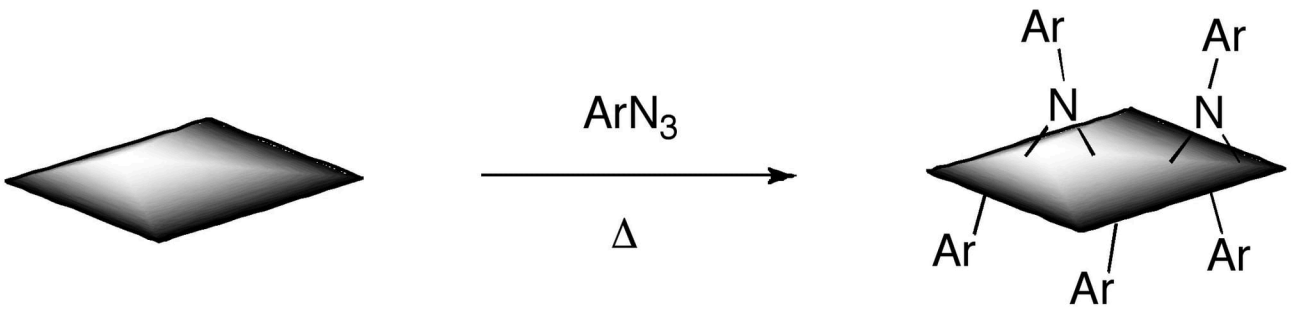
Some methods previously demonstrated for SWNTs have been adapted to GO or graphene. GO carboxylic acid groups have been converted into acyl chlorides followed by amidation with long-chain amines. Additionally, the coupling of primary amines and

amino acids via nucleophilic attack of GO epoxide groups has been reported. Yet another route coupled isocyanates to carboxylic acid groups of GO. Functionalization of partially reduced GO by aryldiazonium salts has also been demonstrated. The Billups reaction has been performed on the intercalation compound potassium graphite (C_8K), as well as graphite fluoride, and most recently GO. Graphene alkylation has been accomplished by treating graphite fluoride with alkyllithium reagents.

ODCB dispersions of graphene may be readily converted to covalently functionalize graphene. Thermal decomposition of benzoyl peroxide is used to initiate radical addition of alkyl iodides to graphene in ODCB dispersions.



Additionally, functionalized graphene with nitrenes generated by thermal decomposition of aryl azides



Bibliography

- P. Blake, P. D. Brimicombe, R. R. Nair, T. J. Booth, D. Jiang, F. Schedin, L. A. Ponomarenko, S. V. Morozov, H. F. Gleeson, E. W. Hill, A. K. Geim, and K. S. Novoselov, *Nano Lett.*, 2008, **8**, 1704.
- J. Chattopadhyay, A. Mukherjee, C. E. Hamilton, J.-H. Kang, S. Chakraborty, W. Guo, K. F. Kelly, A. R. Barron, and W. E. Billups, *J. Am. Chem. Soc.*, 2008, **130**, 5414.
- G. Eda, G. Fanchini, and M. Chhowalla, *Nat. Nanotechnol.*, 2008, **3**, 270.
- M. Y. Han, B. Ozyilmaz, Y. Zhang, and P. Kim, *Phys. Rev. Lett.*, 2008, **98**, 206805.
- Y. Hernandez, V. Nicolosi, M. Lotya, F. M. Blighe, Z. Sun, S. De, I. T. McGovern, B. Holland, M. Byrne, Y. K. Gun'Ko, J. J. Boland, P. Niraj, G. Duesberg, S. Krishnamurthy, R. Goodhue, J. Hutchinson, V. Scardaci, A. C. Ferrari, and J. N. Coleman, *Nat. Nanotechnol.*, 2008, **3**, 563.
- W. S. Hummers and R. E. Offeman, *J. Am. Chem. Soc.*, 1958, **80**, 1339.
- L. Jiao, L. Zhang, X. Wang, G. Diankov, and H. Dai, *Nature*, 2009, **458**, 877.
- D. V. Kosynkin, A. L. Higginbotham, A. Sinitskii, J. R. Lomeda, A. Dimiev, B. K. Price, and J. M. Tour, *Nature*, 2009, **458**, 872.
- D. Li, M. B. Mueller, S. Gilje, R. B. Kaner, and G. G. Wallace, *Nat. Nanotechnol.*, 2008, **3**, 101.
- S. Niyogi, E. Bekyarova, M. E. Itkis, J. L. McWilliams, M. A. Hamon, and R. C. Haddon, *J. Am. Chem. Soc.*, 2006, **128**, 7720.
- Y. Si and E. T. Samulski, *Nano Lett.*, 2008, **8**, 1679.
- L. Staudenmaier, *Ber. Dtsch. Chem. Ges.*, 1898, **31**, 1481.

This page titled 6.7.3: Carbon Nanomaterials is shared under a CC BY 3.0 license and was authored, remixed, and/or curated by Andrew R. Barron (CNX) via source content that was edited to the style and standards of the LibreTexts platform.

6.7.4: Nitrogen Compounds of Carbon

There are a myriad of organic compounds containing carbon-nitrogen bonds, including: amines, imines, and nitriles. However, here we are concerned with the simplest carbon-nitrogen compounds.

Cyanogen

Cyanogen, $(CN)_2$, may be considered the smallest molecular fragment containing carbon and nitrogen (Figure 6.7.4.1a). The reaction chemistry of cyanogen is related to that of the halogens, i.e., F_2, Cl_2, etc. Consequently, cyanogen is called a *pseudo halogen*.

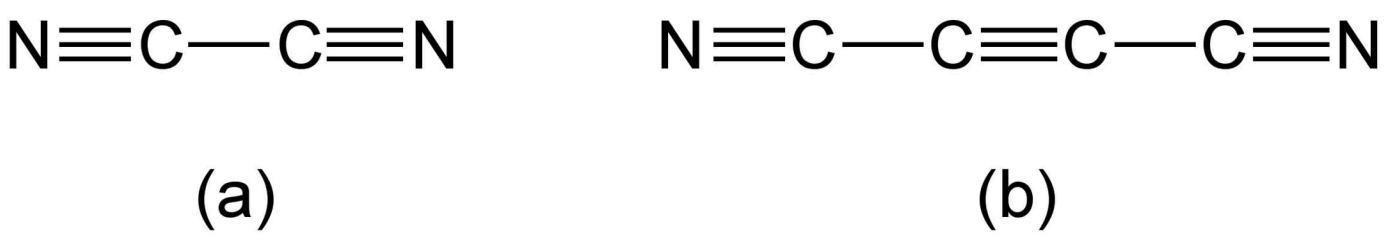


Figure 6.7.4.1: The structures of (a) cyanogen, $(CN)_2$ and (b) dicyanoacetylene (carbon subnitride, C_4N_2).

As shown in Table 6.7.4.1 the bonding in cyanogen is consistent with localization of the π-bonding between carbon and nitrogen given the similarity of the C-N bond distance in cyanogens and acetonitrile. However, there is clearly some π-delocalization associated with the C-C distance given its shortening as compared to ethane.

Table 6.7.4.1: A comparison of the bond distances in selected carbon nitrogen compounds.

Compound	Formula	C-C bond distance (Å)	C-N bond distance (Å)
Cyanogen	$(CN)_2$	1.393	1.163
Hydrogen cyanide	HCN	-	1.154
Acetonitrile	CH_3CN	1.46	1.16
Ethane	C_2H_6	1.535	-
Ethylene	C_2H_4	1.339	-

Cyanogen is produced by the reaction of a mixture of the cyanide and chloride of mercury, (7.4.1).

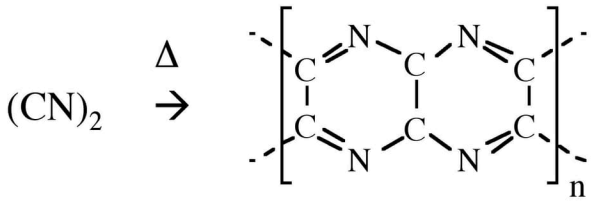
$$\mathrm{Hg(CN)_2 + HgCl_2 \rightarrow (CN)_2 + 2\ Hg + Cl_2} \tag{6.7.4.1}$$

Alternatively, the decomposition of unstable copper(II) cyanide, formed from a copper(II) salts with a Group 1 cyanide, (7.4.2), yields cyanogens, (7.4.3).

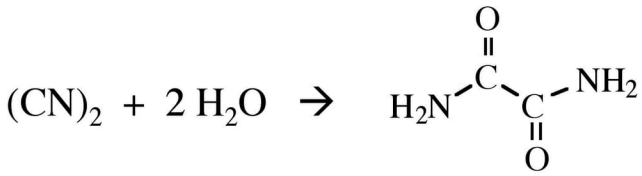
$$\mathrm{CuSO_4 + 2\ KCN \rightarrow Cu(CN)_2 + K_2SO_4} \tag{6.7.4.2}$$

$$\mathrm{2\ Cu(CN)_2 \rightarrow (CN)_2 + 2\ CuCN} \tag{6.7.4.3}$$

Cyanogen is a flammable gas (Mp = -28 °C and Bp = -21 °C) that produces the second hottest flame natural flame (after carbon subnitride, C_4N_2) with a temperature of over 4525 °C when burnt in oxygen. Heating cyanogen in the absence of oxygen results self polymerizes.



Hydrolysis of cyanogen results in addition across the carbon-nitrogen triple bonds and the formation of oxamide. Cleavage of the C-C bond does occur in the presence of base (e.g., KOH), with the formation of cyanide (CN^-) and cyanate (CNO^-) salts, (7.4.4).



$$(CN)_2 + 2\ OH^- \rightarrow CN^- + CNO^- + H_2O \tag{6.7.4.4}$$

Dicyanoacetylene

Dicyanoacetylene (also known as carbon subnitride or by its IUPAC name but-2-ynedinitrile) has the structure shown in Figure 6.7.4.1b, and may be thought of as a dicyanaide substituted acetylene.

At room temperature, dicyanoacetylene is a clear liquid, however, solid dicyanoacetylene has been detected in the atmosphere of Titan (the largest moon of the planet Saturn) by infrared spectroscopy. Dicyanoacetylene is an entropic explosive giving carbon powder and nitrogen gas. In the presence of oxgyen it burns with a bright blue-white flame at a temperature of 4990 °C.

Hydrogen cyanide

Hydrogen cyanide (HCN) is a colorless, highly poisonous, gas (Mp = -13.5 °C and Bp = 25.6 °C). Due to its original isolation from Prussian blue (hydrated ferric ferrocyanide), hydrogen cyanaide is also known by the name of *prussic acid*.

The synthesis of hydrogen cyanide is accomplished commercially by the partial oxidation of methane in the presence of ammonia, (7.4.5), using a platinum catalyst. The heat to activate the reaction is derived from the partial combustion of the methane and ammonia. The resulting aqueous solution is dried by distilled from phosphorus pentoxide (P_2O_5) to yield anhydrous hydrogen cyanide.

$$2\ CH_4 + 3\ O_2 + 2\ NH_3 \rightarrow\ 2\ HCN + 6\ H_2O \tag{6.7.4.5}$$

Hydrogen cyanide may also be formed in the absence of oxygen, (7.4.6); however, in this case the reaction must be heated externally.

$$CH_4 + NH_3 \rightarrow\ HCN + 3\ H_2 \tag{6.7.4.6}$$

Small quantities of hydrogen cyanide for laboratory use may be prepared by the reaction of an acid with a cyanide salt (either potassium or sodium), (7.4.7).

$$KCN + H^+ \rightarrow HCN + K^+ \tag{6.7.4.7}$$

The structure of hydrogen cyanide is shown in Figure 6.7.4.2 along with its isomeric form, hydrogen isocyanide (HNC). While hydrogen cyanide is present in the pits of many fruits, and is generated by burnet moths and some millipedes, hydrogen isocyanide is only found in interstellar space. It is postulated, however, that along with HCN, HNC is an important building block for amino acids and hence life.



Figure 6.7.4.2: The structures of (a) hydrogen cyanaide (HCN) and (b) its isomer hydrogen isocyanide (HNC).

In the liquid state hydrogen cyanide forms strong hydrogen bonds (Figure 6.7.4.3). Hydrogen cyanide is a good solvent for polar compounds due to its high permittivity ($\in_r$) and high dipole moment (2.98 D).

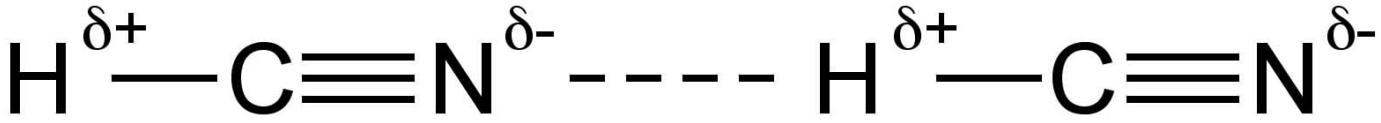


Figure 6.7.4.3: The hydrogen bonding in liquid hydrogen cyanide.

In aqueous solution hydrogen cyanide is a weak acid, (7.4.7), and several salts are known. However, HCN also reacts with water to give ammonium formate via formamide, (7.4.8).

$$\mathrm{HCN + H_2O \rightleftharpoons H_3O^+ + CN^-} \tag{6.7.4.8}$$

$$\mathrm{HCN + H_2O \rightarrow HC(O)NH_2 \xrightarrow{H_2O} HCO_2^- + NH_4^+} \tag{6.7.4.9}$$

In a similar manner to cyanogen's relationship to the halogens, the cyanide anion (CN^-) is considered a *pseudo halide* (i.e., F^-, Cl^-, etc), and as such forms many coordination compounds, e.g., $[Fe(CN)_6]^{3-}$ and $[Ag(CN)_2]^-$.

Assassination, execution, and the Holocaust

Hydrogen cyanide is fatal to humans due to its inhibition of the enzyme cytochrome c oxidase by the cyanide ion (CN^-), which results in the halting of cellular respiration. A concentration of 300 mg/m^3 will kill within 10 minutes, while 3200 mg/m^3 (*ca.* 3500 ppm) will be fatal in about 1 minute.

The symptoms of cyanide poisoning appear similar to a heart attack and this has led to it being the poison of choice for both fictional murder mystery writers as well as the former KGB (*Konitet gosudarstvennoy bezopasnosti* or Committee for State Security) and its predecessor SMERSH (from the contraction *smert shpionam* meaning *death to spies*) in real life. Possibly the most famous use of hydrogen cyanide for assassination was the use of an atomizer mist gun by KGB agent Bohdan Stashynsky for the killing of the Ukranian political writer and anti-communist Lev Rebet in 1957, and later in 1959 that of fellow Ukranian, Stepan Bandera. In both cases the intention was to induce cardiac arrest and make it look like the victim had died of a heart attack.

Without doubt the most notorious use of hydrogen cyanide is in the form of the product Zyklon B, which was originally developed as an insecticide. Dr. Walter Heerdt found that hydrogen cyanide could be absorbed onto substrates such as absorbent pellets (e.g., silica), fibers, or diatomaceous earth (Figure 6.7.4.4). While stable in an airtight container, once opened the hydrogen cyanide is released. The "B" in the trade name comes from the German name for prussic acid (the common name for hydrogen cyanide), i.e., *Blausäure* meaning *blue acid*.

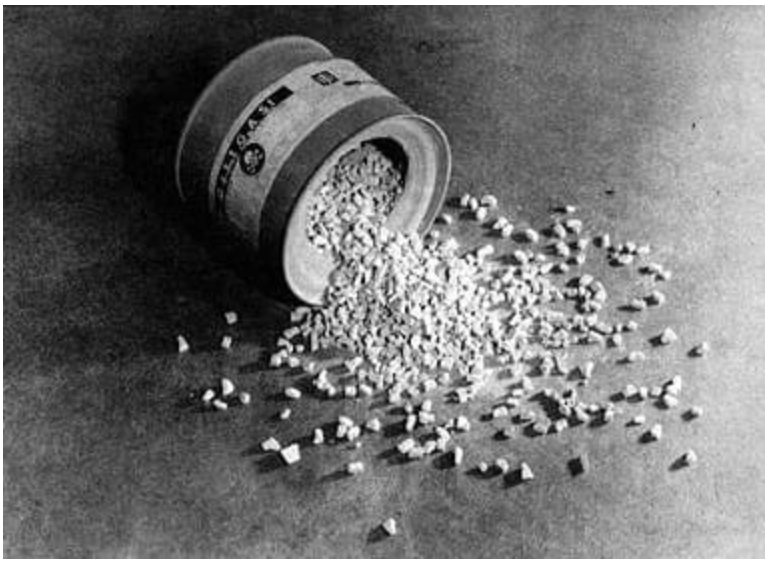


Figure 6.7.4.4: A can of Zyklon B granules.

The first wholesale use of Zyklon B was actually in the US where it was used as early as 1929 to disinfect the freight trains and cloths of Mexican immigrants entering the US. The first use of Zyklon B in the concentration camps during World War II was for a similar purpose (in particular for delousing to control typhus); however, for its use as an insecticide, Zyklon B contained a warning odorant. The deliberate manufacture of Zyklon B without the odorant resulted in the material that was used on a group of 250 gypsy children at the Buchenwald concentration camp in early 1940. Subsequently in September 1940, a similar number of sick Polish prisoners of war and 600 Soviet prisoners of war were killed at Auschwitz (Figure 6.7.4.5). Once these horrific tests were performed, the systematic murder of millions of people, including Jews, gypsies, and homosexuals, was accomplished using Zyklon B at Auschwitz, Majdanek, Sachsenhausen, and one of the Operation Reinhard camps. It is only fitting that many of the architects of the Holocaust themselves died from cyanide, including: Adolf Hitler (in addition to a bullet), Joseph Goebbles, Hermann Göring, and Heinrich Himmler.



Figure 6.7.4.5: The main gate at Auschwitz, through which an estimated two million victims of Nazi genocide passed.

Despite the horror associated with the use of hydrogen cyanide for the Holocaust, it was used by 11 US states for the death penalty (Figure 6.7.4.6). Arizona, Maryland, and Missouri retain the gas chamber as a secondary method of execution though they have lethal injection as the primary method. Potassium cyanide (KCN) pellets are placed into a compartment directly below the chair in the gas chamber . The condemned person is then strapped into the chair, and the airtight chamber sealed. Concentrated sulfuric acid (H_2SO_4) is then poured down a tube onto the cyanide pellets to generate hydrogen cyanide, (7.4.7). Execution by gas chamber is especially unpleasant for the witnesses to the execution due to the physical responses exhibited during the process

of dying, including: convulsions and excessive drooling.



Figure 6.7.4.6: The former gas chamber in San Quentin State Prison, now an execution chamber for lethal injection, in which the State of California executed 192 men and 4 women.

Bibliography

- J. Wu and N. J. Evans, *Astrophys. J.*, 2003, **592**, L79.

This page titled 6.7.4: Nitrogen Compounds of Carbon is shared under a CC BY 3.0 license and was authored, remixed, and/or curated by Andrew R. Barron (CNX) via source content that was edited to the style and standards of the LibreTexts platform.

6.7.5: Carbon Monoxide

Carbon monoxide (CO) is iso-electronic with nitrogen (N_2) and formed through the incomplete combustion of carbon, (7.5.1), or hydrocarbon compounds.

$$2\ C + O_2 \rightarrow\ 2\ CO \tag{6.7.5.1}$$

Carbon monoxide may also be made from steam and coal as part of synthesis gas, (7.4.2). A convenient laboratory preparation of CO is the dehydration of formic acid by sulfuric acid, (7.4.3).

$$C + H_2O \rightarrow CO + H_2 \tag{6.7.5.2}$$

$$HCO_2H \rightarrow CO + H_2O \tag{6.7.5.3}$$

Hazards and toxicity

Carbon monoxide is flammable, (7.4.4), and has an explosive limit of 12.5 – 74% with an auto ignition temperature of 609 °C.

$$2\ CO + O_2 \rightarrow 2\ CO_2 \tag{6.7.5.4}$$

Carbon monoxide is also very toxic; however, it is colorless, odorless, tasteless and non-irritating all of which increase its danger. The incomplete combustion of hydrocarbon (natural gas or heating oil) or carbon sources (coal or charcoal) is a common hazard in the home. In a closed environment (e.g., charcoal grill in room with no, or poor, ventilation) as carbon uses up oxygen in room the formation of toxic carbon monoxide results instead of carbon dioxide (CO_2).Typical sources of CO in the home are shown in Figure 6.7.5.1.

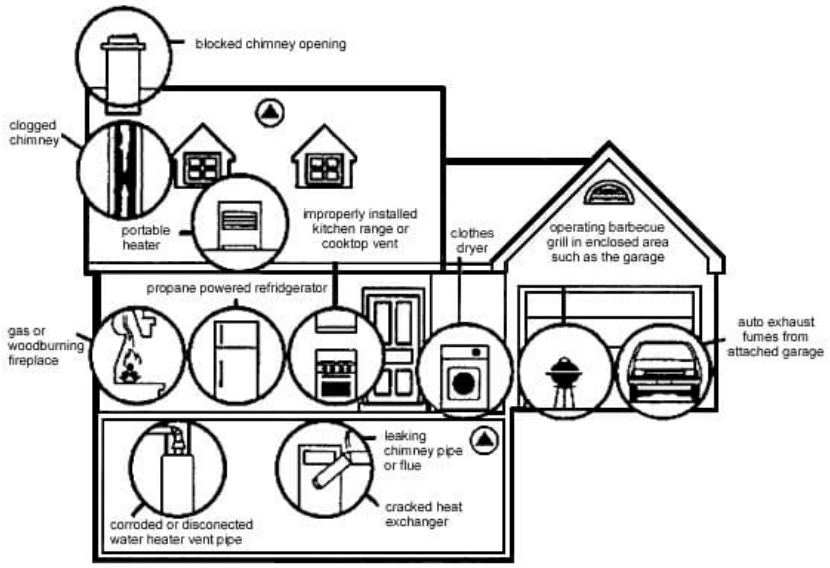


Figure 6.7.5.1: Potential sources of carbon in the home. Copyright: Fire Safety Council.

The toxicity of CO is due to its competition with oxygen at the heme binding site in hemoglobin. The binding affinity for CO is 200 times greater than that for oxygen, meaning that just small amounts of CO dramatically reduces hemoglobin's ability to transport oxygen around the body. The bright red color of the CO-heme complex is the reason that chronic exposure results in the skin adopting a bright red color. The symptoms of CO poisoning include headache, nausea, weakness, and eventually death. When air contains CO levels as low as 0.02%, headache and nausea occur; if the CO concentration is increased to 0.1%, unconsciousness will follow.

Note

Cigarette smoke containing large amounts of carbon monoxide and as a result heavy smokers can have up to 20% of the oxygen-active sites in their blood blocked by CO. However, despite this hazard, cigarettes would be even more deadly if they were not burnt. A key (and often engineered) ingredient in cigarettes is the addictive drug nicotine. Nicotine is an alkaloid (Figure 6.7.5.2a) as is caffeine (Figure 6.7.5.2b) that is in coffee and tea. The lethal dose of caffeine is approximately 10 g, which relates to approximately 70 – 100 cups of coffee (assuming a concentration of 100- 150 mg per cup). Alternatively, a lethal dose of caffeine from cola would require approximately 180 – 280 12 oz bottles, each containing 35 – 44 mg. In comparison nicotine has a lethal dose of 50 mg. This means that 12 cigarettes can provide a lethal does if consumed. The only reason smoking 12 cigarettes do not kill immediately is that the majority of the nicotine is burnt in the smoking of the cigarette. If this were not true smokers would be killed before they could develop a habit!

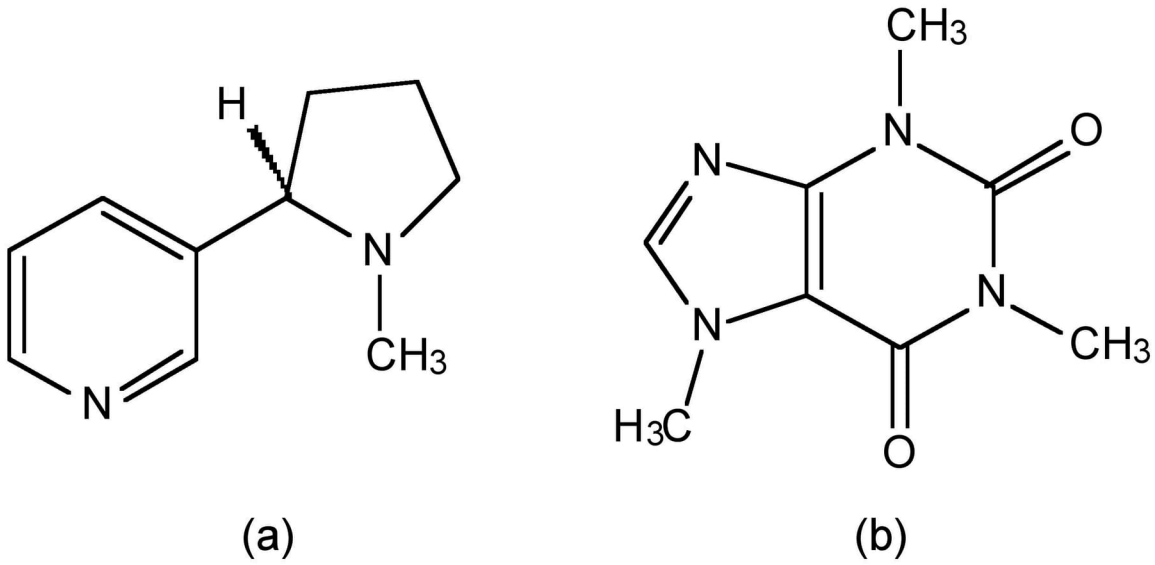


Figure 6.7.5.2: The molecular structures of (a) nicotine and (b) caffeine.

Structure and bonding

The bonding in CO involves 1 σ-bond and 2 sets of π-bonds (Figure 6.7.5.3). The C-O bond distance in carbon monoxide is 1.1 Å and therefore consistent with a triple bond. In comparison a typical C-O single bond is *ca*. 1.43 Å, and an average C-O double bond is *ca*. 1.23 Å. The major absorption band in the infra red spectrum for CO is 2143 cm^{-1}, while for ^{13}CO it is 2099.2 cm^{-1}.

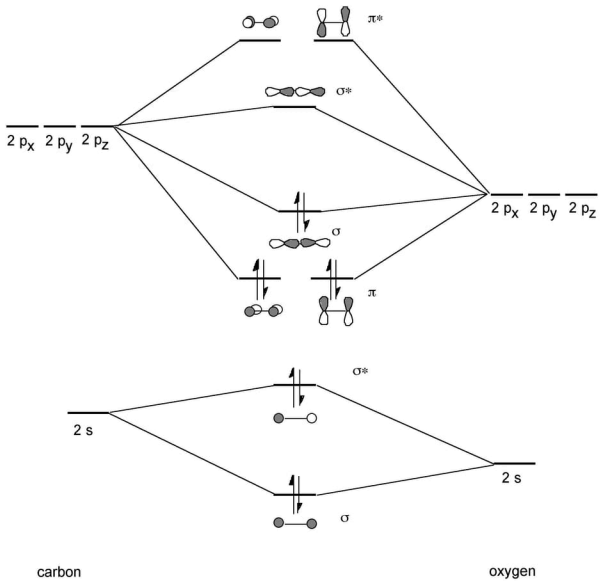


Figure 6.7.5.3: The carbon monoxide molecular orbital diagram.

This page titled 6.7.5: Carbon Monoxide is shared under a CC BY 3.0 license and was authored, remixed, and/or curated by Andrew R. Barron (CNX) via source content that was edited to the style and standards of the LibreTexts platform.

6.7.6: Carbon Dioxide

Carbon dioxide (CO_2) is the most stable oxide of carbon and is formed from the burning of carbon or carbon containing compounds in air or an excess of oxygen, (7.6.1). For industrial applications it is usually prepared from the decomposition of calcium carbonate (limestone), (7.6.2), rather than separation from combustion products.

$$\mathrm{C + O_2 \rightarrow CO_2} \tag{6.7.6.1}$$

$$\mathrm{CaCO_3 \rightarrow CaO + CO_2} \tag{6.7.6.2}$$

Phase chemistry of carbon dioxide

Carbon dioxide does not exists as a liquid under normal atmospheric pressure, but solid CO_2 (also known as *dry ice*) sublimes at -78.5 °C (Figure 6.7.6.1). Dry ice (Figure 6.7.6.2) is commonly used as a refrigerant for food or biological sample preservation.

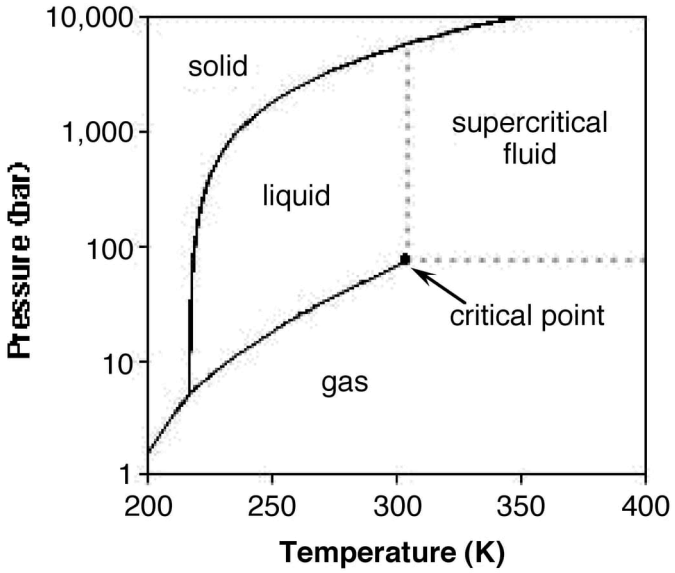


Figure 6.7.6.1: The phase diagram for carbon dioxide.



Figure 6.7.6.2: Photograph of a solid block of *dry ice*.

Note

When dry ice is placed in water (especially heated) sublimation is accelerated, and a low-sinking dense cloud of fog (smoke-like) is created. This is used in fog machines, at theaters, concerts, haunted houses, and nightclubs for dramatic effects (Figure 6.7.6.3). Fog from dry ice hovers above the ground unlike other artificial fog machines (that use partial combustion of oil) where the fog rises like smoke.



Figure 6.7.6.3: Dry ice generated smoke being used during Iron Maiden's *Somewhere Back in Time World Tour*. Copyright: Pyrotek.

Supercritical carbon dioxide

As noted above carbon dioxide usually behaves as a gas in air at standard temperature and pressure (STP = 25 °C and 1 atm) or as a solid when frozen. However, if the temperature and pressure are both increased from STP to be at or above the critical point (Figure 6.7.6.1), carbon dioxide adopts properties midway between a gas and a liquid (T_c = 31.1 °C and P_c = 72.9 atm).

Supercritical CO_2 has become an important industrial solvent due to its role in chemical extraction in addition to its low toxicity and environmental impact. In this regard it is seen as a promising green solvent. One of the biggest applications is the decaffeination of coffee and tea without leaving any residue and allowing the caffeine to be separated and used in other beverage products.

Structure and bonding

Carbon dioxide is a linear molecule due to π-localization. The bonding in CO_2 involves 2 σ-bond and 2 sets of 3 center π-bonds (Figure 6.7.6.4). The C-O bond length of 1.2 Å should be compared to the value observed for organic carbonyls (e.g., ketones, esters, aldehydes) of 1.2 – 1.3 Å.

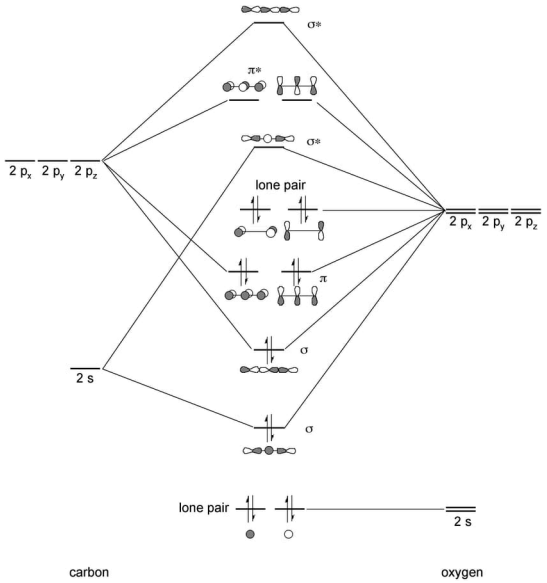


Figure 6.7.6.4: The carbon dioxide molecular orbital diagram.

Dissolution and reaction with water

Although CO_2 has no dipole moment it is very polar (dielectric constant = 1.60 at 0 °C, 50 atm) and consequently dissolves in polar solvents such as water up to a concentration of 18% (0.04 M). Most of it (+99%) is present as solvated CO_2 (Figure 6.7.6.5), and only ca. 0.2% is reacted to form carbonic acid, (7.6.1), with subsequent equilibria resulting in the formation of bicarbonate (HCO_3^-) and carbonate (CO_3^{2-}).

$$H_2O + CO_2 \rightarrow H_2CO_3 \tag{6.7.6.3}$$

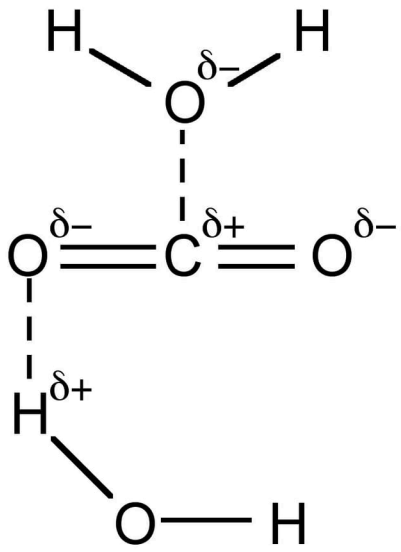


Figure 6.7.6.5: Typical water solvation of carbon dioxide.

The overall reaction involves a series of equilibria. The first equilibrium is the formation of carbonic acid, (7.6.4). The reaction rates, (7.6.5), are on the magnitude of 1 second (i.e., slow), and as a consequence when carbon dioxide is carried in the body an enzyme is present to speed up the reaction.

$$CO_{2(solv)} + H_2O \underset{k_{H_2CO_3}}{\overset{k_{CO_2}}{\rightleftharpoons}} H_2CO_3 \tag{6.7.6.4}$$

$$K = \frac{k_{H_2CO_3}}{k_{CO_2}} = \frac{25}{0.04} = 600 \tag{6.7.6.5}$$

The 2nd equilibrium is as a consequence of first ionization of carbonic acid to form bicarbonate (HCO_3^-), (7.6.6). In contrast to the first reaction, (7.6.4), this reaction is very fast with a K_{eq} = 1.6 x 10^{-4} @ 25 °C.

$$H_2CO_3 \rightleftharpoons HCO_3^- + H^+ \tag{6.7.6.6}$$

The 3rd equilibrium involves the formation of the carbonate ion (7.6.7), and has a K_{eq} = 4.84 x 10^{-11}. Carbonate (CO_3^{2-}) is a delocalized ligand, which can act as a mono or bidentate or bridging group.

$$HCO_3^- \rightleftharpoons CO_3^{2-} + H^+ \tag{6.7.6.7}$$

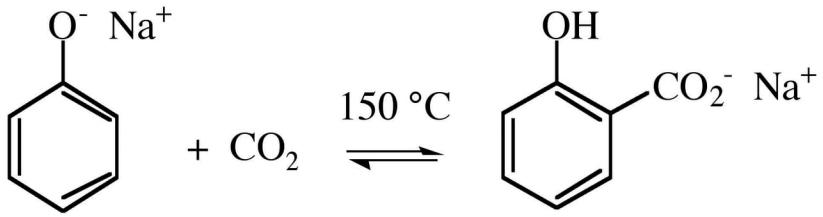
The formation of carbonic acid is the reason that even in the absence of pollutants (such as SO_2) natural rain water is slightly acidic due to dissolved CO_2. The equilibrium associated with carbonic acid is also responsible for the buffering of the pH in blood.

Reaction chemistry

Photosynthesis in plants reduces CO_2 to organic matter but similar reactions have yet to be developed in non-living systems.

Grignards react readily with carbon dioxide to form the carboxylate, which yields the associated carboxylic acid upon hydrolysis, (7.6.8). Similar reactions occur with other organometallic compounds. In addition, CO_2 reacts with alkali metal salts of phenols (phenolates) to yield the hydroxy-carboxylate.

$$RMgX + CO_2 \rightarrow RCO_2MgX \xrightarrow{H_2O} RCO_2H + HOMgX \tag{6.7.6.8}$$



A number of complexes of CO_2 with transition metals are known in which the coordination can occur via the central carbon (Figure 6.7.6.6a) or the C=O bond (Figure 6.7.6.6b). Alternatively, CO_2 can bridge two metal centers.

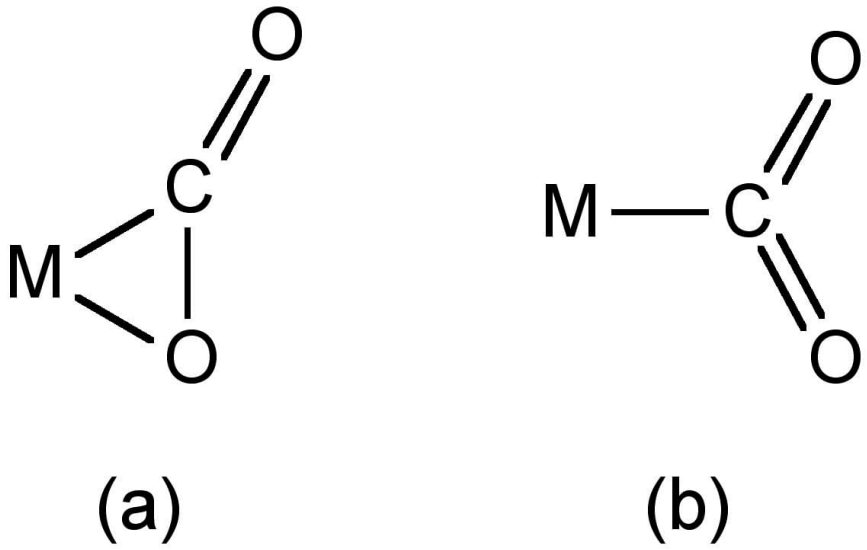


Figure 6.7.6.6: Bonding modes of CO_2 to transition metals.

Global warming and carbon dioxide

Global warming is the process of the observed increase in the average temperature of the Earth's near-surface air and oceans since the mid-20th century. Global surface temperature increased 0.74 °C (1.33 °F) between the start and the end of the 20th century (Figure 6.7.6.7). It is generally agreed that the majority of this temperature increase has occurred since the middle of the 20th century and was caused by increasing concentrations of greenhouse gases resulting from burning fossil fuels (the generation of additional CO_2) and deforestation (the loss of a mechanism for the consumption of CO_2), see Figure 6.7.6.7. While it is appreciated that natural phenomena (including solar radiation and volcanoes) produced most of the warming from pre-industrial times, the magnitude of the changes brought on by global industrialization is more significant.

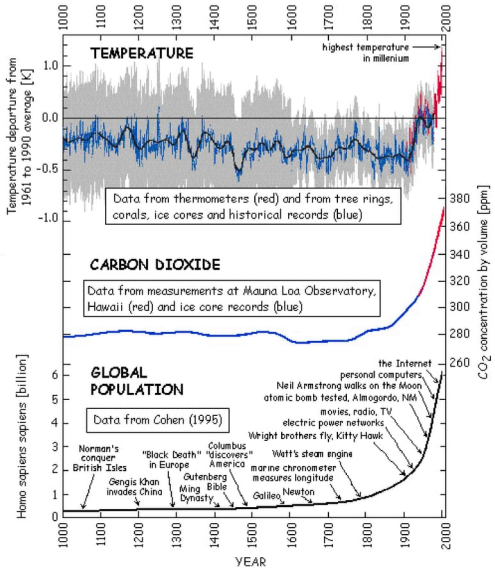


Figure 6.7.6.7: Correlation of Earth average temperature with carbon dioxide and global population.

The Earth's atmosphere has two functions. First, the ozone (O_3) in the upper atmosphere screens harmful UV from reaching the surface of the Earth. Second, as solar radiation penetrates the atmosphere a portion of the heat is then retained as a consequence of the CO_2 in the atmosphere. It is this process that modulates the surface temperature and provides a stable environment for life. The failure or alteration of either of these processes can have a dramatic effect on the livability of a planet.

Consider the relative position of Venus, Earth, and Mars to the Sun (Figure 6.7.6.8). The closer a planet is to the sun the greater the UV radiation and the greater the heating of the planet; however, the temperature is also greatly modulated by the atmosphere. Venus has an atmosphere comprising 95% CO_2 and has a surface temperature of approximately 450 °C. In contrast, while Mars' atmosphere is also 95% CO_2, it is only 1% as dense as that of Earth's, and thus the surface temperatures range from 40 °C during the day (due to radiative heating) to −80 °C at night (due to the lack of retained heat because of the thin atmosphere). These should be compared to Earth's atmosphere which is 0.038% CO_2, which allows for the correct amount of heat to be retained to sustain life. Clearly any significant change in the CO_2 content of the atmosphere will change the global temperatures of a planet.



Figure 6.7.6.8: The relative size and position of the planets from the sun.

Bibliography

- N. Stern, *The Stern Review: The Economics of Climate Change*, HM Treasury, London.
- R. B. Gupta and J.-J. Shim, *Solubility in Supercritical Carbon Dioxide*, CRC Press (2006).
- *Carbon Dioxide Capture and Storage: Special Report of the Intergovernmental Panel on Climate Change*, Cambridge University Press (2005).

This page titled 6.7.6: Carbon Dioxide is shared under a CC BY 3.0 license and was authored, remixed, and/or curated by Andrew R. Barron (CNX) via source content that was edited to the style and standards of the LibreTexts platform.

6.7.7: Suboxides of Carbon

Carbon suboxide

Carbon suboxide is the third oxide of carbon, C_3O_2. It is made from the dehydration of malonic acid, (7.7.1), with P_4O_{10} above 140 °C Like carbon dioxide, the C_3O_2 molecule is linear, with pπ-pπ bonding.

$$\mathrm{CH_2(CO_2H)_2 \rightarrow O{=}C{=}C{=}C{=}O + 2\ H_2O} \tag{6.7.7.1}$$

Gaseous carbon suboxide has an evil smell and while stable at –78 °C it polymerizes at 25 °C. Photolysis of C_3O_2 yields the unstable C_2O. As expected from its synthesis, carbon suboxide reacts slowly with water to form malonic acid, i.e., the reverse of (7.7.1); however, the reaction with stronger nuceophiles such as amines is rapid, (7.7.2).

$$\mathrm{C_3O_2 + 2\ HNR_2 \rightarrow R_2NC(O)CH_2C(O)NR_2} \tag{6.7.7.2}$$

Mellitic acid anhydride

The anhydride of mellitic acid (Figure 6.7.7.1a) may be considered as an oxide of carbon since its chemical formula contains only carbon and oxygen, i.e., $C_{12}O_9$ (Figure 6.7.7.1b).

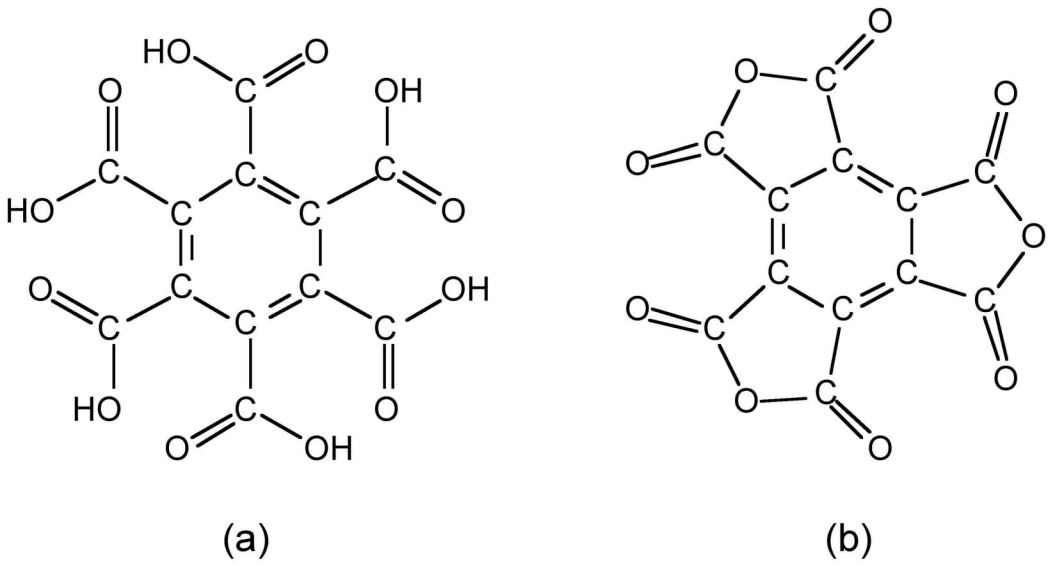


Figure 6.7.7.1: Structures of (a) mellitic acid and (b) its anhydride.

This page titled 6.7.7: Suboxides of Carbon is shared under a CC BY 1.0 license and was authored, remixed, and/or curated by LibreTexts.

6.7.8: Carbon Halides

There are two general classes of carbon halides.

1. Homoleptic halides, e.g., CCl_4, CCl_2F_2, C_6Cl_6, etc.
2. Carbonyl halides, e.g., $Cl_2C{=}O$.

A summary of some simple carbon halides is given in Table 6.7.8.1.

Table 6.7.8.1: Physical properties of simple halogen compounds of carbon.

Compound	Mp (°C)	Bp (°C)	Remarks
CF_4	-185	-128	Very stable gas
CCl_4	-23	76	Colorless liquid, stable
CBr_4	93	190	Pale yellow solid, decomposes upon boiling
CI_4	171	-	Bright red solid, decomposes prior to boiling, sublimed at low pressure
$F_2C{=}O$	-114	-83	Decomposed by H_2O
$Cl_2C{=}O$	-118	8	Phosgene, highly toxic
$Br_2C{=}O$	-	65	Fumes in air

Carbon tetrahalides

The carbon tetrahalides are generally prepared by the direct (thermal) reaction of carbon with the appropriate halogen, (7.8.1); however, specific syntheses are possible for each derivative.

$$\mathrm{C} + 2\ \mathrm{X_2} \rightarrow \mathrm{CX_4} \tag{6.7.8.1}$$

In addition to the direct reaction of fluorine with carbon, CF_4 can be prepared from SiC, (7.8.2). The SiF_4 side product is removed by passing the reaction mixture through NaOH solution, in which SiF_4 reacts to form silicate. The difference in reactivity of SiF_4 and CF_4 is attributable to the lack of an energetically accessible five-coordinate intermediate required for the associative mechanism.

$$\mathrm{SiC} + \mathrm{F_2} \rightarrow \mathrm{SiF_4} + \mathrm{CF_4} \tag{6.7.8.2}$$

Carbon tetrabromide can be obtained by bromination of CH_4 with HBr or Br_2, or by the reaction of CCl_4 with $AlBr_3$, (7.8.3). Carbon tetraiodide (CI4) can be made by the Lewis acid catalyzed halogen exchange reaction, (7.8.4).

$$3\ \mathrm{CCl_4} + 4\ \mathrm{ALBr_3} \rightarrow 3\ \mathrm{CBr_4} + 4\ \mathrm{AlCl_3} \tag{6.7.8.3}$$

$$\mathrm{CCl_4} + 4\ \mathrm{C_2H_5I} \rightarrow \mathrm{CI_4} + 4\ \mathrm{C_2H_5Cl} \tag{6.7.8.4}$$

CF_4 is very stable. In fact, it is so stable that it does not even react with molten sodium. In contrast to CF_4, carbon tetrachloride (CCl_4) reacts readily with alkali metals (K and Na) or other strong reducing agents (e.g., F_2, Al, Ba, Be, and Zn). While CCl_4 is thermodynamically unstable with respect to hydrolysis, it is kinetically stable, and thus finds extensive use as a solvent. Photolysis can result in the transfer of a chloride radical to various substrates. It is also used in the conversion of metal oxides to the chlorides. Carbon tetrabromide (CBr_4) is insoluble in water and other polar solvents, but soluble in benzene. Carbon tetraiodide (CI_4) decomposes thermally, (7.8.5).

$$2\ \mathrm{CI_4} \rightarrow 2\ \mathrm{I_2} + \mathrm{I_2C{=}CI_2} \tag{6.7.8.5}$$

The decreasing stability of CX_4, from fluorine to iodine, is directly related to the C-X bond energy.

Table 6.7.8.2: Bond energies for carbon-halide bonds.

C-X	Bond energy (kJ/mol)
C-F	485
C-Cl	327
C-Br	285
C-I	213

Hazards

Despite its use as a solvent CCl_4 has significant hazardous effects. Inhalation of carbon tetrachloride vapor can cause headaches, mental confusion, depression, fatigue, loss of appetite, nausea, vomiting, and coma. The symptoms can take many hours to appear. The vapor and liquid irritate the eyes, and internal irritation, nausea, and vomiting are caused when taken orally. Chronic effects from prolonged inhalation include bronchitis and jaundice, while skin exposure can cause dermatitis.

Carbon tetrabromide is toxic by inhalation, and the vapor is narcotic if taken in high concentrations. As with CCl_4, CBr_4 can react explosively with alkali metals.

Higher homoleptic halides

Organic compounds that contain only carbon and a halogen are called halocarbons, and these include fluorocarbons and chlorocarbons. The easiest route to fluorocarbons involves the reaction of a hydrocarbon with a high valent fluoride (e.g., CoF_3) or the reaction of a chlorocarbon with SbF_3. In general, chlorocarbons with sp^3 carbon atoms are more stable than those with sp^2 carbon centers. The exception to this is aromatic compounds such as C_6Cl_6.

The physical properties of fluorocarbons range from inert to toxic. Thus, poly(tetrafluoroethylene), $(C_2F_4)_n$, known by either its acronym (PTFE) or its trade name (Teflon), is chemically inert and has a low coefficient of friction (Table 6.7.8.3). As a consequence its uses include coatings on armor-piercing bullets (to stop the wear on the gun barrel), laboratory containers and magnetic stirrers, tubing for corrosive chemicals, and thread seal tape in plumbing applications (plumbers tape). A summary of the physical properties of PTFE is given in Table 6.7.8.3. PTFE is synthesized by the emulsion polymerization of tetrafluoroethylene monomer under pressure through free radical catalyst.

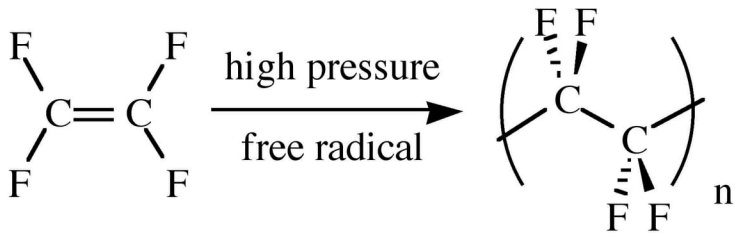


Table 6.7.8.3: Physical properties of poly(tetrafluoroethylene) (PTFE).

Property	Value
Density	2.2 g/cm^3
Melting point	327 °C
Young's modulus	0.5 GPa
Yield strength	23 MPa
Coefficient of friction	0.05 - 0.10
Dielectric constant	2.1
Dielectric strength (1 MHz)	60 MV/m

In contrast with PTFE, octafluoroisobutylene, $(CF_3)_2C{=}CF_2$, is highly toxic, while perfluorodecahydronapthalene ($C_{10}F_8$, Figure 6.7.8.1) is used as a blood substitute component.

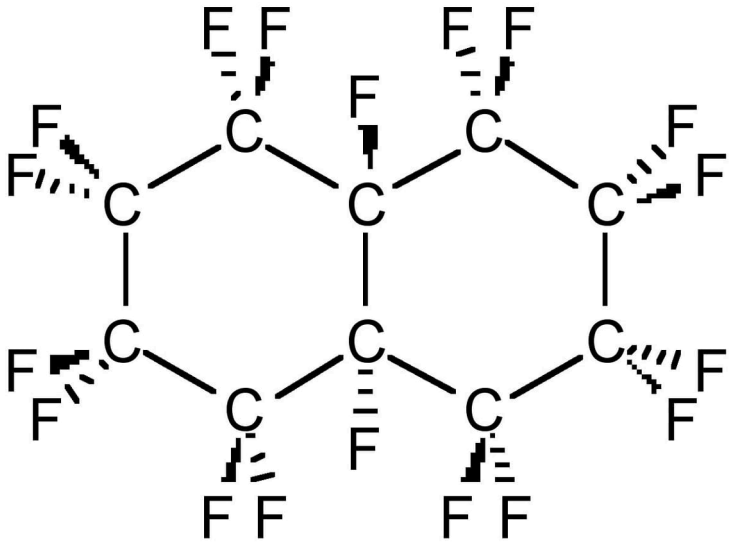


Figure 6.7.8.1: Structure of perfluorodecahydronapthalene.

Mixed halides

Mixed halides are an important class of halocarbon compound. They are synthesized by halide exchange, (7.8.6). The high cost of SbF_3 means that the reaction is generally run with an excess of the chloride.

$$3\ CCl_4 + 2\ SbF_3 \rightarrow 2\ CCl_2F_2 + 2\ SbCl_2 \tag{6.7.8.6}$$

The ordinary name for mixed carbon halide is halon or Freon, although Freon is actually a Du Pont trademark. A list of selected Freon compounds are given in Table 6.7.8.4. Halons are non-toxic, non-flammable, and have no odor. However, it is their very lack of reactivity that has caused a problem.

Table 6.7.8.4: Selected Freons and their applications.

Freon	Formula	Uses
12	CCl_2F_2	Refrigerant
11	CCl_3F	Refrigerant
114	ClF_2C-$CClF_2$	Refrigerant
113	Cl_3C-CF_3	Solvent
13B1	$CBrF_3$	Fire extinguisher
1211	$CBrClF_2$	Fire extinguisher

Environmental impact of chlorofluorcarbon compounds (CFCs)

Chlorofluorcarbon compounds (CFCs) are very stable and are not degraded in the environment. As a consequence they are transported to the stratosphere where they decomposed upon photolysis, (7.8.7). The resulting chloride radical is a catalyst for the decomposition of ozone, (7.8.8), as well as a catalyst for the reaction of ozone with molecular oxygen, (7.8.9).

$$CCl_2F_2 + h\nu \rightarrow CClF_2 + Cl\cdot \tag{6.7.8.7}$$

$$2\ O_3 \xrightarrow{Cl\cdot} 3\ O_2 \tag{6.7.8.8}$$

$$O_3 + O \xrightarrow{Cl\cdot} 2\ O_2 \tag{6.7.8.9}$$

The widespread use of CFCs as refrigerants and propellants meant that by 1986 there were 2.5 billion pounds of CFC being liberated to the atmosphere. This was equivalent to $^1/_2$ lb per person on the planet. Since the ozone layer provides the vital protection to life on the Earth's surface from high energy UV radiation the release of CFC (along with other chemicals) caused a dramatic change in the ozone layer, including the increase in the polar hole in the ozone layer. As a result of the EU called for a complete ban of CFCs (which was followed by other countries). In their place new chemicals with similar refrigerant properties were developed. These compounds contained C-H bonds (e.g., $C_2HCl_2F_3$ and $C_2H_3Cl_2F$) that are readily broken in the lower atmosphere, thus limiting the transport to the stratosphere.

Carbonyl halides

All the carbonyl halides ($X_2C{=}O$, X = F, Cl, Br, I) are known (Table 6.7.8.1). Phosgene ($Cl_2C{=}O$) was first synthesized by John Davy (Figure 6.7.8.2) in 1812 by exposing a mixture of carbon monoxide and chlorine to sunlight, (7.8.10). He named it phosgene from the Greek, *phos* (light) and *gene* (born), in reference to use of light to promote the reaction. The fluoride is also prepared by the reaction of carbon monoxide with the halogen, while the bromide is prepared by the partial hydrolysis of CBr_4 with sulfuric acid.

$$CO + Cl_2 \rightarrow Cl_2C{=}O \tag{6.7.8.10}$$

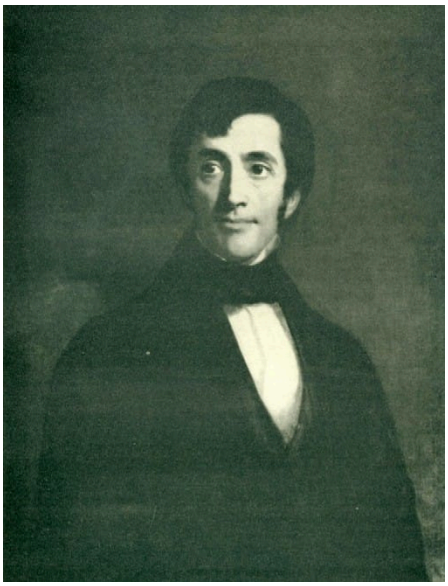


Figure 6.7.8.2: British doctor and chemist John Davy FRS (1790 – 1868) was also the brother of the noted chemist Sir Humphry Davy.

The synthesis of isocyanates from alkyl or aryl amines illustrates the electrophilic character of phosgene and its ability to introduce the equivalent of "CO^{2+}", (7.8.11). This reaction is conducted in the presence of a base such as pyridine that absorbs the hydrogen chloride. Phosgene may also be used to produce acyl chlorides from carboxylic acids, (7.8.12). However, thionyl chloride is more commonly and more safely used in this reaction.

$$RNH_2 + Cl_2C{=}O \rightarrow RN{=}C{=}O + 2\ HCl \tag{6.7.8.11}$$

$$RCO_2H + Cl_2C{=}O \rightarrow RC(O)Cl + HCl + CO_2 \tag{6.7.8.12}$$

Phosgene as a weapon of war

Phosgene is a toxic gas with the smell of "new-mown hay" and was used in chemical warfare during the First World War (Figure 6.7.8.3) where it was a more potent weapon than chlorine. While chlorine was potentially deadly it caused the victim to violently cough and choke (the bodies natural defense to limiting inhalation), in contrast, phosgene caused much less coughing with the result that more of it was inhaled. Phosgene often had a delayed effect; apparently healthy soldiers were taken down with phosgene gas poisoning up to 48 hours after inhalation. A fatal dose of phosgene eventually led to shallow breathing and retching, pulse up to 120, an ashen face and the discharge of four pints of yellow liquid from the lungs each hour for the 48 of the drowning

spasms.



Figure 6.7.8.3: Australian infantry from the 45th Battalion, Australian 4th Division wearing Small Box Respirators (SBR) as protection of chemical warfare agents. Photograph taken at Zonnebeke, on the Ypres sector, 27th September 1917. Copyright: Australian War Memorial.

Although phosgene's boiling point (7.6 °C) meant that is was a vapor, the so-called "white star" mixture of phosgene and chlorine was commonly used on the Somme, because the chlorine supplied the necessary vapor with which to carry the phosgene. A summary of the casualties inflicted by chemical warfare agents during the Great War is shown in Table 6.7.8.5.

Table 6.7.8.5: Casualties from gas attacks during the First World War (including chlorine, phosgene, and mustard gas). British Empire includes troops from United Kingdom, Australia, Canada, India, New Zealand, and South Africa.

Country	Total casualties	Deaths
Russia	419,340	56,000
Germany	200,000	9,000
France	190,000	8,000
British Empire	188,706	8,109
Austria-Hungary	100,000	3,000
USA	72,807	1,462
Italy	60,000	4,627
Others	10,000	1,000

This page titled 6.7.8: Carbon Halides is shared under a CC BY 1.0 license and was authored, remixed, and/or curated by LibreTexts.

6.7.9: Comparison Between Silicon and Carbon

An understanding of the differences between carbon and silicon is important in understanding the relative chemistry of these Group 14 elements.

Size

As expected silicon is larger than carbon due to the presence of a second shell: i.e., C = $1s^2\ 2s^2\ 2p^2$ while Si = $1s^2\ 2s^2\ 2p^6\ 3s^2\ 3p^2$. A comparison of the relative sizes of carbon and silicon are given in Table 6.7.9.1.

Table 6.7.9.1: Atomic, covalent, and van der Waals radii of carbon and silicon.

Element	Atomic radius (Å)	Covalent radius sp^3 (Å)	van der Waal radius (Å)
C	0.70	0.75	1.70
Si	1.10	1.14	2.10

Covalent and van der Waal radii from Royal Society of Chemistry Online Periodic Table. Webelements has a more detailed discussion of all three types of radii, the atomic radii quoted here are empirical.

Coordination number

Carbon is known to have a coordination number of 2, 3, and 4 in its compounds depending on the hybridization. A coordination number of 1 can also be considered for CO and CN^-. Four-coordinate carbon may be considered to be coordinatively saturated. In contrast, in the absence of overwhelming steric bulk, silicon is observed to have coordination numbers of 3, 4, 5, and 6. Examples of five and six-coordinate silicon include $Si(acac)_2Cl$ and SiF_6^{2-}, respectively. Coordination numbers of higher than 4 have been ascribed to the use of low-lying *d* orbitals; however, calculations show these are not significant. Instead, hypervalent silicon is better described by the formation of 3-center molecular orbitals, e.g., Figure 6.7.9.1.

Note

A hypervalent molecule is a molecule that contains one or more typical elements (Group 1, 2, 13-18) formally bearing more than eight electrons in their valence shells.

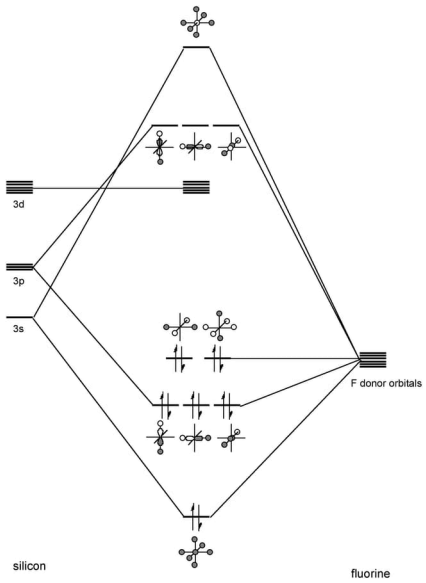


Figure 6.7.9.1: Molecular orbital diagram for SiF_6^{2-}.

Electronegativity

The electronegativities of silicon and carbon are given in Table along with hydrogen. Since carbon is more electronegative than hydrogen the C-H bond is polarized towards carbon resulting in a more protic hydrogen (Figure 6.7.9.2a). In contrast, the lower electronegativity of silicon results in a more hydridic hydrogen (Figure 6.7.9.2b). This difference is reflected in the reaction chemistry of SiH_4 versus CH_4.

Table 6.7.9.2: Selected Pauling electronegativity values. Royal Society of Chemistry Online Periodic Table

Element	Pauling scale
C	2.55
H	2.20
Si	1.90

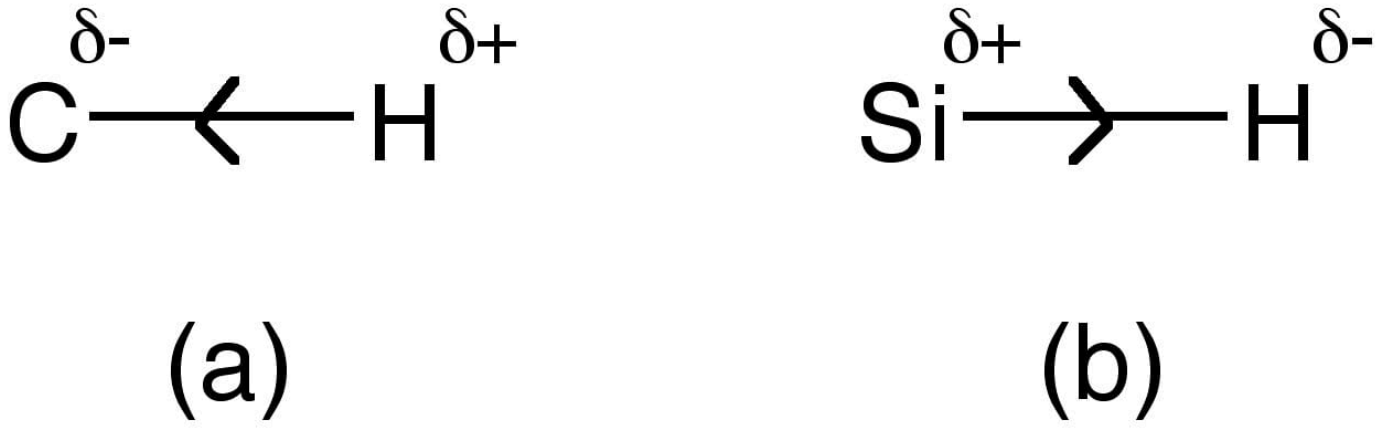


Figure 6.7.9.2: Relative polarization of C-H and Si-H bonds.

Bond energies

The E-E and E-O bond energies for carbon and silicon are given in Table 6.7.9.3. The bond energy for a C-C bond is slightly greater

than for a C-O bond, while the Si-O bond is significantly stronger than the Si-Si bond. This difference is reflected in the chemistry of silicon versus carbon compounds. The chemistry of carbon is dominated by catenation: the ability of a chemical element to form a long chain-like structure via a series of covalent bonds. Although silicon does form Si-Si bonds, they are far more reactive than their C-C analogs, and polymers of silicon are predominantly comprised of Si-O chains (as a result of the very strong bond).

Table 6.7.9.3: Selected bond energies for carbon and silicon. Royal Society of Chemistry Online Periodic Table

Element	E-E bond energy (kJ/mol)	E-O bond energy (kJ/mol)
C	345.6	357.7
Si	222	462

Multiple bonds

While unsaturated compounds for carbon (i.e., alkenes and alkynes) are common, the analogous silicon compounds (disilenes) were only reported in 1981, and disilynes in 2004. The Si=Si double bond lengths are 2.14 - 2.29 Å which is 5 - 10% shorter than the Si-Si single bond lengths. This bond shortening is less than *ca*. 13% in carbon compounds.

Note

The traditional lack of multiple bonds for the Period 3 elements and lower led to the formulation of the double bond rule which states that *chemical elements with a principal quantum number greater than 2 do not form multiple bonds (e.g., double bonds and triple bonds) with themselves or with other elements*. This rule was made obsolete starting from 1981 with the discovery of silicon and phosphorus double bonds. Double bonds that would ordinarily not form can be stabilized with proper functional groups through kinetic stabilization, i.e., either electronically or sterically.

Bibliography

- R. West, M. J. Fink, and J. Michl, *Science*, 1981, **214**, 1343.
- A. Sekiguchi, R. Kinjo, and M. Ichinohe, *Science*, 2004, **305**, 1755.

This page titled 6.7.9: Comparison Between Silicon and Carbon is shared under a CC BY 1.0 license and was authored, remixed, and/or curated by LibreTexts.

6.7.10: Semiconductor Grade Silicon

Introduction

The synthesis and purification of bulk polycrystalline semiconductor material represents the first step towards the commercial fabrication of an electronic device. This polycrystalline material is then used as the raw material for the formation of single crystal material that is processed to semiconductor wafers. The strong influence on the electric characteristics of a semiconductors exhibited by small amounts of some impurities requires that the bulk raw material be of very high purity (> 99.9999%). Although some level of purification is possible during the crystallization process it is important to use as high a purity starting material as possible.

Following oxygen (46%), silicon (L. silicis flint) is the most abundant element in the earth's crust (28%). However, silicon does not occur in its elemental form, but as its oxide (SiO_2) or as silicates. Sand, quartz, amethyst, agate, flint, and opal are some of the forms in which the oxide appears. Granite, hornblende, asbestos, feldspar, clay and mica, etc. are a few of the numerous silicate minerals. With such boundless supplies of the raw material, the costs associated with the production of bulk silicon is not one of abstraction and conversion of the oxide(s), but of purification of the crude elemental silicon. While 98% elemental silicon, known as metallurgical-grade silicon (MGS), is readily produced on a large scale, the requirements of extreme purity for electronic device fabrication require additional purification steps in order to produce electronic-grade silicon (EGS). Electronic-grade silicon is also known as semiconductor-grade silicon (SGS). In order for the purity levels to be acceptable for subsequent crystal growth and device fabrication, EGS must have carbon and oxygen impurity levels less than a few parts per million (ppm), and metal impurities at the parts per billion (ppb) range or lower. Table 6.7.10.1 and Table 6.7.10.2 give typical impurity concentrations in MGS and EGS, respectively. Besides the purity, the production cost and the specifications must meet the industry desires.

Table 6.7.10.1: Typical impurity concentrations found in metallurgical-grade silicon (MGS).

Element	Concentration (ppm)	Element	Concentration (ppm)
aluminum	1000-4350	manganese	50-120
boron	40-60	molybdenum	< 20
calcium	245-500	nickel	10-105
chromium	50-200	phosphorus	20-50
copper	15-45	titanium	140-300
iron	1550-6500	vanadium	50-250
magnesium	10-50	zirconium	20

Table 6.7.10.2: Typical impurity concentrations found in electronic-grade silicon (EGS).

Element	Concentration (ppb)	Element	Concentration (ppb)
arsenic	< 0.001	gold	< 0.00001
antimony	< 0.001	iron	0.1-1.0
boron	≤ 0.1	nickel	0.1-0.5
carbon	100-1000	oxygen	100-400
chromium	< 0.01	phosphorus	≤ 0.3
cobalt	0.001	silver	0.001
copper	0.1	zinc	< 0.1

Metallurgical-grade silicon (MGS)

The typical source material for commercial production of elemental silicon is quartzite gravel; a relatively pure form of sand (SiO_2). The first step in the synthesis of silicon is the melting and reduction of the silica in a submerged-electrode arc furnace. An example of which is shown schematically in Figure 6.7.10.1, along with the appropriate chemical reactions. A mixture of quartzite gravel and carbon are heated to high temperatures (ca. 1800 °C) in the furnace. The carbon bed consists of a mixture of coal, coke, and wood chips. The latter providing the necessary porosity such that the gases created during the reaction (SiO and CO) are able to flow through the bed.

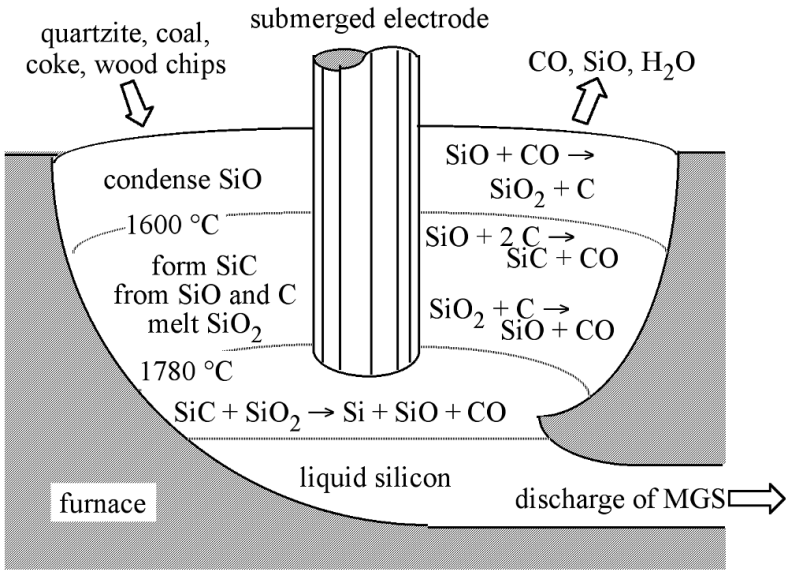


Figure 6.7.10.1: Schematic of submerged-electrode arc furnace for the production of metallurgical-grade silicon (MGS).

The overall reduction reaction of SiO_2 is expressed in (7.10.1), however, the reaction sequence is more complex than this overall reaction implies, and involves the formation of SiC and SiO intermediates. The initial reaction between molten SiO_2 and C, (7.10.2), takes place in the arc between adjacent electrodes, where the local temperature can exceed 2000 °C. The SiO and CO thus generated flow to cooler zones in the furnace where SiC is formed, (7.10.3), or higher in the bed where they reform SiO_2 and C, (7.10.2). The SiC reacts with molten SiO_2, (7.10.4), producing the desired silicon along with SiO and CO. The molten silicon formed is drawn-off from the furnace and solidified.

$$\mathrm{SiO_2(liquid) + 2\ C(solid) \rightarrow Si(liquid) + 2\ CO(gas)} \tag{6.7.10.1}$$

$$\mathrm{SiO_2 + 2\ C \underset{<1600\ ^\circ C}{\overset{>1700\ ^\circ C}{\rightleftharpoons}} SiO + CO} \tag{6.7.10.2}$$

$$\mathrm{SiO + 2C \rightarrow SiC + CO\ (1600\text{ - }1700\ ^\circ C)} \tag{6.7.10.3}$$

'_' allowed only in math mode

The as-produced MGS is approximately 98-99% pure, with the major impurities being aluminum and iron (Table 6.7.10.1), however, obtaining low levels of boron impurities is of particular importance, because it is difficult to remove and serves as a dopant for silicon. The drawbacks of the above process are that it is energy and raw material intensive. It is estimated that the production of one metric ton (1,000 kg) of MGS requires 2500 - 2700 kg quartzite, 600 kg charcoal, 600 - 700 kg coal or coke, 300 - 500 kg wood chips, and 500,000 kWh of electric power. Currently, approximately 500,000 metric tons of MGS are produced per year, worldwide. Most of the production (ca. 70%) is used for metallurgical applications (e.g., aluminum-silicon alloys are commonly used for automotive engine blocks) from whence its name is derived. Applications in a variety of chemical products such as silicone resins account for about 30%, and only 1% or less of the total production of MGS is used in the manufacturing of high-purity EGS for the electronics industry. The current worldwide consumption of EGS is approximately 5 x 10^6 kg per year.

Electronic-grade silicon (EGS)

Electronic-grade silicon (EGS) is a polycrystalline material of exceptionally high purity and is the raw material for the growth of single-crystal silicon. EGS is one of the purest materials commonly available, see Table 6.7.10.2. The formation of EGS from MGS is accomplished through chemical purification processes. The basic concept of which involves the conversion of MGS to a volatile silicon compound, which is purified by distillation, and subsequently decomposed to re-form elemental silicon of higher purity (i.e., EGS). Irrespective of the purification route employed, the first step is physical pulverization of MGS followed by its conversion to the volatile silicon compounds.

A number of compounds, such as monosilane (SiH_4), dichlorosilane (SiH_2Cl_2), trichlorosilane ($SiHCl_3$), and silicon tetrachloride ($SiCl_4$), have been considered as chemical intermediates. Among these, $SiHCl_3$ has been used predominantly as the intermediate compound for subsequent EGS formation, although SiH_4 is used to a lesser extent. Silicon tetrachloride and its lower chlorinated derivatives are used for the chemical vapor deposition (CVD) growth of Si and SiO_2. The boiling points of silane and its chlorinated products (Table 6.7.10.3) are such that they are conveniently separated from each other by fractional distillation.

Table 6.7.10.3: Boiling points of silane and chlorosilanes at 760 mmHg (1 atmosphere).

Compound	Boiling point (°C)
SiH_4	-112.3
SiH_3Cl	-30.4
SiH_2Cl_2	8.3
$SiHCl_3$	31.5
$SiCl_4$	57.6

The reasons for the predominant use of $SiHCl_3$ in the synthesis of EGS are as follows:

1. $SiHCl_3$ can be easily formed by the reaction of anhydrous hydrogen chloride with MGS at reasonably low temperatures (200 - 400 °C);
2. it is liquid at room temperature so that purification can be accomplished using standard distillation techniques;
3. it is easily handled and if dry can be stored in carbon steel tanks;
4. its liquid is easily vaporized and, when mixed with hydrogen it can be transported in steel lines without corrosion;
5. it can be reduced at atmospheric pressure in the presence of hydrogen;
6. its deposition can take place on heated silicon, thus eliminating contact with any foreign surfaces that may contaminate the resulting silicon; and
7. it reacts at lower temperatures (1000 - 1200 °C) and at faster rates than does $SiCl_4$.

Chlorosilane (Seimens) process

Trichlorosilane is synthesized by heating powdered MGS with anhydrous hydrogen chloride (HCl) at around 300 °C in a fluidized-bed reactor, (7.10.5).

'_' allowed only in math mode

Since the reaction is actually an equilibrium and the formation of $SiHCl_3$ highly exothermic, efficient removal of generated heat is essential to assure a maximum yield of $SiHCl_3$. While the stoichiometric reaction is that shown in (7.10.5), a mixture of chlorinated silanes is actually prepared which must be separated by fractional distillation, along with the chlorides of any impurities. In particular iron, aluminum, and boron are removed as $FeCl_3$ (b.p. = 316 °C), $AlCl_3$ (m.p. = 190 °C subl.), and BCl_3 (b.p. = 12.65 °C), respectively. Fractional distillation of $SiHCl_3$ from these impurity halides result in greatly increased purity with a concentration of electrically active impurities of less than 1 ppb.

EGS is prepared from purified $SiHCl_3$ in a chemical vapor deposition (CVD) process similar to the epitaxial growth of Si. The high-purity $SiHCl_3$ is vaporized, diluted with high-purity hydrogen, and introduced into the Seimens deposition reactor, shown schematically in Figure 6.7.10.2. Within the reactor, thin silicon rods called slim rods (ca. 4 mm diameter) are supported by graphite electrodes. Resistance heating of the slim rods causes the decomposition of the $SiHCl_3$ to yield silicon, as described by

the reverse reaction shown in (7.10.5).

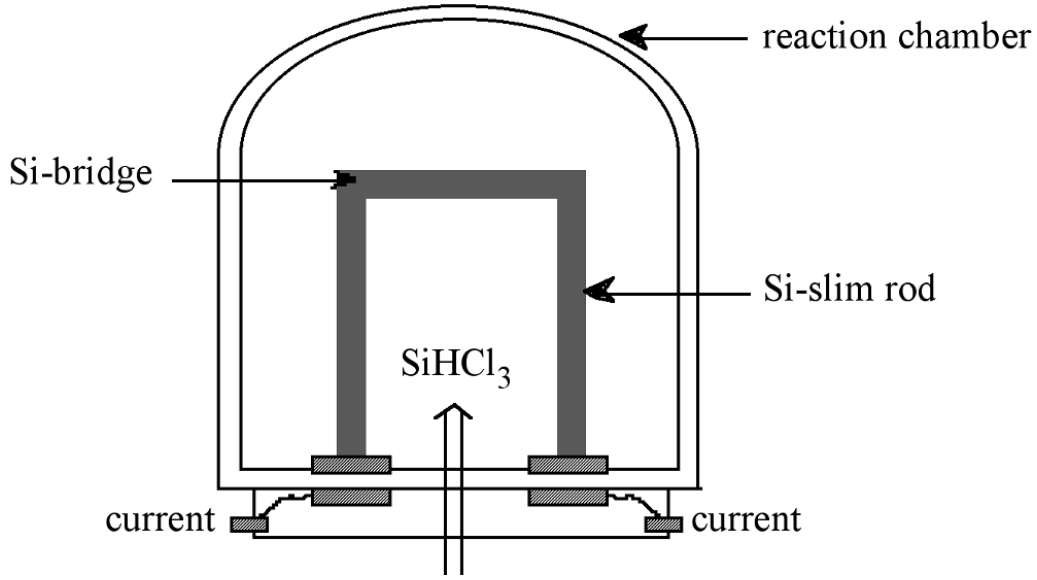


Figure 6.7.10.2: Schematic representation of a Seimens deposition reactor.

The shift in the equilibrium from forming $SiHCl_3$ from Si at low temperature, to forming Si from $SiHCl_3$ at high temperature is as a consequence of the temperature dependence, (7.10.6), of the equilibrium constant, (7.10.7) where ρ = partial pressure, for (7.10.5). Since the formation of $SiHCl_3$ is exothermic, i.e., $\Delta H < 0$, an increase in the temperature causes the partial pressure of $SiHCl_3$ to decrease. Thus, the Siemens process is typically run at ca. 1100 °C, while the reverse fluidized bed process is carried out at 300 °C.

$$\ln K_p = \frac{-\Delta H}{RT} \tag{6.7.10.4}$$

$$K_p = \frac{{}^{\rho}SiHCl_3 \; {}^{\rho}H_2}{{}^{\rho}HCl} \tag{6.7.10.5}$$

The slim rods act as a nucleation point for the deposition of silicon, and the resulting polycrystalline rod consists of columnar grains of silicon (polysilicon) grown perpendicular to the rod axis. Growth occurs at less than 1 mm per hour, and after deposition for 200 to 300 hours high-purity (EGS) polysilicon rods of 150 - 200 mm in diameter are produced. For subsequent float-zone refining the polysilicon EGS rods are cut into long cylindrical rods. Alternatively, the as-formed polysilicon rods are broken into chunks for single crystal growth processes, for example Czochralski melt growth.

In addition to the formation of silicon, the HCl coproduct reacts with the $SiHCl_3$ reactant to form silicon tetrachloride ($SiCl_4$) and hydrogen as major byproducts of the process, (7.10.8). This reaction represents a major disadvantage with the Seimens process: poor efficiency of silicon and chlorine consumption. Typically, only 30% of the silicon introduced into CVD reactor is converted into high-purity polysilicon.

$$HCl + SiHCl_3 \rightarrow SiCl_4 + H_2 \tag{6.7.10.6}$$

In order to improve efficiency the HCl, $SiCl_4$, H_2, and unreacted $SiHCl_3$ are separated and recovered for recycling. Figure 6.7.10.3 illustrates the entire chlorosilane process starting with MGS and including the recycling of the reaction byproducts to achieve high overall process efficiency. As a consequence, the production cost of high-purity EGS depends on the commercial usefulness of the byproduct, $SiCl_4$. Additional disadvantages of the Seimens process are derived from its relatively small batch size, slow growth rate, and high power consumption. These issues have lead to the investigation of alternative cost efficient routes to EGS.

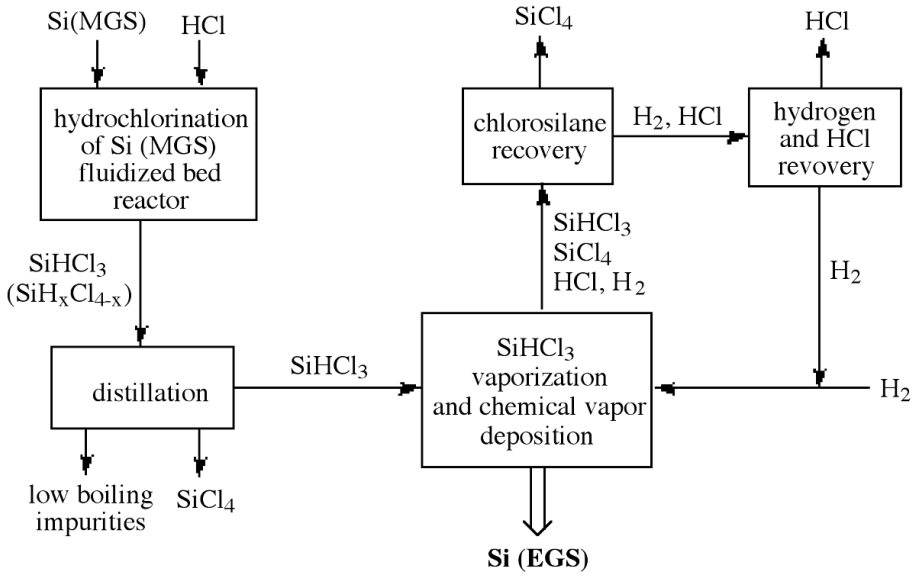


Figure 6.7.10.3: Schematic representation of the reaction pathways for the formation of EGS using the chlorosilane process.

Silane process

An alternative process for the production of EGS that has begun to receive commercial attention is the pyrolysis of silane (SiH_4). The advantages of producing EGS from SiH_4 instead of $SiHCl_3$ are potentially lower costs associated with lower reaction temperatures, and less harmful byproducts. Silane decomposes < 900 °C to give silicon and hydrogen, (7.10.9).

$$SiH_4(vapor) \rightarrow Si(solid) + 2\ H_2(gas) \tag{6.7.10.7}$$

Silane may be prepared by a number of routes, each having advantages with respect to purity and production cost. The simplest process involves the direct reaction of MGS powders with magnesium at 500 °C in a hydrogen atmosphere, to form magnesium silicide (Mg_2Si). The magnesium silicide is then reacted with ammonium chloride in liquid ammonia below 0 °C, (7.10.10).

$$Mg_2Si + 4\ NH_4Cl \rightarrow SiH_4 + 2\ MgCl_2 + 5\ NH_3 \tag{6.7.10.8}$$

This process is ideally suited to the removal of boron impurities (a p-type dopant in Si), because the diborane (B_2H_6) produced during the reaction forms the Lewis acid-base complex, $H_3B(NH_3)$, whose volatility is sufficiently lower than SiH_4, allowing for the purification of the latter. It is possible to prepare EGS with a boron content of ≤ 20 ppt using SiH_4 synthesized in this manner. However, phosphorus (another dopant) in the form of PH_3 may be present as a contaminant requiring subsequent purification of the SiH_4.

Alternative routes to SiH_4 involve the chemical reduction of $SiCl_4$ by either lithium hydride, (7.10.11), lithium aluminum hydride, (7.10.12), or via hydrogenation in the presence of elemental silicon, (7.10.13) - (7.10.16). The hydride reduction reactions may be carried-out on relatively large scales (ca. 50 kg), but only batch processes. In contrast, Union Carbide has adapted the hydrogenation to a continuous process, involving disproportionation reactions of chlorosilanes, (7.10.14) - (7.10.16), and the fractional distillation of silane, Table 6.7.10.3.

$$SiCl_4 + LiH \rightarrow SiH_4 + 4\ LiCl \tag{6.7.10.9}$$

$$SiCl_4 + LiAlH_4 \rightarrow SiH_4 + LiCl + AlCl_4 \tag{6.7.10.10}$$

$$SiCl_4 + 2\ H_2 + Si(98 \rightarrow 4\ SiHCl_3 \tag{6.7.10.11}$$

$$2\ SiHCl_3 \rightarrow SiH_2Cl_2 + 2\ SiHCl_3 \tag{6.7.10.12}$$

$$3\ SiH_2Cl_2 \rightarrow SiH_2Cl + 2\ SiHCl_3 \tag{6.7.10.13}$$

$$2\ SiH_3Cl \rightarrow SiH_4 + SiH_2Cl_2 \tag{6.7.10.14}$$

Pyrolysis of silane on resistively heated polysilicon filaments at 700 - 800 °C yields polycrystalline EGS. As noted above, the EGS formed has remarkably low boron impurities compared with material prepared from trichlorosilane. Moreover, the resulting EGS is less contaminated with transition metals from the reactor container because SiH_4 decomposition does not cause as much of a corrosion problem as is observed with halide precursor compounds.

Granular polysilicon deposition

Both the chlorosilane (Seimens) and silane processes result in the formation of rods of EGS. However, there has been increased interest in the formation of granular polycrystalline EGS. This process was developed in 1980's, and relies on the decomposition of SiH_4 in a fluidized-bed deposition reactor to produce free-flowing granular polysilicon.

Tiny silicon particles are fluidized in a SiH_4/H_2 flow, and act as seed crystal onto which polysilicon deposits to form free-flowing spherical particles. The size distribution of the particles thus formed is over the range from 0.1 to 1.5 mm in diameter with an average particle size of 0.7 mm. The fluidized-bed seed particles are originally made by grinding EGS in a ball (or hammer) mill and leaching the product with acid, hydrogen peroxide, and water. This process is time-consuming and costly, and tended to introduce undesirable impurities from the metal grinders. In a new method, large EGS particles are fired at each other by a high-speed stream of inert gas and the collision breaks them down into particles of suitable size for a fluidized bed. This process has the main advantage that it introduces no foreign materials and requires no leaching or other post purification.

The fluidized-bed reactors are much more efficient than traditional rod reactors as a consequence of the greater surface area available during CVD growth of silicon. It has been suggested that fluidized-bed reactors require $^1/_5$ to $^1/_{10}$ the energy, and half the capital cost of the traditional process. The quality of fluidized-bed polysilicon has proven to be equivalent to polysilicon produced by the conventional methods. Moreover, granular EGS in a free-flowing form, and with high bulk density, enables crystal growers to obtain the high, reproducible production yields out of each crystal growth run. For example, in the Czochralski crystal growth process, crucibles can be quickly and easily filled to uniform loading with granular EGS, which typically exceed those of randomly stacked polysilicon chunks produced by the Siemens silane process.

Zone refining

The technique of zone refining is used to purify solid materials and is commonly employed in metallurgical refining. In the case of silicon may be used to obtain the desired ultimate purity of EGS, which has already been purified by chemical processes. Zone refining was invented by Pfann, and makes use of the fact that the equilibrium solubility of any impurity (e.g., Al) is different in the solid and liquid phases of a material (e.g., Si). For the dilute solutions, as is observed in EGS silicon, an equilibrium segregation coefficient (k_0) is defined by $k_0 = C_s/C_l$, where C_s and C_l are the equilibrium concentrations of the impurity in the solid and liquid near the interface, respectively.

If k_0 is less than 1 then the impurities are left in the melt as the molten zone is moved along the material. In a practical sense a molten zone is established in a solid rod. The zone is then moved along the rod from left to right. If $k_0 < 1$ then the frozen part left on the trailing edge of the moving molten zone will be purer than the material that melts in on the right-side leading edge of the moving molten zone. Consequently the solid to the left of the molten zone is purer than the solid on the right. At the completion of the first pass the impurities become concentrated to the right of the solid sample. Repetition of the process allows for purification to exceptionally high levels. Table 6.7.10.4 lists the equilibrium segregation coefficients for common impurity and dopant elements in silicon; it should be noted that they are all less than 1.

Table 6.7.10.4: Segregation coefficients for common impurity and dopant elements in silicon.

Element	k_0	Element	k_0
aluminum	0.002	iron	8×10^{-6}
boron	0.8	oxygen	0.25
carbon	0.07	phosphorus	0.35
copper	4×10^{-6}	antimony	0.023

Bibliography

- K. G. Baraclough, K. G., in *The Chemistry of the Semiconductor Industry*, Eds. S. J. Moss and A. Ledwith, Blackie and Sons, Glasgow, Scotland (1987).
- L. D. Crossman and J. A. Baker, *Semiconductor Silicon 1977*, Electrochem. Soc., Princeton, New Jersey (1977).
- W. C. O'Mara, Ed. *Handbook of Semiconductor Silicon Technology*, Noyes Pub., New Jersey (1990).
- W. G. Pfann, *Zone Melting*, John Wiley & Sons, New York, (1966).
- F. Shimura, *Semiconductor Silicon Crystal Technology*, Academic Press (1989).

This page titled 6.7.10: Semiconductor Grade Silicon is shared under a CC BY 1.0 license and was authored, remixed, and/or curated by LibreTexts.

6.7.11: Oxidation of Silicon

Note

This module was developed as part of the Rice University course CHEM-496: *Chemistry of Electronic Materials*. This module was prepared with the assistance of Andrea Keys.

Introduction

In the fabrication of integrated circuits (ICs), the oxidation of silicon is essential, and the production of superior ICs requires an understanding of the oxidation process and the ability to form oxides of high quality. Silicon dioxide has several uses:

1. Serves as a mask against implant or diffusion of dopant into silicon.
2. Provides surface passivation.
3. Isolates one device from another (dielectric isolation).
4. Acts as a component in MOS structures.
5. Provides electrical isolation of multi-level metallization systems.

Methods for forming oxide layers on silicon have been developed, including thermal oxidation, wet anodization, chemical vapor deposition (CVD), and plasma anodization or oxidation. Generally, CVD is used when putting the oxide layer on top of a metal surface, and thermal oxidation is used when a low-charge density level is required for the interface between the oxide and the silicon surface.

Oxidation of silicon

Silicon's surface has a high affinity for oxygen and thus an oxide layer rapidly forms upon exposure to the atmosphere. The chemical reactions which describe this formation are:

$$\mathrm{Si_{(s)} + O_{2(g)} \rightarrow SiO_{2(s)}} \tag{6.7.11.1}$$

$$\mathrm{Si_{(s)} + 2\ H_2O_{(g)} \rightarrow SiO_{2(s)} + 2\ H_{2(g)}} \tag{6.7.11.2}$$

In the first reaction a dry process is utilized involving oxygen gas as the oxygen source and the second reaction describes a wet process which uses steam. The dry process provides a "good" silicon dioxide but is slow and mostly used at the beginning of processing. The wet procedure is problematic in that the purity of the water used cannot be guaranteed to a suitable degree. This problem can be easily solved using a pyrogenic technique which combines hydrogen and oxygen gases to form water vapor of very high purity. Maintaining reagents of high quality is essential to the manufacturing of integrated circuits, and is a concern which plagues each step of this process.

The formation of the oxide layer involves shared valence electrons between silicon and oxygen, which allows the silicon surface to rid itself of "dangling" bonds, such as lone pairs and vacant orbitals. These vacancies create mid-gap states between the valence and conduction bands, which prevents the desired band gap of the semiconductor. The Si-O bond strength is covalent (strong), and so can be used to achieve the loss of mid-gap states and passivate the surface of the silicon.

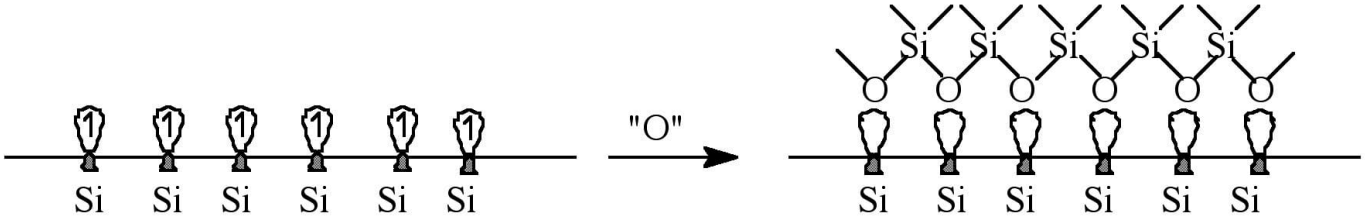


Figure 6.7.11.1: Removal of dangling bonds by oxidation of surface.

The oxidation of silicon occurs at the silicon-oxide interface and consists of four steps:

1. Diffusive transport of oxygen across the diffusion layer in the vapor phase adjacent to the silicon oxide-vapor interface.
2. Incorporation of oxygen at the outer surface into the silicon oxide film.
3. Diffusive transport across the silicon oxide film to its interface with the silicon lattice.
4. Reaction of oxygen with silicon at this inner interface.

As the Si-SiO_2 interface moves into the silicon its volume expands, and based upon the densities and molecular weights of Si and SiO_2, 0.44 Å Si is used to obtain 1.0 Å SiO_2.

Pre-oxidation cleaning

The first step in oxidizing a surface of silicon is the removal of the native oxide which forms due to exposure to open air. This may seem redundant to remove an oxide only to put on another, but this is necessary since uncertainty exists as to the purity of the oxide which is present. The contamination of the native oxide by both organic and inorganic materials (arising from previous processing steps and handling) must be removed to prevent the degradation of the essential electrical characteristics of the device. A common procedure uses a H_2O-H_2O_2-NH_4OH mixture which removes the organics present, as well as some group I and II metals. Removal of heavy metals can be achieved using a H_2O-H_2O_2-HCl mixture, which complexes with the ions which are formed. After removal of the native oxide, the desired oxide can be grown. This growth is useful because it provides: chemical protection, conditions suitable for lithography, and passivation. The protection prevents unwanted reactions from occurring and the passivation fills vacancies of bonds on the surface not present within the interior of the crystal. Thus the oxidation of the surface of silicon fulfills several functions in one step.

Thermal oxidation

The growth of oxides on a silicon surface can be a particularly tedious process, since the growth must be uniform and pure. The thickness wanted usually falls in the range 50 - 500 Å, which can take a long time and must be done on a large scale. This is done by stacking the silicon wafers in a horizontal quartz tube while the oxygen source flows over the wafers, which are situated vertically in a slotted paddle (boat). This procedure is performed at 1 atm pressure, and the temperature ranges from 700 to 1200 °C, being held to within ±1 °C to ensure uniformity. The choice of oxidation technique depends on the thickness and oxide properties required. Oxides that are relatively thin and those that require low charge at the interface are typically grown in dry oxygen. When thick oxides are required (> 0.5 mm) are desired, steam is the source of choice. Steam can be used at wide range of pressures (1 atm to 25 atm), and the higher pressures allow thick oxide growth to be achieved at moderate temperatures in reasonable amounts of time.

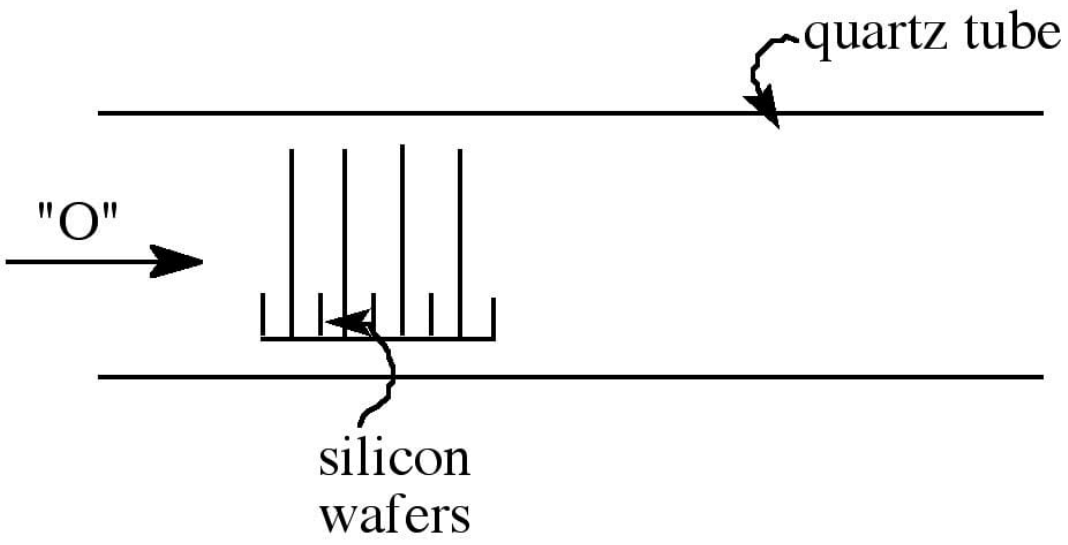


Figure 6.7.11.2: Horizontal diffusion tube showing the oxidation of silicon wafers at 1 atm pressure.

The thickness of SiO_2 layers on a Si substrate is readily determined by the color of the film. Table 6.7.11.1 provides a guidline for thermal grown oxides.

Table 6.7.11.1: Color chart for thermally grown SiO_2 films observed under daylight fluorescent lighting.

Film thickness (μm)	Color	Film thickness (μm)	Color
0.05	tan	0.63	violet-red
0.07	brown	0.68	"bluish"
0.10	dark violet to red-violet	0.72	blue-green to gree
0.12	royal blue	0.77	"yellowish"
0.15	light blue to metallic blue	0.80	orange
0.17	metallic to light yellow-green	0.82	salmon
0.20	light gold	0.85	light red-violet
0.22	gold	0.86	violet
0.25	orange to melon	0.87	blue violet
0.27	red-violet	0.89	blue
0.30	blue to violet blue	0.92	blue-green
0.31	blue	0.95	yellow-green
0.32	blue to blue-green	0.97	yellow
0.34	light green	0.99	orange
0.35	green to yellow-green	1.00	carnation pink
0.36	yellow-green	1.02	violet red
0.37	green-yellow	1.05	red-violet
0.39	yellow	1.06	violet
0.41	light orange	1.07	blue-violet
0.42	carnation pink	1.10	green

0.44	violet-red	1.11	yellow-green
0.46	red-violet	1.12	green
0.47	violet	1.18	violet
0.48	blue-violet	1.19	red-violet
0.49	blue	1.21	violet-red
0.50	blue green	1.24	carnation pink to salmon
0.52	green	1.25	orange
0.54	yellow-green	1.28	"yellowish"
0.56	green-yellow	1.32	sky blue to green-blue
0.57	"yellowish"	1.40	orange
0.58	light orange to pink	1.46	blue-violet
0.60	carnation pink	1.50	blue

High pressure oxidation

High pressure oxidation is another method of oxidizing the silicon surface which controls the rate of oxidation. This is possible because the rate is proportional to the concentration f the oxide, which in turn is proportional to the partial pressure of the oxidizing species, according to Henry's law, (7.11.3), where C is the equilibrium concentration of the oxide, H is Henry's law constant, and p_O is the partial pressure of the oxidizing species.

$$\mathrm{C} = \mathrm{H}_{(\mathrm{pO})} \tag{6.7.11.3}$$

This approach is fast, with a rate of oxidation ranging from 100 to 1000 mm/h, and also occurs at a relatively low temperature. It is a useful process, preventing dopants from being displaced and also forms a low number of defects, which is most useful at the end of processing.

Plasma oxidation

Plasma oxidation and anodization of silicon is readily accomplished by the use of activated oxygen as the oxidizing species. The highly reactive oxygen is formed within an electrical discharge or plasma. The oxidation is carried out in a low pressure (0.05 - 0.5 Torr) chamber, and the the plasma is produced either by a DC electron source or a high-frequency discharge. In simple plasma oxidation the sample (i.e., the silicon wafer) is held at ground potential. In contrast, aniodization systems usually have a DC bias between the sample and an electrode with the sample biased positively with respect to the cathode. Platinum electrodes are commonly used as the cathodes.

There have been at least 34 different reactions reported to occur in an oxygen plasma, however, the vast majority of these are inconsequential with respect to the formation of active species. Furthermore, many of the potentially active species are sufficiently short lived that it is unlikely that they make a significant contribution. The primary active species within the oxygen plasma are undoubtedly O^- and O^{2+}. Both being produced in near equal quantities, although only the former is relevant to plasma aniodization. While these species may be active with respect to surface oxidation, it is more likely that an electron transfer occurs from the semiconductor surface yields activated oxygen species, which are the actual reactants in the oxidation of the silicon.

The significant advatage of plasma processes is that while the electron temperature of the ionized oxygen gas is in excess of 10,000 K, the thermal temperatures required are significantly lower than required for the high pressure method, i.e., < 600 °C. The advantages of the lower reaction temperatures include: the minimization of dopant diffusion and the impediment of the generation of defects. Despite these advantages there are two primary disadvantages of any plasma based process. First, the high electric fields present during the processes cause damage to the resultant oxide, in particular, a high density of interface traps often result. However, post annealing may improve film quality. Second, the growth rates of plasma oxidation are low, typically 1000 Å/h. This growth rate is increased by about a factor of 10 for plasma aniodization, and further improvements are observed if 1 - 3% chlorine is added to the oxygen source.

Masking

A selective mask against the diffusion of dopant atoms at high temperatures can be found in a silicon dioxide layer, which can prove to be very useful in integrated circuit processing. A predeposition of dopant by ion implantation, chemical diffusion, or spin-on techniques typically results in a dopant source at or near the surface of the oxide. During the initial high-temperature step, diffusion in the oxide must be slow enough with respect to diffusion in the silicon that the dopants do not diffuse through the oxide in the masked region and reach the silicon surface. The required thickness may be determined by experimentally measuring, at a particular temperature and time, the oxide thickness necessary to prevent the inversion of a lightly doped silicon substrate of opposite conductivity. To this is then added a safety factor, with typical total values ranging from 0.5 to 0.7 mm. The impurity masking properties result when the oxide is partially converted into a silica impurity oxide "glass" phase, and prevents the impurities from reaching the SiO_2-Si interface.

Bibliography

- M. M. Atalla, in *Properties of Elemental and Compound Semiconductors*, Ed. H. Gatos, Interscience: New York (1960).
- S. K. Ghandhi, *VLSI Fabrication Principles, Silicon and Gallium Arsenide*, Wiley, Chichester, 2nd Ed. (1994).
- S. M. Sze, *Physics of Semiconductor Devices*, 2nd Edition, John Wiley & Sons, New York (1981).
- D. L. Lile, *Solid State Electron.*, 1978, **21**, 1199.
- W. E. Spicer, P. W. Chye, P. R. Skeath, and C. Y. Su, I. Lindau, *J. Vac. Sci. Technol.*, 1979, **16**, 1422.
- V. Q. Ho and T. Sugano, *IEEE Trans. Electron Devices*, 1980, **ED-27**, 1436.
- J. R. Hollanhan and A. T. Bells, *Techniques and Applications of Plasma Chemistry*, Wiley, New York (1974).
- R. P. H. Chang and A. K. Sinha, *Appl. Phys. Lett.*, 1976, **29**, 56.

This page titled 6.7.11: Oxidation of Silicon is shared under a CC BY 1.0 license and was authored, remixed, and/or curated by LibreTexts.

6.7.12: Applications for Silica Thin Films

Introduction

While the physical properties of silica make it suitable for use in protective and optical coating applications, the biggest application of insulating SiO_2 thin films is undoubtedly in semiconductor devices, in which the insulator performs a number of specific tasks, including: surface passivation, field effect transistor (FET) gate layer, isolation layers, planarization and packaging.

The term insulator generally refers to a material that exhibits low thermal or electrical conductivity; electrically insulating materials are also called dielectrics. It is in regard to the high resistance to the flow of an electric current that SiO_2 thin films are of the greatest commercial importance. The dielectric constant (ε) is a measure of a dielectric materials ability to store charge, and is characterized by the electrostatic energy stored per unit volume across a unit potential gradient. The magnitude of ε is an indication of the degree of polarization or charge displacement within a material. The dielectric constant for air is 1, and for ionic solids is generally in the range of 5 - 10. Dielectric constants are defined as the ratio of the material's capacitance to that of air, i.e., (7.12.1). The dielectric constant for silicon dioxide ranges from 3.9 to 4.9, for thermally and plasma CVD grown films, respectively.

$$\epsilon = \frac{C_{material}}{C_{air}} \tag{6.7.12.1}$$

An insulating layer is a film or deposited layer of dielectric material separating or covering conductive layers. Ideally, in these application an insulating material should have a surface resistivity of greater than 10^{13} Ω/cm^2 or a volume resistivity of greater than 10^{11} Ω.cm. However, for some applications, lower values are acceptable; an electrical insulator is generally accepted to have a resistivity greater than 10^5 Ω.cm. CVD SiO_2 thin films have a resistivity of 10^6 - 10^{16} Ω.cm, depending on the film growth method.

As a consequence of its dielectric properties SiO_2, and related silicas, are used for isolating conducting layers, to facilitate the diffusion of dopants from doped oxides, as diffusion and ion implantation masks, capping doped films to prevent loss of dopant, for gettering impurities, for protection against moisture and oxidation, and for electronic passivation. Of the many methods used for the deposition of thin films, chemical vapor deposition (CVD) is most often used for semiconductor processing. In order to appreciate the unique problems associated with the CVD of insulating SiO_2 thin films it is worth first reviewing some of their applications. Summarized below are three areas of greatest importance to the fabrication of contemporary semiconductor devices: isolation and gate insulation, passivation, and planarization.

Device isolation and gate insulation

A microcircuit may be described as a collection of devices each consisting of "an assembly of active and passive components, interconnected within a monolithic block of semiconducting material". Each device is required to be isolated from adjacent devices in order to allow for maximum efficiency of the overall circuit. Furthermore within a device, contacts must also be electrically isolated. While there are a number of methods for isolating individual devices within a circuit (reverse-biased junctions, mesa isolation, use of semi-insulating substrates, and oxide isolation), the isolation of the active components in a single device is almost exclusively accomplished by the deposition of an insulator.

In Figure is shown a schematic representation of a silicon MOSFET (metal-oxide-semiconductor field effect transistor). The MOSFET is the basic component of silicon-CMOS (complimentary metal-oxide-semiconductor) circuits which, in turn, form the basis for logic circuits, such as those used in the CPU (central processing unit) of a modern personal computer. It can be seen that the MOSFET is isolated from adjacent devices by a reverse-biased junction (p^+-channel stop) and a thick oxide layer. The gate, source and drain contact are electrically isolated from each other by a thin insulating oxide. A similar scheme is used for the isolation of the collector from both the base and the emitter in bipolar transistor devices.

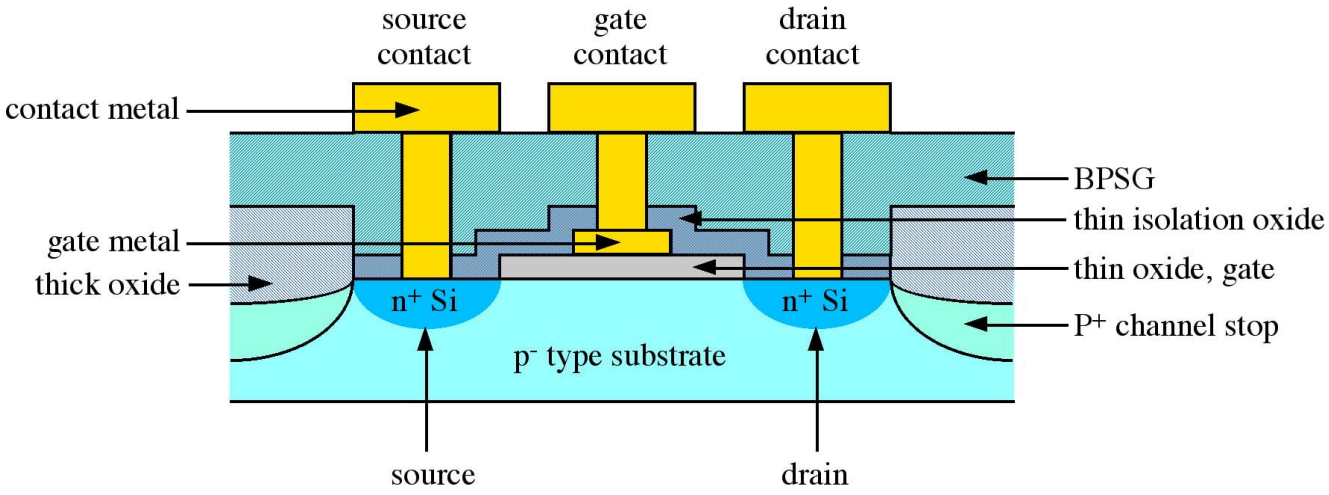


Figure 6.7.12.1: Schematic diagrams of a Si-MOSFET (metal-oxide-semiconductor field effect transistor).

As a transistor, a MOSFET has many advantages over alternate designs. The key advantage is low power dissipation resulting from the high impedance of the device. This is a result of the thin insulation layer between the channel (region between source and drain) and the gate contact, see Figure 6.7.12.1. The presence of an insulating gate is characteristic of a general class of devices called MISFETs (metal-insulator-semiconductor field effect transistor). MOSFETs are a subset of MISFETs where the insulator is specifically an oxide, e.g., in the case of a silicon MISFET device the insulator is SiO_2, hence MOSFET. It is the fabrication of MOSFET circuits that has allowed silicon technology to dominate digital electronics (logic circuits). However, increases in computing power and speed require a constant reduction in device size and increased complexity in device architecture.

Passivation

Passivation is often defined as a process whereby a film is grown on the surface of a semiconductor to either (a) chemically protect it from the environment, or (b) provide electronic stabilization of the surface.

From the earliest days of solid state electronics it has been recognized that the presence or absence of surface states plays a decisive role in the usefulness of any semiconducting material. On the surface of any solid state material there are sites in which the coordination environment of the atoms is incomplete. These sites, commonly termed "dangling bonds", are the cause of the electronically active states which allow for the recombination of holes and electrons. This recombination occurs at energies below the bulk value, and interferes with the inherent properties of the semiconductor. In order to optimize the properties of a semiconductor device it is desirable to covalently satisfy all these surface bonds, thereby shifting the surface states out of the band gap and into the valence or conduction bands. Electronic passivation may therefore be described as a process which reduces the density of available electronic states present at the surface of a semiconductor, thereby limiting hole and electron recombination possibilities. In the case of silicon both the native oxide and other oxides admirably fulfill these requirements.

Chemical passivation requires a material that inhibits the diffusion of oxygen, water, or other species to the surface of the underlying semiconductor. In addition, the material is ideally hard and resistant to chemical attack. A perfect passivation material would satisfy both electronic and chemical passivation requirements.

Planarization

For the vast majority of electronic devices, the starting point is a substrate consisting of a flat single crystal wafer of semiconducting material. During processing, which includes the growth of both insulating and conducting films, the surface becomes increasingly non-planar. For example, a gate oxide in a typical MOSFET (see Figure 6.7.12.1) may be typically 100 - 250 Å thick, while the isolation or field oxide may be 10,000 Å. In order for the successful subsequent deposition of conducting layers (metallization) to occur without breaking metal lines (often due to the difficulty in maintaining step coverage), the surface must be flat and smooth. This process is called planarization, and can be carried out by a technique known as sacrificial etchback. An abrupt step (Figure 6.7.12.2a) is coated with a conformal layer of a low melting dielectric, e.g., borophosphorosilicate glass, BPSG

(Figure 6.7.12.2b), and subsequently a sacrificial organic resin (Figure 6.7.12.2c). The sample is then plasma etched such that the resin and dielectric are removed at the same rate. Since the plasma etch follows the contour of the organic resin, a smooth surface is left behind (Figure 6.7.12.2d). The planarization process thus reduces step height differentials significantly. In addition regions or valleys between individual metallization elements (vias) can be completely filled allowing for a route to producing uniformly flat surfaces, e.g., the BPSG film shown in Figure 6.7.12.1.

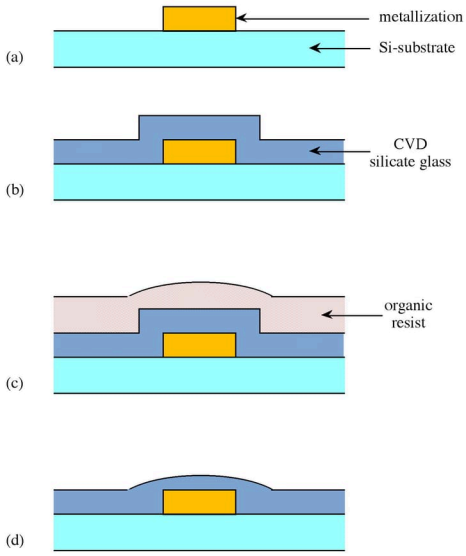


Figure 6.7.12.2: Schematic representation of the planarization process. A metallization feature (a) is CVD covered with silicate glass (b), and subsequently coated with an organic resin (c). After etching the resist a smooth silicate surface is produced (d).

The processes of planarization is vital for the development of multilevel structures in VLSI circuits. To minimize interconnection resistance and conserve chip area, multilevel metallization schemes are being developed in which the interconnects run in 3-dimensions.

Bibliography

- J. L. Vossen and W. Kern, *Phys. Today*, 1980, **33**, 26.
- S. K. Ghandhi, *VLSI Fabrication Principles, Silicon and Gallium Arsenide*, Wiley, Chichester, 2nd Ed. (1994).
- S. M. Sze, *Physics of Semiconductor Devices*, 2nd Edition, John Wiley & Sons, New York (1981).
- W. E. Beadle, J. C. C. Tsai, R. D. Plummer, *Quick Reference Manual for Silicon Integrated Cuircuit Technology*, Wiley, Chichester (1985).
- A. C. Adams and C. D. Capio, *J. Electrochem. Soc.*, 1981, **128**, 2630.

This page titled 6.7.12: Applications for Silica Thin Films is shared under a CC BY 1.0 license and was authored, remixed, and/or curated by LibreTexts.

6.8: Group 15 - The Pnictogens

This page titled 6.8: Group 15 - The Pnictogens is shared under a CC BY 3.0 license and was authored, remixed, and/or curated by Andrew R. Barron (CNX) via source content that was edited to the style and standards of the LibreTexts platform.

6.8.1: The Group 15 Elements- The Pnictogens

The elements

The Group 15 elements have a particular name *pnictogens*. Despite the modern IUPAC notation, the Group 15 elements are still referred to as Group V elements in particular by the semiconductor industry. Table 6.8.1.1 lists the derivation of the names of the Group 15 elements.

Table 6.8.1.1: Derivation of the names of each of the Group 15 (V) elements.

Element	Symbol	Name
Nitrogen	N	Latin *nitrogenium*, where *nitrum* (derived from Greek nitron) means *saltpetre*
Phosphorus	P	From the Greek *phosphoros* meaning *bringer of light*
Arsenic	As	Derived from Syriac *zarniqa* and Persian *zarnikh*, meaning *yellow orpiment*
Antimony	Sb	Greek *anti* and *monos* meaning *not alone*. The symbol Sb from Latin *stibium*
Bismuth	Bi	New Latin *bisemutum* from German *Wismuth*, meaning *white mass*

Note

According to the Oxford English Dictionary, the correct spelling of the element is phosphorus. The word phosphorous is the adjectival form of the P^{3+} valence. In the same way that sulfur forms sulfurous and sulfuric compounds, phosphorus forms phosphorous compounds (e.g., phosphorous acid) and P^{5+} valency phosphoric compounds (e.g., phosphoric acids and phosphates).

Discovery

Nitrogen

Nitrogen was discovered by Rutherford (Figure 6.8.1.1) in 1772. He called it *noxious air* or *fixed air* because there it had been known since the late 18th century that there was a fraction of air that did not support combustion. Nitrogen was also studied by Scheele (Figure 6.8.1.2), Cavendish (Figure 6.8.1.3), and Priestley (Figure 6.8.1.4), who referred to it as *burnt air* or *phlogisticated air*.

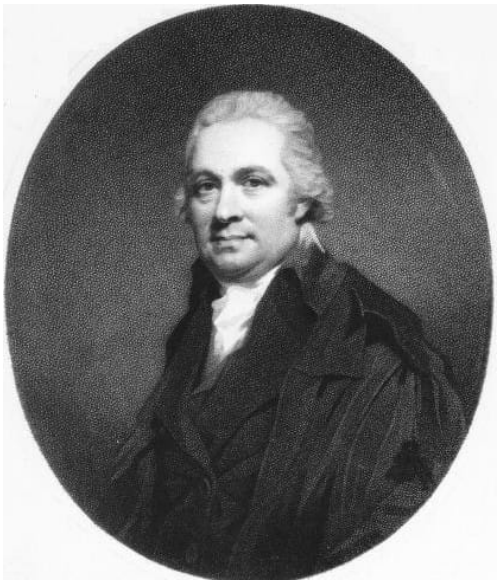


Figure 6.8.1.1: Scottish chemist and physician Daniel Rutherford (1749 - 1819).



Figure 6.8.1.2: Swedish chemist Carl Wilhelm Scheele (1742 – 1786). Isaac Asimov called him "hard-luck Scheele" because he made a number of chemical discoveries before others who are generally given the credit.



Figure 6.8.1.3: British scientist Henry Cavendish FRS (1731 - 1810).

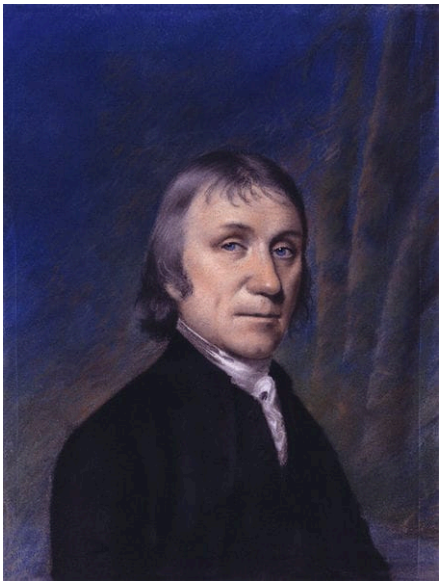


Figure 6.8.1.4: Portrait (by Ellen Sharples) of British clergyman natural philosopher, educator, and political theorist Joseph Priestley (1733 - 1804).

Phosphorus

German alchemist Hennig Brand (Figure 6.8.1.5) was experimenting with urine (which contains dissolved phosphates) in 1669. While attempting to create the fabled philosopher's stone (the legendary alchemical substance capable of turning base metals, such as lead, into gold) by the distillation of salts from urine, he produced a white material that glowed in the dark and burned with a brilliant light. He gave the substance the name *phosphorus mirabilis* (*miraculous bearer of light*). His process involved letting the urine stand for days then boiling it down to a paste which led to a white waxy substance, white phosphorus.



Figure 6.8.1.5: The discovery of phosphorus by German merchant and alchemist Hennig Brand (1630 - 1710) as depicted by Joseph Wright (with significant artistic license with regard to the brightness of the chemiluminescence).

Brand sold the recipe for 200 thaler (a silver coin from whose name the dollar is derived) to D Krafft who toured much of Europe showing it. During his journeys he met Robert Boyle (Figure 6.8.1.6) who without learning the details of the synthesis recreated and improved it by using sand in the reduction of the phosphate, (8.1.1).

$$4\ \mathrm{NaPO_3} + 2\ \mathrm{SiO_2} + 10\ \mathrm{C} \rightarrow 2\ \mathrm{Na_2SiO_3} + 10\ \mathrm{CO} + \mathrm{P_4} \tag{6.8.1.1}$$



Figure 6.8.1.6: British natural philosopher, chemist, physicist, and inventor Robert Boyle (1627 - 1691).

Arsenic

Arsenic sulfides and oxides were known since ancient times. Zosimos (*ca.* 300 AD) describes roasting *sandarach* (realgar, α-As_4S_4) to obtain cloud of arsenious oxide (As_2O_3) that he reduced to metallic arsenic (Figure 6.8.1.7).

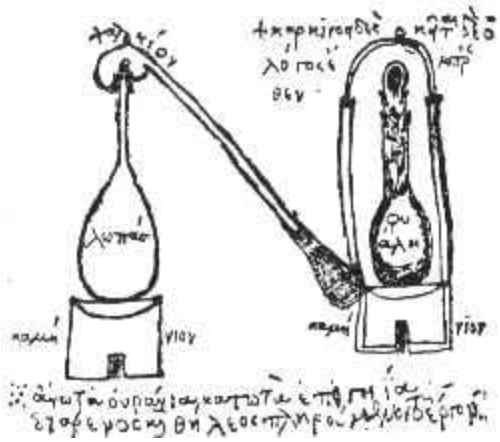


Figure 6.8.1.7: The distillation apparatus of Zosimos.

Antimony

Antimony(III) sulfide, Sb_2S_3 was known as early as 3000 BC. Pastes of Sb_2S_3 powder in fat were used as eye cosmetics in the Middle East. An artifact made of antimony dating to about 3000 BC was found at Tello (part of present-day Iraq), and copper objects plated with antimony from 2500 - 2200 BC have been found in Egypt. The first European description of a procedure for isolating antimony is in the book *De la pirotechnia* by Vannoccio Biringuccio (1480 - 1539).

Bismuth

Since bismuth was known in ancient times, no one person is credited with its discovery. However, the French chemist Claude François Geoffroy (1729 - 1753) demonstrated in 1753 that this metal is distinct from lead and tin.

Abundance

The abundance of the Group 15 elements is given in Table 6.8.1.2.

Table 6.8.1.2: Abundance of the Group 15 elements.

Element	Terrestrial abundance (ppm)
N	25 (Earth's crust), 5 (soil), 0.5 (sea water), 78 x 10^4 (atmosphere)
P	1000 (Earth's crust), 0.65 (soil), 60 x 10^{-3} (sea water), trace (atmosphere)
As	1.5 (Earth's crust), 10 (soil), 16 x 10^{-3} (sea water), trace (atmosphere)
Sb	0.2 (Earth's crust), 1 (soil), 0.3 x 10^{-3} (sea water)
Bi	48 x 10^{-3} (Earth's crust), 0.25 (soil), 400 x 10^{-6} (sea water)

Isotopes

The naturally abundant isotopes of the Group 15 elements are listed in Table 6.8.1.3.

Table 6.8.1.3: Abundance of the non-synthetic isotopes of the Group 15 elements.

Isotope	Natural abundance (%)
Nitrogen-14	99.634
Nitrogen-15	0.0366

Phosphorus-31	100
Arsenic-75	100
Antimony-121	57.36
Antimony-123	42.64
Bismuth-209	100%

Two radioactive isotopes of phosphorus (^{32}P and ^{33}P) have half-lives that make them useful for scientific experiments (14.262 and 25.34 days, respectively). ^{32}P is a β-emitter (1.71 MeV) and is used to produce radiolabeled DNA and RNA probes. Due to the high energy of the β particles which can penetrate skin and corneas, and because any ^{32}P ingested, inhaled, or absorbed is incorporated into bone and nucleic acids extreme care needs to be taken in handling. The lower energy β particles emitted from ^{33}P (0.25 MeV) make it useful for applications such as DNA sequencing.

While bismuth is traditionally regarded as the element with the heaviest stable isotope, ^{209}Bi, it had long been suspected to be unstable on theoretical grounds. In 2003 researchers at the Institut d'Astrophysique Spatiale in Orsay, France, measured the alpha emission half-life of ^{209}Bi to be 1.9×10^{19} years, over a billion times longer than the current estimated age of the universe!

Industrial production of the elements

Nitrogen is the largest constituent of the Earth's atmosphere (78.082% by volume, 75.3% by weight). It is created by fusion processes in stars, and is estimated to be the 7th most abundant element by mass in the universe. Industrial gas produced is by the fractional distillation of liquid air, or by mechanical means using gaseous air (i.e., pressurized reverse osmosis membrane or pressure swing adsorption). Commercial nitrogen is often a byproduct of air processing for industrial concentration of oxygen for steelmaking, etc.

White phosphorus was originally made commercially for the match industry in the 19th century, by distilling off phosphorus vapor from precipitated phosphates, mixed with ground coal or charcoal, (8.1.2). The precipitated phosphates were made from ground-up bones that had been de-greased and treated with strong acids. This process is, however, obsolete due to the submerged-arc furnace for phosphorus production was introduced to reduce phosphate rock. Calcium phosphate (phosphate rock) is heated to 1200 - 1500 °C with SiO_2 and coke (impure carbon) to produce vaporized tetraphosphorus, P_4.

$$\mathrm{Ca_{10}(PO_4)_6F_2 + 15\ C + 9\ SiO_2 \rightarrow 6\ P_{n(g)} + 9\ [(CaO.SiO_2)] + CaF_2 + 15\ CO_{(g)}} \tag{6.8.1.2}$$

Physical properties

The physical properties of the Group 15 elements (Table 6.8.1.3) encompasses a gas (N_2), a non-metallic solid (P_4), metalloids (As and Sb), and a metal (Bi).

Table 6.8.1.3: Selected physical properties of the Group 15 elements.

Element	Mp (°C)	Bp (°C)	Density (g/cm^3)
N	-210.00	-195.79	1.251 g/L (0 °C @ 101.325 kPa)
P	44.2 (white), 610 (black)	280.5 (white), 416 - 590 (sub., red), 620 (sub, violet)	1.823 (white), 2.2 - 2.34 (red), 2.36 (violet), 2.69 (black)
As	817	615 (sub.)	5.727
Sb	630.63	1587	6.697 (solid), 6.53 (liquid)
Bi	271.5	1564	9.78 (solid), 10.05 (liquid)

Vapor phase

Nitrogen forms a dimer in the vapor phase with a triple bond (Figure 6.8.1.8). In the vapor phase above 800 °C tetraphosphorus (P_4) is partially dissociated to P_2.

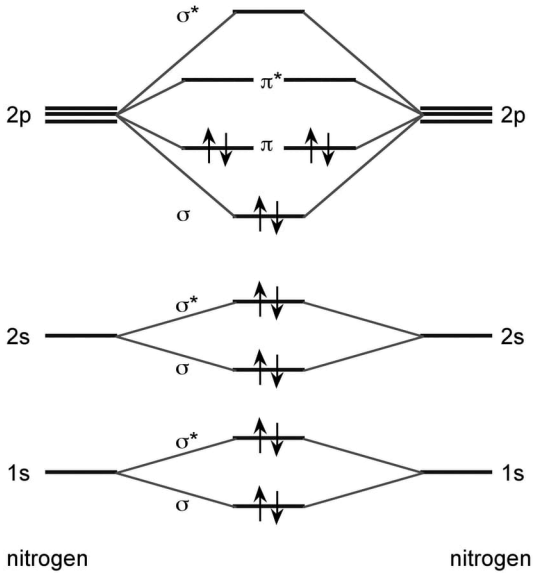


Figure 6.8.1.8: Molecular orbital diagram for the formation of N_2.

Solid state

Phosphorus forms a number of allotropes with very different properties (Figure 6.8.1.9). Red phosphorus is an intermediate phase between the white and violet forms. Scarlet phosphorus is obtained by allowing a solution of white phosphorus in carbon disulfide to evaporate in sunlight. Black phosphorus is formed by heating white phosphorus under high pressures (*ca*. 12,000 atmospheres).



Figure 6.8.1.9: Images of (left to right) white, red, violet and black allotropes of phosphorus.

White phosphorus has two forms, low-temperature β form and high-temperature α form; both of which contain the P4 tetrahedron (Figure 6.8.1.10). White phosphorus is the least stable, the most reactive, most volatile, less dense, and most toxic of the allotropes.

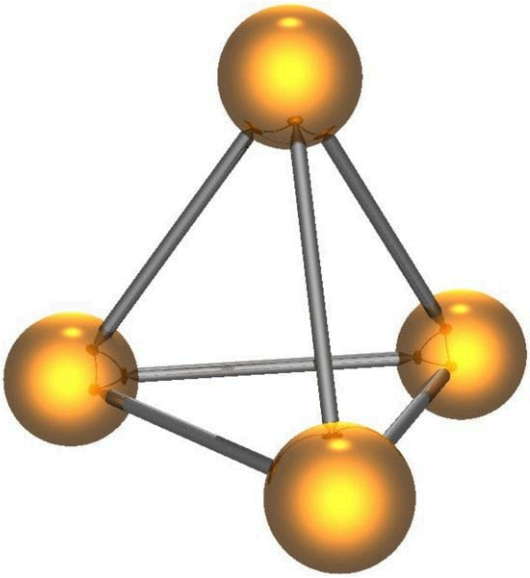


Figure 6.8.1.10: The structure of the P_4 molecule in white phosphorus.

The structural relationship between white and red phosphorus involves breaking one of the P-P bonds in the P_4 unit and forming a bond with a neighboring tetrahedron to give a chain structure (Figure 6.8.1.11). Red phosphorus is formed by heating white phosphorus to 250 °C or by exposing white phosphorus to sunlight. Actually red phosphorus is not a single allotrope, but rather an intermediate phase between the white and violet phosphorus, and most of its properties have a range of values (Table 6.8.1.3).

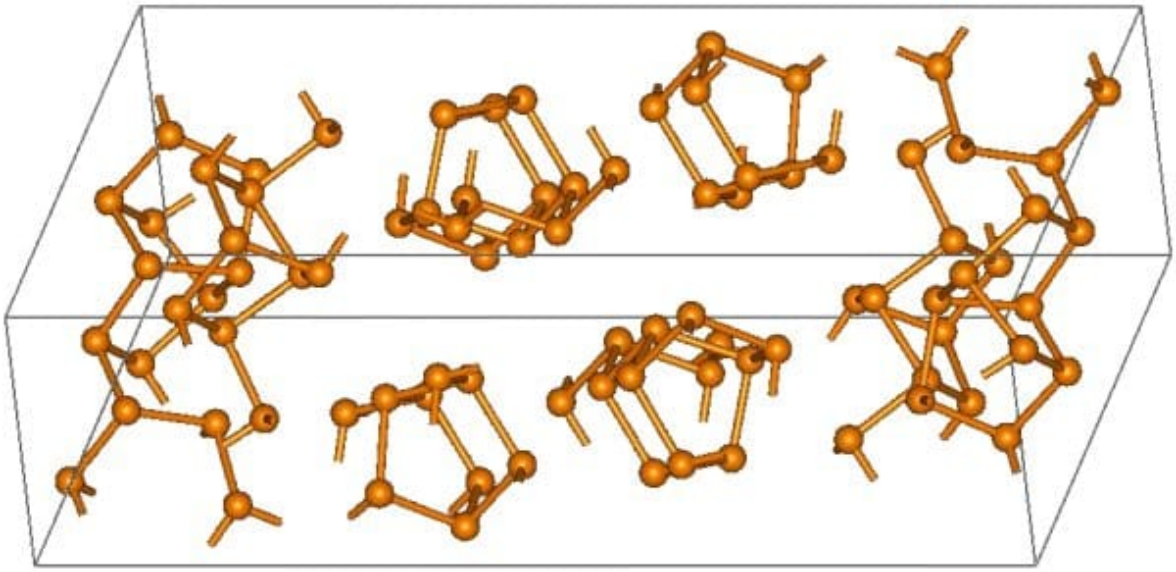


Figure 6.8.1.11: Crystal unit cell of red phosphorus.

Violet phosphorus (Figure 6.8.1.12) is the thermodynamic stable form of phosphorus that is produced by heating red phosphorus above 550 °C. Due to the synthesis being developed by Johann Hittorf (Figure 6.8.1.13) it is sometimes known as *Hittorf*'s *phosphorus*.

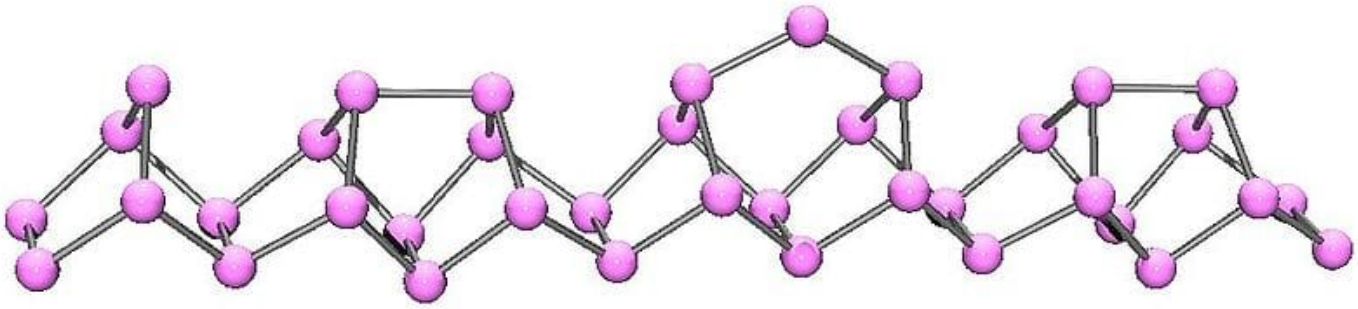


Figure 6.8.1.12: Structure of violet (Hittorf's) phosphorus.



Figure 6.8.1.13: German physicist Johann Wilhelm Hittorf (1824 - 1914).

Black phosphorus is the least reactive allotrope and the thermodynamic stable form below 550 °C. It is also known as β-metallic phosphorus and has a structure somewhat resembling that of graphite (Figure 6.8.1.14).

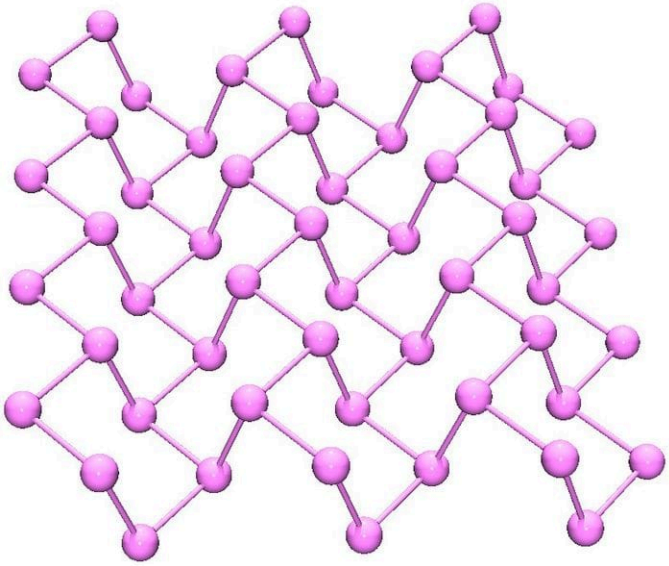


Figure 6.8.1.14: Crystal structure of black phosphorus.

In a similar manner to phosphorus, arsenic has several allotropes some of which a structurally related to those of phosphorus.

Grey arsenic has a structure similar to black phosphorus (Figure 6.8.1.10). Yellow arsenic (As_4) is soft and waxy with a structure similar to too P_4 (Figure 6.8.1.14). Finally, black arsenic is similar in structure to red phosphorus (Figure 6.8.1.11). Antimony and bismuth are both traditional metals and have trigonal hexagonal structures (a = 4.299, c = 11.25 Å, and a = 4.537, c = 11.838 Å, respectively).

Bibliography

- V. Biringuccio, *The Pirotechnia of Vannoccio Biringuccio: The Classic Sixteenth-Century Treatise on Metals and Metallurgy*, Dover Publications (1990).

This page titled 6.8.1: The Group 15 Elements- The Pnictogens is shared under a CC BY 3.0 license and was authored, remixed, and/or curated by Andrew R. Barron (CNX) via source content that was edited to the style and standards of the LibreTexts platform.

6.8.2: Reaction Chemistry of Nitrogen

Despite nitrogen being the inert component of the Earth's atmosphere, dinitrogen undergoes a range of reactions, although it only reacts with a few reagents under standard temperature and pressure. Nitrogen reacts with oxygen in an electric arc, (8.2.1), both in the laboratory and within lightening strikes.

$$\mathrm{N_2 + O_2 \rightarrow 2\ NO} \tag{6.8.2.1}$$

The synthesis of ammonia is accomplished by the Harber process, using an iron oxide (Fe_3O_4) catalyst, (8.2.2), at about 500 °C and 200 atmospheres pressure.

$$\mathrm{N_2 + 3\ H_2 \rightarrow 2\ NH_3} \tag{6.8.2.2}$$

Nitrogen reacts with lithium metal at room temperature to form the nitride, (8.2.3). Magnesium also burns in nitrogen, forming magnesium nitride, (8.2.4).

$$\mathrm{6\ Li + N_2 \rightarrow 2\ Li_3N} \tag{6.8.2.3}$$

$$\mathrm{3\ Mg + N_2 \rightarrow Mg_3N_2} \tag{6.8.2.4}$$

Nitrogen forms complexes with transition metals yielding nitrogeno complexes, (8.2.5). Under some conditions these complexes react to give ammonia, (8.2.6), and as such may give a hint to the action of nitrogenase in which molybdenum in the active site.

$$\mathrm{[(NH_3)_5Ru^{\mathit{II}}(H_2O)]^{2+} + N_2 \rightarrow [(NH_3)_5Ru^{\mathit{II}}(N_2)]^{2+}} \tag{6.8.2.5}$$

$$\mathrm{[W(N_2)_2(PR_3)_4] \xrightarrow{H_2SO_4/MeOH} 2\ NH_3 + N_2\uparrow + W^{\mathit{VI}}\ compounds} \tag{6.8.2.6}$$

This page titled 6.8.2: Reaction Chemistry of Nitrogen is shared under a CC BY 3.0 license and was authored, remixed, and/or curated by Andrew R. Barron (CNX) via source content that was edited to the style and standards of the LibreTexts platform.

6.8.3: Hydrides

Trihydrides of the Group 15 Elements

All five of the Group 15 elements form hydrides of the formula EH_3. Table 6.8.3.1 lists the IUPAC names along with those in more common usage.

Table 6.8.3.1: Traditional and IUPAC (International Union of Pure and Applied Chemistry) names for the Group 15 hydrides.

Compound	Traditional name	IUPAC name
NH_3	Ammonia	Azane
PH_3	Phosphine	Phosphane
AsH_3	Arsine	Arsane
SbH_3	Stibine	Stibane
BiH_3	Bismuthine	Bismuthane

The boiling point and melting point increase increases going down the Group (Table 6.8.3.2) with increased molecular mass, with the exception of NH_3 whose anomalously high melting and boiling points (Figure 6.8.3.1) are a consequence of strong N-H···H hydrogen bonding. A similar (and stronger) effect is observed for the Group 16 hydrides (H_2E).

Table 6.8.3.2: Selected physical properties of Group 15 hydrides.

Compound	Mp (°C)	Bp (°C)	ΔH_f (kJ/mol)	E-H bond energy (kJ/mol)	H-E-H bond angle (°)
NH_3	-77.7	-33.35	-46.2	391	107
PH_3	-133	-87.7	9.3	322	93.5
AsH_3	-116.3	-55	172.2	247	92
SbH_3	-88	-17.1	142.8	255	91.5

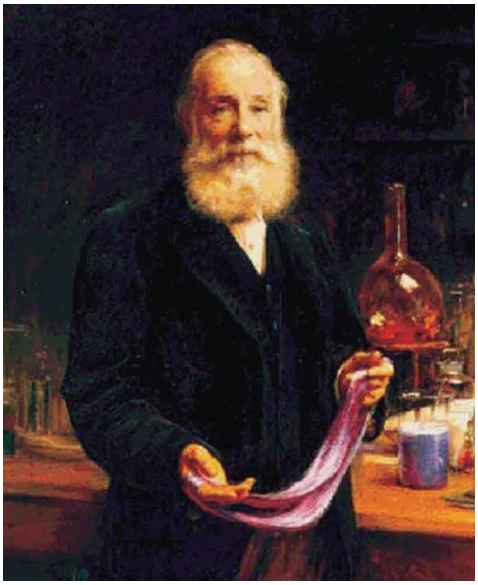


Figure 6.8.3.1: Plot of melting and boiling points of EH_3 (E = N, P, As, and Sb) as a function of molecular mass.

The E-H bond strengths decrease down the group and this correlates with the overall stability of each compound (Table 6.8.3.2). The H-E-H bond angles (Table 6.8.3.2) also decrease down the Group. The H-E-H bond angle is expected to be a tetrahedral ideal of 109.5°, but since lone pairs repel more than bonding pairs, the actual angle would be expected to be slightly smaller. Two possible explanations are possible for the difference between NH_3 and the other hydrides.

1. The N-H bond is short (1.015 Å) compared to the heavier analogs, and nitrogen is more electronegative than hydrogen, so the bonding pair will reside closer to the central atom and the bonding pairs will repel each other opening the H-N-H angle more than observed for PH_3, etc.
2. The accessibility of the 2*s* and 2*p* orbitals on nitrogen allows for hybridization and the orbitals associated with N-H bonding in NH_3 are therefore close to sp^3 in character, resulting in a close to tetrahedral geometry. In contrast, hybridization of the ns and n*p* orbitals for P, As, etc., is less accessible, and as a consequence the orbitals associated with P-H bonding in PH_3 are closer to p in character resulting in almost 90° H-P-H angle. The lower down the Group the central atom the less hybridization that occurs and the closer to pure p-character the orbitals on E associated with the E-H bond.

Ammonia

Ammonia (NH_3) is a colorless, pungent gas (bp = -33.5 °C) whose odor can be detected at concentrations as low 20 – 50 ppm. Its high boiling point relative to its heavier congeners is indicative of the formation of strong hydrogen bonding. The strong hydrogen bonding also results in a high heat of vaporization (23.35 kJ/mol) and thus ammonia can be conveniently used as a liquid at room temperature despite its low boiling point.

WARNING

Ammonia solution causes burns and irritation to the eyes and skin. The vapor causes severe irritation to the respiratory system. If swallowed the solution causes severe internal damage.

Synthesis

Ammonia is manufactured on the industrial scale by the Haber process using the direct reaction of nitrogen with hydrogen at high pressure (10^2 – 10^3 atm) and high temperature (400 – 550 °C) over a catalyst (e.g., α-iron), (8.3.1).

$$\mathrm{N_2 + 3\ H_2 \rightarrow 2\ NH_3} \tag{6.8.3.1}$$

On the smaller scale ammonia is prepared by the reaction of an ammonium salt with a base, (8.3.2), or hydrolysis of a nitride, (8.3.3). The latter is a convenient route to ND_3 by the use of D_2O.

$$\mathrm{NH_4X + OH^- \rightarrow NH_3 + H_2O + X^-} \tag{6.8.3.2}$$

$$\mathrm{Mg_3N_2 + H_2O \rightarrow 3\ Mg(OH)_2 + 2\ NH_3} \tag{6.8.3.3}$$

Structure

The nitrogen in ammonia adopts sp^3 hybridization, and ammonia has an umbrella structure (Figure 6.8.3.2) due to the stereochemically active lone pair.

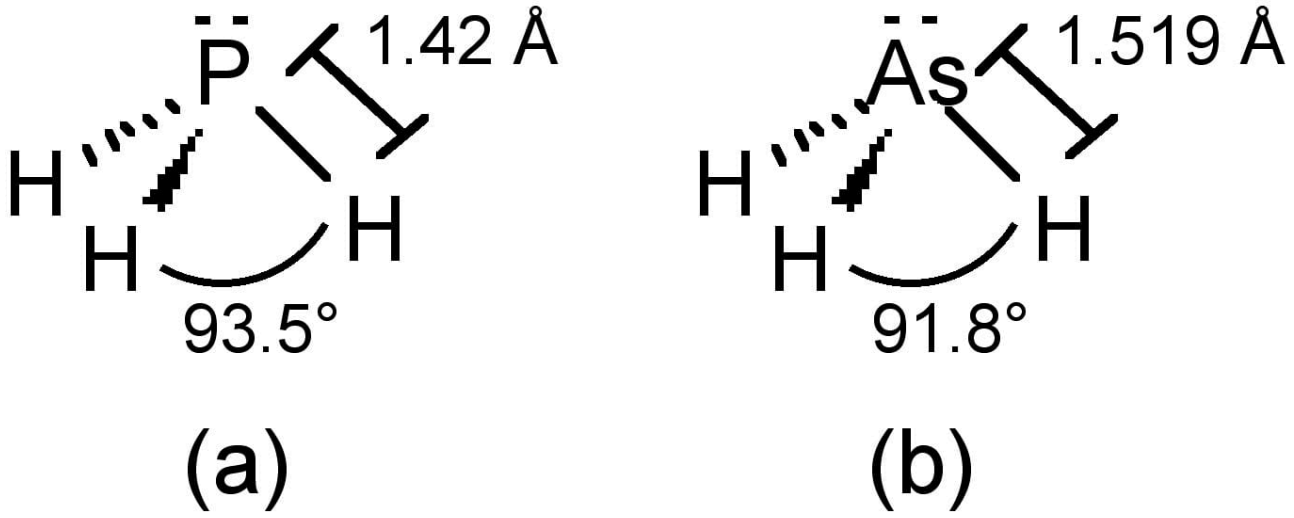
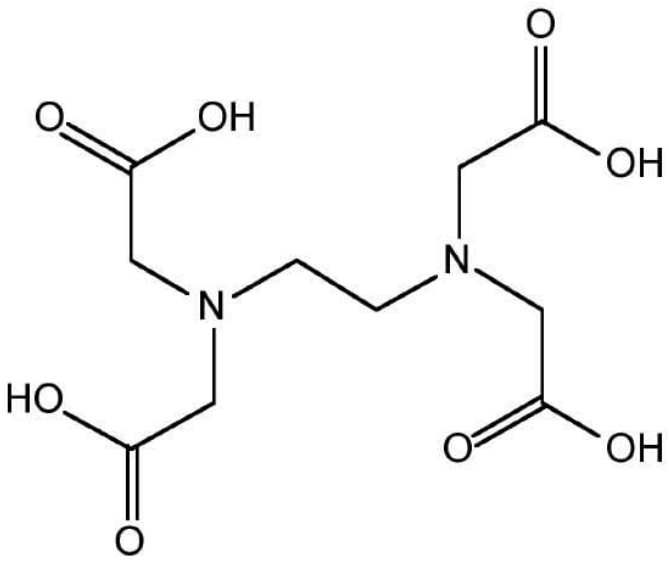


Figure 6.8.3.2: The structure of ammonia.

The barrier to inversion of the umbrella is very low (E_a = 24 kJ/mol) and the inversion occurs 100's of times a second. As a consequence it is not possible to isolate chiral amines in the same manner that is possible for phosphines.



In a similar manner to water, (8.3.4), ammonia is a self-ionizing, (8.3.5); however, the equilibrium constant (K = 10^{-33}) is much lower than water (K = 10^{-14}). The lower dielectric constant of ammonia (16.5 @ 20 °C) as compared to water (80.4 @ 20 °C) means that ammonia is not as good as water as a solvent for ionic compounds, but is better for covalent organic compounds.

$$2\ \mathrm{H_2O} \rightleftharpoons \mathrm{H_3O^+} + \mathrm{OH^-} \tag{6.8.3.4}$$

$$2\ \mathrm{NH_3} \rightleftharpoons \underset{\text{ammonium}}{\textext{}NH_4^+}\t+\und\terset{}{}extamide\mathrm{NH_2^-} \tag{6.8.3.5}$$

Reactions

The similarity of ammonia and water means that the two compounds are miscible. In fact, ammonia forms a series of solid hydrates, analogous to ice in which hydrogen bonding defines the structures (Figure 6.8.3.3). Several hydrates of ammonia are known, including: $NH_3.2H_2O$ (ammonia dihydrate, ADH), $NH_3.H_2O$ (ammonia monohydrate, AMH), and $2NH_3.2H_2O$ (ammonia

hemihydrate, AHH).

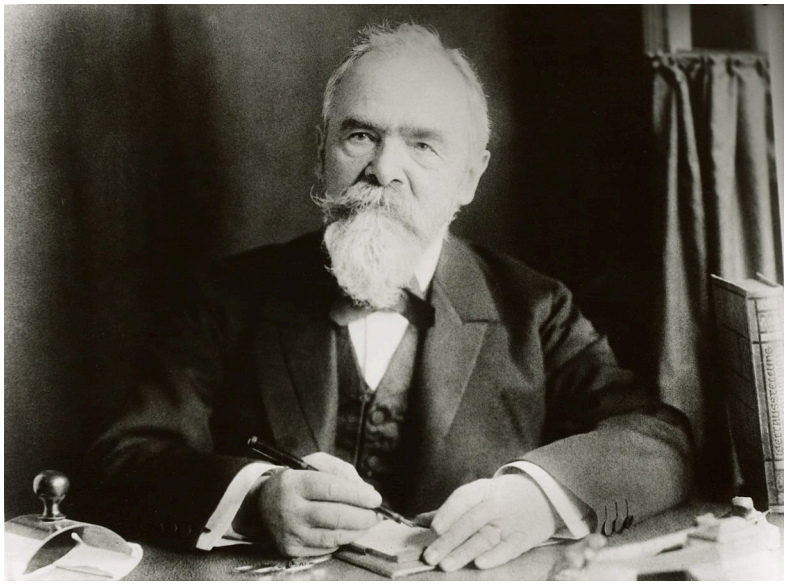


Figure 6.8.3.3: The crystal structure of ammonia monohydrate (ANH-II) with hydrogen atoms omitted. Adapted from A. D. Fortes, E. Suard, M. -H. Lemée-Cailleau, C. J. Pickard, and R. J. Needs, *J. Am. Chem. Soc.*, 2009, **131**, 13508. Copyright: American Chemical Society (2009).

It should be noted that these hydrates do not contain discrete NH_4^+ or OH^- ions, indicating that ammonium hydroxide does not exist as a discrete species despite the common useage of the name. In aqueous solution, ammonia is a weak base (pK_b = 4.75), (8.3.6).

$$\mathrm{NH_{3(aq)} + H_2O_{(l)} \rightleftharpoons NH_{4(aq)}^{+} + OH_{(aq)}^{-}} \tag{6.8.3.6}$$

Note

Ammonia solutions commonly used in the laboratory is a 35% solution in water. In warm weather the solution develops pressure and the cap must be released with care. The 25% solution sold commercially (for home use) is free from this problem.

Ammonia is a Lewis base and readily forms Lewis acid-base complexes with both transition metals, (8.3.7), and main group metals (Figure 6.8.3.4).

$$\mathrm{[Ni(H_2O)_6]^{2+} + 6NH_3 \rightleftharpoons [Ni(NH_3)_6]^{2+} + 6H_2O} \tag{6.8.3.7}$$

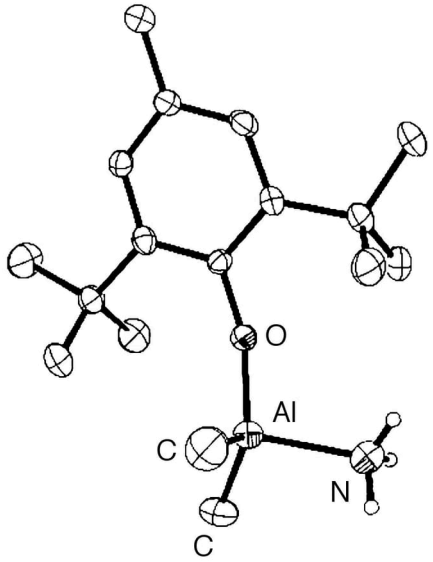


Figure 6.8.3.4: The molecular structure of $AlMe_2(BHT)NH_3$. Hydrogen atoms, except those attached to nitrogen, are omitted for clarity. Adapted from M. D. Healy, J. T. Leman, and A. R. Barron, *J. Am. Chem. Soc.*, 1991, **113**, 2776. Copyright: American Chemical Society.

The formation of stable ammonia complexes is the basis of a simple but effective method of detection: Nessler's reagent, (8.3.8). Using a 0.09 mol/L solution of potassium tetraiodomercurate(II), $K_2[HgI_4]$, in 2.5 mol/L potassium hydroxide. A yellow coloration indicates the presence of ammonia: at higher concentrations, a brown precipitate may form. The sensitivity as a spot test is about 0.3 µg NH_3 in 2 µL.

$$NH_4^+ + 2[HgI_4]^{2-} + 4OH^- \rightarrow HgO\cdot Hg(NH_2)I + 7I^- + 3H_2O \tag{6.8.3.8}$$

Ammonia forms a blue solution with Group 1 metals. As an example, the dissolution of sodium in liquid ammonia results in the formation of solvated Na^+ cations and electrons, (8.3.9) where solv = NH_3. The solvated electrons are stable in liquid ammonia and form a complex: $[e^-(NH_3)_6]$.

$$Na_{(s)} \rightarrow Na_{(solv)} \rightleftharpoons Na^+_{(solv)} + e^-_{(solv)} \tag{6.8.3.9}$$

It is this solvated electron that gives the strong reducing properties of the solution as well as the characteristic signal in the ESR spectrum associated with a single unpaired electron. The blue color of the solution is often ascribed to these solvated electrons; however, their absorption is in the far infra-red region of the spectrum. A second species, Na^-(solv), is actually responsible for the blue color of the solution.

$$2Na_{(solv)} \rightleftharpoons Na^+_{(solv)} + Na^-_{(solv)} \tag{6.8.3.10}$$

The reaction of ammonia with oxygen is highly favored, (8.3.11), and the flammability limit of ammonia is 16 – 25 vol%. If the reaction is carried out in the presence of a catalyst (Pt or Pd) the reaction can be limited to the formation of nitric oxide (NO), (8.3.12).

$$4NH_3 + 3O_2 \rightarrow 2N_2 + 6H_2O \tag{6.8.3.11}$$

$$4NH_3 + 5O_2 \rightarrow 4NO + 6H_2O \tag{6.8.3.12}$$

Ammonium salts

The ammonium cation (NH_4^+) behaves in a similar manner to the Group 1 metal ions. The solubility and structure of ammonium salts particularly resembles those of potassium and rubidium because of their relative size (Table 6.8.3.3). One difference is that ammonium salts often decompose upon heating, (8.3.13).

$$NH_4Cl_{(s)} \rightarrow NH_{3(g)} + HCl_{(g)} \tag{6.8.3.13}$$

Table 6.8.3.3: Ionic radius of the ammonium ion compared to those of potassium and rubidium.

Cation	Ionic radius (Å)
K^+	1.33
NH_4^+	1.43
Rb^+	1.47

The decomposition of ammonium salts of oxidizing acids can often be violent to highly explosive, and they should be treated with care. For example, while ammonium dichromate, $(NH_4)_2Cr_2O_7$, decomposes to give a volcano (Figure 6.8.3.5), ammonium permanganate, $NH_4[MnO_4]$, is friction sensitive and explodes at 60 °C. Ammonium nitrate, $NH_4[NO_3]$, can cause fire if contacted with a combustible material and is a common ingredient in explosives since it acts as the oxygen source due to its positive oxygen balance, i.e., the compound liberates oxygen surplus to its own needs upon decomposition, (8.3.14).

$$\mathrm{NH_4[NO_3] \rightarrow H_2O + N_2 + O} \tag{6.8.3.14}$$



Figure 6.8.3.5: A laboratory demonstration of an ammonium dichromate volcano.

Bibliography

- A. R. Barron, *The Detonator*, 2009, **36**, 60.
- A. D. Fortes, E. Suard, M. -H. Lemée-Cailleau, C. J. Pickard, and R. J. Needs, *J. Am. Chem. Soc.*, 2009, **131**, 13508.
- M. D. Healy, J. T. Leman, and A. R. Barron, *J. Am. Chem. Soc.*, 1991, **113**, 2776.
- A. I. Vogel and G. Svehla, *Textbook of Macro and Semimicro Qualitative Inorganic Analysis*, Longman, London (1979).

Liquid Ammonia as a Solvent

Ammonia has a reasonable liquid range (-77 to –33 °C), and as such it can be readily liquefied with dry ice (solid CO_2, T_{sub} = -78.5 °C), and handled in a thermos flask. Ammonia's high boiling point relative to its heavier congeners is indicative of the formation of strong hydrogen bonding, which also results in a high heat of vaporization (23.35 kJ/mol). As a consequence ammonia can be conveniently used as a liquid at room temperature despite its low boiling point.

Liquid ammonia is a good solvent for organic molecules (e.g., esters, amines, benzene, and alcohols). It is a better solvent for organic compounds than water, but a worse solvent for inorganic compounds. The solubility of inorganic salts is highly dependant on the identity of the counter ion (Table 6.8.3.4).

Table 6.8.3.4: General solubility of inorganic salts in liquid ammonia as a function of the counter ion.

Soluble in liquid NH_3	Generally insoluble in liquid NH_3
SCN^-, I^-, NH_4^+, NO_3^-, NO_2^-, ClO_4^-	F^-, Cl^-, Br^-, CO_3^{2-}, SO_4^{2-}, O^{2-}, OH^-, S^{2-}

The difference in solubility of inorganic salts in ammonia as compared to water, as well as the lower temperature of liquid ammonia, can be used to good advantage in the isolation of unstable compounds. For example, the attempted synthesis of ammonium nitrate by the reaction of sodium nitrate and ammonium chloride in water results in the formation of nitrogen and water due to the decomposition of the nitrate, (8.3.15). By contrast, if the reaction is carried out in liquid ammonia, the sodium chloride side product is insoluble and the ammonium nitrate may be isolated as a white solid after filtration and evaporation below its decomposition temperature of 0 °C, (8.3.16).

$$NaNO_2 + NH_4Cl \xrightarrow{H_2O} NaCl + NH_4(NO_2) \rightarrow N_2 + 2H_2O \tag{6.8.3.15}$$

$$NaNO_2 + NH_4Cl \xrightarrow{NH_3} NaCl \downarrow + NH_4(NO_2) \tag{6.8.3.16}$$

Ammonation

Ammonation is defined as a reaction in which ammonia is added to other molecules or ions by covalent bond formation utilizing the unshared pair of electrons on the nitrogen atom, or through ion-dipole electrostatic interactions. In simple terms the resulting *ammine* complex is formed when the ammonia is acting as a Lewis base to a Lewis acid, (8.3.17) and (8.3.18), or as a ligand to a cation, e.g., $[Pt(NH_3)_4]^{2+}$, $[Ni(NH_3)_6]^{2+}$, $[Cr(NH_3)_6]^{3+}$, and $[Co(NH_3)_6]^{3+}$.

$$SiF_4 + 2NH_3 \rightarrow SiF_4(NH_3)_2 \tag{6.8.3.17}$$

$$BF_3 + NH_3 \rightarrow BF_3(NH_3) \tag{6.8.3.18}$$

Ammonolysis

Ammonolysis with ammonia is an analogous reaction to hydrolysis with water, i.e., a dissociation reaction of the ammonia molecule producing H^+ and an NH_2^- species. Ammonolysis reactions occur with inorganic halides, (8.3.18) and (8.3.19), and organometallic compounds, (8.3.20). In both case the NH_2^- moiety forms a substituent or ligand.

$$P(O)Cl_3 + 6NH_3 \rightarrow P(O)(NH_2)_3 + 3NH_4Cl \tag{6.8.3.19}$$

$$BCl_3 + 6NH_3 \rightarrow B(NH_2)_3 + 3NH_4Cl \tag{6.8.3.20}$$

$$Al(CH_3)_3 + NH_3 \rightarrow \frac{1}{n}[(H_3C)_2Al(NH_2)]_n + CH_4 \tag{6.8.3.21}$$

The reaction of esters, (8.3.21), and aryl halides, (8.3.22), are also examples of ammonolysis reactions.

$$RC(O)OR' + NH_3 \rightarrow RC(O)NH_2 + R'OH \tag{6.8.3.22}$$

$$C_6H_5Cl + 2NH_3 \rightarrow C_6H_5NH_2 + NH_4Cl \tag{6.8.3.23}$$

Homoleptic amides

A homoleptic compound is *a compound with all the ligands being identical*, e.g., $M(NH_2)_n$. A general route to homoleptic amide compounds is accomplished by the reaction of a salt of the desired metal that is soluble in liquid ammonia (Table 6.8.3.4) with a soluble Group 1 amide. The solubility of the Group 1 amides is given in Table 6.8.3.5. Since all amides are insoluble (except those of the Group 1 metals) are insoluble in liquid ammonia, the resulting amide may be readily isolated, e.g., (8.3.23) and (8.3.24).

$$Mn(SCN)_2 + 2KNH_2 \rightarrow Mn(NH_2)_2 \downarrow + 2KSCN \tag{6.8.3.24}$$

$$Cr(NO_3)_3 + 3KNH_2 \rightarrow Cr(NH_2)_3 \downarrow + 3KNO_3 \tag{6.8.3.25}$$

Table 6.8.3.5: Solubility of Group amides in liquid ammonia.

Amide	Solubility in liquid ammonia
$LiNH_2$	Sparingly soluble
$NaNH_2$	Sparingly soluble
KNH_2	Soluble
$RbNH_2$	Soluble
$CsNH_2$	Soluble

Redox reactions

Ammonia is poor as an oxidant since it is relatively easily oxidized, e.g., (8.3.25) and (8.3.26). Thus, if it is necessary to perform an oxidation reaction ammonia is not a suitable solvent; however, it is a good solvent for reduction reactions.

$$4\mathrm{NH_3} + 5\mathrm{O_2} \rightarrow 4\mathrm{NO} + 6\mathrm{H_2O} \tag{6.8.3.26}$$

$$2\mathrm{NH_3} + 3\mathrm{CuO} \rightarrow \mathrm{N_2} + 3\mathrm{H_2O} + 3\mathrm{Cu} \tag{6.8.3.27}$$

Liquid ammonia will dissolve Group 1 (alkali) metals and other electropositive metals such as calcium, strontium, barium, magnesium, aluminum, europium, and ytterbium. At low concentrations (ca. 0.06 mol/L), deep blue solutions are formed: these contain metal cations and solvated electrons, (8.3.27). The solvated electrons are stable in liquid ammonia and form a complex: $[e^-(NH_3)_6]$.

$$\mathrm{Na_{(s)}} \rightarrow \mathrm{Na_{(solv)}} \rightleftharpoons \mathrm{Na^+_{(solv)}} + \mathrm{e^-_{(solv)}} \tag{6.8.3.28}$$

The solvated electrons provide a suitable and powerful reducing agent for a range of reactions that are not ordinarily accomplished, e.g., (8.3.28) and (8.3.29).

$$[\mathrm{Ni(CN)_4}]^{2-} + 2\mathrm{e^-_{(solv)}} \rightarrow [\mathrm{Ni(CN)_4}]^{4-} \tag{6.8.3.29}$$

\[\rm Co_2(CO)_8 + 2 e^-_{(solv)} \rightarrow 2 [Co(CO)_4]^-

Ammonia: From Uses in Agriculture and Beer Production to Prolonging the First World War

One of the cornerstones of the industrial expansion in Germany between 1870 and 1910 (when the population grew from 41 million to 66 million) was the chemicals industry. In particular companies such as Badische Anilin und Soda Fabrik (Baden Aniline and Soda Factory or BASF) had developed their business on the formation of synthetic dyes derived from the chemicals in coal tar.

Coal tar was formed as a by-product of the gasification of coal. A key ingredient of coal tar is naphtha (Table 6.8.3.6) that was used by the rubber industry; however, the remainder was disposed off. It was not long before chemists started to investigate the constituents present in coal tar. One of the first discoveries was by a chemistry student at the Royal College of Chemistry (now Imperial College) in London, William Perkin (Figure 6.8.3.6), who isolated the first synthetic dye: mauveine (Figure 6.8.3.7). This discovery led to an explosion in the chemical industry based on the extraction of compounds from coal tar, which was an essentially free waste product from every gasworks. Nowhere was this research more commercially driven that in Germany.

Table 6.8.3.6: The typical physical properties of naphtha.

Property	Typical value
Molecular weight	100 - 215 g/mol
Specific gravity	0.75 - 0.85 g/cm3
Boiling point	160 - 220 °C

Vapor pressure	5 mmHg
Solubility in water	Insoluble

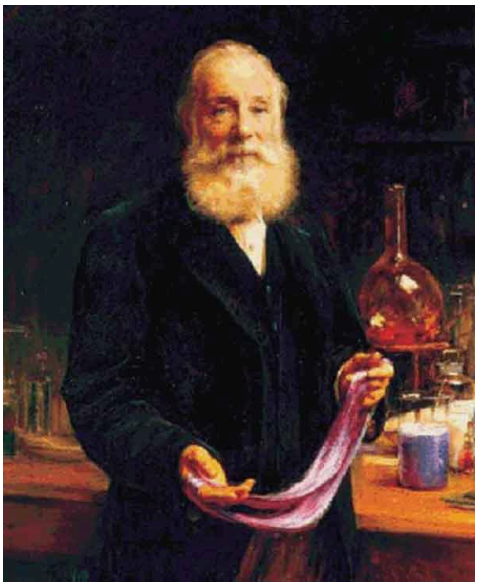


Figure 6.8.3.6: A portrait of English chemist Sir William Perkin (1838 - 1907) holding a sample of cloth dyed with his discovery, mauveine, which is often called *Perkin's purple*.

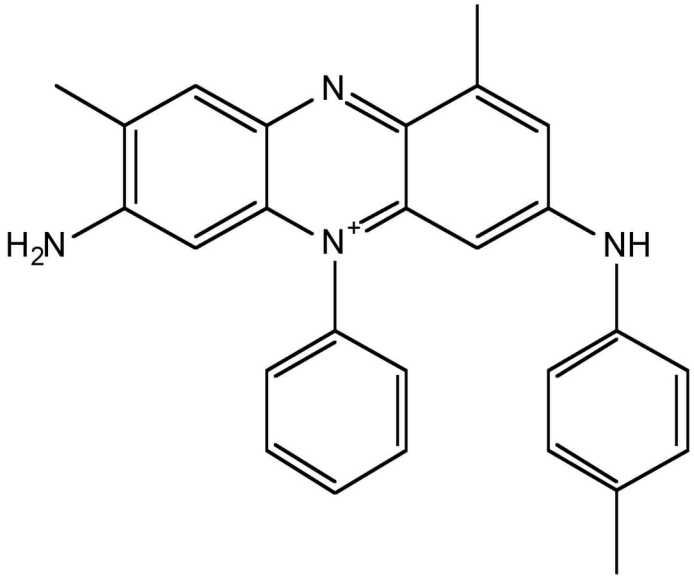


Figure 6.8.3.7: The structure of mauveine-B.

The rapid increase in the German population also put a strain on the countries food resources. What compounded this issue was that the aristocratic Junkers families of East Prussia who owned much of the land in what was known as *Germany's breadbasket*. Junkers grew rye on their estates because the soil was too light for wheat, and since rye was fertilized with potash (potassium oxide, K_2O) of which Germany had vast resources. However, in 1870 grain from the US was becoming cheaper and thus competitive with German rye. To protect their profits the Junkers demanded both subsidies for the export of rye and tariffs for the import of wheat. The result of this was that all the German rye was leaving the country and there was not enough wheat being produced to satisfy the needs of the local population. Sufficient wheat could be grown in Germany if a suitable fertilizer was available.

Sodium nitrate ($NaNO_3$), also known as *Chile saltpeter*, was the most common fertilizer. Unfortunately, by 1900 the deposits looked to be depleted and an alternative was needed. The alternative was found as a component in coal tar. It was known that one of the chemicals that caused the *stink* associated with coal gas and coal tar was ammonia (NH_3). Chemist George Fownes (Figure

6.8.3.8) had suggested that ammonia be turned into a salt and used as a fertilizer. Unfortunately, the amount of ammonia that could be separated from coal tar was still insufficient, so if ammonia could be made on a large enough scale, then large-scale manufacture of a fertilizer could be realized.



Figure 6.8.3.8: British chemist George Fownes, FRS (1815 – 1849).

In 1909 Fritz Haber (Figure 6.8.3.9) presented a method of ammonia synthesis to BASF. His work in collaboration with Carl Bosch (Figure 6.8.3.10) resulted in the process known as the Haber-Bosch process in which nitrogen and hydrogen are mixed at high temperature (600 °C) under pressure (200 atm) over an osmium catalyst, (8.3.30).

$$\mathrm{N_2 + 3H_2 \xrightarrow{Os\ cat} 6NH_3} \tag{6.8.3.30}$$

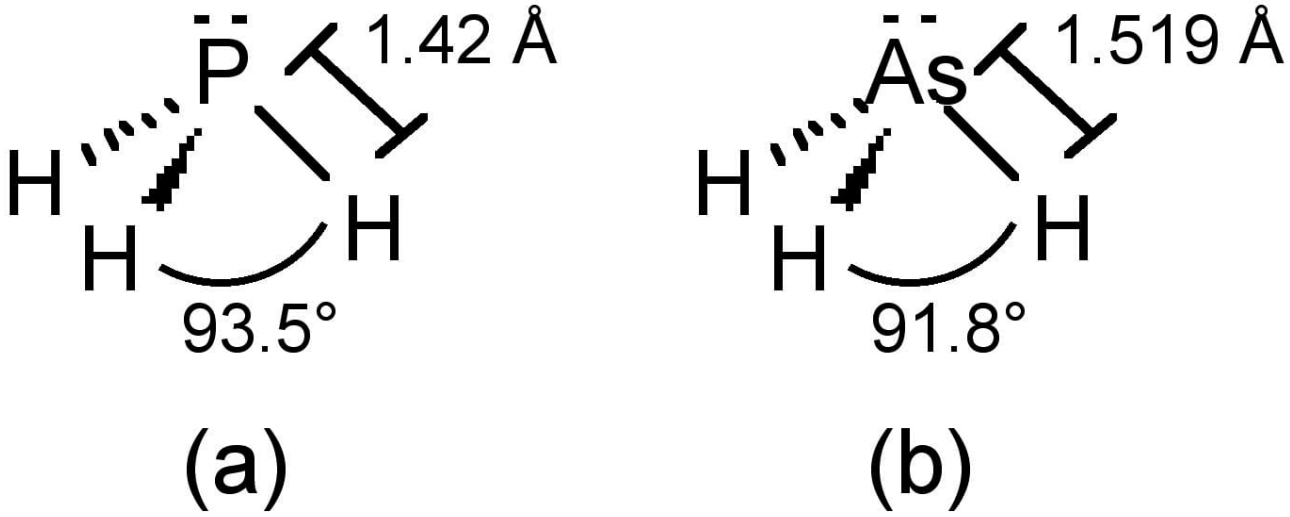


Figure 6.8.3.9: German chemists Fritz Haber (1868 –1934) who received the Nobel Prize in Chemistry in 1918 for his development for synthesizing ammonia.



Figure 6.8.3.10: German chemist Carl Bosch (1874 –1940) who received the Nobel Prize in Chemistry in 1931 for his work in high-pressure chemistry.

It is interesting to note that the realization of the Haber-Bosch process required not only high-pressure vessels to be constructed by the steel industry, but also the liquid forms of nitrogen and hydrogen. As it turned out ammonia was a necessary component for enabling the production of liquid nitrogen and hydrogen, and involved a false hypothesis of what caused malaria, which led to a desire to keep drinks cold.

Long before it was understood the real cause of malaria, John Gorrie (Figure 6.8.3.11), a doctor working in Apalachicola on the Gulf Coast of Florida, was obsessed with finding a cure for malaria. The term *malaria* originated from Medieval Italian: *mala aria* (bad air), and it was associated with swamps and marshlands. Gorrie noticed that malaria was connected to hot humid weather so he began hanging bowl of ice in wards and circulating the air with a fan. However, ice was cut from frozen lakes and rivers in the North East of the US, stored and then shipped all over the world, and Apalachicola was so small that ice was seldom delivered. Gorrie started looking into methods of making ice. It was well known that when a compressed gas expands it takes heat from its surroundings. Gorrie made a steam engine that compressed air in a piston, which when the piston retracted the air cooled. On the next compression stroke the cold air was pushed out across a brine solution (saturated aqueous NaCl) cooling it. When he brought water in contact with the cold brine, it froze creating the first man made ice. On 14 July 1850 Gorrie produced ice for the French Consul to cool the champagne for the celebration of Bastille Day. Just before he died, Gorrie suggested that his (by then) Patented process could be used for cooling food for transport, and it was this application that was used extensively by British merchants to bring meat from Australia to Britain. However, in Germany, Gorrie's invention was more useful for beer.

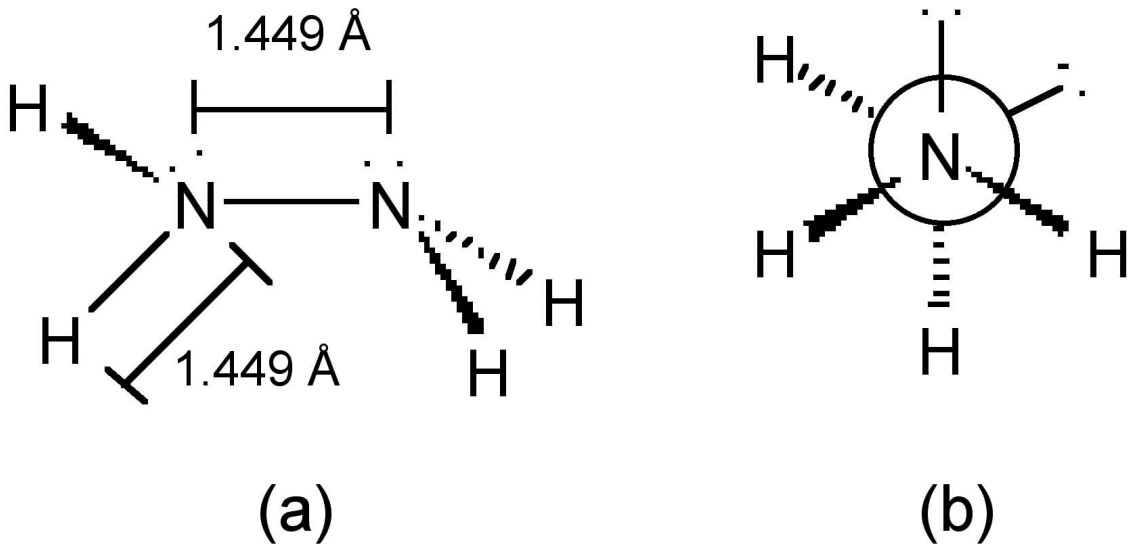


Figure 6.8.3.11: Portrait of American physician and scientist John Gorrie (1803 –1855) is considered the father of refrigeration and air conditioning.

Whereas the British traditionally brewed beer in which the yeast ferments on the surface (*top fermentation*) at a temperature of 60 – 70 °F, in Germany beer was made using *bottom fermentation*. This style of fermentation requires a temperature just above freezing. Traditionally, cold cellars were used to store the fermenting beer, and it is from here the name lager is derived from the German verb *largern*: to store. There had been a law in Germany preventing brewing in the summer, but with Gorrie's process the possibility was to be able to brew beer all year. Carl von Linde (Figure 6.8.3.12) was asked to develop a refrigeration system. He used ammonia instead of air in Gorrie's system, and in 1879 he set up a company to commercialize his ideas. The success of his refrigerator was such that by 1891 there were over 12,000 fridges being used, and more importantly there was now a convenient method of liquefying gases such as hydrogen and nitrogen; both of which were needed for the Haber-Bosch process.

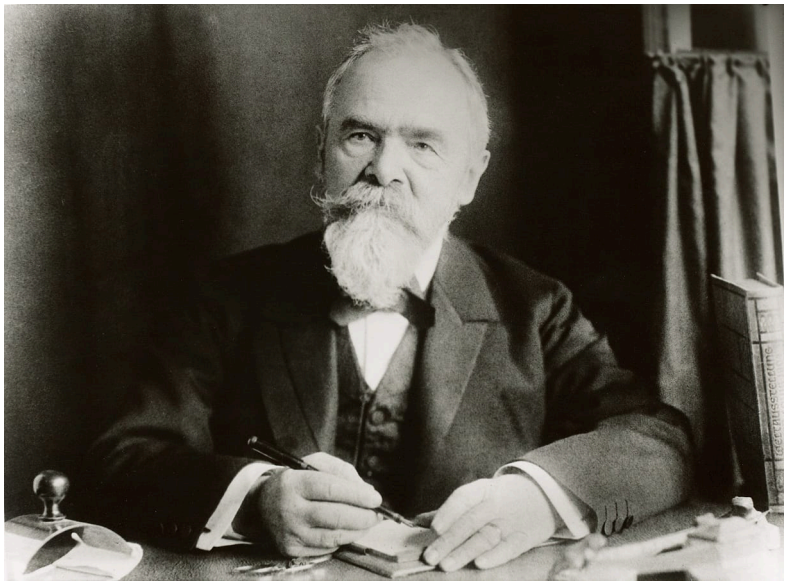


Figure 6.8.3.12: German engineer Carl Paul Gottfried von Linde (1842 - 1934).

As a consequence of the use of ammonia as a refrigerant, it was possible to prepare ammonia on a large industrial scale. Ammonia prepared by the Haber-Bosch process can be converted to nitric acid by the Ostwald process developed by Wilhelm Ostwald (Figure 6.8.3.13). Treatment of ammonia with air over a platinum catalyst yields initially nitric oxide, (8.3.31), and subsequently to nitrogen dioxide, (8.3.32), which dissolves in water to give nitric acid, (8.3.33).

$$4NH_3 + 5O_2 \xrightarrow{\text{Pt cat}} 4NO + 6H_2O \tag{6.8.3.31}$$

$$2NO + O_2 \xrightarrow{\text{Pt cat}} 2NO_2 \tag{6.8.3.32}$$

$$3NO_2 + H_2O \rightarrow 2HNO_3 + NO \tag{6.8.3.33}$$

Addition of soda (sodium hydroxide, NaOH) to nitric acid results in the formation of sodium nitrate, (8.3.34), which was the same fertilizer produced from the deposits in Chile.

$$HNO_3 + NaOH \rightarrow NaNO_3 + H_2O \tag{6.8.3.34}$$



Figure 6.8.3.13: German chemist Friedrich Wilhelm Ostwald (1853 – 1932) received the Nobel Prize in 1909 for his work on catalysis.

Unfortunately, for the Haber-Bosch and Ostwald processes, an even cheaper form of fertilizer was synthesized around the same time using calcium carbide to prepare calcium cyanamide ($CaCN_2$), (8.3.35). As a consequence, the Haber-Bosch process was forgotten until the outbreak of the First World War in 1914.

$$CaC_2 + N_2 \rightarrow CaCN_2 + C \tag{6.8.3.35}$$

Within weeks of the outbreak Germany realized it had only enough explosives for about a year of conflict. This was because the main source of explosives, sodium nitrate was the same source that gave fertilizer, i.e., Chile. Realizing this, the Royal Navy effectively blockaded the supply lines. If Germany did not find another source of Great War would have been over early in 1916, however, it was remembered that the Haber-Bosch process in combination with the Ostwald processes would allow the synthesis of nitric acid, which when mixed with cotton, made nitrocellulose (Figure 6.8.3.14), also known as gun cotton, an explosive, (8.3.36).

$$HNO_3 + C_6H_{10}O_5 \rightarrow C_6H_7(NO_2)_3O_5 + 3H_2O \tag{6.8.3.36}$$



Figure 6.8.3.14: The structure of nitrocellulose.

As a result of the industrial synthesis of ammonia Germany was able to manufacture sufficient explosives to fight until 11 November 1918, by which time almost 10 million were dead, almost 7 million missing, and over 21 million were wounded (Figure 6.8.3.15).



Figure 6.8.3.15: The Douamont Ossuary cemetery and World War I memorial in Verdun, France.

Hydrazine

Hydrazine (N_2H_4) is a colorless liquid with an odor similar to ammonia. Hydrazine has physical properties very close to water, with a melting point of 2 °C and a boiling point of 114 °C. The similarity in its chemistry to water is as a result of strong intermolecular hydrogen bonding.

WARNING

Hydrazine is highly toxic and dangerously unstable, and is usually handled as aqueous solution for safety reasons. Even so, hydrazine hydrate causes severe burns on the skin and eyes. Contact with transition metals, their oxides (e.g., rust), or salts cause catalytic decomposition and possible ignition of evolved hydrogen. Reactions with oxidants are violent.

Synthesis

Hydrazine is manufactured on the industrial scale by the Olin Raschig process using the reaction of a sodium hypochlorite solution with ammonia at 5 °C to form chloramine (NH_2Cl) and sodium hydroxide, (8.3.37). The chloramines solution is the reacted with ammonia under pressure at 130 °C, (8.3.38). Ammonia is used in a 33 fold excess.

$$\mathrm{NH_3 + OCl^- \rightarrow OH^- + NH_2Cl} \tag{6.8.3.37}$$

$$\mathrm{NH_2Cl + OH^- + NH_3 \rightarrow N_2H_4 + Cl^- + H_2O} \tag{6.8.3.38}$$

If transition metals are present then decomposition occurs, (8.3.38), and therefore, ethylenediaminetetraacetic acid (EDTA, Figure $6.8.3.16$) is added to complex the transition metal ions. The as produced hydrazine solution can be concentrated by distillation to give a 65% solution. Anhydrous hydrazine is formed by the distillation from NaOH.

$$\mathrm{2NH_2Cl + N_2H_4 \rightarrow 2NH_4^+ + 2Cl^- + N_2} \tag{6.8.3.39}$$

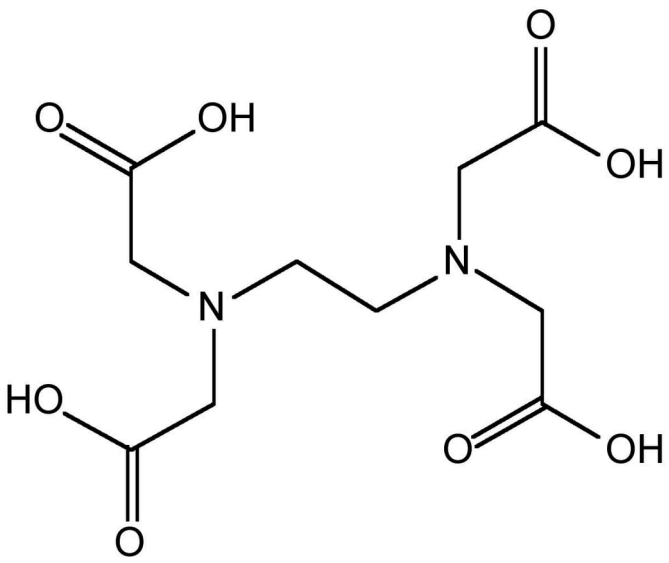


Figure $6.8.3.16$: The structure of ethylenediaminetetraacetic acid (EDTA).

Alternative routes to hydrazine include the oxidation of urea with sodium hypochlorite, (8.3.40), and the reaction of ammonia and hydrogen peroxide, (8.3.41).

$$\mathrm{(H_2N)_2C{=}O + NaOCl + 2NaOH \rightarrow N_2H_4 + H_2O + NaCl + Na_2CO_3} \tag{6.8.3.40}$$

$$\mathrm{2NH_3 + H_2O_2 \rightarrow N_2H_4 + 2H_2O} \tag{6.8.3.41}$$

Structure

The nitrogen atoms in hydrazine adopt sp^3 hybridization (Figure $6.8.3.17$a), and molecule adopts a *gauche* conformation in the vapor, liquid and solid states (Figure $6.8.3.17$b).

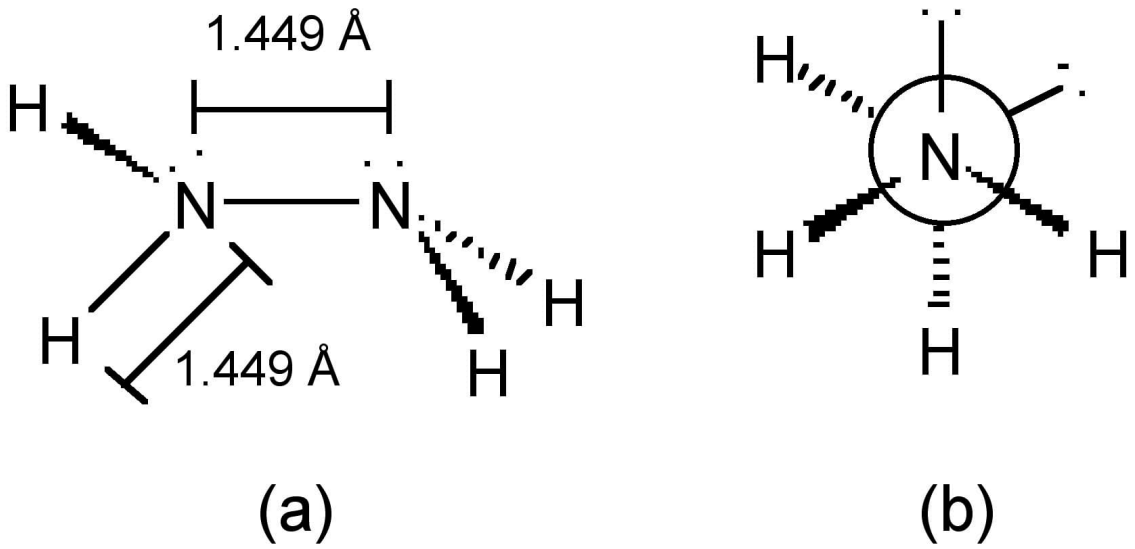


Figure 6.8.3.17: The structure of hydrazine.

In a similar manner to ammonia, (8.3.42), hydrazine is a self-ionizing, (8.3.43). While there is a wide range of salts of the $N_2H_5^+$ cation, only the sodium and potassium salts of $N_2H_3^-$ are stable.

$$2\mathrm{NH_3} \rightleftharpoons \underset{\text{ammonium}}{\mathrm{NH_4^+}} + \underset{\text{amide}}{\mathrm{NH_2^-}} \tag{6.8.3.42}$$

$$2\mathrm{N_2H_4} \rightleftharpoons \mathrm{N_2H_5^+} + \mathrm{N_2H_3^-} \tag{6.8.3.43}$$

Reaction chemistry and uses

Hydrazine is polar, highly ionizing, and forms stable hydrogen bonds, and its resemblance to water is reflected in the formation of aqueous solutions and hydrates. In the solid state the monohydrate is formed, i.e., $N_2H_4.H_2O$. In solution hydrazine acts as a base to form the hydrazinium ion, (8.3.44) where $K_b = 8.5 \times 10^{-7}$. The presence of a second Lewis base site means that hydrazine can be protonated twice to form the hydrazonium ion, (8.3.45) where $K_b = 8.9 \times 10^{-16}$. Salts of the cation $N_2H_5^+$ are stable in water; however, the salts of the dication are less stable.

$$2\mathrm{NH_3} \rightleftharpoons \mathrm{NH_4^+} + \mathrm{NH_2^-} \tag{6.8.3.44}$$

$$\mathrm{N_2H_5^+} + \mathrm{H_2O} \rightleftharpoons \mathrm{N_2H_5^{2+}} + \mathrm{OH^-} \tag{6.8.3.45}$$

The reaction of hydrazine with oxygen is highly favored, (8.3.46), and the explosive limit is 1.8 – 100 vol%.

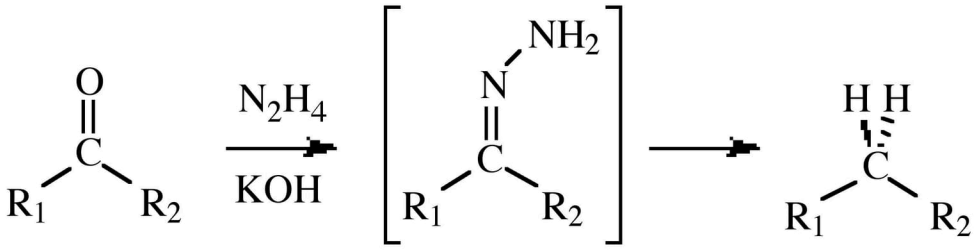
$$\mathrm{N_2H_4} + \mathrm{O_2} \rightarrow \mathrm{N_2} + 2\mathrm{H_2O} \tag{6.8.3.46}$$

Hydrazine is useful in a number of organic reactions for the synthesis of a wide range of compounds used in pharmaceuticals, textile dyes, and in photography, including:

- Hydrazone formation, (8.3.47) and (8.3.48).
- Alkyl-substituted hydrazine synthesis via direct alkylation with alkyl halides.
- Reaction with 2-cyanopyridines to form amide hydrazides, which can be converted using 1,2-diketones into triazines.
- Use in the Wolff-Kishner reduction that transforms the carbonyl group of a ketone or aldehyde into a methylene (or methyl) group via a hydrazone intermediate, (shown below).
- As a building block for the preparation of many heterocyclic compounds via condensation with a range of difunctional electrophiles.
- Cleavage N-alkylated phthalimide derivatives.
- As a convenient reductant because the by-products are typically nitrogen gas and water.

$$2(CH_3)_2C{=}O + N_2H_4 \rightarrow 2H_2O + [(CH_3)_2C{=}N]_2 \quad (6.8.3.47)$$

$$[(CH_3)_2C{=}N]_2 + N_2H_4 \rightarrow 2(CH_3) + 2C{=}NNH_2 \quad (6.8.3.48)$$



Messerschmitt Me 163 Komet

Designed by Alexander Lippisch (Figure 6.8.3.18), the Messerschmitt Me 163B Komet (Figure 6.8.3.19) was the first rocket-powered fighter plane. With a top speed of around 596 mph (Mach 0.83) and a service ceiling of 40,000 ft, the Komet's performance of the Me 163B far exceeded that of contemporary piston engine fighters. However, despite its impressive performance, it was only produced in limited numbers (*ca*. 370 as compared to the 1,430 built of its jet powered compatriot the Me 262) and was not an effective combat airplane.



Figure 6.8.3.18: German pioneer of aerodynamics Alexander Martin Lippisch (1894 – 1976).



Figure 6.8.3.19: The Messerschmitt Me 163B-1.

The Komet was powered by the HWK 109-509 *hot engine* (Figure 6.8.3.20) that used a mixture of a fuel and an oxidizer. The fuel was a mixture of hydrazine hydrate (30%), methanol (57%), and water (13%) that was designated by the code name, *C-Stoff*, that burned with the oxygen-rich exhaust from hydrogen peroxide (*T-Stoff*) used as the oxidizer. The C-Stoff was stored in a glass tank on the plane, while the T-Stoff was stored in an aluminum container. An oxidizing agent cocktail of $CaMnO_4$ and/or K_2CrO_4 was added to the *T-Stoff* generating steam and high temperatures, this in tern reacted violently with the *C-Stoff*. The flow of reagents was controlled by two pumps, to regulate the rate of combustion and thereby the amount of thrust. The violent combustion process resulted in the formation of water, carbon dioxide and nitrogen, and a huge amount of heat sending out a superheated stream of steam, nitrogen and air that was drawn in through the hole in the mantle of the engine, thus providing a forward thrust of approximately 3,800 lbf. Because of the potential hazards of mixing the fuels, they were stored at least $^1/_2$ mile apart, and the plane was washed with water between fueling steps and after missions.

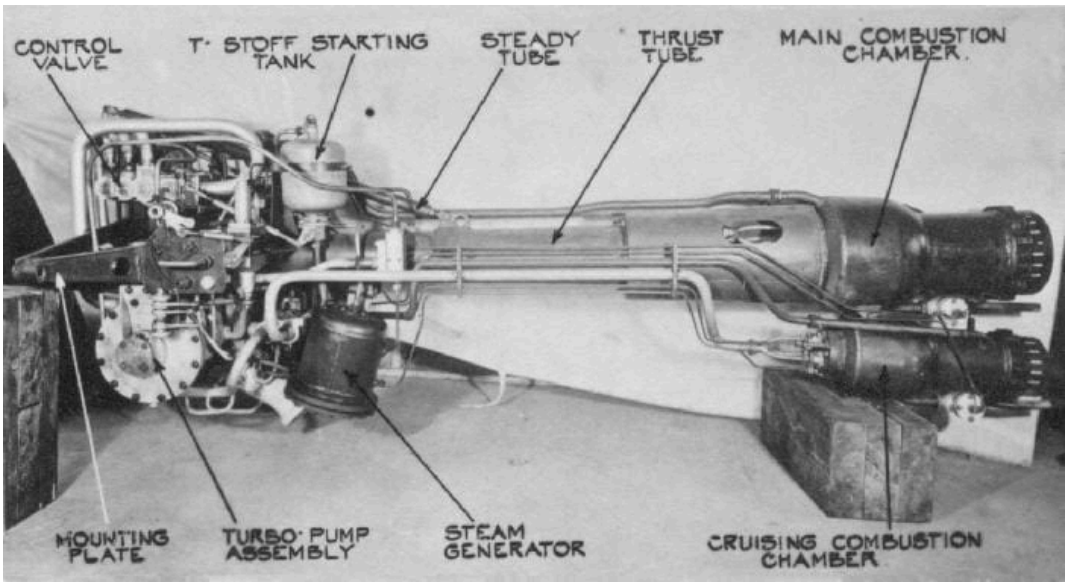


Figure 6.8.3.20: A photograph taken by Professor A. D. Baxter of the HWK 109-509 *hot engine*.

Phosphine and Arsine

Because of their use in metal organic chemical vapor deposition (MOCVD) of 13-15 (III-V) semiconductor compounds phosphine (PH_3) and arsine (AsH_3) are prepared on an industrial scale.

Synthesis

Phosphine (PH_3) is prepared by the reaction of elemental phosphorus (P_4) with water, (8.3.49). Ultra pure phosphine that is used by the electronics industry is prepared by the thermal disproportionation of phosphorous acid, (8.3.50).

$$2P_4 + 12H_2O \rightarrow 5PH_3 + 3H_3PO_4 \tag{6.8.3.49}$$

$$4H_3PO_4 \rightarrow PH_3 + 3H_3PO_4 \tag{6.8.3.50}$$

Arsine can be prepared by the reduction of the chloride, (8.3.51) or (8.3.52). The corresponding syntheses can also be used for stibine and bismuthine.

$$4AsCl_3 + 3LiAlH_4 \rightarrow 4AsH_3 + 3LiAlCl_4 \tag{6.8.3.51}$$

$$4AsCl_3 + 3NaBH_4 \rightarrow 4AsH_3 + 3NaCl + 3BCl_3 \tag{6.8.3.52}$$

The hydrolysis of calcium phosphide or arsenide can also generate the trihydrides.

Structure

The phosphorus in phosphine adopts sp^3 hybridization, and thus phosphine has an umbrella structure (Figure 6.8.3.21a) due to the stereochemically active lone pair. The barrier to inversion of the umbrella (E_a = 155 kJ/mol) is much higher than that in ammonia (E_a = 24 kJ/mol). Putting this difference in context, ammonia's inversion rate is 10^{11} while that of phosphine is 10^3. As a consequence it is possible to isolate chiral organophosphines (PRR'R"). Arsine adopts the analogous structure (Figure 6.8.3.21b).

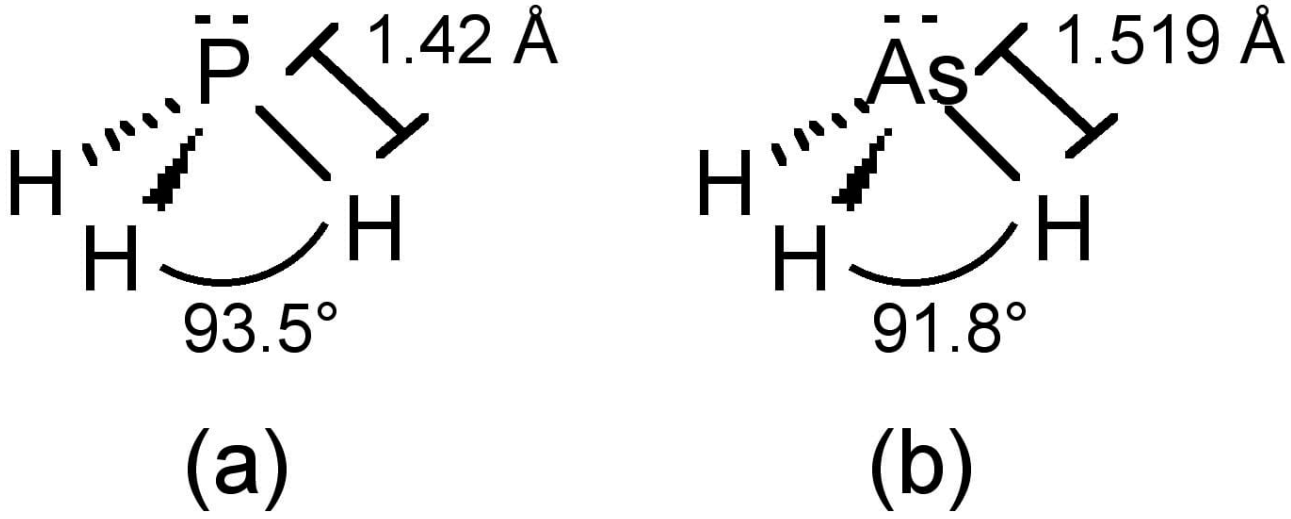


Figure 6.8.3.21: The structures of (a) phosphine and (b) arsine.

Reactions

Phosphine is only slightly soluble in water (31.2 mg/100 mL) but it is readily soluble in non-polar solvents. Phosphine acts as neither an acid nor a base in water; however, proton exchange proceeds via the phosphonium ion (PH_4^+) in acidic solutions and via PH_2^- at high pH, with equilibrium constants $K_b = 4 \times 10^{-28}$ and $K_a = 41.6 \times 10^{-29}$, respectively.

Arsine has similar solubility in water to that of phosphine (i.e., 70 mg/100 mL), and AsH_3 is generally considered non-basic, but it can be protonated by superacids to give isolable salts of AsH_4^+. Arsine is readily oxidized in air, (8.3.53).

$$2AsH_3 + 3O_2 \rightarrow As_2O_3 + 3H_2O \tag{6.8.3.53}$$

Arsine will react violently in presence of strong oxidizing agents, such as potassium permanganate, sodium hypochlorite or nitric acid. Arsine decomposes to its constituent elements upon heating to 250 - 300 °C.

Gutzeit test

The Gutzeit test is the characteristic test for arsenic and involves the reaction of arsine with Ag^+. Arsine is generated by reduction of aqueous arsenic compounds, typically arsenites, with Zn in the presence of H_2SO_4. The evolved gaseous AsH_3 is then exposed to silver nitrate either as powder or as a solution. With solid $AgNO_3$, AsH_3 reacts to produce yellow Ag_4AsNO_3, while with a solution of $AgNO_3$ black Ag_3As is formed.

Hazards

Pure phosphine is odorless, but technical grade phosphine has a highly unpleasant odor like garlic or rotting fish, due to the presence of substituted phosphine and diphosphine (P_2H_4). The presence of P_2H_4 also causes spontaneous combustion in air. Phosphine is highly toxic; symptoms include pain in the chest, a sensation of coldness, vertigo, shortness of breath, and at higher concentrations lung damage, convulsions and death. The recommended limit (RL) is 0.3 ppm.

Arsine is a colorless odorless gas that is highly toxic by inhalation. Owing to oxidation by air it is possible to smell a slight, garlic-like scent when arsine is present at about 0.5 ppm. Arsine attacks hemoglobin in the red blood cells, causing them to be destroyed by the body. Further damage is caused to the kidney and liver. Exposure to arsine concentrations of 250 ppm is rapidly fatal: concentrations of 25 – 30 ppm are fatal for 30 min exposure, and concentrations of 10 ppm can be fatal at longer exposure times. Symptoms of poisoning appear after exposure to concentrations of 0.5 ppm and the recommended limit (RL) is as low as 0.05 ppm.

Bibliography

- R. Minkwitz, A. Kornath, W. Sawodny, and H. Härtner, *Z. Anorg. Allg. Chem.*, 1994, **620**, 753.

This page titled 6.8.3: Hydrides is shared under a CC BY 3.0 license and was authored, remixed, and/or curated by Andrew R. Barron (CNX) via source content that was edited to the style and standards of the LibreTexts platform.

6.8.4: Oxides and Oxoacids

Oxides of Nitrogen

A summary of the physical properties of the oxides of nitrogen is given in Table 6.8.4.1.

Table 6.8.4.1: Physical properties of the oxides of nitrogen.

Oxide	Formula	Mp (°C)	Bp (°C)
Nitrous oxide	N_2O	-90.8	-88.5
Nitric oxide	NO	-163.6	-161.8
Dinitrogen trioxide	N_2O_3	-100.6	3.5 (dec.)
Nitrogen dioxide (dinitrogen tetroxide)	NO_2/N_2O_4	-11.2 (NO_2)	21.2 (N_2O_4)
Nitrogen pentoxide	N_2O_5	30	47

Nitrous oxide

Gaseous nitrous oxide (N_2O) is prepared by the careful thermal decomposition of ammonium nitrate (NH_4NO_2), (8.4.1). Nitrous oxide is a linear molecule (Figure 6.8.4.1a) that is isoelectronic (and isostructural) with carbon dioxide. Despite its use as a power enhancement for automobiles, nitrous oxide is actually not very reactive and a major use is as an aerosol propellant.

$$NH_4NO_2 \xrightarrow{\Delta} N_2O + 2H_2O \tag{6.8.4.1}$$

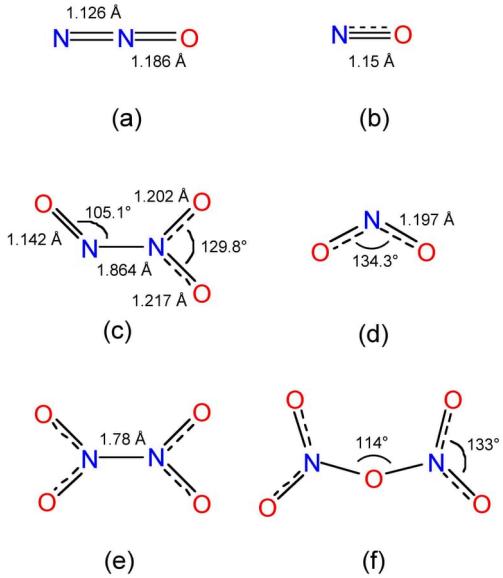


Figure 6.8.4.1: Structures of (a) nitrous oxide, (b) nitric oxide, (c) dinitrogen trioxide, (d) nitrogen dioxide, (e) nitrogen tetroxide, and (f) nitrogen pentoxide.

Nitrous oxide as an anesthetic drug

Nitrous oxide is known as "laughing gas" due to the euphoric effects of inhaling it, a property that has led to its recreational use as a hallucinogen. However, it is as a anesthetic that it has a legitimate application.

The first use of nitrous oxide as anesthetic drug was when dentist Horace Wells (Figure 6.8.4.2) with assistance by Gardner Quincy

Colton (Figure 6.8.4.3) and John Mankey Riggs (Figure 6.8.4.4), demonstrated insensitivity to pain from a dental extraction in December 1844. Wells subsequently treated 12-15 patients, and according to his own record it only failed as an anesthetic in two cases. In spite of these results, the method was not immediately adopted, probably because during his first public demonstration was only partly successful.

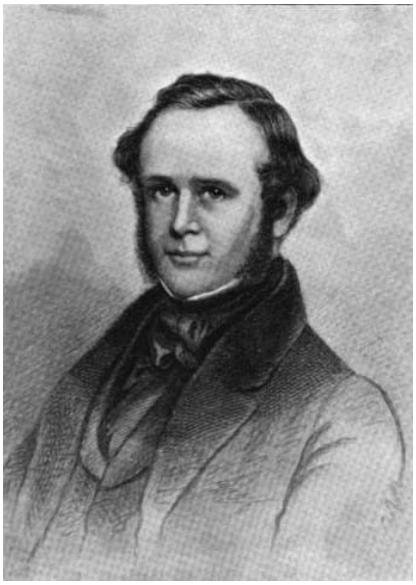


Figure 6.8.4.2: American dentist Horace Wells (1815 - 1848).

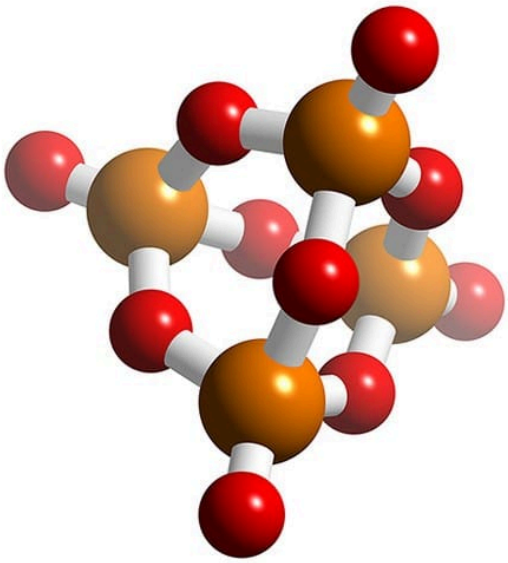


Figure 6.8.4.3: American showman, lecturer, and former medical student Gardner Quincy Colton (1814 - 1898).

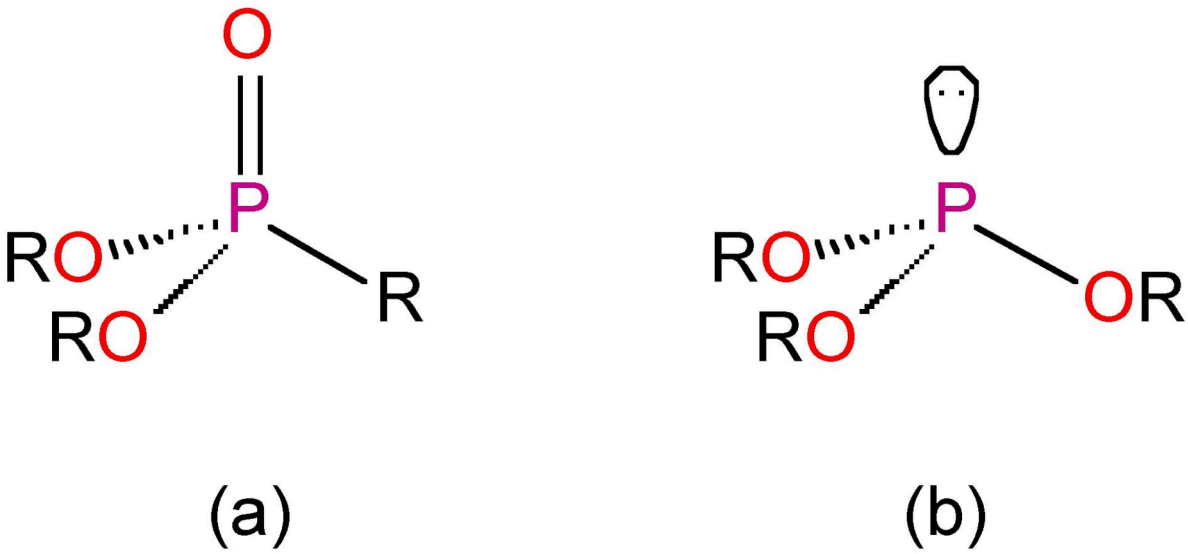


Figure 6.8.4.4: John Mankey Riggs (1811 - 1885) was the leading authority on periodontal disease in the United States, to the point that periodontal disease was known as *Riggs disease*.

The method did not come into general use until 1863, when Colton successfully used it for more than 25,000 patients. As such, the usage of nitrous oxide rapidly became the preferred anesthetic method in dentistry. Because the gas is mild enough to keep a patient in a conscious and conversational state, and yet in most cases strong enough to suppress the pain caused by dental work, it remains the preferred gas anesthetic in today's dentistry.

Nitrous: the secret to more power.

In motorsports, nitrous oxide (often referred to as *nitrous* or *NOS*) allows the engine to burn more fuel, resulting in a more powerful combustion, and hence greater horsepower. The gas itself is not flammable, but it delivers more oxygen (33%) than atmospheric air (21%) by breaking down at elevated temperatures. When N_2O breaks down in during fuel combustion, the decomposition of nitrous is exothermic, contributing to the overall power increase.

Nitrous oxide is stored as a compressed liquid (Figure 6.8.4.5); the evaporation and expansion of liquid nitrous oxide in the intake manifold causes a large drop in intake charge temperature, resulting in a denser charge, further allowing more air/fuel mixture to enter the cylinder. Nitrous oxide is sometimes injected into (or prior to) the intake manifold, whereas other systems directly inject right before the cylinder (direct port injection) to increase power.

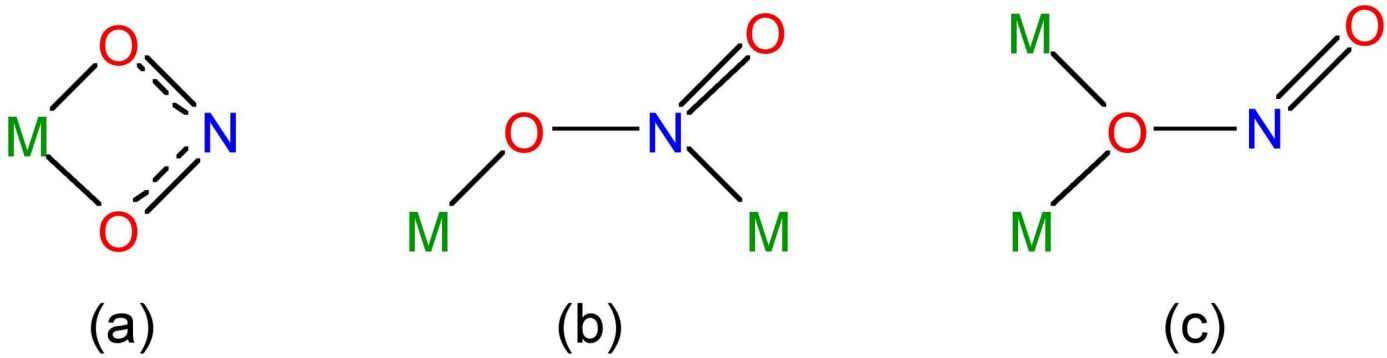


Figure 6.8.4.5: A typical NOS system for automotive use.

One of the major problems of using nitrous oxide in a reciprocating engine is that it can produce enough power to damage or destroy the engine. Very large power increases are possible, and if the mechanical structure of the engine is not properly reinforced, the engine may be severely damaged or destroyed during this kind of operation.

Automotive-grade liquid nitrous oxide differs slightly from medical-grade nitrous oxide in that a small amount of sulfur is added

to prevent substance abuse.

Nitric oxide

Nitric oxide (NO) is formed by the high temperature oxidation of nitrogen, (8.4.2), or the platinum catalyzed oxidation of ammonia at 800 °C, (8.4.3).

$$N_2 + O_2 \rightleftharpoons 2NO \tag{6.8.4.2}$$

$$4NH_3 + 5O_2 \xrightarrow{Pt} 4NO + 6H_2O \tag{6.8.4.3}$$

Nitric oxide (Figure 6.8.4.6b) is electronically equivalent to dinitrogen (N_2) plus an electron, and as a consequence it is paramagnetic with one unpaired electron. The location of the unpaired electron in the π* orbital (Figure 6.8.4.6a) results in a bond order of 2.5 rather than the triple bond observed for N_2 (Figure 6.8.4.6b). The N-O distance of 1.15 Å is intermediate between the triple bond distance in NO^+ (1.06 Å) and the typical double bond distance (*ca.* 1.20 Å). Furthermore, because of the location of the electron it is easy to oxidize nitric oxide to the nitrosonium ion (NO^+), (8.4.4).

$$NO \rightarrow NO^+ + e^- \tag{6.8.4.4}$$

$$2NO + O_2 \rightarrow 2NO_2 \tag{6.8.4.5}$$

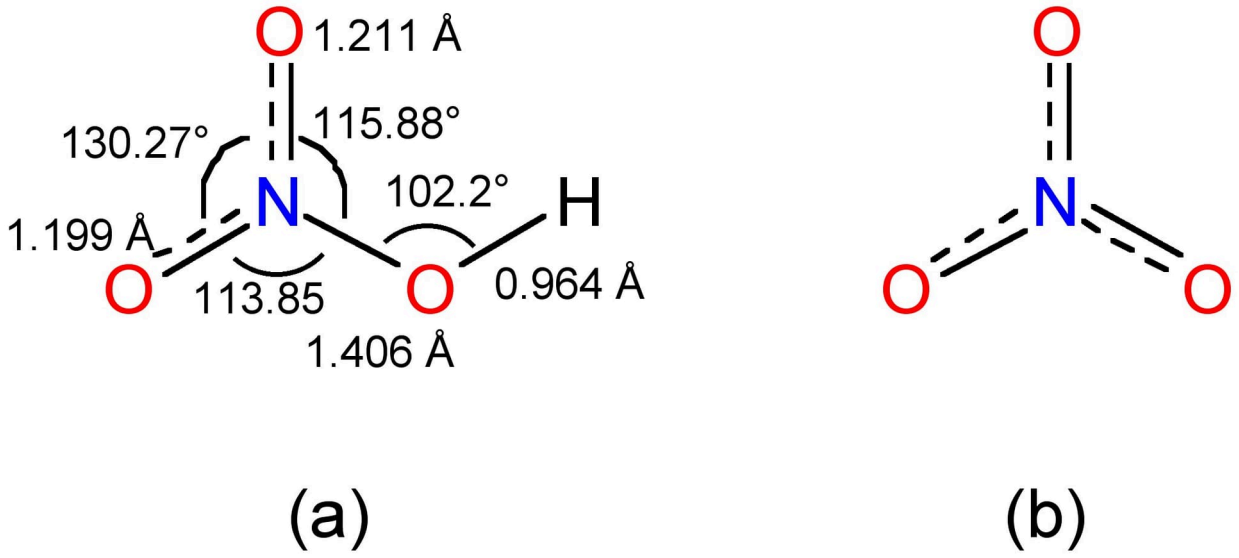


Figure 6.8.4.6: Molecular orbital diagrams for (a) nitric oxide and (b) dinitrogen.

Nitric oxide is unstable to heat, (8.4.6), and oxidation, (8.4.5). It will also react with halogens to form the nitrosyl halides, XNO.

$$3NO \rightarrow N_2O + NO_2 \tag{6.8.4.6}$$

Dinitrogen trioxide

Dinitrogen trioxide (N_2O_3) is formed from the stoichiometric reaction between NO and O_2 or NO and N_2O_4. Dinitrogen trioxide has an intense blue color in the liquid phase and a pale blue color in the solid state. Thermal dissociation of N_2O_3, (8.4.7), occurs above -30 °C, and some self-ionization of the pure liquid is observed, (8.4.8). The asymmetric structure of N_2O_3 (Figure 6.8.4.1c) results in a polar molecule (Figure 6.8.4.7).

$$N_2O_3 \rightleftharpoons NO + NO_2 \tag{6.8.4.7}$$

$$N_2O_3 \rightleftharpoons NO^+ + NO_2^- \tag{6.8.4.8}$$

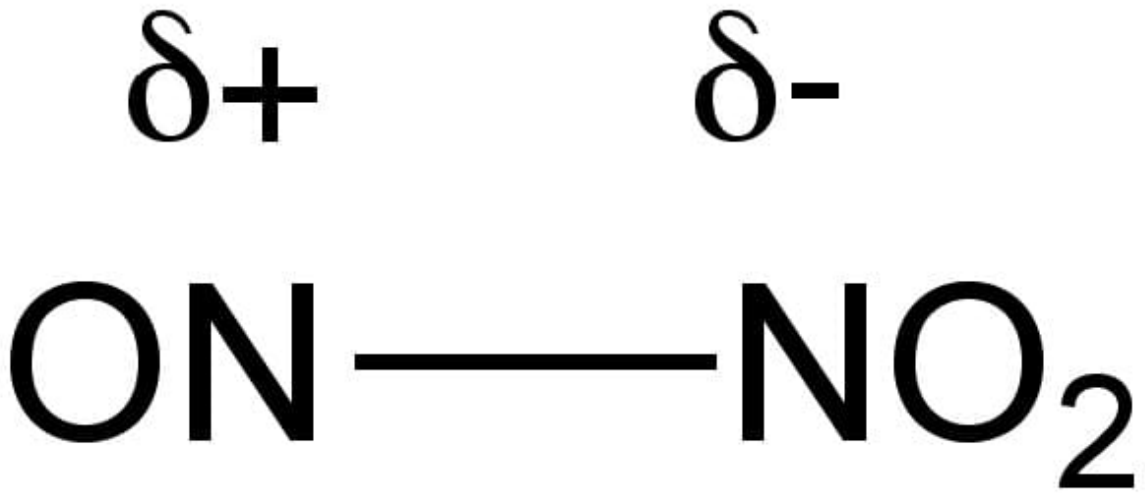


Figure 6.8.4.7: The polarization of the N-N bond in dinitrogen trioxide.

Nitrogen dioxide (and tetroxide)

Formed from the oxidation of nitric oxide, (8.4.9), brown nitrogen dioxide is actually in equilibrium with its colorless dimeric form, nitrogen tetroxide (N_2O_4), (8.4.10).

$$2NO + O_2 \rightleftharpoons 2NO_2 \tag{6.8.4.9}$$

$$\underset{\substack{\text{brown}\\\text{paramagnetic}}}{2NO_2} \rightleftharpoons \underset{\substack{\text{colorless}\\\text{diamagnetic}}}{N_2O_4} \tag{6.8.4.10}$$

Nitrogen dioxide (Figure 6.8.4.1d) is electronically equivalent to the nitrate anion (NO_2^-) less one electron, and as such it is paramagnetic with one unpaired electron. The location of the unpaired electron in a nitrogen sp^2 orbital, and a consequently it forms a dimer through a N-N bond (Figure 6.8.4.1e). Furthermore, it is easy to oxidize nitrogen dioxide to the nitronium ion (NO_2^+), (8.4.11).

$$NO_2 \rightarrow NO_2^+ + e^- \tag{6.8.4.11}$$

Nitrogen dioxide dissolves in water to form a mixture of nitric and nitrous acids, (8.4.12). Nitrogen dioxide acts as an oxidizing agent with the formation of nitrate anion, (8.4.13).

$$2NO_2 + H_2O \rightarrow NO_3^- + NO_2^- + 2H^+ \tag{6.8.4.12}$$

$$2NO_2 + 2I^- \rightarrow I_2 + 2NO_2^- \tag{6.8.4.13}$$

The most common structural form of N_2O_4 (Figure 6.8.4.1e) is planar with a long N-N bond (1.78 Å) that is significantly longer than observed in hydrazine (1.47 Å). Rationalization of this structural effect is obtained from a consideration of the molecular orbitals, which show that the electrons in the σ-bond are actually delocalized over the whole molecule. The rotation about the N-N bond is 9.6 kJ/mol.

Nitrogen pentoxide

The dehydration of nitric acid, with P_2O_5, yields nitrogen pentoxide, (8.4.14), which is an unstable solid at room temperature (Table 6.8.4.1). In the solid state nitrogen pentoxide is actually nitronium nitrate ($NO_2^+NO_3^-$), however, in the vapor phase it exists as a molecular species (Figure 6.8.4.1f) with a bent N-O-N unit. Nitrogen pentoxide is a very powerful nitrating and oxidation agent.

$$2HNO_3 \rightleftharpoons N_2O_5 + H_2O \tag{6.8.4.14}$$

Nitrogen oxides as precursors to smog and acid rain

Nitrogen oxides (NO_x) emissions are estimated to be in the range of 25 - 100 megatonnes of nitrogen per year. Natural sources are thought to make up approximately $^1/_3$ of the total. The generations of NO_x (primarily a mixture of NO_2 and NO) is the main source of smog and a significant contribution to atmospheric pollution; however, NO_x is also responsible for much of the acidity in acid rain.

Atmospheric reactions leading to acid rain

In the dry atmosphere, nitric oxide reacts is oxidized rapidly in sunlight by ozone, (8.4.15). The nitrogen dioxide reacts with the hydroxide radical, formed by the photochemical decomposition of ozone, (8.4.16) and (8.4.17), in the presence of a non-reactive gas molecule such as nitrogen to form nitric acid vapor, (8.4.18). The conversion rate for NO_x to HNO_3 is approximately ten times faster than the equivalent reaction for sulfur dioxide. For example, conversion is essentially complete for a NO_x plume by the time it transverses the North Sea from the UK to Scandinavia.

$$\mathrm{NO + O_2 \rightarrow NO_2 + O_2} \tag{6.8.4.15}$$

$$\mathrm{O_3 + h\nu \rightarrow O* + O_2} \tag{6.8.4.16}$$

$$\mathrm{O* + H_2O \rightarrow 2HO\cdot} \tag{6.8.4.17}$$

$$\mathrm{NO_2 + \cdot OH + N_2 \rightarrow HNO_3 + N_2} \tag{6.8.4.18}$$

At night, conversion takes place via the formation of a nitrate radical, (8.4.19), which subsequently photochemically unstable under sunlight forming nitrogen pentoxide, (8.4.20), that reacts with water on the surface of aerosol particles to form nitric acid, (8.4.21).

$$\mathrm{NO_2 + O_3 \rightarrow NO_3 + O_2} \tag{6.8.4.19}$$

$$\mathrm{NO_2 + NO_3 + N_3 \rightarrow N_2O_5 + N_2} \tag{6.8.4.20}$$

$$\mathrm{N_2O_5 + H_2O \rightarrow 2HNO_3} \tag{6.8.4.21}$$

Both NO and NO_2 are only slightly soluble in water and it is therefore more probable that the nitric acid content of rain is more likely due to the dissolution of nitric acid vapor into raindrops, (8.4.22), rather than a separate reaction.

$$\mathrm{N_2O_5 + H_2O_{(l)} \rightarrow 2HNO_{3(aq)}} \tag{6.8.4.22}$$

Oxoacids of Nitrogen

Nitrous acid

In the gas phase nitrous acid can be made by the following reaction:

$$\mathrm{NO + NO_2 + H_2O \rightleftharpoons 2HNO_2} \tag{6.8.4.23}$$

The gas phase structure as determined by IR spectroscopy is shown in Figure 6.8.4.8a, in which the nitrogen is planar with sp^2 hybridization.

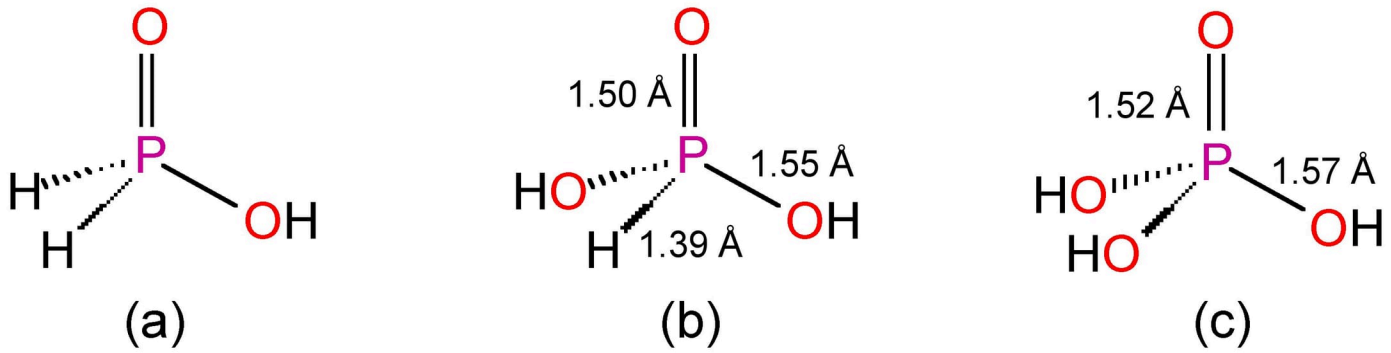


Figure 6.8.4.8

In basic aqueous solution the same reaction results in the formation of the nitrite ion, (8.4.24), which can be precipitated as the Ba^{2+} salt. After separation the addition to sulfuric acid yields a solution of nitrous acid. However, it is not possible to concentrate by heating since decomposition occurs, (8.4.25).

$$NO + NO_2 + 2OH^- \rightleftharpoons 2NO_2^- + H_2O \tag{6.8.4.24}$$

$$3HNO_2 \rightarrow H_3O^+ + NO_3^- + 2NO \tag{6.8.4.25}$$

Nitrous acid is a fairly weak acid in water (pK = 5.22); however, many salts are known of the nitrite ion, NO_2^- (Figure 6.8.4.8b). Complexes of the nitrite ion can be monodentate with bonding via nitrogen (nitro) or an oxygen (nitrito). Both isomers can be isolated in the case of an inert metal, i.e., substitutionally inert d^6 octahedral complexes (Figure 6.8.4.9). Bidentate and bridging modes of coordination are also known for the nitrite anion (Figure 6.8.4.10).

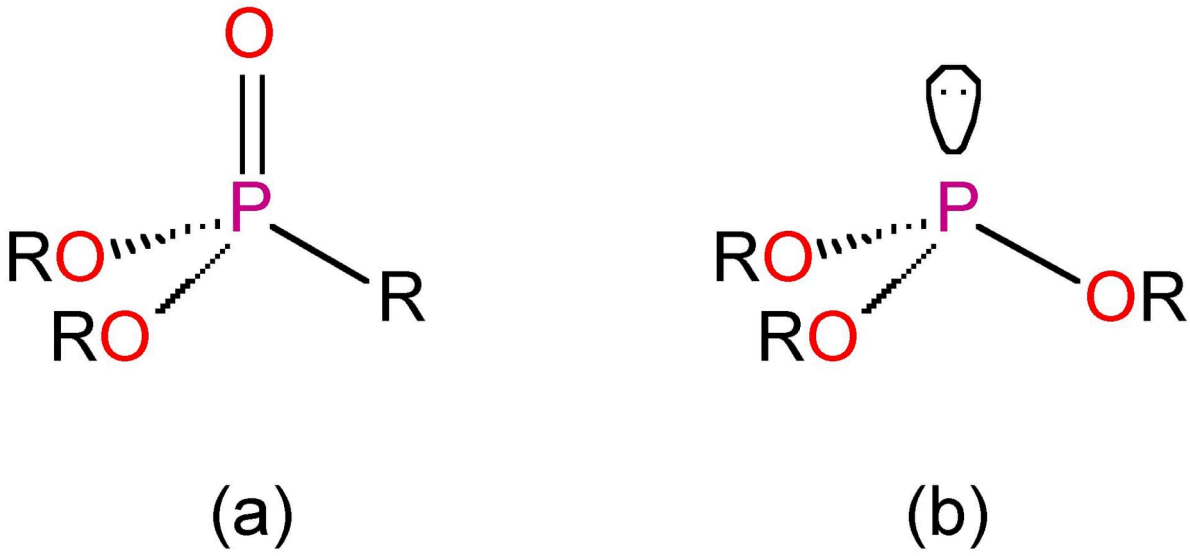


Figure 6.8.4.9: Structures of (a) orange nitro and (b) pink nitrito isomers of $[Co^{III}(NH_3)_5(NO_2)]^{2+}$.

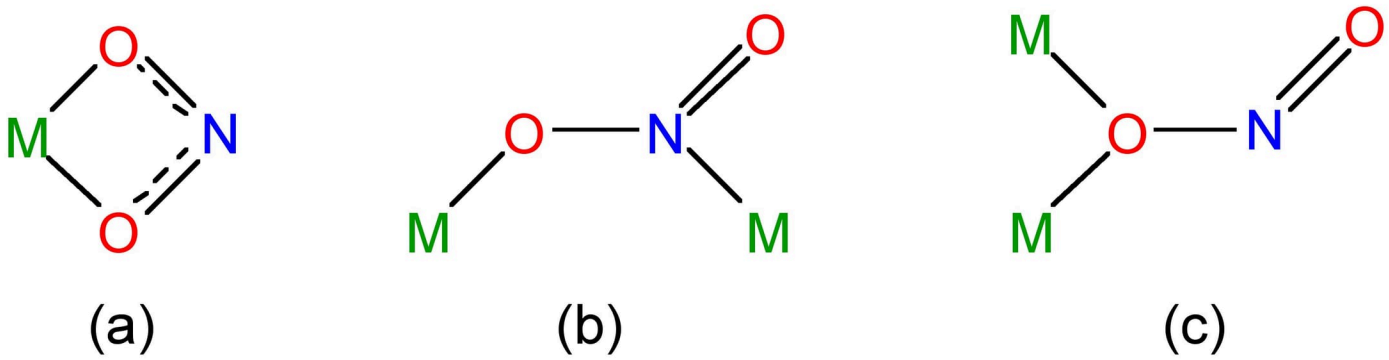


Figure 6.8.4.10: Bidentate (a) and bridging (b and c) modes of coordination of the nitrite anion.

Nitrite can act as either an oxidizing agent, (8.4.26), or a reducing agent, (8.4.27).

$$\mathrm{NO_2^- + 2H^+ + Fe_{2+} \rightarrow NO + H_2O + Fe^{3+}} \tag{6.8.4.26}$$

$$\mathrm{NO_2^- + H_2O + 2Ce^{4+} \rightarrow NO_3^- + 2H^+ + 2Ce^{3+}} \tag{6.8.4.27}$$

The most important use of nitrous acid is in the diazotization reactions in which nitrous acid is generated by acidifying nitrite solution.

Nitric acid

Nitric acid (HNO_3), also known as *aqua fortis* and *spirit of nitre*, is made by the dissolution of nitrogen dioxide in water, (8.4.28). Nitric acid can be concentrated by distillation from concentrated sulfuric acid.

$$\mathrm{3NO_2 + H_2O \rightarrow 2HNO_3 + NO} \tag{6.8.4.28}$$

The structure of HNO_3 in the gas phase is planar at the sp^2 nitrogen (Figure 6.8.4.11a).

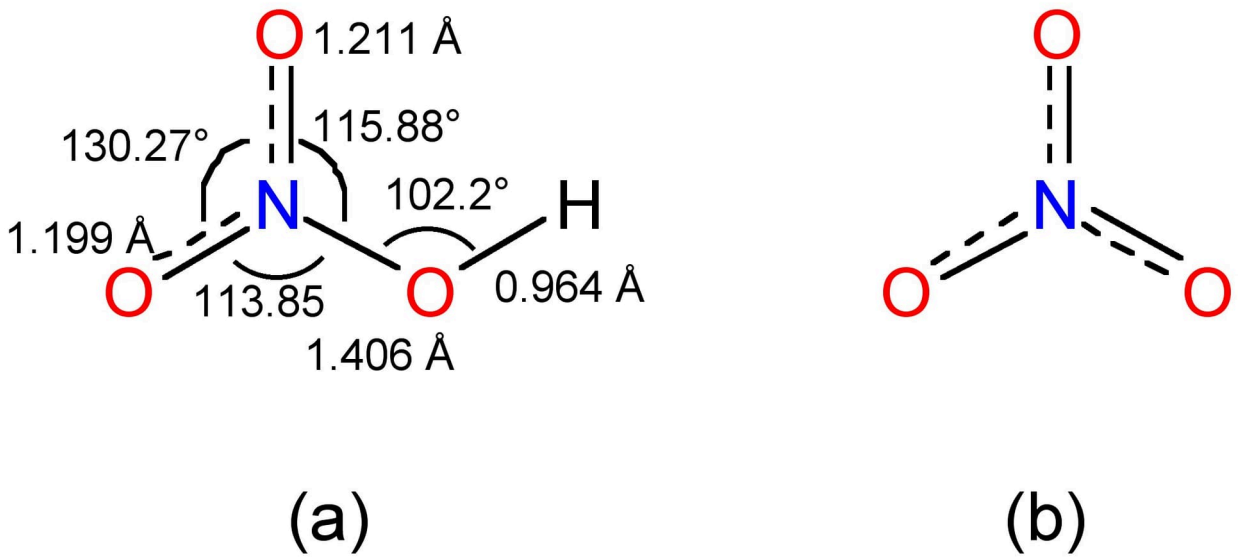


Figure 6.8.4.11: The structures of (a) nitric acid and (b) the nitrate anion.

Pure 100% nitric acid is a very corrosive liquid that is strongly acidic and protonates and dissolves organic species. In the liquid phase it is slightly dissociated, (8.4.29). It is also a powerful oxidizing agent, converting non-metal elements to either the oxide or oxoacid. In contrast with metals it forms either salts or complexes in which the metal is in its highest oxidation state. It is unstable and decomposes upon heating or photolysis.

$$3HNO_3 \rightleftharpoons H_3O^+ + NO_2^+ + 2NO_3^- \tag{6.8.4.29}$$

The pure acid has the highest self ionization of pure liquid acids, (8.4.30). However, the loss of water results, (8.4.31), such that the overall reaction can be described by (8.4.32).

$$2HNO_3 \rightleftharpoons H_2NO_3^+ + NO_3^+ \tag{6.8.4.30}$$

$$H_2NO_3^+ \rightleftharpoons H_2O + NO_2^+ \tag{6.8.4.31}$$

$$HNO_3 \rightleftharpoons NO_3^+ + NO_2^+ + H_2O \tag{6.8.4.32}$$

The common concentration of nitric acid is 70%. While the pure acid is colorless, samples often take on a yellow color due to the photochemical decomposition of nitric acid to give brown NO_2.

$$4HNO_3 \xrightarrow{h\nu} 4NO_2 + 2H_2O + O_2 \tag{6.8.4.33}$$

Note

The term the “acid test” is derived from the medieval practice of debasing of gold and silver currencies (often by the Monarchs who issued them) by debasing with copper. With ducats (Milan), livres (France), florins (Florence), maravedies (Spain) and bezants (Constantinople) in widespread use, and each with a nominal gold or silver content, it was important for a merchant to be able verify the worth of any particular coin. If a drop of dilute nitric acid was placed onto a silver coin adulterated with copper, it turned green, due to the formation of copper(II) nitrate. Conversely, if a gold coin reacted in any way with the nitric acid it was not pure. In both cases the coins failed the “acid test”.

Aqua regia (so called because it dissolves gold) is a mixture of 70% nitric acid and hydrochloric acid in a 1:3 ratio. Aqua regia is a very powerful oxidizing agent (it contains Cl_2) and stablizes some metals as their chloro complexes (Table 6.8.4.2). If HF is added in place of HCl, tantalum may be dissolved with the formation of $[TaF_2]^-$.

Table 6.8.4.2: Metal chloride salts formed by the dissolution of metals in aqua regia.

Metal	**Chloride salt formed**
Au	$[AuCl_4]^-$
Pt	$[PtCl_6]^{2-}$

Fuming nitric acid (100% nitric) is exceedingly corrosive and should not be used. In 100% sulfuric acid, nitric acid acts as a base and gets protonated, (8.4.34) and (8.4.35), and acts as a powerful nitrating agent.

$$HNO_3 + H_2SO_4 \rightarrow ON(OH)_2^+ + HSO_4^- \tag{6.8.4.34}$$

$$ON(OH)_2^+ + HSO_4^- + H_2SO_4 \rightarrow H_3O^+ + NO_2^+ + 2HSO_4^- \tag{6.8.4.35}$$

In water dilute nitric acid is fully ionized, (8.4.36).

$$HNO_3 + H_2O \rightarrow H_3O^+ + NO_3^- \tag{6.8.4.36}$$

The nitrate ion is planar (Figure 6.8.4.11b) and forms many salts and complexes. The nitrate anion is most commonly a monodentate ligand, but can also be a bidentate ligand (Figure 6.8.4.12a) or a bridging ligand (Figure 6.8.4.12b and 12c).

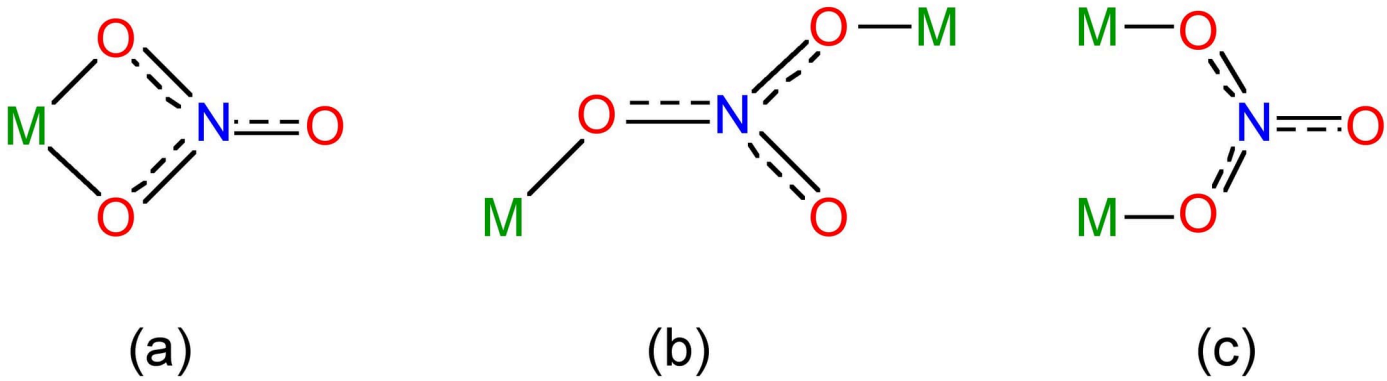


Figure 6.8.4.12: Coordination modes of the nitrate anion.

Phosphorous Oxides

Phosphorous trioxide

The stoichiometric oxidation of white phosphorus yields phosphorous trioxide, (8.4.37).

$$P_4 + 3O_2 \rightarrow 2P_2O_3 \tag{6.8.4.37}$$

Several structural forms of phosphorous trioxide are known, but P_4O_6 is a stable molecule structure (Figure 6.8.4.13), while the rest are polymers.

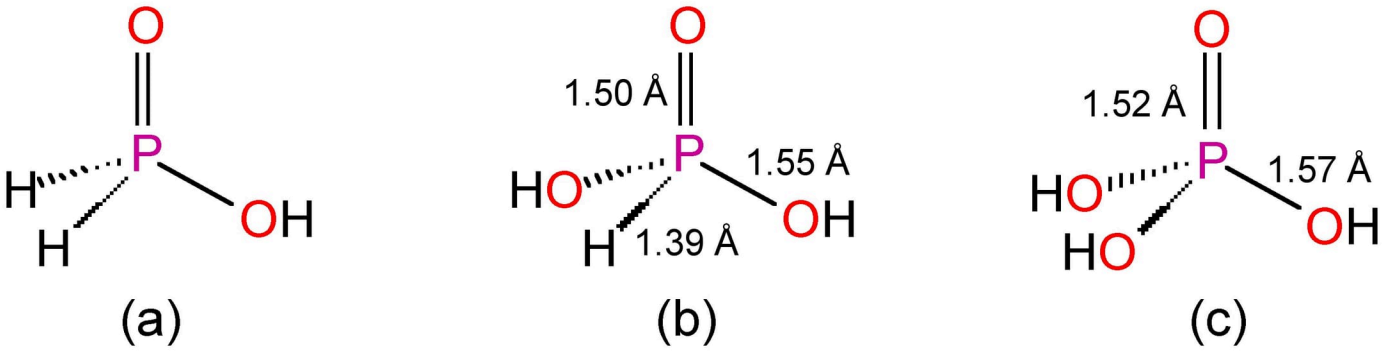


Figure 6.8.4.13: The structure of P_4O_6. Phosphorus atoms are represented by the large spheres, and oxygen atoms by the small spheres (Copyright: Karl Harrison, 2005).

Phosphorous pentoxide

The reaction of white phosphorus with excess oxygen (or the oxidation of phosphorous trioxide) yields phosphorous pentoxide, (8.4.38).

$$P_4 + 5O_2 \rightarrow 2P_2O_5 \tag{6.8.4.38}$$

The structure of hexagonal phosphorous pentoxide is actually that of the dimeric form, P_4O_{10}, and is based upon the structure of P_4O_6, but with P=O units instead of lone pairs (Figure 6.8.4.14). The structure is maintained in the vapor phase; however, other crystalline and glassy forms comprise of a sheet-like structure (Figure 6.8.4.15).

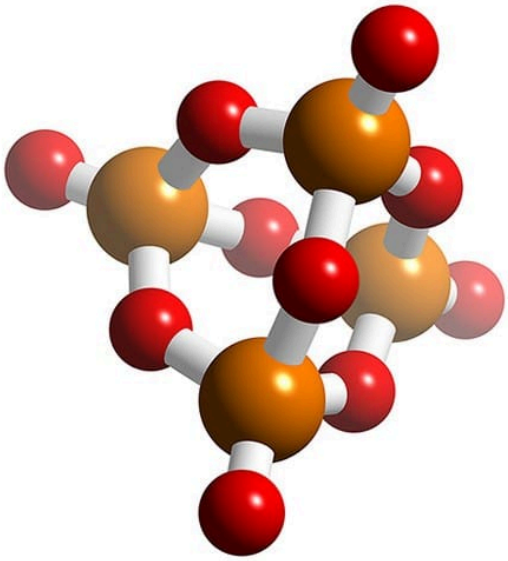


Figure 6.8.4.14: The structure of hexagonal P_4O_{10}. Phosphorus atoms are represented by the large spheres, and oxygen atoms by the small spheres (Copyright: Karl Harrison, 2005).

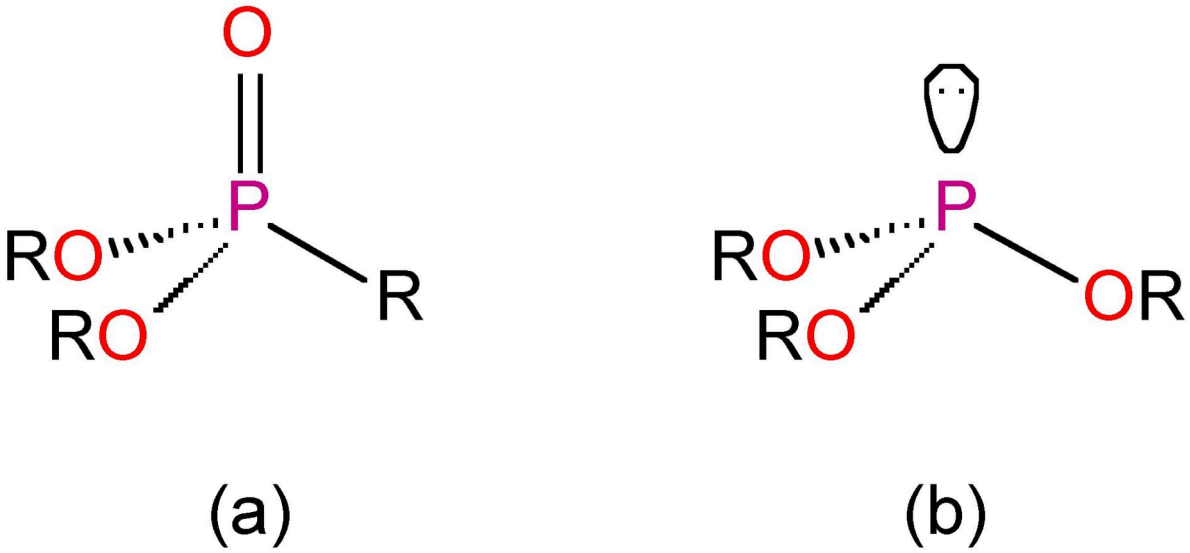


Figure 6.8.4.15: The structure of a sheet in glassy P_4O_{10}.

Phosphorous pentoxide is an excellent drying agent below 100 °C. It reacts with water to form various phosphoric acids, and it will extract water from other 'drying agents', e.g., (8.4.39) and (8.4.40). Phosphorous pentoxide will dehydrate amides to give nitriles, (8.4.41).

$$2HNO_3 \xrightarrow[-H_2O]{P_4O_{10}} N_2O_5 \tag{6.8.4.39}$$

$$H_2SO_4 \xrightarrow[-H_2O]{P_4O_{10}} SO_3 \tag{6.8.4.40}$$

$$RC(O)NH_2 \xrightarrow[-H_2O]{P_4O_{10}} RC \equiv N \tag{6.8.4.41}$$

Oxoacids of Phosphorus

Phosphorous pentoxide (P_2O_5) is an excellent drying agent, and its action is a result of the formation of a range of oxoacids.

Hypophosphorous acid

Hypophosphorous acid, H_3PO_2, is easily prepared pure buy the reaction of white phosphorous with base, followed by acidification, (8.4.42). The pure acid is a solid (Mp = 27 °C) and very soluble in water.

$$\underset{\underset{H_3PO_2}{\downarrow \text{acidify}}}{P_4 + 4OH^- + 4H_2O \rightarrow 4H_2PO_2^- + 2H_2} \tag{6.8.4.42}$$

The structure of H_3PO_2 is determined by X-ray crystallography to be tetrahedral with two hydride ligands and a hydroxide (Figure 6.8.4.16a). The presence of two hydrides is confirmed by NMR spectroscopy. The ^{1}H NMR resonance shows an OH line and a doublet from the P-H with a large one-bond coupling constant to the ^{31}P nucleus. The non-decoupled ^{31}P NMR spectrum shows a triplet (δ = 13 ppm, *J*P-H = 530 Hz) due to the two hydrides.

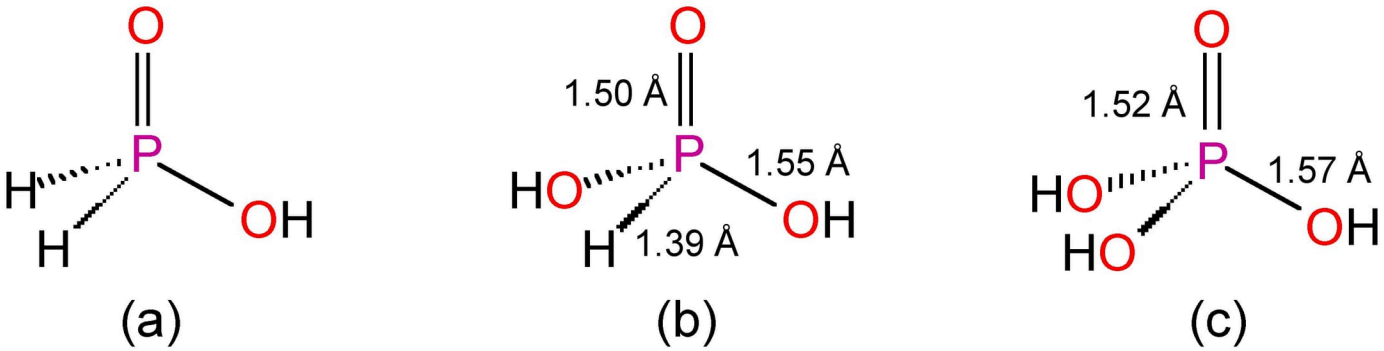


Figure 6.8.4.16: Oxoacids of phosphorous: (a) hypophosphorous acid, (b), phosphorous acid, and (c) phosphoric acid.

In water hypophosphorous acid is a monobasic acid (pK = 1.2), (8.4.43), and it forms a wide range of salts. It is also a powerful reducing agent, but its reaction kinetics is slow.

$$H_2P(O)OH + H_2O \rightleftharpoons H_2P(O)_2^- + H_3O^+ \tag{6.8.4.43}$$

Phosphorous acid

The reaction of P_4O_6 or PCl_3 with water yields phosphorous acid, H_3PO_3; which like hypophosphorous acid is a solid (Mp = 70.1 °C) and very soluble in water. The structure is shown by X-ray crystallography to be comprised of a tetrahedral phosphorus with one hydride and two hydroxides (Figure 6.8.4.16b). ^{31}P NMR spectroscopy demonstrates the presence of a single hydride by the presence of a doublet as a consequence of the phosphorous center being split by a single hydride (δ = 4 ppm, *J*P-H = 700 Hz). The ^{1}H NMR spectrum shows a doublet for the hydride and a single resonance of twice the intensity for the hydroxide.

As expected, in water phosphorous acid is dibasic, (8.4.44). The acid (and the anions) are strong reducing agents, yielding phosphoric acid. They actually react very slowly, and it is thought that this may be due to the reaction being in the tautomeric form, $P(OH)_3$. Although this has not been isolated, the trialkyl derivatives exist in both forms, i.e., esters of phosphoric acids (Figure 6.8.4.17a) and trialkyl phosphates (Figure 6.8.4.17b).

$$HP(O)(OH)_2 \xrightleftharpoons[pK_1 = 1.8]{} [HP(O)_2OH]^- \underset{pK_2=6.7}{\rightleftharpoons} HP(O)_3]^{2-} \tag{6.8.4.44}$$

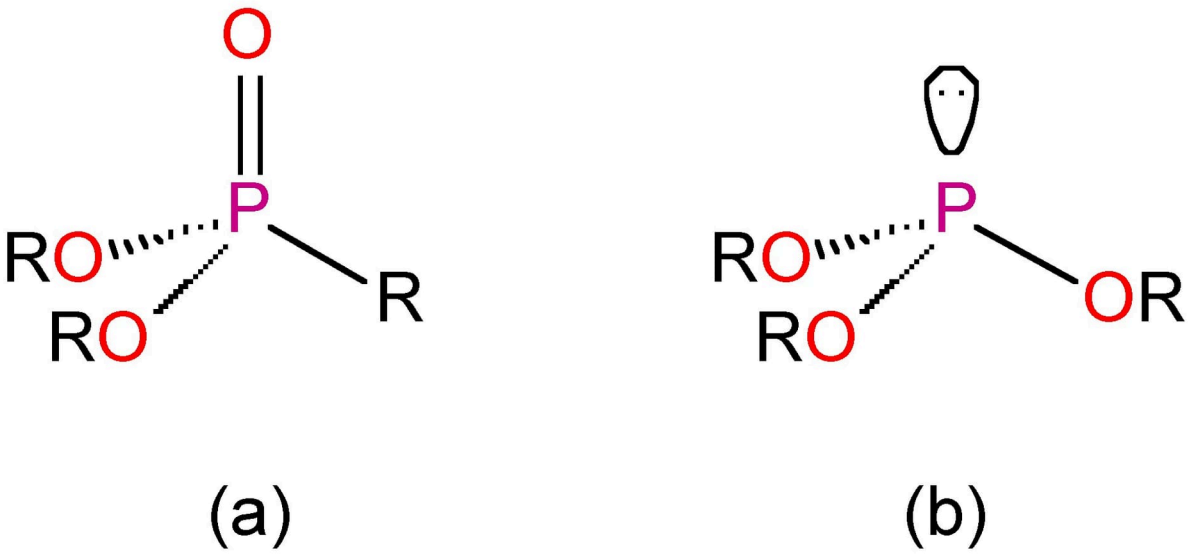


Figure 6.8.4.17: Structures of two tautomeric forms; (a) an ester of phosphoric acid and (b) a trialkyl phosphate.

Ortho phosphoric acid

Orthophosphoric acid (H_3PO_4) is the most common oxoacid of phosphorus (Figure c). The term acid phosphoric acid is commonly used. It is made from the reaction of phosphates with sulfuric acid (H_2SO_4), or from the hydrolysis of P_4O_{10}. The pure acid is a colorless crystalline solid (Mp = 42.35 °C) with extensive hydrogen bonding. The inter-phosphoric acid hydrogen bonding is partially maintained in aqueous solutions above 50% solutions.

Phosphoric acid is very stable and shows no oxidation chemistry below 350 °C. As expected, phosphoric acid is tribasic, (8.4.45). The anions $H_2PO_4^-$ and HPO_4^{2-} have particular names, dihydrogen phosphate and monohydrogen phosphate, respectively.

$$\mathrm{PO(OH)_3} \underset{\mathrm{pK_1=2.15}}{\overset{[}{\rightleftharpoons}} \mathrm{PO_2(OH)_2]^-} \underset{\mathrm{pK_2=7.1}}{\overset{[}{\rightleftharpoons}} \mathrm{PO_3(OH)]^{2-}} \underset{\mathrm{pK_3=12.4}}{\overset{[}{\rightleftharpoons}} \mathrm{PO_4]^{3-}} \tag{6.8.4.45}$$

Many salts of are known for all three anions; those with phosphate (PO_4^{2-}) are often insoluble in water. Many coordination complexes are known, especially with M^{3+} and M^{4+} ions.

Phosphorous esters

The alkyl and aryl homologs of phosphoric acid (i.e., the phosphate triester O=P(OR)$_3$) are prepared by the reaction of P_4O_{10} with the appropriate alcohol. The triesters are good solvents and Lewis basic ligands with coordination via the oxide moiety. The diesters and monoesters can also be made, and they are important in biochemical processes.

Phosphite triesters, P(OR)$_3$, may be made by the reaction of PCl_3 with alcohols or phenols in the presence of an organic base as the acceptor for the HCl formed. Alternatively, they can be prepared directly from white phosphorous, (8.4.46).

$$\mathrm{P_4 + 6OR^- + 6CCl_4 + 6ROH \rightarrow 4P(OR)_3 + 6CHCl_3 + 6Cl^-} \tag{6.8.4.46}$$

Phosphite triesters are readily oxidized to the appropriate phosphate triester, (8.4.47). They also react with alkyl halides to form the dialkyl phosphonate via the Michaelis-Arbusov reaction (8.4.48).

$$\mathrm{2P(OR)_3 + O_2 \rightarrow 2O{=}P(OR)_3} \tag{6.8.4.47}$$

$$\mathrm{P(OR)_3 + R'X \rightarrow O{=}P(OR)_2R' + RX} \tag{6.8.4.48}$$

Polyphosphates

Polyphosphates contain the PO_4 unit, and the simplest example (pyrophosphate or diphosphate, (Figure 6.8.4.18a) can be considered as condensation products of monohydrogen phosphate, (8.4.49). Longer chains can be formed, e.g., the triphosphate $P_3O_{10}^{5-}$ (Figure 6.8.4.18b). The formation and reverse (hydrolysis) reaction are slow, but are readily catalyzed, e.g., by enzymes.

$$2HPO_4^{2-} \xrightarrow{\Delta} [O_3P\text{-}O\text{-}PO_3]^{4-} + H_2O \tag{6.8.4.49}$$

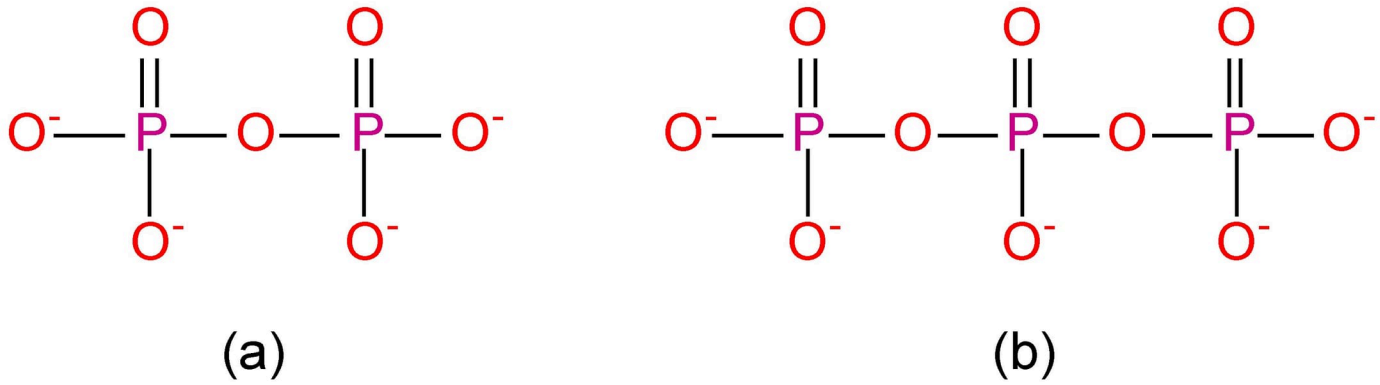
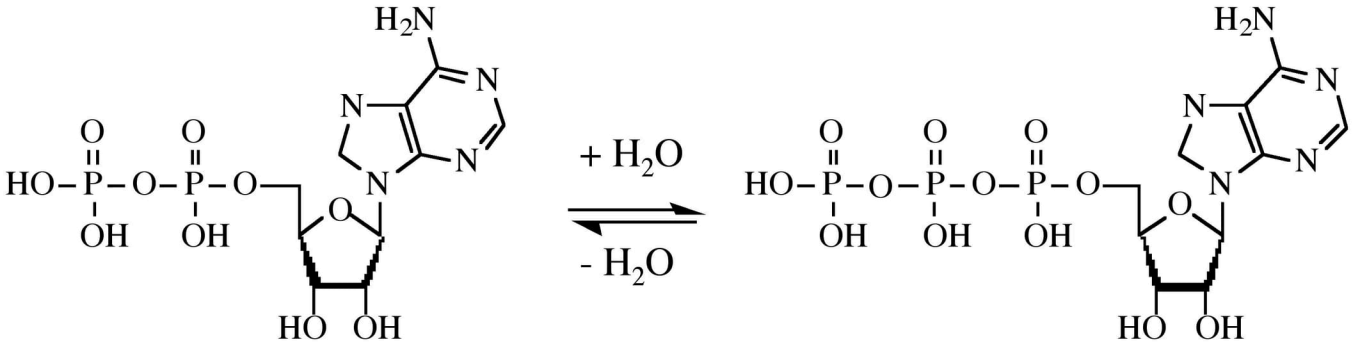


Figure 6.8.4.18: The structures of the (a) diphosphate and (b) triphosphate anions.

The monoesters of the diphosphate and triphosphate are very important in biological processes. In particular the conversion of the triphosphate ATP (adenosine triphosphate) to the diphosphate ADP (adenosine diphosphate) by the transfer of a phosphate group is important in the energetics of biological reactions.



Cyclic polyphosphates

Also known as meta phosphates, cyclic phosphates are also made from fused PO_4 units. The simplest, $P_3O_9^{3-}$, is shown in Figure 6.8.4.19. Slow addition of water to P_4O_{10} results in the formation of the tetrameric polyphosphate, $P_4O_{12}^{4-}$ (Figure 6.8.4.20), which is known as *calgon* due to its ability to complex Ca^{2+} as well as other metals.

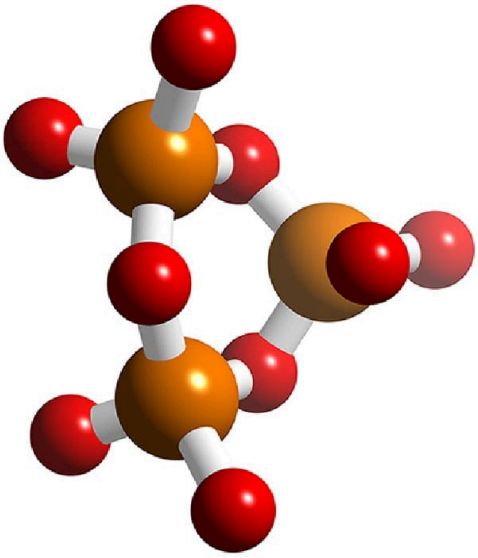


Figure 6.8.4.19: The structure of $P_3O_9^{3-}$. Phosphorus atoms are represented by the large spheres, and oxygen atoms by the small spheres (Copyright: Karl Harrison, 2005).

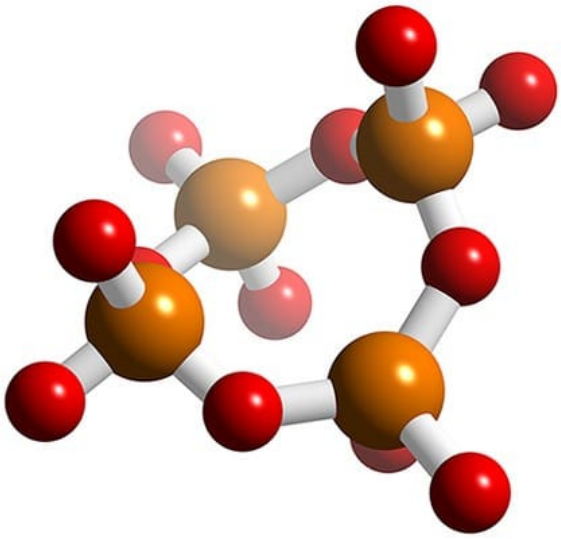


Figure 6.8.4.20: The structure of $P_4O_{12}^{4-}$*calgon*. Phosphorus atoms are represented by the large spheres, and oxygen atoms by the small spheres (Copyright: Karl Harrison, 2005).

This page titled 6.8.4: Oxides and Oxoacids is shared under a CC BY 3.0 license and was authored, remixed, and/or curated by Andrew R. Barron (CNX) via source content that was edited to the style and standards of the LibreTexts platform.

6.8.5: Halides of Phosphorous

Phosphorous trihalides

Phosphorous trihalides, PX_3, are produced from the direct reaction of phosphorous with the appropriate halogen, (8.5.1). The fluoride is readily made from the halide exchange reaction of PCl_3 with fluoride salts, (8.5.2). Mixed trihalides are formed by halide exchange, (8.5.3).

$$P_4 + 6Cl_2 \rightarrow 4PCl_3 \tag{6.8.5.1}$$

$$2PCl_3 + 3CaF_2 \rightarrow 2PF_3 + 3CaCl_2 \tag{6.8.5.2}$$

$$PCl_3 + PBr_3 \rightleftharpoons PCl_2Br + PClBr_2 \tag{6.8.5.3}$$

A summary of the physical properties of the phosphorous trihalides is given in Table 6.8.5.1. All the compounds have a pyramidal structure in the vapor phase and in solution.

Table 6.8.5.1: Selected physical properties of the phosphorous trihalides.

Compound	Mp (°C)	Bp (°C)	P-X (Å)	X-P-X (°)
PF_3	-151.5	-101.8	1.56	96.3
PCl_3	-93.6	76.1	2.04	100
PBr_3	-41.5	173.2	2.22	101
PI_3	61.2	200 (dec.)	2.43	102

The phosphorous trihalides hydrolyze to phosphoric acid, (8.5.4), and undergo alcoholysis to form the trialkyl phosphite derivative, (8.5.5). Phosphorous trifluoride is only slowly hydrolyzed by water, but reacts readily with alakaline solutions. In contrast, phosphorus triiodide is an unstable red solid that reacts violently with water. Phosphorous trichloride in particular is an excellent synthon for most trialkyl phosphines, (8.5.6).

$$PCl_3 + 3H_2O \rightarrow H_3PO_3 + 3HCl \tag{6.8.5.4}$$

$$PCl_3 + 3HOR \rightarrow P(OR)_3 + 3HCl \tag{6.8.5.5}$$

$$PCl_3 + 3RMgBr \rightarrow PR_3 + 3MgBrCl \tag{6.8.5.6}$$

As with other P(III) compounds such as trialkyl phosphines, phosphorous trihalides can be oxidized to the analogous phosphene oxide, e.g., (8.5.7).

$$2PCl_3 + O_2 \rightarrow O{=}PCl_3 \tag{6.8.5.7}$$

Phosphorous trihalides form Lewis acid-base complexes with main group metals, but the bonding to d^n ($n \neq 0$) transition metals occurs in the same manner to that of trialkyl phosphine, i.e., with dπ-pπ back donation. In fact one of the first examples of complexation of phosphorous to a low oxidation metal was the formation of PF_3 complexes with Fe-porphyrin.

Phosphorous pentahalides

The reaction of white phosphorous with excess halogen yields the pentahalides, (8.5.8). However, the pentafluoride is best prepared by halide exchange, (8.5.9).

$$P_4 + 10Cl_2 \rightarrow 4PCl_5 \tag{6.8.5.8}$$

$$2PCl_5 + 5CaF_2 \rightarrow 2PF_3 + 5CaCl_2 \tag{6.8.5.9}$$

The pentaiodide is unknown, however, selected physical properties are given for the others in Table 6.8.5.2.

Table 6.8.5.2: Selected physical properties of phosphorous pentahalides.

Compound	Mp (°C)	Bp (°C)
PF_5	-93.78	-84.5
PCl_5	166.8	160 (subl.)
PBr_5	100	106.0

The structures of the phosphorous pentahalides are all trigonal bipyramidal in the gas phase (Figure 6.8.5.1). Phosphorous pentafluoride maintains the trigonal bipyramidal structure in solid state, but the chloride and bromide are ionic solids, $[PCl_4]^+[PCl_6]^-$ and $[PBr_4]Br$ (Figure 6.8.5.2), respectively. The tetrahedral $[PCl_4]^+$ ion is also formed with the reaction of PCl_5 with other chloride ion acceptors, (8.5.10) and (8.5.11).

$$PCl_5 + TiCl_4 \rightarrow [PCl_4]^+[Ti_2Cl_9]^- \tag{6.8.5.10}$$

$$PCl_5 + NbCl_5 \rightarrow [PCl_4]^+[NbCl_6]^- \tag{6.8.5.11}$$

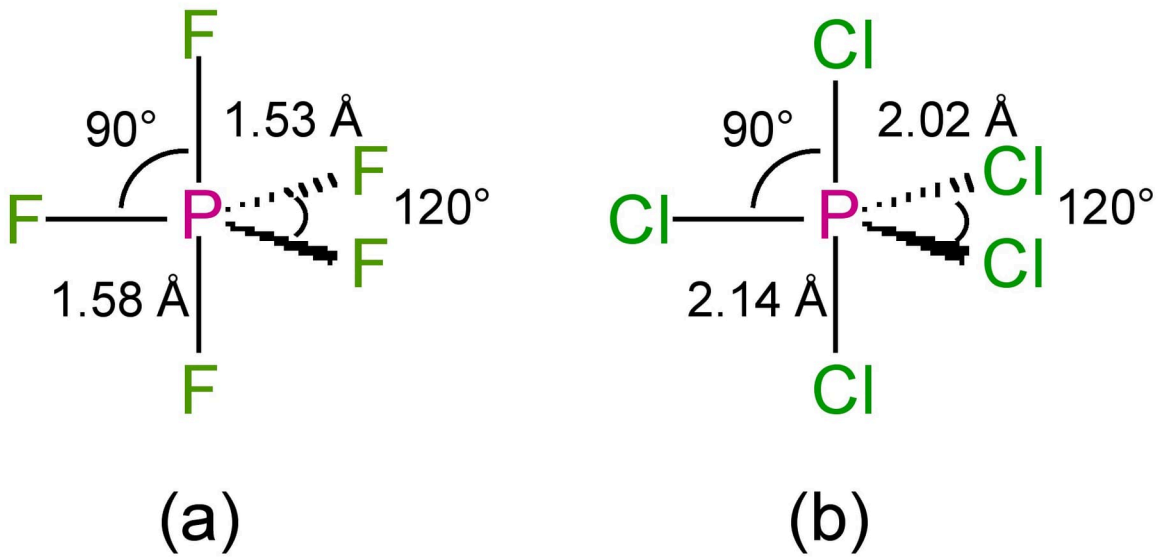


Figure 6.8.5.1: The structures of (a) PF_5 and (b) PCl_5.

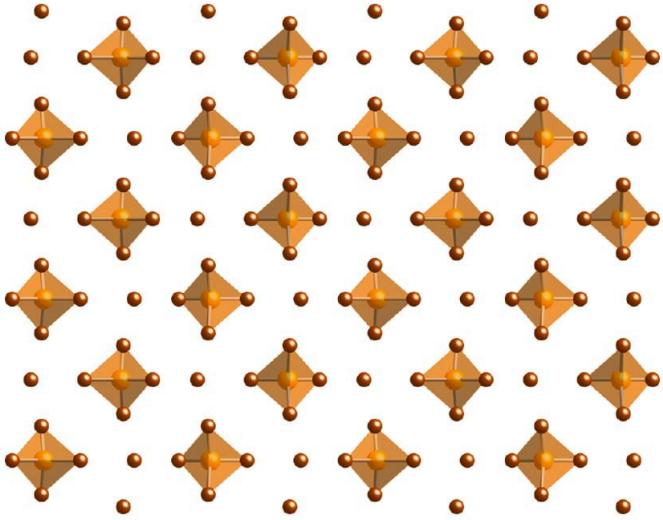


Figure 6.8.5.2: The crystal structure of phosphorous pentabromide.

All of the pentahalides undergo thermal decomposition, (8.5.12).

$$\mathrm{PX_5} \rightleftharpoons \mathrm{PX_3} + \mathrm{X_2} \tag{6.8.5.12}$$

Careful hydrolysis of the pentahalides yields the oxide of the appropriate trihalide, (8.5.13), while excess hydrolysis yields phosphoric acid, (8.5.14).

$$\mathrm{PX_5} + \mathrm{H_2O} \rightarrow \mathrm{O{=}PX_3} + \mathrm{HX} \tag{6.8.5.13}$$

$$\mathrm{PX_5} + 4\mathrm{H_2O} \rightarrow \mathrm{H_3PO_4} + \mathrm{HX} \tag{6.8.5.14}$$

This page titled 6.8.5: Halides of Phosphorous is shared under a CC BY 3.0 license and was authored, remixed, and/or curated by Andrew R. Barron (CNX) via source content that was edited to the style and standards of the LibreTexts platform.

6.9: Group 16

Thumbnail: A sample of sulfur a member of the oxygen group of elements. (Public Domain; Ben Mills).

This page titled 6.9: Group 16 is shared under a CC BY 3.0 license and was authored, remixed, and/or curated by Andrew R. Barron (CNX) via source content that was edited to the style and standards of the LibreTexts platform.

6.9.1: The Group 16 Elements- The Chalcogens

The elements

The Group 16 elements have a particular name chalcogenes. Table 1 lists the derivation of the names of the halogens.

Table 6.9.1.1: Derivation of the names of each of the Group 16(VI) elements.

Element	Symbol	Name
Oxygen	O	Greek *oxys* (*sharp*, from the taste of acids) and *genēs* (producer)
Sulfur (sulphur)	S	From the Latin *sulphurium*
Selenium	Se	Greek *selene* meaning *Moon*
Tellurium	Te	Latin *tellus* meaning *earth*
Polonium	Po	Named after Poland, Latin *Polonia*

Note

In Latin, the word is variously written *sulpur*, *sulphur*, and *sulfur*. It is an original Latin name and not a classical Greek loan, so the *ph* variant does not denote the Greek letter φ. Sulfur in Greek is *thion*, whence comes the prefix *thio-* to donate a sulfur derivative, e.g., a thioketone, $R_2C{=}S$. The simplification of the Latin words *p* or *ph* to an *f* appears to have taken place towards the end of the classical period. The element has traditionally been spelled sulphur in the United Kingdom, India, Malaysia, South Africa, Australia, Ireland, and Canada, but sulfur in the United States. IUPAC adopted the spelling "sulfur" in 1990, as did the Royal Society of Chemistry Nomenclature Committee in 1992.

Discovery

Oxygen

The 2nd century BC Greek writer, Philo of Byzantium, observed that inverting a jar over a burning candle and surrounding the jar's neck with water resulted in some water rising into the neck. He incorrectly ascribed this to the idea that part of the air in the vessel were converted into the element *fire* and thus were able to escape through pores in the glass. Much later Leonardo da Vinci (Figure 6.9.1.1) suggested that this effect was actually due to a portion of air being consumed during combustion.

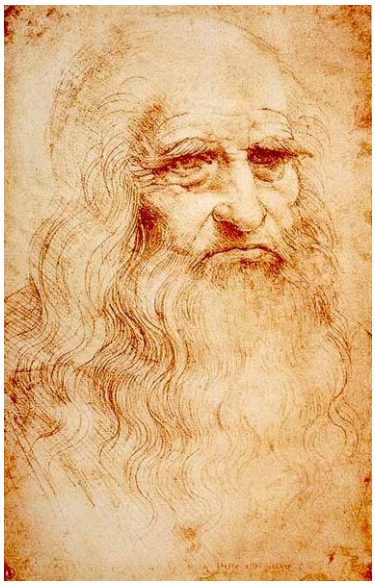


Figure 6.9.1.1: Italian painter, sculptor, architect, musician, scientist, mathematician, engineer, inventor, anatomist, geologist, cartographer, botanist and writer Leonardo di ser Piero da Vinci (1452 - 1519).

By the late 17th century, Robert Boyle (Figure 6.9.1.2) showed that air is necessary for combustion. His work was expanded by English chemist John Mayow (Figure 6.9.1.3) by showing that fire requires only a part of air that he called s*piritus nitroaereus* or just *nitroaereus*.



Figure 6.9.1.2: British natural philosopher, chemist, physicist, and inventor Robert Boyle (1627 - 1691).



Figure 6.9.1.3: English chemist, physician, and physiologist John Mayow FRS (1641–1679).

The reactive nature of nitroaereus was implied by Mayow from his observation that antimony (Sb) increased in weight when heated in air. He also suggested that the lungs separate nitroaereus from air and pass it into the blood and that animal heat and muscle movement result from the reaction of nitroaereus with certain substances in the body; both concepts that were proven to be correct.

Robert Hooke (Figure 6.9.1.4), Ole Borch (Figure 6.9.1.5), Mikhail Lomonosov (Figure 6.9.1.6), and Pierre Bayen (Figure 6.9.1.7) all produced oxygen in experiments in the 17th and the 18th century but none of them recognized it as an element, probably since the prevalence at that time of the phlogiston, and their attempts to fit their experimental observations to that theory.



Figure 6.9.1.4: Portrait of English natural philosopher, architect Robert Hooke FRS (1635 - 1703).



Figure 6.9.1.5: Danish scientist, physician, grammarian, and poet Ole Borch (1626 - 1690).



Figure 6.9.1.6: Russian scientist and writer Mikhail Vasilyevich Lomonosov (1711 - 1765).



Figure 6.9.1.7: French chemist and pharmacist Pierre Bayen (1725 - 1798).

Note

The phlogiston theory was postulated in 1667 by the German alchemist J. J. Becher, and modified in 1731 by the chemist Georg Ernst Stahl. Phlogiston theory stated that all combustible materials were made of two parts. One part, called *phlogiston*, was given off when the substance containing it was burned, while the *dephlogisticated* component was thought to be its true form, or *calx*. Highly combustible materials that leave little residue (e.g., wood) were thought to mostly comprise of phlogiston, while non-combustible substances that corrode (e.g., iron) contained very little phlogiston. Air did not play a role in phlogiston theory, instead, it was based on observations of what happens when something burns, that most common objects appear to become lighter and seem to lose something in the process. However, one observation that overturned phlogiston theory was that metals, gain weight in rusting when they were supposedly losing phlogiston!

Oxygen was first discovered by Carl Wilhelm Scheele (Figure 6.9.1.9) by heating mercuric oxide (HgO). Scheele called the gas *fire air* because it was the only known supporter of combustion. He wrote an account of this discovery in a manuscript (*Treatise on Air and Fire*) submitted in 1775. Unfortunately for Scheele his work was not published until 1777. In August 1774, an experiment conducted by Joseph Priestley (Figure 6.9.1.9) sunlight on mercuric oxide (HgO) inside a glass tube, which liberated a gas he named *dephlogisticated air*. Priestley noted that candles burned brighter in this gas. He even went as far as breathing the gas himself, after which he wrote: "The feeling of it to my lungs was not sensibly different from that of common air, but I fancied that my breast felt peculiarly light and easy for some time afterwards." Priestley published his findings in 1775. Because he published his findings first, Priestley is usually given credit for the discovery of what became known as oxygen.



Figure 6.9.1.8: Swedish chemist Carl Wilhelm Scheele (1742 – 1786). Isaac Asimov called him "hard-luck Scheele" because he made a number of chemical discoveries before others who are generally given the credit.



Figure 6.9.1.9: Portrait (by Ellen Sharples) of British clergyman natural philosopher, educator, and political theorist Joseph Priestley (1733 - 1804).

Interestingly, Lavoisier (Figure 6.9.1.10) claimed to have discovered this new substance independently. However, Priestley visited Lavoisier in October 1774 and told him about his experiment and how he liberated the new gas. Furthermore, Scheele also posted a letter to Lavoisier on September 30, 1774 that described his own discovery. Lavoisier never acknowledged receiving it, however, a copy of the letter was found in Scheele's belongings after his death.



Figure 6.9.1.10: Line engraving (by Louis Jean Desire Delaistre) of the French chemist and biologist Antoine-Laurent de Lavoisier (1743 - 1794) often refereed to as the *father of modern chemistry* due to his extensive contributions.

Raoul Pictet (figure 11) showed that by the evaporation of liquid sulfur dioxide (SO_2), carbon dioxide could be liquefied, which in turn was evaporated to cool oxygen gas enough to liquefy it. Pictet reported his results on December 22, 1877. Two days later, Louis Cailletet (Figure 6.9.1.12) announced his own method of liquefying oxygen. In both cases only a few drops could be produced, making analysis difficult. In 1891 James Dewar (Figure 6.9.1.13) was able to produce enough liquid oxygen to study. However, it was the process developed independently by Carl von Linde (Figure 6.9.1.14) and William Hampson (1854 - 1926).

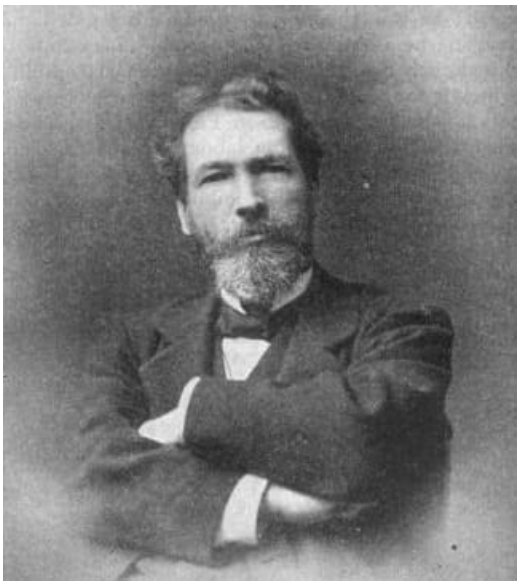


Figure 6.9.1.11: Swiss chemist and physicist Raoul Pierre Pictet (1846 - 1929).

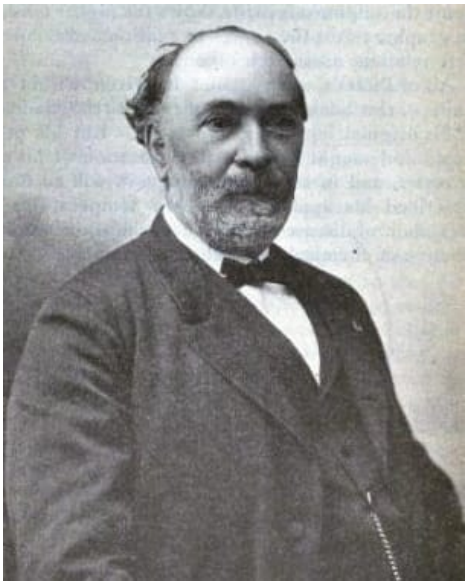


Figure 6.9.1.12: French physicist Louis Paul Cailletet (1832 - 1913).



Figure 6.9.1.13: Scottish chemist and physicist Sir James Dewar FRS (1842 - 1923).

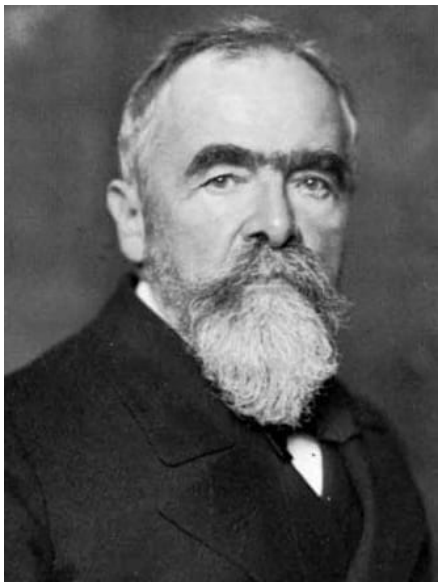


Figure 6.9.1.14: German engineer Carl Paul Gottfried von Linde (1842 - 1934).

Sulfur

Sulfur was known in ancient times and is referred to in the Bible. English translations of the Bible commonly referred to burning sulfur as *brimstone*, giving rise to the name of *fire-and-brimstone* sermons, in which listeners are reminded of the fate of eternal damnation that await the unbelieving and unrepentant. It is from this part of the Bible that Hell is implied to *smell of sulfur* (likely due to its association with volcanic activity). Sulfur ointments were used in ancient Egypt, while it was used for fumigation in Greece. A natural form of sulfur known as *shiliuhuang* was known in China since the 6th century BC. However, it was not until 1777 that Lavoisier (Figure 6.9.1.10) convinced the scientific community that sulfur was an element and not a compound.

Selenium

The element was discovered in 1817 by Berzelius (Figure 6.9.1.15), who found the element associated with tellurium. It was discovered as a byproduct of sulfuric acid production.



Figure 6.9.1.15: Swedish chemist Jöns Jacob Berzelius (1779 - 1848).

Tellurium

Tellurium was discovered in the 18th century in gold ore from the mines in Zlatna, Transylvania. In 1782 Müller von Reichenstein (Figure 6.9.1.16), the Hungarian chief inspector of mines in Transylvania, concluded that the ore was bismuth sulfide. However, the following year, he reported that this was erroneous and that the ore contained mostly gold and an unknown metal very similar to antimony. After three years of work Müller determined the specific gravity of the mineral and noted the radish-like smell of the white smoke evolved when the new metal was heated. Nevertheless, he was not able to identify this metal and gave it the names *aurum paradoxium* and *metallum problematicum*, as it did not show the properties predicted for the expected antimony.



Figure 6.9.1.16: A stamp showing Hungarian mineralogist Franz-Joseph Müller von Reichenstein (1742 - 1825).

In 1789 Kitaibel (Figure 6.9.1.17) also discovered the element independently in an ore from Deutsch-Pilsen which had been regarded as *argentiferous molybdenite*, but later he gave the credit to Müller. In 1798, the name was chosen by Klaproth (Figure 6.9.1.18) who earlier isolated it from the mineral calaverite.



Figure 6.9.1.17: Hungarian botanist and chemist Pál Kitaibel (1757 - 1817).



Figure 6.9.1.18: Figure. German chemist Martin Heinrich Klaproth (1743 –1817).

Polonium

Temporarily called *radium F*, polonium was discovered by Marie Curie and her husband Pierre Curie (Figure 6.9.1.19) in 1898, but it was later named after Marie Curie's native land of Poland. At the time Poland was not an independent country, but partitioned under Russian, Prussian, and Austrian. It was Curie's hope that naming the element after her native land would publicize its lack of independence. Polonium was the first chemical element named to highlight a political controversy.

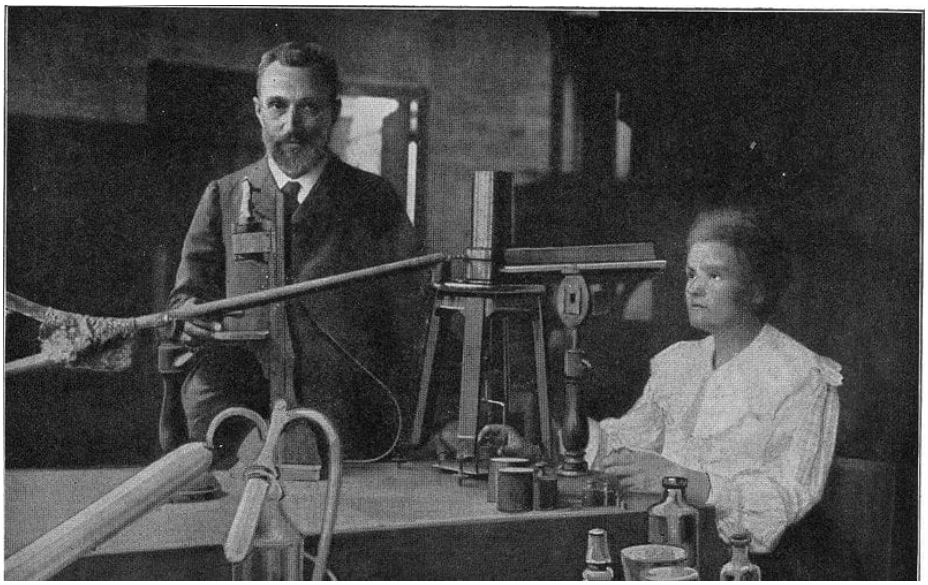


Figure 6.9.1.19: Pierre (1859 - 1906) and Marie Skłodowska-Curie (1867 - 1934) in their Paris laboratory.

Abundance

The abundance of the chalcogenes is given in Table 6.9.1.2.

Table 6.9.1.2: Abundance of Group 16 elements.

Element	Terrestrial abundance (ppm)
O	47 x 10^4 (Earth's crust), constituent of water, 21 x 10^4 (atmosphere)
S	260 (Earth's crust), 870 (sea water), 10^{-3} (atmosphere)
Se	0.05 (Earth's crust), 5 (soil), 0.2 x 10^{-3} (sea water)
Te	5 x 10-3 (Earth's crust), 0.03 (soil), 0.15 x 10^{-6} (sea water)
Po	Trace (Earth's crust)

Isotopes

The naturally abundant isotopes of the Group 16 elements are listed in Table 6.9.1.3. All of the isotopes of polonium are radioactive.

Table 6.9.1.3: Abundance of the non-synthetic isotopes of the Group 16 elements.

Isotope	Natural abundance (%)
Oxygen-16	99.76
Oxygen-17	0.039
Oxygen-18	0.201
Sulfur-32	95.02
Sulfur-33	0.75
Sulfur-34	4.21
Sulfur-36	0.02
Selenium-74	0.87

Selenium-76	9.36
Selenium-77	7.63
Selenium-78	23.78
Selenium-80	49.61
Tellurium-120	0.09
Tellurium-122	2.55
Tellurium-123	0.89
Tellurium-124	4.74
Tellurium-125	7.07
Tellurium-126	18.84
Tellurium-128	31.74
Tellurium-130	34.08

There are 38 known nuclear isomers of tellurium with atomic masses that range from 105 to 142. Tellurium is the lightest element known to undergo alpha decay, with isotopes ^{106}Te to ^{110}Te being able to undergo this mode of decay.

Cigarettes: it is not only the smoke that kills, but also the radioactivity

Ever since the early 1960s, the presence of polonium-210 in tobacco smoke has been known. The world's biggest tobacco firms spent over 40 years trying to find ways to remove the polonium-210 without success: even to this day. However, they also never published the results, keeping the facts of the radioactive hazards from the consumer.

Radioactive polonium-210 is contained in phosphate fertilizers and is absorbed by the roots of plants (such as tobacco) and stored in its tissues. Tobacco plants fertilized by rock phosphates contain polonium-210, which emits alpha radiation estimated to cause about 11,700 lung cancer deaths annually worldwide.

Industrial production of the elements

Sulfur

Elemental sulfur is found near hot springs and volcanic regions in many parts of the world. Volcanic deposits are mined in Indonesia, Chile, and Japan. Significant deposits of sulfur also exist in salt domes along the coast of the Gulf of Mexico, and in eastern Europe and western Asia. The sulfur in these deposits is believed to come from the action of anaerobic bacteria on sulfate minerals. However, fossil-based sulfur deposits from salt domes are the basis for commercial production in the United States, Poland, Russia, Turkmenistan, and Ukraine. Sulfur is mainly extracted from natural sources by two processes: the Sicilian process and the Frasch process.

Sicilian process

First used in Sicily from where it takes its name, the Sicilian process was used in ancient times to get sulfur from rocks present in volcanic regions. The sulfur deposits are piled and stacked in brick kilns built on sloping hillsides, and with airspaces between them (Figure 6.9.1.20). Then powdered sulfur is put on top of the sulfur deposit and ignited. As the sulfur burns, the heat melts the sulfur deposits, causing the molten sulfur to flow down the sloping hillside. The molten sulfur can then be collected in wooden buckets. The sulfur produced by the Sicilian process must be purified by distillation.

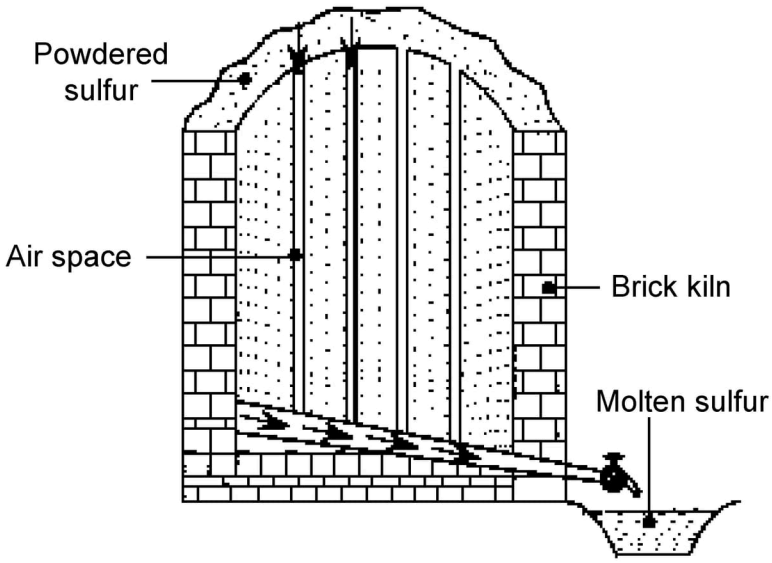


Figure 6.9.1.20: Extraction of sulfur by the Sicilian process.

Frasch process

In 1867, sulfur was discovered in the caprock of a salt dome in Louisiana; however, it was beneath quicksand, which prevented mining. In 1894 Herman Frasch (Figure 6.9.1.21), devised a method of sulfur removal using pipes to bypass the quicksand. The process proved successful, but the high cost of fuel needed to heat the water made the process uneconomic until the 1901 discovery of the Spindletop oil field in Texas (Figure 6.9.1.22) provided cheap fuel oil to the region.



Figure 6.9.1.21: German-born American chemist Herman Frasch (1851 - 1914).



Figure 6.9.1.22: Spindletop oil field in Beaumont, Texas.

In the Frasch process three concentric pipes to extract sulfur at high purity directly out of the ground (Figure 6.9.1.23). Superheated steam (160 °C) is pumped down the outermost pipe, which melts the sulfur. Hot compressed air is pumped down the innermost pipe, which serves to create foam and pressure. The resulting molten sulfur foam is then expelled through the middle pipe. The Frasch process produces sulfur with 99.5% purity, which needs no further purification.

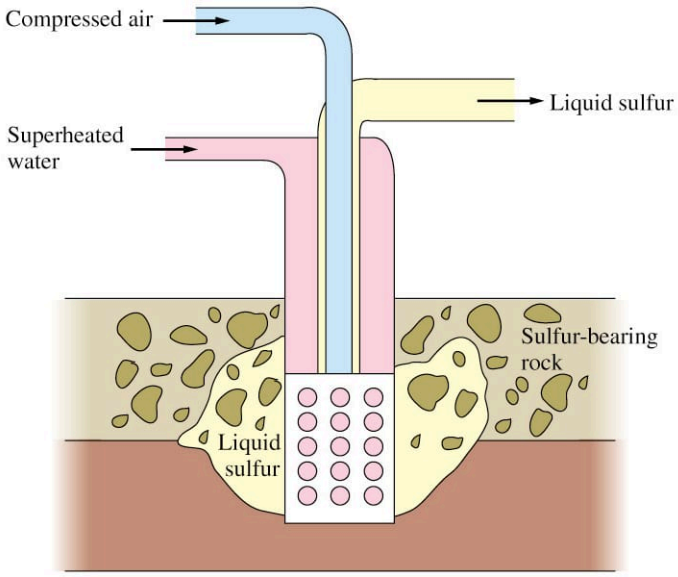


Figure 6.9.1.23: Schematic diagram of the Frasch process.

Most of the world's sulfur was obtained using the Frasch process until the late 20th century, when sulfur recovered from petroleum sources (recovered sulfur) became more commonplace.

Selenium

Elemental selenium is a rare mineral, and most elemental selenium comes as a byproduct of refining copper or producing sulfuric acid. Isolation of selenium begins by oxidation with sodium carbonate to produce selenium dioxide. The selenium dioxide is then mixed with water and the solution is acidified to form selenous acid (oxidation step). Selenous acid is bubbled with sulfur dioxide (reduction step) to give elemental selenium.

Elemental selenium produced by chemical reactions appears as the amorphous red form. When the red form is rapidly melted,

it forms the black, vitreous form. The most thermodynamically stable and dense form of selenium is the electrically conductive gray (trigonal) form, which is composed of long helical chains of selenium atoms (Figure 6.9.1.24). The conductivity of this form is notably light sensitive. Selenium also exists in three different deep-red crystalline monoclinic forms, which is composed of Se_8 molecules, similar to many allotropes of sulfur.

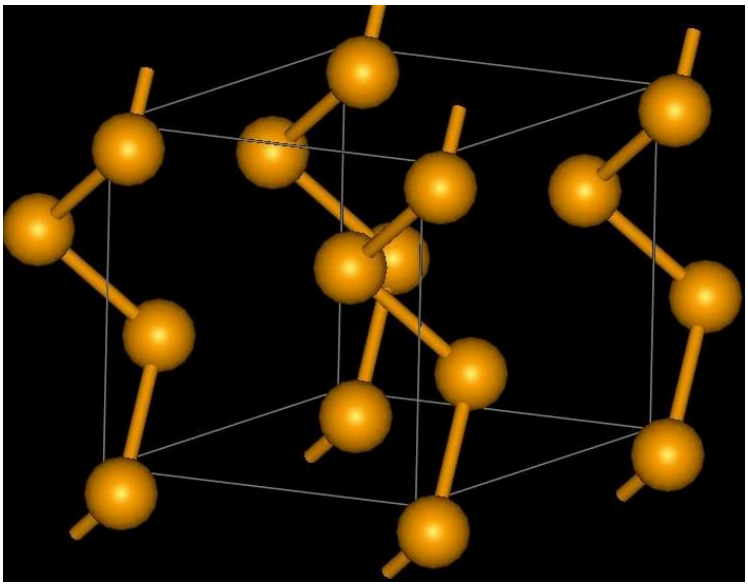


Figure 6.9.1.24: The structure of trigonal selenium.

Tellurium

The principal source of tellurium is from anode sludges produced during the electrolytic refining of copper. Treatment of 500 tons of copper ore typically yields 1 lb (0.45 kg) of tellurium. The anode sludges contain the selenides and tellurides of the noble metals in compounds with the formula M_2Se or M_2Te (M = Cu, Ag, Au). At temperatures of 500 °C the anode sludges are roasted with sodium carbonate (Na_2CO_3) under air. The metals are reduced to the metals, while the tellurium is converted to sodium tellurite, (9.1.1).

$$\mathrm{M_2Te + O_2 + Na_2CO_3 \rightarrow Na_2TeO_3 + 2M + CO_2} \tag{6.9.1.1}$$

Tellurites can be extracted from the mixture with water and are normally present as hydrotellurites $HTeO_3^-$ in solution. Selenates are also formed during this process, but they can be separated by adding sulfuric acid. The hydrotellurites are converted into the insoluble tellurium dioxide while the selenites stay in solution, (9.1.2).

$$\mathrm{HTeO_3^- + OH^- + H_2SO_4 \rightarrow TeO_2 + 2SO_4^{2-} + 2H_2O} \tag{6.9.1.2}$$

The reduction to the metal is done either by electrolysis or by reacting the tellurium dioxide with sulfur dioxide in sulfuric acid, (9.1.3).

$$\mathrm{TeO_2 + 2SO_2 + 2H_2O \rightarrow Te + SO_4^{2-} + 4H^+} \tag{6.9.1.3}$$

Physical properties

The physical properties of the Group 16 elements encompasses a gas (O_2), a non-metallic solid (S_2), and metals (Se, Te, Po), Table 6.9.1.4.

Table 6.9.1.4: Selected physical properties of the Group 16 elements.

Element	Mp (°C)	Bp (°C)	Density (g/cm^3)
O	-218.79	-182.95	1.429 g/L

S	115.21	444.6	1.819
Se	221	685	4.81 (gray), 4.39 (alpha), 4.28 (vitreous)
Te	449.51	988	6.24 (solid), 5.70 (liquid)
Po	254	962	9.196 (alpha), 9.398 (beta)

Vapor phase

The lighter Group 16 elements form X_2 dimers in the vapor phase. Sulfur also forms higher allotropes in the vapor phase (e.g., S_8 and S_6), while selenium and tellurium forms atomic vapor in addition to the dimmers. Unlike dihydrogen, however, the bonding is associated with the molecular orbital combination of the two π-orbitals (Figure 6.9.1.25). All of the dimeric X_2 molecules are paramagnetic.

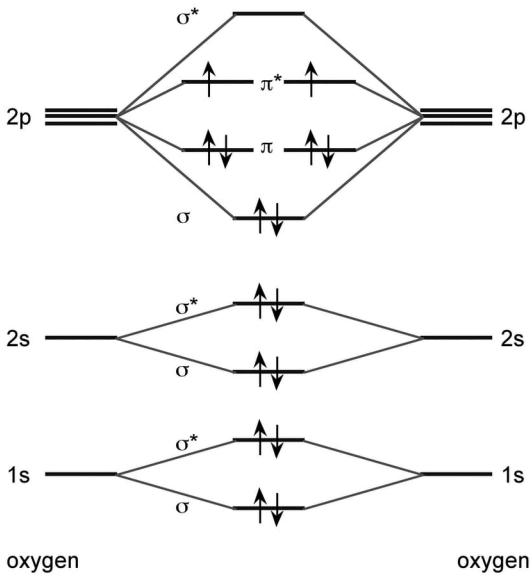


Figure 6.9.1.25: Molecular orbital diagram for the formation of O_2.

Solid state

While sulfur forms over 30 allotropes, the common form of sulfur is cyclooctasulfur (S_8) has three main allotropes: Sα, Sβ, and Sγ. The orthorhombic form (Sα) is more stable up to 95 °C, while the β-form is the thermodynamic form. The lone pairs of electrons make the S-S-S bend (108°), resulting in S_8 having the shape of a crown (Figure 6.9.1.26). When sulfur melts the S_8 molecules break up. When suddenly cooled, long chain molecules are formed in the plastic sulfur that, behave as rubber. Plastic sulfur transform into rhombic sulfur over time.

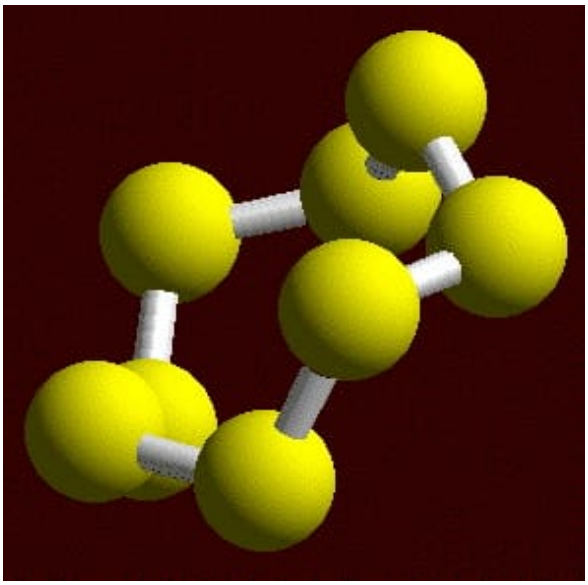


Figure 6.9.1.26: The structure of S_8.

Elemental selenium produced in chemical reactions appears as the amorphous red form. When rapidly melted, it forms the black, vitreous form, which is usually sold industrially as beads. The most thermodynamically stable and dense form of selenium is the electrically conductive gray (trigonal) form, which is composed of long helical chains of selenium atoms (Figure 6.9.1.24). The conductivity of gray selenium is light sensitive and is hence used in photocopiers. Selenium also exists in three different deep-red crystalline monoclinic forms, which are composed of Se_8 molecules, similar to many allotropes of sulfur. Unlike sulfur, however, selenium does not undergo the changes in viscosity when heated.

Tellurium is a crystalline metal with a triginal structure (a = 4.4572 Å, c = 5.929 Å). Polonium has a simple cubic structure in it's a form (a = 3.359 Å)

Compounds of the Group 16 elements.

The chemistry of the Group 16 elements is dominated by the stability of the -2 oxidation state and the noble gas configuration of the X^{2-} anion.

Oxidation state

The electronegativity of oxygen (3.5) results in it having predominantly -2 oxidation state, however, sulfur, selenium and tellurium all for compounds with higher oxidation states, especially with oxygen (Table 6.9.1.5).

Table 6.9.1.5: Examples of oxidation states in compounds of the Group 16 elements.

Element	-2	-1	+4	+6
O	Na_2O, H_2O	H_2O_2	-	-
S	H_2S	H_2S_2	SO_2	H_2SO_4, SO_3
Se	H_2Se	H_2Se_2	SeO_2	SeF_4
Te	H_2Te	$^tBu_2Te_2$	TeO_2	$Te(OH)_6$

Catenation

Catenation is the ability of a chemical element to form a long chain-like structure via a series of covalent bonds. Although oxygen shows this property only in the existence of ozone, sulfur is second only to carbon in exhibiting this mode of combination; the chalcogens beyond sulfur show it to diminishing degrees, polonium having no tendency to catenate.

When aqueous metal sulfide salts are heated with elemental sulfur a range of polysulfide ions are formed, (9.1.4). When alkali polysulfides dissolve in polar solvents (e.g., DMF or DMSO) a deep blue solution is formed. The absorption (λ_{max} = 610 nm) is associated with the radical anion, S_3^-. While, polyselenides and polytellurides are less common, the Se_3^{2-} and Te_3^{2-} ions are known.

$$S^{2-} + nS \rightarrow S^{2-}_{(n+1)} \tag{6.9.1.4}$$

The term *polysulfide* often refers to a class of polymers with alternating chains of several sulfur atoms and hydrocarbon substituents. The general formula is R_2Sn, where n ranges from 2 – 10. For the selenium and tellurium analogs the extent of catenation is far more limited.

Bibliography

- D. Barisic, S. Lulic, and P. Miletic, *Water Research*, 1992, **26**, 607.
- M. Davies, *History of Science,* 1989, **22**, 63.
- T. F. Kelley, *Science*, 1965, **149**, 537.
- M. B. Power, J. W. Ziller, A. N. Tyler, and A. R. Barron, *Organometallics*., 1992, **11**, 1055.

This page titled 6.9.1: The Group 16 Elements- The Chalcogens is shared under a CC BY 3.0 license and was authored, remixed, and/or curated by Andrew R. Barron (CNX) via source content that was edited to the style and standards of the LibreTexts platform.

6.9.2: Ozone

Ozone (O_3) is an allotrope of oxygen that is much less stable than the diatomic molecule (O_2). Ground-level ozone is an air pollutant with harmful effects on the respiratory system, hile the ozone layer in the upper atmosphere filters potentially damaging ultraviolet light from reaching the Earth's surface.

The structure of ozone is bent, with C_{2v} symmetry, similar to water (Figure 6.9.2.1a). The central oxygen has sp^2 hybridization with one lone pair. As a consequence of the bent structure, and the resonance hybridization (Figure 6.9.2.1b) ozone is a polar molecule (dipole moment = 0.5337 D).

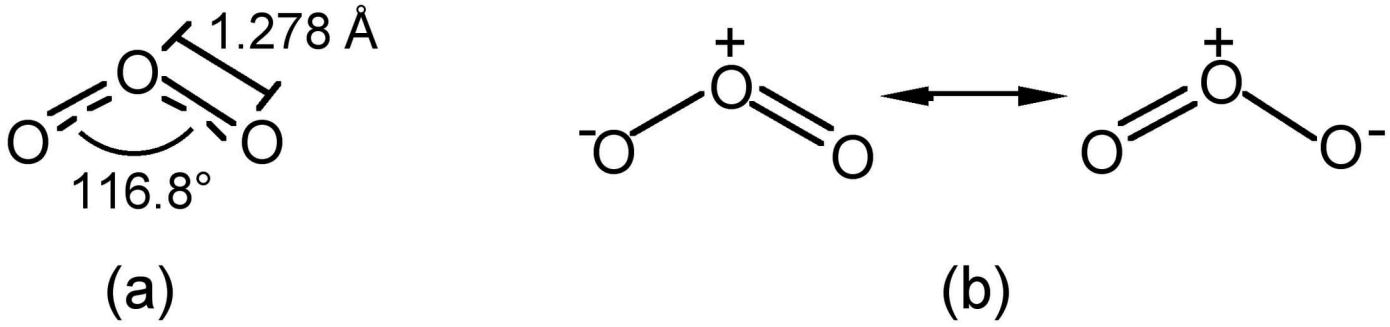


Figure 6.9.2.1: The (a) structural parameters of ozone and (b) its resonance hybridization.

Ozone is made by the exposure of oxygen (O_2) to an electric discharge. Ozone has a characteristic smell can be commonly smelled after a lightening strike; in fact the name ozone comes from the Greek *ozein* meaning *to smell*. In the laboratory, ozone can also be produced by electrolysis using graphite rod cathode, a platinum wire anode, and sulfuric acid (3 M) electrolyte. The half cell reactions are as follows:

$$3H_2O \rightarrow O_3 + 6H^+ + 6e^- \qquad (\Delta E_o = -1.53V) \tag{6.9.2.1}$$

$$6H^+ + 6e^- \rightarrow 3H_2 \qquad (\Delta E_o = 0V) \tag{6.9.2.2}$$

$$2H_2O \rightarrow O_2 + 4H^+ + 4e^- \qquad (\Delta E_o = -1.23V) \tag{6.9.2.3}$$

Ozone is also produced through photolysis of oxygen, (Equation 6.9.2.4 and 6.9.2.5), both in the laboratory and the atmosphere.

$$O_2 \xrightarrow{h\nu} 2O\cdot \tag{6.9.2.4}$$

$$O\cdot + O_2 \rightarrow O_3 \tag{6.9.2.5}$$

Ozone is a very strong oxidizing agent, and will readily oxidize a range of materials, e.g., Equations 6.9.2.6 and 6.9.2.7. It will also oxidize metals (except gold, platinum, and iridium) to their highest oxidation state, e.g., Equation 6.9.2.8.

$$O_3 + CO \rightarrow CO_2 + O_2 \tag{6.9.2.6}$$

$$O_3 + 2I^- + H_2O \rightarrow O_2 + 2OH^- + I_2 \tag{6.9.2.7}$$

$$2Cu^+_{(aq)} + 2H_3O^+_{(aq)} + O_{2(g)} \rightarrow 2Cu^{2+}_{(aq)} + 3H_2O_{(l)} + O_{2(g)} \tag{6.9.2.8}$$

Metal ozanides, which contain the ozonide anion (O_3^-) are explosive and must be stored at cryogenic temperatures. Ozonides for all the alkali metals are known. KO_3, RbO_3, and CsO_3 can be prepared from their respective superoxides.

$$KO_2 + O_3 \rightarrow KO_3 + O_2 \tag{6.9.2.9}$$

Ozone as a modulator of life on Earth

The Earth's atmosphere acts as a source of O_2 and a repository of CO_2, but its also acts as a shield for life. First, nearly all meteorites burn up on entry because of the high temperatures generated by the friction of the atmosphere. Second, the atmosphere acts as a shield for high energy UV radiation.

Although UV radiation converts 7-dehydrocholesterol into vitamin D3 in the skin (Figure 6.9.2.2), and is therefore useful, high energy UV destroys living cells. In fact the darkening we call a suntan is actually the body's mechanism for preventing further UV damage. Sun burn and skin cancer are caused by relatively weak UV light that reaches the Earth's surface, without the atmosphere we would be exposed to high energy UV that would be a hazard to all life on Earth. The Earth's "sun screen" is ozone (O_3). And without ozone in the upper atmosphere there would be no life on Earth.

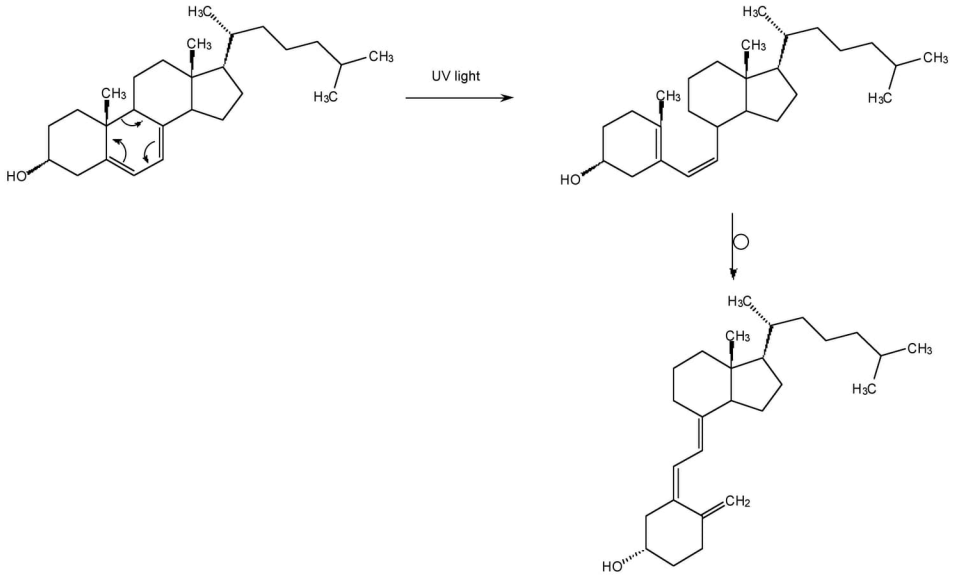


Figure 6.9.2.2: The conversion of 7-dehydrocholesterol (a derivative of cholesterol) to pre-vitamin D3 by photolysis by ultraviolet light, and its subsequent isomerization to vitamin D3.

The ozone layer is located in the lower portion of the stratosphere from approximately 10 km to 50 km above Earth, though the thickness varies seasonally and geographically. This layer contains over 91% of the ozone in Earth's atmosphere and absorbs 93-99% of the sun's high frequency ultraviolet light. The ozone decomposes photolytically to O_2 and molecular oxygen, (9.2.10), and it is this reaction that accounts for the UV protection of the atmosphere. Ozone is naturally regenerated by the exothermic reaction of the molecular oxygen with O_2, (9.2.11).

$$O_3 + h\nu \rightarrow O_2 + O \tag{6.9.2.10}$$

$$O + O_2 \rightarrow O_3 \tag{6.9.2.11}$$

The balance between ozone formation and destruction is thus an important mechanism for the protection of living organisms on the planet. While the ozone layer had been relatively constant on Earth for millions of years, the last 70 have seen a dramatic change including the increase in the polar hole in the ozone layer. The ozone hole is defined geographically as the area where the total ozone concentration is less than 220 Dobson Units.

One Dobson unit refers to a layer of ozone that would be 10 µm (micrometre) that is 1 x 10^{-5} m thick under standard temperature (25 °C) and pressure (1 atmosphere).

The ozone hole has steadily grown in size and length of existence over the past two and half decades. At present the size of ozone hole over Antarctica is estimated to be about 30 million sq.km (Figure 6.9.2.3).

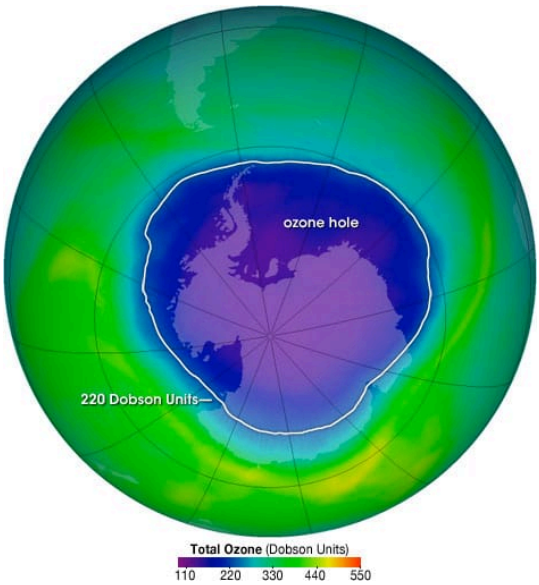


Figure 6.9.2.3: The concentration profile of ozone over Antarctica.

This page titled 6.9.2: Ozone is shared under a CC BY 3.0 license and was authored, remixed, and/or curated by Andrew R. Barron (CNX) via source content that was edited to the style and standards of the LibreTexts platform.

6.9.3: Water - The Fuel for the Medieval Industrial Revolution

Despite the greatest industrial complex of the Roman Empire being the imperial grain mill at Barbegal near Arles in what is now southern France (Figure 6.9.3.1), and the knowledge of gearing used for the mill, the waterwheel (the power source of the Barbegal's power) was little used in the ancient world. This was probably due to the high slave population obviating the need for labor saving devices. However, it may also be that because the Roman Empire was very centralized, they could provide flour on a large scale from a few highly mechanized locations. Upon the fall of the Roman Empire, the knowledge of water power would have been lost were it not for the writing departments of churches and monasteries that continued to operate through the subsequent Dark Ages.



Figure 6.9.3.1: The Barbegal mill as it stands today.

The Barbegal mill is probably the first example of industrial mass production. It consisted of eight pairs of waterwheels positioned on a 65-foot slope (Figure 6.9.3.2). The wheels were turned by water that fell from a reservoir, which in turn was fed by a magnificent aqueduct. The sixteen wheels each powered two grindstones using a set of gear that allowed the horizontal shaft from the wheel to turn a vertical shaft on which the grindstones were positioned. Grain for the mill was imported from as far as Egypt, and the flour production was eight times than that required for the local population of 10,000, resulting in an export business. Unfortunately, upon the fall of Rome the technology of waterpower almost ceased since the small city-states set up had no need for industrial complexes.

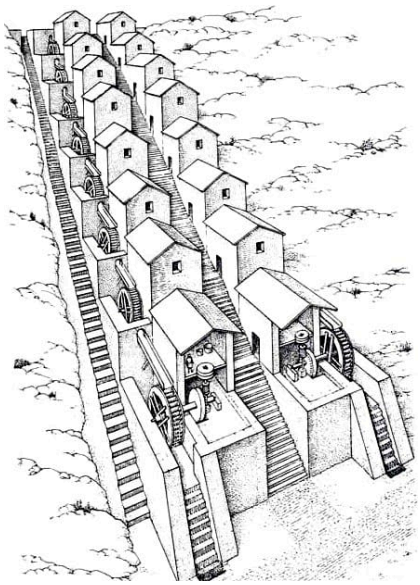


Figure 6.9.3.2: An artist's representation of the overshot waterwheels that are thought to have driven the 16 mills at Barbegal.

There are two general designs of waterwheel. The first is powered by water falling from above the wheel and is called an overshot wheel (Figure 6.9.3.3). The alternative design, the undershot wheel, relied on water flowing on a river or pond such that the current moved the paddles at the bottom of the wheel (Figure 6.9.3.4).

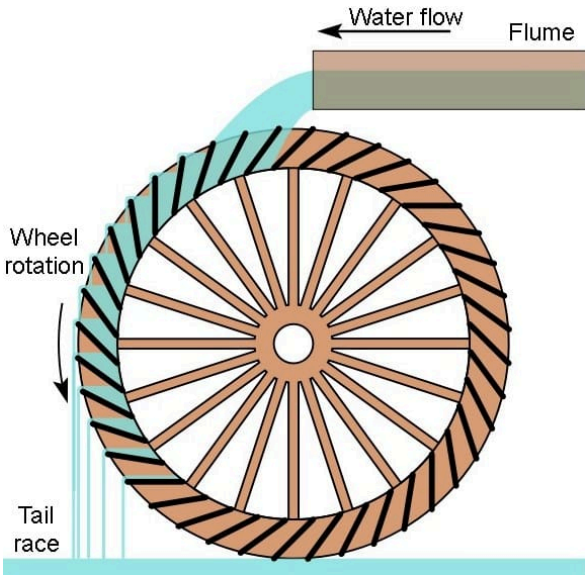


Figure 6.9.3.3: A schematic diagram of an idealized overshot water wheel.

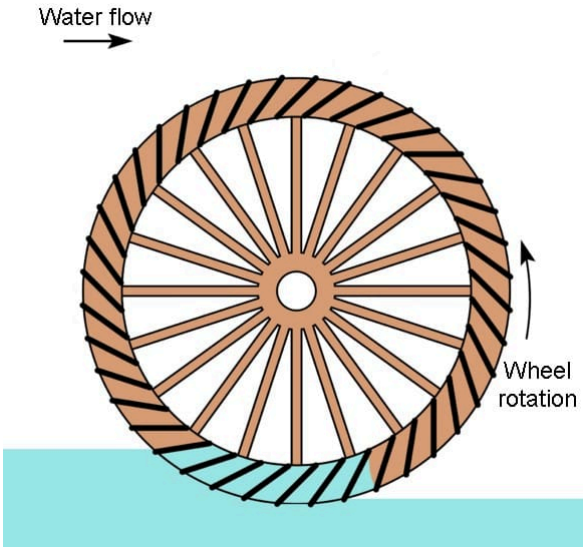


Figure 6.9.3.4: A schematic diagram of an idealized undershot water wheel.

Despite its fall from use, the waterwheel was not forgotten. Due to the writings of 14th century BC engineers, such as Vitruvius (Figure 6.9.3.5), whose texts had been preserved in the libraries in churches and monasteries across Europe, the waterwheel powered mills made a resurgence between the fifth and the tenth century. In most cases mills were owned by the church, since they had the knowledge (from ancient texts) to construct the mills and, possibly just as important, the literacy to develop the accounting system for their profitable use. The church would lease mills to farmers on a time usage, and they would take payment in flour. The owners of waterwheels and their mills were the first barons of industry post the Dark Ages. In fact, the fact that the Saxon word for an aristocrat is *Lord*, which means *loaf giver*, suggests the importance of the waterwheel. By the end of the tenth century the waterwheel was in widespread use across Europe. The Domesday Book (the nationwide census carried out by the Normans after the invasion of England) listed nearly six thousand grain mills in 1089.

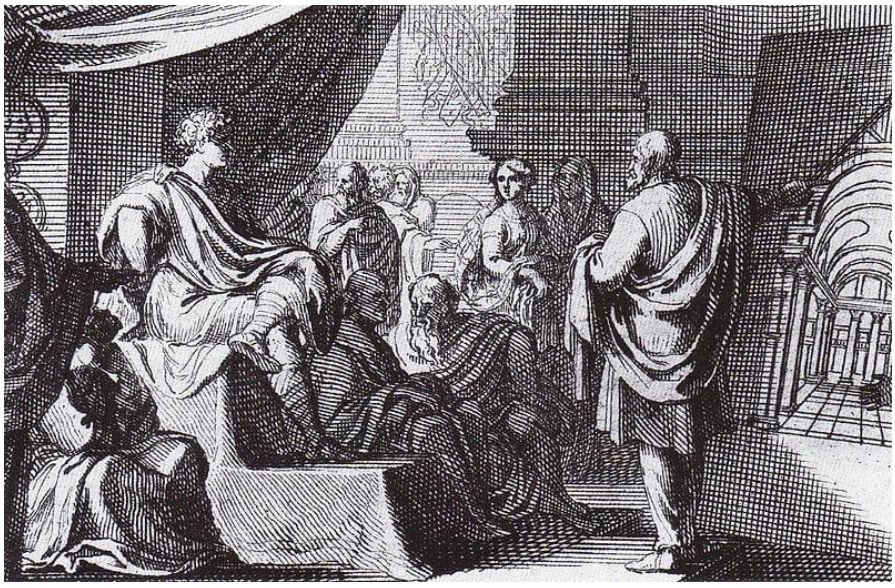


Figure 6.9.3.5: A depiction of Vitruvius (right) presenting De Architectura to the Emperor Augustus.

Despite the large number of waterwheels, the gearing used up until the ninth century was little different to that described by Vitruvius and used at Barbegal. Then around 890 AD the monastery of St Gall a new device was attached to the waterwheel. Instead of gearing to transfer power from horizontal to vertical rotation, a piece of wood was set into the shaft driven by the waterwheel (Figure 6.9.3.6). What had been created was a cam, since as the shaft turns the protruding piece of wood its anything in its way. For example, the first recorded use, by the monks at St Gall, was to crush malt for beer. However, the cam could be made to trip a hammer with every rotation (pounding), or to act on a crank to turn a rotary motion into a horizontal back-and-

forward motion (cutting), or to push down a level and activate a suction pump (raising water from a well), or operate a bellows (for a metal forge). The range of motions meant that waterpower could now be used for a wide range of industries. By the end of the tenth century there were waterwheels powering forge hammers, oil and silk mills, sugar cane crusher, tanning mills pounding leather, grinding stones, ore crushing mills (Figure 6.9.3.7), and as fulling mills for the rapidly expanding trans-European textile industry.

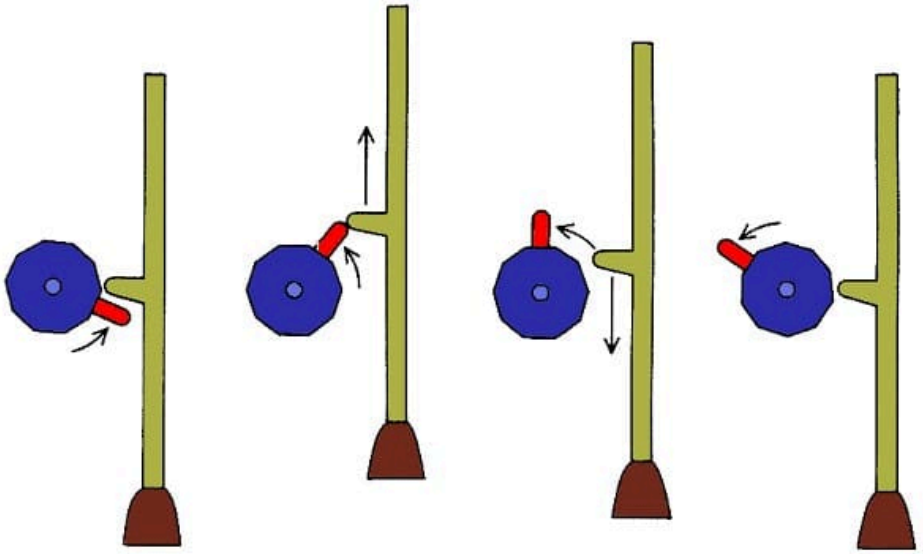


Figure 6.9.3.6: Schematic representation of the transformation of rotary motion into linear motion can be achieved by having a cam on the axle of the wheel



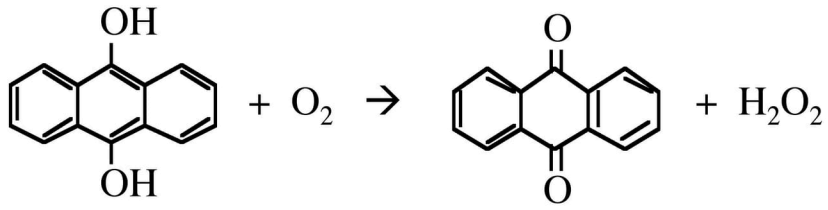
Figure 6.9.3.7: The cam principle as applied to a rock-crushing mill illustrated by Georgius Agricola in his book *De Re Metallica* (1556).

As a consequence of the waterwheel and the cam, the period between the tenth and fourteenth centuries has come to be known as the Medieval Industrial Revolution. It is interesting to note that water played a key role in the driving force during the next Industrial Revolution four hundred years later – the steam engine.

This page titled 6.9.3: Water - The Fuel for the Medieval Industrial Revolution is shared under a CC BY 3.0 license and was authored, remixed, and/or curated by Andrew R. Barron (CNX) via source content that was edited to the style and standards of the LibreTexts platform.

6.9.4: Hydrogen Peroxide

Hydrogen peroxide (H_2O_2) is a very pale blue liquid but appears colorless in dilute solution. It is prepared by the oxidation of anthraquinol (shown below). The hydrogen peroxide is extracted with water from the anthraquinone solution and the 20 - 40% solution is purified by solvent extraction. An alternative process involves the oxidation of isopropanol in either the vapor or liquid phase at 100 °C and *ca*. 15 atm, (9.4.1). The products are separated by fractional distillation.



$$Me_2C(H)OH + O_2 \rightarrow Me_2C(OOH)OH \rightarrow Me_2C{=}O + H_2O_2 \tag{6.9.4.1}$$

In the gas phase H_2O_2 adopts a gauche conformation (Figure 6.9.4.1), but there is only a low barrier to rotation about the O-O bond.

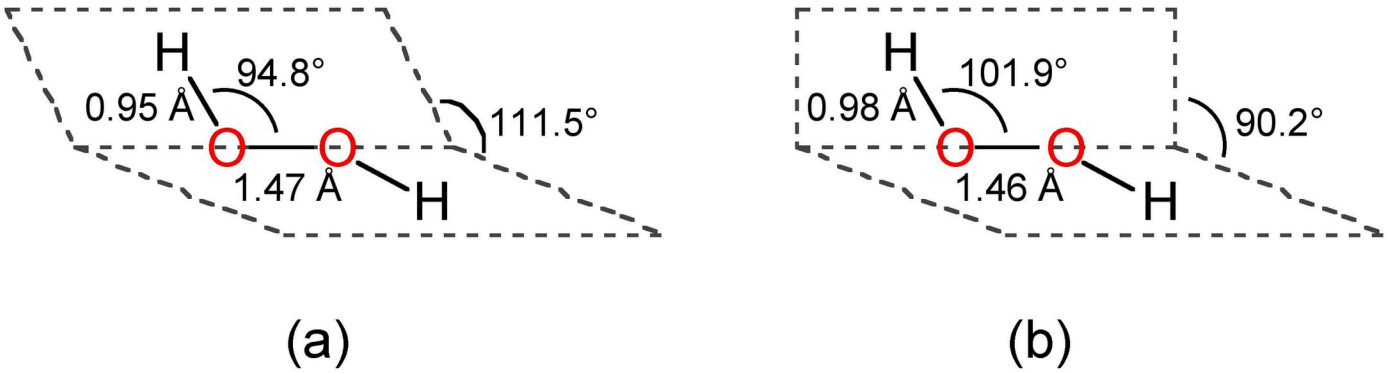


Figure 6.9.4.1: Structure of hydrogen peroxide in (a) the vapor phase and (b) the solid (crystal) phase.

Hydrogen peroxide is a liquid at standard temperature and pressure (25 °C, 1 atm) due to the presence of strong hydrogen bonding similar to found in water. In fact, the liquid range for H_2O_2 (Mp = -0.43 °C, Bp = 150.2 °C) is actually broader than water, and it is slightly more viscous than water. Hydrogen peroxide has a density of 1.44 g/cm^3, and is 10^6 times less basic that water.

As with water, H_2O_2 is a good solvent because of its polar nature and broad liquid temperature range, however, it is dangerous in its pure state due to its facile (ΔH = -99 kJ/mol) auto decomposition, (9.4.2), as well as its strong oxidizing nature.

$$2H_2O_2 \rightarrow 2H_2O + O_2 \tag{6.9.4.2}$$

Hydrogen peroxide is usually sold as 3 - 12% solution for home use; however, laboratory and certain industrial applications require 30% solutions.

Note

Hydrogen peroxide should be stored in a cool, dry, well-ventilated area and away from any flammable or combustible substances. It should be stored in a container composed of non-reactive materials such as stainless steel or glass (other materials including some plastics and aluminum alloys may also be suitable). Because it breaks down quickly when exposed to light, it should be stored in an opaque container, and pharmaceutical formulations typically come in brown bottles that filter out light.

Aqueous solution are weakly acidic (K = 1.5 x 10^{-12}), (9.4.3). However, there is no exchange of oxygen atoms between H_2O_2 and H_2O in the liquid phase.

$$\mathrm{H_2O_2 + H_2O \rightleftharpoons HO_2^- + H_3O^+} \tag{6.9.4.3}$$

As expected hydrogen peroxide is a strong oxidizing agent, (9.4.4), however, it can also act as a reducing agent, (9.4.5).

$$\mathrm{H_2O_3 + 2HI \rightarrow I_2 + 2H_2O} \tag{6.9.4.4}$$

$$\mathrm{5H_2O_2 + 2MnO_4 + 6H^+ \rightarrow 2Mn^{2+} + 8H_2O + 5O_2 \uparrow} \tag{6.9.4.5}$$

This page titled 6.9.4: Hydrogen Peroxide is shared under a CC BY 3.0 license and was authored, remixed, and/or curated by Andrew R. Barron (CNX) via source content that was edited to the style and standards of the LibreTexts platform.

6.9.5: Hydrogen Peroxide Providing a Lift for 007

In the pre-credit sequence of the 1965 film *Thunderball*, James Bond 007 (played by Sean Connery) uses a Jetpack to escape from two gunmen after killing Jacques Bouvar, SPECTRE Agent No. 6 (Figure 6.9.5.1). The Jetpack was also used in the *Thunderball* posters, being the "Look Up" part of the "Look Up! Look Down! Look Out!" tagline (Figure 6.9.5.2). The Jetpack returned in 2002 in *Die Another Day* (in which Pierce Brosnan played Bond) in the Q scene that showcased many other classic gadgets from previous Bond films.



Figure 6.9.5.1: James Bond 007 escaping from gunmen using a Jetpack (Copyright: Eon Productions).



Figure 6.9.5.2: Original poster for *Thunderball* (Copyright Danjaq, LLC and Eon Productions).

The Jetpack was actually a real fully functional device: the Bell Rocket Belt. It was designed for use in the US Army, but was rejected because of its short flying time of 21-22 seconds. Powered by hydrogen peroxide (H_2O_2), it could fly about 250 m and reach a maximum altitude of 18 m, going 55 km/h. Despite its impracticality in the real world, the Jetpack made a spectacular debut in *Thunderball*. Although Sean Connery is seen in close-up during the takeoff and landings (Figure 6.9.5.3), the main flight was actually piloted by Gordon Yeager (Fugre 4) and Bill Suitor (Figure 6.9.5.5).



Figure 6.9.5.3: Close-up shot of Sean Connery as James Bond landing the Jetpack. Note that the harness is not correctly attached, indicating this was a set-up shot for the film rather than a real flight. Presumably the crotch strap would have spoiled the lines of his suit. (Copyright: Eon Productions).



Figure 4: American pilot Gordon Yeager (1927 – 2005).



Figure 6.9.5.5: American rocket pack test pilot Bill Suitor (1944 -).

The Bell Rocket Belt is a low-power rocket propulsion device that allows an individual to safely travel or leap over small distances. All subsequent rocket packs were based on the construction design, developed in 1960-1969 by Wendell Moore. Moore's pack has two major parts:

1. Rigid glass-plastic corset (Figure 6.9.5.6a), strapped to the pilot (Figure 6.9.5.6b). The corset has a tubular metallic frame on the back, on which are fixed three gas cylinders: two with liquid hydrogen peroxide (Figure 6.9.5.6c), and one with compressed nitrogen (Figure 6.9.5.6d). When the pilot is on the ground, the corset distributes the weight of the pack to the pilot's back.
2. The rocket engine, able to move on a ball and socket joint (Figure 6.9.5.6e) in the upper part of the corset. The rocket engine consists of a gas generator (Figure 6.9.5.6f) and two pipes (Figure 6.9.5.6g) rigidly connected with it, which end with jet nozzles with controlled tips (Figure 6.9.5.6h). The engine is rigidly connected to two levers, which are passed under the pilot's hands. Using these levers the pilot inclines the engine forward or back and to the sides. On the right lever is the thrust control turning handle (Figure 6.9.5.6i), connected with a cable to the regulator valve (Figure 6.9.5.6j) to supply fuel to the engine. On the left lever is the steering handle, which controlled the tips of jet nozzles.

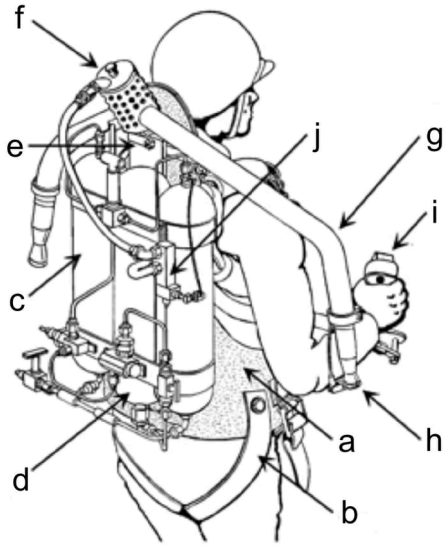


Figure 6.9.5.6: Diagram of the Bell rocket pack (Adapted from US Patent 3,243,144 (1966).

The operating principle of the Jetpack is shown in Figure. The hydrogen peroxide cylinders and compressed nitrogen cylinder are each at a pressure of ca. 40 atm or 4 MPa). To operate the pilot turns the engine thrust control handle, and opens the regulator valve (3 in Figure 6.9.5.7). Compressed nitrogen (1 in Figure 6.9.5.7) displaces liquid hydrogen peroxide (2 in Figure

6.9.5.7), which enters the gas generator (4 in Figure 6.9.5.7). In the gas generator, the hydrogen peroxide contacts the catalyst and is decomposed. The catalyst consists of thin silver plates, covered with a layer of samarium nitrate. The resulting hot high-pressure mixture of steam and gas enters two pipes, which emerge from the gas generator. These pipes are covered with a layer of heat insulator to reduce loss of heat. The hot gas enters the jet nozzles, where first they are accelerated, and then expand, acquiring supersonic speed and creating reactive thrust. The whole construction is simple and reliable; the rocket engine has no moving parts. The pack has two levers, rigidly connected to the engine installation. Pressing on these levers, the pilot deflects the nozzles back, and the pack flies forward. Accordingly, raising this lever makes the pack move back. It is possible to lean the engine installation to the sides (because of the ball and socket joint) to fly sideways.

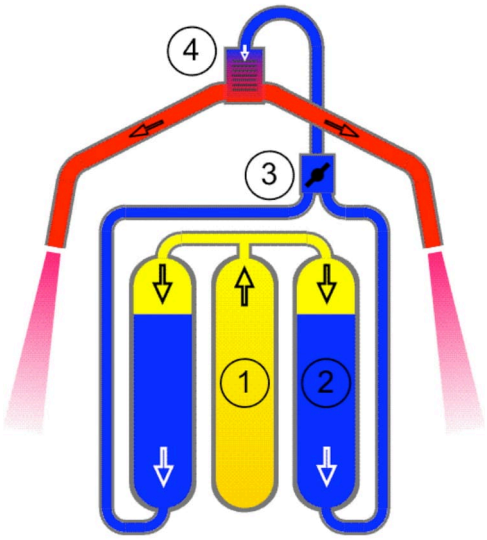


Figure 6.9.5.7: The operating principle of rocket engine.

This page titled 6.9.5: Hydrogen Peroxide Providing a Lift for 007 is shared under a CC BY 3.0 license and was authored, remixed, and/or curated by Andrew R. Barron (CNX) via source content that was edited to the style and standards of the LibreTexts platform.

6.9.6: Comparison of Sulfur to Oxygen

Size

Table 6.9.6.1 summarizes the comparative sizes of oxygen and sulfur.

Table 6.9.6.1: Comparison of physical characteristics for oxygen and sulfur.

Element	Atomic radius (Å)	Covalent radius (Å)	Ionic radius (Å)	van der Waal radius (Å)
Oxygen	0.48	0.66	1.40	1.52
Sulfur	0.88	1.05	1.84	1.80

Electronegativity

Sulfur is less electronegative than oxygen (2.4 and 3.5, respectively) and as a consequence bonds to sulfur are less polar than the corresponding bonds to oxygen. One significant result in that with a less polar S-H bond the subsequent hydrogen bonding is weaker than observed with O-H analogs. A further consequence of the lower electronegativity is that the S-O bond is polar.

Bonds formed

Sulfur forms a range of bonding types. As with oxygen the -2 oxidation state prevalent. For example, sulfur forms analogs of ethers, i.e., thioethers R-S-R. However, unlike oxygen, sulfur can form more than two covalent (non-dative) bonds, i.e., in compounds such as SF_4 and SF_6.

Such hypervalent compounds were originally thought be due to the inclusion of low energy *d* orbitals in hybrids (e.g., sp^3d^2 for SF_6); however, a better picture involves a combination of *s* and *p* ortbitals in bonding (Figure 6.9.6.1). Any involvement of the *d* orbitals is limited to the polarization of the *p* orbitals rather than direct hydridization. In this regard SF_6 represents the archetypal hypervalent molecule. Finally, sulfur can form multiple bonds, e.g., $Me_2S{=}O$.

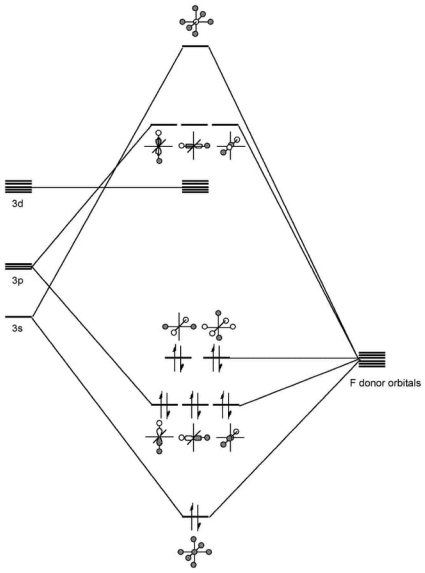


Figure 6.9.6.1: Molecular orbital diagram for SF_6.

Catenation

Catenation is defined as the ability of a chemical element to form a long chain-like structure via a series of covalent bonds. Oxygen's extent of catenation is limited to ozone (O_3) and peroxides (e.g., R-O-O-R). In contrast, the chemistry of sulfur is rich in the formation of multiple S-S bonds.

While elemental sulfur exists as a diatomic molecule (i.e., S_2) in the gas phase at high temperatures, sulfur vapor consists of a mixture of oligomers (S_3 to S_8) as a temperature dependant equilibrium. In the solid state the formation of Sn dominates, and sulfur exists as a range of polymorphs in which extended S-S bonding occurs in either rings of 6 to 20 atoms (e.g., Figure 6.9.6.2) or chains (catenasulfur).

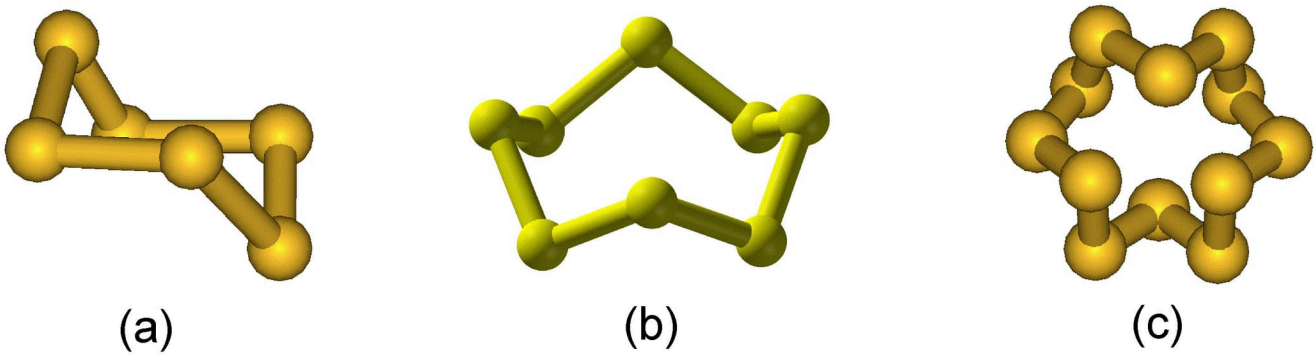


Figure 6.9.6.2: Structures of two polymorphs of sulfur: (a) cyclohexasulfur S_6, (b) cyclooctasulfur S_8, and (b) cyclododecasulfur S_{12}.

The higher level of catenation for sulfur is due to the greater strength of a S-S bond (226 kJ/mol) as compared to the O-O bond (142 kJ/mol). In general the homoleptic bond strength is expected to decrease going down a period of the Periodic Table. The reason for the unexpected weakness of the O-O bond is that the electronegative oxygen atoms repel each other and thus weaken the bond.

This page titled 6.9.6: Comparison of Sulfur to Oxygen is shared under a CC BY 3.0 license and was authored, remixed, and/or curated by Andrew R. Barron (CNX) via source content that was edited to the style and standards of the LibreTexts platform.

6.9.7: Chalconide Hydrides

Dihydrides

The hydrides of sulfur, selenium and tellurium are all extremely toxic gases with repulsive smells. Hydrogen sulfide (H_2S) is very toxic, in fact it is more than 5x as toxic as HCN (Table 6.9.7.1). Hydrogen sulfide is considered a broad-spectrum poison, meaning that it can poison several different systems in the body, although the nervous system is most affected. It forms a complex bond with iron in the mitochondrial cytochrome enzymes, thereby blocking oxygen from binding and stopping cellular respiration. Exposure to low concentrations can result in eye irritation, a sore throat and cough, nausea, shortness of breath, and fluid in the lungs. Long-term, low-level exposure may result in fatigue, loss of appetite, headaches, irritability, poor memory, and dizziness.

Table 6.9.7.1: Toxicity levels for hydrogen sulfide.

Concentration (ppm)	Biological effect
0.00047	Threshold.
10–20	Borderline concentration for eye irritation.
50–100	Eye damage.
100–150	Olfactory nerve is paralyzed and the sense of smell disappears, often together with awareness of danger.
320–530	Pulmonary edema with the possibility of death.
530–1000	Stimulation of the central nervous system and rapid breathing, leading to loss of breathing.
800	Lethal concentration for 50% of humans for 5 minutes exposure (LC50).
+1000	immediate collapse with loss of breathing, even after inhalation of a single breath.

Each of the hydrides is prepared by the reaction of acid on a metal chalcogenide, e.g., (9.7.1) and (9.7.2). The unstable H_2Po has been prepared by the reaction of HCl on Po metal.

$$\mathrm{Fe + S \rightarrow FeS} \tag{6.9.7.1}$$

$$\mathrm{FeS + 2HCl \rightarrow H_2S \uparrow + FeCl_2} \tag{6.9.7.2}$$

The thermal stability and bond strength of the dihydrides follows the trend:

$$\mathrm{H_2S > H_2Se > H_2Te > H_2Po} \tag{6.9.7.3}$$

While H_2Se is thermodynamically stable to 280 °C, H_2Te and H_2Po are thermodynamically unstable.

All the dihydrides behave as weak acids in water. Thus, dissolution of H_2S is water results in the formation of the conjugate bases, (9.7.4) and (9.7.5), with dissociation constants of 10^{-7} and 10^{-17}, respectively.

$$\mathrm{H_2S + H_2O \rightleftharpoons H_3O^+ + SH^-} \tag{6.9.7.4}$$

$$\mathrm{SH^- + H_2O \rightleftharpoons H_3O^+ + S^{2-}} \tag{6.9.7.5}$$

Sulfanes

The propensity of sulfur for catenation means that while the hydrides of oxygen are limited to water (H_2O) and hydrogen peroxide (H_2O_2), the compounds H_2S_n where n = 2 - 6 may all be isolated. Higher homologs are also known, but only as mixtures. All of the sulfanes are yellow liquids whose viscosity increases with increased chain length.

A mixture of lower sulfanes is prepared by the reaction of sodium sulfides (Na_2Sn) with HCl, (9.7.6). From this mixture the compounds H_2S_n where n = 2 - 5 are purified by fractional distillation. However, higher sulfanes are made by the reaction of either

H_2S or H_2S_2 with sulfur chlorides, (9.7.7) and (9.7.8).

$$Na_2S_2 + 2HCl \rightarrow 2NaCl + H_2S_n \tag{6.9.7.6}$$

$$2H_2S + S_nCl_2 \rightarrow 2HCl + H_2S_{n+2} \tag{6.9.7.7}$$

$$2H_2S_2 + S + nCl_2 \rightarrow 2HCl + H_2S_{n+4} \tag{6.9.7.8}$$

This page titled 6.9.7: Chalconide Hydrides is shared under a CC BY 3.0 license and was authored, remixed, and/or curated by Andrew R. Barron (CNX) via source content that was edited to the style and standards of the LibreTexts platform.

6.9.8: Oxides and Oxyacids of Sulfur

Note

Alternative spellings of sulfurous and sulfuric acids are based upon the traditional UK spelling of sulphur, i.e., sulphurous and sulphuric acid.

Sulfur dioxide and sulfurous acid solutions

The combustion of sulfur results in the formation of gaseous sulfur dioxide, (9.8.1).

$$\mathrm{S} + \mathrm{O_2} \rightarrow \mathrm{SO_2} \tag{6.9.8.1}$$

The bent structure of SO_2 is shown in Figure $6.9.8.1$, and as a consequence of the sp^2 hybridization the molecule is polar.

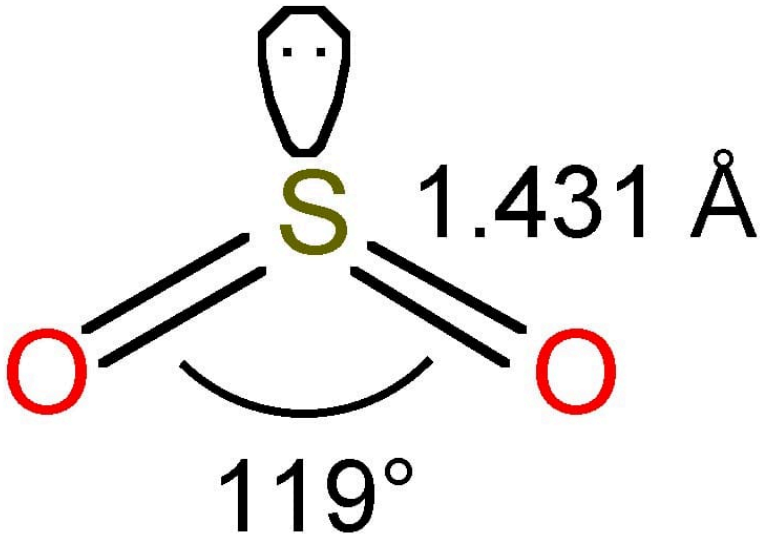


Figure $6.9.8.1$: The structure of sulfur dioxide.

The modest boiling temperature of SO_2 (-10 °C) means that it is readily liquefied and easily kept as a liquid at room temperature under a slight pressure. The liquid is associated by dipole-dipole attractions due to the polar nature of SO_2. Liquid SO_2 is a good solvent due to the polarity of the molecule; as a consequence it readily solubalizes polar compounds and salts. It is also convenient since it is easy to remove from reaction products by evaporation.

Sulfur dioxide is soluble in water forming aqueous solutions where most of the SO_2 is maintained as a hydrogen-bonded hydrate, in a similar manner to that observed for aqueous solutions of carbon dioxide. At equilibrium in neutral water (no added base) a small fraction reacts, to give a mixture of bisulfite (HSO_3^-, Figure $6.9.8.2$a) and sulfite (SO_3^{2-}, Figure $6.9.8.2$b), (9.8.2). The free acid does not to exist.

$$\mathrm{SO_{2(aq)} + H_2O \rightleftharpoons \underset{\underset{\mathrm{H{-}SO_3^-}}{\downarrow}}{\mathrm{HOSO^-_{2(aq)}}} \rightleftharpoons SO^{2-}_{3(aq)}} \tag{6.9.8.2}$$

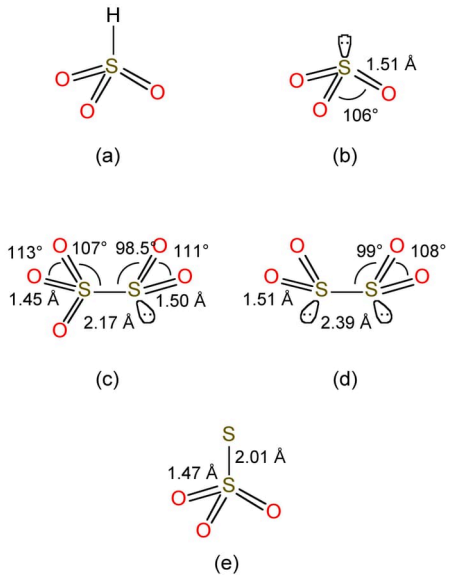


Figure 6.9.8.2: The structures of the (a) bisulfite, (b) sulfite, (c) disulfite, (d) dithionite, and (e) thiosulfate anions.

Bisulfite undergoes a further equilibrium, (9.8.3), to form disulfite, whose structure is shown in Figure 6.9.8.2c.

$$2\mathrm{HSO_3^-} \rightleftharpoons \mathrm{S_2O_5^{2-}} + \mathrm{H_2O} \tag{6.9.8.3}$$

Salts of these anions are known, and complexes of the sulfite ion are known (Figure 6.9.8.3), while SO_2 itself can act as a ligand to heavy metals.

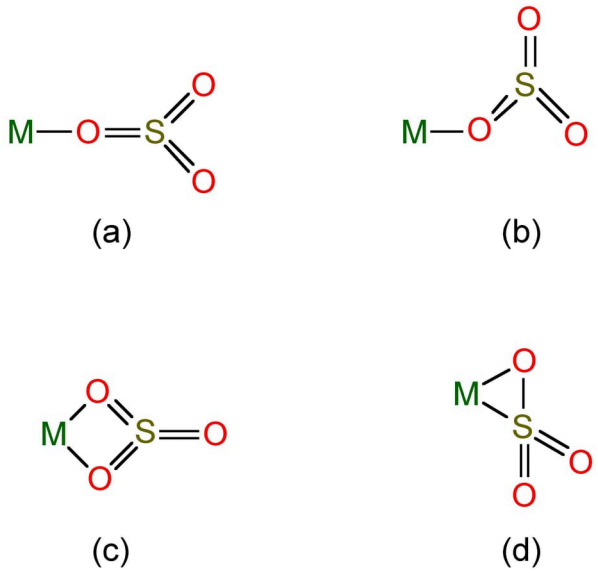


Figure 6.9.8.3: The structural modes of sulfite coordination.

The bisulfite ion has strong reducing properties, e.g., (9.8.4) and (9.8.5).

$$2\mathrm{Fe^{3+}} + \mathrm{SO_3^{2-}} + 2\mathrm{OH^-} \rightarrow 2\mathrm{Fe^{2+}} + \mathrm{H_2O} + \mathrm{SO_4^{2-}} \tag{6.9.8.4}$$

$$2\mathrm{MnO_4^+} + 5\mathrm{SO_3^{2-}} + 6\mathrm{H^+} \rightarrow 2\mathrm{Mn^{2+}} + 3\mathrm{H_2O} + 5\mathrm{SO_4^{2-}} \tag{6.9.8.5}$$

Bisulfite is also reduced by zinc in the presence of additional SO_2, (9.8.6), to form the highly reducing dithionite anion (Figure 6.9.8.2d). Reaction of bisulfite with elemental sulfur yields the thiosulfate anion (Figure 6.9.8.2e), (9.8.7)f.

$$\mathrm{SO_3^{2-}} + \mathrm{SO_2} \xrightarrow{\mathrm{Zn}} \mathrm{S_2O_4^{2-}} \tag{6.9.8.6}$$

$$SO_3^{2-} + S \rightarrow S_2O_3^{2-} \tag{6.9.8.7}$$

Sulfur trioxide and sulfuric acid

Oxidation of sulfur dioxide in the presence of a catalyst (e.g., platinum) yields sulfur trioxide, (9.8.8), which may be condensed to a liquid at room temperature (Bp = 45 °C).

$$2SO_2 + O_2 \xrightarrow{Pt} 2SO_3 \tag{6.9.8.8}$$

Liquid SO_3 exists as a mixture of monomer and trimers (Figure 6.9.8.4a and 4b), while as a solid (Mp = 16.9 °C) it forms polymers (Figure 6.9.8.4c).

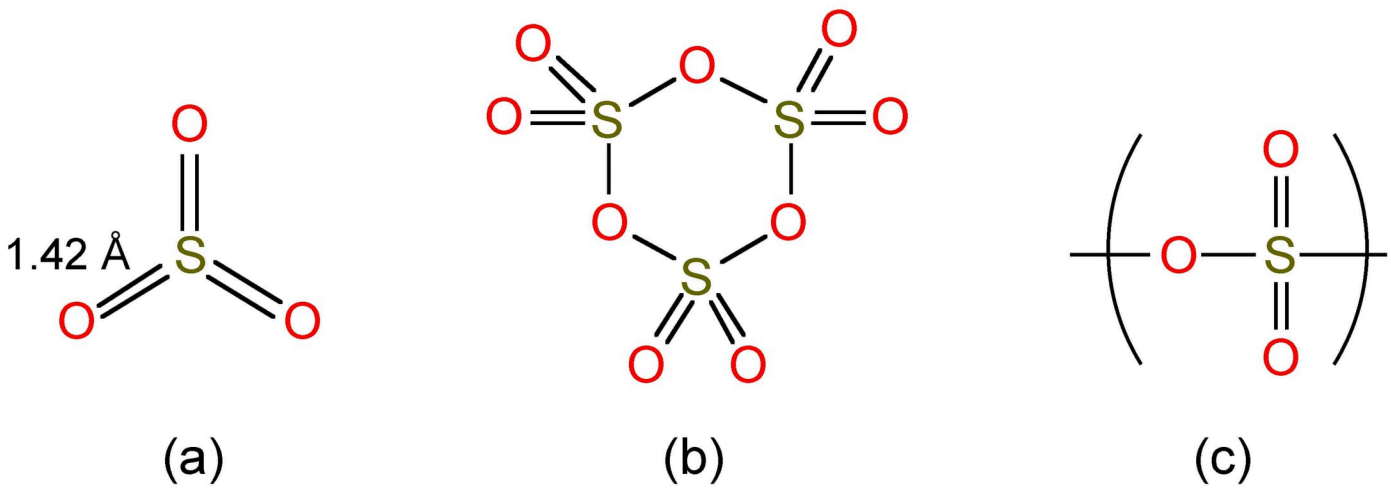


Figure 6.9.8.4: The structure of (a) monomeric, (b) trimeric, and (c) polymeric sulfur trioxide.

The reaction of SO_3 with water results in the formation of sulfuric acid, H_2SO_4, as a viscous, hydrogen bonded liquid. Sulfuric acid is a strong protic acid, which in dilute solutions (in water) reacts as a dibasic acid, (9.8.9), forming bisulfate (HSO_4^-) and sulfate (SO_4^{2-}) anions. A large number of salts are known for both anions. In addition, sulfate is known to act as a monodentate or bidentate ligand in coordination complexes.

$$H_2SO_4 \underset{+H^+}{\overset{-H^+}{\rightleftharpoons}} HSO_4^- \underset{+H^+}{\overset{-H^+}{\rightleftharpoons}} SO_4^{2-} \tag{6.9.8.9}$$

The dissolution of SO_3 in concentrated sulfuric acid yields very corrosive, *fuming* sulfuric acid, which contains some pyrosulfuric acid, (9.8.10).

$$H_2SO_4 + SO_3 \rightleftharpoons H_2S_2O_7 \tag{6.9.8.10}$$

WARNING

The corrosive properties of sulfuric acid are accentuated by its highly exothermic reaction with water. Burns from sulfuric acid are potentially more serious than those of comparable strong acids (e.g., hydrochloric acid), as there is additional tissue damage due to dehydration and particularly secondary thermal damage due to the heat liberated by the reaction with water.

Sulfur as a source of atmospheric pollution and acid rain

Sulfur dioxide is formed as a pollutant during the combustion of sulfur containing fuels, in particular coal. While the emission of SO_2 itself leads to concerns it is its conversion to sulfuric acid in the form of acid rain that has been of concern for several decades. The pathway for the formation of sulfuric acid in the atmosphere is depandant on whether the reaction occurs in dry

atmosphere or in clouds and rain.

Gaseous reactions in a dry atmosphere

In the dry atmosphere, gaseous sulfur dioxide reacts with the hydroxide radical (formed by the photochemical decomposition of ozone, (9.8.11) and (9.8.12), in the presence of a non-reactive gas molecule such as nitrogen, (9.8.12). The sulfurous acid, thus formed reacts with oxygen to generate sulfur trioxide, (9.8.13), which reacts with water to form sulfuric acid, (9.8.14).

$$O_3 + h\nu \rightarrow O* + O_2 \tag{6.9.8.11}$$

$$O* + H_2O \rightarrow 2HO\cdot \tag{6.9.8.12}$$

$$HSO_3 + O_2 \rightarrow HO_2 + SO_3 \tag{6.9.8.13}$$

$$SO_3 + H_2O \rightarrow H_2SO_4 \tag{6.9.8.14}$$

Measurements indicate that the conversion rate of SO_2 to H_2SO_4 is 4% per hour on a clear sunny day, but the rate is slower during the winter.

Liquid phase reactions in clouds and rain

In the liquid phase SO_2 reacts directly with water, (9.8.15). The bisulfite (HSO_3^-) is oxidized by hydrogen peroxide forming a forming bisulfate (HSO_4^-) solution, (9.8.16).

$$2SO_2 + 2H_2O \rightarrow SO_3^{2-} + HSO_3^- + 3H^+ \tag{6.9.8.15}$$

$$HSO_3^- + H_2O_2 \rightarrow HSO_4^- + H_2O \tag{6.9.8.16}$$

Water soluble hydrogen peroxide is formed by the oxidation of water, (9.8.17).

$$HO_2 + HO_2 \rightarrow H_2O_2 + O_2 \tag{6.9.8.17}$$

The HO_2 radical is formed by the photolysis of organic carbonyl compounds, e.g., formaldehyde in (9.8.18) and (9.8.19).

$$H_2C{=}O + h\nu \rightarrow H\cdot + HCO\cdot \tag{6.9.8.18}$$

$$HCO + O_2 \rightarrow HO_2 + CO \tag{6.9.8.19}$$

The conversion rate is independent of pH is very fast: almost 100% per hour in summer. However, the conversion is limited by the supply of hydrogen peroxide, which is often present in much lower levels than SO_2. Thus, a reduction in sulfur dioxide emissions does not always correlate with a reduction of wet acid deposition.

This page titled 6.9.8: Oxides and Oxyacids of Sulfur is shared under a CC BY 3.0 license and was authored, remixed, and/or curated by Andrew R. Barron (CNX) via source content that was edited to the style and standards of the LibreTexts platform.

6.9.9: Sulfur Halides

Sulfur hexafluoride

Sulfur hexafluoride (SF_6) is a gas at standard temperature and pressure (25 °C, 1 atm). The most common synthesis involves the direct reaction of sulfur with fluorine yields SF_6.

$$S + 3F_2 \rightarrow SF_6 \tag{6.9.9.1}$$

It should be noted that while SF_6 is highly stable, SCl_6 is not formed. The explanation of this difference may be explained by a consideration of the Born-Haber cycle shown in Figure 6.9.9.1. A similar cycle may be calculated for SCl_6; however, a combination of a higher dissociation energy for Cl_2 and a lower S-Cl bond energy (Table 6.9.9.1) provide the rational for why SCl_6 is not formed.

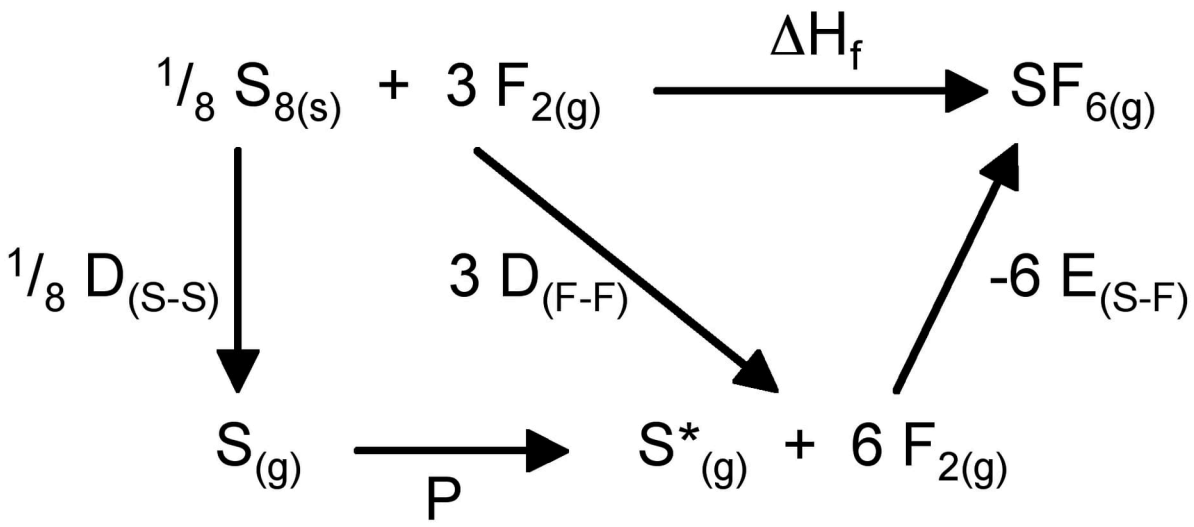


Figure 6.9.9.1: Born-Haber cycle for the formation (ΔH_f) of SF_6: where $D_{(X-Y)}$ = dissociation energy for X-Y bond, $E_{(S-F)}$ = S-F bond energy, and S* indicates 6 coordinate sulfur.

Table 6.9.9.1: Comparison of diatomic bond dissociation and S-X bond energy for the fluorine and chlorine analogs.

Bond dissociation energy	kJ/mol	Bond energy	kJ/mol
$D_{(F-F)}$	158	$E_{(S-F)}$	362
$D_{(Cl-Cl)}$	262	$E_{(S-Cl)}$	235

The S-F bond length (1.56 Å) is very short and consistent with π-bonding in addition to σ-bonding. Like SiF_6^{2-}, SF_6 is an example of a hypervalent molecule (Figure 6.9.9.2).

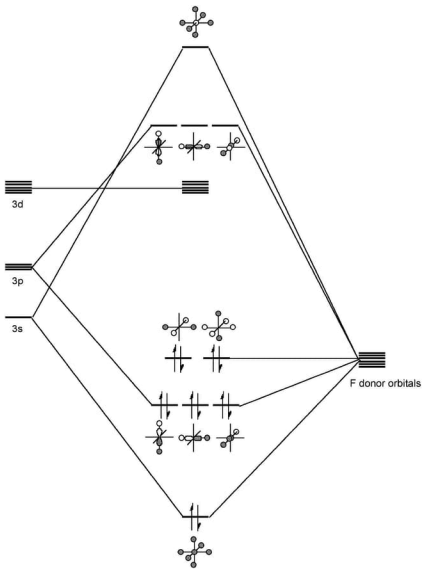


Figure 6.9.9.2: Molecular orbital bonding in SF_6.

Sulfur hexafluoride is an unreactive, non toxic compound. Its inert nature provides one of its applications, as a spark suppressor. The hexafluoride is generally resistant to chemical attack, e.g., no reaction is observed with potassium hydroxide (KOH) at 500 °C. The low reactivity is due to SF_6 being kinetically inert due to:

- Coordination saturation precluding associative reactions with nucleophiles.
- Strong S-F bond (360 kJ/mol) limiting dissociative reactions.

Thermodynamically SF_6 should react with water (ΔH = -460 kJ/mol), but the rate factors are too great. Sulfur hexafluoride can be reduced with sodium in liquid ammonia, (9.9.2), or with $LiAlH_4$. In each of these reactions the mechanism involves the formation of a radical, (9.9.3). The reaction with sulfur trioxide yields SO_2F_2, (9.9.4), however, the reactions with carbon or CS_2 only occur at elevated temperatures (500 °C) and pressure (4000 atm).

$$\mathrm{SF_6 + 8Na \rightarrow Na_2S + 6NaF} \tag{6.9.9.2}$$

$$\mathrm{SF_6 + e^- \rightarrow SF_6^-} \tag{6.9.9.3}$$

$$\mathrm{SF_6 + 2SO_3 \xrightarrow{250\ ^\circ C} 3SO_2F_2} \tag{6.9.9.4}$$

Sulfur monochloride pentafluoride

Although the hexachloride is unknown, it is possible to isolate the monochloride derivative (SF_5Cl) by the oxidative addition of Cl-F across SF_4.

$$\mathrm{SF_4 + ClF \rightarrow SF_5Cl} \tag{6.9.9.5}$$

Sulfur monochloride pentafluoride is a gas (Bp = -21 °C), but unlike SF_6 it is fairly reactive due to the polarization of the S-Cl bond (Figure 6.9.9.3), and as a consequence it reacts with water, (9.9.6).

$$\mathrm{SF_5Cl + 3H_2 \rightarrow SO_3 + 5HF + HCl} \tag{6.9.9.6}$$

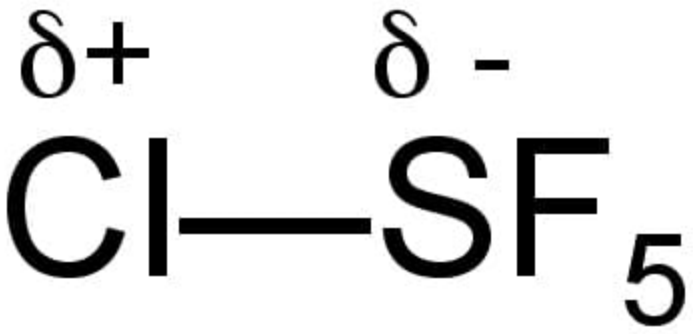


Figure 6.9.9.3: Polarization of the S-Cl bond in SF_5Cl.

Sulfur pentafluoride

Although SF_5 does not exist as a stable molecule, the gaseous dimmer S_2F_{10} (Bp = 29 °C) may be isolated from the photochemical hydrogen reduction of SF_5Cl, (9.9.7).

$$2SF_5Cl + H_2 \xrightarrow{h\nu} S_2F_{10} + 2HCl \tag{6.9.9.7}$$

While the sulfur is octahedral in S_2F_{10} (Figure 6.9.9.4a) the S-S bond is weak and long (2.21 Å versus an expected 2.08 Å for a single S-S bond). Despite the apparently weak S-S bond, S_2F_{10} shows almost no reactivity at room temperature; however, the S-S bond undergoes homoleptic cleavage at high temperatures. The resultant $SF_5^{\cdot}$ radicals disproportionate to give highly reactive fluoride radicals, (9.9.8), which is the source of the highly oxidative properties of S_2F_{10}.

$$2SF_5 \rightarrow 2SF_4 + 2F\cdot \tag{6.9.9.8}$$

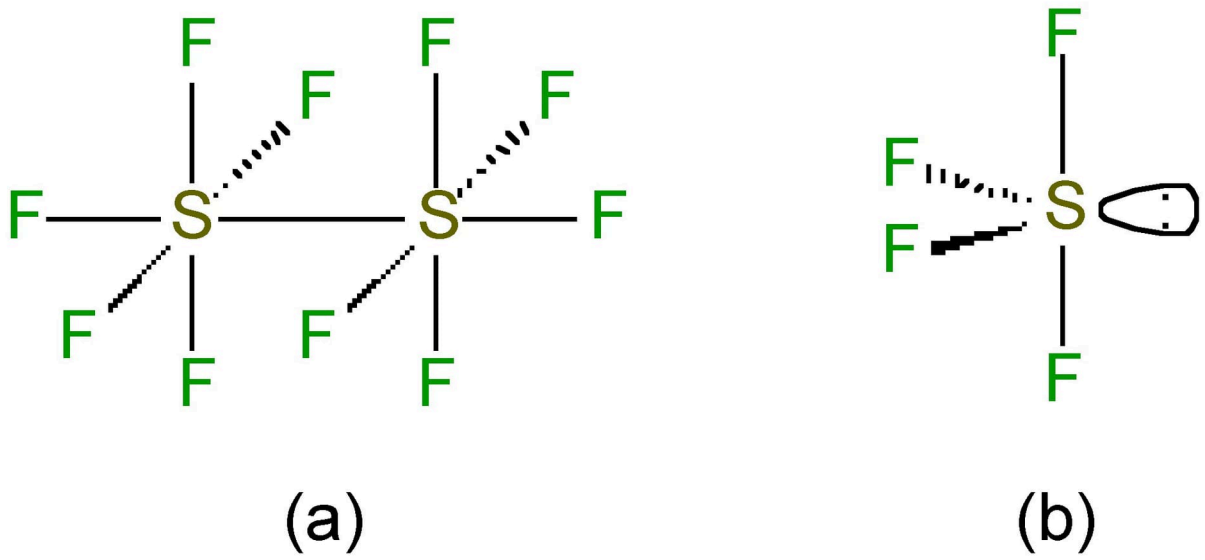


Figure 6.9.9.4: Structures of (a) S_2F_{10} and (b) SF_4.

The $SF_5^{\cdot}$ fragment is stabilized by the addition of an alkyl radical, and thus, there are a large number of RSF_5 derivatives known. Unlike, the chloride analog, these are very stable.

Sulfur tetrafluoride

Sulfur tetrafluoride (SF_4) is prepared from sulfur dichloride and sodium fluoride in acetonitrile solution at 70 - 80 °C.

$$3SCl_2 + 4NaF \rightarrow SF_4 + S_2Cl_2 + 4NaCl \tag{6.9.9.9}$$

The structure of SF_4 (and its substituted derivatives RSF_3) is based upon a trigonal bipyramidal structure with one of the equatorial sites being occupied by a lone pair (Figure 6.9.9.4b). Unlike the hexafluoride, sulfur tetrachloride is a highly reactive compound. It hydrolyzes readily, (9.9.10), and is a useful fluorinating agent (Figure 6.9.9.5).

$$SF_4 + 2H_2O \rightarrow SO_2 + 4HF \tag{6.9.9.10}$$

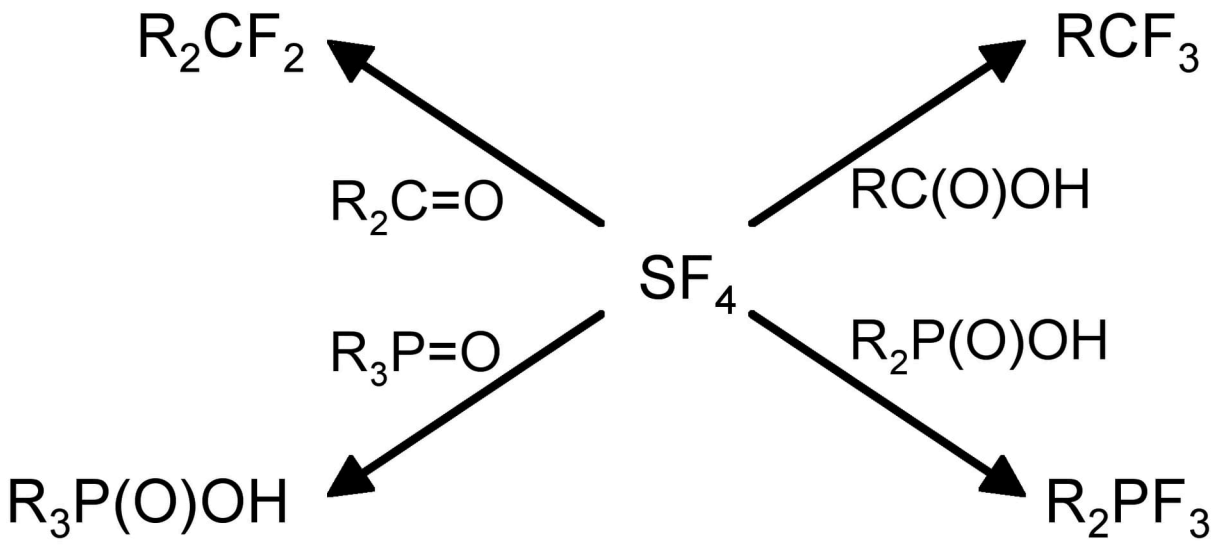


Figure 6.9.9.5: Examples of the use of SF_4 as a fluorinating agent.

Sulfur chlorides

The chlorination of molten sulfur yields the fowl smelling disulfur dichloride (S_2Cl_2). If the reaction is carried out with a catalyst such as $FeCl_3$, SnI_4 or I_2, an equilibrium mixture containing sulfur dichloride (SCl_2) is formed. However, the dichloride dissociates readily, (9.9.11), although it can be isolated as a dark red liquid if it distilled in the presence of PCl_5. The reaction of chlorine at -80 °C with SCl_2 or S_2Cl_2 allows for the formation of SCl_4 as a yellow crystalline compound which dissociates above -31 °C. Sulfur chlorides are readily hydrolyzed. Sulfur chlorides are used to dissolve sulfur (giving species up to $S_{100}Cl_2$) for the vulcanization of rubber.

$$2SCl_2 \rightleftharpoons S_2Cl_2 + Cl_2 \tag{6.9.9.11}$$

In the vapor phase S_2Cl_2 has C_2 symmetry (Figure 6.9.9.6a) while that of SCl_2 has C_{2v} symmetry (Figure 6.9.9.6b).

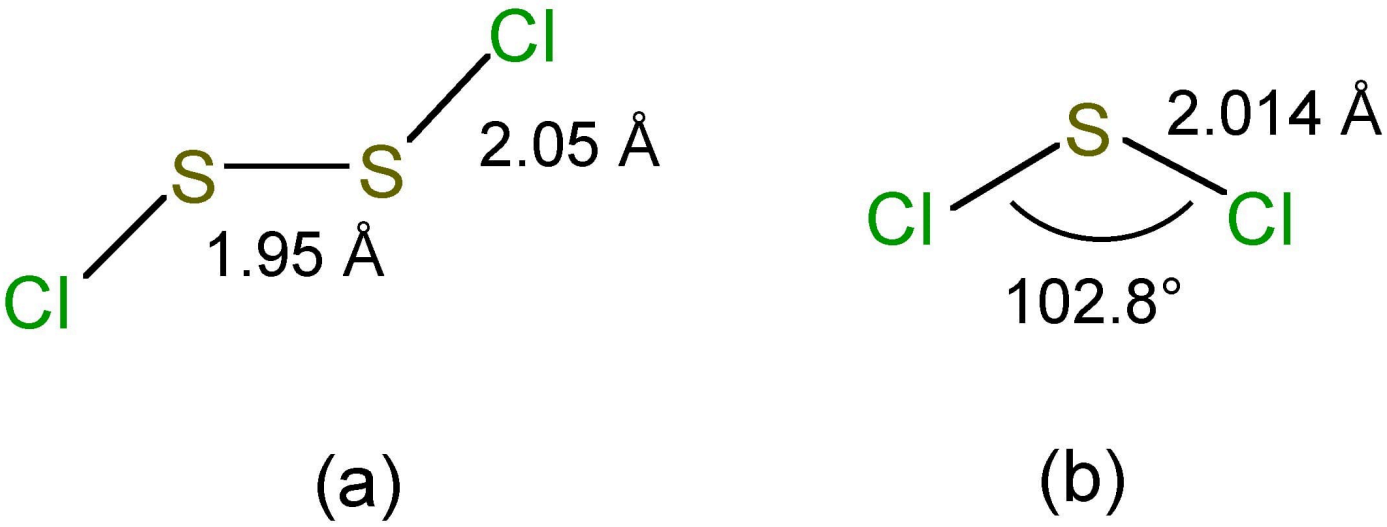


Figure 6.9.9.6: Structures of (a) S_2Cl_2 and (b) SCl_2.

This page titled 6.9.9: Sulfur Halides is shared under a CC BY 3.0 license and was authored, remixed, and/or curated by Andrew R. Barron (CNX) via source content that was edited to the style and standards of the LibreTexts platform.

6.10: The Halogens

Thumbnail: Chlorine gas in an ampoule. (CC-BY-SA; W. Oelen (http://woelen.homescience.net/science/index.html))

This page titled 6.10: The Halogens is shared under a CC BY 3.0 license and was authored, remixed, and/or curated by Andrew R. Barron (CNX) via source content that was edited to the style and standards of the LibreTexts platform.

6.10.1: The Group 17 Elements- The Halogens

The Group 17 elements have a particular name: the *halogens* meaning *born of salt*. This is due to the formation of salts when they form compounds with a metal. Table 6.10.1.1 lists the derivation of the names of the halogens.

Table 6.10.1.1: Derivation of the names of each of the halogens.

Element	Symbol	Name
Fluorine	F	Latin *fluere* meaning *to flow*
Chlorine	Cl	Greek *khlôros* meaning *pale green*
Bromine	Br	Greek *brómos* meaning *stench*
Iodine	I	Greek *odes* meaning *violet* or *purple*
Astatine	At	Greek *astatos*, meaning *unstable*

Discovery

Fluorine

The mineral *fluorspar* (also known as *fluorite*) consists mainly of calcium fluoride and was described in 1530 by Agricola (Figure 6.10.1.1) for its use as a flux. Fluxes are used to promote the fusion of metals or minerals, and it was from this use that fluorine derived its name. In 1670 Heinrich Schwanhard found that when he mixed fluorspar with an acid the fumes produced (hydrogen fluoride) etched the glasses he was wearing. Despite many researchers investigating the chemistry of hydrogen fluoride (HF) the elemental form of fluorine was not isolated until 1886 when Henri Moissan (Figure 6.10.1.2) studied the electrolysis of a solution of potassium hydrogen difluoride (KHF_2) in liquid hydrogen fluoride (HF). The mixture was needed because hydrogen fluoride is a non-conductor. The device was built with platinum/iridium electrodes in a platinum holder and the apparatus was cooled to −50 °C.



Figure 6.10.1.1: German author Georg Bauer (1494 - 1555), whose pen-name was the Latinized Georgius Agricola, was most probably the first person to be environmental conscious.



Figure 6.10.1.2: French chemist Ferdinand Frederick Henri Moissan (1852 - 1907) was awarded the Nobel Prize for his work with fluorine.

The generation of elemental fluorine from hydrofluoric acid proved to be exceptionally dangerous, killing or blinding several scientists who attempted early experiments on this halogen. The victims became known as *fluorine martyrs*.

Chlorine

Archaeological evidence has shown that sodium chloride (known as *table salt*) has been used as early as 3000 BC and brine (the saturated water solution) as early as 6000 BC. It is thought that hydrochloric acid was probably known to alchemist Jābir ibn Hayyān (Figure 6.10.1.3) around 800 AD, while aqua regia (a mixture of nitric acid and hydrochloric acid) began to be used to dissolve gold sometime before 1400 AD. Upon dissolving gold in aqua regia, chlorine gas is released along with other nauseating and irritating gases.



Figure 6.10.1.3: 15th century portrait of Abu Musa Jābir ibn Hayyān (721 - 815), also known by his Latinized name “Gerber”. He was a chemist, alchemist, astronomer and astrologer, engineer, geologist, philosopher, physicist, and pharmacist and physician.

Chlorine was first prepared and studied in 1774 by Carl Wilhelm Scheele (Figure 6.10.1.4), and therefore he is credited for its discovery despite his failing to establish chlorine as an element, mistakenly thinking that it was the oxide obtained from the hydrochloric acid. Regardless of what he believed, Scheele did isolate chlorine by reacting MnO_2 (as the mineral pyrolusite) with HCl, (10.1.1).

$$4HCl + MnO_2 \rightarrow MnCl_2 + 2H_2O + Cl_2 \quad (6.10.1.1)$$



Figure 6.10.1.4: Swedish chemist Carl Wilhelm Scheele (1742 – 1786). Isaac Asimov called him "hard-luck Scheele" because he made a number of chemical discoveries before others who are generally given the credit.

Bromine

Bromine was discovered independently by two chemists Antoine Balard (Figure 6.10.1.5) in 1825 and Carl Jacob Löwig (Figure 6.10.1.6) in 1826.



Figure 6.10.1.5: French chemist Antoine Jérôme Balard (1802 - 1876).



Figure 6.10.1.6: German chemist Carl Jacob Löwig (1803 - 1890).

Balard found bromide salts in the ash of sea weed from the salt marshes of Montpellier. The sea weed was used to produce iodine, but also contained bromine. Balard distilled the bromine from a solution of seaweed ash saturated with chlorine. The properties

of the resulting substance resembled that of an intermediate of chlorine and iodine; with those results he tried to prove that the substance was iodine monochloride (ICl), but after failing to do so he was sure that he had found a new element and named it *muride*, derived from the Latin word *muria* for brine.

In contrast, Löwig isolated bromine from a mineral water spring in Bad Kreuznach. Löwig used a solution of the mineral salt saturated with chlorine and extracted the bromine with Et_2O. After evaporation a brown liquid remained. Unfortunately, the publication of his results were delayed and Balard published first.

Iodine

Iodine was discovered by Bernard Courtois (Figure 6.10.1.7) in 1811 when he was destroying the waste material from the production of saltpeter (KNO_3) during gunpowder production. Saltpeter produced from French niter beds required sodium carbonate (Na_2CO_3), which could be isolated from seaweed washed up on the coasts of Normandy and Brittany. To isolate the sodium carbonate, seaweed was burned and the ash then washed with water; the remaining waste was destroyed by the addition of sulfuric acid (H_2SO_4). After adding too much acid, Courtois observed a cloud of purple vapor that crystallized on cold surfaces making dark crystals. Courtois suspected that this was a new element but lacked the money to pursue his observations. In supplying samples to his friends, Charles Desormes and Nicolas Clément, he hoped his research was to continue. On 29 November 1813, Dersormes and Clément made public Courtois's discovery, describing the substance to a meeting of the Imperial Institute of France.



Figure 6.10.1.7: French chemist Bernard Courtois (1777 - 1838).

Astatine

The existence of *eka-iodine* had been predicted by Mendeleev (Figure 6.10.1.8), but astatine was first synthesized in 1940 by Corson (Figure 6.10.1.9), MacKenzie (Figure 6.10.1.10), and Segrè (Figure 6.10.1.11) at the University of California, Berkeley by bombarding bismuth with alpha particles.

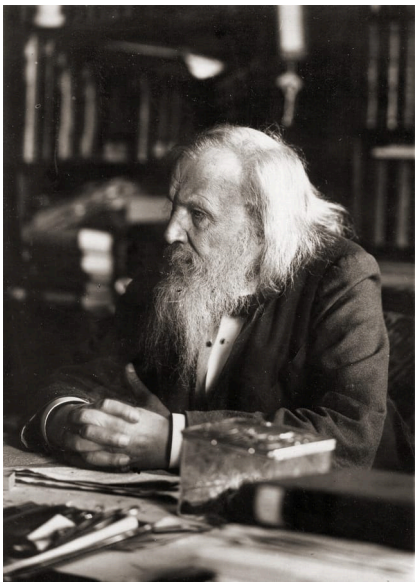


Figure 6.10.1.8: Russian chemist Dmitri Mendeleev (1834 - 1907).



Figure 6.10.1.9: Physicist and President of Cornell University, Dale R. Corson (1914 -).



Figure 6.10.1.10: Physicist Kenneth Ross MacKenzie (1912 - 2002).



Figure 6.10.1.11: Italian physicist Emilio Segrè (1905 - 1989).

Abundance

The abundance of the halogens is given in Table 6.10.1.2.

Table 6.10.1.2: Abundance of the halogens.

Element	Terrestrial abundance (ppm)
F	950 (Earth's crust), 330 (soil), 1.3 (sea water), 6 x 10^{-4} (atmosphere)
Cl	130 (Earth's crust), 50 – 2000 (soil), 1.8 x 10^{4} (sea water)
Br	0.4 (Earth's crust), 5 – 40 (soil), 65 (sea water)
I	0.14 (Earth's crust), 3 (soil), 0.06 (sea water), 60 x 10^{-3} (atmosphere)
At	Trace in some minerals

Isotopes

The naturally abundant isotopes of the halogens are listed in Table 6.10.1.3. All 33 isotopes of astatine are radioactive.

Table 6.10.1.3: Abundance of the major isotopes of the halogens.

Isotope	Natural abundance (%)
Fluorine-19	100
Chlorine-35	75.77
Chlorine-36	trace
Chlorine-37	24.23
Bromine-79	50.69
Bromine-81	49.31
Iodine-127	100%

While ^{19}F is the only naturally abundant isotope of fluorine, the synthetic isotope, ^{18}F, has half life of about 110 minutes, and is commercially an important source of positrons for positron emission tomography (PET). PET is a nuclear medicine imaging technique that produces a 3-D image of processes within the body. The system detects pairs of γ-rays emitted indirectly by a positron-emitting radionuclide (tracer), which is introduced into the body on a biologically active molecule.

Trace amounts of radioactive ^{36}Cl exist in the environment at about 7 x 10^{-11}%. ^{36}Cl is produced in the atmosphere by the interaction of cosmic rays with ^{36}Ar. In the ground ^{36}Cl is generated through neutron capture by ^{35}Cl or muon (an elemental particle similar to an electron) capture by ^{40}Ca. ^{36}Cl decays with a half-life of 308,000 years making it suitable for geologic dating in the range of 60,000 to 1 million years. However, due to the large amounts of ^{36}Cl produced by irradiation of seawater during atmospheric detonations of nuclear weapons between 1952 and 1958, it is also sued as an event marker for 1950s water in soil and ground water.

Iodine has 37 isotopes of iodine, but only one, ^{127}I, is stable. Of the radioactive isotopes, ^{129}I (half-life 15.7 million years) is used for radiometric dating of the first 85 million years of solar system evolution. ^{129}I is also a product of uranium and plutonium fission, and as a consequence of nuclear fuel reprocessing and atmospheric nuclear weapons tests, the natural signal has been swamped. As a consequence it can now be used as a tracer of nuclear waste dispersion into the environment. ^{129}I was used in rainwater studies to track fission products following the Chernobyl disaster.

Due to preferential uptake of iodine by the thyroid, isotopes with short half lives such as ^{131}I can be used for thyroid ablation, a procedure in which radioactive iodine is administered intravenously or orally following a diagnostic scan. The lower energy isotopes ^{123}I and ^{125}I are used as tracers to evaluate the anatomic and physiologic function of the thyroid.

Industrial production.

Industrial production of fluorine involves the electrolysis of hydrogen fluoride (HF) in the presence of potassium fluoride (KF) during which fluorine gas is formed at the anode and hydrogen gas is formed at the cathode (Figure 6.10.1.12). The potassium fluoride (KF) is converted to potassium bifluoride (KHF_2), (10.1.2), which is the electrolyte and intermediate to the fluorine and hydrogen, (10.1.3).

$$\mathrm{HF + KF \rightarrow KHF_2} \tag{6.10.1.2}$$

$$\mathrm{2KHF_2 \rightarrow 2KF + 2F_2 + H_2} \tag{6.10.1.3}$$



Figure 6.10.1.12: The fluorine cell room at F2 Chemicals Ltd, Preston, UK.

The HF is formed as a byproduct of the production of phosphoric acid, since phosphate-containing minerals contain significant amounts of calcium fluorides, which upon treatment with sulfuric acid release hydrogen fluoride, (10.1.4).

$$\mathrm{CaF_2 + H_2SO_4 \rightarrow 2HF + CaSO_4} \tag{6.10.1.4}$$

Chlorine is generally manufactured by electrolysis of a sodium chloride solution (brine). The production of chlorine results in the co-products caustic soda (sodium hydroxide, NaOH) and hydrogen gas (H_2). Chlorine can also be produced by the electrolysis of a solution of potassium chloride, in which case the co-products are hydrogen and caustic potash (potassium hydroxide). There are three industrial methods for the extraction of chlorine by electrolysis of chloride solutions, all proceeding by the same reaction at the cathode, (10.1.5), and anode, (10.1.6), which lead to the overall reaction, (10.1.7), where M = Na or K.

$$\mathrm{2H^+_{(aq)} + 2e^- \rightarrow H_{2(g)}} \tag{6.10.1.5}$$

$$\mathrm{2Cl^-_{(aq)} \rightarrow Cl_{2(g)} + 2e^-} \tag{6.10.1.6}$$

$$\mathrm{2MCl + 2H_2O \rightarrow Cl_2 + H_2 + 2MOH} \tag{6.10.1.7}$$

Bromine exists exclusively as bromide salts in the Earth's crust, however, due to leaching, bromide salts have accumulated in sea water, but at a lower concentration than chloride. The majority of bromine is isolated from bromine-rich brines, which are treated with chlorine gas, flushing through with air. In this treatment, bromide anions are oxidized to bromine by the chlorine gas, (10.1.8).

$$\mathrm{2Br^- + Cl_2 \rightarrow 2Cl^- + Br_2} \tag{6.10.1.8}$$

Two major sources of iodine are used for commercial production: the caliche (a hardened sedimentary deposit of calcium carbonate found in Chile) and the iodine containing brines of gas and oil fields in Japan and the United States. The caliche contains sodium nitrate ($NaNO_3$); in which traces of sodium iodate ($NaIO_3$) and sodium iodide (NaI) are found. During the production of sodium nitrate the sodium iodate and iodide is extracted. Iodine sourced from brine involves the acidification with

sulfuric acid to form hydrogen iodide (HI), which is then oxidized to iodine with chlorine, (10.1.9). The aqueous iodine solution is concentrated by passing air through the solution causing the iodine to evaporate. The iodine solution is then re-reduced with sulfur dioxide, (10.1.10). The dry hydrogen iodide (HI) is reacted with chlorine to precipitate the iodine, (10.1.11).

$$2HI_{(aq)} + Cl_2 \rightarrow I_{2(aq)} + 2HCl_{(aq)} \tag{6.10.1.9}$$

$$I_2 + 2H_2O + SO_2 \rightarrow 2HI + H_2SO_4 \tag{6.10.1.10}$$

$$2HI + Cl_2 \rightarrow I_2 \downarrow + 2HCl \tag{6.10.1.11}$$

Physical properties

The physical properties of the halogens (Table 6.10.1.4) encompasses gases (F_2 and Cl_2), a liquid (Br_2), a non-metallic solid (I_2), and a metallic metal (At).

Table 6.10.1.4: Selected physical properties of the halogens.

Element	Mp (°C)	Bp (°C)	Density (g/cm3)
F	-219.62	-188.12	1.7 x 10^{-3} @ 0 °C, 101 kPa
Cl	-101.5	-34.04	3.2 x 10^{-3} @ 0 °C, 101 kPa
Br	-7.2	58.8	3.1028 (liquid)
I	113.7	184.3	4.933
At	302	337	*ca.* 7

Reactivity

All the halogens are highly reactive and are as a consequence of the stability of the X^- ion are strong oxidizing agents (Table 6.10.1.5).

Table 6.10.1.5: Electrochemical reduction potential for halogens.

Reduction	Reduction potential (V)
$F_2 + 2\ e^- \rightarrow 2\ F^-$	2.87
$Cl_2 + 2\ e^- \rightarrow 2\ Cl^-$	1.36
$Br_2 + 2\ e^- \rightarrow 2\ Br^-$	1.07
$I_2 + 2\ e^- \rightarrow 2\ I^-$	0.53

WARNING

Elemental fluorine (fluorine gas) is a highly toxic, corrosive oxidant, which can cause ignition of organic material. Fluorine gas has a characteristic pungent odor that is detectable in concentrations as low as 20 ppb. As it is so reactive, all materials of construction must be carefully selected and metal surfaces must be passivated. In high concentrations, soluble fluoride salts are also toxic and skin or eye contact with high concentrations of many fluoride salts is dangerous.

Use of chlorine as a weapon

Chlorine gas, also known as *bertholite*, was first used as a weapon in World War I by Germany on April 22, 1915 in the Second Battle of Ypres. At around 5:00 pm on April 22, 1915, the German Army released one hundred and sixty eight tons of chlorine gas over a 4 mile front against French and colonial Moroccan and Algerian troops of the French 45th and 78th divisions (Figure

6.10.1.13). The attack involved a massive logistical effort, as German troops hauled 5730 cylinders of chlorine gas, weighing ninety pounds each, to the front by hand. The German soldiers also opened the cylinders by hand, relying on the prevailing winds to carry the gas towards enemy lines. Because of this method of dispersal, a large number of German soldiers were injured or killed in the process of carrying out the attack. Approximately 6,000 French and colonial troops died within ten minutes at Ypres, primarily from asphyxiation and subsequent tissue damage in the lungs. Many more were blinded. Chlorine gas forms hydrochloric acid when combined with water, destroying moist tissues such as lungs and eyes. The chlorine gas, being denser than air, quickly filled the trenches, forcing the troops to climb out into heavy enemy fire.



Figure 6.10.1.13: The gas attack of the Second Battle of Ypres.

As described by the soldiers it had a distinctive smell of a mixture between pepper and pineapple. It also tasted metallic and stung the back of the throat and chest. The damage done by chlorine gas can be prevented by a gas mask, or other filtration method, making the fatalities from a chlorine gas attack much lower than those of other chemical weapons. The use as a weapon was pioneered by Fritz Haber (Figure 6.10.1.14) of the Kaiser Wilhelm Institute in Berlin, in collaboration with the German chemical conglomerate IG Farben, who developed methods for discharging chlorine gas against an entrenched enemy. It is alleged that Haber's role in the use of chlorine as a deadly weapon drove his wife, Clara Immerwahr, to suicide. After its first use, chlorine was used by both sides as a chemical weapon (Figure 6.10.1.15), but it was soon replaced by the more deadly gases phosgene and mustard gas.



Figure 6.10.1.14: German scientist and Nobel Prize winner Fritz Haber (1868 - 1934).



Figure 6.10.1.15: A poison gas attack, in World War I.

Vapor phase

All the halogens form X_2 dimers in the vapor phase in an analogous manner to hydrogen. Unlike dihydrogen, however, the bonding is associated with the molecular orbital combination of the two p-orbitals (Figure 6.10.1.16). The bond lengths and energies are given in Table 6.10.1.6.

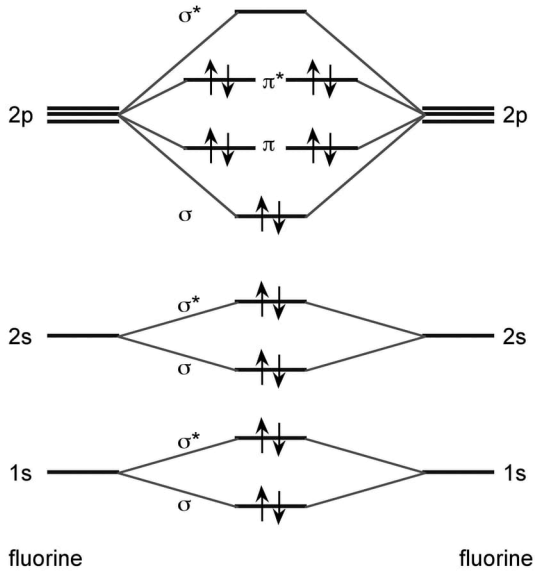


Figure 6.10.1.16: Molecular orbital diagram for the formation of F_2.

Table 6.10.1.6: Bond lengths and energies for halogens.

Element	Bond length (Å)	Energy (kJ/mol)
F_2	1.42	158
Cl_2	1.99	243
Br_2	2.29	193
I_2	2.66	151

Solid state

Iodine crystallizes in the orthorhombic space group Cmca (Figure 6.10.1.17). In the solid state, I_2 molecules still contain short I-I bond (2.70 Å).

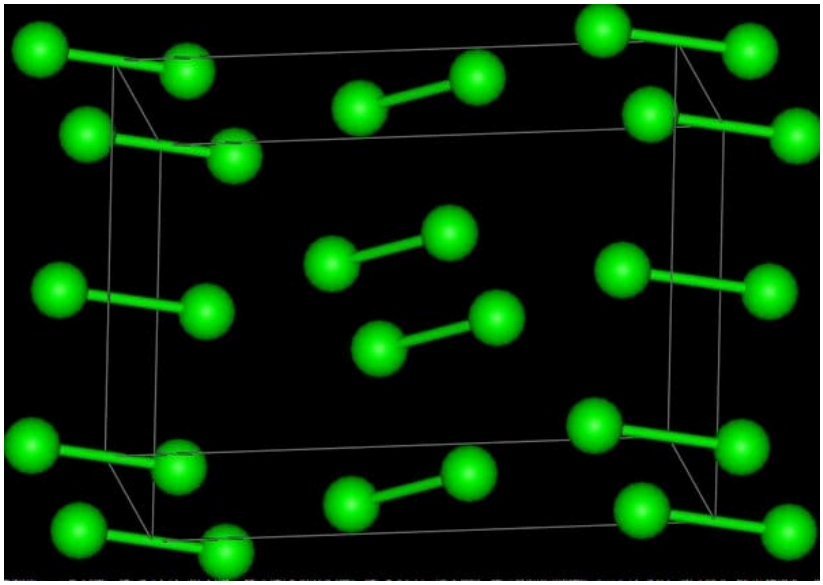


Figure 6.10.1.17: The solid state structure of I_2.

Compounds of the halogens.

The chemistry of the halogens is dominated by the stability of the -1 oxidation state and the noble gas configuration of the X^- anion.

Oxidation state

The use of oxidation state for fluorine is almost meaningless since as the most electronegative element, fluorine exists in the oxidation state of -1 in all its compounds, except elemental fluorine (F_2) where the oxidation state is zero by definition. Despite the general acceptance that the halogen elements form the associated halide anion (X^-), compounds with oxidation states of +1, +3, +4, +5, and +7 are common for chlorine, bromine, and iodine (Table 6.10.1.7).

Table 6.10.1.7: Examples of multiple oxidation states for the halogens.

Element	-1	+1	+3	+4	+5	+7
Cl	HCl	ClF	ClF_3, $HClO_2$	ClO_2	ClF_5, ClO_3^-	$HClO_4$
Br	HBr	BrCl	BrF_3	Br_2O_4	BrF_5, BrO_3^-	BrO_4^-
I	HI	ICl	IF_3, ICl_3	I_2O_4	IO_3^-	IO_4^-

Bibliography

- G. Agricola, *De Re Metallica*, Dover Publications, UK (1950)
- K. Christe, *Inorg. Chem.*, 1986, **25**, 3721.

This page titled 6.10.1: The Group 17 Elements- The Halogens is shared under a CC BY 3.0 license and was authored, remixed, and/or curated by Andrew R. Barron (CNX) via source content that was edited to the style and standards of the LibreTexts platform.

6.10.2: Compounds of Fluorine

Elemental fluorine (F_2) is the most reactive element. Fluorine combines directly with all other elements, except nitrogen and the lighter noble gases. It also reacts with many compounds forming fluorides, and many organic compounds inflame and burn in the gas. The highly reactive nature is due to the weak F-F bond (thermodynamically unstable), which provides a low activation energy to reactions (kinetically unstable). The ΔG for reactions is often large due to the strength of the resulting X-F bonds. The weak F-F bond (158 kJ/mol) is due to the small size (0.5 Å) and high nuclear charge of fluorine that result in a small overlap of the bonding orbitals and a repulsion between the non-bonding orbitals (lone pairs) on the two fluorine atoms.

Ionic salts

The ease of formation of F^- anion is due to the high electron affinity of fluorine (-322 kJ/mol). Since the fluoride ion is small (1.33 Å) and the least polarizable anion (i.e., *hard*) it is stable in ionic lattices with metal cations in a high oxidation state (high charge), e.g., MnF_4 and CrF_5. In general the highest oxidation states for any metal are found with the fluoride salts. The large ionization energies needed to produce the cations are recovered by the high lattice energies.

Covalent compounds

The high electronegativity of fluorine means that it forms a single electron pair bond polar bond with a high ionic character. The polar nature of the bond means that there is a large inductive effect within a molecule. For example, perfluoroethanol (CF_3CF_2OH) has an acidity comparable to acetic acid.

The high strength of X-F bonds (Table 6.10.2.1) is also due to the high ionic character (up to 50%) that results in a high activation energy for bond breaking. In contrast, the low polarizability of the fluorine means that the inter-molecular van der Waals bonds are very weak. Thus, even with very high molecular weights the boiling point can be very low, e.g, WF_6, Bp = 17 °C, Mw = 297.84 g/mol.

Table 6.10.2.1: Typical bond energies for X-F bonds.

Bond	Bond energy (kJ/mol)
C-F	486
N-F	272
P-F	490

A wide range of fluoride complexes may be prepared from both metal (FeF_6^{3-}, RuF_6^-, PtF_6^{2-}, and SnF_6^{2-}) and non-metal (BF_4^-, SiF_6^{2-}, and PF_6^-) fluorides. While many fluorides are salts, when the metal is in its higher oxidation states (e.g., OsF_6 and WF_6), the formation of an ionic lattice with the appropriate cation (i.e., Os^{6+} and W^{6+} respectively) is energetically unfavorable.

Hydrogen fluoride

Hydrogen fluoride (HF) is converted to highly corrosive hydrofluoric acid upon contact with moisture. Pure hydrogen fluoride must be handled in metal or polythene vessels, while aqueous solutions will readily etch and dissolve standard laboratory glassware requiring the use of fluorinated polymer (e.g., Teflon) containers.

Hydrogen fluoride is synthesized by the reaction of a fluoride salt with a concentrated acid, (10.2.1). The HF vapor may be condensed, and then subsequently purified by distillation.

$$CaF_2 + H_2SO_4 \rightarrow CaSO_4 + 2HF \uparrow \tag{6.10.2.1}$$

The H-F bonding in hydrogen fluoride involves an electron pair bond with a high degree of ionic character. This results in a very polar H-F bond and a large dipole moment (1.86 D).

In the vapor phase, hydrogen fluoride is monomeric above 80 °C, but at lower temperatures it associates into oligomers and small polymers, e.g., cyclic $(HF)_6$, as a consequence of strong intermolecular hydrogen bonds. As a pure liquid (Mp = -83 °C, Bp = 19.5 °C) hydrogen fluoride is extensively associated by strong hydrogen bonding to form zig-zag polymers (Figure 6.10.2.1).

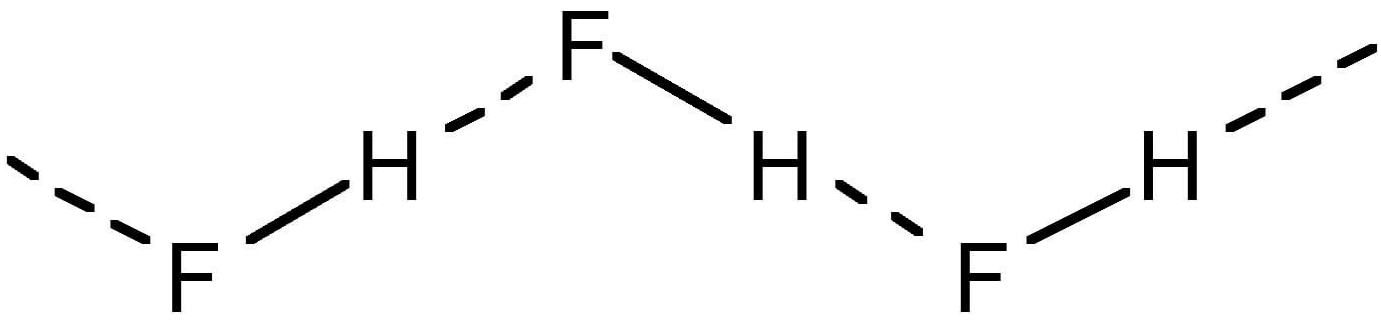


Figure 6.10.2.1: The hydrogen bonding in HF.

Hydrogen fluoride has a high dielectric constant (84.2) and as such is a good solvent for polar molecules. However, it is not a good solvent for salts (even fluorides) because it does not solvate cations too well. Despite this, it is useful as a solvent because it is non-oxidizing and easy to evaporate off products.

In a similar manner to water, hydrogen fluoride self-ionizes, (10.2.2). Salts of H_2F^+ are known and the F- anion is further solvated by the HF to form a series of salts, (10.2.3). The complex anion HF_2^- is also formed in aqueous solutions of hydrogen fluoride (pK = 0.7).

$$2HF \rightleftharpoons H_2F^+ + F^- \tag{6.10.2.2}$$

$$F^- + n\ HF \rightleftharpoons HF_2^- + H_2F_3^- + H_3F_4^-\ \text{etc.} \tag{6.10.2.3}$$

Hydrogen fluoride is actually a weak acid in aqueous solution with a low pK = 3.5. In fact, HF is a weaker acid that the other halogen analogs:

\[\rm HF

This trend is despite the fluorine being more electronegative than the other halogens, but is consistent with the strength of the H-F bond (568 kJ/mol).

Hydrogen fluoride is used as a non-oxidizing acid for the hydrolysis of proteins and acid catalyzed condensation reaction. The stability of its salt (HF_2^-) allow for the study of very strong acids, (10.2.5) and (10.2.6).

$$2HF + R_2C{=}O \rightarrow R_2C{=}OH^+ + HF_2^+ \tag{6.10.2.4}$$

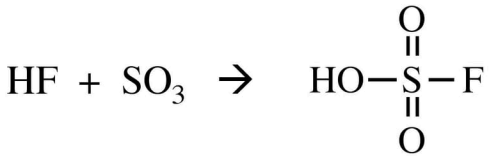
$$2HF + H_2O \rightarrow H_3O^+ + HF_2^- \tag{6.10.2.5}$$

The acidity of HF may be increased sufficiently by the addition of a fluoride acceptor (e.g., SbF_5) to facilitate the reaction with a weak base such as benzene, (10.2.7).

$$C_6H_6 + HF + SbF_5 \rightarrow C_6H_7^+ + SbF_6^- \tag{6.10.2.6}$$

Finally, hydrogen fluoride can be used in the synthesis of other fluorine-containing compounds:

$$6HF + KCl + PCl_5 \rightarrow K[PF_6] + 6HCl\uparrow \tag{6.10.2.7}$$



Organic fluorine compounds

Organic compounds in which some or all of the hydrogen atoms are replaced by fluorine have unique (and often important) properties. The high stability of fluorocarbon compounds is a consequence of the C-F bond energy (486 kJ/mol) in comparison with that of C-H (415 kJ/mol); however, while kinetically stable, fluorocarbons are not necessarily particularly thermodynamically stable.

Replacement of hydrogen with fluorine results in an increased density; since the small size of fluorine means that the minimal distortion or structural change occurs as a result of the substitution. As with metal salts, the weak inter-molecular forces means that completely fluorinated organic compounds have low boiling points. One attribute of the low inter-molecular forces is the low coefficient of friction for fluoropolymers such as polytetrafluoroethylene, commonly known as Teflon (Figure 6.10.2.2).

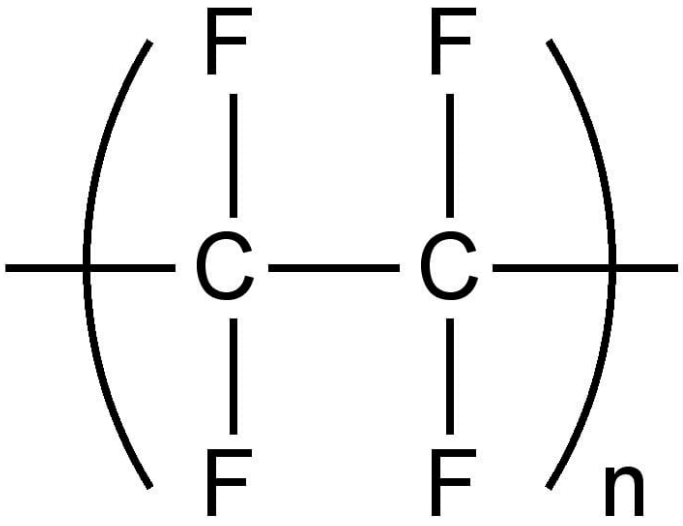


Figure 6.10.2.2: The structure of polytetrafluoroethylene (Teflon).

Synthetic routes to fluorocarbon compounds

The simplest route to a fluorocarbon compounds involves the direct replacement of another halogen by a metal fluoride, (10.2.9). The driving force for this reaction depends on the free-energy difference of MF and MCl, which is related to the difference in lattice energies. Thus, the larger the metal cation, the more favored the reaction. In this regard, AgF and CsF are the most effective fluorination agent.

$$\text{R-Cl} + \text{MF} \rightleftharpoons \text{R-F} + \text{MCl} \tag{6.10.2.8}$$

Anhydrous hydrogen fluoride (HF) reacts with chlorocarbon compounds in the presence of a catalyst such as $SbCl_5$ or CrF_4, (10.2.10). However, elevated temperatures (50 – 150 °C) and high pressures (50 – 500 psi) are required.

$$2\text{CCl}_4 + 3\text{HF} \rightarrow \text{CCl}_2\text{F}_2 + \text{CCl}_3\text{F} + 3\text{HCl} \tag{6.10.2.9}$$

The direct replacement of hydrogen with fluorine is possible if the reaction is carried out under dilute conditions in the presence of a catalyst, (10.2.11).

$$\text{C}_6\text{H}_6 + 9\text{F}_2 \xrightarrow{\text{Cu}} \text{C}_6\text{F}_{12} + 6\text{HF} \tag{6.10.2.10}$$

Sulfur tetrafluoride (SF_4) is a particularly selective fluorination agent. It can be used to convert ketones to difluoro compounds, (10.2.12).

$$2R_2C{=}O + SF_4 \rightarrow R_2CF_2 + SO_2 \tag{6.10.2.11}$$

This page titled 6.10.2: Compounds of Fluorine is shared under a CC BY 3.0 license and was authored, remixed, and/or curated by Andrew R. Barron (CNX) via source content that was edited to the style and standards of the LibreTexts platform.

6.10.3: Compounds of Chlorine

Comparison to fluorine

To appreciate the chemistry of chlorine in comparison to that of fluorine it is necessary to appreciate the differences and trends between the elements. As may be seen in Table 6.10.3.1, chloride is significantly larger than fluorine. In addition while chlorine is an electronegative element its electronegativity is significantly less than that of fluorine, resulting in less polar bonding.

Table 6.10.3.1: Comparison of physical characteristics for fluorine and chlorine.

Element	Ionic radius (Å)	Covalent radius (Å)	van der Waal radius (Å)	Electronegativity
Fluorine	1.33	0.64	1.47	-4.1
Chlorine	1.81	0.99	1.75	-2.9

The X-Cl bond is an electron pair covalent bond with a highly polar nature. In this regard, chlorine is similar to fluorine. However, there are two key features with regard to chlorine's bonding that differentiates it from fluorine.

1. Unlike fluorine, chlorine can form multiple covalent bonds, e.g., ClO_4^- and ClF_3.
2. Unlike fluorine, chlorine can form π-bonds with oxygen, i.e., Cl=O.

The chloride ion (Cl^-) forms salts with ionic lattices (e.g., NaCl) but also forms a wide range of complexes, e.g., $[Fe(H_2O)_5Cl]^{2+}$ and $[RhCl_6]^{3-}$. Chloride also acts as a bridging ligand in which one, two or three chlorides can bridge two metal centers (Figure 6.10.3.1).

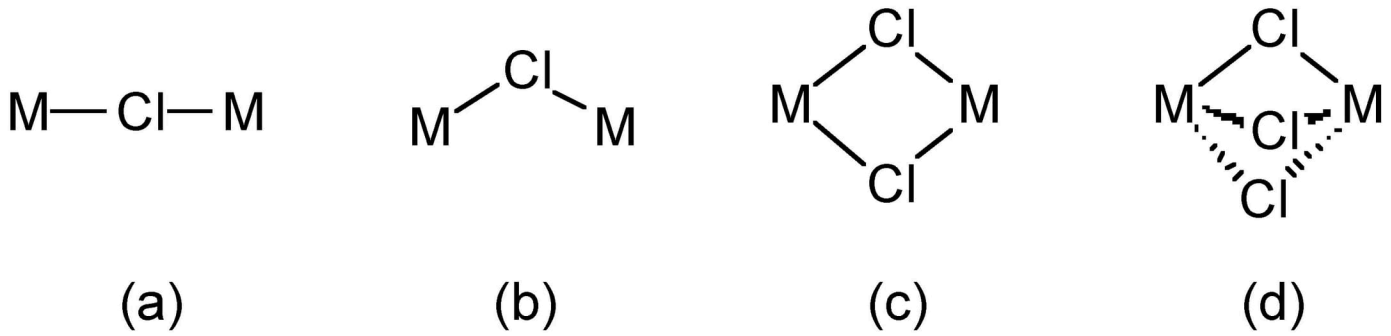


Figure 6.10.3.1: Structures of common halide bridging moieties.

Chloride (and bromide) bridges are usually bent, whereas fluoride bridges can be either linear or bent. As an example, BeF_2 and $BeCl_2$ are isostructural, consisting of infinite chains with bent bridges (Figure 6.10.3.2). In contrast, transition metal pentahalides show different structures depending on the identity of the halide. This, $TaCl_5$ dimerizes with bent bridges (Figure 6.10.3.3a), while TaF_5 forms a cyclic tetramer with linear fluoride bridges (Figure 6.10.3.3b).

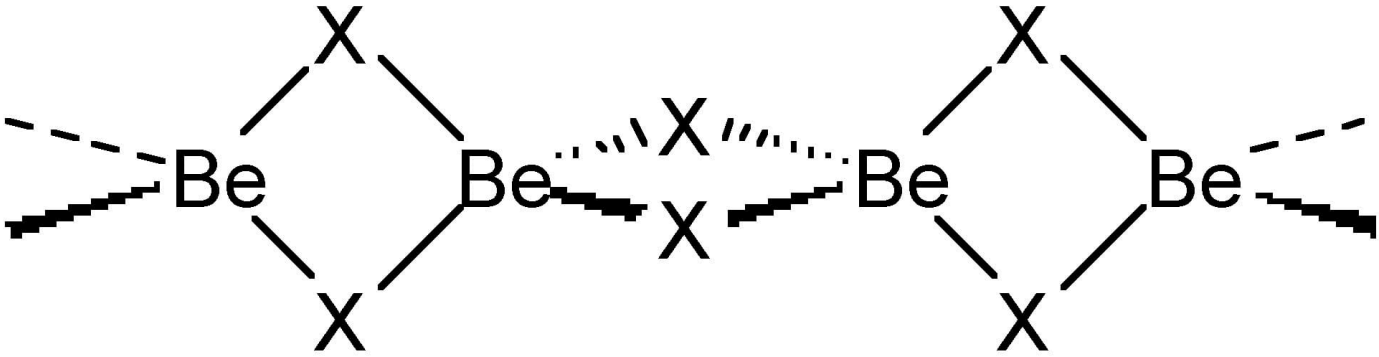


Figure 6.10.3.2: The solid state structure of BeX_2 (X = F or Cl).

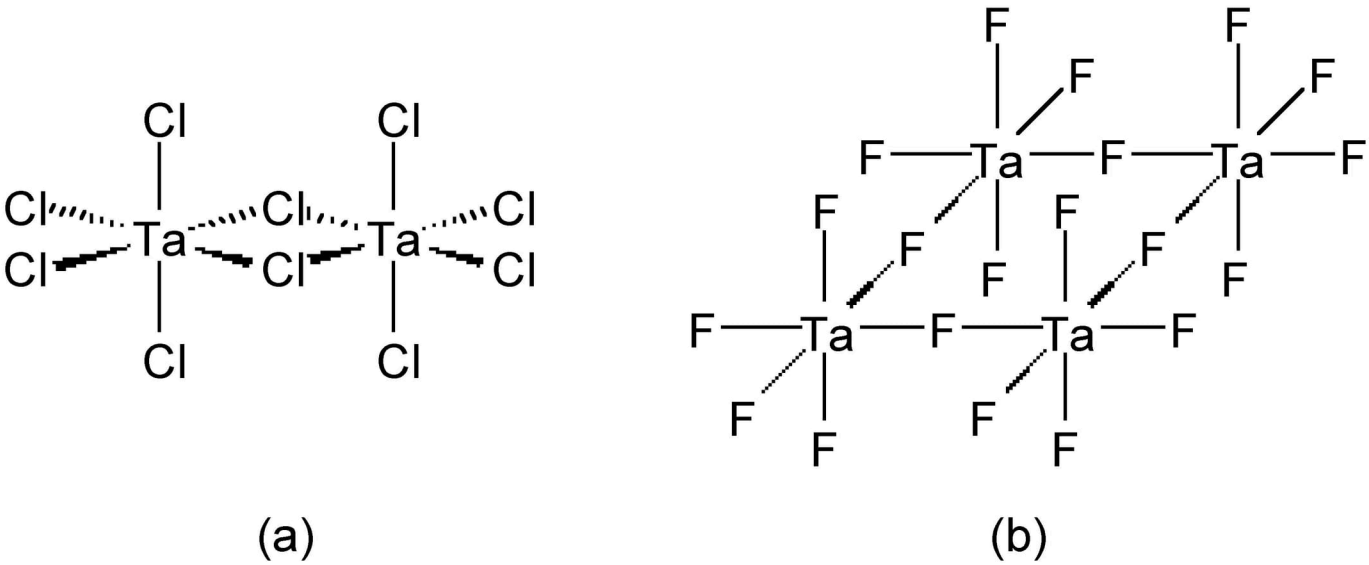


Figure 6.10.3.3: The solid state structure of (a) $TaCl_5$ and (b) TaF_5.

The halide bridge

The bridging halide bonds can be described by both Lewis and molecular orbital (MO) theory. In a simple picture, the lone pair of a terminal halide can be thought to act as a Lewis base donor ligand to the second Lewis acidic metal center. Indeed some bridging halides are asymmetric consistent with this view; however, the symmetrical ones can be described by a resonance form. From a molecular orbital point of view, the bridging halide is represented by a combination of two metal centered orbitals with two halogen orbitals.

Hydrogen chloride

Hydrogen chloride (HCl) is prepared by the reaction of concentrated sulfuric acid (H_2SO_4) with either NaCl or concentrated HCl solution.

Hydrogen chloride is a polar molecule with a dipole of 1.08 D. However, the lower polarity as compared to that of hydrogen fluoride (1.91 D) is consistent with the physical and chemical properties. Hydrogen chloride is a gas at room temperature (Mp = -114.25 °C, Bp = -85.09 °C), and its low boiling point is consistent with weak hydrogen bonding in the liquid state. While self-ionization, (10.3.1), is very small, liquid HCl dissolves some inorganic compounds to give conducting solutions, (10.3.2).

$$3HCl \rightleftharpoons H_2Cl^+ + HCl_2^- \tag{6.10.3.1}$$

$$R_3N + 2HCl \rightleftharpoons R_3NH^+ + HCl_2^- \tag{6.10.3.2}$$

Hydrogen chloride is soluble (and reacts) in water, (10.3.3). The pK_a of the reaction (-7.0) is larger than observed for fluorine (3.2) and as such HCl is a stronger acid than HF.

$$HCl + H_2O \rightleftharpoons H_3O^+ + Cl^- \tag{6.10.3.3}$$

Oxides of Chlorine

Chlorine forms a series of oxides (Table 6.10.3.2) in which the chlorine has the formal oxidation states +1, +4, +6, and +7. The physical properties of the oxides are summarized in Table 6.10.3.2. While, the oxides of chlorine are not very stable (in fact several are shock sensitive and are prone to explode) the conjugate oxyacids are stable.

Table 6.10.3.2: Physical properties of the oxides of chlorine.

Compound	Mp (°C)	Bp (°C)
Cl_2O	-116	4
ClO_2	-5.9	10
Cl_2O_4	-117	44.5
Cl_2O_6	3.5	unstable
Cl_2O_7	-91.5	82

Dichlorine monoxide (Cl_2O, Figure 6.10.3.4a) is a yellowish-red gas that is prepared by the reaction of chlorine with mercury oxide, (10.3.4), or with a solution of chlorine in CCl_4.

$$2Cl_2 + 2HgO \rightarrow HgCl_2 \cdot HgO + Cl_2O \tag{6.10.3.4}$$

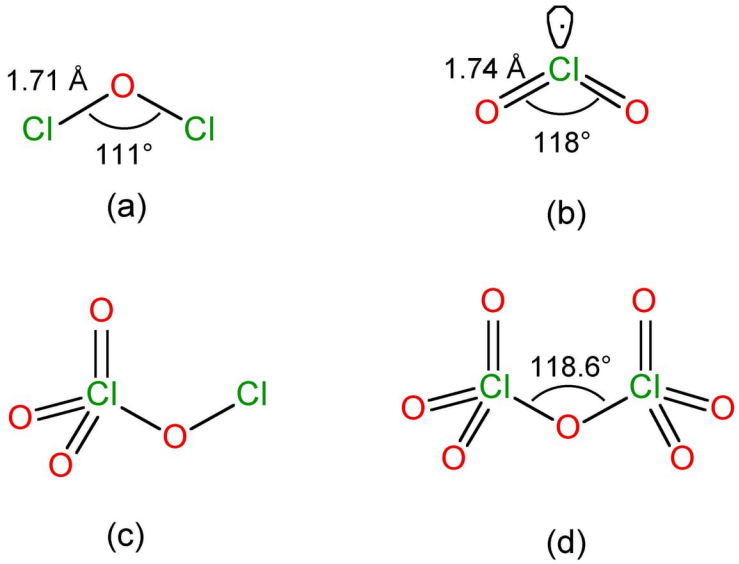


Figure 6.10.3.4: The structure of (a) Cl_2O, (b) ClO_2, (c) Cl_2O_4, and (d) Cl_2O_7.

When heated or subject to a spark, Cl_2O explodes to Cl_2 and O_2. Dichlorine monoxide reacts with water to form an orange-yellow solution of hypochlorous acid, (10.3.5).

$$H_2O_{(g)} + Cl_2O_{(g)} \rightleftharpoons 2HOCl_{(g)} \tag{6.10.3.5}$$

Chlorine dioxide (ClO_2) is a yellowish gas at room temperature and is commonly used in industry as an oxidizing agent. The best synthesis of ClO_2 involves the reduction of potassium chlorate ($KClO_3$) by oxalic acid at 90 °C, since the CO_2 formed acts as a diluent for the highly explosive ClO_2. On an industrial scale ClO_2 is made by the exothermic reaction of sodium chlorate with SO_2 in sulfuric acid, (10.3.6). The photolysis of ClO_2 yields a dark brown solid with the formula Cl_2O_3; however, its facile explosive

decomposition precludes study.

$$2\mathrm{NaClO_3} + \mathrm{SO_2} + \mathrm{H_2SO_4} \rightarrow 2\mathrm{ClO_2} + 2\mathrm{NaHSO_4} \tag{6.10.3.6}$$

The structure of ClO_2 (Figure 6.10.3.4b) is equivalent to SO_2 with one extra electron, resulting in a paramagnetic unpaired electron species. Unusually, despite the unpaired electron configuration, ClO_2 shows no tendency to dimerize. This is unlike the analogous NO_2 molecule.

Dichlorine tetraoxide (Cl_2O_4) is commonly called chlorine perchlorate as a consequence of its structure (Figure 6.10.3.4c). Dichlorine hexaoxide (Cl_2O_6) is an unstable red oil that has the ionic structure in the solid state: $[ClO_2]^+[ClO_4]^-$.

Dichlorine heptoxide (Cl_2O_7) is a relatively stable oil, that is prepared by the dehydration of perchloric acid at -10 °C, (10.3.7), followed by vacuum distillation. The structure of Cl_2O_7 (Figure 6.10.3.4d) has been determined by gas phase electron diffraction.

$$\mathrm{HClO_4} \xrightarrow[-\mathrm{H_2O}]{+\mathrm{P_4O_5}} \mathrm{Cl_2O_7} \tag{6.10.3.7}$$

The reaction of Cl_2O_7 with alcohols and amines yields alkyl perchlorates ($ROClO_3$) and amine perchlorates (R_2NClO_3), respectively.

Fluorides of chlorine

Given the isolobal relationship between the halogens it is not surprising that the mixed dihalogens can be prepared, e.g., ClF, ICl, and BrCl. Chlorine fluoride is a highly reactive gas (Bp = -100.1 °C) that is a powerful fluorinating agent, and is prepared by the oxidation of chlorine by chlorine trifluoride, (10.3.8).

$$\mathrm{Cl_2} + \mathrm{ClF_3} \rightarrow 3\mathrm{ClF} \tag{6.10.3.8}$$

The higher electronegativity of fluorine as compared to chlorine (Table 6.10.3.1), and the ability of chlorine to form more than one bond, means that higher fluorides of chlorine are also known, i.e., ClF_3 and ClF_5. Chlorine trifluoride (CF_3, Bp = 11.75 °C) is a useful fluorinating agent, that is prepared by the high temperature reaction of elemental chlorine and fluorine, is a useful fluorinating age. The gaseous pentafluoride (ClF_5, Bp = -31.1 °C) is prepared by the reaction of potassium chloride with fluorine, (10.3.10).

$$\mathrm{Cl_2} + 3\mathrm{F_2} \xrightarrow{200^\circ\mathrm{C}} 2\mathrm{ClF_3} \tag{6.10.3.9}$$

$$\mathrm{KCl} + 3\mathrm{F_2} \xrightarrow{200^\circ\mathrm{C}} \mathrm{ClF_5} + \mathrm{KF} \tag{6.10.3.10}$$

The structure of ClF_3 is T-shaped with two lone pairs on chlorine (Figure 6.10.3.5a), while that of ClF_5 is square pyramidal with a single lone pair on chlorine (Figure 6.10.3.5b).

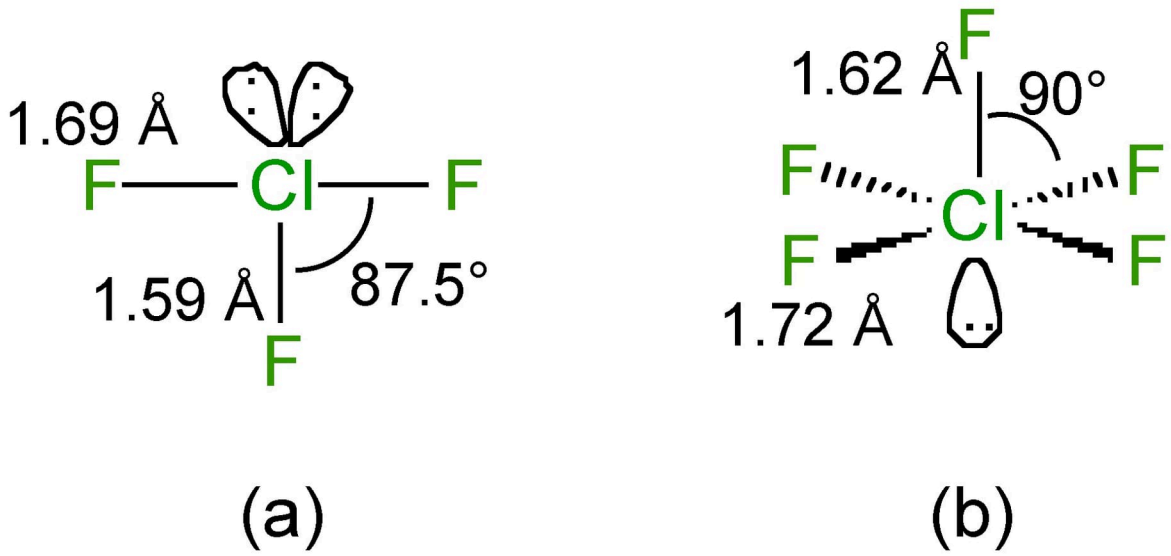


Figure 6.10.3.5: The structures of (a) ClF_3 and (b) ClF_5.

In general the halogen fluorides are very reactive; explosive reactions occur with organic compounds. They are all powerful fluorinating agents when diluted with nitrogen, and the order of reactivity follows:

$$ClF_3 > BrF_3 > BrF_5 > IF_7 > ClF > IF_5 > BrF \tag{6.10.3.11}$$

Like most halogen fluorides, ClF, ClF_3 and ClF_5 all react with strong bases (e.g., alkali metal fluorides) to form anions, (10.3.12) and (10.3.13), and strong acids (e.g., AsF_5 and SbF_5) to form cations, (10.3.14), (10.3.15), and (10.3.16).

$$ClF + CsF \rightarrow Cs^+ + ClF_2^- \tag{6.10.3.12}$$

$$ClF_3 + CsF \rightarrow Cs^+ + ClF_4^- \tag{6.10.3.13}$$

$$2ClF + AsF_5 \rightarrow FCl_2^+ + AsF_6^- \tag{6.10.3.14}$$

$$ClF_3 + AsF_5 \rightarrow ClF_2^+ + AsF_6^- \tag{6.10.3.15}$$

$$ClF_5 + SbF_5 \rightarrow ClF_4^+ + SbF_6^- \tag{6.10.3.16}$$

This page titled 6.10.3: Compounds of Chlorine is shared under a CC BY 3.0 license and was authored, remixed, and/or curated by Andrew R. Barron (CNX) via source content that was edited to the style and standards of the LibreTexts platform.

6.10.4: Oxyacids of Chlorine

Table 6.10.4.1 lists the various oxyacids of chlorine. The relative strengths increase with the number of oxygen atoms since the more there are, the greater is the extent to which the negative charge on the resulting anion can be delocalized.

Table 6.10.4.1: Relative acidity of oxyacids of chlorine.

Oxyacid	Formula	pK_a
Hypochlorous	HOCl	7.5
Chlorous	$HClO_2$	1.9
Chloric	$HClO_3$	-2
Perchloric	$HClO_4$	-10

Hypochlorous acid

Hypochlorous acid (HOCl) can be made pure in the gas phase, (10.4.1), while strong acid solutions can be made from Cl_2O. In contrast, dilute aqueous solutions are obtained with a suspension of mercury oxide to remove the chloride, (10.4.2).

$$H_2O_{(g)} + Cl_2O_{(g)} \rightleftharpoons 2HOCl_{(g)} \tag{6.10.4.1}$$

$$2Cl_2 + 2HgO_{(s)} + H_2O \rightarrow 2HOCl + HgO \cdot HgCl_2 \downarrow \tag{6.10.4.2}$$

Solutions of the anion, OCl^-, are obtained by electrolysis of brine solution; allowing the products to mix at low temperature, (10.4.3).

$$Cl_2 + 2OH^- \rightarrow ClO^- + Cl^- + H_2O \tag{6.10.4.3}$$

The anion (hypochlorite) is a good oxidant, (10.4.4) and (10.4.5), but can undergo disproportionation, (10.4.6); slowly at 25 °C, but fast above 80 °C.

$$ClO^- + NH_3 \rightarrow NH_2Cl + OH^- \tag{6.10.4.4}$$

$$ClO^- + 2I^- + 2H^+ \rightarrow I_2 + Cl^- + H_2O \tag{6.10.4.5}$$

$$3ClO^- \rightarrow 2Cl^- + ClO_3^- \tag{6.10.4.6}$$

Chlorous Acid

Chlorous acid (HOClO) is prepared by the reaction of ClO_2 with base, (10.4.7), followed by the precipitation of the ClO_2^- salt with barium chloride, (10.4.8). The barium salt is dried and then reacted with a calculated amount of H_2SO_4, (10.4.9).

$$2ClO_2 + 2OH^- \rightarrow ClO_2^- + ClO_3^- + H_2O \tag{6.10.4.7}$$

$$2ClO_2^- + BaCl_2 \rightarrow 2Cl^- + Ba(ClO_2)_2 \downarrow \tag{6.10.4.8}$$

$$Ba(ClO_2)_2 + H_2SO_4 \rightarrow Ba(SO_4) + 2HClO_2 \tag{6.10.4.9}$$

The pure acid is unknown since it is too unstable, however, salts can be prepared directly, e.g., (10.4.10).

$$2ClO_2 + Na_2O_2 \rightarrow 2NaClO_2 + O_2 \tag{6.10.4.10}$$

The anion (ClO_2^-) is stable in alkaline solutions but in acid solutions decomposition occurs, (10.4.11).

$$5HClO_2 \rightarrow 4ClO_2 + Cl^- + H^+ + 2H_2O \tag{6.10.4.11}$$

As with hypochlorite, the chlorite anion is a strong oxidant, (10.4.12).

$$ClO_2^- + 4I^- + 4H^+ \rightarrow 2I_2 + 2H_2O + Cl^- \tag{6.10.4.12}$$

Chloric Acid

The chloric anion (ClO_3^-) is made from the reaction of chlorine gas with hot alkali (80 °C) or by the electrolysis of hot NaCl solution.

$$3Cl_2 + 6OH^- \rightarrow ClO_3^- + 5Cl^- + 3H_2O \tag{6.10.4.13}$$

To obtain a solution of the acid, ClO_3^- is precipitated as the barium salt, (10.4.14), which is removed, dried, and suspended in water and treated with a calculated amount of H_2SO_4, (10.4.15). The free acid cannot be isolated and a maximum concentration of only 40% can be obtained in water.

$$2ClO_3^- + BaCl_2 \rightarrow 2Cl^- + Ba(ClO_3)_2 \downarrow \tag{6.10.4.14}$$

$$Ba(ClO_3)_2 + H_2SO_4 \rightarrow Ba(SO_4) + 2HClO_3 \tag{6.10.4.15}$$

The ClO_3^- anion is pyramidal both in solid salts and in solution, and many salts are known; however, those with organic cations are explosive. The anion is a strong oxidizing agent, (10.4.16) and (10.4.17), and it disproportionates slowly in solution, (10.4.18).

$$ClO_3^- + 6I^- + 6H^+ \rightarrow 3I_2 + 3H_2O + Cl^- \tag{6.10.4.16}$$

$$ClO_3^- + 3NO_2^- \rightarrow 3No_3^- + Cl^- \tag{6.10.4.17}$$

$$4ClO_3^- \rightarrow 3ClO_4^- + Cl^- \tag{6.10.4.18}$$

Perchloric Acid

The perchlorate anion (ClO_4^-) is best made by electrolytic oxidation of chlorate in aqueous solution, (10.4.19). Fractional distillation can concentrate the solution to 72.5% which is a constant boiling mixture. This concentration is moderately safe to use, however, 100% perchloric acid may be obtained by dehydration with H_2SO_4.

$$ClO_3^- + H_2O \rightarrow ClO_4^- + 2H^+ + 2e^- \tag{6.10.4.19}$$

WARNING

Perchloric acid is a very dangerous liquid that will explode if traces of metal ions are present. It is also a very strong oxidizing agent that will convert organic compounds to CO_2 and H_2O.

Perchloric acid is a very strong acid that is fully ionized in aqueous solution, such that the salt $[H_3O][ClO_4]$ can be isolated. Many other perchlorate salts are known, but those with organic cations are explosive. Perchlorate salts of metals are often used when studying complex formation in aqueous solution, because ClO_4^- is a very weak ligand (PF_6^- is better) and unlikely to form complexes itself. However, perchlorate does complex with +3 and +4 cations.

This page titled 6.10.4: Oxyacids of Chlorine is shared under a CC BY 3.0 license and was authored, remixed, and/or curated by Andrew R. Barron (CNX) via source content that was edited to the style and standards of the LibreTexts platform.

6.10.5: Bromine Trifluoride as a Solvent

WARNING

Bromine trifluoride is a toxic, colorless, and corrosive liquid with a pungent choking smell that is soluble in sulfuric acid but explodes on contact with water and organic compounds. Vapors severely irritate and may burn the eyes, skin, and respiratory system. The liquid burns all human tissue and causes severe damage.

Bromine trifluoride (BrF_3) has a liquid range similar to water (Mp = 8.8 °C and Bp = 127 °C), and like water it auto ionizes, (10.5.1).

$$\mathrm{BrF_3 \rightarrow BrF_2^+ + BrF_4^-} \tag{6.10.5.1}$$

The products, like those of water's self-ionization, are an acid (BrF_2^+) and a base (BrF_4^-). However, unlike water, BrF_3 reacts with fluoride acids and bases not proton acids and bases. Thus, in BrF_3 a base is a salt that provides F^-, i.e., potassium fluoride (KF) is a base in BrF_3 solution in the same manner as potassium hydroxide (KOH) is a base in water. The product from the reaction of a fluoride donor salt with BrF_3 is the formation of the conjugate base, BrF_4^-, (10.5.2).

$$\mathrm{AgF + BrF_3 \rightarrow Ag^+ + BrF_4^-} \tag{6.10.5.2}$$

Other examples of this type of reaction include:

$$\mathrm{KF + BrF_3 \rightarrow K^+ + BrF_4^-} \tag{6.10.5.3}$$

$$\mathrm{NOF + BrF_3 \rightarrow NO^+ + BrF_4^-} \tag{6.10.5.4}$$

By analogy, an acid in BrF_3 solution is a compound that acts as a fluoride (F^-) acceptor, i.e., a Lewis acid, (10.5.5).

$$\mathrm{SbF_5 + BrF_3 \rightarrow SbF_6^- + BrF_2^+} \tag{6.10.5.5}$$

Exercise 6.10.5.1

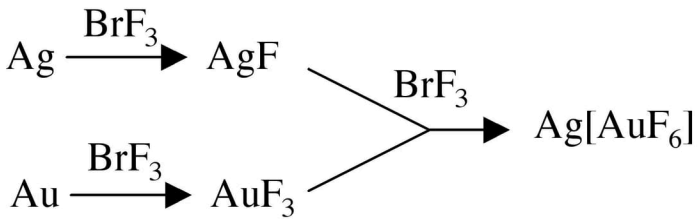
What are the products from the reaction of HF with BrF_3?

Answer available at the end of this section.

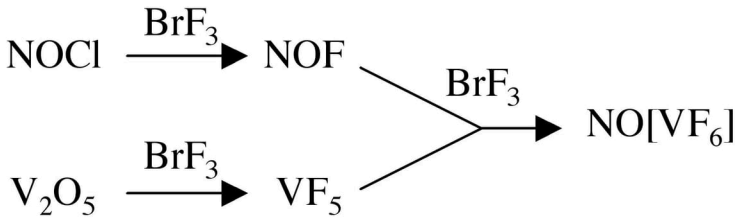
Bromine trifluoride as a fluorinating agent

Bromine trifluoride is a strong fluorinating agent that is able to convert a metal (e.g., vanadium) to its associated fluoride compound, (i.e., VF_5). A wide range of salts and oxides may be converted to fluorides with the metal in a high oxidation state. However, it should be noted that BeO, MgO, and Al_2O_3 form oxo fluorides rather than the fluoride.

The reaction of silver with BrF_3 yields the monofluoride, while the same reaction with gold yields the trifluoride, Eq. If the reactions are combined in BrF_3 solution a mixed metal fluoride salt is formed.



A similar reaction occurs with NOCl and V_2O_5.



Exercise 6.10.5.2

What are the products from the reaction of BrF_3 with (a) Sb_2O_5, (b) KCl, and (c) a mixture of Sb_2O_5 and KCl?

Answer available at the end of this section.

Bibliography

- J. H. Simons, *Inorg. Synth.*, 1950, **3**, 184.

Answers

$$HF + BrF_3 \rightarrow HF_2^- + BrF_2^+ \tag{6.10.5.6}$$

(a) SbF_5, (b) KF, and (c) $K[SbF_6]$.

This page titled 6.10.5: Bromine Trifluoride as a Solvent is shared under a CC BY 3.0 license and was authored, remixed, and/or curated by Andrew R. Barron (CNX) via source content that was edited to the style and standards of the LibreTexts platform.

6.11: Group 18 - The Noble Gases

Thumbnail: Vial of glowing ultrapure neon. (CC SA; Jurii via http://images-of-elements.com/neon.php).

This page titled 6.11: Group 18 - The Noble Gases is shared under a CC BY 3.0 license and was authored, remixed, and/or curated by Andrew R. Barron (CNX) via source content that was edited to the style and standards of the LibreTexts platform.

6.11.1: The Group 18 Elements- The Noble Gases

The elements

The Group 18 elements have a particular name Noble gases. *Noble gas* is translated from the German noun *Edelgas*, first used in 1898 by Hugo Erdmann (1862 - 1910) to indicate their extremely low level of reactivity. The noble gases were often also called the *inert gases*, however, since noble gas compounds are now known this name is no longer used. Table 6.11.1.1 lists the derivation of the names of the Noble gases.

Table 6.11.1.1: Derivation of the names of each of the Group 18(VIII) elements.

Element	Symbol	Name
Helium	He	Greek *helios* meaning the *Sun*
Neon	Ne	From the Greek meaning *new one*
Argon	Ar	From the Greek meaning *inactive*
Krypton	Kr	From the Greek *kryptos* meaning *the hidden one*
Xenon	Xe	From the Greek xenos], meaning *foreigner*, *stranger*, or *guest*
Radon	Rn	From its *radioactive* nature

Discovery

Helium

The first evidence of helium was the observation by astronomer Pierre Janssen (Figure 6.11.1.1) on August 18, 1868 as a bright yellow line with a wavelength of 587.49 nm in the spectrum of the chromosphere of the Sun. On October 20 of the same year, English astronomer Norman Lockyer (Figure 6.11.1.2) observed a yellow line in the solar spectrum, which he named the *D3 Fraunhofer* line because it was near the known *D1* and *D2* lines of sodium. He concluded that it was caused by an element in the Sun unknown on Earth. Lockyer and Edward Frankland (Figure 6.11.1.3) named the element with the Greek word for the Sun, *helios*.

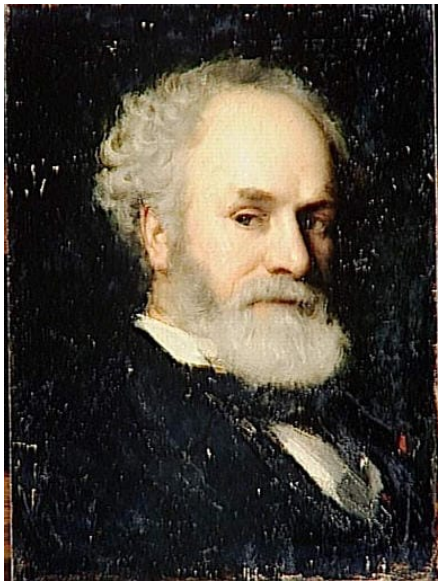


Figure 6.11.1.1: Portrait of French astronomer Pierre Jules César Janssen (1824 - 1907).



Figure 6.11.1.2: English scientist and astronomer Sir Joseph Norman Lockyer, FRS (1836 - 1920).

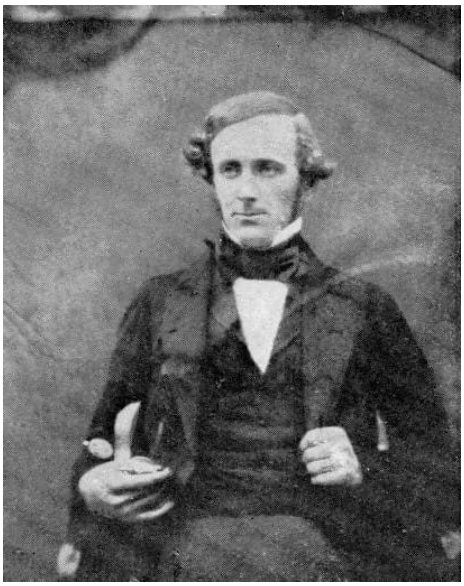


Figure 6.11.1.3: English chemist Sir Edward Frankland, KCB, FRS (1825 - 1899).

On March 26, 1895 British chemist Sir William Ramsay (Figure 6.11.1.4) isolated helium on Earth by treating the mineral cleveite (a radioactive mineral containing uranium and found in Norway) with mineral acids.



Figure 6.11.1.4: Scottish chemist Sir William Ramsay, KCB FRSE (1852 - 1916).

Neon

Neon was discovered in 1898 by Sir William Ramsay (Figure 6.11.1.4) and Morris Travers (Figure 6.11.1.5). When Ramsay chilled a sample of air until it became a liquid, then warmed the liquid and captured the gases as they boiled off. After nitrogen, oxygen, and argon, the three gases that boiled off were krypton, xenon, and neon.



Figure 6.11.1.5: English chemist and founding director of the Indian Institute of Science, Morris William Travers (1872 - 1961).

Argon

In 1785 Henry Cavendish (Figure 6.11.1.6) suspected that argon was present in air but it was not isolated until 1894 by Lord Rayleigh (Figure 6.11.1.7) and Sir William Ramsay (Figure 6.11.1.4) in an experiment in which they removed all of the oxygen, carbon dioxide, water and nitrogen from a sample of clean air.



Figure 6.11.1.6: British scientist Henry Cavendish FRS (1731 - 1810).

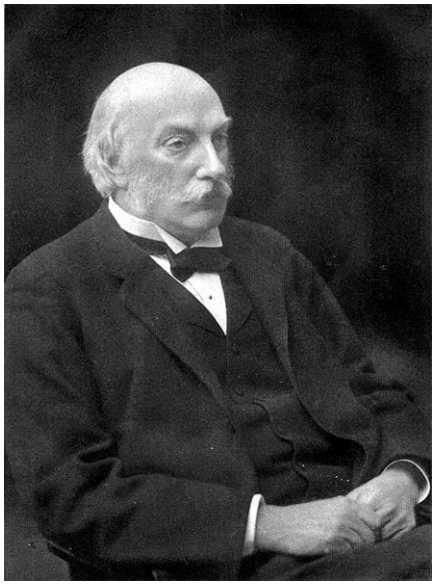


Figure 6.11.1.7: English physicist John William Strutt, 3rd Baron Rayleigh, OM (1842 - 1919).

Krypton

Krypton was discovered in 1898 by Sir William Ramsay (Figure 6.11.1.4) and Morris Travers (Figure 6.11.1.5) in residue left from evaporating nearly all components of liquid air.

Note

In 1960, an international agreement defined the *meter* (m) in terms of wavelength of light emitted by the ^{86}Kr isotope (wavelength of 605.78 nm). This agreement replaced the standard meter located in Paris, which was a metal bar made of a Pt-Ir alloy, and was itself replaced by a definition based on the speed of light, a fundamental physical constant. In October 1983, the *Bureau International des Poids et Mesures* defined the meter as the distance that light travels in a vacuum during $^{1}/_{299,792,458}$ s.

Xenon

Xenon was discovered by William Ramsay (Figure 6.11.1.4) and Morris Travers (Figure 6.11.1.5) on July 12, 1898, shortly after their discovery of krypton and neon.

Radon

Radon was the fifth radioactive element to be discovered after uranium, thorium, radium and polonium. Discovered in 1900 by Friedrich Dorn (Figure 6.11.1.8) after he noticed that radium compounds emanate a radioactive gas that he named *Radium Emanation* (*Ra Em*). Prior to these experiments, in 1899, Pierre and Marie Curie (Figure 6.11.1.9) observed that the *gas* emitted by radium remained radioactive for a month. Later that year, Ernest Rutherford (Figure 6.11.1.10) noticed variations when trying to measure radiation from thorium oxide. In 1901, he demonstrated that the emanations are radioactive, but credited the Curies for the discovery of the element.



Figure 6.11.1.8: German physicist Friedrich Ernst Dorn (1848 - 1916).

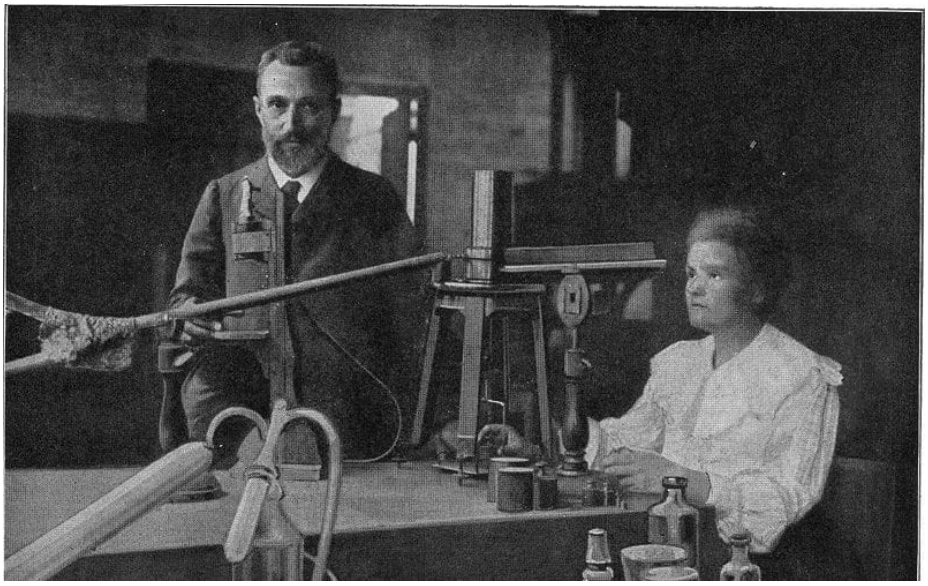


Figure 6.11.1.9: Pierre (1859 - 1906) and Marie Skłodowska-Curie (1867 - 1934) in their Paris laboratory.

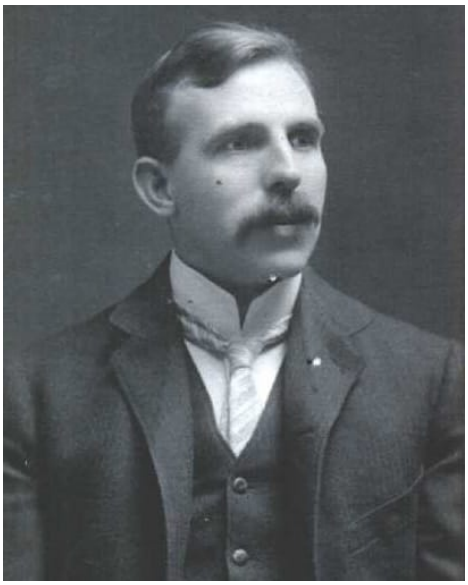


Figure 6.11.1.10: British-New Zealand chemist and physicist Ernest Rutherford, 1st Baron Rutherford of Nelson, OM, FRS (1871 - 1937).

Abundance

The abundance of the Noble gases is given in Table 6.11.1.2.

Table 6.11.1.2: Abundance of Group 18 elements.

Element	Terrestrial abundance (ppm)
He	8×10^{-3} (Earth's crust), 4×10^{6} (sea water), 5 (atmosphere)
Ne	70×10^{-3} (Earth's crust), 0.2 (sea water), 18 (atmosphere)
Ar	1.2 (Earth's crust), 0.45 (sea water), 0.93×10^{4} (atmosphere)
Kr	10×10^{-6} (Earth's crust), 80×10^{-6} (sea water), 1 (atmosphere)
Xe	2×10^{-6} (Earth's crust), 100×10^{-6} (sea water), 90×10^{-3} (atmosphere)

Isotopes

The naturally abundant isotopes of the Group 18 elements are listed in Table 6.11.1.3. All of the isotopes of radon are radioactive.

Table 6.11.1.3: Abundance of the non-synthetic isotopes of the Group 18 elements.

Isotope	Natural abundance (%)
Helium-3	0.000137
Helium-4	99.999863
Neon-20	90.48
Neon-21	0.27
Neon-22	9.25
Argon-36	0.337
Argon-86	0.063
Argon-40	99.600

Krypton-78	0.35
Krypton-80	2.25
Krypton-81	trace
Krypton-82	11.6
Krypton-83	11.5
Krypton-84	57
Krypton-86	17.3
Xenon-124	0.095
Xenon-126	0.089
Xenon-128	1.91
Xenon-129	26.4
Xenon-130	4.07
Xenon-131	21.2
Xenon-132	26.9
Xenon-134	10.4
Xenon-136	8.86
Radon-222	trace

Unlike most elements, helium's isotopic abundance varies greatly by origin, due to the different formation processes. The most common isotope, ^{4}He, is produced on Earth by a decay of heavier radioactive elements. It was also formed in enormous quantities during the *Big Bang*.

Naturally occurring ^{40}K with a half-life of 1.25×10^{9} years, decays to stable ^{40}Ar (11.2%) by electron capture and positron emission, and also to stable ^{40}Ca (88.8%) via beta decay. These properties and ratios are used to determine the age of rocks.

With a half-life of 230,000 years ^{81}Kr is used for dating 50,000 - 800,000 year old groundwater. ^{85}Kr is an inert radioactive noble gas with a half-life of 10.76 years. It is produced in nuclear bomb testing and nuclear reactors. ^{85}Kr is released during the reprocessing of fuel rods from nuclear reactors.

Industrial production of the elements

Helium is extracted by fractional distillation from natural gas, which contains up to 7% helium. Since helium has a lower boiling point than any other element, low temperature and high pressure are used to liquefy nearly all the other gases. The resulting helium gas is purified by successive exposures to lowering temperatures. A final purification step with activated charcoal results in 99.995% pure Grade-A helium.

Argon is produced industrially by the fractional distillation of liquid air, a process that separates liquid nitrogen, which boils at 77.3 K, from argon, which boils at 87.3 K and oxygen, which boils at 90.2 K. Xenon is obtained commercially as a byproduct of the separation of air into oxygen and nitrogen.

Physical properties

The physical properties of the Group 18 elements are given in Table 6.11.1.4.

Table 6.11.1.4: Selected physical properties of the Group 18 elements.

Element	Mp (°C)	Bp (°C)

He	-272.20	-268.93
Ne	-248.59	-246.08
Ar	-189.35	-185.85
Kr	-157.36	-153.22
Xe	-111.7	-108.12
Rn	-71.15	-61.85

All of the Noble gases show characteristic spectral lines (Figure 6.11.1.11 – Figure 6.11.1.15).



Figure 6.11.1.11: Spectral lines of helium.



Figure 6.11.1.12: Spectral lines of neon.



Figure 6.11.1.13: Spectral lines of argon.

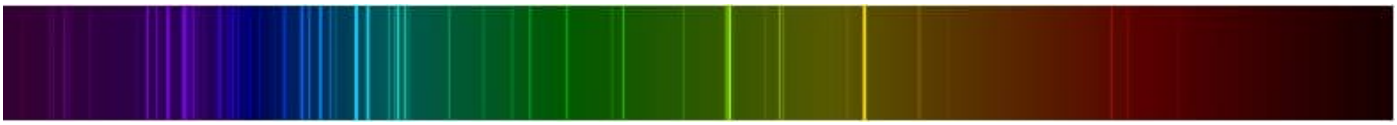


Figure 6.11.1.14: Spectral lines of krypton.



Figure 6.11.1.15: Spectral lines of xenon.

Compounds of the Group 18 elements.

Only a few hundred noble gas compounds have been formed. Neutral compounds of helium and neon have not been formed, while xenon, krypton, and argon have shown only minor reactivity. The reactivity follows the order:

$$\mathrm{Ne} < \mathrm{He} < \mathrm{Ar} < \mathrm{Kr} < \mathrm{Xe} < \mathrm{Rn}$$

Xenon compounds are the most numerous of the noble gas compounds. Oxidation states of +2, +4, +6, and +8 with electronegative elements, e.g., XeF_2, XeF_4, XeF_6, XeO_4, and Na_4XeO_6. Compounds of xenon bound to boron, hydrogen, bromine, iodine, beryllium, sulphur, titanium, copper, and silver have also been observed but only at low temperatures in noble gas matrices, or in supersonic noble gas jets.

Although radon is more reactive than xenon it should form chemical bonds more easily than xenon, however, due to the high radioactivity and short half-life of radon isotopes, only a few fluorides and oxides of radon have been formed.

Krypton is less reactive than xenon, and oxidation states are generally limited to +2, KrF_2. Compounds in which krypton forms a bond to nitrogen and oxygen are only stable below -60 °C and -90 °C, respectively. Krypton atoms chemically bound to other

nonmetals (hydrogen, chlorine, carbon) as well as some late transition metals (copper, silver, gold), but only at low temperatures in noble gas matrices, or in supersonic noble gas jets. Similar conditions were used to obtain the first compounds of argon.

Noble gases also form non-covalent compounds, for example clathrates that consist of an atom trapped within cavities of crystal lattices of organic and inorganic compounds. Noble gases can form endohedral fullerene compounds, in which the noble gas atom is trapped inside a fullerene molecule (Figure 6.11.1.16).

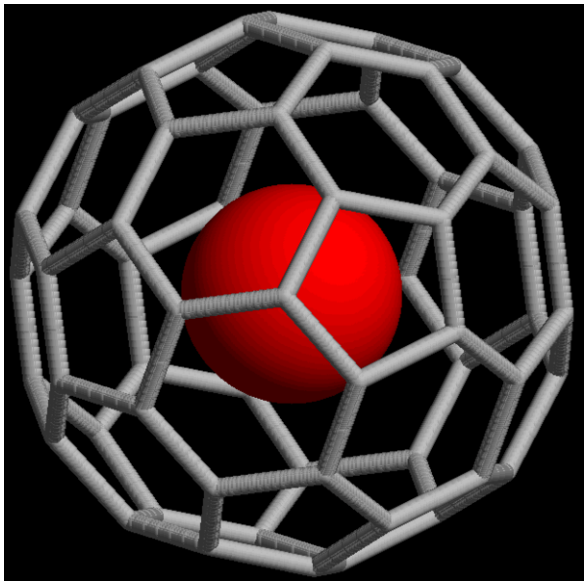


Figure 6.11.1.16: A skeletal structure of He@C_{60}.

Bibliography

- L. Pauling, *J. Am. Chem. Soc.*, 1933, **55**, 1895.
- M. Saunders, H. A. Jiménez-Vázquez, R. J. Cross, and R. J. Poreda, *Science*, 1993, **259**, 1428.

This page titled 6.11.1: The Group 18 Elements- The Noble Gases is shared under a CC BY 3.0 license and was authored, remixed, and/or curated by Andrew R. Barron (CNX) via source content that was edited to the style and standards of the LibreTexts platform.

7: ACID-BASE AND DONOR-ACCEPTOR CHEMISTRY

7.1: Acid-Base Models as Organizing Concepts

7.2: Lewis Concept and Frontier Orbitals

7.2.1: The frontier orbital approach considers Lewis acid-base reactions in terms of the donation of electrons from the base's highest occupied orbital into the acid's lowest unoccupied orbital.

7.2.2: All other things being equal, electron withdrawing groups tend to make Lewis acids stronger and bases weaker while electron donating groups tend to make Lewis bases stronger and acids weaker

7.2.3: The electronic spectra of charge transfer complexes illustrate the impact of frontier orbital interactions on the electronic structure of Lewis acid-base adducts

7.2.4: Bulky groups weaken the strength of Lewis acids and bases because they introduce steric strain into the resulting acid-base adduct.

7.2.5: Frustrated Lewis pair chemistry uses Lewis acid and base sites within a molecule that are sterically restricted from forming an adduct with each other.

7.3: Hard and Soft Acids and Bases

7.3.1: Hard-Hard and Soft-Soft preferences may be explained and quantified in terms of electrostatic and covalent and electronic stabilization on the stability of Lewis acid-base adducts

This page titled 7: Acid-Base and Donor-Acceptor Chemistry is shared under a CC BY 4.0 license and was authored, remixed, and/or curated by Stephen Contakes.

- 6: Acid-Base and Donor-Acceptor Chemistry by Stephen Contakes is licensed CC BY 4.0.

7.1: Acid-Base Models as Organizing Concepts

> In a very real sense, we can make an acid anything we wish. The differences between the various acid-base concepts are not concerned with which is 'right', but which is *most convenient to use in a particular situation*.
>
> James E. Huheey, Ellen A. Keiter, and Richard L. Keiter

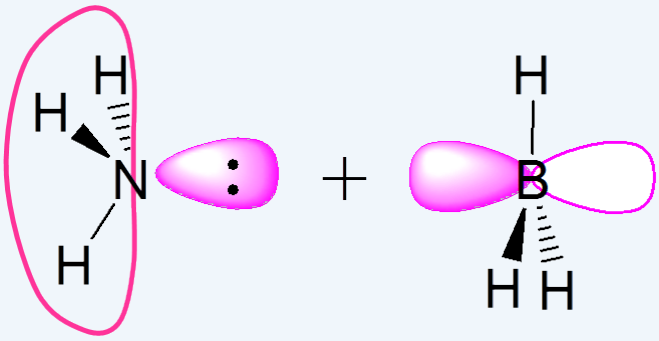
The concept of acids and bases is often associated with the movement of hydrogen ions from one molecule or ion to another. However, a host of acid-base concepts have been developed to help chemists organize and make sense of a wide range of reactions (Table 6.1).

Table 6.1. Summary of major acid-base models.

Definition	Theoretical paradigm and notable features.	Acid	Base	Illustrative sam
Arrhenius (1894)	Interested in what the substance does to the state of an aqueous solution. In particular it assesses proton donation to & removal from water using $[H_3O^+]$ as a proxy. Readily accommodates the pH concept as a measure of the state of a solution.	Increases $[H_3O^+]$	Decreases $[H_3O^+]$	$\underset{acid}{HCl} + H_2O \rightarrow H_3O^+ + Cl^-$ $\underset{base}{NH_3} + H_2O \rightarrow NH_4^+ + OH^-$
Brønsted-Lowry (1923)	Envisions acid-base reactivity in terms of the transfer of an H^+ from one substance to another. Allows for conjugate acids and bases and solvent autoionization.	Donates H^+	Accepts H^+	$\underset{acid}{HCl} + \underset{base}{NH_3} \rightarrow \underset{conj.\ acid}{NH_4^+} + \underset{conj.\ base}{Cl^-}$ $\underset{acid}{HOAc} + \underset{base}{NH_3} \rightarrow \underset{conj.\ acid}{NH_4^+} + \underset{conj.\ base}{OAc^-}$ $\underset{amphoteric}{2\ H_2O} \rightarrow \underset{conj.\ acid}{H_3O^+} + \underset{conj.\ base}{OH^-}$

Definition	Theoretical paradigm and notable features.	Acid	Base	Illustrative sam
Lux-Flood (1939-~47)	Describes reactions involving oxides and oxyanions in terms of the transfer of oxide ion (O^{2-}). Mainly used in geochemistry, although it also can be used to describe some redox reactions.	Oxide acceptor	Oxide donor	$\underset{acid}{SiO_2} + \underset{base}{CaO} \rightarrow CaSiO_3$ $\underset{base}{H_2O} + \underset{acid}{CO} \rightarrow H_2 + CO_2$
Solvent System	Applies aspects of the Arrhenius , Brønsted-Lowry, and Lux-Flood acid base concepts to solvent cation & anion formation in a generalized reaction. Can be used to describe solution chemistry in nonaqueous solvent systems like BrF_3.	Is a solvent cation or increases the solvent cation concentration, often by receiving a lone pair-bearing group	Is a solvent anion or increases the solvent anion concentration, often by donating a lone pair-bearing group	$\underset{acid}{SbF_5} + \underset{base}{BrF_3} \rightarrow \underset{conj.\ base}{SbF_6^-} + \underset{conj.\ acid}{BrF_2^+}$ $\underset{amphoteric}{2\ BrF_3} \rightarrow \underset{conj.\ acid}{BrF_2^+} + \underset{conj.\ base}{BrF_4^-}$

Definition	Theoretical paradigm and notable features.	Acid	Base	Illustrative sam
Lewis (1923)	Envisions acid-base reactivity in terms of electron pair donation. Encompasses the Arrhenius , Brønsted-Lowry, Lux-Flood, and Solvent System definitions and readily integrates with molecular orbital descriptions of chemical reactivity in Frontier orbital theory.	Accepts an electron pair	Donates an electron pair	$:\underset{base}{NH_3} + \underset{acid}{BF_3} \rightarrow H_3N + BF_3$
Nucleophile-Electrophile	Applies the Lewis concept to organic reactivity. Nucleophiles are Lewis bases which tend to react to form a bond with Lewis acid sites called electrophilic centers.	(The electrophile) Tends to react by receiving an electron pair from a nucleophile, forming a bond in the process	(The nucleophile) Donates an electron pair to form a bond to an electrophile	$\underset{base}{Br^-} + \underset{acid}{CH_3-Cl} \rightarrow Br-CH_3 + Cl^-$
Usanovich (1939)	Extends Lewis theory to include the donation and acceptance of any number of electrons, whether through the formation of an adduct or electron transfer.	Accepts electrons	Donates electrons	$:\underset{base}{NH_3} + \underset{acid}{BH_3} \rightarrow \underset{adduct}{H_3N-BH_3}$ $\underset{acid}{Fe^{2+}} + \underset{base}{Zn^0} \rightarrow Fe^0 + Zn^{2+}$

Definition	Theoretical paradigm and notable features.	Acid	Base	Illustrative sam
Frontier Orbital (1960s)	Envisions Lewis Acid-base/ Electrophile-nucleophile reactions in terms of the donation and acceptance of electrons between the reactant's frontier orbitals. Specifically, the reaction is envisioned in terms of donation of the base's HOMO electrons into the acid's LUMO level.	Possesses a LUMO capable of forming an occupied bonding MO on mixing with a base's HOMO.	Possesses an electron-bearing HOMO capable of forming a filled bonding MO on mixing with an acid's LUMO.	 base acid adduct

Some concepts involve defining acids and bases in particular ways that allow for the understanding of particular types of chemical systems. For example, the familiar Arrhenius and Brønsted acid and base concepts used in general chemistry help chemists make sense of the behavior of compounds which can transfer H^+ ions among themselves, often in aqueous solution. However, the solvent system acid-base concept defines acids and bases in terms of the transfer of a lone-pair bearing group and is particularly useful for conceptualizing the reactivity of main group halides, oxides, and related compounds. Some acid-base definitions seek to encompass an extremely wide range of chemical reactions. For instance, the Lewis acid-base definition encompasses the Arrhenius , Brønsted, and solvent system definitions and has also found wide use in inorganic chemistry owing to the ease with which Lewis acid-base interactions may be described by the Frontier Orbital approach in terms of interacting molecular orbitals on the acid and base.

References

Huheey, J. E.; Keiter, E. A.; Keiter, R. L., *Inorganic Chemistry: Principles of Structure and Reactivity. 4th ed.*; HarperCollins: New York, NY, 1993, pg. 318.

This page titled 7.1: Acid-Base Models as Organizing Concepts is shared under a CC BY 4.0 license and was authored, remixed, and/or curated by Stephen M. Contakes.

- 6.1: Acid-Base Models as Organizing Concepts by Stephen M. Contakes is licensed CC BY 4.0.

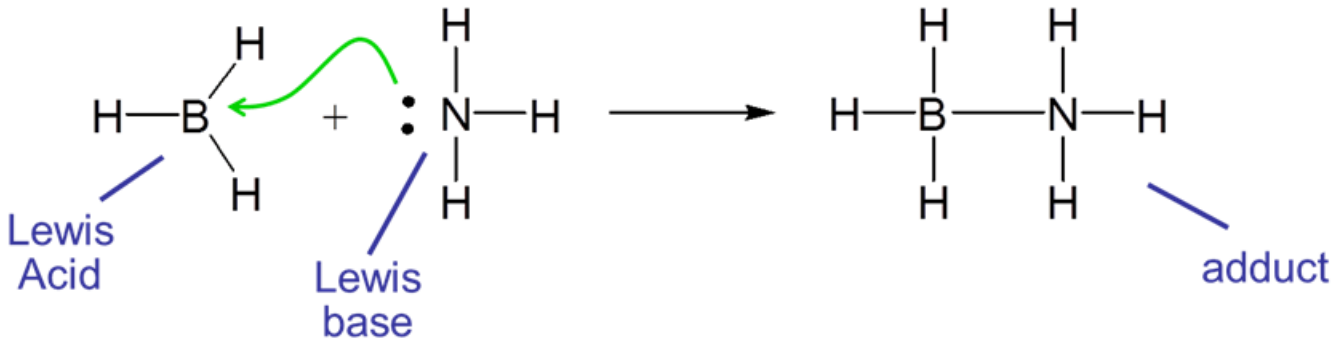
7.2: Lewis Concept and Frontier Orbitals

The Lewis acid-base concept generalizes the Brønsted and solvent system acid base concepts by describing acid-base reactions in terms of the donation and acceptance of an electron pair.

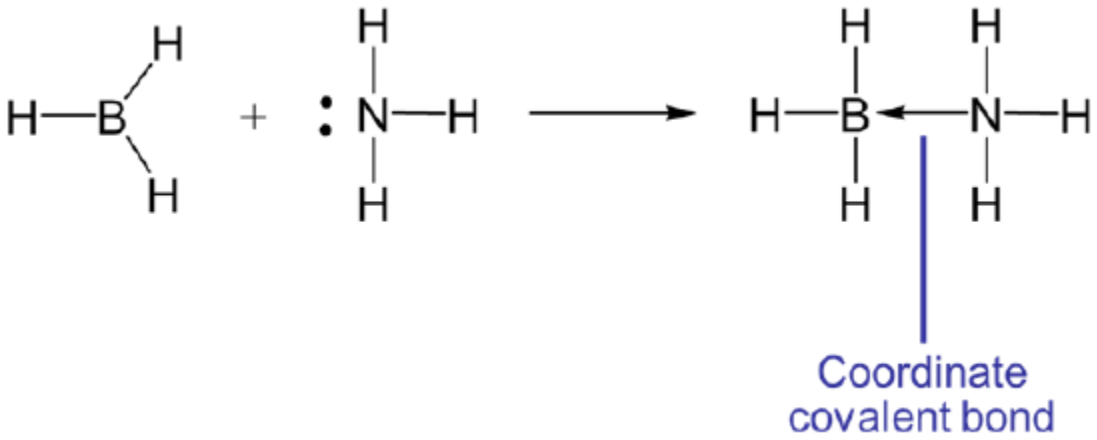
Under the Lewis definition

- **Lewis acids** are electron pair acceptors
- **Lewis bases** are electron pair donors

and in Lewis acid-base reactions, a Lewis base donates an electron pair to the Lewis acid, which accepts it. The reaction between borane, BH_3, and NH_3 is the classic example:



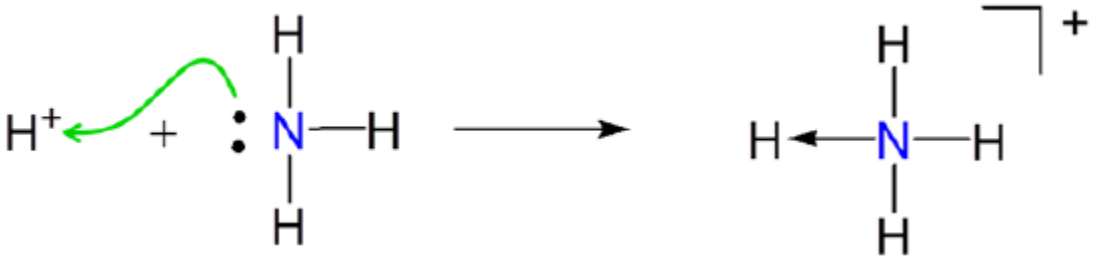
In this case the Lewis acid-base reaction results in the formation of a bond between BH_3, and NH_3. When the acid and base combine to form a larger unit, that unit is said to be an adduct, and the resulting bond is said to be a coordinate covalent or dative bond. Such coordinate covalent bonds are often represented by an arrow that indicates the direction of electron donation from the base to the acid. For instance, the reaction between BH_3 and NH_3 could also have been written as



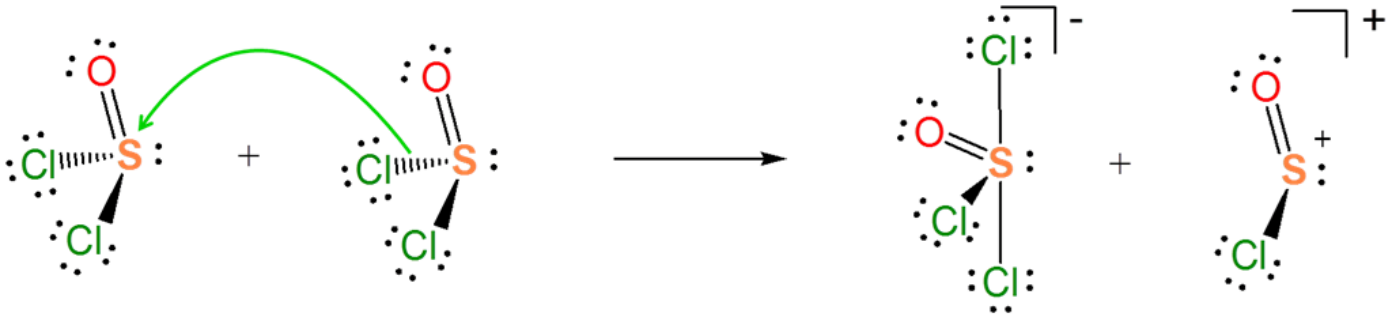
The arrow notation for the coordinate covalent bond is really just a convenient formalism - a bookkeeping tool to help keep track of where the electrons came from and where they might return if the reverse reaction occurs. In actuality a coordinate covalent bond is just an ordinary covalent bond like any other.

For example, in Brønsted acid-base reactions, the hydrogen ion is an acid because it accepts an electron pair from the Brønsted

base. Consequently, under the Lewis acid-base concept, Brønsted acid-base reactions involve the formation of an adduct between H^+ and a base.



The Lewis acid-base concept nicely explains ionization reactions involving nonaqueous solvents. For instance, the autoionization of $SOCl_2$ is an acid-base reaction between two $SOCl_2$ molecules.

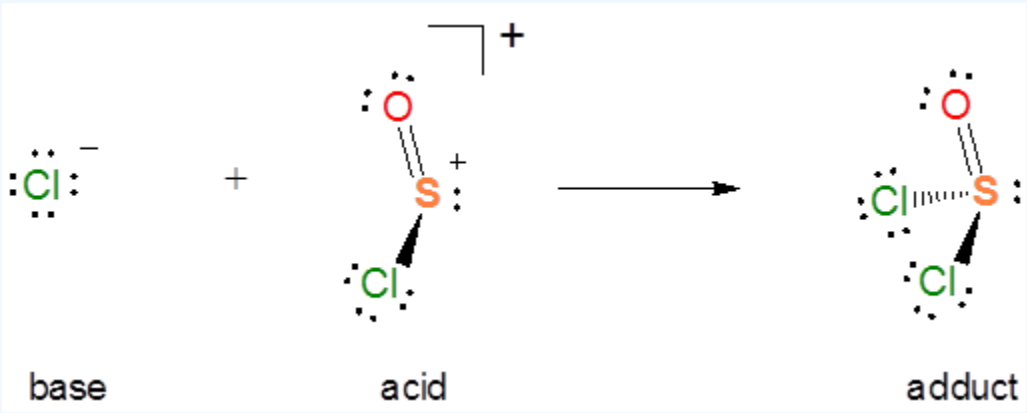


Example 7.2.1

Explain how the autoionization of $SOCl_2$ is a Lewis acid-base displacement reaction.

Solution

In the autoionization of $SOCl_2$ the pair of electrons donated comes from the S-Cl bond, and the S-Cl bond is broken to give a lone pair bearing a Cl^- base and an $SOCl^+$ Lewis acid fragment. If you are having trouble seeing how this works, it can be instructive to consider the reverse of this process. It is a Lewis acid-base reaction to give a Lewis acid-base adduct:

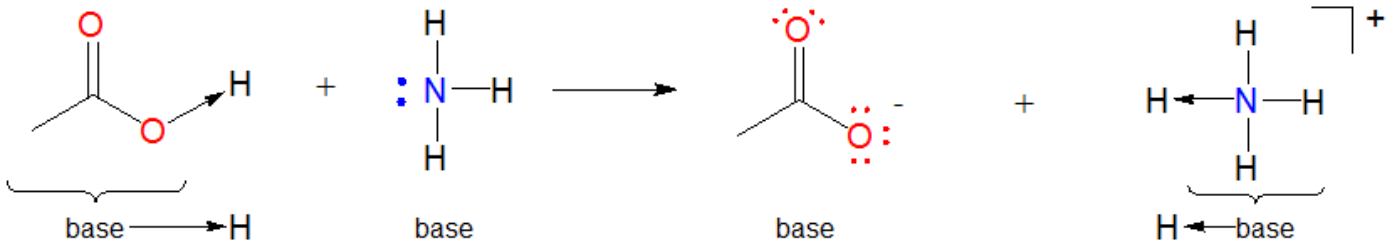


From the autoionization reaction it is also apparent that $SOCl_2$ itself acts as a Lewis acid towards the liberated Cl^-. So the autoionization reaction involves a transfer of the Cl^- base between the two Lewis acids - a Lewis acid-base displacement reaction.



It can be helpful to keep several distinctions in mind when using the Lewis acid-base concept to describe chemical reactions.

1. Many Lewis-Acid base reactions are displacement reactions. This is because the hydrogen ion is usually bound to something at the start of the reaction. In such cases the Lewis acid H^+ unit is transferred from one Lewis base to another :



Such acid-base reactions are sometimes called displacement reactions since the base group in the initial Lewis acid-base complex is displaced by the incoming Lewis base to generate another complex.

2. Substances are sometimes considered amphoteric because they exhibit Lewis acidity and basicity at different types of atomic centers. The classic example is aluminum hydroxide, $\mathrm{Al(OH)_3}$. In water $\mathrm{Al(OH)_3}$ can act as a Lewis acid towards OH^- ion. The reaction occurs by formation of an adduct at $\mathrm{Al(OH)_3}$'s Al^{3+} center:

$$\mathrm{Al(OH)_3 + OH^- \rightarrow Al(OH)_4^-}$$

Notice that in addition to acting as a Lewis acid, in this reaction $Al(OH)_3$

- does not act as a Brønsted acid or base since no H^+ ion transfer occurs
- but does act as an Arrhenius acid since OH^- ion is consumed from solution, decreasing $[OH^-]$ and increasing $[H^+]$

In water $\mathrm{Al(OH)_3}$ also acts as a Lewis base towards H^+ through the lone pairs on its hydroxide ligands.

$$\mathrm{Al(OH)_3 + 3\,H^+ + 3\,H_2O \rightarrow Al(H_2O)_6^{3+}}$$

Notice that in addition to acting as a Lewis base, in this reaction $\mathrm{Al(OH)_3}$ also acts as a

- Brønsted base, since a H^+ ion is transferred onto the OH^- ligand
- Arrhenius base, since H^+ ion is consumed from solution, decreasing $[H^+]$
- Lewis acid at its Al^{3+} center, since Al-O metal-ligand bonds are formed

Substances that rapidly undergo Lewis acid-base reactions are called nucleophiles and electrophiles.

Two factors govern the course of chemical reactions - thermodynamics and kinetics. Thermodyamics determines what possible fates of the reaction can take place while kinetics determines which among those possible fates will take place quickly under a particular set of reaction conditions. Because of this, it can be helpful to distinguish Lewis acids and bases that tend to undergo reaction quickly with one another from those which do so more slowly. For this reason, synthetic chemists use the terms electrophile and nucleophile to refer to Lewis acids and bases that react quickly:

- electrophile - Lewis acids that rapidly react with a given Lewis base or class of Lewis bases are said to be good electrophiles
- nucleophile - Lewis bases that rapidly react with a given Lewis acid or class of Lewis acids are said to be good nucleophiles

The electrophile-nucleophile concept is sometimes referred to as the Ingold-Robinson acid-base concept after two organic chemists who did much to illustrate the utility of thinking about Lewis acid-base reactions in kinetic terms.

Several distinctions that should be kept in mind when using the electrophile-nucleophile/Ingold-Robinson concept to think about chemical reactivity:

1. Whether a given Lewis acid or base is able to react rapidly depends on the reaction conditions and the substrate (substance it is reacting with). This means that in principle, the terms nucleophile and electrophile should not be used without appropriately qualifying what the substances act as a nucleophile or electrophile towards and under what conditions. Unfortunately this is rarely done. In such cases, the conditions and substrate must be inferred from the context. For instance, when you learned that the chloride ion is a good nucleophile when studying organic chemistry, what was meant is that chloride is a good nucleophile towards electrophilic carbon atoms in organic molecules.

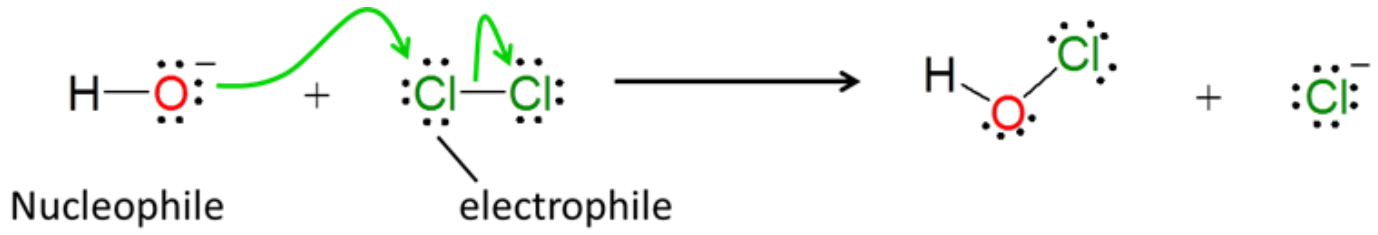
2. Acid and base strength and electrophilicity-nucleophilicity are not exactly the same thing. In many contexts where Lewis acids and bases are classified as electrophilic and nucleophilic substances, it is common to also refer to substances as being good acids or bases on the basis of their Brønsted acidity and basicity. In these contexts, the terms acid and base typically refer to the thermodynamic propensity of a substance to give and accept hydrogen ions while the terms nucleophile and electrophile refer to a substance's kinetic propensity to react with carbon-based Lewis acids and bases, respectively.

A substance may be both a good nucleophile and a strong Brønsted base. For instance, alkyllithium carbanion reagents and alkali metal hydrides are strong bases and good nucleophiles towards electrophilic carbon atoms in organic solvents at moderate temperatures. However, this is not always the case. Under such conditions iodide ion, I^-, is a good nucleophile towards electrophilic carbon atoms but is a poor Brønsted base (it is the conjugate of the strong acid HI). In fact, for the halide ions the order of Brønsted basicity is the opposite of the order of nucleophilicity towards electrophilic carbon:

stronger Brønsted base: F^-, Cl^-, Br^-, I^-: weaker Brønsted base

better nucleophlie: I^-, Br^-, Cl^-, F^-: poorer nucleophile

3. Although the nucleophile-electrophile concept is most often used to describe organic reactions, it is also useful for describing inorganic reactions as well. For instance, the formation of hypochlorite ion in chlorine water possibly involves nucleophilic attack of hydroxide on an electrophilic chlorine atom in an S_N2 type process:



The Usanovich Acid-base Concept

The Usanovich Acid-base concept encompasses a wider range of reactions than the Lewis acid-base concept but is perhaps too general to serve as a convenient framework for understanding reaction chemistry. The Usanovich acid-base concept was developed by the Russian chemist Mikhail Usanovich and extends the Lewis acid-base concept's definition of acids and bases as electron pair donors and acceptors even further. Within the Usanovich definition:

- Acids are anything that accepts electrons, increases cation concentrations, decreases anion concentrations, or reacts with bases
- Bases are anything that donates electrons, increases anion concentrations, decreases cation concentrations, or reacts with acids

These definitions essentially expand the Lewis definition by removing the requirement that the electrons donated or accepted be a pair and practically mean that Usanovich acid-base reactions include Lewis acid-base reactions plus oxidation-reduction reactions. In other words:

- Usanovich acids are Lewis acids plus oxidants
- Usanovich bases are Lewis bases plus reductants

Under this definition BF_3, Fe^{3+}, and $[Fe(CN)_6]^{3-}$ all act as acids, and : NH_3, CN^-, and Zn are all bases:

$$\underset{acid}{BF_3} + \underset{base}{NH_3} \rightarrow F_3B-NH_3$$

$$\underset{acid}{Fe^{3+}} + 6\underset{base}{CN:^-} \rightarrow [Fe(CN)_6]^{3-}$$

$$\underset{acid}{2[Fe(CN)_6]^{3-}} + \underset{base}{Zn} \rightarrow 2[Fe(CN)_6]^{3-} + Zn^{2+}$$

However, notice that while it is easy to think about how any acids might interchangeably react with a given base (and vice versa), under the other acid-base concepts chemists have found it more difficult to think about reactions between oxidants/reductants and Lewis acids and bases. For example, it is difficult to think about how a reaction between BF_3 and Zn metal might occur. Would two Zn donate a pair of electrons to the BF_3? For this reason, most chemists find it more convenient to think about Lewis acid-base and redox reactions under separate categories rather than unite them under the Usanovich definition.

$$\underset{oxidant}{2[Fe(CN)_6]^{3-}} + \underset{reductant}{Zn} \rightarrow 2[Fe(CN)_6]^{3-} + Zn^{2+}$$

Again, it can be helpful to remember Huheey's dictum that deciding between acid-base concepts is not a matter of which concept is the most correct but rather of which is more convenient for a given application.

This page titled 7.2: Lewis Concept and Frontier Orbitals is shared under a CC BY-NC 4.0 license and was authored, remixed, and/or curated by Stephen M. Contakes.

- 6.4: Lewis Concept and Frontier Orbitals by Stephen M. Contakes is licensed CC BY 4.0.

7.2.1: The frontier orbital approach considers Lewis acid-base reactions in terms of the donation of electrons from the base's highest occupied orbital into the acid's lowest unoccupied orbital.

Another way the Lewis-Acid base concept is widely employed for understanding chemical reactivity is through the frontier orbital approach to chemical reactions. The frontier orbital concept conceptualizes chemical bonding and reactivity in terms of the interactions between frontier orbitals on the chemical species undergoing an interaction (*e.g.* molecules, atoms, ions, or groups as they interact to form a bond or undergo a reaction). Frontier orbitals are those at the frontier between occupied and unoccupied. They are often taken to be the highest energy occupied and lowest energy unoccupied molecular orbitals, called the HOMO and LUMO levels. However, it can sometimes be more convenient to think about them as atomic orbitals or Valence Bond approach-derived orbitals. When developing rough qualitative frontier orbital descriptions of the orbital interactions involved in a given system, the choice of what types of orbitals to use is often a matter of what is the most informative and convenient.

In particular, the frontier orbital concept envisions a Lewis acid-base interaction as involving an interaction between some of the frontier orbitals of the Lewis acid and base, specifically the donation of electrons from the base's HOMO level into the acid's LUMO level. For example, in the frontier orbital approach, adduct formation between NH_3 and BH_3 involves the donation of electrons from ammonia's a_1 HOMO into BH_3's a_2'' LUMO level.

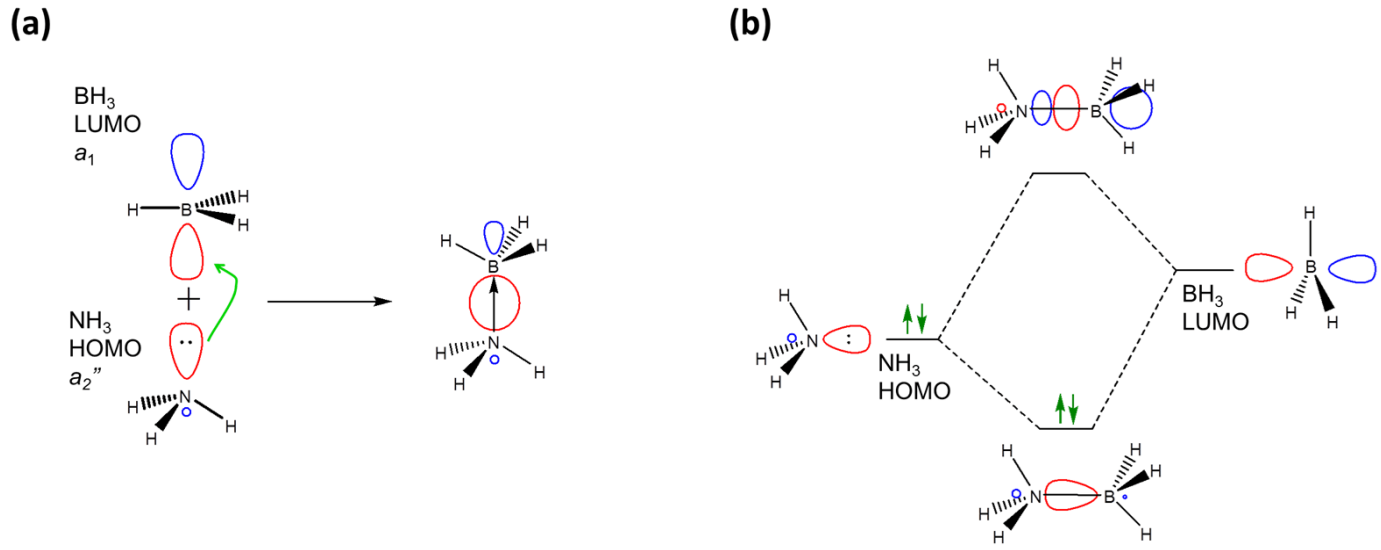


Figure 7.2.1.1. Frontier orbital picture of adduct formation between ammonia and borane. (a) As NH_3 and BH_3 approach one another, interaction between the NH_3 HOMO and BH_3 LUMO gives a bonding MO. (b) Partial molecular orbital diagram for $NH_3 \rightarrow BH_3$ showing the stabilization of the base (NH_3) lone pair in a sigma bonding MO upon adduct formation.

As expected when two orbitals of the appropriate symmetry combine, the result of the interaction is the formation of a lower energy bonding orbital between the acid and base (Figure 7.2.1.1). Since it is occupied by an electron, the net result of the interaction is the lowering of the base's lone pair energy as it interacts with the Lewis acid. In this case the interaction just follows the general pattern for Lewis-Acid base adduct formation, which is:

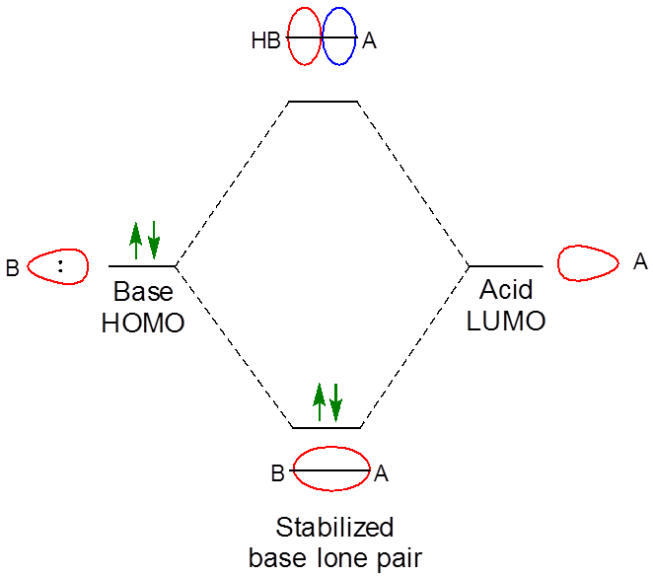
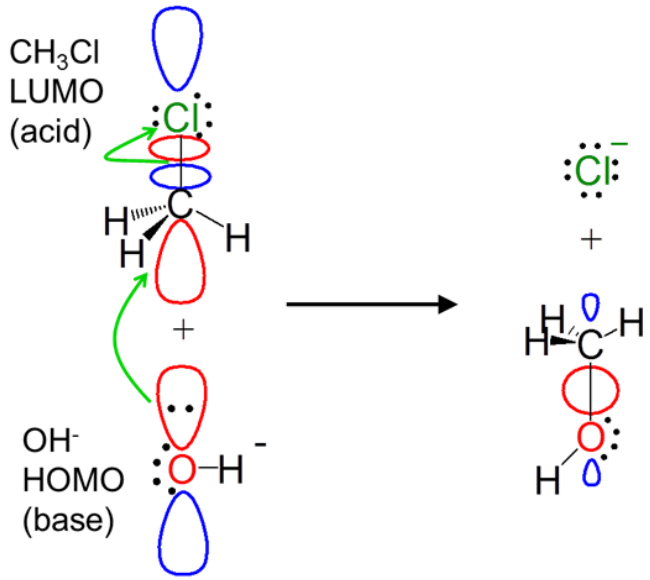


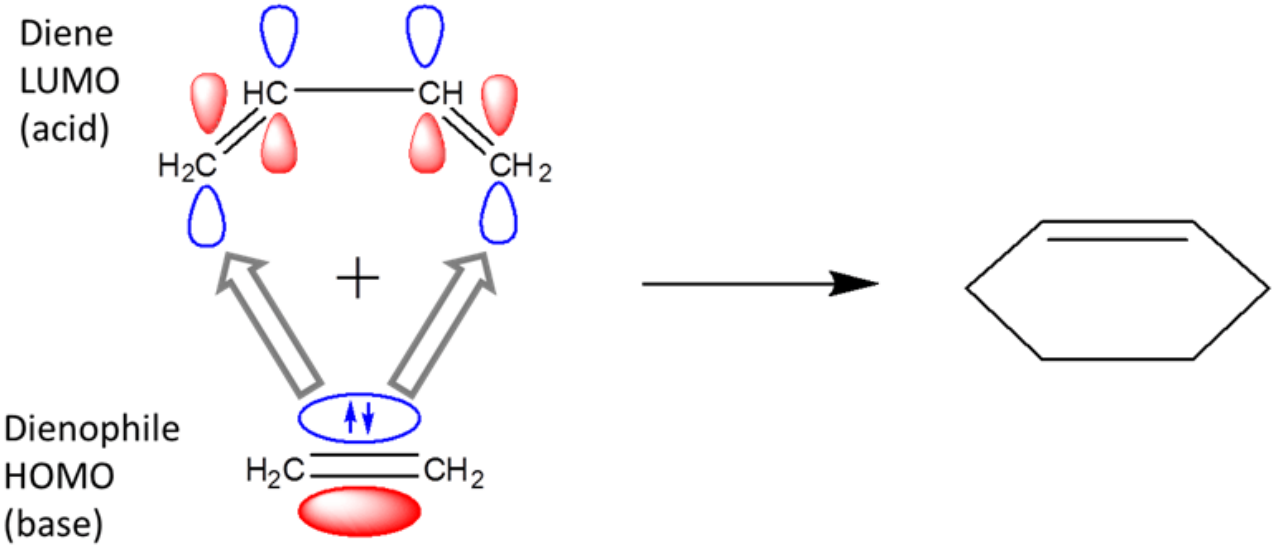
Figure 7.2.1.2. Generalized frontier orbital picture for adduct formation between a Lewis base (B) and a Lewis acid (A) involving stabilization of the lone pair of the base HOMO by formation of a bonding orbital with the acid LUMO. The relative energies of the acid LUMO and base HOMO affect the character of the bonding and antibonding MOs but are otherwise unimportant in determining the general features of the interaction. In some cases the base HOMO is higher in energy; in others the acid LUMO is higher in energy; in still others they are equal in energy. In any case the net result is the stabilization of the base lone pair.

The frontier orbital concept illuminates the orbital interactions involved in reactions. For instance, from a frontier orbital perspective the alkyl halide substitution reaction between hydroxide and CH_3Cl via the S_N2 mechanism involves a Lewis acid-base interaction:

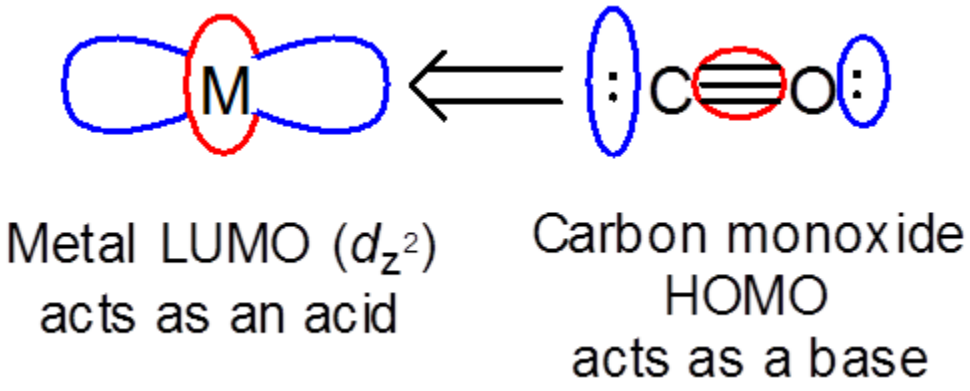


Notice how the frontier orbital approach even explains the displacement of the chloride leaving group. The donation of electrons from the hydroxide HOMO populates the antibonding CH_3Cl LUMO, breaking the C-Cl bond.

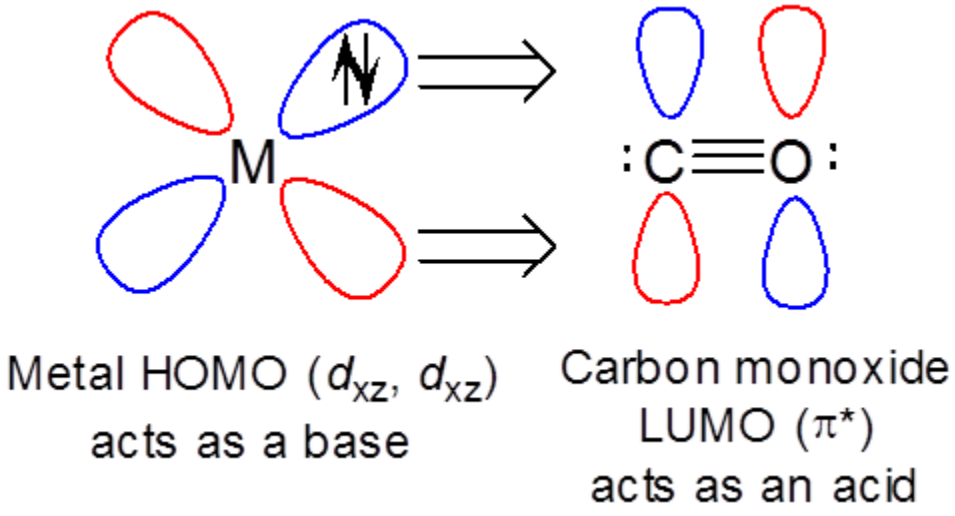
With the frontier orbital approach, it becomes apparent that pericyclic reactions are Lewis acid-base reactions. For example, in the Diels-Alder reaction, the dienophile acts as a Lewis base and the diene as a Lewis acid.



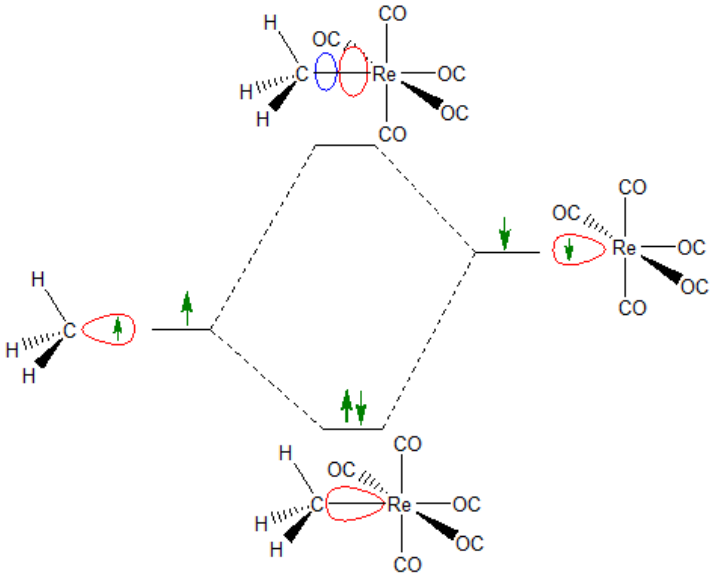
The orbital interactions involved in a given reaction can include both reactants acting as both an acid and base. In these cases the HOMO of each reactant interacts with the LUMO of the other. A good example of this involves Π-type interactions between a metal ion with occupied *d* orbitals and a pi-acceptor ligand. The ligand acts as a base and the metal as an acid to give a M-CO single bond:



However, the metal can also act as a base towards the ligand LUMO (π^*) orbitals.



The frontier orbital concept can also be used to describe interactions between one or more singly occupied frontier orbitals. In fact, when approximate molecular orbital diagrams are being constructed, it can often be helpful to focus on one or two particularly instructive interactions. In these cases, it is sometimes convenient to think about a chemical bond as involving the formation of bonding and antibonding interactions between singly occupied frontier orbitals on different molecular fragments. For instance, when thinking about the chemistry of $CH_3Re(CO)_5$ it can sometimes be helpful to think about the C-Re bond as arising from the interaction between a singly-occupied sp^3 type orbital on a CH_3 group and a singly occupied d^2sp^3 orbital on the Re.



In introducing singly occupied orbitals, the frontier orbital concept formally handles interactions that the Lewis acid-base concept does not, since Lewis acid-base behavior is formally confined to the acceptance and donation of electron *pairs*.

This page titled 7.2.1: The frontier orbital approach considers Lewis acid-base reactions in terms of the donation of electrons from the base's highest occupied orbital into the acid's lowest unoccupied orbital. is shared under a CC BY 4.0 license and was authored, remixed, and/or curated by Stephen M. Contakes.

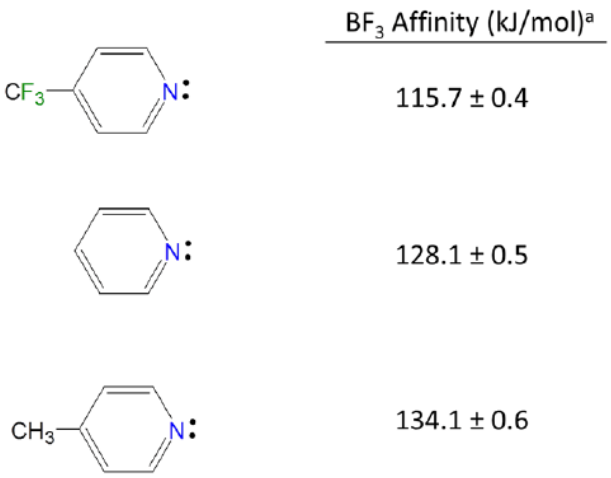
- 6.4.1: The frontier orbital approach considers Lewis acid-base reactions in terms of the donation of electrons from the base's highest occupied orbital into the acid's lowest unoccupied orbital. by Stephen M. Contakes is licensed CC BY 4.0.

7.2.2: All other things being equal, electron withdrawing groups tend to make Lewis acids stronger and bases weaker while electron donating groups tend to make Lewis bases stronger and acids weaker

The electrons donated from a Lewis base to a Lewis acid in a Lewis acid-base reaction are donated and accepted at particular atomic centers. For instance, the formation of an adduct between ammonia and BF_3 involves the donation of the lone pair on the ammonia nitrogen atom to the Lewis acid site on BF_3.



Because Lewis acid-base reactions involve electron donation and acceptance at particular sites, substituent groups which alter the electron density at a site through inductively donating or withdrawing electron density will affect the Lewis acid-base properties of that site. For instance, the BF_3 affinities of 4-substituted pyridines increase slightly as the substituent on the aromatic ring is changed from electron donating Me to electron withdrawing CF_3.



a) Data from Laurence, C.; Gal, J.-F. o., *Lewis basicity and Affinity Scales: Data and Measurement. John Wiley: Chichester, West Sussex, U.K., 2010; pp. 91-101.*

Substituent inductive effects are much as one might predict. Since Lewis bases donate electron pairs and Lewis acids accept them:

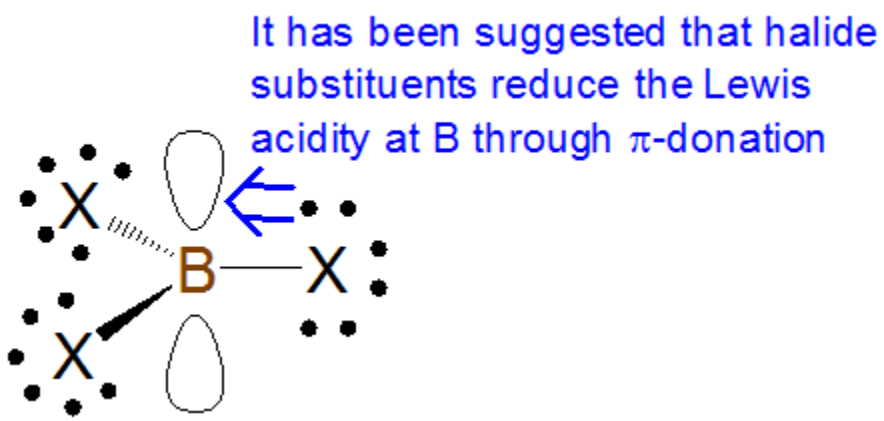
- electron withdrawing substituents tend to decrease the Lewis basicity of basic sites while electron donating substituents increase site Lewis basicity by making them more electron rich.
- electron withdrawing substituents increase the Lewis acidity of acidic sites by making those sites more electron deficient while electron donating substituents tend to decrease Lewis acidity by making sites less electron deficient.

Nevertheless it can be difficult to predict substituent-based trends in Lewis acidity and basicity by inductive effects alone. This is because inductive effects are modest and often exists in competition with other substituent effects, such as

- Steric effects, discussed in section 6.4.7
- Hardness effects, discussed in section 6.6
- π-donation and acceptance effects, which can increase or decrease electron density at a given site as well as create an energy barrier for any structural distortions that might occur upon adduct formation.

Avoid misconceptions about the impact ofπ donation and acceptance on Lewis acid-base affinity

As with σ-based induction effects, π-donation tends to increase Lewis basicity and decrease Lewis acidity while π-withdrawal tends to decrease Lewis basicity and increase Lewis acidity. However, care needs to be taken in assessing the effect of π-donation effects on Lewis acidity and basicity. For example, some textbooks claim that the Lewis acidity of boron trihalides is dominated by the reduction of boron acidity through π-donation from the halide substituents:

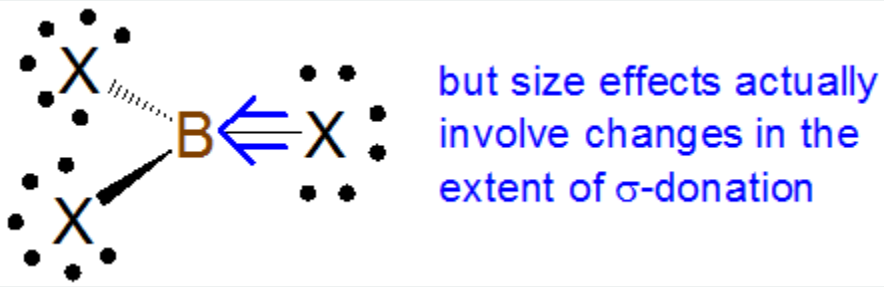


According to this explanation, the extent of this π-donation decreases down the halogen group as the boron-halogen bond distance decreases. This is consistent with the observed trend in Lewis acidity of the boron trihalides towards most bases, which runs counter to that suggested by inductive effects alone:

$$BI_3 > BBr_3 > BCl_3 >> BF_3$$

However, computational work suggests that this explanation is incorrect, since

- atomic size effects are important mainly for substituents in which the connected atom is in row 3+ or higher;
- atomic size effects mainly involve changes in the extent of σ-overlap. In other words, the larger halogens are less able to reduce the electron deficiency at the boron center through σ interactions while π-interactions play little or no role.



References:

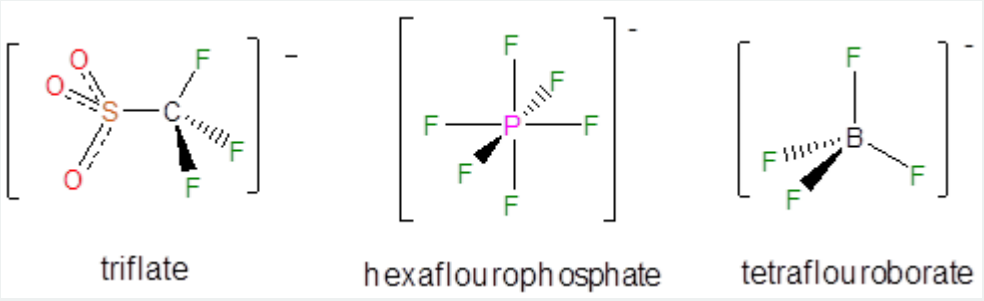
1. Plumley, J. A.; Evanseck, J. D., Periodic Trends and Index of Boron Lewis Acidity. *The Journal of Physical Chemistry A* 2009, 113 (20), 5985-5992.

2. Jupp, A. R.; Johnstone, T. C.; Stephan, D. W., Improving the Global Electrophilicity Index (GEI) as a Measure of Lewis Acidity. *Inorganic Chemistry* 2018, 57 (23), 14764-14771.

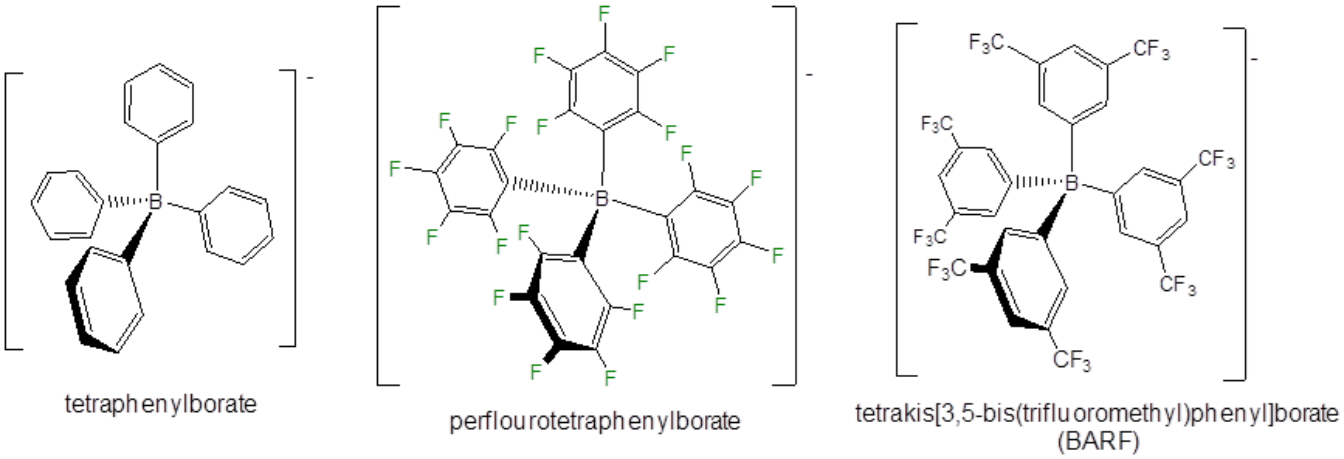
The conjugate bases of many Brønsted superacids have electron-withdrawing substituents that make them such poor Lewis bases that they are useful as noncoordinating anions.

The nonreactivity of Brønsted superacids' conjugate bases towards hydrogen ions is often mirrored in nonreactivity towards other Lewis Acids/electrophiles, most notably metals. This makes these substances useful as inert or noncoordinating ions, although since all are reactive towards suitably electrophilic centers, they are perhaps better understood as weakly coordinating.

A number of noncoordinating anions are commonly used in synthetic and other applications. The conjugate base of perchloric acid, perchlorate, was a common noncoordinating inert anion in classical coordination chemistry and continues to be used widely in electrochemistry. In contrast, the conjugate bases of triflic acid, hexafluoroboric acid, and tetrafluoroboric acid are now more commonly used as counterions for isolating reactive cations.



Even less reactive noncoordination anions include derivatives of tetraphenylborate, particularly those with electron withdrawing substituents.



Other classes of noncoordinating ions include fluoroantimonate clusters, derivatives of the carborane anion ($CB_{11}H_{11}^-$), and fluorinated aluminum tetraalkoxides.

References

Engesser, T. A.; Lichtenthaler, M. R.; Schleep, M.; Krossing, I., Reactive p-block cations stabilized by weakly coordinating anions. *Chemical Society reviews* **2016**, *45 (4)*, 789-899.

This page titled 7.2.2: All other things being equal, electron withdrawing groups tend to make Lewis acids stronger and bases weaker while electron donating groups tend to make Lewis bases stronger and acids weaker is shared under a CC BY 4.0 license and was authored, remixed, and/or curated by Stephen M. Contakes.

- 6.4.2: All other things being equal, electron withdrawing groups tend to make Lewis acids stronger and bases weaker while electron donating groups tend to make Lewis bases stronger and acids weaker by Stephen M. Contakes is licensed CC BY 4.0.

7.2.3: The electronic spectra of charge transfer complexes illustrate the impact of frontier orbital interactions on the electronic structure of Lewis acid-base adducts

When a Lewis acid-base adduct is formed, electron density and negative charge are transferred from the Lewis base to the acid.

The formation of a Lewis-acid base complex involves the transfer of electron density from the base to the acid.



Figure 6.4.2.7.2.3.1.

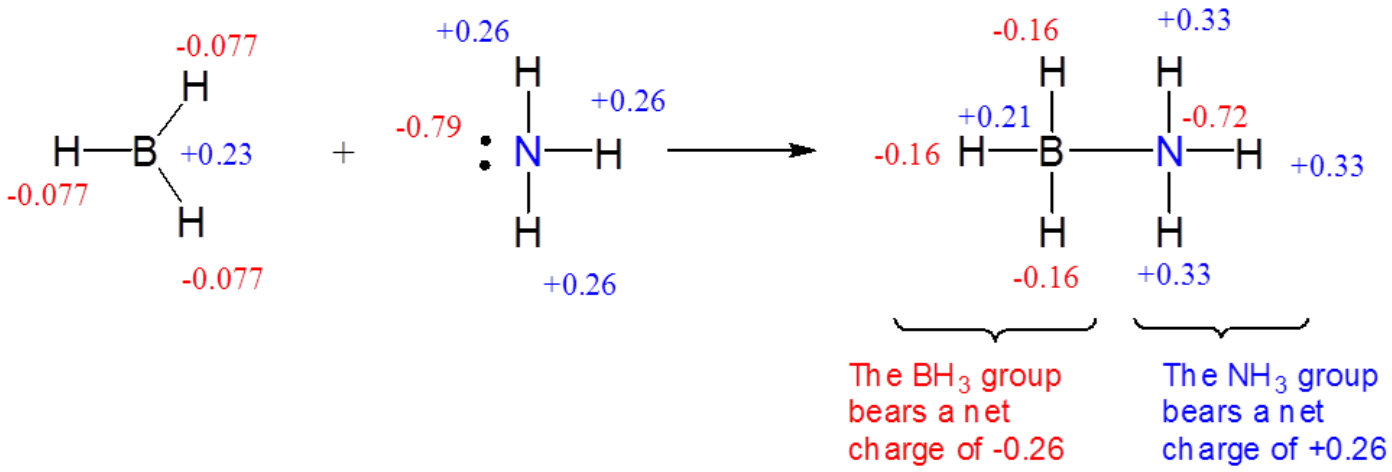


Figure 6.4.2.7.2.3.1. Calculated change in atomic charge distribution upon formation of an adduct between BH_3 and NH_3 in the gas phase. All partial charges were calculated for geometry-optimized molecules at the 6-31G** level.

Weakly bound Lewis acid-base adducts in which charge is incompletely transferred are called charge transfer complexes.

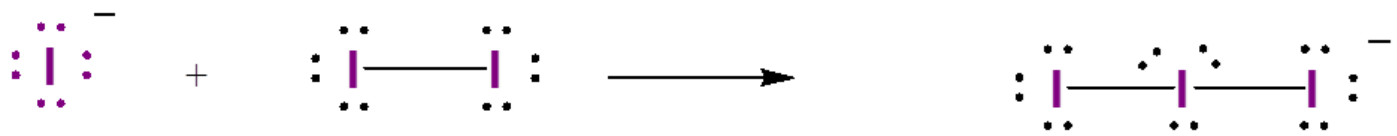
In many weakly bound Lewis acid-base complexes, the transfer of electron density and, consequently, charge from the base group to the acid group is only partial:

$$A + B \rightleftharpoons A^{\delta-}B^{\delta+}$$

Such Lewis acid-base adducts are commonly called **charge transfer complexes (CT complexes)** or **donor-acceptor complexes (DA complexes)**. In these

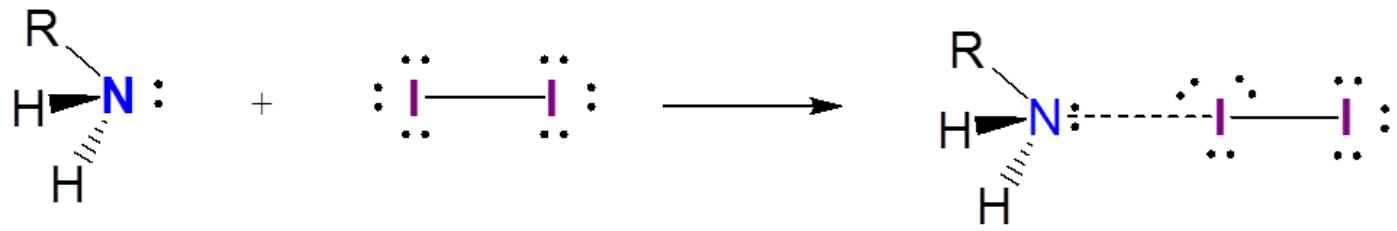
- the base is called the **donor (D)** since it is a net donor of electrons and, consequently, their negative charge
- the acid is called the **acceptor (A)** since it is a net acceptor of electrons and, consequently, their negative charge

A particularly well-known class of charge transfer complexes is the iodine charge transfer complexes. In iodine charge transfer complexes the I_2 acts as a Lewis acid. This is possible since iodine is a Row 3+ element and so is capable of forming hypervalent complexes on reaction with a Lewis base. For example, I_2 reacts with I^- to give the triiodide ion.

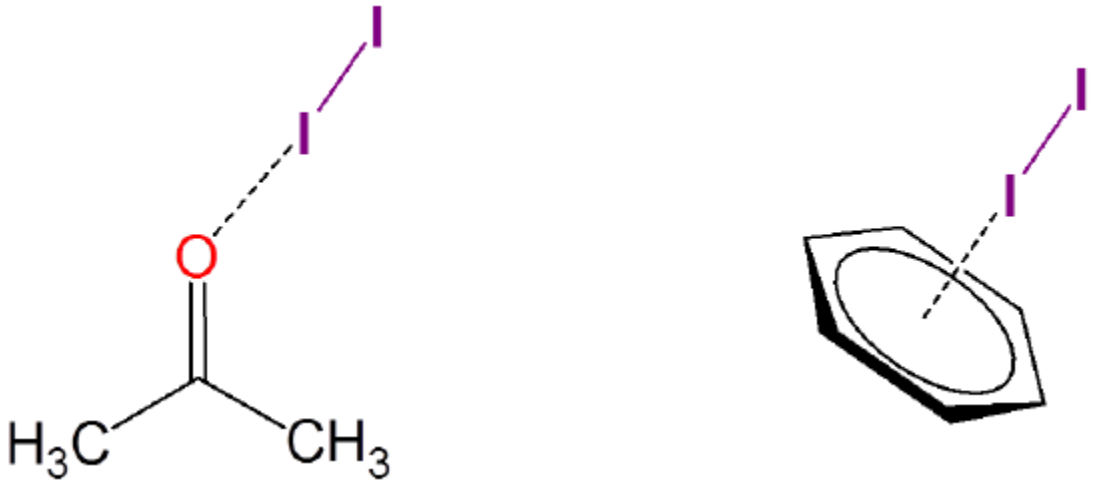


Triiodide is well-known from introductory chemistry from the bright blue color that appears when the triiodide complexes with starch to give the dark blue starch-iodide complex.

In contrast to the stable triiodide anion, iodine charge transfer complexes are only weakly associated. Complexes between iodine and amines are a well known example:

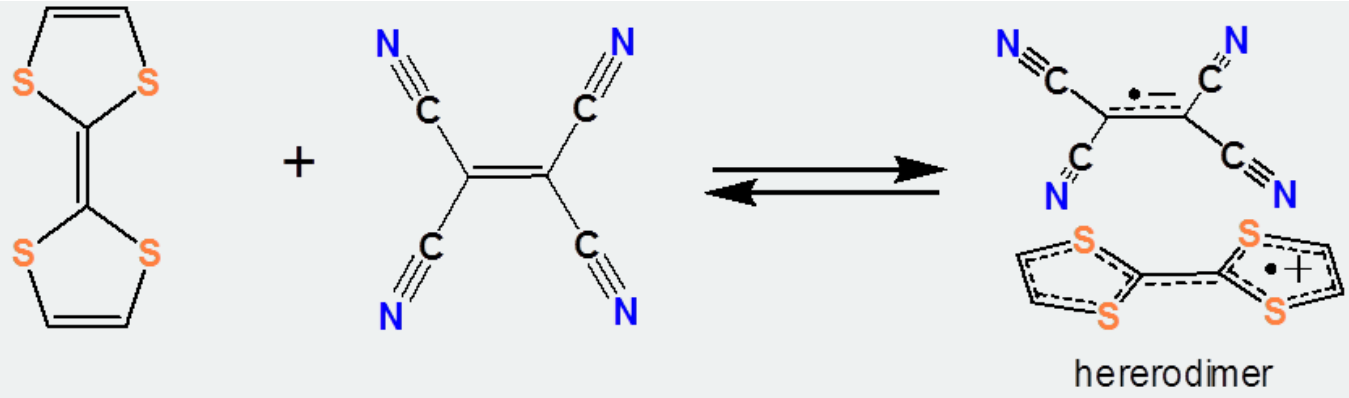


Iodine also forms weakly-associated charge transfer complexes with many solvents. For instance, iodine can weakly associate with both acetone and benzene:

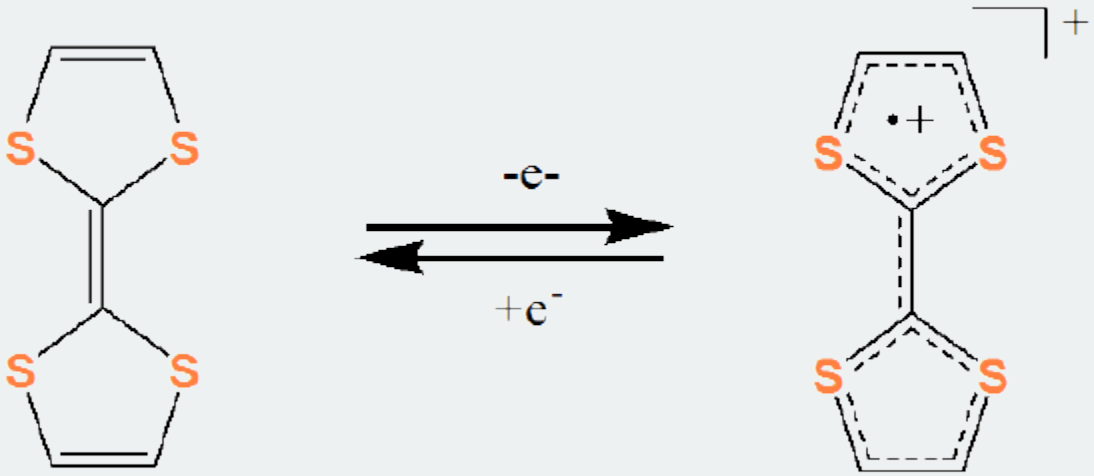


Organic Charge Transfer Complexes

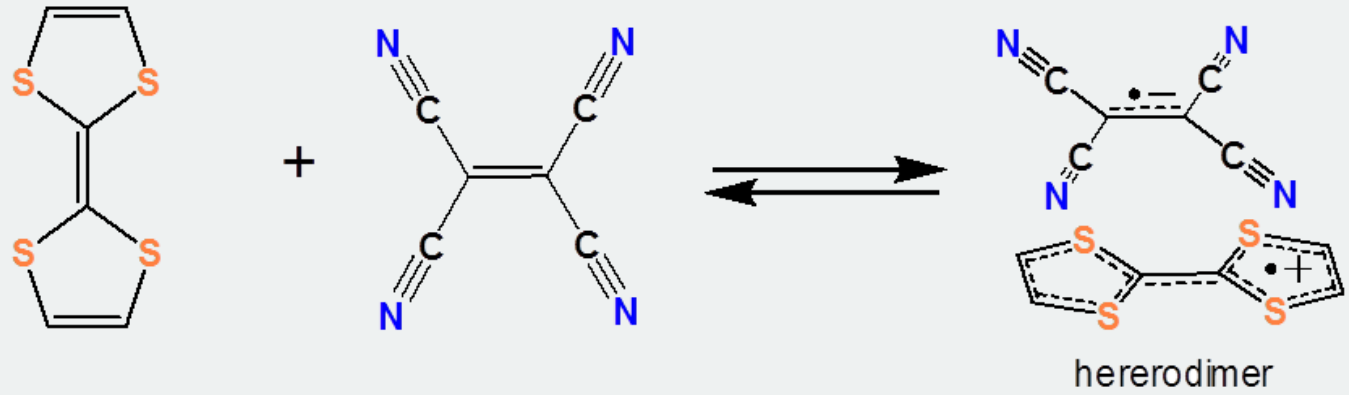
It is worth noting in passing that several organic charge transfer complex systems have been developed in which organic electron donors and acceptors weakly associate with each other. These are of considerable interest for use in molecular electronics applications, and as a result, a large variety of organic electron donors and acceptors have been developed. An example of an organic electron acceptor is tetracyanoethylene (TCNE):



and an example of an organic electron acceptor is tetrathiofulvalene (TTF).



Together they form a charge transfer complex:



Similar organic charge transfer systems have been investigated for use in organic photovoltaic cells. There is considerable interest in developing such organic photovoltaic devices owing to the ease with which organic materials may be fabricated from organic solutions and suspensions.

Charge transfer complexes exhibit charge transfer transitions in which absorption triggers the transfer of an electron from the donor to the acceptor.

When iodine is dissolved in solutions of donor solvents, the striking purple color of molecular iodine is replaced by a yellow-brown color. This is because charge transfer complexes like those formed by I_2 can absorb light in ways that neither the donor nor the acceptor can on their own. Specifically, charge transfer complexes exhibit **charge transfer bands (CT bands)** in their absorption spectra. In the charge transfer transition the initial partial transfer of charge from the donor Lewis base to the acceptor Lewis acid in the charge transfer complex is pushed further by photoexcitation.

$$D^{\delta+} - A^{\delta-} \overset{h\nu_{CT}}{\longrightarrow} D^{+} - A^{-}$$

The nature of these charge transfer transitions is seen from the orbital description of binding for iodine charge transfer complexes. When a donor-I_2 complex forms, the formation of donor-I_2 bonding and antibonding orbitals results in a shift in the $I2\sigma \rightarrow \sigma*$ transition to higher energy, as a new charge transfer band is formed, associated with the excitation of an electron from the largely amine-centered amine-I_2 σ orbital to the largely I_2-centered amine-I_2 $\sigma*$ orbital.

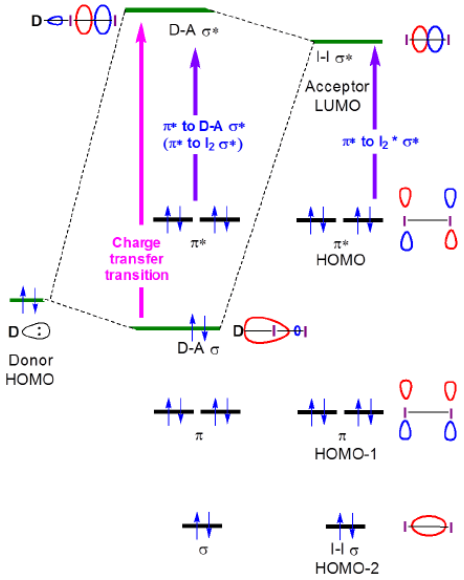


Figure 6.4.2.7.2.3.2. Frontier orbital interactions that give rise to changes in the absorption spectra of iodine when it forms a charge transfer complex with a Lewis base donor.

Solutions of I_2 as mixtures with Lewis bases such as amines and in donor solvents clearly have charge transfer bands in their absorption spectra. Several such spectra are given in Figure 6.4.2.3.

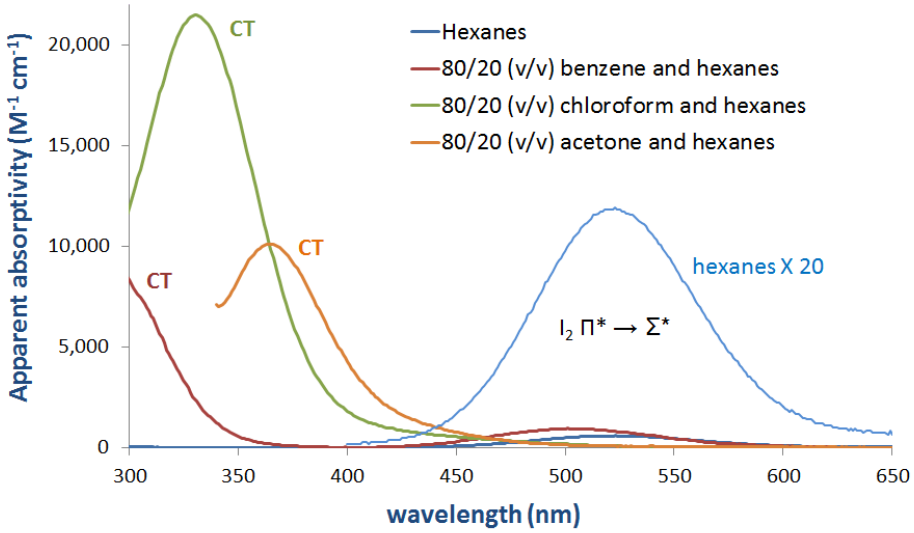


Figure 7.2.3.3. Absorption spectrum of molecular iodine (I_2) in various solvents showing the appearance of a CT band in donor solvents.*

In principle, the energies of both the charge transfer and $I_2\ \pi*\ \rightarrow\ D-A\ \sigma*$ transitions both increase with donor strength, as shown in Figure 6.4.2.4.

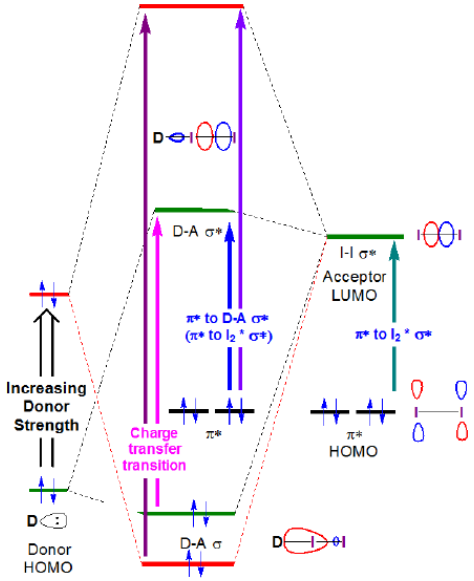


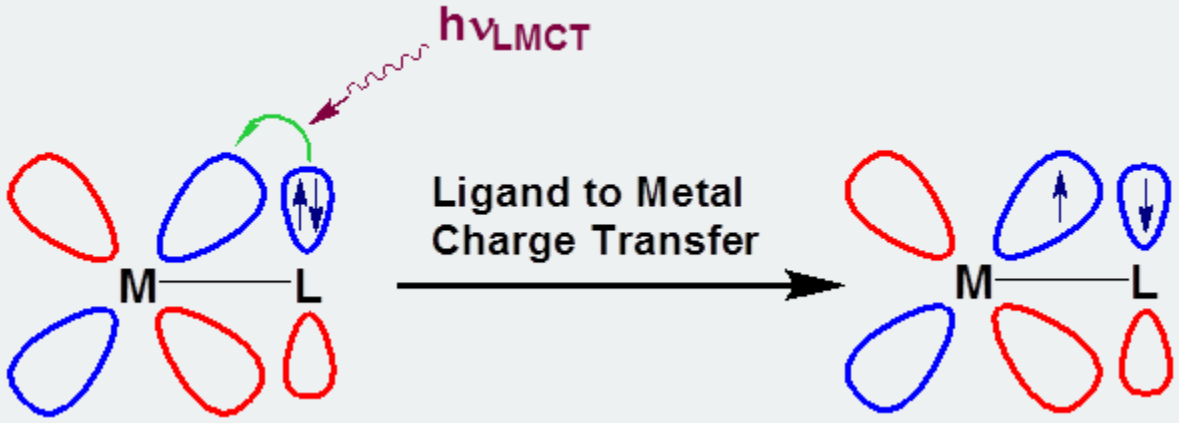
Figure 7.2.3.4. Expected change in the frontier orbital energies associated with I_2 donor acceptor complex formation when the HOMO energy of the donor is increased.

As can be seen in Figure 6.4.2, the charge transfer band energy might be expected to increase as the donor HOMO increases in energy to become closer in energy to the acceptor LUMO. Although care should be taken when interpreting the solution phase spectra of I_2, this expectation is borne out by a cursory and qualitative analysis of the spectra in Figure 6.4.2.3. The CT transition energy shifts towards lower wavelengths (and thus higher energy) as the highest occupied atomic orbital energy for the donor atom increases on going from acetone (oxygen, -15.85 eV) to chloroform (chlorine, -13.67eV) and finally benzene (carbon, -10.66 eV).**

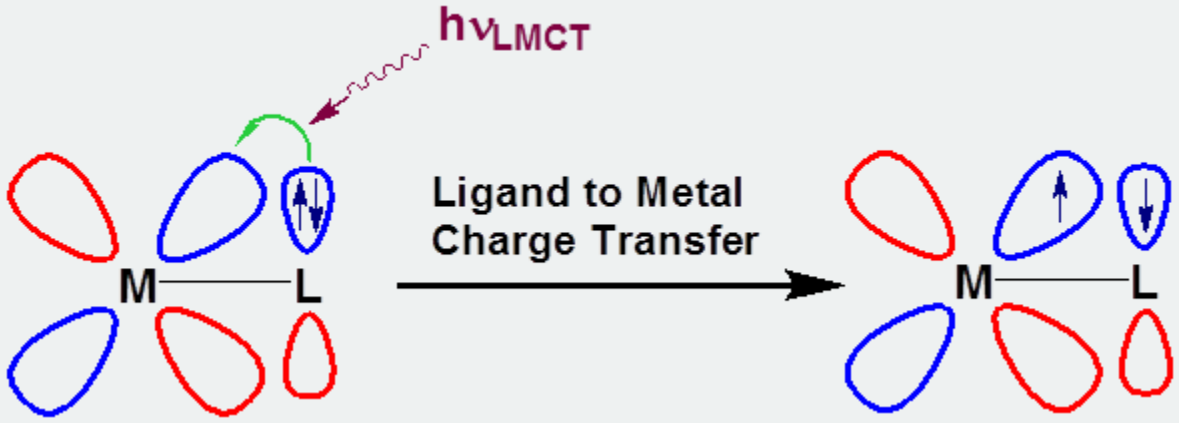
Charge Transfer Bands in Transition Metal Chemistry

Charge transfer transitions are responsible for the intense color of many transition metal complexes. In these cases, however, the weak Lewis acid-base interaction involves incomplete electron donation and acceptance in a $p\pi - d\pi$ (or $p\pi - d\pi *$)-bond between a metal and ligand. The charge transfer bands in the absorption spectra of these complexes involve the transfer of electrons between the metal and ligand. In particular,

- Metal to ligand charge transfer (MLCT or CTTL) bands involve the transfer of an electron from a filled or partly filled metal *d* orbital to a ligand $\pi *$-type orbital.



- Ligand to metal charge transfer (LMCT or CTTM) bands involve the transfer of an electron from a filled or partly filled ligand orbital to a metal *d*-orbital.



- Metal to metal charge transfer bands can be observed in some bimetallic complexes. However, these are usually thought of only as an electron transfer rather than as a shift in the status of a Lewis acid-base interaction.

Because metal-ligand charge transfer bands involve intermolecular electron transfer between the metal and ligand to generate a high energy redox state, the CT excited state is both a better oxidant and reductant than the ground state. Consequently there has been intense research into the development of metal complexes whose charge transfer excited states are powerful oxidants and reductants in the expectation that they will be able to drive the photocatalytic oxidation and reduction of substrates.

* The apparent absorptivity of I_2 in hexanes was calculated from the absorption spectrum of 215 μM I_2 in hexanes. All other apparent absorptivities were calculated from absorption spectra of solutions that were 44 μM in I_2.

** The band positions are not the CT band energies, and the HOMO energies given are atomic energy levels and do not

necessarily correspond to the HOMO of the donor in solution. Because of this and other simplifications this analysis is not intended to replace a rigorous computational analysis of the factors that give rise to CT band positions.

References

1. Meyerstein, D.; Treinin, A., Charge-transfer complexes of iodine and inorganic anions in solution. Transactions of the Faraday Society 1963, 59 (0), 1114-1120.
2. Baskar, A. J. A.; Rajpurohit, A. S.; Panneerselvam, M.; Jaccobb, M.; RoopSingh, D.; Kannappan, V., Experimental and theoretical analysis of substituent effect on charge transfer complexes of iodine and some alkylbenzenes in n-hexane solution at 303K. Chemical Data Collections 2017, 7-8, 80-92.

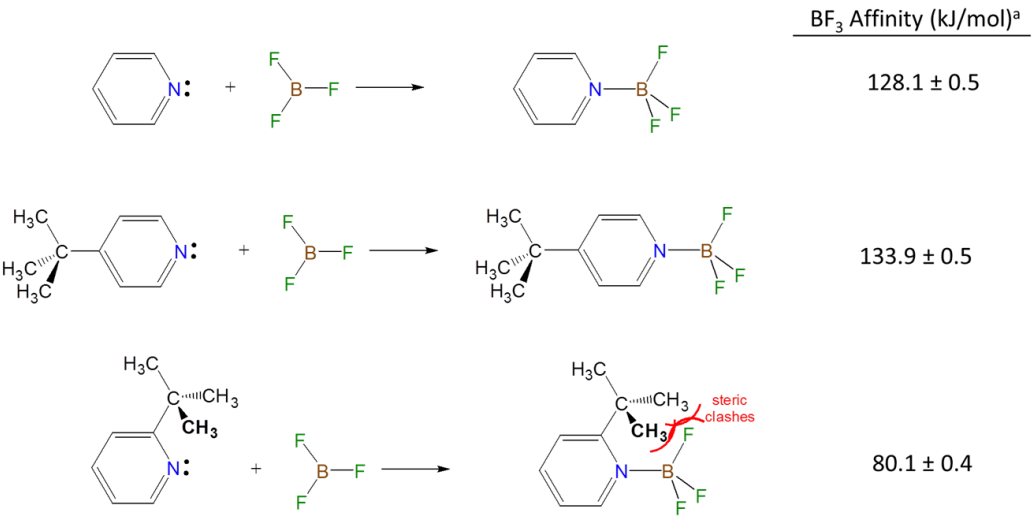
This page titled 7.2.3: The electronic spectra of charge transfer complexes illustrate the impact of frontier orbital interactions on the electronic structure of Lewis acid-base adducts is shared under a CC BY-NC 4.0 license and was authored, remixed, and/or curated by Stephen M. Contakes.

- 6.4.3: The electronic spectra of charge transfer complexes illustrate the impact of frontier orbital interactions on the electronic structure of Lewis acid-base adducts by Stephen M. Contakes is licensed CC BY 4.0.

7.2.4: Bulky groups weaken the strength of Lewis acids and bases because they introduce steric strain into the resulting acid-base adduct.

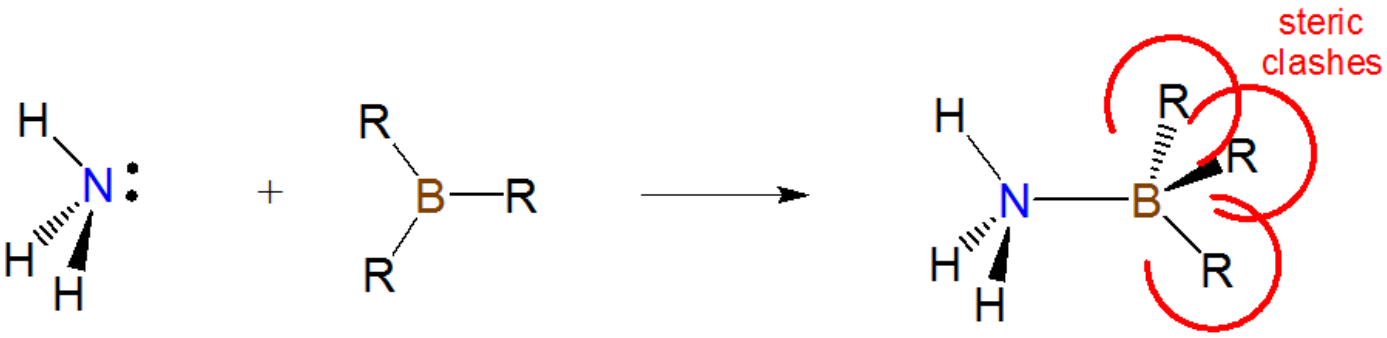
Steric effects can influence the ability of a Lewis acid or base to form adducts by introducing:

- **front strain (F-strain)** whereby bulky groups make it difficult for the Lewis acid and Lewis base centers to approach and interact.



a) Data from Laurence, C.; Gal, J.-F. o., *Lewis basicity and Affinity Scales: Data and Measurement. John Wiley: Chichester, West Sussex, U.K., 2010; pp. 91-101.*

- **back strain (B-strain)** associated with steric interactions that do not directly impede the Lewis acid and base centers from interacting but instead occur as the acid and base rearrange upon adduct formation. For instance, when trivalent boron compounds form adducts with amines, the boron center changes from a more open trigonal geometry to a more hindered tetrahedral one:



- **internal strain (I-strain)** is also associated with the geometry changes incident on adduct formation. However, while B-strain involves direct steric clashes that occur on adduct formation, I-strain is the strain involved in deforming bond and torsional angles away from more stable local geometries. Thus it is more important for Lewis base centers embedded in rings or clusters.

References

1. Alder, R. W., Strain effects on amine basicities. *Chemical Reviews* 1989, 89 (5), 1215-1223.

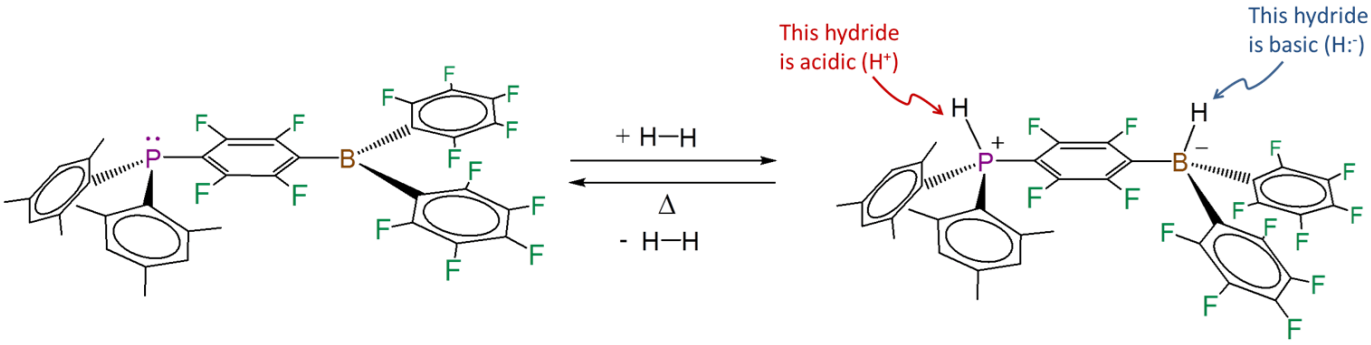
This page titled 7.2.4: Bulky groups weaken the strength of Lewis acids and bases because they introduce steric strain into the resulting acid-base adduct. is shared under a CC BY 4.0 license and was authored, remixed, and/or curated by Stephen M. Contakes.

- 6.4.7: Bulky groups weaken the strength of Lewis acids and bases because they introduce steric strain into the resulting acid-base adduct. by Stephen M. Contakes is licensed CC BY 4.0.

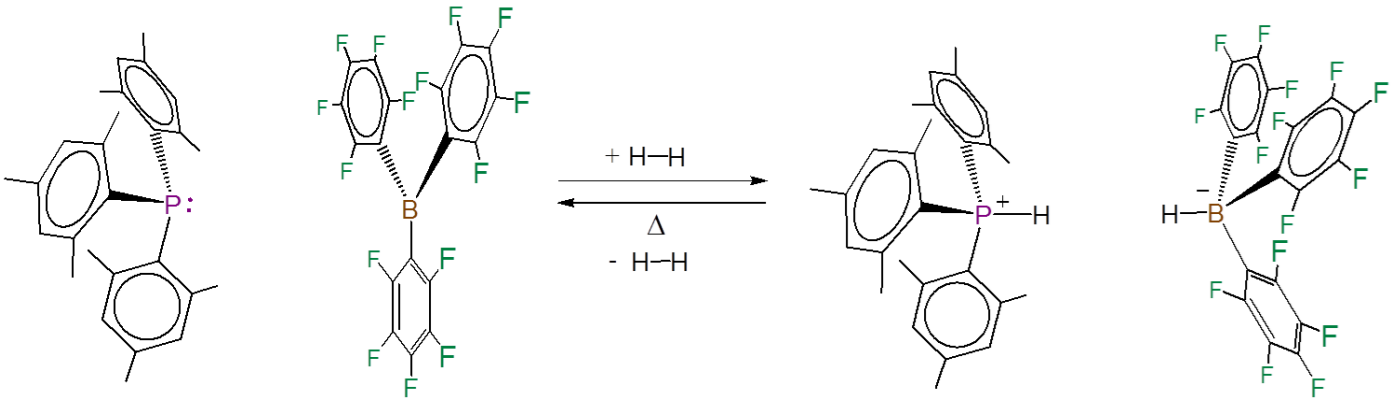
7.2.5: Frustrated Lewis pair chemistry uses Lewis acid and base sites within a molecule that are sterically restricted from forming an adduct with each other.

In certain cases when a Lewis acid-base adduct is sterically hindered from quantitatively forming an adduct (and perhaps even when they are so able), the Lewis acid and Lewis base can act together to heterolytically cleave chemical bonds. In such cases the pair of electrons that would otherwise be donated by the base is said to be a **frustrated Lewis pair (FLP)** and in performing the heterolytic cleavage the Lewis acid and base are said to exhibit **frustrated Lewis pair chemistry**.

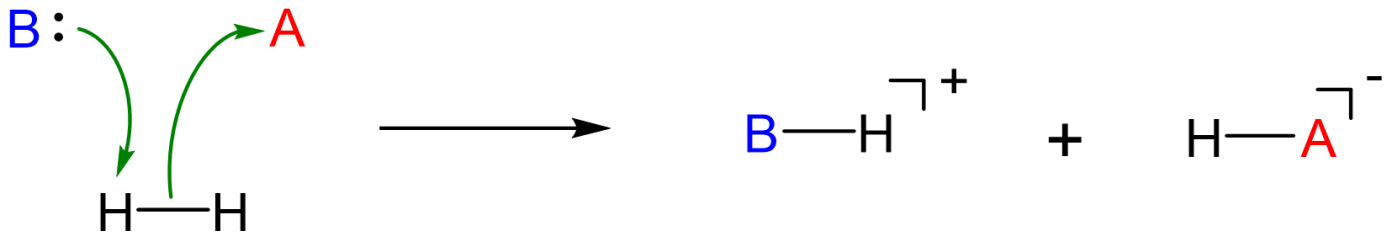
The **Stephan's phosphinoborane** illustrates how FLP chemistry works. It reversibly cleaves dihydrogen to give a zwitterionic species containing both acidic and basic element hydride bonds.



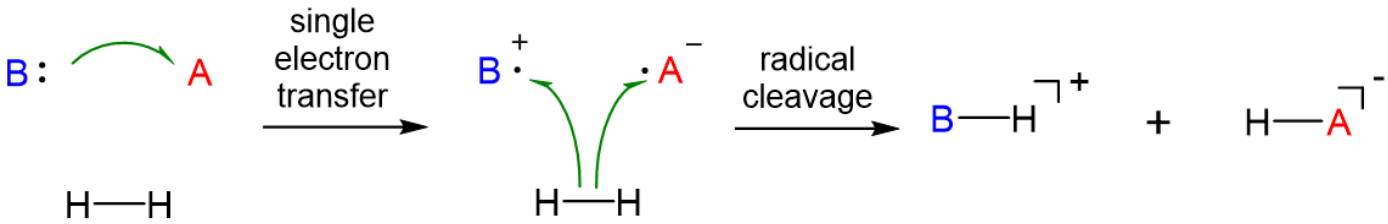
Note that the Lewis acid and base do not need to be part of the same molecule. Hydrogen is also heterolytically cleaved by mixtures of sterically encumbered triarylphosphines and triarylboranes. This time the reaction gives phosphonium and hydroborate ions:



Given the description of FLP systems as frustrated Lewis acid-base adducts, it is natural to think about the cleavage of substrates like H_2 as involving nucleophilic attack by the Lewis base while the Lewis acid acts like an electrophile in a heterolytic cleavage mechanism.



However, only some FLP systems cleave substrates through this mechanism. In others the mechanism involves homolytic cleavage by a diradical intermediate.



In either case, when substrates like H_2 are cleaved by FLPs, they are generally separated into more reactive fragments (e.g., in the case of H_2, H^+ and H^-). Because of this the substrates are said to be activated to undergo further reactions. Because FLP systems can cleave and activate substrates, there is considerable interest in the development of FLP systems that can facilitate reactions of economic or environmental interest. So far FLP systems have been developed that can catalyze various hydrogenations and activate numerous substrates, including CO, SO_2, and N_2.

References

1. Stephan, D. W., Frustrated Lewis Pairs: From Concept to Catalysis. *Accounts of Chemical Research* 2015, 48 (2), 306-316.
2. Fontaine, F.-G.; Stephan D. W., On the concept of frustrated Lewis pairs. *Philosophical Transactions of the Royal Society A: Mathematical, Physical and Engineering Sciences* 2017, 375 (2101), 20170004.
3. Jupp, A. R.; Stephan, D. W., New Directions for Frustrated Lewis Pair Chemistry. *Trends in Chemistry* 2019, 1 (1), 35-48.

This page titled 7.2.5: Frustrated Lewis pair chemistry uses Lewis acid and base sites within a molecule that are sterically restricted from forming an adduct with each other. is shared under a CC BY-NC 4.0 license and was authored, remixed, and/or curated by Stephen M. Contakes.

- 6.4.8: Frustrated Lewis pair chemistry uses Lewis acid and base sites within a molecule that are sterically restricted from forming an adduct with each other. by Stephen M. Contakes is licensed CC BY 4.0.

7.3: Hard and Soft Acids and Bases

Origin of the Hard-Soft Acid-Base Principle

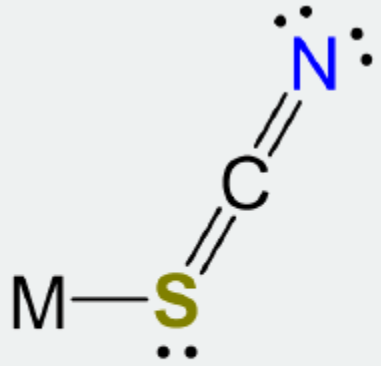
One of the strengths of the Lewis acid-base concept is the readiness with which it illuminates the role that covalent and electrostatic interactions in acid base behavior, specifically through its ability to explain chemical interactions in terms of frontier orbitals and the interactions between charged groups as electrons are donated from a base to an acid. However, simply acknowledging the presence of such interactions does little to illuminate the degree to which each mode of explanation best explains the bonding in a given system? To what extent is a given adduct better described as held together by covalent bonds as opposed to ionic ones - *e.g.* better described as a molecule rather than an ion pair? Moreover, does it even matter, given that the orbitals of quantum mechanics result from the combination of electrons' wavelike behavior with their electrostatic attraction to nuclei in either case?[1] These questions and more are addressed by one of the most important conceptual tools in contemporary inorganic chemistry, the Hard-Soft acid-base principle.

The **Hard-Soft acid-base principle (HSAB principle)** stems from the recognition that some Lewis acids and bases seem to have a natural affinity for one another.* Consider the following:

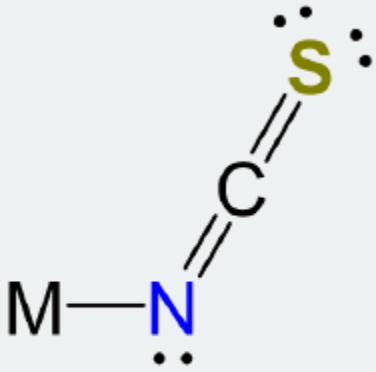
- Some metals are commonly found in nature as salts of chloride or as oxide ores while others are found in combination with sulfur. Geochemists even use the Goldschmidtt classification scheme to classify the halide and oxide formers as lithophiles and the sulfide formers as chalcophiles.
- In living systems small highly charged metals ions like Fe^{3+} are usually found bound to N and O atoms while larger metals with lower charges such as Zn^{2+} are often found attached to at least one S atom. Similarly, metals prefer to bind to one coordination site over the other when forming complexes with ambidentate ligands. The most well-known instances involve complexes of cyanate and thiocyanate, which can coordinate metals through either the N or chalcogen atom. For instance, Cu^{2+} and Zn^{2+} form *N*-thiocyanato complexes in species like $[Cu(NCS)_2(py)_2]$ and $[Zn(NCS)_4]^{2-}$ while their larger cogeners Au^{3+} and Hg^{2+} preferentially forms S-thiocyanato complexes, giving species like $[Hg(SCN)_4]^{2-}$.

Ambidentate ligands

Ambidentate ligands possess multiple coordination sites through which a metal may bind. For instance, thiocyanate may coordinate metals (M) at either the S or N to give *S*-thiocyanato or *N*-thiocyanato complexes.



S-thiocyanato



N-thiocyanato

- The solubility trends for the alklai metal halides and silver halides are opposite, even though both involve salts of formula M^+X^- (salts can be thought of as involving Lewis acid-base adduct formation between the anions and cations). Specifically,

although the silver halides are all relatively insoluble in water, the very modest solubility they possess follows the order:

$$X = F >> Cl > Br > I \text{ (for the solubility of AgX)}$$

In contrast, the much more ample solubility of the alkali metal halides** follows the opposite order. For example, the order for the lithium halides is

$$X = F << Cl < Br << I \text{ (for the solubility of LiX)}$$

Notes

1. Albeit suitably fudged through such niceties as the Aufbau principle and other approximations.

* Despite the fruitfulness of this observation, in general it is important to reduce the potential for observer bias by checking observations like these against compounds reported in the chemical literature and databases like the Inorganic Crystal Structure and Cambridge Crystallographic Databases.

** These are very soluble in water, to the point where some solutions are perhaps better described as solutions of water in the halide.

† This can be predicted based on the relative hardness of BF_3, BR_3, and BH_3 in the list of hard and soft acids. However, for those of you who may be confused as to why H is considered a better electron donor for the purposes of softening a Lewis acid center while alkyl groups are better electron donors for the purposes of stabilizing carbocations in organic chemistry, the dominant effect is the lower electronegativity of H relative to carbon (in CH_3). The effect of electron donation due to hyperconjugation isn't as great for thermodynamically stable bases like BX_3/BR_3.

This page titled 7.3: Hard and Soft Acids and Bases is shared under a CC BY 4.0 license and was authored, remixed, and/or curated by Stephen M. Contakes.

- 6.6: Hard and Soft Acids and Bases by Stephen M. Contakes is licensed CC BY 4.0.

7.3.1: Hard-Hard and Soft-Soft preferences may be explained and quantified in terms of electrostatic and covalent and electronic stabilization on the stability of Lewis acid-base adducts

The Hard Soft Acid Base Principle is a Conceptual Tool for Thinking About Patterns of Lewis Acid-Base Reactivity

The explanation of the trends in metal distribution, halide salt solubility, and preferred metal coordination patterns is rooted in Arland, Chatt, and Davies' observation that *Lewis acids and bases could be classified into two groups based on their propensity to form stable compounds with one another* (*e.g.* acids in a class tend to form more stable adducts with bases in the same class than they did with bases in the other).[1] Arland, Chatt, and Davies somewhat boringly termed these groups class a and class b but today they are known by Ralph Pearson's name for them. Pearson called the class a acids and bases hard and class b acids and bases soft. These terms reflect how "soft" these substance's electron clouds are towards distortion or, in other words, their polarizability (Figure 7.3.1.1). Pearson terms acids and bases which are relatively polarizable **soft** and those which are difficult to polarize **hard.**

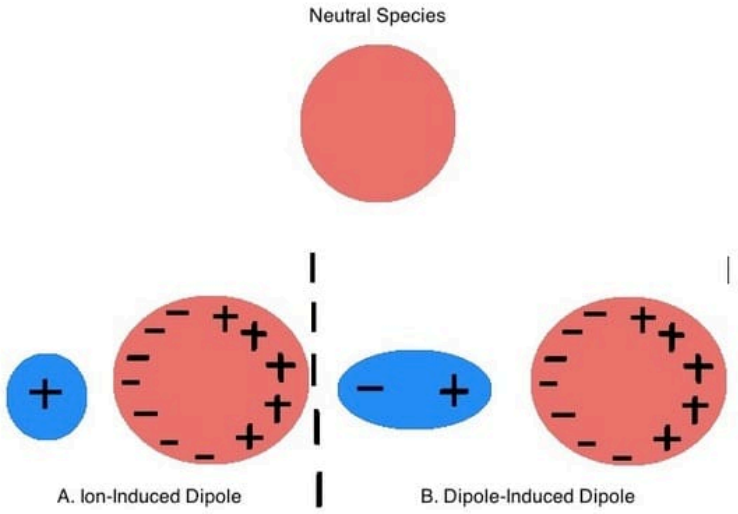


Figure 7.3.1.1: Polarizability refers to the ease with which a substance's electron cloud may be distorted under the action of an electric field. A fragment's polarizability determines the degree to which its electron cloud is distorted by A.) an Ion and B.) a polar molecule to induce a dipole moment. The figure is taken from (and the caption expanded from) Cox, Kelly and Dana Reusser "Polarizability"

Recognizing Hard and Soft Acids and Bases

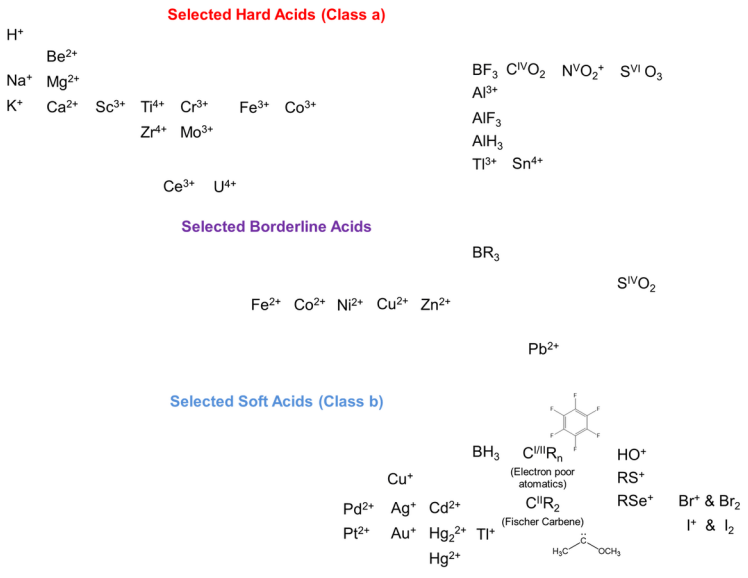
Hard acids and bases come in two varieties:

1. hard acid and base sites that possess few valence electrons and for which polarization therefore involves distorting core electrons, which are difficult to distort because they are close to the nucleus and experience a high nuclear charge. The most common examples of such substances are Lewis acid hard acids towards the left of the periodic table.
2. hard acid and base sites with a high charge density (highly charged relative to size) and/or which are electron deficient. In these cases polarization involves distorting electrons that already experience strong unshielded electrostatic interactions.

Soft acids and bases also come in two varieties

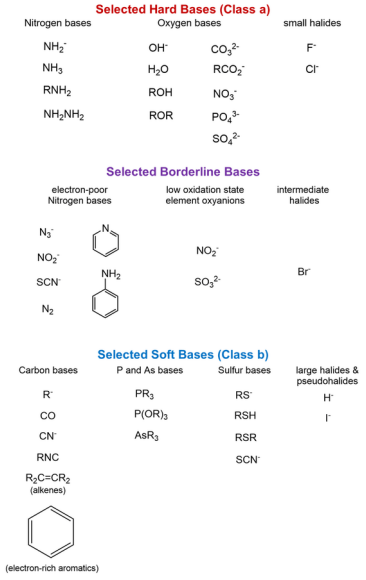
1. soft acids and bases which posses many valence electrons and so are more readily polarized. In consequence, all other things being equal, soft acids and bases are more likely to be found towards the middle or right of the periodic table.
2. soft acids and bases with little charge density and/or which are relatively electron rich.

Note that the hard-soft classification should not be thought of as if all hard acids and bases are equally hard and all soft acids and bases equally soft. There is a graduation in hardness and softness and a number of intermediate acids and bases which do not fit neatly in either category. With this caveat in mind, representative **hard, soft, and borderline acids** are given below. Notice how they illustrate the trends just outlined.



As expected, hard acids tend to be found towards the left side of the periodic table and involve higher oxidation states and/or electron donating substituents while soft acids are more common to the right of the periodic table and involve lower oxidation states and/or electron donating substituents.

Illustrative hard, soft, and borderline bases are given below. Again, notice how these substances illustrate the general trends.



Qualitative Estimation of the Relative Hardness and Softness of Lewis Acids and Bases

As can be seen from the examples above, **hard acids are relatively electron-poor and hard bases electron-rich** since they have comparatively

- small frontier orbitals, reflective of their relatively small atom/ion/fragment sizes
- high (for acids) or low (for bases) oxidation states on the base atom, reflected in a large positive formal charge (for acids) or negative formal charge (for bases)
- low polarizability, due to loss or gain of substantial numbers of electrons, or the localization of
  - positive charge on an electropositive element or an atom bearing electron-withdrawing substituents
  - negative charge on an electronegative element or an atom bearing electron-donating substituents

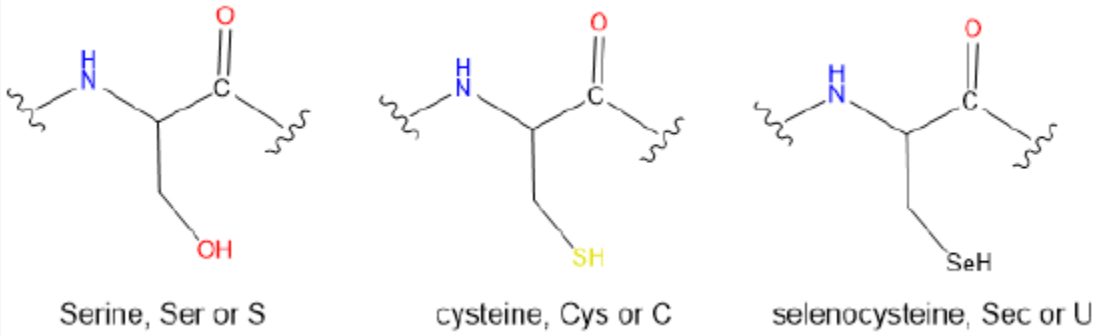
In contrast to hard acids and bases, **soft acids are relatively electron-rich and soft bases larger and more electron poor** since they have comparatively

- large frontier orbitals, reflective of their relatively large atom/ion/fragment sizes
- low oxidation states, often resulting in small or nonexistent atomic charges
- high polarizability, as might be expected of species in which electron-electron repulsions are lower and electrons are spread over a large volume. Sometimes this is indicated by
  - positive charge on an electronegative element or an atom bearing electron-donating substituents
  - negative charge on an electropositive element or an atom bearing electron-withdrawing substituents

Exercise 7.3.1.1

Rank the acids or bases in each set in increasing order of expected hardness.

a. Cr^{2+} and Cr^{3+}
b. H^+, Cs^+, and Tl^+
c. SCN^- (acting as a base at N) and SCN^- (acting as a base at S)
d. AlF_3, AlH_3, $AlMe_3$
e. The side chains of the following proteinogenic amino acids



Answer available at the end of this section.

The Hard-Soft Acid-Base Principle (HSAB Principle)

The **Hard-Soft acid-base principle (HSAB Principle) explains patterns in Lewis acid-base reactivity in terms of a *like reacts with like preference***. Both thermodynamically and kinetically, hard acids prefer hard bases and soft acids soft bases. Specifically,

- Thermodynamically, hard acids form stronger acid-base complexes with hard bases while soft acids form stronger complexes

with soft bases.
- Kinetically, hard acids/electrophiles react more quickly with hard bases/nucleophiles while soft acids/electrophiles react more quickly with soft bases/neucleophiles.

Applications of the HSAB principle include

1. Predicting the equilibrium or speed of *Lewis acid-base metathesis and displacement reactions*. In a Lewis acid-base **metathesis reaction** the acids and bases swap partners

$$\mathrm{A_1 : B_1 + A_2 : B_2 \overset{k_1,\ K_{eq}}{\rightleftharpoons} A_1 : B_2 + A_2 : B_1}$$

For example, the equilibrium position of the metathesis reaction between TlF and $\mathrm{K_2S}$ favors the products:

$$\mathrm{2\,TlF + H_2S \rightleftharpoons Tl_2S + 2\,KF}$$

consistent with the HSAB's hard-hard and soft-soft preference.



The HSAB principle also allows for prediction of the position of displacement reactions, in which a Lewis acid or base forms an adduct using a base or acid from an existing Lewis acid-base complex. In these reactions, the displacement of acid or base from the reactant complex may be thought of as a sort of metathesis reaction, one in which in the unbound acid or base switches places with one in the complex. For example, the reaction between HI and methylmercury cation

$$\mathrm{HI + HgSCH_3^+ \rightleftharpoons CH_3SHgI + H^+}$$

involves displacement of an iodide from HI to give $\mathrm{CH_3HgI}$. The position of the equilibrium favors $\mathrm{CH_3HgI}$ since both $\mathrm{CH_3Hg^+}$ and $\mathrm{I^-}$ are soft, while $\mathrm{H^+}$ is a hard acid.



Exercise 7.3.1.2

Predict the position of equilibrium for the following reaction.

$$\mathrm{Fe_2O_3 + 3\,Ag_2S \rightleftharpoons Fe_2S_3 + 3\,Ag_2O}$$

Answer available at the end of this section.

Exercise 7.3.1.3

Predict whether K for the following equilibria will be <<1, ~1, or >>1.

a. $\mathrm{2\,HF + (CH_3Hg)_2S \rightleftharpoons 2\,CH_3HgF + H_2S}$
b. $\mathrm{Ag(NH_3)_2^+ + 2\,PH_3 \rightleftharpoons Ag(PH_3)_2^+ + 2\,NH_3}$

c. $Ag(PH_3)_2^+ + 2\,H_3B{-}SH_2 \rightleftharpoons 2\,H_3B{-}PH_3 + Ag(SH_2)_2^+$
d. $H_3B{-}NH_3 + F_3B{-}SH_2 \rightleftharpoons H_3B{-}SH_2 + F_3B{-}NH_3$

Answer available at the end of this section.

2. Predicting the relative strengths of a given set of *Lewis acids or bases towards a particular substrate*. Consider, for example, the relative strengths of a BH_3, BMe_3, and BF_3 towards group 15 hydrides like NH_3, PH_3, and AsH_3. Of the boranes listed, the hardest acid BF_3 is the strongest acid towards the hard base NH_3 while BH_3 is the strongest towards AsH_3.[†]

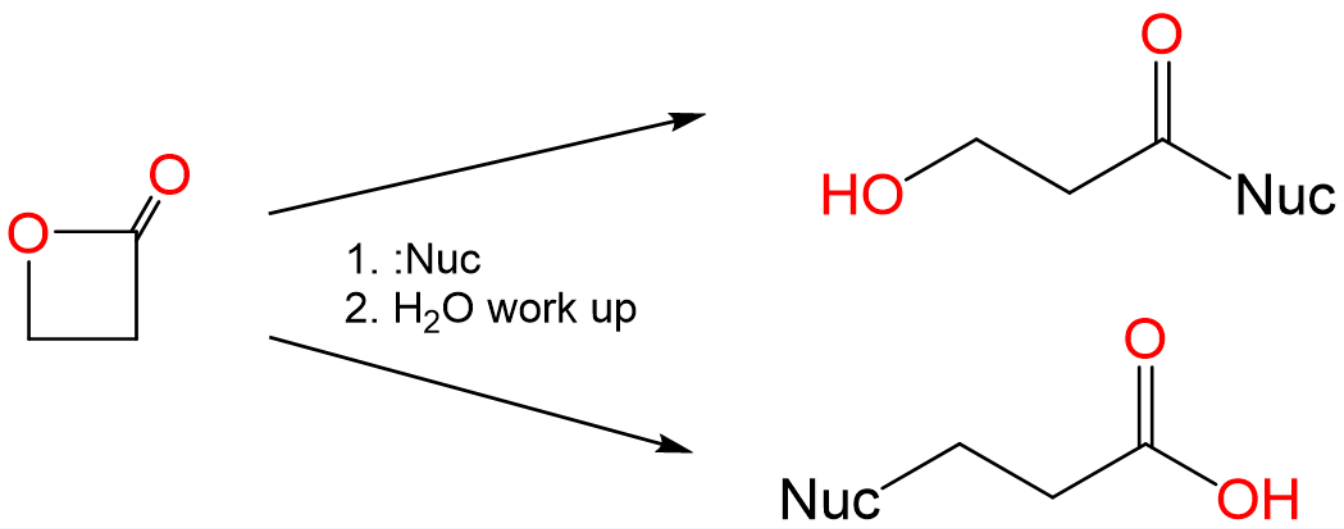
Exercise 7.3.1.4

Which acid will form the most stable complex with CO: BH_3, BF_3, or BMe_3?

Answer available at the end of this section.

Exercise 7.3.1.5

When lactones react with nucleophiles, they can undergo ring opening reactions to give either an alcohol or a carboxylic acid, as shown for propiolactone below:



In the reaction above, sterically unhindered alkoxides give one product and sterically unhindered thioalkoxides the other. Explain why this is the case and predict the products of the reaction between propiolactone and the sodium salts of ethoxide and thioethoxide.

Answer available at the end of this section.

The theoretical interpretation of the hard-soft acid-base principle is that hard-hard preferences reflect superior electrostatic stabilization while soft-soft preferences reflect superior covalent stabilization.

The hard-hard and soft-soft preferences in Lewis acid-base interactions reflect that

- The lone pair of a hard base is strongly stabilized electrostatically by a hard acid.
- The lone pair of a soft base is strongly stabilized by forming a covalent bond with a soft acid.

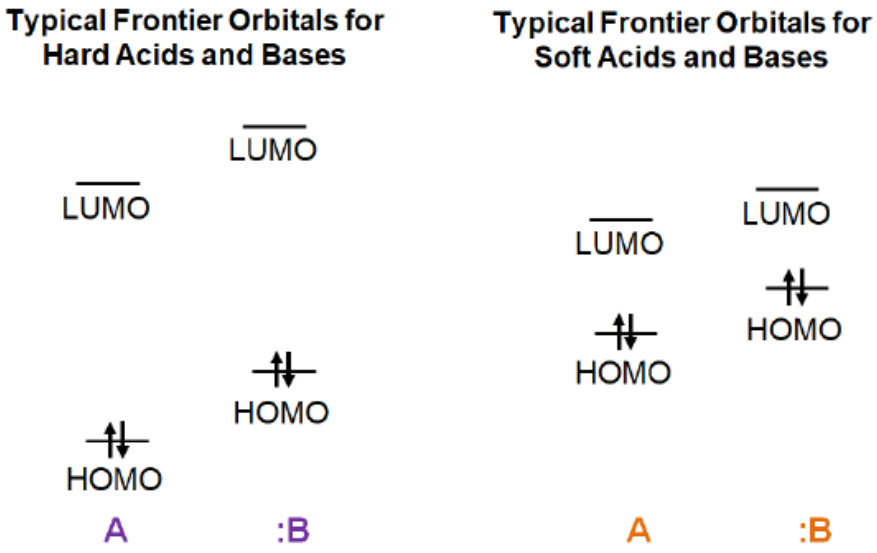
- The lone pair of a hard or soft base is comparatively weakly stabilized by an acid opposite to it in hardness or softness since the overall electrostatic and covalent stabilization of the adduct is comparatively weak.

To see why this is the case it is helpful to divide the contributions to the interaction energy between an acid and a base as follows:

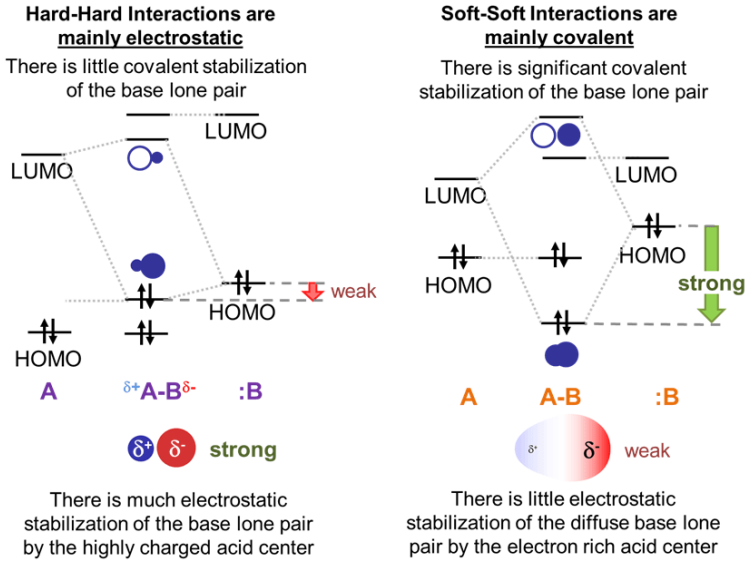
Interaction Energy = Electrostatic attractions and repulsions of partial atomic charges (Ionic term) + Interactions between filled orbitals on one fragment and unfilled orbitals on the other (Covalent term) + Electrostatic repulsions between filled orbitals on the two fragments (Steric term)

Of the three contributions to the interaction energy, only the ionic and covalent terms directly relate to the hardness of the interacting acid and base. One approach to thinking about how hardness influences the ionic and covalent contributions is to consider the frontier orbitals involved in the acid-base interaction. This is sometimes done through the use of the Salem-Klopman equation,[1,*] although in the treatment which follows a more qualitative approach will be employed.

Both hard acids and bases will have comparatively low energy HOMO levels and high energy LUMO levels, with a correspondingly high HOMO-LUMO gap. In contrast, soft acids and bases will have comparatively high-energy HOMO levels and low-energy LUMO levels, giving a comparatively smaller HOMO-LUMO gap.



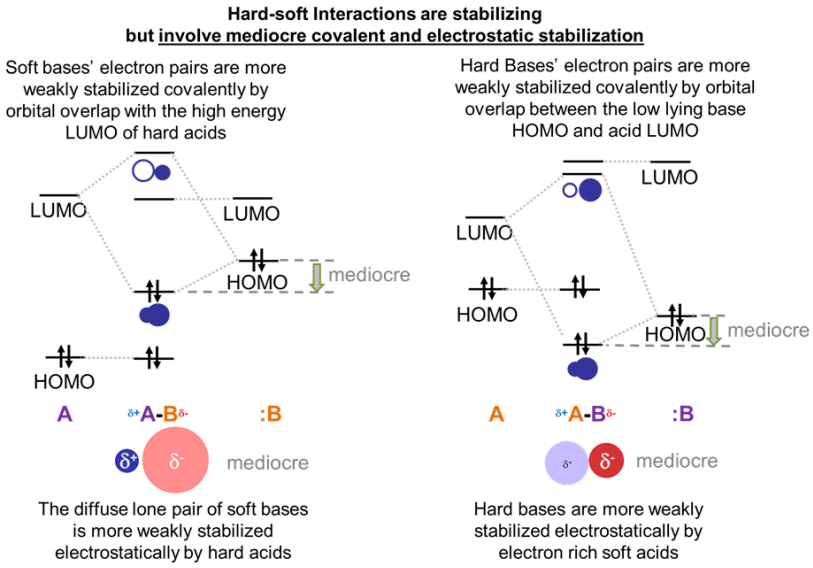
Given this, consider the frontier orbital interactions involved in the formation of an acid-base complex for the possible cases, as illustrated schematically below.



The large gap in energy between hard bases' highly stabilized HOMO lone pairs and the high energy LUMO of hard acids ensures that in **hard acid-hard base adducts the dominant stabilizing interaction will involve electrostatic attraction between the base lone pair and the electropositive Lewis acid center**. Fortunately, since the electron clouds in hard bases are relatively dense and electron rich while hard Lewis acids are highly charged and small, these electrostatic interactions are strong.

In contrast, in **soft acid-soft base adducts, the dominant stabilizing interaction will be covalent.** This is because the small gap in energy between a soft base HOMO and soft acid LUMO enables the formation of a well-stabilized bonding orbital with significant electron density between the acid and base.

The orbitals' interactions between hard acids and soft bases and soft acids and hard bases are intermediate between the hard acid-hard base and soft acid-soft base cases.



This means that the adducts are stable relative to free acid and base – just not as well stabilized as in the hard acid and hard base case. In the case of hard acids and soft bases the hard acids are less able to stabilize the soft bases' relatively diffuse electron pair electrostatically and there isn't as much covalent stabilization as in adducts of soft acids and bases due to the hard acid's high energy.

References

1. Ahrland, S.; Chatt, J.; Davies, N. R., The relative affinities of ligand atoms for acceptor molecules and ions. Quarterly Reviews, Chemical Society 1958, 12 (3), 265-276.

2. Pearson, R. G., Hard and Soft Acids and Bases. Journal of the American Chemical Society 1963, 85 (22), 3533-3539.

3. Fleming, I., Molecular orbitals and organic chemical reactions. Reference ed.; Wiley: Hoboken, N.J., 2010.

Notes

* Despite the fruitfulness of this observation, in general it is important to reduce the potential for observer bias by checking observations like these against compounds reported in the chemical literature and databases like the Inorganic Crystal Structure and Cambridge Crystallographic Databases.

** These are very soluble in water, to the point where some solutions are perhaps better described as solutions of water in the halide.

† This can be predicted based on the relative hardness of BF_3, BR_3, and BH_3 in the list of hard and soft acids. However, for those of you who may be confused as to why H is considered a better electron donor for the purposes of softening a Lewis acid center while alkyl groups are better electron donors for the purposes of stabilizing carbocations in organic chemistry, the dominant effect is the lower electronegativity of H relative to carbon (in CH_3). The effect of electron donation due to hyperconjugation isn't as great for thermodynamically stable bases like BX_3/BR_3.

†† For more on the Salem-Klopman equation see Fleming, I., Molecular orbitals and organic chemical reactions. Reference ed.; Wiley: Hoboken, N.J., 2010; pp. 138-143.

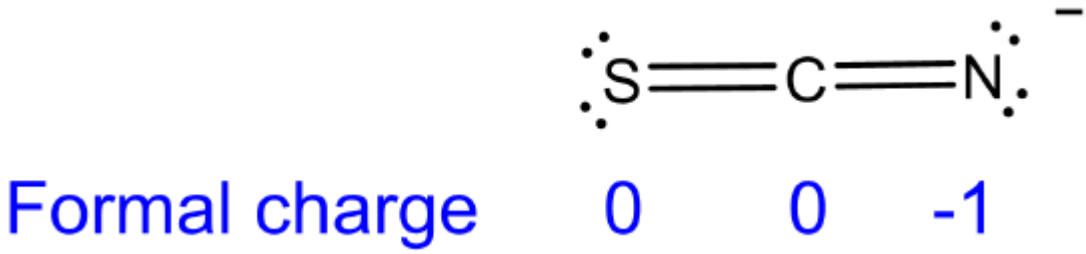
Answers

Exercise 7.3.1.1

(a) $Cr^{2+} < Cr^{3+}$ All other things being equal, hardness increases with oxidation state.

(b) $Tl^+ < Cs^+ < H^+$ The order reflects Cs^+ and Tl^+'s larger size relative to H^+ (which doesn't possess any electrons that can be polarized anyway) and that Tl^+ still possesses two valence electrons while Cs^+ possesses none.

(c) SCN^- (acting as a base at S) < SCN^- (acting as a base at N). The order reflects the greater electronegativity of N than S and N's possession of a more negative formal charge of -1.



(d) $AlH_3 < AlMe_3 < AlF_3$. The hardness increases as the substituents on the Lewis acid Al center become less electron donating and more electron withdrawing (and, incidentally, harder bases) as their electronegativity increases in the order $H^- < CH_3^- < F^-$. Note that the order of electron donating ability for H^- and CH_3^- is the opposite observed for carbocations, for which hyperconjugation plays a larger role.

(e) Sec < Cys < Ser. The hardness increases as the electronegativity of the Lewis base chalcogen increases on going from a selenol to a thiol to an alcohol.

Exercise 7.3.1.2

The equilibrium will favor the reactants (K<1) since the hard-hard and soft-soft interactions in the reactants are more stable than the hard-soft interactions in the products.



Exercise 7.3.1.3

a. K< < 1 since the reactant adducts are hard-hard and soft-soft while the products involve hard-soft interactions.

b. K>>1 since the reactant complex, diamine silver(I), is a complex of a hard base, NH_3, with the soft acid, Ag^+, while the product is a complex of the same soft acid with the soft base phosphine.

c. K~1 since all the adducts amongst the reactants and products involve soft acids and bases.

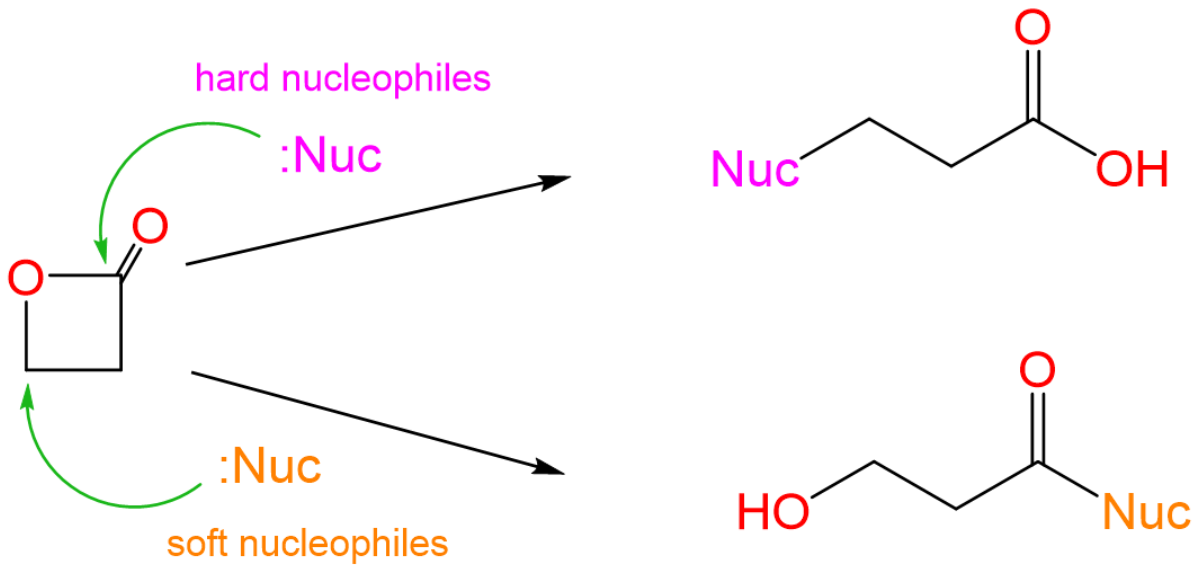
d. K>>1 since BH_3 is a softer acid than BF_3, so it will form a stronger complex with the softer base H_2S while the harder BF_3 forms a stronger complex with the harder base NH_3.

Exercise 7.3.1.4

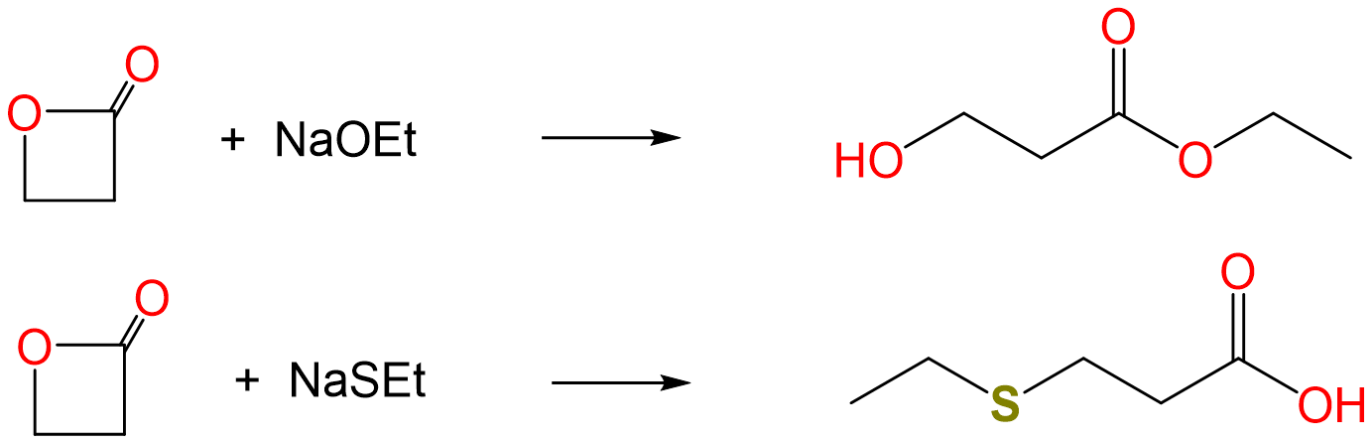
BH_3. Since CO forms complexes primarily through its carbon lone pair, it is a soft base and so will form the strongest complex with the softest Lewis acid.

Exercise 7.3.1.5

The two reaction products correspond to nucleophilic attack at the lactones' two electrophilic carbon centers. Specifically, the acid is produced by attack at the softer C^I center of the CH_2 directly attached to the ester oxygen and the alcohol by nucleophilic attack at the harder C^{III} center of the ester carbonyl.



Consequently, it is reasonable to expect that the harder base ethoxide will nucleophilically attack the harder carbonyl carbon while the softer thioethoxide will attack the softer methylene carbon.



This page titled 7.3.1: Hard-Hard and Soft-Soft preferences may be explained and quantified in terms of electrostatic and covalent and electronic stabilization on the stability of Lewis acid-base adducts is shared under a CC BY-NC 4.0 license and was authored, remixed, and/or curated by Stephen M. Contakes.

- 6.6.2: Hard-Hard and Soft-Soft preferences may be explained and quantified in terms of electrostatic and covalent and electronic stabilization on the stability of Lewis acid-base adducts by Stephen M. Contakes is licensed CC BY 4.0.

8: ORGANOMETALLIC CHEMISTRY (EVANS)

Organometallic (OM) chemistry is the study of compounds containing, and reactions involving, metal-carbon bonds. The metal-carbon bond may be transient or temporary, but if one exists during a reaction or in a compound of interest, we're squarely in the domain of organometallic chemistry. Despite the denotational importance of the M-C bond, bonds between metals and the other common elements of organic chemistry also appear in OM chemistry: metal-nitrogen, metal-oxygen, metal-halogen, and even metal-hydrogen bonds all play a role. Metals cover a vast swath of the periodic table and include the alkali metals (group 1), alkali earth metals (group 2), transition metals (groups 3-12), the main group metals (groups 13-15, "under the stairs"), and the lanthanides and actinides. We will focus most prominently on the behavior of the transition metals, so called because they cover the transition between the electropositive group 2 elements and the more electron-rich main group elements.

8.1: Introduction to Organometallic Chemistry

8.1.1: Resources for Organometallic Chemistry

8.1.2: What is Organometallic Chemistry?

8.2: Organometallic Ligands

8.2.1: Carbenes

8.2.2: Carbon Monoxide

8.2.3: σ Complexes

8.2.4: Dative Ligands of N, O, and S

8.2.5: Metal Alkyls

8.2.6: Metal Hydrides

8.2.7: N-heterocyclic Carbenes

8.2.8: Odd-numbered π Systems

8.2.9: Phosphines

8.2.10: π Systems

8.3: Structural Fundamentals

8.3.1: Ligand Field Theory and Frontier Molecular Orbital Theory

8.3.2: Open Coordination Site

8.3.3: Periodic Trends of the Transition Metals

8.3.4: Predicting the Geometry of Organometallic Complexes

8.3.5: Simplifying the Organometallic Complex (Part 1)

8.3.6: Simplifying the Organometallic Complex (Part 2)

8.3.7: Simplifying the Organometallic Complex (Part 3)

8.4: Fundamentals of Organometallic Chemistry

8.4.1: β-Elimination Reactions

8.4.2: Associative Ligand Substitution

8.4.3: Dissociative Ligand Substitution Reactions

8.4.4: Ligand substitution

8.4.5: Migratory Insertion- 1,2-Insertions

8.4.6: Migratory Insertion- Introduction and CO Insertions

8.4.7: Oxidative Addition- General Ideas

8.4.8: Oxidative Addition of Non-polar Reagents
8.4.9: Oxidative Addition of Polar Reagents
8.4.10: Quirky Ligand Substitutions
8.4.11: Reductive Elimination- General Ideas
8.4.12: The trans/cis Effects and Influences
8.5: Parallels between Main Group and Organometallic Chemistry
8.5.1: Parallels between Main Group and Binary Carbonyl Complexes
8.5.2: The Isolobal Analogy
8.5.2.1: Extensions of the Analogy
8.5.2.2: Some Applications of the Isolobal Analogy
8.5.3: Metal-Metal Bonds
8.5.3.1: Metal-Metal Multiple Bonds
8.5.4: Cluster Compounds
8.5.4.1: Boranes
8.5.4.2: Heteroboranes
8.5.4.3: Metallaboranes and Metallacarboranes
8.5.4.4: Carbonyl Clusters
8.5.4.5: Carbon-Centered Clusters
8.5.4.6: Additional Comments on Clusters
8.5.5: Problems

This page titled 8: Organometallic Chemistry (Evans) is shared under a CC BY-NC-SA 4.0 license and was authored, remixed, and/or curated by Michael Evans.

- Organometallic Chemistry (Evans) by Michael Evans is licensed CC BY-NC-SA 4.0.

8.1: INTRODUCTION TO ORGANOMETALLIC CHEMISTRY

8.1.1: Resources for Organometallic Chemistry

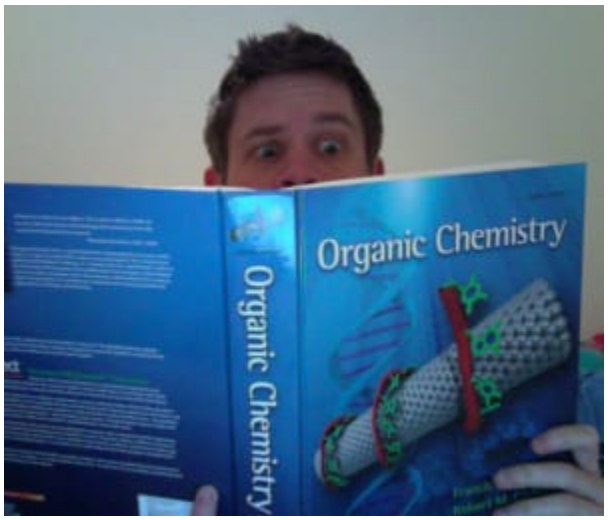
8.1.2: What is Organometallic Chemistry?

This page titled 8.1: Introduction to Organometallic Chemistry is shared under a CC BY-NC-SA 4.0 license and was authored, remixed, and/or curated by Michael Evans.

- 1: Introduction to Organometallic Chemistry by Michael Evans is licensed CC BY-NC-SA 4.0.

8.1.1: Resources for Organometallic Chemistry

Let's face it: organometallic chemistry is a somewhat esoteric subject. Unfortunately, this fact makes it difficult to find cheap, current textbooks on the subject, but there are a few used gems for sale on the Internet. Crabtree's Organometallic Chemistry of the Transition Metals is a short but solid book that's a good jumping-off point for deeper studies. Spessard and Miessler's Organometallic Chemistry is a longer but still informative classic. Hartwig's "biblical" Organotransition Metal Chemistry is a nice reference work, but I wouldn't start off with this back-breaking tome. If you do, skip around and avoid the vast sections of text describing "what's known" with little explanation.



What resources are available for the interested organometallics student?

For the penny-pinching student or layman, there are several good resources for organometallic chemistry on the Web. Nothing as exhaustive as Reusch's Virtual Textbook of Organic Chemistry exists for organometallic chemistry, but the base of resources available on the Web is growing. Rob Toreki's Organometallic HyperTextBook could use a CSS refresh, but contains some nice introductions to different organometallic concepts and reactions. Try the electron-counting quiz!

VIPER is a collection of electronic resources for teaching and learning inorganic chemistry, and includes a nice section on organometallic chemistry featuring laboratory assignments, lecture notes, and classroom activities. Awesome public lecture notes are available from Budzelaar at the University of Manitoba and Shaughnessy at Alabama (Roll Tide?). For practice problems, check out Fu's OpenCourseWare material from MIT and Shaughnessy's problem sets.

This page titled 8.1.1: Resources for Organometallic Chemistry is shared under a CC BY-NC-SA 4.0 license and was authored, remixed, and/or curated by Michael Evans.

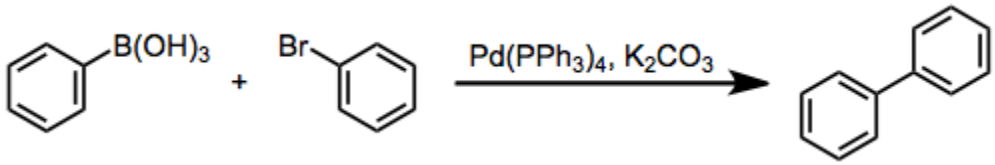
- 1.1: Resources for Organometallic Chemistry by Michael Evans is licensed CC BY-NC-SA 4.0.

8.1.2: What is Organometallic Chemistry?

Let's begin with a few simple questions: what is organometallic chemistry? What, after studying organometallic chemistry, will we know about the world that we didn't know before? Why is the subject worth studying? And what kinds of problems is the subject meant to address? The purpose of this post is to give the best answers I currently know of to these questions. The goal of this otherwise content-free post is twofold: (1) to help motivate us as we move forward (that is, to constantly remind us that there is a point to all this!); and (2) to illustrate the kinds of problems we'll be able to address using concepts from the field. You might be surprised by the spine-chilling power you feel after learning about the behavior of organometallic compounds and reactions!

Put most bluntly, organometallic (OM) chemistry is the study of compounds containing, and reactions involving, metal-carbon bonds. The metal-carbon bond may be transient or temporary, but if one exists during a reaction or in a compound of interest, we're squarely in the domain of organometallic chemistry. Despite the denotational importance of the M-C bond, bonds between metals and the other common elements of organic chemistry also appear in OM chemistry: metal-nitrogen, metal-oxygen, metal-halogen, and even metal-hydrogen bonds all play a role. Metals cover a vast swath of the periodic table and include the alkali metals (group 1), alkali earth metals (group 2), transition metals (groups 3-12), the main group metals (groups 13-15, "under the stairs"), and the lanthanides and actinides. We will focus most prominently on the behavior of the transition metals, so called because they cover the transition between the electropositive group 2 elements and the more electron-rich main group elements.

Why is the subject worth studying? Well, for me, it mostly comes down to synthetic flexibility. There's a reason the "organo" comes first in "organometallic chemistry"—our goal is usually the creation of new bonds in organic compounds. The metals tend to just be along for the ride (although their influence, obviously, is essential). And the fact is that you can do things with organometallic chemistry that you cannot do using straight-up organic chemistry. Case in point:



The venerable Suzuki reaction...unthinkable without palladium!

The establishment of the bond between the phenyl rings through a means other than dumb luck seems unthinkable to the organic chemist, but it's natural for the palladium-equipped metal-organicker. Bromobenzene looks like a potential electrophile at the bromine-bearing carbon, and if you're familiar with hydroboration you might see phenylboronic acid as a potential nucleophile at the boron-bearing carbon. Catalytic palladium makes it all happen! Organometallic chemistry is full of these mind-bending transformations, and can expand the synthetic toolbox of the organic chemist considerably.

To throw another motive into the mix for the non-specialist (or the synthesis-spurning chemist), organometallic chemistry is full of intriguing stories of scientific inquiry and discovery. Exploring how researchers take a new organometallic reaction from "ooh pretty" to strong predictive power is instructive for anyone interested in "how science works," in a practical sense. We'll examine a number of classical experiments in organometallic chemistry, both for their value to the field and their contributions to the general nature of scientific inquiry.

What kinds of problems should we be able to address as we move forward? Here's a bulleted list of the most commonly encountered types of problems in an organometallic chemistry course:

- Describe the structure of an organometallic complex...
- Predict the product of the given reaction conditions...
- Draw a reasonable mechanism based on evidence...
- Devise a synthetic route to synthesize a target organometallic compound...
- Explain the observation(s)...
- Predict the results of a series of experiments...

The first four are pretty standard organic-esque problems, but it's the last two, more general classes that really make organometallic chemistry compelling. Just imagine putting yourself in the shoes of the pioneers and making the same predictions

they did!

There you have it, a short introduction to organometallic chemistry and why it's worth studying. Of course, we'll use the remainder of space in the blog to fully describe what organometallic chemistry really is...but it's helpful to keep these motives in mind as you study. Keep a thirst for predictive power, and it's hard to go wrong with organometallic chemistry!

This page titled 8.1.2: What is Organometallic Chemistry? is shared under a CC BY-NC-SA 4.0 license and was authored, remixed, and/or curated by Michael Evans.

- 1.2: What is Organometallic Chemistry? by Michael Evans is licensed CC BY-NC-SA 4.0.

8.2: ORGANOMETALLIC LIGANDS

8.2.1: Carbenes

8.2.2: Carbon Monoxide

8.2.3: σ Complexes

8.2.4: Dative Ligands of N, O, and S

8.2.5: Metal Alkyls

8.2.6: Metal Hydrides

8.2.7: N-heterocyclic Carbenes

8.2.8: Odd-numbered π Systems

8.2.9: Phosphines

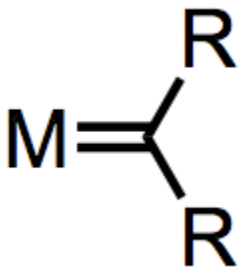
8.2.10: π Systems

This page titled 8.2: Organometallic Ligands is shared under a CC BY-NC-SA 4.0 license and was authored, remixed, and/or curated by Michael Evans.

- 2: Organometallic Ligands by Michael Evans is licensed CC BY-NC-SA 4.0.

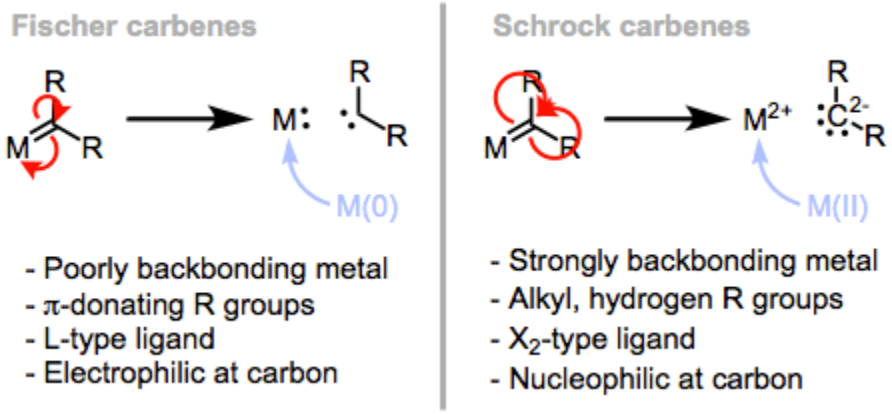
8.2.1: Carbenes

In a previous post, we were introduced to the N-heterocyclic carbenes, a special class of carbene best envisioned as an L-type ligand. In this post, we'll investigate other classes of carbenes, which are all characterized by a metal-carbon double bond. Fischer carbenes, Shrock carbenes, and vinylidenes are usually actor ligands, but they may be either nucleophilic or electrophilic, depending on the nature of the R groups and metal. In addition, these ligands present some interesting synthetic problems: because free carbenes are quite unstable, ligand substitution does not cut the mustard for metal carbene synthesis.



General Properties

Metal carbenes all possess a metal-carbon double bond. That's kind of a given. What's interesting for us about this double bond is that there are multiple ways to deconstruct it to determine the metal's oxidation state and number of d electrons. We could give one pair of electrons to the metal center and one to the ligand, as we did for the NHCs. This procedure nicely illustrates why compounds containing M=C bonds are called "metal carbenoids"—the deconstructed ligand is an L-type carbenoid. Alternatively, we could give both pairs of electrons to the ligand and think of it as an X2-type ligand. The appropriate procedure depends on the ligand's substituents and the electronic nature of the metal. The figure below summarizes the two deconstruction procedures.

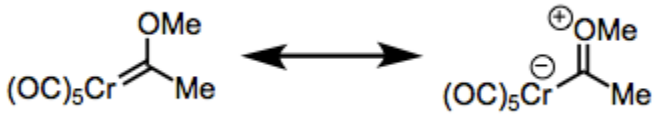


The proper method of deconstruction depends on the electronic nature of the ligand and metal.

When the metal possesses π-acidic ligands and the R groups are π-basic, the complex is best described as an L-type Fischer carbene and the oxidation state of the metal is unaffected by the carbene ligand. When the ligands are "neutral" (R = H, alkyl) and the metal is a good backbonder—that is, in the absence of π-acidic ligands and electronegative late metals—the complex is best described as an X2-type Schrock carbene. Notice that the oxidation state of the metal depends on our deconstruction method! Thus, we see that even the oxidation state formalism isn't perfect.

Deconstruction reveals the typical behavior of the methylene carbon in each class of complex. The methylene carbon of Schrock carbenes, on which electron density is piled through backbonding, is nucleophilic (the 2– charge screams nucleophilic!). On the other hand, the methylene carbon of Fischer carbons is electrophilic, because backbonding is weak and does not compensate for σ-donation from the ligand to the metal. To spot a Fischer carbene, be on the lookout for reasonable zwitterionic resonance

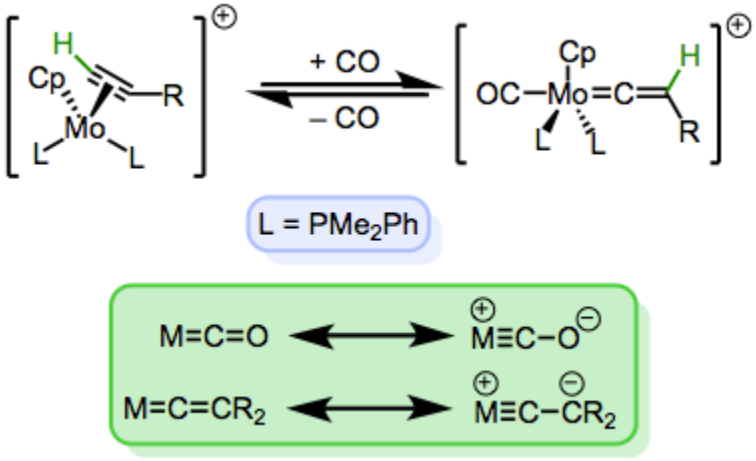
structures like the one at right below.



Thanks to the pi-accepting CO ligands, the metal handles the negative charge well. This is a Fischer carbene.

The clever reader may notice that we haven't mentioned π-acidic R groups, such as carbonyls. Complexes of this type are best described as Fischer carbenes as well, as the ligand is still electrophilic. However, complexes of this type are difficult to handle and crazy reactive (see below) without a π-basic substituent to hold them in check.

Vinylidenes are the organometallic analogues of allenes, and are best described as intermediate in behavior between Fischer and Schrock carbenes. They are electrophilic at the α carbon and nucleophilic at the β carbon—in fact, a nice analogy can be made between vinylidenes and carbon monoxide. Tautomerization to form alkyne π-complexes is common, as the vinylidene and alkyne complexes are often comparable in stability.



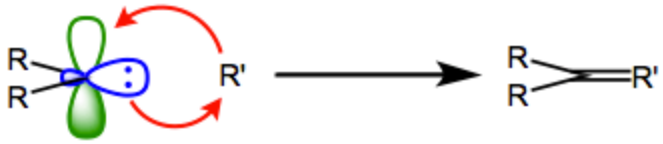
Vinylidene tautomerization, and an analogy between vinylidenes and CO.

Take care when diagnosing the behavior of metal carbenes. In these complexes, there is often a subtle interplay between the R groups on the carbene and other ligands on the metal. In practice, many carbenes are intermediate between the Fischer and Schrock ideals.

Synthesis

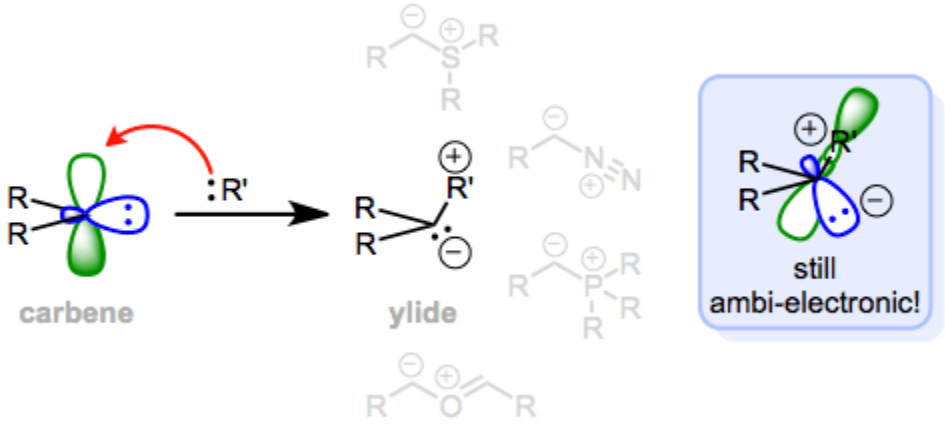
Metal carbenes present a fascinating synthetic problem. A cursory look at the deconstruction procedures above reveals that these complexes cannot be made using ligand substitution reactions, because the free ligands are far too unstable. Although the synthetic methods introduced here will be new for us, the attuned organic chemist will find them familiar. The conceptual foundations of metal carbene synthesis are similar to methods for the synthesis of alkenes in organic chemistry.

In the post on NHCs, we saw that the free carbene is both nucleophilic (via the lone pair in its σ system) and electrophilic (via its empty 2pz orbital). Organic precursors to metal carbenes and alkenes also possess this property—they can act both as nucleophiles and electrophiles. Fundamentally, this "ambi-electronic" behavior is useful for the creation of double bonds. One bond comes from "forward flow," and the other from "reverse flow." Naturally, the other reacting partner also needs to be ambi-electronic for this method to work.



A fundamental paradigm for double bond synthesis: ambi-electronic compounds doing what they do.

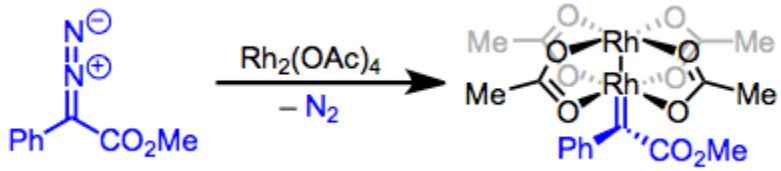
What sets carbene precursors apart from free carbenes? What other kinds of molecules may act as both nucleophiles and electrophiles at the same atom? Watch what happens when we tack a third group onto the free carbene...the figure below shows the result in general and a few specific examples in gray.



A "dative ligand" R' is the difference between a carbene and an ylide. Both are ambi-electronic.

An ylide, which contains adjacent positive and negative charges, results from this purely hypothetical process. Ylides (diazo compounds, specifically) are the most common precursors to metal carbene complexes. Like free carbenes, ylides are ambi-electronic. The electrophilic frontier orbital of an ylide is just the σ* orbital of the bond connecting the charged atoms, which makes sense if we consider the positively charged fragment as a good leaving group (it always is). The lone pair is still nucleophilic. The figure above depicts some of the most famous ylides of organic chemistry, including those used for alkene synthesis (Corey-Chaykovsky and Wittig) and cycloaddition reactions (the carbonyl ylide).

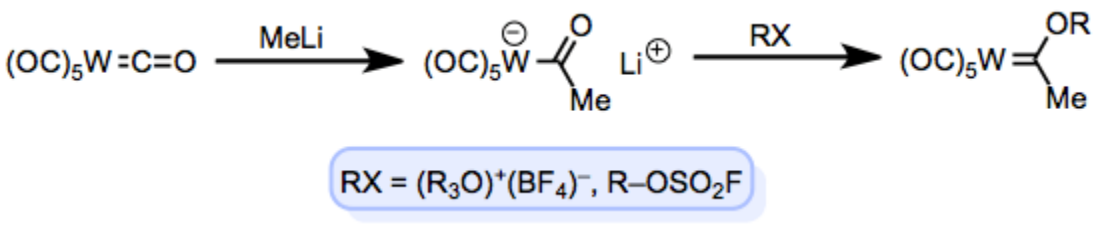
Although diazo compounds are most commonly drawn with charges on the two nitrogen atoms, the diazo carbon is a good nucleophile and can attack electrophilic metal centers to initiate metal carbene formation. A slick 15N kinetic isotope effect study showed that C–N bond cleavage is the rate-limiting step of the reaction below. Visualize the carbanionic resonance structure to kick off the mechanism! Don't think too hard about the structure of rhodium(II) acetate here. Rhodium, copper, ruthenium, and iridium all form carbene complexes with diazo compounds in a similar way.



After association of the nucleophilic carbon to Rh, elimination with loss of nitrogen gas is the slow step of this reaction.

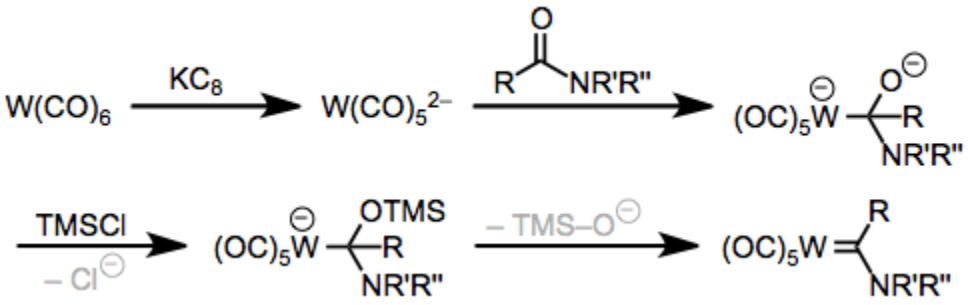
Diazo compounds work well for metal carbene formation when they possess an electron-withdrawing group, which stabilizes the ylide through conjugation. What about Fischer carbenes, which possess electron-donating groups on the carbene carbon? An interesting method that still involves a "push-and-pull" of electron flow (but not ylides) employs metal-CO complexes. Upon addition of a strong nucleophile ("forward flow") to the carbonyl carbon, a metalloenolate of sorts is produced. Treatment with an electrophile RX that prefers oxygen over the metal ("reverse flow") results in an OR-substituted Fischer carbene. Reactions reminiscent of transesterification trade out the OR group for an –SR group (using a thiol) or an –NR2 group (using a secondary

amine).



Fischer's classical route to L-type carbenes.

As counterintuitive as it may seem, it's possible to use metal dianions for the synthesis of Fischer carbenes via a method pioneered by Hegedus and Semmelhack. Potassium intercalated in graphite—the mysterious "KC8"—reduces group 6 metal carbonyl complexes to the corresponding dianions, which subsequently unleash a deluge of electrons on a poor, unsuspecting amide to afford NR2-substituted Fischer carbenes after treatment with trimethylsilyl chloride.

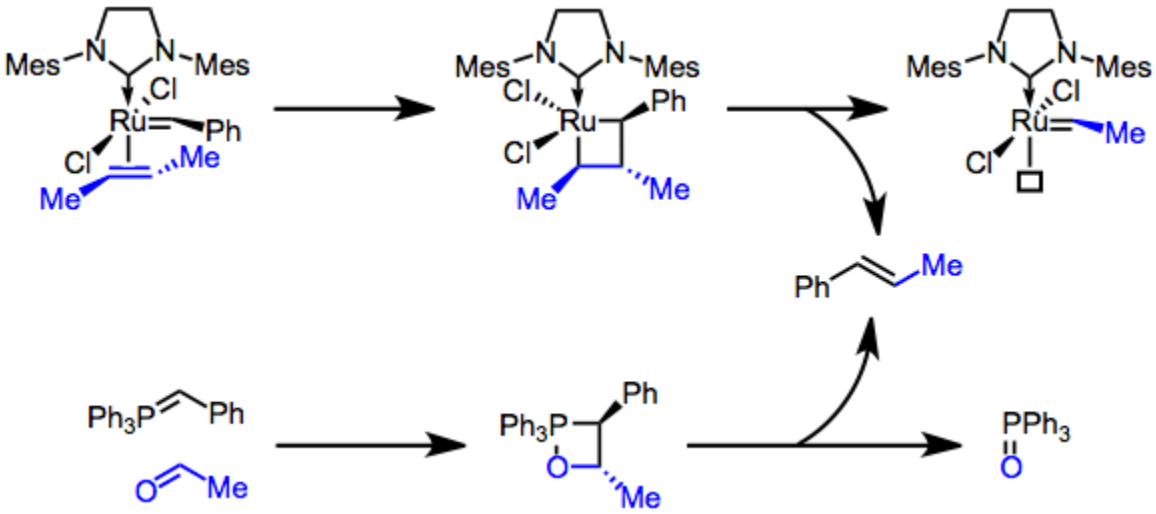


One-directional electron flow for Fischer carbene synthesis: the Hegedus-Semmelhack approach.

For other methods for the synthesis of Fischer carbenes, check out this nice review from the Baran group.

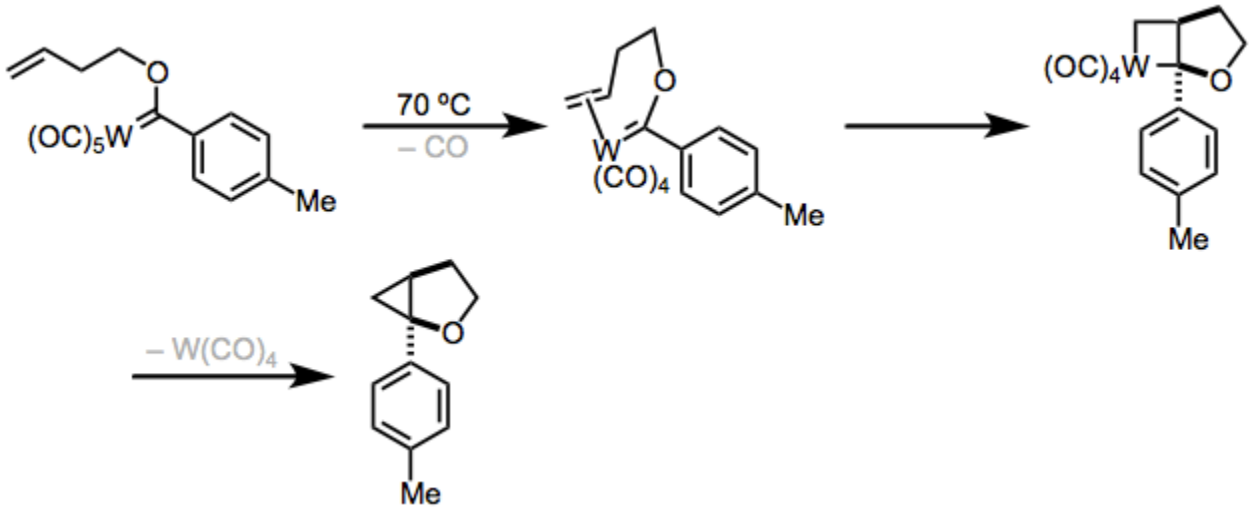
Reactions

In many ways, the reactivity of metal carbenes parallels that of ylides. Olefin metathesis catapulted metal carbenes to international stardom, but in many ways, metathesis is conceptually similar to the Wittig reaction, which employs phosphorus ylides. During both mechanisms, an ylide/carbene hooks up with another doubly bound molecule to form a four-membered ring. This step is followed by what we might call "orthogonal breakdown" to yield two new double bonds.



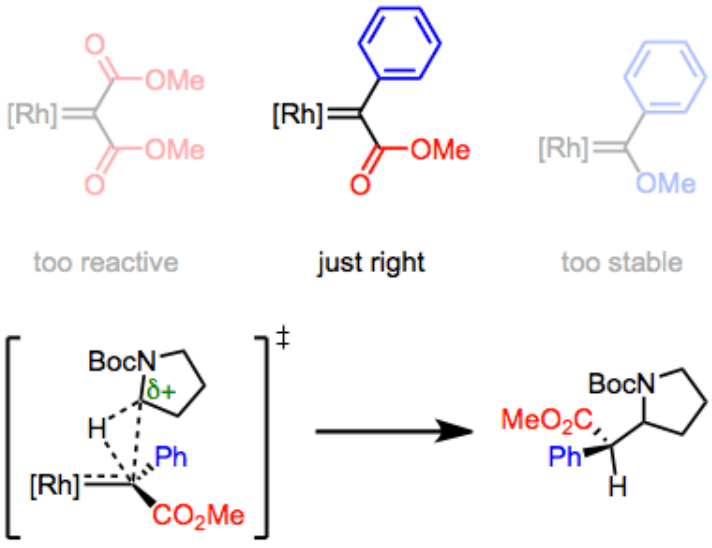
Wittig, Grubbs, and Schrock: Lords of the Chemical Dance. Ambi-electronic molecules are the dancers!

In my opinion, bond insertion reactions are the most interesting processes in which carbenes regularly engage. Bond insertions may be subdivided into cyclopropanation (π-bond insertion) and σ-bond insertion. Evidence suggests that most cyclopropanations take place by a mechanism that overlaps with metathesis—instead of orthogonal breakdown, reductive elimination occurs to release the three carbon atoms as a cyclopropane.



The metallacyclobutane mechanism of cyclopropanation.

σ-Bond insertion involves electron-rich C–H bonds most prominently, suggesting that electrophilic Fischer carbenes should be best for this chemistry. Fischer carbenes incorporating electron-withdrawing groups love to dimerize to form olefins and/or cyclopropanate olefins—how might we put the brakes on this behavior? If we simply tack a π-basic substituent onto the carbene carbon, the reactivity of these complexes is "just right" for C–H insertion. Notably, no covalent organometallic intermediates are involved; the electrophilic carbene carbon snuggles in between C and H in a single step. The transition state of this step resembles the transfer of a hydride from the organic substrate to the carbene, with "rebound" of electron density toward the partial positive charge.



Donor-acceptor carbenoids are the "Goldilocks complexes" of C–H insertion.

Let's end with a nod to the similarity between Fischer carbenes and carboxylic acid derivatives (esters and amides).

Transesterification-type reactions allow the chemist to swap out heteroatomic substituents on the carbene carbon at will (see above). Alkyl substitutents can even be deprotonated at the α carbon, just like esters! When we see the electronic similarities between the M=C bond of a Fischer carbene and the O=C bond of carboxylic acid derivatives, the similar behavior is only natural.

This page titled 8.2.1: Carbenes is shared under a CC BY-NC-SA 4.0 license and was authored, remixed, and/or curated by Michael Evans.

- 2.1: Carbenes by Michael Evans is licensed CC BY-NC-SA 4.0.

8.2.2: Carbon Monoxide

As a young, growing field, organometallic chemistry may be taught in many ways. Some professors (e.g., Shaugnessy) spend a significant chunk of time discussing ligands, while others forego ligand surveys (e.g., White) to dive right in to reactions and mechanisms. I like the ligand survey approach because it lays out many of the general concerns associated with certain ligand sets before organometallic intermediates pop up. With the general concerns in hand, it becomes easier to generate explanations for certain observed effects on reactions that depend on ligands. Instead of generalizing from complex, specific examples in the context of reaction mechanisms, we'll look at general trends first and apply these to reaction intermediates and mechanisms later. This post kicks off our epic ligand survey with carbon monoxide, a simple but fascinating ligand.

General Properties

CO is a dative, L-type ligand that does not affect the oxidation state of the metal center upon binding, but does increase the total electron count by two units. We've recently seen that there are really two bonding interactions at play in the carbonyl ligand: a ligand-to-metal $n \rightarrow d_\sigma$ interaction and a metal-to-ligand $d_\pi \rightarrow \pi^*$ interaction. The latter interaction is called **backbonding**, because the metal donates electron density back to the ligand. To remind myself of the existence of backbonding, I like to use the right-hand resonance structure whenever possible; however, it's important to remember to treat CO as an L-type ligand no matter what resonance form is drawn.

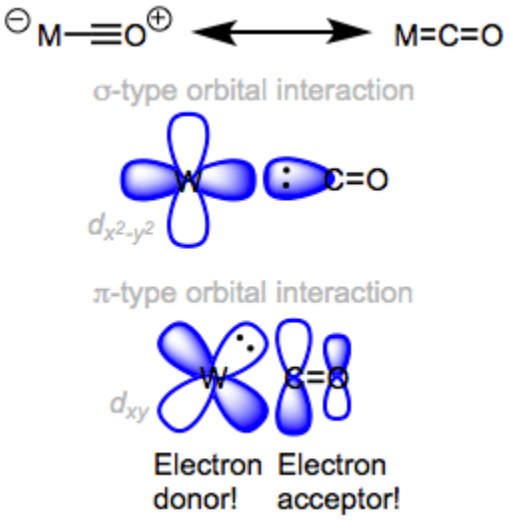


Figure 8.2.2.1: Orbital interactions in M=C=O. (Copyright; Michael Evans)

CO is a fair σ-donor (or σ-base) and a good π-acceptor (or π-acid). The properties of ligated CO depend profoundly upon the identity of the metal center. More specifically, the electronic properties of the metal center dictate the importance of backbonding in metal carbonyl complexes. Most bluntly, *more electron-rich metal centers are better at backbonding to CO*. Why is it important to ascertain the strength of backbonding? I'll leave that question hanging for the moment, but we'll have an answer very soon. Read on!

Infrared spectroscopy has famously been used to empirically support the idea of backbonding. The table below arranges some metal carbonyl complexes in "periodic" order and provides the frequency corresponding to the C=O stretching mode. Notice that without exception, every complexed CO has a stretching frequency lower than that of free CO. Backbonding is to blame! The C–O bond order in complexed carbon monoxide is (almost always) lower than that of free CO.

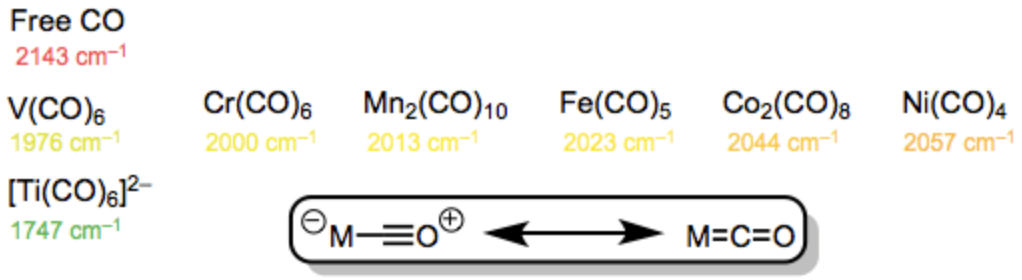


Figure 8.2.2.2: C=O stretching frequencies in metal-carbonyl complexes. Does something seem off here? (Copyright; Michael Evans)

The figure above depicts a clear increase in frequency (an increase in C–O bond order) as we move left to right across the periodic table. This finding may seem odd if we consider that the number of *d* electrons in the neutral metal increases as we move left to right. Shouldn't metal centers with more *d* electrons be better at backbonding (and more "electron rich")? What's going on here? Recall the periodic trend in *orbital energy*. As we move left to right, the *d* orbital energies decrease and the energies of the d_π and π* orbitals separate. As a result, the backbonding orbital interaction becomes worse (remember that strong orbital interactions require well-matched orbital energies) as we move toward the more electronegative late transition metals! We can draw an analogy to enamines and enols from organic chemistry. The more electronegative oxygen atom in the enol is a worse electron donor than the enamine's nitrogen atom.

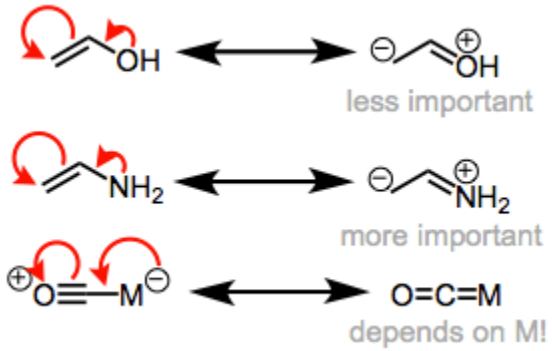


Figure 8.2.2.3: The importance of backbonding depends on the electronegativity of the metal and its electron density. (Copyright; Michael Evans)

Of course, the contribution of other ligands on the metal center to backbonding cannot be forgotten, either. Logically, electron-donating ligands will tend to make the backbond stronger (they make the metal a better electron donor), while electron-withdrawing ligands will worsen backbonding. Adding electron-rich phosphine ligands to a metal center, for instance, *decreases* the CO stretching frequency due to *improved* backbonding.

Carbonyl ligands are famously able to **bridge** multiple metal centers. Bonding in bridged carbonyl complexes may be either "traditional" or delocalized, depending on the structure of the complex and the bridging mode. The variety of bridging modes stems from the different electron donors and acceptors present on the CO ligand (and the possibility of delocalized bonding). Known bridging modes are shown in the figure below.

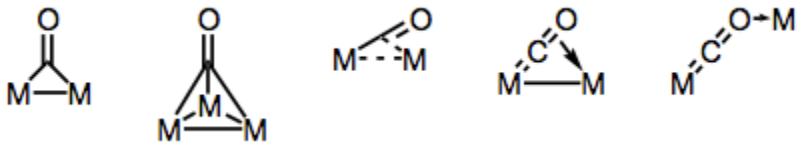


Figure 8.2.2.4: Building bridges with carbonyl ligands! (Copyright; Michael Evans)

Synthesis

Metal carbonyl complexes containing only CO ligands abound, but most cannot be synthesized by the method we all wish worked, bathing the elemental metal in an atmosphere of carbon monoxide (entropy is a problem, as we already discussed for $W(CO)_6$).

This method does work for nickel(0) and iron(0) carbonyls, however.

$M + n\ CO \rightarrow M(CO)_n$ [M = Fe, n = 5; M = Ni, n = 4]

Other metal carbonyl complexes can be prepared by **reductive carbonylation**, the treatment of a high-oxidation-state complex with CO. These methods usually require significant heat and pressure. One example:

$WCl_6 + CO + \text{heat, pressure} \rightarrow W(CO)_6$

Still other methods employ **deinsertion** from organic carbonyl compounds like dimethylformamide. These methods are particularly useful for preparing mixed carbonyl complexes in the presence of reducing ligands like phosphines.

$IrCl_3(H_2O)_3 + 3\ PPh_3 + HCONMe_2 + PhNH_2 \rightarrow IrCl(CO)(PPh_3)_2 + (Me_2NH_2)Cl + OPPh_3 + (PhNH_3)Cl + 2\ H_2O$

The key thing to notice about the reaction above is that the CO ligand is derived from dimethylformamide (DMF).

Reactions

The dissociation of carbonyl ligands is common in reactions that require an open coordination site at the metal. Naturally, the favorability of dissociation is governed by electron density at the metal—weaker backbonding metals lose CO more easily. This is one reason understanding trends in backbonding strength is important!

Like the carbonyl carbon in organic compounds, the carbon of ligated CO is often an exquisite electrophile—particularly when the metal is a poor π-base, leaving the carbonyl carbon starved of electrons. CO ligands are susceptible to nucleophilic attack at the carbonyl carbon in the presence of strong nucleophiles. Treating the adduct with an electrophile yields a Fischer carbene complex. If we imagine M=C=O as an analogue of ketene, this reactivity just corresponds to classic nucleophilic addition across the C=O bond.

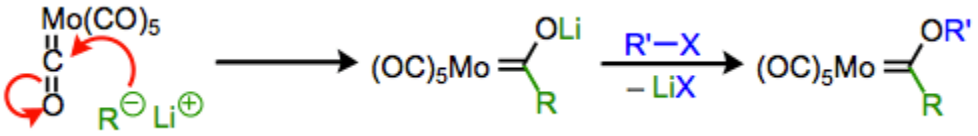


Figure 8.2.2.5: Metal carbene complexes from metal carbonyls via nucleophilic addition. (Copyright; Michael Evans)

Perhaps the most important elementary step in which the CO ligand participates is **migratory insertion**, a step typical of oxidized organic ligands (CO, alkenes, alkynes, etc.). The net result of the process is the insertion of the carbonyl carbon into an M–X bond (X is most commonly C or H, but can be any X-type ligand). An empty coordination site—the strange-looking box in the figure below—is left behind after migration. The **hydroformylation** reaction involves the insertion of CO into an M–C bond as a key step. We'll talk about this fascinating processes in more detail in a later post.

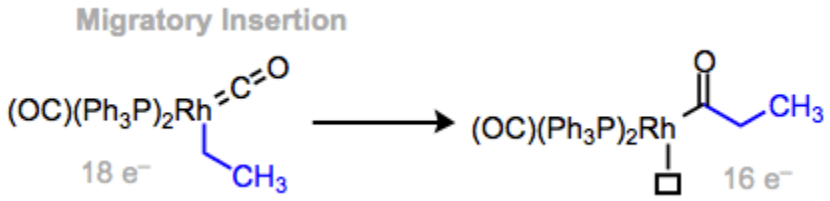


Figure 8.2.2.6: Migratory insertion, a powerful method for C–C bond construction on transition metal centers.Copy and Paste Caption here. (Copyright; Michael Evans)

For CO, it's useful to think about migratory insertion as a sort of intramolecular nucleophilic attack by the X-type ligand on coordinated CO. In this respect its similar to the intermolecular nucleophilic addition process leading to carbenes described above. Just view the carbonyl carbon as an electrophile (as if you don't already!) and it becomes easy to keep these ideas in mind. We'll see migratory insertion in more detail in a future post as well.

This page titled 8.2.2: Carbon Monoxide is shared under a license and was authored, remixed, and/or curated by Michael Evans.

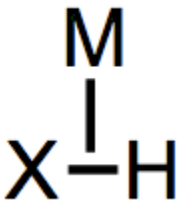
- 2.2: Carbon Monoxide by Michael Evans has no license indicated.

8.2.3: σ Complexes

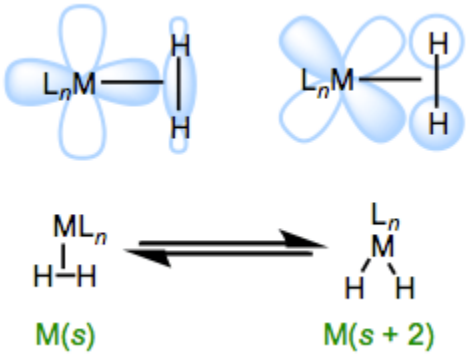
Ligands can, shockingly enough, bind through their σ electrons in an L-type fashion. This binding mode depends as much on the metal center as it does on the ligand itself—to see why, we need only recognize that σ complexes look like intermediates in concerted oxidative additions. With a slight reorganization of electrons and geometry, an L-type σ ligand can become two X-type ligands. Why, then, are σ complexes stable? How can we control the ratio of σ complex to X_2 complex in a given situation? How does complexation of a σ bond change the ligand's properties? We'll address these questions and more in this post.

General Properties

The first thing to realize about σ complexes is that they are highly sensitive to steric bulk. Any old σ bond won't do; hydrogen at one end of the binding bond or the other (or both) is necessary. The best studied σ complexes involve dihydrogen (H2), so let's start there.

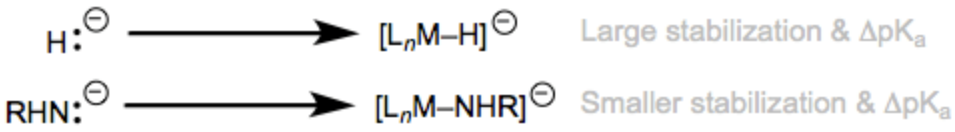


Mildly backbonding metals may bind dihydrogen "side on." Like side-on binding in π complexes, there are two important orbital interactions at play here: σH–H → dσ and dπ → σ*H–H. Dihydrogen complexes can "tautomerize" to $(H)_2$ isomers through oxidative addition of the H–H bond to the metal.



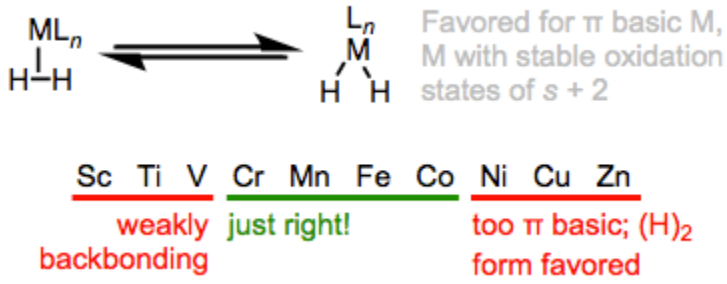
Orbital interactions and L-X_2 equilibrium in σ complexes.

H_2 binding in an L-type fashion massively acidifies the ligand—changes in pKa of over thirty units are known! Analogous acidifications of X–H bonds, which we touched on in a previous post, rarely exhibit ΔpKa > 5. What gives? What's causing the different behavior of X–H and H–H ligands? The key is to consider the conjugate base of the ligand—in particular, how much it's stabilized by a metal center relative to the corresponding free anion. The principle here is analogous to the famous dictum of organic chemistry: consider charged species when making acid/base comparisons. Stabilization of the unhindered anion H– by a metal is much greater than stabilization of larger, more electronegative anions like HO– and NH_2– by a metal. As a result, it's more favorable to remove a proton from metal-complexed H_2 than from larger, more electronegative X–H ligands.



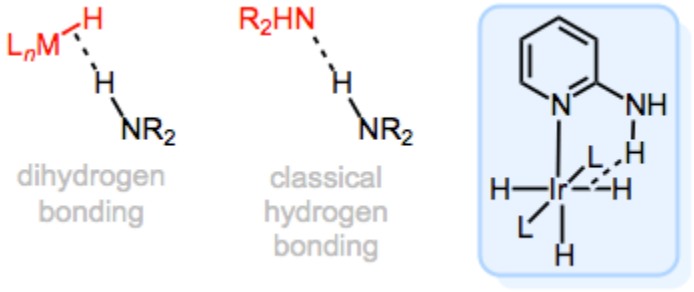
Remarkably large stabilization by an acidic metal fragment, without any counterbalancing from steric factors, explains the extreme acidification of dihydrogen upon metal binding.

The electronic nature of the metal center has two important effects on σ complexes. The first concerns the acidity of H2 upon metal binding. The principle here is consistent with what we've hammered into the ground so far. In the same way cationic organic acids are stronger than their neutral counterparts, σ complexes of electron-poor metals—including (and especially) cations—are stronger acids than related complexes of electron-rich metals. The second concerns the ratio of L-type to X_2-type binding. We should expect more electron-rich metal centers to favor the X2 isomer, since these should donate more strongly into the σ*H–H orbital. This idea was masterfully demonstrated in a study by Morris, in which he showed that H2 complexes of π-basic metal centers show all the signs of X2 complexes, rather than L complexes. More generally, metal centers in σ complexes need a good balance of π basicity and σ acidity (I like to call this the "Goldilocks effect"). Because of the need for balance, σ complexes are most common for centrally located metals (groups 6-9).



Oxidative addition of H2 is important for electron-rich, π-basic metal centers. Groups 6-9 hit the "Goldilocks" spot.

The M–H bond in hydride complexes is a good base—anyone who's ever quenched lithium aluminum hydride can attest to this! Intriguingly, because it's a good base, the M–H bond can participate in hydrogen bonding with an acidic X–H bond, where X is a heteroatom. This kind of bonding, called dihydrogen bonding (since two hydrogen atoms are involved), is best described as a sort of σM–H → σ*X–H orbital interaction. Think of it as analogous to a traditional hydrogen bond, but using a σ bond instead of a lone pair. Crazy, right?!



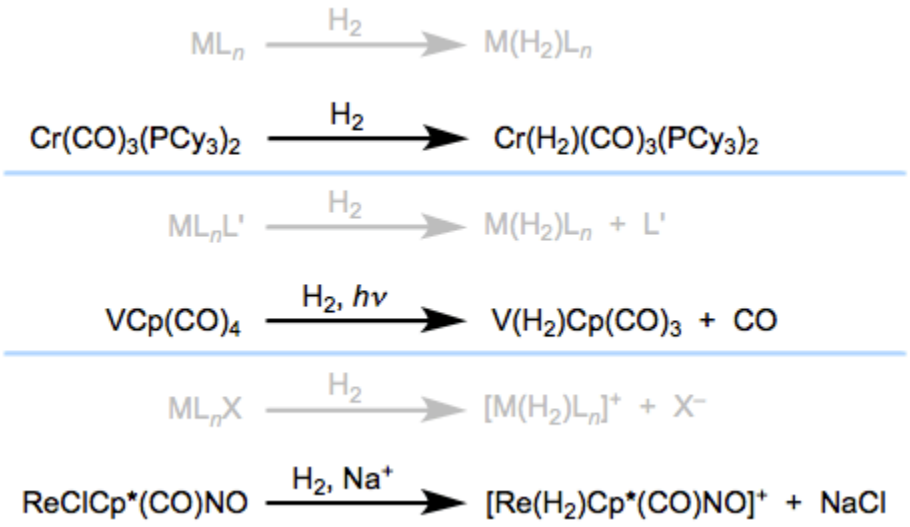
Dihydrogen bonding in metal hydrides: a sort of "interrupted protonation" of M–H.

Other kinds of σ complexes are known, but these are rarer than H–H complexes. One class that we've seen before involve agostic interactions of C–H bonds in alkyl ligands. σ Complexes of inorganic ligands like silanes and stannanes may involve complex bonding patterns, but we won't concern ourselves with those here.

Synthesis

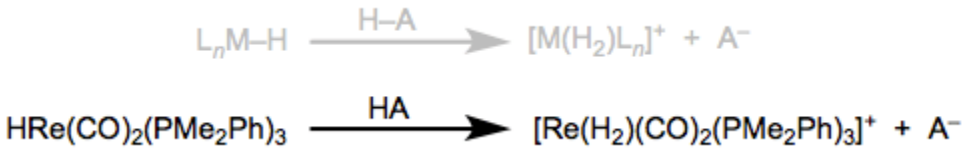
If a metal center with an open coordination site has the "Goldilocks combination" of electronic factors, simply treating it with

dihydrogen gas is enough to form the σ complex. Metals that bear labile L- or X-type ligands can also yield σ complexes upon treatment with H2.



Methods for the synthesis of σ complexes from dihydrogen gas. Displacement of a labile ligand or occupation of a vacant site represent the essence of these methods.

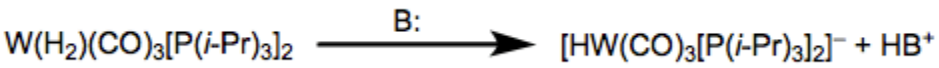
An alternative synthetic method involves the protonation of a basic M–H bond...taking dihydrogen bonding to the extreme! This method is especially nice if a cationic complex is the goal; of course, the metal needs to be π basic to make protonation favorable.



Protonation of an M–H bond for the synthesis of dihydrogen σ complexes.

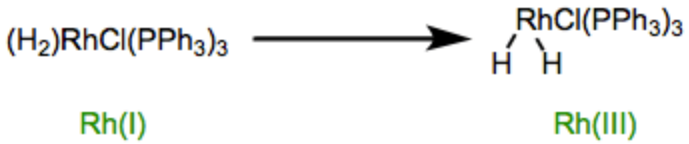
Reactions

Deprotonation of an L-type X–H ligand is probably the simplest reaction of this class of ligands. This process is just the reverse of the synthetic method described above. We can refer to it as heterolytic cleavage, since the X atom that stays bound to the metal holds on to the electrons of the X–H bond. The charge of the product complex is one less than that of the starting material. A variation on this theme involves intramolecular proton transfer.



Deprotonation of dihydrogen complexes produces metal hydrides.

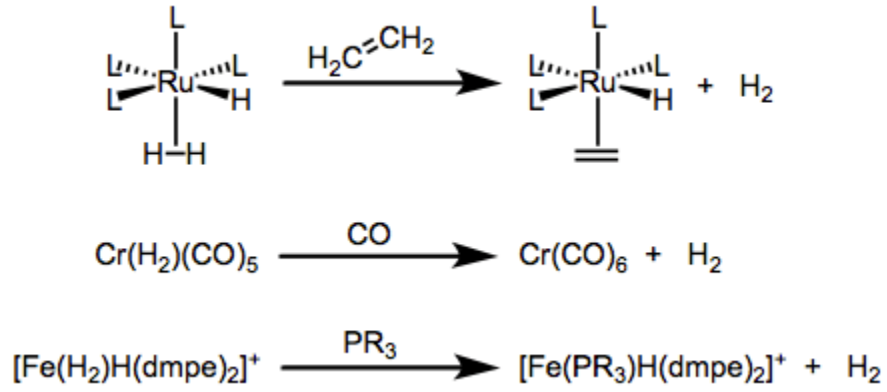
Homolytic cleavage of X–H is also possible, and it can happen in two ways. Intramolecular oxidative addition is the first, and we've seen it already. Since this process is intramolecular and little geometric reorganization is necessary, kinetic barriers tend to be low and the process may be reversible (unless the electronic circumstances of the metal are extreme). This sort of oxidative addition is important for many hydrogenation reactions, such as those employing Wilkinson's catalyst.



Oxidative addition of dihydrogen via a sigma complex. In some cases, this process is a finely balanced equilibrium.

And the second way? In theory at least, intermolecular homolytic cleavage is possible. This process corresponds to one-electron oxidation of two distinct metal centers. Contrast this pattern of electron exchange with intramolecular oxidative addition, which involves two-electron oxidation of a single metal center. This kind of reactivity is rare in practice.

Ligand substitutions with other L-type ligands— including CO, N2, phosphines, and unsaturated organics—are also known. In fact, this process has been implicated in catalytic cycles for some hydrogenation reactions.



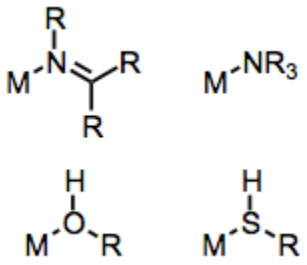
Ligand substitution reactions of sigma complexes. Can you justify the favorability of these reactions?

This page titled 8.2.3: σ Complexes is shared under a CC BY-NC-SA 4.0 license and was authored, remixed, and/or curated by Michael Evans.

- 2.3: σ Complexes by Michael Evans is licensed CC BY-NC-SA 4.0.

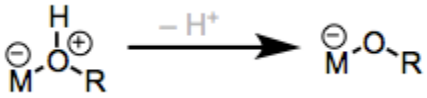
8.2.4: Dative Ligands of N, O, and S

In this post, we'll take a quick look at L-type ligands of nitrogen, oxygen, and sulfur. Ligands of this type are important for at least two reasons: (1) coordination to a metal can modify the reactivity of the bound functional group, and (2) dative coordination is a critical element of organometallic reactions that depend on intramolecular **directing group** effects. "Long-term" ligands containing two-connected nitrogens, such as pyridines and oxazolines, are now among the most commonly used for organometallic reactions. The behavior of coordinated dinitrogen is also a hot research area right now. Although they look boring on the surface, dative ligands of N, O, and S are rich in chemistry!



General Properties

This might be the first class of ligand for which we can reliably say that backbonding is rarely important. Dative coordination of amines and alcohols involves a straightforward n → dσ orbital interaction. Intuitively, we should expect the acidity of amines, alcohols, and thiols to increase upon coordination, because removal of electron density from nitrogen and oxygen through coordination makes these atoms more electrophilic. Consider the charged model of dative bonding at left in the figure below.

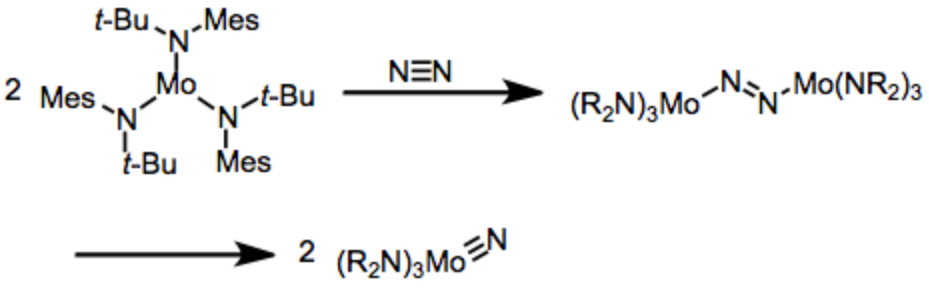


Coordination increases acidity.

Transfer of the lost proton to an organic substrate is an important aspect of hydrogenation reactions employing amine ligands (see below).

Food for thought: why aren't (cheaper) amines found in place of phosphines in organometallic catalysts? History has ruled against tertiary amines, but are there any good reasons why? Yes—for one thing, amine nitrogens are more sterically hindered than analogous phosphorus atoms, because N–C bonds are shorter than P–C bonds. Plus, the cone angles of amines are generally wider than those of phosphines. Getting amines to play nice with hindered metal centers can thus be very difficult.

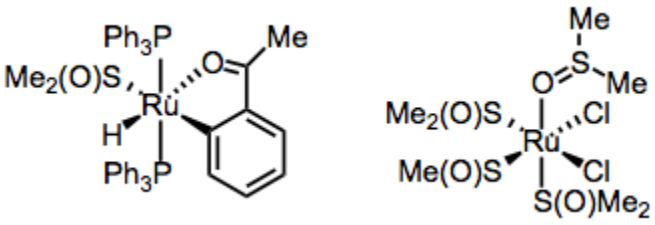
Although dinitrogen (N2) is isoelectronic with carbon monoxide, it's been a tough nut for organometallic chemists to crack. An electron-rich metal center lacking π-acidic ligands is an absolute must for dinitrogen-containing complexes, as the π*NN orbital does not easily participate in backbonding. What sets nitrogen apart from CO is its ability to participate in side-on bonding and bridging through its π system—for this application, dinitrogen's higher-energy orbitals are a perk over CO. While migratory insertion and nucleophilic addition reactions of N2 bound "end-on" (through a non-bonding lone pair) are virtually unknown, functionalization of "side-on" nitrogen ligands is a growing field. Dinitrogen has been known to bridge multiple metals in "end-end," "side-end," and "side-side" modes.



Activation of dinitrogen by molybdenum—a complex containing an "end-end," linear bridging dinitrogen (not shown) is proposed as an intermediate in this mechanism.

Imines are another important class of ligands that fit into this post; unlike carbonyl compounds, imines more commonly bind through the nitrogen atom rather than the π system. These are very common directing groups but are also important for hydrogenation and hydroamination reactions.

DMSO is an interesting, archetypal sulfur-containing ligand that may bind through either S or O. As sulfur is softer and more polarizeable than oxygen, sulfur binds to softer (low-valent) metals and oxygen to harder metal centers.

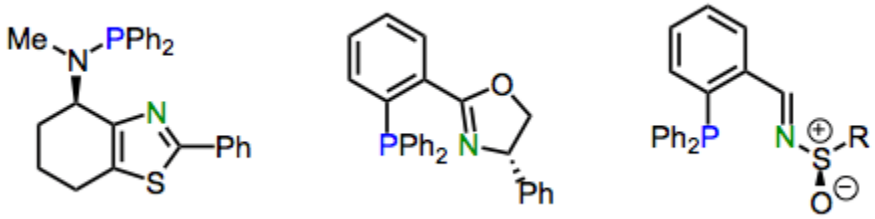


The soft Ru(II) center with hydrocarbyl ligands contains S-bound DMSO, while the harder Ru(II) with chloride ligands includes one O-bound DMSO.

Most ligands binding through dative sulfur require chelation, as M–S bond strengths tend to be low.

Synthesis

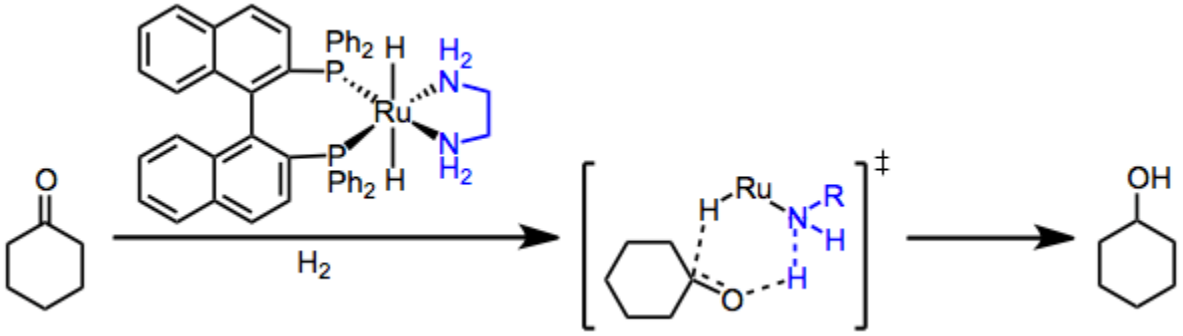
Ligand substitution reactions are most commonly used to load dative ligands of N, O, and S onto metal centers. In some cases, when the heteroatom bears a hydrogen atom, deprotonation can produce a covalent, X-type ligand. Usually, however, these types of ligands are incorporated into organic substrates and used as directing groups—coordination brings the metal center into close contact with a target functional group, such as an alkene, C–H bond, or C–X bond. They may also be part of chelating ligands containing a second, more robust electron donor, like a phosphine.



P,N ligands for organometallic chemistry.

Reactions

I'll showcase only one reaction in this section: the Noyori hydrogenation employing amine ligands as proton donors. The reaction is a nice illustration of the influence of metal coordination on the reactivity of amines.



"External" hydrogenation without substrate binding. The metal is a hydride source, and the ligand a proton source.

Easy, breezy, beautiful, right? Dative ligands of N, O, and S are usually employed as spectators, not actors, so reactions like this are somewhat hard to come by. I'll pass on discussing the reactivity of dinitrogen complexes in detail, but for an interesting recent example of metal-dinitrogen chemistry, check this out.

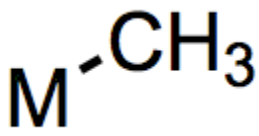
This page titled 8.2.4: Dative Ligands of N, O, and S is shared under a CC BY-NC-SA 4.0 license and was authored, remixed, and/or curated by Michael Evans.

- 2.4: Dative Ligands of N, O, and S by Michael Evans is licensed CC BY-NC-SA 4.0.

8.2.5: Metal Alkyls

Part 1:

With this post we finally reach the defining ligands of organometallic chemistry, alkyls. Metal alkyls feature a metal-carbon σ bond and are usually actor ligands, although some alkyl ligands behave as spectators. Our aim will be to understand the general dependence of the behavior of alkyl ligands on the metal center and the ligand's substituents. Using this knowledge, we can make meaningful comparisons between related metal alkyl complexes and educated predictions about their likely behavior. Because alkyl ligands are central to organometallic chemistry, I've decided to spread this discussion across multiple posts. We'll deal first with the general properties of metal alkyls.



In the Simplifying the Organometallic Complex series, we decomposed the M–C bond into a positively charged metal and negatively charged carbon. This deconstruction procedure is consistent with the relative electronegativities of carbon and the transition metals. It can be very useful for us to imagine metal alkyls essentially as stabilized carbanions—but it's also important to understand that M–C bonds run the gamut from extremely ionic and salt-like ($NaCH_3$) to essentially covalent ($[HgCH_3]^+$). The reactivity of the alkyl ligand is inversely related to the electronegativity of the metal center.

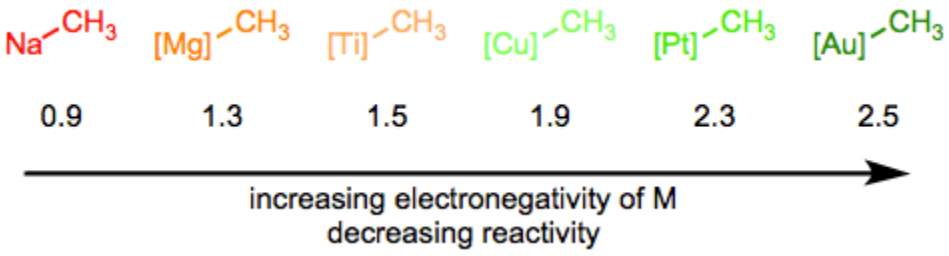


Figure 8.2.5.1: Reactivity decreases as the metal's electronegativity increases. Values given are Pauling electronegativities. (Michael Evans)

The hybridization of the carbon atom is also important, and the trend here follows the trend in nucleophilicity as a function of hybridization in organic chemistry. *sp*-Hybridized ligands are the least nucleophilic, followed by sp^2 and sp^3 ligands respectively.

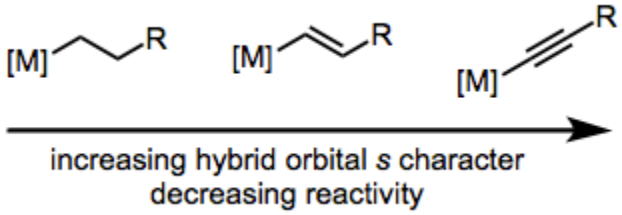
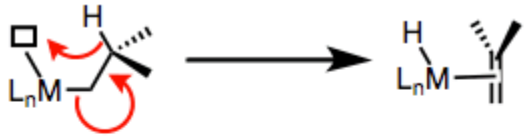


Figure 8.2.5.1: Note that this trend is similar to the nucleophilicity of carbanions as a function of hybridization. (Michael Evans)

The history of transition metal alkyls is an intriguing example of an incorrect scientific paradigm. After several unsuccessful attempts to isolate stable metal alkyls, organometallic chemists in the 1920s got the idea that metal-carbon bonds were weak in general. However, later studies showed that it was *kinetic instability*, not thermodynamic, that was to blame for our inability to isolate metal alkyls. In other words, most metal alkyls are susceptible to decomposition pathways with low activation barriers—the instability of the M–C bond *per se* is not to blame. Crabtree cites typical values of 30-65 kcal/mol for M–C bond strengths.

What are the major decomposition pathways of metal alkyl complexes? **β-hydride elimination** is the most common. Thermodynamically, the ubiquity of β-hydride elimination makes sense—M–C bonds run 30-65 kcal/mol, while M–H bonds tend to be stronger. The figure below summarizes the accepted mechanism and requirements of β-hydride elimination. We'll revisit this fundamental reaction of organometallic complexes in a future post.



1. The β-carbon must bear a hydrogen.
2. M–C and C–H must be *syn coplanar*.
3a. The metal must possess a vacant coordination site and an accessible empty orbital.
3b. The metal must possess 16 or fewer total electrons.
4. For rapid elimination, the metal must be at least d^2.

Figure 8.2.5.1: What kinds of metal alkyl complexes violate the requirements for beta-hydride elimination? (Copyright; author via source)

Kinetically stable metal alkyl complexes violate one of the requirements for β-hydride elimination. Methyl and neopentyl complexes lack β-hydrogens, violating requirement 1. Tightly binding, chelating ligands may be used to prevent the formation of an empty coordination site, violating requirements 3a and 3b. Titanium complexes are known that violate requirement 4 and eliminate only very slowly—back-donation from the metal to the σ^*_{C-H} is required for rapid elimination (see below).

Reductive elimination is a second common decomposition pathway. The alkyl ligand hooks up with a second X-type ligand on the metal, and the metal is reduced by two units with a decrease in the total electron count by two units. I've omitted curved arrows here because different mechanisms of reductive elimination are known. We'll discuss the requirements of reductive elimination in detail in a future post; for now, it's important to note that the thermodynamic stability of C–X versus that of (M–X + M–C) is a critical driving force for the reaction.

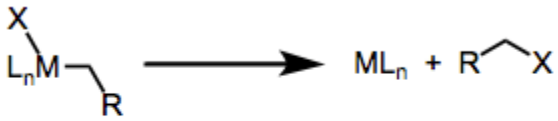


Figure 8.2.5.1: The thermodynamics of reductive elimination can present problems for some alkyl complexes. (Copyright; author via source)

When X = H, reductive elimination is nearly always thermodynamically favorable; thus, isolable alkyl hydride complexes are rare. This behavior is a feature, not a bug, when we consider that hydrogenation chemistry depends on it! On the other hand, when X = halogen reductive elimination is usually disfavored. Reductive elimination of C–C (X = C) can be favored thermodynamically, but is usually slower than the corresponding C–H elimination.

Complexes that cannot undergo β-hydride elimination are sometimes susceptible to **α-elimination**, a mechanistically similar process that forms a metal carbene. This process is particularly facile when the α-position is activated by an adjacent electron donor (Fischer carbenes are the result).

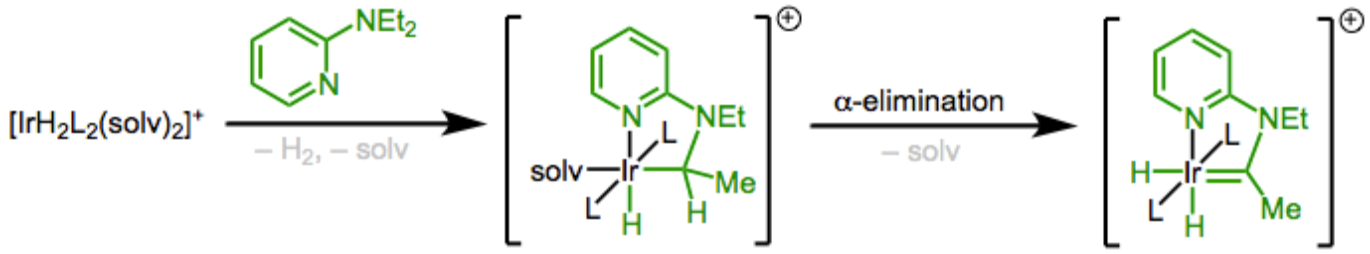


Figure 8.2.5.1: Oxidative addition followed by alpha-elimination, forming a Fischer carbene from an alkyl complex. (Copyright; author via source)

In some metal alkyl complexes, C–H bonds at the α, β, or even farther positions can serve as electron donors to the metal center. This idea is supported by crystallographic evidence and NMR chemical shifts (the donating hydrogens shift to high field). Such interactions are called **agostic interactions**, and they resemble an "interrupted" transition state for hydride elimination. Alkyl complexes that cannot undergo β-hydride elimination for electronic reasons (high oxidation state, d^0 metals) and vinyl complexes commonly exhibit this phenomenon. The fact that β-hydride elimination is slow for d^0 metals—agostic interactions are seen instead—suggests that back-donation from a filled metal orbital to the σ^*_{C-H} is important for β-hydride elimination. Here's an interesting, recent-ish review of agostic interactions.

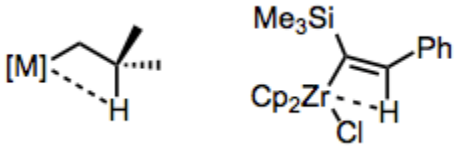


Figure 8.2.5.1: Copy and Paste Caption here. (Copyright; author via source)

In the next post in this series, we'll explore the synthesis of metal alkyl complexes in more detail, particularly clarifying the question: how can we conquer β-hydride elimination?

Part 2:

In this post, we'll explore the most common synthetic methods for the synthesis of alkyl complexes. In addition to enumerating the reactions that produce alkyl complexes, this post will also describe strategies for getting around β-hydride elimination when isolable alkyl complexes are the goal. Here we go!

Properties of Stable Alkyl Complexes

Stable alkyl complexes must be resistant to β-hydride elimination. In the last post we identified four key conditions necessary for elimination to occur:

1. The β-carbon must bear a hydrogen.
2. The M–C and C–H bonds must be able to achieve a *syn* coplanar orientation (pointing in the same direction in parallel planes).
3. The metal must bear 16 total electrons or fewer and possess an open coordination site.
4. The metal must be at least d^2.

Stable alkyl complexes must violate at least one of these conditions. For example, titanium(IV) complexes lacking *d* electrons β-eliminate very slowly. The complex below likely also benefits from chelation (see below).

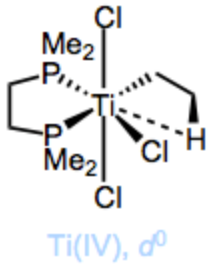


Figure 8.2.5.1: No d electrons here! (Michael Evans)

Complexes have been devised that are unable to achieve the *syn* coplanar orientation required for elimination, or that lack β-hydrogens outright. A few examples are provided below—one has to admire the cleverness of the researchers who devised these complexes. The metallacyclobutane is particularly striking!

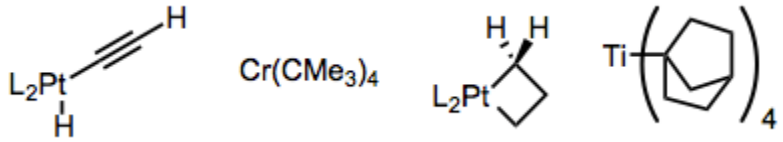


Figure 8.2.5.1: Complexes whose beta-C–H bonds cannot align in a syn coplanar manner with the M–C bond. (Copyright; author via source)

Using tightly binding, chelating ligands or a directing group on the substrate, the formation of 16-electron complexes susceptible to β-hydride elimination can be discouraged. Notice how the hyrdrogen-bonding L_2 ligands in the central complex below hold the metal center in a death grip.

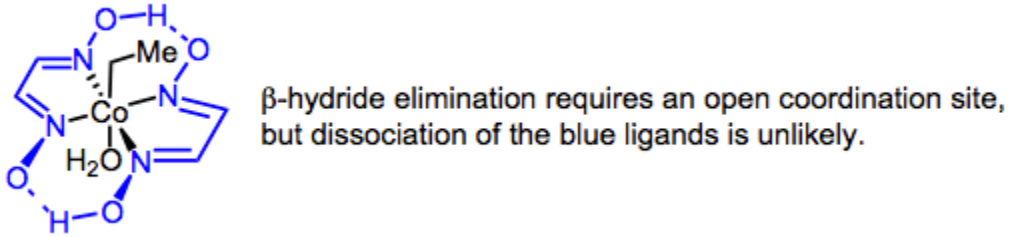


Figure 8.2.5.1: Tightly chelating ligands prevent the opening of a coordination site. (Copyright; author via source)

Finally, it's worth noting that complexes with an open coordination site—such as 16-electron, square-planar complexes of Ni, Pd, and Pt important for cross-coupling—are susceptible to reactions with solvent or other species at the open site. Bulky alkyl ligands help prevent these side reactions. In the example below, the methyl groups of the *o*-tolyl ligands extend into the space above and below the square plane, discouraging the approach of solvent molecules perpendicular to the plane.

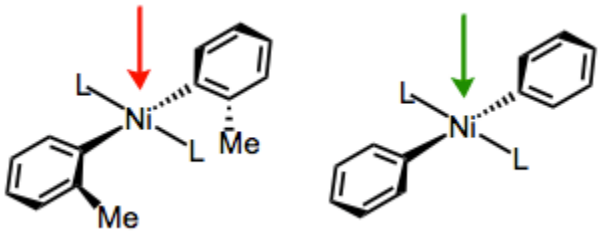


Figure 8.2.5.1: The approach of solvent perpendicular to the square plane is slowed by methyl groups on the aryl ligand. (Copyright; author via source)

Many transition metal complexes catalyze (*E*)/(*Z*) isomerization and the isomerization of terminal alkenes (α-olefins) to internal isomers via β-hydride elimination. This is a testament to the importance of this process for alkyl complexes. Of course, transient alkyl complexes may *appear* to be susceptible to β-hydride elimination, but if other processes are faster, elimination will not occur. Thus, the optimization of many reactions involving alkyl complexes as intermediates has involved speeding up other

processes at the expense of β-hydride elimination—hydrocyanation is a good example.

Synthesis of Alkyl Complexes

The dominant synthetic methods for alkyl complexes are based on nucleophilic attack, electrophilic attack, oxidative addition, and migratory insertion. The first two methods should be intuitive to the organic chemist; the second two are based on more esoteric (but no less important) reactions of organometallic complexes.

Metals bearing good leaving groups are analogous to organic electrophiles, and are susceptible to **nucleophilic attack** by organolithiums, Grignard reagents, and other polarized organometallics. These reactions can be viewed as a kind of **transmetalation**, as the alkyl ligand moves from one metal to another. Electron-withdrawing X-type ligands like –Cl and –Br should jump out as good leaving groups. On the other hand, clean substitution of L-type ligands by anionic nucleophiles is much more rare (anionic complexes would result).

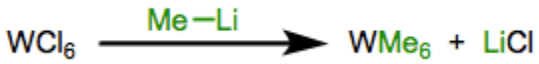


Figure 8.2.5.1: Simple and straightforward: nucleophile attacks electrophilic metal. (Copyright; author via source)

Many anionic metal complexes are nucleophilic enough to attack electrophilic sources of carbon such as alkyl and acyl halides in an **electrophilic attack** mode. An available lone pair on the metal and open coordination site are prerequisites for this chemistry. The charge on the complex increases by one unit (in effect, negative charge is transferred to the electrophile's leaving group). We can classify these as oxidative ligation reactions—notice that the oxidation state of the metal increases by two units.

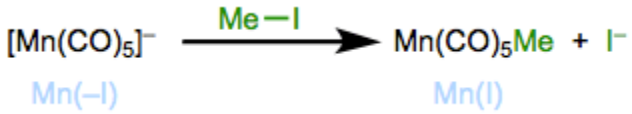


Figure 8.2.5.1: Oxidative ligation for the synthesis of alkyl complexes. Total electron count does not change. (Copyright; author via source)

Oxidative addition results in the cleavage of a W–Z bond and placement of two new X-type ligands (–W and –Z) on the metal center, with an increase in the oxidation state of the metal and the total electron count by two units. Organic halides are extremely common substrates for this reaction, the first step in the mechanism of cross-coupling reactions. The oxidized metal complex containing new alkyl and halide ligands is the final product. Notice that *two* open coordination sites are required (not necessarily simultaneously), the metal center must be amenable to two-electron oxidation, and the number of total electrons of the complex increases by two. In essence, the electrons of the W–Z bond join the complex's party. Take note that there are many known mechanisms for oxidative addition! We'll explore these different mechanisms in detail in a future post.

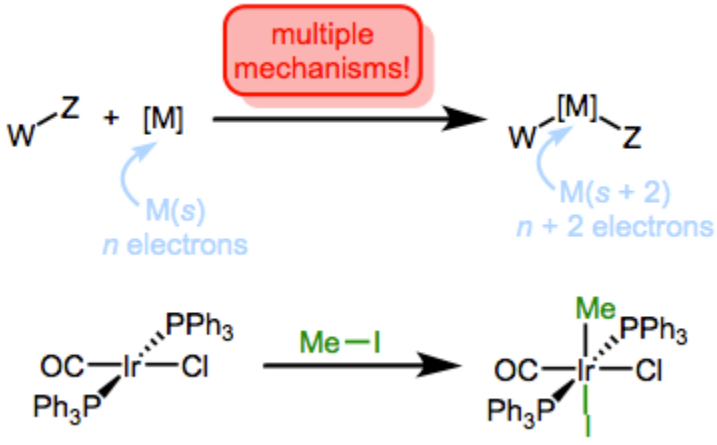


Figure 8.2.5.1: Oxidative addition, with a representative example, for the synthesis of metal alkyl complexes. (Copyright; author via source)

Finally, **migratory insertion** of unsaturated organic compounds is an important method for the synthesis of certain alkyl complexes, and an important step of organometallic reactions that result in addition across π bonds. Migratory insertion is the

microscopic reverse of β-hydride elimination. The clever among you may notice that the use of migratory insertion to synthesize alkyl complexes seems inconsistent with our observation that its reverse is ubiquitous for metal alkyls—shouldn't equilibrium favor the olefin hydride complex? In many cases this is the case; however, there are some notable exceptions. For example, perfluoroalkyl complexes are exceptionally stable (why?), so the insertion of fluoroalkenes is often favored over elimination.

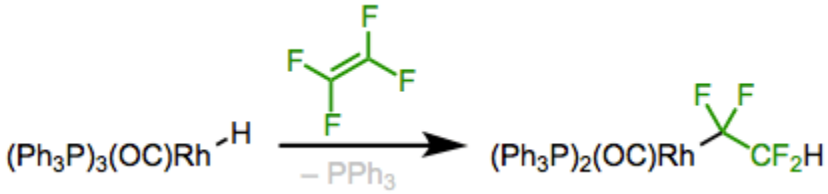


Figure 8.2.5.1: Why does this work? Thank fluorine! (Copyright; author via source)

As we noted above, we can still invoke kinetically stable alkyl complexes as *intermediates* in reactions provided subsequent steps are faster. In the next post, we'll examine the general classes of reactions in which alkyl complexes find themselves the major players, focusing on the specific mechanistic steps that involve the alkyl complex (reductive elimination, transmetalation, migratory insertion, and [naturally] β-hydride elimination).

Part 3:

In this last post on alkyl ligands, we'll explore the major modes of reactivity of metal alkyls. We've discussed β-hydride elimination in detail, but other fates of metal alkyls include reductive elimination, transmetallation, and migratory insertion into the M–C bond. In a similar manner to our studies of other ligands, we'd like to relate the steric and electronic properties of the metal alkyl complex to its propensity to undergo these reactions. This kind of thinking is particularly important when we're interested in controlling the relative rates and/or extents of two different, competing reaction pathways.

Reactions of Metal Alkyl Complexes

Recall that **β-hydride elimination** is an extremely common—and sometimes problematic—transformation of metal alkyls. Then again, there are reactions for which β-hydride elimination is desirable, such as the Heck reaction. Structural modifications that strengthen the M–H bond relative to the M–C bond encourage β-hydride elimination; the step can also be driven by trapping of the metal hydride product with a base (the Heck reaction uses this idea).

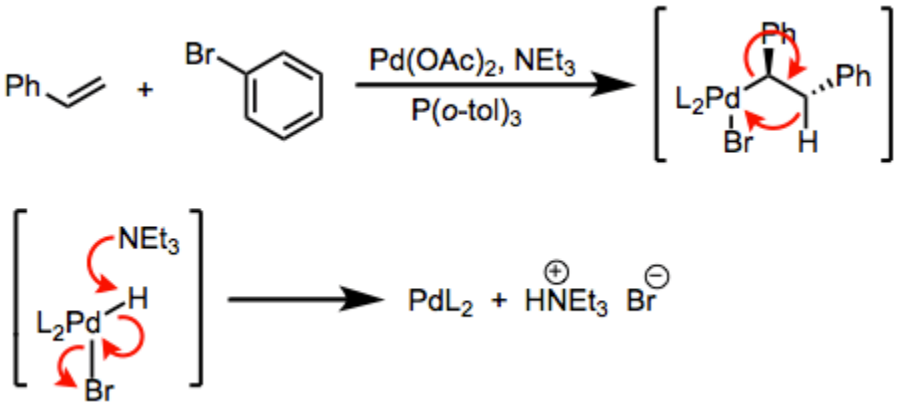


Figure 8.2.5.1: During the Heck reaction, beta-hydride elimination is driven by a base. (Copyright; author via source)

On the flip side, stabilization of the M–C bond discourages elimination and encourages its reverse: migratory insertion of olefins into M–H. Previously we saw the example of perfluoroalkyl ligands, which possess exceptionally stable M–C bonds. The fundamental idea here—that electron-withdrawing groups on the alkyl ligand stabilize the M–C bond—is quite general. Hartwig describes an increase in the "ionic character" of the M–C bond upon the addition of electron-withdrawing groups to the alkyl ligand (thereby strengthening the M–C bond, since ionic bonds are stronger than covalent bonds). Bond energies from organic chemistry bear out this idea to an extent; for instance, see the relative BDEs of Me–Me, Me–Ph, and Me–CCH in this reference. I still find this explanation a little "hand-wavy," but it serves our purpose, I suppose.

Metal alkyls are subject to **reductive elimination**, the microscopic reverse of oxidative addition. The metal loses two covalent ligands, its formal oxidation state decreases by two units, total electron count decreases by two units, and an R–X bond forms. Reductive elimination is favorable when the R–X bond in the organic product is more stable than the M–R and M–X bonds in the starting complex (a thermodynamic issue). It should be noted, however, that the kinetics of reductive elimination depend substantially on the steric bulk of the eliminating ligands. Concerted reductive elimination of R–H usually possesses a lower activation energy than R–R elimination.

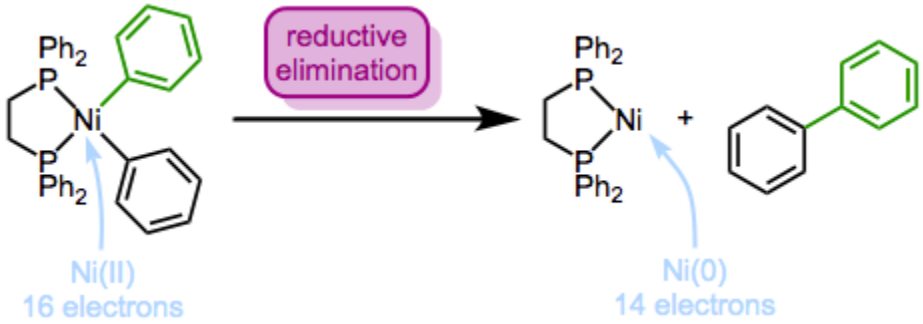


Figure 8.2.5.1: An example of reductive elimination. Intuitively, the electron density at the metal center increases as this step proceeds. (Copyright; author via source)

Transmetalation involves the transfer of an alkyl ligand from one metal to the other. An interesting problem concerns the relative reactivity of metal alkyls toward transmetalation. Assuming similar, uncomplicated ligand sets, which of two metal centers is more likely to hold on to an alkyl ligand? Consider the two situations below.

$$\mathrm{MR + M' \rightleftharpoons M + M'R}$$

$$\mathrm{MR + M'R' \rightleftharpoons MR' + M'R}$$

The first is a *bona fide* transmetalation; the second is really a double replacement reaction. The distinction is rarely drawn in practice, but it's important! The difference is that in the first case, a single-electron transfer of sorts must take place, while in the second case, no redox chemistry is necessary. Favorability in the first case is governed by the relative reduction potentials of M and M' (the reaction goes forward when M' is more easily oxidized than M); in the second case, the relative electropositivities of the metals is key, and other factors like lattice energies may be important. The distinction between transmetalation *per se* and double replacement explains the paradoxical synthetic sequence in the figure below. In practice, both are called "transmetalation." See these slides (page 6) for a summarizing reference.

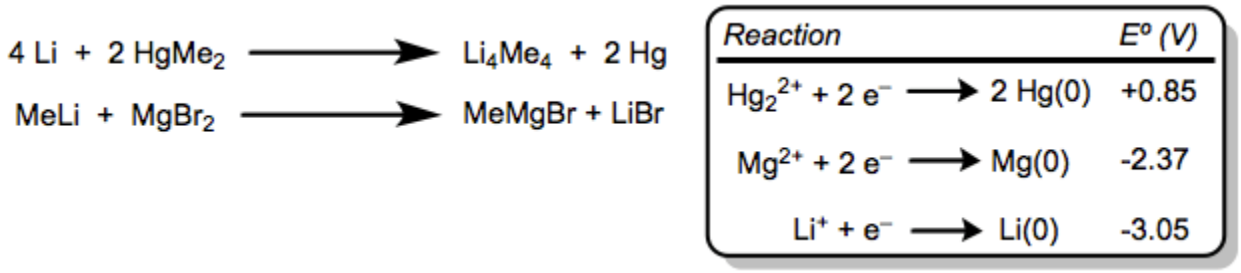


Figure 8.2.5.1: How are both of these reactions favorable? The first is a true transmetalation; the second is a double replacement. (Copyright; author via source)

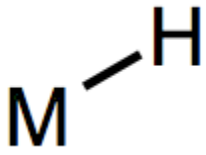
This brings our extended look at metal alkyl complexes to a temporary close. Of course, metal alkyls are *everywhere* in organometallic chemistry...so seeing them again is pretty much inevitable! The next installment in the Epic Ligand Survey series concerns allyl, cyclopentadienyl, and other odd-membered pi systems. These L_nX-type ligands can, like arenes, pile as many as six electrons on the metal center at once.

This page titled 8.2.5: Metal Alkyls is shared under a CC BY-NC-SA 4.0 license and was authored, remixed, and/or curated by Michael Evans.

- 2.5: Metal Alkyls by Michael Evans is licensed CC BY-NC-SA 4.0.

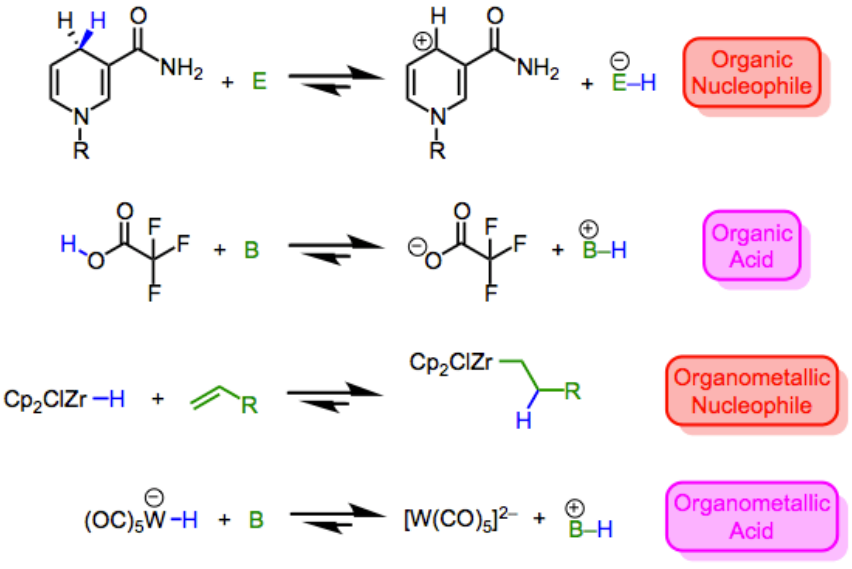
8.2.6: Metal Hydrides

Metal-hydrogen bonds, also known (misleadingly) as **metal hydrides**, are ubiquitous X-type ligands in organometallic chemistry. There is much more than meets the eye to most M-H bonds: although they're simple to draw, they vary enormously in polarization and pKa. They may be acidic or hydridic or both, depending on the nature of the metal center and the reaction conditions. In this post, we'll develop some heuristics for predicting the behavior of M-H bonds and discuss their major modes of reactivity (acidity, radical reactions, migratory insertion, etc.). We'll also touch on the most widely used synthetic methods to form metal hydrides.



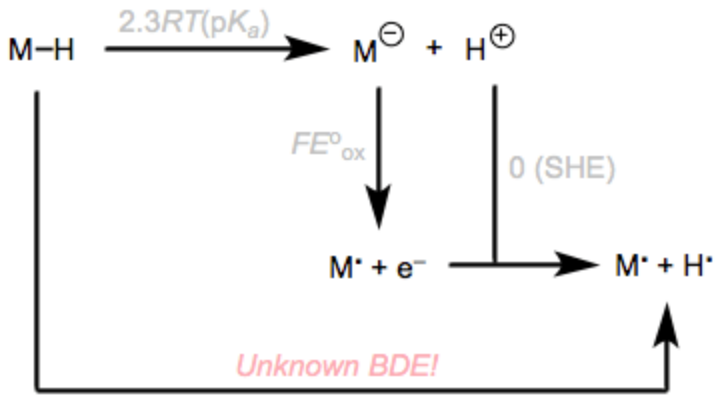
General Properties

Metal hydrides run the gamut from nucleophilic/basic to electrophilic/acidic. Then again, the same can be said of X–H bonds in organic chemistry, which may vary from mildly nucleophilic (consider Hantzsch esters and NADH) to extremely electrophilic (consider triflic acid). As hydrogen is what it is in both cases, it's clear that the nature of the X fragment—more specifically, the stability of the charged fragments X+ and X−—dictate the character of the X–H bond. Compare the four equilibria outlined below—the stabilities of the ions dictate the position of each equilibrium. By now we shouldn't find it surprising that the highly π-acidic W(CO)5 fragment is good at stabilizing negative charge; for a similar reason, the ZrCp2Cl fragment can stabilize positive charge.*



Metal-hydrogen bonds may be either hydridic (nucleophilic) or acidic (electrophilic). The nature of other ligands and the reaction conditions are keys to making predictions.

Let's turn our attention now to *homolytic* M–H bond strength. A convenient thermodynamic cycle allows us to use the acidity of M–H and the oxidation potential of its conjugate base in order to determine bond strength. This clever method, employed by Tilset and inspired by the inimitable Bordwell, uses the cycle in the figure below. BDE values for some complexes are provided as well. From the examples provided, we can see that bond strength increases down a group in the periodic table. This trend, and the idea that bridging hydrides have larger BDEs than terminal M–H bonds, are just about the only observable trends in M–H BDE.

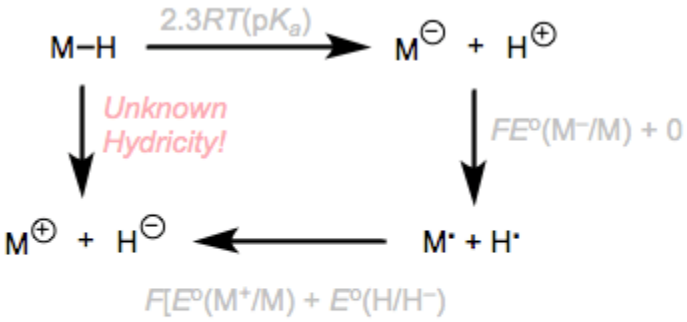


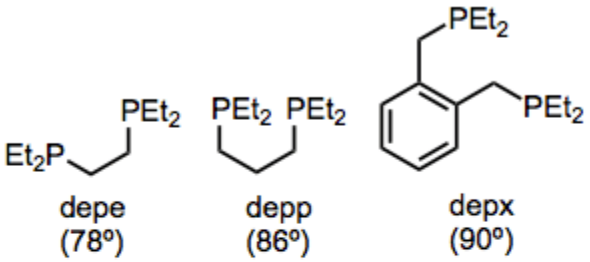
Complex	BDE (kcal/mol)
$CpCr(CO)_3H$	61
$CpMo(CO)_3H$	69
$CpW(CO)_3H$	72
$Mn(CO)_5H$	68
$Re(CO)_5H$	75

A clever cycle for determining BDEs from other known quantities, with select BDE values. I've left out solvation terms from the thermodynamic cycle. For more details, see the Tilset link above.

Why is knowing M-H BDEs useful? For one thing, the relative BDEs of M-C and M-H bonds determine the thermodynamics of β-hydride elimination, which results in the replacement of a covalent M-C bond with an M-H bond. Secondly, complexes containing weak M-H bonds are often good hydrogen transfer agents and may react with organic radicals and double bonds, channeling stannane and silane reductants from organic chemistry.

Hydricity refers to the tendency of a hydride ligand to depart as H–. A similar thermodynamic cycle relates the energetics of losing H– to the oxidation potentials of the conjugate base and the oxidized conjugate base; however, this method is complicated by the fact that hydride loss establishes an open coordination site. I've provided an abridged version of the cycle below. Hydricities are somewhat predictable from the electronic and steric properties of the metal center: inclusion of electron-donating ligands tends to increase hydricity, while electron-withdrawing or acidic ligands tend to decrease it. For five-coordinate hydrides that form 16-electron, square planar complexes upon loss of hydride, the bite angle of chelating phosphines plays an interesting role. As bite angle increases, hydricity does as well.



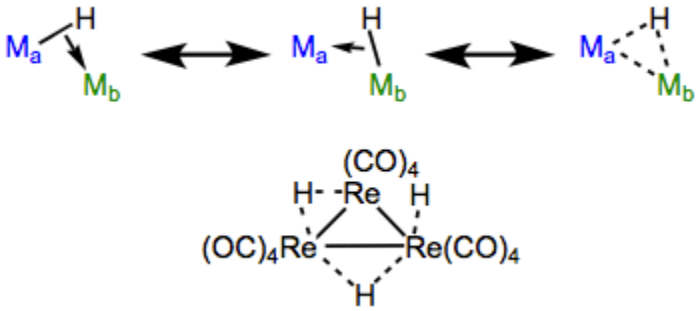


Complex	Hydricity (kcal/mol)
$HPd(depe)_2^+$	43
$HPd(depp)_2^+$	55
$HPd(depx)_2^+$	61

A thermodynamic cycle for hydricity, with some examples. Hydricity and bite angle are well correlated in five-coordinate palladium hydrides.

Bridging hydrides are an intriguing class of ligands. A question to ponder: how can a ligand associated with only two electrons possibly bridge two metal centers? How can two electrons hold three atoms together? Enter the magic of three-center, two-electron bonding. We can envision the M–H sigma bond as an electron donor itself! With this in mind, we can imagine that hydrides are able to bind end-on to one metal (like a standard X-type ligand) and side-on to another (like an L-type π system ligand, but using sigma electrons instead). Slick, no? We'll see more side-on bonding of sigma electrons in a future post on sigma

complexes.



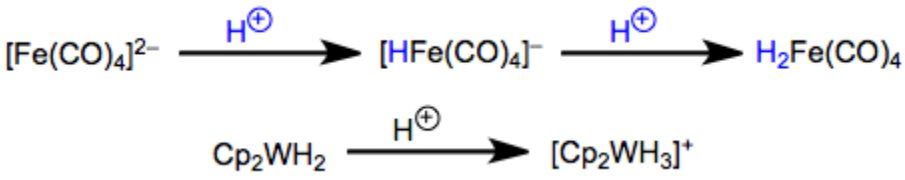
Resonance forms of bridging hydrides, with an example. Sigma complexes like these show up in other contexts, too!

Consistent with the idea that bridging is the result of "end-on + side-on" bonding, bond angles of bridging hydrides are never 180°.

Synthesis

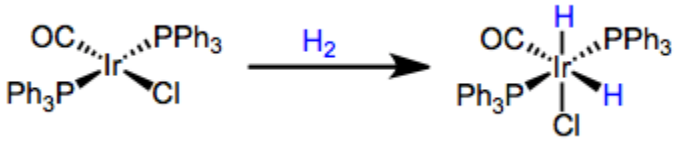
Here we'll discuss four ways to make hydrides: metal protonation, oxidative addition of H2, addition of nucleophilic main-group hydrides (borohydrides, aluminum hydrides, and silanes), and β-hydride elimination.

Just as in organic chemistry, the basicity of an organometallic complex is inversely related to the acidity of its conjugate base. Furthermore, charges have a predictable effect on the basicity of organometallic complexes: negatively charged complexes lacking π-acidic ligands are highly basic. Even neutral complexes containing strong donor ligands, like the tungsten complex below, can be protonated effectively. Notice that protonation is actually a kind of oxidative addition—the oxidation state of Fe in the first reaction below goes from -2 to 0 to +2! All coordination events of isolated electrophiles can also be viewed in this light. Reactions of this type are sometimes called **oxidative ligations** to distinguish them from oxidative addition reactions, which involve the addition of two ligands to the metal center with oxidation.



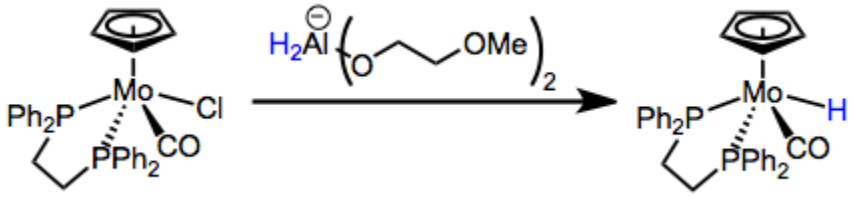
Metal protonation reactions involve the metal center as a base.

Contrast oxidative ligation with the **oxidative addition** of dihydrogen (H2), a second method for the synthesis of hydride complexes. A key requirement here is that the starting metal center is at least d2—two electrons are formally lost from the metal center, and metals can't possess a negative number of d electrons. An open coordination site on the starting material must also be present (or possible through ligand dissociation). The reaction below is a standard example of the addition of H2 to Vaska's complex, but there are some funky variations on this theme. These riffs include third-order homolytic cleavage of H2 by two metal radicals, and oxidative addition followed by deprotonation by the starting complex (apparent heterolytic cleavage).



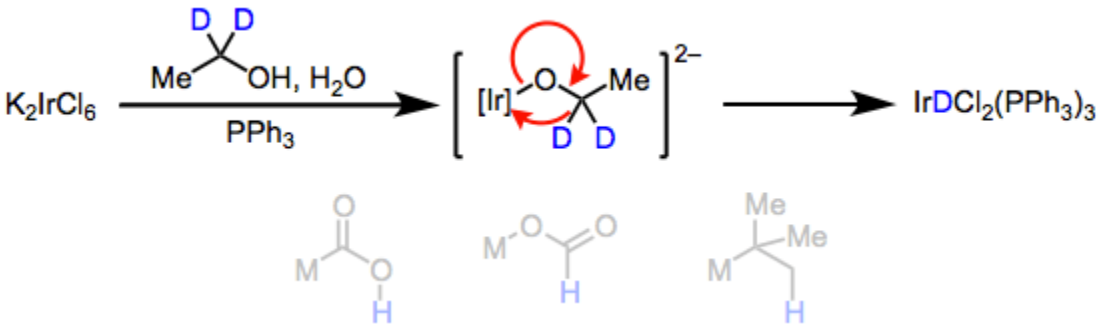
Oxidative addition of dihydrogen for the synthesis of metal hydrides.

Main-group hydrides like borohydrides and aluminum hydrides are great sources of H– for organometallic complexes. These reactions seem more natural than metal protonations, since we often think of metals as electropositive or electrophilic species. Indeed, the combination of main-group sources of nucleophilic hydride with complexes containing metal–leaving group bonds is a very general method for the synthesis of metal hydride complexes. Check out the reaction below—what's the most likely mechanism? Is associative or dissocative substitution more likely? Hint: count electrons!



Nucleophilic substitution with a hydride source. What's the most likely mechanism?

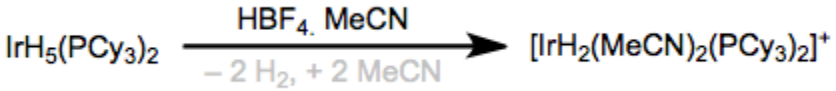
β-hydride elimination forms metal hydride complexes and double bonds within organic ligands. Alkoxide ligands are commonly used for this purpose—elimination to form the hydride complex and aldehyde is more favorable than the reverse, migratory insertion of C=O into the M–H bond. Since the unsaturated byproduct is thrown away, it's desirable to make it something small, cheap, and gaseous. Hydroxycarbonyl, formate, and tert-butyl ligands have been applied successfully with this goal in mind...what are the byproducts?



Beta-hydride elimination for the synthesis of metal hydrides.

Reactions

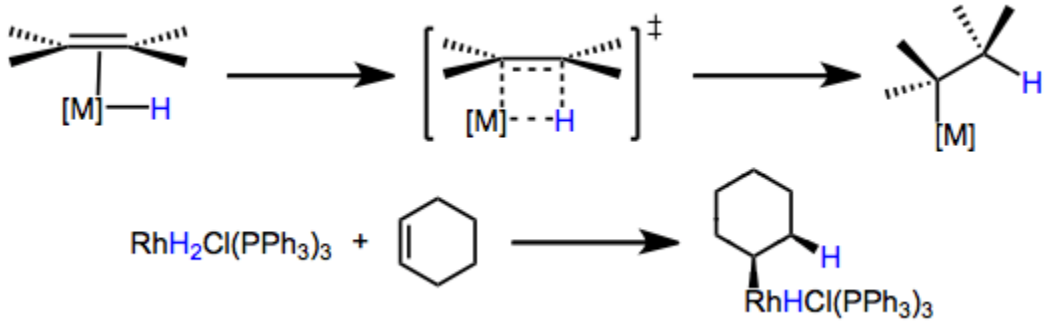
Metal hydrides are characterized by nucleophilic, electrophilic, and radical behavior. The exact behavior of a given metal hydride complex depends on its electronic properties, its M–H bond dissociation energy, and the nature of the reacting partner. Basic metal hydrides react with acids to free up a coordination site on the metal center (file this reaction alongside photolytic M–CO cleavage and M–CO cleavage with amine oxides).



"Protonolysis" generates two open coordination sites with loss of hydrogen gas.

Migratory insertion reactions involving M–H bonds are extremely important in a practical sense (see hydrogenation and hydroformylation), and are conceptually related to nucleophilic hydride transfers from the metal center. We can think of insertions of π bonds into M–H as internal nucleophilic attack by the hydride ligand at one end of the π bond, with coordination of the metal center to the other. The figure below depicts the transition state for migratory insertion of an olefin into M–H and an example reaction. Notice the coplanarity of M, H, and the C=C bond in the transition state for insertion, which determines the cis configuration of the product. The same is required for the microscopic reverse (β-hydride elimination) but this essential geometry

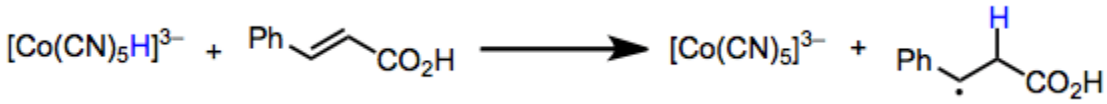
is easily overlooked for β-hydride elimination.



Migratory insertion of an olefin into M–H. Note the relative configuration of M–C and C–H!

It is important to note that insertions of CO into M–H bonds are rare, because such insertions are usually unfavorable thermodynamically.

Finally, the radical behavior of certain metal hydrides in the presence of olefins deserves a nod. The behavior of the cobalt hydride complex in the reaction below is typical of these types of reactions.



Hydrogen atom transfer to olefins. Radical reduction of carbon tetrachloride is a related process.

And there you have it: the properties, synthesis, and reactivity of metal hydrides in a nutshell. Like other ligands we've seen so far, the behavior of hydrides is controlled by the nature of the metal center and its accompanying ligands. However, it's interesting to note that the observed behavior of hydrides often depends on the nature of the reaction conditions, as well. Some complexes display "schizophrenic" behavior, so to speak, putting on their nucleophile hat in the presence of an electrophile and their electrophile hat in the presence of a nucleophile.

This page titled 8.2.6: Metal Hydrides is shared under a CC BY-NC-SA 4.0 license and was authored, remixed, and/or curated by Michael Evans.

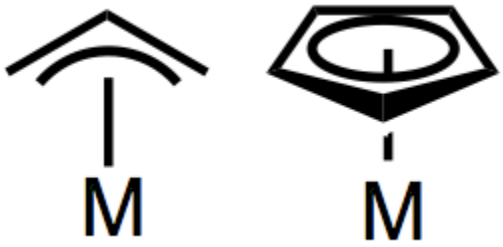
- 2.6: Metal Hydrides by Michael Evans is licensed CC BY-NC-SA 4.0.

8.2.7: N-heterocyclic Carbenes

This page titled 8.2.7: N-heterocyclic Carbenes is shared under a CC BY-NC-SA 4.0 license and was authored, remixed, and/or curated by Michael Evans.

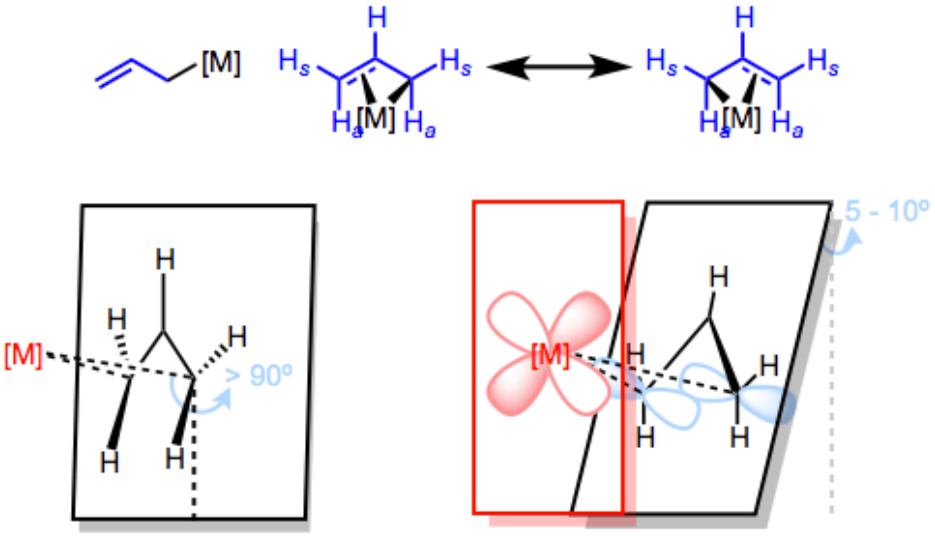
8.2.8: Odd-numbered π Systems

Odd-numbered π systems—most notably, the allyl and cyclopentadienyl ligands—are formally LnX-type ligands bound covalently through one atom (the “odd man out”) and datively through the others. This formal description is incomplete, however, as resonance structures reveal that multiple atoms within three- and five-atom π systems can be considered as covalently bound to the metal. To illustrate the plurality of equally important resonance structures for this class of ligands, we often just draw a curved line from one end of the π system to the other. Yet, even this form is not perfect, as it obscures the possibility that the datively bound atoms may dissociate from the metal center, forming σ-allyl or ring-slipped ligands. What do the odd-numbered π systems really look like, and how do they really behave?



General Properties

Allyls are often actor ligands, most famously in allylic substitution reactions. The allyl ligand is an interesting beast because it may bind to metals in two ways. When its double bond does not become involved in binding to the metal, allyl is a simple X-type ligand bound covalently through one carbon—basically, a monodentate alkyl! Alternatively, allyl can act as a bidentate LX-type ligand, bound to the metal through all three conjugated atoms. The LX or “trihapto” form can be represented using one of two resonance forms, or (more common) the “toilet-bowl” form seen in the general figure above. I don’t like the toilet-bowl form despite its ubiquity, as it tends to obscure the important dynamic possibilities of the allyl ligand.

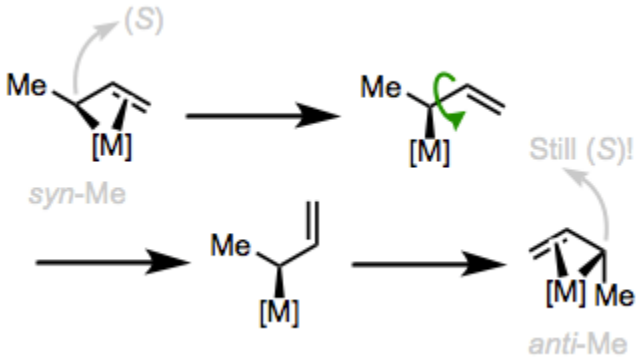


Can we use FMO theory to explain the wonky geometry of the allyl ligand?

The lower half of the figure above illustrates the slightly weird character of the geometry of allyl ligands. In a previous post on even-numbered π systems, we investigated the orientation of the ligand with respect to the metal and came to some logical

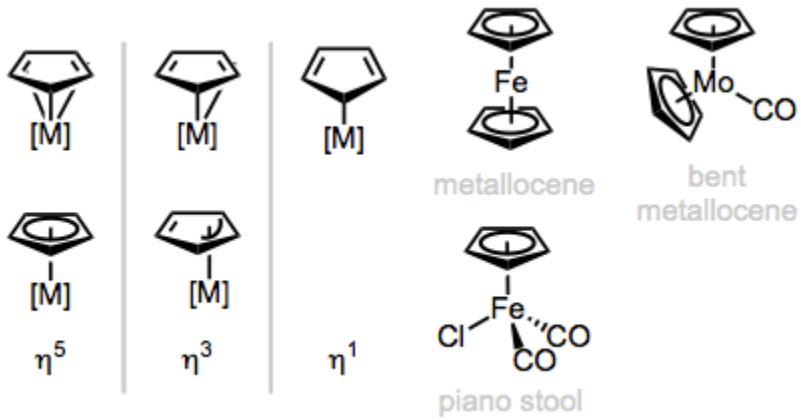
conclusions by invoking FMO theory and backbonding. A similar treatment of the allyl ligand leads us to similar conclusions: the plane of the allyl ligand should be parallel to the xy-plane of the metal center and normal to the z-axis. In reality, the allyl plane is slightly canted to optimize orbital overlap—but we can see at the right of the figure above that π2–dxy orbital overlap is key. Also note the rotation of the anti hydrogens (anti to the central C–H, that is) toward the metal center to improve orbital overlap.

Exchange of the syn and anti substituents can occur through σ,π-isomerization followed by bond rotation and formation of the isomerized trihapto form. Notice that the configuration of the stereocenter bearing the methyl group is unaffected by the isomerization! It should be noted that 1,3-disubstituted allyl complexes almost exclusively adopt a syn,syn configuration without danger of isomerization.



The methylene and central C–H simply change places!

Upon deconstruction, the cyclopentadienyl (Cp) ligand yields the aromatic cyclopentadienyl anion, an L2X-type ligand. Cp is normally an η5-ligand, but η3 (LX) and η1 (X) forms are known in cases where the other ligands on the metal center are tightly bound. η1-Cyclopentadienyl ligands can sometimes be fluxional—the metal has the ability to "jump" from atom to atom. Variations on the Cp theme include Cp* (C5Me5) and the monomethyl version (C5H4Me). Cp may be found as a loner alongside other ligands (in "half-sandwich" or "piano-stool" complexes), or paired up with a second Cp ligand in metallocenes. The piano-stool and bent metallocene complexes are most interesting for us, since these have potential for open coordination sites—plain vanilla metallocenes tend to be relatively stable and boring.

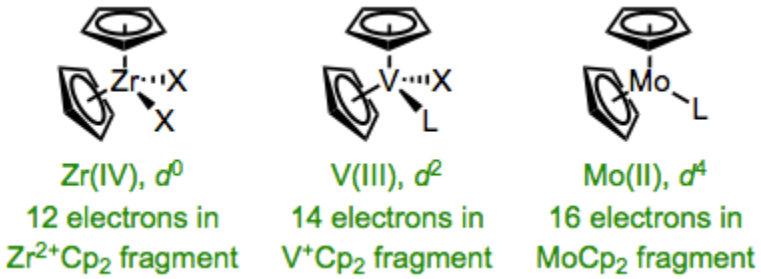


Binding modes of Cp and general classes of Cp complexes.

Research for this post has made me appreciate the remarkable electron-donating ability of the cyclopentadienyl (Cp) ligand, which renders its associated metal center electron rich. The LUMO of Cp is high in energy, so the ligand is a weak π-acid and is, first and foremost, a σ-donor. This effect is apparent in the strong backbonding displayed by Cp carbonyl complexes. Despite its strong donating ability, Cp is rarely an actor ligand unless another ligand shakes things up—check out the nucleophilic reactivity of doubly jazzed-up ferrocene for a nice example.

It's critical to recognize that η5-Cp is a six-electron ligand (!). Because Cp piles on electrons, the numbers of ligands bound to

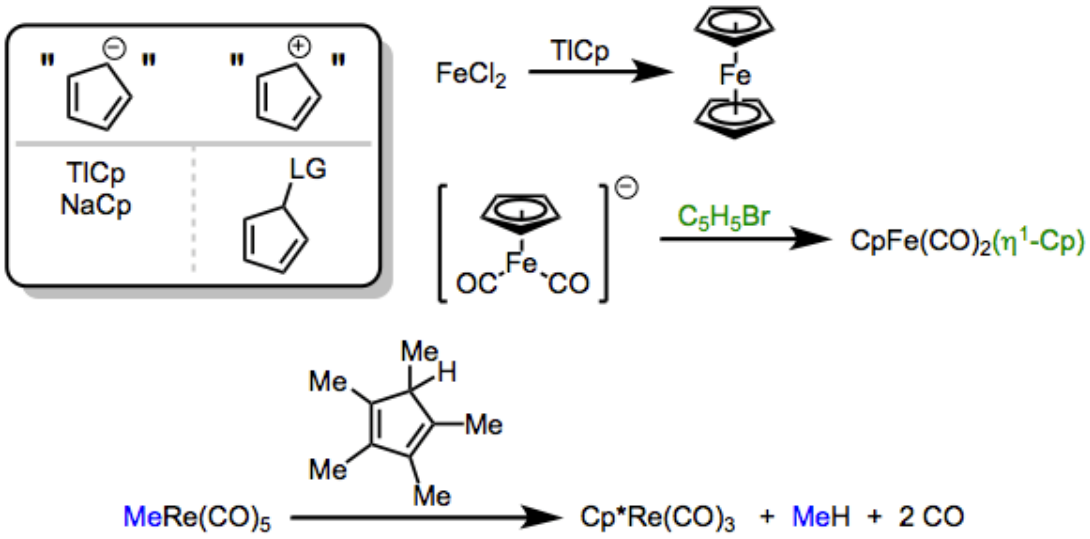
the metal in Cp complexes tend to be lower than we might be used to, especially in bent metallocenes containing two Cp's. Still, the number of ligands we'd expect on the metal center in these complexes is perfectly predictable. We just need to keep in mind that the resulting complexes are likely to contain 16 or 18 total electrons.



By considering the MCp2 fragment, we can predict the nature of ancillary ligands in bent metallocenes.

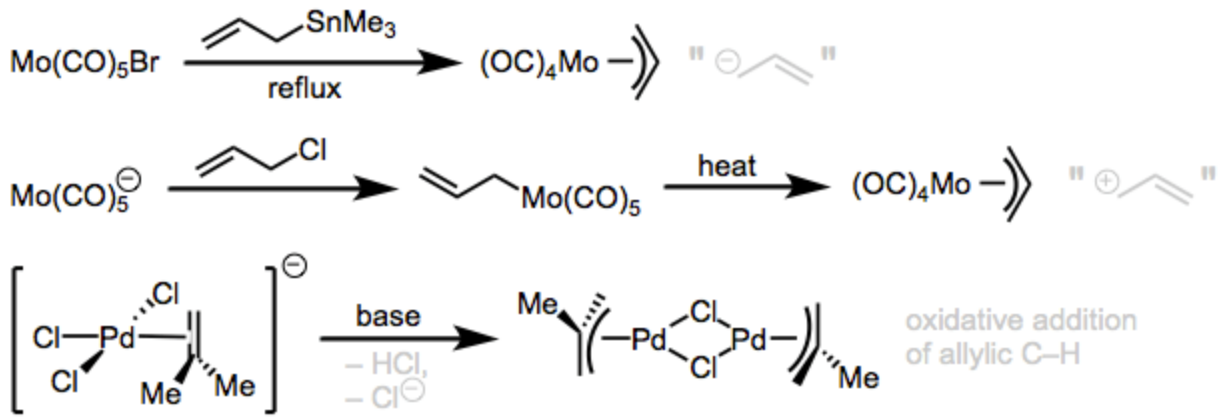
Synthesis

Crabtree cleanly divides methods for the synthesis of Cp complexes into those employing Cp+ equivalents, Cp– equivalents, and the neutral diene. Naturally, the first class of reagents are appropriate for electron-rich, nucleophilic complexes, while the second class are best used in conjunction with electron-poor, electrophilic complexes. The figure below provides a few examples.



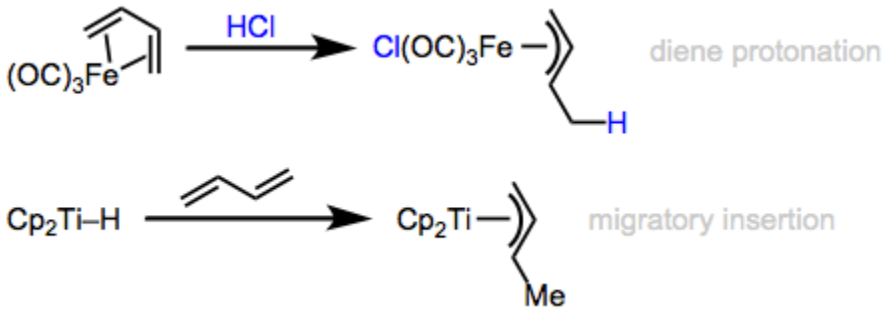
Methods for the synthesis of Cp complexes. The possibilities are exhausted by anionic, cationic, and neutral Cp equivalents!

Methods for synthesizing allyl complexes can also be classified according to whether the allyl donor is a cationic, anionic, or neutral allyl equivalent. In metal-catalyzed allylic substitution reactions, the allyl donor is usually a good electrophile bearing a leaving group displaced by the metal (an allyl cation equivalent). However, similar complexes may be obtained through oxidative addition of an allylic C–H bond to the metal, as in the synthesis of methallyl palladium chloride dimer below. Transmetalation of nucleophilic allyls from one metal to another, which we can imagine as nucleophilic attacks of an anionic allyl group, are useful when the metal is electron-poor.



Nucleophilic, electrophilic, and neutral allyl donors.

Complexes containing conjugated dienes are also viable precursors to allyl complexes. Migratory insertion of a diene into the M–H bond is a nice route to methyl-substituted allyl complexes, for example. Interestingly, analogous insertions of fulvenes do not appear to lead to Cp complexes, but some funky reductive couplings that yield ansa-metallocenes are known. External electrophilic attack (e.g., protonation) and nucleophilic attack on coordinated dienes also result in allyl complexes. In essence, one double bond of the diene becomes a part of the allyl ligand in the product; the other is used as a "handle" to establish the key covalent bond to the allyl ligand.

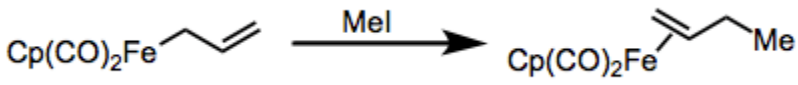


Dienes: brave crusaders in the quest for allyl complexes.

Reactions

Since the Cp ligand is typically a spectator, we'll focus in this section on the reactivity of allyl ligands. As usual, the behavior of the allyl ligand depends profoundly on the nature of its coordinated metal center, which depends in turn on the metal's ancillary ligands. Avoid "tunnel vision" as you study the examples below—depending on the issue at hand, the ancillary ligands may be as important as (or more important than) the actor ligand.

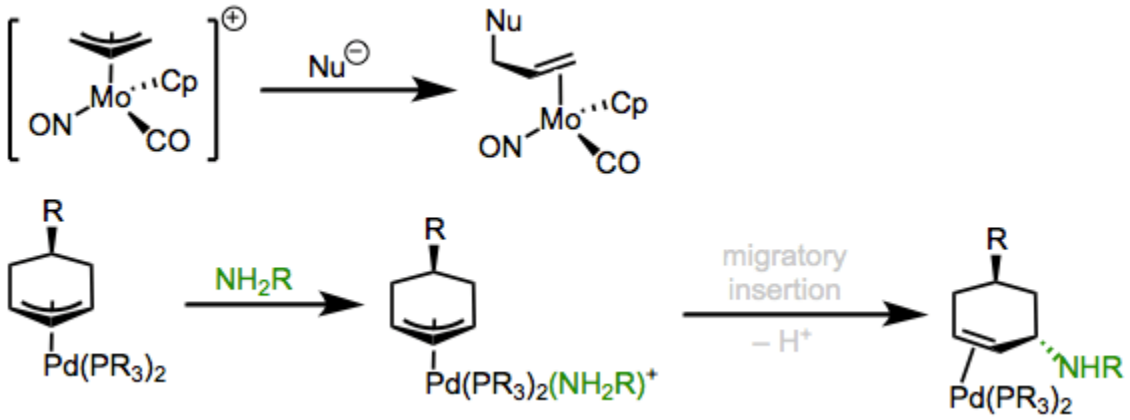
Nucleophilic allyl complexes react with electrophiles like H+, MeI, X+, and acylium ions to yield cationic alkene complexes.



Attack of electrophiles on nucleophilic allyl complexes. Notice the donating Cp ligand!

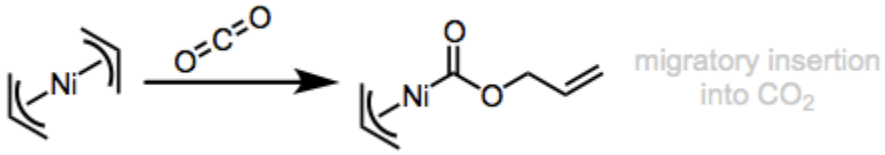
In a conceptually related process, nucleophiles can attack allyl ligands bound to electrophilic metals. This process is key in allylic substitution reactions. In some cases, the nucleophile is known to bind to the metal first, then transfer to the allyl ligand through reductive elimination. Alternatively, direct attack on the allyl ligand may occur on the face opposite the metal. The figure below

illustrates both possibilities.



External and internal attack of nucleophiles on coordinated allyl ligands.

Migratory insertion of allyl ligands is known, and is analogous to insertions involving alkyl ligands (see the figure below). Movement of the allyl ligand toward the coordination site of the dative ligand is assumed. Of course if oxidative addition to form allyl complexes is possible, reductive elimination of allyl ligands with other X-type ligands is also possible. We'll hit on these process in more detail in their dedicated posts.



Like alkyl ligands, allyls can migrate onto dative ligands like CO and π bonds.

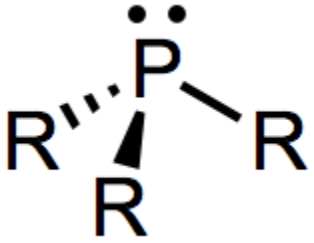
One final post on σ-complexes will bring this series to a temporary close. In the next post, we'll look at ligands that, rather surprisingly, bind through their σ-electrons. These "non-classical" ligands behave like other dative ligands we've seen before, but are important for many reactions that involve main-group single bonds, such as oxidative addition. Before their discovery, the relevance of σ-ligands for reaction mechanisms went unappreciated by organometallic chemists.

This page titled 8.2.8: Odd-numbered π Systems is shared under a CC BY-NC-SA 4.0 license and was authored, remixed, and/or curated by Michael Evans.

- 2.8: Odd-numbered π Systems by Michael Evans is licensed CC BY-NC-SA 4.0.

8.2.9: Phosphines

The epic ligand survey continues with tertiary phosphines, PR_3. Phosphines are most notable for their remarkable electronic and steric tunability and their "innocence"—they tend to avoid participating directly in organometallic reactions, but have the ability to profoundly modulate the electronic properties of the metal center to which they're bound. Furthermore, because the energy barrier to umbrella flipping of phosphines is quite high, "chiral-at-phosphorus" ligands can be isolated in enantioenriched form and introduced to metal centers, bringing asymmetry just about as close to the metal as it can get in chiral complexes. Phosphorus NMR is a technique that Just Works (thanks, nature). Soft phosphines match up very well with the soft low-valent transition metals. Electron-poor phosphines are even good π-acids!

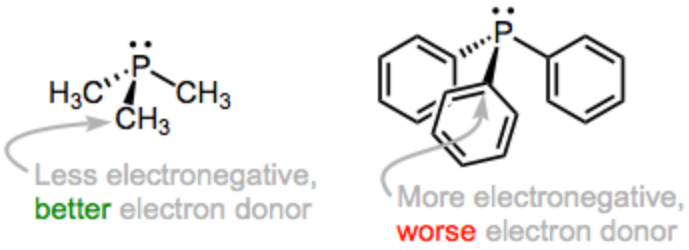


General Properties

Like CO, phosphines are dative, L-type ligands that formally contribute two electrons to the metal center. Unlike CO, most phosphines are not small enough to form more than four bonds to a single metal center (and for large R, the number is even smaller). Steric hindrance becomes a problem when five or more PR_3 ligands try to make their way into the space around the metal. An interesting consequence of this fact is that many phosphine-containing complexes do not possess 18 valence electrons. Examples include $Pt(PCy_3)_2$, $Pd[P(t\text{-}Bu)_3]_2$, and $[Rh(PPh_3)_3]^+$. Doesn't that just drive you crazy? It drives the complexes crazy as well—and most of these coordinatively unsaturated compounds are wonderful catalysts.

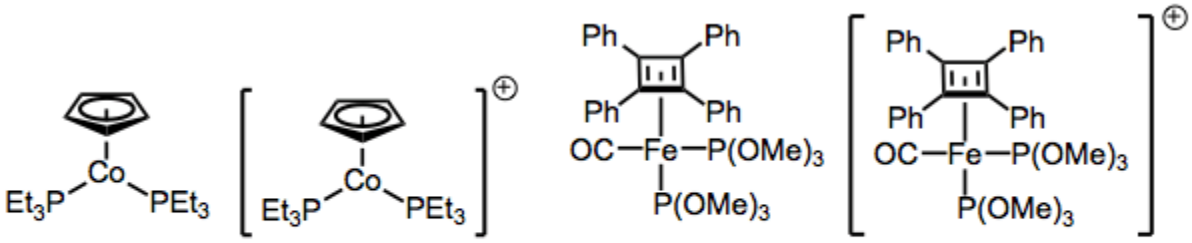
Bridging by phosphines is extremely rare, but ligands containing multiple phosphine donors that bind in an L_n ($n > 1$) fashion to a single metal center are all over the place. These ligands are called chelating or polydentate to indicate that they latch on to metal centers through multiple binding sites. For entropic reasons, chelating ligands bind to a single metal center at multiple points if possible, instead of attaching to two different metal centers (the aptly named chelate effect). An important characteristic of chelating phosphines is bite angle, defined as the predominant P–M–P angle in known complexes of the ligand. We'll get into the interesting effects of bite angle later, but for now, we might imagine how "unhappy" a ligand with a preferred bite angle of 120° would be in the square planar geometry. It would much rather prefer to be part of a trigonal bipyramidal complex, for instance.

The predominant orbital interaction contributing to phosphine binding is the one we expect, a lone pair on phosphorus interacting with an empty metallic d orbital. The electronic nature of the R groups influences the electron-donating ability of the phosphorus atom. For instance, alkylphosphines, which possess P–Csp^3 bonds, tend to be better electron donors than arylphosphines, which possess P–Csp^2 bonds. The rationale here is the greater electronegativity of the sp^2 hybrid orbital versus the sp3 hybrid, which causes the phosphorus atom to hold more tightly to its lone pair when bound to an sp^2 carbon. The same idea applies when electron-withdrawing and -donating groups are incorporated into R: the electron density on P is low when R contains electron-withdrawing groups and high when R contains electron-donating groups. Ligands (and associated metals) in the former class are called electron poor, while those in the latter class are electron rich.



As we add electronegative R groups, the phosphorus atom (and the metal to which it's bound) become more electron poor.

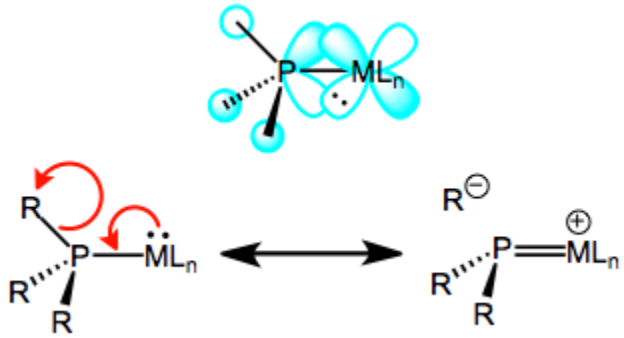
Like CO, phosphines participate in backbonding to a certain degree; however, the phenomenon here is of a fundamentally different nature than CO backbonding. For one thing, phosphines lack a π* orbital. In the days of yore, chemists attributed backbonding in phosphine complexes to an interaction between a metallic dπ orbital and an empty 3d orbital on phosphorus. However, this idea has elegantly been proven bogus, and a much more organicker-friendly explanation has taken its place (no d orbitals on P required!). In an illuminating series of experiments, M–P and P–R bond lengths were measured via crystallography for several redox pairs of complexes. I've chosen two illustrative examples, although the linked reference is chock full of other pairs. The question is: how do we explain the changes in bond length upon oxidation?



M–P	2.218 Å	2.230 Å	**M–P**	2.146 Å	2.261 Å
P–R	1.846 Å	1.829 Å	**P–R**	1.598 Å	1.578 Å

Upon oxidation, M–P bond lengths increase and and P–R bond lengths decrease. Why?

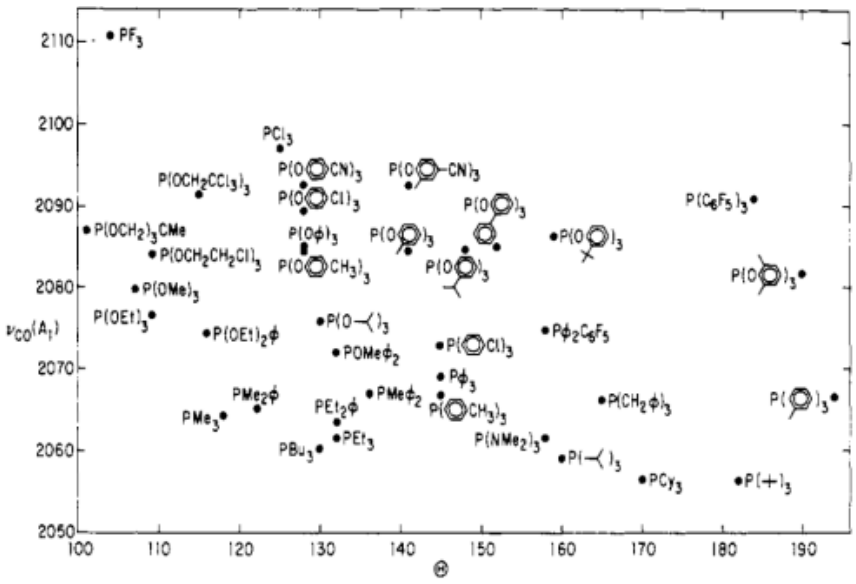
Oxidation decreases the ability of the metal to backbond, because it removes electron density from the metal. This explains the increases in M–P bond length—just imagine a decrease the M–P bond order due to worse backbonding. And the decrease in P–R bond length? It's important to see that invoking only the phosphorus 3d orbitals would not explain changes in the P–R bond lengths, as the 3d atomic orbitals are most definitely localized on phosphorus. Instead, we must invoke the participation of σ*P–R orbitals in phosphine backbonding to account for the P–R length decreases. When all is said and done, the LUMO of the free phosphine has mostly P–R antibonding character, with some 3d thrown into the mix. The figure below depicts one of the interactions involved in M–P backbonding, a dπ → σ* interaction (an orthogonal dπ → σ* interaction also plays a role). As with CO, a resonance structure depicting an M=P double bond is a useful heuristic! Naturally, R groups that are better able to stabilize negative charge—that is, electron-withdrawing groups—facilitate backbonding in phosphines. Electron-rich metals help too.



Backbonding in phosphines, a sigma-bond-breaking affair.

The steric and electronic properties of phosphines vary enormously. Tolman devised some intriguing parameters that characterize the steric and electronic properties of this class of ligands. To address sterics, he developed the idea of cone angle—the apex angle of a cone formed by a point 2.28 Å from the phosphorus atom (an idealized M–P bond length), and the outermost edges of atoms in the R groups, when the R groups are folded back as much as possible. Wider cone angles, Tolman reasoned, indicate greater steric congestion around the phosphorus atom. To address electronics, Tolman used a not-so-old friend of ours—the CO stretching frequency (νCO) of mixed phosphine-carbonyl complexes. Specifically, he used Ni(CO)3L complexes, where L is a tertiary phosphine, as his standard. Can you anticipate Tolman's logic? How should νCO change as the electron-donating ability of the phosphine ligands increases?

Tolman's logic went as follows: more strongly electron-donating phosphines are associated with more electron-rich metals, which are better at CO backbonding (due fundamentally to higher orbital energies). Better CO backbonding corresponds to a lower νCO due to decreased C–O bond order. Thus, better donor ligands should be associated with lower νCO values (and vice versa for electron-withdrawing ligands). Was he correct? Exhibit A...

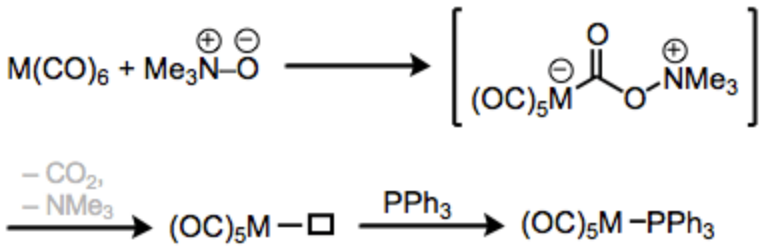


Tolman's map of the steric and electronic properties of phosphine ligands.

Notice the poor ligand trifluorophosphine stuck in the "very small, very withdrawing" corner, and its utter opposite, the gargantuan tri(tert-butyl)phosphine in the "extremely bulky, very donating" corner. Intriguing! One can learn a great deal just by studying this chart.

Synthesis

Phosphine complexes are most commonly made through ligand substitution processes—the exchange of one ligand for another on a metal center. One interesting method utilizes tertiary N-oxides to essentially "oxidize off" a CO ligand, leaving behind an open coordination site that may be filled by a phosphine. Notice that the carbon of CO is behaving as an electrophile in this process. Shi and Basolo masterfully demonstrate that an intermediate amine complex cannot be involved in this mechanism. Irradiation by ultraviolet light is an alternative method to coax the CO ligand off of metal carbonyl complexes.



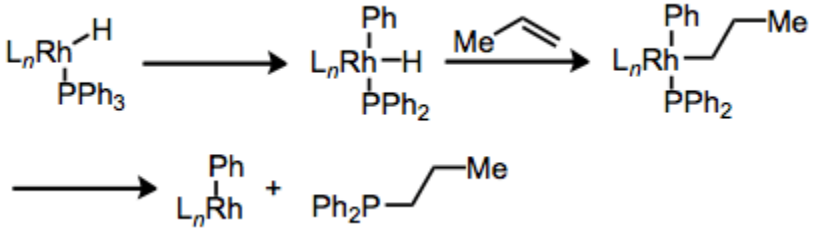
Ligand substitution with the help of trimethylamine oxide.

Methods for synthesizing the phosphine ligands themselves are somewhat beyond our scope, but electrophilic phosphorus chemistry is common, particularly when arylphosphines are the target.

Reactions

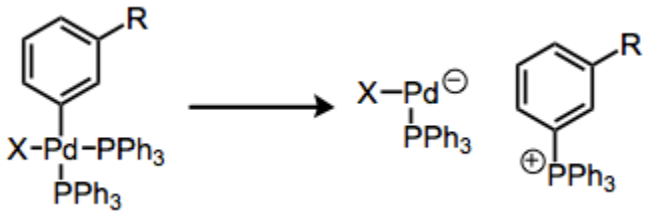
Phosphines are most often spectator ligands, meaning that they don't participate in reactions, but hang on for the ride. There are, however, some important exceptions to this rule. First of all, dissociation of a phosphine ligand is often required to generate a site of coordinative unsaturation before catalytic reactions can begin. Good examples are cross-couplings employing the saturated $Pd(PPh_3)_4$. This complex is actually just a precatalyst that must lose phosphine ligands to enter the catalytic cycle of cross-coupling. Phosphine association is also an important step of many catalytic reactions.

What decomposition pathways are available to phosphine ligands? P–C bond cleavage is a surprisingly common process. In general, the idea is that the metal center can insert into the P–C bond via concerted oxidative addition, then reductively eliminate to establish a new P–C bond. Reductive elimination can even occur after some intermediate steps, as in the example below.



P–C bond cleavage: also known as the "R group shuffle."

Phosphonium salt formation from arylphosphine complexes is a related process. Here, the complex essentially just falls apart after P–C reductive elimination.



Reductive elimination to form phosphonium salts.

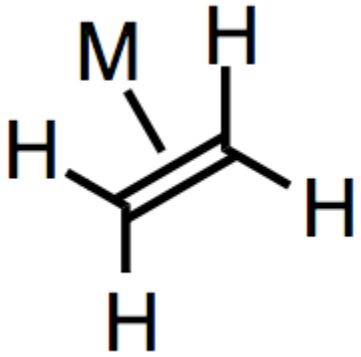
Phosphine ligands are everywhere, and we'll definitely see more of this fascinating class of ligands in the future. They are particularly powerful as the bearers of asymmetry in chiral metal complexes, which are used to prepare enantioenriched organic products.

This page titled 8.2.9: Phosphines is shared under a CC BY-NC-SA 4.0 license and was authored, remixed, and/or curated by Michael Evans.

- 2.9: Phosphines by Michael Evans is licensed CC BY-NC-SA 4.0.

8.2.10: π Systems

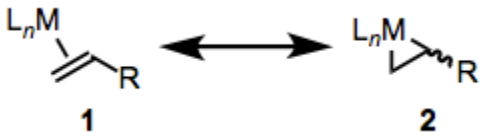
With this post, we finally reach our first class of dative **actor** ligands, **π systems**. In contrast to the **spectator** L-type ligands we've seen so far, π systems most often play an important role in the reactivity of the OM complexes of which they are a part (since they act in reactions, they're called "actors"). π Systems do useful chemistry, not just with the metal center, but also with other ligands and external reagents. Thus, in addition to thinking about how π systems affect the steric and electronic properties of the metal center, we need to start considering the metal's effect on the ligand and how we might expect the ligand to behave as an active participant in reactions. To the extent that structure determines reactivity—a commonly repeated, and extremely powerful maxim in organic chemistry—we can think about possibilities for chemical change without knowing the elementary steps of organometallic chemistry in detail yet.



General Properties

The π bonding orbitals of alkenes, alkynes, carbonyls, and other unsaturated compounds may overlap with dσ orbitals on metal centers. This is the classic ligand HOMO → metal LUMO interaction that we've beaten into the ground over the last few posts. Because of this electron donation from the π system to the metal center, coordinated π systems often act electrophilic, even if the starting alkene was nucleophilic (the **Wacker oxidation** is a classic example; water attacks a palladium-coordinated alkene). The π → dσ orbital interaction is central to the structure and reactivity of π-system complexes.

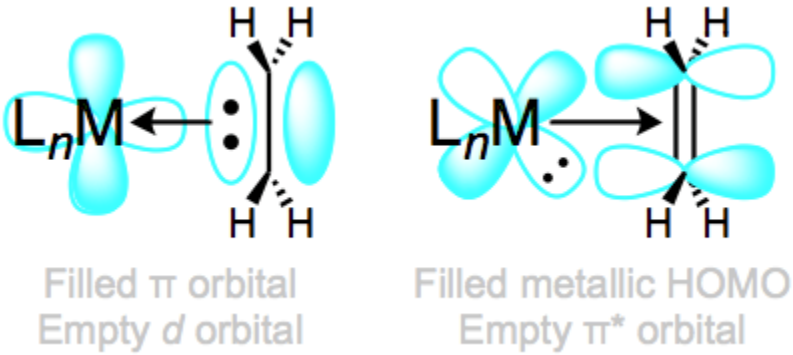
Then again, a theme of the last three posts has been the importance of orbital interactions with the opposite sense: metal HOMO → ligand LUMO. Like CO, phosphines, and NHCs, π systems are often subject to important backbonding interactions. We'll focus on alkenes here, but these same ideas apply to carbonyls, alkynes, and other unsaturated ligands bound through their π clouds. For alkene ligands, the relative importance of "normal" bonding and backbonding is nicely captured by the relative importance of the two resonance structures in the figure below.



Resonance forms of alkene ligands.

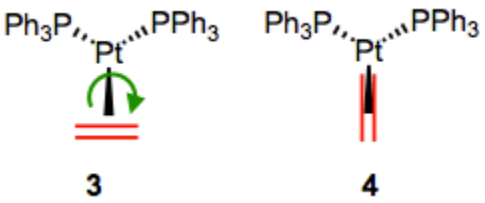
Complexes of weakly backbonding metals, such as the electronegative late metals, are best represented by the traditional dative resonance structure **1**. But complexes of strong backbonders, such as electropositive Ti(II), are often best drawn in the **metallacyclopropane** form **2**. Organic hardliners may have a tough time believing that **1** and **2** are truly resonance forms, but several studies—e.g. of the Kulinkovich cyclopropanation—have shown that independent synthetic routes to metallacyclopropanes and alkene complexes containing the same atoms result in the same compound. Furthermore, bond lengths and angles in the alkene change substantially upon coordination to a strongly backbonding metal. We see an elongation of the C=C bond (consistent with decreased bond order) and some pyramidalization of the alkene carbons (consistent with a change in hybridization from sp2 to sp3). A complete orbital picture of "normal" bonding and backbonding in alkenes is shown in the figure

below.



Normal bonding and backbonding in alkene complexes.

Here's an interesting question with stereochemical implications: what is the orientation of the alkene relative to the other ligands? From what we've discussed so far, we can surmise that one face of the alkene must point toward the metal center. Put differently, the bonding axis must be normal to the plane of the alkene. However, this restriction says nothing about rotation about the bonding axis, which spins the alkene ligand like a pinwheel. Is a particular orientation preferred, or can we think about the alkene as a circular smudge over time? The figure below depicts two possible orientations of the alkene ligand in a trigonal planar complex. Other orientations make less sense because they would involve inefficient orbital overlap with the metal's orthogonal d orbitals. Which one is favored?



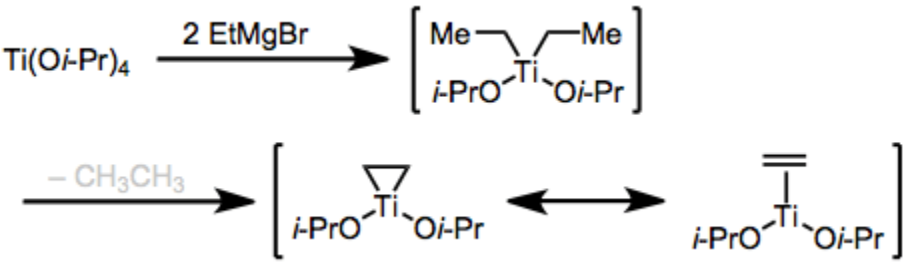
Two limiting cases for alkene orientation in a trigonal planar complex.

First of all, we need to notice that these two complexes are **diastereomeric**. They have different energies as a result, so one must be favored over the other. Naive steric considerations suggest that complex **4** ought to be more stable (in most complexes, steric factors dictate alkene orientation). To dig a little deeper, let's consider any electronic factors that may influence the preferred geometry. We've already seen that electronic factors can overcome steric considerations when it comes to complex geometry! To begin, we need to consider the crystal field orbitals of the complex as a whole. Verify on your own that in this d10, Pt(0) complex, the crystal-field HOMOs are the dxy and dx2–y2 orbitals. Where are these orbitals located in space? In the xy-plane! Only the alkene in **3** can engage in efficient backbonding with the metal center. In cases when the metal is electron rich and/or the alkene is electron poor, complexes like **3** can sometimes be favored in spite of sterics. The thought process here is very similar to the one developed in an earlier post on geometry. However, please note that this situation is fairly rare—steric considerations often either match or dominate electronics where alkenes are concerned.

Synthesis

Alkene and alkyne complexes are most often made via **ligand substitution** reactions, which simply exchange one ligand for another. A nice example of a stable alkene complex synthesized via ligand substitution is [Ir(COD)Cl]2, made from IrCl3 and cyclooctadiene. Similarly, the inimitable Pd2(dba)3 may be prepared from PdCl42– and dibenzylideneacetone (dba). In truth, only a few stable alkene and alkyne complexes find use as organometallic precatalysts and/or catalysts. Substitutions of alkenes for phosphine ligands can be rendered easy, so phosphine precatalysts may be used in reactions that involve intermediate alkene complexes. In addition, unsaturated complexes containing an open coordination site often associate with alkenes and alkynes. Gold(I) chemistry is riddled with examples of this strategy, for example. The unsaturated complexes may be derived from precursors themselves, and the resulting π complexes may be short lived, but that's often the point! Some transformation of the π system is often desired.

I have to mention the metallacyclopropane route to alkene complexes from the Kulinkovich reaction, which is a surprising but awesome transformation. After displacement of two alkoxide ligands on titanium by ethylmagnesium bromide, a process described as either (1) β-hydride elimination followed by reductive elimination, or (2) concerted σ-bond metathesis leads to the liberation of ethane and formation of the alkene complex. The proof that the product is an alkene complex? Other olefins can displace ethylene, and ethylene can come right back in to re-form the product! Ti(II)'s strong backbonding ability almost certainly figures in to the driving force for the ethane-releasing step(s).



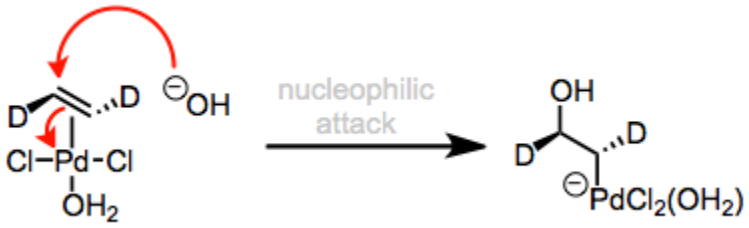
Kulinkovich synthesis of alkene complexes. A remarkable loss of ethane!

Reactions

The reactivity patterns of alkene and alkyne ligands are remarkably similar to those of carbon monoxide: nucleophilic attack and migratory insertion dominate their chemistry. The important issues of **site selectivity** and **stereoselectivity** come into play when considering alkenes and alkynes, however—the fundamental questions are...

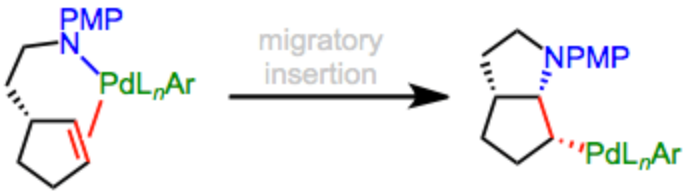
- Which atom gets the nucleophile/migrating group?
- Which atom gets the metal?
- What is the relative orientation of the nucleophile/migrating group and the metal (cis or trans)?

The wide variety of what we might generally call "**atom-metallation**" processes (carbopalladation, carboauration, aminopalladation, oxypalladation, etc.) may involve external nucleophilic addition to the π system, with attachment of the metal to the carbon that was not attacked. The net result is the addition of atom and metal across the π bond, in a trans or anti orientation. The anti orientation results because the nucleophile attacks the face opposite the metal center. A cis orientation of nucleophile and metal is indicative of a migratory insertion pathway (see below). In the example in the following figure, the metal alkyl was converted into a chlorohydrin using copper(II) chloride and LiCl (with stereospecific inversion). Subsequent epoxide formation with NaOH afforded only the cis diastereomer, supporting the trans configuration of the metal alkyl.



Nucleophilic attack on a coordinated alkene or alkyne is always trans, or anti.

Migratory insertion of alkenes and alkynes, like insertions of CO, can be thought of as an internal attack by a nucleophile already coordinated to the metal center. Migratory insertion is the C–C bond-forming step of **olefin polymerization**, and some fascinating studies of this reaction have shown that the alkyl group (the growing polymer chain) migrates to the location of the olefin (not the other way around). Migratory insertion is also important for the **Heck reaction**—in this case, the olefin inserts into a Pd–Csp2 bond. Finally, a large number of metal-catalyzed addition reactions rely on migratory insertion as the key C–X bond-forming step. cis-Aminopalladation is one example.

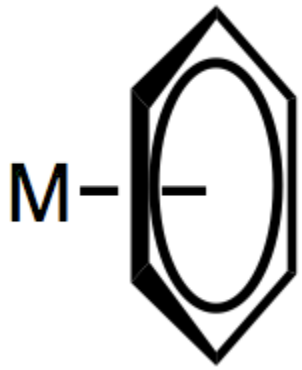


cis-Aminopalladation via migratory insertion. Two new bonds are established with stereospecificity!

Importantly, migratory insertion of alkenes and alkynes into M–X bonds takes place in a syn or cis fashion—the metal and the migrating group (X) end up on the same face of the π system. The site selectivity of migratory insertion may be controlled by either steric factors or the π system's electronics, although the former is more common, I'd say. Electronics are at play in Wacker oxidations of 1-alkenes, for example, which exclusively yield methyl ketones.

Finally, **electrophilic attack** on π systems coordinated to electron-rich metals can also happen, although it's much rarer than nucleophilic attack. Usually these reactions involve coordination of the electrophile to the metal, followed by migratory insertion. We'll hear more about this in a future post on electrophilic attack on coordinated ligands. Coming up next: cyclic π systems!

Arene or **aromatic ligands** are the subject of this post, the second in our series on π-system ligands. Arenes are dative, L-type ligands that may serve either as actors or spectators. Arenes commonly bind to metals through more than two atoms, although η2-arene ligands are known. Structurally, most η6-arenes tend to remain planar after binding to metals. Both "normal" bonding and backbonding are possible for arene ligands; however, arenes are stronger electron donors than CO and backbonding is less important for these ligands. The reactivity of arenes changes dramatically upon metal binding, along lines that we would expect for strongly electron-donating ligands. After coordinating to a transition metal, the arene usually becomes a better electrophile (particularly when the metal is electron poor). Thus, metal coordination can enable otherwise difficult **nucleophilic aromatic substitution** reactions.

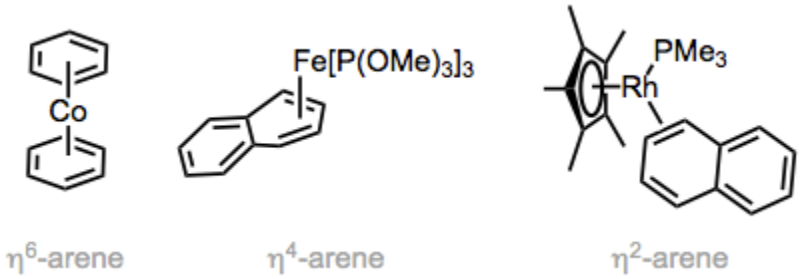


General Properties

The coordination of an aromatic compound to a metal center through its aromatic π MOs removes electron density from the ring. I'm going to forego an in-depth orbital analysis in this post, because it's honestly not very useful (and overly complex) for arene ligands. π → dσ (normal bonding) and dπ → π* (backbonding) orbital interactions are possible for arene ligands, with the former being much more important, typically. To simplify drawings, you often see chemists draw "toilet-bowl" arenes involving a circle and single central line to represent the π → dσ orbital interaction. Despite the single line, it is often useful to think about arenes as L3-type ligands. For instance, we think of η6-arenes as six-electron donors.

Multiple coordination modes are possible for arene ligands. When all six atoms of a benzene ring are bound to the metal (η6-mode), the ring is flat and C–C bond lengths are slightly longer than those in the free arene. The ring is bent and non-aromatic in η4-mode, so that the four atoms bound to the metal are coplanar while the other π bond is out of the plane. η4-Arene ligands show up in both stable complexes (see the figure below) and reactive intermediates that possess an open coordination site. To generate the latter, the corresponding η6-arene ligand undergoes **ring slippage**—one of the π bonds "slips" off of the metal to create an open coordination site. We'll see ring slippage again in discussions of the aromatic cyclopentadienyl and indenyl

ligands.



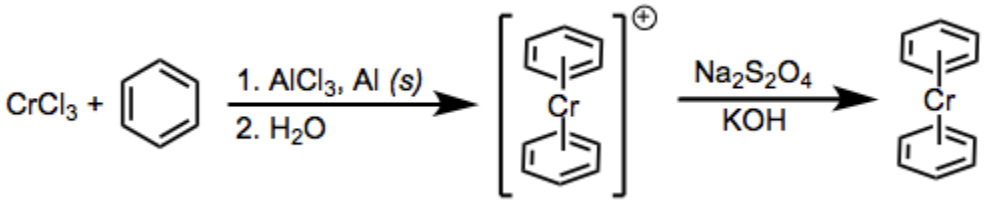
Arene ligands exhibit multiple coordination modes.

Even η2-arene ligands bound through one double bond are known. Coordination of one π bond results in **dearomatization** and makes η2-benzene behave more like butadiene, and furan act more like a vinyl ether. With naphthalene as ligand, there are multiple η2 isomers that could form; the isomer observed is the one that retains aromaticity in the free portion of the ligand. In fact, this result is general for polycyclic aromatic hydrocarbons: binding maximizes aromaticity in the free portion of the ligand. In the linked reference, the authors even observed the coordination of two different rhodium centers to naphthalene—a bridging arene ligand! Other bridging modes include σ, π-binding (the arene is an LX-type ligand, and one C–M bond is covalent, not dative) and L2-type bridging through two distinct π systems (as in biphenyl).

Arene ligands are usually hydrocarbons, not heterocycles. Why? Aromatic heterocycles, such as pyridine, more commonly bind using their basic lone pairs. That said, a few heterocycles form important π complexes. Thiophene is perhaps the most heavily studied, as the desulfurization of thiophene from fossil fuels is an industrially useful process.

Synthesis

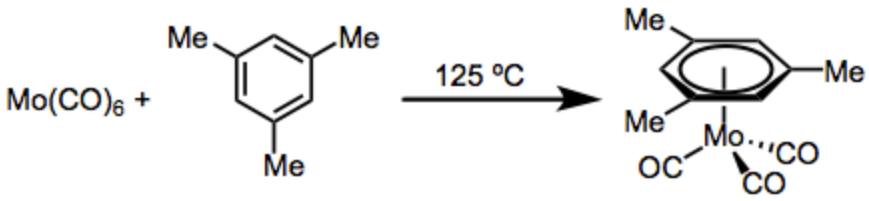
There are two common methods for the stoichiometric synthesis of arene “sandwich” complexes, in which a metal is squished between two arenes. Starting from a metal halide, treatment with a Lewis acid and mild reductant rips off the halogen atoms and replaces them with arene ligands. The scope of this method is fairly broad metal-wise.



The Fischer-Hafner synthesis. Reduction of metal halides in the presence of arene.

A second method, “co-condensation,” involves the simultaneous condensation of metal atom and arene vapor onto a cold (-196 °C) surface.

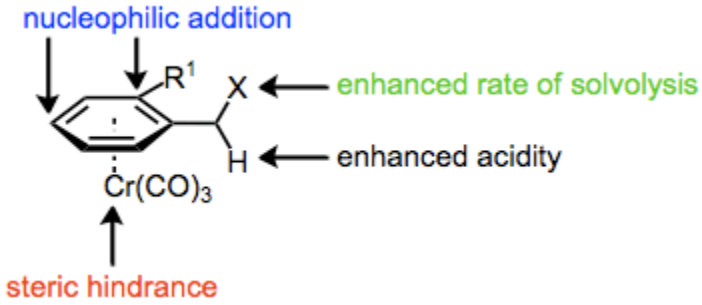
Syntheses of metal arene carbonyl complexes take advantage of the fact that arenes are strongly binding, “chelating” ligands. Infrared spectroscopic studies have shown that a single benzene ligand is a stronger electron donor than three CO ligands—C–O stretching frequencies are lower in metal arene carbonyls than homoleptic metal carbonyls. Since the process is entropically driven, a little heat can get the job done.



Entropically driven synthesis of arene complexes: three molecules for the price of one!

Reactions

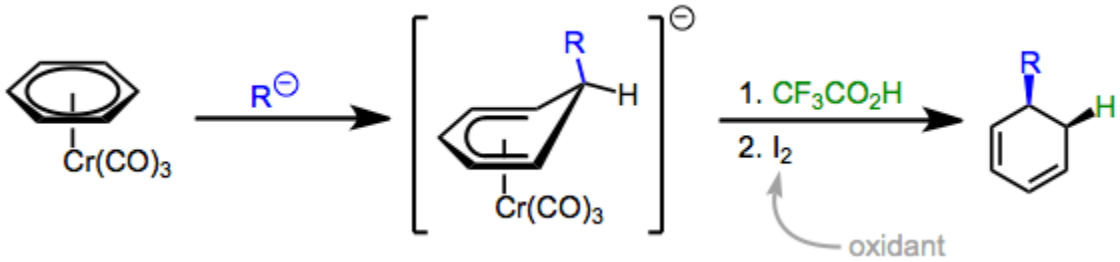
It's important here to distinguish aromatic X-type ligands from the topic of this post, Ln-type arenes bound only through their π systems. The figure below nicely summarizes the typical behavior of arene ligands coordinated through their π clouds. Although the figure is for chromium carbonyls specifically, other metals apply as well. Note the reactivity of the benzylic position: both cations and anions are stabilized by the metal.



The magic of metal coordination: increased acidity and electrophilicity and steric hindrance.

Since the coordination of arenes to metals depletes electron density on the arene, it makes sense that metal-arene complexes should be susceptible to nucleophilic aromatic substitution (NAS). In fact, NAS on metal-coordinated arene ligands has been extensively developed for several different metals. However, all of these NAS methods are stoichiometric because the product ligands are as good as (or better than) the starting ligands at coordinating metal. A stoichiometric amount of another reagent—typically an oxidant—is used to free up the arene. Why are oxidants effective at freeing arene ligands from metal centers? Oxidation worsens the metal's ability to backbond and consequently decreases the enthalpic advantage of arene binding. Entropy is thus able to take over and release the ligand.

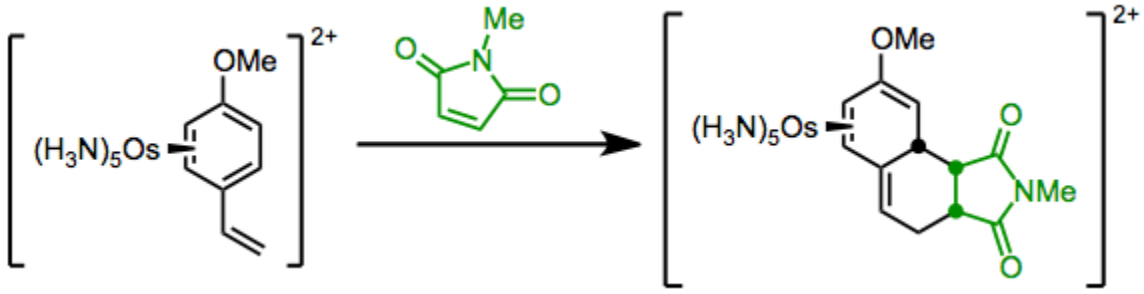
Steric hindrance on the side of the arene bound to the metal is a second important factor to consider. Nucleophilic addition takes place on the face opposite the coordinated metal. If rearomatization through the loss of a leaving group isn't fast, an electrophile can be introduced after nucleophilic addition, resulting in the cis addition of nucleophile and electrophile across an aromatic π bond. Take that, aromaticity!



Aromaticity takes a beating, thanks to chromium!

We already touched a little on the interesting behavior of η_2-arene complexes, which behave more like their analogues possessing one less double bond. Here's a nifty example from Harman of a Diels-Alder reaction in which a substituted styrene is the diene.

Strike two for aromaticity!



Harman's Os(II) arene chemistry. Styrene is uniquely acting like a diene!

If you're interested in learning more about this fascinating chemistry, check out Harman's review (linked above). The behavior of furan is particularly intriguing.

This brings us to the end of our short series on L-type π-system ligands. However, we'll encounter ligands that bear great similarity to alkenes and arenes in the near future. π Systems that contain an odd number of atoms, unlike π systems we've seen so far, are LnX-type ligands with one covalent M–X bond and n dative bonds. We'll return to this interesting class of ligands after finishing off the dative ligands with metal carbenes and introducing a few simple X-type ligands (hydrides, alkyls, alkoxides, etc.).

This page titled 8.2.10: π Systems is shared under a CC BY-NC-SA 4.0 license and was authored, remixed, and/or curated by Michael Evans.

- 2.10: π Systems by Michael Evans is licensed CC BY-NC-SA 4.0.

8.3: STRUCTURAL FUNDAMENTALS

8.3.1: Ligand Field Theory and Frontier Molecular Orbital Theory

8.3.2: Open Coordination Site

8.3.3: Periodic Trends of the Transition Metals

8.3.4: Predicting the Geometry of Organometallic Complexes

8.3.5: Simplifying the Organometallic Complex (Part 1)

8.3.6: Simplifying the Organometallic Complex (Part 2)

8.3.7: Simplifying the Organometallic Complex (Part 3)

This page titled 8.3: Structural Fundamentals is shared under a CC BY-NC-SA 4.0 license and was authored, remixed, and/or curated by Michael Evans.

- 3: Structural Fundamentals by Michael Evans is licensed CC BY-NC-SA 4.0.

8.3.1: Ligand Field Theory and Frontier Molecular Orbital Theory

In this post, we'll begin to explore the molecular orbital theory of organometallic complexes. Some background in molecular orbital theory will be beneficial; an understanding of organic frontier molecular orbital theory is particularly helpful. Check out Fukui's Nobel Prize lecture for an introduction to FMO theory. The theories described here try to address how the approach of ligands to a transition metal center modifies the electronics of the metal and ligands. The last post on geometry touched on these ideas a little, but we'll dig a little deeper here. Notably, we need to address the often forgotten influence of the metal on the ligands—how might a metal modify the reactivity of organic ligands?

This page titled 8.3.1: Ligand Field Theory and Frontier Molecular Orbital Theory is shared under a CC BY-NC-SA 4.0 license and was authored, remixed, and/or curated by Michael Evans.

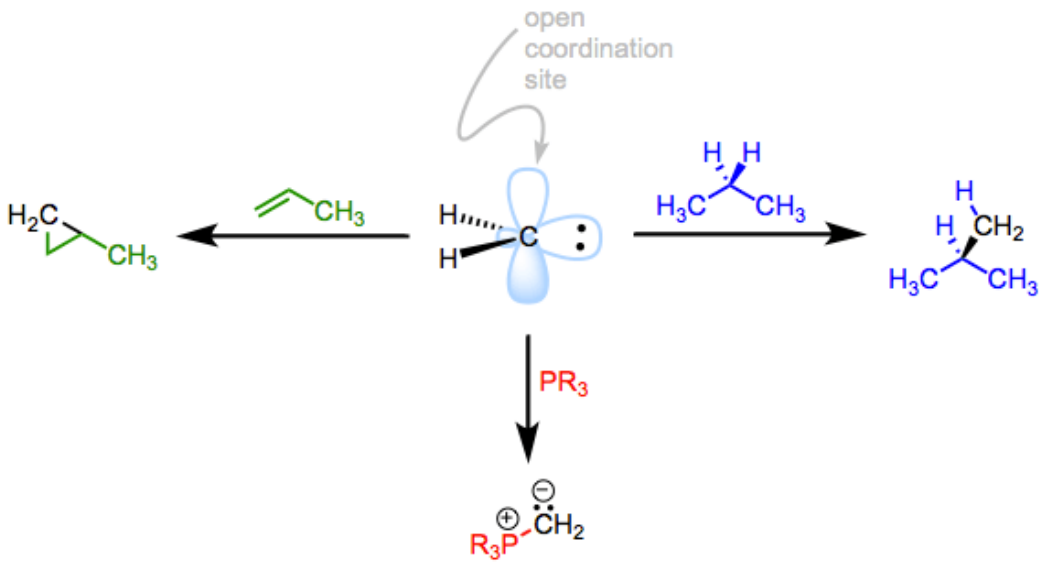
- 3.1: Ligand Field Theory and Frontier Molecular Orbital Theory by Michael Evans is licensed CC BY-NC-SA 4.0.

8.3.2: Open Coordination Site

The concept of coordinative unsaturation can be confusing for the student of organometallic chemistry, but recognizing open coordination sites in OM complexes is a critical skill.

Introduction

Let's begin with a famous example of coordinative unsaturation from organic chemistry.



An analogy from organic chemistry. The reactivity of the carbene flows from its open coordination site.

Carbenes are both nucleophilic and electrophilic, but the essence of their electrophilicity comes from the fact that they don't have their fair share of electrons (8). They have not been saturated with electrons—carbenes want more! To achieve saturation, carbenes may inherit a pair of electrons from a σ bond (σ-bond insertion), π bond (cyclopropanation), or lone pair (ylide formation). Notice that, simply by spotting coordinative unsaturation, we've been able to fully describe the carbene's reactivity! We can do the same with organometallic complexes—open coordination sites suggest specific reactivity patterns. That's why understanding coordinative unsaturation and recognizing its telltale sign (the open coordination site) are essential skills for the organometallic chemist.

Coordinative unsaturation is not just the possession of a coordination number less than 6, or an apparent space in which a ligand might be able to approach. Sixteen or fewer total electrons on the metal center are a second necessity—just as, in the organic case, 6 or fewer electrons on the unsaturated atom are essential. Sixteen or fewer total electrons and coordination number less than 6 add up to a more fundamental synonym for an open coordination site: an empty metal-centered orbital!

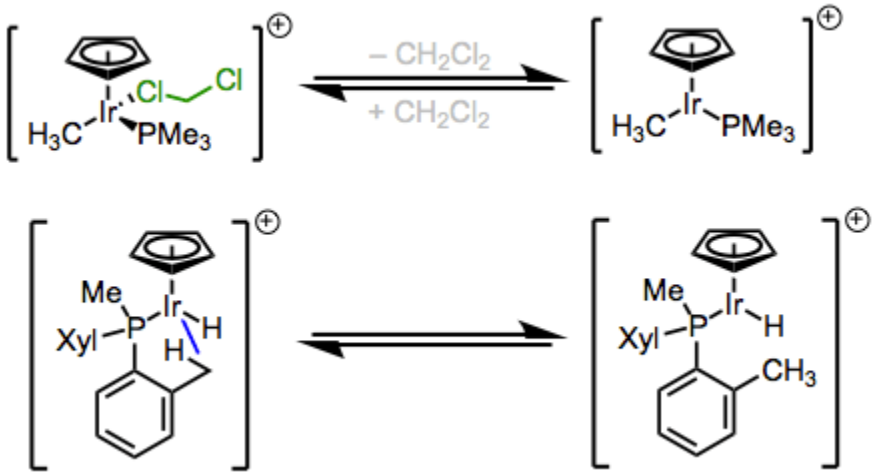
(<= 16 total electrons on M) + (< 6 coordination number on M) = empty d orbital on M

The lesson here is that we can't just look to the geometry of a complex to determine whether it bears an open coordination site—electron counting is essential too.

Like carbenes and carbocations, metal complexes containing open coordination sites don't just hang around. They react rapidly with all kinds of electron sources. Furthermore, you won't see them in stable starting materials or products. Thus, recognizing when a complex has the potential for an open site is important. What are some structural signs that point to the possibility of an open coordination site?

1. Weakly coordinating ligands

Ligand dissociation from an 18-electron complex produces an open coordination site. Solvent ligands and side-on σ ligands—both of which bind relatively weakly to metals—often engage in this process. Try counting electrons in the two pairs of cationic iridium complexes below.



Dissociation of weakly bound ligands reveals open coordination sites.

Dissociation of a π-system ligand may also reveal an open coordination site.

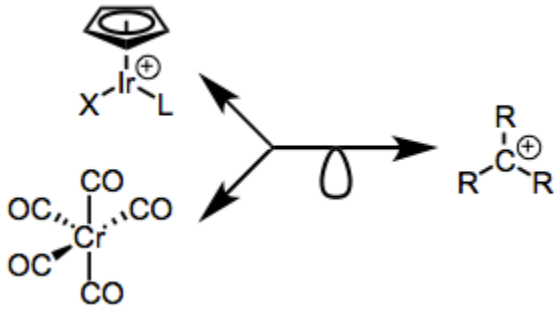
2. Reaction conditions encouraging dissociation

In this category, we might file away photochemical and amine-oxide-mediated dissociations of CO. Conditions like these encourage the loss of a ligand and subsequent replacement with something else, àla S_N1 substitution.

3. Potential for reductive elimination

Reductive elimination is the open coordination site's dream come true: two (sites) for the price of one (step)! Factors affecting the favorability of reductive elimination are beyond the scope of this post, but we can mention a couple here: steric crowding and an electron-poor metal.

Finally, it's important to note that open coordination sites often show up in fragments of OM complexes examined for one reason or another. We can relate these fragments to organic or main-group intermediates using isolobal analogies, powerful conceptual tools that we'll explore in detail in another post. For example, the fragment $(CO)_5Cr$ is isolobal with the organic carbocation—the two sets of frontier MOs are analogous, and both structures have an open coordination site.



All three of these analogous fragments bear an open coordination site.

This page titled 8.3.2: Open Coordination Site is shared under a CC BY-NC-SA 4.0 license and was authored, remixed, and/or curated by Michael Evans.

- 3.2: Open Coordination Site by Michael Evans is licensed CC BY-NC-SA 4.0.

8.3.3: Periodic Trends of the Transition Metals

Periodic trends play a huge role in organic chemistry. Regular changes in electronegativity, atomic size, ionization energy, and other variables across the periodic table allow us to make systematic predictions about the behavior of similar compounds. Of course, the same is true for organometallic complexes! With a firm grip on the periodic trends of the transition metals, we can begin to make comparisons between complexes we're familiar with and those we've never seen before. Periodic trends essentially provide an exponential increase in predictive power. In this post, we'll hit on the major periodic trends of the transition metals and discuss a few examples for which these trends can be handy.

Before beginning, a couple of caveats are in order. First of all, many of the trends across the transition series are not perfectly regular. Hartwig wisely advises that one should consider the transition series in blocks instead of as a whole when considering periodic trends. For instance, general increases in a quantity may be punctuated by sudden decreases; in such a case, we may say that the quantity increases generally, but definite conclusions are only possible when the metals under comparison are close to one another in the periodic table (and we need to be careful about unexpected jumps). Secondly, periodic trends are significantly affected by the identity of ligands and the oxidation state of the metal center, so comparisons need to be appropriately controlled. Using periodic trends to compare a Pd(II) complex and a Ru(III) complex is largely an exercise in futility, but comparing Pt(II) and Pd(II) complexes with similar ligand sets is reasonable. Keep these ideas in mind to avoid spinning your wheels unnecessarily! Alright, let's dive in...

This page titled 8.3.3: Periodic Trends of the Transition Metals is shared under a CC BY-NC-SA 4.0 license and was authored, remixed, and/or curated by Michael Evans.

- 3.3: Periodic Trends of the Transition Metals by Michael Evans is licensed CC BY-NC-SA 4.0.

8.3.4: Predicting the Geometry of Organometallic Complexes

An important issue that we've glossed over until now concerns what organometallic complexes actually look like: what are their typical geometries? Can we use any of the "bookkeeping metrics" we've explored so far to reliably predict geometry? The answer to the latter questions is a refreshing but qualified "yes." In this post, we'll explore the possibilities for complex geometry and develop some general guidelines for predicting geometry. In the process we'll enlist the aid of a powerful theoretical ally, crystal field theory (CFT), which provides some intuitive explanations for geometry the geometry of organometallic complexes.

This page titled 8.3.4: Predicting the Geometry of Organometallic Complexes is shared under a CC BY-NC-SA 4.0 license and was authored, remixed, and/or curated by Michael Evans.

- 3.4: Predicting the Geometry of Organometallic Complexes by Michael Evans is licensed CC BY-NC-SA 4.0.

8.3.5: Simplifying the Organometallic Complex (Part 1)

Organometallic complexes, which consist of centrally located metals and peripheral organic compounds called ligands, are the workhorses of organometallic chemistry. Just like organic intermediates, understanding something about the structure of these molecules tells us a great deal about their expected reactivity. Some we would expect to be stable, and others definitely not! A big part of our early explorations will involve describing, systematically, the principles that govern the stability of organometallic complexes. From the outset, I will say that these principles are not set in stone and are best applied to well controlled comparisons. Nonetheless the principles are definitely worth talking about, because they form the foundation of everything else we'll discuss. Let's begin by exploring the general characteristics of organometallic complexes and identifying three key classes of organic ligands.

When we think of metals we usually think of electropositive atoms or even positively charged ions, and many of the metals of OM chemistry fit this mold. In general, it is useful to imagine organic ligands as electron donors and metals as electron acceptors. When looking at a pair of electrons shared between a transition metal and main-group atom (or hydrogen), I imagine the cationic metal center and anionic main-group atom racing toward one another from oblivion like star-crossed lovers. In the opposite direction (with an important caveat that we'll address soon), we can imagine ripping apart metal–R covalent bonds and giving both electrons of the bond to the organic atom. This heterolytic bond cleavage method reproduces the starting charges on the metal and ligand. Unsurprisingly, the metal is positive and the ligand negative.

FYI, you might see the blue bipyridine referred to as an L2 ligand elsewhere; this just means that a single bipyridine molecule possesses two L-type binding points. Ligands with multiple binding points are also known as chelating or polydentate ligands. Chelating ligands may feature mixed binding modes; for instance, the allyl ligand is of the LX-type. Chelating ligands can also bind to two different metal centers; when they act in this way, they're called bridging ligands. But don't let all this jargon throw you! Deconstruct complexes one binding point at a time, and you cannot go wrong.

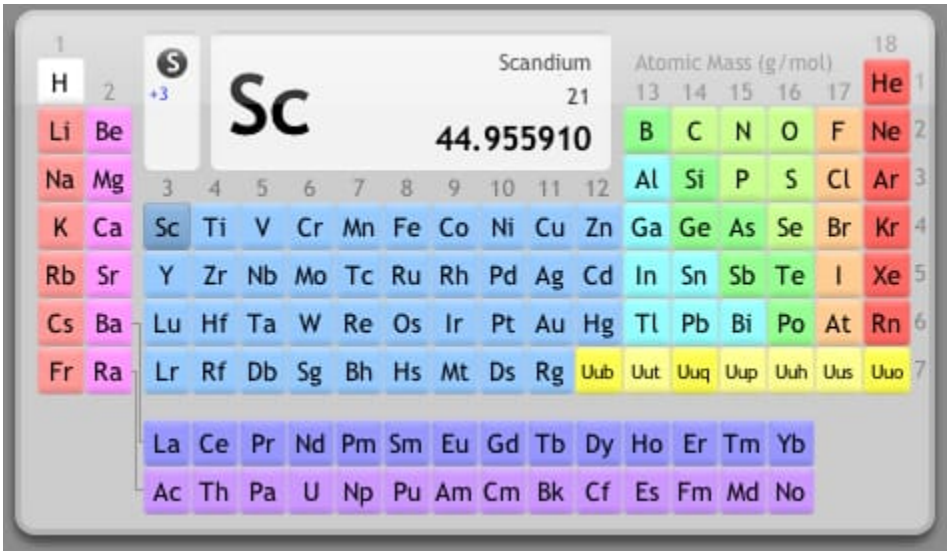
Next, we'll take a closer look at the metal center and expand on the purpose of the deconstruction process described here.

This page titled 8.3.5: Simplifying the Organometallic Complex (Part 1) is shared under a CC BY-NC-SA 4.0 license and was authored, remixed, and/or curated by Michael Evans.

- 3.5: Simplifying the Organometallic Complex (Part 1) by Michael Evans is licensed CC BY-NC-SA 4.0.

8.3.6: Simplifying the Organometallic Complex (Part 2)

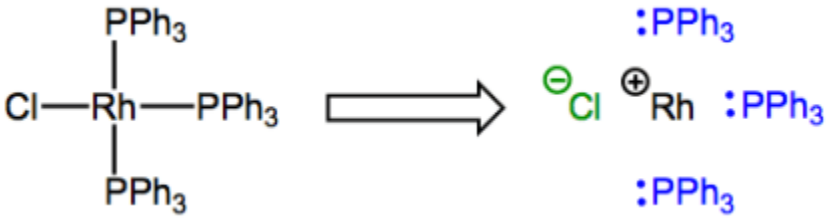
Now it's time to turn our attention to the metal center, and focus on what the deconstruction process can tell us about the nature of the metal in organometallic complexes. We'll hold off on a description of periodic trends of the transition series, but now is a good time to introduce the general characteristics of the transition metals. Check out groups 3-12 in the table below.



The transition metals are colored dark blue in this table.

The transition metals occupy the d-block of the periodic table, meaning that, as we move from left to right across the transition series, electrons are added to the d atomic orbitals. Just like organic elements, the transition metals form bonds using only their valence electrons. But when working with the transition metals, we need to concern ourselves only with the d atomic orbitals, as none of the other valence subshells contain any electrons. Although the periodic table may lead you to believe that the transition metals possess filled s subshells, we imagine metals in organometallic complexes as possessing valence electrons in d orbitals only! The reason for this is somewhat complicated, but has to do with the partial positive charge of complexed metals. Neutral transition metal atoms do, in fact, possess filled s subshells. Why, then, is it important to remember that the valence electrons of complexed metal centers are all d electrons? We will see that the number of d electrons possessed by a complexed metal is in many ways a useful concept. If you find that your counts are off by two, this common mistake is probably the culprit!

Let's turn our attention now to a new complex. I've gone ahead and deconstructed it for us.



Say hello to rhodium (Rh)! Don't fret; it's just a group 9 element.

The complex possesses one X-type and three L-type ligands, so the rhodium atom ends up with a formal charge of +1. The formal charge on the metal center after deconstruction has a very special name that you will definitely want to commit to memory: it's called the oxidation state. It's usually indicated with a roman numeral next to the atomic symbol of the metal (the "+" is implied). In the complex shown above, rhodium is in the Rh(I) or +1 oxidation state. Oxidation state is most useful because changes in oxidation state indicate changes in electron density at the metal center, and this can be a favorable or unfavorable occurrence depending on the other ligands around. We will see this principle in action many, many times! Get used to changes in

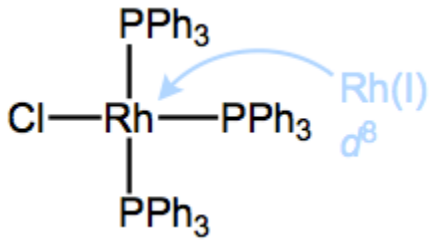
oxidation state as everyday events in organometallic reaction mechanisms. Unlike carbon (with the exception of carbene...what's its oxidation state?!) and other second-row elements, the transition metals commonly exhibit multiple different oxidation states. More on that later, though. For now, training yourself to rapidly identify the oxidation state of a complexed metal is most important. Please note that when a complex possesses an overall charge, the oxidation state is affected by this charge!

oxidation state = number of X-type ligands bound to metal + overall charge of complex

What of this number of d electrons concept? A very useful way to think about "number of d electrons" is as the "number of non-bonding electrons on the metal center," and you're probably familiar with identifying non-bonding electrons from organic chemistry. The numbers of valence electrons of each organic element are set in stone: carbon has four, nitrogen has five, et cetera. Furthermore, using this knowledge, it's straightforward to determine the number of lone pair electrons associated with an atom by subtracting its number of covalent bonds from its total number of valence electrons. E.g., for a neutral nitrogen atom in an amine NR3, 5 – 3 = 2 lone pair electrons, typically. The extension to organometallic chemistry is natural! We can analyze complexed metal centers in the same way, but they tend to have a lot more non-bonding electrons than organic atoms, and the number depends on the metal's oxidation state. For instance, the deconstructed rhodium atom in the figure above has 8 d electrons: 9 valence electrons minus 1 used for bonding to Cl. Dative bonds don't affect d electron count since both electrons in the bond come from the ligand.

number of non-bonding electrons = number of d electrons = metal's group number – oxidation state

Drawing all the non-bonding d electrons out as lone pairs would clutter things up, so they are never drawn...but we must remember that they're around! Why? Because the number of d electrons profoundly affects a complex's geometry. We will return to this soon, but the key idea is that the ligands muck up the energies of the d orbitals as they approach the metal (recall the "star-crossed lovers" idea), and the most favorable way to do so depends on the number of non-bonding electrons on the metal center.



Oxidation state and d electron count: two tools the OM chemist can't live without!

This post introduced us to two important bookkeeping tools, oxidation state and number of d electrons. In the final installment of the "Simplifying the Organometallic Complex" series, we'll bring everything together and discuss total electron count. We'll see that total electron count may be used to draw a variety of insightful conclusions about organometallic complexes.

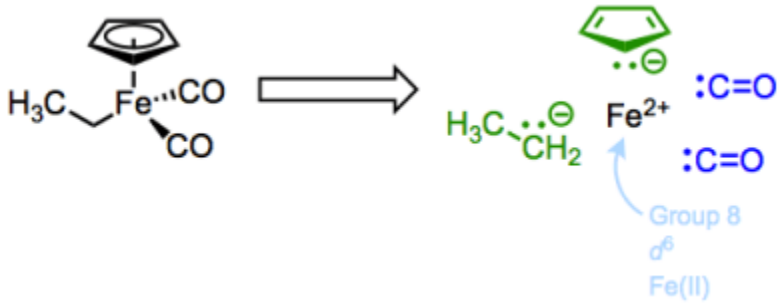
This page titled 8.3.6: Simplifying the Organometallic Complex (Part 2) is shared under a CC BY-NC-SA 4.0 license and was authored, remixed, and/or curated by Michael Evans.

- 3.6: Simplifying the Organometallic Complex (Part 2) by Michael Evans is licensed CC BY-NC-SA 4.0.

8.3.7: Simplifying the Organometallic Complex (Part 3)

So far, we've seen how deconstruction can reveal useful "bookkeeping" properties of organometallic complexes: number of electrons donated by ligands, coordination number, oxidation state, and d electron count (to name a few). Now, let's bring everything together and discuss total electron count, the sum of non-bonding and bonding electrons associated with the metal center. Like oxidation state, total electron count can reveal the likely reactivity of OM complexes—in fact, it is often more powerful than oxidation state for making predictions. We'll see that there is a definite norm for total electron count, and when a complex deviates from that norm, reactions are likely to happen.

Let's begin with yet another new complex. This molecule features the common and important cyclopentadienyl and carbon monoxide ligands, along with an X-type ethyl ligand.



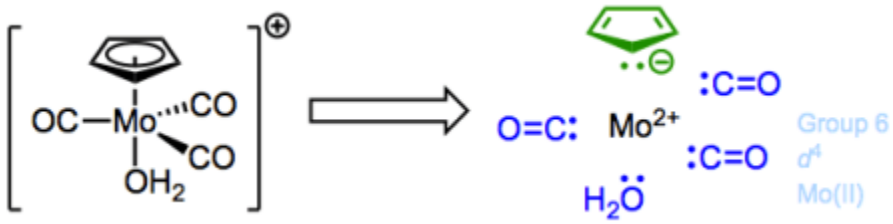
What is the total electron count of this Fe(II) complex?

The Cp or cyclopentadienyl ligand is a polydentate, six-electron L2X ligand. The two pi bonds of the free anion are dative, L-type ligands, which we'll see again in a future post on ligands bound through pi bonds. Think of the electrons of the pi bond as the source of a dative bond to the metal. Since both electrons come from the ligand, the pi bonds are L-type binders. The anionic carbon in Cp is a fairly standard, anionic X-type binder. The carbon monoxide ligands are interesting examples of two-electron L-type ligands—notice that the free ligands are neutral, so these are considered L-type! Carbon monoxide is an intriguing ligand that can teach us a great deal about metal-ligand bonding in OM complexes...but more on that later.

After deconstruction, we see that the Fe(II) center possesses 6 non-bonding d electrons. The total electron count is just the d electron count plus the number of electrons donated by the ligands. Since the d electron count already takes overall charge into account, we need not worry about it as long as we've followed the deconstruction procedure correctly.

total electron count = number of d electrons + electrons donated by ligands

For the Fe(II) complex above, the total electron count is thus 6 + (6 + 2 + 2 + 2) = 18. Let's work through another example: the complex below features an overall charge of +1. Water is a dative ligand—that "2" is very important!

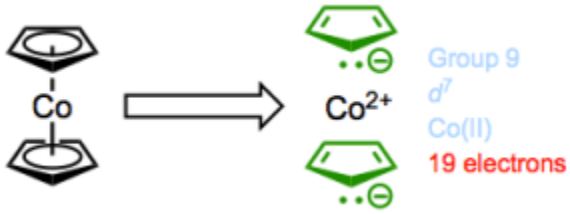


Note that the overall charge is lumped into the oxidation state and d electron count of Mo.

The oxidation state of molybdenum is +2 here...remember that the overall charge factors in to that. When everything is said and done, the total electron count is 4 + (6 + 2 + 2 + 2 + 2) = 18.

What's up with 18?! As it turns out, 18 electrons is a very common number for stable organometallic complexes. So common that the number got its own rule—the 18-electron rule—which states that stable transition-metal complexes possess 18 or fewer electrons. The rule is analogous to organic chemistry's octet rule. The typical explanation for the 18-electron rule points out that there are 9 valence orbitals (1 s, 3 p, 5 d) available to metals, and using all of these for bonding seems to produce the most stable complexes. Of course, as soon as the rule left the lips of some order-craving chemist, researchers set out to find counterexamples to it, and a number of counterexamples are known. Hartwig describes the rule as an "empirical guideline" with little theoretical support. In fact, theoretical studies have shown that the participation of p orbitals in complex MOs is unlikely. I know that's not what you want to hear—but hang with me! The 18-electron rule is still a very useful guideline. It's most interesting, in fact, when it is not satisfied.

One last example...how would you expect the complex below to react?



Cobaltocene: jonesing for chemical change.

If we assume that the 18-electron rule is true, then cobaltocene has a real problem. It possesses 7 + (6 + 6) = 19 total valence electrons! Yet, we can also reason that this complex will probably react to relieve the strain of not having 18 electrons by giving up an electron. Guess what? In practice, cobaltocene is a great one-electron reducing agent, and can be used to prepare anionic complexes through electron transfer.

$$CoCp_2 + ML_n \rightarrow [CoCp_2] + [ML_n]^- \tag{8.3.7.1}$$

This post described how to calculate total electron count and introduced the power of the 18-electron rule for predicting whether a complex will donate or accept electrons. We will definitely see these ideas again! But what happens when the electron counts of two complexes we're interested in comparing are the same? We'll need more information. In the next post, we'll explore the periodic trends of the transition series. Our goal will be to make meaningful comparisons between complexes of different metals.

This page titled 8.3.7: Simplifying the Organometallic Complex (Part 3) is shared under a CC BY-NC-SA 4.0 license and was authored, remixed, and/or curated by Michael Evans.

- 3.7: Simplifying the Organometallic Complex (Part 3) by Michael Evans is licensed CC BY-NC-SA 4.0.

8.4: FUNDAMENTALS OF ORGANOMETALLIC CHEMISTRY

8.4.1: β-Elimination Reactions

8.4.2: Associative Ligand Substitution

8.4.3: Dissociative Ligand Substitution Reactions

8.4.4: Ligand substitution

8.4.5: Migratory Insertion- 1,2-Insertions

8.4.6: Migratory Insertion- Introduction and CO Insertions

8.4.7: Oxidative Addition- General Ideas

8.4.8: Oxidative Addition of Non-polar Reagents

8.4.9: Oxidative Addition of Polar Reagents

8.4.10: Quirky Ligand Substitutions

8.4.11: Reductive Elimination- General Ideas

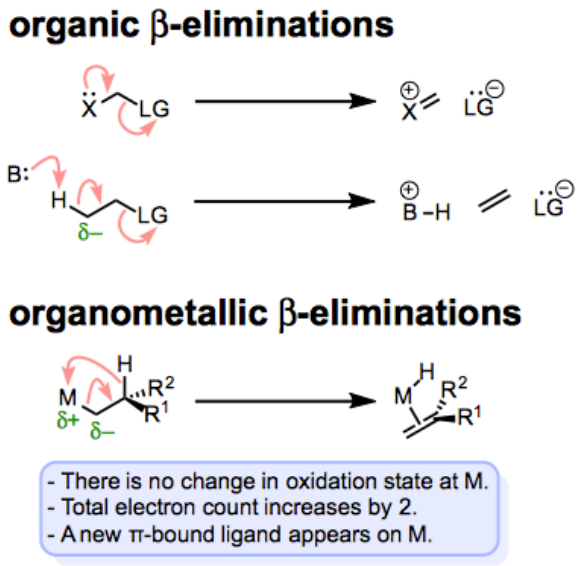
8.4.12: The trans/cis Effects and Influences

This page titled 8.4: Fundamentals of Organometallic Chemistry is shared under a CC BY-NC-SA 4.0 license and was authored, remixed, and/or curated by Michael Evans.

- 4: Fundamentals of Organometallic Chemistry by Michael Evans is licensed CC BY-NC-SA 4.0.

8.4.1: β-Elimination Reactions

In organic chemistry class, one learns that elimination reactions involve the cleavage of a σ bond and formation of a π bond. A nucleophilic pair of electrons (either from another bond or a lone pair) heads into a new π bond as a leaving group departs. This process is called β-elimination because the bond β to the nucleophilic pair of electrons breaks. Transition metal complexes can participate in their own version of β-elimination, and metal alkyl complexes famously do so. Almost by definition, metal alkyls contain a nucleophilic bond—the M–C bond! This bond can be so polarized toward carbon, in fact, that it can promote the elimination of some of the world's worst leaving groups, like –H and –CH3. Unlike the organic case, however, the leaving group is not lost completely in organometallic β-eliminations. As the metal donates electrons, it receives electrons from the departing leaving group. When the reaction is complete, the metal has picked up a new π-bound ligand and exchanged one X-type ligand for another.



Comparing organic and organometallic β-eliminations. A nucleophilic bond or lone pair promotes loss or migration of a leaving group.

In this post, we'll flesh out the mechanism of β-elimination reactions by looking at the conditions required for their occurrence and their reactivity trends. Many of the trends associated with β-eliminations are the opposite of analogous trends in 1,2-insertion reactions. A future post will address other types of elimination reactions.

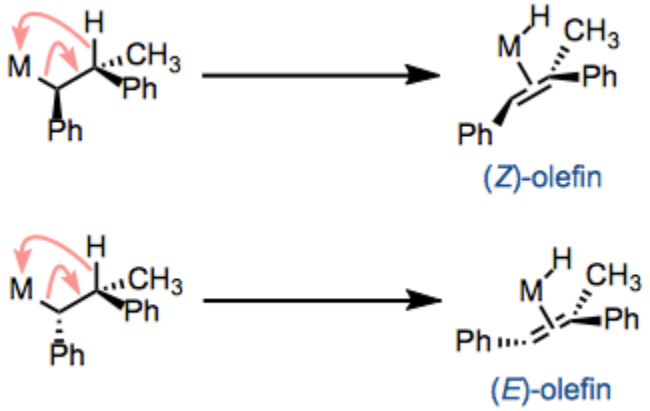
β-Hydride Elimination

The most famous and ubiquitous type of β-elimination is **β-hydride elimination**, which involves the formation of a π bond and an M–H bond. Metal alkyls that contain β-hydrogens experience rapid elimination of these hydrogens, provided a few other conditions are met.

The complex must have an open coordination site and an accessible, empty orbital on the metal center. The leaving group (–H) needs a place to land. Notice that after β-elimination, the metal has picked up one more ligand—it needs an empty spot for that ligand for elimination to occur. We can envision hydride "attacking" the empty orbital on the metal center as an important orbital interaction in this process.

The M–C_α and C_β–H bonds must have the ability to align in a syn coplanar arrangement. By "syn coplanar" we mean that all four atoms are in a plane and that the M–C_α and C_β–H bonds are on the same side of the C_α–C_β bond (a dihedral angle of 0°). You can see that conformation in the figure above. In the syn coplanar arrangement, the C–H bond departing from the ligand is optimally lined up with the empty orbital on the metal center. Hindered or cyclic complexes that cannot achieve this conformation do not undergo β-hydride elimination. The need for a syn coplanar conformation has important implications for eliminations that may

establish diastereomeric olefins: β-elimination is stereospecific. One diastereomer leads to the (E)-olefin, and the other leads to the (Z)-olefin.



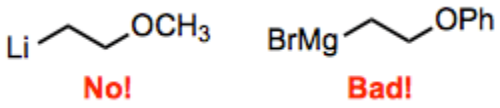
β-elimination is stereospecific. One diastereomer of reactant leads to the (Z)-olefin and the other to the (E)-olefin.

The complex must possess 16 or fewer total electrons. Examine the first figure one more time—notice that the total electron count of the complex increases by 2 during β-hydride elimination. Complexes with 18 total electrons don't undergo β-elimination because the product would end up with 20 total electrons. Of course, dissociation of a loose ligand can produce a 16-electron complex pretty easily, so watch out for ligand dissociation when considering the possibility of β-elimination in a complex. Ligand dissociation may be reversible, but β-Hydride elimination is almost always irreversible.

The metal must bear at least 2 d electrons. Now this seems a bit strange, as the metal has served as nothing but an empty bin for electrons in our discussion so far. Why would the metal center need electrons for β-hydride elimination to occur? The answer lies in an old friend: backbonding. The $\sigma_{C-H} \rightarrow M$ orbital interaction mentioned above is not enough to promote elimination on its own; an $M \rightarrow \sigma^*_{C-H}$ interaction is also required! I've said it before, and I'll say it again: backbonding is everywhere in organometallic chemistry. If you can understand and articulate it, you'll blow your instructor's mind.

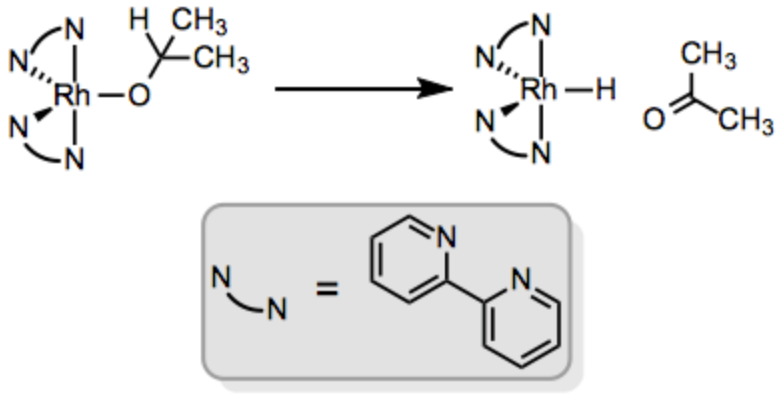
Other β-Elimination Reactions

The leaving group does not need to be hydrogen, of course, and a number of more electronegative groups come to mind as better candidates for leaving groups. β-Alkoxy and β-amino eliminations are usually thermodynamically favored thanks to the formation of strong M–O and M–N bonds, respectively. These reactions are so favored in β-alkoxyalkyl "complexes" of alkali and alkaline earth metals (R–Li, R–MgBr, etc.) that using these as σ-nucleophiles at carbon is untenable. Such compounds eliminate immediately upon their formation. I had an organic synthesis professor in undergrad who was obsessed with this—using a β-alkoxyalkyl lithium or β-alkoxyalkyl Grignard reagent in a synthesis was a recipe for red ink. β-Haloalkyls were naturally off limits too.



Watch out…these are not stable compounds!

The atom bound to the metal doesn't have to be carbon. β-Elimination of alkoxy ligands affords ketones or aldehydes bound at oxygen or through the C=O π bond (this step is important in many transfer hydrogenations, and an analogous process occurs in the Oppenauer oxidation). Amido ligands can undergo β-elimination to afford complexes of imines; however, this process tends to be slower than β-alkoxy elimination.



β-Elimination helps transfer the elements of dihydrogen from one organic compound to another.

Incidentally, I haven't seen any examples in which the β atom is not carbon, but would be interested if anyone knows of an example!

Applications of β-Eliminations

As with many concepts in organometallic chemistry, there are two ways to think about applications of β-elimination. One can take either the "inorganic" perspective, which focuses on the metal center, or the "organic" perspective, which focuses on the ligands.

With the metal center in focus, we can recognize that β-hydride elimination has the wonderful side effect of establishing an M–H bond—a feat generally difficult to achieve in a selective manner via oxidative addition of X–H. If the ligand from which the hydrogen came displaced something more electronegative, the whole process represents reduction at the metal center. For example, imagine rhodium(III) chloride is mixed with sodium isopropoxide, $NaOCH(CH_3)_2$. The isopropoxide easily displaces chloride, and subsequent β-hydride elimination affords a rhodium hydride, formally reduced with respect to the chloride starting material. See p. 236 of this review for more.

With the ligand in focus, we see that the organic ligand is oxidized in the course of β-hydride elimination. Notice that the metal is reduced and the ligand oxidized! A π bond replaces a σ bond in the ligand, and if the conditions are right, this represents a bona fide oxidation (as opposed to a mere elimination). For example, oxidative addition into a C–H bond followed by β-hydride elimination at a C–H bond next door sets up an alkene where two adjacent C–H bonds existed before, an oxidation process. These dehydrogenation reactions are incredibly appealing in a theoretical sense, but still at an early stage when it comes to scope and practicality.

Summary

We already encountered β-hydride elimination in an earlier series of posts on metal alkyl complexes, where we noted that it's a very common decomposition pathway for metal alkyls. β-Hydride elimination isn't all bad, however, as it can be an important step in catalytic reactions that result in the oxidation of organic substrates (dehydrogenations and transfer hydrogenations) and in reactions that reduce metal halides to metal hydrides. The general idea of β-elimination involves the transfer of a leaving group from a ligand to the metal center with simultaneous formation of a π bond in the ligand. β-Elimination requires an open coordination site and at least two d electrons on the metal center, and eliminations of chiral complexes are stereospecific. The leaving group is commonly hydrogen, but need not be—the more electronegative the leaving group, the more favorable the elimination. Stronger π bonds in the product also encourage β-elimination, so eliminations that form carbonyl compounds or imines are common.

In the next post, we'll explore other types of organometallic elimination reactions, which establish π bonds at different positions in metal alkyl or other complexes. α-Eliminations, for example, establish metal-carbon, -oxygen, or -nitrogen multiple bonds, which are generally difficult to forge through other means

Contributors and Attributions

- Dr. Michael Evans (Georgia Tech)

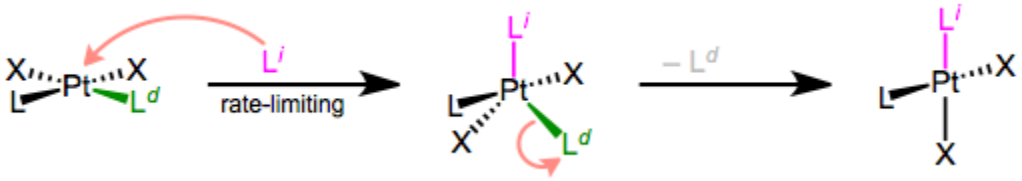
This page titled 8.4.1: β-Elimination Reactions is shared under a CC BY-NC-SA 4.0 license and was authored, remixed, and/or curated by Michael Evans.

- 4.1: β-Elimination Reactions by Michael Evans is licensed CC BY-NC-SA 4.0.

8.4.2: Associative Ligand Substitution

Despite the sanctity of the 18-electron rule to many students of organometallic chemistry, a wide variety of stable complexes possess fewer than 18 total electrons at the metal center. Perhaps the most famous examples of these complexes are 14- and 16-electron complexes of group 10 metals involved in cross-coupling reactions.

Ligand substitution in complexes of this class typically occurs via an associative mechanism, involving approach of the incoming ligand to the complex before departure of the leaving group. If we keep this principle in mind, it seems easy enough to predict when ligand substitution is likely to be associative. But how can we spot an associative mechanism in experimental data, and what are some of the consequences of this mechanism?



The prototypical mechanism of associative ligand substitution. The first step is rate-determining. A typical mechanism for associative ligand substitution is shown above. It should be noted that square pyramidal geometry is also possible for the intermediate, but is less common. Let's begin with the kinetics of the reaction.

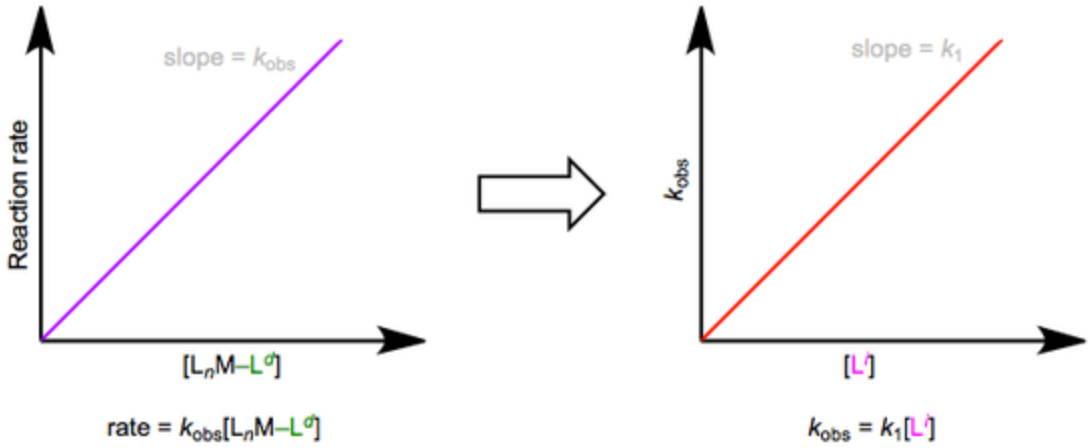
Reaction Kinetics

Reaction kinetics are commonly used to elucidate organometallic reaction mechanisms, and ligand substitution is no exception. Different mechanisms of substitution may follow different rate laws, so plotting the dependence of reaction rate on concentration often allows us to distinguish mechanisms. Associative substitution's rate law is analogous to that of the S_N2 reaction—rate depends on the concentrations of both starting materials.

$$L_nM{-}L^d + L_i \rightarrow L_nM{-}L_i + L^d \tag{8.4.2.1}$$

$$\frac{d[L_nM{-}L^i]}{dt} = rate = k_1[L_nM{-}L^d][L^i] \tag{8.4.2.2}$$

The easiest way to determine this rate law is to use pseudo-first-order conditions. Although the rate law is second order overall, if we could somehow render the concentration of the incoming ligand unchanging, the reaction would appear first order. The observed rate constant under these conditions reflects the constancy of the incoming ligand's concentration ($k_{obs} = k_1[L^i]$, where both k_1 and $[Li]$ are constants). How can we make the concentration of the incoming ligand invariant, you ask? We can drown the reaction in ligand to achieve this. The teensy weensy bit actually used up in the reaction has a negligible effect on the concentration of the "sea" of starting ligand we began with. The observed rate is equal to $k_{obs}[L_nM{-}L^d]$, as shown by the purple trace below. By determining k_{obs} at a variety of $[L^i]$ values, we can finally isolate k_1, the rate constant for the slow step. The red trace below at right shows the idea.



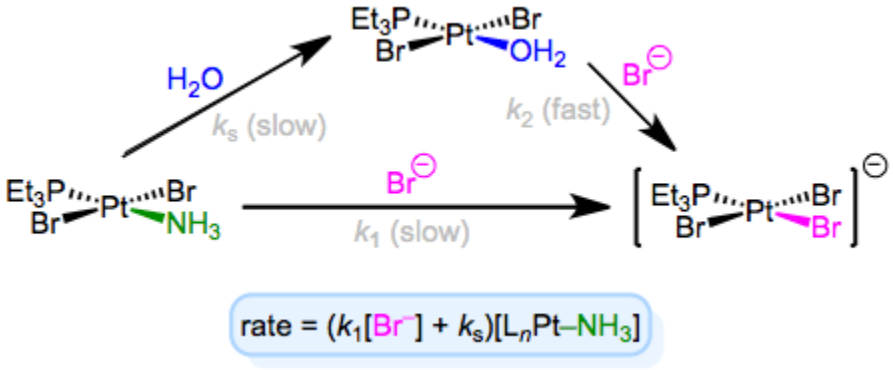
Associative substitution under pseudo-first-order conditions. The reaction is "swamped out" with incoming ligand.

In many cases, the red trace ends up with a non-zero y-intercept...curious, if we limit ourselves to the simple mechanism shown in the first figure of this post. A non-zero intercept suggests a more complex mechanism. We need to add a new term (called k_s for reasons to become clear shortly) to our first set of equations:

$$rate = (k_1[L_i] + k_s)[L_nM–L^d] \tag{8.4.2.3}$$

$$k_{obs} = k_1[L_i] + k_s \tag{8.4.2.4}$$

The full rate law suggests that some other step (with rate ks[LnM–Ld]) independent of incoming ligand is involved in the mechanism. To explain this observation, we can invoke the solvent as a reactant. Solvent can associate with the complex first in a slow step, then incoming ligand can displace the solvent in a fast step. Solvent concentration doesn't enter the rate law because, well, it's drowning the reactants and its concentration undergoes negligible change! An example of this mechanism in the context of Pt(II) chemistry is shown below.



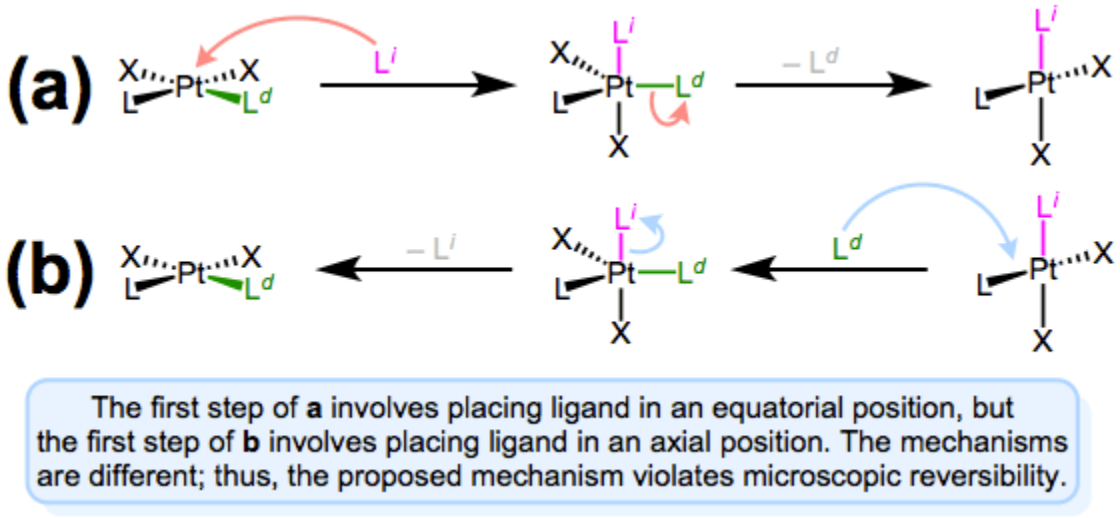
Associative substitution with solvent participation—a head-scratching mechanism for many an organometallic grad student!

As an aside, it's worth mentioning that the entropy of activation of associative substitution is typically negative. Entropy decreases as the incoming ligand and complex come together in the rate-determining step. Dissociative substitution shows the opposite behavior: loss of the departing ligand in the RDS increases entropy, resulting in positive entropy of activation.

Stereochemistry of Substitution

As we saw in discussions of the trans effect, the entering and departing ligands both occupy equatorial positions in the trigonal bipyramidal intermediate. Microscopic reversibility is to blame: the mechanism of the forward substitution (displacement of the leaving by the incoming ligand) must be the same as the mechanism of the reverse reaction (displacement of the incoming by the

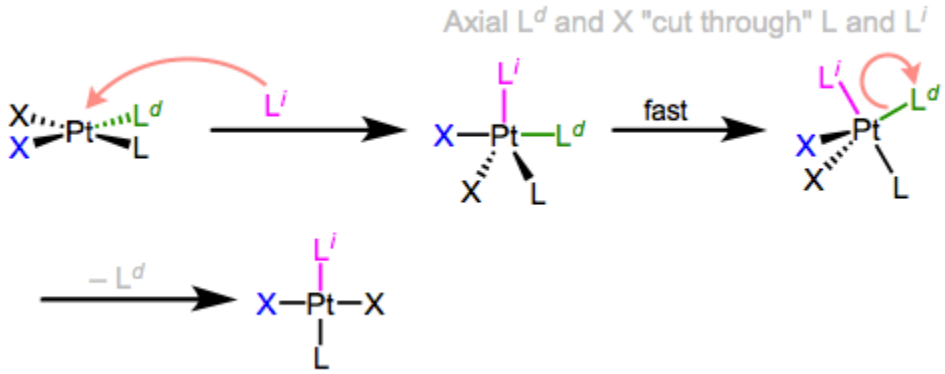
leaving ligand). This can be a confusing point, so let's examine an alternative mechanism that violates microscopic reversibility.



A mechanism involving approach to an axial position and departure from an equatorial position violates microscopic reversibility. Forward and reverse reactions a and b differ!

The figure above shows why a mechanism involving axial approach and equatorial departure (or vice versa) is not possible. The forward and reverse reactions differ, in fact, in both steps. In forward mechanism a, the incoming ligand enters an axial site. But in the reverse reaction, the incoming ligand (viz., the departing ligand in mechanism a) sits on an equatorial site. The second steps of each mechanism differ too—a involves loss of an equatorial ligand, while b involves loss of an axial ligand. Long story short, this mechanism violates microscopic reversibility. And what about a mechanism involving axial approach and axial departure? Such a mechanism is unlikely on electronic grounds. The equatorial sites are more electron rich than the axial sites, and σ bonding to the axial d_{z^2} orbital is expected to be strong. Intuitively, then, loss of ligand from an axial site is less favorable than loss from an equatorial site.

I know what you're thinking: what the heck does all of this have to do with stereochemistry? Notice that, in the equatorial-equatorial mechanism (first figure of this post), the axial ligands don't move at all. The configuration of the starting complex is thus retained in the product. Although retention is "normal," complications often arise because five-coordinate TBP complexes—like other odd-coordinate organometallic complexes—are often fluxional. Axial and equatorial ligands can rapidly exchange through a process called Berry pseudorotation, which resembles the axial ligands "cutting through" a pair of equatorial ligands like scissors (animation!). Fluxionality means that all stereochemical bets are off, since any ligand can feasibly occupy an equatorial site. In the example below, the departing ligand starts out cis to L, but the incoming ligand ends up trans to L.



Berry pseudorotation in the midst of associative ligand substitution.

Associative Substitution in 18-electron Complexes?

Associative substitution can occur in 18-electron complexes if it's preceded by the dissociation of a ligand. For example, changes in the hapticity of cyclopentadienyl or indenyl ligands may open up a coordination site, which can be occupied by a new ligand to kick off associative substitution. An allyl ligand may convert from its π to σ form, leaving an open coordination site where the π bond left. A particularly interesting case is the **nitrosyl ligand**—conversion from its linear to bent form opens up a site for coordination of an external ligand.

Summary

Associative ligand substitution is common for complexes with 16 total electrons or fewer. The reaction is characterized by a second-order rate law, the possibility of solvent participation, and a trigonal bipyramidal intermediate that is often fluxional. An open coordination site is essential for associative substitution, but such sites are often hidden in the dynamism of 18-electron complexes with labile ligands.

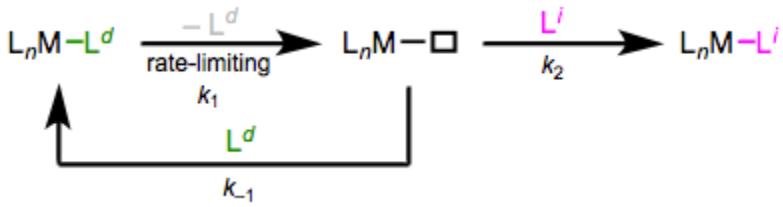
Dr. Michael Evans (Georgia Tech)

This page titled 8.4.2: Associative Ligand Substitution is shared under a CC BY-NC-SA 4.0 license and was authored, remixed, and/or curated by Michael Evans.

- 4.2: Associative Ligand Substitution by Michael Evans is licensed CC BY-NC-SA 4.0.

8.4.3: Dissociative Ligand Substitution Reactions

Associative substitution is unlikely for saturated, 18-electron complexes—coordination of another ligand would produce a 20-electron intermediate. For 18-electron complexes, dissociative substitution mechanisms involving 16-electron intermediates are more likely. In a slow step with positive entropy of activation, the departing ligand leaves, generating a coordinatively unsaturated intermediate. The incoming ligand then enters the coordination sphere of the metal to generate the product. For the remainder of this post, we'll focus on the kinetics of the reaction and the nature of the unsaturated intermediate (which influences the stereochemistry of the reaction). The reverse of the first step, re-coordination of the departing ligand (rate constant k–1), is often competitive with dissociation.



A general scheme for dissociative ligand substitution. There's more to the intermediate than meets the eye!

Reaction Kinetics

Let's begin with the general situation in which k_1 and k_{-1} are similar in magnitude. Since k_1 is rate limiting, k_2 is assumed to be much larger than k_1 and k_{-1}. Most importantly, we need to assume that variation in the concentration of the unsaturated intermediate is essentially zero. This is called the steady state approximation, and it allows us to set up an equation that relates reaction rate to observable concentrations Hold onto that for a second; first, we can use step 2 to establish a preliminary rate expression.

$$\text{rate} = k_2[L_nM\text{–}\lozenge][Li] \tag{1}$$

Of course, the unsaturated complex is present in very small concentration and is unmeasurable, so this equation doesn't help us much. We need to remove the concentration of the unmeasurable intermediate from (1), and the steady state approximation helps us do this. We can express variation in the concentration of the unsaturated intermediate as (processes that make it) minus (processes that destroy it), multiplying by an arbitrary time length to make the units work out. All of that equals zero, according to the SS approximation. The painful math is almost over! Since Δt must not be zero, the other factor, the collection of terms, must equal zero.

$$\Delta[LnM\text{–}\lozenge] = 0 = (k1[LnM\text{–}L^d]\text{–}k\text{–}1[LnM\text{–}\lozenge][L^d]\text{–}k_2[LnM\text{–}\lozenge][Li])\Delta t \tag{2}$$

$$0 = k_1[LnM\text{–}Ld]\text{–}k_{-1}[LnM\text{–}\lozenge][Ld]\text{–}k_2[LnM\text{–}\lozenge][Li] \tag{3}$$

Rearranging to solve for [LnM–◊], we arrive at the following.

$$[LnM\text{–}\lozenge] = k_1\frac{[LnM\text{–}L_d]}{(k_{-1}[L_d] + k_2[Li]} \tag{4}$$

Finally, substituting into equation (1) we reach a verifiable rate equation.

$$\text{rate} = k_2k_1\frac{[LnM\text{–}Ld][Li]}{(k_{-1}[L_d] + k_2[Li]} \tag{5}$$

When k_{-1} is negligibly small, (5) reduces to the familiar equation (6), typical of dissociative reactions like S_N1.

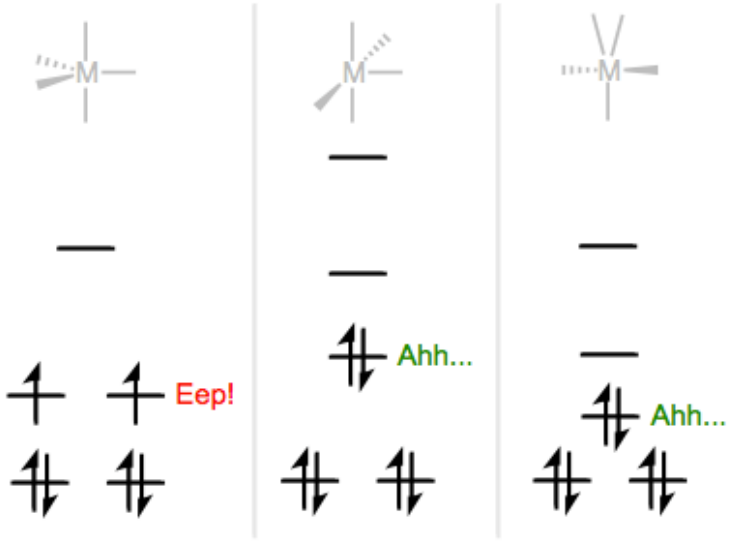
$$\text{rate} = k_1[LnM\text{–}L_d] \tag{6}$$

Unlike the associative rate law, this rate does not depend on the concentration of incoming ligand. For reactions that are better

described by (5), we can drown the reaction in incoming ligand to make $k_2[Li]$ far greater than $k_{-1}[Ld]$, essentially forcing the reaction to fit equation (6).

The Unsaturated Intermediate & Stereochemistry

Dissociation of a ligand from an octahedral complex generates an usaturated ML5 intermediate. When all five of the remaining ligands are L-type, as in Cr(CO)5, the metal has 6 d electrons for a total electron count of 16. The trigonal bipyramidal geometry presents electronic problems (unpaired electrons) for 6 d electrons, as the figure below shows. The orbital energy levels come from crystal field theory. Distortion to a square pyramid or a distorted TBP geometry removes the electronic issue, and so five-coordinate d6 complexes typically have square pyramidal or distorted TBP geometries. This is just the geometry prediction process in action!



TBP geometry is electronically disfavored for d6 metals. Distorted TBP and SP geometries are favored.

When the intermediate adopts square pyramidal geometry (favored for good π-acceptors and σ-donors...why?), the incoming ligand can simply approach where the departing ligand left, resulting in retention of stereochemistry. Inversion is more likely when the intermediate is a distorted trigonal bipyramid (favored for good π-donors). As we've already seen for associative substitution, fluxionality in the five-coordinate intermediate can complicate the stereochemistry of the reaction.

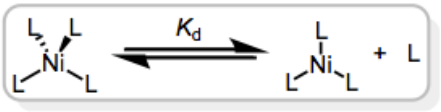
Encouraging Dissocative Substitution

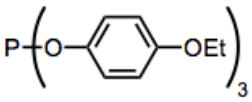
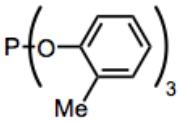
In general, introducing structural features that either stabilize the unsaturated intermediate or destabilize the starting complex can encourage dissociative substitution. Both of these strategies lower the activation barrier for the reaction. Other, quirky ways to encourage dissociation include photochemical methods, oxidation/reduction, and ligand abstraction.

Let's begin with features that stabilize the unsaturated intermediate. Electronically, the intermediate loves it when its d electron count is nicely matched to its crystal field orbitals. As you study organometallic chemistry, you'll learn that there are certain "natural" d electron counts for particular geometries that fit well with the metal-centered orbitals predicted by crystal field theory. Octahedral geometry is great for six d electrons, for example, and square planar geometry loves eight d electrons. Complexes with "natural" d electron counts—but bearing one extra ligand—are ripe for dissociative substitution. The classic examples are d8 TBP complexes, which become d8 square planar complexes (think Pt(II) and Pd(II)) upon dissociation. Similar factors actually stabilize starting 18-electron complexes, making them less reactive in dissociative substitution reactions. d6 octahedral complexes are particularly happy, and react most slowly in dissociative substitutions. The three most common types of 18-electron complexes, from fastest to slowest at dissociative substitution, are:

d8 TBP > d10 tetrahedral > d6 octahedral

Destabilization of the starting complex is commonly accomplished by adding steric bulk to its ligands. Naturally, dissociation relieves steric congestion in the starting complex. Chelation has the opposite effect, and tends to steel the starting complex against dissociation.



L	Cone Angle	K_d
$P(OEt)_3$	109	$< 10^{-10}$
	128	$6 * 10^{-10}$
$P(O\textit{i}\text{-}Pr)_3$	130	$2.7 * 10^{-5}$
	141	$4 * 10^{-2}$
PPh_3	145	huge

As steric bulk on the ligand increases, dissociation becomes more favorable.

I plan to cover the “quirky” methods in a post of their own, but these include strategies like N-oxides for CO removal, photochemical cleavage of the metal–departing ligand bond, and the use of silver cation to abstract halide ligands. Oxidation and reduction can also be used to encourage substitution: 17- and 19-electron complexes are much more reactive toward substitution than their 18-electron analogues.

This page titled 8.4.3: Dissociative Ligand Substitution Reactions is shared under a CC BY-NC-SA 4.0 license and was authored, remixed, and/or curated by Michael Evans.

- 4.3: Dissociative Ligand Substitution Reactions by Michael Evans is licensed CC BY-NC-SA 4.0.

8.4.4: Ligand substitution

Ligand substitution is the first reaction one typically encounters in an organometallic chemistry course. In general, ligand substitution involves the exchange of one ligand for another, with no change in oxidation state at the metal center. The incoming and outgoing ligands may be L- or X-type, but the charge of the complex changes if the ligand type changes. Keep charge conservation in mind when writing out ligand substitutions.

How do we know when a ligand substitution reaction is favorable? The thermodynamics of the reaction depend on the relative strength of the two metal-ligand bonds, and the stability of the departing and incoming ligands (or salt sof the ligand, if they're X type). It's often useful to think of X-for-X substitutions like acid-base reactions, with the metal and spectator ligands serving as a "glorified proton." Like acid-base equilibria in organic chemistry, we look to the relative stability of the two charged species (the free ligands) to draw conclusions. Of course, we don't necessarily need to rely just on primal thermodynamics to drive ligand substitution reactions. Photochemistry, neighboring-group participation, and other tools can facilitate otherwise difficult substitutions.

Ligand substitution is characterized by a continuum of mechanisms bound by associative (A) and dissociative (D) extremes. At the associative extreme, the incoming ligand first forms a bond to the metal, then the departing ligand takes its lone pair and leaves. At the dissociative extreme, the order of events is opposite—the departing ligand leaves, then the incoming ligand comes in. Associative substitution is common for 16-electron complexes (like d8 complexes of Ni, Pd, and Pt), while dissociative substitution is the norm for 18-electron complexes. Then again, reality is often more complicated than these extremes. In some cases, evidence is available for simultaneous dissociation and association, and this mechanism has been given the name interchange (IA or ID).

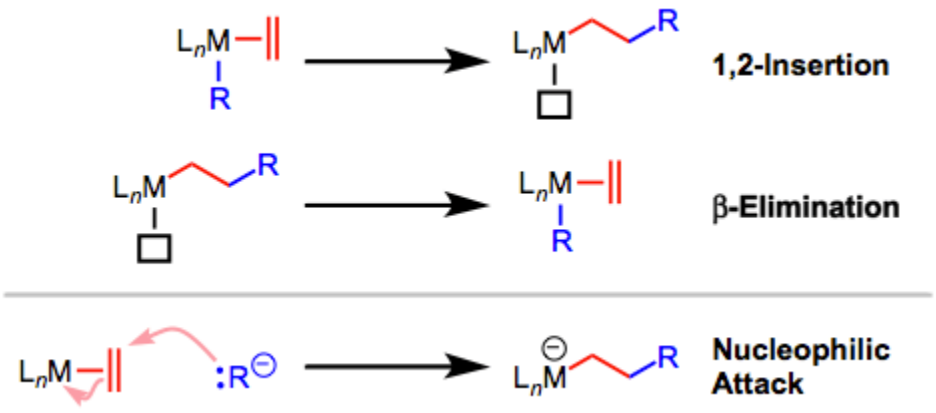
Over the next few posts, we'll explore ligand substitution reactions and mechanisms in detail. We'd like to be able to (a) predict whether a mechanism is likely to be associative or dissociative; (b) propose a reasonable mechanism from given experimental data; and (c) describe the results we'd expect given a particular mechanism. Keep these goals in mind as you learn the theoretical and experimental nuts and bolts of substitution reactions.

This page titled 8.4.4: Ligand substitution is shared under a CC BY-NC-SA 4.0 license and was authored, remixed, and/or curated by Michael Evans.

- 4.4: Ligand substitution by Michael Evans is licensed CC BY-NC-SA 4.0.

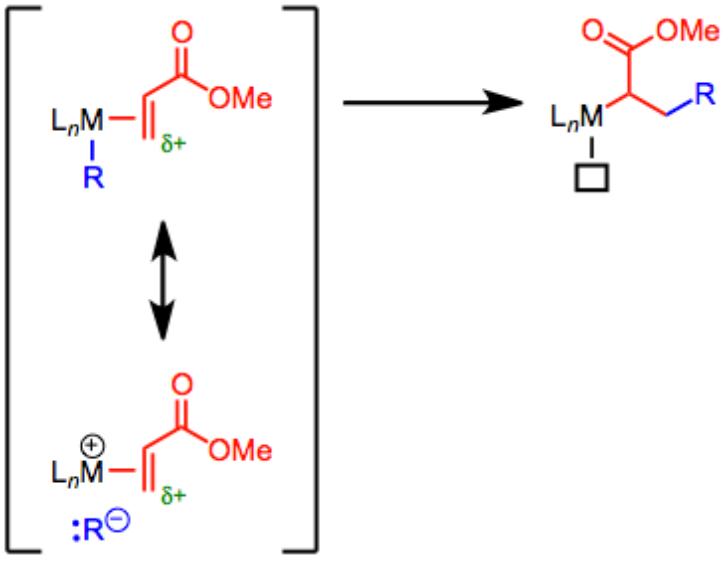
8.4.5: Migratory Insertion- 1,2-Insertions

Insertions of π systems into M-X bonds are appealing in the sense that they establish two new σ bonds in one step, in a stereocontrolled manner. As we saw in the last post, however, we should take care to distinguish these fully intramolecular migratory insertions from intermolecular attack of a nucleophile or electrophile on a coordinated π-system ligand. The reverse reaction of migratory insertion, β-elimination, is not the same as the reverse of nucleophilic or electrophilic attack on a coordinated π system.



1,2-Insertion is distinct from nucleophilic/electrophilic attack on coordinated ligands.

Like 1,1-insertions, 1,2-insertions generate a vacant site on the metal, which is usually filled by external ligand. For unsymmetrical alkenes, it's important to think about site selectivity: which atom of the alkene will end up bound to metal, and which to the other ligand? To make predictions about site selectivity we can appeal to the classic picture of the M–X bond as M+X–. Asymmetric, polarized π ligands contain one atom with excess partial charge; this atom hooks up with the complementary atom in the M–R bond during insertion. Resonance is our best friend here!



The site selectivity of 1,2-insertion can be predicted using resonance forms and partial charges.

A nice study by Yu and Spencer illustrates these effects in homogeneous palladium- and rhodium-catalyzed hydrogenation reactions. Unactivated alkenes generally exhibit lower site selectivity than activated ones, although steric differences between the

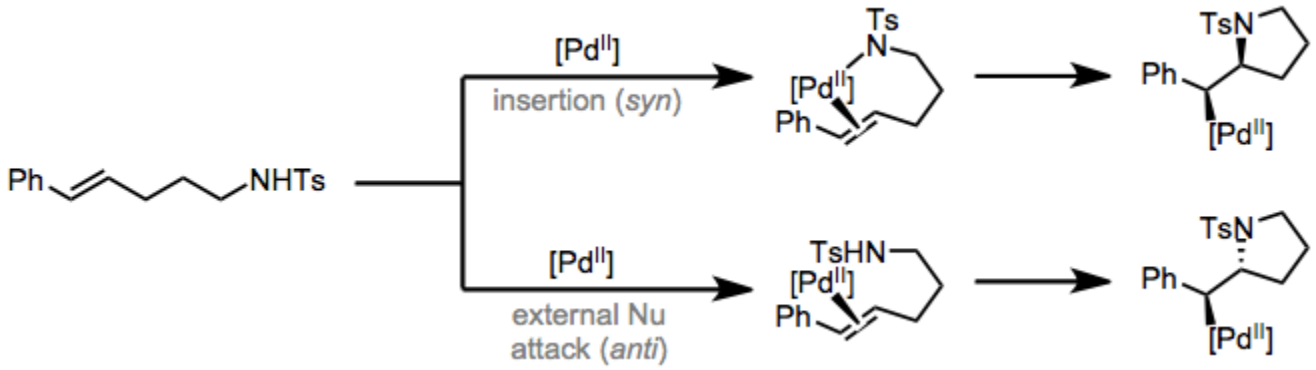
two ends of the double bond can promote selectivity.

Reactivity Trends in 1,2-Insertions

The thermodynamics of 1,2-insertions of alkenes depend strongly on the alkene, but we can gain great insight by examining the structure of the product alkyl. Coordinated alkenes that give strong metal-alkyl bonds after migratory insertion tend to undergo the process. Hence, electron-withdrawing groups, such as carbonyls and fluorine atoms, tend to encourage migratory insertion—remember that alkyl complexes bearing these groups tend to have stable M–C bonds.

Insertions of alkenes into both M–H and M–R (R = alkyl) are favored thermodynamically, but the kinetics of M–R insertion are much slower. This observation reflects a pervasive trend in organometallic chemistry: M–H bonds react more rapidly than M–R bonds. The same is true of the reverse, β-elimination. Even in cases when both hydride and alkyl elimination are thermodynamically favored, β-hydride elimination is much faster. Although insertion into M–R is relatively slow, this elementary step is critical for olefin polymerizations that form polyalkenes (Ziegler-Natta polymerization). This reaction deserves a post all its own!

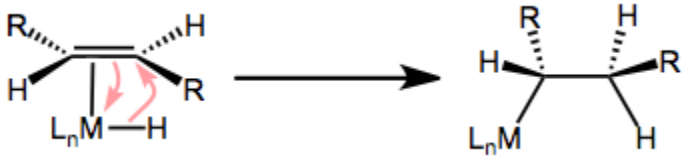
As the strength of the M–X bond increases, the likelihood that an L-type π ligand will insert into the bond goes down. Hence, while insertions into M–H and M–C are relatively common, insertions into M–N and M–O bonds are more rare. Lanthanides and palladium are known to promote insertion into M–N in some cases, but products with identical connectivity can come from external attack of nitrogen on a coordinated π ligand. The diastereoselectivity of these reactions provides mechanistic insight—since migratory insertion is syn (see below), a syn relationship between Pd and N is to be expected in the products of migratory insertion. An anti relationship indicates external attack by nitrogen or oxygen.



The diastereoselectivity of formal insertions provides insight about their mechanisms.

Stereochemistry of 1,2-Insertions

1,2-Insertion may establish two stereocenters at once, so the stereochemistry of the process is critical! Furthermore, 1,2-insertions and β-eliminations are bound by important stereoelectronic requirements. An analogy can be made to the E2 elimination of organic chemistry, which also has strict stereoelectronic demands. For migratory insertion to proceed, the alkene and X-type ligand must be syncoplanar during insertion; as a consequence of this alignment, X and MLn end up on the same face of the alkene after insertion. In other words, insertions into alkenes take place in a syn fashion. Complexes that have difficulty achieving a coplanar arrangement of C=C and M–X undergo insertion very slowly, if at all.



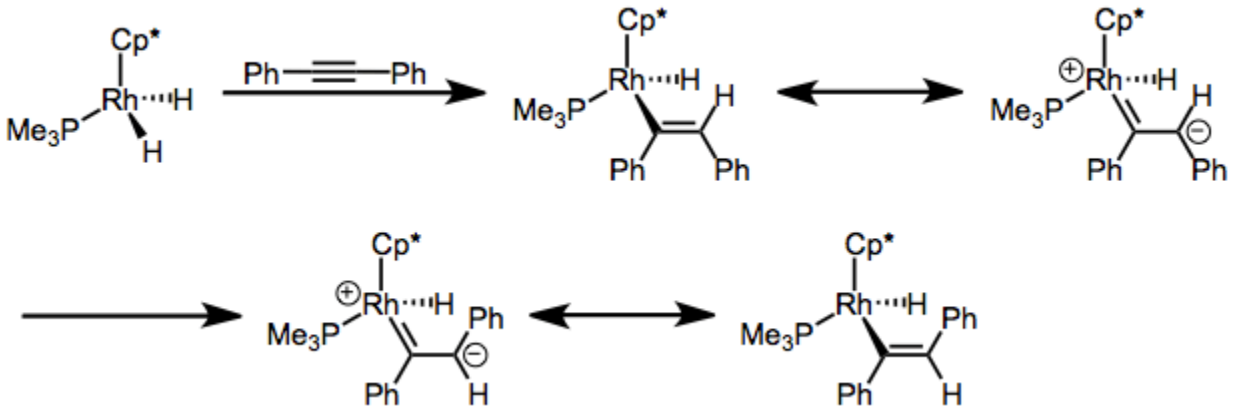
1,2-Insertions take place in a syn fashion. The metal and X end up bound to the same face of the alkene.

This observation has important implications for β-elimination, too—the eliminating X and the metal must have the ability to align

syn.

Insertions of Other π Systems

To close this post, let's examine insertions into π ligands other than alkenes briefly. Insertions of alkynes into metal-hydride bonds are known, and are sometimes involved in reactions that I refer to collectively as "hydrostuffylation": hydrosilylation, hydroesterification, hydrogenation, and other net H–X additions across the π bond. Strangely, some insertions of alkynes yield trans products, even though cis products are to be expected from syn addition of M–X. The mechanisms of these processes involve initial syn addition followed by isomerization to the trans complex via an interesting resonance form. The cis complex is the kinetic product, but it isomerizes over time to the more thermodynamically stable trans complex.



Migratory insertions of alkynes into M–H produce alkenyl complexes, which have been known to isomerize.

The strongly donating Cp* ligand supports the legitimacy of the zwitterionic resonance form—and suggests that the C=C bond may be weaker than it first appears!

Polyenes can participate in migratory insertion, and insertions of polyenes are usually quite favored because stabilized π-allyl complexes result. In one mind-bending case, a coordinated arene inserts into an M–Me bond in a syn fashion!

Have you ever stopped to consider that the addition of methyllithium to an aldehyde is a formal insertion of the carbonyl group into the Li–Me bond? It's true! We can think of these as (very) early-metal "insertion" reactions. Despite this precedent, migratory insertion reactions of carbonyls and imines into late-metal hydride and alkyl bonds are surprisingly hard to come by. Rhodium is the most famous metal that can make this happen—rhodium has been used in complexes for arylation and vinylation, for example. Insertion of X=C into the M–R bond is usually followed by β-hydride elimination, which has the nifty effect of replacing H in aldehydes and aldimines with an aryl or vinyl group.

This page titled 8.4.5: Migratory Insertion- 1,2-Insertions is shared under a CC BY-NC-SA 4.0 license and was authored, remixed, and/or curated by Michael Evans.

- 4.5: Migratory Insertion- 1,2-Insertions by Michael Evans is licensed CC BY-NC-SA 4.0.

8.4.6: Migratory Insertion- Introduction and CO Insertions

Introduction

We've seen that the metal-ligand bond is generally polarized toward the ligand, making it nucleophilic. When a nucleophilic, X-type ligand is positioned *cis* to an unsaturated ligand in an organometallic complex, an interesting process that looks a bit like nucleophilic addition can occur.

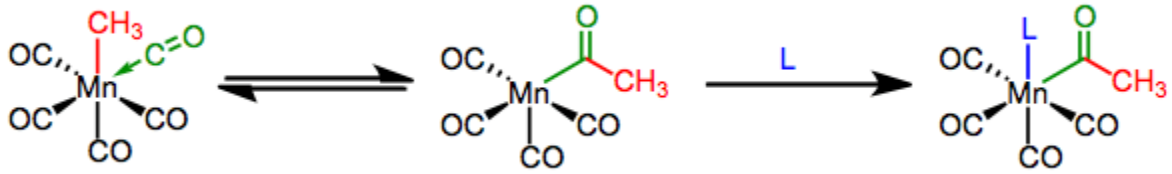


Figure 8.4.6.1: Migratory insertion into a metal-carbon bond. (Michael Evans)

On the whole, the unsaturated ligand appears to insert itself into the M–X bond; hence, the process is called **migratory insertion**. An open coordination site shows up in the complex, and is typically filled by an added ligand. The open site may appear where the unsaturated ligand was *or* where the X-type ligand was, depending on which group actually moved (see below). There is no change in oxidation state at the metal (unless the ligand is an alkylidene/alkylidyne), but the total electron count of the complex decreases by two during the actual insertion event—notice in the above example that the complex goes from 18 to 16 total electrons after insertion. A dative ligand comes in to fill that empty coordination site, but stay flexible here: L could be a totally different ligand or a Lewis base in the X-type ligand. L can even be the carbonyl oxygen itself!

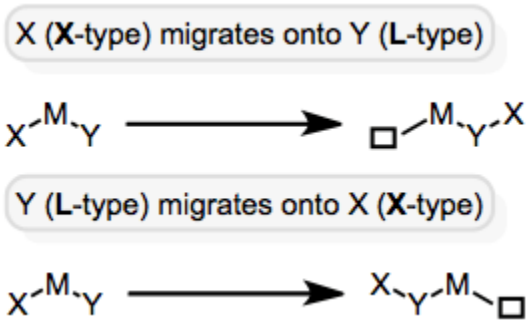


Figure 8.4.6.2: X can migrate onto unsaturated ligand Y, or Y onto X. The former is more common for CO insertions. (Michael Evans)

We can distinguish between two types of insertions, which differ in the number of atoms in the unsaturated ligand involved in the step. Insertions of CO, carbenes, and other η^1 unsaturated ligands are called **1,1-insertions** because the X-type ligand moves from its current location on the metal to one spot over, on the atom bound to the metal. η^2 ligands like alkenes and alkynes can also participate in migratory insertion; these reactions are called **1,2-insertions** because the X-type ligand slides two atoms over, from the metal to the distal atom of the unsaturated ligand.

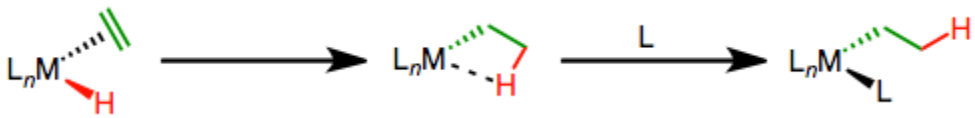


Figure 8.4.6.3: 1,2-insertion of an alkene and hydride. In some cases, an agostic interaction has been observed in the unsaturated intermediate. (Michael Evans)

This is really starting to look like the addition of M and X across a π bond! However, we should take care to distinguish this completely intramolecular process from the attack of a nucleophile or electrophile on a coordinated π system, which is

a different beast altogether. Confusingly, chemists often jumble up all of these processes using words like “hydrometalation,” “carbometalation,” “aminometalation,” etc. Another case of big words being used to obscure ignorance! We’ll look at nucleophilic and electrophilic attack on coordinated ligands in separate posts.

Reactivity Trends in CO Insertions

Certain conditions *must* be met for migratory insertion to occur: the two ligands undergoing the process must be *cis*, and the complex must be stable with two fewer total electrons. Thermodynamically, the formed Y–X and covalent M–Y bonds must be more stable than the broken M–X and dative M–Y bonds for insertion to be favored. When the opposite is true, the microscopic reverse (**elimination** or **deinsertion**) will occur spontaneously.

Migratory aptitudes for insertion into CO have been studied extensively, and the general conclusion here is “it’s complicated.” A few ligands characterized by remarkably stable metal-ligand bonds don’t undergo insertion for thermodynamic reasons—the M–X bond is just too darn strong. Perfluoroalkyl complexes and metal hydrides are two notable examples. Electron-withdrawing groups on the X-type ligand, which strengthen the M–X bond, slow down insertion (likely for thermodynamic reasons though…Hammond’s postulate in action).

What factors affect the relative speed (kinetics) of favorable insertions? Sterics is one important variable. Both 1,1- and 1,2-insertions can relieve steric strain at the metal center by spreading out the ligands involved in the step. In 1,2-insertions, the X-type ligand removes itself completely from the metal! Unsurprisingly, then, bulky ligands undergo insertions more rapidly than smaller ligands. Complexes of the first-row metals tend to react more rapidly than analogous second-row metal complexes, and second-row metal complexes react faster than third-row metal complexes. This trend fits in nicely with the typical trend in M–C bond strengths: first row < second row < third row. Lewis acids help accelerate insertions into CO by coordinating to CO and making the carbonyl carbon more electrophilic. For a similar reason, CO ligands bound to electron-poor metal centers undergo insertion more rapidly than CO’s bound to electron-rich metals. Finally, for reasons that are still unclear, one-electron oxidation often increases the rate of CO insertion substantially.

Although the thermodynamics of alkene 1,2-insertion are more favorable for metal-carbon than metal-hydrogen bonds, M–H bonds react *much* more rapidly than M–C bonds in 1,2-insertions. This fact has been exploited for olefin hydrogenation, which would be much less useful if it had to complete with olefin polymerization (the result of repeated insertion of C=C into M–C) in the same reaction flask! More on that in the next post.

Stereochemistry in CO Insertions

Migratory insertion steps are full of stereochemistry! Configuration at the migrating alkyl group is retainedduring insertion—a nice piece of evidence supporting a concerted, intramolecular mechanism of migration.

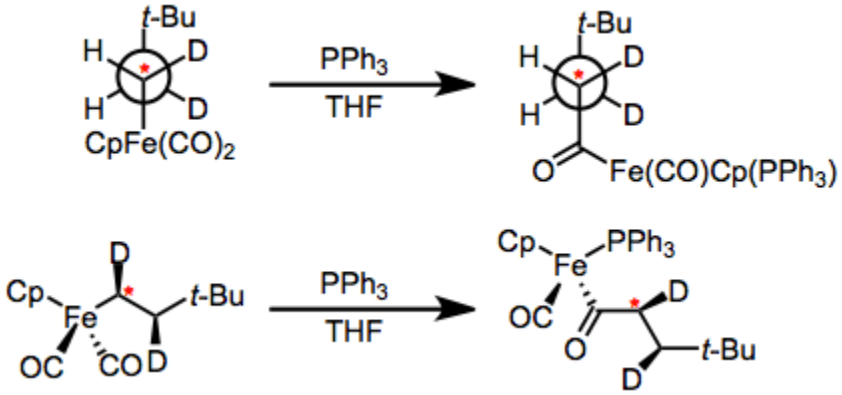


Figure 8.4.6.4: Migratory insertion occurs with retention of configuration at the migrating alkyl group. Two different views of the same reaction are shown here. (Michael Evans)

What about stereochemistry at the metal center? Migratory insertion may create a stereogenic center at the metal—see the iron example above. Whether the X-type ligand moves onto the unsaturated ligand or *vice versa* will impact the configuration of the product complex. Calderazzo’s study of this issue is one of my favorite experiments in all of organometallic chemistry! He took the simple labeled substrate in the figure below and treated it with dative ligand, encouraging insertion. Four products of insertion

are possible, corresponding to reaction of the four CO ligands *cis* to the methyl ligand. Try drawing a few curved arrows to wrap your mind around the four possibilities, and consider both CO migration and Me migration as possible at this point.

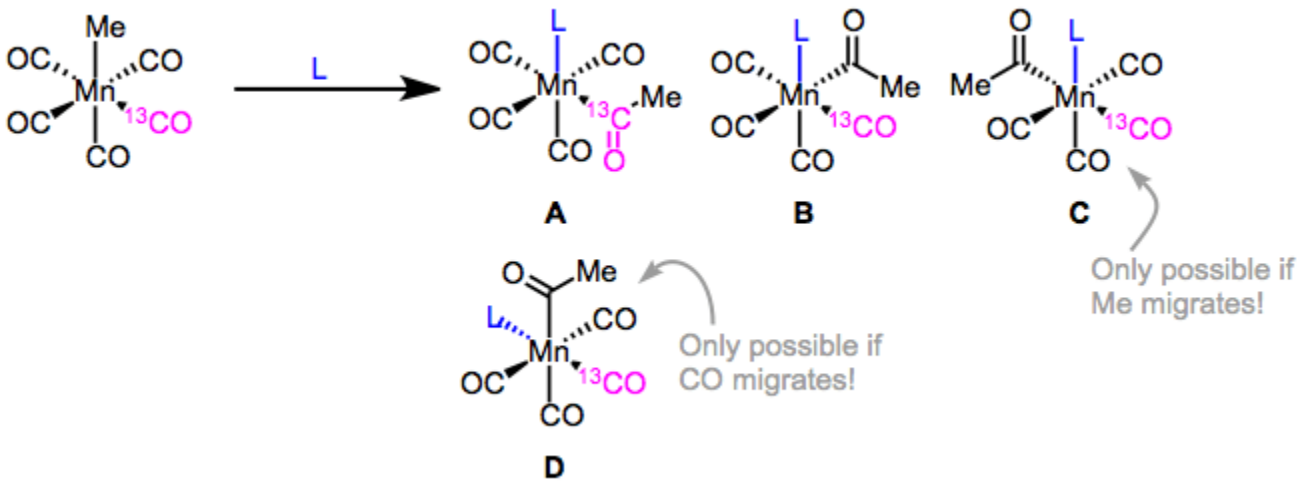


Figure 8.4.6.5: Insertion of the labeled complex shown could produce four products. Calderazzo did not observe product **D**, supporting a mechanism involving Me migration to CO. (Michael Evans)

Note that product **D** is impossible if we only allow the Me group to migrate—the spot *trans* to the labeled CO is another CO ligand, so that spot can only pick up L if CO migrates (not if Me migrates). On the other hand, product **C** must have come from the migration of Me, since the Me group has moved from a *cis* to a *trans*position relative to the labeled CO in product **C**. Calderazzo observed products **A**, **B**, and **C**, but not **D**, supporting a mechanism involving Me migration. Other experiments since support the idea that most of the time, the alkyl group migrates onto CO. Slick, huh?

I won't address insertions into alkylidenes, alkylidynes, and other one-atom unsaturated ligands in this post, as insertions into CO are by far the most popular 1,1 insertions in organometallic chemistry. In the next post, we'll dig more deeply into 1,2-insertions of alkenes and alkynes. Thanks for reading!

This page titled 8.4.6: Migratory Insertion- Introduction and CO Insertions is shared under a CC BY-NC-SA 4.0 license and was authored, remixed, and/or curated by Michael Evans.

8.4.7: Oxidative Addition- General Ideas

A critical difference between the transition metals and the organic elements is the ability of the former to exist in multiple oxidation states. In fact, the redox flexibility of the transition metals and the redox obstinacy of the organic elements work wonderfully together. Why? Imagine the transition metal as a kind of matchmaker for the organic elements. Transition metals can take on additional covalent bonds (oxidation), switch out ligands (substitution), then release new covalent bonds (reduction). The resulting organic products remain unfazed by the metal's redox insanity. Talk about a match made in heaven!

The following series of posts will deal with the first step of this process, oxidation. More specifically, we'll discuss the oxidation of transition metals via formal insertion into covalent bonds, also known as **oxidative addition (OA)**. Although we often think of oxidative addition as an elementary reaction of organometallic chemistry, it is *not* an elementary mechanistic *step*. In fact, oxidative addition can proceed through a variety of mechanisms. Furthermore, any old change in oxidation state does not an oxidative addition make (that almost rhymes...). Formally, the attachment of an electrophile to a metal center (e.g., protonation) represents oxidation, but we shouldn't call this oxidative addition, since two ligands aren't entering the fray. Instead, we call this **oxidative ligation (OL)**.

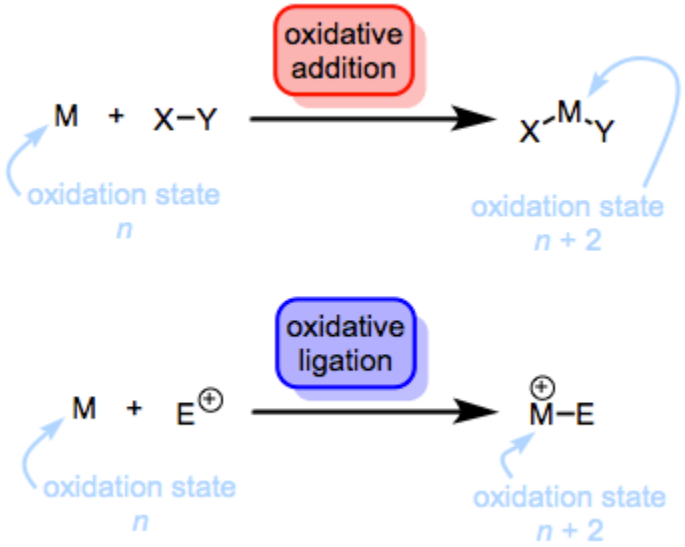


Figure 8.4.7.1: Oxidative addition involves formal bond insertion and the introduction of two new ligands to the metal. Oxidative ligation, OTOH, involves the coordination of only one new ligand, an electrophile. (Michael Evans)

Protonation is (formally) a kind of oxidation. Who knew?! S_N2 reactions with the metal as nucleophile are also oxidative ligations. Of course, if the leaving group comes back and forms a new bond to the metal, we're back to oxidative addition. Both reactions lead to an increase in the oxidation state of the metal by two units and a decrease in the *d* electron count of the metal by two electrons. However, note how the total electron count changes in each case. The total electron count does not change during an oxidative ligation. Think of it this way: the new ligand brings no electrons with it to the complex. On the other hand, the total electron count of the complex actually *increases* by two electrons during oxidative addition. As a result, *eighteen-electron complexes do not undergo oxidative addition*. Carve that sucker on a stone tablet. Seventeen-electron complexes can undergo oxidative addition via bimolecular OA reactions, which leave X on one metal center and Y on another.

What are the mechanisms of oxidative addition, anyway? Let's begin with the "concerted" mechanism, which can be thought of as σ-complex formation followed by insertion. The metal first sidles up to the X–Y bond and a σ complex forms (ligand dissociation may be required first). As we've seen, σ complexes $M(X_2)$ are tautomeric with their $M(X)_2$ forms. When back donation from the metal is strong enough, the σ complex disappears and $M(X)_2$ is all that remains. The metal has been formally oxidized: oxidative addition!

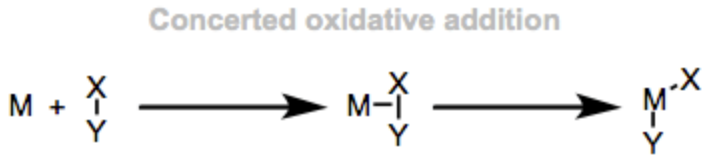


Figure 8.4.7.2: Copy and Paste Caption here. (Copyright; author via source)

There are several variations on this theme. When X and Y are different, the σ complex is skewed and approach to the metal "asynchronous." When the metal isn't a great nucleophile, the reaction may stop at the σ-complex stage.

Other mechanisms of oxidative addition require multiple steps and the formation of polar or radical intermediates. An important two-step, polar mechanism involves S_N2 attack of a nucleophilic metal on an electrophile, followed by coordination of the leaving group to the metal center. What we might call S_N1-type mechanisms, involving dissociation of the electrophile before nucleophilic attack by the metal, also occur (HCl and other strong acids operate like this). Finally, both non-chain and chain radical mechanisms are possible in reactions of metal complexes with alkyl halides. We'll dive into these mechanisms in more detail in upcoming posts.

Hopefully from this general discussion, you've gleaned a few trends. The metal *must* have a stable oxidation state two units higher than its current OS for oxidative addition to occur. For the reaction to work well, the metal typically needs to be electron rich (and in a relatively low oxidation state) and the organic compound needs to be electron poor. To see why, consider that during oxidative addition, the metal formally loses two *d*electrons. Furthermore, the main-group atoms X and Y gain electron density, since the new M–X and M–Y bonds are likely polarized toward X and Y. The metal needs to bear *two* open coordination sites (not necessarily at the same time) for oxidative addition to occur, because two new ligands enter the metal's coordination sphere. Since the new ligands need space, steric hindrance tends to discourage oxidative addition. Oftentimes ligand dissociation is required before oxidative addition can occur; in many of these cases, the rate of dissociation influences the overall rate of the reaction.

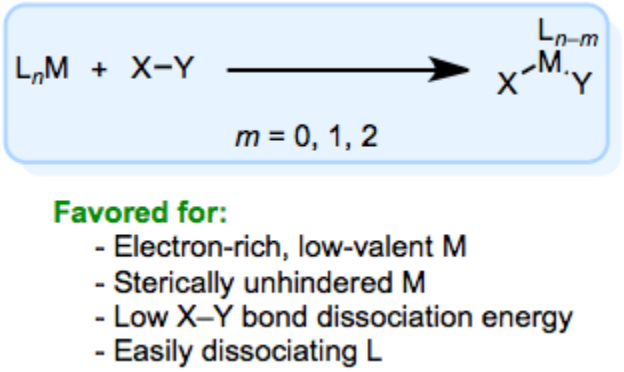


Figure 8.4.7.3: Factors affecting the kinetics and thermodynamics of oxidative addition. (Michael Evans)

This page titled 8.4.7: Oxidative Addition- General Ideas is shared under a CC BY-NC-SA 4.0 license and was authored, remixed, and/or curated by Michael Evans.

8.4.8: Oxidative Addition of Non-polar Reagents

How important are oxidative additions of non-polar reagents? *Very*. The addition of dihydrogen (H_2) is an important step in catalytic hydrogenation reactions. Organometallic C–H activations depend on oxidative additions of C–H bonds. In a fundamental sense, oxidative additions of non-polar organic compounds are commonly used to establish critical metal-carbon bonds. Non-polar oxidative additions get the ball rolling in all kinds of catalytic organometallic reactions. In this post, we'll examine the mechanisms and important trends associated with non-polar oxidative additions.

Oxidative Additions of H_2

Electron-rich metal centers with open coordination sites (or the ability to form them) undergo oxidative additions with dihydrogen gas. The actual addition step is concerted, as we might expect from the dull H_2molecule! However, before the addition step, some interesting gymnastics are going on. The status of the σ complex that forms prior to H–H insertion is an open question—for some reactions it is a transition state, others a discrete intermediate. In either case, the two new hydride ligands end up *cis* to one another. Subsequent isomerization may occur to give a *trans* dihydride.

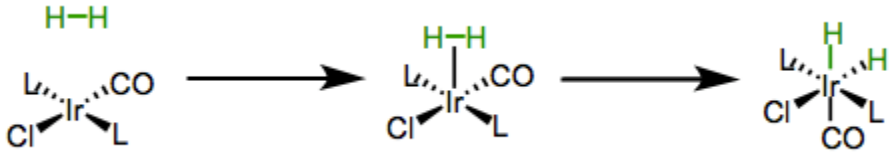


Figure 8.4.8.1: Oxidative addition of dihydrogen to Vaska's complex. Note the *cis*arrangement of the hydride ligands. (Michael Evans)

There's more to this little reaction than meets the eye. For starters, either pair of *trans* ligands in the starting complex (L/L or Cl/CO) may "fold back" to form the final octahedral complex. As in associative ligand substitution, the transition state for folding back is basically trigonal bipyramidal. As we saw before, π-acidic ligands love the equatorial sites of the TBP geometry, which are rich in electrons capable of π bonding. As a consequence, π-acidic ligands get folded back preferentially, and tend to end up *cis* to their *trans* partners in the starting complex.

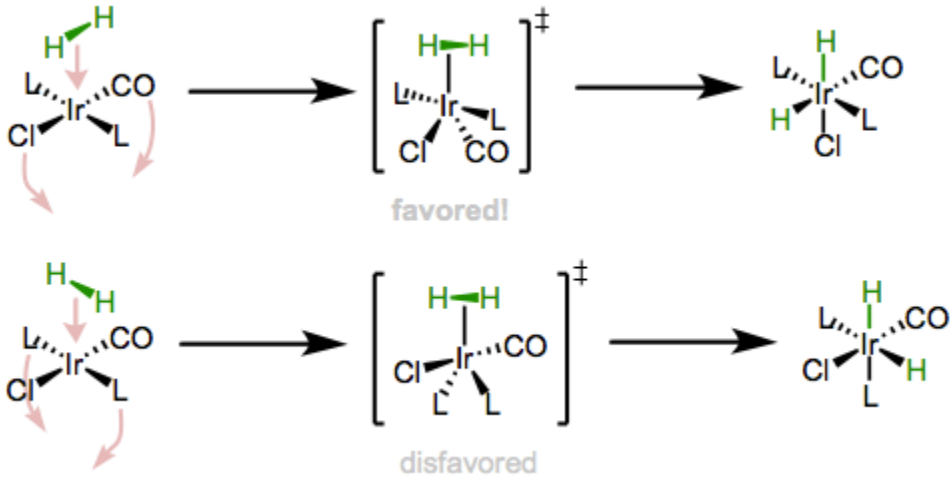


Figure 8.4.8.2: Dihydrogen may approach along two distinct trajectories. Placing π-acidic ligands in the equatorial plane of the TBP transition state is favored. (Michael Evans)

Termolecular oxidative additions of H_2, in which the two H atoms find their way to two different metal centers, are also known, but these suffer from entropic issues, since H_2 is jammed between two metal complexes in the transition state of the (concerted) mechanism.

Oxidative Additions of Silanes (H–Si)

Silanes bearing Si–H bonds may react with organometallic complexes in oxidative addition reactions. Spectroscopic experiments support the intermediacy of a silyl σ complex before insertion. Since the mechanism is concerted, oxidative addition occurs with retention of configuration at Si. The usual pair of forward bonding ($\sigma_{Si-H} \rightarrow d_{\sigma}$) and backbonding ($d_{\pi} \rightarrow \sigma^*_{Si-H}$) orbital interactions are at play here. File this reaction away as a great method for the synthesis of silyl complexes.

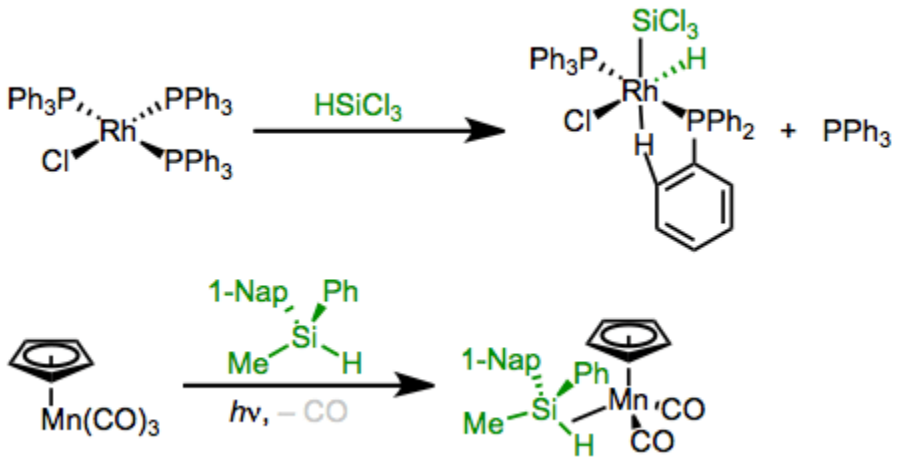


Figure 8.4.8.3: Si–H bonds undergo oxidative addition to electron-rich metal complexes. Electron-poor complexes may stop at the σ complex stage. (Michael Evans)

Oxidative Additions of C–H Bonds

Needless to say, oxidative addition reactions of C–H bonds are highly prized among organometallic chemists. As simple as it is to make silyl complexes through oxidative addition, analogous reactions of C–H bonds that yield alkyl hydride complexes are harder to come by.

The thermodynamics of C–H oxidative addition tell us whether it's favorable, and depend heavily on the nature of the organometallic complex. The sum of the bond energies of the new M–C and M–H bonds must exceed the sum of the energies of the C–H bond and any M–L bonds broken during the reaction (plus, OA is entropically disfavored). For many complexes, the balance is not in favor of oxidative addition. For example, the square planar Vaska's complex (L_2(CO)IrCl; L = PPh_3) seems like a great candidate for oxidative addition of methane—at least to the extent that the product will be six-coordinate and octahedral. However, thermodynamics is a problem:

$$104\ (C–H) - [60\ (Ir–H) + 35\ (Ir–Me)] + 9\ kcal/mol\ (entropy) = 18\ kcal/mol$$

18 kcal/mol is prohibitively high in energy, and playing with the temperature to adjust the entropy factor can't "save" the reaction.

More electron-rich complexes exhibit favorable thermodynamics for insertions of C–H bonds. The example below is so favorable (104 – [75 + 55] + 9 = –17 kcal/mol) that the product is a rock!

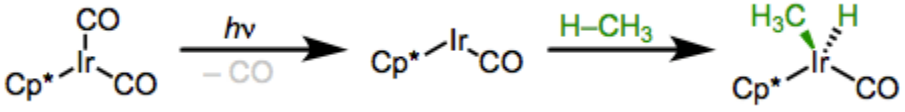


Figure 8.4.8.4: This thermodynamically favorable C–H oxidative addition is helped by the electron-donating Cp* ligand. (Michael Evans)

Arenes undergo C–H oxidative addition faster (and more favorably) than alkanes for several reasons. It seems likely that an intermediate arene π complex and/or C–H σ complex precede insertion, and these complexes ought to be more stable than alkyl σ complexes. In addition, metal-aryl bonds tend to be stronger than metal-alkyl bonds.

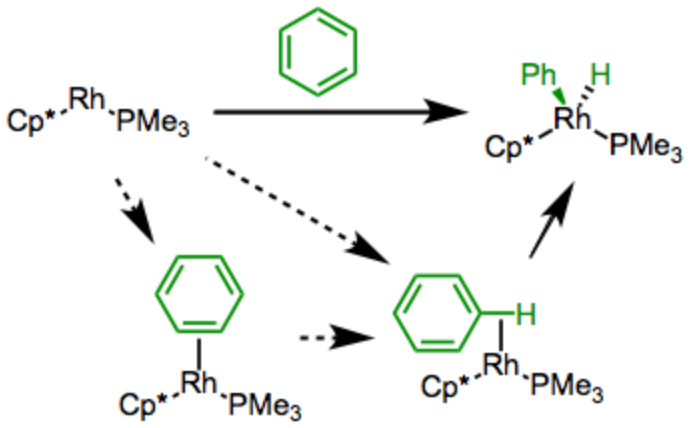


Figure 8.4.8.5: Mechanistic possibilities for the oxidative addition of arene C–H bonds. (Michael Evans)

Your average organic compound is covered in C–H bonds. Thus, for C–H oxidative addition to be synthetically useful, we need to understand how to control the selectivity of the reaction. In most early studies, selectivity for insertion into primary C–H bonds was observed. It became apparent that primary alkyl complexes (*viz*., the observed products) are generally much more stable than secondary alkyl complexes, even though the corresponding primary and secondary σ complexes are comparable in energy. Steric factors are a likely culprit!

Naturally, other strategies for controlling selectivity in C–H "activations" have appeared; however, be aware that these may not involve oxidative addition. Lewis basic directing groups have been used with success to direct oxidative addition to a nearby C–H bond—but these reactions are aided by base and do not involve oxidation. Metal carbenoid insertions into C–H bonds also do not involve oxidation at the metal center. The lesson of these reactions: *be careful*, and don't assume that all alkyl complexes are the result of C–H oxidative addition!

This page titled 8.4.8: Oxidative Addition of Non-polar Reagents is shared under a CC BY-NC-SA 4.0 license and was authored, remixed, and/or curated by Michael Evans.

8.4.9: Oxidative Addition of Polar Reagents

Organometallic chemistry has vastly expanded the practicing organic chemist's notion of what makes a good nucleophile or electrophile. Pre-cross-coupling, for example, using unactivated aryl halides as electrophiles was largely a pipe dream (or possible only under certain specific circumstances). Enter the oxidative addition of polarized bonds: all of a sudden, compounds like bromobenzene started looking a *lot* more attractive as starting materials. **Cross-coupling reactions** involving sp^2– and *sp*-hybridized C–X bonds beautifully complement the "classical" substitution reactions at sp^3 electrophilic carbons. Oxidative addition of the C–X bond is the step that kicks off the magic of these methods. In this post, we'll explore the mechanisms and favorability trends of oxidative additions of polar reagents. The landscape of mechanistic possibilities for polarized bonds is much more rich than in the non-polar case—concerted, ionic, and radical mechanisms have all been observed.

Concerted Mechanisms

Oxidative additions of aryl and alkenyl C_{sp^2}–X bonds, where X is a halogen or sulfonate, proceed through **concerted** mechanisms analogous to oxidative additions of dihydrogen. Reactions of N–H and O–H bonds in amines, alcohols, and water also appear to be concerted. A π complex involving η^2-coordination is an intermediate in the mechanism of insertion into aryl halides at least, and probably vinyl halides too. As two open coordination sites are necessary for concerted oxidative addition, loss of a ligand from a saturated metal complex commonly precedes the actual oxidative addition event.

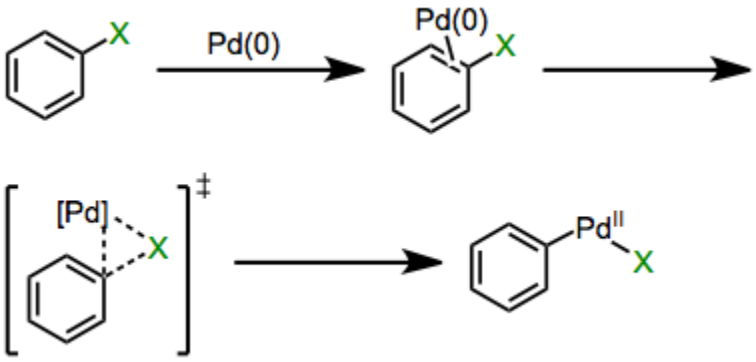


Figure 8.4.9.1: Concerted oxidative addition of aryl halides and sulfonates. (Copyright; author via source)

Trends in the reactivity of alkyl and aryl (pseudo)halides toward oxidative addition are some of the most famous in organometallic chemistry. Aryl iodides are most reactive, followed by bromides, tosylates, and chlorides. To counter the lower electrophilicity of aryl chlorides, electron-rich alkyl phosphine ligands may be used to accelerate reactions of aryl chlorides. These "hot" ligands increase electron density at the metal center, facilitating oxidative addition. Because they tend to be bulkier than aryl phosphines, though, complexes of alkyl phosphines sometimes operate through slightly different mechanisms than aryl phosphine complexes. Although the exact species undergoing oxidative addition may differ (see below), all of the actual oxidative addition events are thought to be concerted.

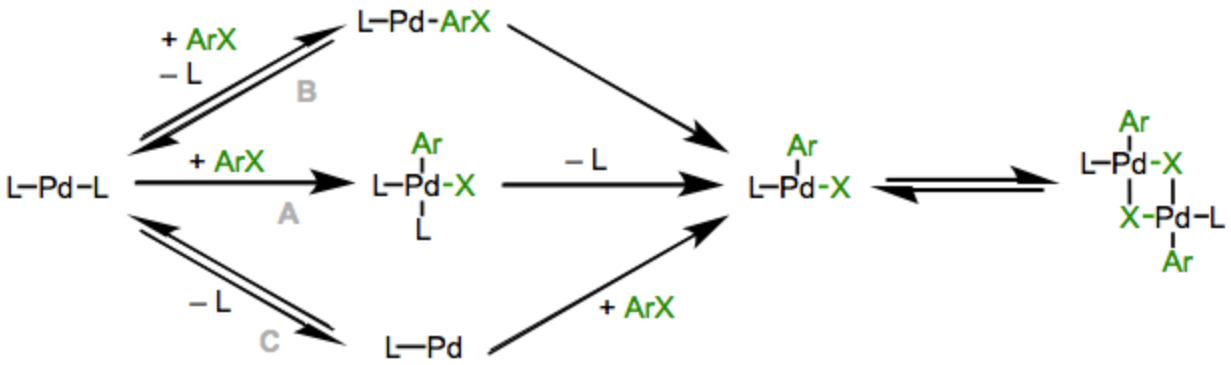


Figure 8.4.9.2: Mechanisms of oxidative addition to palladium(0) phosphine complexes. Much depends on the nature of L. (Copyright; author via source)

Here, as we've seen before, electron-rich organohalides react more slowly than electron-poor compounds. Oxidative addition depletes electron density from the metal center and increases electron density in the organic ligands, so this trend makes sense!

S_N2 and Ionic Mechanisms

Very electrophilic halides often react through ionic mechanisms in which oxidative addition *per se* takes place over multiple steps. As strange as it may be to imagine a metal center as a nucleophile, this exact reactivity is central to the S_N2 and ionic mechanisms of oxidative addition. In a slow step, the metal center attacks the electrophilic atom, displacing halide. Rapid recombination of the positively charged metal complex and negative halide ion yields the product of oxidative addition. In essence, this mechanism involves oxidative ligation followed by association of oppositely charged ions. Loss of a dative ligand is sometimes necessary as an intermediate step, if the metal complex is saturated after the S_N2 step.

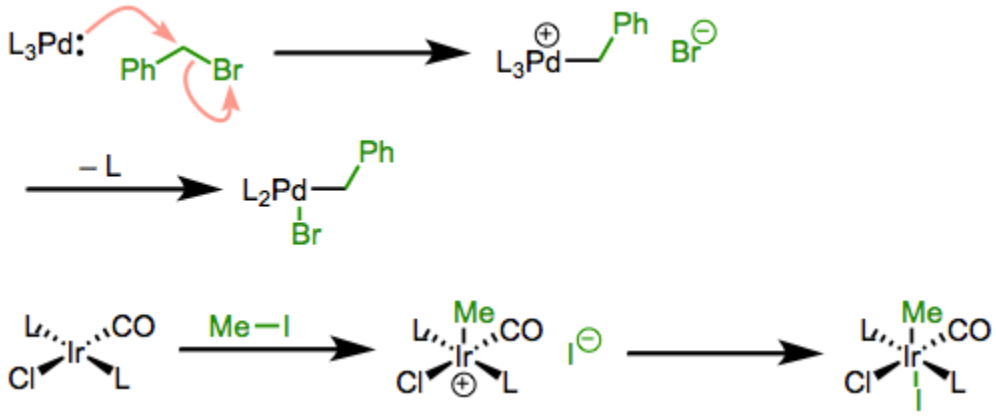


Figure 8.4.9.3: SN2 mechanisms of oxidative addition: oxidative ligation followed by ligand substitution or simple coordination. (Copyright; author via source)

An extremely solid analogy can be drawn between these reactions and classical S_N2 reactions from "sophomore organic" chemistry. Primary halides react most quickly, followed by secondary and tertiary halides. Inversion at carbon is observable in these reactions, and entropy of activation is negative (suggesting an associated transition state). Negatively charged metal complexes kick butt in these reactions, and as electron-withdrawing ligands are added to the metal center, reactivity decreases. Added halide anions can actually accelerate S_N2 oxidative additions—the anion coordinates to the metal center, making it negative and increasing its electron-donating power.

A nice analogy can also be drawn between S_N2-type oxidative additions and oxidative additions of strong acids, which occur basically through the same mechanism (with replacement of hydrogen for carbon). During these so-called "ionic mechanisms," protonation of the metal center usually occurs first, followed by ligand substitution or simple coordination of the conjugate base. In rarer circumstances and for less nucleophilic metal complexes, coordination of the conjugate base can actually occur first, followed by protonation!

Radical Mechanisms

Radicals are sometimes thought of as the bucking broncos of the chemistry world, and as such, radical mechanisms for oxidative additions are more difficult to control and less appealing. For example, one must be careful to use solvents that don't react with the intermediate radicals. Still, a considerable amount of effort has been directed at "taming the wild beast." In some ways, radical reactions offer complementary selectivity to ionic and concerted mechanisms.

Non-chain radical mechanisms involve single-electron transfer from the metal complex to the organohalide, followed by recomination of the resulting radicals. The metallic and organic radicals, when stable, can even be isolated from the reaction as products.

$PtL_2 + RX \rightarrow PtL_2X^{\cdot} + R^{\cdot} +$

$PtL_2X^{\cdot} + R^{\cdot} \rightarrow PtL_2XR$

Reactivity trends here depend on the stability of the intermediate radical species. Tertiary halides react most rapidly, followed by secondary and primary halides. More electron-rich metal centers react more rapidly (are you sick of this trend yet?), since they can more easily donate an electron to the organohalide.

Chain radical mechanisms involve reactions between radical intermediates and even-electron starting materials, resulting in the continuous regeneration of radicals as products form. I like to imagine the radical intermediates as Tom Hanks in *Cast Away*, floating in an ocean of even-electron starting material. A nice example of this reactivity was explored by Hill and Puddephatt in the mid-1980s.

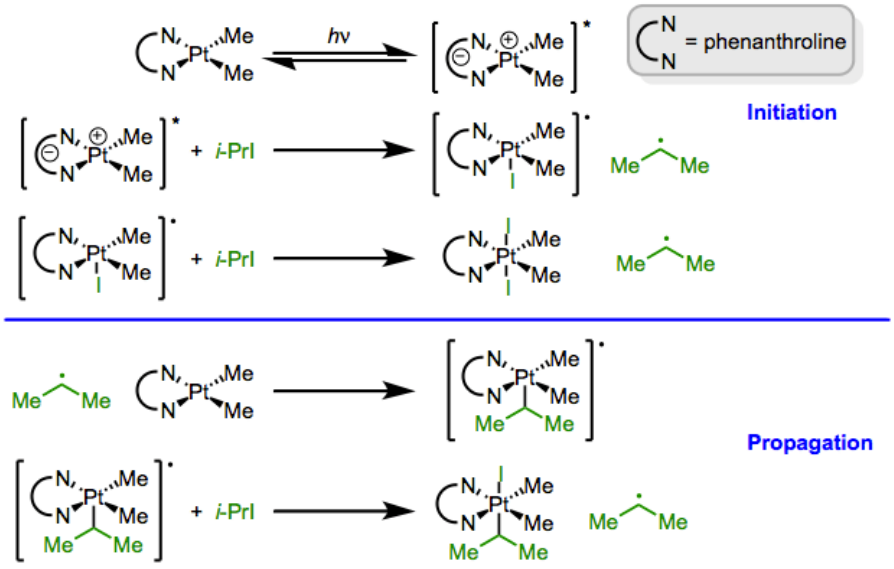


Figure 8.4.9.4: Organometallic complexes can carry out radical chain mechanisms too! Here, isopropyl radical is the propagating radical. (Copyright; author via source)

Excitation of the Pt(II) complex yields a charge-transfer complex that can abstract iodine from isopropyl iodide. A second abstraction event completes the initiation phase. During propagation, isopropyl radical couples with the (unexcited) Pt(II) complex, and the resulting organometallic radical abstracts iodine from the starting organohalide. Free radical scavengers kill the reaction, but interestingly, only the isopropyl radical reacts with radical traps.

Lastly, I'll just mention briefly that **binuclear oxidative additions**, which involve two metal centers "tugging" on the organohalide in concert, often involve radicals and/or one-electron transfers. Here's one example involving chromium, and here's a somewhat more famous example involving cobalt (by Budzelaar!).

Summing up, oxidative additions of polar reagents are critical steps in many organometallic reactions. We've only just barely scratched the surface of this important class of reactions, but a few powerful trends have emerged. In general, more electron-rich OM complexes and more electron-poor polar organics react more rapidly in oxidative additions. Steric hindrance in the

metal complex can also play an interesting role, either by changing the actual species that undergoes oxidative addition or by discouraging oxidative addition altogether. Next up, we'll take a brief look at the microscopic reverse of oxidative addition, **reductive elimination**. Most of the trends and mechanisms associated with reductive elimination are simply the opposite of those for oxidative addition, so our discussions of reductive elimination will be fairly short.

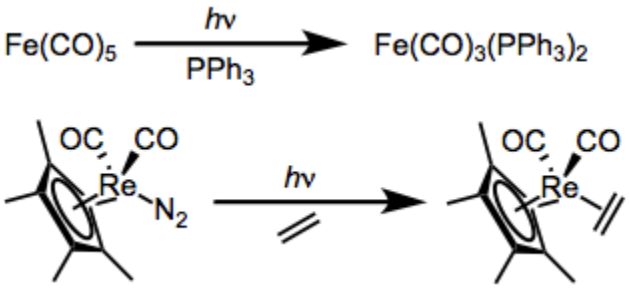
This page titled 8.4.9: Oxidative Addition of Polar Reagents is shared under a CC BY-NC-SA 4.0 license and was authored, remixed, and/or curated by Michael Evans.

8.4.10: Quirky Ligand Substitutions

Over the years, a variety of “quirky” substitution methods have been developed. All of these have the common goal of facilitating substitution in complexes that would otherwise be inert. It’s an age-old challenge: how can we turn a stable complex into something unstable enough to react? Photochemical excitation, oxidation/reduction, and radical chains all do the job, and have all been well studied. We’ll look at a few examples in this post—remember these methods when simple associative or dissociative substitution won’t get the job done.

Photochemical Substitution

Substitution reactions of dative ligands—most famously, CO—may be facilitated by photochemical excitation. Two examples are shown below. The first reaction yields only monosubstituted product without ultraviolet light, even in the presence of a strongly donating phosphine.

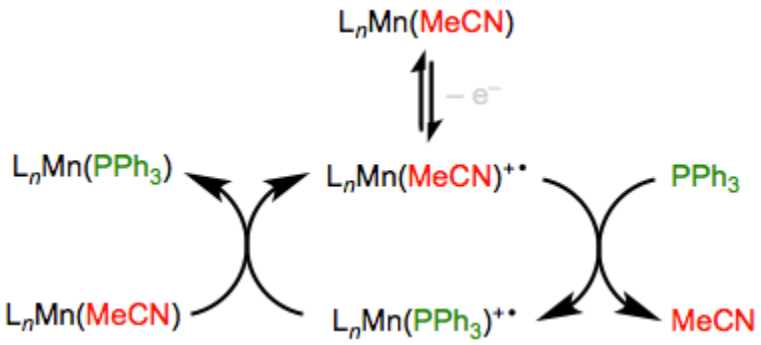


Dissociative photochemical substitutions of CO and dinitrogen.

All signs point to dissociative mechanisms for these reactions (the starting complexes have 18 total electrons each). Excitation, then, must increase the M–L antibonding character of the complex’s electrons; exactly how this increase in antibonding character happens has been a matter of some debate. Originally, the prevailing explanation was that the LUMO bears M–L antibonding character, and excitation kicks an electron up from the HOMO to the LUMO, encouraging cleavage of the M–L bond. A more recent, more subtle explanation backed by calculations supports the involvement of a metal-to-ligand charge-transfer state along with the “classical” ligand-field excited state.

Oxidation/Reduction

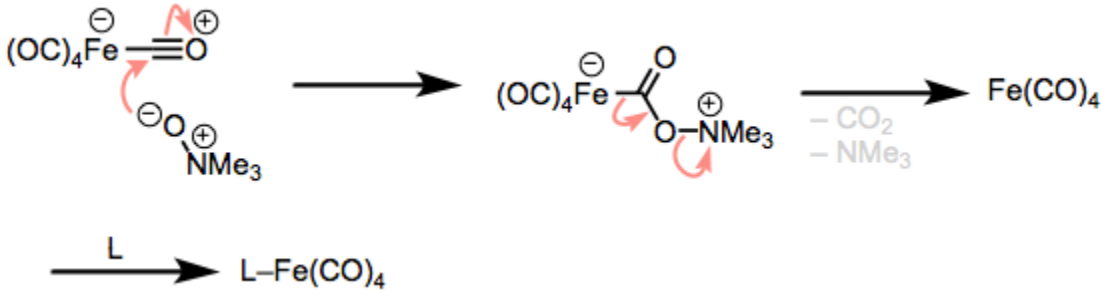
Imagine a screaming baby without her pacifier—that’s a nice analogy for an odd-electron organometallic complex. Complexes bearing 17 and 19 total electrons are much more reactive toward substitution than their even-electron counterparts. Single-electron oxidation and reduction (“popping out the pacifier,” if you will) can thus be used to efficiently turn on substitution. As you might expect, oxidation and reduction work best on electron-rich and electron-poor complexes, respectively. The Mn complex in the oxidative example below, for instance, includes a strongly donating MeCp group (not shown).



Oxidation accelerates substitution in electron-rich complexes through a chain process.

Reduction works well for electron-poor metal carbonyl complexes, which are happy to accept an additional electron.

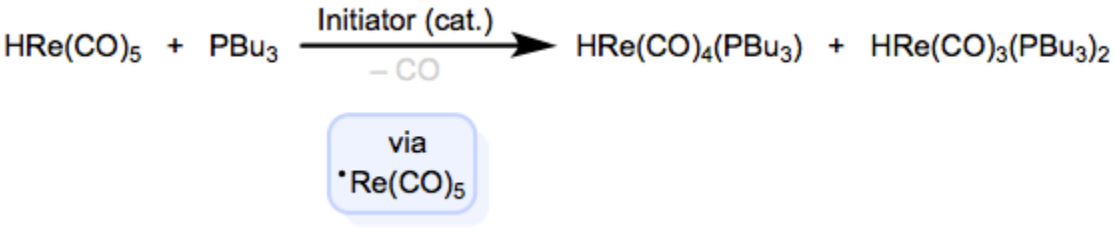
There is a two-electron oxidation method that's also worth knowing: the oxidation of CO with amine oxides. This nifty little method releases carbon dioxide, amine, and an unsaturated complex that may be quenched by a ligand hanging around. The trick is addition to the CO ligand followed by elimination of the unsaturated complex. As the oxidized CO2 and reduced amine float away, the metal complex finds another ligand.



Oxidation of CO with amine oxides. A fun method for dissociative substitution of metal carbonyls!

Radical Chain Processes

Atom abstraction from 18-electron complexes produces neutral 17-electron intermediates, which are susceptible to ligand substitution via radical chain mechanisms. The fact that the intermediates are neutral distinguishes these methods from oxidation-based methods. First-row metal hydrides are great for these reactions, owing to their relatively weak M–H bonds. One example is shown below.



Radical-chain substitution involving atom abstraction.

After abstraction of the hydrogen atom by initiator, substitution is rapid and may occur multiple times. Propagation begins anew when the substituted radical abstracts hydrogen from the starting material to regenerate the propagating radical and form the product. These quirky methods are nice to have in your back pocket when you're backed into a synthetic corner—sometimes, conventional associative and dissociative substitution just won't do the job. In the next post, we'll press on to oxidative addition.

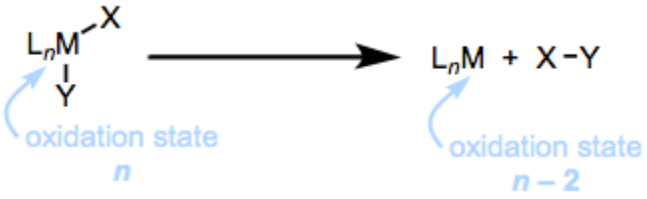
Template:Evans

This page titled 8.4.10: Quirky Ligand Substitutions is shared under a CC BY-NC-SA 4.0 license and was authored, remixed, and/or curated by Michael Evans.

- 4.10: Quirky Ligand Substitutions by Michael Evans is licensed CC BY-NC-SA 4.0.

8.4.11: Reductive Elimination- General Ideas

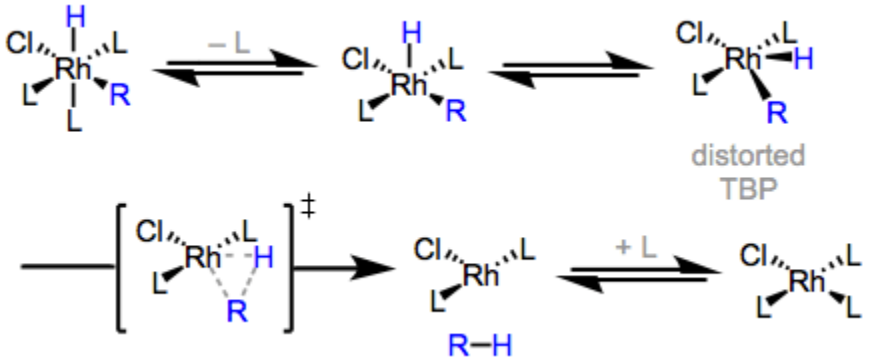
Reductive elimination is the microscopic reverse of oxidative addition. It is literally oxidative addition run in reverse—oxidative addition backwards in time! My favorite analogy for **microscopic reversibility** is the video game Braid, in which "resurrection is the microscopic reverse of death." The player can reverse time to "undo" death; viewed from the forward direction, "undoing death" is better called "resurrection." Chemically, reductive elimination and oxidative addition share the same reaction coordinate. The only difference between their reaction coordinate diagrams relates to what we call "reactants" and "products." Thus, their mechanisms depend on one another, and trends in the speed and extent of oxidative additions correspond to opposite trends in reductive eliminations. In this post, we'll address reductive elimination in a general sense, as we did for oxidative addition.



A general reductive elimination. The oxidation state of the metal decreases by two units, and open coordination sites become available.

During reductive elimination, the electrons in the M–X bond head toward ligand Y, and the electrons in M–Y head to the metal. The eliminating ligands are always X-type! On the whole, the oxidation state of the metal decreases by two units, two new open coordination sites become available, and an X–Y bond forms. What does the change in oxidation state suggest about changes in electron density at the metal? As suggested by the name "reductive," the metal gains electrons. The ligands lose electrons as the new X–Y bond cannot possibly be polarized to both X and Y, as the original M–X and M–Y bonds were. Using these ideas, you may already be thinking about reactivity trends in reductive elimination...hold that thought.

It's been observed in a number of cases that a ligand dissociates from octahedral complexes before concerted reductive elimination occurs. Presumably, dissociation to form a distorted TBP geometry brings the eliminating groups closer to one another to facilitate elimination.

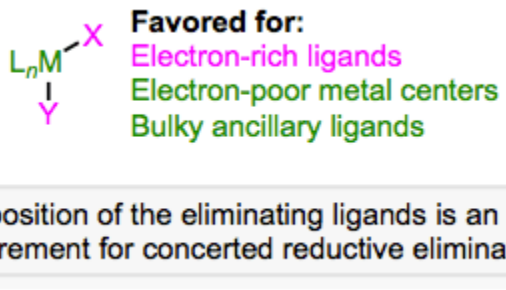


Reductive elimination is faster from five-coordinate than six-coordinate complexes.

Square planar complexes may either take on an additional fifth ligand or lose a ligand to form an odd-coordinate complex before reductive elimination. Direct reductive elimination without dissociation or association is possible, too.

Reactivity trends in reductive elimination are opposite those of oxidative addition. More electron-rich ligands bearing electron-donating groups react more rapidly, since the ligands lose electron density as the reaction proceeds. More electron-poor metal centers—bearing π-acidic ligands and/or ligands with electron-withdrawing groups—react more rapidly, since the metal center gains electrons. Sterically bulky ancillary ligands promote reductive elimination since the release of X and Y can "ease" steric

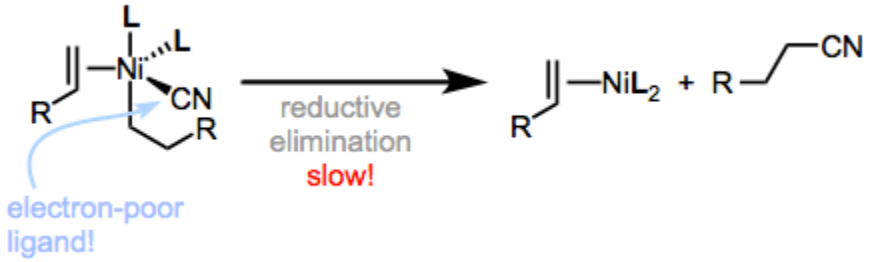
strain in the starting complex. Steric hindrance helps explain, for example, why coordination of a fifth ligand to a square planar complex promotes reductive elimination even though coordination increases electron density at the metal center. A second example: trends in rates of reductive eliminations of alkanes parallel the steric demands of the eliminating ligands: C–C > C–H > H–H.



Reactivity trends for reductive eliminations.

Mechanistic trends for reductive elimination actually parallel trends in mechanisms of oxidative addition, since these two reactions are the microscopic reverse of one another. Non-polar and moderately polar ligands react by concerted or radical mechanisms; highly polarized ligands and/or very electrophilic metal complexes react by ionic (S_N2) mechanisms. The thermodynamics of reductive elimination must be favorable in order for it to occur! Most carbon–halogen reductive eliminations, for example, are thermodynamically unfavorable (this has turned out to be a good thing, especially for cross-coupling reactions).

Reductive elimination is an important step in many catalytic cycles—it usually comes near the "end" of catalytic mechanisms, just before product formation. For some catalytic cycles it's the turnover-limiting step, making it very important to consider! Hydrocyanation is a classic example; in the mechanism of this reaction, reductive elimination of C–CN is the slow step. Electron-poor alkyl ligands, derived from electron-poor olefins like unsaturated ketones, are bad enough at reductive elimination to prevent turnover altogether! Of course, the electronegative CN ligand is not helping things either...how would you design the ancillary ligands L to speed up this step?



Reductive elimination is the turnover-limiting step of hydrocyanation. How would you design L to speed it up?

Contributors and Attributions

- Dr. Michael Evans (Georgia Tech)

This page titled 8.4.11: Reductive Elimination- General Ideas is shared under a CC BY-NC-SA 4.0 license and was authored, remixed, and/or curated by Michael Evans.

- 4.11: Reductive Elimination- General Ideas by Michael Evans is licensed CC BY-NC-SA 4.0.

8.4.12: The trans/cis Effects and Influences

The trans effect is an ancient but venerable observation. First noted by Chernyaev in 1926, the trans effect and its conceptual siblings (the trans influence, cis influence, and cis effect) are easy enough to comprehend. That is, it's simple enough to know what they are. To understand why they are, on the other hand, is much more difficult.

Definitions & Examples

Let's begin with definitions: what is the trans effect? There's some confusion on this point, so we need to be careful. The trans effect proper, which is often called the kinetic trans effect, refers to the observation that certain ligands increase the rate of ligand substitution when positioned trans to the departing ligand. The key word in that last sentence is "rate"—the trans effect proper is a kinetic effect. The trans influence refers to the impact of a ligand on the length of the bond trans to it in the ground state of a complex. The key phrase there is "ground state"—this is a thermodynamic effect, so it's sometimes called the thermodynamic trans effect. Adding to the insanity, cis effects and cis influences have also been observed. Evidently, ligands may also influence the kinetics or thermodynamics of their cis neighbors. All of these phenomena are independent of the metal center, but do depend profoundly on the geometry of the metal (more on that shortly).

Kinetic trans and cis effects are shown in the figure below. In both cases, we see that X1 exhibits a stronger effect than X2. The geometries shown are those for which each effect is most commonly observed. The metals and oxidation states shown are prototypical.

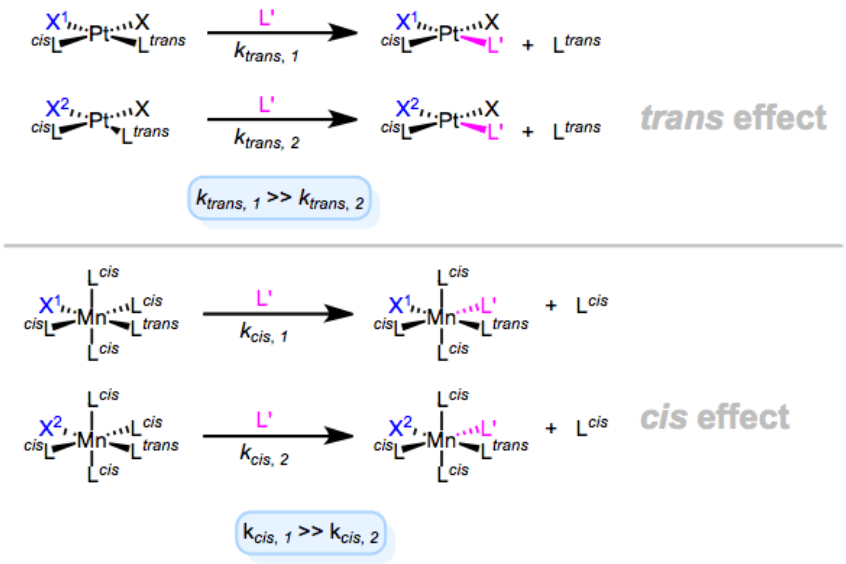


Figure 8.4.12.1: The kinetic trans and cis effects in action. X^1 is the stronger (trans/cis)-effect ligand in these examples.

On to the influences, which are simpler to illustrate since they're concerned with ground states, not reactions. The lengthened bonds below are exaggerated.

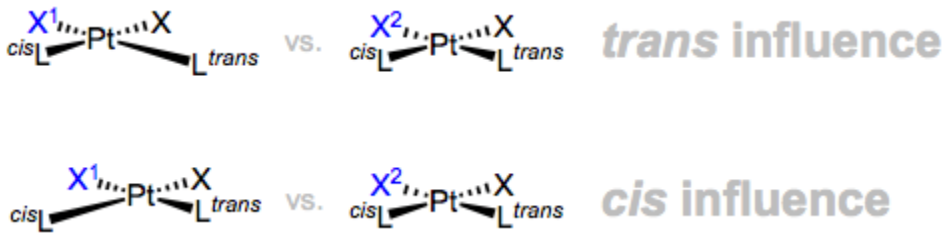


Figure 8.4.12.2: The trans and cis influences in action. Note the elongated bond lengths.

And there we have it folks, the thermodynamic and kinetic cis/trans effects. It's worth keeping in mind that the kinetic trans effect is most common for d8 square planar complexes, and the kinetic cis effect is most common for d6 octahedral complexes (particularly when the departing L is CO). But a lingering question remains: what makes for a strong trans effect ligand?

Origins of Effects & Influences

The trans effect and its cousins are all electronic, not steric effects. So, the electronic properties of the ligand dictate the strength of its trans effect. Let's finally dig into the trans effect series:

(weak) F^-, HO^-, H_2O 3 < py < Cl^- < Br– < I–, SCN^-, NO_2^-, $SC(NH_2)_2$, Ph^- < SO_3^{2-} < PR_3 < AsR_3, SR_2, H_3C^- < H^-, NO, CO, NC^-, C_2H_4 (strong)

What's the electronic progression here? It's clear that electronegativity decreases across the series: F^- < Cl^- < Br^- < I^- < H_3C^-. From a bonding perspective, we can say that ligands with strong trans effects are strong σ-donors (or σ-bases). Yet σ-donation doesn't tell the whole story. What about ethylene and carbon monoxide, which both appear at the top of the heap? Neither of these ligands are strong σ-donors, but their π systems do interact with the metal center through backbonding. Consider the following sub-series: S=C=N– < PR_3 < CO. Backbonding increases across this series, along with the strength of the trans effect. Strong backbonders—better known as π-acceptors or π-acids—exhibit strong trans effects.

Strong trans effect = strong σ-donor + strong π-acceptor

Wonderful! Using these ideas we can identify ligands with strong trans effects. But we can dive deeper down the rabbit hole: why does this particular combination of electronic factors lead to a strong trans effect? To understand this, we need to know the mechanism of the ligand substitution reaction that's sped up by strong trans effect ligands. For 16-electron Pt(II) complexes, associative substitution is par for the course. The incoming ligand binds to the metal first, forming an 18-electron complex (yay!), which jettisons a ligand to yield a new 16-electron product. The mechanism in all its glory is shown in the figure below.

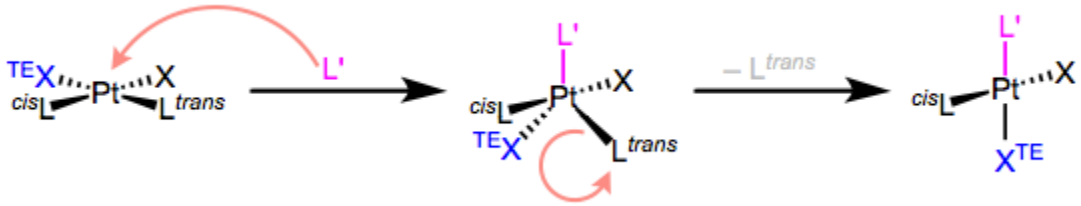


Figure 8.4.12.3: The mechanism of associative ligand substitution of Pt(II) complexes.

Some very important points about this mechanism:

- The incoming ligand always sits at an equatorial site in the trigonal bipyramidal intermediate. More on this another day, but I think of this result as governed by the principle of least motion. Consider the molecular gymnastics that would have to happen to place the incoming ligand in an axial position.
- Two ligands in the square plane are "pushed down" and become the other two equatorial ligands.
- Owing to microscopic reversibility, the leaving group must be one of the equatorial ligands.

The third point reveals that once L' has "pushed down" XTE and Ltrans, Ltrans has no choice but to leave (assuming XTE stays put). Thus, the trans effect has nothing to do with the second step of the mechanism, which is not rate determining anyway. The key is the first step—in particular, the "pushing down" event. Apparently, ligands with strong trans effects like to be pushed down. They like to occupy the equatorial plane of the TBP intermediate. Now here's the kicker: the equatorial sites of the TBP geometry are more π basic than the axial sites. The equatorial plane is just the xy-plane of the metal center, and the d orbitals in that plane (when occupied) are great electron sources for π-acidic ligands. Thus, π-acidic ligands want to occupy those equatorial sites, to receive the benefits of strong backbonding! Boom; strong π-acids encourage loss of the ligand trans to themselves.



Figure 8.4.12.4: The equatorial sites of TBP metals are rich in electrons that can π bond.

What about those pesky σ donors? Well, we can imagine that in a square planar complex, a ligand and its trans partner are competing for donation into the same d orbital. Strong σ donation from a ligand should thus weaken the bond trans to it. Although this is the thermodynamic trans effect (trans influence) in action, the resulting destabilization of the ground state relative to the transition state is a kinetic effect. On the whole, the barrier to substitution of the trans ligand goes down as σ-donating strength goes up.

This idea of "competition for the metal center" is a nice heuristic to use when thinking about the trans and cis influences. The type of metallic orbital involved in M–L bonding determines the strength of L's trans and cis influences on neighboring ligands that also need that metallic orbital for bonding. For example: both influences are large if the metal's s orbital is a significant contributor to M–L bonding, since it's non-directional; the trans influence is much greater than the cis influence when metallic p orbitals are primarily involved in M–L. For a deeper explanation of these ideas, see this paper.

Summing up

Perhaps the most valuable lesson from a study of the trans effect is that many concepts from organometallic chemistry involve more than meets the eye. Geometric effects and influences are real icebergs, in the sense that the observations and trends are easy to grasp, but difficult to explain. We had to dig all the way into the mechanism of associative ligand substitution before a satisfactory explanation emerged!

This page titled 8.4.12: The trans/cis Effects and Influences is shared under a CC BY-NC-SA 4.0 license and was authored, remixed, and/or curated by Michael Evans.

- 4.12: The trans/cis Effects and Influences by Michael Evans is licensed CC BY-NC-SA 4.0.

8.5.1: Parallels between Main Group and Binary Carbonyl Complexes

This page titled 8.5.1: Parallels between Main Group and Binary Carbonyl Complexes is shared under a license and was authored, remixed, and/or curated by LibreTexts.

8.5: PARALLELS BETWEEN MAIN GROUP AND ORGANOMETALLIC CHEMISTRY

8.5.1: Parallels between Main Group and Binary Carbonyl Complexes

8.5.2: The Isolobal Analogy

8.5.2.1: Extensions of the Analogy

8.5.2.2: Some Applications of the Isolobal Analogy

8.5.3: Metal-Metal Bonds

8.5.3.1: Metal-Metal Multiple Bonds

8.5.4: Cluster Compounds

8.5.4.1: Boranes

8.5.4.2: Heteroboranes

8.5.4.3: Metallaboranes and Metallacarboranes

8.5.4.4: Carbonyl Clusters

8.5.4.5: Carbon-Centered Clusters

8.5.4.6: Additional Comments on Clusters

8.5.5: Problems

This page titled 8.5: Parallels between Main Group and Organometallic Chemistry is shared under a license and was authored, remixed, and/or curated by LibreTexts.

- 15: Parallels between Main Group and Organometallic Chemistry has no license indicated.

8.5.2: The Isolobal Analogy

The **isolobal analogy** (aka isolobal principle) is a strategy used in organometallic chemistry to relate the structure of organic and inorganic molecular fragments in order to predict bonding properties of organometallic compounds. Roald Hoffmann described molecular fragments as isolobal: "*if the number, symmetry properties, approximate energy and shape of the frontier orbitals and the number of electrons in them are similar – not identical, but similar*." One can predict the bonding and reactivity of a species from that of a better-understood species **if the two molecular fragments have similar frontier orbitals**; **the highest occupied molecular orbital (HOMO) and the lowest unoccupied molecular orbital (LUMO).** Isolobal compounds are analogues to *isoelectronic compounds* that share the same number of valence electrons and structure.

Isolobal species are indicated with an isolobal arrow symbol; a double-headed arrow with half an orbital (Figure $8.5.2.1$).

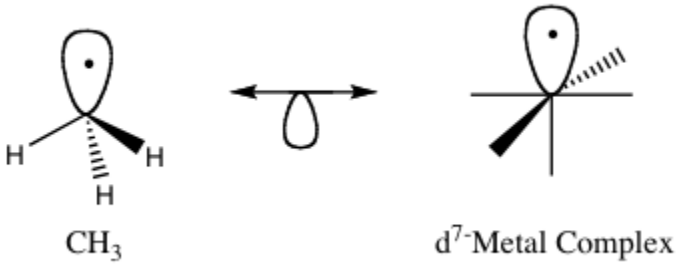


Figure $8.5.2.1$: A methyl radical related to a d^7 metal complex by the isolobal analogy. A double headed arrow with a half orbital indicates that the two structures are related by the isolobal analogy. (public domain)

The concept of isolobality was developed by Roald Hoffmann (Figure $8.5.2.2$), who won the Nobel prize in chemistry in 1981. It comes from the greek words “isos” meaning “similar” and “lobos” meaning lobe. Hence, “isolobal” means “similar lobes”. In his Nobel speech he defined isolobality as follows: “Molecular fragments are isolobal if the number, symmetry properties, approximate energy and shape of the frontier orbitals and the number of electrons in them are similar - not identical, but similar. “ When molecular fragments are isolobal then they can likely be combined to form a stable molecule. Thus, isolobal fragments are compatible building blocks for the construction of stable molecules. We can also say that the concept of isolobality helps us to predict when a stable bond forms. Whenever two molecular fragments are isolobal, then they will likely form stable bonds between them.

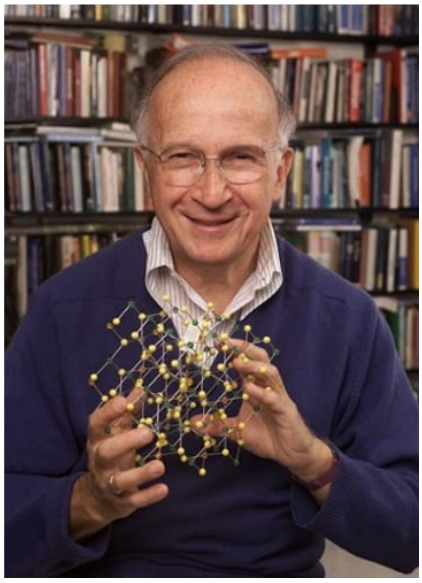


Figure $8.5.2.2$: Roald Hoffman (Attribution: .The original uploader was Xtreambar at English Wikipedia. / Public domain https://commons.wikimedia.org/wiki/F...d_Hoffmann.jpg)

Isolobal Fragments of main group elements

There is a simple means to determine if fragments are isolobal. In main group chemistry the octet rule is a very helpful guide, especially for the period 2 elements (B,C,N,O,F) for which the octet rule holds fairly strictly. The difference between the number "8" and the number of valence electrons (VE) of the molecular fragment is equal to the number of frontier orbitals and the number of electrons in it.

of frontier orbitals = # of electrons in frontier orbitals = 8 – VE

Thus, **when two fragments (of main group elements) have the same number of valence electrons, they can be considered isolobal.** For example, the CH_3 fragment created by homolytic cleavage of a $C–H$ bond from CH_4 is shown in Figure 8.5.2.1. This CH_3 fragment has 7 VE on the carbon, and therefore it has one frontier orbital with one electron it (Figure 8.5.2.1). The same is true for the NH_2 (7 VE) and OH (7 VE) fragments shown in XXX. All of these fragments have 7 VE and one frontier orbital (Figure 8.5.2.3).

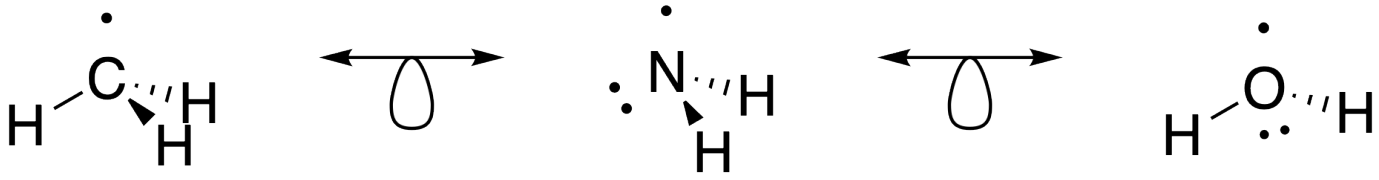


Figure 8.5.2.3: Examples of fragments that are isolobal. These fragments are comprised of main group elements, and all have 7 valence electrons around the central atom, thus they each have one frontier orbital. (CC-BY-SA; Kathryn Haas)

According to the isolobal analogy, it should be possible to combine isolobal fragments to form stable molecules. Let's test this on the fragments shown in Figure 8.5.2.3. All the posible combinations are shown in Figure 8.5.2.4. Two CH_3 fragments can be combined to form an ethane molecule which is known to be stable. The combination of CH_3 andNH_2 gives methylamine which is stable, and the combination of CH_3 and OH gives methanol, which is also stable. TwoNH_2 fragments give hydrazine, H_2N-NH_2 which exists, the combination of$NH_2$and OH gives the known hydroxylamine molecule NH_2OH. The combination of two OH fragments gives hydrogen peroxide H_2O_2.

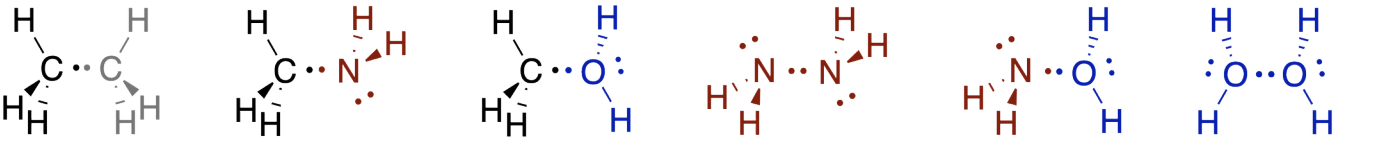


Figure 8.5.2.4: Combinations of isolobal fragments lead to stable molecules (stable enough to exist). (CC-BY-SA; Kathryn Haas)

As another example, a CH_2 fragment is a 6 VE fragment, thus there are 8-6=2 frontier orbitals with overall two electrons in them (Figure 8.5.2.5). An NH-fragment and an O-atom also have 6 VE, and are therefore isolobal to CH_2. In NH there are 5+1=6 valence electrons, and an oxygen atom has 6 valence electrons. We can combine two CH_2 fragments to form ethene $H_2C{=}CH_2$. Combining CH_2 with NH and O, respectively gives methanimine H_2CNH, and formaldehyde $H_2C{=}O$, respectively. Methylene imine is stable in the gas phase, and oligomerizes in higher concentrations to form a hexamer, called urotropine. Other oligomers and polymers are also known. The combination of two NH fragments gives the known molecule diazene $HN{=}NH$, and the combination with an O atom gives $HN{=}O$, which is known as nitroxyl or azanone, and is stable in the gas phase. The combination of two oxygen atoms gives the well known O_2 molecule.

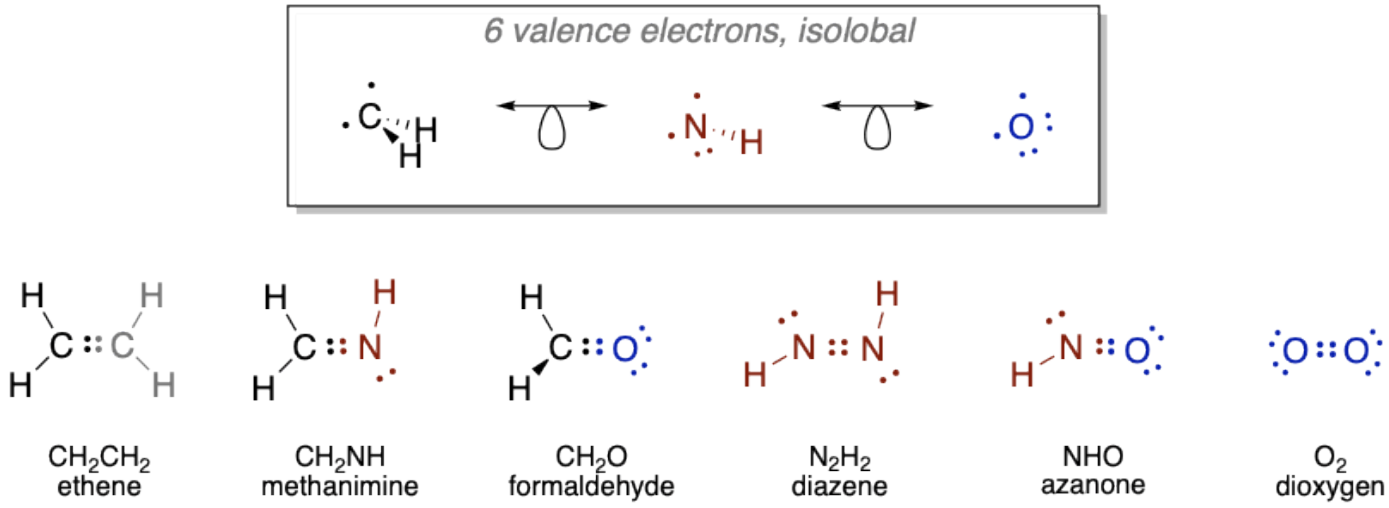


Figure 8.5.2.5: Examples of isolobal fragments of main group elements with 6 valence electrons, and combination of those fragments that result in stable compounds. (CC-BY-SA; Kathryn Haas)

The analogy could also be extended to 5 VE fragments (not shown). The CH fragment has 4+1=5 VE, and an N-atom has 5 VE as well, thus they can be considered isolobal. Two CH fragments give acetylene C_2H_2, and two N atoms give the dinitrogen molecule N_2. The combination of a CH fragment with an N fragment gives H-CN, well known as hydrogen cyanide.

Isolobal fragments of transition elements

In the way the octet rule can help to predict the number of frontier orbitals and the electrons in them for main group element fragments, **the 18 electron rule can be used to predict the number of frontier orbitals and electrons for organometallic fragments**, including carbonyl fragments. The number of frontier orbitals and the number of electrons in them is 18 minus the number of valence electrons the organometallic fragment has:

frontier orbitals = # of electrons in frontier orbitals = 18 – VE

For example, a metal complex with a count of 17 electrons, such as $\mathrm{Mn(CO)_5}$, there is one frontier orbital with one electron. This implies that a 17 VE carbonyl fragment is isolobal to a 7 VE organic fragment such as $\mathrm{CH_3}$. For a 16 VE fragment such as $\mathrm{Fe(CO)_4}$ there are two frontier orbitals with one electron in each of them, and for a 15 VE fragment such as $\mathrm{(CO)_3Co}$ there are three frontier orbitals with overall three valence electrons (Figure 8.5.2.6). Similarly, a 16 VE metal carbonyl fragment is isolobal to a 6 VE fragment such as $\mathrm{CH_2}$, and a 15 VE fragment is isolobal to a 5 VE fragment such as CH (Figure 8.5.2.6).

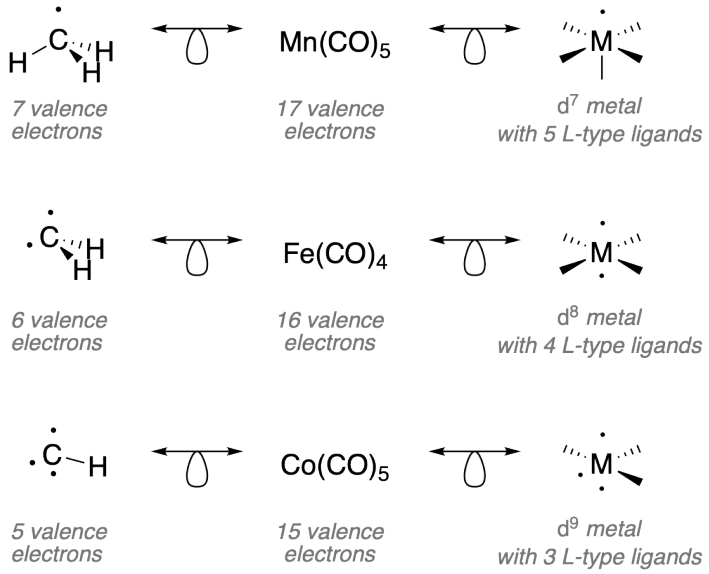


Figure 8.5.2.6: Examples for isolobal metal carbonyl and organic fragments (CC-BY-SA; Kathryn Haas)

It should be possible to combine the isolobal fragments from Figure 8.5.2.6 to form stable molecules. Let us check how well this works (Figure 8.5.2.7). It should be possible to combine the two 17 VE electron fragments such as $\mathrm{Mn(CO)_5}$ to form $\mathrm{(CO)_5Mn{-}Mn(CO)_5}$. This is a known molecule. Remember we encountered it previously when we discussed the homoleptic carbonyls of metals with an odd number of electrons. Combining this fragment with a 7 VE $\mathrm{CH_3}$ fragment leads to $\mathrm{(CO)_5Mn{-}CH_3}$ which is also stable.

Can we also combine two 16 VE electron fragments to form $\mathrm{(CO)_4Fe{=}Fe(CO)_4}$ with an Fe=Fe double bond? The answer is no. Metal-metal double bonds, and also metal-metal triple bonds in carbonyl complexes are not formed. Instead clusters with single bonds are realized. The number of single bonds a metal makes is equal to the number of its frontier orbitals. In the case of 16 VE fragments trimeric clusters with single bonds are formed. In this cluster the two frontier orbitals of each fragment make two single bonds to two other fragments. In contrast, a 16 VE carbonyl fragment such as $\mathrm{(CO)_4Fe}$ can be combined with a 6 VE fragment to form a compound with a Fe=C double bond. A compound with a metal-carbon double bond is called a carbene complex. Similarly, the combination of 15 VE fragments of the type $\mathrm{Co(CO)_3}$ does not lead to a stable $\mathrm{(CO)_3Co{\equiv}Co(CO)_3}$ molecule with a $\mathrm{Co{\equiv}Co}$ triple bond. Instead, nature realizes a tetrameric tetrahedral cluster in which the three frontier orbitals of each 15 VE fragment make three single bonds to the other three 15 VE fragments. In clusters the CO ligands may not only be terminal, they can also be bridging. In the tetrameric Co-cluster, there are are nine terminal and three bridging CO-ligands. The three bridging CO ligands are connecting the three Co atoms at the base triangular face of the tetrahedron. What about the combination of a 15 VE fragment with an organic 5 VE fragment? The combination of a 15 VE fragment such as $Co(CO)_3$ with a 5 VE organic fragment such as CH to does yield stable complexes such as the $\mathrm{(CO)_3Co{\equiv}CH}$ complex with a $\mathrm{Co{\equiv}C}$ triple bond. Complexes with metal-carbon triple bonds are called carbine complexes.

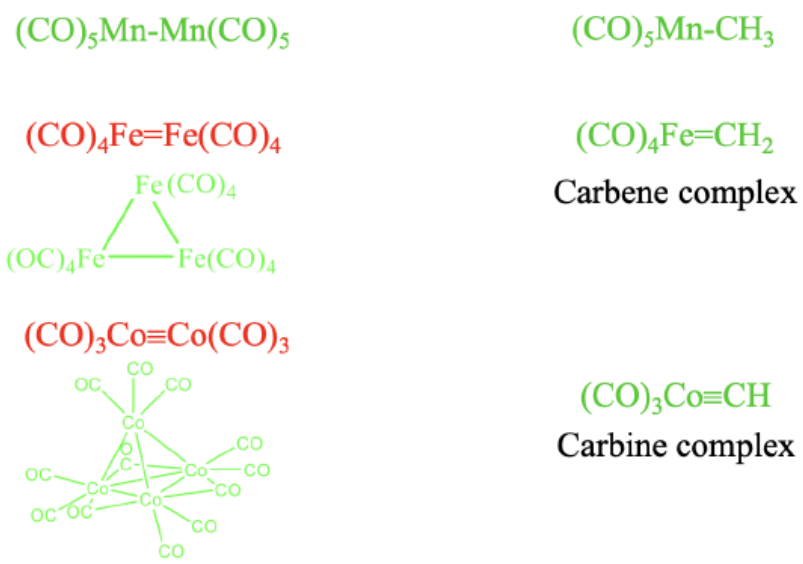


Figure 8.5.2.7: Stable molecules formed from isolobal fragments are shown in green. Species that have not been isolated (they are unstable) are shown in red (Attribution: W. Petz).

Synthesis of Terameric Cluster Carbonyls

How can we make a carbonyl cluster like $((Co(CO)_3)_4$?



Figure 8.5.2.8: Thermal reaction of $Co_2(CO)_8$ leading to $Co_4(CO)_{12}$ (Attribution: W. Petz)

It can be prepared by heating the $Co_2(CO)_8$ to a temperature above 54°C. Above this temperature the reactant loses four CO ligands and rearranges to form the cluster (Fig. 8.5.2.8). Interestingly, the higher homologues of the Co-cluster, the $Rh_4(CO)_{12}$ and the $Ir_4(CO)_{12}$ form spontaneously from the elements. Remember, that we previously determined that the $Rh_2(CO)_8$ and the $Ir_2(CO)_8$ are not stable. Rh and Ir favor the tetrameric clusters with 12 COs over the dimer with 8 CO ligands.

Structures of $Co_4(CO)_{12}$, $Rh_4(CO)_{12}$ and $Ir_4(CO)_{12}$

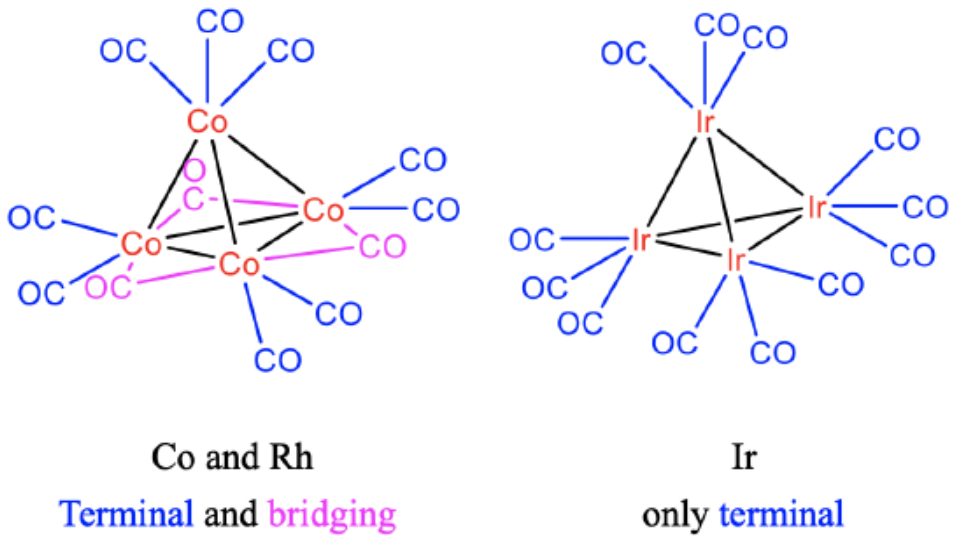


Figure 8.5.2.9: Structures of tetrameric group 9 carbonyl clusters (Attribution: W. Petz)

Like in the Co-cluster, there are 9 terminal and three bridging CO ligands in the $Rh_4(CO)_{12}$ cluster. By contrast, there are only terminal CO ligands in the iridium cluster (Fig.8.5.2.9) . This may be explained by the larger Ir-Ir bond length in comparison to the Co-Co and Rh-Rh bond lengths. The observation reflects the general rule that only 3d and 4d elements have bridging CO ligands, while only terminal ligands are observed in metals with 5d electrons.

Isoelectronic Charged Carbonyl Clusters

The previously discussed clusters were charge-neutral. Can we construct charged isoelectronic ones with different metals, and what is their stability? Let us start with the tetrameric Co-cluster made of four 15 VE fragments. The element left to the Co is the Fe. It has one electron less, therefore $Fe(CO)_3^-$ is the 15 VE electron fragment which is isoelectronic to the neutral $Co(CO)_3$ fragment. Its tetramer would be a $Fe_4(CO)_{12}^{4-}$ cluster. This cluster is not known. The cluster already carries a 4- charge which is too high to support stable Fe-Fe bonds. Each Fe carries formally a 1- negative charge and there is too much electrostatic repulsion between the Fe atoms. Another possibility to realize a 15 VE fragment with Fe is a $(CO)_4Fe^+$ fragment. Here an additional ligand is added contributing two electrons, and one electron is removed resulting in a fragment with a 1+ charge. The fragment could be combined to form an $Fe_4(CO)_{16}^{4+}$ cluster. However, such a cluster is also not stable. This is because the coordination number would be 7, which is too high for a carbonyl. In addition, there is the destabilizing effect of the positive charge on the Fe-C bond. Similarly, tetramers of the 15 VE fragments $Mn(CO)_4$, $Cr(CO)_4^-$ and $(CO)_5Cr^+$ are also not known. Also in these cases, the coordination numbers would be too high. The $Mn(CO)_4$ and the $Cr(CO)_4^-$ would lead to a coordination number of 7, in the case of the $Cr(CO)_5^+$ fragment the coordination number would be even 8. We see here the limitations of the concept of isolobality. The presence of isolobality is not always sufficient to make a stable molecule, also other factors like coordination numbers and charge needs to be considered.What about charged isoelectronic clusters made from 16 VE? We saw previously that the neutral 16 VE $Fe(CO)_4$ fragment gave a $Fe_3(CO)_{12}$ trimer. If we go from the Fe to the Mn, the isoelectronic 16 VE fragment would be a $Mn(CO)_4^-$ fragment because Mn has one electron less than Fe. This fragment can indeed be trimerized to give a stable $Mn_3(CO)_{12}^{3-}$ cluster with a 3- charge. This charge is not too high yet to destabilize the Mn-Mn bond and the coordination number of 6 is ideal for the stability of carbonyls. We could add a ligand and remove two electrons to produce a 15 VE $Mn(CO)_5^+$ fragment. However, in this case the coordination number would become 7 upon trimerization, which is too high to produce a stable cluster. In addition, the positive charge destabilizes the Mn-C bond. Replacing Mn by Cr in $Mn(CO)_5^+$ would give a neutral 16 VE $Cr(CO)_5$ fragment, but its trimer is not stable because also in this case the coordination number becomes too high. Replacing Fe in $Fe(CO)_4$ by Co would require a 1+ charge giving a $Co(CO)_4^+$ 16 VE fragment. Its trimer would have the coordination number 6, but it would carry a 4+ charge which is too high. A $Co(CO)_3^-$ fragment would also have 16 VE, but its trimer is also not known, possibly because the

relatively small coordination number of 5, which is less favorable than a coordination number of 6. Overall we can say as a rule for the stability for carbonyl clusters that there should not be positive charges, and no high negative charges. There should not be high coordination numbers.

Clusters with 16 VE and 6 VE Fragments

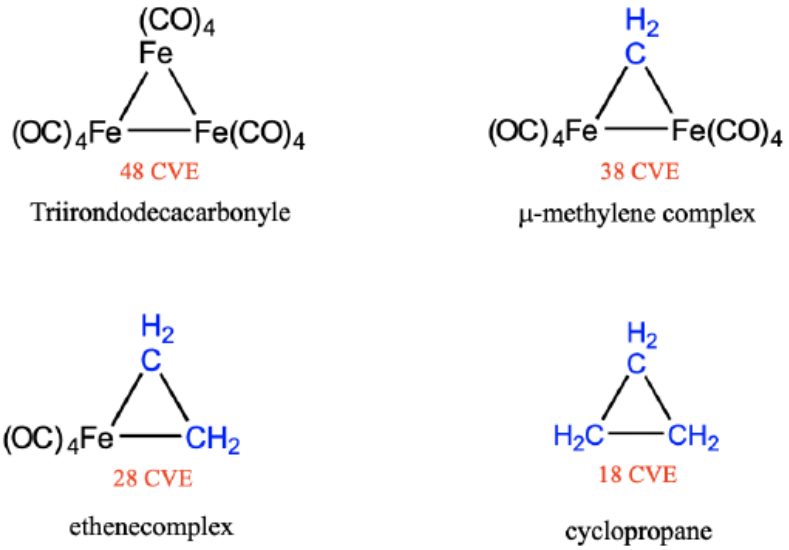


Figure 8.5.2.10: Clusters with 16 VE and 6 VE fragments (Attribution: W. Petz)

The cluster chemistry of carbonyls is even more versatile due to the possibility to substitute 16 and 15 VE fragments by 6 and 5 VE fragments, respectively. For instance, we can replace one 16 VE $Fe(CO)_4$ fragment by a 6 VE CH_2 fragment in the trimeric triiron dodecacarbonyl $Fe_3(CO)_{12}$ cluster (Fig. 8.5.2.10). In the resulting cluster a methylene group bridges two Fe atoms, therefore the complex can be regarded a μ-methylene complex. The substitution reduces the number of cluster valence electrons (CVE) from 48 to 38. A second substitution of another 16 VE tetracarbonyl iron fragment by another 6 VE methylene fragment gives a cluster with two Fe-C bonds and one carbon-carbon bond having 28 cluster valence electrons. This complex can be regarded as a ethene complex in which an ethene molecule binds side-on to a 15 VE $Fe(CO)_4$ fragment. Upon binding, the two Fe-C bonds are formed at the expense of the C-C π-bond and the bond order in the C-C bond is reduced from 2 to 1. If we substitute the last tetracarbonyl iron fragment by a third CH_2 unit, then a completely organic molecule, cyclopropane, results. All the molecules are known to be stable molecules, and their stability can be nicely understood by using the concept of isolobality.

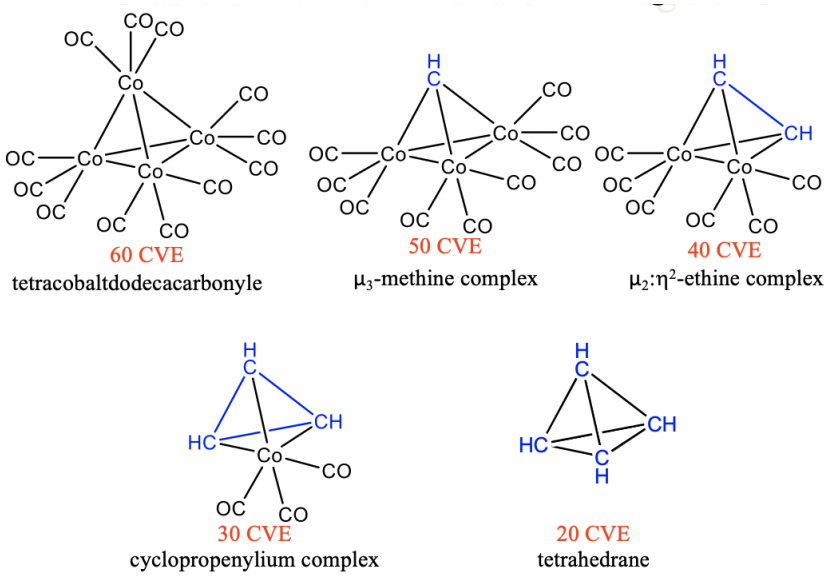


Figure 8.5.2.11: Clusters with 15 VE and 5 VE fragments (Attribution: W. Petz)

Similarly, we can substitute 15 VE tricarbonyl cobalt units by 5 VE CH fragments in tetracobaltdodecacarbonyl $Co_4(CO)_{12}$. A first substitution gives a 50 VE cluster with one CH fragment that makes three bonds to three $Co(CO)_4$ fragments (Fig. 8.5.2.11). Because the CH group bridges three metal atoms it is regarded a μ_3-methine complex. A second substitution produces a 40 VE cluster with an organic CH-CH unit that makes four bonds to two Co atoms of two 15 VE $Co(CO)_3$ fragments. The CH-CH fragment can be considered an ethine molecule binding side-on to a dicobalthexacarbonyl fragment, whereby the two π-bonds in ethine are expended to form four Co-C single bonds. The cluster can be considered a μ_2:η_2-ethine complex because the ethine bridges two Co atoms and both carbons are involved in the bonding with Co. A third substitution leads to a 30 CVE cluster with three CH units binding to one $Co(CO)_3$ fragment. There are three C-C single bonds and three Co-C bonds in the cluster. The three CH units form a cyclopropenylium complex that binds side-on to a $Co(CO)_4$ fragment. A free cyclopropenylium molecule is a 3-ring with three π-electrons that are delocalized in the ring. Therefore, the bond order in a free cyclopropenylium molecule is 1.5. In the complex the three π-electrons are being used to make the three single bonds with the cobalt atoms. The bond order in cyclopropenylium is thereby reduced from 1.5 to 1. Finally, the fourth substitution of a tricarbonyl cobalt fragment by a methine fragment yields the completely organic tetrahedrane molecule. This molecule and the others discussed before are stable. The isolobality concept lets us rationalize these complex structures easily and understand their stability.

Synthesis of Cluster Complexes From Alkynes

The view that the 40 VE clusters are alkyne clusters is not just a formal view. They can be synthesized from alkynes. For instance alkyne-dicobalt clusters are accessible from dicobalt octacarbonyl and alkynes (Fig. 8.5.2.12).

$$Co_2(CO)_8 + RC{\equiv}CR \rightarrow (\mu\text{-}RC{\equiv}CR)Co_2(CO)_6 + 2\ CO$$

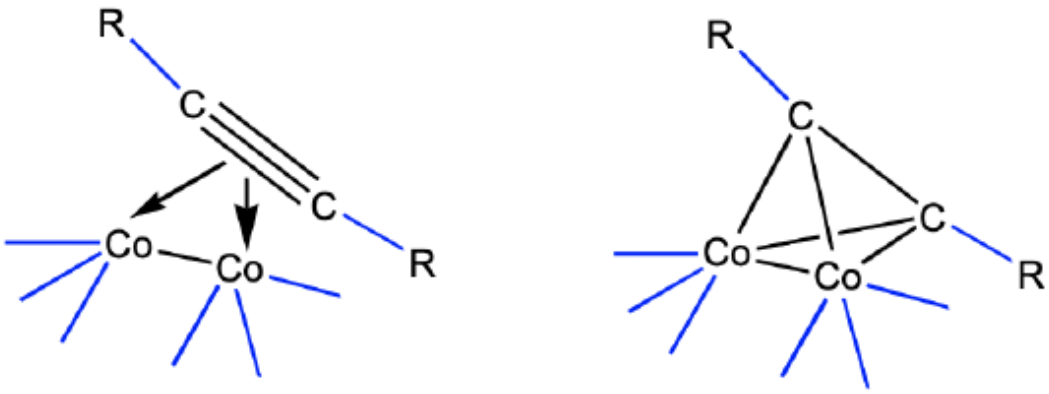
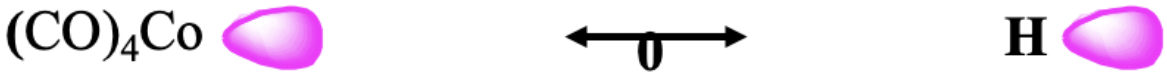


Figure 8.5.2.12: Synthesis of cluster complexes from alkynes (Attribution: W. Petz)

The cluster forms via the donation of the four π electrons of the alkynes into the metal d-orbitals of the dimeric cobalt carbonyl. This leads to a loss of of two CO ligands, and the formation of four Co-C bonds. Under harsher conditions the C-C triple bond can also cleave and this can give access to methine complexes.

Carbonyl Hydrides

Now let us leave the carbonyl cluster compounds and talk about another interesting class of carbonyls: carbonyl hydrides. They can be rationalized by the concept of isolobality as well. A hydrogen atom can be conceived as a species with one frontier orbital containing one electron. In this case the frontier orbital is simply the 1s orbital of the hydrogen. Thus, it should be possible to combine an H atom with a 17 VE carbonyl fragment like tetracarbonyl cobalt.



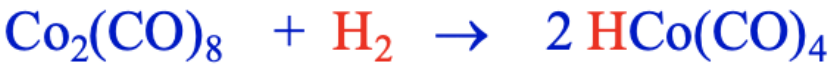
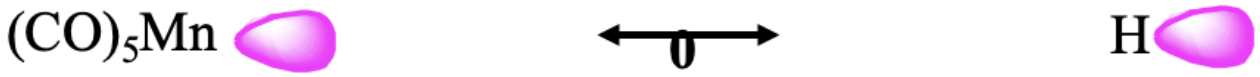


Figure 8.5.2.13: Example for the formation of a cobalt carbonyl hydride (Attribution: W. Petz)

Indeed, one can combine such fragments to form stable carbonyl hydrides such as tetracarbonylhydrido cobalt (0). This molecule can be synthesized by reduction of bis(tetracarbonyl cobalt) (0) with dihydrogen (Fig. 8.5.2.13). Counter-intuitively, this molecule is a strong acid, it has an acidity similar to sulfuric acid. One would think that the Co-H bond would be polarized toward H based on electronegativity arguments. However, this is not the case. The carbonyl fragment has a frontier orbital which is energetically higher than that of H, and thus the bond is polarized toward H. In another view we can explain the high acidity be the fact that the loss of the proton leads to the very stable 18 VE tetrahedral $Co(CO)_4^-$ anion. Thus, loss of the proton occurs easily.



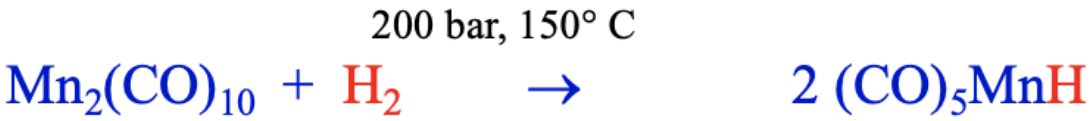


Figure 8.5.2.14: Example for the formation of a manganese carbonyl hydride (Attribution: W. Petz)

Another 17 VE electron fragment is the $Mn(CO)_5$ fragment. Also this fragment can be combined with an isolobal H fragment to form a stable molecule, which has the composition $HMn(CO)_5$ (Fig. 8.5.2.14). It can be prepared from bis(pentacarbonyl manganese) and dihydrogen at 200 bar and 150°C. This carbonyl hydride is a weak acid, it has a similar acidity as H_2S. We could argue that this lower acidity may be because the loss of the proton reduces its coordination number from 6 to 5. The coordination number of 6 is the preferred coordination number for carbonyls and thus the tendency to lose the proton is relatively small. The different metal and the number of carbonyl ligands will likely lead to a different energy of the frontier orbital compared to the previous example, which leads to a different polarity.

Overall, one can tune the properties in carbonyl hydrides from highly acidic to hydridic by choice of the metal the coordination number, and also by the choice of additional ligands L other than carbonyl. The electronic and steric properties of the ligands have an influence on the energy of the HOMO of the fragment, and thus on the polarity of the metal-hydrogen bond, and the acidity.

Sources: https://en.Wikipedia.org/wiki/Isolobal_principle

This page titled 8.5.2: The Isolobal Analogy is shared under a CC BY-SA 4.0 license and was authored, remixed, and/or curated by Kai Landskron & Kathryn Haas.

- 10.3: The Concept of Isolobality, Carbonyl Clusters, and Ligands Related to CO by Kai Landskron is licensed CC BY 4.0.

8.5.2.1: Extensions of the Analogy

The isolobal analogy has applications beyond simple octahedral complexes. It can be used with a variety of ligands, charged species and non-octahedral complexes.

The isolobal analogy can also be used with i**soelectronic fragments** having the same coordination number, which allows **charged species** to be considered. For example, $\mathrm{Re(CO)_5}$ is isolobal with $\mathrm{CH_3}$ and therefore, $\mathrm{[Ru(CO)_5]^+}$ and $\mathrm{[Mo(CO)_5]^-}$are also isolobal with $\mathrm{CH_3}$. Any 17-electron metal complex would be isolobal in this example.

In a similar sense, the **addition or removal of electrons from two isolobal fragments** results in two new isolobal fragments. Since $\mathrm{Re(CO)_5}$ is isolobal with $\mathrm{CH_3}$, $\mathrm{[Re(CO)_5]^+}$ is isolobal with $\mathrm{CH_3{}^+}$.

The analogy applies to other shapes besides tetrahedral and octahedral geometries. The derivations used in octahedral geometry are valid for most other geometries. The exception is square-planar because square-planar complexes typically abide by the 16-electron rule. Assuming ligands act as two-electron donors the metal center in square-planar molecules is d^8. To relate an octahedral fragment, ML_n, where M has a d^x electron configuration to a square planar analogous fragment, the formula ML_{n-2} where M has a d^{x+2} electron configuration should be followed.

Octahedral ML_n	Square Planar ML_n
$d^6:$ $\mathrm{Mo(CO)_5}$	$d^8:$ $\mathrm{[PdCl_3]^-}$
$d^8:$ $\mathrm{Os(CO)_4}$	$d^10:$ $\mathrm{Ni(PR_3)_2}$

Further examples of the isolobal analogy in various shapes and forms are shown

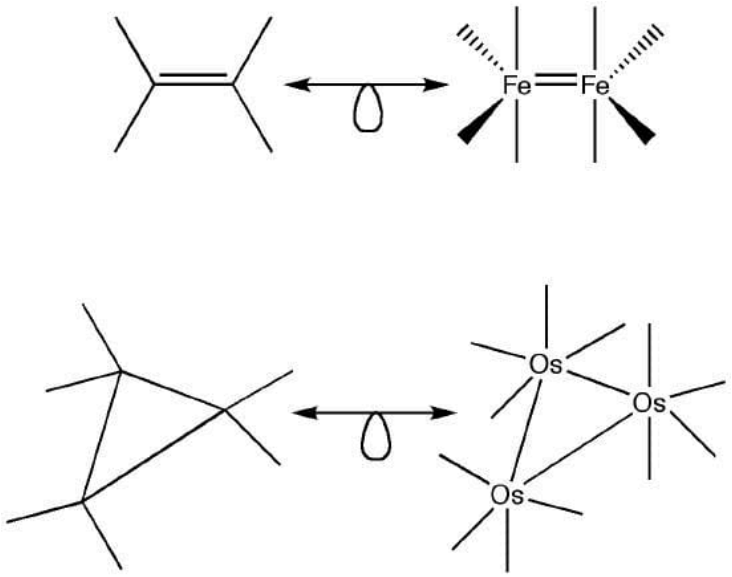


Figure 8.5.2.1.1: Examples of extensions of the isolobal analogy. (Public Domain; Chem507f10grp5via Wikipedia)

Sources: https://en.Wikipedia.org/wiki/Isolobal_principle

This page titled 8.5.2.1: Extensions of the Analogy is shared under a CC BY-SA 4.0 license and was authored, remixed, and/or curated by Wikipedia via source content that was edited to the style and standards of the LibreTexts platform.

8.5.2.2: Some Applications of the Isolobal Analogy

This page titled 8.5.2.2: Some Applications of the Isolobal Analogy is shared under a license and was authored, remixed, and/or curated by Kathryn Haas.

8.5.3: Metal-Metal Bonds

Molecular orbital considerations in Dinuclear Metal Complexes with Multiple M-M Bonds

Let us begin a new chapter and think about dinuclear transition metal complexes with multiple metal-metal bonds. What is the maximum bond order that we could expect? The transition metals have five d-orbitals available, and in order to determine the maximum possible bond order we need to see how they overlap to form molecular orbitals (Fig. 11.1.1).

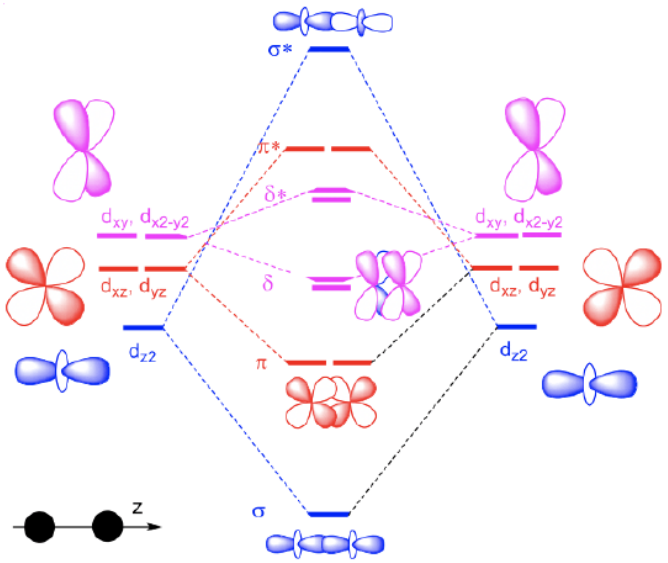


Figure 11.1.1 Molecular orbital overlap of metal d-orbitals forming M-M bonds

If we define the M-M bond axis as the z-axis, then two d_z^2-orbitals can overlap in σ-fashion to form a bonding and an anti-bonding σ-molecular orbital. A d_{xz}, and a d_{yz} can overlap with another d_{xz} and another d_{yz} in π-fashion to form two degenerated bonding π and two degenerated anti-bonding π*-orbitals. π-overlap is smaller than σ-overlap, therefore the split in energy between the bonding and the anti-bonding π-orbitals is smaller than the split between the bonding and the anti-bonding σ-orbitals. The d_{xy} orbital can overlap with another d_{xy} orbital in δ-fashion, and so can the $d_{x^2-y^2}$ with another $d_{x^2-y^2}$. This gives two bonding δ-orbitals and two anti-bonding δ-orbitals. The δ-overlap is even smaller than the π-overlap, therefore the energy split between the bonding and the anti-bonding δ-orbitals is even smaller than those for the π and π*-orbitals. So what would be the maximum bond order that could be achieved? The maximum bond order would be achieved when all bonding MOs were full, and all anti-bonding MOs were empty. We have overall five bonding MOs that we could fill with ten electrons from two metal atoms with d^5-electron configuration. The maximum bond order BO would therefore be BO=5. However, in practice only bond orders up to 4 are well known. This is because the $d_{x^2-y^2}$ orbital is usually too involved in the bonding with the ligands thereby becoming unavailable for metal-metal interactions. The $d_{x^2-y^2}$ orbital makes the strongest interactions with the ligands because most ligands approach on or near the x and the y-axes.

Electron Configurations and Multiple M-M Bonds

We can easily predict now which electron configuration leads to which metal-metal bond order. The bond order increases from 1 to 4 with the electron configuration changing from d^1 to d^4. At d^4 all bonding MOs are full with eight electrons.

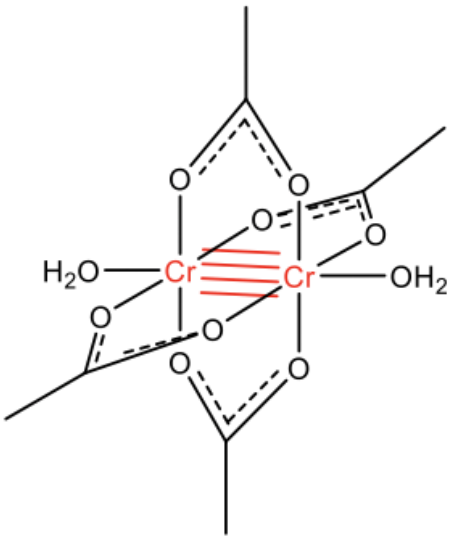


Figure 11.1.2 Tetraacetatodiaquadichromium complex

An example of a complex with a bond order of 4 is the tetraacetatodiaquadichromium complex shown (Fig. 11.1.2). Cr is in the oxidation state +2, which makes the chromium a d^4 species. We can quickly show this by counting the valence electrons. A neutral Cr atom has 6 VE, and an electron configuration $3d^5 4s^1$. There are four acetate ligands having a 1- charge each which gives four negative charges overall. The complex is overall neutral which means that each Cr must have formally a 2+ charge, and the electron configuration is $3d^4$.

d^1	d^2	d^3	d^4	d^5	d^6	d^7	d^8
1	2	3	4	3	2	1	0

Figure 11.1.3 Relationship between metal-metal bond order and electron configuration

With even more electrons in the metal d-orbitals the bond order begins to decrease again as anti-bonding MOs need to be filled (Fig. 11.1.3). The combination of two metals with d^5 electron configuration leads to a triple bond, two d^6-metals give a double bond, and two d^7 metals give a single bond. A metal-metal bond should not exist for two d^8-metals because then the bond order is zero.

Evidence for M-M Multiple Bonds

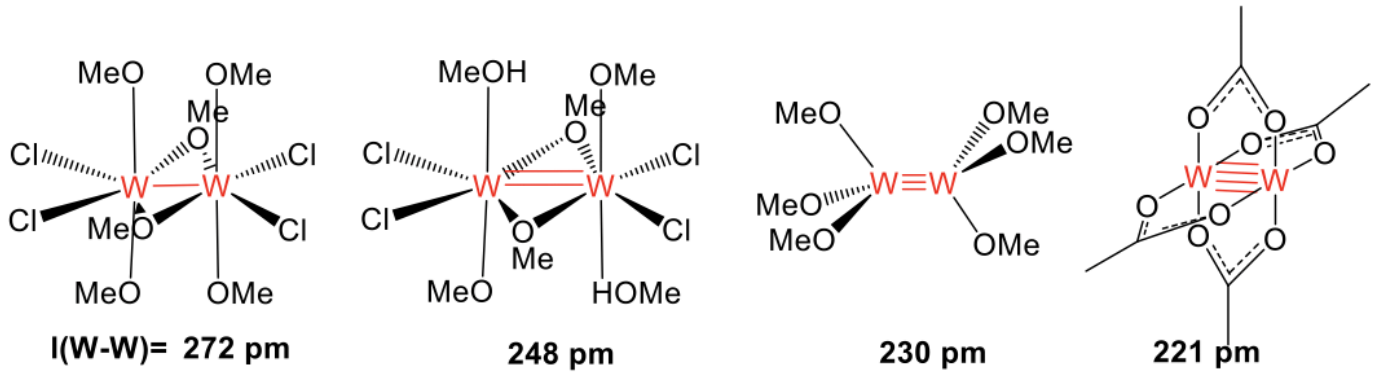


Figure 11.1.4 M-M bond length in four tungsten complexes

What experimental evidence can support the existence of a particular bond order (Fig. 11.1.4)? One argument is the bond length which can be obtained through the crystal structure determination of the complex. The shorter the bond, the higher the bond order. For instance, in the four tungsten complexes shown the bond lengths decrease from 272 pm, to 248 pm, to 230 pm to 221 pm corresponding to a single, double, triple, and quadruple bond, respectively.

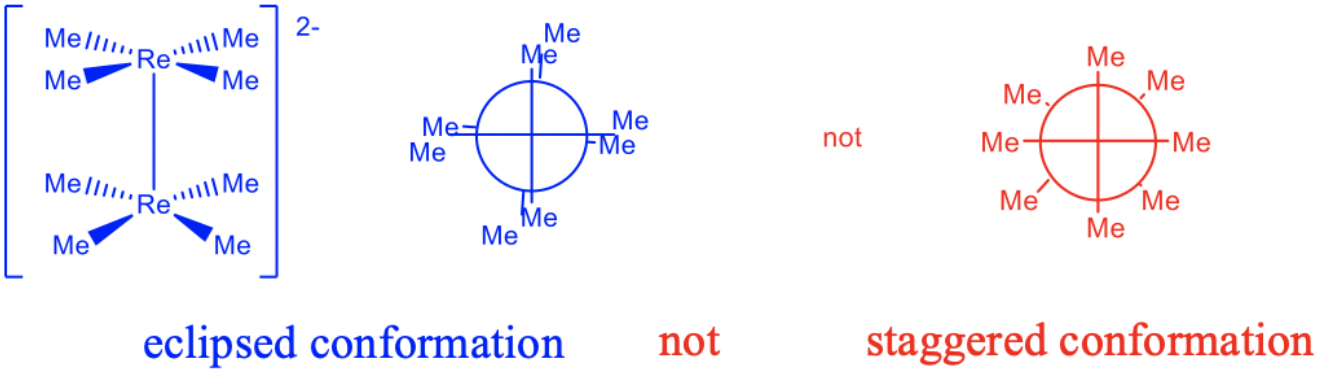


Figure 11.1.5 $ReMe_4$ confirmations

Another hint can be the conformation of a molecule (Fig. 11.1.5). For instance, the two square-planar units of the $Re_2Me_8^{2-}$ complex anion show eclipsed conformation. Steric repulsion arguments would favor the staggered conformation, so there must be a reason why the two $ReMe_4$ units are eclipsed. The rhenium is in the oxidation state +3, thus it is a d^4 species, and we would argue that there may be a Re-Re quadruple bond. This quadruple bond can only form when the d_{xy} orbitals are in eclipsed conformation, and this is only possible when the two $ReMe_4$ fragments are in eclipsed conformation. The very short bond length of 218 pm further supports the existence of the quadruple bond.

Dr. Kai Landskron (Lehigh University). If you like this textbook, please consider to make a donation to support the author's research at Lehigh University: Click Here to Donate.

This page titled 8.5.3: Metal-Metal Bonds is shared under a license and was authored, remixed, and/or curated by LibreTexts.

- 11.1: Complexes with Multiple Metal-Metal Bonds by Kai Landskron is licensed CC BY 4.0.

8.5.3.1: Metal-Metal Multiple Bonds

Molecular orbital considerations in Dinuclear Metal Complexes with Multiple M-M Bonds

Let us begin a new chapter and think about dinuclear transition metal complexes with multiple metal-metal bonds. What is the maximum bond order that we could expect? The transition metals have five d-orbitals available, and in order to determine the maximum possible bond order we need to see how they overlap to form molecular orbitals (Fig. 11.1.1).

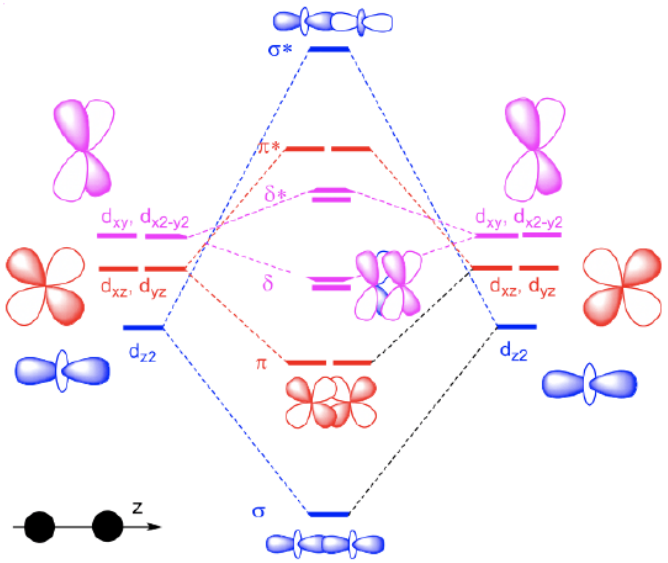


Figure 11.1.1 Molecular orbital overlap of metal d-orbitals forming M-M bonds

If we define the M-M bond axis as the z-axis, then two d_z^2-orbitals can overlap in σ-fashion to form a bonding and an anti-bonding σ-molecular orbital. A d_{xz}, and a d_{yz} can overlap with another d_{xz} and another d_{yz} in π-fashion to form two degenerated bonding π and two degenerated anti-bonding π*-orbitals. π-overlap is smaller than σ-overlap, therefore the split in energy between the bonding and the anti-bonding π-orbitals is smaller than the split between the bonding and the anti-bonding σ-orbitals. The d_{xy} orbital can overlap with another d_{xy} orbital in δ-fashion, and so can the $d_{x^2-y^2}$ with another $d_{x^2-y^2}$. This gives two bonding δ-orbitals and two anti-bonding δ-orbitals. The δ-overlap is even smaller than the π-overlap, therefore the energy split between the bonding and the anti-bonding δ-orbitals is even smaller than those for the π and π*-orbitals. So what would be the maximum bond order that could be achieved? The maximum bond order would be achieved when all bonding MOs were full, and all anti-bonding MOs were empty. We have overall five bonding MOs that we could fill with ten electrons from two metal atoms with d^5-electron configuration. The maximum bond order BO would therefore be BO=5. However, in practice only bond orders up to 4 are well known. This is because the $d_{x^2-y^2}$ orbital is usually too involved in the bonding with the ligands thereby becoming unavailable for metal-metal interactions. The $d_{x^2-y^2}$ orbital makes the strongest interactions with the ligands because most ligands approach on or near the x and the y-axes.

Electron Configurations and Multiple M-M Bonds

We can easily predict now which electron configuration leads to which metal-metal bond order. The bond order increases from 1 to 4 with the electron configuration changing from d^1 to d^4. At d^4 all bonding MOs are full with eight electrons.

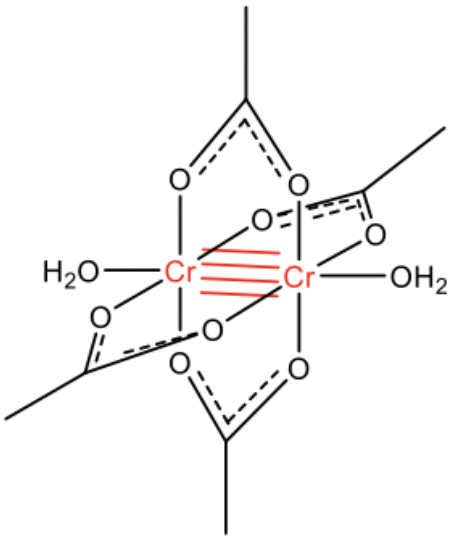


Figure 11.1.2 Tetraacetatodiaquadichromium complex

An example of a complex with a bond order of 4 is the tetraacetatodiaquadichromium complex shown (Fig. 11.1.2). Cr is in the oxidation state +2, which makes the chromium a d^4 species. We can quickly show this by counting the valence electrons. A neutral Cr atom has 6 VE, and an electron configuration $3d^5 4s^1$. There are four acetate ligands having a 1- charge each which gives four negative charges overall. The complex is overall neutral which means that each Cr must have formally a 2+ charge, and the electron configuration is $3d^4$.

d^1	d^2	d^3	d^4	d^5	d^6	d^7	d^8
1	2	3	4	3	2	1	0

Figure 11.1.3 Relationship between metal-metal bond order and electron configuration

With even more electrons in the metal d-orbitals the bond order begins to decrease again as anti-bonding MOs need to be filled (Fig. 11.1.3). The combination of two metals with d^5 electron configuration leads to a triple bond, two d^6-metals give a double bond, and two d^7 metals give a single bond. A metal-metal bond should not exist for two d^8-metals because then the bond order is zero.

Evidence for M-M Multiple Bonds

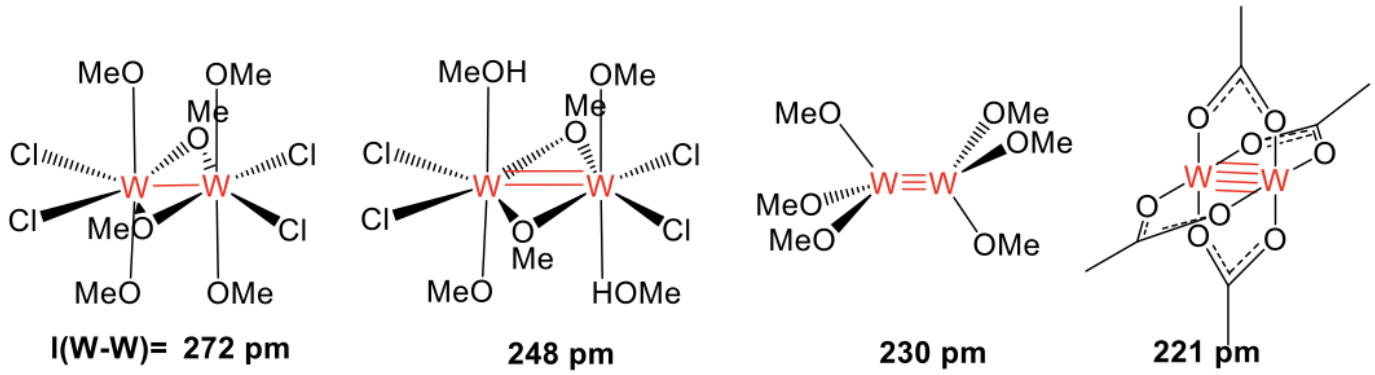


Figure 11.1.4 M-M bond length in four tungsten complexes

What experimental evidence can support the existence of a particular bond order (Fig. 11.1.4)? One argument is the bond length which can be obtained through the crystal structure determination of the complex. The shorter the bond, the higher the bond order. For instance, in the four tungsten complexes shown the bond lengths decrease from 272 pm, to 248 pm, to 230 pm to 221 pm corresponding to a single, double, triple, and quadruple bond, respectively.

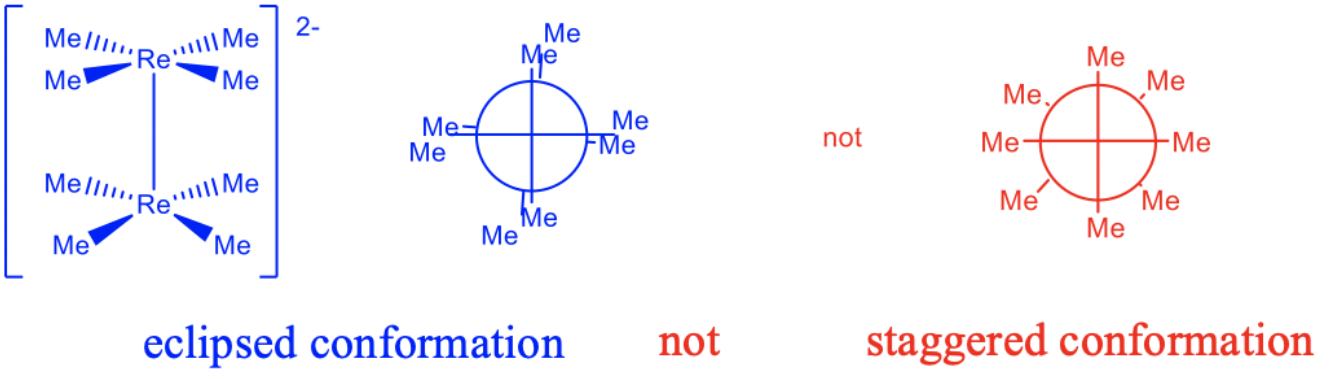


Figure 11.1.5 $ReMe_4$ confirmations

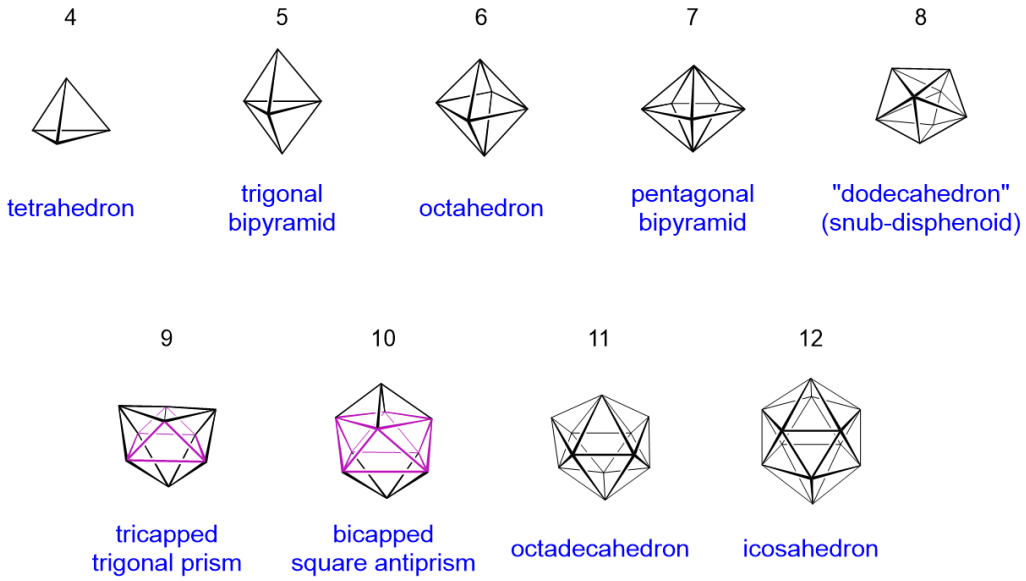
Another hint can be the conformation of a molecule (Fig. 11.1.5). For instance, the two square-planar units of the $Re_2Me_8^{2-}$ complex anion show eclipsed conformation. Steric repulsion arguments would favor the staggered conformation, so there must be a reason why the two $ReMe_4$ units are eclipsed. The rhenium is in the oxidation state +3, thus it is a d^4 species, and we would argue that there may be a Re-Re quadruple bond. This quadruple bond can only form when the d_{xy} orbitals are in eclipsed conformation, and this is only possible when the two $ReMe_4$ fragments are in eclipsed conformation. The very short bond length of 218 pm further supports the existence of the quadruple bond.

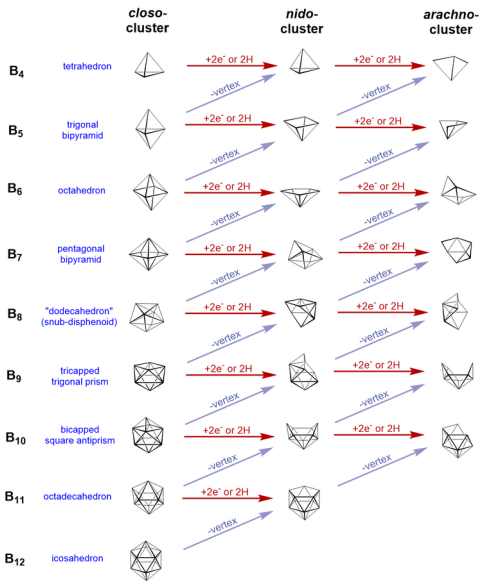
Dr. Kai Landskron (Lehigh University). If you like this textbook, please consider to make a donation to support the author's research at Lehigh University: Click Here to Donate.

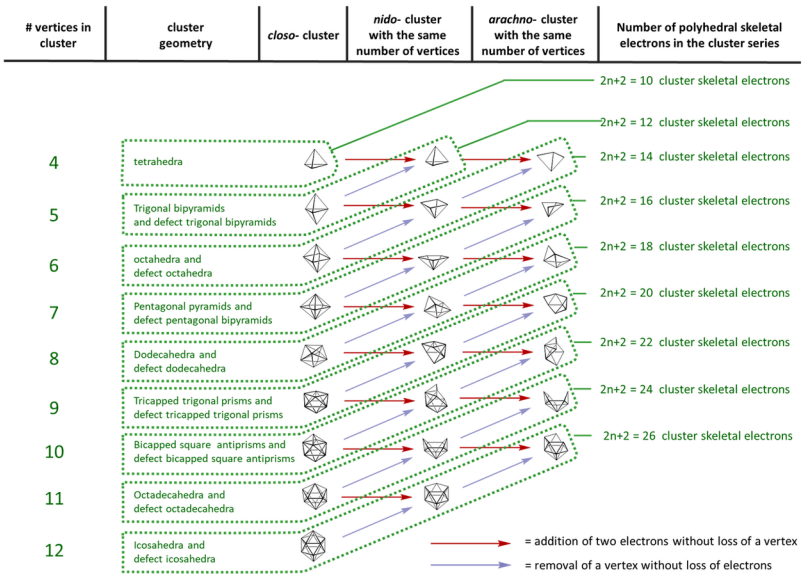
This page titled 8.5.3.1: Metal-Metal Multiple Bonds is shared under a license and was authored, remixed, and/or curated by LibreTexts.

- 11.1: Complexes with Multiple Metal-Metal Bonds by Kai Landskron is licensed CC BY 4.0.

8.5.4: Cluster Compounds







Notes and References

This page titled 8.5.4: Cluster Compounds is shared under a CC BY-SA 4.0 license and was authored, remixed, and/or curated by Stephen M. Contakes.

- 15.4: Cluster Compounds by Stephen M. Contakes is licensed CC BY-SA 4.0.

8.5.4.1: Boranes

Boranes and the Bonding in boranes

Boranes were introduced in Chapter 8 (Section 8.6.1). Boranes are compounds consisting of boron and hydrogen.The most basic example is diborane (B_2H_6), all boranes are electron-deficient compounds. For B_2H_6 usually 14 electrons are needed to form 2c,2e-bonds, but only 12 valence electrons are present. Because of this there are two B-H-B bonds, which have three centers, but only two electrons (3c, 2e bond). This can be interpreted as a molecular orbital that is formed by combining the contributed atomic orbitals of the three atoms. In more complicated boranes not only B-H-B bonds but also B-B-B 3c, 2e-bonds occur. In such a bond the three B-atoms lie at the corners of an equilateral triangle with their sp^3 hybrid orbitals overlapping at its center. One of the common properties of boranes is, that they are flammable or react spontaneously with air. They burn with a characteristic green flame. And they are colorless, diamagnetic substances.

Nomenclature

In neutral boranes the number of boron atoms is given by a prefix and the number of Hydrogen-atoms is given in parentheses behind the name. example: B_5H_{11} -> pentaborane(11), B_4H_{10} -> tetraborane(10) For ions primarily the number of hydrogen-atoms and than the number of boron-atoms is given, behind the name the charge is given in parentheses. example: $[B_6H_6]^{2-}$ -> hexahydrohexaborat(2-)

Wades rule, Structures of boranes

Wades rule helps to predict the general shape of a borane from its formula. Ken Wade developed a method for the prediction of shapes of borane clusters; however, it may be used for a wide range of substituted boranes (such as carboranes) as well as other classes of cluster compounds. Wade's rules are used to rationalize the shape of borane clusters by calculating the total number of skeletal electron pairs (SEP) available for cluster bonding. In using Wade's rules it is key to understand structural relationship of various boranes.

Wade's rules:

The general methodology to be followed when applying Wade's rules is as follows:

I. First, find the number of skeletal electron pairs

1. Determine the total number of valence electrons from the chemical formula, i.e., 3 electrons per B, and 1 electron per H.
2. Subtract 2 electrons for each vertex unit (B-H, C-H in a carborane, etc.).
3. Divide the number of remaining electrons by 2 to get the number of skeletal electron pairs (SEP).

II. Then determine the number of vertices in the parent deltahedron, *n*, from the number of SEP.

n = vertices in the parent deltahedron = SEP -1

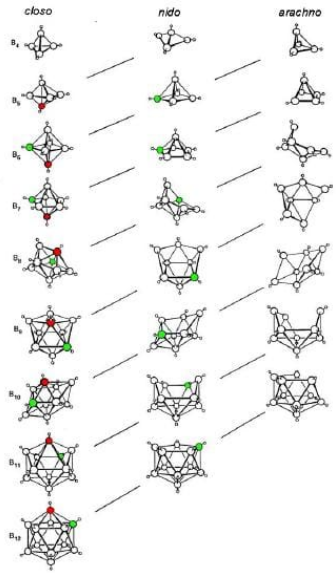
III. Finally, determine whether the cluster is *closo*-, *nido*-, *arachno*-, *hypho*-, *klado*-, or otherwise by comparing the number of vertex atoms with those in the parent deltahedron.

1. When *n* vertex atoms are present (i.e., *n* boron atoms) the cluster has a *closo*- structure, specifically that of the parent deltahedron.
2. When *n*-1 vertex atoms are present (i.e., *n* boron atoms) the cluster has a *nido* structure.
3. When *n*-2 vertex atoms are present (i.e., *n* boron atoms) the cluster has a *arachno* structure.
4. When *n*-3 vertex atoms are present (i.e., *n* boron atoms) the cluster has a *hypho* structure.
5. When *n*-4 vertex atoms are present (i.e., *n* boron atoms) the cluster has a *klado* structure.

6. If there are more vertex atoms than are vertices present in the parent deltahedron then the extra boron occupies a capping position on a triangular face.

Formula Skeletal	Skeletal electron pairs	type
$[\mathrm{B}_n\ \mathrm{H}_n]^{2-}$	n+1	closo
$\mathrm{B}_n\ \mathrm{H}_{n+4}$	n+2	nido
$\mathrm{B}_n\ \mathrm{H}_{n+6}$	n+3	arachno
$\mathrm{B}_n\ \mathrm{H}_{n+8}$	n+4	hype

The polyhedra are always made up of triangular faces, so they are called **deltahedra**. Usually there are three possible structure types:



*Structural relationship between closo, nido, and arachno boranes (and hetero-substituted boranes). The diagonal lines connect species that have the same number of skeletal electron pairs (SEP). Hydrogen atoms except those of the B-H framework are omitted. The red atom is omitted first, the green atom removed second. Adapted from R. W. Rudolph, Acc. Chem. Res., 1976, **9**, 446.*

Closo-boranes

- closed deltahedra without B-H-B 3c,2e-bonds
- thermally stable and moderately reactive.
- example: $[\mathrm{B}_5\mathrm{H}_5]^{2-}$: the ion builds up a trigonal, bipyramidal polyhedron

Nido-boranes

- closo borane with one corner less and addition of two hydrogen-atoms instead
- B-H-B-bonds and B-B-bonds are possible.
- thermally stability lies between closo- and arachno-boranes.
- example: $\mathrm{B}_5\mathrm{H}_9$ its structure can be assumed as the octahedral deltahedron of $[\mathrm{B}_6\mathrm{H}_6]^{2-}$ without one corner tetragonal pyramid

Arachno-boranes

- closo borane deltahedron but with two BH-units removed and two H-atoms added.

- it has to have B-H-B 3c, 2e-bonds.
- thermally unstable at room temperature and highly reactive.
- example: \{\ce{B4H10}\} the structure can be derived from $[B_6H_6]^{2-}$ -> deltahedron with two corners less.

There exist also other structures like the hypho-boranes, but they are less important.

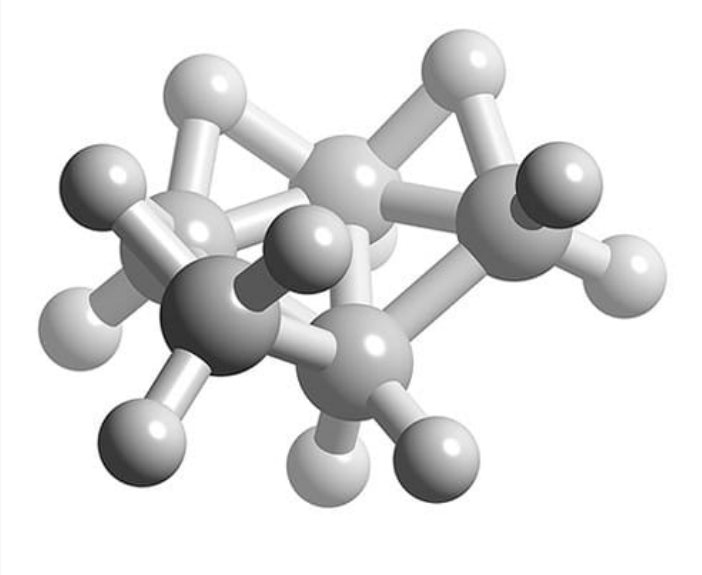
Wade's Rules

Example 8.5.4.1.1: B_5H_{11}

What is the structure of B_5H_{11}?

Solution

1. Total number of valence electrons = (5 x B) + (11 x H) = (5 x 3) + (11 x 1) = 26
2. Number of electrons for each B-H unit = (5 x 2) = 10
3. Number of skeletal electrons = 26 – 10 = 16
4. Number SEP = 16/2 = 8
5. If *n*+1 = 8 and *n*-2 = 5 boron atoms, then *n* = 7
6. Structure of *n* = 7 is pentagonal bipyramid, therefore B_5H_{11} is an *arachno* based upon a pentagonal bipyramid with two apexes missing.



Ball and stick representation of the structure of B_5H_{11}.

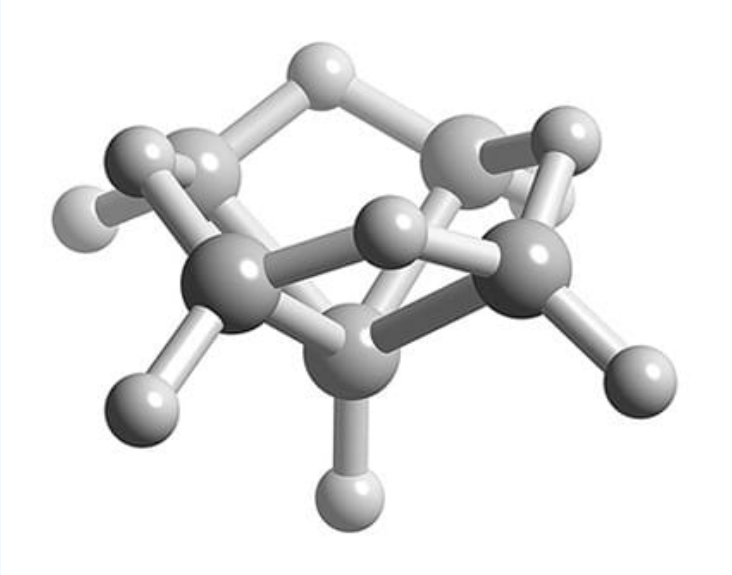
Example 8.5.4.1.2: B_5H_9?

What is the structure of B_5H_9?

Solution

1. Total number of valence electrons = (5 x B) + (9 x H) = (5 x 3) + (9 x 1) = 24
2. Number of electrons for each B-H unit = (5 x 2) = 10
3. Number of skeletal electrons = 24 – 10 = 14
4. Number SEP = 14/2 = 7
5. If *n*+1 = 7 and *n*-1 = 5 boron atoms, then *n* = 6

6. Structure of n = 6 is octahedral, therefore B_5H_9 is a *nido* structure based upon an octahedral structure with one apex missing.

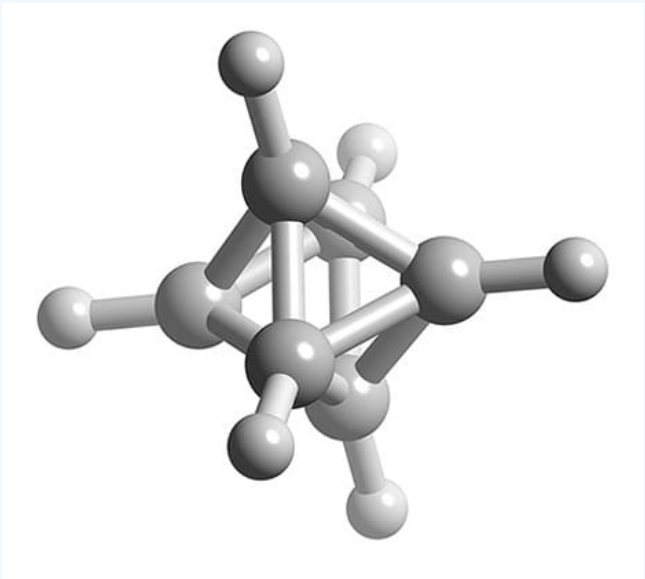


Ball and stick representation of the structure of B_5H_9.

Example 8.5.4.1.3: $B_6H_6^{2-}$

What is the structure of $B_6H_6^{2-}$?

1. Total number of valence electrons = (6 x B) + (3 x H) = (6 x 3) + (6 x 1) + 2 = 26
2. Number of electrons for each B-H unit = (6 x 2) = 12
3. Number of skeletal electrons = 26 – 12 = 14
4. Number SEP = 14/2 = 7
5. If n+1 = 7 and n boron atoms, then n = 6
6. Structure of n = 6 is octahedral, therefore $B_6H_6^{2-}$ is a *closo* structure based upon an octahedral structure.

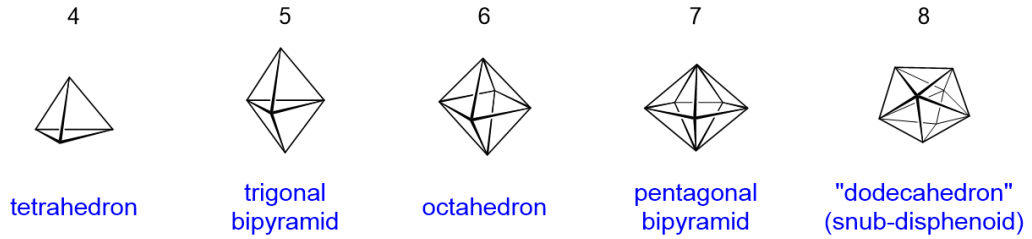


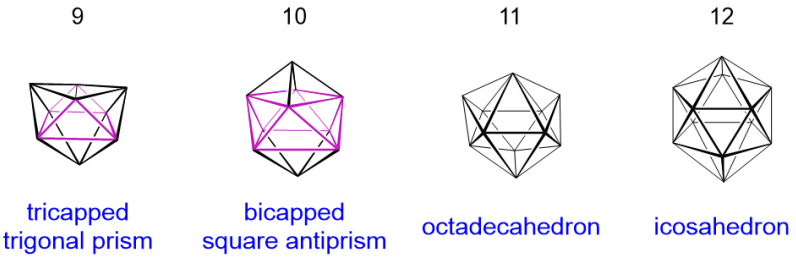
Ball and stick representation of the structure of $B_6H_6^{2-}$.

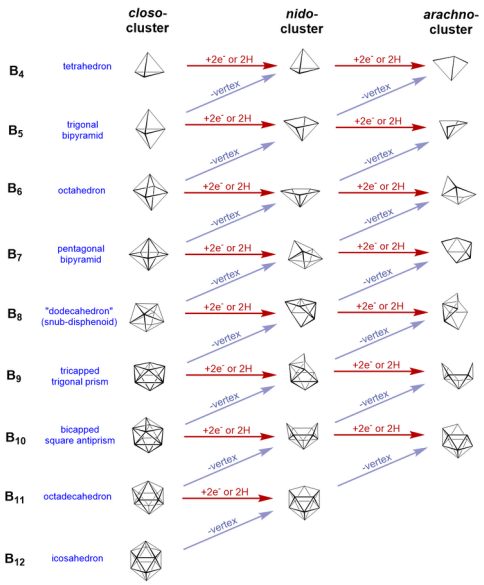
Table 8.5.4.1.1 provides a summary of borane cluster with the general formula $B_nH_n^{x-}$ and their structures as defined by Wade's rules.

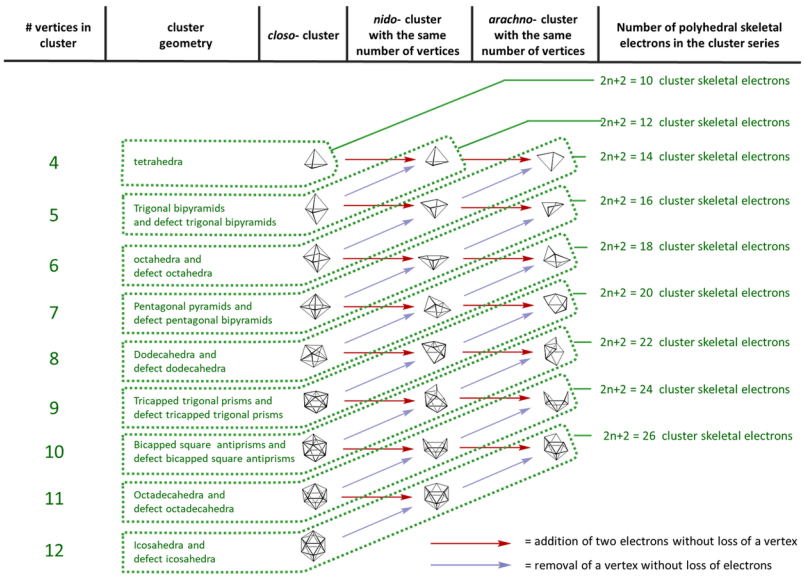
Table 8.5.4.1.1: Wade's rules for boranes.

Type	Basic formula	Example	# of verticies	# of vacancies	# of e- in B + charge	# of bonding MOs
Closo	$B_nH_n^{2-}$	$B_6H_6^{2-}$	n	0	3n + 2	n + 1
Nido	$B_nH_n^{4-}$	B_5H_9	n + 1	1	3n + 4	n + 2
Arachno	$B_nH_n^{6-}$	B_4H_{10}	n + 2	2	3n + 6	n + 3
Hypho	$B_nH_n^{8-}$	$B_5H_{11}^{2-}$	n + 3	3	3n + 8	n + 4









Notes and References

R. W. Rudolph, *Acc. Chem. Res.*, 1976, **9**, 446.

K. Wade, *Adv. Inorg. Chem. Radiochem.*, 1976, **18**, 1.

D. F. Shriver, P. W. Atkins, Inorganic Chemistry Third edition, Oxford University Press, 2001

Patrick O' Malley from the University of Manchester via Wolearn.org (https://www.wolearn.org/pluginfile.php/1492/mod_resource/content/1/Wades_Rules.pdf)

Template:ContribConnectionshttps://archive.cnx.org/contents/ffb...2/wade-s-rules

Contributors and Attributions

Stephen Contakes, Westmont College, made the lower three figures and edited the methodology for applying Wade's rules. He suspects the original text of the page was imported from https://chem.libretexts.org/Bookshelves/Inorganic_Chemistry/Chemistry_of_the_Main_Group_Elements_(Barron)/06%3A_Group_13/6.05%3A_Wades_Rules.

This page titled 8.5.4.1: Boranes is shared under a license and was authored, remixed, and/or curated by LibreTexts.

- 24.5: The Isolobal Principle and Application of Wade's Rules is licensed CC BY-NC-SA 4.0.
- 15.4: Cluster Compounds by Stephen M. Contakes is licensed CC BY-SA 4.0.

8.5.4.2: Heteroboranes

This page titled 8.5.4.2: Heteroboranes is shared under a license and was authored, remixed, and/or curated by LibreTexts.

8.5.4.3: Metallaboranes and Metallacarboranes

This page titled 8.5.4.3: Metallaboranes and Metallacarboranes is shared under a license and was authored, remixed, and/or curated by LibreTexts.

8.5.4.4: Carbonyl Clusters

This page titled 8.5.4.4: Carbonyl Clusters is shared under a license and was authored, remixed, and/or curated by LibreTexts.

8.5.4.5: Carbon-Centered Clusters

This page titled 8.5.4.5: Carbon-Centered Clusters is shared under a license and was authored, remixed, and/or curated by LibreTexts.

8.5.4.6: Additional Comments on Clusters

This page titled 8.5.4.6: Additional Comments on Clusters is shared under a license and was authored, remixed, and/or curated by LibreTexts.

8.5.5: Problems

This page titled 8.5.5: Problems is shared under a license and was authored, remixed, and/or curated by LibreTexts.

9: INTRODUCTION TO SOLID STATE CHEMISTRY

Introduction to Solid State Chemistry is a first-year single-semester college course on the principles of chemistry. This unique and popular course satisfies MIT's general chemistry degree requirement, with an emphasis on solid-state materials and their application to engineering systems.

9.1: The Nature of Crystalline Solids

9.1.1: Crystal Structures of Metals

9.1.2: Ionic and Covalent Solids - Structures

9.1.2.1: Prelude to Ionic and Covalent Solids - Structures

9.1.2.2: Close-packing and Interstitial Sites

9.1.2.3: Structures Related to NaCl and NiAs

9.1.2.4: Tetrahedral Structures

9.1.2.5: Layered Structures and Intercalation Reactions

9.1.2.6: Bonding in TiS_2, MoS_2, and Pyrite Structures

9.1.2.7: Spinel, Perovskite, and Rutile Structures

9.1.2.8: Discussion Questions

9.1.2.9: References

9.2: Bonding in Metals, Semiconductors and Insulators – Band Structure

9.2.1: Prelude to Electronic Properties of Materials - Superconductors and Semiconductors

9.2.2: Periodic Trends- Metals, Semiconductors, and Insulators

9.2.3: Bonding in Metals

9.2.4: Conduction in Metals

9.2.5: Superconductors

9.2.6: Semiconductors- Band Gaps, Colors, Conductivity and Doping

9.2.7: Semiconductor p-n Junctions

9.2.8: Diodes, LEDs and Solar Cells

9.3: X-rays and X-ray Diffraction

9.4: The Imperfect Solid State

9.5: Glasses

9.6: Phase Equilibria and Phase Diagrams

This page titled 9: Introduction to Solid State Chemistry is shared under a CC BY-NC-SA 4.0 license and was authored, remixed, and/or curated by Donald Sadoway (MIT OpenCourseWare).

9.1: The Nature of Crystalline Solids

In an assembly of atoms or molecules a solid phase is formed whenever the interatomic (intermolecular) attractive forces significantly exceed the disruptive thermal forces and thus restrict the mobility of atoms, forcing them into more-or-less fixed positions. From energy considerations it is evident (as discussed in LN-2) that in such solids the atoms or molecules will always attempt to assume highly ordered structures which are characterized by s*ymmetry*. Depending on the nature of the acting interatomic forces, all solids may be subdivided into:

a. Ionic solids (NaCl)
b. Covalent solids (Diamond)
c. Metallic solids (Fe, Ni, etc.)
d. Van der Waals solids (ice, solid He)

Solids as we encounter them in nature may or may not reflect the internally ordered arrangement in their appearance. We find, for example, well-formed quartz crystals, garnets, diamonds and snowflakes which are all characterized by flat bounding planes which intersect at characteristic angles. On the other hand, we also observe rounded stones and man-made cast solid objects with no external evidence of internal order (fig. 1).

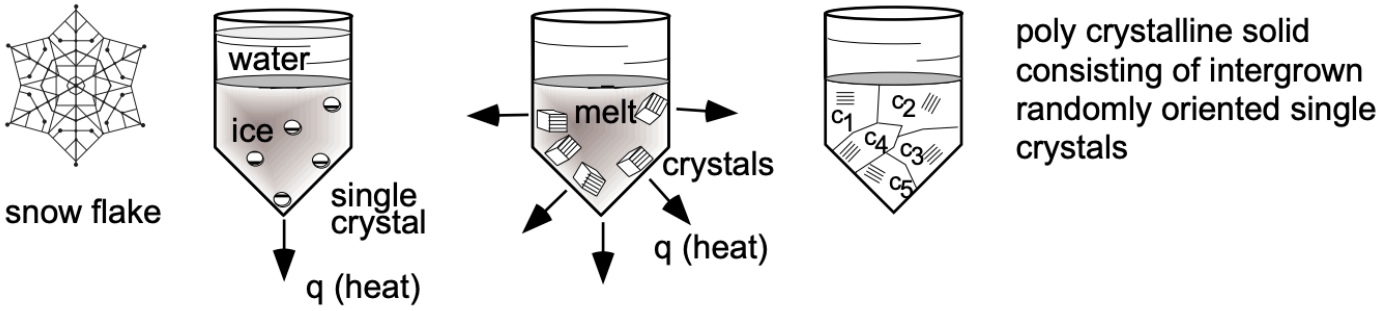


Figure 1 Crystals, internal order and external appearance

To understand the external appearance of the solid state it is necessary to consider the formation of solids from different *phases*. Solids, for example, are formed upon cooling of liquids (melts) - by freezing or solidification; this solidification process normally proceeds in total confinement and the resulting “cast” structure will have an external appearance which reflects in detail the confining geometry (and not the internal order). Moreover, depending on solidification conditions, the solid body may be either a s*ingle crystal* or *polycrystalline*. Polycrystalline solids (in excess of 95% of the solid state encountered) may be thought of as an assembly of microscopic single crystals with random orientation held together like a maze structure by the interwoven irregular shapes of the individual crystals.

A typical example of an "unconfined" phase transformation is the formation of snowflakes where the external boundaries of the solid have assumed *crystalline* appearance, reflecting in detail the internally ordered molecular (H_2O) arrangement. Another unconfined formation of a solid is precipitation from solution (sugar crystals, $CuSO_4$ and the like). Similarly, the formation of crystals from the vapor phase leads to bodies which externally reflect elements of internal order.

CRYSTAL STRUCTURE

From the earlier discussion it should be apparent that, when strong interatomic forces exist, atoms tend to pack closely together - the closeness of packing being particularly pronounced in the solid state. In this case atoms can be regarded as hard spheres and the problem of close packing can be treated as one in which the whole assembly has a tendency toward efficient packing. A little thought or a few simple experiments with ping-pong balls quickly convince us that regular arrangements of the spheres generally lead to more compact assemblies than irregular arrangements (fig. 2). The same principle applies to arrangement of atoms in the solid state. Where strong attractive forces are exerted we find that the atoms or molecules concerned arrange themselves in a regular three-dimensional pattern. It is this regularity which is the basis of crystallinity in materials: i.e., *a crystal structure is nothing more than an orderly array of atoms or molecules*. This definition of a crystal is distinct from the popular concept based on observation of external symmetry of crystals, often seen during the study of elementary chemistry, in which some crystals

appear cubic, others needle-shaped and so on. The regular external shape is obtained only when the conditions of crystallization are favorable to development of flat, geometric faces. In most instances, particularly with metals, these conditions are absent, and the crystals have irregular surfaces even though the internal arrangement is perfectly geometric.

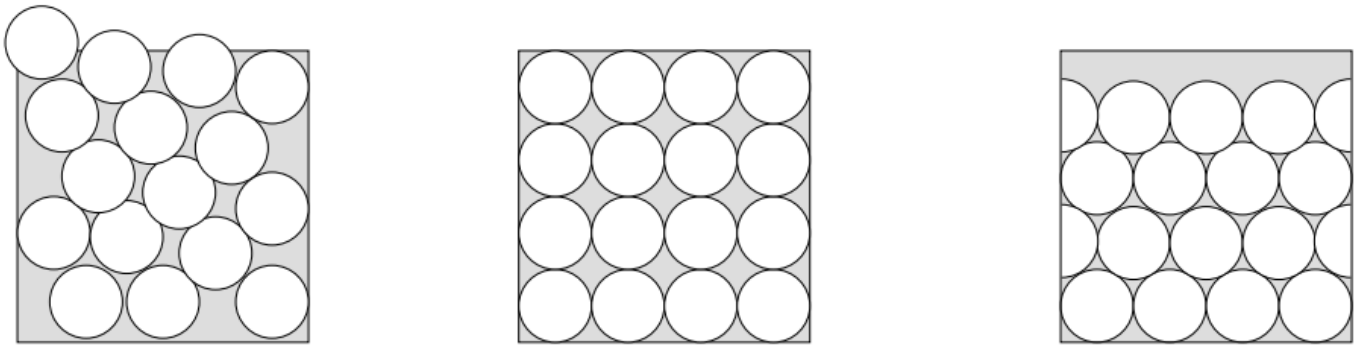


Figure 2 The packing density of ordered systems.

Atomic arrays in crystals are conveniently described with respect to a three-dimensional net of straight lines. Consider a lattice of lines, as in fig. 3, dividing space into equal-sized prisms which stand side-by-side with all faces in contact, thereby filling all space and leaving no voids. The intersections of these lines are points of a **space lattice**, i.e., a *geometrical abstraction* which is useful as a reference in describing and correlating symmetry of actual crystals. These lattice points are of fundamental importance in describing crystals for they may be the positions occupied by individual atoms in crystals or they may be points about which several atoms are clustered. Since prisms of many different shapes can be drawn through the points of a space lattice to partition it into cells, the manner in which the network of reference lines is drawn is arbitrary. It is not necessary that the lines be drawn so that atoms lie only at corners of unit prisms. In fact, it is more convenient to describe some crystals with respect to prisms in which atoms lie at prism centers or at the centers of prism faces as well as at prism corners.

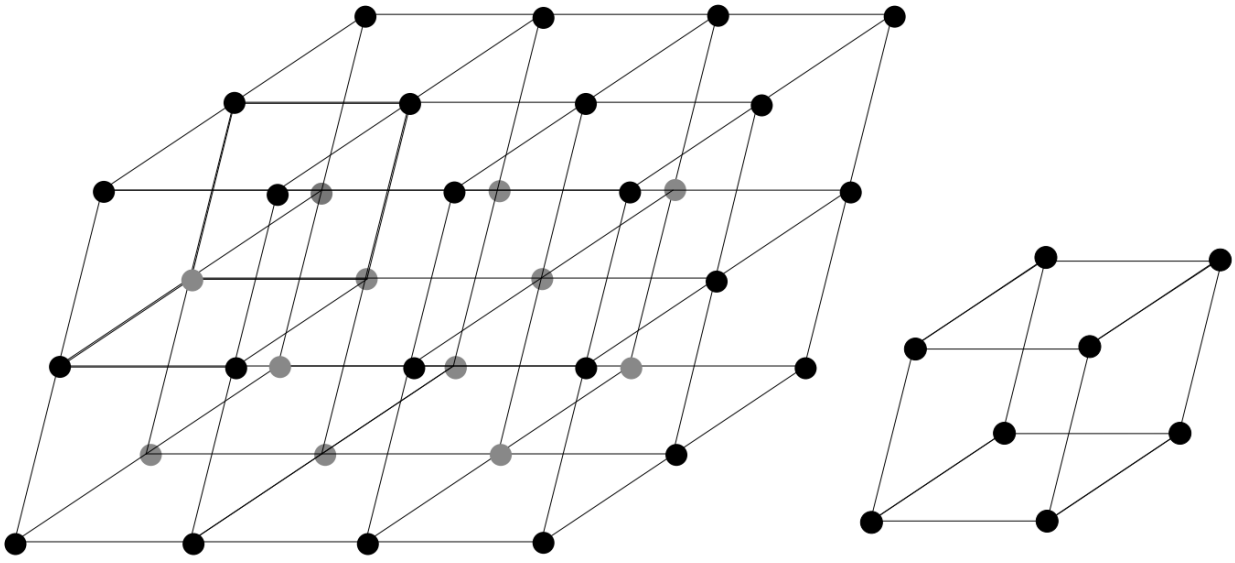


Figure 3 The space lattice

An important characteristic of a space lattice is that every point has identical surroundings: the grouping of lattice points about any given point is identical to the grouping about any other point in the lattice. In other words, if we could move about in the lattice, we would not be able to distinguish one point from another because rows and planes near each point would be identical. If we were to wander among the atoms of a solid metal or chemical compound, we would find the view from any lattice point exactly the same as that from any other.

There are fourteen space lattices (fig. 4). That is, no more than fourteen ways can be found in which points can be arranged in space so that each point has identical surroundings. Of course, there are many more than fourteen ways in which atoms can be arranged in actual crystals; thus there are a great number of crystal *structures*. Too often the term “lattice” is loosely

used as a synonym for “structure”, an incorrect practice which is frequently confusing. The distinction can be clearly seen if we remember that a space lattice is an array of points in space. It is a geometrical abstraction which is useful only as a reference in describing and correlating symmetry of actual crystals. A crystal structure, however, is the arrangement of atoms or molecules which actually exists in a crystal. It is a dynamic, rather than a static, arrangement and is subject to many imperfections. Although any crystal structure has an inherent symmetry which corresponds to one of the fourteen space lattices, one, two or several atoms or molecules in the crystal structure may be associated with each point of the space lattice. This symmetry can be maintained with an infinite number of different actual arrangements of atoms - making possible an endless number of crystal structures.

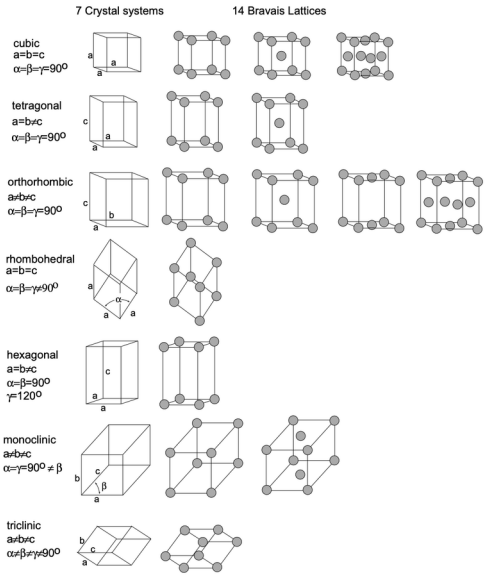


Figure 4 The 7 crystal systems and the 14 Bravais lattices

To specify a given arrangement of points in a space lattice, it is customary to identify a unit cell with a set of coordinate axes, chosen to have an origin at one of the lattice points (fig. 5). In a cubic lattice, for example, we choose three axes of equal length that are mutually perpendicular and form three edges of a cube. Each space lattice has some convenient set of axes, but they are not necessarily equal in length or orthogonal. Seven different systems of axes are used in crystallography, each possessing certain characteristics as to equality of angles and equality of lengths. These seven crystal systems are tabulated in Table I (to be considered in conjunction with fig. 4).

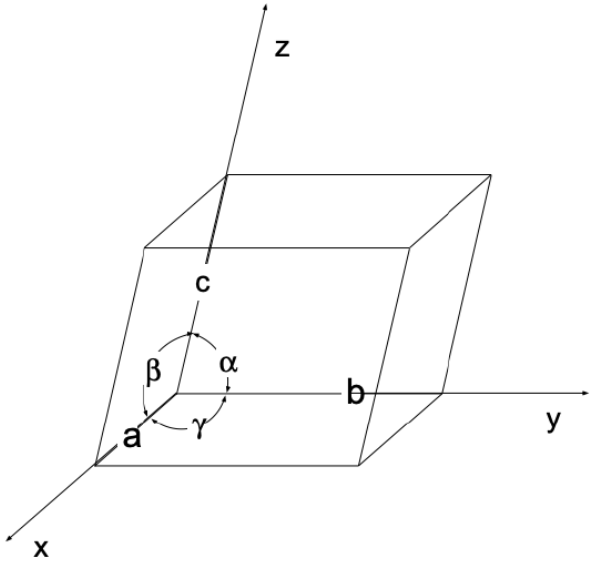


Figure 5 Specification of Unit Cell parameters

Table I. The Seven Crystal Systems

System	Parameters	Interaxial Angles
	$a \neq b \neq c$	$\alpha \neq \beta \neq \gamma$
Triclinic	$a \neq b \neq c$	$\alpha = \gamma = 90^\circ \neq \beta$
Monoclinic	$a \neq b \neq c$	$\alpha = \beta = \gamma$
Orthorhombic	$a = b \neq c$	$\alpha = \beta = \gamma$
Tetragonal	$a = b = c$	$\alpha = \beta = \gamma = 90^\circ$
Cubic	$a = b \neq c$	$\alpha = \beta = 90^\circ, \gamma = 120^\circ$
Hexagonal	$a = b = c$	$\alpha = \beta = \gamma \neq 90^\circ$
Rhombohedral	$a = ch$	

The network of lines through the points of a space lattice (fig. 3) divides it into *unit cells* (see also fig. 4). Each unit cell in a space lattice is identical in size, shape and orientation to every other unit cell. It is the building block from which the crystal is constructed by repetition in three dimensions. The unit cells of the fourteen space lattices are shown in fig. 4. All crystal structures are based on these fourteen arrangements.

The body-centered cubic, face-centered cubic and hexagonal lattices are common and of prime importance in metals. Some of the metals associated with nuclear applications, such as uranium and plutonium, have crystal structures which are more complicated than these three relatively simple types. In general, crystalline ceramics also are more complex.

CELLS VS PRIMITIVE CELLS

In the literature we often find reference to **unit cells** and to **primitive cells**. The primitive cell may be defined as a geometrical shape which, when repeated indefinitely in three dimensions, will fill all space and is the equivalent of one atom. The unit cell differs from the primitive cell in that it is not restricted to being the equivalent of one atom. In some cases the two coincide. For instance, in fig. 4 all fourteen space lattices are shown by their unit cells. Of these fourteen, only seven (which are those?) are also primitive cells.

Primitive cells are drawn with lattice points at all corners, and each primitive cell contains the equivalent of one atom. For instance, a simple cubic unit cell has an atom at each corner. However, at any of these given corners, this atom must be shared with seven other identical cubes which fill the volume surrounding this point. Thus there is effectively only 1/8 of the atom which can be assigned to that particular unit cell. Since there are eight corners in a cube, there is the equivalent of one atom, and thus the primitive cell and unit cell coincide.

Continuing, consider the *body-centered cubic* (BCC) lattice. In this case there is one atom at the center of the cube and one atom contributed by the eight corners. This cell, then, has two atoms and, to avoid confusion, should be termed a unit cell. In the *face-centered cubic* lattice there are six face atoms, but each face atom is shared by two cells. Consequently, each face contributes 1/2 an atom. The faces thus contribute three atoms and the corners one, for a total of four atoms in the unit cell. The face-centered cubic structure (FCC) can also be considered as four interpenetrating simple cubic cells.

In the study of crystals the primitive cell has limited use because the unit cell more clearly demonstrates the symmetrical features of a lattice. In other words, the unit cell can usually be visualized readily whereas the primitive cell cannot. For example, the cubic nature of the face-centered cubic lattice is immediately apparent in the unit cell, but it is not nearly so obvious in the rhombohedral primitive cell.

PACKING OF ATOMS

A crystal structure is a regular array of atoms arranged on one of the fourteen space lattices. The least complicated crystal structures are those having a single atom at each lattice point. Polonium has the simplest structure, being simple cubic. In normal metals, the atoms (or positive ions) are held together by a cloud of free electrons so that each atom tends to be attracted equally and indiscriminately to all its geometrically nearest neighbors by the free electrons passing between them. This condition fosters the formation of closely packed structures of the types which can be demonstrated by efficiently packing uniformly-sized spheres into a given volume.

You can gain a better grasp of packing by conducting an experiment as follows. Assume we have a quantity of small spheres which we are required to efficiently pack into a box (a 'two-dimensional' approach can be made using a handful of pennies). After some shuffling, it is obvious that the closest possible packing is obtained when the spheres are in contact and their centers occupy

positions which correspond to the apices of equilateral triangles (fig. 6). It is also evident that there are two sets of triangles – one set with vertices pointing away from the observer (points up) and the other set with vertices pointing toward the observer (points down).

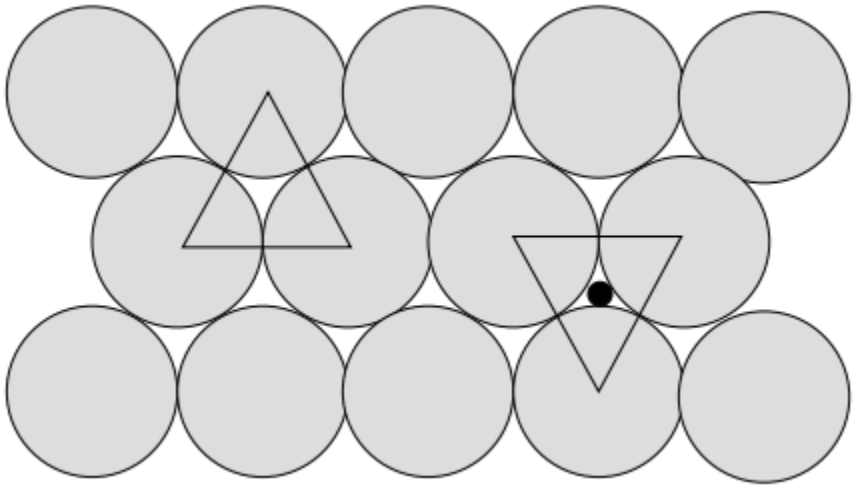


Figure 6 Close packed atomic arrangements

When a second layer is added, there is closest-packing if the spheres in this new layer rest in the hollows formed by the spheres of the first layer. The centers of the spheres in the second layer will lie above the centers of the points-up triangles or above the centers of the points-down triangles, but not both simultaneously. Which set is used is immaterial. For our discussion, however, assume the second layer is centered on the points-up triangles.

When we start adding a third layer, the spheres will again rest in the hollows formed by the spheres in the second layer. And again we have the option of placing the third layer on the points-up or on the points-down triangles. If we center the third layer on the points-down triangles, we find the third layer is directly above the first layer. If additional layers are added using an alternate stacking sequence (i.e., alternately centering the layers on the points-up and the points-down triangles), the sequence can be written as ABABABAB. . . This arrangement of spheres, translated to an arrangement of atoms, is the hexagonal close-packed (HCP) structure - very important, but not discussed in detail here.

Many elements having covalent bonding form arrangements in which the coordination number is (8–N), where N is the number of valence electrons. What, then, is the coordination number of the HCP structure just demonstrated? The geometry of the structure shows that any one atom has twelve equidistant neighbors. It is apparent that if, in any layer, a given sphere is placed in the adjoining layer, it fits in the hollow formed by three spheres and consequently is tangent to three spheres in the adjoining layer. Thus any given atom in the HCP structure is tangent to twelve other atoms – six in its own layer and three each in two adjoining layers.

When the third layer of spheres was added in the above discussion, we assumed this layer was centered on the points-down triangles of the second layer. What happens if the centers of the points-up triangles of the second layer are used instead? The distribution of spheres in the third layer is the same as in the first two layers, but does not lie directly above either of these two layers. If a fourth layer is added, centered on the points-up triangles of the third layer, we find the fourth layer is directly above the first layer and duplicates it completely. The stacking sequence for this structure can be written as ABCABCABC. . . This arrangement has the same density of packing and the same coordination number as the HCP structure. However, it is the face-centered cubic (FCC) structure.

The HCP and FCC crystal structures have the same density of packing and the same coordination number. Therefore we might expect the behavior of the two HCP and FCC structures to be very much alike with regard to physical and mechanical properties. This, however, in most instances is not the case.

The maximum density of packing is found only in the HCP and FCC crystal structures. Why the metallic bond does not always produce one or the other of these two densest arrangements of atoms is as yet subject of intensive studies. The BCC unit cell contains two atoms, and the coordination number is eight. There is partial compensation for this in the fact that there are six next-nearest neighbors at distances only slightly greater than that of the eight nearest neighbors. Some characteristics of cubic structures are given in Table II.

An interesting example of the type of crystal structure obtained in covalently bonded elements which obey the (8–N) coordination number rule (where N is the number of valence electrons) is the diamond structure. This structure is found in carbon, germanium, silicon, and tin at low temperatures and in certain compounds. Each atom has four nearest neighbors – a configuration that is variously called diamond cubic, body-centered tetrahedral or tetrahedral cubic.

TABLE II. Characteristics of Cubic Lattices

	Simple	Body-Centered	Face-Centered
Unit Cell Volume	a^3	a^3	a^3
Lattice Points Per Cell	1	2	4
Nearest Neighbor Distance	a	$\frac{a\sqrt{3}}{2}$	$\frac{a}{\sqrt{2}}$
Number of Nearest Neighbors	6	8	12
Second Nearest Neighbor Distance	$a\sqrt{2}$	a	a
Number of Second Neighbors	12	6	6

Many compounds crystallize in variations of cubic forms. Rock salt (NaCl), for example, is typical of many oxides, fluorides, chlorides, hydrides and carbides. It is sometimes considered as simple cubic with alternate Na and Cl atoms on the cube corners. Actually the structure is two interpenetrating FCC lattices – one of Na and the other of Cl – and the corner of one is located at point 1/2, 0, 0 of the other.

Many other oxides, fluorides and some intermetallic compounds have the fluorite (CaF_2) structure. This is FCC with Ca at the cube corners and face centers and F at all quarter points along the cube diagonals.

LATTICE PLANES AND DIRECTIONS

It is desirable to have a system of notation for planes within a crystal or space lattice such that the system specifies orientation without giving position in space. *Miller indices* are used for this purpose. These indices are based on the intercepts of a plane with the three crystal axes - i.e., the three edges of the unit cell. The intercepts are measured in terms of the edge lengths or dimensions of the unit cell which are the unit distances from the origin along the three axes. For instance, the plane that cuts the x-axis at a distance from the origin equal to one-half the x-dimension of the cell is said to have an x-intercept equal to $1/2$, and if it cuts the y-axis at $1/2$ the y-dimension of the cell, the y-intercept is $1/2$, regardless of the relative magnitudes of the x - and y -dimensions. If a plane is parallel to an axis, it intercepts the axis at infinity.

To determine Miller indices (hkl) of a plane, we take the following steps:

1. Find the intercepts on the three axes in multiples or fractions of the edge lengths along each axis.
2. Determine the reciprocals of these numbers.
3. Reduce the reciprocals to the three smallest integers having the same ratio as the reciprocals.
4. Enclose these three integral numbers in parentheses, e.g., (hkl).

A cube has six equivalent faces. If we have a definite orientation and wish to discuss one specific plane of these six, it is possible to specify this plane by using the proper Miller indices. Parentheses are used around the Miller indices to signify a specific plane. On the other hand, it is often advantageous to talk about planes of a “form” – i.e., a family of equivalent planes such as the six faces of a cube. To do this it is customary to use the Miller indices, but to enclose them in curly brackets (braces). Thus the set of cube faces can be represented as {100} in which

$$\{100\} = (100) + (010) + (001) + (\bar{1}00) + (0\bar{1}0) + (00\bar{1})$$

This notation thus provides a shorthand scheme to avoid writing the indices for all six cube faces.

The utility of the scheme is even more evident in the case of the (110) planes – i.e., the dodecahedral planes (in a cubic system), where

$$\begin{aligned}\{110\} =& (110) + (101) + (011) + (\bar{1}10) + (\bar{1}01) + (0\bar{1}1) \\ &+ (1\bar{1}0) + (10\bar{1}) + (01\bar{1}) + (\bar{1}\bar{1}0) + (\bar{1}0\bar{1}) + (0\bar{1}\bar{1})\end{aligned} \tag{9.1.1}$$

The equivalent form for the orthorhombic system is

$$\begin{aligned}\{110\} &= (110) + (\overline{110}) + (1\overline{1}0) + (\overline{110}) \\ \{101\} &= (101) + (\overline{1}01) + (10\overline{1}) + (\overline{1}0\overline{1}) \\ \{011\} &= (011) + (0\overline{1}1) + (01\overline{1}) + (0\overline{11})\end{aligned} \tag{9.1.2}$$

The octahedral planes for the cube are

$$\begin{aligned}\{111\} =&(111) + (\overline{1111}) + (1\overline{1}1) + (11\overline{1}) \\ &+ (\overline{111}) + (\overline{111\overline{1}}) + (1\overline{11}) + (\overline{111})\end{aligned} \tag{9.1.3}$$

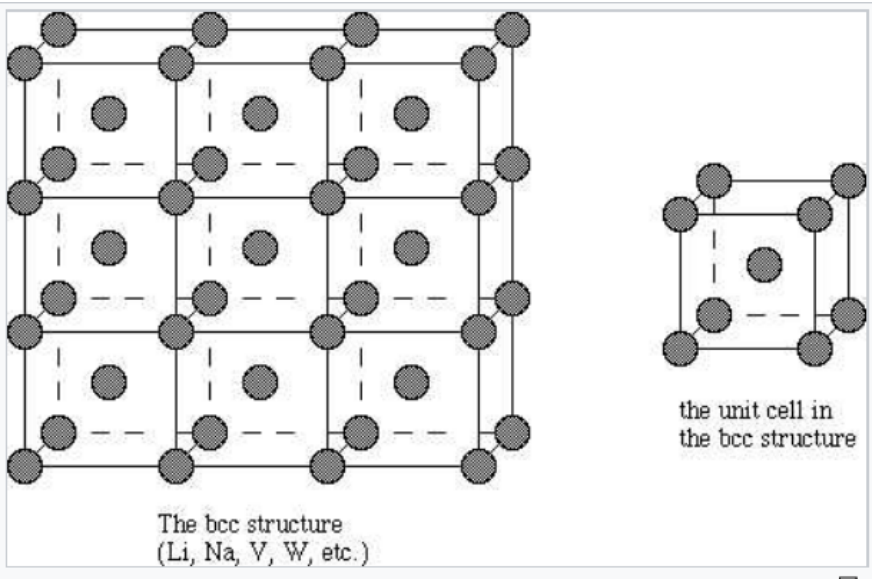
Direction indices are defined in a different manner. A line is constructed through the origin of the crystal axis in the direction under consideration and the coordinates of a point on the line are determined in multiples of lattice parameters of the unit cell. The indices of the direction are taken as the smallest integers proportional to these coordinates and are closed in square brackets. For example, suppose the coordinates are $x = 3a, y = b$ and $z = c/2$, then the smallest integers proportional to these three numbers are 6, 2 and 1 and the line has a [621] direction. As further examples, the x-axis has direction indices [100], the y-axis [010] and the z-axis [001]. A face diagonal of the xy face of the unit cell has direction indices [110], and a body diagonal of the cell has direction indices [111]. Negative indices occur if any of the coordinates are negative. For example, the $-y$ axis has indices [0$\overline{1}$0]. A full set of equivalent directions, i.e., directions of a form, are indicated by carets: $\langle uvw \rangle$.

This page titled 9.1: The Nature of Crystalline Solids is shared under a CC BY-NC-SA 4.0 license and was authored, remixed, and/or curated by Donald Sadoway (MIT OpenCourseWare).

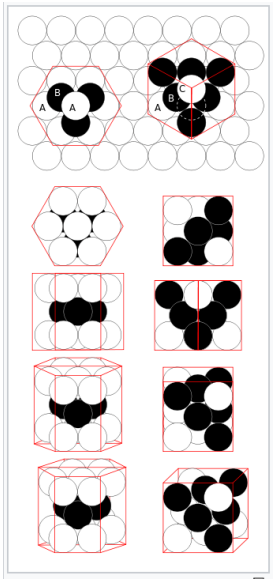
9.1.1: Crystal Structures of Metals

The Crystalline Nature of Metals

All metallic elements (except Cs, Ga, and Hg) are crystalline solids at room temperature. Like ionic solids, metals and alloys have a very strong tendency to crystallize, whether they are made by thermal processing or by other techniques such as solution reduction or electroplating. Metals crystallize readily and it is difficult to form a glassy metal even with very rapid cooling. Molten metals have low viscosity, and the identical (essentially spherical) atoms can pack into a crystal very easily. Glassy metals can be made, however, by rapidly cooling alloys, particularly if the constituent atoms have different sizes. The different atoms cannot pack in a simple unit cell, sometimes making crystallization slow enough to form a glass.



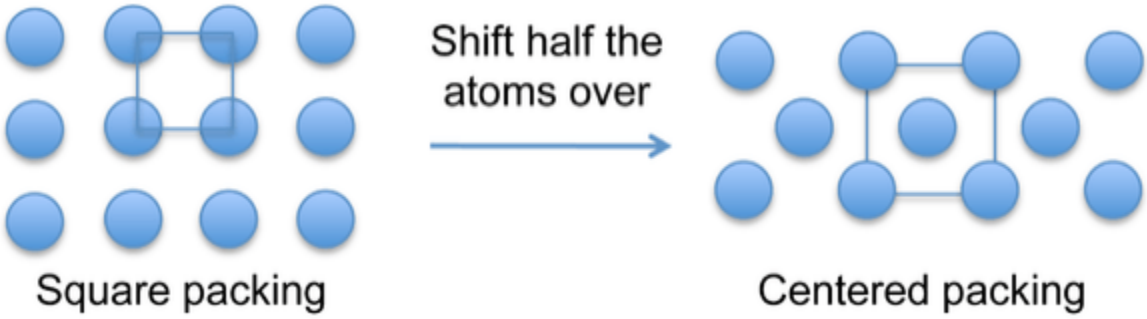
Body-centered cubic



hcp (left) and fcc (right) close-packing of spheres

Crystal structures

Most metals and alloys crystallize in one of three very common structures: body-centered cubic (bcc), hexagonal close packed (hcp), or cubic close packed (ccp, also called face centered cubic, fcc). In all three structures the coordination number of the metal atoms (i.e., the number of equidistant nearest neighbors) is rather high: 8 for bcc, and 12 for hcp and ccp. We can contrast this with the low coordination numbers (i.e., low valences - like 2 for O, 3 for N, or 4 for C) found in nonmetals. In the bcc structure, the nearest neighbors are at the corners of a cube surrounding the metal atom in the center. In the hcp and ccp structures, the atoms pack like stacked cannonballs or billiard balls, in layers with a six-coordinate arrangement. Each atom also has six more nearest neighbors from layers above and below. The stacking sequence is ABCABC... in the ccp lattice and ABAB... in hcp. In both cases, it can be shown that the spheres fill 74% of the volume of the lattice. This is the highest volume fraction that can be filled with a lattice of equal spheres.



Atoms in metallic crystals have a tendency to pack in dense arrangments that fill space efficiently. The simple square packing (above) upon which the simple cubic structure is based is inefficient and thus rare among metallic crystal structures. Body- or face-centered structures fill space more efficiently and more common.

Periodic trends in structure and metallic behavior

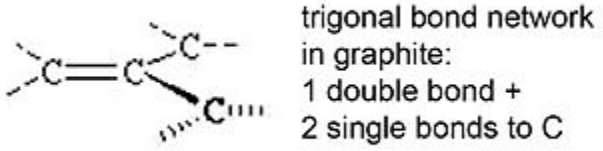
Remember where we find the metallic elements in the periodic table - everywhere except the upper right corner. This means that

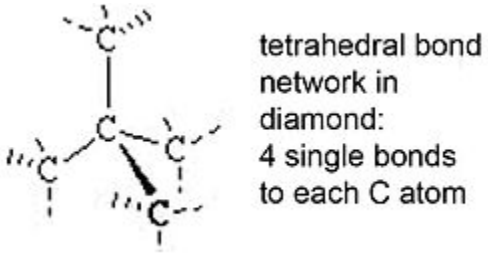
as we go down a group in the p-block (let's say, group IVA, the carbon group, or group VA, the nitrogen group), the properties of the elements gradually change from nonmetals to metalloids to metals. The carbon group nicely illustrates the transition. Starting at the top, the element carbon has two stable allotropes - graphite and diamond. In each one, the valence of carbon atoms is exactly satisfied by making four electron pair bonds to neighboring atoms. In graphite, each carbon has three nearest neighbors, and so there are two single bonds and one double bond. In diamond, there are four nearest neighbors situated at the vertices of a tetrahedron, and so there is a single bond to each one.

The two elements right under carbon (silicon and germanium) in the periodic table also have the diamond structure (recall that these elements cannot make double bonds to themselves easily, so there is no graphite allotrope for Si or Ge). While diamond is a good insulator, both silicon and germanium are semiconductors (i.e., metalloids). Mechanically, they are hard like diamond. Like carbon, each atom of Si and Ge satisfies its valence of four by making single bonds to four nearest neighbors.

The next element under germanium is tin (Sn). Tin has two allotropes, one with the diamond structure, and one with a slightly distorted bcc structure. The latter has metallic properties (metallic luster, malleability), and conductivity about 10^9 times higher than Si. Finally, lead (Pb), the element under Sn, has the ccp structure, and also is metallic. Note the trends in coordination number and conducting properties:

Element	Structure	Coord. no.	Conductivity
C	graphite, diamond	3, 4	semimetal, insulator
Si	diamond	4	semiconductor
Ge	diamond	4	semiconductor
Sn	diamond, distorted bcc	4, 8	semiconductor, metal
Pb	ccp	12	metal





The elements C, Si, and Ge obey the octet rule, and we can easily identify the electron pair bonds in their structures. Sn and Pb, on the other hand, adopt structures with high coordination numbers. They *do not have enough valence electrons* to make electron pair bonds to each neighbor (this is a common feature of metals). What happens in this case is that the valence electrons become "smeared out" or delocalized over all the atoms in the crystal. It is best to think of the bonding in metals as a crystalline arrangement of positively charged cores with a "sea" of shared valence electrons gluing the structure together. Because the electrons are not localized in any particular bond between atoms, they can move in an electric field, which is why metals conduct electricity well. Another way to describe the bonding in metals is nondirectional. That is, an atom's nearest neighbors surround it in every direction, rather than in a few particular directions (like at the corners of a tetrahedron, as we found for diamond). Nonmetals (insulators and semiconductors), on the other hand, have directional bonding. Because the bonding is non-directional and coordination numbers are high, it is relatively easy to deform the coordination sphere (i.e., break or stretch bonds) than it is in the case of a nonmetal. This is why elements like Pb are much more malleable than C, Si, or Ge.

This page titled 9.1.1: Crystal Structures of Metals is shared under a CC BY-SA 4.0 license and was authored, remixed, and/or curated by Chemistry 310 (Wikibook) via source content that was edited to the style and standards of the LibreTexts platform.

- 6.4: Crystal Structures of Metals by Chemistry 310 is licensed CC BY-SA 4.0. Original source: https://en.wikibooks.org/wiki/Introduction_to_Inorganic_Chemistry.

9.1.2: IONIC AND COVALENT SOLIDS - STRUCTURES

Learning Objectives

- Describe many crystal structures in terms of close-packed frameworks with systematic filling of octahedral and tetrahedral holes.
- Represent crystal structures by drawing them in sections.
- Rationalize, using chemical principles, why certain crystal structures are stable for certain compounds but not for others, as well as why certain structural and bonding motifs are preferred for certain compounds relative to others.
- Predict which crystal structures are most favorable for a given composition based on ionicity and periodic trends.
- Explain structure-dependent properties such as ferroelectricity and magnetic ordering based on crystal structures.
- Understand intercalation reactions in layered and open framework solids.
- Predict the preferred formation of normal or inverse spinels using arguments from transition metal chemistry (e.g. crystal field stabilization energies).

Inorganic solids often have simple crystal structures, and some of these structures are adopted by large families of ionic or covalent compounds. Examples of the most common structures include NaCl, CsCl, NiAs, zincblende, wurtzite, fluorite, perovskite, rutile, and spinel. We will develop these structures systematically from the close packed and non-close packed lattices shown below. Some layered structures, such as $CdCl_2$ and CdI_2, can be thought of as relatives of simple ionic lattices with some atoms "missing."

9.1.2.1: Prelude to Ionic and Covalent Solids - Structures

9.1.2.2: Close-packing and Interstitial Sites

9.1.2.3: Structures Related to NaCl and NiAs

9.1.2.4: Tetrahedral Structures

9.1.2.5: Layered Structures and Intercalation Reactions

9.1.2.6: Bonding in TiS_2, MoS_2, and Pyrite Structures

9.1.2.7: Spinel, Perovskite, and Rutile Structures

9.1.2.8: Discussion Questions

9.1.2.9: References

This page titled 9.1.2: Ionic and Covalent Solids - Structures is shared under a CC BY-SA 4.0 license and was authored, remixed, and/or curated by Chemistry 310 (Wikibook) via source content that was edited to the style and standards of the LibreTexts platform.

- 8: Ionic and Covalent Solids - Structures by Chemistry 310 is licensed CC BY-SA 4.0. Original source: https://en.wikibooks.org/wiki/Introduction_to_Inorganic_Chemistry.

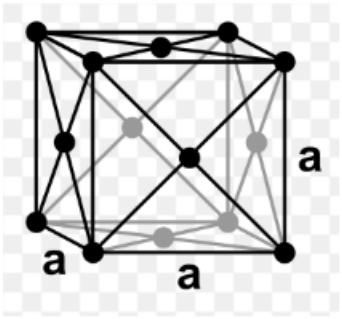
9.1.2.1: Prelude to Ionic and Covalent Solids - Structures

As we noted in our discussion of metal and alloy structures in Chapter 6, there is an intimate connection between the structures and the physical properties of materials. As we "graduate" from simple metal structures based on sphere packings to more complex structures, we find that this is still true. In this chapter we will try to systematize the structures of inorganic solids - metal oxides, halides, sulfides, and related compounds - and develop some rules for which structures to expect based on electronegativity differences, hard-soft acid-base rules, and other periodic trends. We will see that many of these structures are related to the sphere packings that we learned about in Chapter 6.

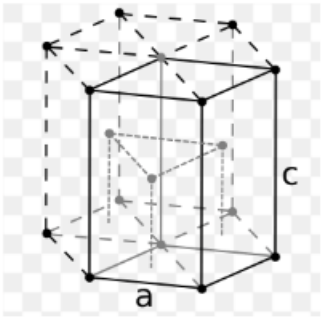


The morphology of twinned crystals of iron pyrite (FeS_2) is related to the underlying cubic symmetry of the unit cell. Like NaCl, the pyrite crystal structure can be thought of as a face-centered cubic array of anions (S_2^{2-}) with cations (Fe^{2+}) occupying all the octahedral holes.

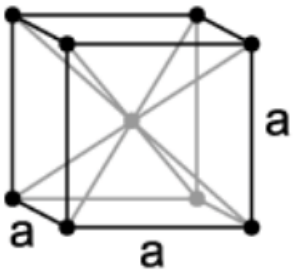
Inorganic solids often have simple crystal structures, and some of these structures are adopted by large families of ionic or covalent compounds. Examples of the most common structures include NaCl, CsCl, NiAs, zincblende, wurtzite, fluorite, perovskite, rutile, and spinel. We will develop these structures systematically from the close packed and non-close packed lattices shown below. Some layered structures, such as $CdCl_2$ and CdI_2, can be thought of as relatives of simple ionic lattices with some atoms "missing."



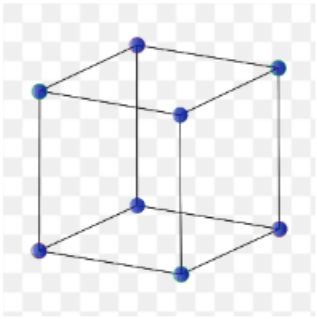
Face-centered cubic (fcc) or cubic close-packed (ccp)



Hexagonal close-packed (hcp)



Body-centered cubic



Simple cubic

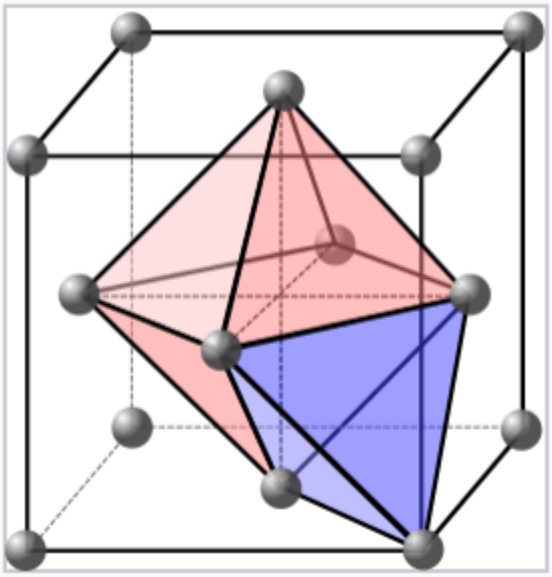
This page titled 9.1.2.1: Prelude to Ionic and Covalent Solids - Structures is shared under a CC BY-SA 4.0 license and was authored, remixed, and/or curated by Chemistry 310 (Wikibook) via source content that was edited to the style and standards of the LibreTexts platform.

- 8.1: Prelude to Ionic and Covalent Solids - Structures by Chemistry 310 is licensed CC BY-SA 4.0. Original source: https://en.wikibooks.org/wiki/Introduction_to_Inorganic_Chemistry.

9.1.2.2: Close-packing and Interstitial Sites

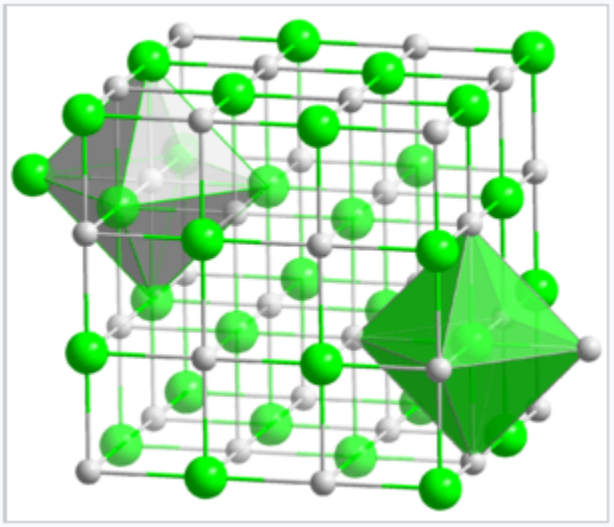
Many common inorganic crystals have structures that are related to cubic close packed (face-centered cubic) or hexagonal close packed sphere packings. These packing lattices contain two types of sites or "holes" that the interstitial atoms fill, and the coordination geometry of these sites is either **tetrahedral** or **octahedral**. An interstitial atom filling a tetrahedral hole is coordinated to four packing atoms, and an atom filling an octahedral hole is coordinated to six packing atoms. In both the hexagonal close packed and cubic close packed lattices, there is one octahedral hole and two tetrahedral holes per packing atom.

Question: Would anions or cations be better as packing atoms?
We might expect that anions, which are often larger than cations, would be better suited to the positions of packing atoms. While this is often true, there are many examples of structures in which cations are the packing atoms, and others in which the distinction is arbitrary. The NaCl structure is a good example of the latter.



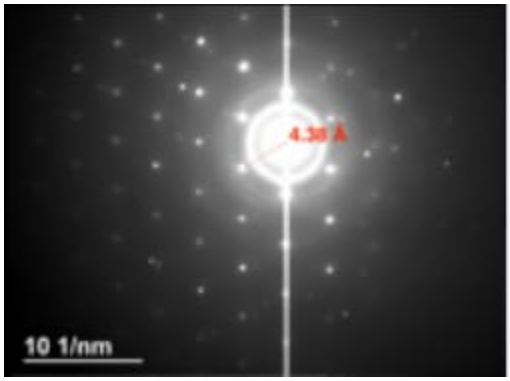
One octahedral and one tetrahedral site in a face-centered cubic unit cell. Each cell contains four packing atoms (gray), four octahedral sites (pink), and eight tetrahedral sites (blue).

In the NaCl structure, shown on the right, the green spheres are the Cl^- ions and the gray spheres are the Na^+ ions. The octahedral holes in a face-centered cubic lattice can be found at fractional coordinates (1/2 1/2 1/2), (1/2 0 0), (0 1/2 0), and (0 0 1/2). There are four of these holes per cell, and they are filled by the chloride ions. The packing atoms (Na^+) have coordinates (0 0 0), (0 1/2 1/2), (1/2 1/2 0), and (1/2 0 1/2). Note that each of the Na^+ positions is related to a Cl^- position by a translation of (1/2 0 0). Another way of stating this is that the structure consists of **two interpenetrating fcc lattices**, which are related to each other by a translation of half the unit cell along any of the three Cartesian axes. We could have equivalently placed the Cl ions at the fcc lattice points and the Na ions in the octahedral holes by simply translating the origin of the unit cell by (1/2 0 0). Thus the distinction between packing and interstitial atoms in this case is arbitrary.



Crystal structure of NaCl. Both the Na^+ and Cl^- ions are octahedrally coordinated.

NaCl is interesting in that it is a three-dimensional checkerboard, and thus there are no NaCl "molecules" that exist in the structure. When this structure was originally solved (in 1913 by using X-ray diffraction) by W. L. Bragg, his interpretation met resistance by chemists who thought that precise integer stoichiometries were a consequence of the valency of atoms in molecules. The German chemist P. Pfeiffer noted in 1915 that 'the ordinary notion of valency didn't seem to apply', and fourteen years later, the influential chemist H. E. Armstrong still found Bragg's proposed structure of sodium chloride 'more than repugnant to the common sense, not chemical cricket'! Nevertheless, Bragg and his father, W. H. Bragg, persevered and used the then-new technique of X-ray diffraction to determine the structures of a number of other compounds, including diamond, zincblende, calcium fluoride, and other alkali halides. These experiments gave chemists their first real look at the atomic structure of solids, and laid the groundwork for X-ray diffraction experiments that later elucidated the structures of DNA, proteins, and many other compounds. For their work on X-ray diffraction the Braggs received the Nobel prize in Physics in 1915.

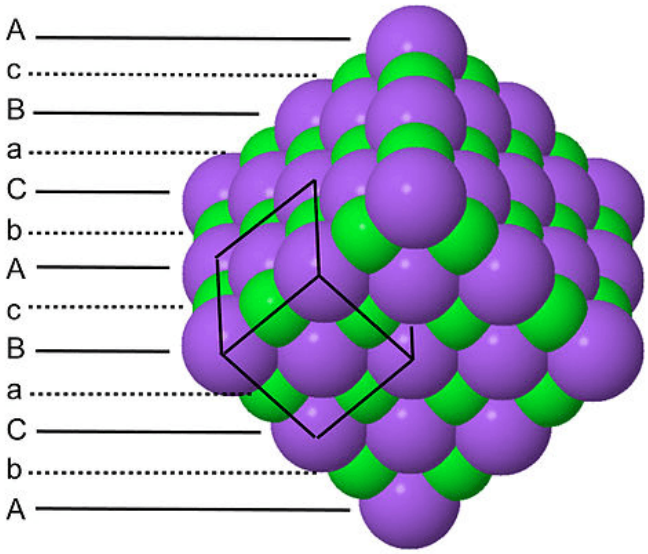


The lattice dimensions and positions of atoms in crystals such as NaCl are inferred from diffraction patterns.

Since each type of atom in the NaCl structure forms a face-centered cubic lattice, there are four Na and four Cl atoms per NaCl unit cell. It is because of this ratio that NaCl has a 1:1 stoichiometry. The shaded green and gray bipyramidal structures in the NaCl lattice show that the Na^+ ions are coordinated to six Cl^- ions, and vice versa. The NaCl structure can be alternatively drawn as a stacking of close-packed layer planes, AcBaCbAcBa... along the body diagonal of the unit cell. Here the uppercase letters represent the packing atoms, and the lower case letters are the interstitial atoms. This layered packing is illustrated below:

NaCl structure

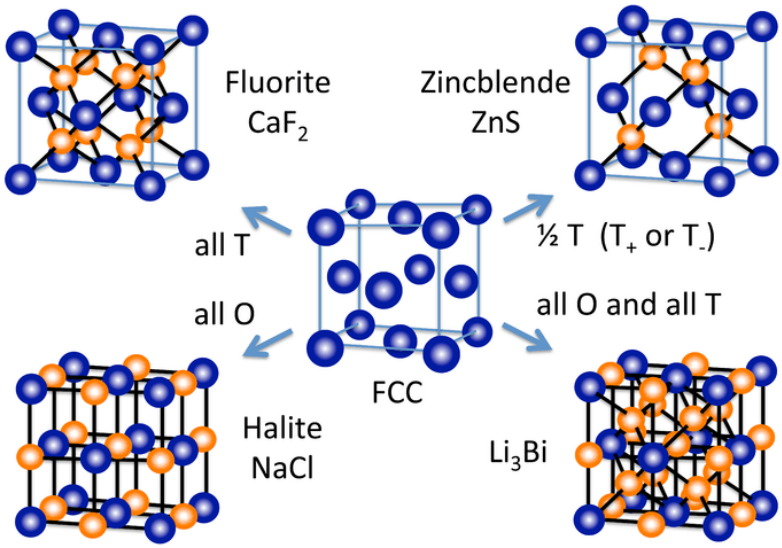
- ---------- A
- - - -c- - - -
- ---------- B
- - - -a- - - -
- ---------- C
- - - -b- - - -
- ---------- A
- - - -c- - - -
- ---------- B
- - - -a- - - -
- ---------- C
- - - -b- - - -
- ---------- A



Note that both the packing atoms and interstitials are stacked in the sequence A-B-C-A-B-C..., in keeping with the fact that each forms a cubic close-packed lattice.

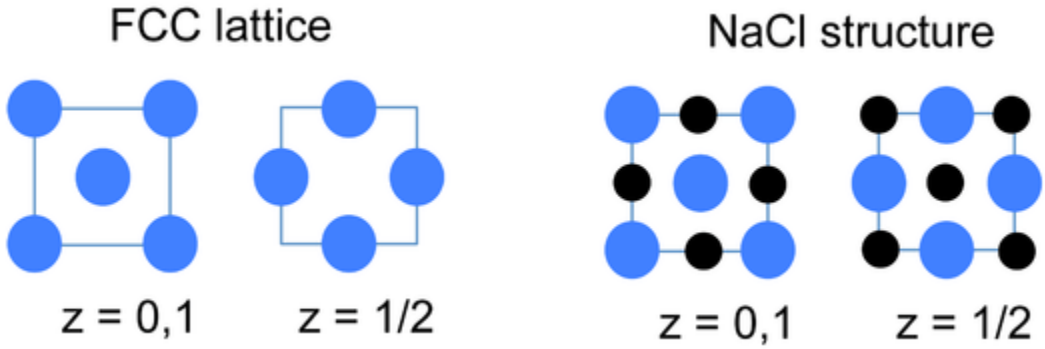
The NaCl structure is fairly common among ionic compounds:

- Alkali Halides (except CsCl, CsBr, and CsI)
- Transition Metal Monoxides (TiO, VO,..., NiO)
- Alkali Earth Oxides and Sulfides (MgO, CaO, BaS... except BeO and MgTe)
- Carbides and Nitrides (TiC, TiN, ZrC, NbC) -these are very stable refractory, interstitial alloys (metallic)



A number of other inorganic crystal structures are formed (at least conceptually) by filling octahedral and/or tetrahedral holes in close-packed lattices. The figure at the right shows some of the most common structures (fluorite, halite, zincblende) as well as a rather rare one (Li_3Bi) that derive from the fcc lattice. From the hcp lattice, we can make the NiAs and wurzite structures, which are the hexagonal relatives of NaCl and zincblende, respectively.

An alternative and very convenient way to represent inorganic crystal structures (especially complex structures such as Li_3Bi) is to draw the unit cell in slices along one of the unit cell axes. This kind of representation is shown at the left for the fcc lattice and the NaCl structure. Since all atoms in these structures have z-coordinates of either 0 or 1/2, only those sections need to be drawn in order to describe the contents of the unit cell. It is a useful exercise to draw some of the fcc compound structures (above) in sections.



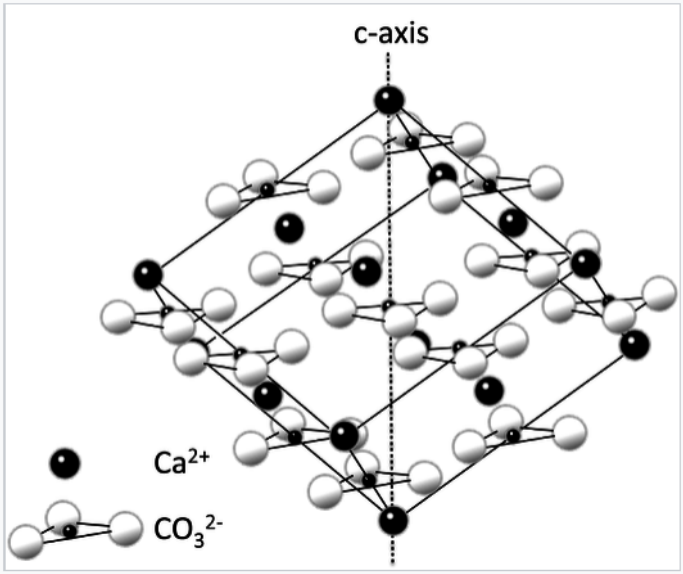
This page titled 9.1.2.2: Close-packing and Interstitial Sites is shared under a CC BY-SA 4.0 license and was authored, remixed, and/or curated by Chemistry 310 (Wikibook) via source content that was edited to the style and standards of the LibreTexts platform.

- 8.2: Close-packing and Interstitial Sites by Chemistry 310 is licensed CC BY-SA 4.0. Original source: https://en.wikibooks.org/wiki/Introduction_to_Inorganic_Chemistry.

9.1.2.3: Structures Related to NaCl and NiAs

There are a number of compounds that have structures similar to that of NaCl, but have a lower symmetry (usually imposed by the geometry of the anion) than NaCl itself. These compounds include:

- FeS_2 (pyrite, "fools gold"): S_2^{2-} (disulfide) and Fe^{2+}
- CaC_2 (a salt-like carbide): Ca^{2+} and linear C_2^{2-} anions
- $CaCO_3$ (calcite, limestone, marble): Ca^{2+} and triangular CO_3^{2-}.



The rhombohedral unit cell of the calcite crystal structure. The hexagonal c-axis is shown.

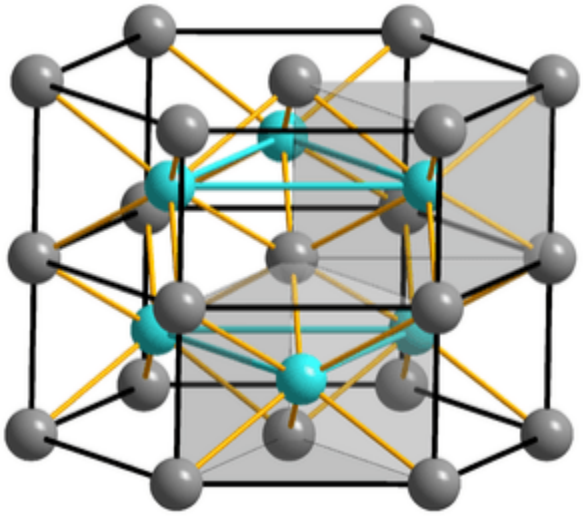
The **calcite** ($CaCO_3$) crystal structure is shown above. Triangular CO_3^{2-} ions fill octahedral holes between the Ca^{2+} ions (black spheres) in a distorted NaCl lattice. As in NaCl, each ion is coordinated by six of the other kind. From this image we can see why the $CaCO_3$ structure has a lower symmetry than that of NaCl. The fourfold rotation symmetry of the NaCl unit cell is lost when the spherical Cl^- ions are replaced by triangular CO_3^{2-} ions. Because of this symmetry lowering, transparent crystals calcite are birefringent, as illustrated below.



Calcite crystals are birefringent, meaning that their refractive indices are different along the two principal crystal directions. This gives rise to the phenomenon of double refraction.

NiAs structure

The NaCl structure can be described a face-centered cubic lattice with all of the octahedral holes filled. What if we start with a hexagonal-close packed lattice rather than a face-centered cubic lattice?



Nickel arsenide crystal structure. The Ni_6As trigonal prisms are shaded gray. One octahedron of six As atoms surrounding a Ni atom is shown in the center of the figure.

This is the structure adopted by **NiAs** and many other transition metal sulfides, phosphides, and arsenides. The cations are shown in gray while the anions are light blue in the figure at the right. The cations are in octahedral coordination, so each cation is coordinated to six anions. The anions are also coordinated to six cations, but they occupy trigonal prismatic sites. In terms of layer stacking, the NiAs structure is AcBcAcBc..., where the A and B sites (the hcp lattice) are occupied by the As atoms, and the c sites, which are eclipsed along the layer stacking axis, are occupied by Ni. Unlike the NaCl structure, where the anion and cation sites are interchangeable, NiAs has unique anion and cation sites. The layer stacking sequence for NiAs is shown below:

- ---------- A
- - - -c- - - -
- ---------- B
- - - -c- - - -
- ---------- A
- - - -c- - - -
- ---------- B
- - - -c- - - -

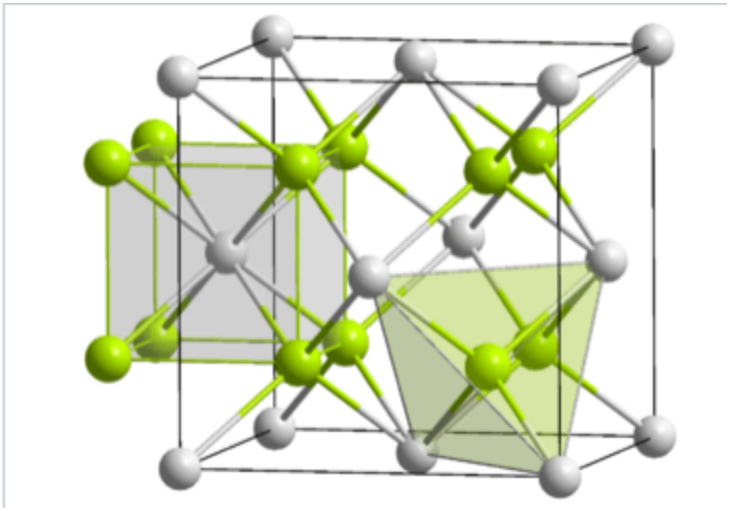
The NiAs structure cannot be adopted by ionic compounds because of the eclipsing cations, because the cation-cation repulsions would be internally destabilizing for an ionic compound. This structure is mainly adopted by covalent and polar covalent MX compounds, typically with "soft" X anions (S, Se, P, As,....) and low-valent transition metal cations. For example, some compounds with the NiAs structure are: MS, MSe, MTe (M=Ti, V, Fe, Co, Ni). Often these are nonstoichiometric or complex stoichiometries with ordered vacancies (Cr_7S_8, Fe_7S_8).

This page titled 9.1.2.3: Structures Related to NaCl and NiAs is shared under a CC BY-SA 4.0 license and was authored, remixed, and/or curated by Chemistry 310 (Wikibook) via source content that was edited to the style and standards of the LibreTexts platform.

- 8.3: Structures Related to NaCl and NiAs by Chemistry 310 is licensed CC BY-SA 4.0. Original source: https://en.wikibooks.org/wiki/Introduction_to_Inorganic_Chemistry.

9.1.2.4: Tetrahedral Structures

In ccp and hcp lattices, there are two tetrahedral holes per packing atom. A stoichiometry of either M_2X or MX_2 gives a structure that fills all tetrahedral sites, while an MX structure fills only half of the sites. An example of an MX_2 structure is **fluorite**, CaF_2, whose structure is shown in the figure at the left. The packing atom in fluorite is Ca^{2+} and the structure is composed of three interpenetrating fcc lattices. It should be noted that the Ca^{2+} ion (gray spheres) as a packing atom defies our "rule" that anions are larger than cations and therefore must be the packing atoms. The fluorite structure is common for ionic MX_2 (MgF_2, ZrO_2, etc.) and M_2X compounds (Li_2O). In contrast, the hcp relative of the fluorite structure is quite rare because of unfavorable close contacts between like-charged ions.



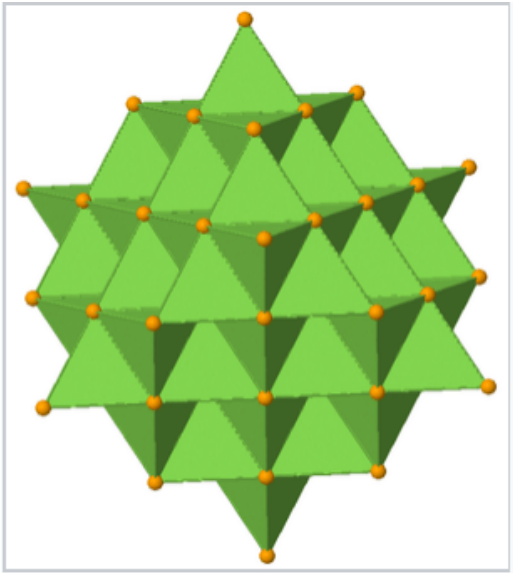
The fluorite (CaF_2) crystal structure showing the coordination environments of the Ca and F atoms

In terms of geometry, Ca^{2+} is in cubic coordination with eight F^- neighbors, and the fluoride ions are tetrahedrally coordinated by four Ca^{2+} ions. The 8:4 coordination geometry is consistent with the 1:2 Ca:F stoichiometry; in all crystal structures the ratio of the coordination numbers is the inverse of the stoichiometric ratio. The three interpenetrating fcc lattices have Ca at 0,0,0 , 1/2,1/2,0 , etc....F at 1/4,1/4,1/4 , 3/4,3/4,1/4 , etc... and F at 3/4,3/4,3/4 , 1/4,1/4/3/4 , etc.

Looking more closely at the tetrahedral sites in fluorite, we see that they fall into two distinct groups: T_+ and T_-. If a tetrahedron is oriented with a vertex pointing upwards along the stacking axis, the site is T_+. Likewise, a tetrahedron with a vertex oriented downward is T_-. The alternation of T_+ and T_- sites allows for efficient packing of ions in the structure. The layer stacking sequence in this structure (including fluoride ions in the T_+ and T_- sites) is:

- ---------- A
- - - -b- - - T_+
- - - -a- - - T_-
- ---------- B
- - - -c- - - T_+
- - - -b- - - T_-
- ---------- C
- - - -a- - - T_+
- - - -c- - - T_-
- ---------- A
- - - -b- - - T_+

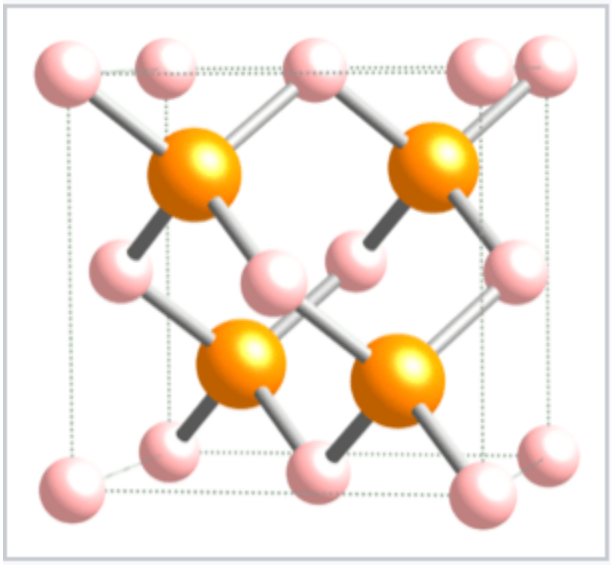
- - - -a- - - T_-



Polyhedral view of the fluorite crystal structure, showing T_+ and T_- Ca_4F tetrahedra. The Ca^{2+} ions are stacked ABCABC... along the body diagonal of the unit cell, which is the vertical direction in this image.

Tetrahedrally bonded compounds with a 1:1 stoichiometry (MX compounds) have only **half** of the tetrahedral sites (either the T_+ or T_- sites) filled. In this case, both the M and the X atoms are tetrahedrally coordinated. The **zincblende** and **wurtzite** structures are 1:1 tetrahedral structures based on fcc and hcp lattices, respectively. Both structures are favored by p-block compounds that follow the octet rule, and these compounds are usually semiconductors or insulators. The zincblende structure, shown below, can be thought of as two interpenetrating fcc lattices, one of anions and one of cations, offset from each other by a translation of 1/4 along the body diagonal of the unit cell. Examples of compounds with the zincblende structure include CuCl, CuI, ZnSe, HgS, BeS, CdTe, AlP, GaP, SnSb, CSi, and diamond. Additionally, the compound $CuInSe_2$ is zincblende in an ordered, doubled unit cell (the chalcopyrite structure). The solid solution compounds $CuIn_{1-x}Ga_xSe_2$ with this structure are among the most widely studied materials for use in efficient thin film photovoltaic cells. Using ZnS as a representative of zincblende, the coordination of both Zn and S atoms is tetrahedral. The layer sequence, which is AbBcCaAbBcC..., results in six-membered ZnS rings that have the same geometry as the "chair" version of cyclohexane. The chair conformation allows for a relatively long distance between opposite atoms in the ring and, as a result, it is more sterically favorable than the boat form. The sequence of close-packed layers in zincblende, filling only the T_+ sites and leaving the T_- sites empty, is shown below:

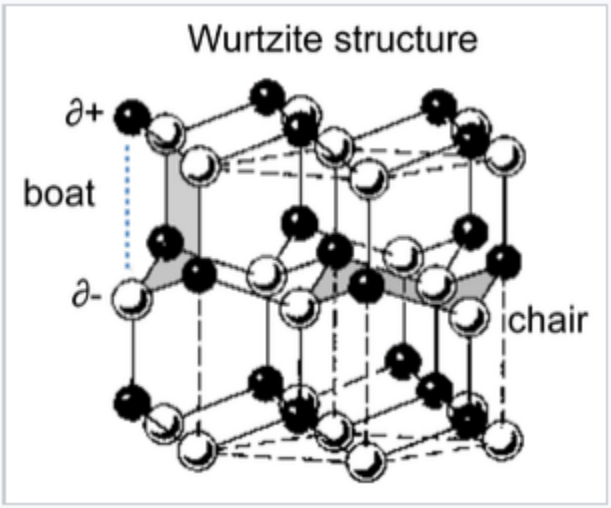
- ---------- A
- - - -b- - - T_+
- - - - - - T_-
- ---------- B
- - - -c- - - T_+
- - - - - - T_-
- ---------- C
- - - -a- - - T_+
- - - - - - T_-



The zincblende unit cell

The wurtzite structure is a close relative of zinc blende, based on filling half the tetrahedral holes in the hcp lattice. Like zincblende, wurtzite contains planes of fused six-membered rings in the chair conformation. Unlike zincblende, however, the rings joining these planes contain six-membered "boat" rings. The boat aligns the anions so that they are directly above the cations in the structure, a less favorable situation sterically but a more favorable one in terms of electrostatics. As a result, the wurtzite structure tends to favor more polar or ionic compounds (e.g., ZnO, $NH_4^+F^-$) than the zincblende structure. As with zincblende, both ions are in tetrahedral (4:4) coordination and there are typically eight valence electrons in the MX compound. Examples of compounds with this structure include: BeO, ZnO, MnS, CdSe, MgTe, AlN, and NH_4F. The layered structure of wurtzite is AbBaAbB and the layer sequence with T_+ sites filled is illustrated below:

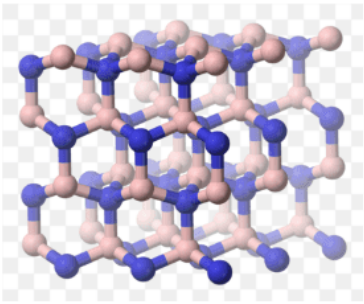
- ---------- A
- - - -b- - - T_+
- - - - - - - T_-
- ---------- B
- - - -a- - - T_+
- - - - - - - T_-
- ---------- A
- - - -b- - - T_+
- - - - - - - T_-
- ---------- B



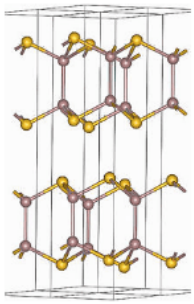
The chair and boat conformations of six-membered ZnS rings in the wurtzite structure.

An interesting consequence of the layer stacking in the wurtzite structure is that the crystals are polar. When cleaved along the c-axis (the stacking axis), crystals of ZnO, ZnS, and GaN have one negatively charged face and an opposite positively charged face. An applied electric field interacts with the crystal dipole, resulting in compression or elongation of the lattice along this direction. For this reason crystals of compounds in the wurtzite structure are typically piezoelectric.

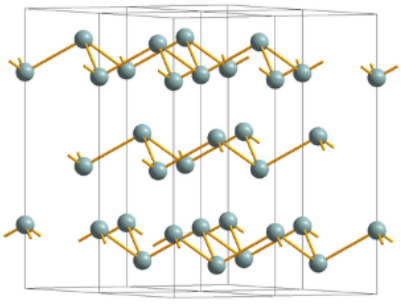
Some compounds are diamorphic and can have either the zincblende or wurtzite structure. Examples of these compounds that have intermediate polarities include CdS and ZnS. SiO_2 exists in polymorphs (crystobalite and tridymite) that resemble zincblende and wurtzite with O atoms midway between each of the Si atoms. The zincblende and wurtzite structures have efficient packing arrangements for tetrahedrally bonded networks and are commonly found in compounds that have tetrahedral bonding. Water, for example, has a tetrahedral hydrogen bonding network and is wurtzite-type. The undistorted wurtzite and zinc blende structures are typically found for AX compounds with eight valence electrons, which follow the octet rule. AX compounds with nine or ten electrons such as GaSe and GaAs crystallize in distorted variants of the wurtzite structure. In GaSe, the extra electrons form lone pairs and this creates layers in the structure, as can be seen in the figure below. To the right of GaSe, the structures of As, Sb, and SbAs show an ever further breakdown of the structure into layers as more valence electrons are added.



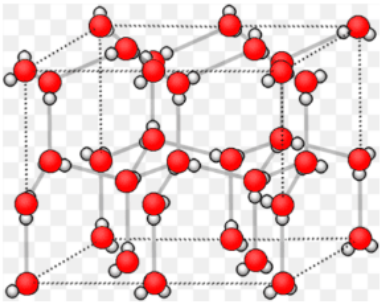
Wurtzite crystal structure



GaSe crystal structure



Crystal structure of Sb, SbAs, and gray As



Crystal structure of hexagonal ice

Hexagonal ice is the most stable polymorph of ice, which is obtained upon freezing at 1 atmosphere pressure. This polymorph (ice-I) has a hcp wurtzite-type structure. Looking at the structure shown at the right, we see that there are irregular arrangements of the O-H---O bonds. In the structure, hydrogen bonding enforces the tetrahedral coordination of each water molecule, resulting in a relatively open structure that is less dense than liquid water. For this reason, ice floats in water.

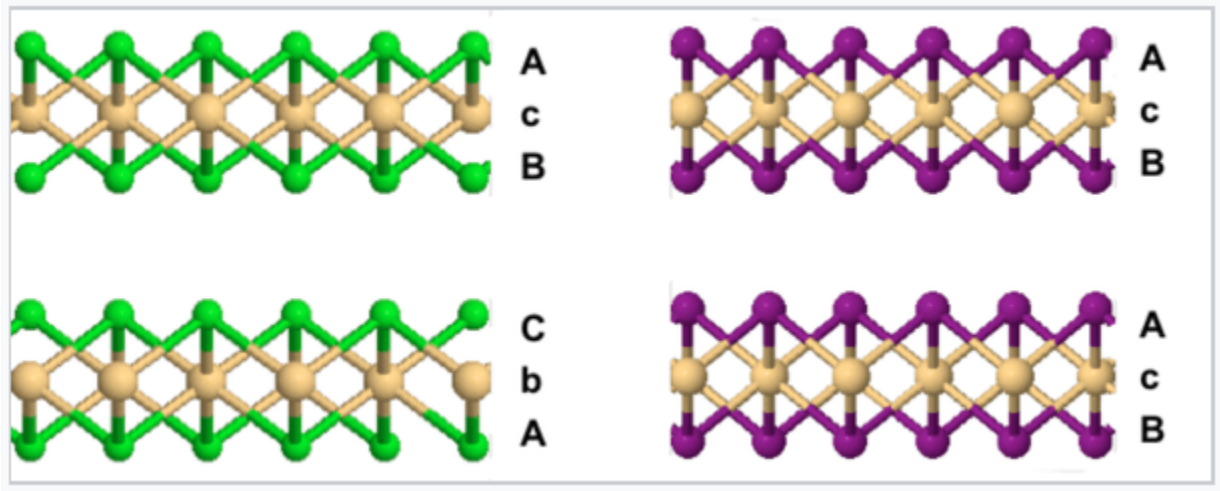
This page titled 9.1.2.4: Tetrahedral Structures is shared under a CC BY-SA 4.0 license and was authored, remixed, and/or curated by Chemistry 310 (Wikibook) via source content that was edited to the style and standards of the LibreTexts platform.

- 8.4: Tetrahedral Structures by Chemistry 310 is licensed CC BY-SA 4.0. Original source: https://en.wikibooks.org/wiki/Introduction_to_Inorganic_Chemistry.

9.1.2.5: Layered Structures and Intercalation Reactions

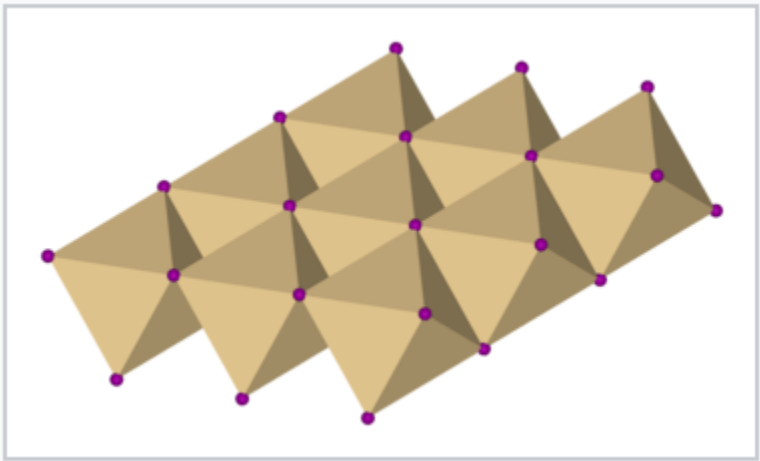
Layered structures are characterized by strong (and typically covalent) bonding between atoms in two dimensions and weaker bonding in the third. A broad range of compounds including metal halides, oxides, sulfides, selenides, borides, nitrides, carbides, and allotropes of some pure elements (B, C, P, As) exist in layered forms. Structurally, the simplest of these structures (for example binary metal halides and sulfides) can be described as having some fraction of the octahedral and/or tetrahedral sites are filled in the fcc and hcp lattices. For example, the $CdCl_2$ structure is formed by filling all the octahedral sites in alternate layers of the fcc lattice, and the CdI_2 structure is the relative of this structure in the hcp lattice.

In the **$CdCl_2$ structure**, the stacking sequence of anion layers is ABCABC...
In the **CdI_2 structure**, the anion stacking sequence is ABAB..., and all the cations are eclipsed along the stacking axis.



Comparison of the $CdCl_2$ (left) and CdI_2 (right) crystal structures

These are examples of **6-3 structures**, because the cations are coordinated by an octahedron of six anions, and the anions are coordinated by three cations to make a trigonal pyramid (like NH_3). Another way to describe these structures is to say that the MX_6 octahedra each share six edges in the MX_2 sheets.



Polyhedral drawing of one layer of the $CdCl_2$ or CdI_2 structure showing edge-sharing MX_6 octahedra

Because these structures place the packing atoms (the anions) in direct van der Waals contact, they are most stable for relatively **covalent** compounds. Otherwise, the electrostatic repulsion between contacting anions would destabilize the structure energetically. More ionic MX_2 compounds tend to adopt the fluorite (CaF_2) or rutile (TiO_2) structures, which are not layered.

Despite the fact that these two structure types are the same at the level of nearest and next-nearest neighbor ions, the CdI_2 structure is much more common than the $CdCl_2$ structure.

$CdCl_2$ structure:

MCl_2 (M = Mg, Mn, Fe, Co, Ni, Zn, Cd)

$NiBr_2$, NiI_2, $ZnBr_2$, ZnI_2

CdI_2 structure:

MCl_2 (M = Ti, V)

MBr_2 (M = Mg, Fe, Co, Cd)

MI_2 (M = Mg, Ca, Ti, V, Mn, Fe, Co, Cd, Ge, Pb, Th)

$M(OH)_2$ (M = Mg, Ca, Mn, Fe, Co, Ni, Cd)

MS_2 (M = Ti, Zr, Sn, Ta, Pt)

MSe_2 (M = Ti, Zr, Sn, V, Pt)

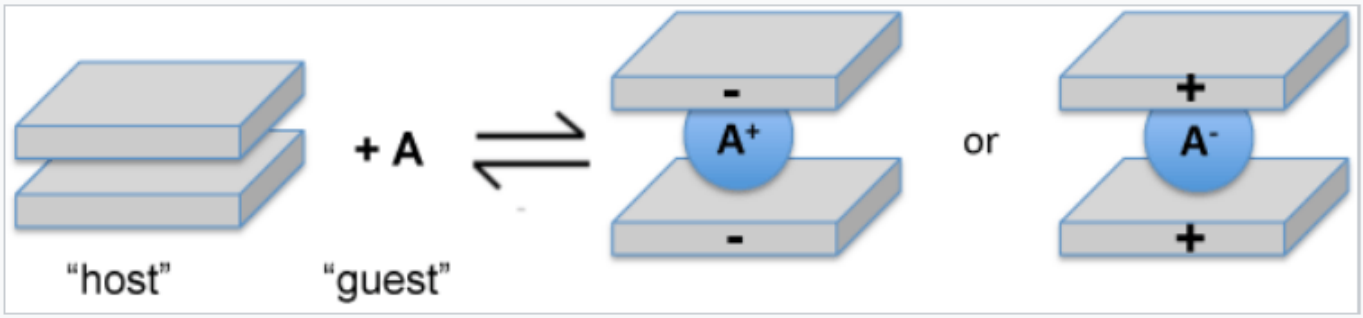
MTe_2 (M = Ti, Co, Ni, Rh, Pd, Pt)

Physically, layered compounds are **soft** and **slippery**, because the layer planes slide past each other easily. For example, graphite, MoS_2, and talc (a silicate) are layered compounds that are used widely as **lubricants** and lubricant additives.

An important reaction of layered compounds is **intercalation**. In intercalation reactions, guest molecules and ions enter the galleries that separate the sheets, usually with expansion of the lattice along the stacking axis. This reaction is typically reversible if it does not perturb the bonding within the sheets. Often the **driving force for intercalation is a redox reaction**, i.e., electron transfer between the host and guest. For example, lithium metal reacts with TiS_2, MoS_2, and graphite to produce $LiTiS_2$, Li_xMoS_2 ($x < 1$), and LiC_6. In these compounds, lithium is ionized to Li^+ and the sheets are negatively charged. Oxidizing agents such as

Br_2, $FeCl_3$, and AsF_5 also react with graphite. In the resulting intercalation compounds, the sheets are positively charged and the intercalated species are anionic.

Intercalation reactions are especially important for electrochemical energy storage in **secondary batteries**, such as **lithium ion** batteries, **nickel-metal hydride** batteries, and **nickel-cadmium** batteries. The reversible nature of the intercalation reaction allows the electrodes to be charged and discharged up to several thousand times without losing their mechanical integrity. In lithium ion batteries, the negative electrode material is typically graphite, which is intercalated by lithium to make LiC_6. Several different oxides and phosphates containing redox active transition metal ions (Mn, Fe, Co, Ni) are used as the positive electrode materials.



Oxidative or reductive intercalation involves the placement of anions or cations between sheets.

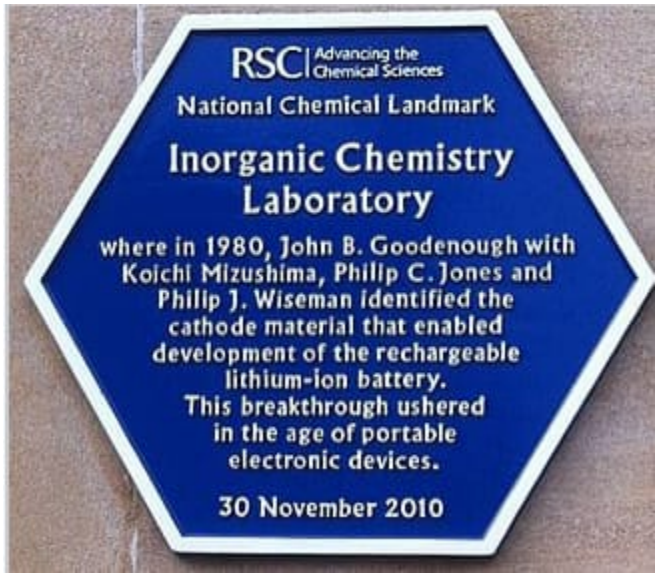
Lithium ion batteries based on CoO_2 were first described in 1980[1] by John B. Goodenough's research group at Oxford. In batteries based on CoO_2, which has the CdI_2 structure, the positive electrode half-reaction is:

$$\mathrm{LiCoO_2} \leftrightharpoons \mathrm{Li_{1-x}CoO_2} + x\,\mathrm{Li^+} + \mathrm{xe^-} \tag{9.1.2.5.1}$$

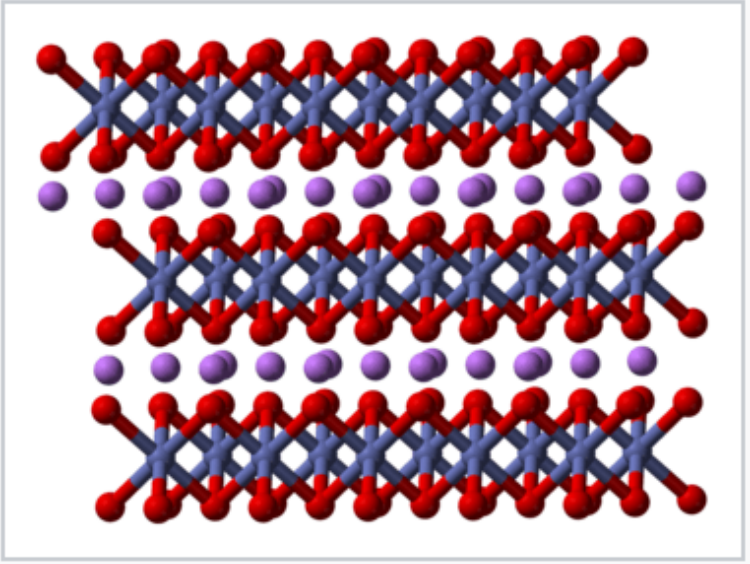
The negative electrode half reaction is:

$$x\,\mathrm{Li^+} + \mathrm{xe^-} + x\,\mathrm{C_6} \leftrightharpoons x\,\mathrm{LiC_6} \tag{9.1.2.5.2}$$

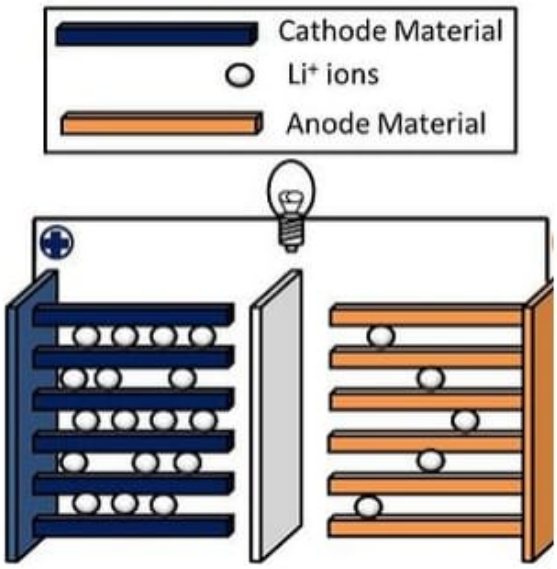
The battery is fully charged when the positive electrode is in the CoO_2 form and the negative electrode is in the LiC_6 form. Discharge involves the motion of Li^+ ions through the electrolyte, forming Li_xCoO_2 and graphite at the two electrodes.



Blue plaque erected by the Royal Society of Chemistry commemorating the development of cathode materials for the lithium-ion battery



Crystal structure of $LiCoO_2$[2]



The lithium ion battery is a "rocking chair" battery, so named because charging and discharging involve moving Li^+ ions from one side to the other. CoO_2 is one example of a positive electrode material that has been used in lithium ion batteries. It has a high energy density, but batteries based on CoO_2 have poor thermal stability. Safer materials include lithium iron phosphate ($LiFePO_4$), and $LiMO_2$ (M = a mixture of Co, Mn, and Ni). These batteries are used widely in laptop computers, portable electronics, cellular telephones, cordless tools, and electric and hybrid vehicles.

A similar intercalation reaction occurs in nickel-cadmium batteries and nickel-metal hydride batteries, except in this case the reaction involves the movement of protons in and out of the $Ni(OH)_2$ lattice, which has the CdI_2 structure:

$$\mathrm{NiO(OH) + H_2O + e^- \longrightarrow Ni(OH)_2 + OH^-} \tag{9.1.2.5.3}$$

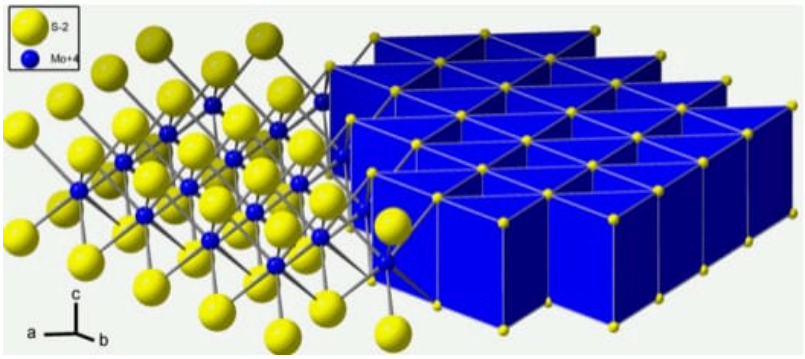
There are many layered compounds that cannot be intercalated by redox reactions, typically because some other stable product is formed. For example, the reaction of layered CdI_2 with Li produces LiI (NaCl structure) and Cd metal.

This page titled 9.1.2.5: Layered Structures and Intercalation Reactions is shared under a CC BY-SA 4.0 license and was authored, remixed, and/or curated by Chemistry 310 (Wikibook) via source content that was edited to the style and standards of the LibreTexts platform.

- 8.5: Layered Structures and Intercalation Reactions by Chemistry 310 is licensed CC BY-SA 4.0. Original source: https://en.wikibooks.org/wiki/Introduction_to_Inorganic_Chemistry.

9.1.2.6: Bonding in TiS_2, MoS_2, and Pyrite Structures

Many layered dichalcogenides, such as TiS_2 and ZrS_2, have the CdI_2 structure. In these compounds, as we have noted above, the metal ions are octahedrally coordinated by S. Interestingly, the structures of MoS_2 and WS_2, while they are also layered, are different. In these cases, the metal is surrounded by a **trigonal prism** of sulfur atoms. NbS_2, TaS_2, $MoSe_2$, $MoTe_2$, and WSe_2 also have the trigonal prismatic molybdenite structure, which is shown below alongside a platy crystal of MoS_2.

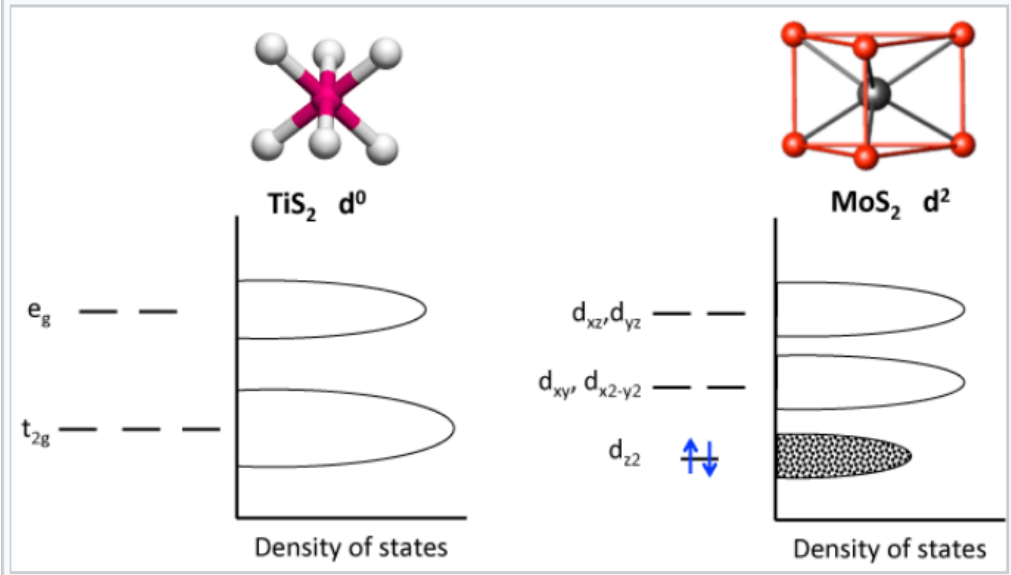




The coordination of the metal ions by a trigonal prism of chalcogenide ions is **sterically unfavorable** relative to octahedral coordination. There are close contacts between the chalcogenide ions, which are eclipsed in the stacking sequence **AbA/BaB/AbA/BaB**... (where "/" indicates the van der Waals gap between layers). What stabilizes this structure?

The molybdenite structure occurs most commonly in MX_2 compounds with a **d^1 or d^2 electron count**. The figure below compares the splitting of d-orbital energies in the octahedral and trigonal prismatic coordination environments:

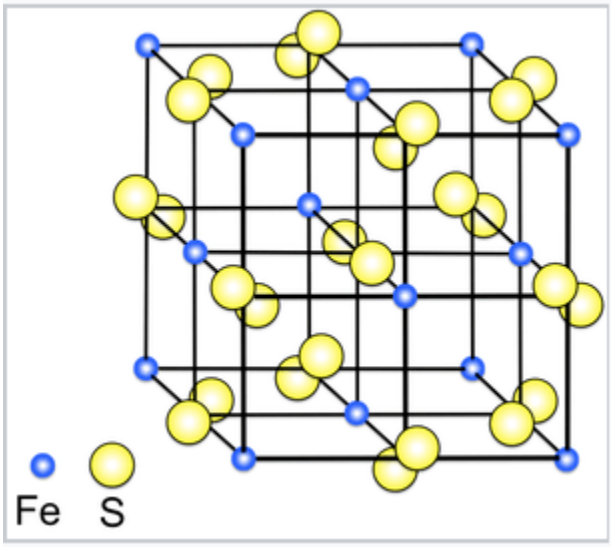
The trigonal prismatic structure is stabilized in MoS_2 by filling the lowest energy band, the d_{z2}. The d_{z2} orbital which points vertically through the triangular top and bottom faces of the trigonal prism, has the least interaction with the sulfide ligands and therefore the lowest energy. The d_{xz} and d_{yz} orbitals, which point at the ligands, have the highest energy. The d_{z2} orbital is lower in energy in this structure than the t_{2g} orbitals are in the octahedral structure of TiS_2.



d-orbital splittings and energy bands in TiS_2 and MoS_2. MoS_2 is a semiconductor with a 1.3 eV gap between its filled and empty bands.

Because it has an unfilled t_{2g} band, TiS_2 is relatively easy to reduce by intercalation with Li. For this reason, $LiTiS_2$ was one of the first intercalation compounds studied by Stanley Whittingham, who developed the concept of the non-aqueous lithium ion battery in the early 1970's.[3] Because it has a filled d_{z2} band, MoS_2 is harder to reduce, but it can be intercalated by reaction with the powerful reducing agent n-butyllithium to make Li_xMoS_2 ($x < 1$). Atoms in the van der Waals planes of these compounds are relatively unreactive, which gives MoS_2 its good oxidative stability and enables its application as a high temperature lubricant. Atoms at the edges of the crystals are however more reactive and in fact are catalytic. High surface area MoS_2, which has a high density of exposed edge planes, is used as a hydrodesulfurization catalyst and is also of increasing interest as an electrocatalyst for the reduction of water to hydrogen.

Layered metal dichalcogenides, including MoS_2, WS_2, and SnS_2, can form closed nanostructures that take the shape of multiwalled onions and multiwalled tubes. These materials were discovered by the group of Reshef Tenne in 1992, shortly after the discovery of carbon nanotubes. Since then nanotubes have been synthesized from many other materials, including vanadium and manganese oxides.



The pyrite (FeS_2) crystal structure. The structure is related to NaCl, with Fe^{2+} and S_2^{2-} ions occupying the cation and anion sites.

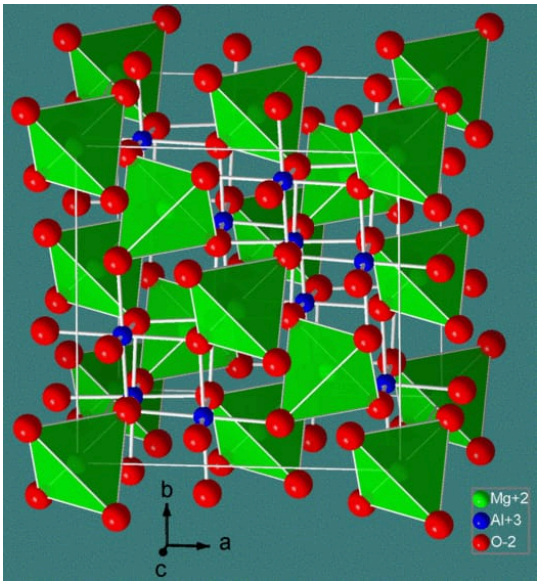
Although early (TiS_2) and late (PtS_2) transition metal disulfides have layered structures, a number of MS_2 compounds in the middle of the transition series, such as MnS_2, FeS_2 and RuS_2, have three-dimensionally bonded structures. For example, FeS_2 has the **pyrite structure**, which is related to the NaCl structure. The reason is that FeS_2 is not $Fe^{4+}(S^{2-})_2$, but is actually $Fe^{2+}(S_2^{2-})$, where S_2^{2-} is the disulfide anion (which contains a single bond like the peroxide anion O_2^{2-}). S^{2-} is too strong a reducing agent to exist in the same compound with Fe^{4+}, which is a strong oxidizing agent. Because FeS_2 is actually $Fe^{2+}(S_2^{2-})$, it is a 1:1 compound and adopts a 1:1 structure.

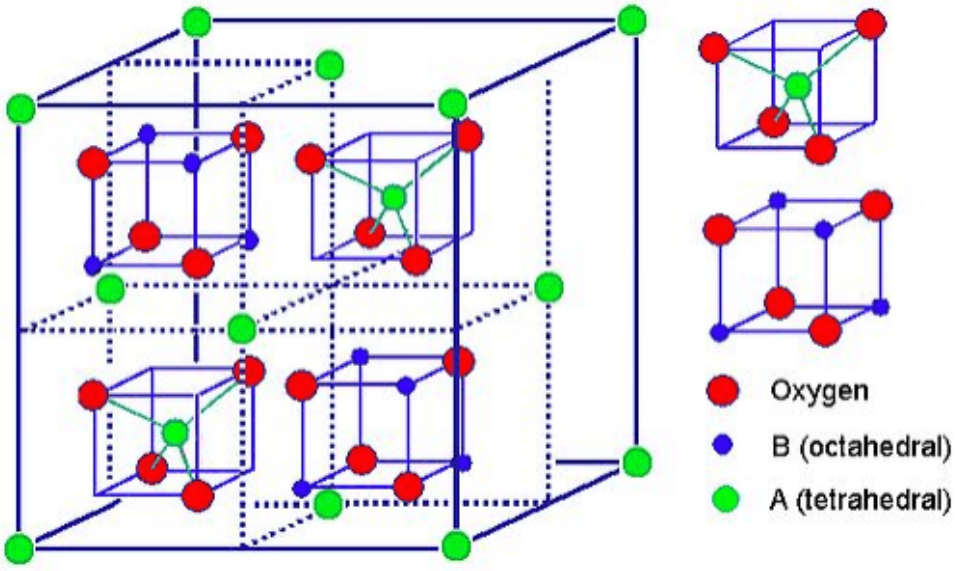
This page titled 9.1.2.6: Bonding in TiS_2, MoS_2, and Pyrite Structures is shared under a CC BY-SA 4.0 license and was authored, remixed, and/or curated by Chemistry 310 (Wikibook) via source content that was edited to the style and standards of the LibreTexts platform.

- 8.6: Bonding in TiS_2, MoS_2, and Pyrite Structures by Chemistry 310 is licensed CC BY-SA 4.0. Original source: https://en.wikibooks.org/wiki/Introduction_to_Inorganic_Chemistry.

9.1.2.7: Spinel, Perovskite, and Rutile Structures

There are three more structures, which are derived from close-packed lattices, that are particularly important because of the material properties of their compounds. These are the **spinel** structure, on which ferrites and other magnetic oxides are based, the **perovskite** structure, which is adopted by ferroelectric and superconducting oxides, and the **rutile** structure, which is a common binary 6:3 structure adopted by oxides and fluorides.





The **spinel structure** is formulated MM'_2X_4, where M and M' are tetrahedrally and octahedrally coordinated cations, respectively, and X is an anion (typically O or F). The structure is named after the mineral $MgAl_2O_4$, and oxide spinels have the general formula AB_2O_4.

In the **normal spinel** structure, there is a close-packed array of anions. The A-site cations fill 1/8 of the tetrahedral holes and the B-site cations fill 1/2 of the octahedral holes. A polyhedral view of the normal spinel unit cell is shown at the left, and a simplified view (with the contents of the back half of the cell removed for clarity) is shown above. Each unit cell contains eight formula units and has a composition $A_8B_{16}O_{32}$.

Inverse spinels have a closely related structure (with the same large unit cell) in which the A-site ions and half of the B-site ions switch places. Inverse spinels are thus formulated $B(AB)O_4$, where the AB ions in parentheses occupy octahedral sites, and the other B ions are on tetrahedral sites. There are also mixed spinels, which are intermediate between the **normal** and **inverse** spinel structure.

Some spinel and inverse spinel AB combinations are:

$A^{2+}B^{3+}$, e.g., $MgAl_2O_4$ (normal spinel)

$A^{4+}B^{2+}$, e.g., $Pb_3O_4 = Pb^{II}(Pb^{II}Pb^{IV})O_4$ (inverse spinel)

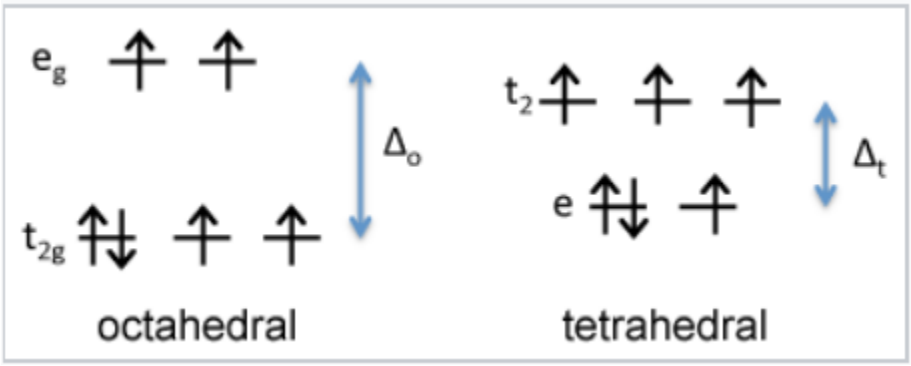
$A^{6+}B^{+}$, e.g., Na_2WO_4 (normal spinel)

Many magnetic oxides, such as Fe_3O_4 and $CoFe_2O_4$, are spinels.

Normal vs. inverse spinel structure

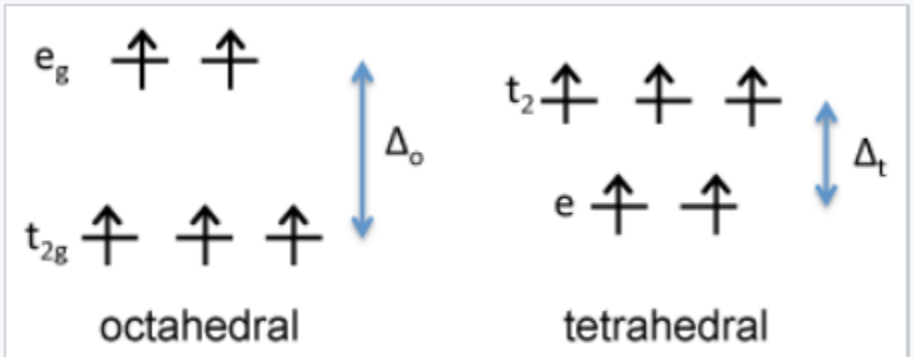
For transition metal oxide spinels, the choice of the normal vs. inverse spinel structure is driven primarily by the **crystal field stabilization energy** (CFSE) of ions in the tetrahedral and octahedral sites. For spinels that contain 3d elements such as Cr, Mn, Fe, Co, and Ni, the electron configuration is typically **high spin** because O^{2-} is a **weak field ligand**.

As an example, we can consider magnetite, Fe_3O_4. This compound contains one Fe^{2+} and two Fe^{3+} ions per formula unit, so we could formulate it as a normal spinel, $Fe^{2+}(Fe^{3+})_2O_4$, or as an inverse spinel, $Fe^{3+}(Fe^{2+}Fe^{3+})O_4$. Which one would have the lowest energy?



d-orbital energy diagram for Fe^{2+}

First we consider the crystal field energy of the **Fe^{2+}** ion, which is d^6. Comparing the tetrahedral and high spin octahedral diagrams, we find that the CFSE in an **octahedral** field of O^{2-} ions is $[(4)(\frac{2}{5}) - (2)(\frac{3}{5})]\Delta_o - P = \mathbf{0.4\Delta_o - P}$. In the **tetrahedral** field, the CFSE is $[(3)(\frac{3}{5}) - (3)(\frac{2}{5})]\Delta_t - P = \mathbf{0.6\Delta_t - P}$. Since Δ_o is about 2.25 times larger than Δ_t, the octahedral arrangement has a larger CFSE and is preferred for Fe^{2+}.



d-orbital energy diagram for Fe^{3+}

In contrast, it is easy to show that **Fe^{3+}**, which is d^5, would have a CFSE of zero in either the octahedral or tetrahedral geometry. This means that Fe^{2+} has a preference for the octahedral site, but Fe^{3+} has no preference. Consequently, we place Fe^{2+} on octahedral sites and **Fe_3O_4 is an inverse spinel**, $Fe^{3+}(Fe^{2+}Fe^{3+})O_4$.

Ferrites are compounds of general formula **$M^{II}Fe_2O_4$**. We can see that magnetite is one example of a ferrite (with M = Fe). Other divalent metals (M = Mg, Mn, Co, Ni, Zn) also form ferrites. Ferrites can be normal or inverse spinels, or mixed spinels, depending on the CFSE of the M^{II} ion. Based on their CFSE, Fe^{2+}, Co^{2+}, and Ni^{2+} all have a strong preference for the octahedral site, so those compounds are all inverse spinels. $ZnFe_2O_4$ is a normal spinel because the small Zn^{2+} ion (d^{10}) fits more easily into the tetrahedral site than Fe^{3+} (d^5), and both ions have zero CFSE. $MgFe_2O_4$ and $MnFe_2O_4$, in which all ions have zero CFSE and no site preference, are mixed spinels. **Chromite** spinels, **$M^{II}Cr_2O_4$**, are always **normal spinels** because the d^3 Cr^{3+} ion has a strong preference for the octahedral site.

Examples of normal and inverse spinel structures:

$MgAl_2O_4$ is a **normal spinel** since both Mg^{2+} and Al^{3+} are non-transition metal ions and thus CFSE = 0. The more highly charged Al^{3+} ion prefers the octahedral site, where it is surrounded by six negatively charged oxygen atoms.

Mn_3O_4 is a **normal spinel** since the Mn^{2+} ion is a high spin d^5 system with zero CFSE. The two Mn^{3+} ions are high spin d^4 with higher CFSE on the octahedral sites (3/5 Δ_O) than on the tetrahedral site (2/5 Δ_t ~ 1/5 Δ_O).

Fe_3O_4 is an **inverse spinel** since the Fe^{3+} ion is a high spin d^5 system with zero CFSE. Fe^{2+} is a high spin d^6 system with more CFSE on an octahedral site than on a tetrahedral one.

$NiFe_2O_4$ is again an **inverse spinel** since Ni^{2+} (a d^8 ion) prefers the octahedral site and the CFSE of Fe^{3+} (a d^5 ion) is zero.

$FeCr_2O_4$ is a **normal spinel** since Fe^{2+} is high spin d^6 ion with $CFSE = [4(\frac{2}{5}) - 2(\frac{3}{5})]\Delta_o = \frac{2}{5}\Delta_o$ on an octahedral site, and Cr^{3+} is a d^3 ion with CFSE = 3(2/5) Δ_O = 6/5 Δ_O. Hence it is more energetically favorable for Cr^{3+} to occupy both of the octahedral sites.

Co_3O_4 is a **normal spinel**. Even in the presence of weak field oxo ligands, Co^{3+} is a low spin d^6 ion with very high CFSE on the octahedral sites, because of the high charge and small size of the Co^{3+} ion. Hence the Co^{3+} ions occupy both octahedral sites, and Co^{2+} occupies the tetrahedral site.

Magnetism of ferrite spinels

Ferrite spinels are of technological interest because of their magnetic ordering, which can be ferrimagnetic or antiferromagnetic depending on the structure (normal or inverse) and the nature of the metal ions. Fe_3O_4, $CoFe_2O_4$, and $NiFe_2O_4$ are all inverse spinels and are ferrimagnets. The latter two compounds are used in magnetic recording media and as deflection magnets, respectively.

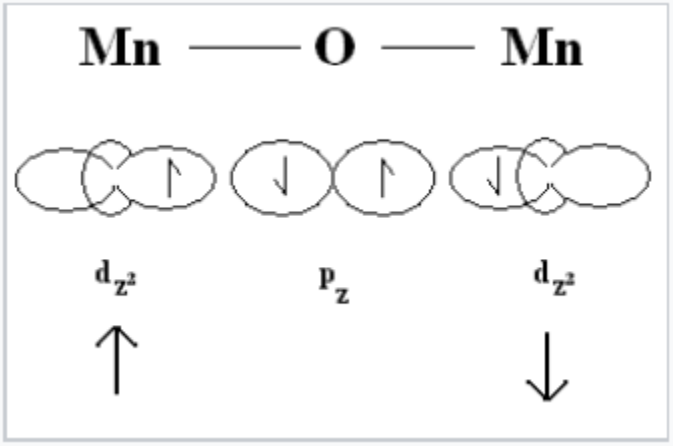
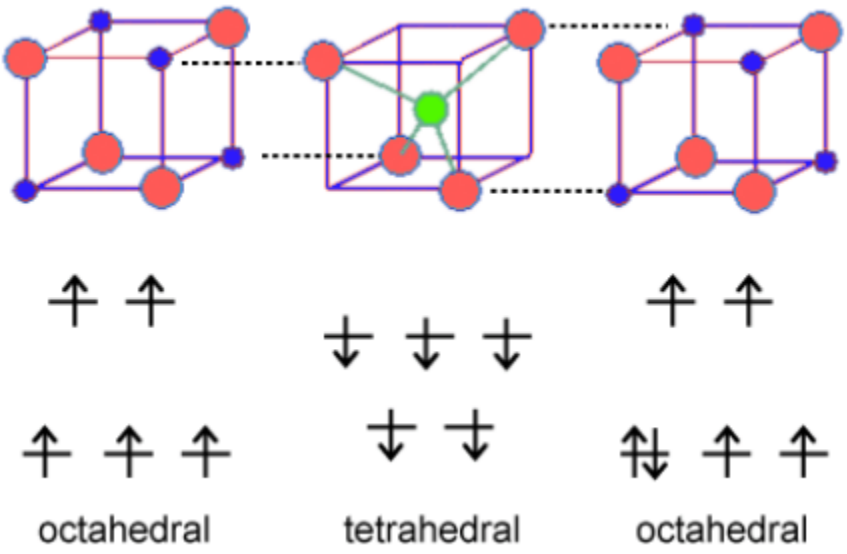


Illustration of antiferromagnetic superexchange between two transition metal cations through a shared oxygen atom.

In order to understand the magnetism of ferrites, we need to think about how the unpaired spins of metal ions are coupled in oxides. If an oxide ion is shared by two metal ions, it can mediate the coupling of spins by superexchange as shown at the right. The coupling can be antiferromagnetic, as shown, or ferromagnetic, depending on the orbital filling and the symmetry of the orbitals involved. The **Goodenough-Kanamori rules** predict the local magnetic ordering (ferromagnetic vs. antiferromagnetic) that results from superexchange coupling of the electron spins of transition metal ions. For ferrites, the strongest coupling is between ions on neighboring **tetrahedral and octahedral sites**, and the ordering of spins between these two sites is reliably **antiferromagnetic**.

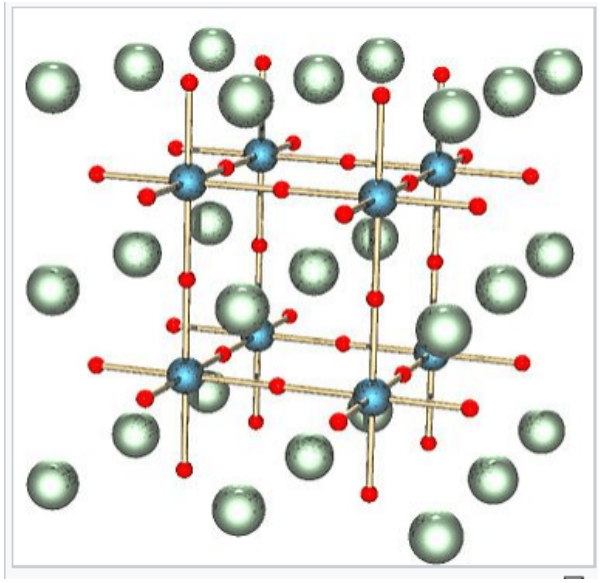


Because all the tetrahedral and octahedral sites in a spinel or inverse spinel crystal are coupled together identically, it works out that ions on the tetrahedral sites will all have one orientation (e.g., spin down) and ions on all the octahedral sites will have the opposite orientation (e.g., spin up). If the number of spins on the two sites is the same, then the solid will be

antiferromagnetic. However, if the **number of spins is unequal** (as in the case of Fe_3O_4, $CoFe_2O_4$, and $NiFe_2O_4$) then the solid will be **ferrimagnetic**. This is illustrated above for Fe_3O_4. The spins on the Fe^{3+} sites cancel, because half of them are up and half are down. However, the four unpaired electrons on the Fe^{2+} ions are all aligned the same way in the crystal, so the compound is ferrimagnetic.

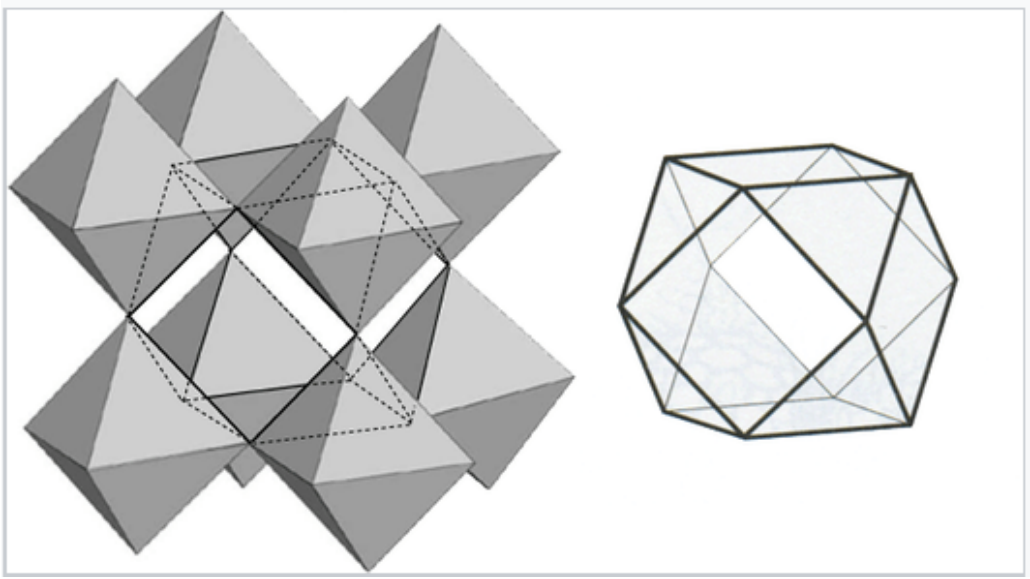
Perovskites are **ternary oxides** of general formula **ABO_3**. More generally, the perovskite formula is ABX_3, where the anion X can be **O, N, or halogen**. The A ions are typically large ions such as Sr^{2+}, Ba^{2+}, Rb^{+}, or a lanthanide 3+ ion, and the B ions are smaller transition metal ions such as Ti^{4+}, Nb^{5+}, Ru^{4+}, etc. The mineral after which the structure is named has the formula $CaTiO_3$.

The perovskite structure has simple cubic symmetry, but is related to the fcc lattice in the sense that the A site cations and the three O atoms comprise a fcc lattice. The B-site cations fill 1/4 of the octahedral holes and are surrounded by six oxide anions.



ABX_3 perovskite structure. A, B, and X are white, blue, and red, respectively.

The coordination of the A ions in perovsite and the arrangement of BO_6 octahedra is best understood by looking at the ReO_3 structure, which is the same structure but with the A-site cations removed. In the polyhedral representation of the structure shown at the right, it can be seen that the octahedra share all their vertices but do not share any octahedral edges. This makes the ReO_3 and perovskite structures flexible, like three-dimensional wine racks, in that the octahedra can **rotate and tilt cooperatively**. Eight such octahedra surround a large **cuboctahedral cavity**, which is the site of the A ions in the perovskite structure. Cations in these sites are coordinated by 12 oxide ions, as expected from the relationship between the perovskite and fcc lattices.



Polyhedral representation of the ReO_3 structure showing the large cuboctahedral cavity that is surrounded by 12 oxygen atoms

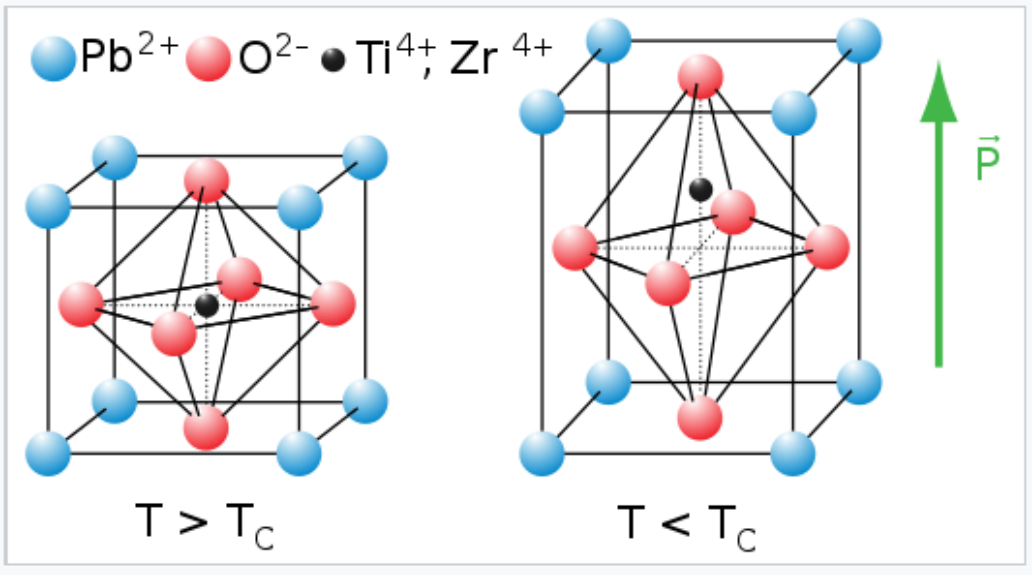
Because the A-site is empty in the ReO_3 structure, compounds with that structure can be reversibly **intercalated** by small ions such as **Li^+ or H^+**, which then occupy sites in the cuboctahedral cavity. For example, smart windows that darken in bright sunlight contain the **electrochromic** material WO_3, which has the ReO_3 structure. In the sunlight, a photovoltaic cell drives the reductive intercalation of WO_3 according to the reaction:

$$x\,\mathrm{H}^+ + \mathrm{xe}^- + \mathrm{WO}_3 \;\leftrightharpoons\; \mathrm{H}_x\mathrm{WO}_3 \qquad (9.1.2.7.1)$$

WO_3 is a light yellow compound containing d^0 W(VI). In contrast, H_xWO_3, which is mixed-valent W(V)-W(VI) = d^1-d^0, has a deep blue color. Such coloration is typical of mixed-valence transition metal complexes because their d-electrons can be excited to delocalized conduction band levels by red light. Because the electrochemical intercalation-deintercalation process is powered by a solar cell, the tint of the windows can adjust automatically to the level of sunlight.

Ferroelectric perovskites

The flexibility of the network of corner-sharing BO_6 octahedra is also very important in ferroelectric oxides that have the perovskite structure. In some perovsites with small B-site cations, such as Ti^{4+} and Nb^{5+}, the cation is too small to fit symmetrically in the BO_6 octahedron. The octahedron distorts, allowing the cation to move off-center. These distortions can be **tetragonal** (as in the example shown at the right), **rhombohedral**, or **orthorhombic**, depending on whether the cation moves towards a vertex, face, or edge of the BO_6 octahedron. Moving the cation off-center in the octahedron creates an **electric dipole**. In ferroelectrics, these dipoles align in neighboring unit cells through cooperative rotation and tilting of octahedra. The crystal thus acquires a net electrical polarization.



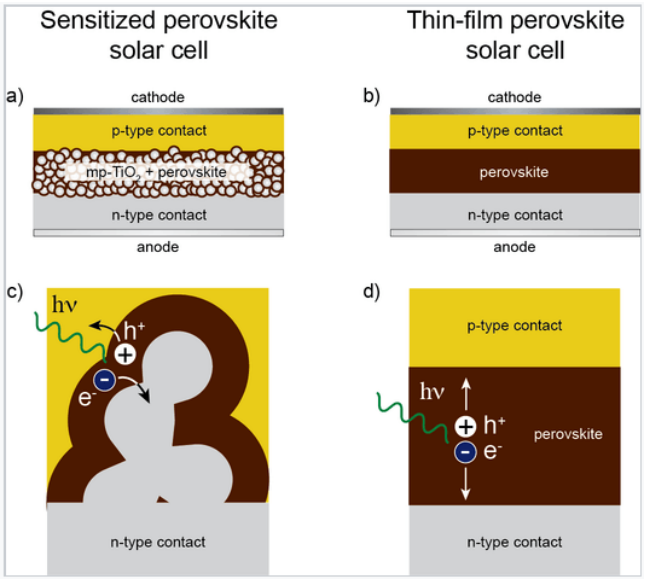
Tetragonal distortion of the perovskite unit cell in the ferroelectric oxide PZT, $PbTi_xZr_{1-x}$

Ferroelectricity behaves analogously to **ferromagnetism**, except that the polarization is electrical rather than magnetic. In both cases, there is a **critical temperature (T_c)** above which the **spontaneous polarization** of the crystal disappears. Below T_c, the electric polarization of a ferroelectric can be switched with a coercive field, and hysteresis loop of polarization vs. field resembles that of a ferromagnet. Above T_c, the crystal is **paraelectric** and has a high dielectric permittivity.

Ferroelectric and paraelectric oxides (along with piezoelectrics and pyroelectrics) have a wide variety of applications as switches, actuators, transducers, and dielectrics for capacitors. **Ferroelectric capacitors** are important in memory devices (FRAM) and in the tuning circuits of cellular telephones. **Multiferroics**, which are materials that are simultaneously ferroelectric and ferromagnetic, are rare and are being now intensively researched because of their potential applications in electrically adressable magnetic memory.

Halide perovskites (ABX_3, X = Cl, Br, I) can be made by combining salts of monovalent A ions (A^+ = Cs^+, NH_4^+, RNH_3^+) and divalent metal salts such as $PbCl_2$ or PbI_2. These compounds have sparked recent interest as light absorbers for **thin film solar cells** that produce electricity from sunlight. Lead and tin halide perovskites can be grown as thin films from solution precursors or by thermal evaporation at relatively low temperatures. In some lead halide perovskites, the mobility of electrons and holes is very high, comparable to that of more expensive III-V semiconductors such as GaAs, which must be grown as very pure single crystals at high temperatures for use in solar cells. Because of their high carrier mobility, some lead halide perovskites are also electroluminescent and are of interest as inexpensive materials for light-emitting diodes (LEDs).

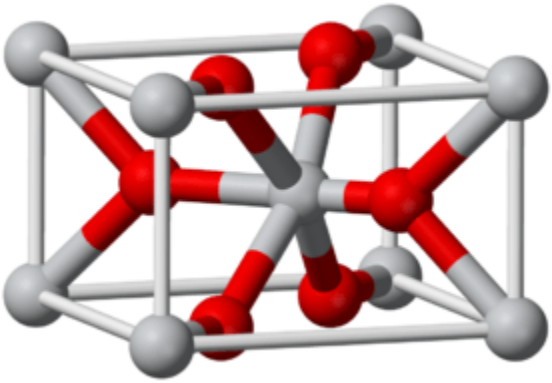
Tin and lead halide perovskites were first studied in the 1990s as materials for thin film electronics,[4] and more recently as light absorbers in dye-sensitized solar cells. Soon after the results on dye-sensitized perovskite cells were reported, it was discovered that halide perovskites could also be used in thin film solid state solar cells. The structures of these solar cells are shown schematically at the right. The highest reported solar power conversion efficiencies of perovskite solar cells have jumped from 3.8% in 2009 [5] to 10.2% in 2012[6] and a certified 20.1% in 2014.[7]. The highest performing cells to date contain divalent lead in the perovskite B cation site and a mixture of methylammonium and formamidinium ions in the perovskite A cation site.



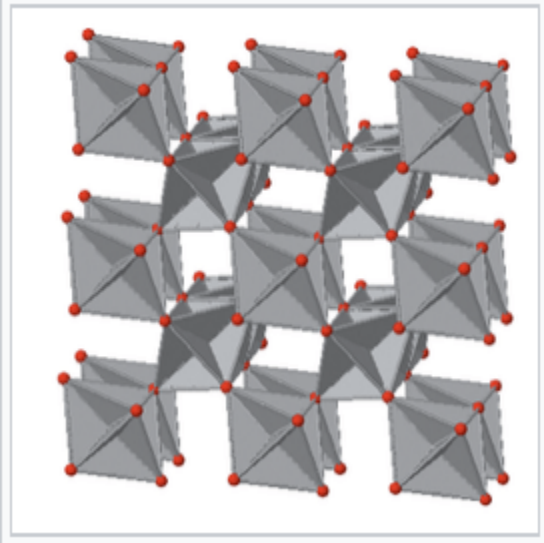
a) Solar cell architecture in which a lead halide perovskite absorber coats a layer of nanocrystalline anatase TiO_2. b) Thin-film solar cell, with a layer of lead halide perovskite sandwiched between two selective contacts. c) Charge generation and extraction in the sensitized architecture and d) in the thin-film architecture.

Despite their very impressive efficiency, perovskite solar cells are stable for relatively short periods of time and are sensitive to air and moisture. Current research is focused on understanding the degradation mechanisms of these solar cells and improving their stability under operating conditions.

The **rutile structure** is an important MX_2 (X = O, F) structure. It is a 6:3 structure, in which the cations are octahedrally coordinated by anions, and as such is intermediate in polarity between the CaF_2 (8:4) and SiO_2 (4:2) structures. The mineral rutile is one of the polymorphs of TiO_2, the others (anatase and brookite) also being 6:3 structures.



The rutile structure can be described as a distorted version of the NiAs structure with half the cations removed. Recall that compounds with the NiAs structure were typically metallic because the metal ions are eclipsed along the stacking axis and thus are in relatively close contact. In rutile, the MO_6 **octahedra share edges** along the tetragonal c-axis, and so some rutile oxides, such as **NbO_2, RuO_2 and IrO_2,** are also **metallic** because of **d-orbital overlap** along that axis. These compounds are important as electrolyzer catalysts and catalyst supports because they combine high catalytic activity with good electronic conductivity.



View down the tetragonal c-axis of the rutile lattice, showing edge-sharing MO_6 octahedra.

Rutile TiO_2, because of its high refractive index, is the base pigment for white paint. It is a wide bandgap semiconductor that has also been extensively researched as an electrode for water splitting solar cells and as a photocatalyst (primarily as the anatase polymorph) for degradation of pollutants in air and water. Self-cleaning glass exploits the photocatalytic properties of a thin film of TiO_2 to remove oily substances from the glass surface and improve the wetting properties of the glass.

This page titled 9.1.2.7: Spinel, Perovskite, and Rutile Structures is shared under a CC BY-SA 4.0 license and was authored, remixed, and/or curated by Chemistry 310 (Wikibook) via source content that was edited to the style and standards of the LibreTexts platform.

- 8.7: Spinel, Perovskite, and Rutile Structures by Chemistry 310 is licensed CC BY-SA 4.0. Original source: https://en.wikibooks.org/wiki/Introduction_to_Inorganic_Chemistry.

9.1.2.8: Discussion Questions

- Using the Liverpool 3D visualization website (http://www.chemtube3d.com/solidstate/_table.htm) determine the anion and cation coordination geometries in cadmium chloride and anatase. Describe the arrangement of octahedra (in terms of whether they share edges, faces, etc.) in these structures.
- Count the number of atoms in the Li_3Bi and ReO_3 unit cells, and determine the coordination environments of each of the ions.
- Silicon, germanium, and many other semiconductors adopt the diamond (or zincblende) structure. Assuming that all the atoms are the same size, calculate the volume fraction of the unit cell that is occupied by the atoms. How does the filling fraction of diamond compare to simple cubic and close-packed structures, and what does this tell us about the relationship between coordination number and density?
- Describe the structural basis of ferroelectricity in barium titanate.

This page titled 9.1.2.8: Discussion Questions is shared under a CC BY-SA 4.0 license and was authored, remixed, and/or curated by Chemistry 310 (Wikibook) via source content that was edited to the style and standards of the LibreTexts platform.

- 8.8: Discussion Questions by Chemistry 310 is licensed CC BY-SA 4.0. Original source: https://en.wikibooks.org/wiki/Introduction_to_Inorganic_Chemistry.

9.1.2.9: References

1. K. Mizushima, P.C. Jones, P.J. Wiseman, J.B. Goodenough (1980). "Li_xCoO_2(0Materials Research Bulletin **15**: 783–789. doi:10.1016/0025-5408(80)90012-4.
2. Yang Shao-Horn, Laurence Croguennec, Claude Delmas, E. Chris Nelson and Michael A. O'Keefe (July 2003). "Atomic resolution of lithium ions in $LiCoO_2$". *Nature Materials* **2** (7): 464–467. doi:10.1038/nmat922. PMID 12806387.
3. M. Stanley Whittingham "Lithium Batteries and Cathode Materials" Chem. Rev., 2004, vol. 104, pp. 4271–4302. DOI: 10.1021/cr020731c
4. Kagan, Cherie R.; Mitzi, David B.; Dimitrakopoulos, C. D. (1999). "Organic-inorganic hybrid materials as semiconducting channels in thin-film field-effect transistors". *Science* **286**: 945-947. doi:10.1126/science.286.5441.945.
5. Kojima, Akihiro; Teshima, Kenjiro; Shirai, Yasuo; Miyasaka, Tsutomu (6 May 2009). "Organometal Halide Perovskites as Visible-Light Sensitizers for Photovoltaic Cells". *Journal of the American Chemical Society* **131** (17): 6050–6051. doi:10.1021/ja809598r. PMID 19366264.
6. Chung, In; Lee, Byunghong; He, Jiaking; Chang, Robert P. H.; Kanatzidis, Mercouri G. (24 May 2012). "All-solid-state dye-sensitized solar cells with high efficiency". *Nature* **485**: 486-489. doi:10.1038/nature11067.
7. IEEE Spectrum, Perovskite Solar Cell Bests Bugbears, Reaches Record Efficiency, 7 January 2015
8. W. Zhang et al. (2013), "Unexpected Stable Stoichiometries of Sodium Chlorides." *Science*, vol. 342, no. 6165, pp. 1502-1505. doi: 10.1126/science.1244989

This page titled 9.1.2.9: References is shared under a CC BY-SA 4.0 license and was authored, remixed, and/or curated by Chemistry 310 (Wikibook) via source content that was edited to the style and standards of the LibreTexts platform.

- 8.10: References by Chemistry 310 is licensed CC BY-SA 4.0. Original source: https://en.wikibooks.org/wiki/Introduction_to_Inorganic_Chemistry.

9.2: Bonding in Metals, Semiconductors and Insulators – Band Structure

INTRODUCTION

Characteristic properties of metals include: (1) electrical conductivity, (2) opaqueness and (3) malleability. A very simple model in which the metallic crystal is viewed as a lattice of positive ions surrounded by a “gas” of free electrons provides a crude understanding of the first and third properties. If the crystal has a gas of free electrons, it is easy to see why the application of an electric field will result in the motion of these electrons and thus for the high electrical conductivity. This model also allows one to explain the malleability of metals, as shown in fig. 1b. When a metallic crystal is subject to forces that displace one plane of atoms with respect to another, the environment of the charged species is left unchanged. In contrast, the displacement of neighboring planes in an ionic crystal as a result of a distorting force will lead to cleavage, largely because of changes in the interaction of the charged species (Figure $9.2.1, left$).

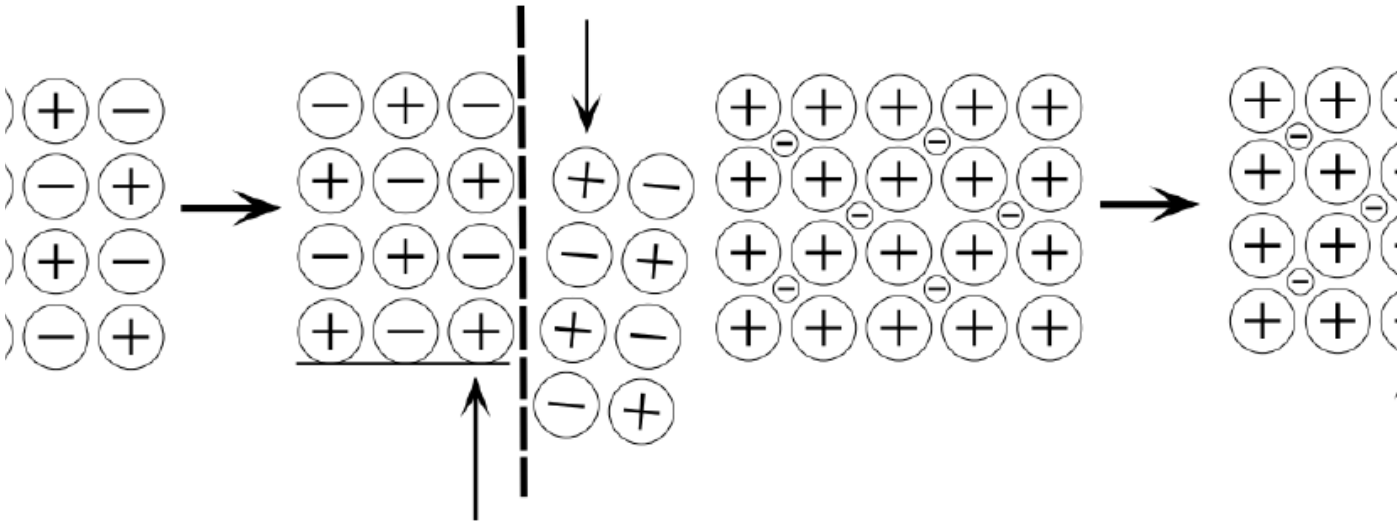


Figure $9.2.1$: Mechanical properties of ionic and metallic crystals. (left) In ionic crystals the displacement of neighboring planes by shear forces frequently results in cleavage largely because of the establishment of repulsive forces in the cleavage plane. (right) In metallic crystals the displacement of neighboring planes does not lead to charge effects; slip is a common phenomenon; metals are malleable.

The **free electron gas theory or Drude–Lorentz (D-L) theory** also explains in principle the nature of the attractive bonding forces which hold the metallic ions (the metal) together: the crystal is held together by electrostatic forces of attraction between the positively charged metal ions and the non-localized, negatively charged electrons - the electron gas. The theory in its original form assumes that the classical kinetic theory of gases is applicable to the *electron gas* ; mutual repulsion between electrons was ignored and the electrons were expected to have velocities which are temperature dependent according to a Maxwell-Boltzmann distribution law.

While the Drude-Lorentz theory of metallic bonding was considered a useful model, several shortcomings soon became apparent. The most notable failure consisted of the unexplainable discrepancy between the observed and predicted specific heats of metals (energy in the form of heat, required to increase the temperature of $1\ \mathrm{g}$ of a given metal by $1^{\circ}\mathrm{C}$). The D-L theory predicted much larger specific heats than are observed (because the Maxwell-Boltzmann energy distribution has no restrictions as to the number of species allowed to have exactly the same energy). [If there are restrictions as to the number of electrons with identical energy (Pauli exclusion principle!), we have to apply a different form of statistics (Fermi-Dirac statistics).]

ENERGY BAND THEORY BASED ON FORMATION OF MOLECULAR ORBITALS

A different model, and one that is more closely related to the models of the chemical bond discussed earlier, is the *band model*. This model, proposed by Bloch before the development of the molecular-orbital approach to chemical bonding, is actually a molecular-orbital model of metallic crystals. The orbitals characteristic of the whole crystal are obtained as linear combinations of the atomic orbitals of the individual atoms.

From the large electrical conductivity of metals, it appears that at least some of the electrons can move freely through the bulk of the metal. Since even lithium with only one valence electron has eight nearest neighbors (crystallizes in a body-centered cubic lattice), it is clear that the atoms can not be bonded to each other by localized electron-pair bonds (for in that case the lithium atom, which altogether has only three electrons, would have to supply eight or even fourteen valence electrons to establish bonding with the nearest and next-to-nearest neighbor atoms). The fact that in a metal lattice one atom can simultaneously interact with a large number of others can be explained by considering that metals constitute an extreme example of *delocalized bonding*.

Conditions in metals are not as easily assessed as in organic hydrocarbon chains because metal lattices are three-dimensional structures. However, several important results from the theory of metallic bonding can be understood on a highly simplified model in which the three-dimensional lattice is replaced by a one-dimensional system. Consider the formation of a linear array of lithium atoms from individual lithium atoms:

$$\mathrm{Li} \rightarrow \mathrm{Li}-\mathrm{Li} \rightarrow \mathrm{Li}-\mathrm{Li}-\mathrm{Li} \rightarrow \mathrm{Li}-\mathrm{Li}-\mathrm{Li}-\mathrm{Li} \rightarrow \ldots \tag{9.2.1}$$

The first stage is the formation of a lithium molecule, Li_2, which is comparable to the hydrogen molecule, H_2. The two lithium atoms are bound together by a pair of valence electrons; each lithium atom supplies its 2s-electron which, through orbital overlap, forms a covalent molecular bond (fig. 2). The molecule formed occurs in lithium vapor and differs from the H_2 molecule only by its greater interatomic distance ($\mathrm{Li}-\mathrm{Li}=2.67 \times 10^{-10}\ \mathrm{m}, \mathrm{H}-\mathrm{H}=0.75 \times 10^{-10}\ \mathrm{m}$) and smaller energy of formation. The larger separation and the consequent reduction in bond energy can be attributed to the size of the Li^{+} atomic core.

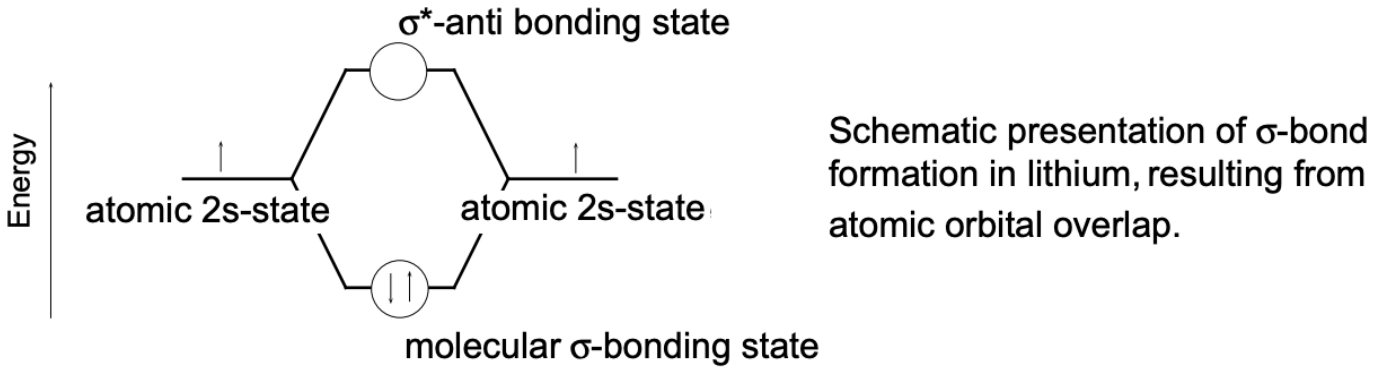


Figure 2 Formation of Li_2 molecule

In the determination of molecular orbital states by **linear combination of atomic orbitals** (LCAO) we obtain more than one solution from the Schrödinger equation. We have so far concentrated mostly on the low energy states, leading to σ or π bonds. We have largely ignored the so-called *antibonding states* which in covalent molecules have energies higher than the original energy states of the isolated reaction partners (presently Li) and, therefore, remain unoccupied (or empty) in two-atomic molecules. In any multi-atom system (such as a piece of metal), the total number of molecular orbital states (electronic states) is always the same as the total number of original atomic states (conservation of electronic states). However, not all of these states are necessarily occupied by electrons.

Consider the hypothetical linear molecule Li_3. Since the valence electron cloud is spherical, the central lithium atom can not give preference to either of its neighbors. The three atomic valence electron clouds overlap to form one continuous distribution and two others with nodes (antibonding states), i.e., three molecular orbitals in all (Fig. 3).

As the length of the chain is increased, the number of electronic states into which the atomic $2s$ state splits also increases, *the number of states always equaling the number of atoms*. The same occurs when lithium chains are placed side-by-side or stacked

on top of each other, so that finally the space lattice of the lithium crystal is obtained. It is of great significance that these electronic states have energies which are bounded by an upper and lower limiting value (see fig. 4). Within these limits the states form an *energy band* of closely spaced values (one gram of lithium contains nearly 10^{23} atoms). Similarly, energy bands can also result from overlapping p and d orbitals. The electronic states (orbitals) within an energy band are filled progressively by pairs of electrons in the same way that the orbitals of an atom were filled in accordance with the Pauli principle. This means that for lithium the electronic states of the 2s band will be exactly half-filled.

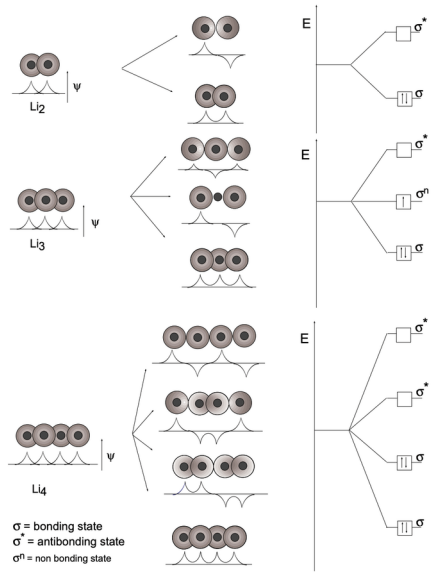


Figure 3 Formation of molecular chains of lithium atoms.

It is of interest to consider why lithium atoms or Li_2 molecules combine to form a metal lattice. In the lithium lattice the smallest distance between neighboring atoms is $3.03 \times 10^{-10}\ \mathrm{m}$, which is larger than in the Li_2 molecule. This reflects the fact that bonds between pairs of atoms in the metal are weaker than they are in the molecule. Nevertheless, the metallic form of lithium is more stable than the molecular form because in the metal one atom has many more neighbors than in the Li_2 molecule. As a result, the binding energy per gram atom of lithium (i.e., per $6.92\ \mathrm{g}$ of lithium) is $163\ \mathrm{kJ}$ for the metal lattice, but only $56\ \mathrm{kJ}$ for one mole of molecule.

> The possibility of hybridization (first advanced by L. Pauling to explain metallic bonding) is also a likely factor for the formation of metallic bonds. Thus strong bonds can be formed when the valence electron clouds become concentrated along the direction in which the bonding partners are situated. According to Pauling the situation can be described by *mesomeric* limiting formulae, just as in the theory of unsaturated carbon compounds. One reason given for hydrogen not forming a metal is its inability to hybridize.

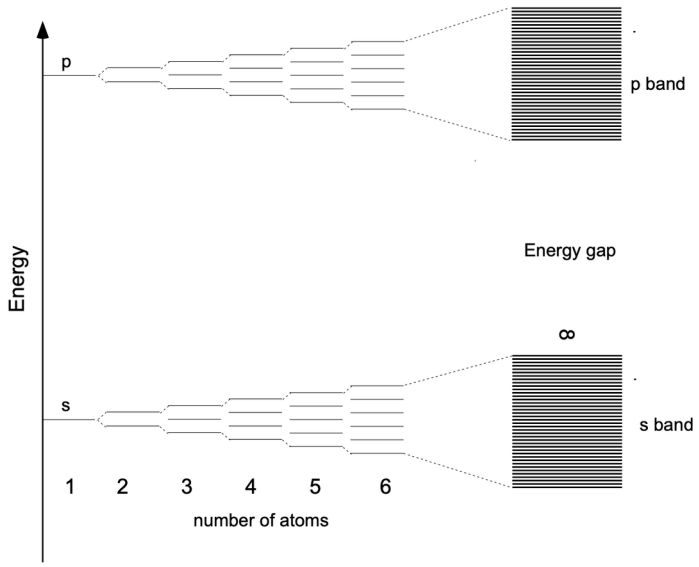


Figure 4 Formation of energy bands from energy levels of constituent atoms

The appearance of bands of allowed electron energies relates to the overlap of electron ψ functions. The width of each energy band is a function of the crystal structure because it determines the number of nearest neighbors in the crystal. Different metal atoms with the same valence, particularly elements in the same group of the periodic table, can often replace each other in arbitrary proportions without altering either the lattice type or the structure of the energy bands. This explains why such metals tend to form a complete series of *solid solutions*. Metallic alloys consist of such solid solutions or of heterogeneous mixtures of such solutions. Within certain limits, even metal atoms of different valence can be interchanged in a lattice.

Structure of Metals

According to the above considerations the band structure of Li metal can be represented as shown in fig. 5. According to previous reasoning, the $2\ \mathrm{s}$ band has N states ($\mathrm{N}=$ number of atoms) and accommodates $n2s$ electrons (where n is the number of electrons per atom in the $2\ \mathrm{s}$ state times N). Thus, this band has only half of the states filled since each state can accommodate two electrons of opposite spin (Pauli exclusion principle). In accordance with the Aufbau principle, the lowest energy states of the band are filled first and the upper states remain empty - but can readily be occupied by electrons upon thermal excitation or the application of an electric field. Since the width of the energy band is of the order of a few volts, spacings of states within the band are of the order of $\sim 10^{-20}\mathrm{eV}\left(1\mathrm{eV}=1.6\times10^{-19}\ \mathrm{J}\right)$, electrons can readily acquire the energy necessary to move into excited states, be accelerated, and move through the metal as *conducting electrons*. Partly filled bands thus constitute *conduction bands*.

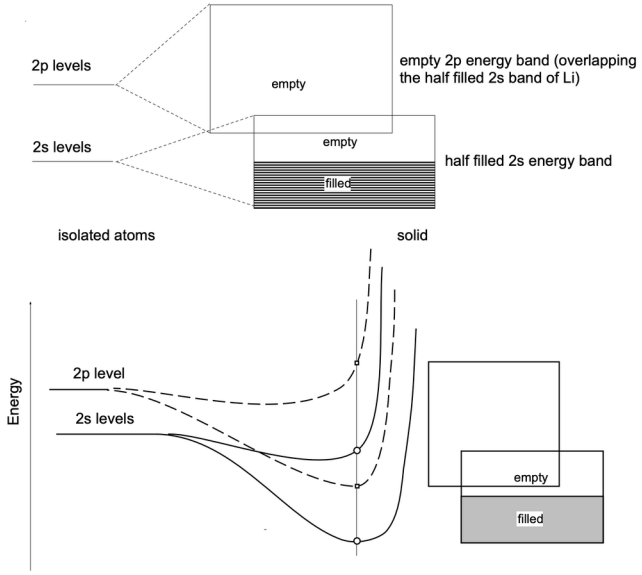


Fig. 5 Schematic energy band configuration for Li .

The conduction mechanism in Mg, for example, appears complicated by the fact that each $3s$ state of the valence shell in the atoms is doubly occupied $(3s^2)$. Thus the $3s$ band must be filled completely and no electronic conduction would in principle be expected. Electronic conduction, however, is observed because of a partial overlap of the $3s$ and the empty $3p$ bands. With this overlap, electrons can be activated into empty $3p$ states and exhibit conduction, as in the partly filled s band in Li.

Structure of Insulators and Semiconductors (Molecular Crystals)

The same band model can also account for the lack of conductivity in covalent crystals, such as diamond. In the diamond crystal, with a two-electron bond between every atom and each of its neighbors, the bonding molecular orbitals form a band at much lower energies than the energy of the atomic sp^3 hybrid orbitals, and the antibonding orbitals form a band at energies much higher than the energy of the atomic orbitals. Also, since each atom contributes four orbitals and four electrons, there are just enough electrons to fill the bonding orbitals (corresponding to an electron pair bond joining every atom to each of its neighbors) and the only vacant orbitals are those in the high energy band of antibonding orbitals (see fig. 6).

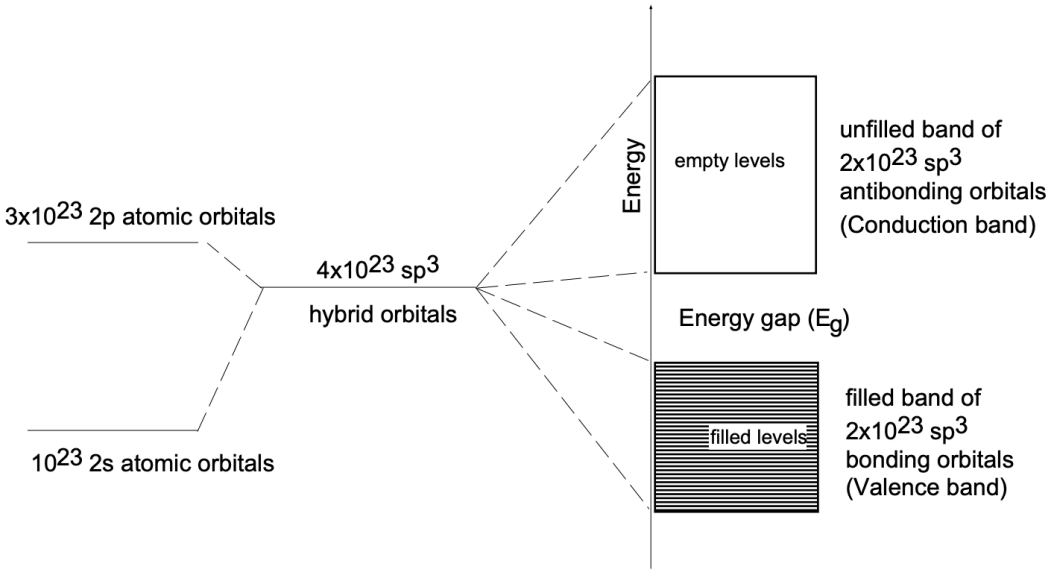


Fig. 6 Band structure of insulators and semiconductors (molecular crystals); the conditions depicted reflect a molar crystal of carbon (diamond).

Both insulators and semiconductors have the same basic band structure — the primary difference is the *width* of the forbidden energy gap $(\mathrm{E_g})$ between the valence and the conduction band.

Insulators, generically, are materials with very high resistivity (see Table I), comprising glasses, polymers, refractories, composites, liquids and gases. In the present context, an insulator is a molecular crystal, such as diamond (C) or sapphire, with a band gap (E_g) in excess of $4\mathrm{eV}$ (arbitrary value). Generally such materials will not conduct electricity since their valence band is filled and the energy required to transfer electrons from the valence band to the empty conduction band is far in excess of both the thermal energies at room temperature and the energy provided by radiation of the visible spectrum ($2\mathrm{eV}$). Therefore, insulators (in single crystal form) are normally transparent (colorless); however, if light is excessively or totally scattered at internal heterogeneities (such as grain boundaries), they may be translucent and even opaque. It should also be recognized that impurities $\left(\mathrm{Cr}^{3+}\right.$ in $\left.\mathrm{Al_2O_3}\right)$ or particular point defects (color centers) may impart a color to the transparent insulator crystals. The color arises because of partial absorption of white light and selective transmission of the other portions of the visible spectrum.

Semiconductors: The conventional semiconductors, silicon (Si) and germanium (Ge), have a band gap $(\mathrm{E_g})$ of 1.1 and $0.7\mathrm{eV}$ respectively and therefore absorb visible radiation; they are opaque (fig. 7). Considering the statistical nature of the thermal energy distribution in the solid matrix (Maxwell-Boltzmann), a significant number of electrons in the valence band will, at room temperature, acquire sufficient energy to cross the existing energy gap and thus provide for *semiconductivity*. The conductivity will therefore increase with temperature, contrary to metallic systems, until electron scattering effects, due to increased lattice vibrations (which decrease the mobility of electrons), begin to dominate.

The value of semiconductors for solid state device fabrication lies in the fact that the number and type of conducting electric charge carriers [electrons are n-type (negative), holes are p-type (positive)] can be controlled through incorporation of appropriate *dopant elements*. Thus the substitutional incorporation of Group V elements (Sb, As, P) provides for shallow donor levels in the band gap at about $0.01\mathrm{eV}$ from the conduction band. The substitutional incorporation of Group III elements (B, Al) generates *acceptor levels* in the band gap at about $0.01\mathrm{eV}$ from the valence band. The two types of impurities are almost completely ionized at room temperature and give rise to *extrinsic* n-type and p-type conductivity – the basis for the formation of *junction devices* such as diodes and transistors (fig. 8).

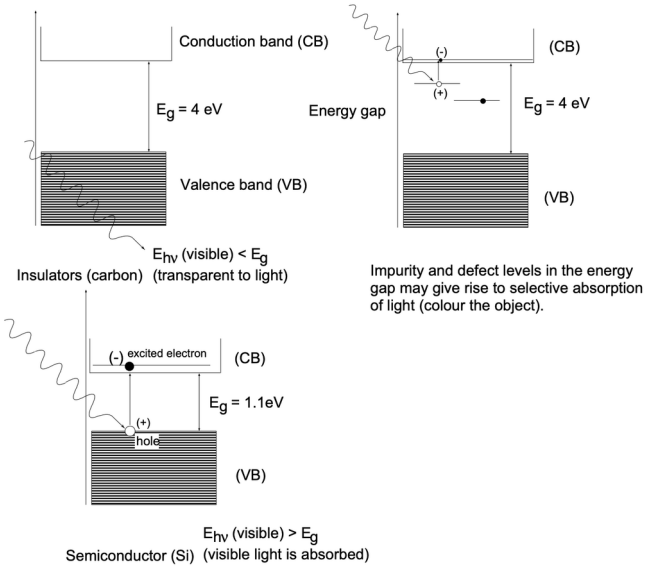


Fig. 7 Optical behavior of insulators and semiconductors

Of increasing importance are compound *III-V (adamantine) semiconductors*, such as GaAs, InSb, InP and GaP (compounds of Group III and Group V elements). Together these compounds provide eight valence electrons and, by sp^3 hybridization, are able to form a diamond-like, covalent crystal structure with semiconductor properties. These

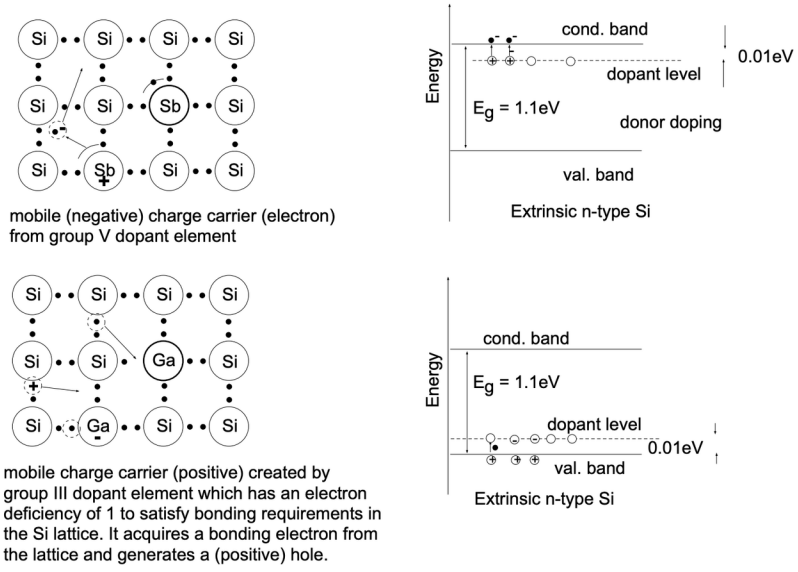


Fig. 8 Extrinsic p- and n-type semiconductors.

compounds (GaAs, for example) exhibit electron mobilities which are higher than those of silicon and, therefore, are of considerable interest for advanced device technology.

Table I. ELECTRICAL RESISTIVITIES OF METALS AND NONMETALS AT $20^{\circ}C$*

Metals	Resistivity, 10^{-8} ohm–m**	Nonmetals	Resistivity, ohm–m**
Silver	1.6	Semiconductors	
Copper	1.67	Silicon	1000.0
Gold	2.3	Germanium	0.09
Aluminum	2.69	Insulators	
Magnesium	4.4	Diamond	10^{10}–10^{11}
Sodium	4.61	Quartz	1.2×10^{12}
Tungsten	5.5	Ebonite	2×10^{13}
Zinc	5.92	Sulfur	4×10^{13}
Cobalt	6.24	Mica	9×10^{13}
Nickel	6.84	Selenium	2×10^{14}
Cadmium	7.4	Paraffin wax	3×10^{16}
Iron	9.71		
Tin	12.8		
Lead	20.6		
Uranium	29		
Zirconium	41		
Manganin	44		
Titanium	55		
Lanthanum	59		
96%Iron–4%Si	62		
Cerium	78		
Nichrome	100		

*From *American Institute of Physics Handbook*, Dwight E. Gray, ed. McGraw-Hill, New York (1963), pp. 4–90; 9–38.

**Note the different units in the two columns

APPENDIX

Approximate Energy Values for Some Events and Reactions

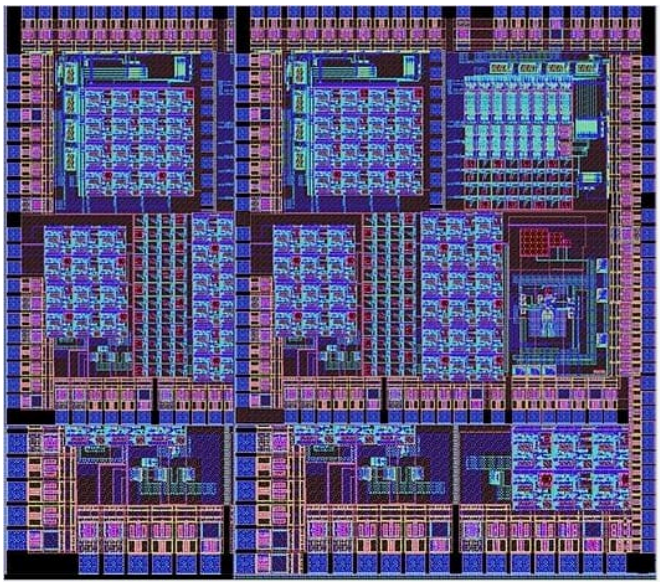
Solar Energy Emission	$\sim 10^{30}$ kJ/ day
Convertible Solar Energy on Earth	$\sim 10^{18}$ kJ/ year
Energy Consumption on Earth	$\sim 8 \times 10^{17}$ kJ/ year
Super-Nova Explosion	$\sim 10^{39}$ kJ
100 Mega-Ton H-Bomb Explosion	$\sim 10^{15}$ kJ
Atlas Blast-Off	$\sim 10^{8}$ kJ
Lethal X-Ray Dose	~ 1 kJ
25¢ Piece Falling from Pocket	$\sim 10^{-4}$ kJ
Bee's Wing Beat	$\sim 10^{-6}$ kJ
Moonlight/Face/Second	$\sim 10^{-8}$ kJ

This page titled 9.2: Bonding in Metals, Semiconductors and Insulators – Band Structure is shared under a CC BY-NC-SA 4.0 license and was authored, remixed, and/or curated by Donald Sadoway (MIT OpenCourseWare).

- 1.3: Bonding in Metals, Semiconductors and Insulators – Band Structure by Donald Sadoway is licensed CC BY-NC-SA 4.0. Original source: https://ocw.mit.edu/courses/3-091sc-introduction-to-solid-state-chemistry-fall-2010/pages/syllabus/.

9.2.1: Prelude to Electronic Properties of Materials - Superconductors and Semiconductors

In Chapter 6 we developed an energy band picture for metals, starting from atomic orbitals and building up the molecular orbitals of the solid metallic crystal. This treatment gave us a useful picture of how electrons behave in metals, moving at very fast speed between scattering events, and migrating in an electric field at a slow drift velocity. It also taught us that a metal is something with a partially filled band, meaning that the Fermi level cuts through one of its bands of orbitals. An insulator or a semiconductor has a similar band picture, except that the bands are either completely full or completely empty. In this case the Fermi level lies in the gap between fully occupied and unoccupied bands. We will see in this chapter that the properties of semiconductors (along with their useful electronic applications) depend on the addition of small amounts of impurities ("dopants") that change the position of the Fermi level, resulting in conduction by electrons or "holes."



Modern integrated circuits contain billions of nanoscale transistors and diodes that are essential for logic and memory functions. Both kinds of devices rely on junctions between crystalline silicon regions that contain a few parts per million of boron or phosphorus impurities.

While the band picture works well for most crystalline materials, it does not tell us the whole story of conduction in solids. That is because the band model (like MO theory) is based on a *one-electron* model. This was an approximation we made at the very beginning of our discussion of MO theory: we used hydrogen-like (one-electron) solutions to the Schrödinger equation to give us the shapes of s, p, d, and f atomic orbitals. In a one-electron atom, these orbitals are degenerate within a given shell, and the energy differences between, e.g., 2s and 2p orbitals arise only when we consider the energy of an electron in the field of other electrons in the atom. Moving from atoms to molecules, we made linear combinations to generate one-electron molecular orbitals (and, in solids, one-electron energy bands). But as in multi-electron atoms, life is not so simple for real molecules and solids that contain many electrons. Electrons repel each other and so their movement in molecules and in solids is ***correlated***. While this effect is weak in a "good" metal such as sodium - where the wavefunctions are highly delocalized - it can be quite important in other materials such as transition metal oxides. Correlated electron effects give rise to **metal-insulator transitions** that are driven by small changes in temperature, pressure, or composition, as well as to **superconductivity** - the passage of current with zero resistance at low temperatures. In this chapter we will develop some simple models to understand these interesting and important electronic properties of solids.

This page titled 9.2.1: Prelude to Electronic Properties of Materials - Superconductors and Semiconductors is shared under a CC BY-SA 4.0 license and was authored, remixed, and/or curated by Chemistry 310 (Wikibook) via source content that was edited to the style and standards of the LibreTexts platform.

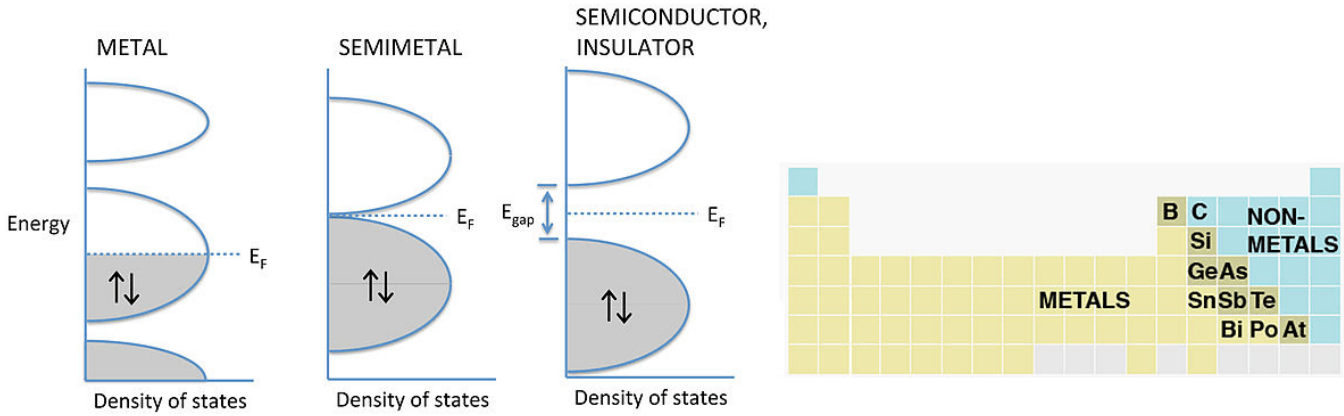
- 10.1: Prelude to Electronic Properties of Materials - Superconductors and Semiconductors by Chemistry 310 is licensed CC BY-SA 4.0. Original source: https://en.wikibooks.org/wiki/Introduction_to_Inorganic_Chemistry.

9.2.2: Periodic Trends- Metals, Semiconductors, and Insulators

As we consider periodic trends in the electronic properties of materials, it is important to review some of the key bonding trends we have learned in earlier chapters:

- Going down the periodic table, atoms in solids tend to adopt structures with higher coordination numbers.
- The second row of the periodic table is special, with strong s-p hybridization and π-bonding between atoms.
- Electrons in higher quantum shells are less strongly bound, so the energy difference between bonding and antibonding orbitals becomes smaller for heavier atoms.

We also know that most of the elements in the periodic table are metals, but the elements in the top right corner are insulating under ordinary conditions (1 atm. pressure) and tend to obey the octet rule in their compounds.



At the transition between metals and non-metals in the periodic table we encounter a crossover in electronic properties, as well as in other properties such as the acidity of the oxides (see Ch. 3). The group of elements at the border is loosely referred to as the metalloids. Several of these elements (such as C, Sn, and As) can exist as different allotropes that can be metals, insulators, or something in between.

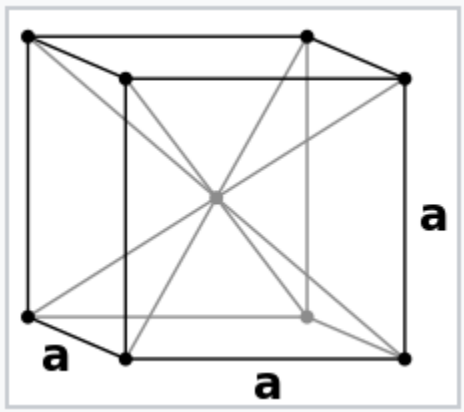
A more rigorous delineation of the electronic properties of these elements (and of many compounds) can be made by considering their band structures and the **temperature dependence of the electronic conductivity**. As we have previously discussed, metals have partially filled energy bands, meaning that the Fermi level intersects a partially filled band. With increasing temperature, metals become poorer conductors because lattice vibrations (which are called phonons in the physics literature) scatter the mobile valence electrons. In contrast, semiconductors and insulators, which have filled and empty bands, become better conductors at higher temperature, since some electrons are thermally excited to the lowest empty band. The distinction between insulators and semiconductors is arbitrary, and from the point of view of metal-insulator transitions, all semiconductors are insulators. We typically call an insulator a semiconductor if its band gap (E_{gap}) is less than about 3 eV. A semimetal is a material that has a band gap near zero, examples being single sheets of sp^2-bonded carbon (graphene) and elemental Bi. Like a narrow gap semiconductor, a semimetal has higher conductivity at higher temperature.

This page titled 9.2.2: Periodic Trends- Metals, Semiconductors, and Insulators is shared under a CC BY-SA 4.0 license and was authored, remixed, and/or curated by Chemistry 310 (Wikibook) via source content that was edited to the style and standards of the LibreTexts platform.

- 10.4: Periodic Trends- Metals, Semiconductors, and Insulators by Chemistry 310 is licensed CC BY-SA 4.0. Original source: https://en.wikibooks.org/wiki/Introduction_to_Inorganic_Chemistry.

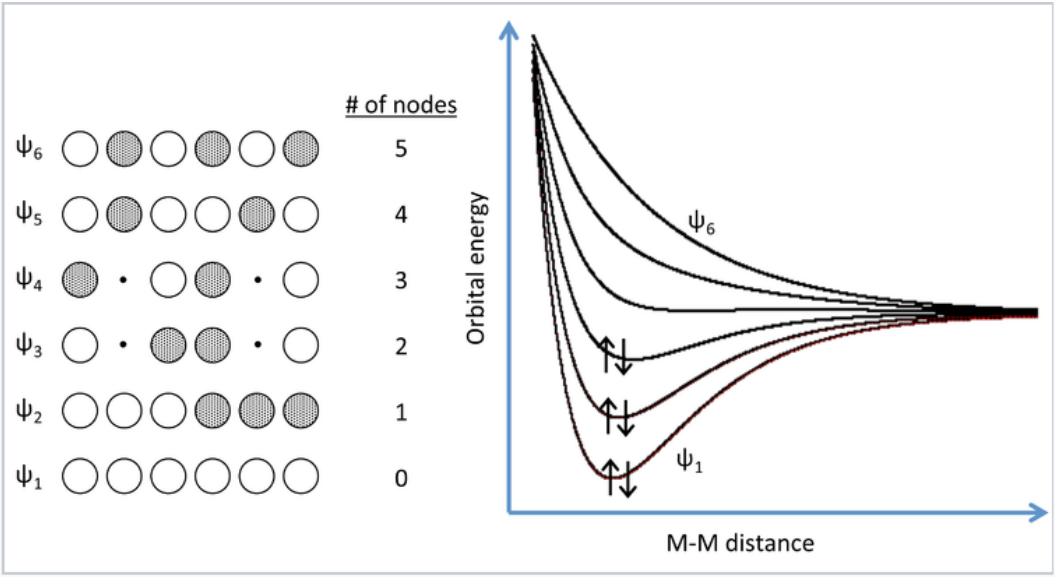
9.2.3: Bonding in Metals

The electron pair description of chemical bonds, which was the basis of the octet rule for p-block compounds, breaks down for metals. This is illustrated well by Na metal, the structure of which is shown at the left. Na has too few valence electrons to make electron pair bonds between each pair of atoms. We could think of the Na unit cell as having eight no-bond resonance structures in which only one Na-Na bond per cell contains a pair of electrons.



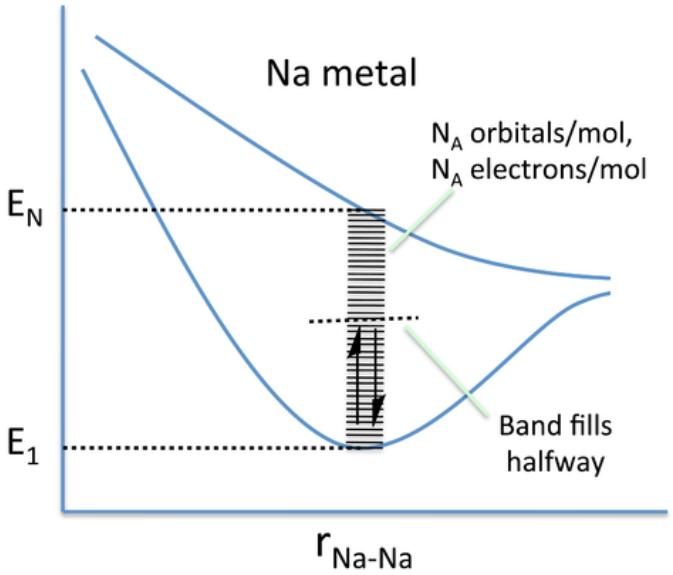
Sodium metal crystallizes in the body-centered cubic structure, in which each atom has eight nearest neighbors. Since the electronic configuration of Na is $[Ar]3s^1$, there are only two valence electrons per unit cell that are shared among eight Na-Na bonds. This means that the Na-Na bond order is 1/8 in Na metal.

A more realistic way to describe the bonding in metals is through **band theory**. The evolution of energy bands in solids from simple MO theory (Chapter 2) is illustrated at the right for a chain of six Na atoms, each of which has one 3s valence orbital and contributes one valence electron. In general, **n** atomic orbitals (in this case the six Na 3s orbitals) will generate **n** molecular orbitals with **n-1** possible nodes. In Chapter 2, we showed that the energy versus internuclear distance graph for a two hydrogen atom system has a low energy level and a high energy level corresponding to the bonding and antibonding molecular orbitals, respectively. These two energy levels were well separated from each other, and the two electrons in H_2 energetically prefer the lower energy level. If more atoms are introduced to the system, there will be a number of additional levels between the lowest and highest energy levels.



MO picture for a linear chain of six Na atoms. Three of the six MOs can accommodate all six valence electrons. Adding more atoms to the chain makes more molecular orbitals of intermediate energy, which eventually merge into a continuous band of orbitals. For Na, the 3s band is always half-filled because each MO can accommodate two electrons.

In band theory, the atom chain is extrapolated to a very large number - on the order of 10^{22} atoms in a crystal - so that the different combinations of bonding and anti-bonding orbitals create "bands" of possible energy states for the metal. In the language of physics, this approach of building the bands from discrete atomic orbitals is called the "tight-binding" approximation. The number of atoms is so large that the energies can be thought of as a continuum rather than a series of distinct levels. A metal will only partially fill this band, as there are fewer valence electrons than there are energy states to fill. In the case of Na metal, this results in a half-filled 3s band.



Nearly free electron model

In metals, the valence electrons are delocalized over many atoms. The total energy of each electron is given by the sum of its kinetic and potential energy:

$$E = KE + PE$$

$$E \approx p^2/2m + V$$

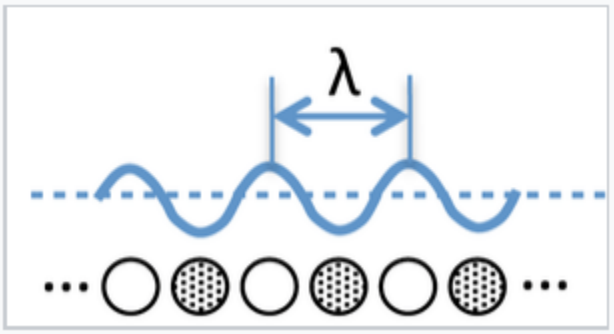
where **p** is the momentum of the electron (a vector quantity), m is its mass, and V is an average potential that the electron feels from the positive cores of the atoms. This potential holds the valence electrons in the crystal but, in the free electron model, is essentially uniform across the crystal.

Electron wavelength and wavenumber

What are the consequences of this model for band theory? For a hypothetical infinite chain (i.e., a 1D crystal) of Na atoms, the molecular orbitals at the bottom of the 3s band are fully bonding and the *wavelength* of electrons (2x the distance between nodes) in these orbitals is very long. At the top of the band, the highest orbital is fully antibonding and the wavelength is 2 times the distance between atoms (2a), since there is one node per atom. Remember that the **wavelength of an electron (λ)** is inversely proportional to its momentum p, according to the de Broglie relation **λ = h/p**.

For a (nearly) free electron, the kinetic energy can be expressed in terms of its wavelength, using $KE = p^2/2m$ and the de Broglie relation:

$$KE = \frac{p^2}{2m} = \frac{h^2}{2m\lambda^2} \tag{9.2.3.1}$$



We can think of the wavelength of an electron in a molecular orbital as twice the distance between nodes. If there are N atoms in a linear chain, the wavelength of the nth orbital is given by λ = 2Na/n, where a is the distance between atoms.

At this point, it is convenient to define the **wavenumber** of the electron as **k**, which has units of inverse length and is inversely proportional to λ. **k** is also directly proportional to the momentum **p**. Like **p**, **k** is a vector quantity. In a 1D crystal, **k** can be either positive or negative, corresponding to an electron moving to the left or right along the chain.

$$k = \frac{2\pi}{\lambda} = \frac{2\pi p}{h} \text{ where h is Planck's constant} \tag{9.2.3.2}$$

The most important property of **k** is that it is *directly proportional to the number of nodes* **n** in a molecular orbital within the band. For a 1D crystal of sodium atoms that contains **N** unit cells, each separated by a distance a, a molecular orbital with n nodes has a wavelength λ = 2Na/n and the wavenumber k = πn/Na. We can see from this definition that k = 0 at the bottom of the band (where λ is infinite) and k = π/a at the top of the band where the MO contains **N** nodes and λ = 2a.

Energies of orbitals in a metallic crystal

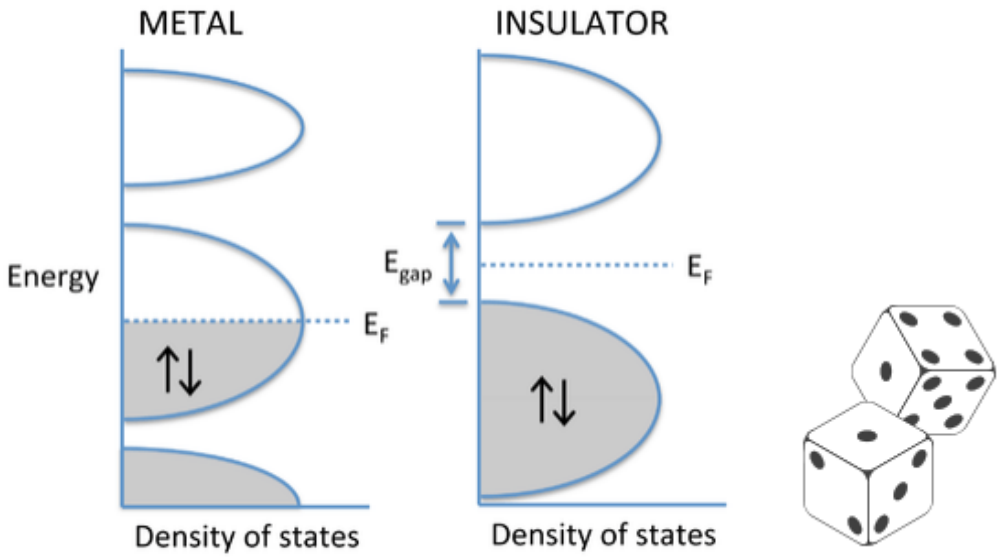
Electrons with long wavelengths do not "feel" the individual atoms in the lattice and so they behave as if they are *nearly free* (but confined to the crystal). Near the bottom of the band, the electron energy increases *parabolically* with the number of nodes ($KE \propto \mathbf{n}^2$), since the momentum **p** is directly proportional to **n**. Because **p** is also directly proportional to **k**, we can write:

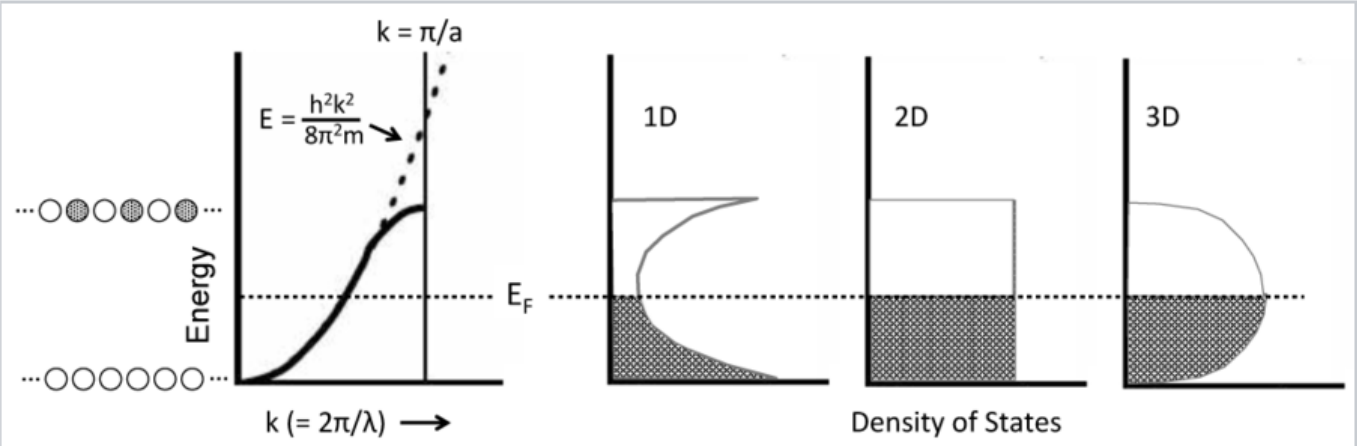
$$KE = \frac{p^2}{2m} = \frac{h^2k^2}{8\pi^2 m} \tag{9.2.3.3}$$

This parabolic relationship is followed as long as the electron wavelength is long compared to the distance between atoms. Near the top of the band, the wavelength becomes shorter and the electrons start to feel the positively charged atomic cores. In particular, the electrons prefer to have the maxima in their wavefunctions line up with the atomic cores, which is the most electrostatically favorable situation. The electron-atom attraction lowers the energy and causes the E vs. k curve to deviate from the parabolic behavior of a "free" electron as shown in the figure below.

Density of States (DOS)

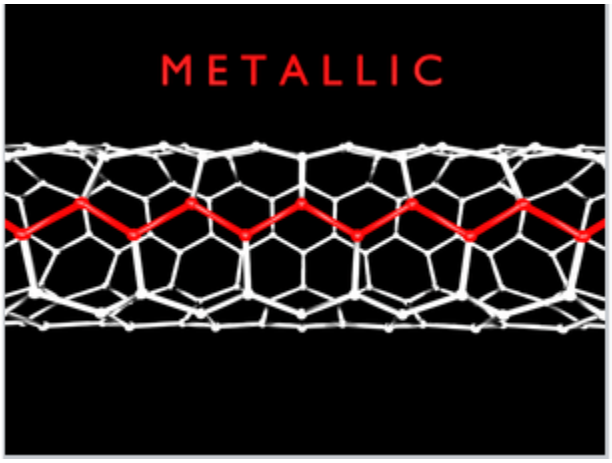
The density of states is defined as the number of orbitals per unit of energy within a band. Because of the parabolic relation between E and k, the density of states for a 1D metallic crystal is highest near the bottom and top of the energy band where the slope of the E vs. k curve is closest to zero. The shape of the DOS curve is different in crystals of higher dimensionality as shown in the figure in the left, because statistically there are more ways to make an orbital with N/2 nodes than there are with zero or N nodes. The situtation is analogous to the numbers you can make by rolling dice. With one die, the numbers 1-6 have equal probability. However, with two dice there is only one way to make a two (snake eyes) or a twelve (boxcars), but many ways to make a seven (a winner!).





Electrons in metals follow a parabolic dispersion curve, where the energy increases with the square of the wavenumber, k. Near the top of the band, the dispersion curve deviates from the parabolic dotted line. Because there is one MO for each value of k, the number of orbitals per unit energy (the density of states, DOS) is highest at the bottom and top of the band for a 1D chain of atoms. The density of states is constant with energy for a 2D crystal, and has a maximum in the middle of the band for a 3D crystal. At low temperature, all the MOs below the Fermi level E_F are occupied, and all the MOs above it are empty.

While most of the time we will talk about 3D crystals that have their maximum DOS near the middle of the energy band, there are examples of quasi-1D systems, such as carbon nanotubes. Metallic carbon nanotubes have strong optical absorption bands that correspond to transitions between the two regions of high DOS (the van Hove singularities) near the bottom and top of the bands.



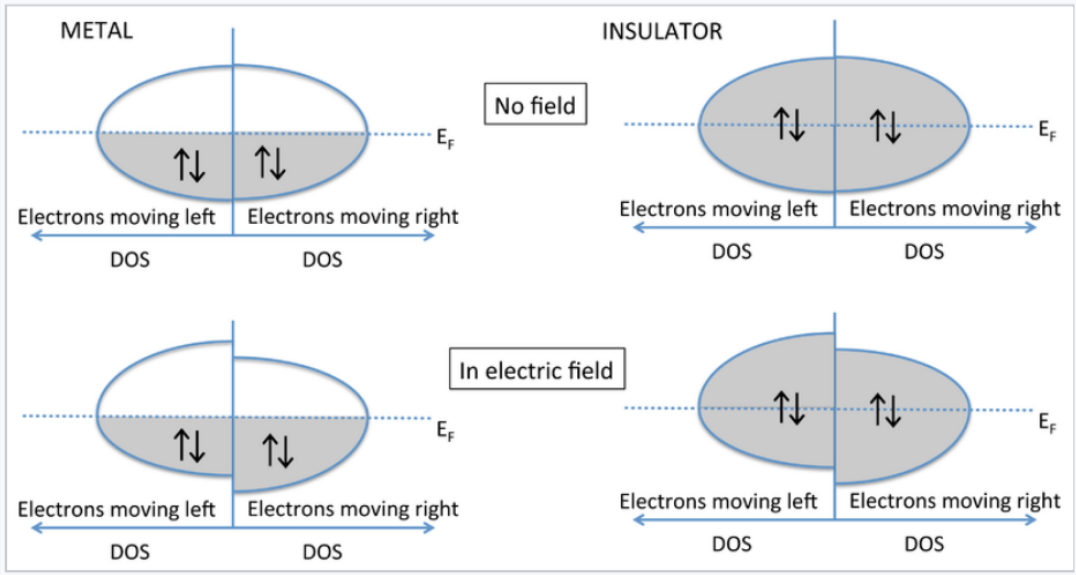
Single-walled carbon nanotubes with "armchair" chirality are metallic and have characteristic sharp absorption bands in the infrared. Prof. Millie Dresselhaus (below) did foundational research on the electronic properties of carbon nanotubes and other low-dimensional conductors.



Metals, semiconductors, and insulators

The degree to which bands fill determines whether a crystalline solid is a metal, semiconductor, or insulator. If the highest occupied molecular orbitals lie within a band - i.e., if the Fermi level E_F cuts through a band of orbitals - then the electrons are free to change their speed and direction in an electric field and the solid is metallic. However, if the solid contains just enough electrons to completely fill a band, and the next highest set of molecular orbitals is empty, then it is a semiconductor or insulator. In this case, there is an energy gap between the filled and empty bands, which are called the valence and conduction bands, respectively. Although the distinction is somewhat arbitrary, materials with a large gap (> 3 eV) are called insulators, and those with smaller gaps are called semiconductors. We will learn more about the properties of semiconductors in Chapter 10.

Why don't insulators conduct electricity? The energy vs. DOS diagram below shows what happens when an electric field is applied to a metal or an insulator. In this case we have changed the diagram to show explicitly the energies of electrons moving left and right. These energies are the same in the absence of an electric field. Once we apply a field (e.g., by putting a voltage across a metal wire), the electrons moving in the direction of the field have lower energy than those moving in the opposite direction. In the case of the metal, the populations of electrons moving with and against the electric field are different, and there is a net flow of current. Note that this can happen only when the Fermi level cuts through a partially filled band. With a semiconductor or insulator, the valence band is filled and the conduction band is empty. Applying an electric field changes the energies of electrons traveling with and against the field, but because the band is filled, the same number are going in both directions and there is no net current flow.



E vs. DOS diagrams comparing the behavior of metals and insulators in an applied electric field.

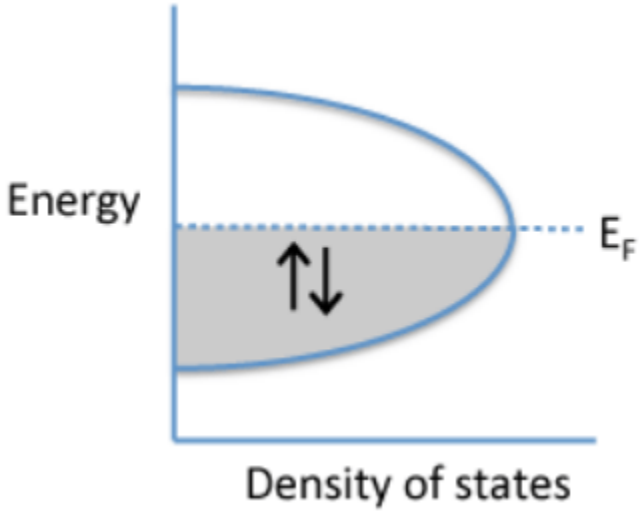
Note that in this picture, all the molecular orbitals extend over the entire crystal. The valence electrons are *delocalized,* even in the case of a semiconductor or insulator. However, there can be no net movement of electrons unless the band is partially filled.

This page titled 9.2.3: Bonding in Metals is shared under a CC BY-SA 4.0 license and was authored, remixed, and/or curated by Chemistry 310 (Wikibook) via source content that was edited to the style and standards of the LibreTexts platform.

- 6.5: Bonding in Metals by Chemistry 310 is licensed CC BY-SA 4.0. Original source: https://en.wikibooks.org/wiki/Introduction_to_Inorganic_Chemistry.

9.2.4: Conduction in Metals

In metals, the valence electrons are in molecular orbitals that extend over the entire crystal lattice. As we will learn in Chapter 7, metals are almost always crystalline and the individual crystal grains are typically micron size. This means that the spatial extent of the orbitals is *very large* compared to the size of the atoms or the unit cell. The diagram at the left shows a generic plot of electron energy vs. density of states for a metal such as Na, Cu, or Ag. In these cases, there are N orbitals for N electrons, and each orbital can accommodate two electrons. Therefore the Fermi level, which corresponds to the energy of the highest occupied MO at zero temperature, is somewhere in the middle of the band of orbitals. The energy level spacing between orbitals is very small compared to the thermal energy kT, so we can think of the orbitals as forming a continuous band.



Classically, if the electrons in this band were free to be thermally excited, we would expect them to have a specific heat of 3R per mole of electrons. However, experimentally we observe that C_p is only about 0.02 R per mole. This suggests that *only about 1%* of the electrons in the metal can be thermally excited at room temperature. However, essentially *all* of the valence electrons are free to move in the crystal and contribute to electrical conduction. To understand this apparent paradox, we need to recall that the electrons exist in *quantized energy levels*.

Because of quantization, electrons in metals have a Fermi-Dirac distribution of energies. In this distribution, most of the electrons are spin-paired, although the individual electrons in these pairs can be quite far apart since the orbitals extend over the entire crystal. A relatively small number of electrons at the top of the Fermi sea are unpaired by thermal excitation. This is the origin of the Pauli paramagnetism of metals.

How fast are electrons traveling in a typical metal? Because of the bell shape of the E vs. DOS curve, most of the electrons have $E \approx E_F$. At the midpoint energy (E_F) of the band, the MO's have one node for every two atoms. We can calculate the de Broglie wavelength as twice the distance between nodes and thus:

> **λ = 4a** at the midpoint of the band.

where **a** is the interatomic spacing. Since a typical value of **a** is about 2 Å, we obtain the **de Broglie wavelength λ ≈ 8 Å**.

Using the de Broglie relation $p = h/\lambda$, we can write:

$$\mathbf{p = \frac{h}{\lambda} = m_e v_F} \tag{9.2.4.1}$$

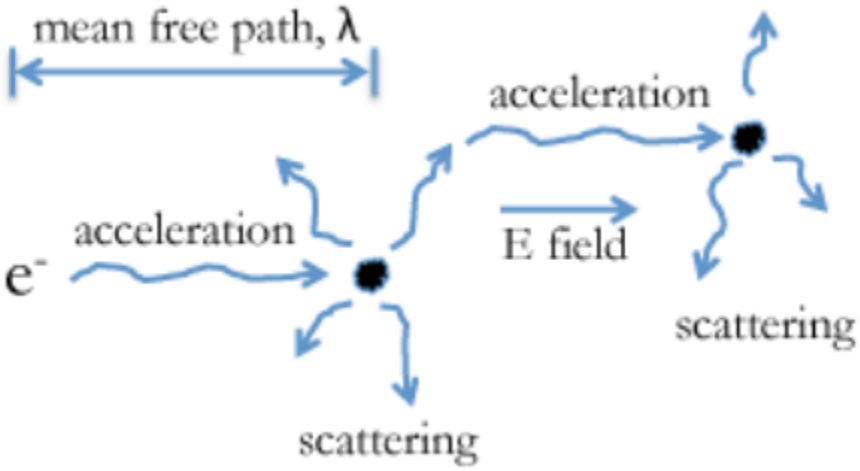
where $\mathbf{m_e}$ is the mass of the electron and $\mathbf{v_F}$ is the velocity of electrons with energy E_F.

Solving for $V_F = \frac{h}{m_e \lambda}$ we obtain $\mathbf{v_F} = \frac{(6.62\times10^{-34} Js)}{(9.1\times10^{-31} kg)(8\times10^{-10} m)} = \mathbf{1.0 \times 10^6 m/s}$

Experimental values of v_F are 1.07 x 10^6 and 1.39 x 10^6 m/s for Na and Ag, respectively, so our approximations are pretty good.

How fast are electrons moving in metals? Really, really fast!! **1,000,000 meters per second!** This is about 1/300 the speed of light, and about 3000 times the speed of sound in air (3 x 10^2 m/s).

However, the **drift velocity** of electrons in metals - the speed at which electrons move in applied electric field - is quite slow, on the order of 0.0001 m/s, or .01 cm/s. You can easily outrun an electron drifting in a metal, even if you have been drinking all night and have been personally reduced to a very slow crawl.



In order to understand the great disparity between the Fermi velocity and the drift velocity of electrons in metals, we need to consider a picture for the scattering of electrons, and their acceleration in an electric field, as shown at the left. If we apply a voltage across a metal (e.g., a metal wire), the electrons are subjected to an electric field **E**, which is the voltage divided by the length of the wire. This electric field exerts a force on the electron, causing it to accelerate. However, the electron is frequently scattered, mostly by phonons (lattice vibrations). Each time the electron is scattered its acceleration starts all over again. The time between scattering events is **τ** and the distance the electrons travel between scattering events is the **mean free path**, **λ**. (Note that this is NOT the same λ as the de Broglie wavelength, they just unfortunately have the same symbol!)

We can write the force on the electron as:

$$\mathbf{F} = \mathbf{eE} = \mathbf{m_e a} = \frac{\mathbf{m_e v_{drift}}}{\tau} \tag{9.2.4.2}$$

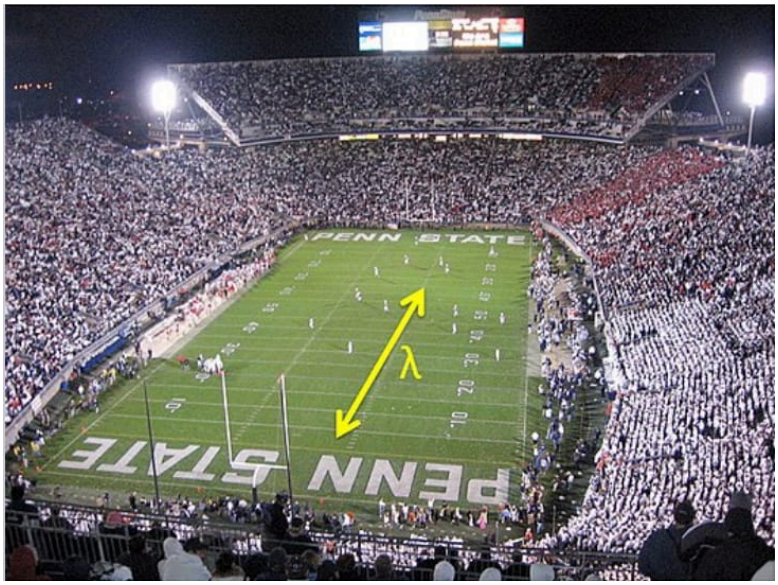
In this equation, **a** is the acceleration in the electric field, $\mathbf{m_e}$ is the mass, and v_{drift} is the **drift velocity** of the electron.

Experimentally, the mean free path is typically obtained by measuring the scattering time. For an electron in Cu metal at 300 K, the scattering time τ is about 2 x 10^{-14} s. From this we can calculate the mean free path as:

$$\lambda = \mathbf{v_{avg}}\tau \approx \mathbf{v_F}\tau = (1 \times 10^6 m/s)(2 \times 10^{-14}) = \mathbf{40nm} \tag{9.2.4.3}$$

The mean free path (40 nm = 400 Å) is quite long compared to the interatomic spacing (2 Å). To put it in perspective, if the interatomic spacing were scaled to the length of a football (0.3 m), the mean free path would be over half the length of the football field (60 m). Thus an electron travels a fairly long way between scattering events and scarcely notices the atomic structure of the metal in which it is traveling.

To summarize, electrons are traveling in metals at the Fermi velocity v_F, which is very, very fast (10^6 m/s), but the flux of electrons is the same in all directions. That is, they are *going nowhere fast*. In an electric field, a very small but directional *drift velocity* is superimposed on this fast random motion of valence electrons.



For ordinary metals, the mean free path of a valence electron (λ) is quite long relative to the interatomic spacing, represented in this analogy as the length of a football.

We can calculate the drift velocity of electrons as the acceleration in the electric field times the scattering time:

From F = ma, we obtain the acceleration (a) as:

$$\mathbf{a} = \frac{\mathbf{F}}{\mathbf{m_e}} = \frac{\mathbf{eE}}{\mathbf{m_e}} \tag{9.2.4.4}$$

And thus,

$$\mathbf{v_{drift}} = \mathbf{a}\tau = \frac{\mathbf{eE}\tau}{\mathbf{m_e}} \tag{9.2.4.5}$$

If we divide both sides of this equation by the magnitude of the electric field (**E**), we obtain the **mobility (μ)**:

$$\mu = \frac{\mathbf{v_{drift}}}{\mathbf{E}} = \frac{\mathbf{e}\tau}{\mathbf{m_e}} \tag{9.2.4.6}$$

μ has units of velocity/field = cm/s / V/cm = cm^2/Vs

An important consequence of the calculation of v_{drift} is **Ohm's Law**, V = iR. From the equations above, we can see that the drift velocity increases linearly with the applied electric field. The drift velocity (cm/s) is proportional to the current (i, coul/s), and the electric field (E, V/cm) is proportional to the voltage (V):

$$\mathbf{Current\ (i)} = \mathbf{nev_{drift}} \times \mathbf{area} \tag{9.2.4.7}$$

$$\mathbf{Voltage\ (V)} = \mathbf{E} \times \mathbf{length} \tag{9.2.4.8}$$

Here **n** is the density of valence electrons (#/cm^3) and **e** is the charge of the electron (coul). Combining these equations with our equation for v_{drift} we obtain:

$$V = i(\frac{m_e}{ne^2\tau})\frac{(}{length}area) = iR \tag{9.2.4.9}$$

Thus, V = iR, where R is the combination of the two terms in parentheses. The first of these is the **resistivity**, ρ, and the second is a geometrical factor.

The **conductivity (σ)** of a metal, which is the inverse of ρ, is proportional to μ, which in turn is proportional to τ (and λ):

$$\sigma = \mathrm{ne}\mu = \frac{\mathrm{ne}^2\tau}{\mathrm{m_e}} \tag{9.2.4.10}$$

We can use this equation to work out the conductivity of a specific metal (Cu), for which n = 8.5 x 10^{22} cm^{-3} and τ = 2 x 10^{-14} s. Putting in the numbers for m_e and e, we obtain σ = 7 x 10^5 Ω^{-1} cm^{-1} for Cu, in good agreement with the measured value (6 x 10^5 $\Omega^{-1}cm^{-1}$).

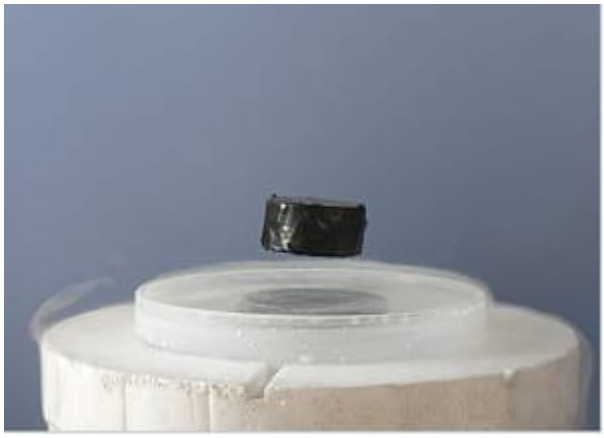
This page titled 9.2.4: Conduction in Metals is shared under a CC BY-SA 4.0 license and was authored, remixed, and/or curated by Chemistry 310 (Wikibook) via source content that was edited to the style and standards of the LibreTexts platform.

- 6.6: Conduction in Metals by Chemistry 310 is licensed CC BY-SA 4.0. Original source: https://en.wikibooks.org/wiki/Introduction_to_Inorganic_Chemistry.

9.2.5: Superconductors

Superconductivity refers to the flow of electrical current in a material with zero resistance. Such materials are very important for use in electromagnets, e.g., in magnetic resonance imaging (MRI) and nuclear magnetic resonance (NMR) machines, because once the current starts flowing in the coils of these magnets it doesn't stop. Magnetic levitation using superconductors - which, below a critical field strength, are perfect diamagnets that are not penetrated by magnetic flux lines - is also potentially relevant to future technologies such as magnetically levitated trains.

The phenomenon of superconductivity, first discovered in Hg metal in 1911 by Onnes, continues to be only partially understood. It is of great interest to physicists as a macroscopic quantum phenomenon, and to chemists and materials scientists who try to make better superconductors (especially those that superconduct at higher temperatures) and devices derived from them, such as superconducting quantum interference devices (SQUIDs), which are extremely sensitive magnetometers.

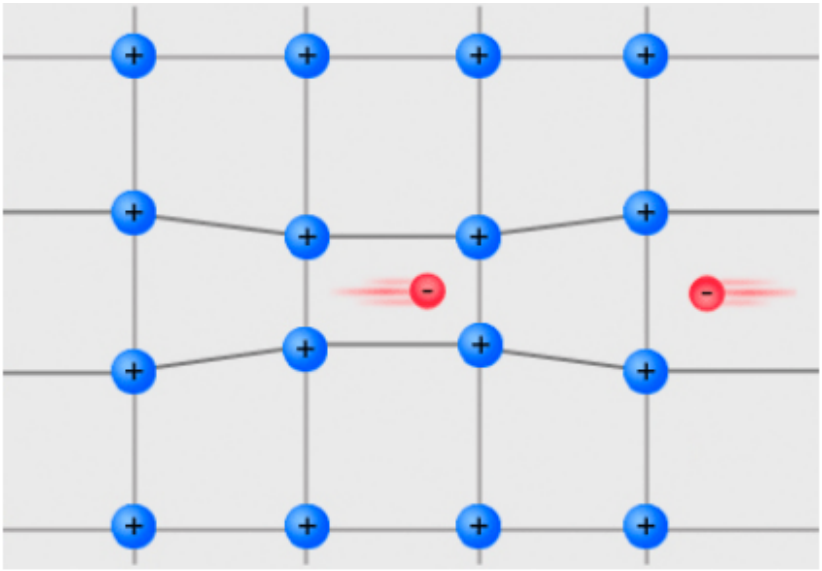


A magnet levitating above a high-temperature superconductor, cooled with liquid nitrogen. Persistent electric current flows on the surface of the superconductor, excluding the magnetic field of the magnet. This current effectively forms an electromagnet that repels the magnet.

Spin pairing and zero resistance

The transition from the metallic to the superconducting state is related to the quantum phenomena of Bose-Einstein condensation and superfluidity. Individual electrons have spin = 1/2, and as such are fermions (particles with half-integer spin). Because of the Pauli exclusion principle, no more than two fermions can occupy the same quantum state (such as an orbital in a molecule or a solid). The familiar consequence of this rule is the aufbau filling of orbitals with spin-paired electrons in each energy level. In contrast, particles with integer spins - which are called bosons - do not have this restriction, and any number of bosons can occupy the same quantized energy level.

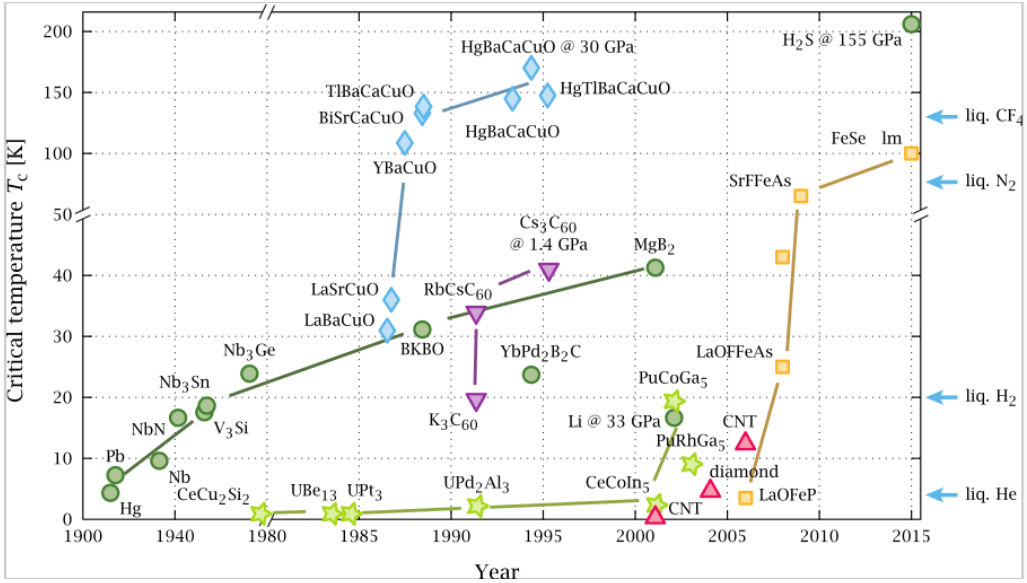
Superconductivity occurs when electrons spin pair into so-called Cooper pairs, which can travel through the lattice together. The electrons in a Cooper pair, although spin-paired, have a long-distance relationship: the spatial extent of a Cooper pair is a few nanometers in cuprate superconductors, and up to one micron in low T_c superconductors such as aluminum. Because its overall spin angular momentum is zero, a Cooper pair is a boson. When the temperature is low enough, the Cooper pairs "condense" into the lowest energy level. The second lowest energy level - which is typically a few meV above the ground state - is not accessible to them as long as the energy gap is larger than the thermal energy, kT. The scattering of electrons by the lattice then becomes forbidden by energy conservation because scattering dissipates energy, and the Cooper pairs cannot change their energy state. Thus the resistance (which arises from scattering, as we learned in Ch. 6) drops abruptly to zero below T_c. However, the Cooper pairs can be broken apart when they move fast, and thus superconductors turn back into normal metals (even below T_c) above some critical current density j_c. This phenomenon is also related to the critical magnetic field, H_c, that quenches superconductivity.



A trampoline for electrons

What causes electrons, which repel each other because of their negative charge, to pair up and travel together in superconductors? The mechanism - which must involve some kind of attractive interaction between electrons - is well understood for "conventional" superconductors which have relatively low transition temperatures, but is not yet known with certainty for high temperature oxide superconductors. In conventional, or BCS superconductors, the spin pairing is mediated by the lattice as shown in the figure at the left. A strong electron-lattice interaction causes a distortion in the lattice as an electron moves through. This elastic deformation is felt as an attractive force by a second electron moving in the opposite direction. This can be thought of as analogous to the interaction of two people jumping on a trampoline. The weight of the first person on the trampoline creates a "well" that attracts the second one, and they tend to move together (even if they don't like each other). Strange as this interaction seems, it is supported experimentally by isotope effects on T_c and by quantitative predictions of T_c values in conventional superconductors.

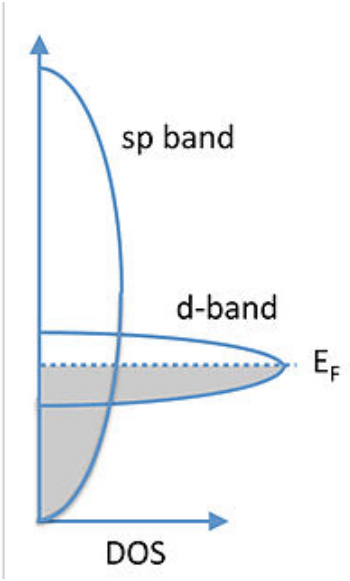
Bad metals make good superconductors. All superconductors are "normal" metals - with finite electrical resistance - above their critical transition temperature, T_c. If you ask where in the periodic table one might look for superconductors, the answer is surprising. The most conductive metals (Ag, Au, Cu, Cs, etc.) make the worst superconductors, i.e., they have the lowest superconducting transition temperatures, in many cases below 0.01 K. Conversely "bad" metals, such as niobium alloys, certain copper oxides, $K_xBa_{1-x}BiO_3$, MgB_2, FeSe, and alkali salts of C_{60}^{n-} anions, can have relatively high transition temperatures.



Timeline of superconducting materials, showing T_c vs. year of discovery.

We observe that most good superconductors appear in composition space very **near a metal-insulator transition**. In terms of our microscopic picture, orbital overlap in superconductors is poor, just barely enough to make them act as metals ($\Delta \approx U$) above T_c. In the normal state, superconductors with high T_c - which can be as high as 150 K - are typically "bad" metals. An important characteristic of such metals is that the **mean free path** of electrons (in the normal state, above T_c) is on the order of the lattice spacing, i.e., **only a few Å**. In contrast, we learned in Ch. 6 that good metals such as Au, Ag, and Cu have electron mean free paths that are two orders of magnitude longer (ca. 40 nm). In a bad metal, the electron "feels" the lattice rather strongly, whereas in a good metal, the electrons are insensitive to small changes in the distance between metals atoms.

What does the band picture look like for a bad metal? The key point is that because orbital overlap is poor, the metal has a **high density of states** at the Fermi level. This is a universal property of high temperature superconductors and provides a clue of where to look for new and improved superconducting materials. Recall that transition elements in the middle of the 3d series (Cr, Fe, Co, Ni) were magnetic because of poor orbital overlap and weak d-d bonding. The elements below these - especially Nb, Ta, and W - have just barely enough d-d orbital overlap to be on the metallic side of the metal-insulator transition and to be "bad" metals. Carbides and nitrides of these elements are typically superconducting, with the carbon and nitrogen atoms serving to adjust the valence electron density, as illustrated in the table below.



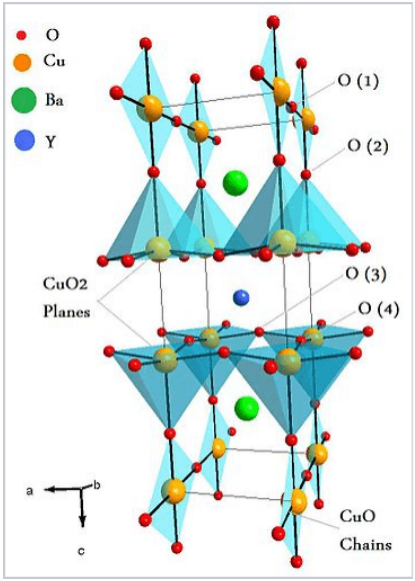
Generic E vs. DOS for a bad metal.

Compound	NbC	Mo_2N	TaC	VN	NbN	TaN	Nb_3Ge
T_c (K)	11.1	5.0	9.7	7.5	15.2	17.8	22.3

High T_c superconductors

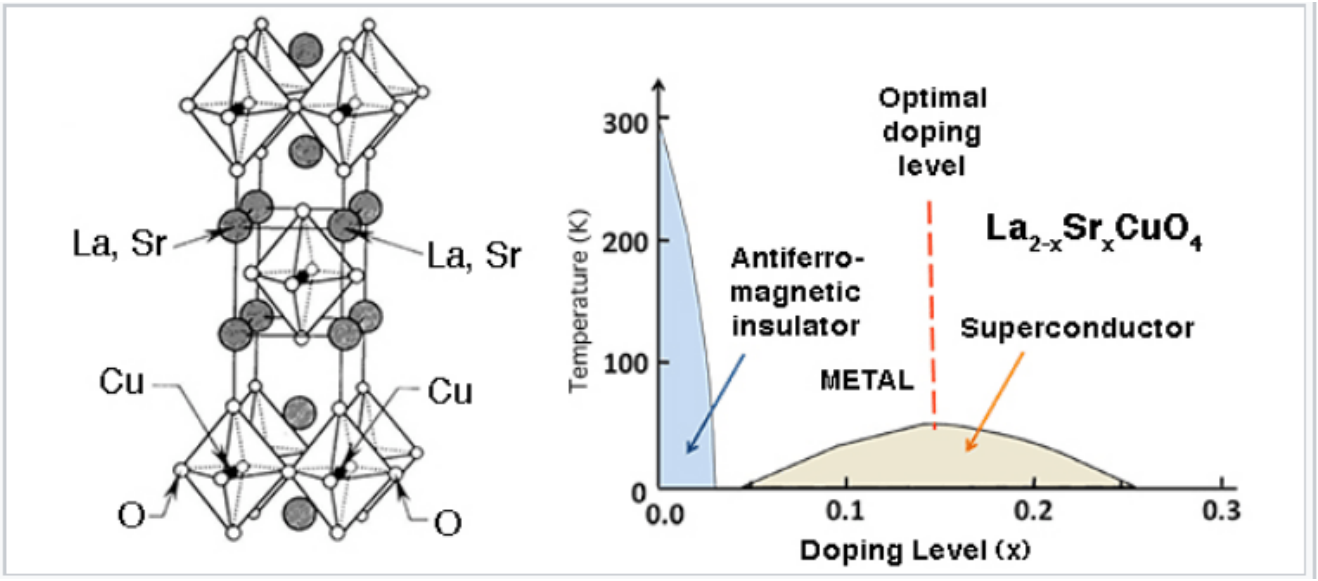
In addition to having weak orbital overlap in the metallic state - which results in a high DOS at E_F - high temperature superconductors also typically contain elements in mixed oxidation states (for example, $Cu^{2+/3+}$ or $Bi^{3+/5+}$) that are close in energy to the O^{2-}/O^- couple in the lattice. At ambient pressure, cuprate superconductors have the highest known T_c values, ranging between about 35 and 150 K. The crystal structures of these materials are almost all variants of the perovskite lattice, as shown at the right for the 1-2-3 superconductor $YBa_2Cu_3O_{7-\delta}$. An ideal perovskite lattice would have formula $ABO_3 = A_3B_3O_9$. In $YBa_2Cu_3O_{7-\delta}$, Y and Ba occupy the A cation sites, Cu occupies the B sites, and two of the nine O atoms are missing.

The $YBa_2Cu_3O_{7-\delta}$ lattice consists of mixed-valent copper(II/III) oxide sheets capped by oxygen atoms to form CuO_5 square pyramids. These sheets encapsulate the Y^{3+} cations. Copper(II) oxide ribbons that share the apical oxygen atoms of the square pyramids run in one direction through the structure. In $YBa_2Cu_3O_{7-\delta}$ and related materials, one component of the structure (here the Cu-O ribbons) acts as a **charge reservoir** to control the doping of the planar CuO_2 sheets, which are the elements of the structure that carry the supercurrent. Cuprate superconductors with Bi, Tl, or Hg-containing charge reservoir layers and multiple, eclipsed CuO_2 sheets in the unit cell tend to have the highest T_c values.



Crystal structure of $YBa_2Cu_3O_{7-\delta}$ (YBCO), the first superconductor with T_c above the boiling point of liquid nitrogen.

The connection between the metal-insulator transtion and superconductivity is nicely illustrated in the phase diagram of $La_{2-x}Sr_xCuO_4$, the first cuprate superconductor, which was discovered in 1986 by Georg Bednorz and K. Alex Müller. This compound has a rather simple structure in which rocksalt La(Sr)O layers are intergrown with perovskite $La(Sr)CuO_3$ layers. Undoped La_2CuO_4 contains only Cu^{2+} ions and is an antiferromagnetic insulator. As a small amount of Sr^{2+} is substituted for La^{3+}, some of the Cu^{2+} is oxidized to Cu^{3+}, and the lattice is doped with holes. As the doping level increases, the antiferromagnetic phase undergoes a first-order phase transition to a "bad" metal, and at slightly higher doping density the superconducting phase appears. The proximity of the superconducting phase to the metal-insulator transition is a hallmark of cuprate superconductors. A maximum T_c of 35K is observed at x = 0.15. Doping at higher levels moves the Fermi level beyond the point of highest DOS in the d-band of Cu and the superconducting phase then gradually disappears. It is interesting to compare this phase diagram with that of V_2O_3 (above), which also undergoes an antiferromagnetic insulator to "bad" metal transition as it is doped.



Crystal structure and phase diagram of the cuprate superconductor $La_{2-x}Sr_xCuO_4$. (LSCO)

This page titled 9.2.5: Superconductors is shared under a CC BY-SA 4.0 license and was authored, remixed, and/or curated by Chemistry 310 (Wikibook) via source content that was edited to the style and standards of the LibreTexts platform.

- 10.3: Superconductors by Chemistry 310 is licensed CC BY-SA 4.0. Original source: https://en.wikibooks.org/wiki/Introduction_to_Inorganic_Chemistry.

9.2.6: Semiconductors- Band Gaps, Colors, Conductivity and Doping

Semiconductors, as we noted above, are somewhat arbitrarily defined as insulators with **band gap energy ≤ 3.0 eV** (~290 kJ/mol). This cutoff is chosen because, as we will see, the conductivity of undoped semiconductors drops off exponentially with the band gap energy and at 3.0 eV it is very low. Also, materials with wider band gaps (e.g. $SrTiO_3$, E_{gap} = 3.2 eV) do not absorb light in the visible part of the spectrum

There are a number of places where we find semiconductors in the periodic table:

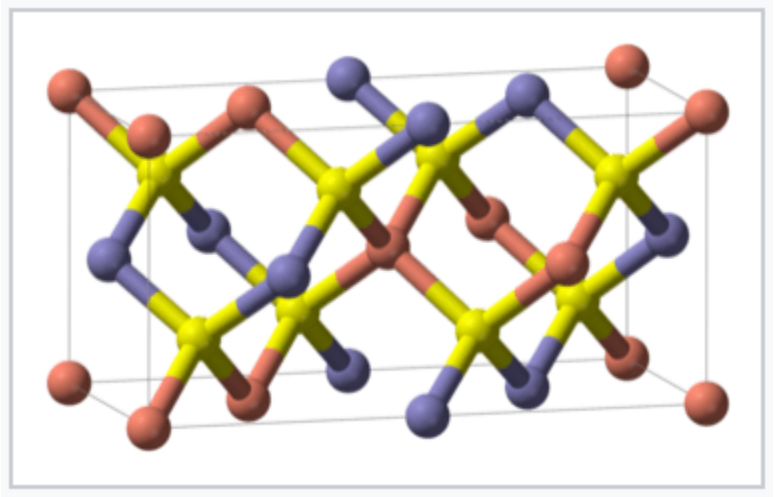
- Early transition metal oxides and nitrides, especially those with d^0 electron counts such as TiO_2, TaON, and WO_3
- Oxides of later 3d elements such as Fe_2O_3, NiO, and Cu_2O
- Layered transition metal chalcogenides with d^0, d^2 and d^6 electron counts including TiS_2, ZrS_2, MoS_2, WSe_2, and PtS_2
- d^{10} copper and sliver halides, e.g., CuI, AgBr, and AgI
- Zincblende- and wurtzite-structure compounds of the p-block elements, especially those that are isoelectronic with Si or Ge, such as GaAs and CdTe. While these are most common, there are other p-block semiconductors that are not isoelectronic and have different structures, including GaS, PbS, and Se.



A 2" wafer cut from a GaAs single crystal. GaAs, like many p-block semiconductors, has the zincblende structure.

The **p-block octet semiconductors** are by far the most studied and important for technological applications, and are the ones that we will discuss in detail.

Zincblende- and wurtzite-structure semiconductors have 8 valence electrons per 2 atoms. These combinations include 4-4 (Si, Ge, SiC,...), 3-5 (GaAs, AlSb, InP,...), 2-6 (CdSe, HgTe, ZnO,...), and 1-7 (AgCl, CuBr,...) semiconductors. Other variations that add up to an octet configuration are also possible, such as $Cu^{I}In^{III}Se_2$, which has the **chalcopyrite** structure, shown at the right.



The **chalcopyrite structure** is adopted by ABX_2 octet semiconductors such as $Cu^{I}In^{III}Se_2$ and $Cd^{II}Sn^{IV}P_2$. The unit cell is doubled relative to the parent **zincblende structure** because of the ordered arrangement of cations. Each anion (yellow) is coordinated by two cations of each type (blue and red).

How does the **band gap energy** vary with **composition**? There are two important trends

(1) Going **down a group** in the periodic table, the gap **decreases**:

C (diamond) > Si > Ge > α-Sn

E_{gap} (eV): 5.4 1.1 0.7 0.0

This trend can be understood by recalling that E_{gap} is related to the **energy splitting between bonding and antibonding orbitals**. This difference decreases (and bonds become weaker) as the principal quantum number increases.

(2) For isoelectronic compounds, **increasing ionicity** results in a **larger band gap**.

Ge < GaAs < ZnSe

0.7 1.4 2.8 eV

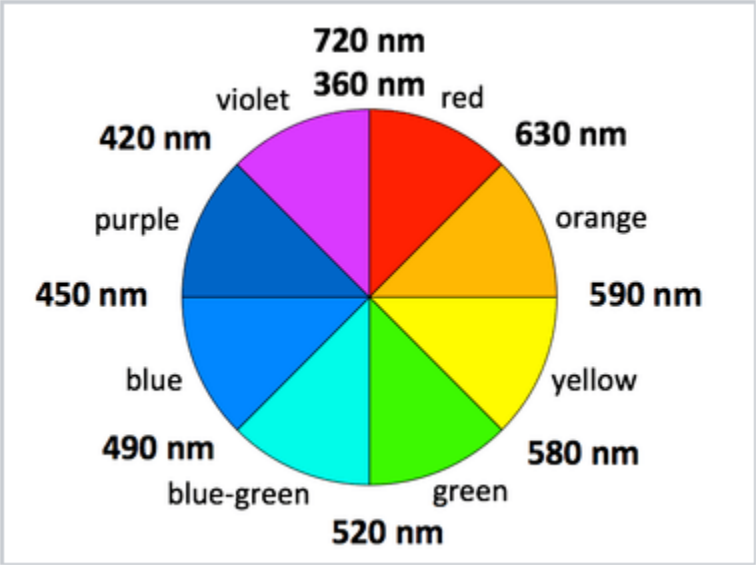
Sn < InSb < CdTe < AgI

0.0 0.2 1.6 2.8 eV

This trend can also be understood from a simple MO picture, as we discussed in Ch. 2. As the electronegativity difference $\Delta\chi$ increases, so does the energy difference between bonding and antibonding orbitals.

The band gap is a very important property of a semiconductor because it determines its color and conductivity. Many of the applications of semiconductors are related to band gaps:

- Narrow gap materials ($Hg_xCd_{1-x}Te$, VO_2, InSb, Bi_2Te_3) are used as infrared photodetectors and thermoelectrics (which convert heat to electricity).
- Wider gap materials (Si, GaAs, GaP, GaN, CdTe, $CuIn_xGa_{1-x}Se_2$) are used in electronics, light-emitting diodes, and solar cells.



Color wheel showing the colors and wavelengths of emitted light.

Semiconductor solid solutions such as $GaAs_{1-x}P_x$ have band gaps that are intermediate between the end member compounds, in this case GaAs and GaP (both zincblende structure). Often, there is a linear relation between composition and band gap, which is referred to as **Vegard's Law**. This "law" is often violated in real materials, but nevertheless offers useful guidance for designing materials with specific band gaps. For example, red and orange light-emitting diodes (LED's) are made from solid solutions with compositions of $GaP_{0.40}As_{0.60}$ and $GaP_{0.65}As_{0.35}$, respectively. Increasing the mole fraction of the lighter element (P) results in a larger band gap, and thus a higher energy of emitted photons.

Colors of semiconductors

The color of absorbed and emitted light both depend on the band gap of the semiconductor. Visible light covers the range of approximately 390-700 nm, or 1.8-3.1 eV. The **color of emitted light** from an LED or semiconductor laser corresponds to the band gap energy and can be read off the color wheel shown at the right.



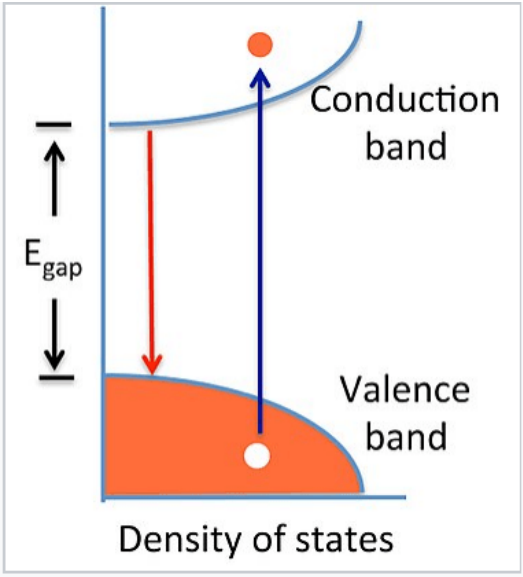
Fe_2O_3 powder is reddish orange because of its 2.2 eV band gap

The color of **absorbed light** includes the band gap energy, but also all colors of higher energy (shorter wavelength), because electrons can be excited from the valence band to a range of energies in the conduction band. Thus semiconductors with band gaps in the infrared (e.g., Si, 1.1 eV and GaAs, 1.4 eV) appear black because they absorb all colors of visible light. Wide band gap semiconductors such as TiO_2 (3.0 eV) are white because they absorb only in the UV. Fe_2O_3 has a band gap of 2.2 eV and thus absorbs light with $\lambda < 560$ nm. It thus appears reddish-orange (the colors of light reflected from Fe_2O_3) because it absorbs green, blue, and violet light. Similarly, CdS (E_{gap} = 2.6 eV) is yellow because it absorbs blue and violet light.

Electrons and holes in semiconductors

Pure (undoped) semiconductors can conduct electricity when electrons are promoted, either by heat or light, from the valence band to the conduction band. The promotion of an **electron** (e^-) leaves behind a **hole** (h^+) in the valence band. The hole, which is the absence of an electron in a bonding orbital, is also a mobile charge carrier, but with a positive charge. The motion of holes in the lattice can be pictured as analogous to the movement of an empty seat in a crowded theater. An empty seat in the middle of a row can move to the end of the row (to accommodate a person arriving late to the movie) if everyone moves over by one seat. Because the movement of the hole is in the opposite direction of electron movement, it acts as a positive charge carrier in an electric field.

The opposite process of excitation, which creates an electron-hole pair, is their recombination. When a conduction band electron drops down to recombine with a valence band hole, both are annihilated and energy is released. This release of energy is responsible for the emission of light in LEDs.



An electron-hole pair is created by adding heat or light energy E ≥ E_{gap} to a semiconductor (blue arrow). The electron-hole pair recombines to release energy equal to E_{gap} (red arrow).

At equilibrium, the creation and annihilation of electron-hole pairs proceed at equal rates. This dynamic equilibrium is analogous to the dissociation-association equilibrium of H^+ and OH^- ions in water. We can write a mass action expression:

$$n \times p = K_{eq} = n_i^2$$

where n and p represent the number density of electrons and holes, respectively, in units of cm^{-3}. The intrinsic carrier concentration, n_i, is equal to the number density of electrons or holes in an undoped semiconductor, where n = p = n_i.

Note the similarity to the equation for water autodissociation:

$$[H^+][OH^-] = K_w$$

By analogy, we will see that when we increase n (e.g., by doping), p will decrease, and vice-versa, but their product will remain constant at a given temperature.

Temperature dependence of the carrier concentration. Using the equations $K_{eq} = e^{(\frac{-\Delta G^o}{RT})}$ and $\Delta G^o = \Delta H^o - T\Delta S^o$, we can write:

$$n \times p = n_i^2 = e^{(\frac{\Delta S^o}{R})} e^{(\frac{-\Delta H^o}{RT})} \tag{9.2.6.1}$$

The entropy change for creating electron hole pairs is given by:

$$\Delta S^o = Rln(N_V) + Rln(N_V) = Rln(N_C N_V) \tag{9.2.6.2}$$

where N_V and N_C are the effective density of states in the valence and conduction bands, respectively.

and thus we obtain

$$n_i^2 = N_C N_V e^{(-\Delta H^o RT)} \tag{9.2.6.3}$$

Since the volume change is negligible, $\Delta H^o \approx \Delta E^o$, and therefore $\frac{\Delta H^o}{R} \approx \frac{E_{gap}}{k}$, from which we obtain

$$n_i^2 = N_C N_V e^{(\frac{-E_{gap}}{kT})} \tag{9.2.6.4}$$

and finally

$$\mathbf{n = p = n_i = (N_C N_V)^{\frac{1}{2}} e^{(\frac{-E_{gap}}{2kT})}} \tag{9.2.6.5}$$

For pure Si (E_{gap} = 1.1 eV) with N ≈ 10^{22}/cm^3, we can calculate from this equation a carrier density n_i of approximately 10^{10}/cm^3 at 300 K. This is about 12 orders of magnitude lower than the valence electron density of Al, the element just to the left of Si in the periodic table. Thus we expect the conductivity of pure semiconductors to be many orders of magnitude lower than those of metals.

Conductivity of intrinsic semiconductors

The conductivity (σ) is the product of the number density of carriers (n or p), their charge (e), and their mobility (μ). Recall from Chapter 6 that μ is the ratio of the carrier drift velocity to the electric field and has units of cm^2/Volt-second. Typically electrons and holes have somewhat different mobilities (μ_e and μ_h, respectively) so the conductivity is given by:

$$\sigma = ne\mu_e + pe\mu_h \tag{9.2.6.6}$$

For either type of charge carrier, we recall from Ch. 6 that the mobility μ is given by:

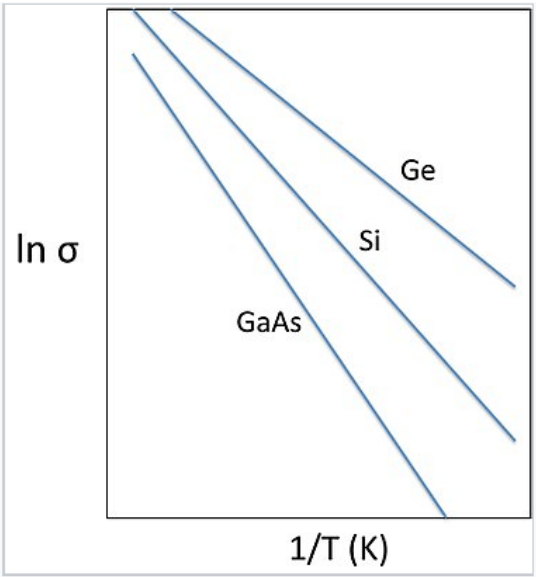
$$\mu = \frac{v_{drift}}{E} = \frac{e\tau}{m} \tag{9.2.6.7}$$

where e is the fundamental unit of charge, τ is the scattering time, and m is the effective mass of the charge carrier.

Taking an average of the electron and hole mobilities, and using n = p, we obtain

$$\sigma = \sigma_o e^{(\frac{-E_{gap}}{2kT})},\ where\ \sigma_o = 2(N_C N_V)^{\frac{1}{2}} e\mu \tag{9.2.6.8}$$

By measuring the conductivity as a function of temperature, it is possible to obtain the activation energy for conduction, which is E_{gap}/2. This kind of plot, which resembles an Arrhenius plot, is shown at the right for three different undoped semiconductors. The slope of the line in each case is -E_{gap}/2k.



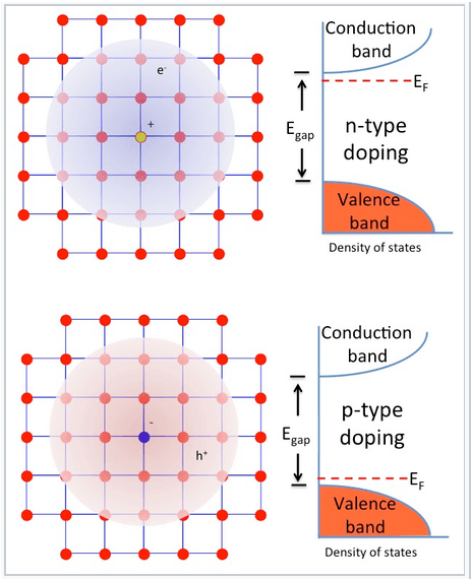
Plots of ln(σ) vs. inverse temperature for intrinsic semiconductors Ge (E_{gap} = 0.7 eV), Si (1.1 eV) and GaAs (1.4 eV). The slope of the line is -E_{gap}/2k.

Doping of semiconductors. Almost all applications of semiconductors involve controlled **doping**, which is the substitution

of impurity atoms, into the lattice. Very small amounts of dopants (in the parts-per-million range) dramatically affect the conductivity of semiconductors. For this reason, very pure semiconductor materials that are carefully doped - both in terms of the concentration and spatial distribution of impurity atoms - are needed.

n- and p-type doping. In crystalline Si, each atom has four valence electrons and makes four bonds to its neighbors. This is exactly the right number of electrons to completely fill the valence band of the semiconductor. Introducing a phosphorus atom into the lattice (the positively charged atom in the figure at the right) adds an extra electron, because P has five valence electrons and only needs four to make bonds to its neighbors. The extra electron, at low temperature, is bound to the phosphorus atom in a hydrogen-like molecular orbital that is much larger than the 3s orbital of an isolated P atom because of the high dielectric constant of the semiconductor. In silicon, this "expanded" Bohr radius is about 42 Å, i.e., 80 times larger than in the hydrogen atom. The energy needed to ionize this electron – to allow it to move freely in the lattice - is only about 40–50 meV, which is not much larger the thermal energy (26 meV) at room temperature. Therefore the Fermi level lies just below the conduction band edge, and a large fraction of these extra electrons are promoted to the conduction band at room temperature, leaving behind fixed positive charges on the P atom sites. The crystal is **n-doped**, meaning that the majority carrier (electron) is negatively charged.

Alternatively, boron can be substituted for silicon in the lattice, resulting in **p-type** doping, in which the majority carrier (hole) is positively charged. Boron has only three valence electrons, and "borrows" one from the Si lattice, creating a positively charged hole that exists in a large hydrogen-like orbital around the B atom. This hole can become delocalized by promoting an electron from the valence band to fill the localized hole state. Again, this process requires only 40–50 meV, and so at room temperature a large fraction of the holes introduced by boron doping exist in delocalized valence band states. The Fermi level (the electron energy level that has a 50% probability of occupancy at zero temperature) lies just above the valence band edge in a p-type semiconductor.



n- and p-type doping of semiconductors involves substitution of electron donor atoms (light orange) or acceptor atoms (blue) into the lattice. These substitutions introduce extra electrons or holes, respectively, which are easily ionized by thermal energy to become free carriers. The Fermi level of a doped semiconductor is a few tens of mV below the conduction band (n-type) or above the valence band (p-type).

As noted above, the doping of semiconductors dramatically changes their conductivity. For example, the intrinsic carrier concentration in Si at 300 K is about 10^{10} cm^{-3}. The mass action equilibrium for electrons and holes also applies to doped semiconductors, so we can write:

$$n \times p = n_i^2 = 10^{20} cm^{-6} \; at \; 300K \tag{9.2.6.9}$$

If we substitute P for Si at the level of one part-per-million, the concentration of electrons is about 10^{16} cm^{-3}, since there are approximately 10^{22} Si atoms/cm^3 in the crystal. According to the mass action equation, if n = 10^{16}, then p = 10^4 cm^{-3}. There are

three consequences of this calculation:

- The density of carriers in the doped semiconductor (10^{16} cm^{-3}) is much higher than in the undoped material (~10^{10} cm^{-3}), so the conductivity is also many orders of magnitude higher.
- The activation energy for conduction is only 40–50 meV, so the conductivity does not change much with temperature (unlike in the intrinsic semiconductor)
- The minority carriers (in this case holes) do not contribute to the conductivity, because their concentration is so much lower than that of the majority carrier (electrons).

Similarly, for p-type materials, the conductivity is dominated by holes, and is also much higher than that of the intrinsic semiconductor.

Chemistry of semiconductor doping. Sometimes it is not immediately obvious what kind of doping (n- or p-type) is induced by "messing up" a semiconductor crystal lattice. In addition to substitution of impurity atoms on normal lattice sites (the examples given above for Si), it is also possible to dope with vacancies - missing atoms - and with interstitials - extra atoms on sites that are not ordinarily occupied. Some simple rules are as follows:

- For substitutions, adding an **atom to the right** in the periodic table results in **n-type** doping, and an atom to the **left** in **p-type** doping.

  For example, when TiO_2 is doped with Nb on some of the Ti sites, or with F on O sites, the result is n-type doping. In both cases, the impurity atom has one more valence electron than the atom for which it was substituted. Similarly, substituting a small amount of Zn for Ga in GaAs, or a small amount of Li for Ni in NiO, results in p-type doping.

- **Anion vacancies** result in **n-type** doping, and **cation vacancies** in **p-type** doping.

  Examples are anion vacancies in CdS_{1-x} and WO_{3-x}, both of which give n-type semiconductors, and copper vacancies in $Cu_{1-x}O$, which gives a p-type semiconductor.

- **Interstitial cations** (e.g. Li) donate electrons to the lattice resulting in **n-type** doping. Interstitial anions are rather rare but would result in p-type doping.

Sometimes, there can be both p- and n-type dopants in the same crystal, for example B and P impurities in a Si lattice, or cation and anion vacancies in a metal oxide lattice. In this case, the two kinds of doping **compensate** each other, and the doping type is determined by the one that is in higher concentration. A dopant can also be present on more than one site. For example, Si can occupy both the Ga and As sites in GaAs, and the two substitutions compensate each other. Si has a slight preference for the Ga site, however, resulting in n-type doping.

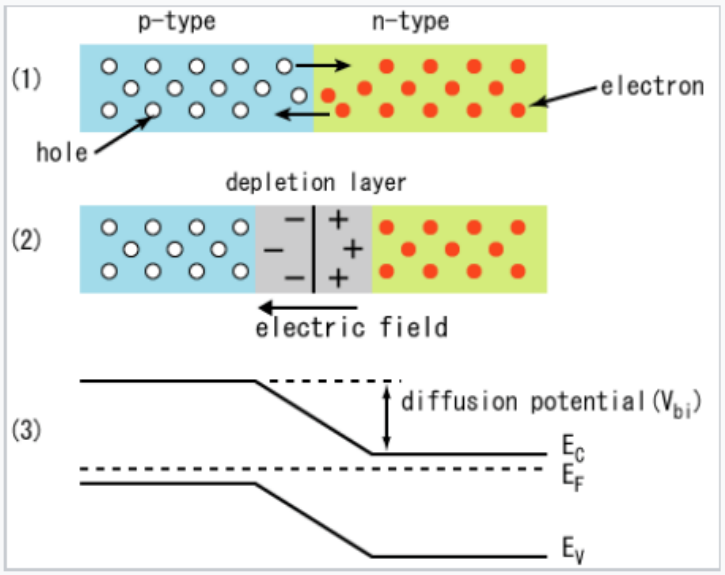
This page titled 9.2.6: Semiconductors- Band Gaps, Colors, Conductivity and Doping is shared under a CC BY-SA 4.0 license and was authored, remixed, and/or curated by Chemistry 310 (Wikibook) via source content that was edited to the style and standards of the LibreTexts platform.

- 10.5: Semiconductors- Band Gaps, Colors, Conductivity and Doping by Chemistry 310 is licensed CC BY-SA 4.0. Original source: https://en.wikibooks.org/wiki/Introduction_to_Inorganic_Chemistry.

9.2.7: Semiconductor p-n Junctions

Semiconductor p-n junctions are important in many kinds of electronic devices, including diodes, transistors, light-emitting diodes, and photovoltaic cells. To understand the operation of these devices, we first need to look at what happens to electrons and holes when we bring p-type and n-type semiconductors together. At the junction between the two materials, mobile electrons and holes annihilate each other, leaving behind the fixed + and - charges of the electron donor and electron acceptor dopants, respectively. For example, on the n-side of a silicon p-n junction, the positively charged dopants are P^+ ions and on the p-side the negatively charged dopants are B^-. The presence of these uncompensated electrical charges creates an electric field, the **built-in field** of the p-n junction. The region that contains these charges (and a very low density of mobile electrons or holes) is called the **depletion region**.

The electric field, which is created in the depletion region by electron-hole recombination, repels both the electrons (on the n-side) and holes (on the p-side) away from the junction. The concentration gradient of electrons and holes, however, tends to move them in the opposite direction by diffusion. At equilibrium, the flux of mobile carriers is zero because the field-driven migration flux is equal and opposite to the concentration-driven diffusion flux.



When p-type and n-type semiconductors are joined, electrons and holes are annihilated at the interface, leaving a depletion region that contains positively and negatively charged donor and acceptor atoms, respectively. At equilibrium, the Fermi level (E_F) is uniform throughout the junction. E_F lies just above the valence band on the p-type side of the junction and just below the conduction band on the n-type side.

The width of the depletion layer depends on the screening length in the semiconductor, which in turn depends on the dopant density. At high doping levels, the depletion layer is narrow (tens of nanometers across), whereas at low doping density it can be as thick as 1 µm. The depletion region is the only place where the electric field is nonzero, and the only place where the bands bend. Elsewhere in the semiconductor the field is zero and the bands are flat.

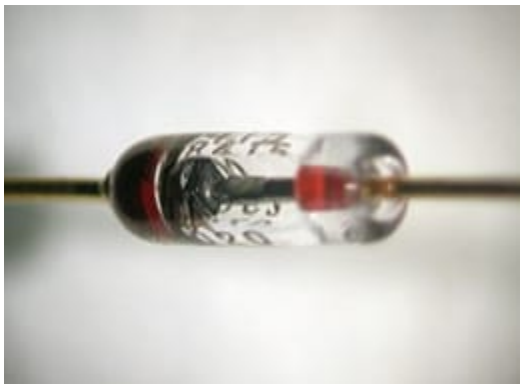
In the middle of p-n junction, the Fermi level energy, E_F, is halfway between the valence band, VB, and the conduction band, CB, and the semiconductor is intrinsic ($n = p = n_i$)

This page titled 9.2.7: Semiconductor p-n Junctions is shared under a CC BY-SA 4.0 license and was authored, remixed, and/or curated by Chemistry 310 (Wikibook) via source content that was edited to the style and standards of the LibreTexts platform.

- 10.6: Semiconductor p-n Junctions by Chemistry 310 is licensed CC BY-SA 4.0. Original source: https://en.wikibooks.org/wiki/Introduction_to_Inorganic_Chemistry.

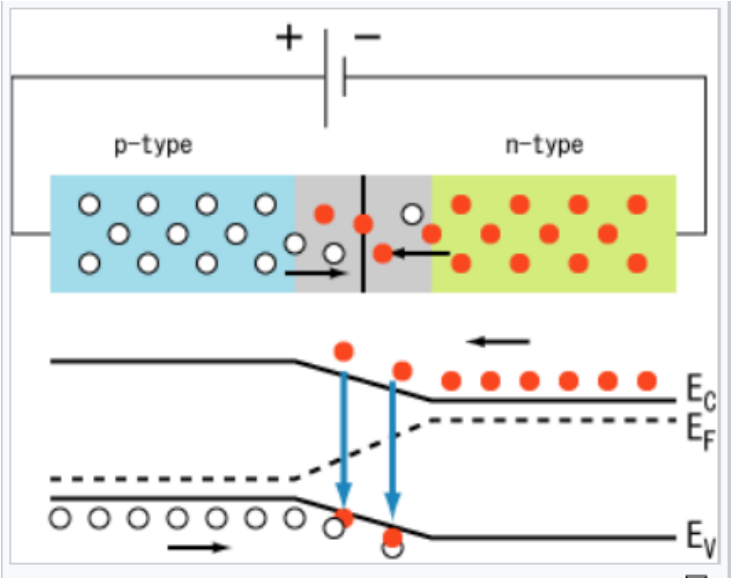
9.2.8: Diodes, LEDs and Solar Cells

Diodes are semiconductor devices that allow current to flow in only one direction. Diodes act as rectifiers in electronic circuits, and also as efficient light emitters (in LEDs) and solar cells (in photovoltaics). The basic structure of a diode is a junction between a p-type and an n-type semiconductor, called a p-n junction. Typically, diodes are made from a single semiconductor crystal into which p- and n- dopants are introduced.



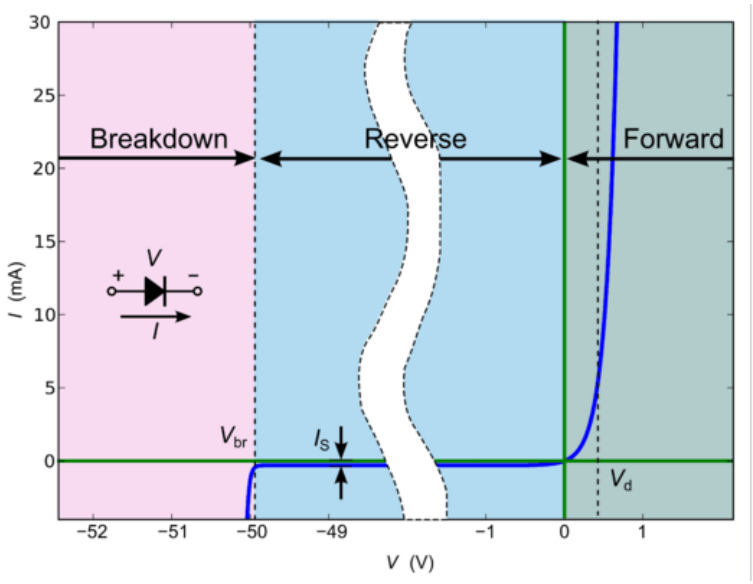
Closeup of a diode, showing the square-shaped semiconductor crystal *(black object on left)* (John Maushammer, Wikipedia, CC-BY-SA)

If the n-side of a diode is biased at positive potential and the p-side is biased negative, electrons are drawn to the n-side and holes to the p-side. This reinforces the built in potential of the p-n junction, the width of the depletion layer increases, and very little current flows. This polarization direction is referred to as "back bias." If the diode is biased the other way, carriers are driven into the junction where they recombine. The electric field is diminished, the bands are flattened, and current flows easily since the applied bias lowers the built-in potential. This is called "forward bias."



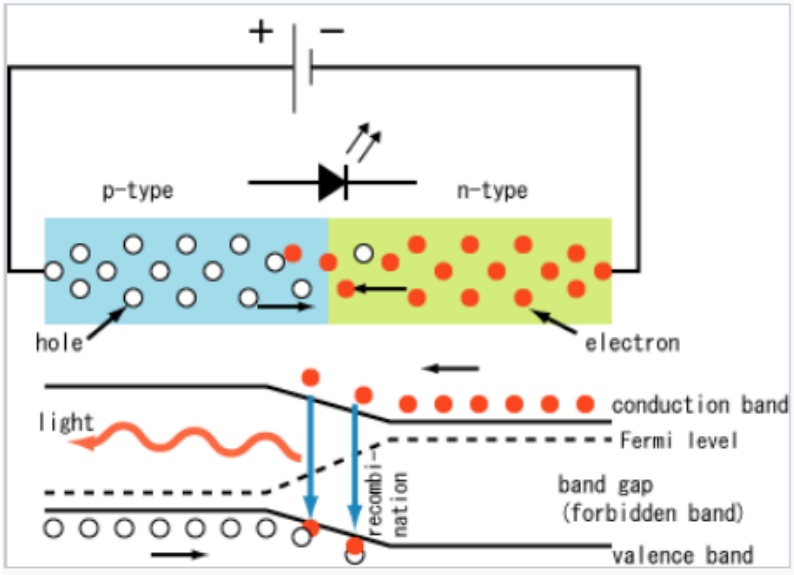
Electrons (red) and holes (white) in a forward-biased diode. (S-kei. Wikipedia, CC-BY-SA)

The figure on the left illustrates a forward-biased diode, through which current flows easily. As electrons and holes are driven into the junction (black arrows in lower left figure), they recombine (downward blue arrows), producing light and/or heat. The Fermi level in the diode is indicated as the dotted line. There is a drop in the Fermi level (equal to the applied bias) across the depletion layer. The corresponding diode i-V curve is shown on the right. The current rises exponentially with applied voltage in the forward bias direction, and there is very little leakage current under reverse bias. At very high reverse bias (typically tens of volts) diodes undergo avalanche breakdown and a large reverse current flows.



Diode i-V curve

A **light-emitting diode** or **LED** is a kind of diode that converts some of the energy of electron-hole recombination into light. This radiative recombination process always occurs in competition with non-radiative recombination, in which the energy is simply converted to heat. When light is emitted from an LED, the photon energy is equal to the bandgap energy. Because of this, LED lights have pure colors and narrow emission spectra relative to other light sources, such as incandescent and fluorescent lights. LED lights are energy-efficient and thus are typically cool to the touch.



Light-emitting diode (LED). (S-kei. Wikipedia, CC-BY-SA)

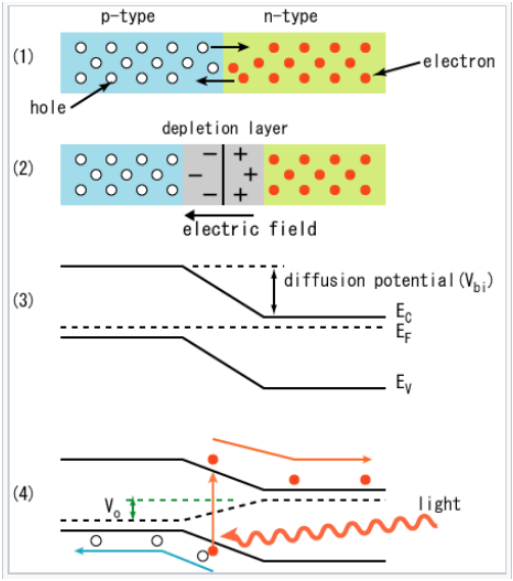
Direct-gap semiconductors such as GaAs and GaP have efficient luminescence and are also good light absorbers. In direct gap semiconductors, there is no momentum change involved in electron-hole creation or recombination. That is, the electrons and holes originate at the same value of the momentum wavevector **k**, which we encountered in Ch. 6. **k** is related to the momentum (also a vector quantity) by **p** = h**k**/2π. In a direct-gap semiconductor, the top of the valence band and the bottom of the conduction band most typically both occur at **k** = 0. Since the momentum of the photon is close to zero, photon absorption and emission are strongly allowed (and thus kinetically fast). Polar semiconductors such as GaAs, GaN, and CdSe are typically direct-gap materials. **Indirect-gap** semiconductors such as Si and Ge absorb and emit light very weakly because the valence band maximum and conduction band minimum do not occur at the same point in k-space. This means that a lattice vibration (a phonon) must also be created or annihilated in order to conserve momentum. Since this "three body" (electron, hole, phonon) process has low probability, the radiative recombination of electrons and holes is slow relative to non-radiative decay - the thermalization of electron-hole energy as lattice vibrations - in indirect-gap semiconductors. The momentum selection rule thus prevents light absorption/emission and there are no pure Si LEDs or Si-based lasers.



Prof. Shuji Nakamura holding a blue LED.

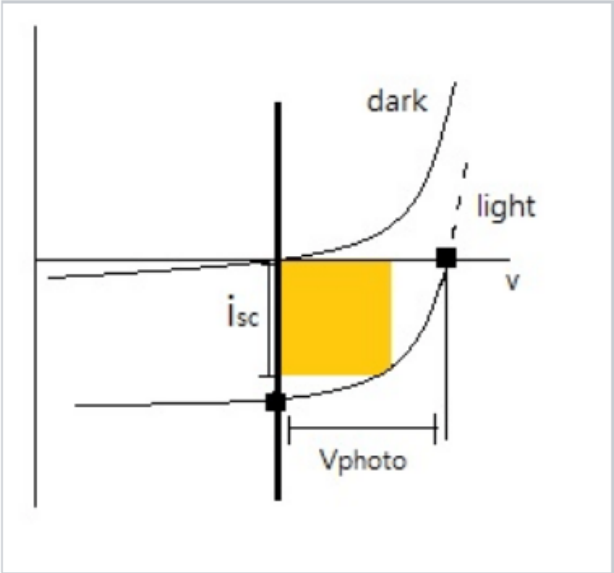
While red, orange, yellow, and green LEDs can be fabricated relatively easily from AlP-GaAs solid solutions, it was initially very difficult to fabricate blue LEDs because the best direct gap semiconductor with a bandgap in the right energy range is a nitride, GaN, which is difficult to make and to dope p-type. Working at Nichia Corporation in Japan, Shuji Nakamura succeeded in developing a manufacturable process for p-GaN, which is the basis of the blue LED. Because of the importance of this work in the development of information storage (Blu-Ray technology) and full-spectrum, energy-efficient LED lighting, Nakamura shared the 2014 Nobel Prize in Physics with Isamu Asaki and Hiroshi Amano, both of whom had made earlier contributions to the development of GaN diodes.

A **Solar cell**, or photovoltaic cell, converts light absorbed in a p-n junction directly to electricity by the photovoltaic effect. Photovoltaics is the field of technology and research related to the development of solar cells for conversion of solar energy to electricity. Sometimes the term solar cell is reserved for devices intended specifically to capture energy from sunlight, whereas the term photovoltaic cell is used when the light source is unspecified.



Photovoltaic effect in a semiconductor p-n junction. (S-kei. Wikipedia, CC-BY-SA)

Photocurrent in p-n junction solar cells flows in the diode reverse bias direction. In the dark, the solar cell simply acts as a diode. In the light, the photocurrent can be thought of as a constant current source, which is added to the i-V characteristic of the diode. The relationship between the dark and light current in a photovoltaic cell is shown in the diagram at the left.

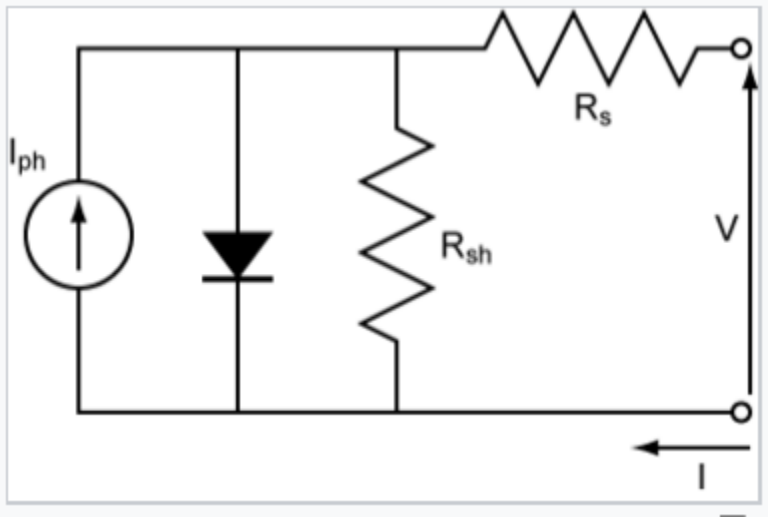


Current-voltage characteristic of a solar cell in the dark and under illumination with band gap light. The short-circuit photocurrent is indicated as i_{sc}, and the open-circuit photovoltage is V_{photo}. The maximum power generated by the solar cell is determined by the area of the orange box.

The built-in electric field of the p-n junction separates e^- h^+ pairs that are formed by absorption of bandgap light in the depletion region. The electrons flow downhill, towards the n-type side of the junction, the holes flow uphill towards the p-side. If $h\nu \geq E_{gap}$, light can be absorbed by promoting an electron from the valence band to the conduction band. Any excess energy is rapidly

thermalized. Light with hν > E_g thus can store only E_g worth of energy in an e^- h^+ pair. If light is absorbed outside of depletion region, i.e., on the n- or p-side of the junction where there is no electric field, minority carriers must diffuse into the junction in order to be collected. This process occurs in competition with electron-hole recombination. Because impurity atoms and lattice defects make efficient recombination centers, semiconductors used in solar cells (especially indirect-gap materials such as Si, which must be relatively thick in order to absorb most of the solar spectrum) must be very pure. Most of the cost of silicon solar cells is associated with the process of purifying elemental silicon and growing large single crystals from the melt.

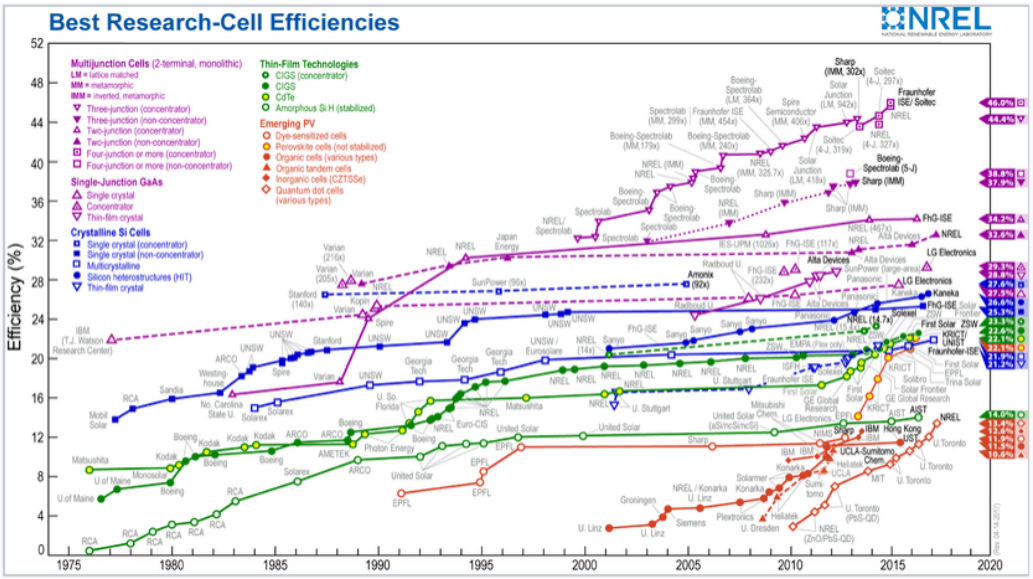
In the photodiode i-V curve above, V_{photo} is typically only about 70% of the bandgap energy E_{gap}. The photocurrent is limited by the photon flux, the recombination rate, and the re-emission of absorbed light.[6] The area of the orange rectangle indicates the power generated by the solar cell, which can be calculated as P = i x V. In good single crystal or polycrystalline solar cells made of Si, GaAs, CdTe, $CuIn_xGa_{1-x}Se_2$, or $(CH_3NH_3)PbI_3$ the quantum yield (the ratio of short circuit photocurrent to photon flux) is close to unity.



The equivalent circuit of a p-n junction solar cell, which results in the "light" i-V curve shown in the figure above. The solar cell is effectively a diode with a reverse-bias current source provided by light-generated electrons and holes. The shunt resistance (R_{sh}) in the equivalent circuit represents parasitic electron-hole recombination. A high shunt resistance (low recombination rate) and low series resistance (R_s) are needed for high solar cell efficiency.

Solar cells have many current applications. Individual cells are used for powering small devices such as electronic calculators. Photovoltaic arrays generate a form of renewable electricity, particularly useful in situations where electrical power from the grid is unavailable such as in remote area power systems, Earth-orbiting satellites and space probes, remote radio-telephones and water pumping applications. Photovoltaic electricity is also increasingly deployed in grid-tied electrical systems.

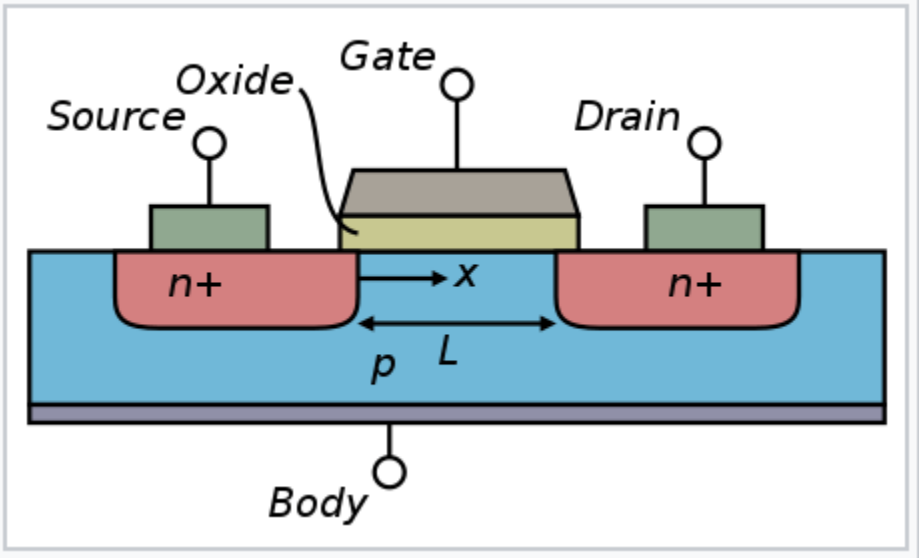
The cost of installed photovoltaics (calculated on a per-watt basis) has dropped over the past decade at a rate of about 13% per year, and has already reached grid parity in Germany and a number of other countries.[7] Photovoltaic grid parity is anticipated in U.S. power markets in the 2020 timeframe.[8] A major driver in the progressively lower cost of photovoltaic power is the steadily increasing efficiency of solar cells, which is shown in the graphic at the right. Higher efficiency solar cells require less area to deliver the same amount of power, and this lowers the "balance of system" costs such as wiring, roof mounting, etc., which scale as the area of the solar panels. Progress towards higher efficiency reflects improved processes for making photovoltaic materials such as silicon and gallium arsenide, as well as the discovery of new materials. Silicon solar cells are a mature technology, so they are now in the flat part of the learning curve and are approaching their maximum theoretical efficiencies. Newer technologies such as organic photovoltaics, quantum dot solar cells, and lead halide perovskite cells are still in the rising part of the learning curve.



Reported timeline of solar cell energy conversion efficiencies since 1976 (National Renewable Energy Laboratory)

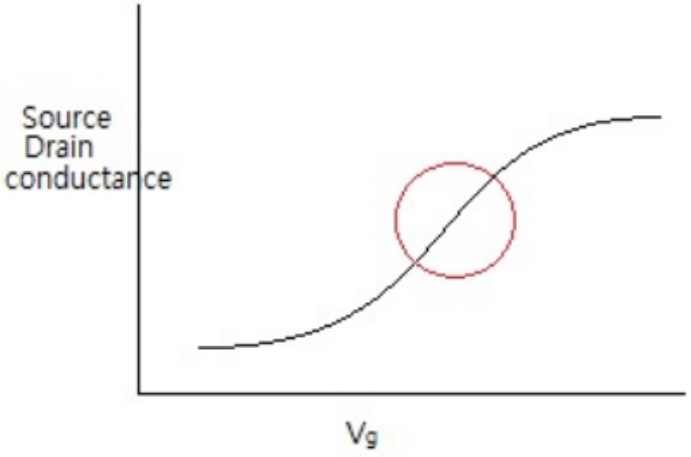
A **field effect transistor (FET)** is a transistor that uses an electric field to control the width of a conducting channel and thus the current in a semiconductor material. It is classified as unipolar transistor, in contrast to bipolar transistors.

Field effect transistors function as current amplifiers. The typical structure of Si-based FETs is one in which two n-type regions (the source and the drain) are separated by a p-type region. An oxide insulator over the p-type region separates a metal gate lead from the semiconductor. This structure is called a metal-oxide-semiconductor FET (or MOSFET). When voltage is applied between source and drain, current cannot flow because either the n-p or the p-n junction is back-biased. When a positive potential is applied to the gate, however, electrons are driven towards the gate, and locally the semiconductor is "inverted" to n-type. Then the current flows easily between the n-type source and drain through the n-channel. The current flow between the source and drain is many times larger than the current through the gate, and thus the FET can act as an amplifier. Current flow can also represent a logical "1," so FETs are also used in digital logic.



Cross section of an n-type MOSFET

In electronic devices such as microprocessors, field-effect transistors are kept in the off-state most of the time in order to minimize background current and power consumption. The FET shown above, which has n-type source and drain regions, is called an NMOS transistor. In a PMOS transistor, the source and drain regions are p-type and the gate is n-type. In **CMOS** (complementary metal-oxide semiconductor) integrated circuits, both NMOS and PMOS transistors are used. CMOS circuits are constructed in such a way that all PMOS transistors must have either an input from the voltage source or from another PMOS transistor. Similarly, all NMOS transistors must have either an input from ground or from another NMOS transistor. This arrangement results in low static power consumption.



Transistors are most useful in the range of gate voltage (indicated by the red circle in the figure at the left) where the source-drain current changes rapidly. In this region it is possible to effect a large change in current between source and drain when a small signal is applied to the gate. An important figure of merit for FETs is the **subthreshold slope**, which is the slope a plot of log(current) vs. V_{gate}. An ideal subthreshold slope is one decade of current per 60 mV of gate bias. Typically, a decade change in source-drain current can be achieved with a change in gate voltage of ~70 mV. The performance of FETs as switches and amplifiers is limited by the subthreshold slope, which in turn is limited by the capacitance of the gate. It is desirable to have

a very high gate capacitance, which requires a thin insulating oxide, but also to have a small leakage current, which requires a thick oxide. A current challenge in the semiconductor industry is to continue to scale FETs to even smaller nanoscale dimensions while maintaining acceptable values of these parameters. This is being done by developing new gate insulator materials that have higher dielectric constants than silicon oxide and do not undergo redox reactions with silicon or with metal gate leads. Only a few known materials (such as hafnium oxynitride and hafnium silicates) currently meet these stringent requirements.

This page titled 9.2.8: Diodes, LEDs and Solar Cells is shared under a CC BY-SA 4.0 license and was authored, remixed, and/or curated by Chemistry 310 (Wikibook) via source content that was edited to the style and standards of the LibreTexts platform.

- 10.7: Diodes, LEDs and Solar Cells by Chemistry 310 is licensed CC BY-SA 4.0. Original source: https://en.wikibooks.org/wiki/Introduction_to_Inorganic_Chemistry.

9.3: X-rays and X-ray Diffraction

HISTORICAL INTRODUCTION

X-rays were discovered during the summer of 1895 by Wilhelm Röntgen at the University of Würtzburg (Germany). Röntgen was interested in the *cathode rays* (beams of electrons) developed in discharge tubes, but it is not clear exactly which aspects of cathode rays he intended to study. By chance he noticed that a fluorescent screen $(\mathrm{ZnS} + \mathrm{Mn}^{++})$ lying on a table some distance from the discharge tube emitted a flash of light each time an electrical discharge was passed through the tube. Realizing that he had come upon something completely new, he devoted his energies to investigating the properties of the unknown ray " X " which produced this effect. The announcement of this discovery appeared in December 1895 as a concise ten page publication.

The announcement of the discovery of X-rays was received with great interest by the public. Röntgen himself prepared the first photographs of the bones in a living hand, and use of the radiation was quickly adopted in medicine. In the succeeding fifteen years, however, very few fundamental insights were gained into the nature of X-radiation. There was some indication that the rays were waves, but the evidence was not clear-cut and could be interpreted in several ways. Then, at the University of Munich in 1912, Max von Laue performed one of the most significant experiments of modern physics. At his suggestion, Paul Knipping (who had just completed a doctoral thesis with Röntgen) and Walter Friedrich (a newly appointed assistant to Sommerfeld) directed a beam of X-rays at a crystal of copper sulfate and attempted to record the scattered beams on a photographic plate. The first experiment was unsuccessful. The result of a second experiment was successful. They observed the presence of spots produced by diffracted X-ray beams grouped around a larger central spot where the incident X-ray beam struck the film. This experiment demonstrated conclusively that X-radiation consisted of waves and, further, that the crystals were composed of atoms arranged on a *space lattice*.

ORIGIN OF X-RAY SPECTRA

The interpretation of X–ray spectra according to the Bohr theory (LN-1) of electronic levels was first (and correctly) proposed by W. Kossel in 1920: the electrons in an atom are arranged in shells (K, L, M, N, corresponding to n = 1, 2, 3, 4, ..., etc.). Theory predicts that the energy differences between successive shells increase with decreasing n and that the electron transition from n = 2 to n = 1 results in the emission of very energetic (short wavelength) radiation (fig. 1), while outer shell transitions (say, from $n = 5$ to $n = 4$) yield low energy radiation (long wavelength). For hydrogen, you recall, the wave number of the emitted radiation associated with a particular electron transition is given by the Rydberg equation:

$$\bar{v} = \left(\frac{1}{n_i^2} - \frac{1}{n_f^2} \right) R$$

For "hydrogen-like" atoms with the atomic number Z (containing one electron only) the corresponding Rydberg equation becomes:

$$\bar{v} = \left(\frac{1}{n_i^2} - \frac{1}{n_f^2} \right) RZ^2$$

From this relationship it is apparent that the energy difference associated with electron transitions increases strongly with the atomic number and that the wavelength of radiation emitted during such transitions moves with increasing Z from the $10^{-7}\ \mathrm{m}$ range to the $10^{-10}\ \mathrm{m}$ range (radiation now defined as X-rays).

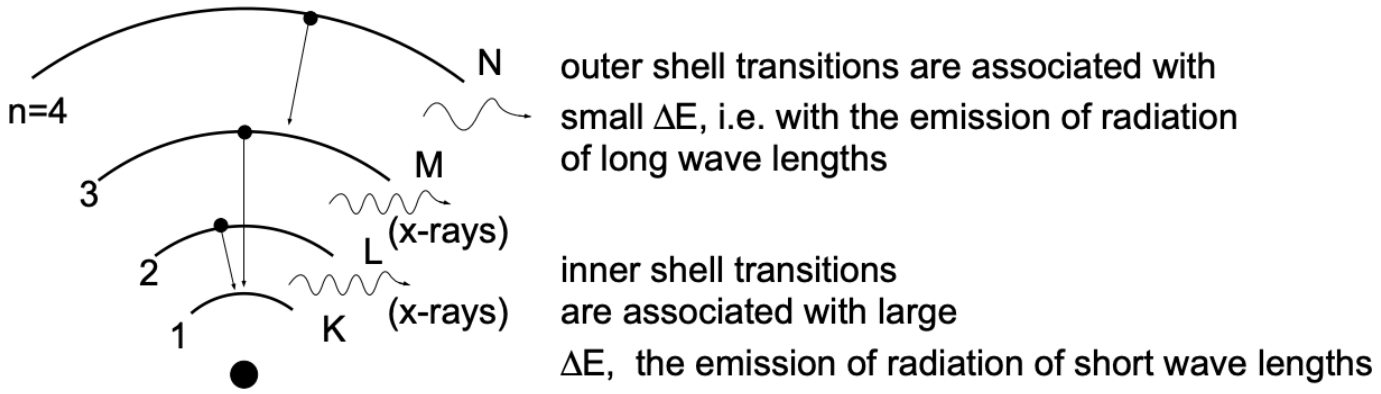


Figure 1 X-rays are generated by inner shell electron transitions

To bring about such inner shell transitions requires the generation of an *electron vacancy*: an electron must be removed, for example from the K shell $(\mathrm{n}=1)$, of an atom. Such a vacancy is conveniently produced in an X-ray tube by an electron beam (generated by a heated filament which is made a cathode) impinging, after being subjected to an accelerating potential of several kV, into a target material made anode (fig. 2). The impinging electrons will transfer part of their energy to electrons of the target material and result in electronic excitation. If the energy of the arriving electrons is high enough, some may knock out a K shell electron in the target and thus generate a vacancy. [It should be clear that a $\mathrm{K} \rightarrow \mathrm{L}$ excitation cannot take place since the L shell is filled: excitation must involve $(n=1) \rightarrow (n=\infty)$.] When such a vacancy is generated, it can readily be filled by an electron from the L shell or the M shell of the same atom. These internal electron transitions give rise to the emission of "characteristic" X-radiation which, because of its short wavelength, has extremely high "penetrating" power.

Since an electron beam is used to generate X-rays, the X-ray tube has to be evacuated: to dissipate the energy flux arriving at the target, the anode support (onto which the target is mounted) is water-cooled.

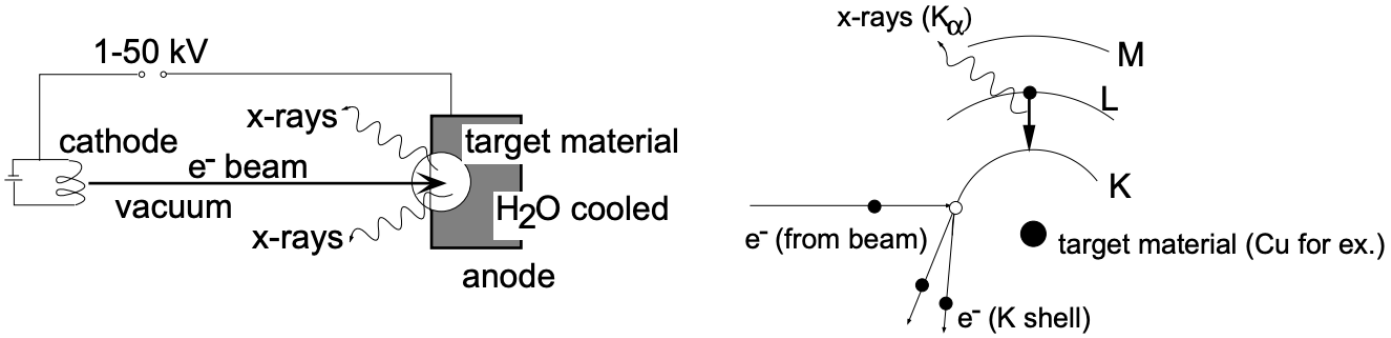


Figure 2 Generation of x-rays

Under standard operating conditions, the characteristic radiation emitted by the target comprises two sharp lines, referred to as K_α and K_β lines (fig. 3). They are associated, respectively, with electron transitions from $n=2$ to $n=1$ and from $n=3$ to $n=1$.

Emitted X-ray spectra were extensively studied by H.G.J. Moseley who established the relationship between the wavelength of characteristic radiation and the atomic number Z of the radiation emitting target material (fig. 4). Experimentally he found that the K_α lines for various target materials (elements) exhibit the relationship:

$$\lambda K_\alpha \propto \frac{1}{Z^2} \quad \left(\bar{v} K_\alpha \propto Z^2\right)$$

Moseley's empirical relationship (which reflects a behavior in agreement with the Rydberg equation) can be quantified. While the energy levels associated with outer electron transitions are significantly affected by the "screening" effect of inner electrons (which is variable and cannot as yet be determined from first principles), the conditions associated with X-ray generation are simple. Very generally, the screening effect of the innermost electrons on the nuclear charge is accounted for in an effective nuclear charge $(Z-\sigma)$ and the Rydberg equation assumes the form:

$$\bar{v} = \left(\frac{1}{n_i^2} - \frac{1}{n_f^2} \right) R(Z - \sigma)^2$$

where $\sigma =$ screening effect

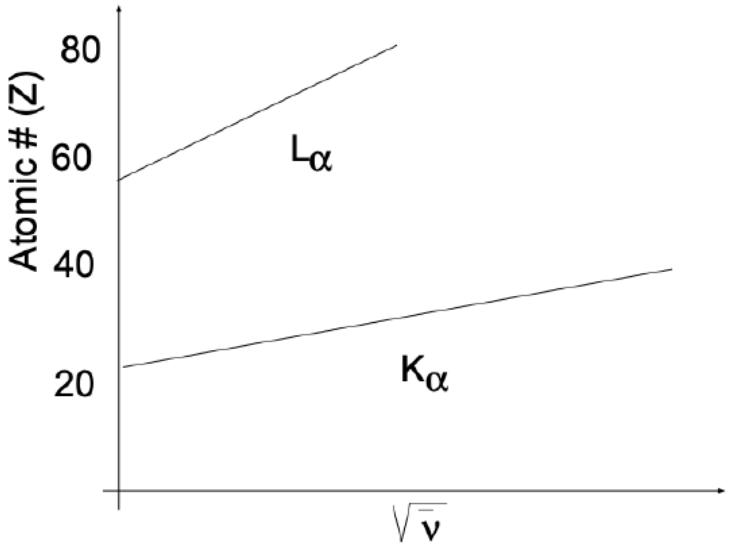


Figure 4 Moseley relationship for K_α and L_α radiation

Considering the transition $n_2 \rightarrow n_1$, screening of the full nuclear charge is only provided by the one electron remaining in the K shell. Thus it is possible to use the ν modified Rydberg equation, taking $\sigma = 1$. Accordingly, we have:

$$\bar{v}K_\alpha = \left(\frac{1}{2^2} - \frac{1}{1^2} \right) R(Z-1)^2 = -\frac{3}{4} R(Z-1)^2$$

where: $\mathrm{R} =$ Rydberg constant and $\mathrm{Z} =$ atomic number of the target material. [The minus sign (-) only reflects radiative energy given off by the system.]

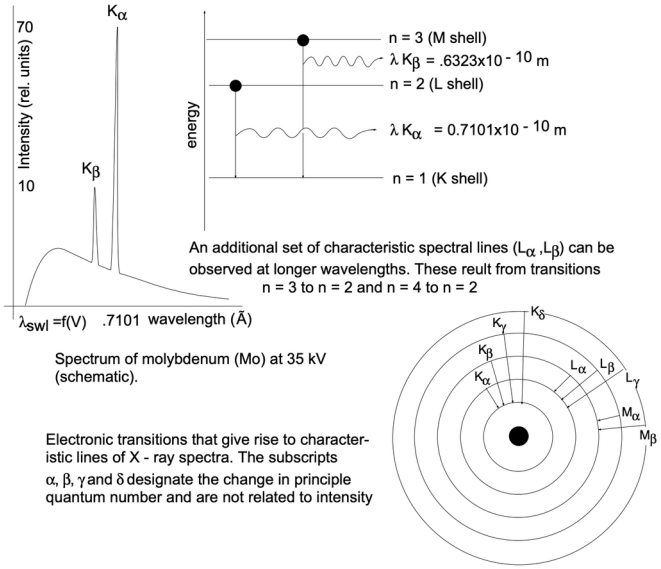


Figure 3 Electronic transitions giving rise to characteristic X- ray spectra.

Similarly, for the characteristic L_α series of spectral lines ($n = 3$ to $n = 2$) we find, after removal of one L electron, that the screening of the electrons in the K shell and the remaining electrons in the L shell reduces the nuclear charge by 7.4 (empirical value).

$$\overline{\nu}\mathrm{L}_{\alpha}=\left(\frac{1}{3^2}-\frac{1}{2^2}\right)\mathrm{R}(\mathrm{Z}-7.4)^2=-\frac{5}{36}\mathrm{R}(\mathrm{Z}-7.4)^2$$

A second look at the X-ray spectrum of a Mo target, obtained with an electron accelerating potential of $35\mathrm{kV}$ (fig. 5), shows that the characteristic radiation $(\mathrm{K}_{\alpha},\mathrm{K}_{\beta})$ appears superimposed on a continuous spectrum (continuously varying λ) of lower and varying intensity. This continuous spectrum is referred to as **bremsstrahlung** (*braking radiation*) and has the following origin. Electrons, impinging on the target material, may lose their energy by transferring it to orbiting electrons, as discussed above; in many instances, however, the electrons may come into the proximity of the force fields of *target nuclei* and, in doing so, will be "slowed down" or decelerated to a varying degree,

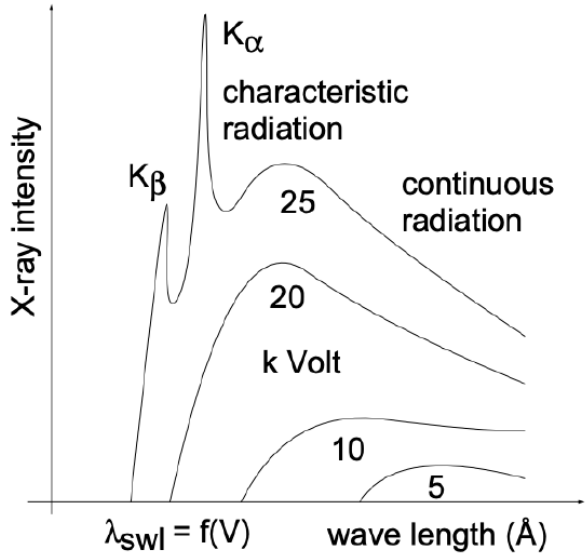
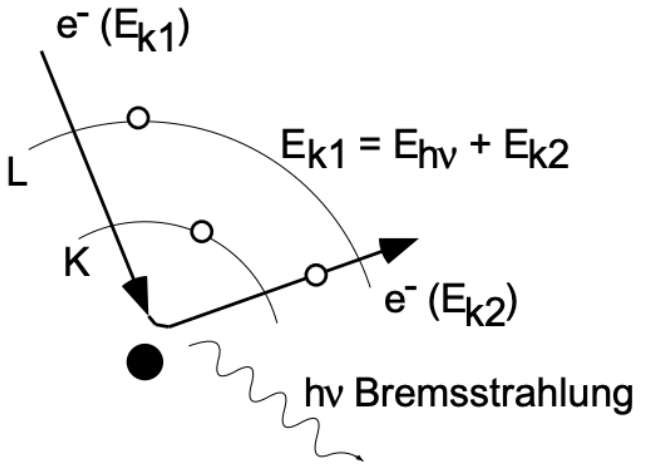


Figure 5 X-ray spectrum of Mo target as a function of applied Voltage.

ranging from imperceptible deceleration to total arrest. The energy lost in this slowing down process is emitted in the form of radiation (braking radiation, or bremsstrahlung). This energy conversion, as indicated, can range from partial to complete (fig. 6). The



for $E_{k2}=0$, $E_{(h\nu)max}=E_{k1}=\lambda_{SWL}=h\nu=eV$; $\lambda_{swl}=hc/eV$

Figure 6 Origin of Bremsstrahlung; the continuous part of the X-ray spectrum

incident electrons have an energy of $\mathrm{e}\cdot\mathrm{V}$ (electronic charge times accelerating Voltage) in the form of kinetic energy $(\mathrm{mv}^2/2)$, and their total energy conversion gives rise to a *Shortest Wavelength* (SWL) - the cut-off of the continuous spectrum for decreasing values of λ (fig. 5). Analytically, we have:

$$eV = h\nu_{max} = h\frac{c}{\lambda_{SWL}} \quad ; \quad \lambda_{SWL} = \frac{hc}{eV}$$

From this relationship it is evident that the cut-off of the continuous spectrum toward decreasing λ''s (λ_{SWL}) is controlled by the accelerating potential (fig. 5).

"FINE STRUCTURE" OF CHARACTERISTIC X-RAYS

It is customary to consider the characteristic X-ray spectral lines as discrete lines $(K_\alpha, K_\beta, L_\alpha, L_\beta$, etc.). In reality, they are not discrete since the electron shells involved in the associated electron transitions have energy *sublevels* (s, p, d orbitals). These sublevels give rise to a "fine structure" insofar as the K_α lines are doublets composed of $K_{\alpha 1}$ and $K_{\alpha 2}$ lines. Similarly, L_α, L_β, etc., exhibit a fine structure.

These considerations suggest that X-ray spectra contain information concerning the energetics of electronic states. Obviously, analysis of X-rays emitted from a target of unknown composition can be used for a quantitative chemical analysis. [This approach is taken routinely in advanced scanning electron microscopy (SEM) where X-rays, generated by the focused electron-beam, are analyzed in an appropriate spectrometer.]

In fundamental studies it is also of interest to analyze soft (long λ) X-ray spectra. For example, take the generation of X-rays in sodium (Na). By generating an electron vacancy in the K shell, a series of K_α and K_β lines will result. The cascading electron generates vacancies in the $2p$ level, which in turn can be filled by electrons entering from the 3s level (generation of "soft" X-rays). If the X-rays are generated in a Na vapor, the $3s \rightarrow 2p$ transition will yield a sharp line; on the other hand, if X-rays are analyzed in sodium metal, the same transition results in the emission of a continuous broad band, about 30Å in width. This finding confirms the existence of an *energy band* (discussed earlier).

An analysis of the width and intensity distribution of the X-ray band provides experimental data concerning the energy band width and the energy state density distribution within the energy band (fig. 7).

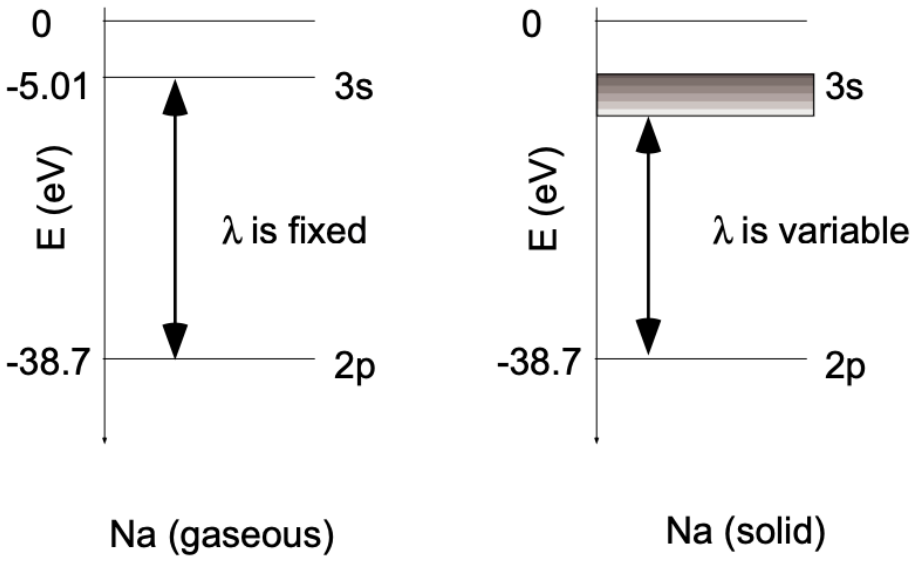


Figure 7 Soft X-rays from 3s - 2p transitions in solid Na and Na vapor

X-RAYS FOR STRUCTURAL ANALYSIS

The extensive use of X-rays for the analysis of atomic structural arrangements is based on the fact that waves undergo a phenomenon called *diffraction* when interacting with systems (diffracting centers) which are spaced at distances of the same order of magnitude as the wavelength of the particular radiation considered. X-ray diffraction in crystalline solids takes place because the atomic spacings are in the 10^{-10} m range, as are the wavelengths of X-rays.

DIFFRACTION AND BRAGG'S LAW

The atomic structure of crystalline solids is commonly determined using one of several different X-ray diffraction techniques. Complementary structure information can also be obtained through electron and neutron diffraction. In all instances, the radiation used must have wavelengths in the range of 0.1 to 10Å because the resolution (or smallest object separation distance) to which any radiation can yield useful information is about equal to the wavelength of the radiation, and the average distance between adjacent atoms in solids is about $10^{-10}\ \mathrm{m}(1\text{Å})$. Since there is no convenient way to focus X-rays with lenses and to magnify images, we do not attempt to look directly at atoms. Rather, we consider the interference effects of X-rays when scattered by the atoms, comprising a crystal lattice. This is analogous to studying the structure of an optical diffraction grating by examining the interference pattern produced when we shine visible light on the grating. (The spacing of lines on a grating is about 0.5 to 1 μm and the wavelength of visible radiation ranges from 0.4 to 0.8 μm.) In the optical grating the ruled lines act as scattering centers, whereas in a crystal it is the atoms (more correctly, the electrons about the atom) which scatter the incident radiation.

The geometrical conditions which must be satisfied for diffraction to occur in a crystal were first established by Bragg. He considered a monochromatic (single wavelength) beam of X-rays with coherent radiation (X-rays of common wave front) to be incident on a crystal, as shown in fig. 8. Moreover, he established that the atoms which

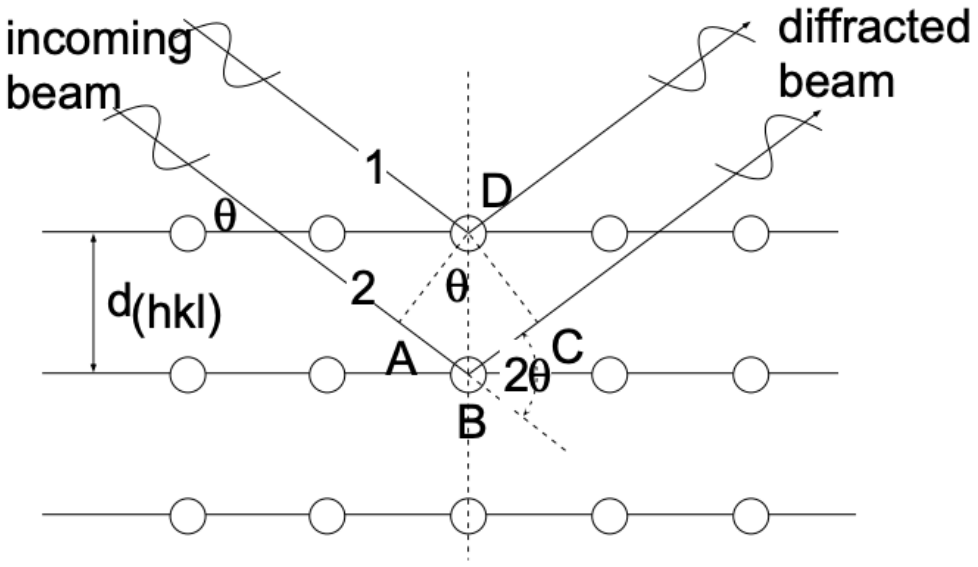


Figure 8 Bragg's law, assuming the planes of atoms behave as reflecting planes.

constitute the actual scattering centers can be represented by sets of parallel planes (in which the atoms are located) which act as mirrors and "reflect" the X-rays. In cubic systems the spacing of these planes, $\mathrm{d}_{(\mathrm{hkl})}$ (see $\mathrm{LN}-4$), is related to the lattice constant

(a):

$$\mathrm{d}_{(\mathrm{hkl})}=\frac{\mathrm{a}}{\sqrt{\mathrm{h}^2+\mathrm{k}^2+\mathrm{I}^2}} \tag{1}$$

For constructive interference of the scattered X-rays (the appearance of a diffraction peak) it is required that the beams, scattered on successive planes, be "in phase" (have again a common wave front) after they leave the surface of the crystal. In terms of the beams labeled 1 and 2 in fig. 8 this requires that the distance $\overline{\mathrm{AB}}+\overline{\mathrm{BC}}$ be equal to an integral number of wavelengths (λ) of the indicent radiation. Accordingly:

$$\overline{\mathrm{AB}}+\overline{\mathrm{BC}}=\mathrm{n}\lambda \quad (\mathrm{n}=1,2,3,\ldots)$$

Since $\overline{\mathrm{AB}}=\overline{\mathrm{BC}}$ and $\sin\theta=\frac{\overline{AB}}{d_{(hk)}}\ \left[\overline{AB}=d_{(hk)}\sin\theta\right]$:

$$\mathrm{n}\lambda=2\ \mathrm{d}_{(\mathrm{hkl})}\sin\theta \tag{2}$$

This relation is referred to as *Bragg's Law* and describes the angular position of the diffracted beam in terms of λ and $d_{(hkl)}$. In

most instances of interest we deal with first order diffraction ($n = 1$) and, accordingly, Bragg's law is:

$$\lambda = 2d_{(hkl)} \sin\theta$$

[We are able to make $n = 1$ because we can always interpret a diffraction peak for $n = 2, 3, \ldots$ as diffraction from (nh $nknl$) planes - i.e., from planes with one-nth the interplanar spacing of $d_{(\mathrm{hkl})}$.].

If we consider fig. 8 as representative for a "diffractometer" set-up (fig. 11), we have a collimated beam of X-rays impinging on a (100) set of planes and at 2θ to the incident beam a detector which registers the intensity of radiation. For a glancing incident beam (small θ) the detector will register only background radiation. As θ increases to a value for which $2d\sin\theta = \lambda$, the detector will register high intensity radiation - we have a diffraction peak. From the above it is evident that the diffraction angle (θ) increases as the interplanar spacing, $\mathrm{d}_{(\mathrm{hkl})}$, decreases.

The diffraction experiment as presently considered is intended to provide quantitative information on the volume (the lattice constant a) and shape characteristics (SC, BCC, FCC) of the unit cell. The intensity of diffraction peaks depends on the phase relationships between the radiation scattered by all the atoms in the unit cell. As a result, it happens quite often that the intensity of a particular peak, whose presence is predicted by Bragg's law, is zero. (This is because Bragg's law deals not with atom positions, but only with the size and shape of the unit cell.) For example, consider the intensity of the (100) diffraction peak of a crystal which has a BCC unit cell. The phase relationships show that the X-rays scattered at the top and bottom faces of the unit cell, (100) planes, interfere constructively, but are 180° out of phase with the X-rays scattered by the atom at the center of the unit cell. The resultant intensity is therefore zero. The rules which govern the presence of particular diffraction peaks in the different cubic Bravais lattices (SC, BCC and FCC) are given in Table I.

TABLE I. *Selection Rules for Diffraction Peaks in Cubic Systems*

Bravais Lattice	Reflections Present	Reflections Absent
Simple Cubic	All	None
Body-Centered Cubic	$(\mathrm{h}+\mathrm{k}+\mathrm{l}) =$ even	$(\mathrm{h}+\mathrm{k}+\mathrm{l}) =$ odd
Face-Centered Cubic	h, k, l unmixed (either all odd or all even)	h, k, l mixed

The rules given are strictly true only for unit cells where a single atom is associated with each lattice point. (Unit cells with more than one atom per lattice point may have their atoms arranged in positions such that reflections cancel. For example, diamond has an FCC Bravais lattice with two atoms per lattice point. All reflections present in diamond have unmixed indices, but reflections such as {200}, {222} and {420} are missing. The fact that all reflections present have unmixed indices indicates that the Bravais lattice is FCC – the extra missing reflections give additional information as to the exact atom arrangement.)

A hypothetical diffraction experiment: A material is known to be of simple cubic structure; determine a, the lattice constant, by X-ray diffraction. In theory, the question may be answered by placing the crystal into a diffractometer, rotating it into all possible positions relative to the incident X-ray beam and recording all diffracting 2θ values. From the above we know that the smallest observed θ value must correspond to diffraction on $\{100\}$ planes and also that $d_{(100)} = a$. We may now use Bragg's equation to determine a, the lattice constant:

$$\begin{aligned} \lambda &= 2d\sin\theta = 2a\sin\theta \\ a &= \frac{\lambda}{2\sin\theta} \end{aligned} \tag{9.3.1}$$

There are two simplifying assumptions in this problem: (1) we know the system is SC and (2) we are able, through rotation, to bring all planes present into diffraction conditions.

EXPERIMENTAL APPROACHES TO X-RAY DIFFRACTION

In the context of this course we are interested in making use of X-ray diffraction for the purpose of (a) identifying (cubic) crystal systems, (b) determining the lattice constant, a, and (c) identifying particular planes or meaningful orientations. The possible

approaches can, in principle, be identified through an examination of Bragg's law. The Bragg condition for particular $\mathrm{d}_{(\mathrm{hkl})}$ values can be satisfied by adjusting either one of two experimental variables: (a) λ, the wavelength of the X-ray beam used, or (b) θ, the orientation of the crystal planes relative to the incident X-rays.

(a) Fixed θ, Variable λ: One means of satisfying Bragg's law is to irradiate a stationary single crystal (θ fixed for all planes within the crystal) with an X-ray beam of "white" radiation, which contains the characteristic and continuous spectrum produced by an X-ray tube. (For λ variable we have the simultaneous exposure of a crystal to a range of λ values). Each set of planes will reflect (diffract) the particular λ which satisfies the Bragg condition for the fixed θ. The diffracted beams may conveniently be recorded with a Polaroid camera or, alternately, with an electronic imaging device. It is possible to analyze either the transmitted or the back-reflected X-rays. This experimental procedure is referred to as the **Laue technique** (fig. 9); it is mostly conducted in the back-reflection mode. Note that the approach taken makes it possible to determine the values of θ for each reflection, but not the corresponding λ. Therefore, the technique cannot be used, for example, to determine lattice constants. However, it is very valuable if particular planes or crystal orientations are to be identified.

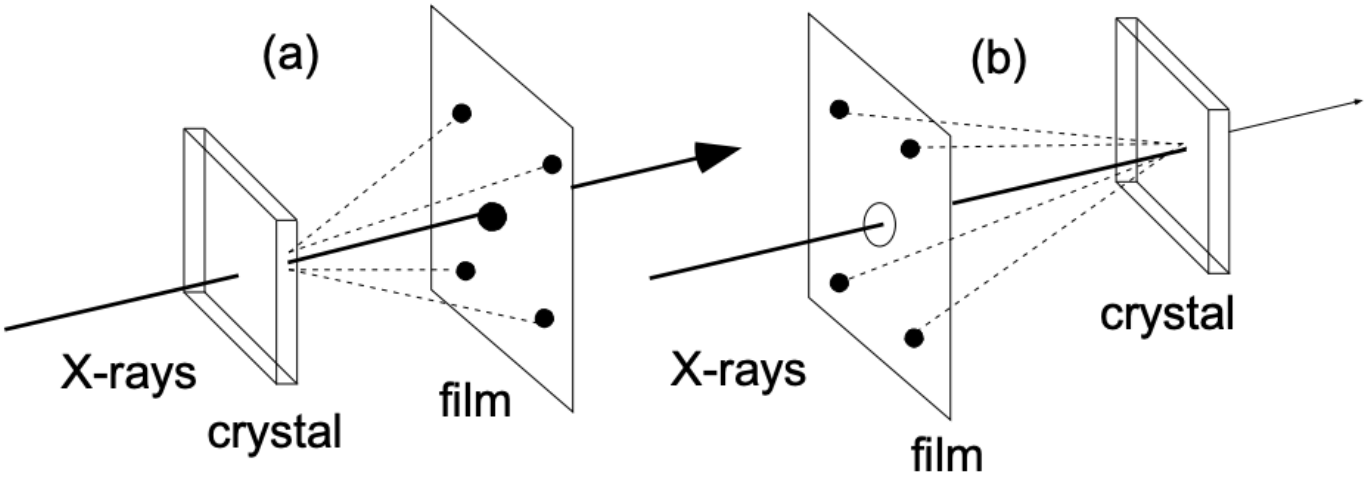


Figure 9: Laue diffraction in (a) transmission and (b) back-reflection mode. Long

This is a figure with information about the process described in this section.

The figure has several sections of important information:

- This is the description of the first section.
- The middle section of the figure contains this information.
- The third and final section of the figure has this information.

(b)Fixed λ (Monochromatic X-Rays), Variable θ: The basic prerequisite for this approach is the availability of a monochromatic X -radiation of known wavelength (λ). Such radiation can be conveniently obtained by using a crystal (i.e., its diffracting property) as a filter or monochromator (fig. 10). Filter action is achieved by positioning the crystal in such a way that the unfiltered radiation emitted by the X-ray tube becomes incident at an angle, θ, on a set of low index planes which satisfy Bragg's law for the highest intensity radiation (K_α) emitted. The condition of a fixed λ and variable θ is experimentally used in two techniques. Using a **diffractometer** (fig. 11), we place a sample (ground to a powder) into the center of a rotating stage and expose it to a monochromatic X-ray beam. The sample is rotated into diffraction condition and the diffraction angle determined.

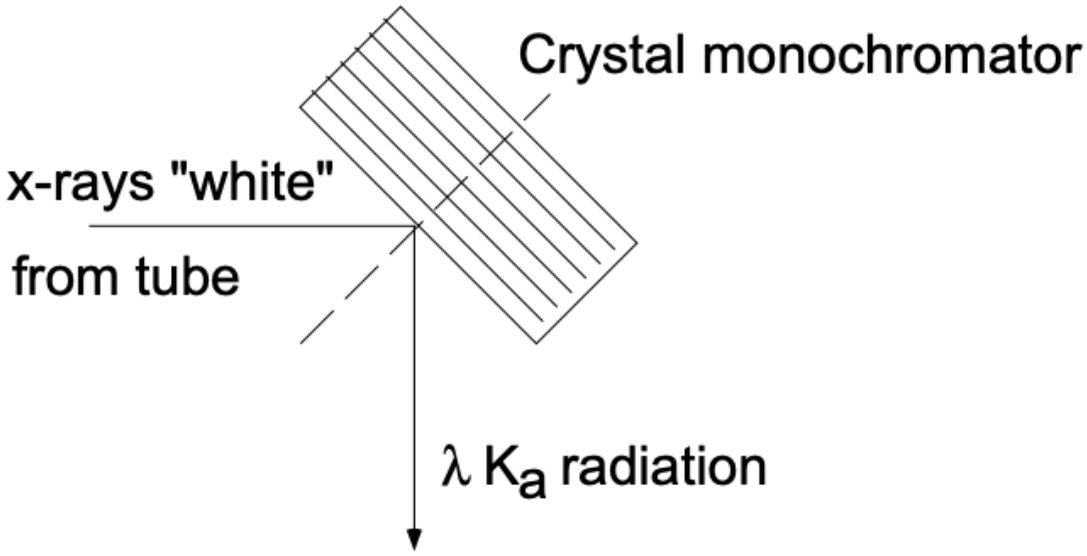


Figure 10 Isolation of monochromatic radiation from target radiation

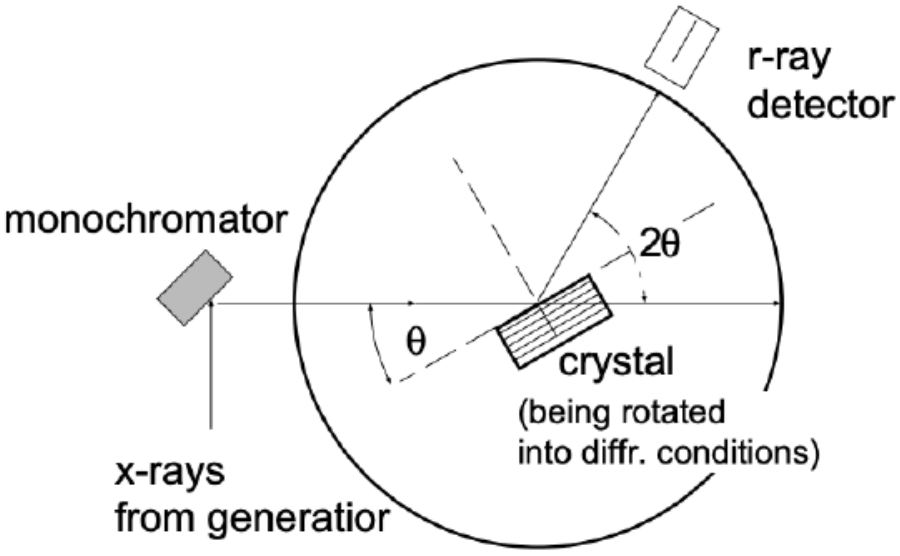


Figure 11 X-ray Diffractometer setup.

In the **Debye-Scherrer method** (fig.12) the sample is ground to a powder and placed (in an ampoule) into the center of a Debye-Scherrer camera. Exposed to monochromatic X-rays, in this way a large number of diffracted cone-shaped beams are generated such that the semiangles of the cones measure 2θ, or twice the Bragg angle for the particular diffracting crystallographic planes. The reason diffracted beams are cone-shaped is that the planes in question (within the multitude of randomly oriented grains) give rise to diffraction for any orientation around the incident beam as long as the incident beam forms the appropriate Bragg angle with these planes – thus there is a rotational symmetry of the diffracted beams about the direction of the incident beam. Those planes with the largest interplanar spacing have the smallest Bragg angle, θ.

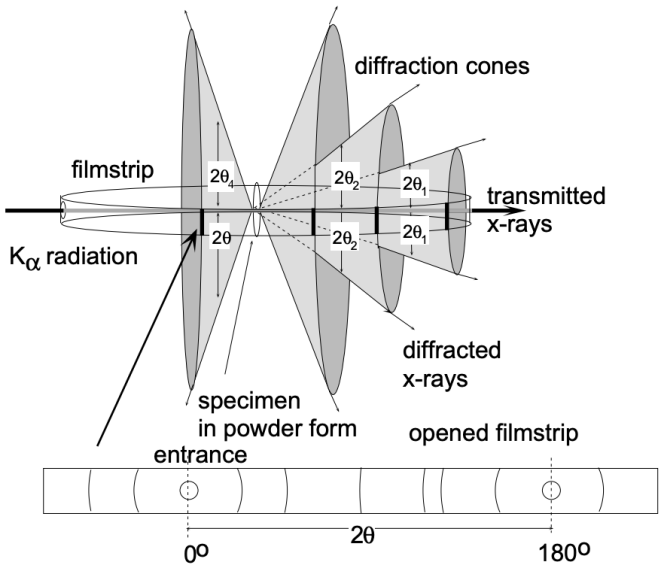


Figure 12 Debye-Scherrer powder diffraction setup and analysis

In a Debye-Scherrer arrangement, after exposing a powder of a crystalline material to monochromatic X-rays, the developed film strip will exhibit diffraction patterns such as indicated in fig. 12. Each diffraction peak (dark line) on the film strip corresponds to constructive interference at planes of a particular interplanar spacing $[\mathrm{d}_{(\mathrm{hkl})}]$. The problem now consists of "indexing" the individual lines - i.e., determining the Miller indices (hkl) for the diffraction lines:

$$\begin{aligned} \text{Bragg:} \quad \lambda &= 2\ \mathrm{d}_{(\mathrm{hkl})} \sin\theta \qquad ;\mathrm{d}_{(\mathrm{hkl})} = \frac{\mathrm{a}}{\sqrt{\mathrm{h}^2+\mathrm{k}^2+\mathrm{l}^2}} \\ \lambda^2 &= 4\ \mathrm{d}^2_{(\mathrm{hkl})} \sin^2\theta \qquad ;\mathrm{d}^2_{(\mathrm{hkl})} = \frac{\mathrm{a}^2}{\left(\ \mathrm{h}^2+\mathrm{k}^2+\mathrm{l}^2\right)} \end{aligned} \tag{9.3.2}$$

Substitution and rearrangement of above yields:

$$\frac{\sin^2\theta}{\left(h^2+k^2+|^2\right)} = \frac{\lambda^2}{4a^2} = \text{ const.}$$

Accordingly, we find that for all lines (θ values) of a given pattern, the relationship

$$\frac{\sin^2\theta_1}{\left(h^2+k^2+|^2\right)_1} = \frac{\sin^2\theta_2}{(h^2+k^2+\mathrm{I}^2)_2} = \frac{\sin^2\theta_3}{(h^2+k^2+\mathrm{I}^2)_3} = \text{ const.}$$

holds. Since the sum $(h^2+k^2+l^2)$ is always integral and $\lambda^2/4a^2$ is a constant, the problem of indexing the pattern of a cubic system is one of finding a set of integers $(h^2+k^2+l^2)$ which will yield a constant quotient when divided one by one into the observed $\sin^2\theta$ values. (Certain integers such as $7, 15, 23$, etc. are impossible because they cannot be formed by the sum of three squared integers.)

Indexing in step-by-step sequence is thus performed as follows: θ values of the lines are obtained from the geometric relationship of the unrolled film strip. Between the exit hole of the X-ray beam $(2\theta = 0^\circ)$ and the entrance hole $(2\theta = 180^\circ)$ the angular relationship is linear (fig. 12). The increasing θ values for successive lines are indexed $\theta_1, \theta_2, \theta_3$, etc., and $\sin^2\theta$ is determined for each. If the system is simple cubic we know that all planes present will lead to diffraction and the successive lines (increasing θ) result from diffraction on planes with decreasing interplanar spacing: (100), (110), (111), (200), (210), (211), (220), etc. From equation (3) above we recognize:

$$\frac{\sin^2\theta_1}{1} = \frac{\sin^2\theta_2}{2} = \frac{\sin^2\theta_3}{3} = \frac{\sin^2\theta_4}{4} = \frac{\sin^2\theta_5}{5} = \text{ const.}$$

If the system is BCC, however, we know from the selection rules that only planes for which $(h+k+l) =$ even will reflect. Thus:

$$\frac{\sin^2\theta_1}{2} = \frac{\sin^2\theta_2}{4} = \frac{\sin^2\theta_3}{6} = \frac{\sin^2\theta_4}{8} \text{ etc. } = \text{ const.}$$

[SC can be differentiated from BCC through the fact that no sum of three squared integers can yield 7, but 14 can be obtained from planes (321)].

For FCC systems, the selection rules indicate reflections on planes with unmixed h,k,l indices:

$$\frac{\sin^2\theta_1}{3} = \frac{\sin^2\theta_2}{4} = \frac{\sin^2\theta_3}{8} == \text{ const.}$$

After proper indexing, the constant is obtained:

$$\frac{\sin^2\theta}{(h^2+k^2+L^2)} = \text{ const.}$$

and the particular Bravais lattice is identified. The lattice constant of the unit cell is subsequently obtained, knowing the wavelength of the incident radiation:

$$\begin{aligned} \frac{\sin^2\theta}{(\mathrm{h}^2+\mathrm{k}^2+\mathrm{I}^2)} &= \text{const.} = \frac{\lambda^2}{4\mathrm{a}^2} \\ a^2 &= \frac{\lambda^2}{4\sin^2\theta}\left(h^2+k^2+1^2\right) \\ a &= \frac{\lambda}{2\sin\theta}\sqrt{\left(h^2+k^2+1^2\right)} \end{aligned} \tag{9.3.3}$$

This page titled 9.3: X-rays and X-ray Diffraction is shared under a CC BY-NC-SA 4.0 license and was authored, remixed, and/or curated by Donald Sadoway (MIT OpenCourseWare).

- 1.5: X-rays and X-ray Diffraction by Donald Sadoway is licensed CC BY-NC-SA 4.0. Original source: https://ocw.mit.edu/courses/3-091sc-introduction-to-solid-state-chemistry-fall-2010/pages/syllabus/.

9.4: The Imperfect Solid State

INTRODUCTION

Real crystals are never perfect: they always contain a considerable density of defects and imperfections that affect their physical, chemical, mechanical and electronic properties. The existence of defects also plays an important role in various technological processes and phenomena such as annealing, precipitation, diffusion, sintering, oxidation and others. It should be noted that defects do not necessarily have adverse effects on the properties of materials. There are many situations in which a judicious control of the types and amounts of imperfections can bring about specific characteristics desired in a system. This can be achieved by proper processing techniques. In fact, “defect engineering” is emerging as an important activity.

All defects and imperfections can be conveniently considered under four main divisions: *point defects*, *line defects* or dislocations, *planar defects* or interfacial or grain boundary defects, and *volume defects*. We can also add here *macroscopic* or *bulk defects* such as pores, cracks and foreign inclusions that are introduced during production and processing of the solid state. Point defects are inherent to the equilibrium state and thus determined by temperature, pressure and composition of a given system. The presence and concentration of other defects, however, depend on the way the solid was originally formed and subsequently processed.

Briefly consider the effects of *imperfections* or crystal defects on a few important properties of solids. The electrical behavior of semiconductors, for example, is largely controlled by crystal imperfections. The conductivity of silicon can thus be altered in type (n or p) and by over eight orders of magnitude through the addition of minute amounts of electrically active dopant elements. In this case, each atom of dopant, substitutionally incorporated, represents a point defect in the silicon lattice. The fact that such small amounts of impurity atoms can significantly alter the electrical properties of semiconductors is responsible for the development of the transistor and has opened up the entire field of solid state device technology. Practically none of the semiconducting properties that led to these engineering accomplishments are found in a “perfect” crystal. They are properties peculiar to the defective solid state.

The existence of dislocations (line defects) in crystals provides a mechanism by which permanent change of shape or mechanical deformation can occur. A crystalline solid free of dislocations is brittle and practically useless as an engineering material. While the existence of dislocations in crystals insures ductility (ability to deform), the theoretical strength of crystalline solids is drastically reduced by their presence.

We should recognize that dislocations play a central role in the determination of such important properties as strength and ductility. In fact, virtually all mechanical properties of crystalline solids are to a significant extent controlled by the behavior of line imperfections.

The ability of a ferromagnetic material (such as iron, nickel or iron oxide) to be magnetized and demagnetized depends in large part on the presence of two-dimensional imperfections known as *Bloch walls*. These interfaces are boundaries between two regions of the crystal which have a different magnetic state. As magnetization occurs, these defects migrate and by their motion provide the material with a net magnetic moment. Without the existence of Bloch walls all ferromagnetic materials would be permanent magnets. In fact, electromagnets would not exist if it were not for this type of defect.

The presence of surface defects such as cracks causes brittle materials like glass to break at small applied stresses. This fact is familiar to anyone who has broken a glass tube by first filing a small notch (or crack) into the surface. Removal of cracks from the surface of glass either by etching in hydrofluoric acid or by flame polishing almost always raises the fracture strength. For example, glass in the absence of any surface cracks has a fracture strength of $\sim 10^{10} \mathrm{Newton} / \mathrm{m}^2$ (as opposed to real glass which has a fracture strength of $\sim 0^7$ Newton $/ \mathrm{m}^2$).

POINT DEFECTS

Formation of Point Defects

An incontrovertible law of nature states: “Nothing is perfect”. This law applies to humans as well as to the inorganic world of crystalline solids and can be formulated as the 2nd law of thermodynamics:

$$\mathrm{F} = \mathrm{H} - \mathrm{TS} \tag{1}$$

where F is the free energy of a given system, H is the heat content or enthalpy and TS is the entropy, or disorder, term. If a reaction takes place at a temperature T, we find the change in $\mathrm{F}(\Delta \mathrm{F})$ related to a change in $\mathrm{H}(\Delta \mathrm{H})$, the heat content, and possibly also a change in TS $(T \Delta S)$. Such is the case when defects are formed in a perfect solid: The energy distribution in a solid (Maxwell-Boltzmann) suggests that a number of individual atoms may acquire enough thermal energy to be displaced from the equilibrium lattice site into an interstitial position. This process of point defect formation requires energy and leads to lattice strain which constitutes, as discussed earlier, an increase in the heat content of the system (ΔH is positive and increases linearly with the number of defects formed). The departure from perfection by the generation of defects leads to disorder (ΔS is positive). The magnitude of disorder generated (ΔS) is very large during the initial step from perfection to slight disarray, but the increase in disorder (with a given number of defects generated) decreases as the overall disorder increases.

Correspondingly the term $T \Delta S$ drops rapidly at the beginning and then flattens out. The net result (fig. 1), free energy, exhibits a minimum for a certain number of defects in the

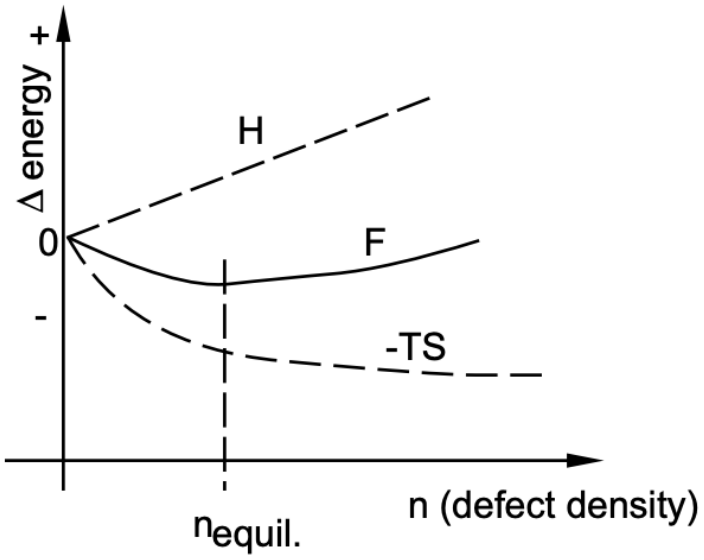


Figure 1 Thermodynamics of point defect formation

solid [equilibrium defect density = f (temperature)]; the F_{minimum} suggests also that the transition from perfection to equilibrium defect structure is spontaneous: it occurs naturally!

While the detailed mechanisms for the formation of atomic vacancies in solids are still the subject of extensive research, the associated equilibrium energetics are clear: calculations of the thermal energy of atoms in a lattice show that the average vibrational energy of lattice atoms is much less than $1 \mathrm{eV}$ (the approximate energy change associated with vacancy formation, i.e., the least amount of energy required to form a vacancy) at room temperature. Therefore a lattice atom will only acquire the energy $\Delta \mathrm{H}_{\mathrm{d}}$, the energy required to form the defect, upon the occurrence of a large energy fluctuation. Since the relative probability of an atom having an energy $\Delta \mathrm{H}_d$ or more in excess of the ground state energy is $e^{-\Delta H_d / kT}$, the probability that an atomic site is vacant varies in the same way. In a (molar) crystal containing N atomic sites, the number n_{d} of vacant sites is, therefore,

$$\mathrm{n_d} = \mathrm{ANe}^{-\Delta \mathrm{H_d/kT}} \tag{2}$$

where

- n_{d} is the number of defects (in equilibrium at T)
- N is the total number of atomic sites per mole
- $\Delta \mathrm{H}_{\mathrm{d}}$ is the energy necessary to form the defect
- T is the absolute temperature (K)
- k is the Boltzmann constant
- A is a proportionality constant

Point Defects in “Pure” Metallic Systems

Point defects in “pure” crystalline metals are defects of atomic dimensions, such as impurity atoms, the absence of a matrix atom and/or the presence of a matrix atom in the wrong place. Some of these point defects are shown in fig. 2. An impurity atom that occupies a normal lattice site is called a *substitutional impurity atom* and an impurity atom found in the interstice between matrix atoms is called an *interstitial impurity atom*. Whether a foreign atom will occupy a substitutional

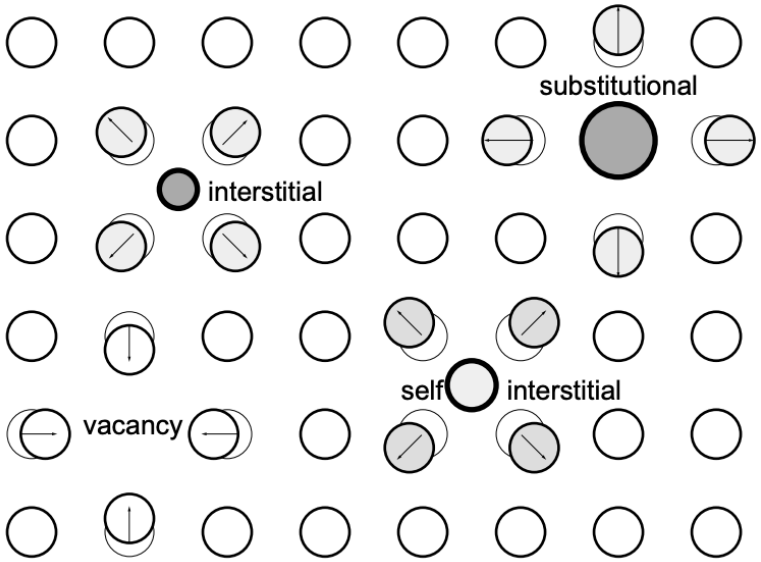


Figure 2 Point defects in crystalline solids

or interstitial site depends largely on the size of the atom relative to the size of the site. Small atoms are usually interstitial impurities, while larger atoms are usually substitutional impurities.

A *vacancy* is an atom site, normally occupied in the perfect crystal, from which an atom is missing. Often the term “vacancy” is used to denote a so-called *Schottky defect*, which is formed when an atom or an ion leaves a normal lattice site and repositions itself in a lattice site on the surface of the crystal. This may be the result of atomic rearrangement in an existing crystal at a high temperature when atomic mobility is high because of increased thermal vibrations. A vacancy may also originate in the process of crystallization as a result of local disturbances during the growth of new atomic planes on the crystal surface. Vacancies are point defects of a size nearly equal to the size of the original (occupied) site; the energy of the formation of a vacancy is relatively low - usually less than 1 eV.

The number of vacancies at equilibrium at each temperature in a crystal can be determined from eq. (2), in which $\Delta \mathrm{H_d}$ is the energy necessary to take an atom from a regular site of the crystal and place it on the surface for a Schottky-type defect. When a solid is heated a new higher equilibrium concentration of vacancies is established, usually first at crystal surfaces and then in the vicinity of dislocations and grain boundaries which provide sites for the atoms which have left their normal lattice site. Vacancies gradually spread throughout the crystal (from the surfaces into the bulk). On cooling the vacancy concentration is lowered by "diffusion of vacancies" to grain boundaries or dislocations, which act as sinks. In both cases, the new equilibrium vacancy concentration is established only after a finite amount of time. The rate at which vacancies move from point to point in the lattice decreases exponentially with decreasing temperature. Thus, on very rapid cooling (quenching) from a high temperature near the melting point most of the vacancies do not have time to diffuse to sinks and are said to be "frozen in". This gives a considerably greater ("non-equilibrium") concentration of vacancies in quenched specimens than that indicated by the thermal equilibrium value.

The concentration of vacant lattice sites in pure materials is very small at low temperatures - about one vacancy every 10^8 atom sites - and increases with increasing temperature to about one vacancy every 10^3 sites at the melting temperature. Vacancies are important because they control the rate of matrix (or substitutional) atom diffusion - i.e., atoms are able to move around in a crystalline solid primarily because of the presence of vacancies. (The mechanism by which they move is the same as that associated with moving a car in a filled parking lot to the exit). This is shown schematically in fig. 3. S*elf-interstitials* are generally not encountered in close-packed

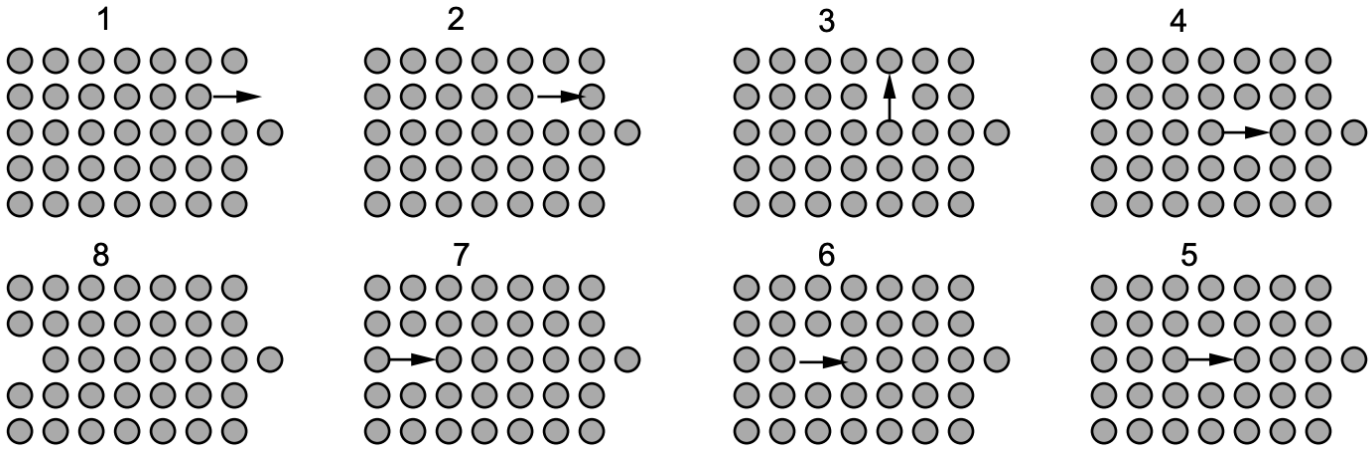


Figure 3 Dynamics of vacancy movements in a close packed solid

metallic systems, but may be introduced by irradiation. For example, high-energy neutrons from atomic fission can knock metal atoms from their regular sites into interstitial sites, creating vacancy-interstitial pairs.

Point Defects in Ionic Solids

Point defects in ionic structures differ from those found in pure elements because of the charge neutrality requirement. For example, in a pure monovalent ionic material a cation vacancy must have associated with it either a cation interstitial or an anion vacancy to maintain charge neutrality. Similar requirements hold for anion vacancies. A vacancy pair defect (migration of a cation and an anion to the surface) is usually called a *Schottky imperfection*, and a vacancy-interstitial pair defect is referred to as a *Frenkel imperfection* (an anion or cation has left its lattice position, which becomes a vacancy, and has moved to an interstitial position). These two types of imperfections are shown in fig. 4. Self-interstitials are much more common in ionic structures than in pure elements because many ionic compounds have relatively large interstitial sites available. That is, there are often interstitial sites in the unit cell that have nearly the

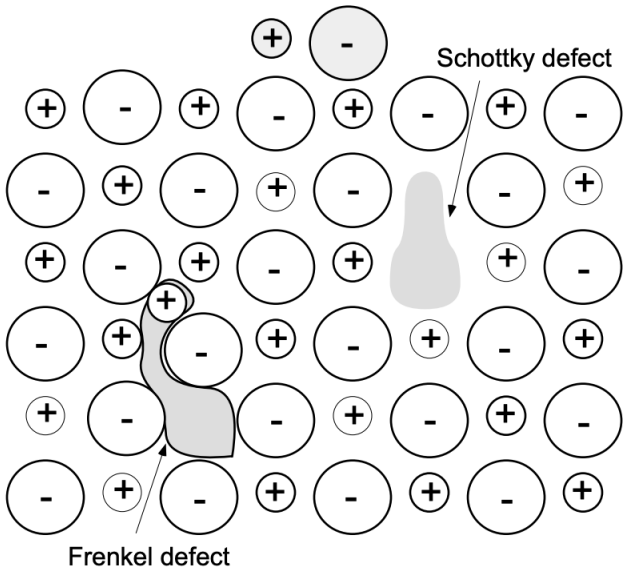


Figure 4 Point defects in ionic solids

same surroundings as normal atom sites. (For example, in BeO the Be atoms fill only one-half the available tetrahedral sites, leaving four possible cation interstitial sites per unit cell. Thus a Be atom could go from a regular lattice site to an almost equivalent interstitial site with little distortion of the lattice.)

Foreign atoms in ionic crystals produce defects that also must maintain charge neutrality. For example, in NaCl a monovalent cation, such as lithium, may simply replace one of the sodium ions as a substitutional impurity. But a divalent cation, such as

calcium, replacing a sodium ion must be accompanied by either a cation vacancy or an anion interstitial if charge neutrality is to be maintained. Correspondingly, monovalent impurity cations in a divalent structure (e.g., Na in MgO) must be accompanied by an appropriate number of cation interstitials or anion vacancies.

Point Defects in Covalently Bonded Solids

Substitutional impurities in covalently bonded materials can create a unique imperfection in the electronic structure if the impurity atom is from a group in the periodic table other than the matrix atoms. For example, you already considered Group V and Group III elements in a Group IV matrix, such as As or B in Si.

When foreign atoms are incorporated into a crystal structure, whether in substitutional or interstitial sites, we say that the resulting phase is a *solid solution* of the matrix material (solvent) and the foreign atoms (solute). The term “solid solution”, however, is not restricted to the low solute contents of doped semiconductor systems; there are many solid solutions, such as metallic alloys, that comprise a wide composition range.

LINE DEFECTS

Line imperfections, or *dislocations*, in crystalline solids are defects that produce lattice distortions centered about a line. A dislocation is simply the edge of an extra inserted fractional plane of atoms (fig. 5). Normally the symbol ⊥ is used to represent a *positive*

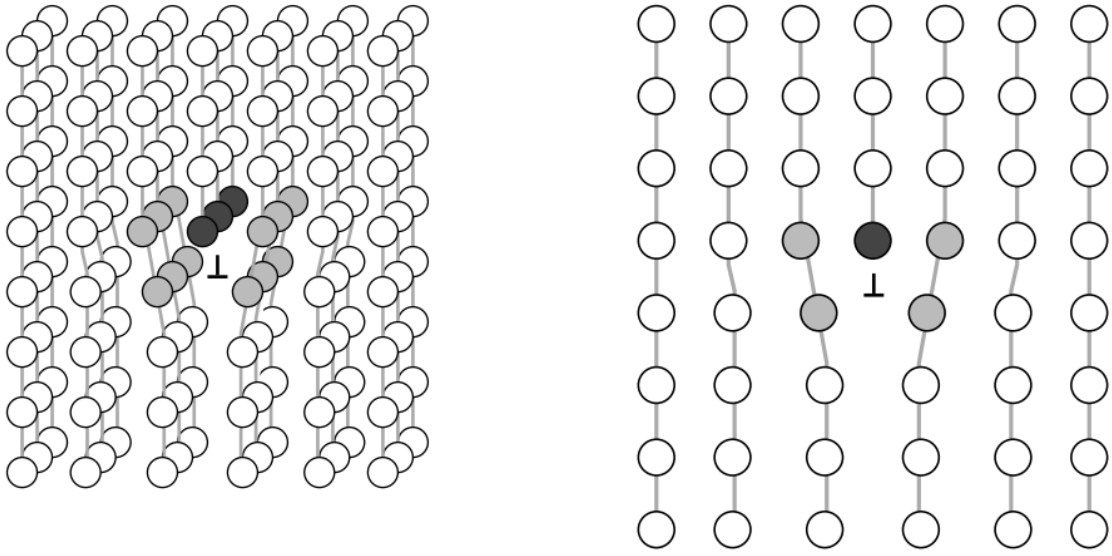


Figure 5 Schematic presentation of a dislocation; the last row of atoms (dark) in the inserted fractional plane

dislocation (extra fractional plane) and ⊤ is used to represent a *negative dislocation* (missing fractional plane).

The importance of dislocations is readily demonstrated in the deformation of crystalline materials. The plane in which a dislocation moves through the lattice is called a *slip plane*. With an applied shear stress the dislocation moves, atomic row by atomic row, and one part of the crystal is displaced relative to the other. When the dislocation has passed through the crystal, the portion of the crystal above the *slip plane* has shifted one atomic distance relative to the portion below the slip plane. In other words, the motion of the dislocation has caused the crystal to change its shape - to be permanently deformed (fig. 6).

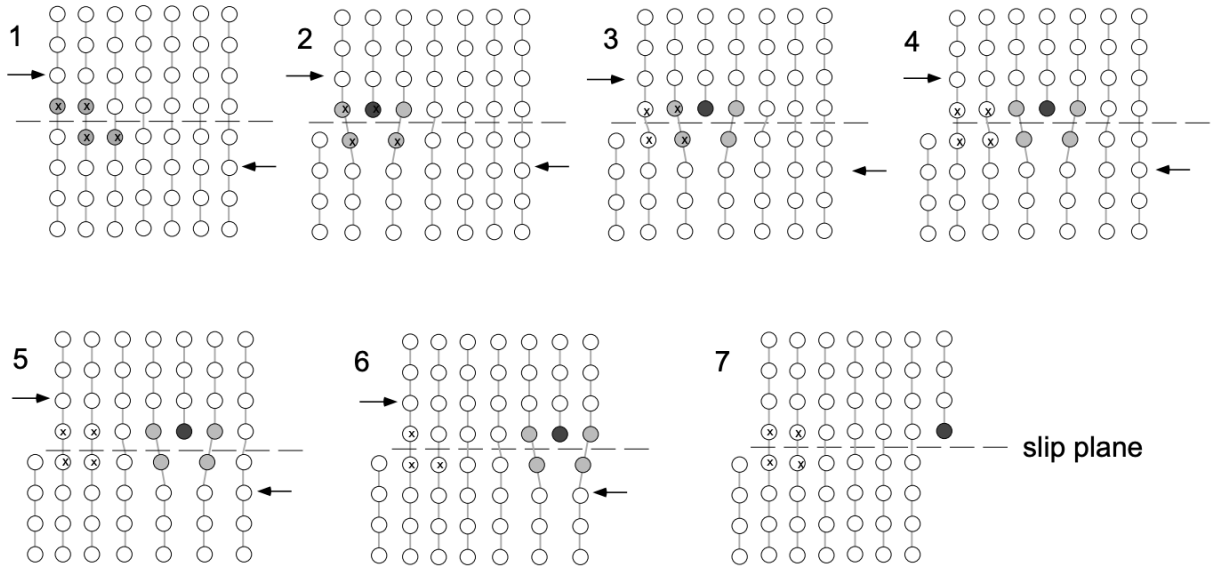


Figure 6 Plastic deformation of crystalline solid by slip associated with stress induced motion of dislocation

Please note: on either side of the dislocation the crystal lattice is essentially perfect, but in the immediate vicinity of the dislocation the lattice is severely distorted. For a positive edge dislocation, the presence of the extra half plane causes the atoms above the slip plane to be put in compression, while those below the slip plane are put in tension. Consequently, the edge dislocation will have a stress field around it that is compressive above the slip plane and tensile below the slip plane.

Plastic Deformation By Slip:

When single crystals of metal (or semiconductor) are pulled in tension, they will begin to deform (elongate) plastically at relatively low stress levels, and "blocks" of the crystals slide over one another because of dislocation motion. Simultaneously, so-called *slip lines* appear on their surface. It is found that deformation by slip occurs most easily on planes with high atomic density and with large interplanar spacing, while the direction of slip is in all instances an atomically "close-packed direction". For FCC structures we therefore observe as the primary slip system {111} planes in direction, while in BCC structures the primary slip occurs on {110} planes in directions. (It should be noted that an alternate deformation mechanism is "deformation twinning", presently not to be considered.)

Dislocation Climb:

Climb is the name given to the motion of dislocations when the extra "half" plane is extended farther into a crystal or partially withdrawn from it. Clearly, the climb process is not a motion of the plane, but rather its growth or shrinking as a result of the addition of atoms or "vacancies" respectively from the environment of the dislocation (fig. 7).

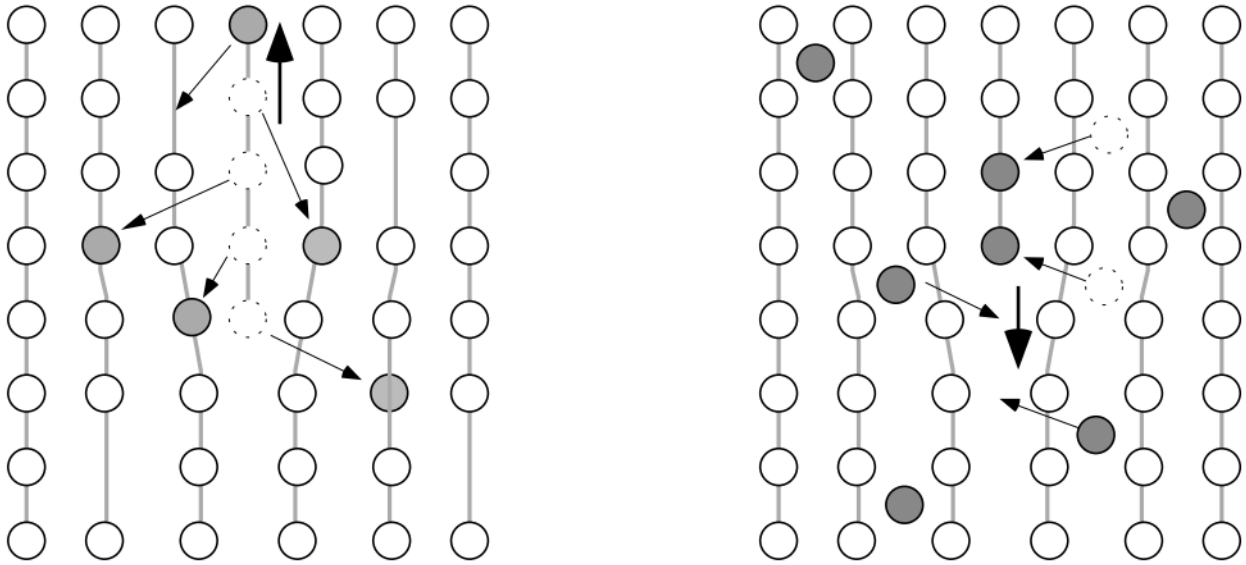


Figure 7 Dislocation climb by (a) loss of atoms to surrounding vacancies and (b) incorporation of interstitial atoms.

Multiplication of Dislocations:

Since during slip each dislocation leaves the matrix, macroscopic deformation could not take place given normal dislocation densities in the range of $10^6 - 10^8/\mathrm{cm}^3$. Examination of the deformed crystals indicates that multiplication of dislocations takes place during deformation. While there are a multitude of multiplication mechanisms, the one most extensively studied is the Frank-Read Source (not to be discussed in detail).

Dislocation Interactions:

The relative ease with which dislocations move across a solid matrix can be attributed to the severe displacements of atoms in the core of dislocations. If these local stresses are reduced, the mobility of dislocations - and thus the ease of slip - is reduced. It is found that impurities in the vicinity of dislocation cores tend to reduce the local distortion energy of the dislocations and thus stabilize the system against slip. In many systems impurities are intentionally added (e.g., solid solution hardening) to increase the strength of materials. Similarly, micro-precipitates tend to impede dislocation motion (e.g., precipitation hardening).

INTERFACIAL IMPERFECTIONS

The several different types of interfacial, or planar imperfections, in solids can be grouped into the following categories:

1. Interfaces between solids and gases, which are called *free surfaces;*
2. Interfaces between regions where there is a change in the electronic structure, but no change in the periodicity of atom arrangement, known as *domain boundaries;*
3. Interfaces between two crystals or grains of the same phase where there is an orientation difference in the atom arrangement across the interface; these interfaces are called *grain boundaries;*
4. Interfaces between different phases, called *phase boundaries,* where there is generally a change of chemical composition and atom arrangement across the interface.

Grain boundaries are peculiar to crystalline solids, while free surfaces, domain boundaries and phase boundaries are found in both crystalline and amorphous solids.

Free Surfaces

Because of their finite size, all solid materials have free surfaces. The arrangement of atoms at a free surface differs slightly from the interior structure because the surface atoms do not have neighboring atoms on one side. Usually the atoms near the surface have the same crystal structure but a slightly larger lattice parameter than the interior atoms.

Perhaps the most important aspect of free surfaces is the *surface energy* (γ) associated with surfaces of any solid. The source of

this surface energy may be seen by considering the surroundings of atoms on the surface and in the interior of a solid. To bring an atom from the interior to the surface, we must either break or distort some bonds - thereby increasing the energy. The surface energy is defined as the increase in energy per unit area of new surface formed. In crystalline solids, the surface energy depends on the crystallographic orientation of the surface - those surfaces that are planes of densest atomic packing are also the planes of lowest surface energy. This is because atoms on these surfaces have fewer of their bonds broken or, equivalently, have a larger number of nearest neighbors within the plane of the surface. Typical values of surface energies of solids range from about 10^{-1} to $1\ \mathrm{J/m^2}$. Generally, the stronger the bonding in the crystal, the higher the surface energy.

Surface energies can be reduced by the adsorption of foreign atoms or molecules from the surrounding atmosphere. For example, in mica the surface energy of freshly cleaved material in a vacuum is much higher than the surface energy of the same surface cleaved in air. In this instance, oxygen is adsorbed from the air to partially satisfy the broken bonds at the surface. Impurity atom adsorption makes it almost impossible to maintain atomically clean surfaces. As a result, surface properties such as electron emission, rates of evaporation and rates of chemical reactions are extremely dependent on the presence of any adsorbed impurities. These properties will be different if the measurements are made under conditions giving different surface adsorption.

Grain Boundaries

Grain boundaries separate regions of different crystallographic orientation. The simplest form of a grain boundary is an interface composed of a parallel array of edge dislocations. This particular type of boundary is called a tilt boundary because the misorientation is in the form of a simple tilt about an axis, parallel to the dislocations. Tilt boundaries are referred to as low-angle boundaries because the angle of misorientation is generally less than 10°.

When a grain boundary has a misorientation greater than 10° or 15°, it is no longer practical to think of the boundary as being made up of dislocations because the spacing of the dislocations would be so small that they would lose their individual identity. The grain boundary represents a region a few atomic diameters wide where there is a transition in atomic periodicity between adjacent crystals or grains.

Grain boundaries have an interfacial energy because of the disruption in atomic periodicity in the vicinity of the boundary and the broken bonds that exist across the interface. The interfacial energy of grain boundaries is generally less than that of a free surface because the atoms in a grain boundary are surrounded on all sides by other atoms and have only a few broken or distorted bonds.

Solids with grain boundaries are referred to as *polycrystalline*, since the structure is composed of many crystals - each with a different crystallographic orientation. In the case of iron the grain boundary structure can be revealed by preferential chemical attack (*etching*) at the grain boundaries, while the grain structure in polyethylene is revealed by the use of polarized light. The grain structure is usually specified by giving average grain diameter or by using a scheme developed by the American Society for Testing and Materials (ASTM). In the ASTM procedure the grain size is specified by a “grain size number” (n) where

$$N = 2^{n-1} \tag{9.4.1}$$

with N equal to the number of grains per square inch when the sample is viewed at 100X magnification. For example, at a magnification of $X = 100$, a material with grain size number 8 will show 128 grains per inch ^{2} - this material in effect has (at $X = 1$) 1.28×10^6 grains per square inch. If the grains are approximately square in cross section, this corresponds to an average grain dimension of $8.8 \times 10^{-4}\mathrm{in}^*$.

In polycrystalline samples the individual grains usually have a random crystallographic orientation with respect to one another, and the grain structure is referred to as *randomly oriented*. In some instances, however, the grains all have the same orientation to within a few degrees. In this instance the material is said to have a *preferred orientation* or *texture*.

Phase Boundaries

A *phase* is defined as a *homogeneous, physically distinct and mechanically separable portion of the material with a given chemical composition and structure*. Phases may be substitutional or interstitial solid solutions, ordered alloys or compounds, amorphous substances or even pure elements; a crystalline phase in the solid state may be either polycrystalline or exist as a single crystal.

Solids composed of more than one element may - and often do - consist of a number of phases. For example, a dentist's drill, something painfully familiar to all of us, consists of a mixture of small single crystals of tungsten carbide surrounded by a matrix of cobalt. Here the cobalt forms a continuous phase. Polyphase materials such as the dentist's drill are generally referred to as

composite materials. Composite materials have great importance in the engineering world because they have many attractive properties that set them apart from single-phase materials. For example, the dentist's drill has good abrasive characteristics (due to the hard carbide particles) and good toughness and impact resistance (due to the continuous cobalt matrix). Neither the tungsten carbide nor the cobalt has both abrasion resistance and impact resistance, yet the proper combination of the two phases yields a composite structure with the desired properties.

*

ASTM has as yet not issued specifications in SI units!

The nature of the interface separating various phases is very much like a grain boundary. Boundaries between two phases of different chemical composition and different crystal structure are similar to grain boundaries, while boundaries between different phases with similar crystal structures and crystallographic orientations may be analogous to low-angle grain boundaries in both energy and structure.

The concept of a solid consisting of a continuous phase and a discontinuous phase (or phases) leads to a simple classification of the various types of composite materials. Table 1 gives this classification, which is based on the structure (whether amorphous or crystalline) of the continuous and discontinuous phases.

TABLE 1

Classification of Composite or Multiphase Materials

Continuous Phase	Discontinuous Phase (or Phases)	Examples
Crystalline	Crystalline	All metallic systems such as cast iron, steel, soft solder, etc.; most natural rocks such as granite and marble.
Crystalline	Amorphous	None of practical significance.
Amorphous	Crystalline	Most man-made ceramics such as building bricks and electrical insulator porcelain, concrete, partially crystalline polymers, some polymer-crystalline particle composites.
Amorphous	Amorphous	Fiberglass, asphalt, wood, hydrated cement, other gels.

This page titled 9.4: The Imperfect Solid State is shared under a CC BY-NC-SA 4.0 license and was authored, remixed, and/or curated by Donald Sadoway (MIT OpenCourseWare).

- 1.6: The Imperfect Solid State by Donald Sadoway is licensed CC BY-NC-SA 4.0. Original source: https://ocw.mit.edu/courses/3-091sc-introduction-to-solid-state-chemistry-fall-2010/pages/syllabus/.

9.5: Glasses

INTRODUCTION

When a liquid phase is cooled to below its freezing temperature, it usually transforms into a crystalline solid, i.e. it crystallizes. Some liquids, because of complex molecular configuration or slow molecular transport, do not “crystallize” (assume an ordered configuration) upon being cooled to low temperatures, but instead form a rigid disordered network, known as glass, which is very similar in structure to that of the liquid. Most metals and alkali halides crystallize easily upon cooling through the freezing temperature because the structural rearrangement from the liquid to the crystalline state is simple and bonding is nondirectional. At temperatures just above the freezing temperature, most metals and molten salts have fluidities approximately equivalent to that of water at room temperature. Thus, the required structural rearrangements can take place relatively easily.

In contrast, many inorganic silicates form glasses upon cooling because the fluidity at and even above the freezing temperature is very low. This glass formation is related to the high silicon-oxygen single-bond energies and the directional bonding requirements imposed by sp^3 hybridization of silicon. The disordered liquid cannot flow easily and thus cannot undergo the rearrangements required for crystallization. Moreover, the fluidity decreases very rapidly as the temperature is lowered. [For large organic and polymeric liquids, crystallization is difficult because of their chain lengths. In polymer systems the intermolecular bonding (Van der Waals) is weak and expected to permit individual molecules to readily slide past one another. Thus, it is the "difficult" structural rearrangement required for crystallization that induces glass formation in these systems.]

The fluidity of liquids (the reciprocal of the viscosity) is a measure of their ability to flow. In turn, the viscosity (η) (fig. 1) is a measure of their resistance to flow.

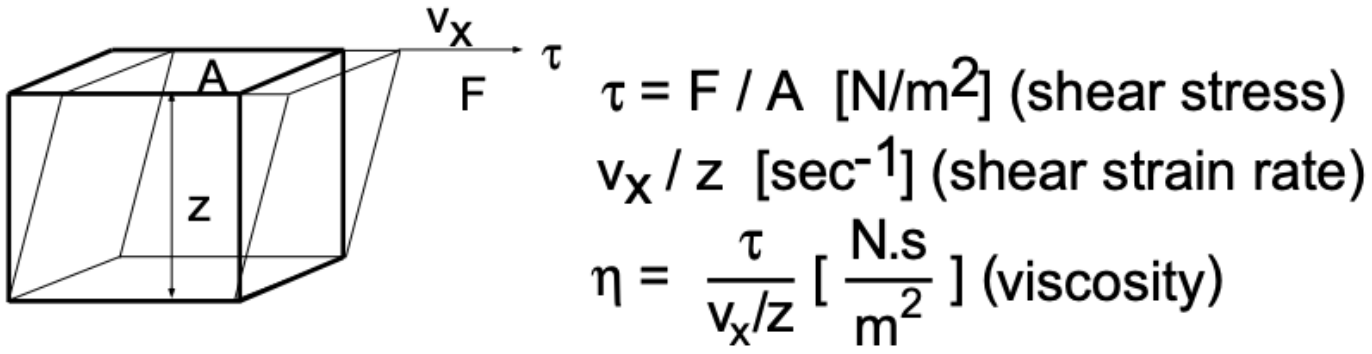


Figure 1 Dimensional analysis of viscosity

Viscosity is formulated as the ratio of an applied shear stress to the resultant shear-strain rate - its dimensions are Newton seconds per meter^2. Liquid flow, involving the motion of molecules past one another, requires the breaking and making of new bonds. Thus the fluidity, like chemical reactions and diffusion in solids (to be discussed later) is expected to exhibit an exponential temperature dependence and may be modelled as:

$$\frac{1}{\eta} \propto e^{-}\left(\frac{\text{Bond Energy}}{kT}\right) \tag{9.5.1}$$

It is noteworthy that inorganic glasses occur in nature as do organic glasses (such as the sap from trees) whereas metallic glasses do not occur naturally and have been manufactured only within the last two decades. The major obstacle to achieving metallic glasses was our inability to cool metallic melts to room temperature at rates high enough so that ordering (and thus crystallization) is prevented.

The *glass transition* point, T_g, (temperature at which a supercooled liquid becomes a glass) is for glasses what the melting point, T_m, is for crystalline solids. Characteristic for almost all glass-forming materials is that at T_g a change in the temperature dependence of the density $(\Delta \mathrm{V}/\Delta \mathrm{T})$ takes place [where the viscosity is in the range 10^4 to $10^6 \mathrm{Ns/m}^2$ (the viscosity of $\mathrm{H_2O}$ is $1.5 \times 10^{-3} \mathrm{Ns/m}^2$, or about nine orders of magnitude less)]. At higher temperatures (lower viscosities) the structural units are able to

reorganize themselves quickly as a quasi-equilibrium liquid. At temperatures below T_g reorganization among the structural units virtually ceases and the resulting rigid material is referred to as a glass. The experimental value obtained for T_g depends on the time scale of the experiment. On slow cooling, for example, the structural units have more time to reorganize and, thus, T_g is lower (fig. 2).

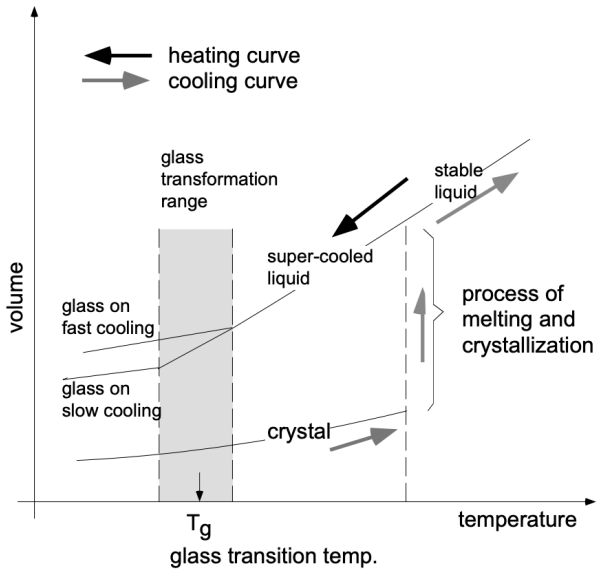


Figure 2 Volume changes associated with heating and cooling in systems susceptible to glass formation.

METALLIC GLASSES

The existence of metallic glasses shows the generality of the glass-forming process. In addition, the physical picture in this case is especially simple. Even with the highest presently attainable cooling rates (up to $10^{7^{\circ}}\mathrm{C/s}$), no "pure" metal has yet been obtained in a glassy state. However, if the liquid is an alloy of two (or more) metals whose atoms differ greatly in size, the crystallization process is more difficult and can be prevented in many instances by extremely rapid cooling of the melt $\left(10^{6^{\circ}}\mathrm{C/sec}\right)$. The two experimental techniques for rapid cooling are (1) propelling a liquid drop at high velocity and "splatting" it against a cooled copper surface, (2) flattening a liquid drop between a piston and an anvil or between two rolls and (3) "spinning" the melt by transferring it in a continuous mode onto a rapidly rotating, cooled wheel (fig. 3). X-ray patterns of the solidified alloys are similar to those of liquid metals - this and other evidence suggest that they are "amorphous", that their structure is that of a glass.

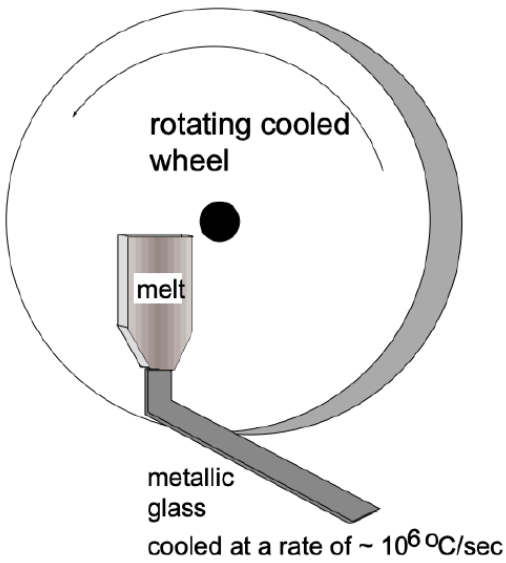


Figure 3 Production of metalic glass by melt spinning

Another method for preparing metallic glasses is by vacuum deposition onto a substrate cooled to approximately 80K. Again, pure metals crystallize under these conditions, but suitable alloys form glasses, some of which are stable when brought to room temperature. An example is the silver-copper system in which the two solid metals have only about eight percent solubility in each other. If a melt containing 50 wt.% silver and 50 wt.% copper is slowly cooled, two crystalline phases are produced. When this same alloy is obtained by vacuum deposition, a metastable metallic glass is formed. Initially the glass has metallic electrical conductivity comparable to that of the liquid alloy. When the glass is heated for $1/2$ hour at $380\ \mathrm{K}$, it converts to a crystalline, metastable face-centered cubic solid solution. Only on heating at about $500\ \mathrm{K}$ does the equilibrium, two-phase structure form. Many pure nonmetallic elements, however, such as S, Se, Ge and Si, form a stable glass under suitable conditions.

THE GLASSY STATE

The properties and chemical composition of the glass used for optical purposes differ greatly from those of the glass used for baking dishes. Likewise, the glass used for window panes differs from the glass used for artwork or optical purposes. However, (most) inorganic glasses have one thing in common: they are ceramic materials (compounds that contain metallic and non-metallic elements, most often oxygen) with the amorphous structure of a frozen liquid.

Quartz glass is not crystalline at room temperature because the rearrangement of interatomic bonds between Si and O required for the establishment of order is impeded: the viscosity of glass is so high at room temperature that millions of years would be required for it to crystallize (see above). Hence, glass can be viewed as a perfectly rigid "liquid", being exceptional in that its extraordinarily high viscosity slows down its flow properties even on an expanded time scale.

Upon cooling of liquid “glass” we observe that $\Delta V/\Delta T$ (the contraction with lowering of T) changes. This may be seen by following the three basic steps in the production of glass: (1) the melting of quartz sand (minute crystals of silica), (2) the shaping of the glass while in a viscous state and (3) the controlled cooling of the shaped article. The $\mathrm{SiO_4}$ tetrahedra in the sand (crystals) are arranged in an ordered pattern (fig. 4), but in the molten state the crystal matrix breaks up into strings and rings of tetrahedra in irregular patterns (fig. 5). Because the temperature is very high, the groupings continually break up and reform, making the mass fluid.

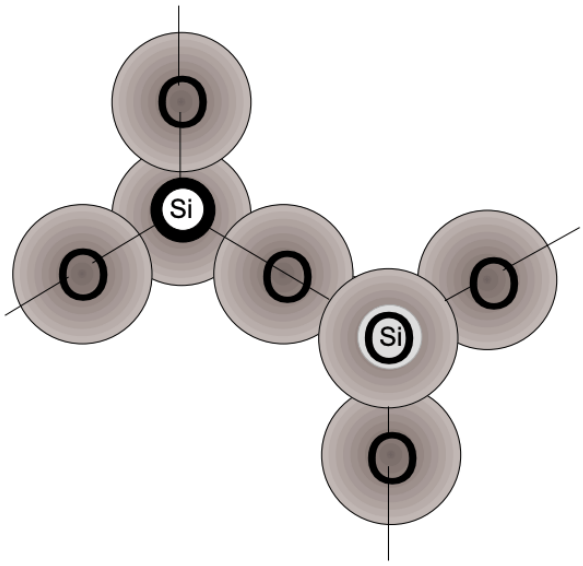


Figure 4 Basic Si - O - Si - units as established with $\mathrm{sp^3}$ hybridization of Si

Upon cooling of molten $\mathrm{SiO_2}$ the tetrahedra form larger groupings and the glass becomes more viscous, permitting it to be shaped by blowing, rolling, pressing, etc. With continuing cooling, larger groupings of tetrahedra form as their kinetic energy decreases. These two phenomena are responsible for the increase in viscosity and the shrinkage that takes place during the cooling period. Beyond the glass transformation temperature changes in configuration of the tetrahedra virtually cease because the glass, to all intents and purposes, has lost its fluidity.

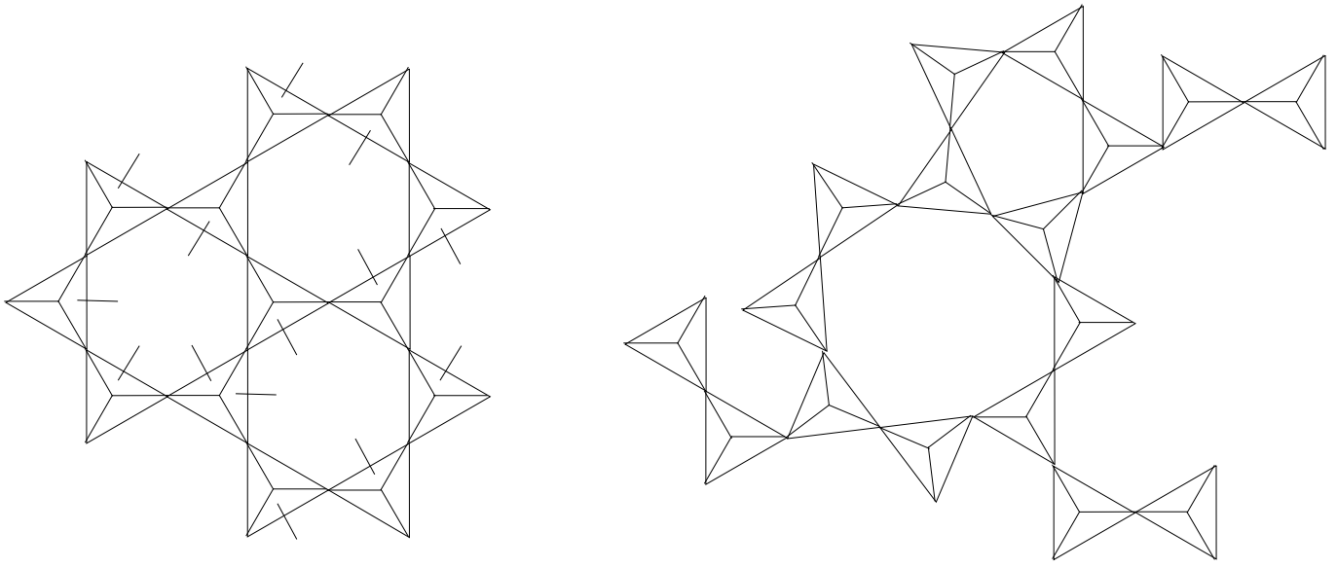


Figure 5 Two-dimensional view of tetrahedra as in silicondioxide structures: (a) in crystalline, ordered structures and (b) in disordered glassy (amorphous) structures.

OXIDE GLASSES

The bonding forces responsible for the formation of network structure in crystalline SiO_2 produce similar networks in glasses of other oxides such as B_2O_3 and P_2O_5 which are thus also considered as primary *network formers* (the present discussion will be limited to silica glasses). If an oxide, such as Na_2O, is added to silica glass, a bond in the network is broken and the relatively mobile sodium ion becomes a part of the structure (fig. 6). Examples of such *network modifiers* are $N_2O, K_2O, Li_2O, CaO, MgO$ and PbO.

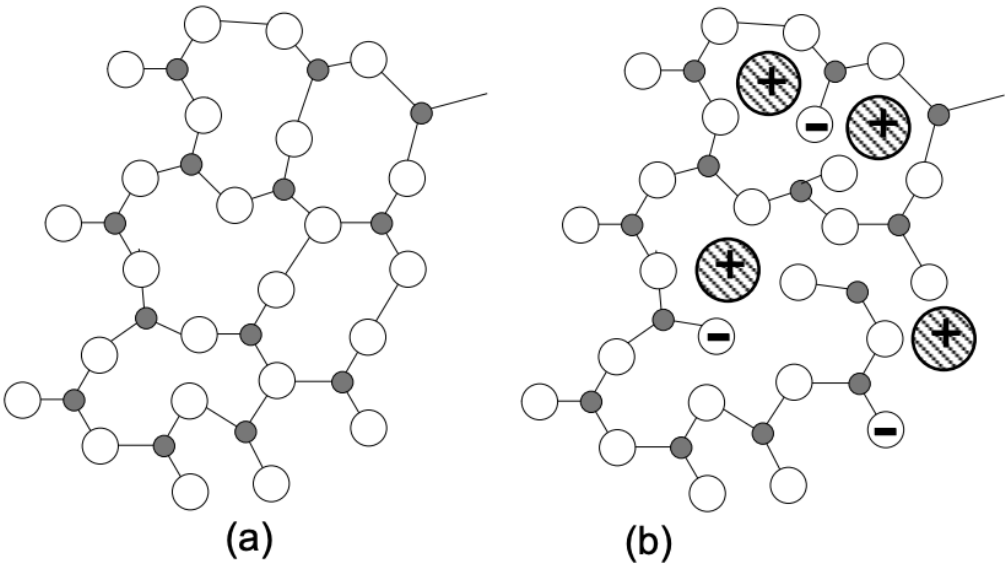


Figure 6 Schematic glass networks; (a) SiO_2 network (b) SiO_2 network modified through addition of Na_2O.

With increase in the amount of modifier, the average number of oxygen-silicon bonds forming bridges between silicon between silicon atoms decreases as follows:

O/Si Ratio in Glass	Bridging-O-Si Bonds/Si atom
2.0	4 (fig. 7)

O/Si Ratio in Glass	Bridging-O-Si Bonds/Si atom
2.5	3
3.0	2

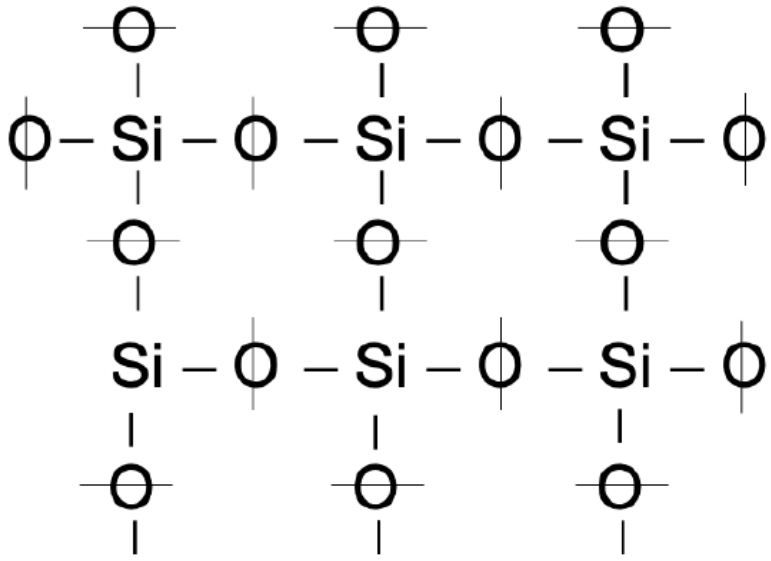


Figure 7 Schematic of SiO_2 network; the O to Si ratio is 2 : 1 as indicated by the chemical formula

Two bridging bonds per silicon atom will correspond, for example, to a linear chain structure, and any further increase in modifier would reduce the length of the chain. The principal effect of a modifier is to lower the melting and working temperature by decreasing the viscosity. An excess of modifier can make the structural units in the melt sufficiently simple and mobile that crystallization occurs in preference to the formation of a glass.

The compositions and properties of typical glasses are listed in Table 1. Soda-lime glass not only has the advantage of being made from inexpensive raw materials, but also the practical convenience of low working temperatures (fig. 8). Most glass-forming operations (pressing, drawing, etc.) begin at the temperature corresponding to the working point, but can continue while the glass cools.

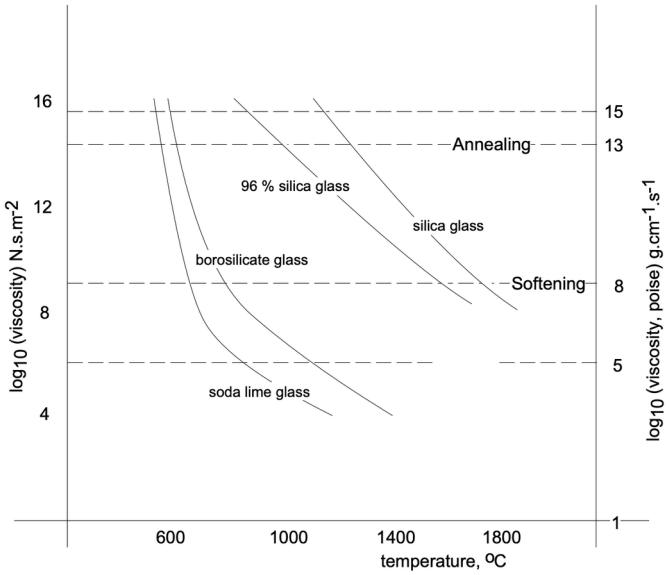


Figure 8 Important temperatures in fabrication of silicate glasses (the temperatures are related to viscosity which in turn controls workability)

ANNEALING OF GLASS

In order to relieve the internal stresses that may develop during glass formation, all commercial glassware is annealed (slowly cooled) immediately after shaping. This slow cooling operation is carried out in industry by placing the shaped objects on a conveyor belt which transports them first through a reheating zone and then through sections having successively lower temperatures in a furnace called the *lehr*.

TABLE 1. Typical Oxide Glasses

	Composition, w/o								
Type	SiO_2	Na_2O	K_2O	CaO	MgO	B_2O_3	Al_2O_3	Other	Properties or uses
Soda-lime	72	14		9	4		1		Window glass
Silica glass (fused quartz)	99.5+								High-temperature applications; low coefficient of expansion
96% silica glass	96.3	<0.2	<0.2			2.9	0.4		Comparable to fused quartz
Borosilicate	80.5	3.8	0.5			12.9	2.2		Resistant to heat and to chemicals
Light flint optical	54	1	8					37PbO	High index of refraction
Surface-strengthened glass	55	16	2	2		2	19	$4TiO_2$	Cookware
Glass-ceramic	56				15		20	$9TiO_2$	Radomes

The transformation of a liquid to a glass actually takes place over a range of temperatures at which the glass shrinks (thermal contraction). The glass does not undergo a change from disordered liquid structure to crystal structure as iron does at its transformation temperature; in glass, the transformation temperature is the temperature below which viscosity prevents any further configurational changes. Any contraction beyond the transformation temperature range is due only to the lower kinetic energy of the groupings.

The transformation temperature of a given “glass composition” depends on its constituents and upon the rate of cooling. Slow cooling results in a lower transformation range because the tetrahedra will have more time to rearrange (to some degree). This results in tighter packing of tetrahedra as the mass reaches its transformation range. When the glass reaches room temperature, its volume will be smaller when cooled slowly than glass melt which has been cooled rapidly. Hence, slower cooling from the melt results in a denser glass. (See fig. 2.)

Glass is thermodynamically unstable at room temperature because configuration changes (which require eons of years to come about!) would result in a lower free energy configuration. However, the changes are so slow that they may be considered negligible.

PROPERTIES OF GLASSES

The strong covalent bonds that exist between the atoms of inorganic glasses plus the lack of crystal structure give glass unusual characteristics. Thus, quartz glass is:

1. (a) Chemically stable;
2. (b) A poor conductor of heat and electricity;
3. (c) Inherently transparent;
4. (d) Inherently strong.

Chemical Stability

All glasses are immune to oxidation (decay) because their atoms are fully oxidized. Glass composed of 100 percent silica

tetrahedra is extraordinarily inert. It resists the action of most acids (the most notable exception is hydrofluoric acid, utilized to etch glass), but it is attacked by strong alkalis. (The bottles containing liquid alkalis on a chemist's shelf have a clouded surface.)

Conductivity

The ability of a material to conduct electricity is dependent upon the presence of electrons in the conduction band, separated in glasses by as much as 10eV from the valence band. Because the electrons in glass are tightly bonded, glass is a very poor conductor of electricity - in fact, the large energy gap makes glass an excellent insulator. Glass is also a poor conductor of heat. Thus, hot common glass may crack when cold water is poured onto it because the surface exposed to the cold water will shrink while the dimensions of the interior remain unaffected.

Strength

Glass is harder than many types of steel and is also very elastic, as evidenced by the speed and accuracy with which glass marbles rebound when they meet.

Glass has "no" crystal structure, and hence the phenomenon of slip cannot take place. This, together with the strong bonding between atoms, gives glass a very high compressive strength and a theoretical tensile strength of about $10^7 \mathrm{kN/m^2}$ (significantly higher than that of steel). (Glass fibers with an actual tensile strength of $4 \times 10^7 \mathrm{kN/m^2}$ have been produced.) Since glass has a "liquid structure" it may be considered "saturated with dislocations". [If a piece of metal has a very high dislocation density (eg., due to cold working) the dislocations interfere with each other's movements. Therefore, with increasing dislocation density a piece of metal becomes harder and stronger, but also more brittle.] Since the molecular structures in glass are unable to move, the presence of minute cracks or imperfections in glass permits stress concentrations to localize and exceed the bond strength between atoms - common glass will crack. Thus, in actual practice, the strength of glass is, by a factor of 100 to 1000, less than the theoretical strength, and glass is brittle. For example, a freshly made electric light bulb may not crack when initially dropped, but its surface becomes damaged and, after it rebounds and strikes the floor a few more times, it breaks.

The inherent high strength of fibrous glass is utilized in the fiberglass sections employed for boats and automobile bodies. Before being pressed into shape fiberglass is mixed with a synthetic resin which serves to protect the fibers from scratching. Since the fibers thus retain their high strength, fiberglass sections are very strong for their weight.

STRENGTHENED GLASS

The glass scientist has produced objects made of glass which can be struck with a hammer or dropped from a tall building without breaking. Two techniques are employed in strengthening glass - one physical and one chemical. Both techniques are based on the fact that, when there is the slightest imperfection (minute scratch) on the surface, glass remains extraordinarily strong in compression but becomes weak in tension. Thus the strengthening treatment consists of *prestressing* a glass object by inducing compressive strains in its exterior and thereby enabling it to counteract any tensile stresses which develop under tension.

In physical prestressing, the shaped object is heated to just below its softening point (surface flows are annealed out) and its surface is then chilled by means of a blast of air or an oil bath. Under these conditions the exterior of the glass cools and contracts immediately, but since glass is a poor conductor of heat the interior will not contract - the glass will not crack because the interior remains plastic. When the interior starts to cool, it cannot contract because the exterior has already set, but, in attempting to contract, the interior continues to draw the exterior together. A built-in compressive stress then develops in the outer layers of the glass. When a tensile stress is applied to this glass, it is counteracted by these compressive stresses. Thus the prestressed glass will not shatter until the surface compression is exceeded.

As long as its surface remains intact, prestressed glass continues to be strong and shock-resistant. However, if a deep scratch develops on the surface, the tensile stresses set up in the interior by the surface compression are released and the glass will shatter into thousands of tiny particles. Therefore prestressed articles must be cut to exact size and all holes drilled prior to prestressing. Among the many uses for this type of glass are plate-glass doors, side windows of automobiles and portholes of ships.

Ion exchange is a chemical technique for prestressing glass objects. The first step is to place the shaped object into a molten salt bath containing potassium ions, which replace the sodium ions on the surface of the glass. The potassium ions are larger than the sodium ions and, in accommodating them, the surface of the glass becomes more crowded - thus inducing compressive strains on the exterior. Glass of this type, characterized by very high strength, is useful for a great variety of applications. Its

flexural strength can be as high as $10^6 \mathrm{kN/m^2}$ compared with $10^5 \mathrm{kN/m^2}$ for untreated glass.

DEVITRIFICATION OF GLASS

Under certain conditions glass will become “contaminated” with crystalline particles. A glass in this condition is termed *devitrified*, which is simply another way of stating that it has partially or completely crystallized. Devitrified glass, unless of the very special variety that is deliberately produced, is undesirable since the crystalline areas form large crystals and are extremely weak and brittle, as well as being translucent only. Crystalline segregations in glass are known as stones

RECRYSTALLIZED GLASS (GLASS CERAMICS)

Recrystallized glass, also known as polycrystalline glass, is commonly produced by adding nucleating agents to the glass batch. Subsequently the glass can be formed into a desired shape by any of the conventional glass forming processes and then be heat-treated to promote recrystallization. Recrystallized glass possesses increased impact strength, hardness and thermal shock resistance compared with conventional non-crystalline glasses. One commonplace application of a recrystallized glass is in the manufacture of the so-called refrigerator-to-oven cooking dishes.

COLORED GLASSES

We recognize that glass is normally colorless due to the fact that all electrons are “tightly bonded” and no electronic excitations in the energy range of the visible light spectrum are possible. Glass, however, may be made to absorb selectively in the visible spectrum (thus becoming colored) by any one of three processes:

(1) Addition of ions of transition metals. Such ions provide electronic excitation possibilities to visible light. Typical ions added are:

$$\begin{array}{ll} \mathrm{Cr^{++}} & \text{blue} \\ \mathrm{Cr^{+++}} & \text{green} \\ \mathrm{Co^{++}} & \text{pink} \\ \mathrm{Mn^{++}} & \text{orange} \\ \mathrm{Fe^{++}} & \text{blue-green} \end{array} \tag{9.5.2}$$

(2) Addition of colloidal particles (ϕ 40 to 2000Å). These small particles, while not impeding light transmission (because of their small size) exhibit selective absorption and complementary reflection. Au particles (at 10^{-4} $\mathrm{g/cm^3}$) give colors which vary with particle size:

$$\begin{array}{lll} \mathrm{Au} & \phi 4-10 \text{ nm} & \text{pink} \\ \mathrm{Au} & \phi 10-75 \text{ nm} & \text{ruby} \\ \mathrm{Au} & \phi 75-110 \text{ nm} & \text{green} \\ \mathrm{Au} & \phi 110-170 \text{ nm} & \text{brown} \end{array} \tag{9.5.3}$$

(3) Addition of colored crystals. Some glasses are colored by means of crystals dispersed throughout. An example is the scarlet glass made by the early Egyptians (brought about by the addition of red copper oxide). Another example is red color from the addition of red $\mathrm{Pb_2CrO_6}$ whereas $\mathrm{Cr_2O_3}$ yields green color.

GLASS FIBER

Glass fiber, or fiberglass* as it is commonly known, is glass in fiber form. It is made by one of several processes, each of which involves the drawing out of the filaments from glass in the viscous state. Modern technical developments date from World War I when Germany had to find a substitute for asbestos as insulating material.

The process whereby continuous filament glass fiber is made is particularly interesting. The glass batch is melted in the glass tank furnace and the molten glass is molded into ordinary sized marbles. These marbles are fed into an electric furnace which has a platinum-alloy bushing containing many tiny holes. When the glass marbles reach the holes, the glass flows through them and is drawn down vertically, forming individual filaments. These filaments can then be twisted into a “yarn” and spun on normal textile spindles as required. About one third of an ounce of glass produces about one hundred miles of filament at a rate of about

6,000 feet per minute.

Glass wool, on the other hand, is produced by a different process. The most common technique, known as the Crown process, produces a thick matte of short glass fibers which are held together by a polymer binder. In the Crown method, a thick stream of molten glass is poured into a rapidly rotating steel dish that has tiny vents around its periphery. The glass is forced through these vents by centrifugal force, forming relatively short fibers with diameters of about 0.0007 cm. The matte is then passed through curing ovens where the binder sets and is then cut into sizes suitable for insulation.

*

Fiberglass is really a registered trade name.

SHEET AND PLATE GLASS PRODUCTION

The main types of flat glass produced are drawn sheet and float glass. The processes involved are highly automated.

Flat drawn glass is used for windows and other applications where accuracy of thickness and a high surface finish are not vital. In this process the molten glass is drawn up vertically from the end of a large rectangular tank furnace, the thickness of the drawn sheet being controlled principally by the size of the slot in the steel form held just above the surface of the molten glass. A steel starting dummy is used to commence the drawing action, but this is cracked off once it passes through. Once started, this process is continuous, the cooled and solidified sheet merely being cracked off in suitable lengths once it leaves the rolls.

The *float process* is the most recent advance in the production of plate glass with a high surface finish. In the float process, flat, fire-finished, stress-free glass is formed by preventing contact between the glass sheet and anything solid. The glass leaves the glass-tank in a continuous molten strip and is floated immediately onto the surface of a bath of molten tin. The tin bath is surrounded by a non-oxidizing atmosphere and, while in this atmosphere, the glass is heated sufficiently to prevent the development of internal stresses. As the glass sheet leaves the float bath chamber it enters an annealing furnace. Glass produced by the float process is free from distortion and has fire-finished surfaces that are smoother and flatter than those of normal polished plate glass.

This page titled 9.5: Glasses is shared under a CC BY-NC-SA 4.0 license and was authored, remixed, and/or curated by Donald Sadoway (MIT OpenCourseWare).

- 1.7: Glasses by Donald Sadoway is licensed CC BY-NC-SA 4.0. Original source: https://ocw.mit.edu/courses/3-091sc-introduction-to-solid-state-chemistry-fall-2010/pages/syllabus/.

9.6: Phase Equilibria and Phase Diagrams

PHASE EQUILIBRIA AND PHASE DIAGRAMS

Phase diagrams are one of the most important sources of information concerning the behavior of elements, compounds and solutions. They provide us with the knowledge of phase composition and phase stability as a function of temperature (T), pressure (P) and composition (C). Furthermore, they permit us to study and control important processes such as phase separation, solidification, sintering, purification, growth and doping of single crystals for technological and other applications. Although phase diagrams provide information about systems *at equilibrium*, they can also assist in predicting phase relations, compositional changes and structures *in systems not at equilibrium*.

GASES, LIQUIDS AND SOLIDS

Any material (elemental or compound) can exist as a gas, a liquid or a solid, depending on the relative magnitude of the attractive interatomic or intermolecular forces vs the disruptive thermal forces. It is thus clear that the stability (existence) of the different states of aggregation, which are referred to as *phases*, is a function of temperature and pressure (since with increased pressure the atoms, for exampled of a gas phase, are closer spaced and thus subject to increased interatomic attraction).

In general terms, a “phase” is a homogeneous, physically distinct, mechanically separable portion of a material with a given chemical composition. To illustrate this definition, let us look at a few examples of common multi-phase systems. Ice cubes in water constitute a two-phase system (ice and liquid water), unless we include the vapor above the glass in our system, which would make it a three-phase system. A mixture of oil and water would also be a two-phase system. Just as oil and water represent two distinct liquid phases, two regions of a solid with distinctly different composition or structure separated by boundaries represent two solid phases.

If we look at a one-component system, such as liquid water, we recognize that because of the energy distribution of the water molecules, some water molecules will always possess sufficient energy to overcome the attractive forces on the surface of $\mathrm{H_2O}$ and enter into the gas phase. If thermal energy is continuously supplied to a liquid in an open container, the supply of high energy molecules (which leave the liquid phase) is replenished and the temperature remains constant - otherwise the loss of high energy molecules will lower the temperature of the system. The total quantity of heat necessary to completely "vaporize" one mole of a liquid at its boiling point is called its *molar heat of vaporization*, designated by $\Delta \mathrm{H_V}$. Similarly, the heat required to completely melt one mole of a solid (the heat required to break the bonds established in the solid phase) is called the *(latent) heat of fusion* ($\Delta \mathrm{H_V}$).

Visualize a liquid in a sealed container with some space above the liquid surface. Again, some of the most energetic liquid molecules will leave the liquid phase and form a "gas phase" above the liquid. Since gas molecules will thus accumulate in the gas phase (at a constant temperature), it is inevitable that as a result of collisions in the gas phase some molecules will re-enter the liquid phase and a situation will be established whereby the rate of evaporation will equal the rate of condensation – i.e., a dynamic equilibrium between the liquid and gas phase will exist. The established pressure in the gas phase is referred to as the *equilibrium vapor pressure*, which is normally significantly less for solids than for liquids.

For obvious reasons it is desirable to know for any given material the conditions (P, T) under which the solid state, the liquid state and the gaseous state are stable, as well as the conditions under which the solid and liquid phases may coexist. These conditions are graphically presented in *equilibrium phase diagrams*, which can be experimentally determined.

ONE-COMPONENT PHASE DIAGRAM

Figure 1 illustrates the temperatures and pressures at which water can exist as a solid, liquid or vapor. The curves represent the points at which two of the phases coexist in equilibrium. At the point T_t vapor, liquid and solid coexist in equilibrium. In the fields of the diagram (phase fields) only one phase exists. Although a diagram of this kind delineates the boundaries of the phase fields, it does not indicate the quantity of any phase present.

It is of interest to consider the slope of the liquid/solid phase line of the $\mathrm{H_2O}$ phase diagram. It can readily be seen that if ice $-$ say at $-2^{\circ}\mathrm{C}$ $-$ is subjected to high pressures, it will transform to liquid $\mathrm{H_2O}$. (An ice skater will skate not on ice, but on water.)

This particular pressure sensitivity (reflected in the slope of the solid/liquid phase line) is characteristic for materials which have a higher coordination number in the liquid than in the solid phase $(\mathrm{H_2O}, \mathrm{Bi}, \mathrm{Si}, \mathrm{Ge})$. Metals, for example have an opposite slope of the solid/liquid phase line, and the liquid phase will condense under pressure to a solid phase.

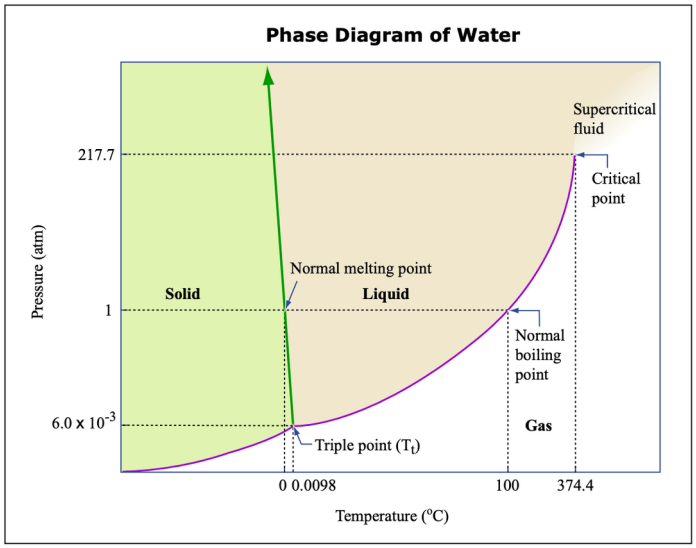


Image by MIT OpenCourseWare.

Fig. 1 Pressure/Temperature Diagram for Water. (Not drawn to scale.)

PHASE RULE AND EQUILIBRIUM

The phase rule, also known as the Gibbs phase rule, relates the number of components and the number of degrees of freedom in a system at equilibrium by the formula

$$F = C - P + 2 \tag{1}$$

where F equals the number of degrees of freedom or the number of independent variables, C equals the number of components in a system in equilibrium and P equals the number of phases. The digit 2 stands for the two variables, temperature and pressure.

$$\mathrm{CaCO_3(\ s) \leftrightarrows CaO(s) + CO_2(\ g)} \tag{2}$$

There are also three different chemical constituents, but the number of components is only two because any two constituents completely define the system in equilibrium. Any third constituent may be determined if the concentration of the other two is known. Substituting into the phase rule (eq. [1]) we can see that the system is univariant, since $F = C - P + 2 = 2 - 3 + 2 = 1$. Therefore only one variable, either temperature or pressure, can be changed independently. (The number of components is not always easy to determine at first glance, and it may require careful examination of the physical conditions of the system at equilibrium.)

The phase rule applies to dynamic and reversible processes where a system is heterogeneous and in equilibrium and where the only external variables are temperature, pressure and concentration. For one-component systems the maximum number of variables to be considered is two - pressure and temperature. Such systems can easily be represented graphically by ordinary rectangular coordinates. For two-component (or binary) systems the maximum number of variables is three pressure, temperature and concentration. Only one concentration is required to define the composition since the second component is found by subtracting from unity. A graphical representation of such a system requires a three-dimensional diagram. This, however, is not well suited to illustration and consequently separate two-coordinate diagrams, such as pressure vs temperature, pressure vs composition and temperature vs composition, are mostly used. Solid/liquid systems are usually investigated at constant pressure, and thus only two variables need to be considered – the vapor pressure for such systems can be neglected. This is called a condensed system and finds considerable application in studying phase equilibria in various engineering materials. A condensed system will be represented by the following modified phase rule equation:

$$F = C - P + 1 \tag{3}$$

where all symbols are the same as before, but (because of a constant pressure) the digit 2 is replaced by the digit 1, which stands for temperature as variable. The graphical representation of a solid/liquid binary system can be simplified by representing it on ordinary rectangular coordinates: temperature vs concentration or composition.

PHASE DIAGRAM

With the aid of a suitable calorimeter and energy reservoir, it is possible to measure the heat required to melt and evaporate a pure substance like ice. The experimental data obtainable for a mole of ice is shown schematically in fig. 2. As heat is added to the solid, the temperature rises along line "a" until the temperature of fusion (T_f) is reached. The amount of heat absorbed per mole during melting is represented by the length of line " b ", or $\Delta \mathrm{H_F}$. The amount of heat absorbed per mole during evaporation at the boiling point is represented by line " d ". The reciprocal of the slope of line "a", (dH/dT), is the heat required to change the temperature of one mole of substance (at constant pressure) by $1^{\circ}\mathrm{CF.(dH/dT)}$ is the molar heat capacity of a material, referred to as " $\mathrm{C_p}$ ". As the reciprocal of line "a" is C_p (solid), the reciprocals of lines "c" and "e" are C_p (liquid) and C_p (vapor) respectively.

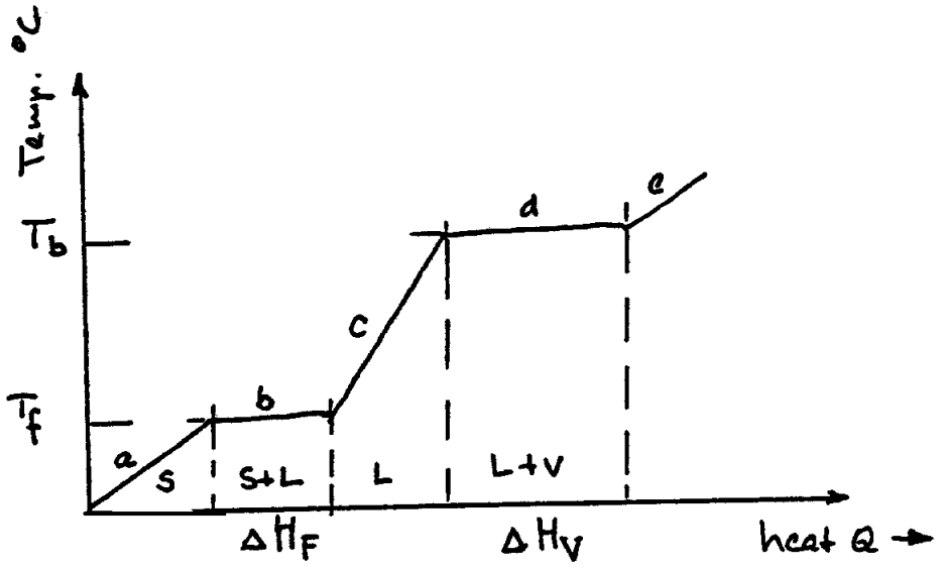


Fig. 2 H vs T Diagram for Pure $\mathrm{H_2O}$. (Not to scale.)

From a thermodynamic standpoint, it is important to realize that fig. 2 illustrates the energy changes that occur in the system during heating. Actual quantitative measurements show that 5.98 kJ of heat are absorbed at the melting point (latent heat of fusion) and 40.5 kJ per mole (latent heat of evaporation) at the boiling point. The latent heats of fusion and evaporation are unique characteristics of all pure substances. Substances like Fe, Co, Ti and others, which are allotropic (exhibit different structures at different temperatures), also exhibit latent heats of transformation as they change from one solid state crystal modification to another.

ENERGY CHANGES

When heat is added from the surroundings to a material system (as described above), the energy of the system changes. Likewise, if work is done on the surroundings by the material system, its energy changes. The difference in energy $(\Delta \mathrm{E})$ that the system experiences must be the difference between the heat absorbed (Q) by the system and the work (W) done on the surroundings. The energy change may therefore be written as:

$$\Delta \mathrm{E} = \mathrm{Q} - \mathrm{W} \tag{4}$$

If heat is liberated by the system, the sign of Q is negative and work done is positive. Q and W depend on the direction of change, but $\Delta \mathrm{E}$ does not. The above relation is one way of representing the **First Law of Thermodynamics** which states that the energy of a system and its surroundings is always conserved while a change in energy of the system takes place. The energy change, $\Delta \mathrm{E}$, for a process is independent of the path taken in going from the initial to the final state.

In the laboratory most reactions and phase changes are studied at constant pressure. The work is then done solely by the pressure

(P), acting through the volume change, $\Delta \mathrm{V}$.

$$\mathrm{W} = \mathrm{P}\Delta \mathrm{V} \quad \$and\$ \quad \Delta \mathrm{P} = 0 \tag{5}$$

Hence:

$$\mathrm{Q} = \Delta \mathrm{E} + \mathrm{P}\Delta \mathrm{V} \tag{6}$$

Since the heat content of a system, or the *enthalpy* H, is defined by.

$$\mathrm{H} = \mathrm{E} + \mathrm{PV} \tag{7}$$

$$\Delta \mathrm{H} = \Delta \mathrm{E} + \mathrm{P}\Delta \mathrm{V} \tag{8}$$

so that:

$$\Delta \mathrm{H} = \mathrm{Q} - \mathrm{W} + \mathrm{P}\Delta \mathrm{V} \tag{9}$$

or

$$\Delta \mathrm{H} = \mathrm{Q} \tag{10}$$

Reactions in which $\Delta \mathrm{H}$ is negative are called *exothermic* since they liberate heat, whereas *endothermic* reactions absorb heat. Fusion is an endothermic process, but the reverse reaction, crystallization, is an exothermic one.

ENTROPY AND FREE ENERGY

When a gas condenses to form a liquid and a liquid freezes to form a crystalline solid, the degree of internal order increases. Likewise, atomic vibrations decrease to zero when a perfect crystal is cooled to $0^{\circ}\mathrm{K}$. Since the term *entropy*, designated by S, is considered a measure of the degree of disorder of a system, a perfect crystal at $0^{\circ}\mathrm{K}$ has zero entropy.

The product of the absolute temperature, T, and the change in entropy, $\Delta \mathrm{S}$, is called the entropy factor, T $\Delta \mathrm{S}$. This product has the same units (Joules/mole) as the change in enthalpy, $\Delta \mathrm{H}$, of a system. At constant pressure, P, the two energy changes are related to one another by the Gibbs free energy relation:

$$\Delta \mathrm{F} = \Delta \mathrm{H} - \mathrm{T}\Delta \mathrm{S} \tag{11}$$

where

$$\mathrm{F} = \mathrm{H} - \mathrm{TS} \tag{12}$$

The natural tendency exhibited by all materials systems is to change from one of higher to one of lower free energy. Materials systems also tend to assume a state of greater disorder whereby the entropy factor $\mathrm{T}\Delta \mathrm{S}$ is increased. The free energy change, $\Delta \mathrm{F}$, expresses the balance between the two opposing tendencies, the change in heat content $(\Delta \mathrm{H})$ and the change in the entropy factor $(T\Delta S)$.

If a system at constant pressure is in an equilibrium state, such as ice and water at $0^{\circ}\mathrm{C}$, for example, at atmospheric pressure it cannot reach a lower energy state. At equilibrium in the ice-water system, the opposing tendencies, $\Delta \mathrm{H}$ and $\mathrm{T}\Delta \mathrm{S}$, equal one another so that $\Delta \mathrm{F} = 0$. At the fusion temperature, $\mathrm{T_F}$:

$$\Delta \mathrm{S_F} = \frac{\Delta \mathrm{H_F}}{\mathrm{T_F}} \tag{13}$$

Similarly, at the boiling point:

$$\Delta S_v = \frac{\Delta H_v}{T_v} \tag{14}$$

Thus melting or evaporation only proceed if energy is supplied to the system from the surroundings.

The entropy of a pure substance at constant pressure increases with temperature according to the expression:

$$\Delta S = \frac{C_p \Delta T}{T} \quad (\text{since } : \Delta H = C_p \Delta T \ ) \tag{15}$$

where $\mathrm{C_p}$ is the heat capacity at constant pressure, $\Delta \mathrm{C_p}, \Delta \mathrm{H}, \mathrm{T}$ and $\Delta \mathrm{T}$ are all measurable quantities from which $\Delta \mathrm{S}$ and $\Delta \mathrm{F}$ can be calculated.

F vs T

Any system can change spontaneously if the accompanying free energy change is negative. This may be shown graphically by making use of F vs T curves such as those shown in fig. 3.

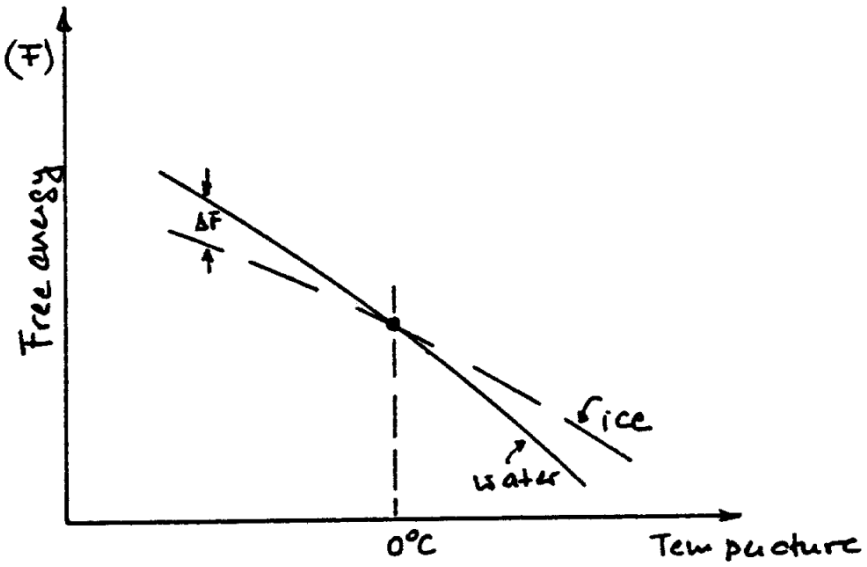


Fig. 3 Free energy is a function of temperature for ice and water.

The general decrease in free energy of all the phases with increasing temperature is the result of the increasing dominance of the temperature-entropy term. The increasingly negative slope for phases which are stable at increasingly higher temperatures is the result of the greater entropy of these phases.

PHASE DIAGRAMS (TWO-COMPONENT SYSTEMS)

SOLID SolutionS

A solution can be defined as a homogeneous mixture in which the atoms or molecules of one substance are dispersed at random into another substance. If this definition is applied to solids, we have a *solid solution*. The term “solid solution” is used just as “liquid solution” is used because the solute and solvent atoms (applying the term solvent to the element in excess) are arranged at random. The properties and composition of a solid solution are, however, uniform as long as it is not examined at the atomic or molecular level.

Solid solutions in alloy systems may be of two kinds: substitutional and interstitial. A substitutional solid solution results when the solute atoms take up the positions of the solvent metal in the crystal lattice. Solid solubility is governed by the comparative size of the atoms of the two elements, their structure and the difference in electronegativity. If the atomic radii of a solvent and solute differ by more than 15% of the radius of the solvent, the range of solubility is very small. When the atomic radii of two elements are equal or differ by less than 15% in size and when they have the same number of valency electrons, substitution of one kind of atom for another may occur with no distortion or negligible distortion of the crystal lattice, resulting in a series of homogeneous solid solutions. For an unlimited solubility in the solid state, the radii of the two elements must not differ by more than 8% and both the solute and the solvent elements must have the same crystal structure.

In addition to the atomic size factor, the solid solution is also greatly affected by the electronegativity of elements and by the

relative valency factor. The greater the difference between electronegativities, the greater is the tendency to form compounds and the smaller is the solid solubility. Regarding valency effect, a metal of lower valency is more likely to dissolve a metal of higher valency. Solubility usually increases with increasing temperature and decreases with decreasing temperature. This causes precipitation within a homogeneous solid solution phase, resulting in hardening effect of an alloy. When ionic solids are considered, the valency of ions is a very important factor.

CONSTRUCTION OF EQUILIBRIUM PHASE DIAGRAMS OF TWO-COMPONENT SYSTEMS

To construct an equilibrium phase diagram of a binary system, it is a necessary and sufficient condition that the boundaries of one-phase regions be known. In other words, the equilibrium diagram is a plot of solubility relations between components of the system. It shows the number and composition of phases present in any system under equilibrium conditions at any given temperature. Construction of the diagram is often based on solubility limits determined by thermal analysis – i.e., using cooling curves. Changes in volume, electrical conductivity, crystal structure and dimensions can also be used in constructing phase diagrams.

The solubility of two-component (or binary) systems can range from essential insolubility to complete solubility in both liquid and solid states, as mentioned above. Water and oil, for example, are substantially insoluble in each other while water and alcohol are completely intersoluble. Let us visualize an experiment on the water-ether system in which a series of mixtures of water and ether in various proportions is placed in test tubes. After shaking the test tubes vigorously and allowing the mixtures to settle, we find present in them only one phase of a few percent of ether in water or water in ether, whereas for fairly large percentages of either one in the other there are two phases. These two phases separate into layers, the upper layer being ether saturated with water and the lower layers being water saturated with ether. After sufficiently increasing the temperature, we find, regardless of the proportions of ether and water, that the two phases become one. If we plot solubility limit with temperature as ordinate and composition as abscissa, we have an isobaric [constant pressure (atmospheric in this case)] phase diagram, as shown in fig. 4. This system exhibits a *solubility gap*.

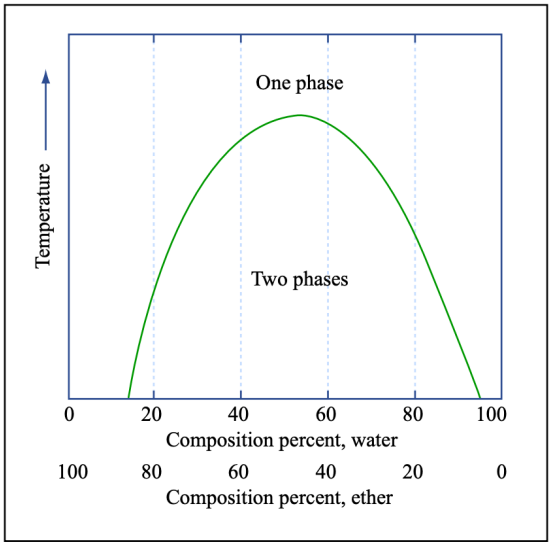


Image by MIT OpenCourseWare.

Fig. 4 Schematic representation of the solubilities of ether and water in each other.

COOLING CURVES

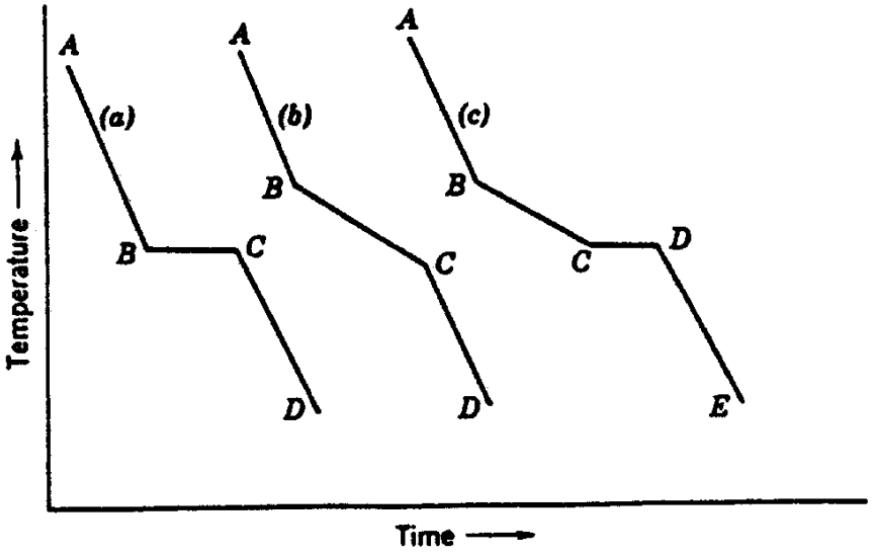


Fig. 5 Cooling curves: (a) pure compound; (b) binary solid solution; (c) binary eutectic system.

SOLID Solution EQUILIBRIUM DIAGRAMS

Read in Jastrzebski: First two paragraphs and Figure 3-4 in Chapter 3-8, "Solid Solutions Equilibrium Diagrams," pp. 91-92.

Read in Smith, C. O. The Science of Engineering Materials. 3rd ed. Englewood Cliffs, NJ: Prentice-Hall, 1986. ISBN: 9780137948840. Last two paragraphs and Figure 7-8 in Chapter 7-3-1, "Construction of a Simple Equilibrium Diagram," pp. 247-248.

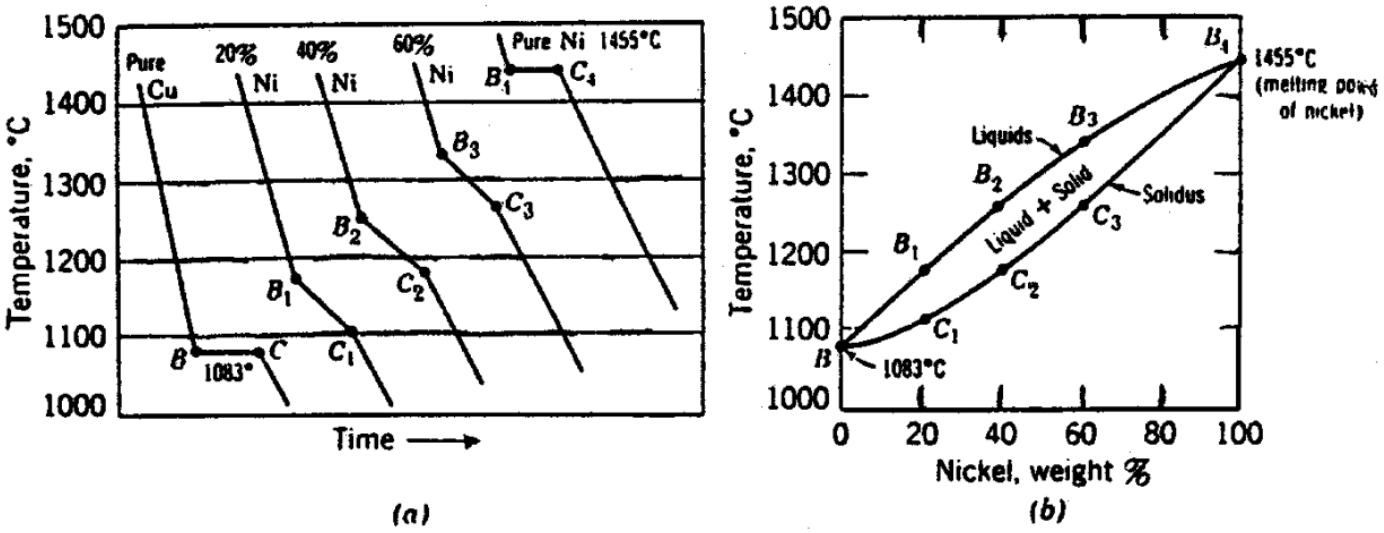


Fig. 6 Plotting equilibrium diagrams from cooling curves for Cu-Ni solid solution alloys. (a) Cooling curves; (b) equilibrium diagram.

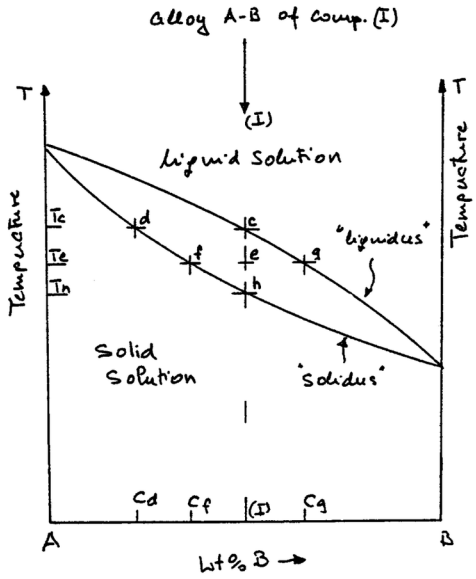


Fig. 7

INTERPRETATION OF PHASE DIAGRAMS

From the above discussion we can draw two useful conclusions which are the only rules necessary for interpreting equilibrium diagrams of binary systems.

Rule 1 - Phase composition: To determine the composition of phases which are stable at a given temperature we draw a horizontal line at the given temperature. The projections (upon the abscissa) of the intersections of the isothermal line with the liquidus and the solidus give the compositions of the liquid and solid, respectively, which coexist in equilibrium at that temperature. For example, draw a horizontal temperature line through temperature T_e in fig. 7. The T_e line intersects the solidus at f and the liquidus at g, indicating solid composition of $f\%$ of B and $(100-f)\%$ of A. The liquid composition at this temperature is $\mathrm{g}\%$ of B and $(100-\mathrm{g})\%$ of A. This line in a two-phase region is known as a tie line because it connects or "ties" together lines of one-fold saturation - i.e., the solid is saturated with respect to B and the liquid is saturated with respect to A.

Rule 2 - The Lever Rule: To determine the relative amounts of the two phases, erect an ordinate at a point on the composition scale which gives the total or overall composition of the alloy. The intersection of this composition vertical and a given isothermal line is the fulcrum of a simple lever system. The relative lengths of the lever arms multiplied by the amounts of the phase present must balance. As an illustration, consider alloy I in fig. 7. The composition vertical is erected at alloy I with a composition of $e\%$ of B and $(100-e)\%$ of A. This composition vertical intersects the temperature horizontal (T_e) at point e. The length of the line "$f-e-g$" indicates the total amount of the two phases present. The length of line "$e-g$" indicates the amount of solid. In other words:

$$\begin{aligned} \frac{\mathrm{eg}}{\mathrm{fg}} \times 100 &= \%\text{ of solid present} \\ \frac{\mathrm{fg}}{\mathrm{fg}} \times 100 &= \%\text{ of liquid present} \end{aligned} \tag{9.6.1}$$

These two rules give both the *composition* and the *relative quantity* of each phase present in a two-phase region in any binary system in equilibrium regardless of physical form of the two phases. The two rules apply only to two-phase regions.

ISOMORPHOUS SYSTEMS

An isomorphous system is one in which there is complete intersolubility between the two components in the vapor, liquid and solid phases, as shown in fig. 9. The $\mathrm{Cu}-\mathrm{Ni}$ system is both a classical and a practical example since the monels, which enjoy extensive commercial use, are $\mathrm{Cu}-\mathrm{Ni}$ alloys. Many practical materials systems are isomorphous.

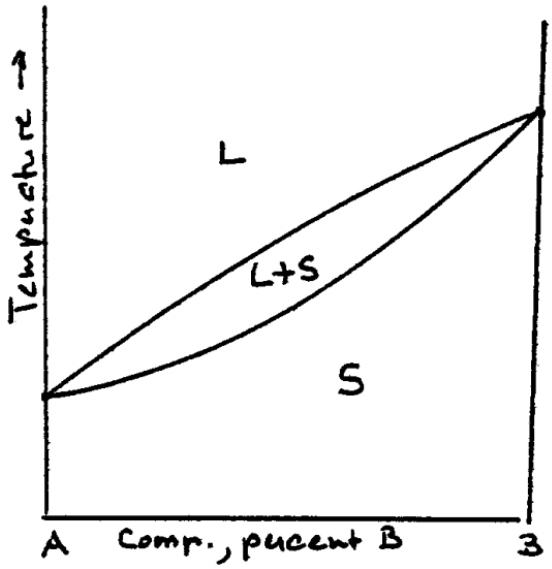


Fig. 9 Schematic phase diagram for a binary system, A-B, showing complete intersolubility (isomorphism) in all phases.

INCOMPLETE SOLUBILITY

Read in Smith, C. O. The Science of Engineering Materials. 3rd ed. Englewood

Cliffs, NJ: Prentice-Hall, 1986. ISBN: 9780137948840.

Chapter 7-3-5, "Incomplete Solubility," pp. 252-253.

EUTECTIC SYSTEMS

Read in Smith: Chapter 7-3-6, "Eutectic," pp. 253-256.

EQUILIBRIUM DIAGRAMS WITH INTERMEDIATE COMPOUNDS

Read in Jastrzebski, Z. D. *The Nature and Properties of Engineering Materials*. 2nd ed.

New York, NY: John Wiley & Sons, 1976. ISBN: 9780471440895.

Chapter 3-11,"Equilibrium Diagrams with Intermediate Compounds," pp. 102-103.

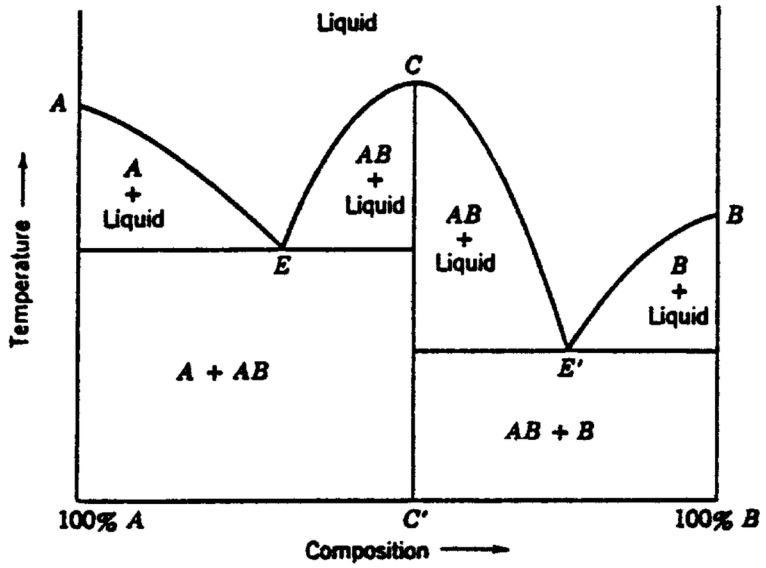


Fig. 15 Binary system showing an intermediate compound. C is the melting point (maximum) of the compound AB having the composition C'. E is the eutectic of solid A and solid AB. E' is the eutectic of solid AB and solid B.

TWO-COMPONENT SYSTEMS

A pressure-temperature diagram is extremely useful when one wishes to discuss a one-component system. A component in this case is an element or compound (for example, Fe, MgO, or $\mathrm{H_2O}$). As long as there is only one component present, the system may be adequately described by the two variables, pressure and temperature. In a two-component system, a third variable is needed; this is composition. The two-component system may be described by a three dimensional pressure - temperature composition diagram. It is however in the framework of this course not appropriate to deal with the complexities of the 3D phase diagram at this point and, since most materials are used under isobaric (constant pressure) conditions, we will first discuss an isobaric two-dimensional diagram of temperature versus composition. At a later point we will explain how the one component pressure-temperature and the isobaric two-component temperature-composition diagrams may be combined to construct the three-dimensional pressure-temperature-composition diagram of a two-component system.

Temperature-composition diagrams

A two-component temperature-composition diagram at constant pressure is called a binary phase diagram or equilibrium diagram. Temperature is plotted as the ordinate and composition as the abscissa. In the system AB, the composition is usually expressed in terms of the mole fraction of B, x_B, or the weight percent of B, w/o B. (The mole fraction of B is equal to the number of moles of B divided by the sum of the number of moles of A plus the number of moles of B. The weight percent of B is equal to the product of 100 and the weight of B divided by the sum of the weights of A and B.) The composition need not be specified in terms of A since the sum of the mole fraction of B and the mole fraction of A is equal to one, and the sum of the weight percent of A and the weight percent of B is equal to 100. For pure A, both x_B and w/o B are zero; and for pure B they are one and 100, respectively.

A typical binary phase diagram (Figure 1) indicates those phases present in equilibrium at any particular temperature and composition at the constant pressure for which the phase diagram was determined. At low temperatures, the only phase present is the solid designated by S in the phase diagram. Pure A melts at the temperature T_{fA} and pure B melts at the temperature T_{fB} Alloys of composition between pure $A\,(x_B = 0)$ and pure $B\,(x_B = 1)$ exist only in the solid state of aggregation until the temperature of the solidus line is reached. The solidus is represented in the phase diagram by the lower curve extending from $\mathrm{T_{fA}}$ to $\mathrm{T_{fB}}$. Below the solidus temperature only solid exists; but above the solidus, there is a two-phase region $(L + S)$ in which both liquid and solid phases are in equilibrium. The liquid-plus-solid region extends from the solidus temperature over a finite temperature interval for all alloys of the system AB. The extent of the temperature interval reduces to zero for the pure components A and B. since according to the one-component pressure-temperature diagram, at any particular pressure there is

only one temperature at which liquid and solid are in equilibrium.

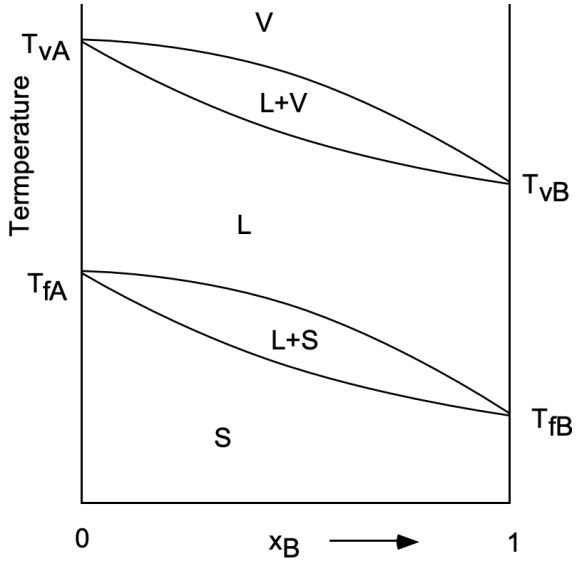


Figure 1 • Binary Phase Diagram. A binary phase diagram is an isobaric temperature composition diagram. In this case there is complete volubility in the solid, liquid, and vapor states of aggregation, and only one phase is found for each state of aggregation. At low temperatures, the material of any composition is solid; at higher temperatures there is a two-phase liquid-plus-solid region, a liquid region, a liquid-plus-vapor region and, at very high temperatures, an all-vapor region.

The upper boundary of the liquid-plus-solid region is the liquidus temperature. Above this temperature, any alloy of the system exists as a liquid phase until the temperature increases to that level at which vaporization begins. The pure compositions A and B vaporize completely at T_{vA} and T_{vB}, because the liquid and vapor phases for a pure component at constant pressure can be in equilibrium at only one temperature. Alloys of intermediate composition do not completely vaporize at any one temperature but over a finite temperature interval.This is shown in the phase diagram of Figure 1 by the liquid-plus-vapor $(L+V)$ region. At temperatures above this region, only the vapor phase exists.

Metallurgists or materials scientists are more often concerned with the liquid and solid phases and less often with the vapor phase. For this reason, and the fact that it is difficult to determine vapor phase diagrams, most binary diagrams extend no higher in temperature than the all-liquid region.

Cooling through a two-phase field

Solidification or melting of an intermediate alloy may be illustrated by the enlarged view of a two-phase field shown in Figure 2.

If an alloy of composition $\mathrm{x_o}$, originally liquid at temperature $\mathrm{T_1}$, is cooled, it remains liquid until the temperature reaches the liquidus temperature at point 2. At this temperature T_2, the first particle of solid appears. This solid does not have the same composition as the parent liquid. The composition of the first solid formed at $\mathrm{T_2}$ is found by constructing an isothermal line from 2 to $2'$. This isotherm is called a tie-line. The composition of the solid and liquid phases in equilibrium at a particular temperature is given by the intersection of the tie-line at that temperature with the solidus and liquidus curves, respectively. Thus at temperature T_2, the solid has the composition $\times 2'$ and the liquid the composition x_2 (where $x_2 = x_0$).

Upon further cooling to T_3, the composition of the liquid has shifted to the left along the liquidus to $\times 3$, and the composition of the solid has shifted to the left along the solidus to $x3'$ because at T_3, the only liquid and solid compositions that can be in equilibrium with one another are $x3$ and $x3'$ respectively.

Despite the fact that both liquid and solid have compositions different from the alloy composition, the overall alloy (liquid and solid together) retains its original composition x_0. As the temperature approaches the solidus temperature $\mathrm{T_5}$, the solid composition approaches x', (where ${x_5}' = x_0$) and the last quantity of liquid of composition x_5 freezes. At temperatures below the solidus, the solid composition remains unchanged, for example, at $\mathrm{T_6}$ the solid composition is $\mathrm{x_0}$.

The above analysis applies only to solidification at such a slow rate of cooling that equilibrium is achieved at every temperature.

This is not always the case, however.

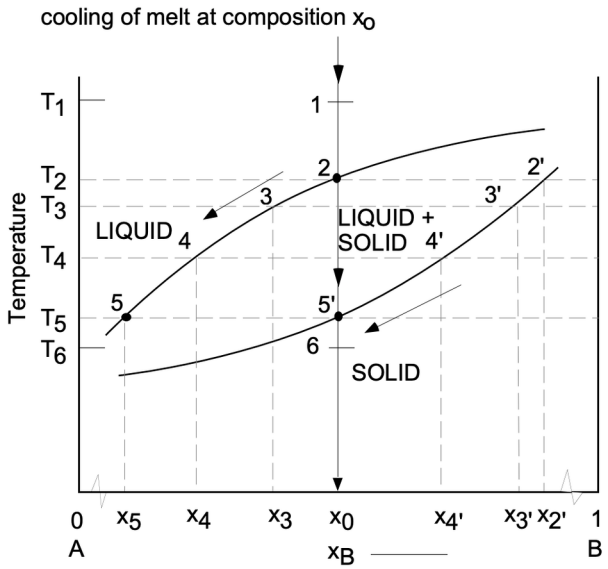


Figure 2 · Cooling Through a Two-Phase Field. As an alloy of composition x_0 is cooled from the liquid region through the two-phase liquid-plus-solid field, the first particle of solid forms at temperature T_2 and is of composition x_2,. The composition of the solid is given by the intersection of the isothermal tie line with the solidus, and the composition of the liquid by the intersection of the tie-line with the liquidus. As the temperature is decreased, the composition of the solid and of the liquid shifts to the left until at $\mathrm{T_5}$ the solid is of composition $\mathrm{x_0}$ and the last of the liquid freezes.

lever law

To determine exactly how much liquid and solid are present at any given temperature, let us derive a relation known as the "lever law." If one mole of alloy of composition x_0 is chosen as a basis, then, at any temperature T. the fraction of liquid f_L is found as follows: The sum of the fractions of liquid and solid must equal one, that is,

$$f_S + f_L = 1$$

The number of moles of B present in the alloy must be the same as the number of moles of B present in the solid phase plus the number of moles of B present in the liquid phase, that is,

$$x_O = x_S f_S = xL f_L$$

Since

$$f_S = 1 - f_L$$

we may substitute and obtain

$$x_O = x_S - x_S fL + x_L f_L$$

On rearranging and solving for $\mathrm{f_L}$ we find that

$$f_L = (x_S - x_0) / (x_S - xL) .$$

This relation is called the "lever law" because the fraction of one of the two phases present is equal to the opposite side of the tie-line $(\mathrm{x_S - x_O})$ divided by the entire tie-line $(x_S - x_L)$ In this way the tie-line acts as though it were a lever whose fulcrum is at the point x_0. In a similar way it is found that

$$f_s = (x_O - x_L) / (x_S - xL) .$$

This page titled 9.6: Phase Equilibria and Phase Diagrams is shared under a CC BY-NC-SA 4.0 license and was authored, remixed, and/or curated by Donald Sadoway (MIT OpenCourseWare).

- 1.10: Phase Equilibria and Phase Diagrams by Donald Sadoway is licensed CC BY-NC-SA 4.0. Original source: https://ocw.mit.edu/courses/3-091sc-introduction-to-solid-state-chemistry-fall-2010/pages/syllabus/.

INDEX

A

absorption spectra
2.1.2: Discovery of Subatomic Particles and the Bohr Atom

acids
1.3: History of Inorganic Chemistry

alchemy
1.3: History of Inorganic Chemistry

angular momentum quantum number
2.2.2: Quantum Numbers and Atomic Wave Functions

anions
2.3.3: Covalent and Ionic Radii

atom charge
3.1.3: Formal Charge

atomic mass
2.1.1: The Periodic Table

atomic number
2.3.1: Ionization energy

atomic orbital
2.2.2: Quantum Numbers and Atomic Wave Functions

atomic physics
2.1.2: Discovery of Subatomic Particles and the Bohr Atom
2.2: The Schrödinger equation, particle in a box, and atomic wavefunctions

atomic radius
2.2.4: Shielding
2.3: Periodic Properties of Atoms
2.3.3: Covalent and Ionic Radii
2.4: Problems
3.2.4: Ligand Close Packing

atomic size trends
2.3.3: Covalent and Ionic Radii

atomic structure
2.2.2: Quantum Numbers and Atomic Wave Functions
2.2.3: Aufbau Principle
2.2.4: Shielding
2.3: Periodic Properties of Atoms
2.3.1: Ionization energy
2.3.2: Electron Affinity

atomic theory
2: Atomic Structure

atomic theory milestones
2.1: Historical Development of Atomic Theory

atoms
2.1: Historical Development of Atomic Theory
3.1: Lewis Electron-Dot Diagrams

Aufbau principle
2.2.3: Aufbau Principle

AXmEn
3.2.1: Lone Pair Repulsion

B

bases
1.3: History of Inorganic Chemistry

benzene
3.1.1: Resonance

beryllium
3.1.4: Lewis Fails to Predict Unusual Cases - Boron and Beryllium

boiling point
3.4: Hydrogen Bonding

bond
3.3: Molecular Polarity

bond angle variation
3.2.1: Lone Pair Repulsion

bond angles
3.2: Valence Shell Electron-Pair Repulsion
3.2.1: Lone Pair Repulsion
3.2.2: Multiple Bonds
3.2.3: Electronegativity and Atomic Size Effects
3.2.4: Ligand Close Packing

bond length
3.1.4: Lewis Fails to Predict Unusual Cases - Boron and Beryllium

bond lengths
3.2.3: Electronegativity and Atomic Size Effects
3.2.4: Ligand Close Packing

bond polarity
3.2.3: Electronegativity and Atomic Size Effects

bonding
3.1: Lewis Electron-Dot Diagrams
3.1.4: Lewis Fails to Predict Unusual Cases - Boron and Beryllium

bonding electrons
3.1.3: Formal Charge

bonding geometry
3.2: Valence Shell Electron-Pair Repulsion

bonding theories
3.1.2: Breaking the octet rule with higher electron counts (hypervalent atoms)

boron
3.1.4: Lewis Fails to Predict Unusual Cases - Boron and Beryllium

Bronze Age
1.3: History of Inorganic Chemistry

C

carbon
1.2: Inorganic vs Organic Chemistry

carbon nanotubes
1.2: Inorganic vs Organic Chemistry

carbonate ion
3.1.1: Resonance

cations
2.3.3: Covalent and Ionic Radii

central atom
3.2: Valence Shell Electron-Pair Repulsion
3.2.1: Lone Pair Repulsion

charge
3.3: Molecular Polarity

chemical behavior
2.1.1: The Periodic Table

chemical bonding
3.1.2: Breaking the octet rule with higher electron counts (hypervalent atoms)
3.1.3: Formal Charge
3.2.2: Multiple Bonds
3.2.4: Ligand Close Packing
3.4: Hydrogen Bonding

chemical bonds
3.1.1: Resonance
3.2.3: Electronegativity and Atomic Size Effects

chemical change
2.1: Historical Development of Atomic Theory

chemical disciplines
1: Introduction to Inorganic Chemistry

chemical elements
1.1: What is Inorganic Chemistry?

chemical properties
1.2: Inorganic vs Organic Chemistry

chemical reactions
1.3: History of Inorganic Chemistry

chemistry
1.3: History of Inorganic Chemistry
2.1.1: The Periodic Table
2.3: Periodic Properties of Atoms
3.1: Lewis Electron-Dot Diagrams

chemistry of life
1.1: What is Inorganic Chemistry?

comprehension assessment
1: Introduction to Inorganic Chemistry

conduct electricity
1.1: What is Inorganic Chemistry?

coordination number
3.2.4: Ligand Close Packing

coulombs law
2.2.4: Shielding

covalent
3.3: Molecular Polarity

covalent bond
3.4: Hydrogen Bonding

covalent character
2.3.3: Covalent and Ionic Radii

D

Dalton's Atomic Theory
2.1: Historical Development of Atomic Theory

definition
1.5: Practice problems

delocalized electrons
3.1.1: Resonance

dipole
3.3: Molecular Polarity

dipole moment
3.1.4: Lewis Fails to Predict Unusual Cases - Boron and Beryllium

dipole moments
3: Simple Bonding Theory

dual nature
2.2: The Schrödinger equation, particle in a box, and atomic wavefunctions

E

effective nuclear charge
2.2.4: Shielding
2.3.3: Covalent and Ionic Radii

electrical conductivity
1.2: Inorganic vs Organic Chemistry

electron
3.1: Lewis Electron-Dot Diagrams

electron affinity
2.3: Periodic Properties of Atoms
2.3.1: Ionization energy
2.3.2: Electron Affinity
2.4: Problems

electron behavior
2: Atomic Structure

electron configuration
2.2.2: Quantum Numbers and Atomic Wave Functions
2.2.3: Aufbau Principle
2.3.2: Electron Affinity

electron geometry
3.2.1: Lone Pair Repulsion

electron groups
3.2: Valence Shell Electron-Pair Repulsion

electron pair repulsion
3.2: Valence Shell Electron-Pair Repulsion
3.2.3: Electronegativity and Atomic Size Effects

electron removal
2.3.1: Ionization energy

electron shielding
2.2.4: Shielding

electronegativity
2.2.4: Shielding
2.3: Periodic Properties of Atoms
2.3.2: Electron Affinity
2.4: Problems
3.2.3: Electronegativity and Atomic Size Effects
3.3: Molecular Polarity

elemental properties
2.1.1: The Periodic Table

elements
1.4: Perspectives
2.1: Historical Development of Atomic Theory

emission spectra
2.1.2: Discovery of Subatomic Particles and the Bohr Atom

empirical evidence
3.2.1: Lone Pair Repulsion

endothermic
2.3.2: Electron Affinity

energy levels
2.1.2: Discovery of Subatomic Particles and the Bohr Atom
2.2: The Schrödinger equation, particle in a box, and atomic wavefunctions
2.2.4: Shielding

equation
2.2.1: Particle in a Box

exothermic
2.3.2: Electron Affinity

F

first ionization energy
2.3.1: Ionization energy

fluorine
2.4: Problems

formal charge
3: Simple Bonding Theory
3.1.3: Formal Charge

functional groups
3.4: Hydrogen Bonding

G

geometry
3.1.4: Lewis Fails to Predict Unusual Cases - Boron and Beryllium

geometry prediction
3.2: Valence Shell Electron-Pair Repulsion
3.2.2: Multiple Bonds

ground state
2.2.3: Aufbau Principle

group families
2.3: Periodic Properties of Atoms

H

Hamiltonian
2.2.1: Particle in a Box

Hamiltonian operator
2.2: The Schrödinger equation, particle in a box, and atomic wavefunctions

Heisenberg uncertainty principle
2.2: The Schrödinger equation, particle in a box, and atomic wavefunctions

historical development
2: Atomic Structure

history
1.4: Perspectives
2.1.1: The Periodic Table

history of atomic theory
2.1: Historical Development of Atomic Theory

history of chemistry
1: Introduction to Inorganic Chemistry

Hund's rule
2.2.3: Aufbau Principle

hybrid orbital theory
3.1.2: Breaking the octet rule with higher electron counts (hypervalent atoms)

hydrogen
2.1.2: Discovery of Subatomic Particles and the Bohr Atom

Hydrogen atom
2.2.2: Quantum Numbers and Atomic Wave Functions

hydrogen bond
3.4: Hydrogen Bonding

hydrogen bonding
3: Simple Bonding Theory
3.4: Hydrogen Bonding

hypervalent atoms
3: Simple Bonding Theory

I

infrared
2.1.2: Discovery of Subatomic Particles and the Bohr Atom

inorganic chemistry
1: Introduction to Inorganic Chemistry
1.1: What is Inorganic Chemistry?
1.2: Inorganic vs Organic Chemistry
1.4: Perspectives
1.5: Practice problems

inorganic compounds
1.5: Practice problems

interdisciplinary fields
1.1: What is Inorganic Chemistry?

intermolecular forces
3.4: Hydrogen Bonding

ion charge
3.1.3: Formal Charge

ionic
3.3: Molecular Polarity

ionic radius
2.3.3: Covalent and Ionic Radii

ionization energy
2.2.4: Shielding
2.3: Periodic Properties of Atoms
2.3.1: Ionization energy
2.3.2: Electron Affinity
2.4: Problems
3.2.3: Electronegativity and Atomic Size Effects

ionization potential
2.3.1: Ionization energy

iron
1.3: History of Inorganic Chemistry

isolobal analogy
8.5.2: The Isolobal Analogy

J

John Newlands
2.1.1: The Periodic Table

K

kinetic energy
2: Atomic Structure
2.2.1: Particle in a Box

L

law of conservation of matter
2.1: Historical Development of Atomic Theory

law of definite proportions
2.1: Historical Development of Atomic Theory

law of multiple proportions
2.1: Historical Development of Atomic Theory

law of octaves
2.1.1: The Periodic Table

LCP theory
3.2.4: Ligand Close Packing

Lewis
3.1: Lewis Electron-Dot Diagrams

Lewis structure
3.1.3: Formal Charge

Lewis structures
3.1.1: Resonance
3.1.2: Breaking the octet rule with higher electron counts (hypervalent atoms)
3.2: Valence Shell Electron-Pair Repulsion

Lewis theory
3.1.4: Lewis Fails to Predict Unusual Cases - Boron and Beryllium

ligand close packing
3.2.4: Ligand Close Packing

line spectrum
2.1.2: Discovery of Subatomic Particles and the Bohr Atom

lone pairs
3.2.1: Lone Pair Repulsion
3.2.2: Multiple Bonds

M

materials
1.4: Perspectives
materials science
1.2: Inorganic vs Organic Chemistry
measurement
2.3.3: Covalent and Ionic Radii
measurements
2.3.2: Electron Affinity
melting point
2.3: Periodic Properties of Atoms
Mendeleev
2.1.1: The Periodic Table
metal ions
1: Introduction to Inorganic Chemistry
metallic character
2.3: Periodic Properties of Atoms
metallurgy
1.3: History of Inorganic Chemistry
metals
1.2: Inorganic vs Organic Chemistry
1.3: History of Inorganic Chemistry
1.5: Practice problems
microscopic properties of matter
2.1: Historical Development of Atomic Theory
model
2.2.1: Particle in a Box
molecular geometry
3.2: Valence Shell Electron-Pair Repulsion
3.2.1: Lone Pair Repulsion
3.2.2: Multiple Bonds
3.2.3: Electronegativity and Atomic Size Effects
molecular interactions
3.4: Hydrogen Bonding
molecular orbitals
3.1.2: Breaking the octet rule with higher electron counts (hypervalent atoms)
molecular polarity
3: Simple Bonding Theory
molecular shape
3.1.2: Breaking the octet rule with higher electron counts (hypervalent atoms)
3.2.1: Lone Pair Repulsion
Molecular Shapes
3.2: Valence Shell Electron-Pair Repulsion
molecular stability
3.1.1: Resonance
molecular structures
3.2.4: Ligand Close Packing
molecule
3.1: Lewis Electron-Dot Diagrams
3.1.3: Formal Charge
molecules
3.3: Molecular Polarity
moment
3.3: Molecular Polarity

N

nanomaterials
1.2: Inorganic vs Organic Chemistry
nitrate ion
3.1.1: Resonance
nitrogen
2.4: Problems
noble gases
2.4: Problems
nuclear charge
2.3.3: Covalent and Ionic Radii

O

octahedral geometry
3.2.2: Multiple Bonds
octet
3.1: Lewis Electron-Dot Diagrams
octet rule
3: Simple Bonding Theory
3.1.2: Breaking the octet rule with higher electron counts (hypervalent atoms)
3.1.4: Lewis Fails to Predict Unusual Cases - Boron and Beryllium
orbital energy levels
2.2.3: Aufbau Principle
organic
3.1: Lewis Electron-Dot Diagrams
organic chemistry
1: Introduction to Inorganic Chemistry
1.1: What is Inorganic Chemistry?
1.2: Inorganic vs Organic Chemistry
organic molecule
3.4: Hydrogen Bonding
organometallic catalysts
1.2: Inorganic vs Organic Chemistry
organometallic compounds
1: Introduction to Inorganic Chemistry
1.1: What is Inorganic Chemistry?
ozone
3.1.1: Resonance

P

Pauli exclusion principle
2.2.3: Aufbau Principle
periodic table
1.1: What is Inorganic Chemistry?
2: Atomic Structure
2.1.1: The Periodic Table
2.2.3: Aufbau Principle
2.2.4: Shielding
2.3.2: Electron Affinity
2.3.3: Covalent and Ionic Radii
3.1.2: Breaking the octet rule with higher electron counts (hypervalent atoms)
3.2.3: Electronegativity and Atomic Size Effects
periodic trends
2: Atomic Structure
2.3: Periodic Properties of Atoms
2.3.1: Ionization energy
2.4: Problems
polarity
3.3: Molecular Polarity
Polyatomic Ions
3.1.3: Formal Charge
potential energy
2: Atomic Structure
2.2.1: Particle in a Box
practice problems
1: Introduction to Inorganic Chemistry
predictions
1.4: Perspectives
principal quantum number
2.2.2: Quantum Numbers and Atomic Wave Functions
properties
2.1.1: The Periodic Table
protein structure
3.4: Hydrogen Bonding

Q

quantum mechanics
2: Atomic Structure
2.2: The Schrödinger equation, particle in a box, and atomic wavefunctions
2.2.1: Particle in a Box
2.2.2: Quantum Numbers and Atomic Wave Functions
quantum numbers
2.2: The Schrödinger equation, particle in a box, and atomic wavefunctions
2.2.2: Quantum Numbers and Atomic Wave Functions
2.2.3: Aufbau Principle
questions
1.5: Practice problems

R

reactions
1.4: Perspectives
reactivity
1: Introduction to Inorganic Chemistry
1.4: Perspectives
reading
1.5: Practice problems
research
1.4: Perspectives
resonance
3: Simple Bonding Theory
3.1.1: Resonance
resonance structures
3.1.1: Resonance
3.1.4: Lewis Fails to Predict Unusual Cases - Boron and Beryllium
rule
3.1: Lewis Electron-Dot Diagrams
Rydberg equation
2.1.2: Discovery of Subatomic Particles and the Bohr Atom

S

Schrödinger
2.2.1: Particle in a Box
Schrödinger equation
2.2: The Schrödinger equation, particle in a box, and atomic wavefunctions
2.2.2: Quantum Numbers and Atomic Wave Functions
second ionization energy
2.3.1: Ionization energy
selenium
2.4: Problems
spectral lines
2.1.2: Discovery of Subatomic Particles and the Bohr Atom
steel
1.3: History of Inorganic Chemistry
steric number
3.2.2: Multiple Bonds
3.2.4: Ligand Close Packing
structure
1.4: Perspectives
sulfur
2.4: Problems

T

tetrahedral geometry
3.2.2: Multiple Bonds
textbook
1.5: Practice problems
theories
1.4: Perspectives
transition metals
2.2.3: Aufbau Principle
trends
2.3.2: Electron Affinity
trigonal bipyramidal
3.2.2: Multiple Bonds

U

ultraviolet
2.1.2: Discovery of Subatomic Particles and the Bohr Atom
understanding
1.5: Practice problems
unshared electrons
3.1.3: Formal Charge

V

valence
3.1: Lewis Electron-Dot Diagrams
valence bond theory
3.1.2: Breaking the octet rule with higher electron counts (hypervalent atoms)
valence electron configuration
3.1.4: Lewis Fails to Predict Unusual Cases - Boron and Beryllium
valence electrons
2.2.4: Shielding
2.3.1: Ionization energy
3: Simple Bonding Theory
3.1.2: Breaking the octet rule with higher electron counts (hypervalent atoms)
3.1.3: Formal Charge
VSEPR
3.2: Valence Shell Electron-Pair Repulsion
3.2.1: Lone Pair Repulsion
3.2.4: Ligand Close Packing
VSEPR Theory
3: Simple Bonding Theory
3.2.2: Multiple Bonds
3.2.3: Electronegativity and Atomic Size Effects

W

water
3.3: Molecular Polarity
wave
2.2.1: Particle in a Box
Wavefunction
2.2: The Schrödinger equation, particle in a box, and atomic wavefunctions
2.2.1: Particle in a Box
2.2.2: Quantum Numbers and Atomic Wave Functions

This page titled Index is shared under a Public Domain license and was authored, remixed, and/or curated by Yulia Zaikina.

GLOSSARY

S

Sample Word 1 | Sample Definition 1

This page titled Glossary is shared under a license and was authored, remixed, and/or curated by Yulia Zaikina.

DETAILED LICENSING

Overview

Title: Advanced Inorganic Chemistry CHEM-5020: Fall 2026

Webpages: 259

Applicable Restrictions: Noncommercial

All licenses found:

- CC BY 3.0: 29.7% (77 pages)
- CC BY-NC-SA 4.0: 26.3% (68 pages)
- CC BY-SA 4.0: 16.6% (43 pages)
- Undeclared: 10.8% (28 pages)
- CC BY 1.0: 5.4% (14 pages)
- CC BY-NC 4.0: 4.6% (12 pages)
- CC BY 4.0: 3.1% (8 pages)
- Public Domain: 1.5% (4 pages)
- CC BY-NC 3.0: 1.2% (3 pages)
- CC BY-NC-SA 3.0: 0.8% (2 pages)

By Page

- Advanced Inorganic Chemistry CHEM-5020: Fall 2026 - *Undeclared*
  - Front Matter - *Undeclared*
    - TitlePage - *CC BY-NC-SA 4.0*
    - InfoPage - *Public Domain*
    - Table of Contents - *Public Domain*
    - Licensing - *Public Domain*
  - 1: Introduction to Inorganic Chemistry - *Undeclared*
    - 1.1: What is Inorganic Chemistry? - *CC BY-NC-SA 4.0*
    - 1.2: Inorganic vs Organic Chemistry - *CC BY-NC-SA 4.0*
    - 1.3: History of Inorganic Chemistry - *CC BY-NC-SA 4.0*
    - 1.4: Perspectives - *CC BY-NC-SA 4.0*
    - 1.5: Practice problems - *CC BY-NC-SA 4.0*
  - 2: Atomic Structure - *Undeclared*
    - 2.1: Historical Development of Atomic Theory - *Undeclared*
      - 2.1.1: The Periodic Table - *Undeclared*
      - 2.1.2: Discovery of Subatomic Particles and the Bohr Atom - *CC BY-NC-SA 3.0*
    - 2.2: The Schrödinger equation, particle in a box, and atomic wavefunctions - *CC BY-NC-SA 4.0*
      - 2.2.1: Particle in a Box - *CC BY-NC-SA 4.0*
      - 2.2.2: Quantum Numbers and Atomic Wave Functions - *CC BY-NC-SA 4.0*
      - 2.2.3: Aufbau Principle - *CC BY-NC-SA 4.0*
      - 2.2.4: Shielding - *CC BY-NC-SA 4.0*
    - 2.3: Periodic Properties of Atoms - *Undeclared*
      - 2.3.1: Ionization energy - *CC BY-NC-SA 3.0*
      - 2.3.2: Electron Affinity - *CC BY-NC 4.0*
      - 2.3.3: Covalent and Ionic Radii - *CC BY-NC 4.0*
    - 2.4: Problems - *Undeclared*
  - 3: Simple Bonding Theory - *Undeclared*
    - 3.1: Lewis Electron-Dot Diagrams - *CC BY-NC 4.0*
      - 3.1.1: Resonance - *CC BY-NC 3.0*
      - 3.1.2: Breaking the octet rule with higher electron counts (hypervalent atoms) - *CC BY-NC 4.0*
      - 3.1.3: Formal Charge - *CC BY-NC 4.0*
      - 3.1.4: Lewis Fails to Predict Unusual Cases - Boron and Beryllium - *CC BY-NC 4.0*
    - 3.2: Valence Shell Electron-Pair Repulsion - *CC BY-NC-SA 4.0*
      - 3.2.1: Lone Pair Repulsion - *CC BY-NC-SA 4.0*
      - 3.2.2: Multiple Bonds - *CC BY-NC-SA 4.0*
      - 3.2.3: Electronegativity and Atomic Size Effects - *CC BY-NC-SA 4.0*
      - 3.2.4: Ligand Close Packing - *CC BY-NC-SA 4.0*
    - 3.3: Molecular Polarity - *CC BY 4.0*
    - 3.4: Hydrogen Bonding - *CC BY-NC-SA 4.0*
  - 4: Symmetry and Group Theory - *CC BY 4.0*
    - 4.1: Symmetry Elements and Operations - *CC BY-NC-SA 4.0*
    - 4.2: Point Groups - *CC BY-NC-SA 4.0*

- 4.2.1: Groups of Low and High Symmetry - *CC BY-NC-SA 4.0*
- 4.2.2: Other Groups - *CC BY-NC-SA 4.0*
- 4.3: Properties and Representations of Groups - *CC BY-NC-SA 4.0*
  - 4.3.1: Matrices - *CC BY-NC-SA 4.0*
  - 4.3.2: Representations of Point Groups - *CC BY-NC-SA 4.0*
  - 4.3.3: Character Tables - *CC BY-NC-SA 4.0*
- 4.4: Examples and Applications of Symmetry - *Undeclared*
  - 4.4.1: Chirality - *CC BY-NC 4.0*
  - 4.4.2: Molecular Vibrations - *CC BY-NC 4.0*
- 4.5: Problems (under construction) - *CC BY-NC-SA 4.0*

◦ 5: Molecular Orbitals - *CC BY-SA 4.0*
- 5.1: Formation of Molecular Orbitals from Atomic Orbitals - *CC BY-SA 4.0*
  - 5.1.1: Molecular Orbitals from s Orbitals - *CC BY-NC 3.0*
  - 5.1.2: Molecular Orbitals from p Orbitals - *CC BY-NC 3.0*
  - 5.1.3: Molecular orbitals from d orbitals - *CC BY-SA 4.0*
  - 5.1.4: Nonbonding Orbitals and Other Factors - *CC BY-SA 4.0*
- 5.2: Homonuclear Diatomic Molecules - *CC BY-SA 4.0*
  - 5.2.1: Molecular Orbitals - *CC BY-SA 4.0*
  - 5.2.2: Orbital Mixing - *CC BY-SA 4.0*
  - 5.2.3: Diatomic Molecules of the First and Second Periods - *CC BY-SA 4.0*
  - 5.2.4: Photoelectron Spectroscopy - *CC BY-SA 4.0*
- 5.3: Heteronuclear Diatomic Molecules - *CC BY-SA 4.0*
  - 5.3.1: Orbital ionization energies - *CC BY-SA 4.0*
  - 5.3.2: Polar bonds - *CC BY-SA 4.0*
  - 5.3.3: Ionic Compounds and Molecular Orbitals - *CC BY-SA 4.0*
- 5.4: Larger (Polyatomic) Molecules - *CC BY-SA 4.0*
  - 5.4.1: Bifluoride anion - *CC BY-SA 4.0*
  - 5.4.2: Carbon Dioxide - *CC BY-SA 4.0*
  - 5.4.3: H_2O - *CC BY-SA 4.0*
  - 5.4.4: NH_3 - *CC BY-SA 4.0*
  - 5.4.5: CO_2 (Revisted with Projection Operators) - *CC BY-SA 4.0*
  - 5.4.6: BF_3 - *CC BY-SA 4.0*
- 5.5: Problems - *CC BY-SA 4.0*

◦ 6: Chemistry of the Main Group Elements (Barron) - *CC BY 3.0*
- 6.1: General Concepts and Trends - *CC BY 3.0*
  - 6.1.1: Fundamental Properties - Oxidation State - *CC BY 3.0*
  - 6.1.2: Fundamental Properties - Ionization Energy - *CC BY 3.0*
  - 6.1.3: Fundamental Properties - Electron Affinity - *CC BY 3.0*
  - 6.1.4: Fundamental Properties - Electronegativity - *CC BY 3.0*
  - 6.1.5: Structure and Bonding - Valence Shell Electron Pair Repulsion (VSEPR) Theory - *CC BY 3.0*
  - 6.1.6: Structure and Bonding - Crystal Structure - *CC BY 3.0*
  - 6.1.7: Structure and Bonding - Stereochemistry - *CC BY 3.0*
  - 6.1.8: Acids, Bases, and Solvents - Choosing a Solvent - *CC BY 3.0*
  - 6.1.9: Chemical Reactivity - The Basics of Combustion - *CC BY 3.0*
  - 6.1.10: Periodic Trends for the Main Group Elements - *CC BY 3.0*
- 6.2: Hydrogen - *CC BY 3.0*
  - 6.2.1: Discovery of Hydrogen - *CC BY 3.0*
  - 6.2.2: The Physical Properties of Hydrogen - *CC BY 3.0*
  - 6.2.3: Synthesis of Molecular Hydrogen - *CC BY 3.0*
  - 6.2.4: Atomic Hydrogen - *CC BY 3.0*
  - 6.2.5: The Proton - *CC BY 3.0*
  - 6.2.6: Hydrides - *CC BY 3.0*
  - 6.2.7: The Hydrogen Bond - *CC BY 3.0*
  - 6.2.8: Isotopes of Hydrogen - *CC BY 3.0*
  - 6.2.9: Nuclear Fusion - *CC BY 3.0*
  - 6.2.10: Storage of Hydrogen for Use as a Fuel - *CC BY 3.0*
- 6.3: Group 1 - The Alkali Metals - *CC BY 3.0*
  - 6.3.1: The Alkali Metal Elements - *CC BY 3.0*
  - 6.3.2: Compounds of the Alkali Metals - *CC BY 3.0*
  - 6.3.3: The Anomalous Chemistry of Lithium - *CC BY 3.0*
  - 6.3.4: Organolithium Compounds - *CC BY 3.0*
- 6.4: Group 2 - The Alkaline Earth Metals - *CC BY 3.0*
  - 6.4.1: The Alkaline Earth Elements - *CC BY 3.0*
  - 6.4.2: Calcium the Archetypal Alkaline Earth Metal - *CC BY 3.0*
  - 6.4.3: Differences for Beryllium and Magnesium - *CC BY 3.0*
  - 6.4.4: Organometallic Compounds of Magnesium - *CC BY 3.0*
- 6.5: Group 12 - *CC BY 3.0*
  - 6.5.1: The Group 12 Elements - *CC BY 3.0*
  - 6.5.2: Cadmium Chalcogenide Nanoparticles - *CC BY 3.0*
  - 6.5.3: Organometallic Chemistry of Zinc - *CC BY 3.0*
  - 6.5.4: Organomercury Compounds - *CC BY 3.0*
  - 6.5.5: The Myth, Reality, and History of

Mercury Toxicity - *CC BY 3.0*
- 6.6: Group 13 - *CC BY 3.0*
  - 6.6.1: The Group 13 Elements - *CC BY 3.0*
  - 6.6.2: Trends for the Group 13 Compounds - *CC BY 3.0*
  - 6.6.3: Borides - *CC BY 3.0*
  - 6.6.4: Boron Hydrides - *CC BY 3.0*
  - 6.6.5: Wade's Rules - *CC BY 3.0*
  - 6.6.6: Trends for the Oxides of the Group 13 Elements - *CC BY 3.0*
  - 6.6.7: Boron Oxides, Hydroxides, and Oxyanions - *CC BY 1.0*
  - 6.6.8: Aluminum Oxides, Hydroxides, and Hydrated Oxides - *CC BY 1.0*
  - 6.6.9: Ceramic Processing of Alumina - *CC BY 1.0*
  - 6.6.10: Boron Compounds with Nitrogen Donors - *CC BY 1.0*
  - 6.6.11: Properties of Gallium Arsenide - *CC BY 1.0*
  - 6.6.12: Electronic Grade Gallium Arsenide - *CC BY 1.0*
  - 6.6.13: Chalcogenides of Aluminum, Gallium, and Indium - *CC BY 1.0*
  - 6.6.14: Group 13 Halides - *CC BY 1.0*
- 6.7: Group 14 - *CC BY 3.0*
  - 6.7.1: The Group 14 Elements - *CC BY 3.0*
  - 6.7.2: Carbon Black- From Copying to Communication - *CC BY 3.0*
  - 6.7.3: Carbon Nanomaterials - *CC BY 3.0*
  - 6.7.4: Nitrogen Compounds of Carbon - *CC BY 3.0*
  - 6.7.5: Carbon Monoxide - *CC BY 3.0*
  - 6.7.6: Carbon Dioxide - *CC BY 3.0*
  - 6.7.7: Suboxides of Carbon - *CC BY 1.0*
  - 6.7.8: Carbon Halides - *CC BY 1.0*
  - 6.7.9: Comparison Between Silicon and Carbon - *CC BY 1.0*
  - 6.7.10: Semiconductor Grade Silicon - *CC BY 1.0*
  - 6.7.11: Oxidation of Silicon - *CC BY 1.0*
  - 6.7.12: Applications for Silica Thin Films - *CC BY 1.0*
- 6.8: Group 15 - The Pnictogens - *CC BY 3.0*
  - 6.8.1: The Group 15 Elements- The Pnictogens - *CC BY 3.0*
  - 6.8.2: Reaction Chemistry of Nitrogen - *CC BY 3.0*
  - 6.8.3: Hydrides - *CC BY 3.0*
  - 6.8.4: Oxides and Oxoacids - *CC BY 3.0*
  - 6.8.5: Halides of Phosphorous - *CC BY 3.0*
- 6.9: Group 16 - *CC BY 3.0*
  - 6.9.1: The Group 16 Elements- The Chalcogens - *CC BY 3.0*
  - 6.9.2: Ozone - *CC BY 3.0*
  - 6.9.3: Water - The Fuel for the Medieval Industrial Revolution - *CC BY 3.0*
  - 6.9.4: Hydrogen Peroxide - *CC BY 3.0*
  - 6.9.5: Hydrogen Peroxide Providing a Lift for 007 - *CC BY 3.0*
  - 6.9.6: Comparison of Sulfur to Oxygen - *CC BY 3.0*
  - 6.9.7: Chalconide Hydrides - *CC BY 3.0*
  - 6.9.8: Oxides and Oxyacids of Sulfur - *CC BY 3.0*
  - 6.9.9: Sulfur Halides - *CC BY 3.0*
- 6.10: The Halogens - *CC BY 3.0*
  - 6.10.1: The Group 17 Elements- The Halogens - *CC BY 3.0*
  - 6.10.2: Compounds of Fluorine - *CC BY 3.0*
  - 6.10.3: Compounds of Chlorine - *CC BY 3.0*
  - 6.10.4: Oxyacids of Chlorine - *CC BY 3.0*
  - 6.10.5: Bromine Trifluoride as a Solvent - *CC BY 3.0*
- 6.11: Group 18 - The Noble Gases - *CC BY 3.0*
  - 6.11.1: The Group 18 Elements- The Noble Gases - *CC BY 3.0*
- 6.12: Front Matter - *Undeclared*
  - 6.12.1: Table of Contents - *Undeclared*

◦ 7: Acid-Base and Donor-Acceptor Chemistry - *CC BY 4.0*
- 7.1: Acid-Base Models as Organizing Concepts - *CC BY 4.0*
- 7.2: Lewis Concept and Frontier Orbitals - *CC BY-NC 4.0*
  - 7.2.1: The frontier orbital approach considers Lewis acid-base reactions in terms of the donation of electrons from the base's highest occupied orbital into the acid's lowest unoccupied orbital. - *CC BY 4.0*
  - 7.2.2: All other things being equal, electron withdrawing groups tend to make Lewis acids stronger and bases weaker while electron donating groups tend to make Lewis bases stronger and acids weaker - *CC BY 4.0*
  - 7.2.3: The electronic spectra of charge transfer complexes illustrate the impact of frontier orbital interactions on the electronic structure of Lewis acid-base adducts - *CC BY-NC 4.0*
  - 7.2.4: Bulky groups weaken the strength of Lewis acids and bases because they introduce steric strain into the resulting acid-base adduct. - *CC BY 4.0*
  - 7.2.5: Frustrated Lewis pair chemistry uses Lewis acid and base sites within a molecule that are sterically restricted from forming an adduct with each other. - *CC BY-NC 4.0*
- 7.3: Hard and Soft Acids and Bases - *CC BY 4.0*
  - 7.3.1: Hard-Hard and Soft-Soft preferences may be explained and quantified in terms of electrostatic and covalent and electronic stabilization on the stability of Lewis acid-

base adducts - *CC BY-NC 4.0*
- 8: Organometallic Chemistry (Evans) - *CC BY-NC-SA 4.0*
  - 8.1: Introduction to Organometallic Chemistry - *CC BY-NC-SA 4.0*
    - 8.1.1: Resources for Organometallic Chemistry - *CC BY-NC-SA 4.0*
    - 8.1.2: What is Organometallic Chemistry? - *CC BY-NC-SA 4.0*
  - 8.2: Organometallic Ligands - *CC BY-NC-SA 4.0*
    - 8.2.1: Carbenes - *CC BY-NC-SA 4.0*
    - 8.2.2: Carbon Monoxide - *Undeclared*
    - 8.2.3: σ Complexes - *CC BY-NC-SA 4.0*
    - 8.2.4: Dative Ligands of N, O, and S - *CC BY-NC-SA 4.0*
    - 8.2.5: Metal Alkyls - *CC BY-NC-SA 4.0*
    - 8.2.6: Metal Hydrides - *CC BY-NC-SA 4.0*
    - 8.2.7: N-heterocyclic Carbenes - *CC BY-NC-SA 4.0*
    - 8.2.8: Odd-numbered π Systems - *CC BY-NC-SA 4.0*
    - 8.2.9: Phosphines - *CC BY-NC-SA 4.0*
    - 8.2.10: π Systems - *CC BY-NC-SA 4.0*
  - 8.3: Structural Fundamentals - *CC BY-NC-SA 4.0*
    - 8.3.1: Ligand Field Theory and Frontier Molecular Orbital Theory - *CC BY-NC-SA 4.0*
    - 8.3.2: Open Coordination Site - *CC BY-NC-SA 4.0*
    - 8.3.3: Periodic Trends of the Transition Metals - *CC BY-NC-SA 4.0*
    - 8.3.4: Predicting the Geometry of Organometallic Complexes - *CC BY-NC-SA 4.0*
    - 8.3.5: Simplifying the Organometallic Complex (Part 1) - *CC BY-NC-SA 4.0*
    - 8.3.6: Simplifying the Organometallic Complex (Part 2) - *CC BY-NC-SA 4.0*
    - 8.3.7: Simplifying the Organometallic Complex (Part 3) - *CC BY-NC-SA 4.0*
  - 8.4: Fundamentals of Organometallic Chemistry - *CC BY-NC-SA 4.0*
    - 8.4.1: β-Elimination Reactions - *CC BY-NC-SA 4.0*
    - 8.4.2: Associative Ligand Substitution - *CC BY-NC-SA 4.0*
    - 8.4.3: Dissociative Ligand Substitution Reactions - *CC BY-NC-SA 4.0*
    - 8.4.4: Ligand substitution - *CC BY-NC-SA 4.0*
    - 8.4.5: Migratory Insertion- 1,2-Insertions - *CC BY-NC-SA 4.0*
    - 8.4.6: Migratory Insertion- Introduction and CO Insertions - *CC BY-NC-SA 4.0*
    - 8.4.7: Oxidative Addition- General Ideas - *CC BY-NC-SA 4.0*
    - 8.4.8: Oxidative Addition of Non-polar Reagents - *CC BY-NC-SA 4.0*
    - 8.4.9: Oxidative Addition of Polar Reagents - *CC BY-NC-SA 4.0*
    - 8.4.10: Quirky Ligand Substitutions - *CC BY-NC-SA 4.0*
    - 8.4.11: Reductive Elimination- General Ideas - *CC BY-NC-SA 4.0*
    - 8.4.12: The trans/cis Effects and Influences - *CC BY-NC-SA 4.0*
  - 8.5: Parallels between Main Group and Organometallic Chemistry - *Undeclared*
    - 8.5.1: Parallels between Main Group and Binary Carbonyl Complexes - *Undeclared*
    - 8.5.2: The Isolobal Analogy - *CC BY-SA 4.0*
      - 8.5.2.1: Extensions of the Analogy - *CC BY-SA 4.0*
      - 8.5.2.2: Some Applications of the Isolobal Analogy - *Undeclared*
    - 8.5.3: Metal-Metal Bonds - *Undeclared*
      - 8.5.3.1: Metal-Metal Multiple Bonds - *Undeclared*
    - 8.5.4: Cluster Compounds - *CC BY-SA 4.0*
      - 8.5.4.1: Boranes - *Undeclared*
      - 8.5.4.2: Heteroboranes - *Undeclared*
      - 8.5.4.3: Metallaboranes and Metallacarboranes - *Undeclared*
      - 8.5.4.4: Carbonyl Clusters - *Undeclared*
      - 8.5.4.5: Carbon-Centered Clusters - *Undeclared*
      - 8.5.4.6: Additional Comments on Clusters - *Undeclared*
    - 8.5.5: Problems - *Undeclared*
- 9: Introduction to Solid State Chemistry - *CC BY-NC-SA 4.0*
  - 9.1: The Nature of Crystalline Solids - *CC BY-NC-SA 4.0*
    - 9.1.1: Crystal Structures of Metals - *CC BY-SA 4.0*
    - 9.1.2: Ionic and Covalent Solids - Structures - *CC BY-SA 4.0*
      - 9.1.2.1: Prelude to Ionic and Covalent Solids - Structures - *CC BY-SA 4.0*
      - 9.1.2.2: Close-packing and Interstitial Sites - *CC BY-SA 4.0*
      - 9.1.2.3: Structures Related to NaCl and NiAs - *CC BY-SA 4.0*
      - 9.1.2.4: Tetrahedral Structures - *CC BY-SA 4.0*
      - 9.1.2.5: Layered Structures and Intercalation Reactions - *CC BY-SA 4.0*
      - 9.1.2.6: Bonding in TiS_2, MoS_2, and Pyrite Structures - *CC BY-SA 4.0*
      - 9.1.2.7: Spinel, Perovskite, and Rutile Structures - *CC BY-SA 4.0*
      - 9.1.2.8: Discussion Questions - *CC BY-SA 4.0*

        - 9.1.2.9: References - *CC BY-SA 4.0*
    - 9.2: Bonding in Metals, Semiconductors and Insulators – Band Structure - *CC BY-NC-SA 4.0*
        - 9.2.1: Prelude to Electronic Properties of Materials - Superconductors and Semiconductors - *CC BY-SA 4.0*
        - 9.2.2: Periodic Trends- Metals, Semiconductors, and Insulators - *CC BY-SA 4.0*
        - 9.2.3: Bonding in Metals - *CC BY-SA 4.0*
        - 9.2.4: Conduction in Metals - *CC BY-SA 4.0*
        - 9.2.5: Superconductors - *CC BY-SA 4.0*
        - 9.2.6: Semiconductors- Band Gaps, Colors, Conductivity and Doping - *CC BY-SA 4.0*
        - 9.2.7: Semiconductor p-n Junctions - *CC BY-SA 4.0*
        - 9.2.8: Diodes, LEDs and Solar Cells - *CC BY-SA 4.0*
    - 9.3: X-rays and X-ray Diffraction - *CC BY-NC-SA 4.0*
    - 9.4: The Imperfect Solid State - *CC BY-NC-SA 4.0*
    - 9.5: Glasses - *CC BY-NC-SA 4.0*
    - 9.6: Phase Equilibria and Phase Diagrams - *CC BY-NC-SA 4.0*
- Back Matter - *Undeclared*
    - Index - *Public Domain*
    - Glossary - *Undeclared*
    - Detailed Licensing - *Undeclared*

This page titled Advanced Inorganic Chemistry CHEM-5020: Fall 2026 is shared under a license and was authored, remixed, and/or curated by Yulia Zaikina.